THE INTERACTOME OF TRANSGLUTAMINASE-2 IN KIDNEY FIBROSIS

Uncovering a mechanism for TG2 unconventional secretion in chronic kidney disease

Giulia Furini

A thesis submitted in partial fulfilment of the
requirements of Nottingham Trent University
for the degree of Doctor of Philosophy

February 2017

Declaration

To the greatest of all teachers:

Loredana Facchini

"Nonna"

29/01/1930 – 01/12/2013

Abstract

Increased release and activity of transglutaminase-2 (TG2) in the tubulointerstitial space has been correlated with the progression of kidney fibrosis during chronic kidney disease (CKD), a condition for which there is no cure. TG2 extracellular activity contributes to kidney fibrosis by determining matrix deposition and resistance to degradation, through calcium dependent protein transamidation and matrix recruitment of latent TGF-β1, however, the mechanism of TG2 secretion from kidney cells is still unknown. This study aims at elucidating the mechanism of TG2 trafficking in CKD as a way to control its release and ultimately limit fibrosis progression. The murine unilateral ureteric obstruction (UUO) model of renal fibrosis was employed. Firstly, the UUO proteome was resolved and the effect of TG2-KO elucidated by quantitative proteomics of kidney homogenates. This led to the identification of markers of CKD strongly upregulated at an advanced stage of UUO, some of which were dysregulated in TG2-null kidneys, and allowed to set a background for subsequent analyses. Secondly, the TG2 interactome was generated by developing an original approach, based on quantitative mass spectrometry of TG2 immunoprecipitates. This highlighted a significant association of TG2 with a large cluster of vesicular proteins which increased post-UUO, forming the hypothesis that TG2 could be secreted by extracellular vesicles (EV) in CKD. The hypothesis was tested in a model of established tubular epithelial cells (TEC), which revealed TG2 in EV mainly of intraluminal origin (exosomes). The involvement of cell surface heparan sulfate proteoglycan (HSPG) syndecan-4 in the secretion pathway of TG2 was also investigated, and a dual role was ascribed to the proteoglycan, supporting both TG2 secretion and extracellular retention of the enzyme, with promotion of TGF-β1 activation.

In conclusion, this study has shown a novel Sdc4-dependent secretion pathway for TG2 by TECs via extracellular vesicles, which is relevant to CKD condition.

Acknowledgements

First of all, I would like to express my gratitude to my Director of Studies, Dr Elisabetta Verderio Edwards, for accepting me in her lab and always guiding me through the project. A great thank you to my other supervisors, Prof Ellen Billet, Prof Graham Ball and Prof Timothy Johnson for always being enlightening with your comments.

The experimental work of this thesis would have been impossible without the contribution of many people. I would like to thank David Boocock, Claire Coveney and Amanda Miles for their help in the proteomic work. A big thank you also goes to former members of my group, that have contributed to my project with the optimization of protocols, and the creation of plasmids and specific cell lines: Dr Izhar Burhan, Dr Alessandra Scarpellini, and Raghavendran Ramaswamy, Dr Nina Schroeder. A lot of time would have been lost without your help. A special thanks to Nina, who was a friend from day one and a great example to whom I aspire. I am so glad that cases of life have brought us to work together for a while, and I will always treasure those moments.

A big thanks to the members of my research group, Grace, Pauline and Elisa, for being supportive to my work and putting up with my madness and my music. A great thank you goes also to all the members of staff and students of the first floor of IBRC, for always helping me when I needed and being ready to share a joke and a smile. Asli, Lindsey, Cheryl, James, Yegor, Tom, Nick, Joseph, Danielle, Dr Dickenson and Dr Nelson, and all the ones that I'm forgetting. You all made my time here so much better. To Murali, in particular, goes some huge thanks, every lab should have a person like you. My gratitude also goes to Eric, for being my morning laugh and unknowingly giving me great lessons of life.

To Fal, the best friend one could wish for and the person I will miss the most. Thanks, simply for being you, splendid and genuine, with a gigantic heart. Thank you for all the laughs and coffees, and for all your little, but huge, gestures of friendship.

A big thank you goes to my amazing flatmates, Christina and Aimee, which were always there for me, amazing listeners, real soulmates and great masters of the chocolate cookie therapy.

To my crazy, wonderful family goes all my gratitude for always supporting me and making me feel their great love while away. All, in one way or another, you have taught me that the important things in life are not in the grades you take home. I am proud to be your daughter, niece and sister.

Finally, to my new family goes the biggest of my thanks, and all my heart: Lorenzo, you crashed into my life 3 years ago, and completely overturned it. You have a way to get me that no one has ever had, and you make me want to be the best person in the world. Thanks for putting up with all this, the distance, the extreme proximity, the moments of panic and those of acute silliness. You're the strongest person I know and my favourite human being. Thank you, my love.

Publications

Published articles

- Burhan I, Furini G, Lortat-Jacob H, Atobatele AG, Scarpellini A, Schroeder N, Atkinson J, Maamra M, Nutter FH, Watson P, Vinciguerra M, Johnson TS, Verderio EA. Interplay between transglutaminases and heparan sulphate in progressive renal scarring. Sci Rep. 2016 Oct 3;6:31343. doi: 10.1038/srep31343. PubMed PMID: 27694984; PubMed Central PMCID: PMC5046136.
- Verderio EA, Furini G, Burhan I, Johnson TS. Transglutaminases: Expression in Kidney and Relation to Kidney Fibrosis. In Transglutaminases, Multiple Functional Modifiers and Targets for New Drug Discovery. Springer ISBN 978-4-431-55823-1

Articles in preparation

- Furini G, Schroeder N, Huang L, Boocock D, Coveney C, Tonoli E, Ball G, Verderio C, Johnson TS, Verderio EA. Quantitative proteomics reveals a syndecan-4 dependent externalisation pathway for transglutaminase-2 via extracellular vesicles in kidneys post-unilateral ureteric obstruction.
- Huang L, Furini G, Burhan I, Ramaswamy R, Scarpellini A, Verderio EA, Johnson TS. HSPG syndecan-4 acts "in trans" in the recruitment of transglutaminase-2 (TG2) from cell to cell.
- Verderio EA , Furini G. Spotlight on the TG2-heparan sulphate interaction.

Published abstracts

- Furini, G., Schroeder, N., Huang, L., Boocock, D., Johnson, T.S. and Verderio, E.A., 2015. FP013QUANTITATIVE PROTEOMICS BY SWATH-MS REVEALS AN ENDOSOMAL TRANSPORT HUB OF PROTEINS WHICH INTERACT WITH TG2 IN A MODEL OF EXPERIMENTAL KIDNEY FIBROSIS. Nephrology Dialysis Transplantation, 30(suppl 3), pp.iii70-iii70

Conference communications

- Gordon Research Conference - Transglutaminases in Human Disease Processes - Barga (Italy) 29 June -4 July 2014: Giulia Furini, Nina Schroeder, Izhar Burhan , Raghavendran Ramaswamy, Timothy S. Johnson, Elisabetta A.M. Verderio. Cell surface trafficking of Transglutaminase-2 in renal tubular epithelial cells: role of Syndecan-4. Poster presentation.
- ERA-EDTA Conference 2015 – London 28-31 May 2015: Giulia Furini, Nina Schroeder, Linghong Huang, David Boocock, Timothy S. Johnson, Elisabetta A. M. Verderio. Quantitative proteomics by SWATH-MS reveals an endosomal transport hub of proteins which interact with TG2 in a model of experimental kidney fibrosis. Poster presentation (Awarded by paper selection committee) and Oral presentation (Nominated for the Renal association young investigator award)
- Kidney Research UK Fellows Day – York, 14-15 September 2015: Giulia Furini, Nina Schroeder, Linghong Huang, David Boocock, Timothy S. Johnson, Elisabetta AM Verderio. Mapping the transglutaminase-2 interactome by SWATH-MS reveals an endosomal transport hub of proteins which interact with TG2 in a model of experimental kidney fibrosis. Oral presentation.
- East Midlands Proteomic workshop – Coventry, 18 November 2015: Giulia Furini, Nina Schroeder, Linghong Huang, Graham Ball, David Boocock, Timothy S. Johnson, Elisabetta A. M. Verderio. Quantitative proteomics by SWATH-MS reveals an endosomal transport hub of proteins which interact with TG2 in a model of experimental kidney fibrosis. Poster presentation.

Abbreviations

Abbreviation	Name
A	Alanine
AAN	Aristolochic Acid Nephropathy
AB	Antibody
Abs	Absorbance
Akt	Protein Kinase B
AMPK	5' AMP-Activated Protein Kinase
Anxa	Annexin
APS	Ammonium Persulfate
Arf	ADP Ribosylation Factor
a-SMase	Acid Sphingomyelinase
ATM/ATR	Ataxia-Telangiectasia Mutated Kinase / ATM- And RAD3-Related Kinase
ATP	Adenosine Triphosphate
BCA	Bicinchoninic Acid
BSA	Bovine Serum Albumin
BTC	Biotin Cadaverine or N-(5-Aminopentyl)Biotinamide Trifluoroacetate Salt
C	Cysteine
C(FC)	Confidence of Fold Change
CCV	Clathrin Coated Vesicles
CDK	Cyclin-Dependent Kinase
CKD	Chronic Kidney Disease
Ct	Cycle Threshold (qPCR)
D	Aspartic Acid
DAPI	4',6-Diamidino-2-Phenylindole
DDA	Data Dependent Acquisition
DEPC	Diethylpyrocarbonate
DIA	Data Independent Acquisition
Dk	Donkey
DMEM	Dulbecco's Modified Eagle's Medium
DMSO	Dimethyl Sulfoxide
DN	Diabetic Nephropathy
dNTP	Deoxyucleoside Triphosphate
DSS	Disuccinimidyl Suberate
DTT	1,4-Dithiothreitol
E	Glutamic Acid
ECL	Enhanced Chemiluminescence
ECM	Extracellular Matrix
EDTA	Ethylenediaminetetraacetic Acid
EGF	Epithelial Growth Factor
ER	Endoplasmic Reticulum
ESKF	End Stage Kidney Failure
F	Phenylalanine
FAK	Focal Adhesion Kinase
FC	Fold Change
FGF	Fibroblast Growth Factor
FITC	Fluorescein Isothiocianate
Flot2	Flotillin 2
FN	Fibronectin

FXIIIa	Factor XIII A
G	Glycine
GO	Gene Ontology
gplTG2	Guinea Pig Liver TG2
GTP	Guanosine Triphosphate
H	Histidine
HBM	Heparin Binding Mutant
Hepase	Heparitinase
His6-rhTG2	Histidine Tagged Recombinant TG2 (Produced in E. Coli) - Identical to Rh-TG2
HRP	Horseradish Peroxidase
HS	Heparan Sulfate
HSP	Heat Shock Proteins
HSPG	Heparan Sulfate Proteoglycan
I	Isoleucine
IF	Immunofluorescence
Ig	Immunoglobulins
ILV	Intraluminal Vesicles
IP	Immunoprecipitation
K	Lysine
KO	Knock Out
L	Leucine
LB	Lysogeny Broth
LDH	Lactate Dehydrogenase
log2(FC)	Logarithm Base 2 Of Fold Change
LRP	Lipoprotein Receptor-Related Protein
M	Methionine
MS	Mass Spectrometry
Ms	Mouse
MV	Microvesicles (Ectosomes)
MVB	Multivesicular Bodies
N	Asparagine
NEM	N-Ethylmaleimide
NF-kB	Nuclear Factor Kappa-Light-Chain-Enhancer of Activated B Cells
NSF	N-Ethylmaleimide-Sensitive Factor
n-SMase	Neutral Sphingomyelinase
NTU	Nottingham Trent University
OGP	Octyl B-D-Glucopyranoside
ON	Overnight (15 h)
P	Proline
PBS	Phosphate Buffer Saline
PCR	Polymerase Chain Reaction
PDGF	Platelet Derived Growth Factor
Pen/Strep	Penicillin-Streptomycin
PFA	Paraformaldehyde
PIP	Phosphoinositide
PKA	Protein Kinase A Or Camp-Dependent Protein Kinase
PKC	Protein Kinase C
PLA	Phospholipase A
Q	Glutamine
qPCR	Quantitative PCR

R	Arginine
RAAS	Renin Angiotensin Aldosterone System
Rb	Rabbit
Rh-TG2	Histidine Tagged Recombinant TG2 (Produced in E. Coli)- Identical to His6-Rhtg2
RIPA	Radio Immunoprecipitation Assay
RT	Reverse Transcription
RT-PCR	Reverse Transcription - Polymerase Chain Reaction
S	Serine
SD	Standard Deviation from the Mean
Sdc4	Syndecan 4
SDS	Sodium Dodecyl Sulphate
SEM	Standard Error from The Mean
SM	Sphingomyelin
SNARE	Soluble NSF Attachment Protein (Snap) Receptor
SNx	Subtotal Nephrectomy
STZ	Streptozotocin
SWATH	Sequential Window Acquisition Of All Theoretical Fragment-Ion Spectra
T	Threonine
TAE	Tris-EDTA
TMB	3,3,5,5-Tetramethylbenzidine
TBST	Tris Buffer Saline – Tween
TBS	Tris Buffer Saline
TCA	Trichloroacetic Acid
TE	Tris-Acetate-EDTA
TEC	Tubular Epithelial Cells
TEMED	Tetramethylethylenediamine
TG	Transglutaminase (Family)
TG2	Transglutaminase 2
TGF-β	Transforming Growth Factor -B
TMB	3,3,5,5-Tetramethylbenzidine
TNF	Tumour Necrosis Factor
TRIS	Tris(Hydroxymethyl) Aminomethane
UUO	Unilateral Ureteric Obstruction
V	Valine
VEGF	Vascular Endothelial Growth Factor
W	Tryptophan
WB	Western Blot
Y	Tyrosine
β-Me	B-Mercaptoethanol

Contents

Chapter I: General introduction

1.1 CHRONIC KIDNEY DISEASE (CKD) AND KIDNEY FIBROSIS

1.1.1 Chronic kidney disease

Chronic kidney disease (CKD) is a pathology characterised by progressive loss of kidney structure and function over time. It is a general term defining a heterogeneous group of disorders affecting kidney structure and function through different mechanisms (Levey and Coresh 2012).

The most common measurement of kidney function in diagnostic is the glomerular filtration rate (GFR), that measures the flow rate of plasma filtration through the kidney. Normally, GFR is approximated by a measure of creatinine clearance (estimated GFR, eGFR), calculated as the ratio between creatinine concentration in the collected urine and its plasma concentration, multiplied for urine flow rate. Cystatin C (CysC) has also been highlighted as a possible marker for GFR, with a more stable rate of production by the body and a better correlation with the loss of filtration ability (Lopez-Giacoman and Madero 2015, Shlipak, Mattes and Peralta 2013). The eGFR formula is normally corrected to normalise the results depending on people's body size, age, ethnicity and sex (Levey, et al. 2009, Levey, et al. 1999). As a customary practice, the eGFR is divided for the body size area of an average man (1.73 m^2) and expressed in ml/min/1.73 m^2. In physiological conditions, GFR is normally around 100-130 mL/min/1.73 m^2 in men and 90-120 ml/min/1.73 m^2 in women. Interestingly, after age 40, GFR tends to naturally decrease of 0.4-1.2 mL/min per year, which approximately means a reduction of kidney function of the 0.5-1% per year (Bochud 2015).

Five stages of CKD have been defined depending on the GFR: as the disease progresses, GFR goes from values ≥ 90 ml/min/1.73 m^2 (stage 1) to 60-89 ml/min/1.73 m^2 (stage 2), 30-59 ml/min/1.73 m^2 (stage 3), 15-29 ml/min/1.73 m^2 (stage 4), and finally to GFR < 15 ml/min/1.73m^2 (stage 5), which is considered as an end stage kidney failure (ESKF), requiring replacement therapy (Eknoyan, et al. 2013). Urine abnormalities such as albuminuria (Eknoyan, et al. 2013) and proteinuria are also employed to define the gravity of the disease. As a general rule, individuals with GFR <60 ml/min/1.73 m^2 (stage 3) for at least 3 months are regarded as patients with CKD, independently from the presence of kidney damage (Eknoyan, et al. 2013, Inker, et al. 2014).

CKD is a significant health issue worldwide, as it affects more than the 10% of the world's population, an epidemic comparable with the one of diabetes (Eckardt, et al. 2013) . In Europe, CKD prevalence goes from 5.1 to 7.0% for stages 1 and 2 combined, from 4.5 to 5.3% for stage 3, from 0.1 to 0.4% for the last stages. Similar numbers can be detected in the United States (Coresh, et al. 2007, de Jong, et al. 2008). The more exposed groups are the elderly, given the natural loss of kidney function with the progression of age, leading to an approximate loss of 30% of kidney function as the age of 70 (Bochud 2015). Some ethnic groups are also more prone to the disease, such as the Afro-Caribbean groups, probably because of a genetic predisposition, and this is connected to a higher risk of hypertension in these groups (Kopp, et al. 2011, Kao, et al. 2008).

There is no cure for CKD, and the only treatments for end-stage CKD patients are dialysis or kidney transplant. Even if only a low percentage CKD patients are at the end stage, CKD treatment is a socio-economic burden for the health system, given the extremely high costs of replacement therapy and dialysis, and the disrupting effect that these treatments have on the life of a patient (Klein, et al. 2011). Typically, at the initial stages there are no symptoms, and the early signs of the disease are generally underestimated or not diagnosed.

Despite being mainly known for their function in the urinary system, kidneys play a series roles in the regulation of body functions, being directly related to the balance of blood composition and pressure (Schnaper and Kopp 2003). Kidney function goes beyond the well-known excretory one: through plasma filtering, excretion of waste and reabsorption of water and nutrients, kidneys play a crucial part in maintaining body balance, controlling blood osmolality in response to antidiuretic hormone (ADH, secreted by the pituitary gland, hypothalamus), acid-base balance (reabsorption of bicarbonate from urine, excrete hydrogen ions H^+ and NH_4^+ into urine), clearing of toxins, etc. (Schnaper and Kopp 2003). In addition to these roles, kidneys perform endocrine functions secreting a series of hormones such calcitriol, erythropoietin and renin, the latter involved in the regulation of angiotensin and aldosterone level and blood pressure through the renin-angiotensin-aldosterone system (RAAS).

Given the crucial roles of kidneys in the maintenance of body homeostasis and clearing of circulating toxic molecules, it is well known that CKD can have damaging effects not only on the excretory system. In particular, CKD affects the cardiovascular system even at its earliest stages, when not many visible symptoms of renal damage are present (Herzog, et al. 2011, Gansevoort, et al. 2013).

Because the kidney is involved in many other physiological and pathological processes in the body, kidney diseases are classically divided in primary diseases, originating in the kidney or mainly located in the kidney, and secondary diseases, which have other origins but lead to CKD.

Examples of primary kidney disease are congenital diseases (e.g. mutations affecting mesangial cells or podocytes), some kinds of diabetic-independent glomerulonephritis, urinary tract infection, etc. (Eckardt, et al. 2013). Most end-stage patients are affected by monogenic disorders such as polycystic kidney disease, which is the main genetic cause of CKD (Devuyst, et al. 2012).

The nephrons are the structural and functional units of the kidneys (**Fig. 1.1**). Each nephron is composed of a corpuscle, that filters the blood and is composed by a capillary tuft called glomerulus and a surrounding Bowman's capsule, and a tubule, that perform both the functions of secretion and reabsorption (**Fig. 1.1, Table 1.1**). Kidney diseases can be distinguished into glomerular conditions, if they initially affect the glomerular portion of the nephron, and tubular diseases, if they start from the tubules (**Fig. 1.1**). Glomerular diseases are the large majority of the diseases leading to CKD, as the glomerulus is the filtering part of the nephron receiving the blood from the system. Even if starting from the glomerulus, the disease eventually compromises the tubular portion during its progression (Kaissling, LeHir and Kriz 2013).
On the other side, few primarily tubular diseases have been reported, which are generally triggered by a form of acute kidney injury whose repair processes become chronic and lead to the formation *foci* of tubulointerstitial fibrosis (Kaissling, LeHir and Kriz 2013). Some toxic substances, ischemia and ureteric obstruction are considered causes of tubular diseases (Kaissling, LeHir and Kriz 2013).

Diabetic nephropathy (DN) and hypertension-associated CKD are the most common causes of ESKF in developed societies (Maezawa, Takemoto and Yokote 2015, Levey and Coresh 2012, Eckardt, et al. 2013). DN is perhaps the most studied type of CKD, given its frequency in the population and its importance in public health. Hyperglycaemia can lead to kidney damage through many ways: it affects the integrity of endothelial basement membrane of glomerulus, the production of nitric oxide, it promotes the activation of RAAS, the release of reactive oxygen species (ROS) and the upregulation of cytokine mediators such as transforming growth factor-β (TGF-β) and vascular endothelial growth factor (VEGF) (Nakagawa, et al. 2011, Broekhuizen, et al. 2010, Nieuwdorp, et al. 2006, Kuwabara, et al. 2010). Hypertension produces a renal damage by increasing blood pressure in the renal capillaries, and ROS production.
Because of its effect on diabetes and hypertension, obesity may be regarded as an important risk factor for CKD (Chen, et al. 2004, Hsu, et al. 2009).

A **Location and structure of the kidney**

The picture is displaying copyright protected material from Pearson Education (USA) and Encyclopaedia Britannica (www.britannica.com).**Permission** to include in the electronic version of the thesis was **not obtained**.

B **Structure of the nephron**

The picture is displaying copyright protected material from Pearson Education (USA). **Permission** to include in the electronic version of the thesis was **not obtained**.

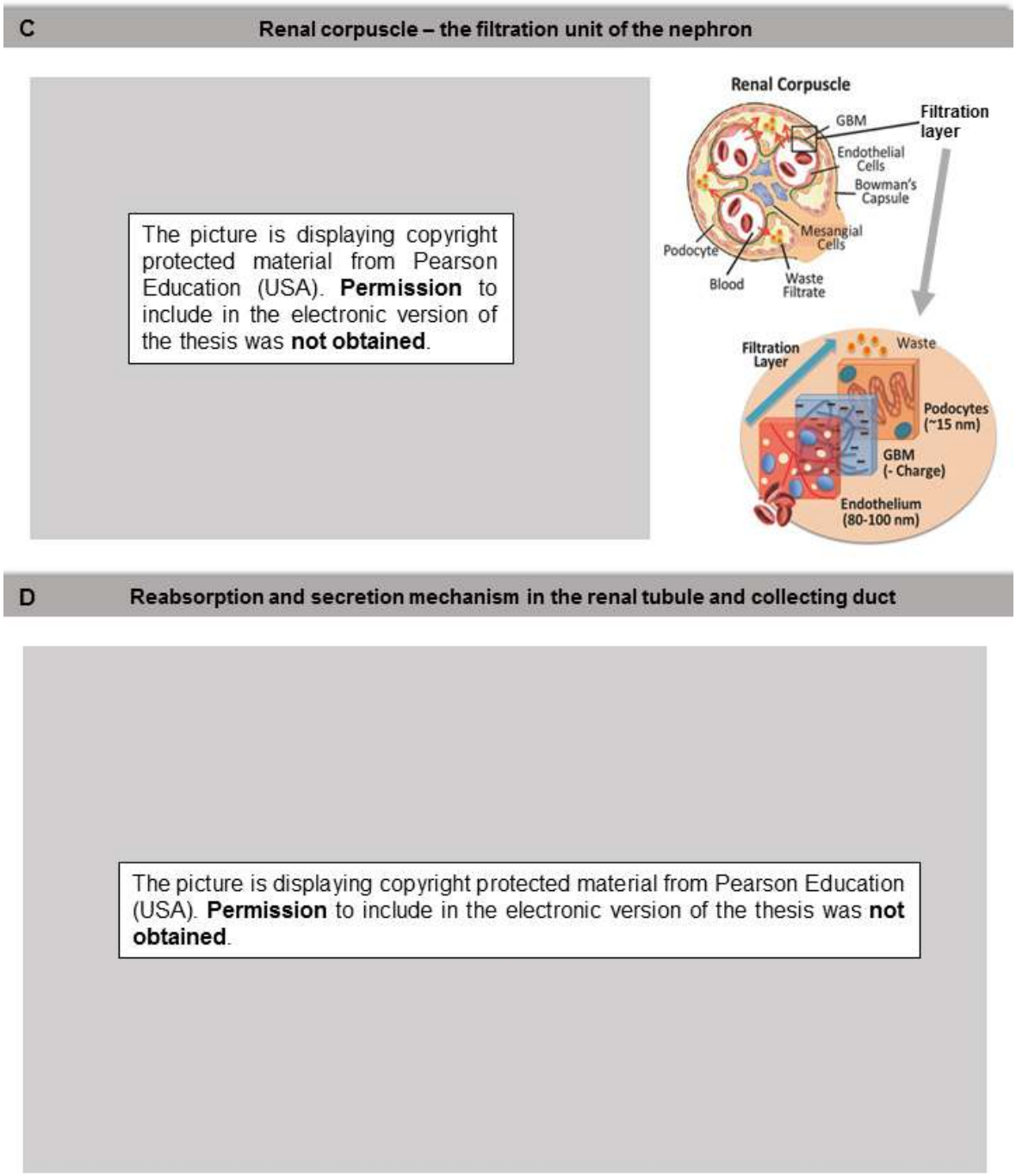

Figure 1.1: Kidney structure and main components. (A) Location and anatomy of the human kidney: The kidneys are "beans shaped" multi-lobed organs located at the back of the abdomen outside the peritoneal cavity. On longitudinal section, the kidney can be distinct into a cortical area, on the outside, and a medullar area in the inside. Picture adapted from (Marieb and Hoehn 2007). Internal anatomy of the kidney, obtained from Encyclopaedia Britannica (www.britannica.com). **(B)** Representative structure of the nephron and distinction between cortical nephrons and juxtamedullary nephrons, from (Marieb and Hoehn 2007). **(C)** Structure of the renal corpuscle: renal corpuscles occupy only 3 -5% of the total kidney (Schnaper and Kopp 2003). They are characterised by a capillary tuft called glomerulus that receives blood-to-filter from the renal afferent arterioles, filters it through a process of ultrafiltration driven by the high pressure in the capillaries, and drains the filtered blood in into an efferent arteriole. The external part of the renal corpuscle is known as the Bowman's capsule and receives the filtered material (ultrafiltrate) that will subsequently flow along the renal tubule (Patton 2015). Distinction into three filtration layers: capillary endothelial cells, characterised by pores (fenestrae); the thick glomerular basement membrane (GBM) characterised by a large glycocalyx, acting as a negatively charged barrier protecting form the filtration of negative molecules such as serum

albumin; the podocyte layer, specialized foot processed (pedicels) cells that surround the capillary tuft. Mesangial cells are specialised cells with characteristics between macrophages and vascular smooth muscle cells (Schnaper and Kopp 2003, Patton 2015) located in the interstitial space between capillaries and involved in glomerular contraction. Pictures obtained from (Marieb and Hoehn 2007) and (Lee, et al. 2015a). Permission to reproduce the picture on the right has been granted by John Wiley and Sons. **(D)** Schematic representation of the renal tubule and collecting duct, with distinctive pattern of reabsorption and secretion: at the proximal convoluted tubule (PCT) mostly reabsorption happens, and salts, water and molecules such as glucose and amino acids are reabsorbed into peritubular capillaries. At the level of the loop of Henle the water and salt exchange takes place: the descending limb of the loop of Henle, permeable to water, allows water to exit freely by osmosis into the interstitial space until tonic equilibrium. The thin ascending limb, impermeable to water, is characterised by a series of transporters that actively pump sodium (Na^+) and other ions out from the filtrate into the interstitial capillaries (reabsorption) (Patton 2015). At the level of distal convoluted tubule (DCT), active transport of ions in both directions happens, and is generally is controlled by hormones. Potassium (K^+) is secreted from the blood to the ultrafiltrate, while calcium (Ca^{2+}) and Na^+ (controlled by aldosterone) are generally reabsorbed in the blood stream (Patton 2015). Exchanges of hydrogen (H^+) and ammonium (NH_4) (secreted) and bicarbonate ions (HCO_3^-, reabsorbed) also happen at this level and control plasma pH. The collecting duct system departs from the distal tubules and descends into the medullar area, where high levels of Na^+ drive water reabsorption through ADH-controlled aquaporins, leading to urine concentration (Patton 2015). Picture obtained from (Marieb and Hoehn 2007).

Table 1.1: Cellular components of the nephron. All cells of the nephron can be affected by CKD.

Location	Cellular types
Renal corpuscle	• Mesangial cells (intraglomerular, between capillaries) • Fenestrated endothelial cells (capillaries) • Podocytes (outer layer of glomerulus) • Epithelial cells (Bowman's capsule)

Tubules	• Tubular epithelial cells (TECs).
	  ○ Proximal convoluted tubule (PCT): cuboidal epithelial cells with brush border (microvilli). Bigger than DCT cells.
	  ○ Descending limb of Loop of Henle: cuboidal epithelial cells (thick) + Squamous epithelial cells (thin).
	  ○ Ascending limb of Loop of Henle: cuboidal epithelial cells (thick) + Squamous epithelial cells (thin).
	  ○ Distal convoluted tubule (DCT): cuboidal epithelial cells without brush border (microvilli). Smaller than PCT cells.
	• Interstitial Fibroblasts /Myofibroblast

Juxtaglomerular apparatus *(Located between afferent arteriole and DCT)*	• Juxtaglomerular cells: specialised smooth muscle cells (known to secrete renin). • Epithelial cells (*Macula densa* – cortical ascending loop of Henle). • Mesangial cells (extraglomerular)
Vascular system	• Endothelial cells • Smooth muscle cells • Leucocytes • Platelets

In summary, several factors can determine CKD, going from diabetes, increase in intravascular pressure (hypertension), ureteric obstruction, toxic molecules, immune complexes, mechanical insult, genetic mutations, etc. However, even if the aetiologies of CKD are multiple, the main feature that unites all these diseases is a progressive scarring, or fibrosis, of the

kidney, that can initiate in any part of the nephron and leads to progressive disruption of renal parenchyma and to the organ functional loss, being the main event associated with the progression of CKD to ESKF (Liu 2006).

1.1.2 Kidney fibrosis

There is a general agreement in literature that kidney fibrosis is the main common event that characterize the progression of virtually any kind of CKD to its end stages and is considered the main cause of the progressive kidney function loss observed in CKD (Liu 2006). Kidney fibrosis is a progressive and irreversible pathological process which, as any other type of tissue fibrosis, may be regarded as an abnormal wound healing process, determined by chronic insult of the organ and inflammation. The main characteristics of kidney fibrosis are the accumulation of sclerotic tissue and collapse of renal parenchyma that lead to kidney failure (Duffield 2014). Fibrotic kidneys show an excessive accumulation and deposition of a pathological extracellular matrix (ECM), mainly consisting of collagen I and III, but also collagen IV (deposited in the basement membrane) and V, fibronectin (FN), laminin, and heparan sulphate proteoglycans (HSPGs). Matrix build up is accompanied by a progressive loss of functional cells and vasculature that lead to the loss of renal parenchyma (Hewitson 2012, Liu 2006, Duffield 2014). While in physiological conditions, ECM synthesis is part of a reparative process, upon CKD the excessive synthesis and deposition results in an accumulation of scarring tissue that is destructive for the organ function. Parenchyma collapse is caused by cell loss as well as accumulation and contraction of ECM fibres, leading to a smaller size of the fibrotic organ, in which the scarring tissue results more concentrated (Hewitson 2009).

As causes of CKD are multiple, and can principally affect the glomerulus, the tubules, and the vascular system, renal fibrosis can start in different parts of the nephron depending on the initial site of insult. Generally, kidney fibrosis can be distinguished into glomerulosclerosis, if it affects the glomerulus, or tubulointerstitial fibrosis, if it affects the tubular interstitium (**Table 1.2**). Since most of nephron volume is made by the tubule (~95%), renal fibrosis is generally observed as a tubulointerstitial fibrosis, that happens simultaneously with the tubular structure loss (Kaissling, LeHir and Kriz 2013).

Glomerulosclerosis is characterised by the thickening of the glomerular basement membrane, mesangial cells proliferation and matrix accumulation in the mesangial space (mainly collagen IV) and podocyte loss. Matrix accumulation impairs the filtration function of the glomerulus and leads to a general hardening of the glomerulus with progressive occlusion. Tubulointerstitial fibrosis is instead characterised by accumulation of interstitial matrix, fibroblast proliferation and activation, tubular damage and tubular atrophy, as well as capillary loss. Accumulation of interstitial matrix within tubules and capillaries impairs their

reabsorption/secretion functions (**Table 1.2**). In some cases, vascular sclerosis can be observed, with matrix accumulation, thickening of the tunica media, smooth muscle cells proliferation and loss of elasticity (**Table 1.2**).

As the disease progresses, leading to ESKF, fibrosis affects all parts of the nephron resulting into widespread fibrotic lesions at glomerular, tubular and vascular level.

Table 1.2: Main events in kidney fibrosis.

Location	Progression	End stage
Renal corpuscle (Glomerulosclerosis)	• Mesangial cells proliferation • Thickening glomerular basement membrane (GBM) • Thickening of Bowman's capsule • Podocyte loss • Matrix accumulation in the glomerulus ("hardening") • Progressive occlusion by fibrous tissue accumulation at the proximal tubular level • Capillary loss	• Complete occlusion of the glomerulus • Fibrotic "hard" glomerulus. • Loss of cells
Tubules (Tubulointerstitial Fibrosis)	• Fibroblast/myofibroblast proliferation • EMT and EndMT • Tubular epithelial cell loss • Thickening tubular basement membrane (TBM) • Matrix accumulation in the interstitial space. • Expansion of interstitial space • Tubular atrophy • Capillary loss	• Tubular loss • Virtually a-cellular sclerotic tissue
Vascular system (Vascular Sclerosis)	• Matrix accumulation inside the vessel • Thickening of the tunica media, • Smooth muscle cells proliferation • Loss of elasticity of the vessel • Vascular calcification can be observed	• Sclerotic vessels • Calcified vessels

1.1.2.1 Cellular mechanisms of kidney fibrosis

At a cellular level, the mechanism of fibrosis shares most pathways with wound healing (Verderio, Johnson and Griffin 2004). The main difference is that, in this case, the continuous insult and inflammation (chronic) lead to a perpetuation of the healing response, that results in an excessive accumulation of ECM beyond the level occurring in the normal wound healing response, as well as disruption of the cellular systems.

The main events that characterize kidney fibrosis can be distinguished into inflammatory infiltration, fibrogenic response (glomerulosclerosis and tubulointerstitial fibrosis) and cell death (with tubular atrophy, capillary loss and podocyte loss), and eventually lead to parenchymal disruption (Liu 2006).

After the initial injury (insult), kidney resident cells activate and start an inflammatory response, with production and secretion of proinflammatory cytokines and chemokines. Proinflammatory cytokines and chemokines recruit inflammatory cells by chemotactic gradient, leading to infiltration of neutrophils, monocytes/macrophages as well as T cells. These cells produce both inflammatory and pro-fibrotic cytokines and injurious molecules such as reactive oxygen species (ROS). Main pro-fibrotic cytokines are thought to be TGF-β [1.1.2.2] and platelet-derived growth factor (PDGF) (Hewitson 2012). These cytokines mainly act in the profibrotic response; however, they are also suggested to contribute to macrophage recruitment in the site of injury. Being the process regarded as an uncontrolled wound response, other factors might co-participate, such as fibroblast growth factors 1 (FGF1, acidic) and 2 (FGF2, basic) and vascular endothelial growth factor (VEGF), interleukins (IL) and tumour necrosis factor α (TNFα) (Grazul-Bilska et al., 2003; Schultz & Wysocki, 2009; Werner & Grose, 2003).

Pro-fibrotic cytokines and growth factors stimulate the activation of the resident mesenchymal cells, their proliferation, and influence ECM-proteins synthesis by these cells. In all kidney compartments, fibrosis is associated with at least one type of mesenchymal cells: the interstitial fibroblast, the glomerular mesangial cells and vascular smooth muscle cells (Liu 2006, Hewitson 2012); these cells are phenotypically similar and, when activated, both mesangial cells and fibroblasts acquire smooth muscle cells features with *de novo* synthesis of smooth muscle actin (α-SMA)(Darby and Hewitson 2007, Johnson, et al. 1991). These activated cells are the principal source of ECM components, in particular collagens I and III and FN (Liu 2006) and also provide mechanical strength for the contraction of the ECM, thus increasing its density (Hewitson 2012). In addition to α-SMA, intermediate filaments proteins are associated with the mesenchymal phenotype, such as desmin and vimentin (Raats and Bloemendal 1992). Particularly important are the activated renal interstitial fibroblast, regarded as myofibroblast. Myofibroblast are recognized by α-SMA (stress fibres) and elevated contractile proprieties and

are identified virtually all types of kidney fibrosis. α-SMA is crucial for cell adhesion and maturation of focal adhesion sites (Hinz, et al. 2003) and is fundamental for the contractile proprieties of myofibroblasts (Hinz, et al. 2001b, Hinz, et al. 2001a). Contraction of myofibroblasts seems to depend on a Rho-Kinase pathway that involves myosin phosphatases (Tomasek, et al. 2002).

Myofibroblast expression is largely correlated with the progression of the disease (Hewitson 2012). While in normal wound healing they contribute to the mechanical tension required for wound closure, but disappear by apoptosis as the scar is formed, during kidney fibrosis they remain and proliferate in the tissue, leading matrix synthesis and deposition as well as tissue contraction (Darby and Hewitson 2007).

Interestingly, resident interstitial peritubular fibroblasts have been suggested not to be the only fount of myofibroblast activation, as other cells such as pericytes/perivascular fibroblasts and bone marrow derived cells (fibrocytes) can be activated to myofibroblasts (Meran and Steadman 2011, Lin, et al. 2008) .

Phenotypical activation of resident cells is not the only source of myofibroblasts in kidney fibrosis. In the context of fibrosis, when the pro-fibrotic stimuli are intense and maintained for long times, they not only promote fibroblast activation in a way that is similar to wound-healing, but also induce transition of tubular epithelial cells (TECs) to mesenchymal features through a process that is referred as epithelial to mesenchymal transition (EMT) (Quaggin and Kapus 2011). EMT is a mechanism through which the epithelial cells, in this case the tubular ones, loose adhesion as well as cell polarity and acquire mesenchymal features with the ability to migrate and invade the area. The process of EMT starts with the loss of adhesive proprieties in the stimulated (or injured) epithelial cells, followed by expression of α-SMA and cytoskeletal modifications, disruption of tubular basement membrane and finally migration and invasion (Liu 2004). EMT is characterized by loss of epithelial markers such as E-cadherin, desmoplakin, cytokeratin, and *de novo* expression of mesenchymal markers such as α-SMA, N-cadherin, OB-cadherin (a better marker of activated fibroblasts), vimentin and fibroblast specific protein 1(FSP1, or S100A4)(Zeisberg and Neilson 2009). Translocation of β-catenin from the membrane to the cytosol and then to the nucleus, where it is involved in transcriptional regulation, is another symptom of cells undergoing EMT (Zeisberg and Neilson 2009).

Interestingly, also injured endothelial cells have been suggested to transition to mesenchymal features through similar mechanism. Endothelial to mesenchymal transition (EndMT) has been observed in different types of renal fibrosis model such as the unilateral ureteric obstruction (UUO), the streptozotocin-induced DN as well as in diabetic kidney biopsies (Li and Bertram 2010, Zeisberg, et al. 2008).

While myofibroblastic activation of the resident cells is an early response of the kidney tissue to pro-fibrotic stimuli and it is also observed in wound healing processes, transition (EMT) of the TECs is thought to happen at a later time (Liu 2006, Efstratiadis, et al. 2009).

Proliferative mesenchymal myofibroblastic cells deriving from both processes produce a substantial amount of collagen (mainly of subtypes I and III) and FN and have contractile proprieties (α-SMA). Continuous deposition of ECM protein by these cells result in the progressive accumulation of a fibrous scar. The fibrous scar as well as the myofibroblast contraction is thought to induce mechanical injury in the kidney, that determine reduced vascularisation (capillary loss), cell atrophy and death and finally parenchymal collapse.
Pro-fibrotic cytokines and growth factors are not only produced by infiltrating leucocytes but also by stimulated epithelial cells, endothelial cells, and by fibroblasts/myofibroblasts, thus perpetuating the fibrotic response. Interestingly it has been seen that, if kidney injury is chronic or persistent, as in many cases of CKD, injured epithelial cells show an arrest in cell cycle between the G2 and M phase and that G2/M-arrested proximal tubular epithelial cells (TECs) can upregulate the production of profibrotic cytokines (especially TGF-β) via a JNK (c-jun NH2-terminal kinase) signalling pathway (Yang, et al. 2010).

Reduced vascularisation is a consequence of tissue fibrosis and leads to hypoxia, which itself has been suggested to act as a profibrotic stimulus, mostly by aim of the hypoxia-inducible factor-1 (HIF1), being involved in both EMT and TGF-β activation. This favours the progression of the disease through a positive feedback loop in which hypoxia is both effect and promoter of fibrosis (Tanaka and Nangaku 2010, Kimura, et al. 2008, Higgins, et al. 2007, Zhang, et al. 2003, Higgins, et al. 2008).
Proteinuria is another well-known consequence of kidney disease, frequently employed as a marker of renal function loss: the breakage of the glomerular barrier leads to leakage of proteins into the urine. At the same time, uremic proteins might be adequately filtered and might accumulate in blood; as these proteins are toxic, they can result in tubular inflammation in a self-sustained loop that promotes fibrosis (Hewitson 2012, Ihle, et al. 1989).

In many CKD conditions, vascular calcification can also be observed and has been linked with elevated risk of mortality. Vascular calcification can be observed in 30-65% of patients with stage 3-5 CKD and in most end stage patients (Moe and Chen 2008). It is considered as a response to hyperphosphatemia, uraemia, inflammation and hyperglycaemia, in which vascular smooth muscle cells acquire chondrocyte/osteoblast-like features and produce "matrix vesicles" from which calcification starts. This process is usually referred as Chronic Kidney Disease-Mineral Bone Disorder (CKD-MBD) (Moe and Chen 2008). Reduced Calcitriol

production by proximal tubular cells is a cause of vascular calcification, as calcitriol is and activated form of Vitamin D that controls calcium absorption and phosphate secretion by the kidney.

Other complications of CKD include anaemia, due to a reduced production of erythropoietin by interstitial fibroblasts around the proximal tubule of the kidney.

1.1.2.2 Transforming growth factor β (TGF-β): the main pro-fibrotic cytokine in kidney fibrosis

Transforming growth factor β (TGF-β1, -β2, -β3) is a family of growth factors necessary for several cellular processes including wound healing, fibrosis and metastatic cancers. TGF-β is synthesized as an immature pro-peptide composed by an N-terminal signal peptide, a latency associated peptide (LAP), and the TGF-β peptide. By proteolysis, mature TGF-β is produced, dimerizes as an ~25 kDa dimer and remains connected with the LAP peptide by non-covalent bonds, forming in what is called small latent TGF-β complex (Annes, Munger and Rifkin 2003, Worthington, Klementowicz and Travis 2011). This complex associates to a larger peptide called latent TGF-β binding protein (LTBP), which is required for secretion, by disulphide bonds. As a result, TGF-β is secreted and accumulates in the matrix as an inactive latent complex referred to as the large latent TGF-β complex, in which the cytokine is complexed with the two other proteins, LAP and LTBP (Annes, Munger and Rifkin 2003, Worthington, Klementowicz and Travis 2011). This complex is unable to bind cell surface receptors, and TGF-β must be released from LAP to be activated.

TGF-β activation by release of the protein can be mediated by different processes, with integrin-mediated activation being the more described. LAP contains Arg-Gly-Asp (RGD) domains for integrin binding, and integrins are known as the main inducers of TGF-β activation, by promoting mechanical tension or by simultaneously binding proteases and LAP (Wipff and Hinz 2008, Hinz 2015, Worthington, Klementowicz and Travis 2011). Moreover, activation can be mediated by proteolytic cleavage of LAP, performed by proteases such as plasmin or matrix metalloproteases (MMPs), ROS-mediated structural modification of LAP and thrombospondin interaction with TGF-β (Annes, Munger and Rifkin 2003). Thrombospondin is a matrix glycoprotein known to be upregulated by TGF-β and has been involved in its activation upon kidney disease (Daniel, et al. 2004). Acid treatment that denatures LAP leads to TGF-β activation *in vitro* (Annes, Munger and Rifkin 2003).

Once activated, TGF-β binds two serine/threonine kinase receptors (TGFβRI and TGFβRII) resulting in TGFβRI phosphorylation by TβRII, which is constitutively phosphorylated. Phosphorylation of the receptor leads to signal transduction by activation of the Smad signalling pathway, involved in the transcriptional regulation of several proteins. Briefly, the

phosphorylated TGFβRI receptor recruits and phosphorylates R-Smads (receptor regulated Smads: Smad2 or Smad3). Smad2/3 then associate to Smad4 (common Smad) and form a heterodimer that enters the nucleus and acts as a transcription factor. The TGF-β/Smad signalling is regulated at different stages, both pre-receptor and post-receptor, by regulation of TGF-β gene expression, activation through different mechanisms, receptor expression and post receptor Smad signalling.

Genes upregulated by TGF-β through Smads are FN, collagen, HSPGs (Kolm, et al. 1996), transglutaminase-2 (TG2) and other wound healing - associated proteins such as thrombospondin and tenascin, while it downregulates proteins associated with matrix degradation, such as some MMPs and plasmin (Varga, Rosenbloom and Jimenez 1987, Ignotz and Massague 1986, Roberts, et al. 1990).

Upregulation of TGF-β has been identified in virtually any kind of CKD. It has been proven to stimulate activation of both mesangial cells and interstitial fibroblasts, and transition of TECs to myofibroblast *in vitro* (Fan, et al. 1999, Liu 2006, Liu 2004). Exogenous TGF-β has been shown to lead to renal fibrosis, while its inhibition has a protective role in CKD (Liu 2006).

In kidney disease, both TGF-β expression and activation by release from the latent complex are upregulated, and also the expression of TGF-β receptors has been suggested to be increased (Böttinger 2007, Bottinger and Bitzer 2002, Lan 2011). All these elements lead to an upregulation of TGF-β/Smad signalling. Moreover, some Smad corepressors, known to control the effect of Smad signalling in healthy kidneys, have been suggested to be downregulated upon kidney fibrosis (Yang, et al. 2003), further increasing the cytokine mediated signalling response. TECs express the largest number of TGF-β receptors, hence they have been suggested to be the main target of the cytokine, leading to EMT (Liu 2004).

Glucose and angiotensin II (AngII) have been suggested as possible TGF-β inducers, as well as proteinuria and ischemia, while other profibrotic factors, such as connective tissue growth factor (CTGF), have been suggested as downstream effectors of TGF-β. CTGF has been suggested to be induced by TGF-β and determine myofibroblast differentiation and proliferation (Duncan, et al. 1999, Gupta, et al. 2000, Kothapalli, et al. 1997).

1.1.2.3 Other factors in kidney fibrosis

Beyond cytokines and growth factors, other molecules can be involved in the promotion of kidney fibrosis. For example, as reported before, there is a direct association between diabetes and CKD, as an increased glucose concentration is known to determine a fibrotic response (Lam, et al. 2003, Li, et al. 2003). Kidney fibrosis has also been suggested to be under the control of the RAAS, putting the pathological process in correlation with blood pressure and hypertension.

There is an association between cardiovascular diseases and kidney fibrosis, which is both direct and indirect. On a side, in fact, fibroblast proliferation and ECM deposition is upregulated by AngII, that also has inflammatory proprieties and induces TGF-β (Ruiz-Ortega and Egido 1997, Ruster and Wolf 2006), but also aldosterone and renin have been proposed to play profibrotic / profibrogenic roles independently from hypertension (Ruster and Wolf 2006). On the other side, hypertension itself induces stress injury in the kidney tissues, indirectly leading to fibrosis. In line with these findings, the control of blood pressure has been suggested to be renoprotective in models of kidney fibrosis (Lewis, et al. 2001).

Studies of hypertensive kidney disease have highlighted the presence of renal oxidative stress leading to promotion of fibrotic matrix accumulation, and that the oxidative stress is induced by prolonged exposure to AngII (Zhao, et al. 2008). Moreover, uremic proteins retained when the kidney progressed to failure have been suggested to be toxic in the context of cardiac disease (Vanholder, et al. 2003).

MMPs and plasminogen/plasmin are proteins involved in matrix remodelling and resolution of the wound healing process. During wound healing, MMPs are released together with their inhibitors (tissue inhibitors of matrix metalloproteases, TIMPs) and control matrix remodelling by degrading existing matrix (Schultz and Wysocki 2009). However, some extracellular proteases have been associated with the progression of kidney fibrosis by acting as signalling molecules, more than simple degrading enzymes (Zhao, et al. 2013). For example, gelatinase-A (MMP-2) has been suggested to promote EMT *in vitro*, and to determine fibrosis if overexpressed in mice (Zhao, et al. 2013). Also, MMP-3 has been involved in the process, by activating Rac1 small GTPase, which leads to the production of ROS (Zhao, et al. 2013). TGF-β -induced shedding of E-cadherin by MMPs has been suggested to induce a signalling pathway mediated by β-catenin, which promotes EMT (Zheng, et al. 2009). Increased MMP-9 activity has been involved in disruption of tubular basement membrane, which promotes EMT of TECs, and tissue-type plasminogen activator (tPA) has been suggested to induce MMP-9 activation (Cheng and Lovett 2003, Radisky, et al. 2005, Yang, et al. 2002, Zheng, et al. 2009).

1.1.2.4 Fibronectin (FN) in cell adhesion and matrix accumulation

FN is a principal component of ECM, necessary for cell adhesion, migration and adhesion-associated signal transduction. FN is a matrix glycoprotein that organises into insoluble fibres though self-association sites; by arranging itself into an insoluble extracellular matrix, FN provides a structure on which cells can adhere and spread.

FN can bind cell surface adhesion receptors such as integrins, through its RGD domains, and heparan sulphate (HS) chains of HSPGs, though its heparin-binding sites. This interaction leads to the activation of adhesion dependent signalling pathways on the cells, that promote

cytoskeletal remodelling necessary for the cell movement. Engagement of FN by cell surface HSPG syndecan-4 (Sdc4) triggers focal adhesion and stress fibres formation, providing the contractile strength for cell movements, through signalling routes that largely depend on protein kinase Cα (PKCα) activation. A specific description of HSPGs involvement in cell matrix adhesion and signal transduction will be provided in Chapter VI.
In addition to its importance in cell adhesion, adhesion-associated signal transduction and cell spreading, FN binding to cell surface receptors is also needed for FN polymerisation from soluble FN dimers into insoluble FN fibrils. Adhesion-mediated cell mechanical contraction, stimulated by Rho family of small GTPases, favours FN assembly into a fibrillar matrix by inducing ECM tension, FN stretching and subsequent exposure of otherwise hidden self-assembly sites (Zhong, et al. 1998, Huveneers, et al. 2008).

In inflammatory conditions, fragmentation of FN leads to release of free RGD sequences, that interfere with FN matrix binding to integrins and lead to cell detachment and detachment-associated cell death, also known as anoikis (Hadden and Henke 2000); this also promotes apoptosis by activating caspase-3 (Buckley, et al. 1999). These free RGD peptides are normally released in large number during matrix remodelling, necessary in both wound healing and angiogenesis, and they are sharply released in kidney fibrosis, due to the activity of specific MMPs (Wang, et al. 2010, Verderio, et al. 2003).

1.1.3 Experimental models of chronic kidney disease inducing fibrosis

As reported before, CKD represents a heterogeneous group of diseases with many aetiologies, characterised by recurrent or progressive injury of the glomerulus, the tubulointerstitium or the vasculature. The most disparate events can affect kidney physiology, ranging from immune events, to inflammatory responses, to toxic substances, to metabolic impairment or genetic predisposition. For this reason, many animal experimental models of CKD exist in renal research, that employ one or more CKD causes to induce the fibrotic response (**Table 1.3**).

Animal models of CKD can be distinguished into spontaneous models and acquired models. Spontaneous models are generally characterised by a low reproducibility and elevated gender and strain bias (Yang, Zuo and Fogo 2010). Some spontaneous models, for example, employ the simply aging of animals, mostly rats, which is linked to a natural decrease of renal functionality (Goldstein, Tarloff and Hook 1988). Aging of experimental animals primarily determines glomerulosclerosis, with thickening of the GBM, followed by tubulointerstitial disease and tubular atrophy, at a rate that is gender and genetic background - dependent and is not always reproducible (Schmitt, et al. 2009). Other models involve for example mice with *Lupus nephritis*, an immune complex – mediated glomerular disease le followed by interstitial responses, or spontaneously hypertensive rats (SHR), rats characterised by hyper-contracting smooth muscle vascular cells leading to excessive vasoconstriction and developing glomerulosclerosis and tubulointerstitial fibrosis as a secondary disease (Santiago-Raber, et al. 2004, Ofstad and Iversen 2005).

Some genetic engineered models have also been produced to mimic specific CKD conditions, as in case of transgenic animals with toxin-induced podocyte depletion (comparable to a genetic focal and segmental glomerulosclerosis, FSGS) or the HIV-associated nephropathy (HIVAN) transgenic mice model, both determining glomerular damage and sclerosis as a primary effect.

Generally reproducible and reliable are the acquired models of CKD. Many acquired models have been developed in the last decades, simulating different types of human conditions lading to fibrosis. Ablation models, obstructive models, and metabolic models mimicking DN are among the more largely employed.

Subtotal nephrectomy (SNx), also regarded as a 5/6 nephrectomy model, is a model inducing glomerulosclerosis by removal of one kidney and ablation of 2/3 of the other, and is sometimes referred to as the "remnant kidney model" (Shimamura and Morrison 1975, Anderson, et al. 1985, Griffin, Picken and Bidani 1994, Kren and Hostetter 1999). Generally, in this model, hypertension and strong upregulation of the RAAS system are observed (Anderson, et al. 1985, Griffin, Picken and Bidani 1994, Greene, Kren and Hostetter 1996, Remuzzi, et al. 2005). Normally, glomerular sclerosis resembling to FSGS and early interstitial fibrosis can be

observed 8 weeks post SNx, while high levels of glomerular sclerosis and tubulointerstitial fibrosis are detected at 3 months post-ablation (Ma, et al. 2005, Johnson, et al. 1997b, Burhan, et al. 2016). Progressive renal insufficiency and hypertension are observed in this model, and detectable by an increases in proteinuria, serum creatinine and systolic blood pressure, with proteinuria strongly correlating with scarring index (Johnson, et al. 1997b).

Unilateral ureteric obstruction (UUO) model is one of the main models employed in the study of CKD, as it allows rapid induction of a tubulointerstitial response (Chevalier, Forbes and Thornhill 2009). In this model, surgical obstruction of one ureter determines urine retention and reduced blood flow, with a rapid (days to weeks) development of tubulointerstitial inflammation and fibrosis, and end stage kidney failure reached in less than a month (Ucero, et al. 2014, Chevalier, Forbes and Thornhill 2009, Scarpellini, et al. 2014). Specific description of this CKD model will be provided in chapter III.

Aristolochic acid nephropathy (AAN) model is a good model of CKD in mice, with mechanisms resembling to the human disease (Huang, et al. 2013, Scarpellini, et al. 2014). AAN is a disease characterised progressive renal interstitial fibrosis often linked with urothelial cancer and associated with aristolochic acid (AA) containing plant extracts (Aristolochia spp.), reported to be nephrotoxic and carcinogenic since last century (Gokmen and Lord 2012, Debelle, Vanherweghem and Nortier 2008). It was first described in 1993 in a Belgian study on women developing tubulointerstitial fibrosis after assumption of a slimming regimen containing extracts from this family (Vanherweghem, et al. 1993). It is sometimes referred as Chinese herbs nephropathy given the frequent substitution of botanical products AA-containing herbs in Chinese. Murine AAN models with administration of a series of AA doses induce an early tubulointerstitial fibrosis, with the proximal tubule being the main target of AA and male being more affected that female (Huang, et al. 2013, Lebeau, et al. 2005).

Other animal models of CKD might involve the employment of puromycin aminonucleoside (PAN), inducing nephrotic syndrome or Cyclosporine A, determining kidney fibrosis by upregulation of pro-fibrotic pathways such as RAAS system and TGF-β signalling pathway (Gherardi, Vecchia and Calandra 1980, Bing, et al. 2006).

Animal models of diabetes have also been employed to study fibrotic development [reviewed in (Rüster and Wolf 2010, Alpers and Hudkins 2011)]. Glomerular injury and endothelial dysfunction are the main effects of diabetes in kidney, however, also tubulointerstitial effects can be observed (Nakagawa, et al. 2011). One of the most used models of DN is the Streptozotocin (STZ) - induced model of Type I diabetes (Tesch and Allen 2007). STZ is a chemical known to be particularly toxic to the pancreatic beta-cells; STZ treatment determines hyperglycaemia, oxidative stress, and albuminuria in a dose-dependent manner. A number of low concentration doses, instead of a single more concentrated dose, are required to produce an effect comparable to diabetes, as STZ has been shown to produce nephrotoxic effects

independently from its effect on hyperglycaemia, making the interpretation of results difficult when high levels are employed (Tesch and Allen 2007).

The db/db mouse model, on the other side, is characterized by of leptin receptor deficiency, and is one of the mostly employed model of Type II diabetes in the study of DN (Sharma, McCue and Dunn 2003).

Table 1.3: Experimental models of CKD.

Model	Principle	Initial fibrotic effect	Advantages	Disadvantages
Ageing	Spontaneous, loss of kidney function with age	Glomerulosclerosis	Spontaneous	Gender and strain dependent. Not reproducible.
Lupus nephritis	Spontaneous, immune complex-mediated	Glomerulosclerosis	Spontaneous	Gender and strain dependent.
spontaneously hypertensive rats (SHR)	Spontaneous, excessive vasoconstriction	Glomerulosclerosis and tubulointerstitial fibrosis as secondary effect	Spontaneous	Gender and strain dependent. Fibrosis as secondary effect.
Toxin-induced podocyte depletion	Genetically engineered model, loss of podocyte barrier.	Glomerulosclerosis (FSGS)	Good model for podocyte loss - glomerular damage	Employment of drugs /toxins.
HIV-associated nephropathy (HIVAN)	Genetically engineered model, mimics nephropathy resulting from kidney infection with HIV or from antiretroviral drugs effect	Glomerulosclerosis (FSGS)	-	Gender and strain dependent.
Subtotal nephrectomy (SNx) or 5/6 nephrectomy model	Acquired model, ablation (removal of one kidney and ablation of 2/3 of the other)	Glomerulosclerosis (FSGS)	Reproducible, well described by proteinuria, does not require drugs/toxins	Slow, elevated hypertension observed.
Unilateral ureteric obstruction (UUO)	Acquired model, surgical obstruction of one ureter	Tubulointerstitial fibrosis	Reproducible, Rapid, does not require drugs /toxins. Determines tubular damage as a primary result. Presence of contralateral kidney as a control.	Does not reflect the slow progression of kidney fibrosis hat generally happens in clinical conditions. Urine accumulation affect detection.
Aristolochic acid nephropathy (AAN)	Acquired model, nephrotoxic effect of aristolochic acid (AA)	Tubulointerstitial fibrosis	Reproducible, well representative of human conditions. Determines tubular damage as a primary result.	Employment of drugs /toxins. Can also determine a carcinogenic response.
Puromycin aminonucleoside (PAN)	Acquired model, nephrotoxic (nephrotic syndrome), podocyte loss.	Glomerulosclerosis	Reproducible, Representative of podocyte loss and glomerular alterations	Employment of drugs /toxins.
Cyclosporine A	Acquired model, induction of pro-fibrotic pathways (mainly RAAS, ROS and TGF-β)	Tubulointerstitial fibrosis and endothelial dysfunction.	Reproducible, activates main pathways leading to kidney fibrosis.	Employment of drugs /toxins, secondary effects. Requires low last diet.
Streptozotocin (STZ) - induced model	Acquired model, type I diabetes. STZ is toxic for pancreatic β cells.	Glomerulosclerosis (DN)	Reproducible DN model. Well correlates with hyperglycaemia and loss of kidney function/kidney damage.	Employment of drugs /toxins. Can also determine nephrotoxicity independently from diabetes.
db/db model	Genetically engineered model, type II diabetes. Model of leptin receptor deficiency.	Glomerulosclerosis (DN)	Reproducible DN model	-

1.2 TRANSGLUTAMINASE FAMILY

1.2.1 The transglutaminase family (TG)

The transglutaminase (TG) family (EC 2.3.2.13, "Protein-glutamine γ-glutamyltransferase") is a family of enzymes with calcium (Ca^{2+})-dependent transamidating activity, which leads to post translational modification of proteins (**Table 1.4**). In humans, nine TGs have been identified, of which eight are catalytically active (TG1-7 and Factor XIII) and one is catalytically inactive (Erythrocyte membrane protein band 4.2) (Eckert, et al. 2014). TG isoforms originated by an early gene duplication event that gave rise to two separate lineages, one containing TG1, TG4 and FXIII, more closely related, and one containing the other TG members (Lorand and Graham 2003a).

Of the TG members, transglutaminase-2 (TG2) has been the most characterised, as ubiquitously expressed and generally present in cells in higher amount. Availability of TG genetic knock out models have contributed to the understanding of specific gene functions, but also highlighted the complexity if their role and regulation. In the following pages, the enzymatic reaction catalysed by the TG family is reviewed and the roles of the individual isozymes summarised with an emphasis on the TG2 family member.

Table 1.4: Members of the transglutaminase (TG) family. Members of the transglutaminase family and proprieties in human. Adapted from (Eckert et al., 2014). Proteins identified as expressed in rat kidney by our group (Burhan, et al. 2016) are highlighted (**Kidney**)

Protein name	Protein ID	Alternative names	Gene	Gene locus	MW (kDa)	Main location in humans	Main function(s)
Transglutaminase-1	TG1	Keratinocyte TG, TGk, particulate TG	*tgm1*	14q11.2	110	Epidermis, squamous epithelia (Membrane-bound keratinocytes) **Kidney**	Keratinocyte Differentiation, Cornified envelope formation
Transglutaminase-2	TG2	Tissue TG, TGc, liver TG, endothelial TG, erythrocyte TG, Ghα	*tgm2*	20q11-12	77	Ubiquitous **Kidney**	Cell adhesion, matrix stabilization, cell death, signal transduction, etc.
Transglutaminase-3	TG3	Epidermal TG, TGE, callus TG, hair follicle TG, bovine snout TG	*tgm3*	20q11-12	77	Hair follicle, epidermis, brain (keratinocytes) **Kidney**	Keratinocyte differentiation, Cornified envelop stabilization, hair growth
Transglutaminase-4	TG4	Prostate TG. TGp androgen-regulated major secretory protein, vesiculase, dorsal prostate protein 1	*tgm4*	3q21-22	77	Prostate	Reproduction, (semen coagulation) – in rodents. Prostate cancer (EMT)
Transglutaminase-5	TG5	TGx	*tgm5*	15q15.2	81	Foreskin keratinocytes, epithelial barrier lining, skeletal muscular striatum	Keratinocyte Differentiation, Cornified envelope formation
Transglutaminase-6	TG6	TGy	*tgm6*	20q11	78	Testis, lung, brain **Kidney**	Poorly understood, Cancer
Transglutaminase-7	TG7	TGz	*tgm7*	15q15.2	81	Ubiquitous but predominately in testis and lung **Kidney**	Poorly understood, Cancer
Factor XIIIa	FXIIIA	Fibrin-stabilizing factor, fibrinoligase, plasma TG, Laki-Lorand factor	*f13a1*	6q24-25	83	Platelets, placenta, synovial fluid, chondrocytes, astrocytes, macrophages, osteoclasts and osteoblasts	Blood coagulation, wound healing, bone synthesis
Erythrocyte membrane protein band 4.2	Band4.2	B4.2, ATP-binding erythrocyte membrane protein band 4.2	*epb42*	15q15.2	72	Erythrocyte membranes, cone marrow, spleen	Membrane integrity, cell attachment, signal transduction

1.2.2 Transglutaminase reactions

TG members catalyse the formation of intra- or inter-molecular covalent isopeptide bonds between the ε-amine group of a peptide-bound lysine residue (Lys) and the γ-carboxamide group of a peptide-bound glutamine (Gln) residue, with release of ammonia (NH_3). This reaction is also known as crosslinking reaction and the resulting ε-(γ-glutamyl)lysine isopeptide bond is highly resistant to proteolysis (Lorand and Graham 2003b).

The catalytic reaction that characterise the TG family relies on a well-conserved catalytic site, is identical between all enzymatically active TGs, of which cysteine is the most important residue (**Fig. 1.2A**). Interestingly, some cysteine proteases, such as papain, cathepsin and caspase I also share a similar catalytic domain (Takahashi, Takahashi and Putnam 1986).

The crosslinking reaction consists of two steps: upon calcium activation, cysteine (Cys) -SH group attacks the free acyl group of the glutamine residues (γ-carboxamide group) and forms an intermediate thioester with release of NH_3, then the thioester reacts with the free amino group of the acyl acceptor lysine (**Fig. 1.2B**). All enzymatically active TGs can also accept free primary amines/polyamines as donors, mediating amine incorporation and polyamination (**Fig. 1.2B**). Moreover, in presence of H_2O, they catalyse deamidation of glutamine residues to glutamate in the absence of amine donors (**Fig. 1.2B**) (Lorand and Graham 2003b).

Some TG, such as TG1, can also perform an esterification reaction, that can link a Gln residue to the aliphatic chain of ceramide and fatty acid (Nemes, et al. 1999) (**Fig. 1.2B**).

An isopeptidase activity, that reverts the crosslinking one, has been observed only *in vitro* (Lorand and Graham 2003b, Király, et al. 2016).

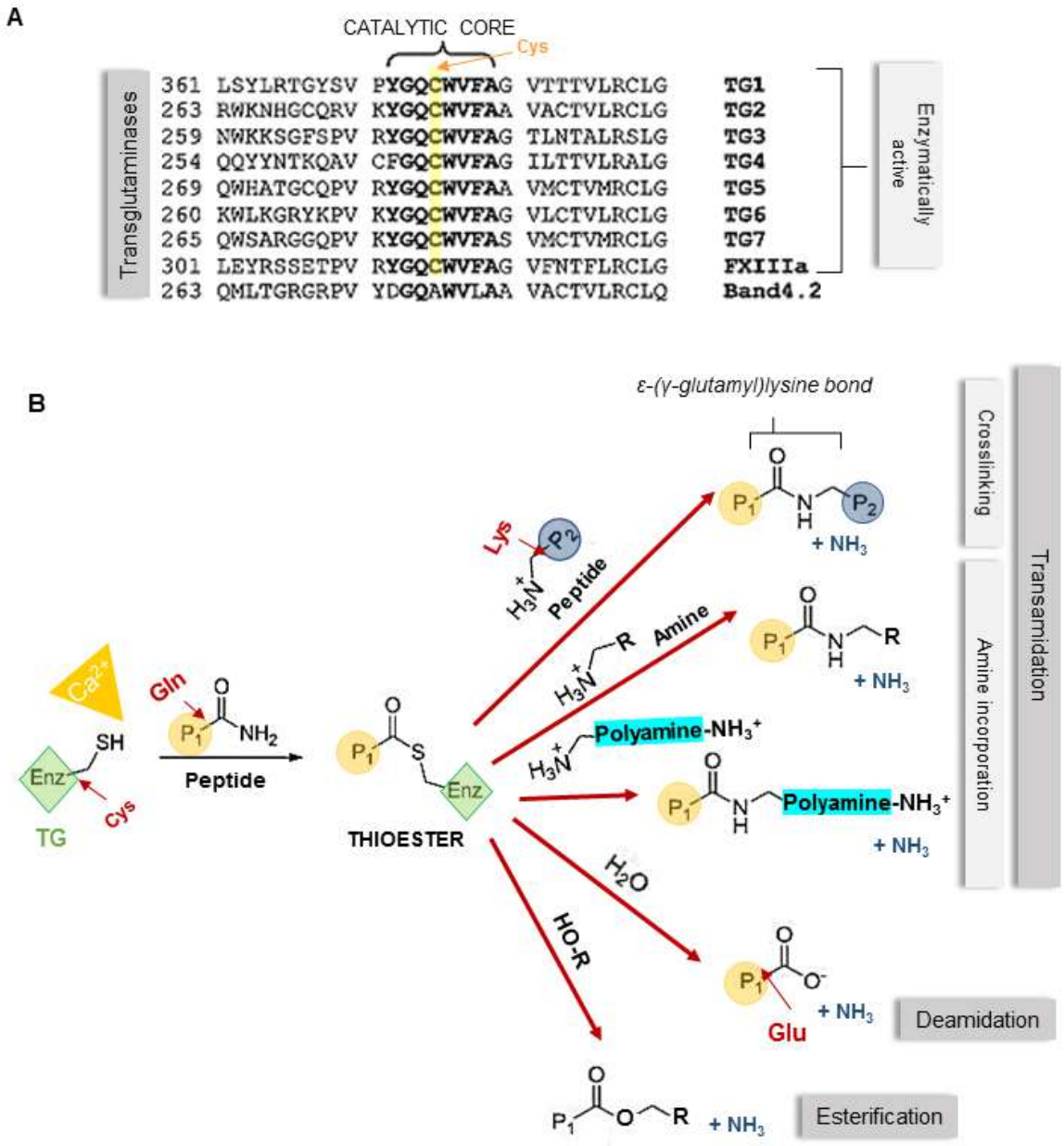

Figure 1.2: The transglutaminase (TG) family. (A) The transamidating catalytic site is conserved among TG members, with exclusion of inactive TG Erythrocyte membrane protein band 4.2 (Band 4.2). Catalytic Cysteine is highlighted in yellow and identified by an arrow. Picture adapted from (Eckert, et al. 2014). Permission to reproduce this picture has been granted by The American Physiological Society. **(B)** Enzymatic reactions catalysed by the TG family, described in [1.2.2]. Picture adapted from (Klöck, DiRaimondo and Khosla 2012). Enz=Enzyme (TG), P = Peptide or Protein. Permission to reproduce this picture has been granted by Springer.

1.2.3 Transglutaminase 1 (TG1)

Transglutaminase-1 (TG1), or Keratinocyte TG, is a membrane-bound protein mainly located in keratinocytes of squamous epithelia, lower female genital tract and upper digestive tract. TG1 is associated with the inner side of the plasma membrane via an amino-terminal lipid (fatty acid) linkage that anchors it to the inner side of the plasma membrane (Phillips, et al. 1993).

TG1 is upregulated at the last stages of keratinocytes differentiation and its activity is fundamental for the formation of the cornified envelope on the cytosolic side of the plasma membrane at these stages, promoting the formation of large protein complexes by crosslinking (Steinert, Chung and Kim 1996, Kalinin, Kajava and Steinert 2002).

Besides being activated by calcium, as all the enzyme members of TG family, TG1 is also activated by proteolysis, resulting in 3 fragments of 10, 33 and 67 kDa which are released in the cytosol (Kim, Chung and Steinert 1995, Sturniolo, et al. 2003, Eckert, et al. 2009, Steinert, Chung and Kim 1996). The proteolysis has been suggested to be mediated by proteins such as the cytosolic calcium-dependent calpain ant the lysosomal cathepsin D (Kim and Bae 1998, Egberts, et al. 2004). The tumour suppressor protein tazarotene-induced gene 3 (TIG3) is a known activator of TG1 in epidermis (Sturniolo, et al. 2003, Eckert, et al. 2009).

TG1 gene mutations lead to *lamellar ichthyosis*, an autosomal recessive skin disorder characterised by abnormal cornification (Huber, et al. 1995, Candi, et al. 1998, Matsuki, et al. 1998). Even if also TG3 and TG5 are localised in the same area and known to contribute to keratinocyte differentiation and formation of the cornified envelope, they fail to compensate the cornified envelope defects of TG1-null mice (Hitomi 2005). Because of the loss of the skin barrier function, TG1-knock out is lethal in neonatal mice (Matsuki, et al. 1998).

1.2.4 Transglutaminase-3 (TG3)

Transglutaminase-3 (TG3), also known as epidermal TG, is mainly identified in epidermis, hair follicle and brain (Hitomi, et al. 2001). Together with TG1 and TG5, it is well expressed in differentiating keratinocytes (Hitomi, et al. 2001, Candi, Schmidt and Melino 2005, Hitomi 2005). It participates to the stabilisation of the cornified envelope together with TG1 (Candi, Schmidt and Melino 2005), even if its presence is not crucial for the formation of a skin barrier (John, et al. 2012). Importantly, it crosslinks keratin and other proteins at the hair follicle supporting hair growth. TG3-null mice have thinner hair, but no significant difference in barrier function or wound healing (John, et al. 2012). TG3 appears to be downregulated during psoriasis, a skin disease associated with altered keratinocyte differentiation, *and lamellar ichthyosis* (Candi, et al. 2002).

Similarly, to TG1, TG3 is activated by proteolysis, which is mediated by Cathepsin L and controlled by the cysteine protease inhibitor cystatin M/E (Cheng, et al. 2006). The 77 kDa precursor protein is cleaved into two domains (50 + 27 kDa), that remain non/covalently joined in the active enzyme (Kim, et al. 1990, Hitomi, Ikeda and Maki 2003). Similarly to TG2, TG3 is able to bind and hydrolyse GTP (Ahvazi, et al. 2004) and, in certain conditions, it has been shown to be secreted by the cells (Sardy, et al. 2002).

1.2.5 Transglutaminase-4 (TG4)

Transglutaminase-4 (TG4), or prostate TG, is specifically present in prostate, prostatic fluids and seminal plasma (Dubbink, et al. 1998, Jiang and Ablin 2011). The enzyme is involved in the formation of the copulatory plug, and TG4-null mice experience lower fertility (Jiang and Ablin 2011). Similarly to TG2 and FXIIIa, TG4 can be secreted (Lorand and Graham 2003b, Jiang and Ablin 2011). TG4 has been correlated with the malignancy of prostate cancer cells and has been associated with EMT in prostate cancer (Jiang and Ablin 2011).

1.2.6 Transglutaminase-5 (TG5)

Transglutaminase-5 (TG5) is mainly localised in keratinocytes and skeletal muscle cells, even if it has been suggested to be present in other tissues (Candi, et al. 2002, Candi, et al. 2004). It is probably involved in the formation of cornified cell envelope and keratinocyte differentiation together with TG1 and TG3 (Candi, et al. 2001). TG5 appears to be upregulated in both *ichthyosis vulgaris* and *lamellar ichthyosis* skin syndromes (Candi, et al. 2002). Mutations in *Tgm5* gene causing enzyme inactivation determine the "peeling skin syndrome" (Cassidy, et al. 2005).

Similarly to TG1 and TG3, TG5 is activated by proteolysis of an 81kDa precursor, resulting in a 53 kDa active peptide (Pietroni, et al. 2008). Similarly to TG2, also TG5 shows GTP binding, and its transamidating activity is inhibited by both GTP and ATP binding (Candi, et al. 2004).

1.2.7 Transglutaminase-6 (TG6) and transglutaminase-7 (TG7)

Transglutaminase-6 (TG6) and transglutaminase-7 (TG7) are less understood TG isoforms. Both are localised in human testes and lungs, and have been detected in mice brain (Eckert, et al. 2014). Both have been also involved in cancer: TG6 has been detected in human tumour cells with neuronal morphology (Thomas, et al. 2013), while TG7 has been associated with a poor outcome of breast cancer (Jiang, et al. 2003).

1.2.8 Factor XIIIa (FXIIIa)

Factor XIIIa (FXIIIa) is one of the most studied TG members and is found in plasma and platelets, but also in macrophages, astrocytes, chondrocyte, dermal dendritic cells, osteoblasts, hearth cells and eyes and synovial fluid (Eckert, et al. 2014). The enzyme is mainly known for its crucial role in the blood coagulation cascade (Ariens, et al. 2002).

FXIII is 83 kDa and is expressed as an heterotetramer composed of two catalytically active subunits (FXIIIa) and two non-catalytic subunits (FXIIIb) that act as carrier proteins. By thrombin-initiated proteolysis mechanism, supported by Ca^{2+}, the catalytical subunit is dissociated from the carrier one, resulting in an active enzyme. The resulting catalytically free "a" subunit is activated by Ca^{2+} (as the other TG members) and plays an important role in blood clot formation by crosslinking of fibrin (Ariens, et al. 2002), which is itself converted from fibrinogen by thrombin.

To promote stabilisation of the fibrin matrix, FXIIIa crosslinks the plasminogen activator inhibitor-2 (PAI2) and α2-antiplasmin (α2-AP), two inhibitors of fibrinolysis, to fibrin, localising them in the blood clot area where they interfere with to plasmin-mediated lysis (Ritchie, et al. 2000). FXIIIa has also been shown to be able to crosslink thymosin-β4 (Tβ4) in the ECM after the release of the protein by thrombin-activated platelets. In this way Tβ4 can be held in the matrix where it contributes to different wound healing steps and promotes the activation of TGF-β (Huff, et al. 2002, Telci and Griffin 2006).

Together with its well-known role in blood coagulation, FXIII has also been suggested to be involved in inflammatory responses: FXIIIa, for example, plays a role in hypertension-associated angiogenesis by mediating monocyte adhesion (AbdAlla, et al. 2004).

Importantly, as TG2 and TG4, Factor XIIIa can be found in extracellular space where it performs its catalytic activity supported by high calcium levels. The mechanism of FXIII secretion has not been elucidated yet, it might involve action of the "b" subunit or might be only dependent on passive stress-induced cell leakage (Muszbek, et al. 2011).

FXIIIa-null mice are characterised by uncontrolled bleeding and, similarly to TG2-null mice, impaired wound healing. They also experience reduced angiogenesis and tissue remodelling defects, in a way that is similar to TG2-null mice (Koseki-Kuno, et al. 2003, Muszbek, et al. 2011, Dardik, Loscalzo and Inbal 2006, Inbal and Dardik 2006).

1.2.9 Erythrocyte membrane protein band 4.2

Erythrocyte membrane protein band 4.2 (Band 4.2) is a 72-kDa catalytically inactive TG member. It lacks the active cysteine that characterises the catalytic site of the other TG isoforms, which is substituted by an alanine (Satchwell, et al. 2009, Eckert, et al. 2014) (**Fig. 1.2A**).

It is a component of the membrane-proximal cytoskeleton of erythrocytes; together with proteins such as spectrin, ankyrin and band 3 (anion exchanger 1, to which band4.2 interacts in living red blood cells), it mediates cortical cytoskeleton attachment to the membrane, playing an important role in the stabilisation of cell and the maintenance of membrane integrity (Satchwell, et al. 2009). Defects in 4.2 expression are involved in hereditary spherocytosis an haemolytic anaemia form of blood disease characterized by the production of spherical blood cells (spherocytes) rather than bi-concave. Band 4.2-null mice are characterised by spherocytosis and defects in ion transport in the cells, by altered regulation of anion exchanger function (band 3) (Peters, et al. 1999, Satchwell, et al. 2009).

1.3 TRANSGLUTAMINASE-2 (TG2)

1.3.1 Transglutaminase-2 (TG2) structure and function in the cell

TG2, or tissue transglutaminase, is the most ubiquitous isoenzyme of the TG family, present virtually in all tissues and cell types and involved in a large spectrum of physiological and pathological events. TG2 was the first described member of the TG family (Mycek, et al. 1959) and, as all the members of the family, it is characterised by a Ca^{2+}-dependent transamidation activity that mediates post translational modification of protein through crosslinking, as well as amine incorporation and deamidation. In addition to the well-known transamidating role of TG2, the enzyme is characterised by Ca^{2+}-independent enzymatic activities, such as GTP and ATP binding and hydrolysis, kinase and protein disulphide isomerase, and non-enzymatic roles as a structural protein in the ECM.

As a result of its multiple function and ubiquity, TG2 has been involved in disparate pathophysiological processes and in a large spectrum of human diseases. As we will see in the next paragraphs, TG2 enzymatic activity has been suggested to be largely controlled by the cells and activated in response to specific stimuli. In physiological conditions, TG2 knock-out mice appear viable, fertile and do not show any developmental abnormality (De Laurenzi and Melino 2001, Nanda, et al. 2001), suggesting that, *in vivo*, TG2 activation is mainly a response to transient or chronic stress condition.

1.3.1.1 TG2 localisation in the cell

Even if TG2 has been described as mainly cytosolic, the enzyme has also been shown to be located on the cell surface and extracellular space, where it contributes to the stabilisation and the deposition of the extracellular matrix (Upchurch, et al. 1991, Barsigian, Stern and Martinez 1991, Belkin 2011, Zemskov, et al. 2006). TG2 lacks a leader peptide (signal peptide) necessary for endoplasmic reticulum (ER) targeting and ER-to-Golgi classical protein secretion (Ichinose, et al. 1990, Ikura, et al. 1988), and also lacks Golgi associated protein modifications such as acetylation and glycosylation (Ichinose, et al. 1990, Ikura, et al. 1988). For these reasons, TG2 has been suggested to be secreted though a non-classical pathway that has not yet completely elucidated (Chou, et al. 2011, Belkin 2011). Shading light on the mechanism of TG2 export by living cells will be one of the main focuses of this Thesis and the description of the state of research on TG2 unconventional secretion will be provided in Chapter V.

Localisation of TG2 has also been reported in the nucleus and in mitochondria (Grazia Farrace, et al. 2002, Furutani, et al. 2016). It has been seen that, in some cell lines such as neuroblastoma cells, TG2 is largely found in the nucleus and can reach up to the 7% of the total enzyme (Lesort,

et al. 1998). Moreover, histones have been shown to be substrates for TG2 activity (Kim, et al. 2002, Mishra, et al. 2006, Ballestar, Boix-Chornet and Franco 2001).

1.3.1.2 TG2 structure and key domains

In humans, the TG2 gene (*Tgm2*) is composed by a total of 13 exons and 12 introns. The most commonly expressed form of TG2 and the only reported in literature as endogenously expressed at a protein level is sometimes referred as TGM2_V1 (Phatak, et al. 2013), or full length TG2. This is a 687 amino acids long monomeric protein of ~78 kDa. TG2 is characterised by four domains: the N-terminal β-Sandwich domain covers the residues from 1 to 139 and does not include a signal peptide for ER-targeting, the α/β catalytic domain, from residue 140 to 454, and two C-terminal β-barrel domains, β1 from residue 479 to residue 585 and β2 from 586 to the C terminal end (**Fig. 1.3**).

The N-terminal β-sandwich domain has been associated with cell adhesion and migration functions of TG2 and does not have enzymatic activity. The N-terminal β-sandwich domain contains a specific binding site for FN in which peptide 88-WTATVVDQQDCTLSLQLTT-106 has been suggested to be crucial for the binding and probably important for the enzyme secretion (Jeong, et al. 1995, Gaudry, et al. 1999, Hang, et al. 2005, Chou, et al. 2011).

The catalytic domain of TG2 is well conserved among the members of the TG family. A catalytic triad formed by Cys277-His335-Asp358 forms the catalytic core (Fesus and Piacentini 2002). Tryptophan residue Trp241 is also situated close to the catalytic core and is important for TG2 transamidating activity, as it has been involved in the stabilisation of reaction intermediates, and is also conserved in other TG members (Iismaa, et al. 2003). Trp-332, on the other side, might be involved in the negative regulation of the activity (Murthy, et al. 2002).

The C- terminal β-barrel domain 1 is involved in binding and hydrolysation of both GTP and ATP, and, together with the core domain and the C- terminal β-barrel 2, regulates the G-protein function of TG2 (Liu, Cerione and Clardy 2002, Kanchan, Fuxreiter and Fésüs 2015, Nakaoka, et al. 1994). TG2 has been shown to be able to bind ATP in the same binding pocket of GTP: the residues Arg476, Arg478, Val479 and Tyr583 have been shown to bind both ATP and GDP by hydrogen bonds, while Ser482 and Arg580 bind only GTP, and Cys230 and Cys370 only ATP (Han, et al. 2010). Kojima and colleagues have recently proposed the sequences responsible for TG2 shuttling between nucleus and cytosol in an hepatocellular carcinoma (HCC) cell line, locating them in the β-barrel domains: a nuclear localization signal (NLS) in the β barrel-1 domain of TG2 (466-AEKEETGMAMRIRV-479) and a leucine-rich nuclear export signal (NES) β barrel-2 domain (657-LHMGLHKL-664) (Shrestha, et al. 2015).

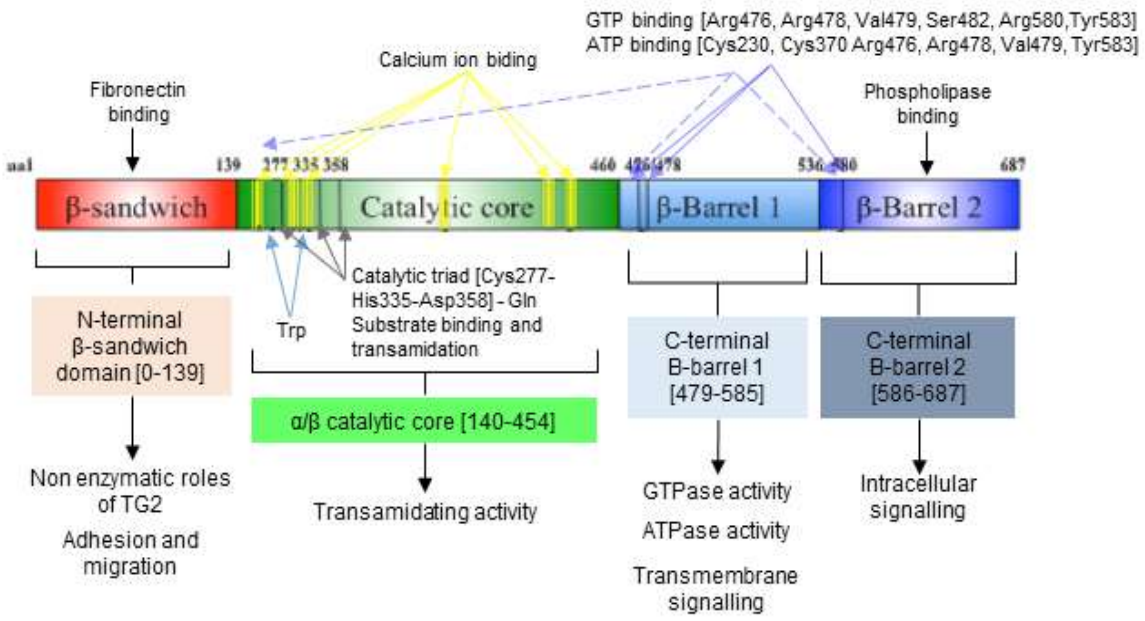

Figure 1.3: TG2 structure and domains. Schematic of TG2 domains with their localisation and associated functions. Important aminoacidic residues have been highlighted. Adapted from (Kanchan, Fuxreiter and Fésüs 2015). Permission to reproduce this picture has been granted by Springer.

TG2 is characterized by at least 4 different isoforms or splice forms, determined by alternative splicing of the transcript. In addition to the canonical full length TG2, or TGM2_V1, 3 isoforms have been reported in literature at mRNA level and have been recently renamed by Phatak and colleagues as TGM2_V2 (short), TGM2_V3 (very short) and TGM2_V4 (a and b, deleted form) (Phatak, et al. 2013). TGM2_V2 and TGM2_V3 are generated by intron retention and result in truncated isoforms with a different C-terminus: TGM2_V2 is a 548 amino acids long protein with a molecular mass of ~62 kDa, TGM2_V3 is a 349 amino acids long protein with a predicted molecular mass of ~38 kDa (Fraij, et al. 1992, Fraij and Gonzales 1996, Antonyak, et al. 2006). TGM2_V4 isoforms a and b are generated by an atypical splicing event resulting in a protein with a size similar to the full length TG2 but with a different C-terminal side (Lai, et al. 2007). In humans, the alterative isoforms lack the C-terminal GTP regulatory domain that controls the access of Ca^{2+} to the active site, and consequently the enzyme is predicted to be constitutively active (Begg, et al. 2006).

Only few studies have been conducted on the role of TG2 isoforms in disease: a higher isoforms expression was detected at mRNA level in cancer cells compared to the normal cells, suggesting an increased level of alternative splicing (Phatak, et al. 2013). Moreover, higher levels of TGM2_V2 expression have been reported upon Alzheimer's disease, in parallel with an increase in crosslinking activity (Citron, et al. 2001). In the rat SNx model of chronic kidney disease generating fibrosis, our group recently demonstrated an upregulation of TG2 alternative

isoform at a transcript level, as well as the canonical TG2 transcript, during the progression of kidney fibrosis (Burhan, et al. 2016).

1.3.1.3 TG2 enzymatic activities in the cell

TG2 possesses multiple activities although it is mostly known for protein transamidation. Several substrate proteins of TG2- mediated transamidation have been reported and collected in the TRANSDAB database (http://genomics.dote.hu/wiki/) (Csősz, Meskó and Fésüs 2009), which currently contains 161 substrates for TG2 enzymatic activity (Appendix **, Table I**).
TG2-crosslinked products are highly resistant to proteolytic degradation and mechanical tension, and can reach large molecular sizes (Griffin, Casadio and Bergamini 2002). In addition to protein crosslinking with formation of ε-(γ-glutamyl)lysine bonds, the transamidation activity of TG2 also determines amine incorporation, typically by incorporating polyamines into peptide-bound glutamine residues. TG2 has also well-known deamidation activity, which has been largely implicated in the modification of gluten peptide gliadin, leading to immune T-cell response in celiac disease (Dørum, et al. 2009, Sollid and Jabri 2011, Anderson, et al. 2000, Klöck, DiRaimondo and Khosla 2012, Arentz-Hansen, et al. 2000).

In addition to its calcium-dependent crosslinking activity, TG2 is able to bind and hydrolyse GTP, acting as a G-protein (referred as Gh) (Nakaoka, et al. 1994). As a G-protein, TG2 has been involved in the regulation phospholipase C (PLCδ1). When not hydrolysing GTP, TG2 has been reported to bind PLCδ1 and inhibit its phospholipase activity, while GTP binding to TG2 allows the dissociation of the two proteins and PLCδ1 activation (Feng, Rhee and Im 1996). TG2 has been shown to couple different receptors to PLC, such as α1b- and α1d-adrenoreceptors, thromboxane and oxytocin receptors. Interestingly, the GTPase activity of TG2 in the activation of PLC has been suggested to contribute to fibroblast adhesion and spreading during wound healing, independently from the crosslinking and non-enzymatic TG2 extracellular roles (Stephens, et al. 2004).

Studies have proposed that TG2 can also act as a protein disulphide isomerase (PDI) in physiological conditions, and that this specific function is involved, in mitochondria, with the correct assembly and folding of the complexes of the respiratory chain (Hasegawa, et al. 2003, Mastroberardino, et al. 2006). Specific substrates are in complex I (NADH–ubiquinone oxidoreductase), complex II (succinate–ubiquinone oxidoreductase) and complex IV (cytochrome c oxidase). This function does not require calcium, hence it would function also when the crosslinking activity of the enzyme is inhibited (Mastroberardino, et al. 2006, Hasegawa, et al. 2003). In support of this notion, TG2-null mice have been reported to have

altered number of disulphide bonds in the respiratory chain complexes, that results in a reduced ATP productions and lethargy of the mice (Mastroberardino, et al. 2006). Accordingly, TG2 overexpression has been proved to induce mitochondrial hyperpolarisation, while its loss determines results in a loss of balance between complex I and II of mitochondrial respiratory system (Grazia Farrace, et al. 2002, Battaglia, et al. 2007). A possible physiological role for TG2 in the context of glucose tolerance was suggested, as TG2-null mice were shown to have a weakened insulin secretion upon glucose simulation, similar to some diabetic responses. This role of TG2 was associated with its involvement in the regulation in the respiratory chain activation lading to ATP production, through its disulphide isomerase function (Bernassola, et al. 2002, Mastroberardino, et al. 2006).

Mishra and colleagues firstly proposed that TG2 is also able to perform serine-kinase activity and phosphorylate insulin-like growth factor-binding protein-3 in breast cancer cells, with a possible anti-apoptotic role (Mishra and Murphy 2004). This activity, again, is not dependent on calcium binding, and even seems to be inhibited by the Ca^{2+}-dependent crosslinking activity of the enzyme (Mishra and Murphy 2004). TG2 kinase activity has been proposed to be induced by protein kinase A (PKA)-mediated phosphorylation, which would also interfere with the enzyme transamidating activity (Mishra, Melino and Murphy 2007). TG2 phosphorylation at serine-216 by PKA has been suggested to create a binding site for 14-3-3 protein family members, with possible roles in signal transduction and apoptosis and a possible involvement in TG2 regulation itself (Mishra and Murphy 2006).

1.3.1.4 The allosteric regulation of TG2 enzymatic activity by calcium, GTP and redox proteins

In the past few decades, several studies have focused on the conformational regulation of TG2 structure by mutually exclusive binding of Ca^{2+} or GTP. TG2 transamidating activity has been suggested to depend on an enzyme "open" tertiary conformation with exposed catalytic domain, which is promoted by Ca^{2+} ions, while GTP binding instead favours TG2 maintenance in a "closed", inactive, conformation (**Fig. 1.4**).

In absence of calcium or at a low calcium level (<100 μM), the active site of TG2 is hidden in a cleft between the N-terminal region and the C-terminal region, covered by the β-barrel domain and hence inaccessible to glutamine donors (Casadio, et al. 1999, Jang, et al. 2014, Liu, Cerione and Clardy 2002) (**Fig. 1.4**). This conformation is regarded as a "close", inactive, TG2 conformation.

Calcium binding determines a "relaxation" of the molecule, to an "open", active, conformation exposing the active sites to substrates (Casadio, et al. 1999, Jang, et al. 2014, Liu, Cerione and Clardy 2002). TG2 can bind 6 Ca^{2+} ions on 6 negatively charged asparagine (Asp) and glutamine (Gln) -rich binding sites. It has been suggested that calcium binding does not determine a complete opening of the TG2 structure, but allows a destabilisation of the structure and the opening of a deep "substrate channel" where glutamine substrates can access to the catalytic core. Binding of glutamine substrates and formation of the acyl-enzyme intermediate allow further opening of the structure to permit correct positioning of the amine donor (Pinkas, et al. 2007, Király, Demény and Fésüs 2011).

GTP binding negatively regulates transamidating activity of TG2 by binding the enzyme in its closed conformation (Liu, Cerione and Clardy 2002, Jang, et al. 2014). Differently from calcium, GTP binding does not directly induce conformational changes in the proteins, but stabilises TG2 into the close structure, that can be reversed by Ca^{2+}- binding, when present at an adequate concentration (>100 μM) (Di Venere, et al. 2000, Casadio, et al. 1999). GTP binding favours stability by masking the "destabilizing residue" Arg579 and favouring the maintenance of the closed conformation, also secured by a Cys277–Tyr516 hydrogen bond (Begg, et al. 2006); on the contrary, Ca^{2+} binding allows destabilisation of the molecular structure and subsequent relaxation by exposing Arg579 and breaking the hydrogen bond (Király, Demény and Fésüs 2011). To note, ATP can also bind TG2 in its close conformation possibly contributing to the stability of the structure (Han, et al. 2010).

The intracellular environment has a relatively high concentration of GTP (50 - 300μM) and ATP (8-11 mM) (Smethurst and Griffin 1996, Király, Demény and Fésüs 2011), and relatively low concentrations of Ca^{2+} (~100nM) (Bronner 2001), hence TG2 crosslinking activity is thought to be inhibited in the cytosol, where TG2 would be acting as a G-protein or be inactive. Only when levels of Ca^{2+} are raised to about 100 μM, the transamidating activity of the enzyme can be detected (Smethurst and Griffin 1996).

Extracellular calcium levels, on the other side, reach millimolar concentrations (~1-1.5 mM) (Bronner 2001, Király, Demény and Fésüs 2011), thus allowing TG2 activation. However, despite the high extracellular levels of calcium and the low GTP, extracellular TG2 has been suggested to be mostly enzymatically inactive *in vivo* in unstressed conditions, and to be almost exclusively activated upon injury or mechanical stress (Siegel, et al. 2008). This is in line with the theory of a TG2 association with stress conditions, supported by the healthy phenotype of TG2-null mice in physiological conditions (De Laurenzi and Melino 2001).

One of the reasons of TG2 inactivity in the extracellular space is the reversible oxidation of "open" TG2 at three cysteine residues (Cys230, Cys370 and Cys371), with formation of a disulphide bond between Cys370 and Cys371 (Stamnaes, et al. 2010), that can happen in the highly oxidizing extracellular environment. These disulphide bonds inhibit Ca^{2+} binding to one

of the sites, and stabilize an inactive, oxidised conformation of TG2. TG2 oxidation is almost exclusively localised in the extracellular space: intracellularly, the reducing environment as well as the abundance of reduced glutathione tend to interfere with the formation of disulphide bonds (**Fig. 1.4**).

Moreover, nitric oxide can inhibit TG2 activity by determining cysteine S-nitrosylation (S-nitrosothiols formation), in a process that is controlled by extracellular calcium levels (Lai, et al. 2001). This modification has been shown to prevent TG2 activity both *in vitro* and *in vivo* in blood vessels, where it limits TG2 dependent vascular calcification and hypertension (Lai, et al. 2001, Santhanam, et al. 2010). Nitrosylation can affect also tyrosine residues of TG2 and was suggested to inhibit its activity in fibroblasts (Telci, et al. 2009) (**Fig. 1.4**).

Thiol reductases such as thioredoxin have been demonstrated to be able to activate TG2 in the extracellular matrix by reducing the Cys disulphide bonds (Jin, et al. 2011). Interestingly, thioredoxin can be secreted by monocytes in response to interferon-γ (IFN-γ), a pro-inflammatory cytokine, and is sufficient to activate the extracellular TG2 (Jin, et al. 2011). In line with this, the employment of the reducing agent DTT has been shown to revers TG2 inactivation caused by oxidation (Stamnaes, et al. 2010) (**Fig. 1.4**). In addition to reducing agents, also mechanical stress associated with cell contraction has been suggested to induce changes on extracellular TG2 conformation, favouring its activation (Huelsz-Prince, et al. 2013, Belkin 2011).

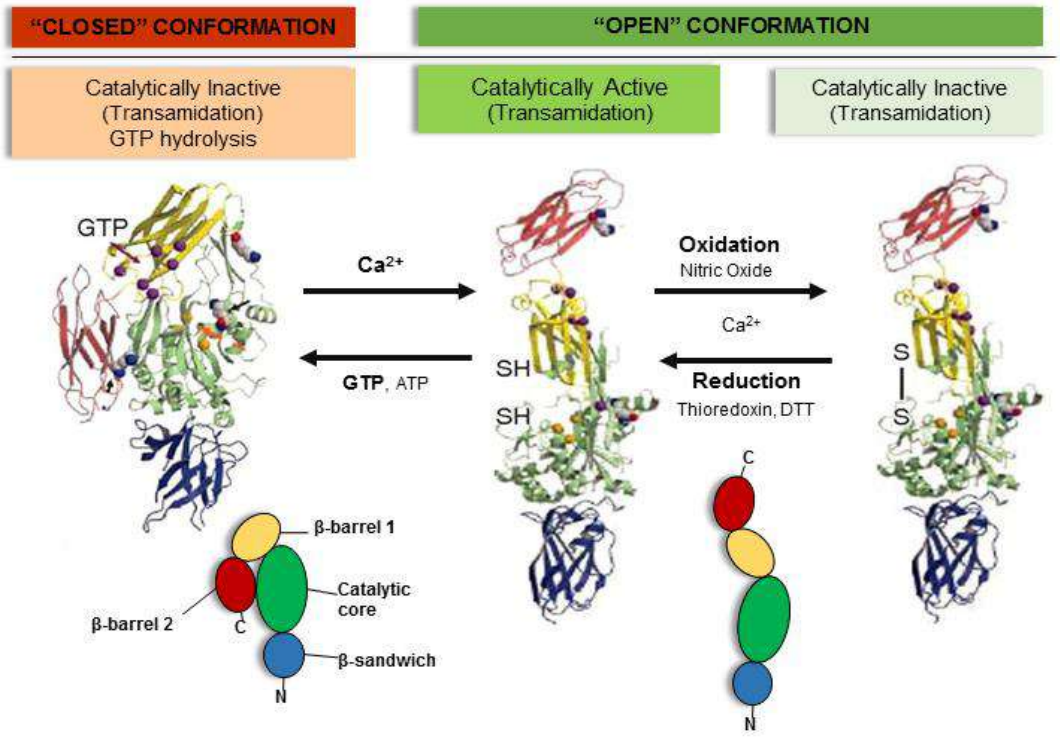

Figure 1.4: The allosteric regulation of TG2 catalytic activity by calcium, nucleosides and redox reactions. Adapted from (Eckert, et al. 2014, Pinkas, et al. 2007). Permission to reproduce these pictures has been granted by The American Physiological Society and Rowena Matthews (Michigan, USA).

1.3.1.5 Regulation of TG2 expression

Even if detected in many cell types, TG2 has been frequently regarded as a stress-associated protein, the expression of which is upregulated by several physiological and pathological stress-associated factors. Many growth factors and inflammatory cytokines have been shown to induce transcription of TG2 mRNA.

TGF-β1, the main pro-fibrotic cytokine involved in the processes of wound healing and fibrosis, upregulates TG2 expression in different cell types (George, et al. 1990, Quan, et al. 2005), and the effect is observable even at low levels of cytokine (1ng/ml) (Quan, et al. 2005). Similarly, cytokines such as interleukin 6 (IL6) and tumour necrosis factor α (TNFα) have also been associated with the enzyme transcription, the latter through induction of nuclear factor κB (NFκB) transcription factor, to which TG2 transcription promoter is sensitive (Suto, Ikura and Sasaki 1993, Kuncio, et al. 1996, Ikura, et al. 1994).

TG2 promoter has an NF-κB binding motif that induces TG2 transcription. Moreover, TG2 is itself able to activate NF-kB through induction of polymerization of NF-κB inhibitory protein, IκBa, with a role in stress response and in the promotion of cell survival in cancer cells; indeed, TG2 inhibition reduces NF-κB activation (Ientile, Caccamo and Griffin 2007, Cao, et al. 2008).

TG2 is upregulated in response to glutamate receptor activation and oxidative stress with release of ROS, which are features neurodegenerative diseases such as Alzheimer's disease and Huntington's disease (Campisi, et al. 2003, Ientile, Caccamo and Griffin 2007).

Other molecules known to induce TG2 transcription are retinoids such as retinoic acid (Piacentini, et al. 1992, Nagy, et al. 1996), and the hypoxia inducible factor HIF-1 (Jang, et al. 2010), which is upregulated upon low oxygen conditions. HIF-1 increases TG2 expression with anti-apoptotic consequences on hypoxic tumour cells, and TG2 has been shown to be upregulated in response to ischemia or hypoxia in different models (Jang, et al. 2010, Filiano, et al. 2010, Tolentino, et al. 2004).

1.3.2 Intracellular TG2 is involved in the regulation of cell death

TG2 has been for long time associated with apoptotic processes inside the cells. TG2 expression and activity has been shown to be upregulated in cells undergoing apoptosis (Piacentini, et al. 2005). Pro-apoptotic stimuli, such as retinoic acid, increase TG2 expression, and TG2 inhibition in the presence of calcium has been suggested to be protective against dell death, in presence of the same stimuli (Oliverio, et al. 1999).

TG2-dependent crosslinking, following increases in intracellular calcium, has been suggested to be involved in the stabilisation of dying cells, preventing loss of intracellular components. The type of cell death induced by TG2 has been suggested to be independent from the normal pathways of apoptosis and necrosis, as the cells are not characterised by classical apoptotic

features (cell shrinkage, chromatin condensation, etc.) neither show fragmentation of DNA (Verderio, et al. 1998, Nicholas, et al. 2003). TG2 determines cell death by inducing cross-linking of intracellular proteins in the presence of calcium.

In the context of renal scarring (Section 1.4), it was observed how TG2 determines intracellular crosslinking in TECs, that were dead but did not show apoptotic morphology and DNA fragmentation (Johnson, et al. 1997a).

In 2003, Nicholas and colleagues showed how intracellular TG2 crosslinking activity happens in response to necrotic stimuli associated with inflammation and wound healing/fibrosis (Nicholas, et al. 2003). Loss of calcium homeostasis during inflammation and wound repair (increase in intracellular Ca^{2+}) led to induction of TG2 crosslinking activity inside the cells, that was mostly localised in the perinuclear area and inside the nucleus. This crosslinking activity was suggested to form shell-like structures around the nuclei, that were comparable to micro-scars or to the TG1-mediated cornified envelope, and were proposed to help trapping the DNA and avert its fragmentation, thus preventing necrotic death and tissue disruption, in a mechanism that is alternative and independent from cell apoptosis (Nicholas, et al. 2003). Similar results were obtained upon UV light - induced upregulation of TG2 activity in dermal fibroblasts (Gross, Balklava and Griffin 2003). This is particularly important in situation of inflammation and tissue repair, limiting necrosis and inflammation and promoting the preservation of the tissue integrity after damage. In hepatic cells, TG2 has been suggested to induce apoptosis through crosslinking and inactivation of the transcription factor SP1 in the nucleus (Tatsukawa, et al. 2009).

Increased intracellular calcium levels and subsequent increase in intracellular TG2-mediated crosslinking and amine incorporation have been associated with different conditions of the brain such as ageing, Alzheimer's disease and Huntington's disease (Jeitner, et al. 2009).

Some authors have suggested that TG2 might be protective against apoptosis in a GTP-dependent manner, favouring survival (Antonyak, et al. 2001, Antonyak, et al. 2006). This might mean that, at the initial stages of infection, when calcium balance is conserved, TG2 upregulation might contribute to cell survival, while, if the stimulus is kept and induces intracellular rise in calcium, TG2 might lead to specific crosslinking-dependent cell death (Nicholas, et al. 2003). In general, TG2 transamidating activity has been suggested to either facilitate or inhibit apoptosis, depending on the tissue and the specific stimuli, while the GTPase function of TG2 has been shown to generally inhibit apoptosis (Fésüs and Szondy 2005).

1.3.3 Extracellular TG2 plays both enzymatic and non-enzymatic roles

As reported before, even if most of TG2 expression is localised in the cytoplasm, a relatively consistent portion of the TG2 (10-20%) is found in the extracellular space, both on the cell surface and extracellular matrix (Zemskov, et al. 2006). In a study on Swiss 3T3 fibroblasts with TG2 expression controlled by a tet-inducible promoter, Dr Verderio and colleagues showed that increased expression of TG2 leads to an increased export and localisation in the extracellular space (Verderio, et al. 1998). Even if in some cases a stress-induced, passive release of TG2 as result of cell damage has been observed (Kawai, et al. 2008), this is thought not to be the only mechanism of TG2 release, as TG2 export has been observed from living and healthy cells *in vitro* (Verderio, et al. 1998).

TG2 is known to be exported by the cells through a still not completely clarified unconventional secretion (Belkin 2011): a description of current hypotheses of TG2 unconventional export will be provided in Chapter V.

Once exported, the enzyme can be found both on the cell surface and extracellular matrix where TG2 co-localises with FN and acts as a Ca^{2+}-dependent transamidating protein (Gaudry, et al. 1999, Verderio, et al. 1998). It also has a structural non-enzymatic role in the ECM, as a protein scaffold with direct consequences on cell adhesion, spreading and survival (Kanchan, Fuxreiter and Fésüs 2015, Belkin 2011) (**Fig. 1.5**).

1.3.3.1 Crosslinking activity of TG2 in the extracellular space is necessary for ECM deposition and resistance

Extracellular TG2 has been shown to covalently crosslink ECM proteins, contributing to ECM deposition and resistance (Aeschlimann and Thomazy 2000). FN, collagens (I, II, III, V, XI), fibrinogen/fibrin, laminin and nidogen are well known substrates of TG2 transamidating activity in the extracellular matrix and cell basement membrane (Verderio, Johnson and Griffin 2004, Barsigian, Stern and Martinez 1991, Verderio, et al. 1998, Jones, et al. 1997, Chau, et al. 2005, Aeschlimann and Paulsson 1991). Particularly important in this context is the role for TG2 in the deposition of a FN matrix by crosslinking soluble monomers, as it provides an environment for cell adhesion and spreading (Jones, et al. 1997, Verderio, et al. 1998). Crosslinking activity of ECM proteins by TG2 has been involved in the promotion of matrix stabilisation, deposition and resistance to proteolytic decay, as well as in the regulation of cell adhesion and movement, by providing a platform of adhesion and migration of cells, like fibroblast or endothelial cells. Since FN matrix assembly acts as start for the polymerisation of other structures, such as fibrillin, TG2 has been suggested to favour not only remodelling of existing matrix, but also initial assembly of novel ECM.

Interestingly, TG2 has also been suggested to crosslink itself to vascular endothelial growth factor receptor (VEGFR), with a role in the modulation of endothelial cell response to VEGF and a potential role in angiogenesis (Dardik and Inbal 2006).
It is important to remember that, while crosslinking activity of TG2 can be well detected *in vitro* upon TG2 export (Verderio, et al. 1998), extracellular TG2 activity *in vivo* is likely to be mostly silent in physiological conditions, due to oxidation/nitrosylation in non-reducing environment, and it is thought to be transiently activated by stress signals or mechanical tension when TG2 is released in the ECM.

1.3.3.2 Non enzymatic roles of extracellular TG2: a scaffold protein necessary for RGD independent adhesion and spreading

The process of cell adhesion and subsequent migration requires the interaction between cell surface receptors, of which the most characterized are Integrins and syndecans, and the extracellular matrix proteins such as FN (RGD cell binding site). Cell surface-matrix interaction leads to different signalling pathways involved in cytoskeletal reorganization, with formation of focal adhesion (FA) and stress fibres. Integrin binding and clustering mediate the process of cell attachment by inducing focal adhesion kinase (FAK) auto-phosphorylation (Tyr397), which in turn leads to FAK activation by further phosphorylation at Tyr576 and Tyr577, by creating a binding site for Src kinase. Autophosphorylation alone does not support FA, which require formation of FAK-Src complex and subsequent Src-mediated activation of the protein. FAK activation, subsequently, regulates both small GTPases Rac and Rho activation (Huveneers and Danen 2009), which are important for migration and stress fibre formation. Transient RhoA downregulation by FAK though activation of small GTPase activating protein p190RhoGAP (Ren, et al. 2000, Arthur and Burridge 2001, Holinstat, et al. 2006) is necessary for transient release of adhesion tension during cell migration.
Cell surface HSPG syndecan-4 (Sdc4) binding to matrix proteins has been involved in the Tyr397-phosphorylation of FAK (Wilcox-Adelman, Denhez and Goetinck 2002), and might also indirectly activate Src-dependent phosphorylation of FAK through PKCα activation (Gatesman, et al. 2004); an outline of HSPGs/Sdc4 involvement in focal adhesion and spreading will be provided on Chapter VI.

In the extracellular space, TG2 can contribute to cell-matrix adhesion and adhesion-dependent signalling through a non-enzymatic "scaffold" role that involves forming a complex with FN, an additional extracellular TG2 function which is independent from its transamidating activity or any other enzymatic activity (Verderio, et al. 2003). TG2 binding site for FN is located on its N-terminal beta sandwich domain (Jeong, et al. 1995, Gaudry, et al. 1999, Hang, et al. 2005).

Extracellular TG2 is able to bind soluble FN at 2:1 stoichiometry on the FN N-terminal gelatin binding domain (Radek, et al. 1993). TG2 promotes FN auto-assembly as well as crosslinking-dependent deposition in the extracellular space in response to stimuli such as TGF-β, and in cooperation with α5β1 integrins (Akimov and Belkin 2001b). Furthermore, TG2 binding to FN has been suggested to protect the enzyme from proteolytic degradation that in the extracellular environment is thought to be mediated specifically by membrane-type MMPs (MT-MMPs subtypes 1-3)(Belkin, et al. 2001)

The TG2-FN matrix complex has been suggested to play an important role in mediating RGD-independent cell adhesion by counteracting stress- or tissue remodelling-associated loss of cell adhesion, and resulting in increased cell survival despite matrix fragmentation (Verderio, et al. 2003). TG2-FN heterocomplex promotes RGD independent cell adhesion by binding to cell surface HSPGs chains and inducing adhesion-dependent cell signalling such as FAK activation (Verderio, et al. 2003). Both integrins and cell surface proteoglycans have been suggested to cooperate with TG2 in the promotion of RGD independent cell adhesion to FN (**Fig. 1.5**). Binding of matrix TG2 to cell surface HSPG Sdc4 induces receptor clustering and subsequent protein kinase Cα (PKCα)- induced signalling (Wang, et al. 2010, Telci, et al. 2008), which in turn would induce β1-integrin clustering and co-signalling (Wang, et al. 2010, Telci, et al. 2008). Indirect association with another HSPG, syndecan-2 (Sdc2), has been reported to be involved the process of cell adhesion in HOB cells, and promote cytoskeletal regulation and FN deposition (Wang, et al. 2010, Wang, Telci and Griffin 2011) (**Fig. 1.5**).

The group of Alex Belkin has proposed that TG2 is also able to directly bind integrins (β1 and β3 mainly) at 1:1 stoichiometry, and, when complexed to extracellular FN, TG2 would act as an integrin-associated co-receptor for the gelatin domain of FN, promoting RGD-independent cell attachment and integrin-dependent cell signalling in this way (Akimov, et al. 2000) (**Fig. 1.5**).

On the cell surface, TG2 has also been shown to interact with other receptors. For example, it has been suggested to bind platelet-derived growth factor receptor (PDGFR) and link it to β1 integrins. Though this function TG2 was proposed to favour receptor clustering, that in turn regulate cell migration (Zemskov, et al. 2009) (**Fig. 1.5**).

Low density lipoprotein (LDL) receptor-related proteins 5 and 6 (LRP5, LRP6) have also been suggested to interact with TG2 on smooth muscle cells, and TG2 binding to these proteins has been suggested to activate the β-catenin signalling pathway, favouring calcification (Faverman, et al. 2008) (**Fig. 1.5**).

LRP1, another member of the family, is an interesting partner of TG2 on the cell surface and a well-known endocytic receptor. TG2 binding to LRP1 has been suggested to promote the enzyme internalisation and degradation through clathrin and/or caveolae-lipid rafts mediated endocytosis (**Fig. 1.5**). Its deletion leads to TG2 upregulation on the cell surface and increased

adhesion and cell-matrix interactions (Zemskov, et al. 2007). LRP1 also regulates endocytosis of other TG2 associated partners such as FN and β1/β3 integrins (Salicioni, et al. 2004, Salicioni, et al. 2002). Localisation of TG2 and β1-integrins in lipid rafts and caveolae might increase the interaction of these particular endocytosis-associated cell domains to the matrix (Zemskov, et al. 2007, Eckert, et al. 2014).

G-protein coupled receptor GPR56 is another binding partner of TG2 on the cell surface, with a role in cancer regulation. GPR56 overexpression has been suggested to inhibit cancer proliferation through a TG2 dependent mechanism which also involves NF-κB (Xu, et al. 2006, Kausar, et al. 2010).

TG2 non-enzymatic interactions are not exclusively associated with adhesion, survival and spreading: the protein has also been suggested to interact with several partners both outside (ECM, cell surface) and inside the cells (cytosol, nucleus), in relation to cell signalling and inflammatory response, and to the control of TG2 activity itself, either directly or by regulation of calcium levels. An exhaustive list of TG2 binding partners and proposed consequences of this interaction has been recently reviewed by Kanchan and colleagues (Kanchan, Fuxreiter and Fésüs 2015) (Appendix **, Table II**). TG2 has also been involved in the regulation of expression and activity of matrix metalloproteases (MMPs) through a non-enzymatic function. For example, TG2 expression was suggested to inhibit MMP-9 transcription by binding c-Jun in the nucleus and inhibiting the Jun-Fos complex binding to the AP-1 transcription site (Ahn, et al. 2008).

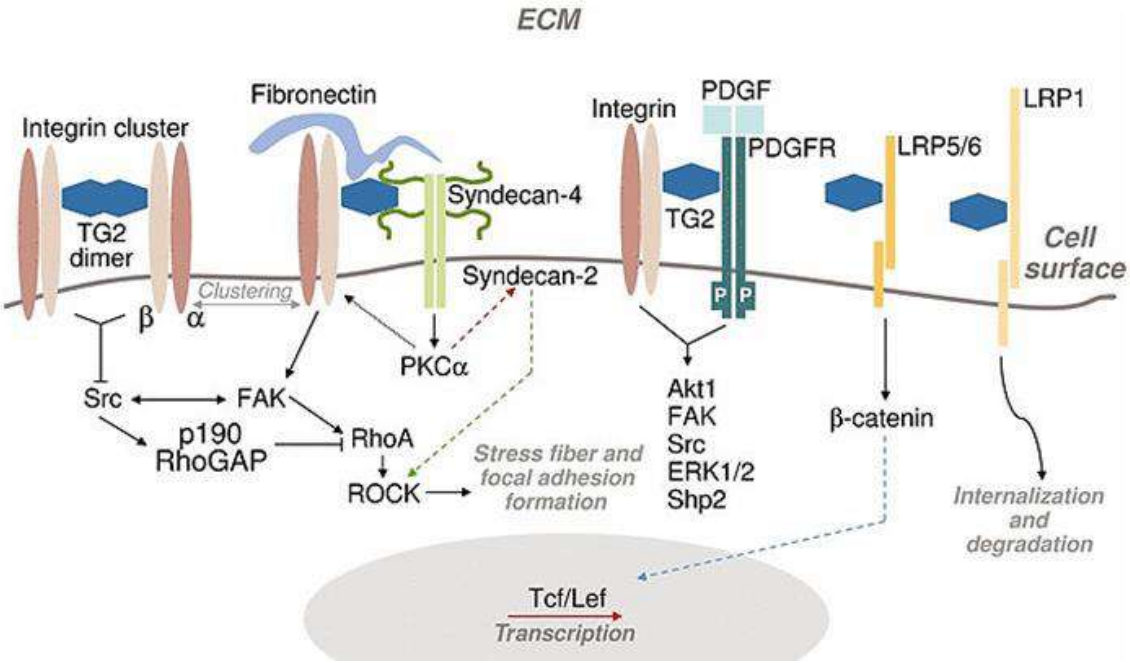

Figure 1.5: Some non-enzymatic functions of TG2 in the extracellular space. From (Belkin 2011). Permission to reproduce this picture has been granted by John Wiley and Sons.

1.3.4 TG2 as a key wound healing protein

In the past few decades, many studies have demonstrated the importance of transglutaminase family members in wound healing, with particular interest on TG2 implication in the process.

Firstly, TG2 is induced and secreted upon tissue injury. Early work in a human fibroblasts monolayer showed that TG2 is deposited in the matrix and associates with FN upon simulation of wound (Upchurch, et al. 1991), where it persists for hours.

Secondly, TG2 expression is upregulated by a series of cytokines that are also induced by platelets and inflammatory cells upon wound repair. Among these, TGF-β, interleukins and TNF-α are well known. Haroon et al. showed a TG2 upregulation in rats upon wound in parallel with cytokine production such as TGF-β, VEGF, TNF-α, IL-6, etc. TG2 deposited in the site of wound already one day after injury in the provisional fibrin matrix, where it performs its crosslinking activity (Haroon, et al. 1999).

Thirdly, on fibroblast monolayer, TGF-β treatment leads to upregulation of both TG2 and FN and stabilizes tissue inflammation by promoting the formation of a proliferative FN matrix (granulation tissue) by crosslinking (Quan, et al. 2005). When acting as a matrix crosslinking enzyme, TG2 has been shown to confer higher stability to the tissue and resistance to both mechanical and chemical matrix degradation (Johnson, et al. 1999).

Extracellular TG2 crosslinking of FN mediates deposition and stabilisation of the granulation tissue, favouring the stabilisation of the inflammatory wound and providing a matrix for fibroblast migration (Quan, et al. 2005).

The crosslinking activity of TG2 is known to play roles also at the earlier stages of wound healing by crosslinking fibrin and FN, as well as at the last stages of scar formation, by crosslinking different collagen isotypes. TG2 has been shown to stabilise the Factor XIII-deposited fibrin blood clot, as non-reducible glutamyl-lysine bounds produced by TG2 have been identified both in the provisional matrix after blood coagulation and during inflammation, and in the granulation tissue produced by fibroblasts to stabilize the inflammatory response.

Therefore, TG2 can act at different stages of the wound healing process, targeting different mechanisms associated with tissue repair (**Table 1.5**). Particularly important is the role for TG2 in the proliferative phase of wound healing, where it has been shown to play roles in granulation tissue formation and fibroblast migration, as well as angiogenesis and epithelization.

The importance for TG2 in the wound healing process has been confirmed by knockout studies, in which TG2-null mice showed delayed wound healing and impaired adhesion of isolated fibroblasts (De Laurenzi and Melino 2001, Nanda, et al. 2001).

TG2 is released by both macrophages and endothelial cells invading the fibrin clot (Haroon, et al. 1999, Murthy, et al. 1991) and has been shown to be upregulated by increased local

concentration of thrombin in endothelial cells (Auld, et al. 2001). Differently from FXIIIa, TG2 does not need thrombin for its activation, therefore can continue its crosslinking activity even after thrombin disappears from the healing area (Verderio, Johnson and Griffin 2004). In line with this is the finding that XIIIa deficiency does not lead to a strong wound healing impairment (~15%) (Muszbek, Yee and Hevessy 1999).

TG2 has also been shown to support scar formation by crosslinking collagen I, II and III as well as promoting lysyl oxidase (LOX) - independent crosslinking of collagen V and XI (Verderio, Johnson and Griffin 2004, Kleman, et al. 1995), leading to collagen matrix remodelling and formation of large collagen bundles, providing resistance to mechanical tension as well as conferring resistance to proteolytic degradation by at least some MMP such as MMP-1 (Johnson, et al. 1999).

TG2 is also known to perform non-enzymatic roles in wound healing, promoting adhesion and migration of fibroblasts on FN in an RGD independent manner (Balklava, et al. 2002, Verderio, et al. 2003, Telci, et al. 2008, Wang, et al. 2010), which is particularly crucial in the context of injury and tissue remodelling, when the activation of proteases for matrix reorganisation leads to the release of numerous interfering RGD- fragments from FN.

TG2 has also been suggested to promote angiogenesis during wound repair (Haroon, et al. 1999), even if a correct balance of the enzyme concentration and activity is necessary for this function. A downregulation of TG2 was observed at the first hours of capillary formation by endothelial cells in a 3D collagen matrix, suggesting that the maintenance of low TG2 is required at the beginning of angiogenesis (Bell, et al. 2001). In line with this finding, excessive TG2 activity inhibits angiogenesis by promoting matrix accumulation (Griffin, et al. 2002, Jones, et al. 2006).

In addition to the abovementioned roles of TG2 in matrix deposition and stabilisation or fibroblast migration, TG2 also plays a role in the inflammatory phase of wound healing with both anti-inflammatory and pro-inflammatory functions. In a non-enzymatic manner, acting as a scaffold protein, TG2 has been seen to promote monocyte recruitment in the site of wound, by favouring their migration on the FN matrix (Akimov and Belkin 2001a). TG2 is particularly expressed in macrophages and, in these cells, has been shown to be important for phagocytosis of dead cells and subsequent release of TGF-β (Szondy, et al. 2003). By intracellular Ca^{2+}-mediated crosslinking, TG2 can contribute to contain inflammation, preventing/limiting leaking from dying cells (Verderio, et al. 1998, Nicholas, et al. 2003).

Interestingly, TG2 has also been suggested to act as a promoting agent for inflammation at the very initial stages after damage. In fact, it TG2 promotes the activation of the secretory phospholipase A2 (sPLA2) by crosslinking or amine incorporation (Cordella-Miele, Miele and Mukherjee 1990, Cordella-Miele, et al. 1993). sPLA2 is an important enzyme in the inflammatory response, as it catalyses the production of arachidonic acid from cell membrane

phospholipids, necessary to produce inflammatory and thrombogenic eicosanoids by the cyclooxygenase pathway.

Table 1.5: Main factions of TG2 and other members of TG family in the wound repair process.

PHASES of WOUND REPAIR	KNOWN FUNCTIONS OF TG2	KNOWN FUNCTIONS OF OTHER TG FAMILY MEMBERS
Haemostasis	• Stabilisation of provisional matrix of Fibrin and FN . • Matrix incorporation of Plasminogen inhibitors (PAI2, α2-AP).	• Fibrin clot formation (FXIIIa). • Matrix incorporation of Plasminogen inhibitors (PAI2, α2-AP) (FXIIIa).
Inflammation	• Monocyte adhesion and migration. • TGF-β activation. • Activation of sPLA2.	
Proliferation / Matrix deposition	• Crosslinking and stabilisation of extracellular matrix (Collagen and FN). • Resistance to / prevention of matrix protease digestion. • Promotion of cell adhesion, migration and proliferation (Fibroblasts). • RDG-independent cell adhesion prevents cell death and favours spreading. • TGF-β activation. • Regulation of angiogenesis.	• Re-epithelisation by promoting keratinocyte differentiation (TG1, TG3, TG5).
Remodelling and resolution of the wound	• Stabilisation of ECM (collagen mainly). • Resistance to / prevention of matrix protease digestion. • Cell death (intracellular crosslinking).	

1.3.5 TG2 roles in disease

TG2 has been associated with a series of pathological conditions, such as celiac disease, cystic fibrosis, heart fibrosis, lung fibrosis, hepatic disease, arthritis, cardiovascular diseases and artherosclerosis etc. (Iismaa, et al. 2009). Several reports have involved TG2 in the development of chronic kidney disease, as will be described in section 1.4.

In the nervous system, TG2 has been attributed roles in neuronal differentiation, synaptic modulation, release of neurotransmitters, and long-term potentiation (Jeitner, et al. 2009). TG2 has been associated with neurodegenerative diseases such as Alzheimer Disease (Wilhelmus, et al. 2009) and Huntington disease (Mastroberardino, et al. 2002), as well as in ischemic neuronal loss (Ientile, et al. 2004). The involvement of TG2 in neurodegenerative diseases has been suggested to be associated with the promotion of accumulation of insoluble protein aggregates in both cytoplasm and nucleus. Through similar processes, TG2 has been involved in Parkinson's disease (Junn, et al. 2003).

Even though TG2 has been for long regarded as a pro-apoptotic factor, in the past few decades, several studies have described a role for TG2 in cancer [reviewed in (Mangala and Mehta 2005, Eckert, et al. 2014)], where it promotes malignancy and proliferation by having both anti-

anoikis effects and anti-apoptotic effects, ultimately favouring cell survival (Mangala, et al. 2007, Mann, et al. 2006, Verma and Mehta 2007, Verderio, et al. 2003).

TG2 expression in cancer is related with enhanced drug-resistance, invasion and migration and has been strongly associated with the promotion of EMT, with evidences in breast and ovarian cancer, and human epidermal cancer stem cells (Fisher, et al. 2015, Shao, et al. 2009, Cao, et al. 2012, Kumar, et al. 2012, Eckert, et al. 2015). The closed, GTP-binding structure of TG2 has been suggested to be necessary for the events (Fisher, et al. 2015, Kumar, et al. 2012, Eckert, et al. 2015). TG2 has also been suggested to control MMP-2 (Gelatinase A) in ovarian cancer (Satpathy, et al. 2009), which has been highlighted as a mediator of cancer cells invasiveness and promotion of metastasis (Kenny, et al. 2008).

Interestingly, TG2 activation of NF-κB has been implicated many of the TG2-mediated events in cancer promotion, including EMT and survival /drug resistance (Mann, et al. 2006, Verma and Mehta 2007, Shao, et al. 2009, Jang, et al. 2010, Cao, et al. 2008). In many tumour cell lines, TG2 expression is induced by the hypoxic environment in an HIF-1 dependent manner (Jang, et al. 2010), which promotes malignant cell growth in solid tumours.

In the extracellular space, TG2 promotes cancer cells cell survival and spreading, especially by its scaffold role and interaction with ECM. Recently, Matei and colleagues revealed the importance of TG2-mediated modifications of the ECM in aggressive pancreatic cancer (Lee, et al. 2015b). TG2 secretion and large collagen crosslinking in the pancreatic stroma was suggested to induce ECM-mechanical tension leading to specific signal transduction for the promotion of mesenchymal cells proliferation (Lee, et al. 2015b). As a confirmation, TG2-KO in pancreatic cancer cells significantly reduces xenograft tumour size in mice, compared to WT cancer cells (Lee, et al. 2015b).

At the light of the more recent findings, it is clear that many disorders in which TG2 has been implicated are driven by changes introduced by increased TG2 synthesis and export in the ECM.

1.4 TRANSGLUTAMINASE-2 IN KIDNEY FIBROSIS

In the past few decades, TG2 has been associated with kidney fibrosis through a series of processes involving extracellular matrix accumulation and stabilization, activation of the profibrotic cytokine TGF-β, cell death, etc. This section will provide a comprehensive outline of the main studies of TG2 involvement in kidney disease (**Table 1.6-1.7**). A summary of TG2 main roles in Kidney fibrosis progression is found in **Table 1.8**.

1.4.1 Transglutaminase-2 expression in kidney

In a healthy kidney TG2 is the more expressed member of the TG family, even if other members of the family, such as TG1, TG3, TG6 and TG7, have been identified in the organ both at an mRNA level and protein level (Deasey, Shanmugasundaram and Nurminskaya 2013, Burhan, et al. 2016).

A recent work from our group employing a rat model of SNx, showed how, even if other members of TG family are expressed in kidney and upregulated upon kidney fibrosis (mainly TG1 and TG3), TG2 is the most expressed TG isoform in kidney and significantly correlates with the loss of renal function (Burhan, et al. 2016). Even if implicated in the process of wound healing in other organs, FXIIIa was not detected as expressed in kidney in this study (Burhan, et al. 2016).

Apart from TG2, the only other member of TG family studied in kidneys is TG1, that has been shown to localize on cadherin-based adherens junctions of kidney TECs (Hiiragi, et al. 1999) and to be important in the regulation of their proliferation through the JAK2-Stat-3 signalling pathway (Zhang, et al. 2009, Ponnusamy, et al. 2009).

As reported before, TG2-null mice are phenotypically normal (De Laurenzi and Melino 2001); the disruption of the gene also does not affect the renal phenotype, as TG2-null mice have normal sized kidneys, no histological differences, and GFR is similar to WT mice (Shweke, et al. 2008). This, in line with our previous general observations, suggests that TG2 has mostly a pathological role in kidney. TG1, however, results upregulated in TG2-null mice (Deasey, Shanmugasundaram and Nurminskaya 2013), suggesting a possible compensatory role. Moreover, levels of TG1, 3, 6 and 7 have been shown to increase in response to TG2 KO in mice (unpublished data TS Johnson/E Verderio).

1.4.2 Transglutaminase-2 association with kidney fibrosis models

In the past few decades, a number of studied have suggested an association between TG2 and the development of kidney fibrosis upon CKD (**Table 1.6**). In all these studies, TG2 has been observed to localize and perform its crosslinking activity in the interstitial space, and, depending on the type of kidney damage, to act in both tubular and glomerular area.

The first suggestion on the involvement of TG2 in the pathological process of kidney fibrosis was published in 1997 by Johnson and colleagues employing a rat SNx model (Johnson, et al. 1997b). In this model, an increase in both TG2 expression and activity was observed as the disease progressed, and the authors hypothesized that TG2 could introduce qualitative changes in the ECM that could slow down matrix degradation by proteases (Johnson, et al. 1997b). In this way, TG2 could shift the extracellular equilibrium to matrix deposition, reducing the proteolytic turnover. As employment of paraffin embedded section, in which the fixation is performed prior to immunohistochemical staining, was suggested to be unsuitable for extracellular TG2 detection (Verderio, et al. 1998), in 1999, the same group (Johnson, et al. 1999) performed TG2 staining on SNx kidney cryosections, proven to be better for detection of extracellular TG2 (Verderio, et al. 1998), together with an *in situ* TG activity assay developed by Verderio and colleagues (Verderio, et al. 1998). They showed that TG2 antigen and activity were abundantly located in the extracellular space in the SNx model, colocalising with the expanded ECM (Johnson, et al. 1999). By addition of exogenous enzyme, TG2 was suggested to stabilise the extracellular collagen against degradation by the action of MMP-1. In the same study, analysis of TG2 expression by mRNA hybridisation suggested that TG2 was mainly produced by proximal TECs and less by the glomerular cells. TG2 was also shown to be expressed by renal fibroblast that proliferate in the tubular interstitium after injury, while the presence of TG2 in blood vessels didn't correlate with the disease (Johnson, et al. 1999). Interestingly, in a retrospective study on the rat SNx model, our group showed that all TG members known to be expressed in kidney steadily increased upon SNx, with a peak at 90 days post-treatment, in line with the loss of renal function. However, at this time-point TG2 expression largely exceeded the other TGs, confirming the leading role of this enzyme (Burhan, et al. 2016).

In a rat model of DN induced by STZ, TG2 was observed to be accumulated in the ECM (Skill, et al. 2001). As DN is primarily a glomerular disease, glomeruli were isolated and analysed for TG2 antigen and ε-(γ-glutamyl)lysine crosslink bound accumulation, identifying an accretion of active TG2 in the glomerular basement membrane (GBM). Even if both tubules and glomeruli showed an increase in TG2 activity [ε-(γ-glutamyl)lysine crosslink] after injury, in the tubules no overall changes in TG2 expression was noticed, meaning that the increase in the extracellular activity was not associated with a *de novo* synthesis of TG2 protein but probably

only to an increase in the enzyme export (Skill, et al. 2001). The same authors developed an *in vitro* model of diabetic nephropathy induced by high glucose levels on opossum kidney (OK) proximal TECs (up to 36 mM, for 96 h), and showed an increase in TG2 expression and crosslinking products upon glucose stress, together with the increase deposition of several ECM proteins, especially FN and total collagen (Skill, et al. 2004). The increase in ECM deposition induced by glucose appeared significantly correlated with the increase in ε-(γ-glutamyl)lysine crosslink bounds, confirming the involvement of the enzyme in matrix accumulation (Skill, et al. 2004).

Some years later, the STZ model was induced on uninephrectomized (UNx) rats by Huang and colleagues, to accelerate the process of kidney fibrosis. In this model, both tubulointerstitial fibrosis and glomerulosclerosis were detected, and increased progressively up to eight months post administration of STZ; TG2 activity was several-fold increased at eight months post treatment, with progressive accumulation of crosslinking products, and was significantly higher than control rats and UNx untreated rats (Huang, et al. 2009). Employment of a specific TG inhibitor was shown to be protective against the progression of disease in this model (Huang, et al. 2009).

In a rat model of FSGS by injection of PAN, the induction of disease led to an increase of TG2 expression and crosslinking activity mainly in the glomeruli, and was accompanied by an increase in FN deposition and reduction in MMP-9 activation (Liu, et al. 2006).

The UUO model on C57BL/6 mice (described in Chapter III) was also employed in the analysis of TG2 implications on CKD by different groups. This model was shown to induce tubulointerstitial fibrosis in only 12 days after treatment, and the development of disease was accompanied by a significant increase in TG2 expression that appeared strongly increased in both tubulointerstitium and periglomerular area (Shweke, et al. 2008). The expression of TG2 correlated with the development of tubulointerstitial fibrosis, detected by an increase in collagen I expression and deposition, myofibroblasts infiltration monocyte adhesion and macrophage infiltration (Shweke, et al. 2008). Interestingly, TG2 was shown to partially co-localise with infiltrated macrophages upon UUO, suggesting that the enzyme could be secreted by different cell types during CKD (Shweke, et al. 2008).

Importantly, an increased expression of TG2 in in renal tubular cells and deposition in the tubulointerstitial space was also identified when the same surgery was performed in Wistar rats, in parallel with increased immunostaining of CTGF, which was suggested to partially co-localize with the enzyme in the tubulointerstitium, and FN (Chen, Huang and Yu 2005).

In a recent study by our group, both UUO model, which induce a rapid tubulointerstitial fibrosis, and AAN model, which induces a tubulointerstitial fibrosis more similar to the human disease (Huang, et al. 2013), were analysed on the C57BL/6 mice strain. In both models, a progressive accumulation of TG2 was detected in the tubulointerstitial space. Increase in

tubulointerstitial TG2 was suggested to result from an augmented export of the enzyme and re-distribution of the protein from the cytosol to the extracellular space, as its total level, when detected by Western blot, was found to not significantly vary upon treatment (Scarpellini, et al. 2014).

As reported above, vascular calcification can be detected on advanced CKD, and it is typical of the mineral bone disorder- associated CKD (CKD-MBD)(Moe, et al. 2009). When arterial calcification was induced using the Cy/+ rat model, that spontaneously develops CKD with all the features of CKD-MBD, TG2 expression and activity of TG2 was shown to be upregulated in both vascular smooth muscle cells and pathological matrix vesicles derived by these cells (Chen, et al. 2013). TG2 was shown to be involved in the calcification of both cells and vesicles, as the general TG inhibitor cystamine slowed down calcification in smooth muscle vascular cells, matrix vesicles and aorta rings isolated from these rats (Chen, et al. 2013).

1.4.3 Transglutaminase-2 in CKD patients

The importance of TG2 in the development of kidney fibrosis has been reported not only in animal models of CKD, but also in human pathology, using biopsies from patients with various kinds of CKD (**Table 1.6**).

The first study to investigate TG2 expression and activity in human biopsies was published in 2003 by Johnson and colleagues. In this study, they examined changes in both TG2 expression and products of TG2 post-translational modification [ε-(γ-glutamyl)lysine crosslink] in renal scarring using biopsies by a number of patients with different nephropathies, both proliferative and non-proliferative, with different levels of scarring. Diseases considered included crescentic glomerulonephritis (CGN), DN, IgA nephropathy (IgAN), FSGS and ESKF, to mention some (Johnson, et al. 2003). A significant correlation between the level of interstitial fibrosis (evaluated by Masson's trichrome - MT staining) and TG2 extracellular expression/*in situ* activity was identified in biopsies characterized by diverse levels of tissue scarring (from mild to severe) (Johnson, et al. 2003). Upregulation of TG2 mRNA was detected in mainly in TECs, but also in interstitial and mesangial cells from these patients, and was associated with an increased expression of soluble TG2, that well correlated with the level of tissue scarring especially in proliferative diseases.

In 2004, a further study employed renal biopsies from 16 DN patients, that showed an increase in TG2 and ε-(γ-glutamyl)lysine crosslink compared to the healthy kidney, as detected by immunofluorescent staining and confocal microscopy. Both TG2 antigen and activity correlated with the level of tissue scarring measured by MT staining, and localised in peritubular and periglomerular areas of the kidneys (El Nahas, et al. 2004).

Interestingly, in both studies mentioned, some level of intracellular TG2 crosslinking activity was detected in TECs upon fibrosis, that suggests a TG2-mediated cell death upon kidney injury (Johnson, et al. 2003, El Nahas, et al. 2004), as a cellular response to loss of calcium homeostasis (Verderio, et al. 1998, Nicholas, et al. 2003). This agrees with what already observed by Johnson and colleagues in 1997, that first proposed a TG2-induced/mediated cell death of tubular cells in the ablation model of CKD (Johnson, et al. 1997b).

Other studies of TG2 expression on human kidney biopsies were undertaken on patients with IgAN, which is a well-known type of proliferative glomerulopathy. In a first study (Ikee, et al. 2007), glomerular staining of TG2 correlated well with the loss of kidney function as detected in different ways (creatinine clearance and serum creatinine, protein excretion, glomerulosclerosis, mesangial cell proliferation), and tubular staining of TG2 was well identified and significantly correlated with markers of tubular dysfunction such as N-acetyl-β-glucosaminidase (Bazzi, et al. 2002) and urinary β2-microglobulin (Peterson, Evrin and Berggard 1969). TG2 staining was shown to be high in interstitial fibrotic lesions and in the proximity of vascular poles, as well as on glomerular crescents, that sometimes form in this kind of disease (Tumlin, Lohavichan and Hennigar 2003).

Whereas it correlated with a series of markers of renal function, TG2 expression didn't correlate with TGF-β staining (Ikee, et al. 2007). In a mouse model of the same disease, TG2 was suggested to be involved in mesangial cells activation by promoting the deposition of IgA on the mesangial cell surface, in a complex with the soluble CD89 protein, which directly binds transferrin receptor. This binding, in turn, induces TG2 expression on the mesangial cell surface which upregulates transferrin receptor, in a positive loop that potentiates mesangial activation upon IgA - CD89 administration (Berthelot, et al. 2012).

In a study of kidney biopsies from patients affected by membranous nephropathy (MN), a primary cause of glomerular disease and one of the common causes of nephrotic syndrome in adults, TG2 expression was increased and preceded the development of fibrosis. However, it was not affected by an immunosuppressive treatment (Papasotiriou, et al. 2012).

TG2 was also analysed as a potential early marker of chronic allograft dysfunction after kidney transplant, which is similar to other forms of CKD and characterised by chronic inflammation and development of fibrosis. Chronic allograft nephropathy (CAN) can be detected in up to 40% of grafts already few months after transplant and is the most common cause transplant failure. It is usually detected too late, by allograft fibrosis, which is led by ECM expansion. To determine if TG2 could be a potential early marker of allograft rejection and subsequent CAN, TG2 expression was examined on sequential biopsies at different stages post-kidney transplant (Johnson, et al. 2004). TG2 and its crosslinking products were shown to be absent in kidney biopsies at implantation, but increased early after transplantation in the tubulointerstitium and mesangium of almost half of the biopsies, and were present in all patients with established

CAN (Johnson, et al. 2004). Importantly, increase in TG2 was detectable before fibrosis and better correlated with the outcome of kidney transplant than other predictors such as collagen staining, α-SMA and MT staining, at the implantation and early after transplant. For this reason, it was suggested to be a potential marker of allograft scarring at the earlier stages of disease (Johnson, et al. 2004). In a subsequent study with a larger cohort, TG2 expression was reported to increase with allograft scarring, observed as a rise in tubulointerstitial fibrosis and tubular atrophy. Its expression was suggested to correlate with both increased expression of TGF-β and with the tissue inhibitor of matrix metalloproteinase-1 (TIMP-1), suggesting that both matrix deposition and reduced degradation contribute to the development of interstitial fibrosis and tubular atrophy in this conditions (Mengel, et al. 2008).

Interestingly, the role of TG2 in chronic allograft rejection has also been studied *in vivo* employing an animal model of allogenic renal transplantation, where kidneys were transplanted from a donor Lewis rat to a receiver Fisher rat (allografts), or to another Lewis rat as a control (isographs) (Shrestha, et al. 2014). In this model, allogenic transplant led to a progressive dysregulation in the parameters of renal function, such as loss of creatinine clearance, increased serum creatinine, hypertension, etc. In parallel, a rise in TG2 expression/activity was observed in the allografts, with increased export in the tubulointerstitium and periglomerular space, and a distribution that mirrored the one of myofibroblasts, while no changes where observed in the controls (Shrestha, et al. 2014). Intriguingly, for the first time, ε-(γ-glutamyl)lysine crosslinked products were also observed be progressively excreted in the allograft urine (Shrestha, et al. 2014), suggesting TG2 activity as a possible easily detectable marker of renal stress.

There is growing interest in urinary biomarkers of CKD as possible predictors of the disease at its early stages, as most of the current markers are mainly representative of the later stages of established disease. In a recent study from Johnson's group, TG2 expression was analysed on urine samples of ~300 patients with distinct types of CKD followed for a minimum of three years (da Silva Lodge, El Nahas and Johnson 2013). Urinary TG2 expression was analysed by sandwich ELISA and was found to be on average 41 times greater than the controls. Higher expression was identified in diabetic nephropathy patients and in general patients with progressive or rapidly progressive disease were showing to have higher TG2 excretion than individuals with non-progressive CKD (da Silva Lodge, El Nahas and Johnson 2013). Increase in TG2 urinary expression could be detected at the early stages of the disease (stage 2), suggesting the enzyme as a possible early marker; moreover, from the statistical analysis of the data, the ratio of TG2:creatinine resulted as an even better predictor of progressive CKD than the ratio of albumin over creatinine (da Silva Lodge, El Nahas and Johnson 2013).

In summary, these studies showed how TG2 is expressed and exported in the interstitial space in in patients affected by a variety of CKDs, and is active as a matrix crosslinker, contributing

to ECM stabilisation. For this reason, TG2 was suggested as a potential clinical target against the development of fibrosis. In the next paragraph, a series of studies involving TG2 deletion or TG chemical inhibition will be shown, which confirmed a potential protective role of TG2 targeting against CKD..

Table 1.6: Studies of transglutaminase-2 in CKD.

	Models of CKD with upregulated extracellular TG2 expression and / or activity	Reference
EXPERIMENTAL MODEL	Subtotal Nephrectomy (SNx) in Rat	(Johnson et al. 1997) (Johnson et al. 1999) (Johnson et al. 2007) (Burhan et al., 2016)
	Unilateral Ureteric Obstruction (UUO) in Rat	(Chen et al. 2005)
	Unilateral Ureteric Obstruction (UUO) in mouse	(Shweke et al. 2008) (Scarpellini et al. 2014)
	Aristolochic Acid Nephropathy (AAN) in mouse	(Scarpellini et al. 2014)
	CKD-Mineral Bone Disorder (CKD-MBD), Cy/+ rat	(Chen et al. 2013)
	STZ- induction of diabetic nephropathy in Rat	(Skill et al. 2001) (Huang et al. 2009) (Huang et al. 2010)
	Rat Fisher-Lewis model of chronic allograft nephropathy	(Shrestha et al. 2014)
	Puromycin aminonucleoside (PAN)-induced rat model of focal and segmental glomerulosclerosis	(Liu et al. 2006)
HUMAN BIOPSIES	Human biopsies with different types of CKD	(Johnson et al. 2003)
	Human biopsies at different stages of diabetic nephropathy	(Johnson et al. 2003) (El Nahas et al. 2004)
	Human biopsies at different stages of allograft rejection	(Johnson et al. 2004)
	Human biopsies at different stages of Membranous Nephropathy (MN)	(Papasotiriou et al. 2012)
	Human biopsies of IgA nephropathy (IgAN)	(Johnson et al. 2003) (Ikee et al. 2007)
CELL SYSTEMS	Tubular epithelial cells (TEC)	(Skill et al. 2004) (Fisher et al. 2009) (Huang et al. 2010) (Chou et al. 2011)
	Vascular smooth muscle cells (VSMC) from Cy/+ rat	(Chen et al. 2013)

1.4.4 Transglutaminase inhibition and TG2 specific knock out have a protective role against the progression of CKD

Given the involvement of TG2 in the process of kidney fibrosis, a number of studies have tested its potential as a clinical target against the progression of disease either by employing TG inhibitors or by knocking down the protein, in both *in vivo* and *in vitro* experimental models (**Table 1.7**).

The first study on the possible effect of TG inhibition on kidney fibrosis was performed by Skill and colleagues on an *in vitro* OK TECs model of DN induced by high glucose levels, where contemporaneous increase in TG2 extracellular expression/activity and matrix deposition were observed (Skill, et al. 2004). In this study, they employed two pan-inhibitors of TGs: one, 1,3-dimethyl-2[(oxopropyl)thio]-imidazolium (synthesized in house and named NTU283), is a potent TG inhibitor with no specificity for any TG family member over another and initially developed by Merk as a FXIIIa inhibitor (Castelhano, et al. 1990, Freund, et al. 1994). NTU283 is suggested to be highly cell soluble and to easily enter the cells. The second one, a carboxybenzoyl-glutamylglycine analogue [N-benzyloxycarbonyl-L-phenylalanyl-6-dimethylsulfonium-5-oxo-L-norleucine or NTU281), was developed by Griffin's group as pan-inhibitor of TGs (Griffin, Coutts and Saint 2004); it is less cell permeable, hence mostly limited to the extracellular space. Application of these TG inhibitors suggested for the first time a direct implication of TG in matrix deposition and stabilisation, with collagen III suggested as the main target of the enzymes' crosslinking activity (Skill, et al. 2004). The same compounds were employed on the experimental rat ablation model of CKD (SNx). These compounds were delivered locally to the kidney by intra renal infusion with a subcutaneous osmotic mini-pump, and confirmed a protective effect of TG inhibition against both glomerulosclerosis and tubulointerstitial fibrosis (detected by collagen deposition and MT staining), interstitial cell proliferation, and loss of renal function (detected by creatinine clearance, proteinuria and albuminuria) (Johnson, et al. 2007).

Few years later, Huang and colleagues employed NTU281 on the STZ model of DN performed on UNx rats (Huang, et al. 2009), delivering the compound to the animals by direct intrarenal infusion for eight months. While untreated animals presented extensive renal fibrosis, and were showing ESKF at the end of the experimental time, rats treated with NTU281 showed a significant reduction of glomerulosclerosis and tubulointerstitial fibrosis detected by MT staining and collagen accumulation, accompanied by a significant amelioration of kidney function (Huang, et al. 2009).

Despite the employment of these TG inhibitors were shown to have positive effect against the development of fibrosis in animal models or cultured cells, they are not specific for TG2, and might lead to other pathologic effects by affecting other members of the TG family, if delivered

systemically. For example, by inhibiting TG1, these compounds were shown to impede terminal differentiation of keratinocytes that could cause parakeratosis (Harrison, et al. 2007). Similarly, attempts to use these inhibitors systemically have resulted in longer bleeding times in some analysed animals (TS Johnson personal communication).

In addition to these pan-inhibitor studies, a series of studies employing specific knock out of TG2 (TG2-KO) confirmed that TG2 inhibition alone was sufficient to slow down the development of fibrosis. In a model of mice UUO, specific TG2-KO appeared protective against the progression of tubulointerstitial fibrosis (Shweke, et al. 2008). The knock out led to a reduced collagen deposition and myofibroblasts / macrophage infiltration, that were associated with a lowered activation of TGF-β (Shweke, et al. 2008). The effect of TG2-KO was also studied *in vitro* using primary TECs from TG2-null mice and was paired to an analysis of TG2 overexpression in opossum kidney (OK) TECs (Fisher, et al. 2009). From this study, TG2 was proven to accelerate ECM deposition with higher resistance to proteolytic digestion, as both features were increased in TG2 overexpressing cells and reduced by TG2-KO (Fisher, et al. 2009). Similar positive effects of TG2-KO against fibrosis were observed in other organs such as in lung and liver (Olsen, et al. 2011, Zhao, et al. 2011), suggesting a conserved mechanism in different fibrotic conditions.

Taken altogether, these studies propose TG2 as a possible target against the development of kidney fibrosis. For this reason, the development of a specific inhibitor of TG2 activity was suggested to be important to provide a potentially highly effective clinical tool against the development of fibrosis. Unfortunately, however, the pharmacological development of this inhibitor is extremely challenging, given the high homology of TG2 catalytic domain with the other members of TG family, and the conserved catalytic core. In the past few decades, several academic groups and R&D companies have registered patents on TG2 small molecule inhibitors, while more recently the development of antibodies as TG2 inhibitors has appeared promising [reviewed in (Verderio, et al. 2015)].
As an increased export of the enzyme has been observed upon fibrosis, an alternative approach would be to block the enzyme trafficking to the cell surface, interfering with TG2 binding to potential secretion partners.

Table 1.7: Studies of transglutaminase inhibition or TG2-deletion in CKD progression.

Type of treatment	Reference
TG inhibitors	(Skill et al. 2004) (Chen et al. 2005) (Johnson et al. 2007) (Huang et al. 2009) (Huang et al. 2010) (Chen et al. 2013)
TG2 knock-out	(Shweke et al. 2008) (Fisher et al. 2009) (Scarpellini et al. 2014)

1.4.5 TG2 mediated TGF-β activation and its importance in progressive kidney scarring

TG2 crosslinking activity has been suggested to play a double fibrogenic role in the development of fibrosis: one is a direct role in the stabilization of ECM, already mentioned in the previous paragraphs, while the second is a role in the recruitment of large latent TGF-β complex to the matrix and activation of TGF-β.

Since the end of the last century, TG2 has been known to be involved in the recruitment of the large latent TGF-β1 complex and TGF-β1 activation by crosslinking of LTBP-1 large binding protein to the extracellular matrix (Nunes, et al. 1997, Kojima, Nara and Rifkin 1993, Verderio, et al. 1999). Interestingly, in fibroblasts, TG2 has also been suggested to induce TGF-β expression at mRNA and protein level through NF-κB activation and subsequent transcriptional regulation (Telci, et al. 2009). Treatment of TG2-expressing Swiss 3T3 fibroblasts with TG inhibitors or inhibition of TG2 activity by nitric oxide (NO) resulted in reduction in NF-κB activation and TGF-β1 expression and activation, and subsequent lowering of ECM protein synthesis and deposition (Telci, et al. 2009). In addition, TGF-β1 has been suggested to upregulate TG2 expression in different cell types (George, et al. 1990, Quan, et al. 2005). This suggest that both TG2 and TGF-β1 are involved in a positive feedback loop in which they reciprocally induce their expression and activation (Belkin 2011).

The hypothesis of TG2 involvement in the upregulation of TGF-β activation during CKD arised from different studies involving KO of the enzyme. Initial findings were provided by Shweke and colleagues on the UUO mice model of experimental kidney fibrosis (Shweke, et al. 2008). While in healthy control mice the TG2-KO didn't significantly affect the amount of activated TGF-β1, when measured by Quantikine TGF-β1 ELISA kit by R&D Systems, upon UUO (12 days post-surgery), the development of renal fibrosis was associated with a consistent increase in active TGF-β1, that was significantly lower in TG2-null mice subjected to the same treatment (Shweke, et al. 2008). Comparable results were obtained by Fisher and colleagues using TG2-null primary TECs and TG2-overexpressing TECs (Fisher, et al. 2009), where TG2 modulation

was shown to significantly affect TGF-β activation when measured by mink lung epithelial cells (MLEC) bioassay (Abe, et al. 1994).

A significant increase in TGF-β was also observed by our group in the AAN model of kidney fibrosis in a recent study (Scarpellini et al. 2014). Interestingly, in this study, the knock out of the HSPG Sdc4 was accompanied by a decrease in TGF-β1 activity in fibrotic mice (Scarpellini et al. 2014). Even if a possible role for cell surface HSPGs such as Sdc4 in TGF-β activation has been suggested, for example by regulating the distribution of the large latent complex, the importance of Sdc4 for the cytokine regulation was suggested to be indirect, by promoting TG2 externalisation and retention, which in turn promotes TGF-β activation. In support to this, in recent work by our group, addition of exogenous TG2 on tubular epithelial cells was shown to be sufficient to induce TGF-β activation, and the effect was reduced by employment of a chemical antagonist of HS chains (Burhan, et al. 2016).

Recent findings on the role of HSPGs interaction with TG2 in progressive renal scarring will be described in the next section. However, the significance of this interaction for the enzyme trafficking and extracellular retention by kidney cells has not yet been completely understood, and will be the focus of Chapter VI.

Table 1.8: Summary of the main roles of transglutaminase-2 in the progression of kidney fibrosis

Roles of transglutaminase-2 in CKD	Reference
Formation of ε-(γ-glutamyl)lysine crosslinks (detected by exhaustive proteolytic digestion)	(Johnson et al. 1997) (Skill et al. 2001) (Skill et al. 2004) (Shrestha et al. 2014)
Formation of ε-(γ-glutamyl)lysine crosslinks (detected by immunocytochemistry/immunofluorescence)	(Johnson et al. 1997) (Johnson et al. 1999) (Skill et al. 2001) (Johnson et al. 2003) (El Nahas et al. 2004) (Johnson et al. 2004) (Liu et al. 2006) (Chen et al. 2013) (Shrestha et al. 2014)
Extracellular transamidating activity (amine incorporation assay)	(Johnson et al. 1999) (Skill et al. 2001) (Johnson et al. 2003) (Johnson et al. 2004) (Liu et al. 2006) (Johnson et al. 2007) (Shweke et al. 2008) (Huang et al. 2009)
ECM deposition	(Skill et al. 2004) (Chen et al. 2005) (Johnson et al. 2007) (Shweke et al. 2008) (Fisher et al. 2009) (Huang et al. 2009) (Chen et al. 2013) (Vascular calcification) (Scarpellini et al. 2014)
Matrix resistance to proteolytic turnover	(Johnson et al. 1999) (Fisher et al. 2009)
Myofibroblasts infiltration	(Johnson et al. 2007) (Shweke et al. 2008) (Huang et al. 2009)
Immune cell infiltration	(Johnson et al. 2007) (Shweke et al. 2008)
Intracellular protein crosslinking	(Johnson et al. 1997) (El Nahas et al. 2004) (Johnson et al. 2004)
Activation of TGF-β	(Shweke et al. 2008) (Fisher et al. 2009) (Huang et al. 2010) (Scarpellini et al. 2014) (Burhan et al. 2016)

1.5 TRANSGLUTAMINASE-2 INTERACTION WITH HEPARAN SULPHATE PROTEOGLYCANS AND INVOLVEMENT IN KIDNEY FIBROSIS

1.5.1 The families of heparan sulfate proteoglycans (HSPGs)

Heparan sulfate proteoglycans (HSPGs) are a cell surface/ECM superfamily of proteoglycans characterised by a core protein associated with one or more covalently attached heparan sulfate (HS) chains, a specific type of glycosaminoglycan (GAG) chain (Esko, Kimata and Lindahl 2009). In mammals, approximately 17 HS proteoglycans have been identified and can be distinguished into nine families depending on their location, core protein and type of HS/GAG chains (Sarrazin, Lamanna and Esko 2011). In general, HSPGs can be divided into two large categories, cell surface membrane-associated proteoglycans and secreted extracellular matrix HSPGs (located in the basement membrane) (**Table 1.9**).

The most well-known cell surface HSPGs are the syndecans (four members, Sdc1-4) and the glypicans (six members, Gpc1-6). Syndecans are a family of transmembrane proteoglycans characterised by a small cytoplasmic domain, a transmembrane portion and a larger extracellular domain with two – to – five GAG chains, that are mainly HS but can include one or two chondroitin sulfate (CS) chains (Sdc1 an Sdc3), a different type of sulfated GAG chain. Glypicans, on the other side, are covalently bound to the cell surface by a glycosylphosphatidylinositol (GPI) phospholipid linkage. The core protein has a globular cysteine rich structure and is characterised by only HS chains in number of one to three (Esko, Kimata and Lindahl 2009, Tumova, Woods and Couchman 2000). Minor forms of cell surface HSPGs include fibroblasts' betaglycan, or TGF-β receptor III (TGFBR3), a large part-time proteoglycan with HS and CS chains, CD44v3, an isoform of CD44 antigen in limphocytes, characterised by one HS chain (Sarrazin, Lamanna and Esko 2011), and Neuropilin-1, another large part-time proteoglycan characterised by HS or CS chains that act as co-receptor in VEGF signalling (**Table 1.9**).

Extracellular matrix (secreted) HSPGs are located in the basement membrane of different cell types and include perlecan, agrin, and collagen type XVIII (endostatin) (Sarrazin, Lamanna and Esko 2011). Perlecan is a large HSPG with a protein core of 400 kDa and one-to-four HS chains. In rare cases CS chains have been observed on perlecan (Kvist, et al. 2006). Agrin is smaller and characterised by only HS chains; it is localised in the basement membrane and is regarded to as the main component of the kidney glomerular basement membrane in humans (Groffen, et al. 1998). Collagen XVIII is a particular basement membrane collagen with one-to-three HS chains, that can be cleaved to form endostatin, a short fragment involved in angiogenesis inhibition (**Table 1.8**).

Interestingly, one last HSPG family, serglycin, is a family of small (10-19 kDa) proteoglycans localised on cytoplasmic storage granules and secretory vesicles of hematopoietic cells, mast cells and endothelial cells (Kolset and Tveit 2008, Pejler, Åbrink and Wernersson 2009). Serglycin is characterised by the presence of CS chains and, notably, it is the only HSPG to show heparin chains (Schaefer, et al. 2004) (**Table 1.9**).

Table 1.9: Heparan sulfate proteoglycans (HSPGs). Table adapted from (Sarrazin, Lamanna and Esko 2011). HS = Heparan sulfate, CS = Chondroitin sulfate. Numbers in brackets indicate the number of chains.

	HSPG Family	Members	Location	Core mass (KDa)	GAG Chains
CELL SURFACE HSPGs	Syndecan	4 : Sdc1, Sdc2, Sdc3, Sdc4	Cell Surface (Transmembrane)	22-43	HS (2-4) + CS (1-2)
	Glypican	6: Gpc1, Gpc2, Gpc3, Gpc4, Gpc5, Gpc6	Cell Surface (GPI-Bound)	57-69	HS (1-3)
	CD44v3	1	Cell Surface (Transmembrane)	37	HS (1)
	Betaglycan or Transforming growth factor beta receptor III (TGFBR3) (part-time PG)	1	Cell Surface (Transmembrane)	110	HS/CS (1-2)
	Neuropilin-1 (part-time PG)	1	Cell Surface (Transmembrane)	130	HS/CS (1)
SECRETED HSPGs	Perlecan	1	Basement membrane	400	HS (1-4)
	Agrin	1	Basement membrane	212	HS (2-3)
	Collagen XVIII	1	Basement membrane	150	HS (1-3)
	Serglycin	1	Secretory granules/vesicles	10–19	Heparin/CS (10–15)

1.5.2 HSPGs in wound healing, fibrosis and kidney disease

Syndecan family has been suggested to play many roles in the process of tissue repair after injury. Sdc4 and Sdc1 have been well described as upregulated during inflammatory conditions, leading to angiogenesis and wound repair (Gallo, et al. 1997). Moreover, Sdc2 has also been suggested to play a role in wound healing by modulation of TGF-β signalling (Chen, Klass and Woods 2004). Growth factors such as FGF2 have been shown to be key mediators of wound healing by interaction with both Syndecans and tyrosine receptors.

Sdc4 activity in wound healing is directly correlated with its ligand-mediated oligomerisation and activation of specific small GTPases in cooperation with β1 integrins. In case of injury, Sdc4 supports cell proliferation and migration to close the wound: the increase of Sdc4 expression

in the wound area correlates with an increase in cell proliferation, that depends on growth factor stimulation (FGF2 binding) and subsequent PKCα activation (Chapter VI).
Sdc1 role in wound healing, on the other side, is associated with the promotion of cell adhesion and negative control of mesenchymal transformation.
Both Sdc4 and Sdc1-null mice show defects in wound healing. Sdc4-null mice show delayed wound healing, which in general depends on altered proliferation and motility of fibroblasts. Sdc4-null mice are unable to produce a proper granulation tissue and novel vascularisation (angiogenesis) in the wound area during the healing process, which depends on a loss of the proliferative capacity of the cells (Echtermeyer, et al. 2001). On the other side, Sdc1-KO mice show defects in wound healing mostly determined by dysregulated re-epithelisation (Stepp, et al. 2002).
Syndecan shedding has been shown to be involved in the regulation of wound healing. During inflammation, HS chains of Syndecans can bind chemokines, which can induce MMP-dependent shedding of Syndecan ectodomains. Apparently, both Sdc1 and Sdc4 shedded ectodomains have been found to accumulate in dermal wound fluids (Subramanian, Fitzgerald and Bernfield 1997), but their involvement in the healing process were suggested as different. Sdc1 shed ectodomains, produced for example by MMP-7, favour cell migration and facilitate wound closure, while at the same time promoting re-epithelisation (Chen, et al. 2009, Endo, et al. 2003, Su, et al. 2008). Sdc4 shedding, on the other side, reduces proliferation and controls FGF2 signalling (Bass and Humphries 2002).

As tissue scarring can be described as an uncontrolled wound healing, it appears likely that Syndecans could be involved in the regulation of tissue fibrosis.
The involvement of Syndecans in tissue fibrosis has been well-studied in heart disease (infarction, hypertension, etc.) and associated with cardiac fibrosis. During cardiac fibrosis, Sdc1 and Sdc4 have been suggested to be upregulated by inflammatory response and to contribute to pro-fibrotic signalling (cell migration/proliferation/adhesion) by binding ECM proteins such as cytokines and growth factors but also FN and collagens, and transducing the signal to the intracellular space. On the other side, ectodomain shedding during inflammation leads to cardiac rupture by ECM degradation, and directly correlates with a bad outcome of myocardial infarction (Schellings, et al. 2010, Lunde, et al. 2016).
In pulmonary fibrosis, shedding of Sdc1 promotes neutrophil chemotaxis and fibrogenesis.
Sdc4 has been suggested to be required for the formation of a myofibroblast phenotype in fibrosis and to induce ECM contraction mediated by fibroblast, transducing TGF-β signalling and activating ERK response during chronic fibrosis (Chen, et al. 2005, Matsui, et al. 2011).

In kidneys, expression of Sdc1, Sdc2 and Sdc4 has been detected, among which Sdc4 was reported to be the most abundant syndecan of kidney tissue, Sdc1 was described as highly expressed and Sdc2 as less expressed (Kim, et al. 1994).

Association of Sdc4/HSPGs with CKD has been reported in the past (Yung, et al. 2001, Morita, et al. 1994, Fan, et al. 2003). Loss of endothelial glycocalyx is another feature of CKD and has been shown to be largely associated with Sdc1 shedding in CKD (Padberg, et al. 2014, Zeng, et al. 2014).

Importantly, also Sdc2 has been shown to be upregulated in some studies of kidney fibrosis: the expression of Sdc2 was increased in parallel with TGF-β upon DN, moreover, it was shown to be upregulated in a model of unilateral nephrectomy where Sdc4 expression was abolished, suggesting a compensatory effect of this family member (Ruiz, et al. 2012, Chen, Klass and Woods 2004).

Recently, in a rat model of CKD obtained by SNx, Sdc4 appeared as the highest expressed syndecan in fibrotic kidneys, increasing in parallel with the loss of kidney function and peaking at a level of advanced fibrosis (90 days post-SNx), when the process becomes irreversible (Burhan, et al. 2016). Knockout of Sdc4 in two mouse model of CKD obtained by UUO or AAN resulted in a striking reduction of fibrosis compared to WT mice (Scarpellini, et al. 2014).

Altogether, these findings suggest that Sdc4 is overexpressed during the progression of CKD and might play a role in supporting fibrosis, which is in line with the protective role of its knock out and the reduced wound healing in Sdc4-null cells (Echtermeyer, et al. 2001).

A recent work has suggested a significant role for HS chain sulfation state in the binding and extracellular localisation of cytokines and growth factors and in promoting their association with their receptors during kidney disease. In this study, the level of sulfation was associated with the progression of kidney fibrosis in the context of chronic allograft rejection after kidney transplant. They suggested that the level of 6-O-sulfated glucosamine residues is upregulated by in kidney TECs upon allograft rejection, that associates with an increased binding of FGF2 and ERK activation. In the same study, the increase in 6-O-sulfation in fibrotic kidneys was confirmed employing a mouse UUO model (Alhasan, et al. 2014).

1.5.3 TG2 interaction with HSPGs is involved in TG2 extracellular roles and in the enzyme release

Lately, different studies have focused on the relationship between extracellular TG2 and cell surface HSPGs.

Different studies from our group at NTU suggested that TG2 is able to bind HS chains / heparin with high affinity (comparable with the affinity of TG2 for FN) and that the interaction of TG2 with cell surface HS chains of syndecans has two main consequences: it mediates the RDG-independent cell adhesion to FN-TG2 heterocomplex and it favours cell surface trafficking and ECM distribution of TG2 (Scarpellini, et al. 2009, Verderio, Scarpellini and Johnson 2009, Verderio and Scarpellini 2010).

Between 2003 and 2008, works from Griffin's group suggested that, in case of apoptosis mediated by matrix fragmentation with loss of RGD-dependent cell adhesion (anoikis), TG2 is able to rescue cell adhesion of fibroblasts and epithelial cells by promoting RGD-independent cell adhesion to FN, and that this critically depends on TG2-FN heterocomplex binding to Sdc4 HS chains, leading to PKCα activation and FAK signalling (Verderio, et al. 2003, Telci, et al. 2008), which requires β1-integrins (Wilcox-Adelman, Denhez and Goetinck 2002).

The role of HSPG in cell adhesion is particularly important in situations of cell stress that determine an over-secretion of TG2 and an over-deposition in the ECM. This happens during pathophysiological events such as wound healing, organ fibrosis or cancer development.

Other studies form Griffin's group confirmed the requirement of Sdc4 for RGD-independent cell adhesion to TG2-FN heterocomplex, while proposing a that also Sdc2 was required for the process, as its deletion was leading to reduced cell attachment and spreading both in control cell or cells cultured in presence of RGD peptide, that TG2-FN homodimer alone couldn't compensate. Interestingly, however, they suggested that Sdc2 didn't directly bind TG2 but acted as a downstream PKCα -dependent signal that regulates actin cytoskeleton (Wang, Telci and Griffin 2011, Wang, et al. 2010) .

In an *in vitro* study employing mouse dermal fibroblast (MDFs), Scarpellini and colleagues showed an elevated affinity of TG2 for HS chains and heparin. They suggested that cell surface HSPGs could act as receptors for TG2 via HS chains, and that binding to cell surface HSPGs significantly controls TG2 trafficking to the cell surface, allowing its extracellular activity (Scarpellini, et al. 2009, Scarpellini 2009). Sdc4 null-MDFs showed a significant abolishment of TG2 export, as well as treatment with a HS chemical antagonist (Surfen) (Schuksz, et al. 2008) or HS digestion by bacterial Heparitinase (Scarpellini, et al. 2009, Scarpellini 2009).

1.5.4 TG2 interaction with HSPGs in models of CKD

Knowing the pivotal role of TG2 export to the cell surface during the progression of CKD, shown in the previous section, the effect of Sdc4 on TG2 trafficking and development of fibrosis was studied *in vivo* employing Sdc4 null mice subjected to 2 two different experimental models of CKD in mice: UUO and AAN. In these models, knock-out of Sdc4 appeared to be protective against the progression of CKD and specifically against the accumulation of fibrotic tissue, by negatively controlling TG2 export and activity on the cell surface (Scarpellini, et al. 2014).

In a recent work, our group analysed expression levels of TG and syndecan family members in a rat model of kidney fibrosis obtained by SNx (Burhan, et al. 2016), showing a correlation between Sdc4 and TG2 expression during the progression of the disease, as well as a co-localisation of the two in the interstitial space and peritubular area of fibrotic kidney tissue, which was abolished by interference with HS chains.

Moreover, in both studies, a possible role for Sdc4 in favouring TG2-mediated TGF-β activation was investigated by measuring the percentage of activated TGF-β via MLEC bioassay (Abe, et al. 1994) in Sdc4-null tissues or after pre-treatment with the Hs antagonist Surfen (Scarpellini, et al. 2014, Burhan, et al. 2016).

Taken altogether, these results confirm a direct binding between TG2 and HS chains of HSPGs and specifically suggested Sdc4 as the main receptor of TG2 on the cell surface, favouring TG2 secretion to the cell surface and localisation in the extracellular space upon injury, where it can perform its enzymatic and non-enzymatic activities in the promotion of fibrosis progression, including TGF-β activation (Verderio, et al. 2015). Once exported, TG2 can probably interact with the HS chains of other extracellular HSPGs such as basement membrane Perlecan or directly with matrix FN, that are likely to contribute to the enzyme trafficking in the extracellular space and localisation in the matrix.

Until now, the importance of HSPGs/Sdc4 for cell surface trafficking of TG2 has been studied *in vitro* in dermal fibroblasts or *in vivo* in models of kidney disease. However, the specific mechanism of TG2-HS/Sdc4 interaction and involvement in the enzyme export has never been investigated employing kidney cell lines. Analysis of HSPGs/Sdc4 role in TG2 export in renal cell types is the aim of Chapter VI and will be described further on.

1.6 HYPOTHESES AND SPECIFIC OBJECTIVES

In this chapter, we have provided some background on the role of TG2 in ECM remodelling and deposition in the context of CKD. TG2 was defined as a possible clinical target against the progression of kidney fibrosis, and the hypothesis of a therapy against CKD targeting TG2 secretion from kidney cells was arisen. As TG2 is characterized by a still not completely clarified unconventional secretion, that might involve TG2 association with different molecular partners and pathways for protein release, we believe that the elucidation of TG2 network of interactions (interactome) in kidneys at the cell-matrix interface would be the quickest conceivable way to identify TG2 - associated partners on its way to secretion by kidney cells. To achieve this purpose, we defined an original proteomic approach that combines TG2-immunoprecipitation (IP) with a high-resolution mass spectrometry (MS) approach. The highly descriptive SWATH data independent acquisition (DIA) was chosen as the MS data collection approach for this study.

We hypothesised that this approach would allow us to define specific TG2-associated partners in the context of kidney fibrosis and that, among these partners, some would lead us to deduce hypotheses for TG2 unconventional secretion from kidney cells in CKD conditions, that would subsequently be tested *in vitro* using kidney immortalized cell lines. As a number of studies from our group have highlighted HSPGs, and specifically Sdc4, as binding partners for TG2, and have suggested an involvement of Sdc4 in TG2 trafficking from kidney cells in *in vivo* models of CKD, we also hypothesised that HSPGs/Sdc4 could be key participants in the pathway of TG2 unconventional secretion from kidney cells.

The main objectives of this studies are:

- The definition of the kidney proteome by SWATH acquisition MS in an experimental model of CKD, that serves to elucidate the context for the subsequent analyses of TG2 associated partners. The experimental model chosen for this study is the UUO model of tubulointerstitial fibrosis.
- The production of the TG2 interactome in in the same experimental model using the abovementioned approach, combining TG2-IP and high-resolution SWATH acquisition MS.
- The analysis of functional distribution and pathway representation of TG2 specifically associated partners at the cell-matrix interface, in order to produce possible hypotheses for the pathway of TG2 unconventional secretion from kidney cells in the context of CKD.
- The *in vitro* validation of the produced hypothesis/hypotheses for TG2 unconventional secretion from kidney cells by, employment of immortalised cell lines.
- The *in vitro* validation of the possible involvement of HSPGs/Sdc4 in TG2 secretion from kidney cells and extracellular retention *in vitro* by employment of immortalised cell lines.

Chapter II: General material and methods

2.1 REAGENTS AND MATERIAL

2.1.1 Cell culture reagents and material

2.1.1.1 Reagents

Table 2.1: Reagents employed for cell culture.

Reagent	Product code	Company	Storage
D-Glucose	G8270	Sigma	RT
DMEM with 1 g/L glucose w/o L-Glutamine	BE12-707F	Lonza	4°C
DMEM with 4.5 g/L glucose w/o L-Glutamine	BE12-614F	Lonza	4°C
DMEM:F-12 1:1 Mixture w/15mM Hepes, w L-Glutamine	BE12-719F	Lonza	4°C
Ethylenediaminetetraacetic acid solution 0.5 M pH 8.0	3690	Sigma	4°C
G418 (Geneticin) (CAS: 108321-42-2) 100 mg/ml solution in HEPES	ant-gn-5	Invivogen	-20°C
G418 Sulfate (lyophilised powder) [potency = 800 µg/mg]	345810	Merk	Stock solution 100 mg/ml in sterile distilled water, filtered (stored at -20°C)
Gibco ™ Foetal Bovine Serum, qualified, E.U.-approved, South America origin	11573397	Thermo Fisher Scientific	-20°C
L-Glutamine solution [200 mM L-glutamine (100X)]	G7513	Sigma	-20°C
MycoAlert Plus Mycoplasma Detection Kit	LT07-701	Lonza	4°C, -20°C once prepared
Mycoplasma removal agent (MRA) [50 µg/ml]	BUF035	AbD Serotec	RT
Penicillin-Streptomycin (Pen/Strep) [10,000 units/ml penicillin and 10 mg/ml streptomycin (100X)]	P4333	Sigma	-20°C
Trypan Blue solution	93595	Sigma	RT
Trypsin solution [2.5% (v/w) trypsin (10X)]	59427C	Sigma	-20°C
Zeocin (lyophilised powder)	ant-zn-1p	Invivogen	Stock solution 100 mg/ml in sterile distilled water, filtered (stored at -20°C)

2.1.1.2 Plasticware

- Sterile plastic serological pipettes, Pasteur pipettes and pipette tips were supplied by Sarstedt.
- T25, T75 and T155 flasks were supplied by Sarstedt.
- Cryotube vials were supplied by Sarstedt.
- Lab-Tek 8-well (0.82cm^2/well) radiation sterilised glass chamber slides were supplied by Thermo Scientific Nunc (10051021, Fisher)

2.1.2 Laboratory reagents

2.1.2.1 Enzymes

- Guinea pig liver TG2 (T5398, Sigma): Purity of powder = 85% (850 µg/mg). Units of enzymatic activity = 2.5 U/mg (1U = formation of 1 µM hydroxamate/min from N-alpha-CBZ-GLN-GLY and hydroxylamine, at pH 6.0, 37°C (GROSSOWICZ, et al. 1950). A 1mg/ml pure TG2 solution (2,5 U/ml) was prepared in ultrapure water, taking into account protein purity, and stored at -20°C.
- Recombinant human hexahistidine-tagged human TG2 produced in *E.coli* (His6-rhTG2) (T002, Zedira, Germany). Purity of powder = 90% (900 µg/mg). Units of enzymatic activity = 0.59 U/mg /mg (1U = formation of 1.0 µM hydroxamate/min from N-alpha-CBZ-GLN-GLY and hydroxylamine, at pH 6.0, 37°C). A 1mg/ml pure TG2 solution (590 mU/ml) was prepared in ultrapure water, taking into account protein purity, and stored at -20°C.
- Heparinase III (or Heparitinase I, HepI) from *Flavobacterium heparinum* (CAS: 37290-86-1) (H8891 Sigma): Units of enzymatic activity = 30 Sigma Units (U)/mg (1U = formation of 1 µM of unsaturated uronic acid /h using bovine kidney Heparan Sulfate as substrate, at pH 7.5, 25°C), equivalent to 0.05 IU/mg (1 IU = 600 Sigma U). A 5 IU/ml stock solution in an appropriate Hep I buffer [20 mM Tris-HCl, 50 mM NaCl, 4 mM CaCl, 0.01% (w/v) BSA, pH 7.5] as suggested by the manufacturer and stored at -80°C.

2.1.2.2 Antibodies

Table 2.2: Primary antibodies. Rb=Rabbit, Ms=Mouse WB= Western Blot, IF=Immunofluorescence, NE=Not employed

Antigen	Antibody	Code	Company	WB	IF
Phospho-(Ser) PKC Substrate (P-S3-101)	Rb monoclonal	6967	Cell Signalling Technology	1:1000	NE
Actin	Rb polyclonal	A2066	Sigma	1:2500	NE
Clathrin Heavy Chain (D3C6)	Rb monoclonal	4796	Cell Signalling Technology	1:500	1:400
Collagen 1	Rb polyclonal	ab34710	Abcam	NE	1:500
Cyclophilin-A	Rb polyclonal	ab41684	Abcam	1:1000	NE
EGFP	Rb polyclonal	ab290	Abcam	1:2500	1:500
Flotillin 2	Ms monoclonal	610383	BD Transduction Laboratories	1:5000	NE
Hemagglutinin (HA)	Rb polyclonal	C29F4	Cell Signalling Technology	1:1000	1:500
His6-Peroxidase	Ms monoclonal	11965085001 ROCHE	Roche, Sigma	1:1000	NE
phospho($pSer_{425}$)-Smad3	Rb polyclonal	SAB4300253	Sigma	NE	1:75
Phospho-(Ser) CDKs Substrate (P-S2-100)	Rb monoclonal	9477	Cell Signaling Technology	1:1000	NE
Phospho-(Ser/Thr) ATM/ATR Substrate (S*/T*QG) (P-S/T2-100)	Rb monoclonal	6966	Cell Signaling Technology	1:1000	NE
Phospho-(Ser/Thr)AMPK Substrate (P-S/T2-102)	Rb monoclonal	5759	Cell Signaling Technology	1:1000	NE
Phospho-Akt Substrate (RXRXXS/T)(110B7E)	Rb monoclonal	9614	Cell Signaling Technology	1:1000	NE

Phospho-PKA Substrate (RRXS/T) (100G7E)	Rb monoclonal	9624	Cell Signalling Technology	1:1000	NE
Phospho-tyrosine	Ms monoclonal	610430	BD Transduction Laboratories	1:250	NE
Smad 3	Rb polyclonal	9513	Cell Signalling Technology	NE	1:75
Syndecan-4 (Sdc4)	Rb polyclonal	ab24511	Abcam	1:500	1:50
Transglutaminase 2 (TG2)	Rb polyclonal	ab80563	Abcam	1:1000	NE
Transglutaminase 2 (TG2)	Rb polyclonal	ab421	Abcam	1:500	NE
Transglutaminase 2 (TG2) - IA12	Ms monoclonal	IA12	University of Sheffield, UK	1:5000	1:400
Transglutaminase 2 (TG2)[Cub7402]	Ms monoclonal	ab2386	Abcam	NE	1:150
α-Smooth muscle actin [1A4]	Ms monoclonal	ab7817	Abcam	1:1000	NE
β-Tubulin	Rb polyclonal	ab6046	Abcam	1:2000	NE

Table 2.3: Secondary antibodies

Secondary antibodies for Western Blot	Product code	Company	Dilution
Donkey anti-rabbit IgG HRP	P0448	Dako	1:2000
Donkey anti-mouse IgG-HRP	P0447	Dako	1:1000
Goat anti-rabbit IgG HRP	7074	Cell Signalling Technology	1:2000

Secondary antibodies for Immunofluorescence	Product code	Company	Dilution	Excitation	Emission	
Donkey anti-rabbit IgG H&L (Alexa Fluor®488)	A21206	Molecular probes / Invitrogen	1:1000	499	519	Green
Donkey anti-rabbit IgG H&L (Alexa Fluor®568)	A10042	Molecular probes / Invitrogen	1:1000	579	603	Red
Goat anti-mouse IgG DyLight®594	A11032	Molecular probes / Invitrogen	1:1000	591	618	Red
Sheep anti-mouse - FITC	76257	Sigma	1:250	495	519	Green

2.1.2.3 Chemicals and reagents

General chemicals were obtained from Sigma or Melford unless otherwise stated. **Table 2.4** reports the list of Chemicals, Kits and Reagents employed for this thesis. Composition of the main Buffers is reported in the Appendix of this thesis (**Table III**).

Table 2.4: Chemicals and reagents. NA = Not available, RT = Room temperature

Name	CAS Number	Product code	Company	Form	Storing T(°C)	Notes
1,4-Dithiothreitol (DTT)	578517	MB1015	Melford	lyophilized powder	4°C	Stock 100 mM in water (-20°C)
1,4-Dithiothreitol (DTT) (Molecular grade)	578517	18064-014	Invitrogen	Solution (0.1M)	-20 °C	In SuperScript® II Reverse Transcriptase kit
100 bp DNA Ladder	NA	G2101	Promega	Solution	-20 °C	Ready-to-load ladder stock by mixing 1:4:1 volumes of 100bp DNA ladder, ultrapure water and Blue/Orange 6X Loading Dye (Primega)
3,3′,5,5′-tetramethylbenzidine (TMB)	54827-17-7	T9281	Sigma	lyophilized powder	4°C	Stock solution 10mg/ml in DMSO (stored at 4°C)
Agarose	9012-36-6	AGR100	Web Scientific	lyophilized powder	RT	
Albumine fom Bovine Serum (BSA) Purity > 96%	9048-46-8	A4503	Sigma	lyophilized powder	4°C	Heat inactivated at 56°C/30 min
Amaxa Nucleofector™ kit V	NA	VCA 1003	Lonza	Solution kit	4°C	
Amiloride hydrochloride hydrate	2016-88-8	A7410	Sigma	lyophilized powder	RT	Stock solution 25 mg/ml (94 mM) in water (stored at -20°C)
Ammonium Persulfate (APS)	7727-54-0	A0502	Melford	lyophilized powder	RT	
Ampicillin	7177-48-2	A9518	Sigma	lyophilized powder	4°C	Stock solution 100 mg/ml in sterile water (stored at -20°C)
BCA Assay Kit Reagent A / Bicinchoninic Acid Solution [1% (w/v) BCA, 2%(w/v) Na2CO3, 0.16% (w/v) NaK tartrate, 0.4%(w/v) NaOH, 0.95%(w/v) NaHCO3]	NA	B9643	Sigma	Solution	RT	
BCA Assay Kit Reagent B [4% (w/v) CuSO4]	7758-98-7	C2284	Sigma	Solution	RT	
Bio-Safe Coomassie Stain	6104-58-1	161-0786	Bio-Rad	Solution	RT	Based on Coomassie brilliant blue G-250
Biotin Cadaverine or N-(5-Aminopentyl)biotinamide trifluoroacetate salt	NA	A5348	Sigma	lyophilized powder	4°C	50 mM in DMSO (stored at 4°C)
bis-2-methyl-4-amino-quinolyl-6-carbamide or Surfen hydrate	NA	S6951	Sigma	lyophilized powder	4°C	Stock solution 30 mM in DMSO (stored at -20°C in the dark in glass containers)
Blue/Orange 6X Loading Dye	NA	G1881	Promega	Solution	-20 °C	
Bradford Reagent	NA	B6916	Sigma	Solution	4°C	Based on Coomassie brilliant blue G-250
Bromophenol Blue	115-39-9	B5525	Sigma	lyophilized powder	RT	
Calcium Chloride (CaCl2)	10043-52-4	C3881	Sigma	lyophilized powder	RT	
cOmplete EDTA-free Protease Inhibitors	NA	0000000 1187358 0001 Roche	Sigma	Tablets	4°C	Dissolve 1 tablet in 50 ml
Deoxycholic Acid (Sodium Deoxycholate)	302-95-4	D6750	Sigma	lyophilized powder	RT	0.1 %(w/v) deoxycholic acid in PBS (stored at -20°C)

DharmaFECT I ®	NA	T-2001-01	Thermo Scientific	Solution	4°C	
Diethylpyrocarbonate (DEPC)	1609-47-8	D5758	Sigma	Solution	4°C	
Dimethyl sulfoxide (DMSO)	67-68-5	FIND	FIND	Solution	RT	
dNTPs mix	NA	U1511	Promea	Solution	-20 °C	
Ethanol (Nuclease free)	64-17-5	D7023	Sigma	Solution	RT	
Ethidium Bromide	1239-45-8	1510	Sigma	Solution	RT	
Ethylenediaminetetraacetic acid (EDTA)	60-00-4	ED	Sigma	lyophilized powder	RT	Stock solution 500 mM pH 8 (stored at RT)
ExtrAvidin®−Peroxidase	NA	E2886	Sigma	Solution	4°C	
EZ-Chemiluminescence Detection Kit for HRP	NA	K1-0170	Geneflow	Solution KIT	4°C	
Fibronectin from human plasma	86088-83-7	F1056	Sigma	lyophilized powder	-20 °C	Stock 1mg/ml solution in ultrapure water was dissolved by incubation at 37 °C for 30 minutes (stored at -20°C)
First-Strand buffer, 5X	NA	18064-014	Invitrogen	Solution	-20 °C	In SuperScript® II Reverse Transcriptase kit
Fluorescein isothiocianate (FITC) - Cadaverine	NA	A10466	Invitrogen	lyophilized powder	4°C	Stock solution 50 mM
Glacial Acetic Acid	64-19-7	A360OB17	Fisher	Solution	RT	
Glycerol	56-81-5	G5516	Sigma	Solution	RT	
Glycine	56-40-6	G0709	Melford	lyophilized powder	RT	
GW4869	6823-69-4	D1692	Sigma	lyophilized powder	RT	Stock solution 5 mM in DMSO (stored at -20°C)
Hydrogen peroxide H_2O_2	7722-84-1	H1009	Sigma	Solution	4°C	
IGEPAL CA-630	9002-93-1	I8896	Sigma	Solution	RT	
Imipramine hydrochloride	113-52-0	I0899	Sigma	lyophilized powder	RT	Stock slution 50 mg/ml (158 mM) in sterile water (stored at -20°C)
iQ™ SYBR® Green Supermix	NA	170-8880	Biorad	Solution	-20 °C	
Isopropanol	67-63-0	P749017	Fisher	Solution	RT	
Kanamycin	25389-94-0	H815	Gibco	lyophilized powder	4°C	Stock solution 25 mg/ml in sterile water (stored at -20°C)
LB Broth, Lennox	NA	BP1427	Fisher Scientific	lyophilized powder	RT	
Methanol	67-56-1	M40017	Fisher	Solution	RT	
N,N,N′,N′-Tetramethylethylenediamine (Temed)	110-18-9	T9281	Sigma	Solution	RT	
N-ethylmaleimide	128-53-0	E3876	Sigma	lyophilized powder	RT	Stock solution 100 mM (12.5 mg/ml) (stored at -20°C)
Nitrocellulose membrane	9004-70-0	1620115	Bio-Rad	Membrane	RT	
N-Octyl-Beta-Glucopyranoside (OGP)	29836-26-8	O8001	Sigma	lyophilized powder	RT	
Paraformaldehyde (PFA)	30525-89-4	P6148	Sigma	lyophilized powder	RT	3% (w/v) solution in PBS pH 7.4 (dissolves at approx. 60°C)
Phosphatase Inhibitor Cocktail 2	NA	P5726	Sigma	Solution	4°C	
Phosphatase Inhibitor Cocktail 3	NA	P0044	Sigma	Solution	4°C	
Phosphate-Citrate Buffer with Urea Hydrogen Peroxide	NA	P4560	Sigma	Tablets	4°C	Dissolve 1 tablet in 10 ml
Pierce™ Crosslink Magnetic IP/Co-IP Kit	NA	88805	Thermo Scientific	Kit	4°C	
Pierce™ LDH Cytotoxicity Assay kit	NA	88953	Thermo Scientific	Kit	-20 °C, 4°C	
PIP Strips™ Membranes	NA	P-23750	Molecular Probes® - Thermo Scientific	Phospholipid Membrane	4°C	
Ponceau S	6226-79-5	P3504	Sigma	lyophilized powder	RT	

Potassium Chloride (KCl)	7447-40-7	P9541	Sigma	lyophilized powder	RT	
Potassium dihydrogen phosphate	7778-77-0	P5504	Sigma	lyophilized powder	RT	
Prism Ultra Protein Ladder (10-245 kDa)	NA	ab116028	Abcam	Solution	-20 °C	
Protease inhibitor cocktail	NA	P8340	Sigma	DMSO Solution	-20°C	
ProteaseMAX™ Surfactant	NA	V2071	Promega	lyophilized powder	-20 °C	1% (w/v) in 50 mM TEAB (stored at -20°C in small volume aliquots - avoid thaw-freeze cycles)
Protogel - 30% Acrylamide/Bis-acrylamidesolution (37.5:1 ratio)	79-06-1	A2-0072	Geneflow	Solution	RT	
QIAGEN Plasmid Midi Kit	NA	12143	Qiagen	Solution KIT	RT	RNase A-supplemented Buffer P1 stored at 4°C
QIAprep Spin Miniprep Kit	NA	27104	Qiagen	Solution KIT	RT	RNase A-supplemented Buffer P1 stored at 4°C
Random primers	NA	C1181	Promega	Solution	-20 °C	
siRNA Buffer, 5X	NA	B-002000-UB	Thermo Scientific	Solution	4°C	
Sodium Cloride (NaCl)	7647-14-5	S7653	Sigma	lyophilized powder	RT	Stock solution 1M in water (stored at RT)
Sodium Dodecyl Sulphate (SDS)	151-21-3	B2008	Melford	lyophilized powder	RT	
Sodium Hydroxide (NaOH)	1310-73-2	50523	Duchefa Biochemie	lyophilized powder	RT	Stock solution 1M in water (stored at RT)
Sodium Phosphate Dibasic Heptahydrate (Na2HPO4)	7782-85-6	S2317	Melford	lyophilized powder	RT	1M solution in distilled water (dissolves at approx. 50°C)
Sulphuric acid H2SO4	7664-93-9	59160PB	Fisher	Solution	RT	
SuperScript® II Reverse Transcriptase	NA	18064-014	Invitrogen	Solution	-20 °C	
TGF-β Recombinant	NA	240B	RD Systems	Solution	-80°C	
Tissue Transglutaminase Pico-Assay Kit	NA	M003	Zedira	Kit	4°C	
tri-ethyl ammonium bicarbonate (TEAB) [1M solution]	15715-58-9	T7408	Sigma	Solution	RT	
Triton-X100	9002-93-1	X100	Sigma	Solution	RT	
Trizma Base / TRIS [Tris(hydroxymethyl) aminomethane]	77-86-1	B2005	Melford	lyophilized powder	RT	
Trypsin, MS Grade		V5280	Promega	lyophilized powder	-20 °C	1 mg/ml in 50 mM acetic acid (stored at -20°C of -80°C for long term storage)
Tween® -20	9005-64-5	P1379	Sigma	Solution	RT	
Urea	57-13-6	U5128	Sigma	lyophilized powder	RT	
VECTASHIELD® Mounting Medium	NA	H-1000	Vectorlab	Solution	4°C	
VECTASHIELD® Mounting Medium with DAPI	NA	H-1200	Vectorlab	Solution	4°C	
β-Mercaptoethanol or 2-Mercaptoethanol	60-24-2	M3148	Sigma	Solution	4°C	

2.1.3 Laboratory equipment

Table 2.5: Laboratory equipment.

Instrument	Company
Amaxa Nucleofactor electroporation machine	Lonza
Amaxa® Nucleofactor™ Device	Lonza
Avanti J 301 High speed centrifuge	Beckman Coulter
Corbett Research Thermal Cycler	Qiagen
Electrophoresis kit MultiSUB Choice 15x15cm	SLS
Electrophoresis tank Multi SUB Mini	Geneflow
Eppendorf refrigerated centrifuge 5417R	Eppendorf
GyroStir 280H Magnetic Hotplate Stirrer	Sciquip
Harrier 18/80 Centrifuge	Sanyo
Heating Block QBT4	Grant
LAS4000 imaging system	GE Healthcare
Leica TCS confocal microscope	Leica
Mini PROTEAN® Gel casting system	Bio-Rad
Mini PROTEAN® Tetra Cell	Bio-Rad
Model 680 Spectrophotometer (plate reader)	Biorad
MSH280 Pro Stirrer	Sciquip
NanoDrop® 8000	Thermo Scientific
Olympus BX61 fluorescent microscope	Olympus
Optima L100 XP Ultracentrifuge	Beckman Coulter
Polarstar Optima Luminometer	BMG Labtech
Power pack	Bio-Rad
SciQuip Orbital Shaker Basic O3	Sciquip
Soniprep 150 Sonicator	MSE
Syngene U:Genius transilluminator	Genflow
TC 3000X Thermocycler	Techne
Triple TOF 5600 +	Sciex
Ts100 Eclipse Optical Microscope	Nikon
U:Genius transilluminator	Syngene
Ultra Turrax T25 homogeniser	Merk
Water bath	Grant

2.1.4 List of companies

Table 2.6: Companies.

Company	Address
Abcam	Cambridge, UK
AbD Serotec	Oxford, UK
BD Biosciences	Oxford, UK
Beckman Coulter	High Wycombe
Bemis	Londonderry, UK
Bio-Rad	Hemel Hempstead, UK
BMG Labtech	Ortenberg, Germany
BMG Labtech	Aylesbury, UK
Cell Signaling Technology	Laiden,The Netherlands
DakoCytomation	Glostrup, Denmark
Eksigent	California, USA
Eppendorf UK	Stevenage, UK
Fisher Scientific	Loughborough, UK
GE Healthcare	Bucks, UK
Geneflow	Lichfield, UK
Invitrogen	Paisley, UK
Invivogen	Toulouse, France
Leica	Solms, Germany
Life Technologies	Paisley, UK
Lonza	Wokingham, UK
Melford	Ipswich, UK
Merk Millipore	Nottingham, UK
New England Biolabs	Hitchin, UK
New Objective Inc.	Massachusetts, USA
Promega	Southampton, UK
Qiagen	Crawley, UK
Reytest	Straubenhardt, Germany
Sarstedt	Leicester, UK
Sartorius Stedim	Epsom, UK
Scientific Laboratory Supplies	Nottingham, UK
SCIEX	Canada
Sciquip	Shrewsbury , UK
Sigma	Dorset, UK
Syngene	Cambridge, UK
Thermo Scientific	Paisley, UK
Vectorlab	Peterborough, UK
VWR	Lutterworth, UK
Web Scientific	Cheshire, UK
Zedira GmbH	Darmstadt, Germany

2.2 METHODS

2.2.1 Cell culture

2.2.1.1 Cell lines

For the *in vitro* experiments performed in this thesis, two commercially available immortalised rat renal cell lines were employed: NRK52E tubular epithelial cells (TECs), an immortalised cell line of adherent epithelial cells obtained from rat proximal renal tubules, and NRK49F fibroblasts, an adherent cell line of rat kidney fibroblasts obtained by isolation from the same mixed culture from which the NRK52E are produced. Both NRK52E TECs and NRK49F renal fibroblasts were obtained from the European Collection of Authenticated Cell Cultures (ECACC) (UK).

In some experiments, a stable cell line of NRK52E clones overexpressing EGFP-tagged TG2 was employed (referred as EGFP-TG2 overexpressing clones or EGFP-TG2 clones). These clones were produced in Dr Verderio Laboratory (NTU) by former Research Assistant Raghavendran Ramaswamy, by stably transfecting NRK52E cells with a specific pEGFP-N1-TG2 plasmid (**Appendix, Fig. II**), expressing a human TG2 cDNA chimeric protein with a C-terminal EGFP tag, with green fluorescence. Briefly, NRK52E wild type (WT) cells were transfected by electroporation with 10μg of pEGFP-N1-TG2 plasmid, and clones resistant to the selective antibiotic G418 (Geneticin®, an analogue of neomycin, was employed in this case) were isolated and screened for TG2 expression and activity. In this thesis, specifically, clones #C5 and clone #E6 were employed: these clones had already been fully characterized in Dr Verderio laboratory (NTU). For the aims of this thesis, characterisation of TG2 expression and activity was repeated for the clones employed to confirm the preservation of their characteristics.

2.2.1.2 Culture conditions

NRK52E cells were cultured in Dulbecco's modified Eagle's medium (DMEM) with 4.5 g/L glucose supplemented with 5% (v/v) filtered (0.2 μm) heat-inactivated Foetal Bovine Serum (FBS), 2mM L-glutamine, 100 IU/mL penicillin and 100 μg/mL streptomycin. This medium composition will be referred as complete medium throughout the thesis.

EGFP-TG2 overexpressing clones were maintained in the same medium, with the addition of 700 μg/ml G418 (Geneticin®) to preserve the stringency of the clonal selection.

NRK49F cells were cultured in the same DMEM medium supplemented with 10% (v/v) filtered (0.2 μm) heat inactivated FBS, 2mM L-glutamine 100 IU/mL penicillin and 100 μg/ml. All cultures were kept at 37°C and 5% CO_2 in air.

Culture conditions could vary in specific experiments, by keeping the cells in lower glucose concentration employing Dulbecco's modified Eagle's medium (DMEM) with 1 g/L glucose (Lonza) or using lower concentrations of FBS to slow down cell growth. siRNA transfections were performed in absence of antibiotics (no penicillin, streptomycin or selective antibiotics) and the corresponding medium is regarded as complete antibiotic-free medium.

2.2.1.3 Cell passaging

90-95% confluent cell monolayers cells were washed one time with pre-warmed (37°C) sterile PBS pH 7.4 [137mM NaCl, 2.7 mM KCl, 10 mM Na_2HPO_4 and 1.8mM KH_2PO_4, pH 7.4 (autoclaved at 121 °C for 20 min)] and incubated with trypsin/EDTA solution [0.25% (w/v) trypsin, 2 mM EDTA in PBS, pH 7.4] for 5 min at 37°C (approximately 1 ml for a T75 flask). Trypsin solution was prepared by diluting 2.5% (w/v) trypsin stock solution with nine volumes of sterile PBS pH 7.4 and adding 1:250 of 500 mM sterile EDTA solution. Solution was sterile filtered (0.2 μm) and aliquots (~10 ml) were stored at -20°C until needed. In-use solution can be kept in the fridge for a short amount of time.

After incubation with trypsin/EDTA solution, cells were dislodged by gently tapping the flask and at least five volumes of complete medium were added to inactivate trypsin. Cell suspension was transferred to a 15ml conical bottom tube and cells were pelleted by centrifugation at 500g for 5 minutes. Cell pellet was re-suspended in 1 ml complete medium and the desired dilution of cells was re-seeded in a new flask containing fresh culture medium. For routine culture of NRK49F and NRK52E cells, cell passaging was usually performed at 1:10 dilution, and cells were again confluent in approximately three days.

2.2.1.4 Cell counting

Cell counting was performed using an Improved Neubauer Chamber hemocytometer of 0.1 mm thickness (HAE2112, Scientific Laboratory Supplies). 10μl of cell suspension were loaded in the chamber after placing an appropriate cover slip. Cells were counted under the microscope at 10x magnification, and at least four 4x4 quadrants at the angles (yellow in **Fig.2.1**) were considered. Average number of cells was calculated for all quadrants considered, and the number of cells per ml was approximated by multiplying the average number by 10^4 (**Fig.2.1**). In specific experiments where high precision was necessary, cell suspension was diluted in nine volumes of trypan blue before counting. In this case, the final cell number takes into count the dilution factor and the resulting number was multiplied by 10^5.

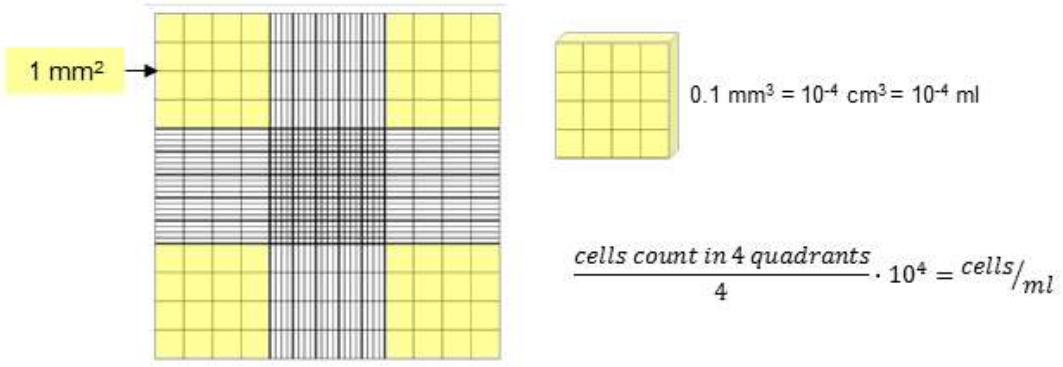

Figure 2.1: Hematocytometer grid employed for cell counting and cell number calculation. The chamber has a thickness of 0.1 mm. It is characterized by nine big squares of 1 mm^2 (volume of 0.1 mm^3 = 10^{-4} ml). 4 quadrants (yellow) were counted for each measurement and averaged. The cell counted in each quadrant (number of cells for 0.1 mm^2 = number of cells in 10^{-4} ml) were multiplied for 10^4 (10,000) to have a reliable approximation of the number of cells per ml.

2.2.1.5 Cryopreservation of cells and resuscitation of frozen cells

In order to freeze cells for cryopreservation, approximately 1 million cells were pelleted by centrifugation as described above. All supernatant was carefully removed and the pellets re-suspended in 1ml of freezing solution [10% dimethyl sulfoxide in FBS; sterile filtered (0.2 µm)]. Cell suspension was transferred into sterile cryovials and frozen at -80°C for a day, before moving them to liquid nitrogen for long term storage. This gradual freezing prevents substantial cell death due to thermic shock.

In order to thaw frozen cells stored in liquid nitrogen, cryovials were recovered from the liquid nitrogen storage and quickly defrosted at 37°C until little ice remained. The outside of the vial was sterilised with 70% (v/v) ethanol, then the thawed mixture was transferred to 10 ml pre-warmed complete medium. Cells were recovered by centrifugation (500g for 5 min), then medium was carefully removed and pelleted cells were transferred to a T25 flask containing fresh complete medium. Medium was changed the day after to remove every trace of DMSO.

2.2.1.6 Routine test for mycoplasma detection

In order to check cultured cells for mycoplasma contamination, MycoAlert Plus Mycoplasma Detection Kit from Lonza was employed, following the manufacturer's instructions. Briefly, the cells were kept in culture for at least 2 days before collecting the conditioned medium for testing. Medium was quickly centrifuged at 200g for 5 min to pellet floating cells and 100 µl of cleared supernatant where transferred in a white 96-well plate suitable for luminescence. 100 µl MycoAlert® PLUS Reagent was added, the plate was incubated for 5 min in the dark at room temperature, then luminescence was read (Read A - spontaneous luminescence) using Polarstar Optima Luminometer (BMG Labtech). 100 µl MycoAlert® PLUS Substrate was then added on the top and the plate incubated again for 10 min in the dark at room temperature.

Luminescence was read for the second time (Read B) and the ratio Read B / Read A calculated. A ratio lower than 1 signifies absence of mycoplasma while a ratio higher than 1.2 means mycoplasma contamination. A value between 1 and 1.2 requires quarantine of the cells and re-testing in one or two days.

In case of mycoplasma contamination, 0.5 µg/ml Mycoplasma Removal Agent (MRA) (AbD Serotec) was added to culture medium for a week and maintained at each cell passaging. After the end of the week, cells were cultured in the absence of MRA for another week before re-testing for mycoplasma.

2.2.1.7 LDH cytotoxicity assay

To assess cytotoxicity of specific compounds, LDH assay was performed using Pierce LDH Cytotoxicity Assay kit (Thermo Scientific) and following the manufacturer's protocol. LDH Cytotoxicity assay is based on the detection of the activity of lactate dehydrogenase (LDH) in the conditioned medium, as LDH is a cytosolic enzyme released in the culture media as a consequence of plasma membrane damage. The assay is based on two reactions: the conversion of lactate to pyruvate by LDH, with production of NADH, and the reduction of tetrazolium salt (INT) to a red formazan product, which employs the produced NADH and is catalysed by the enzyme diaphorase. Red formazan absorbs at 490 nm, and its level is directly proportional to the amount of LDH released by the cells.

To determine the optimal number of cells to employ, a serial dilution of cells (0-20,000 cells/well) was either untreated or lysed with the appropriate lysis buffer provided by the kit. The assay was performed on the conditioned medium following the manufacturer's instruction, and absorbance was measured at 490 nm (red formazan, signal) using a plate reader spectrophotometer. Absorbance at 680 nm was measured as well and subtracted from the Abs490 as the background signal. Abs 490nm – Abs 680 is the measure of LDH release; LDH release from untreated cells is regarded as spontaneous LDH release, while LDH release in the medium of lysed cells is regarded as the maximum LDH release for the specific number of cells, and should be proportional to the cell number.

LDH release values were plotted against the initial number of cells and the optimal number of cells was chosen within the area of linear growth of the maximum LDH - spontaneous LDH trendline.

To perform cytotoxicity assay, 7,500 cells/well were cultured in a 96-well plate in presence of the treatment required by the specific experiment (e.g. chemical compound with unknown cytotoxicity), the assay was performed on the conditioned medium following the manufacturer instruction and LDH release was measured as Abs490 – Abs 680 nm.

2.2.2 Kidney material

For the aims of this thesis either C57BL/6J mice kidneys (Chapter III, IV and VI) or Wistar rats kidneys (Chapter VI) were employed. All animals were bred at Nottingham Trent University (NTU) animal house by licenced technicians. $TG2^{-/-}$ (TG2-null) C57BL/6J mice (De Laurenzi and Melino 2001) were obtained from Prof. Gerry Melino (University of Tor Vergata, Rome) and backcrossed with WT mice at NTU animal house by licenced technicians. After sacrifice, kidneys were stored in Liquid nitrogen.

2.2.3 Total protein extraction

2.2.3.1 Lysis buffers

Cell lysates or tissue lysates utilised in this thesis were produced in different lysis buffers depending on the specific requirements of the subsequent experiments. Composition of lysis buffers and associated experimental procedures are reported in **Table 2.7**.

Table 2.7: Specific composition of the lysis buffers employed and corresponding subsequent experimental procedures. WB=Western Blot, IP=Immunoprecipitation, MS=Mass Spectrometry.

Name	Composition	Employed for			
		WB	*IP*	*Activity assay*	*MS*
IGEPAL- containing Lysis Buffer	20 mM Tris-HCl, 150 mM NaCl, 5 mM EDTA, 1% (v/v) IGEPAL CA-630, 0.5% (w/v) deoxycholic acid, 0.1% (w/v) SDS, pH 7.4	■			
Radioimmunoprecipitation assay buffer (RIPA buffer)	50 mM Tris HCl, 150 mM NaCl, 1% (vv) NP40, 0.5% Sodium Deoxicholate, 0.1% SDS, pH 8	■			
Sucrose – Based Lysis buffer	250 mM sucrose, 2 mM EDTA, and 5 mM Tris-HCl, pH 7.4	■		■	
IP Lysis/Wash buffer (Thermoscientific)	250mM Tris-HCl, 150mM NaCl, 1mM EDTA, 1% NP40, 5% glycerol pH 7.4		■		
Proteomics Lysis Buffer	9.5 M urea, 2%(w/v) DTT, 1% (w/v) N-Octyl-Beta-Glucopyranoside (OGP)				■

2.2.3.2 Total protein extraction from cells

In order to obtain total protein extract from kidney cells, 80-90% confluent monolayers were washed with PBS pH 7.4 and harvested by either trypsinization or cell scraping depending on the experiments. Cell scraping was performed with disposable cell scrapers in a small layer of PBS pH 7.4 (0.5-3 ml depending on the dimension of the culture flask) to favour detachment and is advisable in the experiments where the preservation of membrane proteins is necessary. Cell pellet was collected by centrifugation at 500 g for 5 min and re-suspended in 200µl - 1 ml of the appropriate lysis buffer containing protease inhibitors. Unless otherwise stated, 1:100

dilution of Protease Inhibitor Cocktail (P8340, Sigma) was employed. Cells were incubated for 15 minutes on ice, sonicated on ice (3 repetition for 5 sec, 1 min hold) using a probe sonicator with amplitude set to 5 µm. Lysate was incubated again for 20 min on ice, then a brief centrifugation (1,000 g for 5 min) was employed to remove un-lysed particulate material. If not immediately used, cell lysates were stored at -80°C.

2.2.3.3 Total protein extraction from mouse or rat kidney tissue

10% (w/v) mouse or rat kidney homogenates were produced by either grinding the organ in liquid nitrogen or by mechanical homogenisation using an Ultra Turrax T25 tissue homogenizer (Merck). To perform homogenisation in liquid nitrogen, kidneys or kidney portions were grinded with cold sterile pestle and mortar making sure the tissue was always maintained under a liquid nitrogen coat. The paste obtained was collected with a sterile scalpel and transferred in a new microcentrifuge tube containing the appropriate volume of lysis buffer (100 µl for each mg of kidney tissue).

Mechanical homogenisation with Ultra Turrax T25 tissue homogenizer (Merck) was performed in an appropriate volume of lysis buffer (100 µl for each mg of kidney tissue) on ice, 3 times for 10 sec or until complete homogenization.

In both cases, the mixture was incubated on ice for 20 min, then centrifuged at 4°C for 10 min at 1000 g remove un-lysed particulate material. If not immediately used, tissue homogenates were stored at -80°C.

2.2.4 Protein quantification

2.2.4.1 Preparation of bovine serum albumin (BSA) standard curve

A standard curve of known protein concentrations was produced prior to each protein quantification assay by preparing a serial dilution of bovine serum albumin (BSA) to 1 mg/ml, 0.75 mg/ml, 0.5 mg/ml, 0.25 mg/ml, 0.125 mg/ml and 0 mg/ml (blank) in cell lysis buffer.

2.2.4.2 Bicinchoninic acid (BCA) protein quantification assay

BCA quantification assay was performed using a commercially available BCA quantification assay reagents kit. BCA working solution was prepared immediately before the assay by combining Reagent A [1% (w/v) BCA, 2%(w/v) Na_2CO_3, 0.16% (w/v) NaK tartrate, 0.4%(w/v) NaOH, 0.95%(w/v) $NaHCO_3$] and Reagent B [4% (w/v) $CuSO_4$] in 50:1 proportion. 25 µl of samples (in triplicates) or BSA standards (0-1 mg/ml) (in duplicates) were incubated with 200 µl of BCA working solution in a 96/well plate. The plate was incubated 30 min at 37°C in the dark and the absorbance was measured at 570 nm using a 96 well plate reader

(spectrophotometer). The unknown sample concentration was obtained by plotting the absorbance values on the BSA standard curve of known protein concentration.

2.2.4.3 Bradford protein quantification assay

Bradford quantification assay was performed using the commercially available Bradford reagent from Sigma. 5 µl of samples (in triplicates) or BSA standards (0-1 mg/ml) (in duplicates) were incubated with 250 µl of Bradford reagent in a 96/well plate. The plate was incubated 15 min at room temperature in the dark and the absorbance is measured at 570 nm using a 96 well plate reader (spectrophotometer). The unknown sample concentration was obtained by plotting the absorbance values on the BSA standard curve of known protein concentration.

2.2.5 Immunoprecipitation (IP)

Immunoprecipitation (IP) is a procedure used to precipitate a desired antigen from a pool of proteins. IP was performed using Pierce™ Crosslink Magnetic IP/Co-IP Kit (88805, Thermo Scientific), following the Manufacturer's protocol with some modifications in the length of the incubation steps.

Briefly, 2.5 µg of antibody against the desired protein were incubated with 20 µl of 10mg/mL (200 µg) Pierce Protein A/G Magnetic Beads for one hour at room temperature in constant rotation, then covalently attached to the beads by crosslinking, using 20µM disuccinimidyl suberate (DSS) crosslinker provided in the kit for 3 h at room temperature in constant rotation. Cell or tissue lysates were produced using the specific IP Lysis/Wash Buffer provided by the kit. Equal amounts of total proteins (0.75-1 mg cell lysate/kidney tissue lysate, depending on the experiment) were the applied on the beads overnight (15 h) at 4°C in constant rotation to allow the antigen to bind, then the bound antigen was eluted in 40-90 µl elution buffer pH 2.0, provided by the kit, for 5 min at room temperature. 0.1 volumes of neutralisation buffer pH 8.5 were added to neutralize the pH of the elution. The final solution contains the target protein (precipitated) and the co-associated ones (co-precipitated). Ideally, the antibody (Immunoglobulins) would not be eluted since it is covalently linked to the magnetic beads. If not immediately used, immunoprecipitated (IP) proteins were stored at -80°C.

2.2.6 SDS - polyacrylamide gel electrophoresis (SDS-PAGE)

In order to separate proteins depending on theirs size, denaturing SDS - Polyacrylamide Gel Electrophoresis (SDS-PAGE) was performed using the Mini PROTEAN® cell for 1-D vertical mini gel (8.3 x 7.3 cm) electrophoresis system from Bio-Rad.

2.2.6.1 Preparation of polyacrylamide gel for SDS-PAGE

1.5 mm thick mini SDS-polyacrylamide gels (83 x 73 x 1.5 mm) were prepared on a Mini PROTEAN® gel casting system (Bio-Rad). 8-12% (w/v) acrylamide/bis-acrylamide resolving gel solution was prepared immediately before gel casting as described in **Table 2.8**, poured between Mini PROTEAN® III glass plates (a 1.5 mm thick spacer plate and a short plate) (Web Scientific) until 1.5/2 cm from the top, covered with 1 ml of isopropanol, and let polymerize for 15-20 min or until completely solid. Approximately 8 ml of resolving solution is required for each gel.

Table 2.8: Composition of one SDS-PAGE resolving gel containing either 8%, 10% or 12% acrylamide/bis-acrylamide. 8 ml were used to prepare one mini PROTEAN® gel.

Composition of one 1.5 mm thick Resolving gel (8 ml)			
Components	**ml**		
	8%	**10%**	**12%**
ProtoGel (30%) (30% acrylamide / bisacrylamide solution at 37.5:1 Ratio) (Geneflow)	2.1	2.7	3.2
Resolving buffer 4X [1.5 mM Tris HCl, 0.4% SDS, pH 8.8]	2.0	2.0	2.0
Distilled H2O	3.9	3.3	2.8
10% (w/v) ammonium persulphate (APS)	0.08	0.08	0.08
N,N,N′,N′-Tetramethylethylenediamine (TEMED) (Sigma)	0.008	0.008	0.008

Isopropanol was removed, then 5% (w/v) acrylamide/bis-acrylamide stacking gel (prepared as described in **Table 2.9**) was poured on the top. 10-well combs (Bio-Rad) were immediately inserted to form the sample wells and stacking gel was let to polymerize until solid (approximately 15-20 min). Approximately 2.5 ml of stacking solution is necessary for each gel.

Table 2.9: Composition of one SDS-PAGE stacking gel containing 5% acrylamide/bis-acrylamide. 3 ml were used to prepare one mini PROTEAN® gel.

Composition of one 1.5 mm thick Stacking gel (3 ml)	
Components	**ml**
	5%
ProtoGel (30%) (30% acrylamide / bisacrylamide solution at 37.5:1 Ratio) (Geneflow)	0.5
Stacking buffer 4X [0.5 M Tris HCl, 0.4% SDS, pH 6.8]	0.8
Distilled H2O	1.8
10% (w/v) ammonium persulphate (APS)	0.03
N,N,N′,N′-Tetramethylethylenediamine (TEMED) (Sigma)	0.003

2.2.6.2 Preparation of samples for SDS-PAGE electrophoresis in reducing conditions

Ready-to-load samples were prepared by adding 1/3 volume of 4X reducing and denaturing sample buffer [4X Laemmli buffer: 250 mM Tris-HCl pH 6.8; 40% (v/v) glycerol; 8% (v/v) SDS; 20%(v/v) β-mercaptoethanol (β-ME); 0.008%(w/v) bromophenol blue] to protein samples and warming them up at 98°C for 10 min on a heating block. Samples were cooled at room temperature and briefly spun to collect all material before loading.

2.2.6.3 Protein separation by gel electrophoresis

SDS-PAGE gels were placed into the appropriate Mini PROTEAN® running modules and inserted into the buffer tank containing electrophoresis buffer [25mM Tris-HCl, 192mM glycine; 0.1%(w/v) SDS]. Samples were loaded into the gel wells, together with approximately 2.5 µl of pre-stained protein ladder [Prism Ultra Protein Ladder (10-245 kDa) (ab116028)] was also added on a lane. Samples were separated by electrophoresis, first at a constant voltage of 100V till the samples surpass the stacking gel, then at a constant voltage of 150V until the end.

2.2.6.4 Coomassie blue staining of SDS-PAGE protein gels

To visualize the protein resolved by SDS-PAGE, some gels were stained using BioSafe™ Coomassie Stain from Bio-Rad, following the manufacturer's instructions.

2.2.7 Western blot

In order to determine the expression of target proteins in specific lysates, proteins separated by SDS-PAGE were screened for expression of particular antigens by Western blot (WB).

2.2.7.1 Protein transfer to a nitrocellulose membrane

The proteins separated by SDS-PAGE were transferred electrophoretically from the SDS-polyacrylamide gel onto a 0.45 µm pore–size nitrocellulose membrane (1620115, Bio-Rad) using a Rad Mini Trans-Blot® wet blotting system (Bio-Rad). To assemble the transfer "sandwich" necessary for wet blotting, six pieces of 3 mm Whatman® cellulose chromatography paper (WHA3030861, Sigma) and one piece of nitrocellulose were cut big enough to have the same size as the gel (approximately 9 cm x 7 cm). Nitrocellulose membrane was hydrated in ultrapure water for 5 min, then, together with Whatman® papers and two fibre pads, was pre-saturated in transfer buffer [48 mM Tris, 39 mM glycine, 0.0375% (w/v) SDS, 20% (v/v) methanol] for few minutes. Transfer buffer was freshly prepared from a 10X

stock buffer [480 mM Tris, 390 mM glycine,0.375% (w/v) SDS] by adding 20% (v/v) methanol (200 ml on one litre of final buffer) on the day of use. Elements were assembled in the mini gel holder (Bio-Rad) in this order, starting from the negative electrode (black): fibre pad, three papers, protein gel, nitrocellulose, three papers, and fibre pad. The gel holder was then placed in the Mini Trans-Blot Central Core (Bio-Rad), making sure to pair negative and positive sides, and the structure placed in the buffer tank filled with transfer buffer, together with a Bio-Ice cooling unit to keep the system cold during transfer. Electrophoretic transfer of the samples was then performed at the constant current of 180 mA for 75 min.

2.2.7.2 Membrane staining with Ponceau red

To reveal the bands on the nitrocellulose membrane, Ponceau red staining [0.1% (w/v) Ponceau S, 5% (v/v) glacial acetic acid] was used, immersing the membranes for 2 min in the solution and then quickly rinsing it with water to wash out the excessive stain.
Membranes were then washed with Tris buffered saline buffer (TBS) [25 mM Tris-HCl, 150 mM NaCl and 2 mM KCl, pH 7.4] to remove the stain before the blocking step.

2.2.7.3 Immunoprobing

Nitrocellulose membranes with transferred proteins were incubated in blocking buffer, 5% (w/v) non-fat milk in TBST [25mM Tris-HCl, 150mM NaCl, 2mM KCl, 0.1%(v/v) Tween-20], for one hour at room temperature in constant shaking. The blocking step is necessary to prevent the aspecific binding of the antibody in the subsequent steps.
After blocking, membranes were incubated with the appropriate dilution of primary antibody (**Table 2.2**) in blocking buffer, overnight (15 h) at 4°C in gentle rotation.
The following day the antibody in blocking buffer was recovered (primary antibodies in blocking buffer were stored at -20°C and re-used few times before disposal); membranes were washed three times for 10 min with TBST and incubated with the appropriate dilution of horseradish peroxidase (HRP)-conjugated secondary antibody in blocking buffer (**Table 2.3**) for 2 h at room temperature in gentle rotation. In some experiment, an HRP-conjugated primary antibody was used. In this case the incubation was performed for 2 h at room temperature or overnight (15 h) at 4°C in gentle rotation.
The membrane was then washed again with TBST (3 times/10 min each) and the immunoreactive bands developed by enhanced chemiluminescence (ECL) using EZ-Chemiluminescence Detection Kit for HRP (K1-0170) from Geneflow, following the manufacturer's instructions. EZ-ECL substrate needs to be prepared fresh before membrane development: for a full size membrane (approximately 9 cm x 7 cm), approximately 500 µl of reagent A (luminol and enhancer) were mixed with the same amount of reagent B (stable

peroxide solution) and let equilibrate for 5 min before employment. Nitrocellulose membrane was placed protein-side facing upwards on a dark background in the LAS4000 imaging system (GE Healthcare), EZ-ECL mixture was pipetted on it homogeneously and incubated for 1 min in the dark. Excessive solution was drained out and chemiluminescent image acquisition was performed in the LAS4000 imaging system with exposure time going from 30 sec to 30 min, depending on the specific experiment.

2.2.7.4 Stripping and re-probing

Membrane stripping is a procedure employed to remove the antibodies bound to specific proteins transferred on the nitrocellulose membrane, allowing to re-probe the same proteins with a second antibody. Different stripping buffers exist in biochemistry, with variable strength. For the aims of this thesis, a 0.5 M NaOH solution was employed as a quick stripping buffer. After development, membranes were incubated for 8 min with the solution in constant rotation at room temperature, then washed with TBST, the first time quickly to remove all NaOH, followed by 3 times for 5 min. Stripped membranes need to be blocked again in blocking buffer for 1 h before proceeding with immunoprobing as described above.

2.2.7.5 Quantification of protein expression by gel densitometry

The intensity of selected bands was evaluated by using 2D densitometry evaluation on AIDA (Advanced image Data Analyser) image analyser (Raytest, Germany) and following the manufacturer's instruction. Intensity of the target protein in the sample was normalised for band intensity of a loading control protein, which expression was not affected by the treatment (housekeeping protein). Loading controls employed in this thesis were β-tubulin, actin or cyclophilin-A (**Table 2.2**), deepening on the specific experiment performed.

2.2.8 Immunofluorescent staining of cell monolayers

2.2.8.1 Cell culture in an 8-well chamber slide

In order to immunodetect specific antigens in kidney cell monolayers, fluorescent immunostaining (IF) was performed. To perform fluorescent immunostaining, kidney cells were cultured in an 8-well chamber slide: approximately 20,000 cells were seeded in each well in approximately 300 µl culture medium, treatments were performed as required by the specific experiments, and cells were allowed to grow until approximately 90% confluent.

2.2.8.2 Fixation of cells with or without permeabilization

Once cells reached the desired confluence, medium was removed and cells washed with approximately 500µl of sterile PBS pH 7.4, 3 times for 5 min. After washing, cells were either fixed with paraformaldehyde [3% (w/v) PFA] but not permeabilized or fixed with 3% (w/v) PFA and permeabilized with Triton-X100 depending on the specific aim of the experiment. In the first case, in fact, only the antigen present extracellularly and on the cell surface would be immunodetected by the antibodies, while in the second case, cells would be permeable to the antibody itself, allowing the detection of intracellular antigen.

As PFA is not soluble at room temperature (dissolves at approximately 60°C in PBS), 3% (w/v) PFA solution was prepared fresh before the experiment by mixing the appropriate amount of paraformaldehyde powder in PBS pH 7.4 and letting it dissolve using a magnetic stirrer on an hot plate, under the chemical hood (PFA fumes might be toxic if inhaled), until completely clear. The solution was let to cool down to room temperature before using it to fix the cells.

Fixation of cells without permeabilization was performed incubating the cells with 200µl/well of 3%(w/v) PFA solution for 8 min at room temperature. Cell monolayer was washed with PBS pH 7.4 (3 x 5min) before proceeding with the blocking step.

Fixation and permeabilization was instead performed by incubating the cells with 200µl/well of 3%(w/v) PFA solution for 20 min at room temperature. Cell monolayer was washed two times with PBS pH 7.4, then incubated with 200 µl/well of 0.1% (v/v) Triton X100 in PBS pH 7.4 for 15 min at room temperature. Cell monolayer was washed with PBS pH 7.4 (3 x 5min) before proceeding with the blocking step.

2.2.8.3 Immunoprobing

After fixation / fixation-permeabilization of the cell monolayer, chamber slides were saturated with 200µl/well of blocking buffer [3%(w/v) BSA in PBS pH7.4] for one hour at room temperature or 30 min at 37°C. The blocking step is necessary to prevent the aspecific binding of the antibody in the subsequent steps.

After blocking, cell monolayers were incubated with ~100 µl/well of the appropriate dilution of primary antibody (**Table 2.2,** dilutions for IF) in blocking buffer, overnight (15 h) at 4°C. The following day the cell monolayers were washed with PBS pH 7.4 (3 x 5 min, as described above) and incubated with the appropriate dilution of fluorochrome-conjugated secondary antibody in blocking buffer (**Table 2.3,** fluorochrome-conjugated secondary antibodies) with emission at a specific wavelength, for 2 h at room temperature, protected from light. After incubation, chamber slide was washed again three times with PBS pH 7.4 and the wells removed, leaving the glass slide.

The slide was then mounted using few microliters of a 1:1 dilution of VECTASHIELD® mounting medium with DAPI and without DAPI (Vectorlab), enough to cover all wells. Using this solution, the cell nuclei will be stained with DAPI (4',6-diamidino-2-phenylindole) and appear blue on the fluorescent microscope. Slides were stored in the dark at 4°C for short-term storage and at -20°C for long-term storage.

As a negative control, to rule out any aspecific staining, primary antibody was omitted from one well / treatment, and cells incubated with the secondary antibody alone. Absence of a fluorescent signal after washing-out of the antibody would confirm the specificity of the signal observed in the other wells.

Images were acquired using a Leica TCS confocal microscope (Leica, Germany) at a magnification going from 10X magnification in dry conditions to 63X magnification with immersion oil. Quantification of fluorescent signals was performed with ImageJ open source software (Schindelin, et al. 2015) on at least eight non-overlapping images per treatment.

2.2.9 Transglutaminase activity assay

2.2.9.1 Total TG2 activity assay

In order to determine the TG2 activity of cell and tissue lysates, TG transamination activity was assessed by measuring the enzyme ability of incorporating biotinylated cadaverine (BTC) on immobilised fibronectin (FN), using a modification of the established method by Jones and colleagues (Jones, et al. 1997) (**Fig. 2.2**).

To perform the assay, a 96-well plate was coated with 100µl/well of 5µg/ml human plasma fibronectin (FN) (Sigma) in 50 mM Tris-HCl pH 7.4, overnight (15 h) at 4°C. The plates were washed 3 times with 200 µl/well Tris-HCl pH 7.4, then blocked with 100µl of 3% (w/v) BSA in 50mM Tris-HCl pH 7.4 for 30 min at 37°C or 1h at RT (**Fig. 2.2A**).

In the meantime, protein samples for TG2 activity assay were prepared following the standard lysis protocol and employing a sucrose based lysis buffer [250 mM sucrose, 2 mM EDTA, and 50 mM Tris-HCl, pH 7.4] containing protease inhibitors (1:100 dilution of Protease Inhibitor Cocktail, Sigma). Together with protein samples, also a standard curve of known concentrations of guinea pig liver TG2 (gplTG2) was prepared by performing a serial dilution of stock TG2 (Sigma) to obtain 100, 75, 50, 25, 12.5, 6.25, 3.125 and 0 ng/well. This standard curve would be necessary to relate the specific absorbance to pure TG2 transamidation activity.

After blocking with BSA, the plate was washed again three times with 50 mM Tris-HCl pH 7.4, then 60 µg/well of cell lysate were incubated in triplicates in presence of freshly added 0.1 mM biotin cadaverine [BTC, or N-(5-Aminopentyl)biotinamide trifluoroacetate salt] for 2 h at 37°C in Reaction buffer containing calcium [5 mM $CaCl_2$, 10 mM 1,4-Dithiothreitol (DTT), 50mM Tris-HCl pH 7.4 + 0.1 mM BTC] in a final volume of 100µl/well. Background activity (to be subtracted from the TG2 activity) was measured for each sample in triplicates by replacing $CaCl_2$ with 5 mM EDTA [5 mM EDTA, 10 mM DTT, 50mM Tris-HCl pH 7.4 + 0.1 mM BTC]. Standard curve (0-100 ng/well) was also loaded in duplicates in both reaction buffers in a final volume of 100µl/well and incubated as well for 2 h at 37°C **(Fig. 2.2B)**.

After a wash with 10 mM EDTA in PBS to stop the reaction and three washes with Tris-HCl pH 7.4, the amount of cross-linked BTC was revealed by incubation with 100 µl of a 1:5000 dilution of ExtrAvidin®−Peroxidase in blocking buffer, followed by three other washes with Tris-HCl pH 7.4 **(Fig. 2.2C)**.

Subsequently, the plate was equilibrated for 10 min with 100µl of 50mM phosphate-citrate buffer, containing 0.014% (v/v) H_2O_2, pH 5.0. Buffer was prepared fresh for each experiment by dissolving one tablet Phosphate-citrate buffer/urea H_2O_2 (Sigma) in 10 ml distilled H_2O. At the end of equilibration, the buffer was substituted with 100µl developing solution [50 mM phosphate-citrate buffer, 0.014% (v/v) H_2O_2 pH 5.0 containing 7.5% w/v 3,3′,5,5′-

tetramethylbenzidine (TMB)]. Developing solution was prepared freshly before development by adding 75 µl of 10mg/ml 3,3′,5,5′-tetramethylbenzidine TMB stock solution in DMSO to 10 ml of 50 mM phosphate-citrate buffer, 0.014% (v/v) H_2O_2 pH 5.0 **(Fig.2D)**. If the phosphate-citrate buffer containing H_2O_2 (Sigma) was old, 10 ml of developing solution were also supplemented with 5µl of 30% H_2O_2. The development was observed by the colour of the solution shifting to blue **(Fig.2.2D)**, and was stopped by adding 0.5 volumes of 2.5N sulphuric acid (H_2SO_4), that turns the solution to a stable yellow colour **(Fig. 2.2E)**.

The absorbance was then measured at 450 nm using a 96-well plate reader (spectrophotometer). The specific activity of TG2 in mU was calculated by subtracting the mean absorbance value in presence of EDTA from the mean absorbance value in presence of calcium, and plotting the unknown samples resulting values on the gplTG2 standard curve of known concentrations to infer the amount of TG2 specific activity (mU/ml).

2.2.9.2 Extracellular TG2 activity assay

In order to measure TG2 activity outside the cells, extracellular TG2 activity assay (sometimes regarded as cell surface TG2 activity assay) was performed according to (Jones, et al. 1997). The principle of the experiment is identical to the Total TG2 activity assay. In this case, however, the ability of TG2 of incorporating biotin cadaverine (BTC) **(Fig.2.2)** in FN is measured on living cells, limiting the TG2 activity detected to the cell surface/extracellular one. To perform the assay, a 96-well plate was coated with 50µl/well of 5 µg/ml human plasma FN in 50mM Tris-HCl pH 7.4, overnight (15 h) at 4°C. The wells were washed three times with 200 µl/well Tris-HCl pH 7.4, then blocked with 100µl of 3% (w/v) BSA in 50mM Tris-HCl pH 7.4 for 30 min at 37°C or 1h at room temperature **(Fig.2.2A)**.

To harvest cells for the assay, approximately 80-90% confluent cell monolayers were washed once with PBS pH 7.4 then detached with a trypsin-free buffer [5 mM EDTA in sterile PBS pH 7.4] in gentle shaking at 37°C. Reaction was stopped with complete culture medium and cell pellet collected by centrifugation at 500g for 5 min. A cells suspension of 200,000 cells/ml in serum free-medium containing 10mM 1,4-Dithiothreitol (DTT) prepared ready to be supplemented with BTC and loaded on the plate.

Once blocking step was over, wells were washed two times with 50mM Tris-HCl pH 7.4 and a last one with serum-free culture medium. Appropriate amount of cell suspension was supplemented with 0.1 mM BTC, and 100 µl/well (corresponding to 20,000 cells/well) were incubated in triplicates or quadruplicates, depending on the experiment, for 2 h at 37°C, to allow the amine incorporation reaction to happen **(Fig. 2.2B)**. As a negative control, serum free medium with 10 mM DTT was applied in triplicates and incubated as above.

The reaction was stopped with 2 washes with sterile PBS pH 7.4, and cell monolayer was incubated for 10 min with freshly prepared 0.1% (w/v) sodium deoxycholate in PBS pH 7.4 in

gentle rotation, to lyse the cells and leave only the FN-BTC extracellular matrix. After three washes with Tris-HCl pH 7.4, the amount of cross-linked BTC was revealed by incubation with 100 µl of a 1:5000 dilution of ExtrAvidin®−Peroxidase (E2886, Sigma) in 50 mM Tris-HCl pH 7.4 containing 1.5 % (w/v) BSA for 1 h at 37°C followed by three other washes with Tris-HCl pH 7.4 **(Fig.2.2C)**.

The plate was developed with 100µl developing solution [50 mM phosphate-citrate buffer, 0.014% v/v H_2O_2 pH 5.0 containing 7.5% w/v 3,3′,5,5′-tetramethylbenzidine (TMB)] as described before **(Fig.2.2D)**. The development was detected by the colour of the solution shifting to blue, and was stopped by adding 0.5 volumes of 2.5N Sulphuric acid (H_2SO_4), that turns the solution to a stable yellow colour **(Fig.2.2E)**. The absorbance was then measured at 450 nm using a 96-well plate reader (spectrophotometer).

2.2.9.3 In situ TG2 activity assay

In order to visualise TG2 activity *in situ*, incorporation of fluorescein isothiocianate (FITC) - conjugated cadaverine by a cell monolayer was measured as described by Verderio and colleagues (Verderio, et al. 1998). Briefly, approximately 20,000 cells/well were seeded in an 8-well chamber slide and cultured in 300 µl culture medium until ~70% confluent. Medium was replaced with 250 µl/well of complete medium containing 0.5 mM FITC-cadaverine and cells were incubated for 4 -15 h (ON) depending on the experiment. Cell monolayer was gently washed three times with 500 µl PBS pH 7.4 for 5 min, then cell fixed with 200 µl cold 90% (v/v) methanol in PBS pH 7.4 at -20°C for 10 min. After fixation, chamber slide was washed 4 times with PBS pH 7.4 for 8 min and slide mounted with 1:1 dilution of VECTASHIELD® mounting medium with DAPI and without DAPI as described before [2.2.8.2]

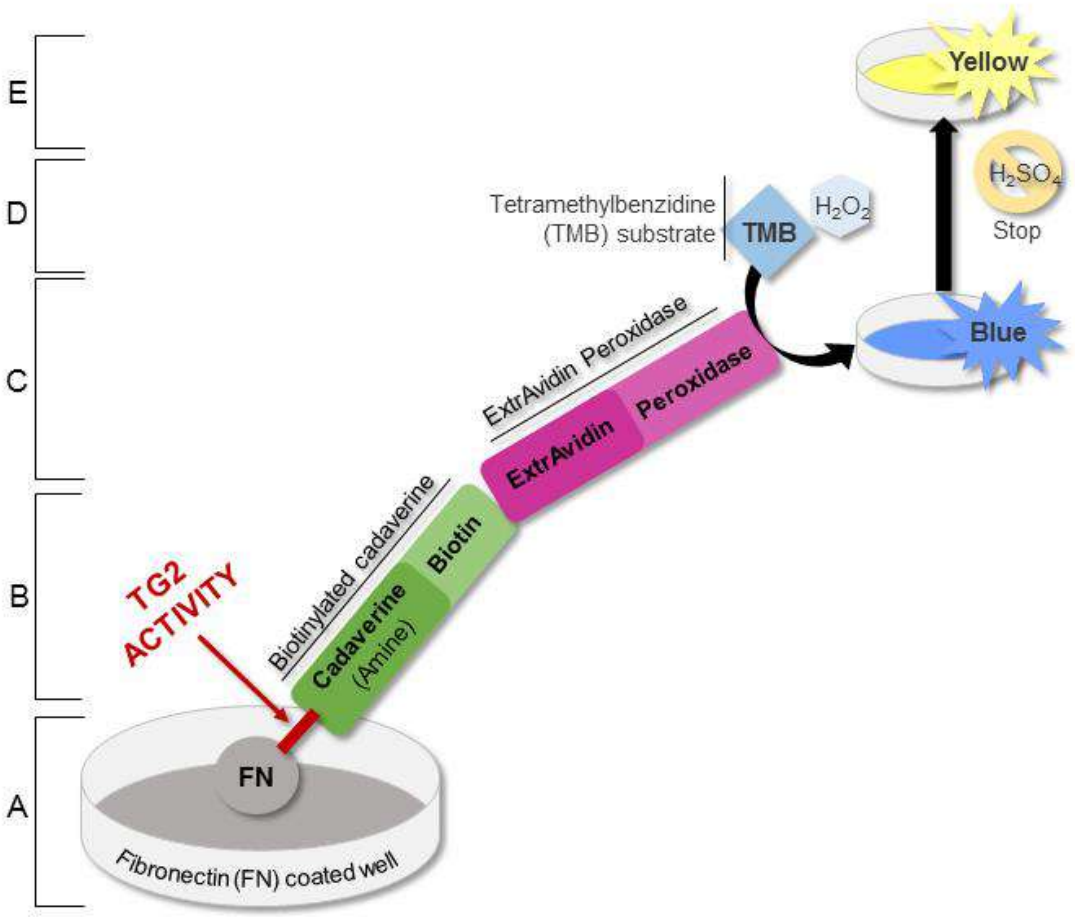

Figure 2.2: Outline of TG2 activity plate assay performed in this thesis. A= Fibronectin (FN) coating; B=Amine (BTC) incorporation by TG2; C=Incubation with ExtrAvidin® peroxidase that binds biotin; D=Development with TMB substrate (peroxidase-dependent colorimetric reaction that turns the solution blue); E = Reaction stopped with sulphuric acid (H_2SO_4) that turns the solution to a stable yellow colour (read at 450 nm).

2.2.10 Cell transfection

2.2.10.1 Transfection of plasmid DNA by electroporation

In specific experiments, cell transfection of cDNA was performed to induce expression of specific proteins by the cells. Electroporation is an easy method used to introduce DNA in the cells by applying a transient electrical field that briefly opens the pores of the cells, allowing exogenous DNA to enter. Amaxa® Nucleofector™ technology, in particular, is a cell-type specific transfection technique based on electroporation, that allows a delivery of DNA directly to the nucleus, transiently opening also the nuclear membrane, hence allowing a higher transfection efficiency.

Following Amaxa® Nucleofector™ manufacturer's suggestions, one million of exponentially growing NRK52E cells or EGFP-TG2 overexpressing NRK52E clones were harvested by centrifugation as described before and re-suspended in 100 µl of supplemented Nucleofector™ solution V form Amaxa Nucleofector™ kit V. Supplemented Nucleofector™ solution was prepared at room temperature shortly before the experiment by mixing one volume of supplement to 4.5 volumes of Nucleofector™ solution V. For a single reaction, 82 µl of Nucleofector™ solution V were supplemented with 18 µl of supplement, to have 100 µl of total reaction volume.

5 µg of the chosen mammalian transfection plasmid (**Table 2.10**) were added to the cell suspension and the whole suspension transferred in the certified electroporation cuvette provided in the kit. As a control, a mock transfection (no plasmid added) was performed, following the same procedure. When performing transient transfections of TG2 and TG2 mutants with the pEGFP-N1-TG2 plasmid (Chapter VI), a control transfection with the empty pEGFP-N1 vector (ClonTech #6085-1), in addition to the mock transfection, was performed.

The cuvette was placed in the cuvette holder of the Amaxa® Nucleofactor™ device and the electric field was transiently applied. Program T-027 of the electroporation device was employed for transfection, as suggested by the manufacturer for this specific cell line. The cuvette was carefully removed and 500 µl of complete DMEM was quickly added on the mixture. Without re-suspending, the sample was gently transferred into a 6-well plate containing 2 ml of pre-warmed complete DMEM medium using the supplied sterile plastic pipettes. Expression of the plasmid was allowed to proceed for 48 h at 37°C in 5% CO_2 before harvesting the cells.

In every experiment, a transfection with 5 µg of pEGFP-N1 empty vector (Clonetech) was carried out to evaluate the transfection efficiency: after 48 h cells were observed under confocal fluorescent microscope and the ratio between fluorescent cells (green emission) and total cells (bright field) was calculated. Generally, transfection efficiency comprised between 65 and 85% was obtained. Moreover, the efficiency of the specific cDNA transfection was

assessed at transcript level by quantitative real time PCR (qRT-PCR) or at protein level by Western blot.

Table 2.10: Mammalian transfection plasmids employed in this thesis for transfection of NR52E cells.

cDNA	Transfection plasmid	Antibiotic resistance
Human Syndecan 4 (Sdc4)	pcDNA3.1(+)_Sdc4 (Scarpellini, 2009)	Ampicillin
Human Syndecan 4 tagged with Hemagglutinin (HA-Sdc4)	pcDNA3_HA-Sdc4 (unpublished)	Ampicillin
Human Transglutaminase 2 tagged with Enhanched Green fluorescent protein (EGFP-TG2 (sometimes referred as EGFP.-TG2(WT)]	pEGFP-N1-TG2(WT) (Scarpellini, 2009)	Kanamycicn
Heparin binding mutant Human Transglutaminase 2 (mutation M1c, Lortat-Jacob et al, 2012) tagged with Enhanched Green fluorescent protein [EGFP-TG2(M1c)]	pEGFP-N1-TG2(M1c) (Unpublished)	Kanamycicn
Heparin binding mutant Human Transglutaminase 2 (mutation M3, Lortat-Jacob et al, 2012) tagged with Enhanched Green fluorescent protein [EGFP-TG2(M3)]	pEGFP-N1-TG2(M3) (Unpublished)	Kanamycicn
Enhanched Green fluorescent protein alone (Transfection control)	EGFP-N1 plasmid (6085-1, Clontech, California, US)	Kanamycicn
None (Control)	Mock transfection	/

2.2.10.2 Transfection of siRNA

Small interfering RNA (siRNA) transfection is a cell transfection technique used to transiently interfere with the expression of selected genes. In this case, a vector-free approach of siRNA transfection, based on DharmaFECT® 1 transfection reagent, was used. In order to perform knock out of selected gene expression on NRK52E cells or NRK52E EGFP-TG2 overexpressing clones, approximately 300,000 cells/well were plated in a 6-well plate and cultured overnight (15 h) in an antibiotic-free DMEM medium specifically prepared for siRNA transfection [DMEM containing 4.5 g/L glucose, 5%(v/v) FBS and 2 mM L-glutamine].

The day after, a transfection solution containing 100 nM siRNA (**Table 2.11**) and DharmaFECT® 1 was prepared; volumes reported in the protocol are considered for the preparation of a 4 ml final transfection solution, which was enough to transfect tree wells of a 6-well plate (approximately 1.3 ml/well). Preparation of siRNA transfection solutions was performed in nuclease-free conditions, and, when necessary, nuclease-free water [diethylpyrocarbonate (DEPC)- treated water prepared by incubation of distilled H_2O with 0.1% (v/v) DEPC overnight under the chemical hood, followed by autoclaving at 121 °C for 20 min] was employed to dilute siRNA stocks and reagents.

Briefly, a 2 µM solution of the specific siRNA employed (**Table 2.11**) was prepared in 200 µl of siRNA Buffer [60 mM KCl, 6 mM HEPES-pH 7.5, 200 uM $MgCl_2$, diluted from 5X siRNA buffer

stock (B-002000-UB, GE Dharmacon, Thermo Scientific) with nuclease-free water], then further diluted to 1μM by adding one volume (200 μl) of serum free DMEM. At the same time, 400 μl of 2.5% (v/v) DharmaFECT® 1 solution in serum-free DMEM was prepared by mixing 10 μl of DharmaFECT® 1 transfection reagent (T-2001-01, GE Dharmacon, Thermo Scientific) to 390 μl of medium. The two separate solutions were incubated for 5 min at room temperature, then combined 1:1 (total volume = 800 μl) and incubated again 20 min at room temperature. The final solution was diluted 5 times with 3.2 ml of complete antibiotics-free DMEM medium. Culture medium was removed from the cultured cells and replaced with approximately 1.3 ml of transfection medium. Following transfection, incubation was protracted for 24 or 48 h depending on the experiment.

In all experiments performed, both a specific gene-targeting siRNA and a non-targeting control scrambled siRNA (**Table 2.11**) were used, to rule out any effect on gene expression determined by the transfection procedure itself. After transfection, the efficiency of knock down at a transcript level or at a protein level was assessed.

Table 2.11: siRNA employed in this thesis for transfection of NRK52E cells.

Knock – out of	SiRNA
Rat Syndecan 4 (Sdc4)	Rat Sdc4 Targeting siRNA [ON-TARGETplus Rat Sdc4 (24771) siRNA - Individual (J-087816-05-0005, Dharmacon,Thermo Scientific)]
Rat Clathrin (Cltc)	Rat Cltc Targeting siRNA [ON-TARGETplus Rat Cltc (54241) siRNA – SMARTpool (L-090659-02-0005, Dharmacon, Thermo Scientific)]
/ (Control)	Non-targeting scrambled control siRNA [ON-TARGETplus Non-targeting siRNA #1 (D-001810-01-05, Dharmacon, Thermo Scientific)]

2.2.11 Amplification of plasmid DNA

2.2.11.1 Preparation of LB Broth (Lennox) culture medium and LB-Agar plates

Lennox lysogeny broth (LB, sometimes referred as Luria Bertani broth) (Bertani 1951) was prepared by mixing 20 g of granulated Fisher BioReagents™ LB Broth Lennox to 1 L of distilled water and autoclaving it (121 °C for 20 min). The final solution contained 5 g/L yeast extract, 10 g/L tryptone and 5g/L NaCl, and its pH was approximately 7.

LB-agar plates containing specific selective antibiotics were also prepared. To prepare 20 Agar plates, 500 ml of LB Broth [0.5% (w/v) yeast extract, 1% (w/v) tryptone and 0.5% (w/v) NaCl, pH~7] were mixed with 1.5% (w/v) of agarose. The mixture was autoclaved (121 °C for 20 min) to sterilise it and dissolve the agarose, and let cool down to approximately 50°C before adding the antibiotics. Autoclaved solution was opened in sterile conditions (over Bunsen flame) and the appropriate amount of the selective antibiotic [100 μg/ml ampicillin or 50 μg/ml kanamycin depending on the specific antibiotic resistance carried by the plasmid the

cells were transformed with, **Table 2.10**] was added. Rapidly, the mixture was poured in bacterial culture Petri dishes (~25 ml/dish) and let solidify at room temperature in sterile conditions. Plates were incubated cover side- down at 37°C for 1 h to avoid contaminations. If not used immediately, plates were sealed with Parafilm M® (Bemis) and stored cover side - down at 4°C in the dark, wrapped in aluminium foil, for no longer than one month. On the day of use, plates were pre-warmed at 37°C for approximately 30 min before employment.

2.2.11.2 *Transformation of DH5α competent cells with plasmid DNA*

In order to transform bacterial *E.coli* cells with plasmid DNA and allow plasmid DNA replication in this system, 50 µl of Subcloning Efficiency™ chemically competent DH5α™ cells (18265-017, Invitrogen) were taken from -80°C storage and slowly thawed on ice. Once defrosted, cells were incubated with approximately 20 ng of desired expression plasmid (**Table 2.10**), on ice for 30 min. After this time, a heat shock of exactly 45 sec at 42°C was performed in a water bath, followed by a 2 min incubation on ice. 950 µl of pre-warmed LB b broth was added on the top, and the tube was incubated for one hour at 37°C at 200 rpm constant shaking. Different volumes of the transformed cells (200-50 µl) were then plated on LB Agar plates containing the selective antibiotic (**Table 2.10**) and plates were incubated cover-side down at 37°C overnight. Antibiotic-resistant colonies were observed the day after. A mock transformation (no plasmid added) was performed every time to confirm whether the antibiotic resistance was carried by the plasmid.

2.2.11.3 Glycerol stock of bacterial colonies

In order to store transformed bacteria, an isolated antibiotic-resistant bacterial colony was picked with a sterile tip to inoculate 10 ml of LB broth containing the selective antibiotic [100 µg/ml ampicillin or 50 µg/ml kanamycin depending on the specific resistance carried by the plasmid used (**Table 2.10)**] in an appropriate sized container (must be at least 5 times bigger than the medium volume, to allow enough oxygen to be available). The preparation was then incubated overnight at 37°C at 200 rpm constant shaking. The resulting bacterial culture was used to prepare 1 ml frozen stocks containing 15% (v/v) glycerol in sterile cryovials (850 µl bacterial culture + 150 µl glycerol), stored at -80°C.

When transformed bacteria were needed, the glycerol stock was gently thawed on ice and, when still partially frozen, a small portion was taken with a sterile loop and used to inoculate selective LB broth.

2.2.11.4 Amplification and extraction of plasmid DNA

2.2.11.4.1 Miniprep of plasmid DNA:

A single bacterial colony from agar plate or glycerol stock was used to inoculate 5 ml of selective LB broth [100 μg/ml ampicillin or 50 μg/ml kanamycin depending on the specific resistance carried by the plasmid used (**Table 2.10)**], and incubated 6-8 h at 37°C at 200 rpm constant shaking. Bacteria were pelleted by centrifugation (6000g for 15 min at 4°C), then plasmid were isolated using the QIAprep Spin Miniprep Kit (Qiagen), following the manufacturer protocol. Plasmid DNA was eluted in 50 μl nuclease-free distilled water unless otherwise stated. Concentration was measured by NanoDrop® 8000 spectrophotometer (Thermo Scientific).

Purity of the plasmid preparation was also assessed with the NanoDrop® 8000 spectrophotometer by the 260/280 and 260/230 absorbance ratio. All nucleotides (RNA, ssDNA and dsDNA) absorb at 260 nm, while proteins, ethanol and other possible contaminants of the extracted plasmid absorb around 280 nm; EDTA and carbohydrate absorb around 230 nm, while phenol contributes to both 230 nm and 280 nm absorbance. DNA preparations with 260/280 around 1.8 and 260/230 ratio around 2-2.2 were regarded as pure (Thermo Fisher Scientific, NanoDrop products 2008).

2.2.11.4.2 Midiprep of plasmid DNA:

A single bacterial colony from agar plate or glycerol stock was used to inoculate 5 ml of selective LB broth [100 μg/ml ampicillin or 50 μg/ml kanamycin depending on the specific resistance carried by the plasmid used (**Table 2.10)**], and incubated 6-8 hr at 37°C at 200 rpm constant shaking. The whole bacterial culture was then transferred in a bigger flask containing 100 ml selective LB broth and left at the same conditions overnight (15 h). Bacteria were pelleted by centrifugation (6000g for 15 min at 4°C), then plasmid were isolated using the Qiagen Plasmid Midi Kit (12143, Qiagen) and following the manufacturer protocol. Plasmid DNA was eluted in 40 μl Tris-EDTA (TE) Buffer [10 mM Tris-HCl, 1 mM EDTA, pH 8.0] unless otherwise stated. Concentration and purity of DNA was measured by NanoDrop® 8000.

2.2.11.5 Sequencing of plasmid DNA

To confirm the correct sequence of plasmid DNA, purified plasmids were sequenced by Sanger sequencing by Source BioScience Overnight Service™ (EVCHT50, Source BioScience).

A minimum of 5 μl of 100 ng/μl plasmid DNA, in either 10 mM Tris HCl pH 8.5 or nuclease – free water, were sent for sequencing. Sequencing primers were provided by the company and depended on the specific vector employed. Sequencing results were analysed by BLAST (Basic

Local Alignment Search Tool, https://blast.ncbi.nlm.nih.gov/Blast.cgi) or Clustal Omega (http://www.ebi.ac.uk/Tools/msa/clustalo) open source sequencing tools.

2.2.12 Total RNA extraction from kidney cells

In order to measure the level of transcription of particular genes, total RNA was extracted from cells. RNA extraction was performed using GenElute™ Mammalian Total RNA Miniprep Kit (Sigma), a column-based RNA purification kit, following the manufacturer's instructions.

To extract RNA, approximately 5 million of exponentially growing cells were employed. Cells were detached by trypsinization as described above, and centrifuged at 500 g for 5 min to obtain cell pellets. Traces of serum were carefully removed by washing the cell pellet once with sterile PBS pH 7.4, and pelleting them again by centrifugation. Cell pellet was lysed with 250 µL of the lysis solution containing β-ME (provided by the kit), and filtered through GenElute filtration column by centrifugation at ~16,000 × g for 2 min. Lysate was supplemented with 250 µl of 70% (v/v) ethanol and placed into a GenElute binding column. A series of brief high speed spins and washes were performed as required by the protocol, and the RNA was eluted in 50 µL of the elution solution by ~16,000 × g centrifugation for 1 min. Extracted RNA was stored at -80°C.

After purification, the amount and quality of the RNA obtained was determined by NanoDrop® 8000 (Thermo Scientific). Between 10 and 20 µg RNA were usually obtained from 1 million cultured cells. RNA preparations with 260/280 ration around 2 and 260/230 ratio around 2-2.2 were regarded as pure (Thermo Fisher Scientific, NanoDrop products 2008).

2.2.13 Reverse transcription

2 µg of total RNA obtained was reverse transcribed using "random primers" (C1181 Promega) and 200 units (100U/µg RNA) of SuperScript® II reverse transcriptase (Invitrogen) at 42°C for 50 min.

Briefly, for each reaction (final volume 20 µl), 2 µg of total RNA was incubated with 25 µg/ml of random primers (Promega) and 250 µM dNTP's (Promega) in a total volume 13 µl at 65°C for 5 min, then quickly chilled on ice. 4 µl of 5X First-Strand buffer and 2 µl of 0.1 M DTT (final concentration 10mM), provided with the transcriptase, were added, and the solution incubated at 25°C for 2 min. 200 units (1 µl) of SuperScript® II reverse transcriptase (18064-014, Invitrogen) were then added, to a final volume of 20 µl. The mixture was incubated in a table top standard thermocycler at 25°C for 10 min, then 42°C for 50 min, and finally at 70°C for 15 min, to allow for reverse transcription. The reverse transcribed cDNA was stored at -20°C until needed.

2.2.14 Quantitative real time PCR (qRT-PCR)

2.2.14.1 qRT-PCR Reaction

To measure the level of expression of the gene of interest, equal volumes of cDNA obtained by reverse transcription were amplified by quantitative PCR (qPCR) using iQ™ SYBR® Green Supermix (170-8880, Biorad). This ready-to-use mix is 2X concentrated and contains 50 U/ml hot-start iTaq™ DNA polymerase, 6 mM $MgCl_2$, 0.4 mM dNTPs, SYBR® Green I dye, enhancers, stabilizers and fluorescein.

Primers for specific gene amplification were found from literature (Brucato, et al. 2000, Kim, et al. 1994, Ahmad, et al. 2007), checked for quality and melting proprieties using Sigma OligoEvaluator™ (http://www.oligoevaluator.com) and obtained from Sigma as customized Easy Oligos (OLIGOS, Sigma). Lyophilized primers were resuspended in nuclease-free water at a 100µM stock concentration. These solutions where then further diluted in nuclease-free water at a 20µM working concentration. The specific primers employed in this thesis are reported in **Table 2.12.**

1µl of cDNA was added to 6.25 µl of 2X iQ™ SYBR® Green Supermix (Biorad), 400 nM forward primer and 400 nM reverse primer in nuclease free water (DEPC-treated), to the final volume of 12.5 µl, into suitable nuclease free Strip tubes (981103, Qiagen). The amplification was performed in triplicates. A no-template control reaction (in triplicates) was included to rule out any buffer contamination. cyclophilin-A (CycA) (**Table 2.12**) was selected as housekeeping gene, employed to normalize the values and perform a relative quantification.

PCR reactions were carried out in a Corbett Rotor-Gene 6000 rotary analyser (Qiagen). Thermal cycles performed for the specific amplifications presented in this thesis are reported in **Table 2.13**: an initial denaturation of 10 min at 95°C was followed by 40 cycles of denaturation at 95°C for 30 sec, annealing at 58°C for 20 sec and elongation at 72°C for 20 sec. At the end of the last cycle, a ramp temperature rise from 72°C to 95°C (5 seconds each °C) was performed to produce melting curves. Melting curves are fundamental to confirm the specificity of the amplification and the absence of contamination in the reagents (no-template control).

Once the last step was over, fluorescence (SYBR Green) data were obtained as graphs of fluorescence signal accumulation over cycle. A fluorescence threshold (background level) was arbitrarily chosen in every experiment and "cycle threshold" (Ct) values were calculated by the software as the intersection points of the fluorescence curves with the threshold chosen. The Ct value can be defined as the number of cycles necessary for the fluorescent signal to cross the threshold, and is proportional to the amount target cDNA in the sample: the higher is the gene expression in the sample analysed, the lower will be the Ct value, and vice versa.

In some cases, the amplification product (end-point) of the PCR reaction was further analysed by agarose gel electrophoresis [2% (w/v)] to confirm the specificity of the amplification as well as the absence of contamination in the reagents (no-template control).

Table 2.12: Primers employed for specific gene amplification by qRT-PCR. Primers were checked for quality and melting proprieties using Sigma OligoEvaluator™ (http://www.oligoevaluator.com) and obtained from Sigma as 100 µM customed Easy Oligos.

Primers					
Target Gene	**Name**	**Sequence 5'-3'**	**Tm**	**Product size**	**Reference**
Syndecan-4 Sdc4	Sdc4 FW	5'-GAGTCGATTCGAGAGACTGA-3'	54	366 bp	(Kim, et al. 1994, Brucato, et al. 2000)
	Sdc4 RV	5'-AAAAATGTTGCTGCCCTG-3'	56		
Cyclophilin-A (CycA)	Rat CycA FW	5'-AGCATACAGGTCCTGGCATC-3'	54	127 bp	(Ahmad, et al. 2007)
	Rat CycA RV	5'-TTCACCTTCCCAAAGACCAC-3'	52		

Table 2.13: Thermal cycles employed for specific gene amplification by qRT-PCR using primers reported in Table 2.12. PCR reactions were carried out in a Corbett Rotor-Gene 6000 rotary analyser (Qiagen).

Thermocycler conditions			
Cycles	**Step**	**T (°C)**	**Time**
1	Denaturation	95°C	10 min
40	Denaturation	95°C	30 sec
	Annealing	58 °C	20 sec
	Elongation	72 °C	20 sec
1	Melt	72 - 95°C	Hold sec on 1st step, hold 5 sec on next steps

2.2.14.2 Relative quantification of transcript expression

Once Ct values were obtained for each replica of each sample, the $2^{-\Delta\Delta Ct}$ relative quantification method (Livak and Schmittgen 2001) was manually applied to calculate the level of expression of the target gene.

Ct values obtained were averaged within the 3 replicas of each sample. Mean Ct values for the housekeeping gene (that is proportional the total cDNA loaded, hence should be constant among the different samples) was subtracted from the mean Ct values for the target gene, obtaining a normalised ΔCt value (1). Subsequently, a ΔΔCt value was calculated as the difference between the gene of interest and a calibrator (2), which is arbitrarily chosen and can be, for example, the untreated sample; the final result will be the level of expression of each

sample relatively to this calibrator. Finally, the relative expression from the calibrator was calculated as $2^{-\Delta\Delta CT}$ (3). Standard errors were calculated as described in (Livak and Schmittgen 2001).

$$(1)\ \Delta Ct = Ct_{target\ gene} - Ct_{housekeeping\ gene} \rightarrow \Delta Ct_{normalised\ CycA} = Ct_{target\ gene} - Ct_{CycA}$$

$$(2)\ \Delta\Delta Ct = \Delta Ct - \Delta Ct_{calibrator}$$

$$(3)\ \%\ Expression_{\ target\ gene\ relatively\ to\ the\ calibrator} = 2^{-\Delta\Delta Ct} \cdot 100$$

2.2.15 Preparation and loading of an electrophoresis agarose gel

In order to separate amplified DNA samples depending on their size, DNA electrophoresis was performed on an agarose gel.

Agarose gel was prepared by mixing 2% (w/v) agarose to a volume of Tris-acetate-EDTA (TAE) buffer (40mM Tris, 20mM acetic acid, 1mM EDTA, pH 8.5) sufficient to fill the gel casting tray. Agarose was dissolved by warming up the mixture in the microwave and, after cooling down the final solution to approximately 50°C, ethidium bromide (10 mg/ml, Sigma) was added to a final concentration of 0.5 µg/ml (5 µl in 100 ml of gel mixture). The gel was then poured into the gel tray containing the well combs and let solidify.

Once solidified, the gel was placed in the electrophoresis chamber, containing a suitable amount of TAE buffer, loading the wells on the negative side (black, as DNA is negatively charged and runs to the positive side). Samples amplified with iQ™ SYBR® Green Supermix are already in a blue loading buffer, in other cases, samples to load were prepared by adding a 1:5 dilution of Blue/Orange 6X loading dye (G1881, Promega). DNA samples were loaded in the wells and electrophoresis was performed by applying a constant voltage of 100 -150 V for at least 30 min.

Together with the samples, 6µl of 100kb DNA ladder was run. 100kb DNA ladder was prepared as suggested by the manufacturer, by mixing 1:4:1 volumes of 100 bp DNA ladder (G2101, Promega), ultrapure water and Blue/Orange 6X loading dye and is necessary to determine the size of the separated fragments and an approximate concentration. Once the run was completed, DNA fragments were visualized under UV light (U:Genius transilluminator, Syngene).

2.2.16 Statistical analysis

All experiments were undertaken at least three times (three independent experiments) unless otherwise stated. Data were expressed as means ± standard deviation (SD), unless otherwise stated. Statistical analysis of the differences between data sets was performed on Office Excel by Student's t-test (two-tailed distribution, unequal variance), unless otherwise stated. A p-value lower than 0.05 was regarded as significant (* = $p<0.05$, ** = $p<0.01$, *** = $p<0.001$, **** = $p<0.0001$).

2.2.17 Protein and nucleotide sequence alignments

Protein and nucleotide sequence alignments were performed employing the distinct functions available on the SDSC (San Diego Supercomputer Centre) Biology Workbench bioinformatic platform (http://workbench.sdsc.edu).

Chapter III: Proteomic analysis of differentially expressed proteins in the unilateral ureteric obstruction (UUO) model of CKD

3.1 AIMS OF THE CHAPTER

The aim of this chapter is to perform a proteomic analysis of the UUO model by employing quantitative mass spectrometry and, in this manner, identify proteins significantly overexpressed or underexpressed upon obstructive nephropathy. Functional enrichment analysis will give an idea of the functional classes and biological pathways affected by the disease, while interaction analysis will provide a picture of the possible connections between the proteins. This novel library of proteins differentially expressed by UUO will be a valuable tool for the identification of markers of advanced tubulointerstitial fibrosis. Furthermore, it will be useful to set a baseline for the TG2-interactome analysis described Chapter IV.
Given the protective role of TG2-KO against the progression of fibrosis observed both *in vitro* and *in vivo* in different models of kidney disease, the analysis of possible variations in protein expression in the TG2-null phenotype subjected to UUO is another aim of this chapter, that might provide information on the role of TG2 in the progression of disease.

3.2 INTRODUCTION

3.2.1 Unilateral ureteric obstruction (UUO) model of CKD

The unilateral ureteric obstruction (UUO) is an experimental model of CKD largely employed in rodents (Chevalier, Forbes and Thornhill 2009). It is a good model to produce a rapid tubular and interstitial response, with proliferation and activation of interstitial fibroblasts, increased deposition of an interstitial matrix mainly composed of collagen I, III, IV, fibronectin (FN) and heparan sulphate proteoglycans (HSPGs), interstitial fibrosis and tubular atrophy (Nagle, et al. 1973, Sharma, et al. 1993). The UUO procedure mimics the effect of human congenital obstructive nephropathy, one of the most important causes of renal impairment in the children (Seikaly, et al. 2003).
While the majority of models of CKD including the ablation models and the diabetic nephropathy models generally lead to glomerular injury and glomerulosclerosis as a primary response, less models have been designed to determine a primary tubulointerstitial disease,

which is particularly important, taking into consideration that the progression of renal insufficiency better correlates with this tubulointerstitial fibrosis, comparing to the glomerular response (Schainuck, et al. 1970). UUO is the best known experimental model with a primary tubulointerstitial effect, even if other experimental models, including ischemia/reperfusion or employment of specific nephrotoxins and immune complexes have been suggested to determine a fibrotic response starting from the tubules (Chevalier, Forbes and Thornhill 2009). Advantages of UUO are the absence of toxins and the availability of the contralateral kidney as a genetically identical control (Chevalier, Forbes and Thornhill 2009).

UUO is produced by surgical incision of abdomen and exposure and obstruction of one of the ureters, usually the left, with two separate knots (one proximal and one distal) or by employment of surgical clips, generally cutting the space between the obstructions (Ucero, et al. 2014). The obstructed kidney experience urine retention and quickly develops the tubulointerstitial injury while the contralateral kidney (non-obstructed kidney) undergoes a series of compensatory changes (Ucero, et al. 2014). The contralateral kidney can be employed as a control but it cannot be employed as a healthy non-treated control, as it compensates for the organ loss (Chevalier 1990). For this reason, a Sham operation, in which the ureter is exposed but not ligated, is usually employed as a healthy control (Ucero, et al. 2014).

The procedure induces extremely rapid responses, with reduced GFR and blood flow already observable within one day, and hydronephrosis, large immune response and cell death within a week (Chevalier, Forbes and Thornhill 2009, Vaughan, et al. 2004).

The organ responses to the UUO leading to a rapid development of CKD in the experimental animals can be divided into three phases: inflammatory response, tubular cell injury and cell death (by both apoptosis and necrosis), and tubulointerstitial fibrosis (Chevalier, Forbes and Thornhill 2009, Ucero, et al. 2014) (**Fig. 3.1**).

Inflammatory response starts immediately after obstruction (~12 h) and is mainly characterized by macrophage infiltration and activation in the interstitial space. Infiltrated macrophages produce a large number of cytokines responsible for fibroblast recruitment and activation as well as for tubular cell death. Two population of macrophages can be observed in this model: the classically activated (M1) and the alternatively activated (M2) (Duffield 2014, Ricardo, van Goor and Eddy 2008). The firsts have a classical inflammatory phenotype and are involved in the promotion of cell death, while the others are involved in tissue healing and resolution of the inflammation, and mediate cell proliferation as well as ECM deposition and sclerotic tissue accumulation (Duffield 2014, Ricardo, van Goor and Eddy 2008).

Upregulation of AngII has also been observed as an early response to UUO (Klahr and Morrissey 1998), with production of reactive oxygen species (ROS) and upregulation of NF-κB (Esteban, et al. 2004), and has been directly involved in the development of tubular injury and tubulointerstitial fibrosis (Ishidoya, et al. 1995, Kaneto, et al. 1994).

TNF-α upregulation by M1 macrophages is also observed and associated with tubular cell death (Misseri, et al. 2005) and NF-κB activation (Meldrum, et al. 2006). NF-κB activation, in turn, promotes macrophage infiltration and upregulates the expression of cytokines and growth factors (Sanz et al., 2010), with TGF-β as the most important factor upregulated in this system (Kaneto, Morrissey and Klahr 1993, Scarpellini, et al. 2014).

TGF-β favours both tubular epithelial cell death and EMT / EndMT, leading to myofibroblast proliferation and fibrosis through Smad3 activation (Sato, et al. 2003, Inazaki, et al. 2004, Ucero, et al. 2014, Chevalier, Forbes and Thornhill 2009).

Tubular cell death is already observed 24 h post-UUO, and involves both apoptotic and necrotic pathways (Ucero, et al. 2014). Tubular dilatation with loss of parenchymal structure is largely evident two weeks post-UUO, sometimes preceded by G2/M cell cycle arrest with abnormal deposition of extracellular matrix (Yang, et al. 2010).

Substantial interstitial fibroblast proliferation and differentiation/activation of interstitial fibroblasts is already evident few days post-surgery (Eddy, et al. 2012, Matsuo, et al. 2005), with expression of myofibroblast markers by day three post-UUO. Subsequently, the tubules undergo a process of dilatation, with deposition of ECM and expansion of the interstitial space, and atrophy, with apoptotic flattened epithelial cells and exposed remnant tubular basement membrane (TBM) where the epithelial cells are lost. Blood vessels might look widened as well, as endothelial cells undergo apoptosis and transformation, with consequent capillary loss and ischemia/hypoxia in the organ.

The presence of glomerular injury and glomerulosclerosis upon UUO remains controversial: having been always regarded as a tubulointerstitial model, an effect on the glomerulus has been generally unheeded. However, in some works, development of proteinuria suggests a secondary glomerular injury, contributing to the outcome of disease (Tapmeier, et al. 2008, Chevalier, Forbes and Thornhill 2009). An effect in the glomeruli is sometimes absent or less evident, mostly characterized by thickening of Bowman's capsule and reduction in the glomerular size, that happens after tubular fibrosis is established and the disease approaches end-stage (around three weeks post-surgery) (Scarpellini, et al. 2014).

In conclusion, the UUO model is a highly reproducible model leading to tubular injury and extended fibrosis in a relatively short period. Early apoptotic and fibrotic response can be already observed at three days post-UUO, including large fibroblast proliferation and activation and a significant increase in collagen expression. By day seven, a significant loss of tubular integrity and accumulation of deposited extracellular collagen are observable (early-CKD) and an established fibrosis with parenchymal damage is present at two weeks post-UUO (late-CKD) (Eddy, et al. 2012, Shweke, et al. 2008). At 21 days, an established kidney fibrosis and parenchymal loss, comparable to the last stages of CKD, can be observed (Scarpellini, et al. 2014, Zhao, et al. 2015a).

Upon histological observation, UUO kidneys are generally characterised by a large interstitial space rich of matrix, with detection of fibroblasts/myofibroblasts and inflammatory cells. Epithelial cells undergoing atrophy usually look flattened or disappear showing the TBM. Also the blood vessels are widened, while the glomeruli are less affected by the process. Only when the disease reaches its end-stages, a glomerular loss and reduction in size, with podocyte death and exposed glomerular basement membrane (GBM) might be observed (Ucero, et al. 2014, Scarpellini, et al. 2014).

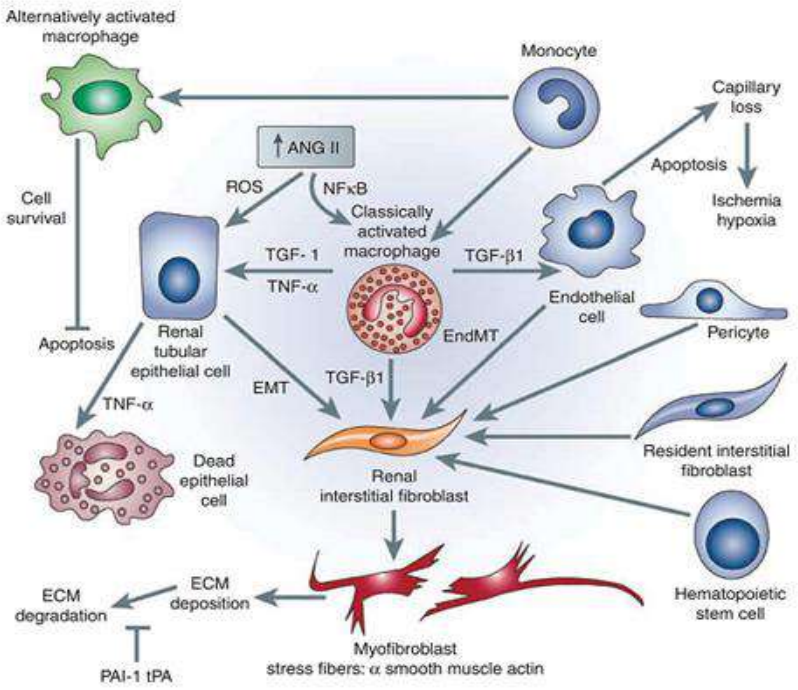

Figure 3.1: Cellular response to unilateral ureteric obstruction (UUO) leading to tubulointerstitial fibrosis and tubular injury. Activation of interstitial macrophages with cytokine release and induction of the renin-angiotensin system (RAS), with AngII production, are key elements in the development of interstitial fibrosis and renal failure upon UUO. The figure represents the main cellular responses to inflammation and AngII rise leading to both epithelial and endothelial cell loss and interstitial fibroblast recruitment, proliferation and activation. Epithelial and endothelial cell transition (EMT and EndMT) contribute to myofibroblast proliferation. Increased deposition of ECM by activated fibroblasts leads to accumulation of sclerotic tissue. Proteases inhibitors and activators such as plasminogen activator (tPA) and plasminogen activator inhibitor (PAI) are involved in the control of matrix degradation. Picture obtained from (Chevalier, Forbes and Thornhill 2009). Permission to reproduce this picture has been granted by Elsevier.

3.2.2 Proteomic studies of CKD employing mass spectrometry (MS)

Despite a large number of studies have aimed to analyse kidney fibrosis progression and identify early or late biomarkers of disease, few works have been published employing a non-hypothesis driven proteomic approach, by mass spectrometric (MS) analysis of kidney tissue or urine (Klein, et al. 2011). In this section, some representative MS analyses of CKD models will be presented, with particular focus on the most recent proteomic studies of the UUO model (**Table 3.1**).

In 2008, a study aimed to determine possible urinary biomarkers of glomerulosclerosis was performed on patients with different diseases targeting the glomerulus (diabetic nephropathy or DN, focal and segmental glomerulosclerosis or FSGS, *lupus nephritis*, membranous nephropathy) (Varghese, et al. 2007). 2-D gel electrophoresis (2-DE) followed by protein spot quantification, and statistical analysis employing the artificial neural network (ANN) algorithm, led to the individuation of 21 possible spots as predictor biomarkers of glomerular diseases, that were identified by MS using either matrix-assisted laser desorption/ionization (MALDI) – time of flight (TOF) tandem MS (MS/MS) approach or linear ion trap quadrupole (LTQ) MS. Most of these proteins were plasma proteins, possibly due to blood leakage into the urine, such as α-1 antitrypsin, transferrin, albumin, and α-1 microglobulin (Varghese, et al. 2007).

In 2009, a proteomic study performed on whole kidney lysates of streptozotocin (STZ)-treated diabetic rats, employing isobaric tag for relative and absolute quantitation (i-TRAQ™) labelling and liquid chromatography tandem ms (LC-MS/MS), identified 330 proteins in diabetic kidneys, of which 88 were significantly altered by DN (Gong, et al. 2009). importantly, a number of proteins associated with redox regulation were either upregulated or downregulated by the disease in this model, including subtypes of glutathione s-transferase and glutathione peroxidase. Basement membrane (BM)-associated proteins such as collagen VI and the hspg perlecan were upregulated by the disease, as well as the cytoskeletal protein actinin. Proteins involved in apoptosis were also identified, such as clusterin and voltage dependent anion selective channel 1 (Gong, et al. 2009).

In 2010, Cummings and colleagues performed a MS analysis to define mediators of tubulointerstitial fibrosis and tubular damage in DN, employing a transgenic OVE26 mice model of type 1 diabetes (Cummins, et al. 2010), a model of progressive DN showing TGF-β -mediated tubulointerstitial fibrosis (Powell, et al. 2009). 2-DE followed by an LC-MS/MS analysis of tubule extracts from kidneys with pro-fibrotic / fibrotic phenotypes led the group to the identification of 476 proteins differentially expressed upon fibrosis. The main finding of this study was the identification of TGF-β -related proteins among the differentially expressed candidates, such as β-catenin (downregulated) and glycogen synthase kinase 3 (GSK3)-β,

together with TGF-β upregulation itself. Grb2-related adaptor protein (GRAP) was upregulated upon disease in the tubules and identified for the first time as a member of the TGF-β signalling pathway by an *in vitro* validation (Cummins, et al. 2010). A number of proteins associated with metabolism and oxidative stress were also highlighted by this study (Cummins, et al. 2010). Interestingly, the redox protein thioredoxin (TXN) was also upregulated in kidney in these diabetic mice (Cummins, et al. 2010).

On a similar model, few years before, another group identified 41 proteins differentially expressed in diabetic disease by 2-D gel and MS on whole kidney tissues (Thongboonkerd, et al. 2004). Among these proteins, they highlighted a downregulation of elastase IIIB and an upregulation of monocyte/neutrophil elastase inhibitor, suggesting an increase in elastin deposition in the kidney (Thongboonkerd, et al. 2004). Subsequent biochemical analysis indeed confirmed the alterations in the renal elastin-elastase system in type 1 diabetic nephropathy (Thongboonkerd, et al. 2004). Other interesting findings were the upregulation of proteins associated with myofibroblast activation (vimentin, tropomyosin, myosin, etc.) and protease inhibitors (antithrombin-IIIb, serine protease inhibitor EIA or serpin, etc.), as well as the identification of complement proteins (inflammatory response) and calcium binding proteins such as calmodulin and calbindin (Thongboonkerd, et al. 2004).

In a study employing the rat SNx model of CKD, in 2005, Xu and colleagues performed MS on isolated glomerular tissue collected by laser capture microdissection (LCM) (Xu, et al. 2005). MALDI-MS led to the detection of 1473 distinct protein peaks, of which 251 were identified as significantly differentially expressed protein compared to the controls. Among these proteins, thymosin-β4 was identified as the main protein marker of sclerosis, with a proposed direct involvement in the fibrotic process (Xu, et al. 2005).

3.2.2.1 Mass spectrometric studies of the UUO model

Few proteomic studies employing MS have been performed in the UUO model in recent years and, as far as we are concerned, none of these works has been performed employing the highly sensitive and quantitative SWATH data acquisition approach employed in this Thesis (**Table 3.1**).

In 2015, Yuan et al. published a study in Scientific Reports (Yuan, et al. 2015) with the aim of identifying specific urinary biomarkers of obstructive nephropathy. In their study, they employed male Sprague-Dawley rats in which UUO was performed in the left kidney, and Sham operated rats that were used as controls. The expression of proteins was analysed by MS at one week and three weeks post-surgery on three randomly selected male rats per treatment and exclusively on urinary proteins, obtained by acetone precipitation of cleared urine, collected at the abovementioned time-points from the residual left ureter. Data were collected by LC-MS/MS using a shotgun approach on a Triple TOF 5600 mass spectrometer (SCIEX). To

determine which proteins were significantly altered by UUO, fold change analysis on spectral counts was performed, and proteins with a p-value ≤ 0.05 and at least 2-fold change from the control were regarded as significantly altered by UUO. They identified 7 proteins significantly increased by UUO after one week and 19 significantly overexpressed at three weeks, compared to the sham operated control. Only two proteins were found upregulated both after one week and three weeks. They considered the proteins upregulated at one week as possible biomarkers of renal tubular injury, while the ones overexpressed at three weeks, when the development of CKD has already reached a high grade of severity, were considered as markers of UUO-induced renal interstitial fibrosis. Among these proteins, the main urine biomarkers highlighted by the study were vimentin, α-actinin-1, moesin, annexin a1 and clusterin, all correlated with the progression of disease. Vimentin is a marker of EMT and mesenchymal cell activation. α-actinin-1 has been described as a marker of a series of nephropathies and is an element of the glomerular filtration barrier (Renaudineau, et al. 2007). Moesin is a cytoskeletal protein recently associated with CKD (Chen, et al. 2014), while annexin A1 is involved in inflammatory processes as well as in apoptosis. Clusterin has been associated with both acute kidney injury and aging of the organ (Fuchs and Hewitt 2011, Trougakos and Gonos 2006).

In the same year, Zhao and colleagues published a study on the International Journal of Clinical Experimental Pathology (Zhao, et al. 2015b). Also this study was performed in Sprague-Dawley rats, of both sexes in this case, but the rats were subjected to UUO of left kidney for a shorter time (12, 24 and 72 h)(Sham operation as control) and MS was performed on whole kidney tissue rather than urine. Total lysates of six left kidneys/treatment were pooled together and separated by 2-D gels in three replicas, and relative volume of spots (% of total volume) was quantified by 2-D gel analysis software. The spots with a significant ($p \leq 0.05$) alteration in size of at least 1.5-fold were analysed by MALDI-TOF/TOF MS and, as a result, 39 proteins were identified as significantly differentially expressed upon UUO, of which some were individuated as underexpressed and some as overexpressed. The proteins identified were associated with cytoskeletal regulation, signalling, apoptosis etc. However, a number of proteins associated with mitochondrial energy production and glucose metabolism were recognised, which are typical of a healthy living and proliferating cell.

The main result of this paper was the identification of a number of antioxidant proteins, such as glutathione S-transferase, glutathione peroxidase, peroxiredoxin and aldose reductases, upregulated at the earlier time points (12 and 24 h). The authors explained this as the effect of an immediate oxidative stress due to a reduction in blood/oxygen supply (hypoxia or ischemia), which leads to release of ROS. This antioxidative response of the cell appeared to happen early after obstruction. On the contrary, no sign of upregulation of antioxidant proteins was identified at 72 h post-UUO, and even a downregulation of glutathione S-transferase and peroxidase was reported at this time-point.

Table 3.1: Some representative proteomic studies of CKD employing MS, with number (nº diff) of differentially expressed proteins detected upon disease.

Reference	Animal and Treatment	Sample	N (samples)	Technique	nº diff	Main findings
Varghese et al., 2007	Human, patients with Either diabetic nephropathy, FSGS, lupus nephritis, membranous nephropathy and proteinuria >3 g/d	Urine	32	2-DE + MALDI-TOF MS/MS or 2-DE+ LTQ linear ion trap MS a	**20**	*Plasma proteins in urine*
Gong et al., 2009	Mice, STZ-Treated	Tissue	4/group	iTRAQ™ labelling + LC-MS/MS	**88**	*Redox regulation, Apoptosis, ECM proteins*
Thongboonkerd et al., 2004	Mice, OVE26 type 1 diabetic (Diabetic nephropathy)	Tissue	5/group	2-DE + MALDI-TOF	**41**	*Elastin accumulation, Myofibroblast actovation, chaperone proteins*
Cummins et al., 2010	Mice, OVE26 type 1 diabetic (Diabetic nephropathy)	Tissue (Tubules)	2/group	2-DE + LC-MS/MS	**476**	*TGF-β signalling pathway*
Xu et al., 2005	Rat, SNx 12 weeks	Tissue (Glomeruli)	6 Rats 30-50 glomeruli/group	MALDI-MS	**251**	*Thymosin β4*
Yuan et al., 2015	Rats, UUO 1 week and 3 weeks	Urine	3/group	LC-MS/MS	**23**	*Vimentin, Alpha-actinin-1, Moesin, Annexin A1 and Clusterin*
Zhao et al., 2015	Rats, UUO 12, 24 and 72 hours	Tissue	3/group	2-DE+ MALDI-TOF/TOF	**39**	*Antioxidant proteins (Glutathione S-transferase, Glutathione peroxidase, Peroxiredoxin and Aldose reductases) upregulated at the earlier time points*

2-DE: 2-dimension gel electrophoresis; MS: Mass spectrometry; MS/MS: Tandem mass spectrometry; LC: Liquid chromatography; iTRAQ™: Isobaric Tag for Relative and Absolute Quantitation; MALDI: Matrix-Assisted Laser Desorption/Ionization; TOF: Time of Flight

3.3 EXPERIMENTAL PROCEDURES

3.3.1 Experimental model

3.3.1.1 TG2-null (TG2-KO) mice and wild type (WT) inbred C57BL/6J mice

In this study both TG2-null (TG2-KO) mice and wild type (WT) inbred C57BL/6J mice were employed. TG2-null mice were obtained with an homologous recombination approach as reported by De Laurenzi and Melino in 2001 (De Laurenzi and Melino 2001). This approach is based on the employment of a targeting pPNT plasmid with neomycin (Geneticin) resistance that deletes a portion of exon 5, exon 6, all intron 5 and the beginning of intron 6 of *Tgm2* sequence (**Fig. 3.2**). In order to produce TG2-null mice, the linearized vector needs to be inserted into embryonic stem cells, that are then selected with neomycin and ganciclovir. Positive clones are injected into C57BL/6J blastocysts and then transferred into pseudo-pregnant females (De Laurenzi and Melino 2001). Mice were obtained from Prof. Gerry Melino, they were backcrossed at least six times with WT mice at the Nottingham Trent University (NTU) animal house by licenced technicians, then genotyped in house by Dr Alessandra Scarpellini. All experimental procedures were carried out under licence in accordance with regulations laid down by Her Majesty's Government, UK (animals scientific procedures act ASPA, 1986), and were approved by NTU ethical review committee (ASPA ethical review process).

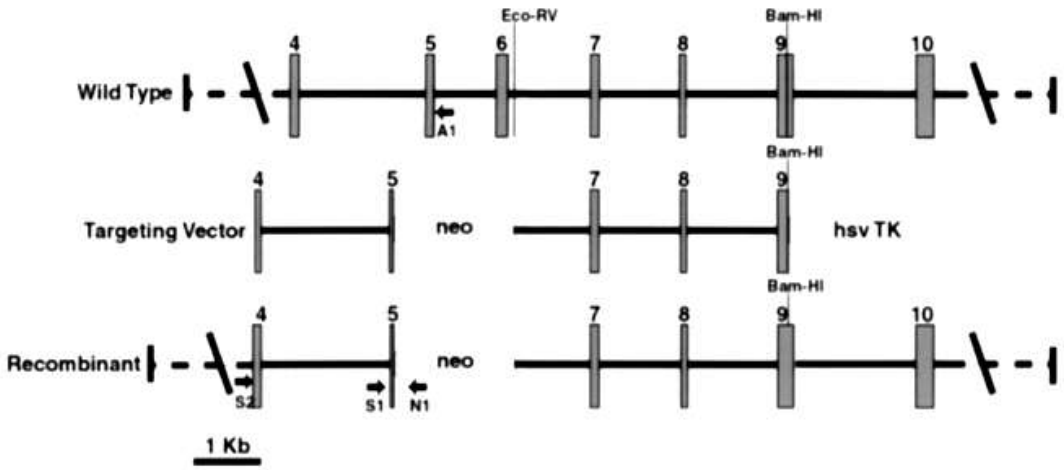

Figure 3.2: Obtainment of TG2-null mice using an homologous recombination approach. The figure, obtained from De Lurenzi and Melino (De Laurenzi and Melino 2001), shows how TGM2 sequence appears in WT mice (wild type) and in TG2-null mice (recombinant), where a part of the sequence, namely all intron 5 and exon 6 and a portion of exon 5 and intron 6, has been deleted. The targeting vector necessary for recombination is shown as well. Permission to reproduce this picture has been granted by The American Society for Microbiology.

3.3.1.2 Execution of unilateral ureteric obstruction (UUO) on WT and TG2-KO mice

Experimental UUO was performed on both strains as described by Vielhauer et al. (Vielhauer, et al. 2001). The procedure was carried out at University of Sheffield (UK) by alicenced technician (Dr Linghong Huang). Mice were anaesthetized with 5% (v/v) fluorothane and the anaesthesia was maintained with 2% (v/v) fluorothane during the surgical process, the left ureter of the mice was obstructed using a ligating clip (Hemoclip Plus, Weck Closure Systems), while the muscle wall was sealed with single cross-over stitching using dissolvable stitches. ADEPT® adhesion reduction solution [4%(w/v) icodextrin] (Baxter Healthcare, Illinois, USA) was dispensed in the peritoneum in order to prevent post-surgical adhesions prior to closing. After the procedure, buprenorphine, an opioid-derivate, was administered to the mice at 10 mg/kg for 40 h for pain-relief. The animals were allowed to eat and drink without restrictions. Mice were sacrificed and kidneys harvested 21 days post-operation. Kidneys were snap-frozen and stored in liquid nitrogen until needed. When needed, left kidneys were removed from liquid nitrogen and employed for the different experiments as described in 3.3.1.3.

All experimental procedures were carried out under licence in accordance with regulations laid down by Her Majesty's Government, UK (animals scientific procedures act ASPA, 1986), and were approved by the University of Sheffield animal ethical review committee (ASPA ethical review process).

3.3.1.3 Numerical dimension of the study

For the aims of this thesis, a total of 32 WT and 32 TG2-KO inbred C57BL/6J mice were employed. Half of these mice (16 WT and 16 TG2-KO) were subjected to UUO and the remaining to a Sham operation for 21 days. Samples were distributed as follows in the different experiments (**Fig. 3.3**):

1. **Validation of the UUO model**: 6 WT Sham operated kidneys (3 females and 3 males), 6 WT UUO kidneys (3 females and 3 males), 6 TG2-KO Sham operated kidneys (3 females and 3 males) and 6 TG2-KO UUO kidneys (3 females and 3 males), all randomly selected, were employed for the validation of the UUO model. Specifically:
    a. One WT female Sham operated kidney quarter, one WT female UUO kidney quarter, one TG2-KO female Sham operated kidney quarter and one TG2-KO female UUO kidney quarter were paraffin embedded, sectioned and stained for histological analysis as described in 3.3.2.
    b. Six WT Sham operated kidney quarters (three females and three males), six WT UUO kidney quarters (three females and three males), six TG2-KO Sham operated kidney quarters (three females and three males) and six TG2-KO UUO kidney

quarters (three females and three males) were homogenized and employed for Western blotting as described in 3.3.3.

c. Three WT Male Sham operated kidney quarters, three WT Male Sham operated kidney quarters, three TG2-KO Male Sham operated kidney quarters and three TG2-KO Male UUO kidney quarters were homogenized and tested for TGF-β1 activity as described in 3.3.4.

2. **Proteomic analysis of the UUO model**: Halves from four WT Sham operated kidneys (three females and one male), four WT UUO kidneys (three females and one male), four TG2-KO Sham operated kidneys (three females and one male) and four WT TG2-KO kidneys (three females and one male) were employed for the SWATH-MS proteomic analysis of the UUO model on total kidney lysate described in paragraphs 3.3.5 and 3.3.6, in order to have 4 biological replicas to compare for each group.
3. **TG2-interactome in the UUO model** (described in Chapter IV): for this study, only male mice were employed to reduce gender/hormonal bias. A total 12 WT Sham operated kidneys, 12 WT UUO kidneys, 12 TG2-KO Sham operated kidneys (necessary as Sham operated background for the analysis) and 12 TG2-KO UUO kidneys (necessary as UUO-background for the analysis) were homogenized, fractionated, pooled in pairs and TG2-immunoprecipitated (TG2-IP) as described in the next chapter. SWATH acquisition-MS proteomic analysis was then performed on 5 TG2-IP samples while the sixth ones of each group were combined and used for the production of the spectral library.

As this was the first time a proteomic study was performed on the UUO model of kidney fibrosis employing the highly sensitive SWATH-data independent acquisition approach, no data were available to perform a power calculation prior to the experiments, in order to determine the minimal number of required biological replicas. For this reason, an arbitrary number of kidneys was chosen for each MS experiment basing on the advice of the NTU proteomic group of John Van Geest Cancer Research Centre and the limited number of kidneys available. Power calculation was performed *a posteriori* to confirm the adequacy of the employed sample size as described in 3.3.9.

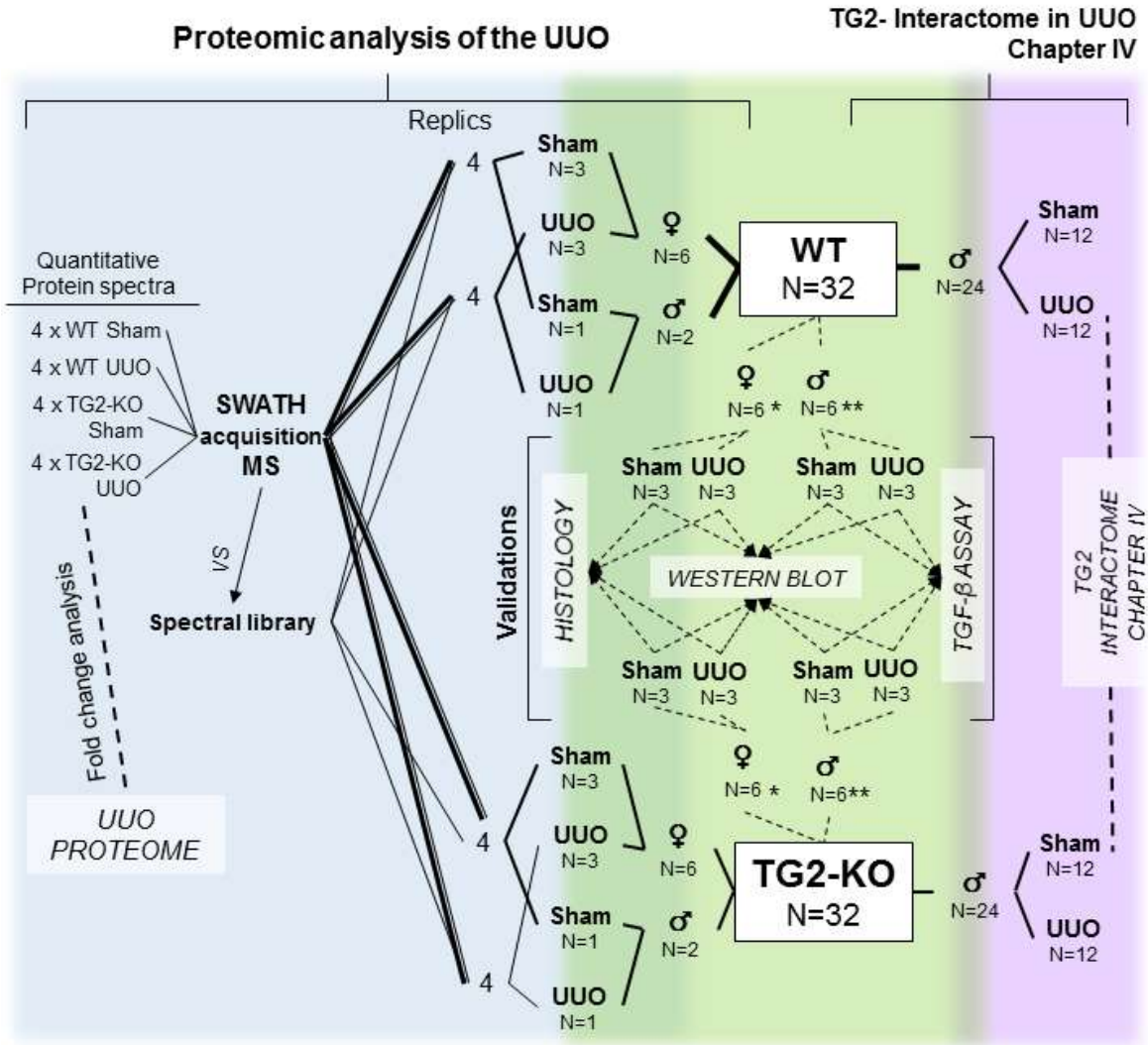

Figure 3.3: Distribution of kidney samples in the different experiment performed. Graphical representation of distribution of the 32 WT kidneys (16 Sham-operated and 16 UUO, 21 days) and the 32 TG2-null kidneys (16 Sham-operated and 16 UUO, 21 days) in the SWATH - MS experiments described in Chapter III (UUO-Proteome) and IV (TG2-interactome in UUO) as well as in the validation histological and biochemical experiments described in Chapter III. In the validation experiments, portions from the same kidneys used in the SWATH acquisition-MS experiments were employed. Legend:* = quarters of the same kidneys used for the SWATH proteomic analysis of UUO (3 females). ** = a quarter from the same kidney used for the SWATH proteomic analysis of UUO (1 male) was employed while the other 2 kidney replicas were portions of kidneys used for the SWATH TG2-interactome study of Chapter IV.

3.3.2 Haematoxylin and eosin (H&E) staining and Masson's trichrome (MT) staining

Haematoxylin and eosin (H&E) staining is one of the main type of staining employed in histology, allowing a general detection of tissue morphology. Haematoxylin is a blue/purple natural stain derived from the Logwood tree wood. In its original form, haematoxylin has a low staining capacity, hence it is usually oxidised to haematein and combined with aluminium, used as a mordant for the dye, to form haemalum. Most haematoxylin stainings [Mayer (Mayer 1891), Ehrlich's (Ehrlich 1886), Harris (Harris 1900), Gill's (Gill, Frost and Miller 1974) etc.], are based on the formation of this metal-dye complex. In other cases, such as Weigert's haematoxylin (Weigert 1904), the metal employed is iron; these are used when the subsequent stains are acidic. Haematoxylin binds acidic and negatively charged compounds such as DNA and RNA (basophils), that will be stained in blue/purple. Other basophil compounds in the cells will have a purple-red colour. Eosin is a synthetic pink/red staining derived from fluorescein. It is an acidic compound that binds to basic and cationic complexes such as positively charged aminoacidic chains (eosinophiles); for this reason, it mainly stains cytoplasm and extracellular compounds: cytoplasm and muscular fibres are stained in red or dark red, while collagen and mitochondria will have a pink colour.

Masson's trichrome (MT) staining is a three-colour staining procedure and it is one of the most common stainings employed for the detection of organ fibrosis. This staining allows to detect simultaneously nuclei, cytoplasm and collagen/bone and determine the accumulation of the last over the others. It is based on three different stainings: first, the abovementioned Weigert's iron haematoxylin (Weigert 1904), that stains the nuclei in brown/dark blue, a second solution, containing acid fuchsin and xylidine Ponceau, is used to stain the cytoplasm in pink, and finally a third staining, that can be green or blue, will stain the fibrillar collagen.

H&E staining and MT staining were performed on paraffin-embedded kidney sections. Normally, kidneys, or kidney portions, should be fixed in formalin from fresh, as soon as they are extracted from the mice. This is because a freezing-thawing process might introduce ruptures in the kidney tissue that will affect the integrity of the final section. In this case, unfortunately, not having freshly extracted kidneys, we had to employ frozen samples (kidney quarters) stored in liquid nitrogen. To make the thawing process as delicate as possible, we proceeded as follows: kidneys were removed from liquid nitrogen and directly placed in dry ice (-78.5°C) for transferring to the freezer. The organs were kept at -80°C for 1 h, then placed in dry ice (-78.5°C) and transferred at -40°C for 2 h and finally at -20°C for 2 h. Transfers from freezers were as quick as possible, and performed in ice. Kidneys were then left to thaw on ice for 45 min and in the fridge (4°C) for 30 min. Finally, they were allowed to reach room temperature on the bench for additional 30 min. Once defrosted, kidneys were fixed in 10%

formalin [4% (w/v) PFA] in PBS pH 7.4 for 36 h, at room temperature and in gentle rotation (60 rpm). After fixation, they were washed 3 times with PBS pH 7.4 and left in PBS until paraffin embedding. The day after, samples were delivered to the University of Sheffield (UK), where paraffin embedding, sectioning and staining were carried out at the Department of Infection, Immunity & Cardiovascular Disease by Dr Fiona J. Wright.

Pictures of stained kidney slides were taken by the author at NTU with an Olympus BX61 fluorescent microscope (Olympus, Japan), set on bright field acquisition, with Cell^F imaging system software (Olympus, Japan). For quantification of kidney fibrosis from MT staining, the % area of the different colours (dark blue, red/pink, light blue) was quantified on Cell^F following the manufacturer's guidelines, on at least 24 different fields per treatment, making sure to include both tubular and glomerular areas of the kidney. The "phase selection" function of the software was used to determine the areas and the level of fibrosis was measured either as a ratio of phase 2 (collagen, light blue) over phase 1 (cytoplasm, red/pink) or as a ratio of phase 2 (collagen, light blue) over phase 3 (nuclei, dark blue).

3.3.3 Immunoprobing of TG2 and the fibrosis marker α-smooth muscle actin in kidney lysates

10% (w/v) kidney homogenates were prepared in a sucrose based lysis buffer [0.32 M sucrose, 5mM Tris-HCl, 2mM EDTA, pH 7.4] containing 1:100 (v/v) protease inhibitors cocktail (P8340, Sigma). Mechanical homogenization was performed on ice using an Ultra Turrax T25 Homogenizer (Merck).

Equal amounts of proteins were resolved by 12% (w/v) acrylamide/bis-acrylamide SDS-PAGE under reducing condition. Immunodetection of the proteins of interest was performed by Western blot as described in the general methods using the antibodies reported in **Table 3.2** in blocking buffer [5% (w/v) non-fat milk in TBST pH 7.4]. Immunoreactive bands were detected by enhanced chemiluminescence (EZ-Chemiluminescence Detection Kit for HRP, Geneflow) after incubation with an appropriate HRP-conjugated secondary antibody (**Table 3.2**) in blocking buffer as described in the general methods. Image acquisition was performed with a LAS4000 imaging system (GE Heathcare) and comparison of protein band intensity was obtained by Aida Image Analyzer v.4.03 (Raytest, Germany), following the manufacturer's instructions.

Table 3.2: List of antibodies employed on whole kidney lysates to validate the UUO model on WT and TG2-null mice. The table shows the details of primary and secondary antibodies employed for Western blot immunodetection on whole kidney lysates. Details of dilution used in blocking buffer [5% (w/v) non-fat milk in TBST pH 7.4] are reported in the table.

Primary antibodies	Company	Dilution
Mouse monoclonal anti-transglutaminase-2 (TG2) (IA12)	University of Sheffield (UK)	1: 5000
Mouse monoclonal anti-alpha-smooth muscle actin (α-SMA) [1A4] (ab7817)	Abcam (UK)	1:1000
Rabbit polyclonal anti-cyclophilin-A (ab41684)	Abcam (UK)	1:1000
Rabbit polyclonal anti-β-tubulin (ab6046)	Abcam (UK)	1:2000
Secondary antibodies	**Company**	**Dilution**
Goat anti-rabbit IgG HRP-conjugated	Dako (Denmark)	1:2000
Goat anti-mouse IgG HRP-conjugated	Dako (Denmark)	1:1000

3.3.4 Detection of TGF-β1 activity in kidney homogenates by mink lung epithelial cell (MLEC) bioassay

In order to measure TGF-β1 activity of the total kidney homogenates, the mink lung epithelial cell (MLEC) bioassay (Abe, et al. 1994) was performed as described before (Scarpellini, et al. 2014, Huang, et al. 2010a). A 10% (w/v) kidney homogenate was prepared in homogenization buffer [0.25 M sucrose, 10 mM Tris-HCl, 1 mM $MgCl_2$, 2 mM EDTA, pH 7.4] containing 1:100 (v/v) protease inhibitors cocktail (P8340, Sigma). Mechanical homogenization was performed on ice using an Ultra Turrax T25 homogenizer (Merck). Each homogenate was centrifuged at 1000 g for 5 min at 4°C to remove large particulates, then the supernatant diluted 1:10 in sterile-filtered (2 μm, Sartorius Stedim) serum-free DMEM with 0.1% (w/v) BSA. 100 μl of this solution was applied to the MLEC in a 96-well plate ($5x10^4$ cells/well) and incubated for 22 h. Cells were then washed twice with PBS and lysed in 1X Reporter Lysis Buffer (Promega). 50 μl of cell lysate were mixed to an equal volume of luciferase substrate (Promega) and light emission was measured with Polarstar Optima luminometer (BMG Labtech). Total TGF-β1 was also measured by acid treatment of the kidney homogenate prior incubation with the MLEC system (Van Waarde, et al. 1997). The experiments were performed by Dr. Nina Schroeder at NTU, analysis and interpretation of results was performed by the author.

3.3.5 Sample preparation for mass spectrometry (MS) analysis in whole kidney lysates

Sham operated and UUO kidneys from both WT and TG2-KO mice (four per treatment, of both genders) were collected from the liquid nitrogen storage and quickly ground in liquid nitrogen using pestle and mortar, in sterile conditions and avoiding cross-contamination. A 10% (w/v) tissue homogenate was prepared in "proteomics lysis buffer" containing 9.5 M urea, 2%(w/v) DTT, 1% (w/v) N-Octyl-Beta-Glucopyranoside (OGP) and protease inhibitors (Sigma). Sonication (amplitude 5 μm, 5 sec, 3 times) was performed to induce mechanical breakage of the tissue. Equal amounts of total protein extracts (50 μg) were diluted in 50 mM tri-ethyl ammonium bicarbonate (TEAB) containing a final concentration of 0.02% (w/v) ProteaseMAX™ surfactant trypsin enhancer (Promega). Proteins were subjected to reduction (5 mM DTT, 56°C for 20 min) and alkylation (15 mM iodoacetamide at room temperature for 15 min), then trypsin digested overnight at 37°C using 0.02 mg/ml MS grade trypsin (Promega) and 0.01% (w/v) ProteaseMAX™ surfactant in a thermomixer. Samples were vacuum concentrated to dryness and resuspended in 20 μl of 5% (v/v) acetonitrile/0.1% (v/v) formic acid for MS analysis.

3.3.6 Mass spectrometry (MS)

3.3.6.1 Mass spectrometry (MS), library production and SWATH data independent acquisition (DIA)

The samples were analysed by reverse-phase high-performance liquid chromatography electrospray ionization tandem mass spectrometry (RP-HPLC-ESI-MS/MS) using the TripleTOF 5600+ mass spectrometer from SCIEX (Canada). The instrument is available for university staff and students at the proteomics facility lab of the John Van Geest Cancer Research Centre, NTU, and MS runs have been performed by Dr David Boocock, assisted by Clare Coveney and Dr Amanda Miles, using the samples prepared by the author.

The mass spectrometer was used in two different modalities depending on the stage of the experiment: shotgun data dependent acquisition (DDA) was employed for spectral library construction, while SWATH - data independent acquisition (DIA) [described in (Gillet, et al. 2012)] was used for the acquisition of quantitative data.

Regarding the liquid chromatography, RP-HPLC mobile phases were solvent A [2% (v/v) acetonitrile, 5% (v/v) DMSO in 0.1% (v/v) formic acid in LC/MS grade water] and solvent B [LC/MS grade acetonitrile containing 5% (v/v) DMSO and 0.1% (v/v) formic acid]. Samples were directly injected onto an YMC Triart-C18 column (25 cm, 2μm, 300 um i.d) at 5 μl/min using microflow LC system (Eksigent ekspert nano LC 425) using an increasing linear gradient

of solvent B over solvent A going from 2% to 40% in a total time of 60 min (SWATH-DIA) or 120 min (spectral library production by DDA). Regeneration and re-equilibration of the column were performed by loading 90% solvent B for 10 mins followed by 5% solvent B for 10 min. Auto calibration was performed by the MS every 4 samples using an injection of a standard of 25 pmol β-Galactosidase digest. The electrospray ionisation, then, was carried out using PicoTip® nanospray emitters uncoated SilicaTips™ (New Objective Inc., USA), with voltage set to +2400 V.

First, a spectral library was produced by DDA on a pool of all samples in high sensitivity mode. DDA mass spectrometry files were searched using ProteinPilot 5 (SCIEX, Canada): the analysis was conducted by the software with an exhaustive identification strategy, searching the UniProt Swiss-Prot database (January 2015 release) for murine species. The generated file was imported into PeakView 2.0 software (SCIEX, Canada) as an ion library and spiked in iRT retention time standards (Biognosys, Switzerland), after filtering for false discovery rate (FDR) of 1% and excluding shared peptides.

SWATH-DIA was then performed on 4 kidney extracts per phenotype and treatment (WT or TG2-KO, UUO or Sham). Data independent detection was performed using 40 variable SWATH windows: during different cycles, the initial survey scan (TOF-MS) is performed for each window (SWATH), and the following MS/MS experiment is carried on the totality of the precursors detected in the SWATH using ion collision energy [reference for the method is provided in (Gillet, et al. 2012)]. Spectral alignment and targeted data extraction from the SWATH data was performed in PeakView 2.0 using the abovementioned reference spectral library generated by DDA. SWATH data was processed using an extraction window of 5 min and applying these parameters: maximum 6 peptides/protein, maximum 6 transitions, peptide confidence of >99%, exclude shared peptides, and XIC width set at 75 ppm.

3.3.6.2 Targeted data extraction and fold change analysis

Quantitation and fold change analysis between the different phenotype/treatment combinations were carried out using the OneOmics cloud processing software from SCIEX, employing weighted average of proteins spectral results among the different biological replica to calculate fold change and relative significance. The outcome of the experiment is a list of protein identification names (IDs), with $\log_2$ of fold change (FC) values (1), absolute FC values (2), p-values of FC [p-value(FC)] and confidence level of FC [C(FC)], all calculated by the software.

$$\log_2[FC_{\,A\,vs\,B}\,(X)] = \log_2 \frac{Mean\ Intensity\ of\ protein\ X\ in\ treatment\ A}{Mean\ Intensity\ of\ protein\ X\ in\ treatment\ B}$$

$$Abs\ FC_{A\,vs\,B}(X) = 2^{|\log_2[FC_{\,A\,vs\,B}\,(X)]|}$$

Under suggestion of Dr David Boocock and the SCIEX technical assistance for the software, confidence level was chosen to be a better measurement of the significance of the fold change, over the most commonly used p-value. In fact, in the software, the C(FC) takes into account the variance among the values and the number of peptides identified per protein, while the p-value(FC), which is calculated in an unweighted manner, does not. While in the confidence level all the values are weighted by their variance (obtained by multiple linear regression, MLR), in the case of the p-values all the values are considered equally, regardless of the variance between measurements. This means that, in cases where there is a large variance between measures or the number measures are low, lower p-values might be an artefact of the high variance among the measurements and not the effect of the change itself, while in the case of confidence all the values that have low reproducibility are weighted out. As a general rule, fold changes with a C(FC) higher than the 0.80 (80%) were regarded as highly significant. Values with confidence between 0.80 (80%) and 0.5 (50%) were acceptable but less significant, and values with C(FC) lower than 0.5 should not be considered as significant. In the analyses performed in this thesis, data were regarded as significantly differentially expressed upon treatment at C(FC) higher than 0.80 (80%).

3.3.7 Bioinformatic analysis

Once a list of significant proteins was obtained, it was analysed with a series of bioinformatics approaches aimed to define the overrepresented functions, biological process and pathways for the differentially expressed proteins, and determine protein-protein interactions.

Full names of the proteins were obtained by manual search of protein IDs on UniProtKB (http://www.uniprot.org/uniprot) database.

Functional classification and functional overrepresentation analysis were performed using two different open source bioinformatics resources: DAVID (Database for Annotation, Visualization, and Integrated Discovery) bioinformatics resource 6.7 (http://david.abcc.ncifcrf.gov) (Dennis, et al. 2003) and PANTHER (Protein ANalysis THrough Evolutionary Relationships) database (http://www.pantherdb.org) (Mi, Muruganujan and Thomas 2013). In both cases, the whole *Mus musculus* genome was employed as background gene list.

3.3.7.1 Functional classification

Functional classification was performed using the Gene Ontology (GO) terms for Biological Process, Molecular Function and Cellular Component in addition to PANTHER Protein Class terms and PANTHER pathways. Gene Ontology (GO, http://geneontology.org) is a project that unifies the scientific terminology of gene product attributes / proprieties across the different

species. It provides a clear and organized vocabulary (ontology) of terms representing gene product properties. These terms are defined, standardized and associated with specific codes, so that gene products are clearly associated with a series of specific annotations depending on their functions. GO contains roughly 25,000 terms, that are species-aspecific, hence can be applied to a wide range of species both bacterial or eukaryotic. GO terms are organised in larger general groups in which are nested narrower groups of more specific terms (child terms). At the top level, GO terms are divided in three different major ontologies, describing:

- Biological Processes: multi-step complete processes performed by groups of molecules having specific function and acting together. Metabolic processes, cell organization processes, signalling events etc. are part of this group.
- Molecular Functions: differently from biological processes, are single elemental activities that are performed by a molecule. For example, catalytic activity, binding, hydrolysis, kinase activity etc. are in this group.
- Cellular components: portions of the cell or the extracellular environment in which the gene products can be detected.

GO terms associated with the proteins in the list were identified using PANTHER and were visualized in pie charts as percentage of representation of the specific GO annotation term (hits of that specific annotation term, or class) over the total number of class hits (for all the annotation terms individuated in the list of proteins.

It is important to remember that the percentage of representation is considered over the total class hits and not over the total amount of proteins: in fact, since a protein ID might fit in more than one GO annotation (class hit) or in no one, the total number of class hits is generally different from the total number of proteins.

The same analysis was performed using PANTHER Protein Class annotation terms, a set of descriptors that identify classes of proteins (for example Cytoskeletal proteins, Kinases, Transcription factors, Chaperones, Signalling molecules, etc.) and PANTHER pathways, annotation terms associated with biological pathways at the whole organism level. For both groups, the different terms/keywords have been searched and organised using PANTHER bioinformatics tool and even if they generally overlap (protein can fall in different terms) and interact, they are not nested in classes and sub-classes or pathways and sub-pathways.

3.3.7.2 Statistical overrepresentation test

Functional overrepresentation test was performed in PANTHER using the same GO terms (Biological Process, Molecular Function, Cellular Component), PANTHER Protein class and PANTHER Pathways annotations, to determine the enrichment of specific classes comparing to the same terms representation in the entire *Mus musculus* genome (Mi, et al. 2013).

The overrepresentation analysis allows, given a list of proteins uploaded by the user, to determine which annotation terms are significantly over-represented or under-represented. It is also referred as enrichment analysis.

The statistical overrepresentation test is based on the comparison of annotation terms' distribution in the user's list of proteins with the distribution of the same annotation terms in the reference list, that is usually the organism genome and should contain all the proteins in the user's list. An expected value (which represent the null hypothesis H_0) (1) and an observed value (2) are calculated for each annotation term X individuated by the user's list, as follows. Being N the total number of genes in the reference list, K the total number of genes in the user's uploaded list, n(X) the number of genes belonging to annotation term X in the reference list and k(X) the number of genes belonging to the annotation term X in the user's list, the values are calculated as:

$$(1)\ Expected\ \ value\ for\ \ X = \frac{N\ genes\ in\ the\ reference\ list\ \epsilon\ X}{tot\ N\ genes\ in\ the\ reference\ list} \cdot tot\ N\ genes\ in\ the\ user's\ list$$

$$= \frac{n(X)}{N} \cdot K$$

$$(2)\ Observed\ value\ for\ X = \ N\ genes\ in\ the\ user's\ list\ \epsilon\ X = k(X)$$

At this point the H_0 hypothesis is that the annotation term X is distributed in the same way in the User's list and in the reference list, hence $\frac{Observed\ value\ for\ X}{Expected\ value\ for\ X} = 1$.

If $\frac{Observed\ value\ for\ X}{Expected\ value\ for\ X} > 1$ there is an overrepresentation, or enrichment, if $\frac{Observed\ value\ for\ X}{Expected\ value\ for\ X} < 1$ there is an underrepresentation.

The statistical method used to calculate if this change is significant is called binomial test.

The null hypothesis H_0 (3) of this test is that the annotation term is distributed equally in the reference and in the User's list, hence probability P(X) of finding a gene from the annotation term X in the User's list is the same probability of finding the annotation term in the Reference list.

$$(3)\ H_0: P(X) = \frac{N\ genes\ in\ the\ reference\ list\ \epsilon\ X}{tot\ N\ genes\ in\ the\ reference\ list} = \frac{n(x)}{N}$$

Knowing the hypothesis, the p-value (p) of the difference is calculated using this formula for a binomial distribution (4).

$$(4)\ p = \sum \binom{K}{k(x)} P(X)^{k(X)} \left(1 - P(X)\right)^{K-k(X)}$$

In this thesis, a p-value lower than 0.05 was regarded as significant.

To confirm the findings obtained with PANTHER, ranking of significantly enriched functions, with fold change enrichment and relative p-value, was also obtained on DAVID bioinformatic

tool by statistical overrepresentation analysis, selecting the GO terms for Biological Process (GOTERM_BP_FAT), Molecular Function (GOTERM_MF_FAT) and Cellular Component (GOTERM_CC_FAT). Again, a p-value lower than 0.05 was considered significant.

Pathway overrepresentation analysis was performed as well in DAVID comparing the representation of the different Kyoto Encyclopaedia of Genes and Genomes (KEGG, http://www.genome.jp/kegg) terms (KEGG_PATHWAY) in the user's list to the expected pathway representation in mice. This analysis was coupled to the statistical overrepresentation analysis performed with PANTHER using the PANTHER Pathway keywords.

3.3.7.3 Investigation of protein interactions using STRING

In order to identify clusters and networks of interacting proteins, known and reported protein-protein interactions in the list of candidates were analysed using STRING (Search Tool for the Retrieval of Interacting Genes/Proteins) v10 database (http://string-db.org) (Szklarczyk, et al. 2015), that contains both known and predicted and both direct and indirect protein interactions. The network was produced by using confidence level greater than 0.4 (mild confidence, set by default by the software) and by removing all the unconnected proteins. The network was exported, and re-organized using the open source software Cytoscape v. 3.0.2 (http://www.cytoscape.org).

3.3.8 Statistical residual analysis in the protein spectral data obtained by SWATH-MS acquisition.

3.3.8.1 Linear regression

In statistics, a linear regression analysis is an analysis performed to identify the relationship between a dependent variable y and an independent, or explanatory, variable x, and, secondly, to infer how strongly dependent variable y can be predicted from an independent variable x. Given a series of n paired x and y numerical data, represented by points in the cartesian plane, the linear regression analysis individuates the best-fitting straight line through the points, called regression line (1). This line gives the predicted value y' for a given independent variable x.

$$t: y' = f(x) \qquad t: y' = mx + q$$

The vertical distance between the point $P_i(x_i; y_i)$ and t is the error from the predicted value and is called residual (2). The regression line is defined as the line that minimizes the mean of the squared residuals (3).

$$residual = y - y'$$

$$average\ residuals = {\sum_{i=1}^{n}(y_i - y'_i)^2}/{n}$$

The coefficient of correlation r is a key descriptor of the strength of the linear correlation between x and y and is defined as the mean of the product of standardized values for x and y (4, 5). The coefficient of correlation r is a value that goes from -1 to 1.

$$standardized\ x_i = x_i^* = \frac{x_i - average(x)}{sd(x)} \qquad standardized\ y_i = y_i^* = \frac{y_i - average(y)}{sd(y)}$$

$$correation\ coefficient\ r = {\sum_{i=1}^{n}(x_i^* \cdot y_i^*)}/{n}$$

In normal linear model, the square root of r (called R^2 or R-squared) is the fraction of variance explained (variance of the population-error variance). The higher is the value, the higher is the dependency of y from x.

3.3.8.2 Analysis of residuals

The analysis of residuals can be used to determine how significant is the difference of given y from its predicted value y'. For this reason, for the aims of this study, it can be used an alternative method, different from the fold change analysis, to determine which proteins are significantly altered in the UUO model compared to the Sham.

To achieve this purpose, the protein intensity data obtained by quantitation with the abovementioned OneOmics cloud processing software (SCIEX) were first normalized within each sample dataset in order to be comparable among samples. For the aims of this thesis, UUO values for a given protein were considered as dependent variables (y) and Sham operated values for the same protein as the independent variables (x). Regression plots were produced in excel for each pair of samples (UUO-1 vs Sham-1, … , UUO-4 vs Sham-1, UUO-1 vs Sham-2, … , UUO-4 vs Sham-2, … , UUO-4 vs Sham-4; a total of 16 pairs) and standardized residuals plots (difference between standardized y and standardized y', calculated for each protein) were obtained as well for each samples. The mean standardized residual of every protein was calculated by averaging the standard residuals of all 16 pairs of samples for each protein in the list (6).

$$Mean\ standard\ residual\ (protein\ X) = {\sum_{i=1}^{16}(y_{X,i}^* - y'^*_{X,i})^2}/{16}$$

The distribution of residuals in the group of proteins approximates a normal standard Gaussian distribution ($m = 0;\ \sigma = 1$). The more distant the mean standard residuals are from m=0 the more significant will be the difference from the predicted values. Because of the proprieties of

the normal standard distribution, a value of higher than 1.96 or lower than -1.96 means a p-value of approximately 0.05 (it is exactly 0.05 if we have $n \to \infty$ number of samples).
The absolutes of the mean residuals can be plotted on a normal standard distribution in Office Excel (NORM.S.DIST function) to infer probability values (p-values).
For this specific study on protein expression, the outcome of the residual analysis can be interpreted in this way: positive mean of residuals indicates that the protein is overexpressed in UUO (dependent variable y) compared to its predicted value, negative mean of residuals implies that the protein is underexpressed in UUO compared to its predicted value, p-value lower than 0.05 means that this difference is significant.

3.3.9 Power analysis

In statistics, the power of an experiment is the ability of the experiment to detect an effect if it exists and it is defined as the probability that the experiment to rejects H_0 (null hypothesis, no effect) if H_1 (alternative hypothesis, effect) is true.
The power is equal to $1 - \beta$, where β is the probability of type II error, a false negative, that means the probability to accept H_0 (null hypothesis, no effect) even if H_1 is true. The higher is the power of the experiment, the higher will be the ability of that particular experimental design to properly detect the effect the researcher is investigating, if that effect exists, and consequentially, the lower will be the rate of false negatives.
The power calculation, or power analysis, is a test usually performed during the experimental design, to determine *a priori* the minimum sample size necessary to have a trustable result, before sacrificing any sample. The power analysis is based on these six variables:

- The effect size of the biological process
- The standard deviation
- The significance level (usually α = 0.05)
- The desired power of the experiment, usually between 95 and 80%
- The sample size
- The alternative hypothesis (one-sided test vs two-sided test)

Knowing this, the test is employed to calculate the minimum sample size knowing all the other variables and the desired power of the experiment. This kind of test is performed *a priori*, and the necessary information are obtained from previous studies on the same biological effect (literature). A series of statistical software and on-line tools allow to perform the power analysis automatically, by introducing some key statistical descriptors obtained by previous literature, mainly standard deviations, means and correlations, the significance level (usually α = 0.05) and the desired power of the experiment, which is usually higher than 80%. Knowing

these values *a priori*, the outcome of the test is the minimal number of samples necessary to get the desired power.

Unfortunately, in some cases, no previous data are available for carrying out an *a priori* power calculation before sacrificing any sample. This is the case of the SWATH-MS proteomic study on UUO performed in this thesis, because no proteomic studies have been performed before in this model with such a sensitive system. In addition to this, when working with large spectral datasets, information such as standard deviations are difficult to obtain from literature, or even to analyse all together, as to every single protein detected is associated with its own standard deviation among the different experimental replica, and the total number of proteins detected by SWATH-DIA can easily reach thousands. In these cases, a pilot study must be performed with an arbitrary number of individuals, and the power calculation has to be performed *a posteriori* using the outcome of this study, to determine if it allows a sufficient power, knowing the statistical variables obtained from the study itself (standard deviation, means, correlation between treated and untreated response, etc.…), or whether more individuals are necessary.

The SWATH-MS experiment performed in this chapter on four independent kidneys/treatment can be considered as a pilot study performed by arbitrarily choosing the sample size. After the list of significantly overexpressed/underexpressed proteins was obtained in the study, a power analysis was performed on series of candidates, to determine the power of the experiment and decide whether the number of samples were enough for the study to be statistically acceptable. The power calculation was performed using the Dell Statistica software (Dell, Texas, USA) and asking the software to compare two different means (UUO or Sham) of dependent samples by T-test.

3.4 RESULTS

3.4.1 Validation of kidney fibrosis in the UUO model by histological analysis

As described above in this chapter, UUO leads to a rapid development of tubulointerstitial fibrosis, with enlarged and atrophied tubules, exposed basement membrane and accumulation of extracellular matrix in the interstitium. Given the rapidity of the process, clear differences should be seen by histological stainings of kidney sections between Sham Operated and UUO kidneys at 21 days post-operation, comparable to advanced-to-end stage level of kidney disease.

To observe morphological changes and fibrotic tissue accumulation between healthy and fibrotic kidneys in C57BL/6J mice subjected to 21 days UUO, both H&E staining and MT staining were performed. In 2014, our group already demonstrated the development of fibrosis on a similar model of UUO performed for 21 days on the same mice strain, by MT staining as well as collagen staining, and results are published (Scarpellini, et al. 2014). For this reason, this analysis has merely validating purposes, aimed to provide a confirmation of a developed fibrosis in our samples.

3.4.1.1 Haematoxylin and eosin (H&E) staining of UUO and Sham-operated kidney sections

In order to qualitatively observe differences in kidney morphology upon UUO, H&E staining of paraffin embedded sections was performed and pictures were obtained as described in 3.3.2. In order to cover as much renal parenchyma as possible, pictures were taken both on the renal cortex and on the renal medulla. The staining highlighted a neat alteration in the organ morphology upon 21 days UUO (**Fig. 3.4**).

In Sham operated kidneys (21 days), histology of the organ appeared healthy in both its glomerular and tubular portion (**Fig. 3.4A**). Renal corpuscle (**Fig. 3.4A** black square bracket; **Fig. 3.4C,** SHAM) appeared normally shaped: glomerulus was well vascularized with observable mesangial cells, while Bowman's capsule appeared normal, with an intact podocyte layer and a clear undisrupted Bowman's space (black arrow individuates one). In some cases, a continuum with the proximal convoluted tubule was seen.

Proximal (**P**) and distal (**D**) convoluted tubules, in the cortical area, were normally shaped (**Fig. 3.4A**) and a tight association of tubules could be observed. At a closer look (**Fig 3.4D**), proximal tubules (**P**) were roughly bean-shaped with a strong eosinophilic stain, while distal tubules (**D**) appeared round in section and with a more intense nuclear stain. In the renal medulla (**Fig. 3.4A**, M), descending and ascending loops of Henle and collecting ducts were clearly distinguishable and outlined by epithelial cells. In general, Sham-operated kidneys appeared

well vascularised, with clear peritubular and glomerular capillaries outlined by endothelial cells.

As expected, sections from kidneys at 21 days post-UUO showed a disruption of the renal structure typical of an advanced-to-end stage tubulointerstitial fibrosis (**Fig. 3.4B**). Cortical tubules (**Fig. 3.4B; Fig. 3.4D,** UUO) were mostly atrophied and lost their tight association, with formation of empty spaces between them, loss of a clear epithelial border and a larger interstitial space. Medullar tubules (**Fig. 3.4B**, M), as well, completely lost their structure and tight association, making difficult to distinguish the different parts. A general paler pink colour characterized the totality of UUO sections (**Fig. 3.4B; Fig. 3.4C-D,** UUO) and this is in agreement with the fact that H&E typically stains fibrillary collagen in a lighter red/pink, comparing to the darker red of cytoplasmic staining (Fischer, et al. 2008). Considering this, a paler colour would reflect the general cell flattening/loss and contemporaneous ECM accumulation. Peritubular capillaries were not as distinguishable as before. As reported before, the effect of UUO on glomerular cells is generally slower, being a model that affects primarily the tubules. In line with the theory, in the sections obtained a part of renal corpuscles (**Fig. 3.4B** black square bracket individuates one, **Fig. 3.4C-UUO**) were still showing the typical structure and a clear vascularisation, even if they were perhaps experiencing a process of podocyte atrophy and scarring, hence displaying a lighter eosinophilic staining. Some glomeruli (**Fig. 3.4B**, **Fig. 3.4C-UUO**, asterisk to identify one) showed a focal glomerulosclerosis, with loss of capillary structure and typical glomerular sclerotic area rich in fibrous tissue.

In conclusion, H&E staining allowed to detect obvious differences in renal morphology at 21-days post UUO, compared to the Sham operated controls, with tubular atrophy and structural loss being the main observable features. The level of kidney damage can be considered similar to the later stages of an obstructive kidney disease (Huang, et al. 2006), even if, given the particular technique and the rapidity of the process, comparison with human disease is difficult (Chevalier, Forbes and Thornhill 2009). At the same time, from the histological appearance of the kidney tissue, Sham operated mice seem to have physiologically normal nephron structures and vascularisation, and can be safely referred as healthy mice, while UUO mice at 21 days can be referred as fibrotic mice.

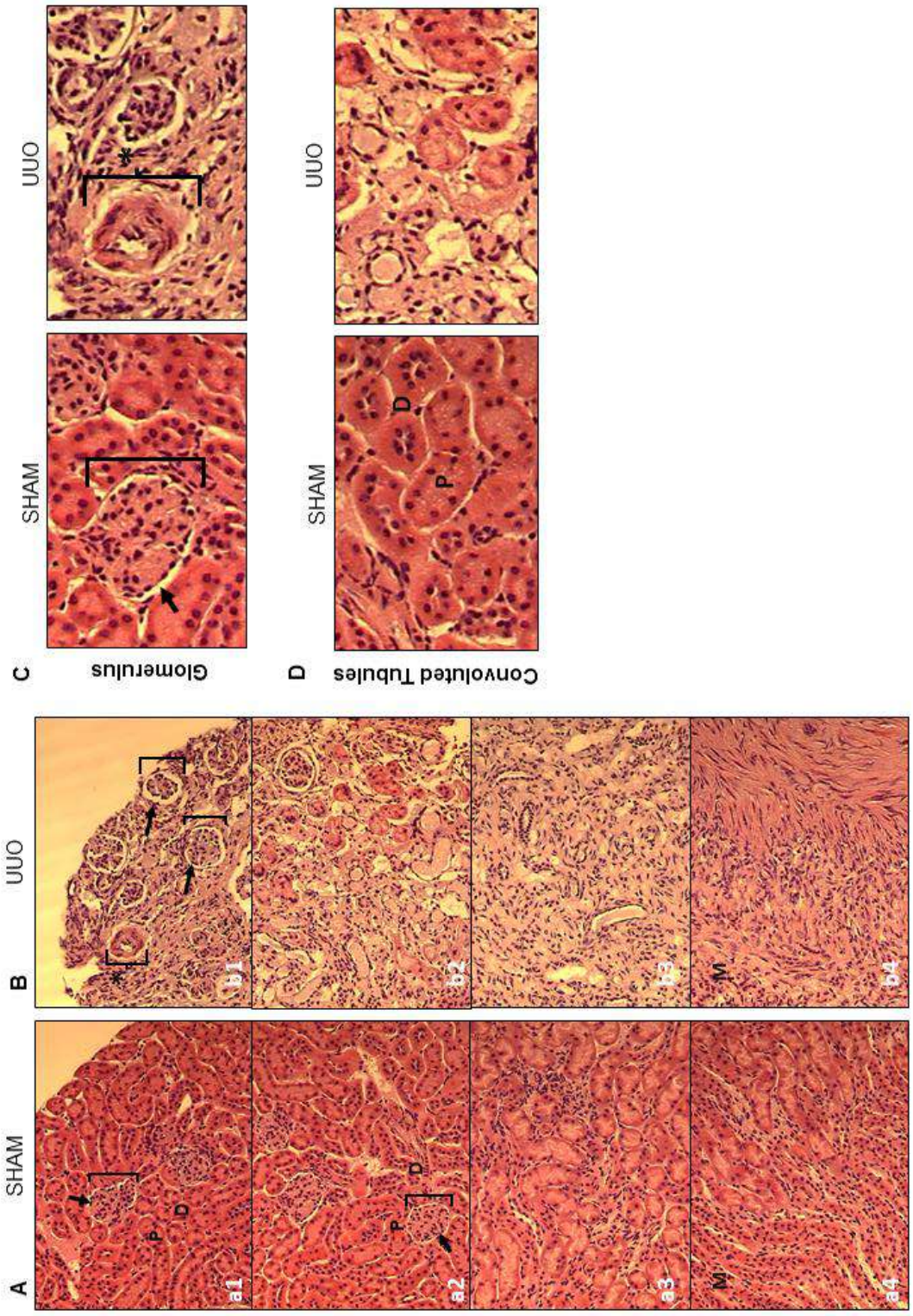

Figure 3.4: Haematoxylin and Eosin (H&E) staining of kidney sections from UUO and Sham operated kidneys at 21 days post-surgery. H&E staining of paraffin sections was performed at the Department of Infection, Immunity & Cardiovascular Disease of the University of Sheffield by Dr Fiona J. Wright. Pictures were taken with an Olympus BX61 fluorescent microscope with Cell^F imaging system software (Olympus, Japan). **(A,B)** Representative images at 20X magnification of Sham (A) and UUO (B) kidneys at 21 days post-surgery. **(C)** Close up (80X) of Glomeruli. **(D)** Close Up (80X) of Proximal and Distal convoluted tubules in the cortical area. Legend: 1,2 = mostly cortical area; 3,4 = mostly medullar area; square bracket = renal corpuscle; arrow = Bowman's space; P = proximal convoluted tubule; D = distal convoluted tubule; M = medulla; * = sclerotic glomerulus.

3.4.1.2 Masson's trichrome (MT) staining of UUO and Sham-operated kidney sections

Masson's Trichrome (MT) staining, a well-established method to quantify the level of scarring in diseased kidneys, was performed on Sham-operated and UUO mice at 21 days post-surgery and pictures were obtained using an Olympus BX61 microscope as described in 3.3.2. Focus was put on both cortical and medullar area, making sure to include sufficient glomeruli and tubules in the pictures (**Fig. 3.5**). Similarly to the H&E staining, MT confirmed a substantial alteration in the organ morphology. In addition, dual-staining of collagen and plasma or collagen and nuclei allows to perform a quantification of kidney fibrosis (fibrotic tissue) as a result of fibrillary collagen accumulation and simultaneous flattening and/or loss of structural cells (**Fig. 3.6**).

In Sham operated kidneys (21 days), normal glomeruli and tubules were observed (**Fig. 3.5A**), with the typical morphology of a healthy organ, as described in the previous section. Large red staining identified the cellular structures; tubules were tightly associated and had a clear epithelial border in both the cortical and the medullar area (**Fig. 3.5A; Fig 3.5D**). The renal corpuscle (**Fig. 3.5A** - black square bracket identifies one, **Fig. 3.5C**) was characterized by properly distributed mesangial cells and podocytes, in red, around the well vascularized capillary system of the glomerulus and enclosed in the typical Bowman's space (black arrow). Kidneys appeared well vascularised both in the glomeruli and around the tubules. Little blue staining for fibrillary tissue was noted, limited to the interstitial space (**Fig. 3.5A; Fig. 3.5D** - white thick arrows identifies an example), the intramesangial ECM (**Fig. 3.5A; Fig. 3.5C** - white thin arrows identifies an example) and the basement membranes of both TECs and glomerular cells (**Fig. 3.5A; Fig. 3.5C** - white triangles identify some examples).

Upon fibrosis (21 days post-UUO), a clear disruption of kidney parenchyma was observed in the MT staining (**Fig. 3.5B**). The plasma staining (red) was strongly reduced compared to the Sham operated kidneys: flattening and loss of tubular cells, and consequent tubular atrophy, was evident, while the reduced staining in the glomeruli might identify a loss in mesangial cells and podocytes. Tubules which lost their tight association and peritubular capillaries borders were less distinguishable from the remnant tubules and appeared enlarged (**Fig. 3.5B, Fig. 3.5C**).

Signs of glomerulosclerosis and corpuscular loss were evident in the cortex with loss of capillary structure and accumulation of sclerotic fibrillary tissue (white thin arrows to identify an example) among the few remnant mesangial cells. However, as shown with the H&E staining, glomerular sclerosis and loss is slower than tubulointerstitial fibrosis in this model, and some intact glomeruli were still present at 21 days post-UUO (black square bracket individuates one)(**Fig. 3.5B, Fig. 3.5C**). The blue staining was strongly augmented in UUO sections, in both cortical and medullar area, and revealed an accumulation of fibrous tissue mostly in the tubulointerstitial space (**Fig. 3.5B, Fig. 3.5D** - white thick arrows identify an

example), but also in atrophied corpuscles (**Fig. 3.5B, Fig. 3.5C** - white thin arrows to identify an example). Following cell loss (TECs and podocytes), exposed basement membranes (white triangles identify an example) were also evident in both tubular and glomerular sections. At a close look (**Fig. 3.5, Fig. 3.5D**), the location of cells, identified by dark brown stained nuclei, was also altered by fibrosis, possibly showing fibroblasts/myofibroblasts in the interstitial space, where they produce abundant matrix, as well as loss of the tubular epithelial border.

Quantification of the different staining colours was performed with Cell^F software and the ratio of collagen over cytoplasm was measured to evaluate the accumulation of fibrotic tissue (**Fig. 3.6A**). Significant collagen accumulation was identified at 21 days post-UUO (10.76±3.13 fold from WT Sham, equalised to 1; p=0.002 **). A similar result was obtained by quantifying the level of collagen over the number of cells (brown staining of the nuclei) (**Fig. 3.6B**), with a 3.19 ± 0.68 -fold increase in collagen deposition at 21 days post-UUO compared to Sham-operated healthy controls (p=0.0003 ***).

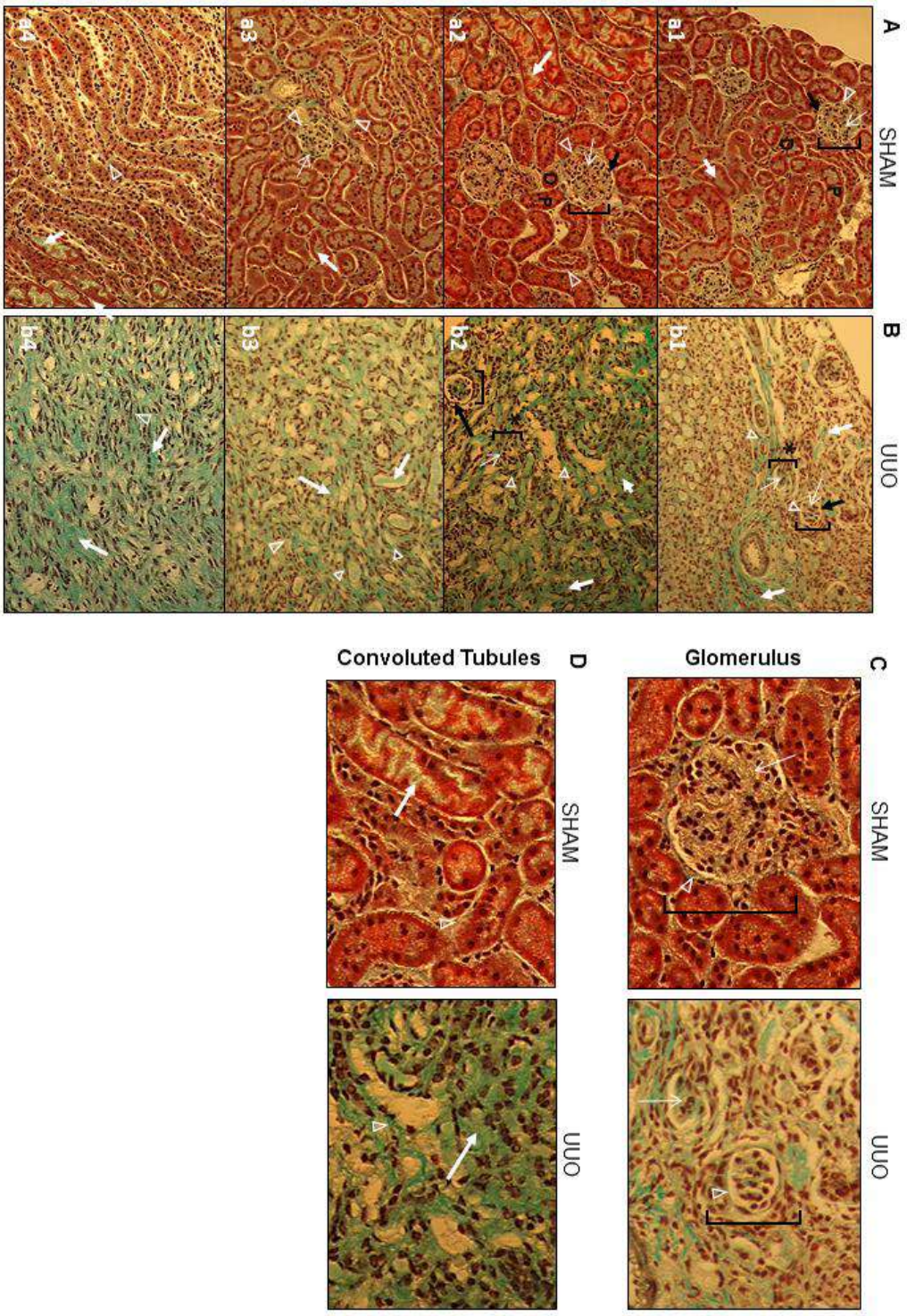

Figure 3.5: Masson's Trichrome (MT) staining of kidney sections from UUO and Sham operated kidneys at 21 days post-surgery. MT staining of paraffin sections was performed at the Department of Infection, Immunity & Cardiovascular Disease of the University of Sheffield by Dr Fiona J. Wright. Pictures were taken with an Olympus BX61 fluorescent microscope with Cell^F imaging system software (Olympus, Japan). **(A,B)** Representative images at 20X magnification of Sham (A) and UUO (B) kidneys at 21 days post-surgery. **(C)** Close up (80X) of Glomeruli. **(D)** Close Up (80X) of Proximal and Distal convoluted tubules in the cortical area. Legend: 1,2 = mostly cortical area; 3,4 = mostly medullar area; square bracket = renal corpuscle; arrow = Bowman's space; P = proximal convoluted tubule; D = distal convoluted tubule; * = sclerotic glomerulus; thick white arrow = interstitial space; thin white arrow = intraglomerular matrix; white triangles = basement membrane.

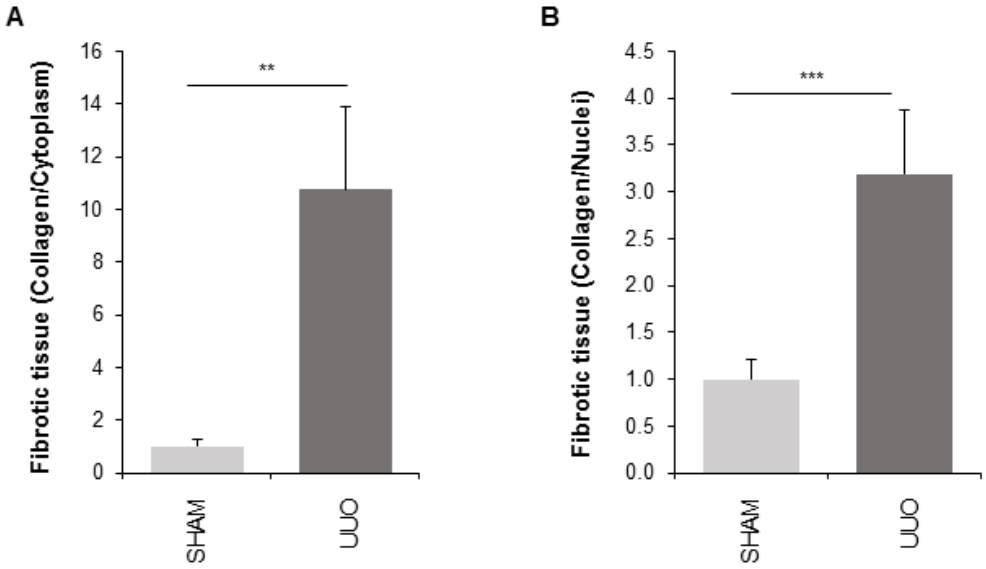

Figure 3.6: Quantification of renal fibrosis by Masson's trichrome (MT) staining. In order to quantify the level of fibrosis WT mice subjected to UUO, quantification of MT-stained sections was performed with Cell^F imaging system software (Olympus, Japan). The level of fibrosis was measured as **(A)** ratio of phase 2 (collagen, light blue) over phase 1 (cytoplasm, pink) or as **(B)** ratio of phase 2 (collagen, light blue) over phase 3 (nuclei, brown). Data represent mean ratio values expressed relative to the WT Sham operated control (equalised to 1) ± SEM, n=24 different fields per treatment covering both cortical and medullar areas. Significance of the differences between treatments was determined by T-test: * = $p<0.05$, ** = $p<0.01$, *** = $p<0.001$, **** = $p<0.0001$.

3.4.2 Expression of the fibrosis marker α-smooth muscle actin (α-SMA) in kidneys subjected to UUO

α-SMA is a well-established marker of myofibroblasts proliferation during fibrosis progression. In order to validate the development of fibrosis in wild type kidneys subjected to UUO (21 days), whole kidney lysates were immunoprobed for α-SMA by Western blotting. At the same time, the expression TG2 was measured on the same lysates using a specific mouse monoclonal anti-TG2 antibody. In all experiments, constitutively expressed cyclophilin-A (CypA) was employed as a loading control.

Previous studies on CKD have reported a predisposition to fibrosis development in adult males comparing to females. A series of studies have showed in the past that the progression of some non-diabetic renal diseases is faster in men then in women of the same age (Seliger, Davis and Stehman-Breen 2001, Neugarten 2002, Silbiger and Neugarten 2008), suggesting a possible involvement of male sex hormones in the process or a possible protective role of female hormones. Similar gender bias was also observed in aging animals and other spontaneous *in vivo* rodent models of CKD [reviewed in (Herrera 2010)]. This is generally not the same in

diabetic kidney diseases, where the impact of sex on the outcome in kidney is much more variable and might be associated with altered hormone levels during diabetes in either genders (Maric 2009). With this in mind, gender bias in protein expression was investigated as well by probing N=3 randomly selected kidneys per treatment from each sex.

3.4.2.1 TG2 expression in whole kidney lysates

In male mice, UUO determined a small but not significant increase in the expression of TG2 at 21-days post-surgery comparing to the healthy mice (**Fig. 3.7A,B**): a 1.39 ± 1.14 fold change increase, in fact, was measured comparing to the sham operated control (equalized to 1) (p=0.61 not significant). In females (**Fig. 3.7D,E**), again, a small increase in TG2 signal was observed at 21-days post UUO, corresponding to a 1.51 ± 0.19 -fold change comparing to the sham-operated control. Again, the difference was not significant by T-test (p=0.16).

These data suggest that, even if TG2 protein expression might increase upon fibrosis, the enzyme is not necessarily up-regulated in a significant manner upon CKD, in agreement with a previous study performed by our group in the UUO and AAN model of kidney fibrosis (Scarpellini, et al. 2014).

Curiously, in some cases, and especially in female mice, a double band between 75 and 80 kDa was observed with the employed antibody, of which only the bottom band, more intense (asterisk), should be specific for the full length form of TG2.

3.4.2.2 α-SMA expression in whole kidney lysates

α-SMA signal was up-regulated at 21-days post-UUO in WT mice of both genders. α-SMA signal (~37 kDa) was absent or minimal in Sham operated kidneys, and strongly increased upon treatment. This is in agreement with previous studies where the myofibroblast marker was investigated in UUO [eg. (Xue, et al. 2003, Inazaki, et al. 2004)].

In male mice (**Fig. 3.7 A,C**), 21-days UUO determined an average 22-fold increase in α-SMA expression comparing to the healthy controls, and varied in a range from ~12 to ~32-fold changes from Sham in the different samples (mean fold increase = 22.7±8.99-fold change from Sham, p=0.05). In female mice (Fig. 3.6 D,F), UUO showed a ~5-fold increase in α-SMA comparing with the Sham operated control (4.83±2.21), that was however not significant (p=0.24) given the variability of expression. The lower expression of α-SMA in female mice might reflect a gender bias in fibrosis development in this model, with a partial protection in female.

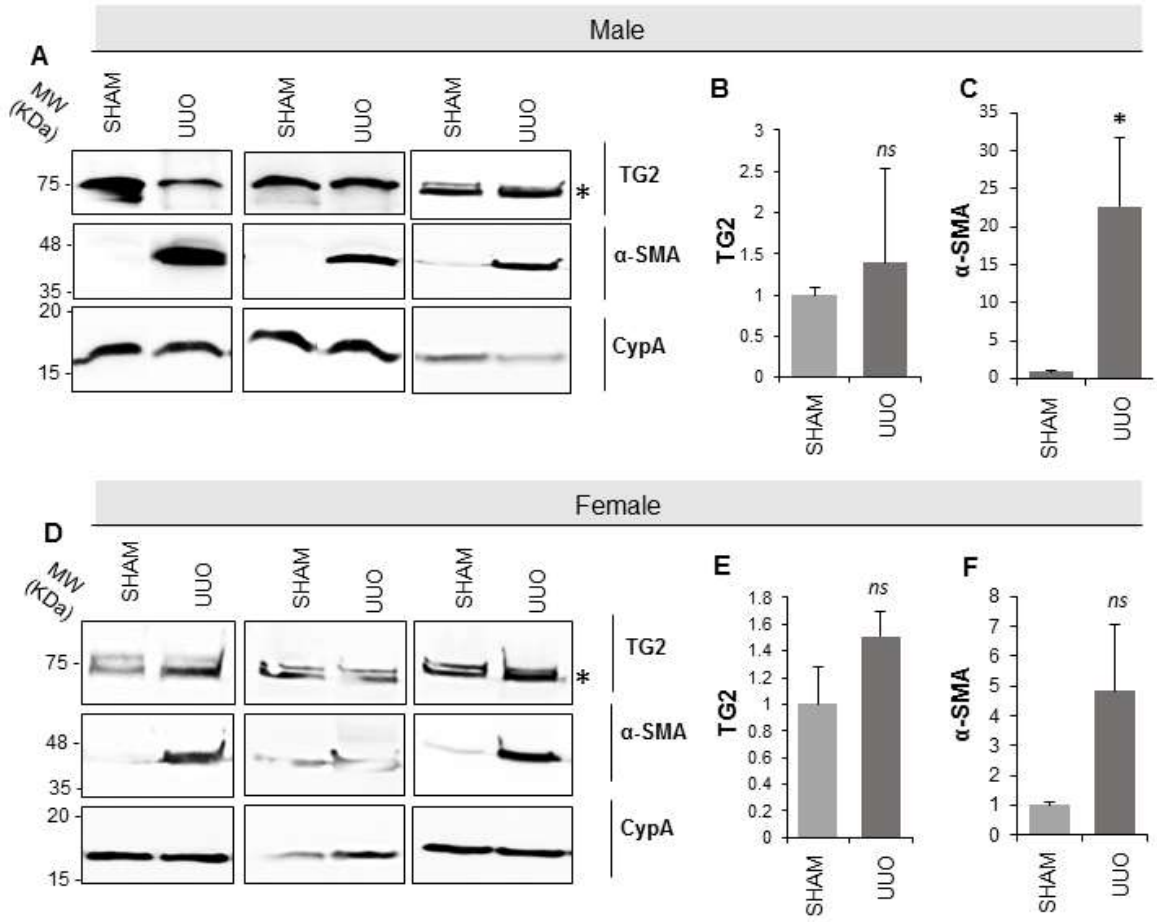

Figure 3.7: Expression of TG2 and fibrosis marker α smooth muscle actin (α-SMA) in kidney lysates from the UUO model at 21-days. Expression of TG2 and fibrosis marker α-SMA was detected by Western blot using the specific antibodies reported in Table 3.2. Experiment was performed on three different male kidneys/treatment (A-C) or three different female kidneys/treatment (D-F). Specific blots are shown on the left (A,D). Intensity of immunoreactive bands was quantified by densitometric analysis and normalised to constitutively expressed cyclophilin-A (CypA). The graphs represent mean normalised densitometric measurements expressed relative to the Sham operated control (equalised to 1) ± SD, n = 3 kidney lysates per group, in either male (B,C) or female (D,F) mice. Significance of the differences between treatments was determined by T-test: * = $p<0.05$, ** = $p<0.01$, *** = $p<0.001$, **** = $p<0.0001$, ns = not significant.

3.4.3 TGF-β activation in the UUO model

TGF-β1 is a known mediator of tubulointerstitial fibrosis, influencing the expression of a number of fibrogenesis-associated proteins. TGF-β activity is known to be increased during fibrosis and sustain the progression of fibrosis (Roberts, et al. 1986, Böttinger 2007). In order to validate the increased activation of the cytokine upon UUO, the TGF-β activity bioassay on the mink lung epithelial cells (MLEC) system was performed on whole kidney lysates from both WT and TG2-null mice, subjected to UUO or Sham operation (**Fig. 3.8**). As expected, TGF-β activation, measured as active TGF-β / total TGF-β, was virtually null in sham operated kidneys. In fact, TGF-β is usually secreted the interstitial space as a response to inflammation, with infiltration of inflammatory cells that release the cytokine, a phenomenon that is generally transient or limited in physiological conditions. UUO for 21 days determined a strong significant increase in TGF-β activity, in agreement with previous measurement performed in the same model (Scarpellini, et al. 2014, Shweke, et al. 2008).

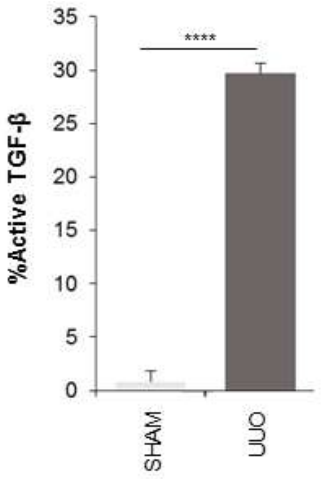

Figure 3.8: Level of active TGF-β in kidney lysates from the UUO model in WT mice. In order to measure the activation of TGF-β in the UUO model (21 days), active and total TGF-β were assessed using 100 µl of 10% (w/v) kidney lysate or acid-treated lysate, both 10 times diluted, on the MLEC system, as described in 3.3.4. The experimental data was collected by Dr Nina Schroeder at NTU. Data represent the mean % of active TGF-β ± SD, N=3. Significance of the differences between treatments was determined by T-test: * = $p<0.05$, ** = $p<0.01$, *** = $p<0.001$, **** = $p<0.0001$

3.4.4 Proteomic analysis by SWATH-MS reveals a series of proteins differentially expressed in UUO mice

3.4.4.1 Definition of a list of proteins differentially expressed by UUO

Quantitative MS analysis employing a SWATH-DIA approach allows to achieve a large coverage of a sample's proteome, with a much higher sensitivity than the targeted data acquisition approach or the shotgun-DDA approach and allowing to perform quantification of protein expression and quantitative comparisons among different samples (Gillet, et al. 2012).

With the aim of determining proteins differentially expressed by UUO, SWATH-MS was performed on four randomly selected Sham operated kidneys and four randomly selected UUO kidneys, all harvested at 21 days post-surgery and belonging to both genders. Samples preparation and SWATH acquisition-MS was performed as described in 3.3.6, and the spectral analysis resulted in the detection of 2106 proteins expressed in the different samples.

Fold change (FC) in proteins' expression between UUO and Sham operated mice were calculated by SCIEX OneOmics processing software. The outcome of the OneOmics FC analysis between UUO and Sham operated samples, at a confidence of fold change [C(FC)] up to 0.5, can be found in the Supplementary information of this thesis (**Suppl. Table 3.1**).

A C(FC) threshold of 0.8 (80%) was chosen to define the list of significant differentially expressed proteins upon UUO, when compared to the Sham operated control. As a result, of the 2106 proteins expressed in the different samples, as detected by SWATH acquisition-MS, 653 were identified as differentially expressed at 21 days post-UUO [C(FC) ≥0.8]. Of these proteins, 195 were upregulated upon UUO (**Suppl. Table 3.5**), while 458 (**Suppl. Table 3.6**) were downregulated by the treatment. Protein IDs were manually searched on UniProtKB and full protein names included in the lists.

Table 3.3 and **3.4** highlight some of the most interesting proteins arose from a preliminary overview of the differentially expressed proteins at 21 days post-UUO.

3.4.4.2 Preliminary observation of the UUO-overexpressed proteins

Even before performing any kind of functional analysis on the proteins, it was already evident that many of the 195 proteins upregulated upon UUO were directly associated with the process of kidney fibrosis (highlighted in **Table 3.3**).

As expected, collagens were identified as upregulated by UUO (**Table 3.3** and **Fig. 3.9A**). Among the collagen subtypes identified, collagen type XII (COCA1_MOUSE), which is known to interact with collagen I, was identified as the most upregulated at 21 days post-UUO, with an ~16 fold increase from the Sham operated controls, followed by collagen I and collagen III, both approximately 7.7-fold upregulated. Relative protein quantification performed by the software, basing on the normalized protein spectra, highlighted collagen I as the more

expressed collagen in UUO kidneys, followed by collagen III and collagen IV, the mayor structural component of the GBM (**Fig. 3.9A**). ECM glycoproteins fibronectin (FN, FINC_MOUSE), fibrillins and fibulins were all strongly upregulated by the disease, with fold increase from the Sham operated conditions going from ~6 (FBLN5_MOUSE) to ~11 (FBN1_MOUSE) (**Table 3.3**). The strong fibulin 1 upregulation agrees with previous studies of mice UUO (Schaefer, et al. 2004). Among these matrix glycoproteins, "EGF-containing fibulin-like protein" (FBLN3_MOUSE), also known as fibulin 3, is able to bind epithelial growth factor receptor (EGFR) activating EGFR-signalling pathway, possibly acting as a profibrotic cytokine in the promotion of kidney fibrosis. Fibronectin and fibrillin 1 showed the highest expression in the group, when relative protein expression was investigated (**Fig. 3.9A**). Interestingly, small leucin rich matrix proteoglycan (SLRP) biglycan was upregulated, together with other SLRPs mimecan and lumican (**Table 3.3, Fig. 3.9A**), in agreement with previous findings on mice subjected to UUO (Schaefer, et al. 2004), and in human biopsies, were it was present both in the glomerulus and in areas of tubulointerstitial fibrosis (Stokes, et al. 2000). Basement membrane laminins, nidogen and HSPGs, including agrin, known to be the main HSPG in the GBM (Groffen, et al. 1998), perlecan, and collagen XVIII /endostatin, were also upregulated by the disease (**Table 3.3, Fig. 3.9A**). Basement membrane HSPGs have been suggested to be involved in the maintenance of the glomerular filtration barrier (Kvist, et al. 2006, Morita, et al. 2005, Miosge, et al. 2003), and may be upregulated in response to injury.

A few proteases and proteases inhibitors, as expected, were overexpressed upon UUO (**Table 3.3**) and might be involved in matrix remodeling and stabilization. Among these, antitrypsin was highly overexpressed (~8 -fold) and known to be upregulated in models of kidney disease (Bergin, et al. 2012, Navarro-Munoz, et al. 2012).

Several markers of fibroblast proliferation and myofibroblast activation were also identified as upregulated at 21 days post-UUO in our model (**Table 3.3**). In agreement with previous studies (Xue, et al. 2003, Inazaki, et al. 2004), as well as with the protein immunoprobing in whole kidney lysates [3.4.2], α-SMA (ACTA_MOUSE) was upregulated in UUO (**Table 3.3**). Moreover, other markers such as vimentin (Yuasa, et al. 2014, Grone, et al. 1987, Johnson, et al. 1991, Ofstad and Iversen 2005, Zou, et al. 2006), desmin (Zou, et al. 2006, Johnson, et al. 1991, Yuasa, et al. 2014) and vinculin (a marker of focal adhesion sites)/talin (Humphries, et al. 2007) were significantly induced at 21-days post-UUO in this model (**Table 3.3**). Calponin is another marker of myofibroblast proliferation (Yuasa, et al. 2014, Choi, Nam and Cha 2014, Lee, et al. 2010, Sugenoya, et al. 2002) with a possible protective role in the glomerulus (Sugenoya, et al. 2002), and one of its isoforms (CNN1_MOUSE) resulted more than 8-fold upregulated upon UUO at 21-days post UUO. Different tropomyosins and myosins were also overexpressed in UUO kidneys, in agreement with their role in cell contraction (Tomasek, et al. 2002) (**Table 3.3**). Relative protein quantification performed by the software, basing on the

normalized spectra, highlighted vimentin as the more expressed marker in UUO kidneys, followed by α-SMA (**Fig. 3.9B**).

Other proteins that might be directly associated with the progression of fibrosis upon UUO are lipid binding proteins such as apolipoproteins (**Table 3.3**). Expression of APOA and mutations in APOE have been associated with the progression of CKD in different models (Kopp, et al. 2011, Boes, et al. 2006, Hsu, et al. 2005). APOE might have a protective function in the glomerulus (Hsu, et al. 2005). Clusterin (CLUS_MOUSE) is an apolipoprotein suggested to be upregulated different types of acute and chronic kidney diseases, where it might play and antiapoptotic role (Chevalier, et al. 1996), and was more than 5-fold increased in the model (**Table 3.3**). Fatty acid binding protein, a lipid binding protein already shown to be upregulated in serum upon kidney disease (Górski, et al. 1997, Yamamoto, et al. 2007) was also identified in this model (**Table 3.3**).

Proteins involved in inflammatory response appeared upregulated in response to UUO at 21-days, among which complement proteins C3 and C4 (Stegall, Chedid and Cornell 2012, Welch, Beischel and Witte 1993) and numerous members of the annexin family were identified (**Table 3.3**). Annexin 1-6 were all upregulated at 21 days post-UUO; annexin 1 was strongly overexpressed (ANXA1_MOUSE, 8-fold overexpressed) and is known to be involved in inflammatory response as well as being a marker of cells undergoing apoptosis (Arur, et al. 2003). Also annexin 5 (ANXA5_MOUSE) is frequently employed as a marker of apoptotic cells in commercial kits and has also been involved in coagulation; similarly, annexin 4 (ANXA4_MOUSE) has been suggested as an early marker of apoptosis (Herzog, et al. 2004). Above all, annexin 2 (ANXA2_MOUSE) is an interesting protein in the context of kidney injury as well as being characterized by an unconventional secretory route [reviewed in Chapter V]. It has been suggested to bind and control plasmin (Ma and Fogo 2009, Fitzpatrick, et al. 2000) and to be upregulated in models of tubular injury and necrosis (Cheng, et al. 2005)

A number of serum proteins were overexpressed in the UUO proteome (**Table 3.3**), in line with previous studies (Filip, et al. 2015). In particular, serum β-2-microglobulin has been demonstrated to markedly increase in patients with chronic renal failure (Blumberg and Burgi 1987, Peterson, Evrin and Berggard 1969, Varghese, et al. 2007). To note, other immunoglobulins were upregulated by UUO and are displayed in **Suppl. Table 3.5**.

Uromodulin appeared as the most overexpressed protein in our UUO model at 21 days post-surgery (UROM_MOUSE, more than 16-fold overexpressed) (**Table 3.3**). The upregulation of this protein in kidneys upon CKD is a novel finding, as the protein is involved in the regulation of tubular structures and is normally present in physiological conditions. However, as uromodulin is the most common protein in the urine of healthy individuals (Bleyer, Zivna and Kmoch 2011, Devuyst 2013, Nagaraj and Mann 2011), urine retention determined by the UUO

procedure might lead to a strong accumulation of the protein in the kidney, which has been associated with forms of CKD (Scolari, et al. 2004, Rampoldi, et al. 2003).

An interesting protein showing a strong increase in expression upon UUO was transgelin (TAGL_MOUSE), more than 9-times upregulated in comparison with the Sham operated control (**Table 3.3**). Transglelin has been recently suggested as a marker of proliferating cells, upregulated during the progression of fibrosis in both glomerular and tubular cells in different models of kidney disease, including obstructive nephropathy (Inomata, et al. 2011, Gerolymos, et al. 2011, Sakamaki, et al. 2011, Daniel, et al. 2012, Karagianni, et al. 2013). Periostin was also strongly overexpressed at 21-days post UUO: this protein has been largely studied in the context of renal disease and associated with both glomerulosclerotic and tubulointerstitial kidney diseases (Guerrot, et al. 2012, Mael-Ainin, et al. 2014, Sen, et al. 2011, Wallace, et al. 2014, Satirapoj, et al. 2012) (**Table 3.3**).

Moesin, galectin-1, retinol-binding protein and myoferlin were among the other interesting proteins overexpressed in the UUO proteome when compared to Sham operated conditions (**Table 3.3**), in agreement with their proposed involvement in CKD models (Henderson, et al. 2008, Chen, et al. 2014, Pallet, et al. 2014). Thymosin β-4 is known to promote stabilisation of fibrin clots in wound repair (Huff, et al. 2002, Telci and Griffin 2006), and was as well overexpressed in the disease together with fibrinogen isoforms (**Table 3.3**).

In summary, these first general observations are already indicatory of the development of a large tubulointerstitial fibrosis upon UUO, highlighting most of the main markers and structural molecules. Interestingly, TG2 (TGM2_MOUSE) was detected as significantly overexpressed by UUO with this technique, even if with only a small fold increase from the Sham operated healthy conditions (FC= +1.71) (**Table 3.3**).

Table 3.3: Highlight of interesting protein groups identified as significantly overexpressed in kidneys at 21 days post-UUO. Comprehensive list of protein can be found in the Supplementary material (**Suppl. Table 3.5**). In increasing shades of red the absolute fold change increase of UUO from Sham operated condition, in increasing shades of yellow the confident of fold change C(FC). A C(FC) higher than 80% (0.8) was regarded as significant.

Highlighted	Examples		FC (UUO/Sham)	C(FC)
Collagens	Collagen alpha-1(I) chain	CO1A1_MOUSE	7.61	0.96
	Collagen alpha-1(III) chain	CO3A1_MOUSE	7.72	0.92
	Collagen alpha-1(IV) chain	CO4A1_MOUSE	2.67	0.88
	Collagen alpha-2(IV) chain	CO4A2_MOUSE	4.50	0.80
	Collagen alpha-1(VI) chain	CO6A1_MOUSE	4.78	0.88
	Collagen alpha-2(VI) chain	CO6A2_MOUSE	4.76	0.94
	Collagen alpha-1(XII) chain	COCA1_MOUSE	15.92	0.82
	Collagen alpha-1(XIV) chain	COEA1_MOUSE	4.62	0.81
Extracellular Matrix glycoproteins	Fibronectin	FINC_MOUSE	7.85	0.84
	Fibrillin-1	FBN1_MOUSE	10.84	0.89
	Fibrillin-2	FBN2_MOUSE	7.26	0.94
	Fibulin-2	FBLN2_MOUSE	9.65	0.81
	Fibulin-5	FBLN5_MOUSE	5.81	0.84
	EGF-containing fibulin-like extracellular matrix protein 1 (Fibulin 3)	FBLN3_MOUSE	6.33	0.80
	Emilin-1	EMIL1_MOUSE	4.42	0.82
	Biglycan	PGS1_MOUSE	8.73	0.86
	Mimecan	MIME_MOUSE	6.67	0.83
	Lumican	LUM_MOUSE	6.55	0.87
Basement membrane	Laminin subunit alpha-5	LAMA5_MOUSE	2.26	0.83
	Laminin subunit beta-1	LAMB1_MOUSE	1.85	0.85
	Laminin subunit gamma-1	LAMC1_MOUSE	1.85	0.93
	Nidogen-1	NID1_MOUSE	2.10	0.92
	Agrin	AGRIN_MOUSE	2.16	0.92
	Basement membrane-specific heparan sulfate proteoglycan core protein	PGBM_MOUSE	1.80	0.81
	Collagen alpha-1(XVIII) chain	COIA1_MOUSE	2.57	0.96
Proteases	Cathepsin D	CATD_MOUSE	2.65	0.82
	Cathepsin Z	CATZ_MOUSE	2.53	0.86
	Hemopexin	HEMO_MOUSE	4.60	0.86
Protease inhibitor	Alpha-1-antitrypsin 1-1	A1AT1_MOUSE	3.07	0.86
	Alpha-1-antitrypsin 1-2	A1AT2_MOUSE	7.86	0.82
	Alpha-1-antitrypsin 1-4	A1AT4_MOUSE	2.72	0.83
	Antithrombin-III	ANT3_MOUSE	2.27	0.86
	Kininogen-1	KNG1_MOUSE	3.09	0.91
	Serpin B6	SPB6_MOUSE	3.56	0.89
	Serpin H1	SERPH_MOUSE	6.19	0.94
Marker Myofibroblasts	Actin, aortic smooth muscle	ACTA_MOUSE	3.17	0.94
	Vimentin	VIME_MOUSE	8.56	0.90
	Desmin	DESM_MOUSE	5.98	0.94
	Vinculin	VINC_MOUSE	2.33	0.94
	Talin-1	TLN1_MOUSE	1.78	0.82
	Calponin-1	CNN1_MOUSE	8.59	0.80
	Calponin-2	CNN2_MOUSE	6.15	0.80
	Tropomyosin alpha-1 chain	TPM1_MOUSE	4.28	0.84
	Tropomyosin alpha-4 chain	TPM4_MOUSE	4.19	0.91
	Myosin light chain kinase, smooth muscle	MYLK_MOUSE	2.59	0.80
	Myosin light polypeptide 6	MYL6_MOUSE	2.53	0.92
	Myosin regulatory light chain 12B	ML12B_MOUSE	2.33	0.83
	Myosin regulatory light polypeptide 9	MYL9_MOUSE	3.08	0.98
	Myosin-9	MYH9_MOUSE	2.61	0.99

	Myosin-10	MYH10_MOUSE	3.27	0.85
	Myosin-11	MYH11_MOUSE	3.28	0.87
Lipid-binding proteins	Apolipoprotein A-I	APOA1_MOUSE	2.46	0.92
	Apolipoprotein A-IV	APOA4_MOUSE	2.50	0.82
	Apolipoprotein E	APOE_MOUSE	3.31	0.87
	Beta-2-glycoprotein 1 (Apolipoprotein H)	APOH_MOUSE	2.50	0.80
	Clusterin (Apolipoprotein J)	CLUS_MOUSE	5.35	0.81
	Fatty acid-binding protein, adipocyte	FABP4_MOUSE	1.82	0.85
Inflammation	Complement C3	CO3_MOUSE	2.59	0.87
	Complement C4-B	CO4B_MOUSE	3.44	0.86
	H-2 class II histocompatibility antigen, A-U alpha chain	HA2U_MOUSE	8.32	0.80
	Annexin A1	ANXA1_MOUSE	8.17	0.84
	Annexin A2	ANXA2_MOUSE	3.76	0.90
	Annexin A3	ANXA3_MOUSE	4.73	0.83
	Annexin A4	ANXA4_MOUSE	1.78	0.85
	Annexin A5	ANXA5_MOUSE	2.29	0.84
	Annexin A6	ANXA6_MOUSE	2.71	0.89
Plasma proteins	Beta-2-microglobulin	B2MG_MOUSE	2.88	0.82
	Serotransferrin	TRFE_MOUSE	3.78	0.91
	Creatine kinase B-type	KCRB_MOUSE	7.56	0.83
	Serum albumin	ALBU_MOUSE	2.98	0.92
	Vitamin D-binding protein	VTDB_MOUSE	3.13	0.93
Other	Uromodulin	UROM_MOUSE	16.34	0.85
	Transgelin	TAGL_MOUSE	9.27	0.89
	Transgelin-2	TAGL2_MOUSE	3.04	0.88
	Periostin	POSTN_MOUSE	8.04	0.80
	Moesin	MOES_MOUSE	1.52	0.81
	Galectin-1	LEG1_MOUSE	6.15	0.87
	Retinol-binding protein 1	RET1_MOUSE	5.56	0.83
	Myoferlin	MYOF_MOUSE	4.99	0.86
	Fibrinogen alpha chain	FIBA_MOUSE	4.64	0.90
	Fibrinogen beta chain	FIBB_MOUSE	4.00	0.86
	Fibrinogen gamma chain	FIBG_MOUSE	4.45	0.85
	Thymosin beta-4	TYB4_MOUSE	4.35	0.88
	Transglutminase 2	TGM2_MOUSE	1.71	0.90

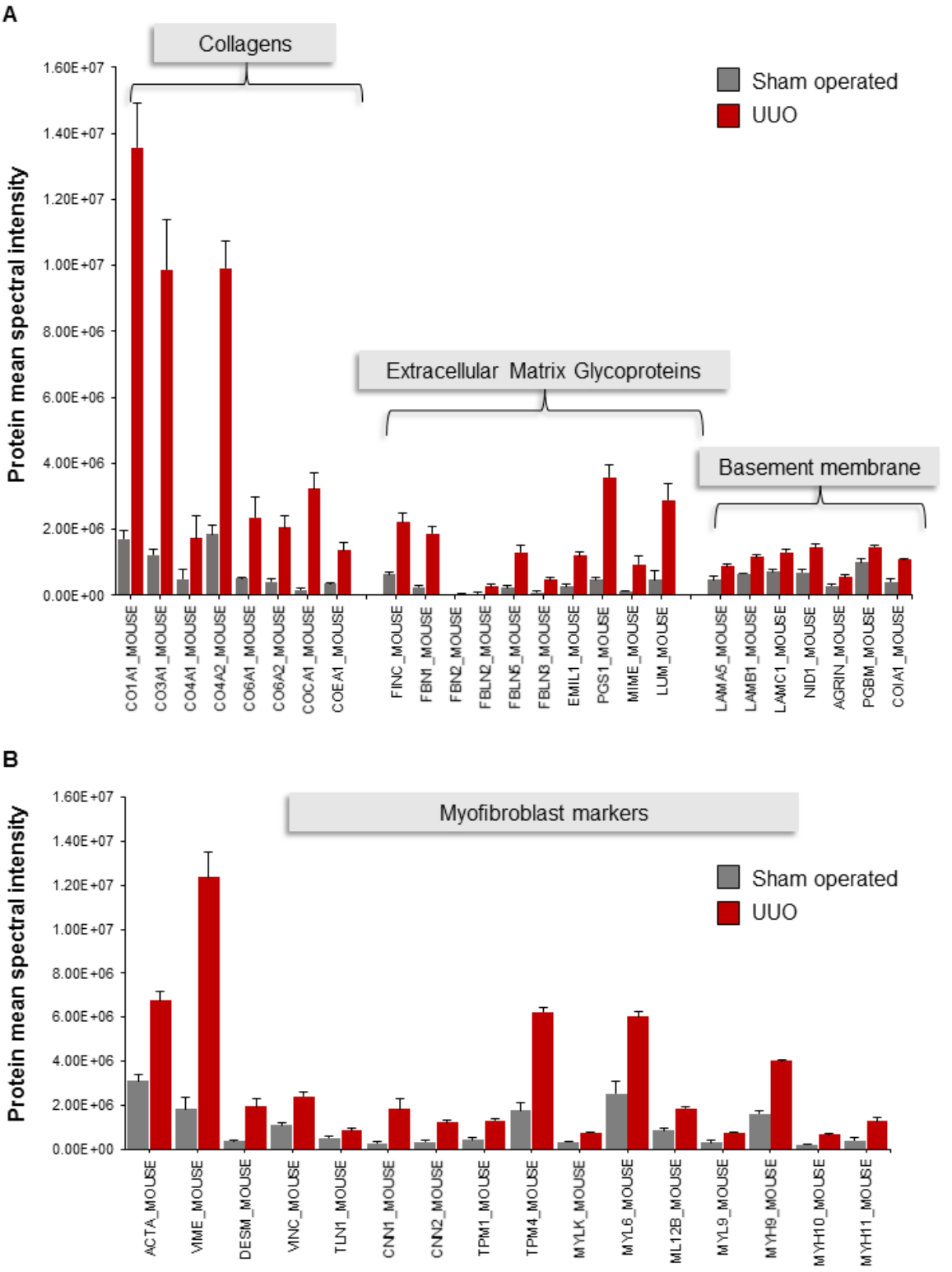

Figure 3.9: Relative protein expression of markers of fibrotic tissue deposition and myofibroblasts proliferation identified as overexpressed in mice subjected to 21 days – UUO. Column charts show the mean relative intensity as calculated by OneOmics software from the SWATH-MS data (SCIEX, Canada) ± SD, N=4 samples per treatment. **(A)** Extracellular matrix and basement membrane proteins: collagens, ECM glycoproteins and basement membrane components including HSPGs**. (B)** Markers of fibroblast proliferation and myofibroblasts differentiation. Significance of the differences between spectral means was determined by T-test; all differences resulted significant at $p<0.01$

3.4.4.3 Preliminary observation of the UUO-underexpressed proteins

The 458 proteins identified as underexpressed at 21 days post-UUO (**Suppl. Table 3.6**), appeared mostly metabolic and in large part associated with mitochondrial functions. They included a great number of enzymes involved in glycolysis / Krebs cycle, cytochrome subunits, ATP and NAD(P)H metabolism but also fatty acid and lipid metabolism. Some metabolic proteins such as glucose-6-phosphatase (G6PC_MOUSE), mitochondrial kynurenine/alpha-aminoadipate aminotransferase (AADAT_MOUSE) or hydroxyacid oxidase 2 (HAOX2_MOUSE) were more than 40-fold underexpressed in UUO conditions (**Suppl. Table 3.6**).

The strong downregulation of a large number of metabolic and regulative proteins is possibly linked to a substantial loss in kidney cells by apoptosis/necrosis, that happens during the progression of experimental UUO (Ucero, et al. 2014, Chevalier, Forbes and Thornhill 2009) and is highly established at this time point (21 days). However, few groups of proteins were selected from the list as interesting in the context of kidney physiology and are displayed in **Table 3.4**.

A number of UUO-downregulated proteins, for examples, were found associated with the control of normal kidney functions. A number of them were involved in transport through the tubular membrane: solute carrier family proteins (S12A1_MOUSE, S13A3_MOUSE, S22AI_MOUSE, S22A2_MOUSE, GTR1_MOUSE) can mediate the uptake of proteins, drugs and neurotransmitters from the blood to the tubular cells, while sodium/glucose cotransporter 2 and Na(+)/H(+) exchange regulatory cofactor NHE-RF3 and chloride intracellular channel protein 5 are important for ion transport along the tubule (**Table 3.4**).

The calcium-binding protein calbindin (CALB1_MOUSE) was also strongly downregulated in this model upon UUO (**Table 3.4**); it is known to be downregulated by ageing of or nephrotoxic stress on the kidney (Steiner, et al. 1996, Armbrecht, et al. 1989, Sooy, Kohut and Christakos 2000, Hoffmann, et al. 2010) and might be involved in the control of physiological renal calcium absorption.

Tubular osmolality - associated proteins such as aquaporins (involved in the regulation of tubular water permeability) and L-xylulose reductase were also underexpressed at 21-days post UUO, together with other proteins in different ways associated with the control of kidney excretion (PGES2_MOUSE, PTGR2_MOUSE, ST1D1_MOUSE) (**Table 3.4**).

A considerable underexpression in proteins involved in the control of blood pressure and Angiotensin metabolism was also noted upon 21 days UUO. Argininosuccinate synthase and cystathionine gamma-lyase were both strongly downregulated by UUO, as well as angiotensin-converting enzymes (ACE_MOUSE and TMM27_MOUSE) and angiotensin-processing enzymes (AMPN_MOUSE, AMPE_MOUSE and NEP_MOUSE) (**Table 3.4**). The latter are possibly linked to a dysregulation of the RAAS system upon UUO (Klahr and Morrissey 1998, Chevalier, Forbes and Thornhill 2009, Ucero, et al. 2014).

Interestingly, a substantial number of antioxidant enzymes was found underexpressed at 21 days post-UUO, including glutathione synthases, s-transferases, reductases, peroxidases, as well as thioredoxins, superoxide dismutase species, peroxidases and catalase (**Table 3.4**).

Few proteins know to be involved ECM digestion, such as meprin and basigin, were several-fold underexpressed in UUO mice at 21 days compared to the Sham operated control (**Table 3.4**), and also alpha-enolase, reported to promote both plasminogen activation and hypoxia tolerance, was more than 2-fold downregulated (**Table 3.4**).

Cadherin-16, known as kidney-specific cadherin, was also downregulated by UUO in a substantial manner (**Table 3.4**), and, being involved in the maintenance of tissue structure, might be associated with a large epithelial cell loss and transition.

Curiously, to conclude, while moesin was identified as upregulated by UUO, ezrin and radixin, the other two ERM-proteins, involved in cytoskeletal-plasma membrane association, were found significantly downregulated. A recent proteomic study on STZ-treated diabetic rats similarly highlighted ezrin downregulation upon disease, in line with our observations (Gong, et al. 2009).

To summarize, the proteins identified as underexpressed in mice kidneys subjected to 21-days UUO were represented by a large percentage of proteins in different ways associated with cell metabolism and energy production, but also included a few proteins directly involved in the control of kidney functionality and physiological response to stress. Among these, the substantial downregulation of antioxidant protein is an interesting finding that might be worth investigating in future, to understand if it is correct considering it a genuine stress response to UUO or it is more likely to be a mere effect of cell death.

In the next sections, a functional analysis of the proteins overexpressed and underexpressed in the UUO-associated proteome will be provided, with the aim of highlighting specific clusters of proteins significantly upregulated or downregulated in the model.

Table 3.4: Highlight of interesting protein groups identified as significantly underexpressed in kidneys at 21 days post-UUO. Comprehensive list of protein can be found in the Supplementary material (**Suppl. Table 3.6**). In increasing shades of red the absolute fold change decrease of UUO from Sham operated condition, in increasing shades of yellow the confident of fold change C(FC). A C(FC) higher than 80% (0.8) was regarded as significant

Highlighted	Examples		FC (Sham/UUO)	C(FC)
Kidney Function	Solute carrier family 12 member 1	S12A1_MOUSE	6.91	0.96
	Solute carrier family 13 member 3	S13A3_MOUSE	9.52	0.88
	Solute carrier family 22 member 18	S22AI_MOUSE	9.86	0.90
	Solute carrier family 22 member 2	S22A2_MOUSE	12.29	0.81
	Solute carrier family 2, facilitated glucose transporter member 1	GTR1_MOUSE	2.58	0.80
	Sodium/glucose cotransporter 2	SC5A2_MOUSE	16.23	0.80
	Na(+)/H(+) exchange regulatory cofactor NHE-RF3	NHRF3_MOUSE	10.71	0.86
	Chloride intracellular channel protein 5	CLIC5_MOUSE	4.18	0.85
	Calbindin	CALB1_MOUSE	32.07	0.91
	Aquaporin-1	AQP1_MOUSE	6.91	0.80
	Aquaporin-3	AQP3_MOUSE	6.51	0.90
	L-xylulose reductase	DCXR_MOUSE	5.92	0.88
	Prostaglandin E synthase 2	PGES2_MOUSE	6.29	0.89
	Prostaglandin reductase 2	PTGR2_MOUSE	3.79	0.89
	Sulfotransferase 1 family member D1	ST1D1_MOUSE	13.74	0.85
Blood pressure - RAAS independent	Argininosuccinate synthase	ASSY_MOUSE	21.28	0.88
	Cystathionine gamma-lyase	CGL_MOUSE	16.04	0.86
Control Angiotensin	Angiotensin-converting enzyme	ACE_MOUSE	12.66	0.91
	Collectrin	TMM27_MOUSE	14.41	0.85
	Aminopeptidase N	AMPN_MOUSE	3.83	0.95
	Glutamyl aminopeptidase	AMPE_MOUSE	4.21	0.87
	Neprilysin	NEP_MOUSE	8.05	0.90
Antioxidant enzymes	Catalase	CATA_MOUSE	12.62	0.94
	Glutathione peroxidase 1	GPX1_MOUSE	3.45	0.92
	Glutathione peroxidase 3	GPX3_MOUSE	1.54	0.83
	Glutathione reductase, mitochondrial	GSHR_MOUSE	2.33	0.80
	Glutathione S-transferase A2	GSTA2_MOUSE	17.14	0.85
	Glutathione S-transferase A3	GSTA3_MOUSE	10.63	0.81
	Glutathione S-transferase A4	GSTA4_MOUSE	3.61	0.86
	Glutathione S-transferase kappa 1	GSTK1_MOUSE	12.27	0.82
	Glutathione S-transferase Mu 1	GSTM1_MOUSE	2.37	0.89
	Glutathione S-transferase Mu 5	GSTM5_MOUSE	3.27	0.87
	Glutathione S-transferase P 1	GSTP1_MOUSE	1.77	0.94
	Glutathione S-transferase theta-2	GSTT2_MOUSE	5.84	0.87
	Glutathione synthetase	GSHB_MOUSE	5.17	0.82
	Microsomal glutathione S-transferase 3	MGST3_MOUSE	7.12	0.84
	Peroxiredoxin-1	PRDX1_MOUSE	2.03	0.91
	Peroxiredoxin-5, mitochondrial	PRDX5_MOUSE	6.30	0.91
	Peroxiredoxin-6	PRDX6_MOUSE	2.23	0.94
	Superoxide dismutase [Cu-Zn]	SODC_MOUSE	3.33	0.94
	Superoxide dismutase [Mn], mitochondrial	SODM_MOUSE	11.66	0.93
	Copper chaperone for superoxide dismutase	CCS_MOUSE	2.75	0.99
	Thioredoxin reductase 2, mitochondrial	TRXR2_MOUSE	4.29	0.83
	Thioredoxin, mitochondrial	THIOM_MOUSE	4.90	0.90
	Thioredoxin-dependent peroxide reductase, mitochondrial	PRDX3_MOUSE	5.23	0.90
Anti-fibrotic	Meprin A subunit alpha	MEP1A_MOUSE	7.15	0.88
	Meprin A subunit beta	MEP1B_MOUSE	14.72	0.82
	Basigin	BASI_MOUSE	4.09	0.87
	Alpha-enolase	ENOA_MOUSE	2.51	0.98
Other	Cadherin-16	CAD16_MOUSE	19.54	0.92
	Radixin	RADI_MOUSE	2.79	0.83
	Ezrin	EZRI_MOUSE	3.13	0.96

3.4.4.4 Functional distribution of UUO-overexpressed and -underexpressed proteins

Functional classification of the differentially expressed proteins identified by SWATH-MS was performed in PANTHER as described in 3.3.7, investigating the GO terms for Biological Processes, Molecular Functions and Cellular Components as well as the PANTHER Protein class terms. Results were visualized in pie charts as percentage of representation of the different annotation classes in the list.

The GO annotations for Biological Processes (**Fig. 3.10A**) revealed that the majority of proteins significantly lowered by UUO have a role in metabolism: 69.9% of the proteins underexpressed by UUO were falling into the "metabolic process" (GO:0008152) annotation term. This was more than the half (55.2%) of the total class hits, which means that most of the metabolic proteins were only associated with this annotation term (**Fig. 3.10A**). On the other side, the 45.9% of the UUO- overexpressed proteins were in some way associated with metabolic processes, but they represent only the 17.5% of the total annotation term hits (**Fig. 3.10A**): this means that these proteins were associated not exclusively with metabolism but also to other processes (they fall in more than one annotation term). Among the Biological processes more represented in UUO, "cellular component organization or biogenesis" (GO:0071840) and cellular process (GO:0009987) covered more than a quarter of the total class hits [10.1% (26.5% of proteins) and 20.1% (53.0% of proteins), respectively], while they were less represented among the 458 proteins underexpressed in UUO [2.6% (3,3% of the proteins) and 11.6% (14.7% of the proteins), respectively] (**Fig. 3.10A**). Interestingly, there was also a higher amount of proteins associated with immune system [immune system process (GO:0002376) 11.4%], apoptosis [apoptotic process (GO:0006915), 2.7%] and adhesion [biological adhesion (GO:0022610), 10.8%] upon UUO induction, which were lower in the list of UUO-underexpressed proteins (**Fig. 3.10A**).

A

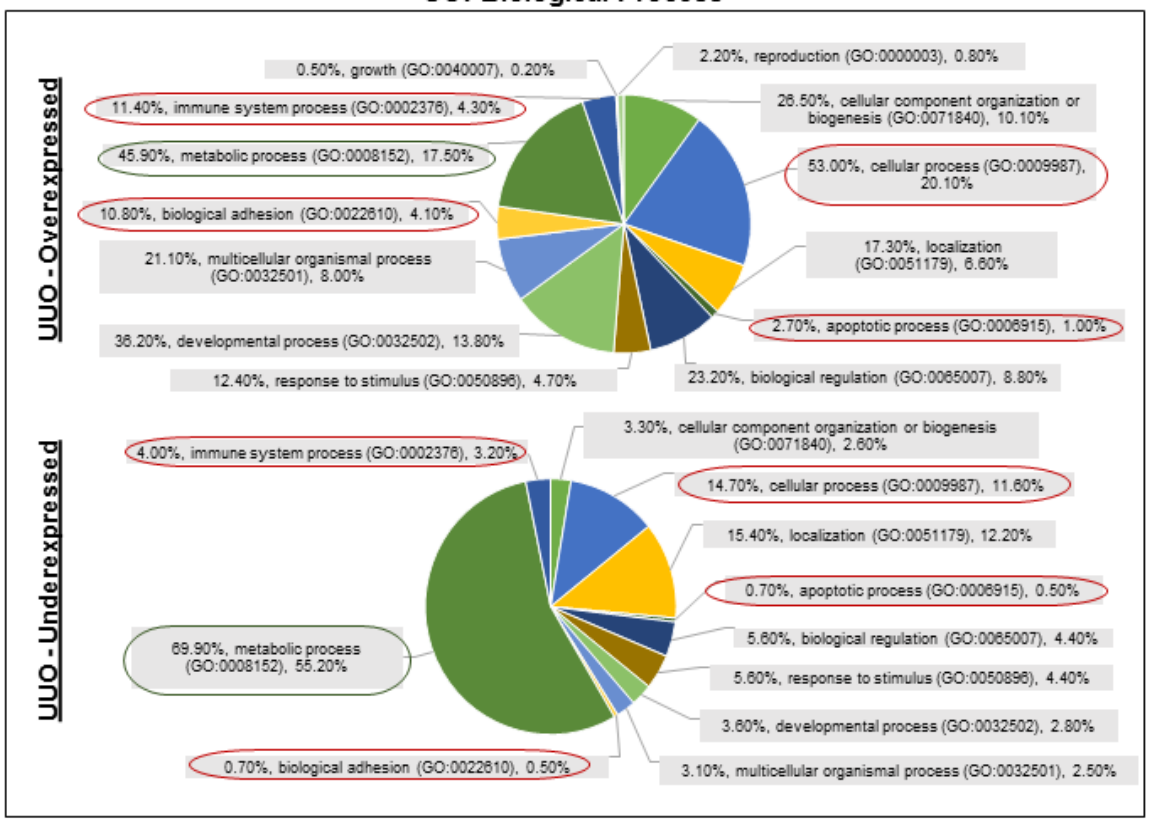

Among the GO terms for Molecular Functions (**Fig.3.10B**), a high percentage of proteins (31.9%) was associated with structural activity [structural molecule activity (GO:0005198)] in the UUO model and was possibly mostly associated with the substantial amount of proteins attributable to the cytoskeleton (**Suppl. Table 3.5**) and to the smooth muscle/mesenchymal phenotype of the cells (**Table 3.8**); they represented the 22.9% of total class hits among the UUO-overexpressed proteins, in contrast to only the 5.7% in the UUO-underexpressed list (**Fig.3.10B**). "Binding" (GO:0005488) molecular function was also associated with the UUO-overexpressed proteins, covering the 42.2% of the proteins (30.2% of total class hits) against the 10.5% of the opposite group (11.1% of total class hits) (**Fig.3.10B**). This might be directly linked to many adhesion proteins and proteins involved in nuclear acid binding among the UUO-overexpressed members of the proteome (**Suppl. Table 3.5**).

As expected, "Catalytic activity" (GO:0003824) function was less represented in the group of proteins overexpressed in the UUO model (29.7% of the proteins, 21.3% of total class hits) in comparison to a substantial representation in the UUO-underexpressed proteins, where the 61.4% of members belong to this annotation term (64.9% of total class hits) (**Fig.3.10B**). In addition, ability to be involved in antioxidant response is also lowered by the UUO, with the "antioxidant activity" (GO:0016209) annotation term being present only in the list of UUO-

underexpressed proteins (2.1% of total class hits) (**Fig.3.10B**), in line with previous observations [3.4.4.3].

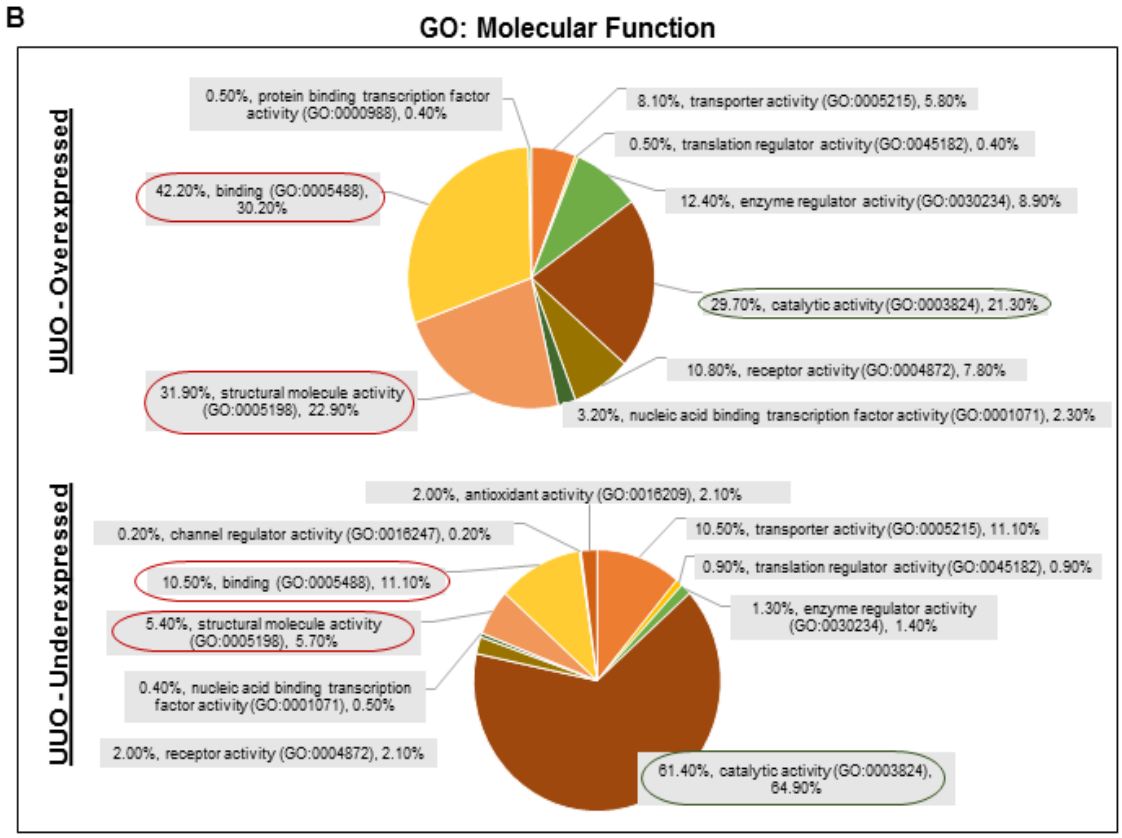

Cellular compartments were also analyzed (**Fig.3.10C**) with the same approach. The UUO-overexpressed proteins were characterized by a substantial amount of proteins belonging to extracellular region (GO:0005576) (17.6% of total class hits) or extracellular matrix (GO:0031012) (9.3% of total class hits), that were considerably lower among the UUO-underexpressed proteins (1.9% and 1.3% respectively) (**Fig.3.10C**). In the latter group, on the other hand, a great amount of proteins was not associated at all with any cell component (around the 65% of proteins) and the remaining were belonging mostly to membranes (GO:0016020, 15.0% of total class hits), organelles (GO:0043226, 23.1% of total class hits) and cell parts, including the plasma membrane (GO:0044464, 45.0% of total class hits) (**Fig.3.10C**).

C

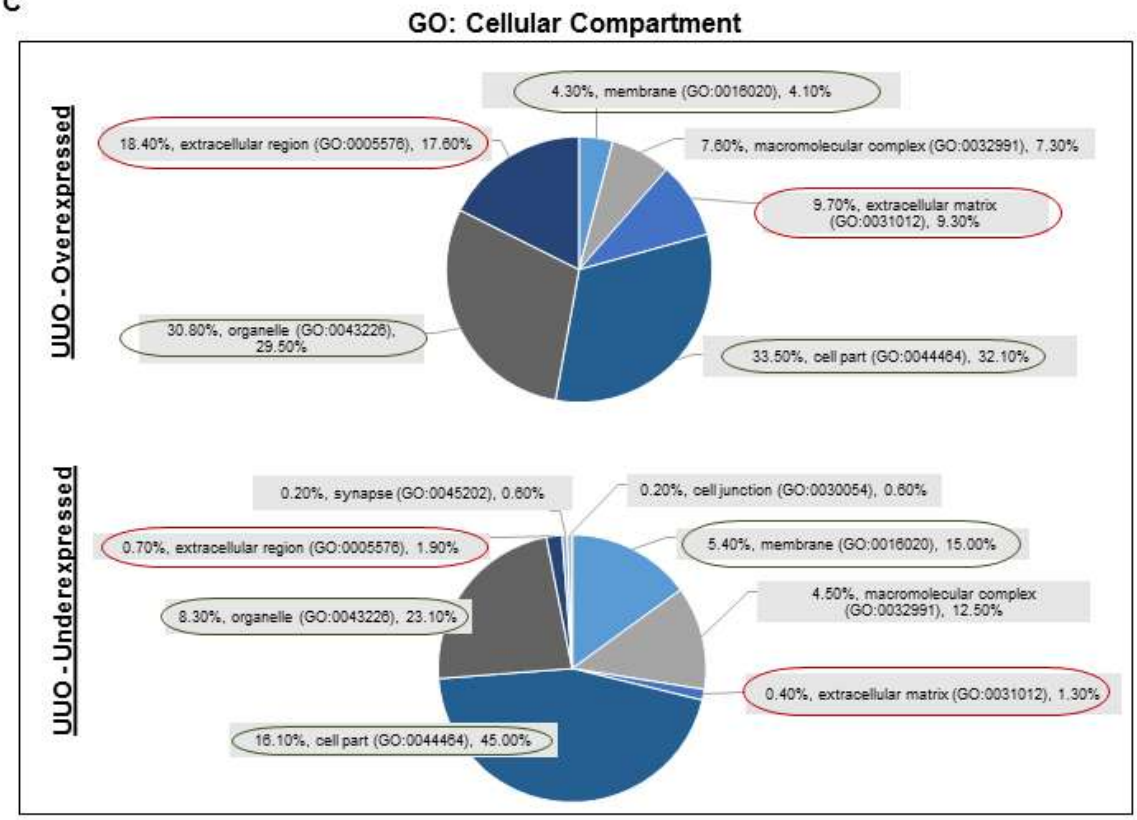

Finally, PANTHER Protein Class annotation terms (**Fig.3.10D**) allowed to determine more specifically to which functional group the proteins were belonging. The four classes more represented in the UUO-overexpressed list were “extracellular matrix protein” (PC00102, 8.3%), “receptor” (PC00197, 8.3%, almost exclusively for cytokines), “enzyme modulator” (PC00095, 10.3%) and, above all, “cytoskeletal protein” (PC00085, 20.2%) (**Fig.3.10D**).

In line with the previous findings, the PANTHER Protein classes more represented among the UUO-underexpressed proteins were mostly oxidoreductases (PC00176, 24.5%), together with other metabolism-associated proteins such as transferases (PC00220, 12.4%), hydrolases (PC00121, 11.0%) and transporters (PC00227, 8.2%), of which most are associated with the mitochondrial membrane (**Fig.3.10D**).

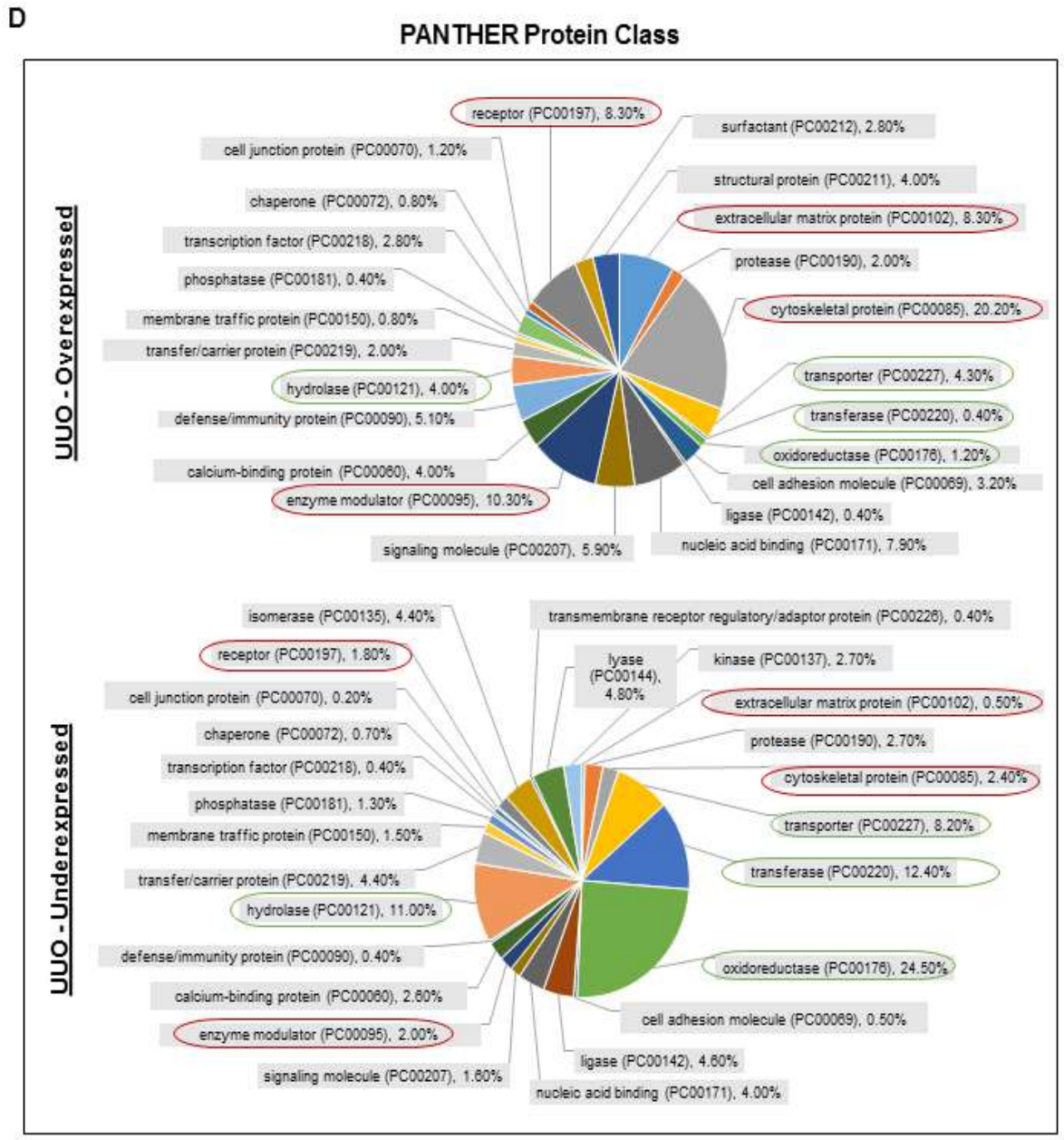

Figure 3.10: Functional distribution of UUO-overexpressed and -underexpressed proteins. ***(starts in previous pages)*** Functional distribution of UUO-Overexpressed and -Underexpressed proteins was investigated by PANTHER (http://www.pantherdb.org) using the annotation term ontologies for **(A)** PANTHER GO-slim Biological Process, **(B)** PANTHER GO-slim Molecular Function, **(C)** PANTHER GO-slim Cellular Component, **(D)** PANTHER Protein Class. Labels to be read as: % proteins belonging to the class over the number of proteins in the list, annotation term (Class), % proteins belonging to the class over the total number of class hits (for all the annotation terms individuated in the list of proteins = 100%). For PANTHER protein class only annotation term (Class) and % proteins belonging to the class over the total number of class hits are displayed. Red circles indicate terms more represented in the UUO-overexpressed protein list, green circles indicate terms more represented in UUO-underexpressed protein list, black circles indicate terms similarly represented in both lists.

The distribution of different biological pathways was also investigated using the PANTHER Pathways annotation terms on PANTHER Database (**Table 3.5, Table 3.6**).

In order of coverage, the more represented pathways among the UUO-overexpressed proteins at 21 days post-surgery (**Table 3.5**) were "Integrin signaling pathway" (P00034, 15.5%),

"Inflammation mediated by chemokine and cytokine signaling pathway" (P00031, 12.7%), "Cytoskeletal regulation by Rho GTPase" (P00016, 9.2%) and "Blood coagulation" (P00011, 6.3%), while in the UUO-underexpressed the main pathways (**Table 3.6**) were "Glycolysis" (P00024, 6.4%), "Huntington disease" (P00029, 5.7%), "TCA cycle" (P00051, 5.7%) and "De novo purine biosynthesis" (P02738, 4.5%).

Table 3.5: PANTHER Pathways representation in UUO-overexpressed proteins. Pathways represented in UUO-overexpressed proteins were investigated by PANTHER (http://www.pantherdb.org) using the annotation term ontologies for PANTHER Pathways. The table shows the pathways distribution in UUO-overexpressed proteins. The number of proteins belonging to the class and the percentage of representation over the total class hits are in increasing shades of red (the higher, the more intense).

PANTHER Pathways	n	%
Integrin signaling pathway (P00034)	22	15.50%
Inflammation mediated by chemokine and cytokine signaling pathway (P00031)	18	12.70%
Cytoskeletal regulation by Rho GTPase (P00016)	13	9.20%
Blood coagulation (P00011)	9	6.30%
Huntington disease (P00029)	7	4.90%
Nicotinic acetylcholine receptor signalling pathway (P00044)	6	4.20%
Gonadotropin releasing hormone receptor pathway (P06664)	5	3.50%
Alzheimer disease-presenilin pathway (P00004)	4	2.80%
Cadherin signaling pathway (P00012)	4	2.80%
Nicotine pharmacodynamics pathway (P06587)	3	2.10%
Heterotrimeric G-protein signaling pathway-Gi alpha and Gs alpha mediated pathway (P00026)	3	2.10%
Wnt signaling pathway (P00057)	3	2.10%
FAS signaling pathway (P00020)	3	2.10%
Dopamine receptor mediated signaling pathway (P05912)	3	2.10%
CCKR signaling map (P06959)	3	2.10%
Metabotropic glutamate receptor group III pathway (P00039)	2	1.40%
5HT1 type receptor mediated signaling pathway (P04373)	2	1.40%
Heterotrimeric G-protein signaling pathway-rod outer segment phototransduction (P00028)	2	1.40%
Plasminogen activating cascade (P00050)	2	1.40%
Endothelin signaling pathway (P00019)	2	1.40%
Enkephalin release (P05913)	2	1.40%
Muscarinic acetylcholine receptor 2 and 4 signaling pathway (P00043)	2	1.40%
Metabotropic glutamate receptor group II pathway (P00040)	2	1.40%
Beta2 adrenergic receptor signaling pathway (P04378)	1	0.70%
Axon guidance mediated by semaphorins (P00007)	1	0.70%
Beta1 adrenergic receptor signaling pathway (P04377)	1	0.70%
GABA-B_receptor_II_signaling (P05731)	1	0.70%
p53 pathway (P00059)	1	0.70%
Heterotrimeric G-protein signaling pathway-Gq alpha and Go alpha mediated pathway (P00027)	1	0.70%
Vitamin D metabolism and pathway (P04396)	1	0.70%
Vasopressin synthesis (P04395)	1	0.70%
General transcription by RNA polymerase I (P00022)	1	0.70%
FGF signaling pathway (P00021)	1	0.70%
EGF receptor signaling pathway (P00018)	1	0.70%
Parkinson disease (P00049)	1	0.70%
Opioid proopiomelanocortin pathway (P05917)	1	0.70%
Opioid prodynorphin pathway (P05916)	1	0.70%
Histamine H2 receptor mediated signaling pathway (P04386)	1	0.70%
Opioid proenkephalin pathway (P05915)	1	0.70%
Cell cycle (P00013)	1	0.70%
Metabotropic glutamate receptor group I pathway (P00041)	1	0.70%
Cortocotropin releasing factor receptor signaling pathway (P04380)	1	0.70%
Pyrimidine Metabolism (P02771)	1	0.70%

Table 3.6: PANTHER Pathways representation in UUO-underexpressed proteins. Pathways represented in UUO-underexpressed proteins were investigated by PANTHER (http://www.pantherdb.org) using the annotation term ontologies for PANTHER Pathways. The table shows the pathways distribution in UUO-underexpressed proteins. The number of proteins belonging to the class and the percentage of representation over the total class hits are in increasing shades of green (the higher, the more intense).

PANTHER Pathways	N	%
Glycolysis (P00024)	10	6.40%
Huntington disease (P00029)	9	5.70%
TCA cycle (P00051)	9	5.70%
De novo purine biosynthesis (P02738)	7	4.50%
ATP synthesis (P02721)	6	3.80%
Wnt signaling pathway (P00057)	5	3.20%
Cadherin signaling pathway (P00012)	5	3.20%
Fructose galactose metabolism (P02744)	5	3.20%
Pyruvate metabolism (P02772)	5	3.20%
Alzheimer disease-presenilin pathway (P00004)	4	2.50%
Inflammation mediated by chemokine and cytokine signaling pathway (P00031)	4	2.50%
Parkinson disease (P00049)	4	2.50%
Cytoskeletal regulation by Rho GTPase (P00016)	4	2.50%
Apoptosis signaling pathway (P00006)	3	1.90%
Arginine biosynthesis (P02728)	3	1.90%
N-acetylglucosamine metabolism (P02756)	3	1.90%
Methylmalonyl pathway (P02755)	3	1.90%
Nicotinic acetylcholine receptor signaling pathway (P00044)	3	1.90%
De novo pyrmidine ribonucleotides biosythesis (P02740)	3	1.90%
Pyrimidine Metabolism (P02771)	3	1.90%
De novo pyrimidine deoxyribonucleotide biosynthesis (P02739)	2	1.30%
Integrin signalling pathway (P00034)	2	1.30%
Pentose phosphate pathway (P02762)	2	1.30%
Asparagine and aspartate biosynthesis (P02730)	2	1.30%
Heterotrimeric G-protein signaling pathway-Gi alpha and Gs alpha mediated pathway (P00026)	2	1.30%
Aminobutyrate degradation (P02726)	2	1.30%
O-antigen biosynthesis (P02757)	2	1.30%
Vitamin B6 metabolism (P02787)	2	1.30%
Leucine biosynthesis (P02749)	2	1.30%
Heme biosynthesis (P02746)	2	1.30%
Gamma-aminobutyric acid synthesis (P04384)	2	1.30%
Succinate to proprionate conversion (P02777)	2	1.30%
Glutamine glutamate conversion (P02745)	2	1.30%
Dopamine receptor mediated signaling pathway (P05912)	2	1.30%
Salvage pyrimidine ribonucleotides (P02775)	2	1.30%
Coenzyme A biosynthesis (P02736)	1	0.60%
Phenylethylamine degradation (P02766)	1	0.60%
Hypoxia response via HIF activation (P00030)	1	0.60%
Nicotine pharmacodynamics pathway (P06587)	1	0.60%
Ascorbate degradation (P02729)	1	0.60%
Heterotrimeric G-protein signaling pathway-Gq alpha and Go alpha mediated pathway (P00027)	1	0.60%
Vitamin D metabolism and pathway (P04396)	1	0.60%
Transcription regulation by bZIP transcription factor (P00055)	1	0.60%
Alanine biosynthesis (P02724)	1	0.60%
Methylcitrate cycle (P02754)	1	0.60%
FGF signaling pathway (P00021)	1	0.60%
Acetate utilization (P02722)	1	0.60%
Valine biosynthesis (P02785)	1	0.60%
TGF-beta signaling pathway (P00052)	1	0.60%
Methionine biosynthesis (P02753)	1	0.60%
FAS signaling pathway (P00020)	1	0.60%
Tryptophan biosynthesis (P02783)	1	0.60%
Plasminogen activating cascade (P00050)	1	0.60%
Threonine biosynthesis (P02781)	1	0.60%
Endothelin signaling pathway (P00019)	1	0.60%
EGF receptor signaling pathway (P00018)	1	0.60%
Isoleucine biosynthesis (P02748)	1	0.60%
Blood coagulation (P00011)	1	0.60%

Formyltetrahydroformate biosynthesis (P02743)	1	0.60%
Angiotensin II-stimulated signaling through G proteins and beta-arrestin (P05911)	1	0.60%
Salvage pyrimidine deoxyribonucleotides (P02774)	1	0.60%
CCKR signaling map (P06959)	1	0.60%
Pyridoxal phosphate salvage pathway (P02770)	1	0.60%
Gonadotropin releasing hormone receptor pathway (P06664)	1	0.60%

3.4.4.5 Statistical overrepresentation test on UUO-overexpressed and -underexpressed proteins

In order to determine which GO terms were significantly enriched or downregulated upon UUO in comparison with their distribution in the whole *Mus Musculus* gene expression, a statistical overrepresentation test was performed employing both PANTHER and DAVID bioinformatics tools. Results from the test performed by PANTHER are shown in **Table 3.7 – 3.10**. As for the previous paragraph, the GO terms for Biological Process, Molecular Function and Cellular Component, in addition to PANTHER Protein Class terms, were analysed. A series of annotation terms were found significantly enriched upon UUO (in the list of UUO-overexpressed proteins) with a p-value of the analysis lower than 0.05 (in bold in the different tables). Other terms were significantly enriched among the UUO-underexpressed protein ($p \leq 0.05$), therefore we can consider them significantly reduced by UUO at 21-days post-surgery.

Within the Biological Processes, a number of terms were significantly enriched upon UUO ($p \leq 0.05$) (in bold in **Table 3.7**). Several terms were found associated with cell adhesion (black arrows), a feature that is strongly represented in interstitial fibroblast/myofibroblasts, RNA modification/translation (grey arrows) and inflammation mediated by cytokines (white arrows). A significant reduction, in line with the previous results reported in 3.4.4.3-3.4.4.4, was found in a series of catalytic/metabolic processes (asterisks, *).

Molecular Functions (**Table 3.8**) significantly enriched by UUO where associated with cytoskeletal organisation and actin binding (black arrows) and regulation of enzymatic activities in cells (white arrows), which were mostly proteolytic. Significantly enriched were also “extracellular matrix structural constituent” GO term (GO:0005201) (light grey arrow) and the "mRNA binding” function (GO:0003729) (dark grey arrow), which is in line with the previous annotation terms identified above for Biological processes and associated with splicing and translation mechanisms. Reduced proteins were again mostly metabolic (asterisks, *), and some of them were directly related to redox regulation (**).

Cellular components overrepresented in the list of proteins differentially expressed by UUO are displayed in **Table 3.9**. This analysis clearly identified that cytoskeletal (dark arrows) and extracellular proteins (grey arrows), most of which belonging to the ECM, were enriched upon UUO, confirming what seen by a preliminary examination of protein names [3.4.4.2]. On the

other hand, UUO-underexpressed protein significantly represented the cytoplasmic and mitochondrial compartments of the cells (asterisk, *), in line with previous speculations [3.4.4.3].

Finally, PANTHER Protein classes significantly modulated by UUO were investigated, and results are shown in **Table 3.10**. PANTHER classes enriched by UUO were again associated with cytoskeletal organisation and actin binding (black arrows) and extracellular matrix composition and organisation (light grey arrow). In addition to these, also regulation of proteolytic activity (white arrows) and mRNA splicing/processing (dark grey arrows) were enriched by UUO. Classes of proteins whose annotation keys were significantly lowered during UUO were as usual metabolic (asterisks, *) and in part associated with redox regulation (**).

Similar outcomes were also obtained by investigating the GO terms in DAVID bioinformatics resource, and results can be found in the appendix of this thesis (**Suppl. Table 3.7 – 3.12**).

In conclusion, these analyses statistically confirmed that functions associated with cytoskeletal assembly and regulation, extracellular matrix dynamics, cell adhesion, inflammatory response and transcriptional modulation are significantly enriched at 21 days post-UUO, while significantly underrepresented in the model are functions associated with cell metabolism and redox regulation.

Table 3.7: GO Biological Process overrepresentation test on UUO-overexpressed and -underexpressed proteins performed by PANTHER. Statistical overrepresentation test was performed by PANTHER (http://www.pantherdb.org) using the annotation terms for PANTHER GO-slim Biological Process. Legend: Black arrows =terms associated with cell adhesion; grey arrows = terms associated with RNA modification and translation; white arrows = terms associated with inflammation. * = terms associated with catalytic/metabolic processes. +, red = overrepresented term (fold change from expected value H_0 >1); -, green = underrepresented term (fold change from expected value H_0 <1). In increasing shades of grey = fold change from the expected value H_0 (the more intense, the higher the fold change). In increasing shades of blue = p-value (the more intense, the lower the p-value). A p-value lower than 0.05 was regarded as significant.

Significantly enriched GO Terms : Biological process

	PANTHER GO-Slim Biological Process	UUO-Overexpressed			UUO-Underexpressed		
			Fold change	p-value		Fold change	p-value
	anatomical structure morphogenesis (GO:0009653)	+	8.06	1.72E-21	-	0.68	1.00E+00
	cellular component organization (GO:0016043)	+	4.99	9.72E-19	-	0.55	1.00E+00
	cellular component morphogenesis (GO:0032989)	+	8.54	1.27E-18	-	0.53	1.00E+00
	cellular component organization or biogenesis (GO:0071840)	+	4.55	4.14E-17	-	0.58	1.00E+00
	developmental process (GO:0032502)	+	3.28	5.64E-17	-	0.32	1.55E-06
	muscle contraction (GO:0006936)	+	8.58	2.33E-08	-	0.66	1.00E+00
	system process (GO:0003008)	+	3.06	1.30E-07	-	0.47	1.44E-01
	cellular process (GO:0009987)	+	1.68	2.69E-07	-	0.47	5.16E-14
➡	cell-cell adhesion (GO:0016337)	+	5.67	2.85E-06	-	0.41	1.00E+00
	mesoderm development (GO:0007498)	+	3.93	6.38E-06	-	0.21	7.90E-02
	single-multicellular organism process (GO:0044707)	+	2.57	8.87E-06	-	0.38	1.99E-03
	multicellular organismal process (GO:0032501)	+	2.57	9.40E-06	-	0.38	1.88E-03
➡	cell-matrix adhesion (GO:0007160)	+	12.34	1.57E-05	-	< 0.2	1.00E+00
➡	mRNA processing (GO:0006397)	+	6.21	1.91E-05	-	< 0.2	9.09E-01
➡	biological adhesion (GO:0022610)	+	4.18	2.05E-05	-	0.26	6.41E-01
➡	cell adhesion (GO:0007155)	+	4.17	4.61E-05	-	0.27	9.77E-01
➡	RNA splicing, via transesterification reactions (GO:0000375)	+	9.07	4.89E-05	-	< 0.2	1.00E+00
	homeostatic process (GO:0042592)	+	6.96	4.99E-05	+	1.68	1.00E+00
➡	RNA splicing (GO:0008380)	+	8.87	5.98E-05	-	< 0.2	1.00E+00
⇨	cytokinesis (GO:0000910)	+	9.96	9.26E-05	-	< 0.2	1.00E+00
	regulation of liquid surface tension (GO:0050828)	+	15.36	1.09E-04	-	< 0.2	1.00E+00
➡	mRNA splicing, via spliceosome (GO:0000398)	+	7.1	1.33E-04	-	< 0.2	1.00E+00
	cellular component movement (GO:0006928)	+	4.17	4.38E-04	-	0.22	1.00E+00
	ectoderm development (GO:0007398)	+	3.3	4.30E-03	-	0.32	1.00E+00
	endocytosis (GO:0006897)	+	4.13	4.56E-03	-	0.66	1.00E+00
	regulation of catalytic activity (GO:0050790)	+	2.56	5.38E-03	-	0.31	2.05E-02
	regulation of molecular function (GO:0065009)	+	2.51	7.41E-03	-	0.35	4.59E-02
	muscle organ development (GO:0007517)	+	4.58	8.00E-03	-	< 0.2	6.31E-01
	intracellular protein transport (GO:0006886)	+	2.57	1.19E-02	-	0.72	1.00E+00
	system development (GO:0048731)	+	2.37	1.30E-02	-	< 0.2	2.14E-05
	protein transport (GO:0015031)	+	2.5	1.75E-02	-	0.7	1.00E+00
⇨	macrophage activation (GO:0042116)	+	5.58	2.50E-02	-	0.29	1.00E+00
	fatty acid metabolic process (GO:0006631)	+	3.83	2.92E-01	+	8.5	9.57E-24
	cell cycle (GO:0007049)	+	2.03	6.18E-01	-	0.27	5.85E-03
	phosphate ion transport (GO:0006817)	-	< 0.2	1.00E+00	+	4.53	4.77E-02
	nucleobase-containing compound metabolic process (GO:0006139)	+	1.09	1.00E+00	-	0.61	2.99E-02
	nervous system development (GO:0007399)	+	1.85	1.00E+00	-	< 0.2	2.19E-02
*	glycolysis (GO:0006096)	-	< 0.2	1.00E+00	+	10.31	7.07E-03
*	ferredoxin metabolic process (GO:0006124)	-	< 0.2	1.00E+00	+	24.91	5.32E-03
*	gluconeogenesis (GO:0006094)	-	< 0.2	1.00E+00	+	16.61	3.48E-03
	response to stimulus (GO:0050896)	+	1.08	1.00E+00	-	0.49	3.21E-03
*	steroid metabolic process (GO:0008202)	+	1.83	1.00E+00	+	4.28	1.92E-04
*	purine nucleobase metabolic process (GO:0006144)	-	< 0.2	1.00E+00	+	6.57	1.07E-04
	cation transport (GO:0006812)	-	< 0.2	1.00E+00	+	2.75	8.83E-05
*	vitamin metabolic process (GO:0006766)	-	< 0.2	1.00E+00	+	11.59	5.87E-06
*	vitamin biosynthetic process (GO:0009110)	-	< 0.2	1.00E+00	+	14.46	4.54E-06
	ion transport (GO:0006811)	-	0.5	1.00E+00	+	2.76	2.89E-06
*	monosaccharide metabolic process (GO:0005996)	-	0.81	1.00E+00	+	6.02	5.91E-07
	response to toxic substance (GO:0009636)	-	< 0.2	1.00E+00	+	10.87	4.84E-07
	regulation of transcription from RNA polymerase II promoter (GO:0006357)	-	0.67	1.00E+00	-	< 0.2	3.75E-07
*	acyl-CoA metabolic process (GO:0006637)	-	< 0.2	1.00E+00	+	19.29	7.66E-10
	regulation of nucleobase-containing compound metabolic process (GO:0019219)	-	0.6	1.00E+00	-	< 0.2	3.07E-10
*	cellular amino acid biosynthetic process (GO:0008652)	-	< 0.2	1.00E+00	+	10.72	2.74E-10
*	tricarboxylic acid cycle (GO:0006099)	-	< 0.2	1.00E+00	+	26.1	2.50E-10
	cell communication (GO:0007154)	+	1.22	1.00E+00	-	0.28	2.16E-10
*	cellular amino acid catabolic process (GO:0009063)	-	< 0.2	1.00E+00	+	14.1	1.29E-10
	transcription from RNA polymerase II promoter (GO:0006366)	-	0.65	1.00E+00	-	< 0.2	9.04E-11
	transcription, DNA-dependent (GO:0006351)	-	0.58	1.00E+00	-	< 0.2	1.46E-12
	regulation of biological process (GO:0050789)	-	0.84	1.00E+00	-	< 0.2	5.00E-13
	biological regulation (GO:0065007)	+	1.27	1.00E+00	-	0.3	3.79E-13
*	primary metabolic process (GO:0044238)	+	1.1	1.00E+00	+	1.58	1.92E-13
	RNA metabolic process (GO:0016070)	+	1.04	1.00E+00	-	< 0.2	2.68E-15
*	carbohydrate metabolic process (GO:0005975)	-	0.42	1.00E+00	+	5.09	7.68E-22
*	fatty acid beta-oxidation (GO:0006635)	-	< 0.2	1.00E+00	+	32.7	1.37E-22
*	coenzyme metabolic process (GO:0006732)	-	< 0.2	1.00E+00	+	15.41	2.55E-23
	cellular amino acid metabolic process (GO:0006520)	-	< 0.2	1.00E+00	+	8.34	5.40E-24
	lipid metabolic process (GO:0006629)	+	1.12	1.00E+00	+	4.18	3.73E-25
*	oxidative phosphorylation (GO:0006119)	-	< 0.2	1.00E+00	+	23.19	1.92E-25
*	metabolic process (GO:0008152)	+	1.21	1.00E+00	+	1.84	2.72E-40
*	respiratory electron transport chain (GO:0022904)	-	< 0.2	1.00E+00	+	13.11	3.61E-44
*	generation of precursor metabolites and energy (GO:0006091)	-	< 0.2	1.00E+00	+	13.4	6.16E-59

Table 3.8: GO Molecular Function overrepresentation test on UUO-overexpressed and -underexpressed proteins performed by PANTHER. Statistical overrepresentation test was performed by PANTHER (http://www.pantherdb.org) using the annotation terms for PANTHER GO-slim Molecular Function. Legend: Black arrows = terms associated with cytoskeletal organisation and actin binding; white arrows = terms associated with regulation of enzymatic activities in cells; light grey arrow = "extracellular matrix structural constituent"; Dark grey arrow = "mRNA binding"; * = metabolic terms; ** = redox regulation-associated terms. +, red = overrepresented term (fold change from expected value H_0 >1); -, green = underrepresented term (fold change from expected value H_0 <1). In increasing shades of grey = fold change from the expected value H_0 (the more intense, the higher the fold change). In increasing shades of blue = p-value (the more intense, the lower the p-value). A p-value lower than 0.05 was regarded as significant.

Significantly enriched GO Terms : Molecular Function

	PANTHER GO-Slim Molecular Function	UUO-Overexpressed			UUO-Underexpressed		
			Fold change	p-value		Fold change	p-value
➡	**structural molecule activity (GO:0005198)**	+	6.7	4.94E-30	+	1.12	1.00E+00
➡	**structural constituent of cytoskeleton (GO:0005200)**	+	8.58	4.39E-27	+	1	1.00E+00
➡	**actin binding (GO:0003779)**	+	10.38	1.11E-09	+	1.07	1.00E+00
➡	**cytoskeletal protein binding (GO:0008092)**	+	7.42	1.39E-07	-	0.77	1.00E+00
	protein binding (GO:0005515)	+	2.23	1.73E-06	-	0.5	1.44E-03
⇨	**extracellular matrix structural constituent (GO:0005201)**	+	14.87	2.46E-06	-	< 0.2	1.00E+00
	binding (GO:0005488)	+	1.64	1.55E-04	-	0.41	8.49E-14
➡	**mRNA binding (GO:0003729)**	+	7.65	6.03E-04	-	< 0.2	1.00E+00
⇨	**peptidase inhibitor activity (GO:0030414)**	+	5.03	1.06E-03	-	< 0.2	4.99E-01
⇨	**enzyme inhibitor activity (GO:0004857)**	+	3.96	2.65E-03	-	0.23	1.00E+00
	calcium ion binding (GO:0005509)	+	3.89	3.16E-03	+	1.72	1.00E+00
⇨	**enzyme regulator activity (GO:0030234)**	+	2.63	4.28E-03	-	0.28	1.35E-02
	hydrolase activity (GO:0016787)	+	1.94	1.06E-02	+	1.34	1.00E+00
	peptidase activity (GO:0008233)	+	2.83	2.16E-02	+	1.1	1.00E+00
	transferase activity (GO:0016740)	-	0.3	4.30E-01	+	2.22	4.49E-08
	DNA binding (GO:0003677)	-	0.4	9.29E-01	-	< 0.2	1.62E-07
*	amino acid transmembrane transporter activity (GO:0015171)	-	< 0.2	1.00E+00	+	5.11	3.64E-02
	transaminase activity (GO:0008483)	-	< 0.2	1.00E+00	+	10.38	2.39E-02
*	nucleotide kinase activity (GO:0019201)	-	< 0.2	1.00E+00	+	6.84	1.56E-02
	transporter activity (GO:0005215)	+	1.45	1.00E+00	+	1.87	5.57E-03
	cation transmembrane transporter activity (GO:0008324)	-	< 0.2	1.00E+00	+	2.87	2.40E-03
	ligase activity (GO:0016874)	-	0.56	1.00E+00	+	2.9	5.16E-04
*	anion channel activity (GO:0005253)	-	< 0.2	1.00E+00	+	16.61	3.70E-04
*	peroxidase activity (GO:0004601)	-	< 0.2	1.00E+00	+	12.46	3.48E-04
*	carbohydrate kinase activity (GO:0019200)	-	< 0.2	1.00E+00	+	11.72	1.02E-04
**	antioxidant activity (GO:0016209)	-	< 0.2	1.00E+00	+	14.46	3.45E-06
	nucleic acid binding (GO:0003676)	-	0.96	1.00E+00	-	0.38	1.70E-06
*	proton-transporting ATP synthase activity, rotational mechanism (GO:0046933)	-	< 0.2	1.00E+00	+	22.14	8.29E-07
	receptor activity (GO:0004872)	+	1.24	1.00E+00	-	0.23	4.39E-07
	transferase activity, transferring acyl groups (GO:0016746)	+	2.86	1.00E+00	+	5.9	8.35E-08
	racemase and epimerase activity (GO:0016854)	-	< 0.2	1.00E+00	+	11.78	3.03E-08
	sequence-specific DNA binding transcription factor activity (GO:0003700)	-	0.51	1.00E+00	-	< 0.2	1.27E-08
*	hydro-lyase activity (GO:0016836)	-	< 0.2	1.00E+00	+	12.92	1.82E-09
*	acetyltransferase activity (GO:0016407)	-	< 0.2	1.00E+00	+	9.52	1.32E-09
	isomerase activity (GO:0016853)	+	1.33	1.00E+00	+	6.33	1.03E-09
	nucleic acid binding transcription factor activity (GO:0001071)	-	0.46	1.00E+00	-	< 0.2	4.57E-10
*	hydrogen ion transmembrane transporter activity (GO:0015078)	-	< 0.2	1.00E+00	+	16.22	9.16E-11
*	lyase activity (GO:0016829)	-	0.62	1.00E+00	+	6.61	1.63E-11
*	catalytic activity (GO:0003824)	+	1.22	1.00E+00	+	2.53	5.54E-60
**	oxidoreductase activity (GO:0016491)	-	0.7	1.00E+00	+	9.73	8.41E-89

Table 3.9: GO Cellular Component overrepresentation test on UUO-overexpressed and -underexpressed proteins, performed by PANTHER. Statistical overrepresentation test was performed by PANTHER (http://www.pantherdb.org) using the annotation terms for PANTHER GO-slim Cellular Component. Legend: Dark arrows = cytoskeletal proteins; grey arrows = extracellular proteins; * = cytoplasmic and mitochondrial proteins. +, red = overrepresented term (fold change from expected value H_0 >1); -, green = underrepresented term (fold change from expected value H_0 <1). In increasing shades of grey = fold change from the expected value H_0 (the more intense, the higher the fold change). In increasing shades of blue = p-value (the more intense, the lower the p-value). A p-value lower than 0.05 was regarded as significant.

Significantly enriched GO Terms : Cellular component

	PANTHER GO-Slim Cellular Component	UUO-Overexpressed			UUO-Underexpressed		
			Fold change	p-value		Fold change	p-value
➡	cytoskeleton (GO:0005856)	+	8.39	1.56E-28	-	0.72	1.00E+00
➡	actin cytoskeleton (GO:0015629)	+	11.57	2.73E-23	-	0.87	1.00E+00
	organelle (GO:0043226)	+	3.62	1.91E-16	-	0.97	1.00E+00
⇨	extracellular region (GO:0005576)	+	5.71	1.19E-14	-	0.21	1.35E-02
	intracellular (GO:0005622)	+	2.91	1.24E-13	+	1.18	1.00E+00
⇨	extracellular matrix (GO:0031012)	+	8.42	4.37E-10	-	0.39	1.00E+00
	cell part (GO:0044464)	+	2.39	7.47E-10	+	1.15	1.00E+00
➡	intermediate filament cytoskeleton (GO:0045111)	+	15.87	5.79E-08	-	< 0.2	1.00E+00
⇨	extracellular space (GO:0005615)	+	60.32	9.14E-04	-	< 0.2	1.00E+00
*	cytoplasm (GO:0005737)	-	0.93	1.00E+00	+	2.11	2.80E-03
*	mitochondrial inner membrane (GO:0005743)	-	< 0.2	1.00E+00	+	8.46	8.19E-05
*	proton-transporting ATP synthase complex (GO:0045259)	-	< 0.2	1.00E+00	+	22.14	2.32E-07
	mitochondrion (GO:0005739)	+	1.11	1.00E+00	+	7.31	6.50E-08

Table 3.10: PANTHER Protein Class overrepresentation test on UUO-overexpressed and -underexpressed proteins, performed by PANTHER. Statistical overrepresentation test was performed by PANTHER (http://www.pantherdb.org) using the annotation terms for PANTHER Protein Class. Legend: Black arrows = terms associated with cytoskeletal organisation and actin binding; light grey arrows = terms associated with extracellular matrix composition and organisation; white arrows = proteolytic activity; dark grey arrows = mRNA splicing/processing. * = metabolic terms; ** = redox regulation-associated terms. +, red = overrepresented term (fold change from expected value H_0 >1); -, green = underrepresented term (fold change from expected value H_0 <1). In increasing shades of grey = fold change from the expected value H_0 (the more intense, the higher the fold change). In increasing shades of blue = p-value (the more intense, the lower the p-value). A p-value lower than 0.05 was regarded as significant.

Significantly enriched Protein Class (PANTHER)

	PANTHER Protein Class	UUO-Overexpressed			UUO-Underexpressed		
			Fold change	p-value		Fold change	p-value
➡	cytoskeletal protein (PC00085)	+	7.82	1.99E-28	-	0.82	1.00E+00
➡	actin family cytoskeletal protein (PC00041)	+	11.33	2.49E-25	-	0.89	1.00E+00
⇨	extracellular matrix protein (PC00102)	+	6.76	1.92E-09	-	0.4	1.00E+00
➡	non-motor actin binding protein (PC00165)	+	9.05	4.09E-08	-	1	1.00E+00
➡	intermediate filament (PC00129)	+	14.19	7.22E-07	-	< 0.2	1.00E+00
⇨	extracellular matrix structural protein (PC00103)	+	14.87	2.99E-06	-	< 0.2	1.00E+00
⇨	serine protease inhibitor (PC00204)	+	8.79	1.52E-05	-	< 0.2	1.00E+00
➡	mRNA splicing factor (PC00148)	+	9.89	2.06E-05	-	< 0.2	1.00E+00
➡	mRNA processing factor (PC00147)	+	7.99	3.86E-05	-	< 0.2	1.00E+00
	surfactant (PC00212)	+	15.36	1.01E-04	-	< 0.2	1.00E+00
➡	structural protein (PC00211)	+	7.31	3.11E-04	-	< 0.2	1.00E+00
⇨	extracellular matrix linker protein (PC00101)	+	23.2	6.28E-04	-	< 0.2	1.00E+00
➡	actin and actin related protein (PC00039)	+	20.8	1.06E-03	-	< 0.2	1.00E+00
⇨	protease inhibitor (PC00191)	+	4.7	2.51E-03	-	< 0.2	4.04E-01
⇨	enzyme modulator (PC00095)	+	2.22	2.48E-02	-	0.39	2.52E-02
➡	actin binding motor protein (PC00040)	+	10.22	3.03E-02	-	< 0.2	1.00E+00
	antibacterial response protein (PC00051)	+	5.95	4.21E-02	-	< 0.2	1.00E+00
*	transferase (PC00220)	-	< 0.2	4.95E-02	+	2.67	4.96E-11
*	nucleotide kinase (PC00172)	-	< 0.2	1.00E+00	+	6.23	3.35E-02
*	transaminase (PC00216)	-	< 0.2	1.00E+00	+	10.38	2.91E-02
	G-protein coupled receptor (PC00021)	-	< 0.2	1.00E+00	-	< 0.2	1.39E-02
	transporter (PC00227)	+	1.15	1.00E+00	+	1.93	4.81E-03
	nucleic acid binding (PC00171)	+	1.03	1.00E+00	-	0.47	3.34E-03
**	peroxidase (PC00180)	-	< 0.2	1.00E+00	+	11.96	2.87E-03
	transfer/carrier protein (PC00219)	+	1.41	1.00E+00	+	2.79	1.92E-03
	anion channel (PC00049)	-	< 0.2	1.00E+00	+	14.23	1.08E-03
*	carbohydrate kinase (PC00065)	-	< 0.2	1.00E+00	+	11.25	8.17E-04
*	hydrolase (PC00121)	-	0.77	1.00E+00	+	1.91	2.85E-04
*	ligase (PC00142)	-	0.31	1.00E+00	+	3.18	1.29E-04
	receptor (PC00197)	+	1.43	1.00E+00	-	0.28	4.20E-05
*	mitochondrial carrier protein (PC00158)	-	< 0.2	1.00E+00	+	9.61	7.16E-06
*	cation transporter (PC00068)	-	< 0.2	1.00E+00	+	4.87	1.06E-06
	acyltransferase (PC00042)	+	1.28	1.00E+00	+	7.95	3.05E-07
*	epimerase/racemase (PC00096)	-	< 0.2	1.00E+00	+	12.03	5.59E-09
	transcription factor (PC00218)	-	0.55	1.00E+00	-	< 0.2	2.07E-09
*	acetyltransferase (PC00038)	-	< 0.2	1.00E+00	+	9.41	1.90E-09
*	ATP synthase (PC00002)	-	< 0.2	1.00E+00	+	15.06	1.86E-09
*	isomerase (PC00135)	-	< 0.2	1.00E+00	+	6.99	5.53E-11
*	hydratase (PC00120)	-	< 0.2	1.00E+00	+	35.17	6.73E-13
*	lyase (PC00144)	-	< 0.2	1.00E+00	+	8.25	1.26E-13
*	oxidase (PC00175)	-	0.83	1.00E+00	+	9.28	2.02E-15
**	reductase (PC00198)	-	0.6	1.00E+00	+	10.61	1.60E-27
***	dehydrogenase (PC00092)	-	0.91	1.00E+00	+	16.29	3.41E-73
	oxidoreductase (PC00176)	-	0.56	1.00E+00	+	10.38	1.77E-91

3.4.4.6 Statistical overrepresentation test of PANTHER Pathways and KEGG Pathways upregulated or downregulated upon UUO

In order to determine which molecular pathways were significantly enriched by UUO, statistical overrepresentation analysis was carried out using both PANTHER Pathways annotation terms of PANTHER bioinformatic tool and KEGG pathways annotation terms on DAVID database (**Table 3.11, 3.12**).

PANTHER Pathways significantly enriched by UUO (**Table 3.11**) were "Integrin signalling pathway" (P00034), "Cytoskeletal regulation by Rho GTPase" (P00016), "Inflammation mediated by chemokine and cytokine signalling pathway" (P00031), "Blood coagulation" (P00011) and "Nicotinic acetylcholine receptor signalling pathway" (P00044). Pathways significantly underexpressed (**Table 3.11**) were almost exclusively related to metabolism aimed to energy production. Examples of these were "Fructose galactose metabolism" (P02744), "ATP synthesis" (P02721), "Glycolysis" (P00024) and, as the more significant, "TCA cycle" (P00051).

Table 3.11: PANTHER Pathway overrepresentation test on UUO-overexpressed and -underexpressed proteins. Statistical overrepresentation test was performed by PANTHER (http://www.pantherdb.org) using the annotation terms ontologies for PANTHER Pathways. Legend: +, red = overrepresented term (fold change from expected value H_0 >1); -, green = underrepresented term (fold change from expected value H_0 <1). In increasing shades of grey = fold change from the expected value H_0 (the more intense, the higher the fold change). In increasing shades of blue = p-value (the more intense, the lower the p-value). A p-value lower than 0.05 was regarded as significant.

Significantly enriched Pathways (PANTHER)

PANTHER Pathways	UUO-Overexpressed			UUO-Underexpressed		
		Fold change	p-value		Fold change	p-value
Integrin signalling pathway (P00034)	+	15.08	4.41E-17	-	0.57	1.00E+00
Cytoskeletal regulation by Rho GTPase (P00016)	+	16.69	3.20E-10	+	2.12	1.00E+00
Inflammation mediated by chemokine and cytokine signaling pathway (P00031)	+	8.86	6.19E-10	-	0.81	1.00E+00
Blood coagulation (P00011)	+	19.05	2.73E-07	-	0.87	1.00E+00
Nicotinic acetylcholine receptor signaling pathway (P00044)	+	7.78	2.19E-02	+	1.61	1.00E+00
Methylmalonyl pathway (P02755)	-	< 0.2	1.00E+00	+	29.89	2.39E-02
De novo purine biosynthesis (P02738)	-	< 0.2	1.00E+00	+	8.72	3.15E-03
Fructose galactose metabolism (P02744)	-	< 0.2	1.00E+00	+	20.76	8.35E-04
Pyruvate metabolism (P02772)	-	< 0.2	1.00E+00	+	22.65	5.49E-04
ATP synthesis (P02721)	-	< 0.2	1.00E+00	+	27.18	1.99E-05
Glycolysis (P00024)	-	< 0.2	1.00E+00	+	16.07	1.92E-07
TCA cycle (P00051)	-	< 0.2	1.00E+00	+	40.76	4.02E-10

Overrepresented KEGG Pathways when analyzed by DAVID (**Table 3.12**) were in line with the previous analysis of PANTHER Pathways. The most enriched pathways upon UUO (**Table 3.12A**) were associated with cell adhesion and cytoskeletal dynamics [Focal adhesion (mmu04510), Tight junction (mmu04530), Regulation of actin cytoskeleton (mmu04810)], to the extracellular matrix system [ECM-receptor interaction (mmu04512)], to mRNA splicing [Spliceosome (mmu03040)] and to inflammation and wound healing [Complement and coagulation cascades (mmu04610), Leukocyte transendothelial migration (mmu04670), Fc gamma R-mediated phagocytosis (mmu04666)]. A series of disease pathways that can be related to inflammation and scarring were also enriched in this model, these pathways were associated with heart diseases [Dilated cardiomyopathy (mmu05414), Viral myocarditis (mmu05416), Hypertrophic cardiomyopathy (mmu05410)] or other pathologies [Small cell lung cancer (mmu05222), Systemic lupus erythematosus (mmu05322)]. Vascular smooth muscle contraction (mmu04270) pathway was also enriched by UUO, possibly related to the mesenchymal cells activation and contraction characterizing fibrosis.

KEGG pathways underexpressed by UUO (**Table 3.12B**) were again mostly metabolic and associated with energy supply to the organism, including sugar, lipids and aminoacid metabolism [for example, Glycolysis/Gluconeogenesis (mmu00010), TCA cycle (mmu00020), Oxidative phosphorylation (mmu00190), Starch and sucrose metabolism (mmu00500), Fructose and mannose metabolism (mmu00051), Fatty acid metabolism (mmu00071), Synthesis and degradation of ketone bodies (mmu00072), Arginine and proline metabolism (mmu00330), Tryptophan metabolism (mmu00380) etc.]. This is in agreement with findings in section 3.4.4.4 and 3.4.4.5. Some disease pathways were also found downregulated by UUO (enriched in UUO-underexpressed group): specifically, these were Parkinson's disease (mmu05012), Huntington's disease (mmu05016) and Alzheimer's disease (mmu05010).

Table 3.12: KEGG overrepresentation test on UUO-overexpressed and -underexpressed proteins performed on DAVID. Statistical overrepresentation test was performed in DAVID (http://david.abcc.ncifcrf.gov) using the annotation terms ontologies KEGG Pathways. The number of proteins belonging to the annotation term and fold change from the expected value H_0 are in increasing shades of red for the UUO-overexpressed proteins (the higher the more intense)(A) and of green for the UUO-underrepresented proteins (the higher the more intense)(B). The p-value is shown in increasing shades of blue (the more intense, the lower the p-value). A p-value lower than 0.05 was regarded as significant.

Significantly enriched Pathways (KEGG)

A	Kegg Pathways in UUO-Overexpressed	Count	%	PValue	Fold Enrichment
	mmu04510:Focal adhesion	18	9.5	1.29E-09	6.36
	mmu04810:Regulation of actin cytoskeleton	17	9.0	3.82E-08	5.48
	mmu04512:ECM-receptor interaction	11	5.8	1.89E-07	9.27
	mmu04610:Complement and coagulation cascades	9	4.8	8.72E-06	8.40
	mmu03040:Spliceosome	10	5.3	5.41E-05	5.64
	mmu05414:Dilated cardiomyopathy	7	3.7	1.78E-03	5.32
	mmu04530:Tight junction	8	4.2	2.79E-03	4.15
	mmu04670:Leukocyte transendothelial migration	7	3.7	6.42E-03	4.12
	mmu05222:Small cell lung cancer	6	3.2	6.72E-03	4.94
	mmu05416:Viral myocarditis	6	3.2	1.02E-02	4.47
	mmu04666:Fc gamma R-mediated phagocytosis	6	3.2	1.21E-02	4.28
	mmu05322:Systemic lupus erythematosus	6	3.2	1.48E-02	4.08
	mmu04270:Vascular smooth muscle contraction	6	3.2	2.67E-02	3.50
	mmu05410:Hypertrophic cardiomyopathy (HCM)	5	2.6	3.03E-02	4.17

B	Kegg Pathways in UUO-Underexpressed	Count	%	PValue	Fold Enrichment
	mmu00190:Oxidative phosphorylation	69	15.9	1.40E-55	10.5
	mmu05012:Parkinson's disease	61	14.0	6.05E-44	9.0
	mmu05016:Huntington's disease	60	13.8	2.47E-33	6.5
	mmu05010:Alzheimer's disease	57	13.1	2.08E-30	6.2
	mmu00280:Valine, leucine and isoleucine degradation	32	7.4	3.40E-30	13.7
	mmu00640:Propanoate metabolism	20	4.6	4.22E-18	13.1
	mmu00020:Citrate cycle (TCA cycle)	20	4.6	1.04E-17	12.7
	mmu00650:Butanoate metabolism	21	4.8	4.36E-17	11.2
	mmu00010:Glycolysis / Gluconeogenesis	24	5.5	6.62E-14	7.0
	mmu00071:Fatty acid metabolism	20	4.6	9.70E-14	8.8
	mmu00480:Glutathione metabolism	21	4.8	1.80E-13	8.0
	mmu00620:Pyruvate metabolism	16	3.7	4.84E-10	7.7
	mmu04260:Cardiac muscle contraction	20	4.6	5.83E-09	5.1
	mmu00330:Arginine and proline metabolism	16	3.7	2.74E-08	6.0
	mmu00380:Tryptophan metabolism	14	3.2	3.77E-08	6.9
	mmu00310:Lysine degradation	12	2.8	3.69E-06	5.8
	mmu00410:beta-Alanine metabolism	9	2.1	6.65E-06	8.1
	mmu00250:Alanine, aspartate and glutamate metabolism	10	2.3	1.06E-05	6.6
	mmu00072:Synthesis and degradation of ketone bodies	6	1.4	6.51E-05	11.8
	mmu00630:Glyoxylate and dicarboxylate metabolism	7	1.6	8.24E-05	8.6
	mmu03320:PPAR signaling pathway	14	3.2	1.39E-04	3.5
	mmu00062:Fatty acid elongation in mitochondria	5	1.1	3.81E-04	12.3
	mmu00903:Limonene and pinene degradation	6	1.4	6.29E-04	7.9
	mmu00520:Amino sugar and nucleotide sugar metabolism	9	2.1	1.39E-03	4.0
	mmu00030:Pentose phosphate pathway	7	1.6	1.54E-03	5.3
	mmu00500:Starch and sucrose metabolism	8	1.8	1.84E-03	4.4
	mmu00051:Fructose and mannose metabolism	8	1.8	2.18E-03	4.3
	mmu00982:Drug metabolism	11	2.5	4.16E-03	2.9
	mmu00260:Glycine, serine and threonine metabolism	7	1.6	4.71E-03	4.3
	mmu00270:Cysteine and methionine metabolism	7	1.6	5.52E-03	4.2
	mmu00980:Metabolism of xenobiotics by cytochrome P450	10	2.3	5.55E-03	3.0
	mmu00052:Galactose metabolism	6	1.4	1.03E-02	4.4
	mmu00360:Phenylalanine metabolism	5	1.1	2.27E-02	4.5
	mmu00400:Phenylalanine, tyrosine and tryptophan biosynthesis	3	0.7	2.30E-02	11.8
	mmu00450:Selenoamino acid metabolism	5	1.1	2.64E-02	4.3
	mmu00053:Ascorbate and aldarate metabolism	4	0.9	3.70E-02	5.3
	mmu01040:Biosynthesis of unsaturated fatty acids	5	1.1	4.48E-02	3.7
	mmu00350:Tyrosine metabolism	6	1.4	4.49E-02	3.0

3.4.4.7 Protein-protein interaction analysis performed on String

To determine if the proteins overexpressed or underexpressed in UUO, and possibly belonging to some key significantly altered classes or pathways, were also able to directly or indirectly interact between themselves, interactions among the UUO- underexpressed or overexpressed proteins were investigated using the STRING bioinformatic tool, a database that collects all the known and reported protein-protein interactions.

The network of interaction obtained for the UUO-overexpressed proteins is reported in **Fig. 3.11**. Among the proteins enriched in UUO, a series of clusters of interacting proteins was detected. To confirm our initial observations [3.4.4.2], a significant group of interacting ECM components was identified, composed by a large cluster of collagens (**a**), but also including a number of fibrillins, fibulins (**b**), laminins (**c**), and FN (**d**). The already mentioned small extracellular proteoglycans and HSPGs (**e**), the latter associated with the glomerular and tubular basement membrane, were directly associated with the other matrix proteins in the network.

By functional analysis, cytoskeletal organisation and regulation of actin polymerisation were highlighted as a significantly represented protein functions among the UUO-overexpressed proteins [3.4.4.4 – 3.4.4.5], suggesting a substantial promotion of cytoskeletal remodelling in fibrotic conditions. In agreement with this, a large cluster of proteins associable to cytoskeletal organisation was identified, consisting of mostly actin types or proteins directly associated with actins (**f**). Among these proteins, some are known markers of mesenchymal cells such as α-SMA, vimentin and desmin (**g**), in agreement with fibroblasts proliferation and activation to myofibroblasts phenotype associated with the rapid fibrosis progression in UUO.

Hubs of proteins associated with inflammation, such as complement proteins (**h**) as well as a considerable group of annexins (**i**), are also identified by the network, in agreement with their suggested involvement in stress response or cell death during the progression of kidney fibrosis [3.4.4.1]. In line with what we already highlighted in **Table 3.3**, a significant cluster of serine protease inhibitors of the serpin superfamily was also identified (**j**), and might suggest a role for these proteins in the promotion of fibrosis by slowing down fibrolytic processes.

Finally, a node of proteins involved in RNA binding, regulation of mRNA maturation and splicing is evident in the interaction network (**k**) as already suggested by functional analysis [3.4.4.4 – 3.4.4.5] and might highlight an altered or even alternative regulation of protein expression upon CKD.

When protein-protein interactions in UUO-underexpressed proteins were analyzed (**Fig. 3.12**), the resulting network was extremely rich in interactions compared to the interactions in UUO-overexpressed proteins. A main cluster of metabolic proteins, mostly cytoplasmic or mitochondrial, with few sparse protein connections around, was obtained, suggesting that the metabolism-associated proteins are the most altered in the fibrotic kidney.

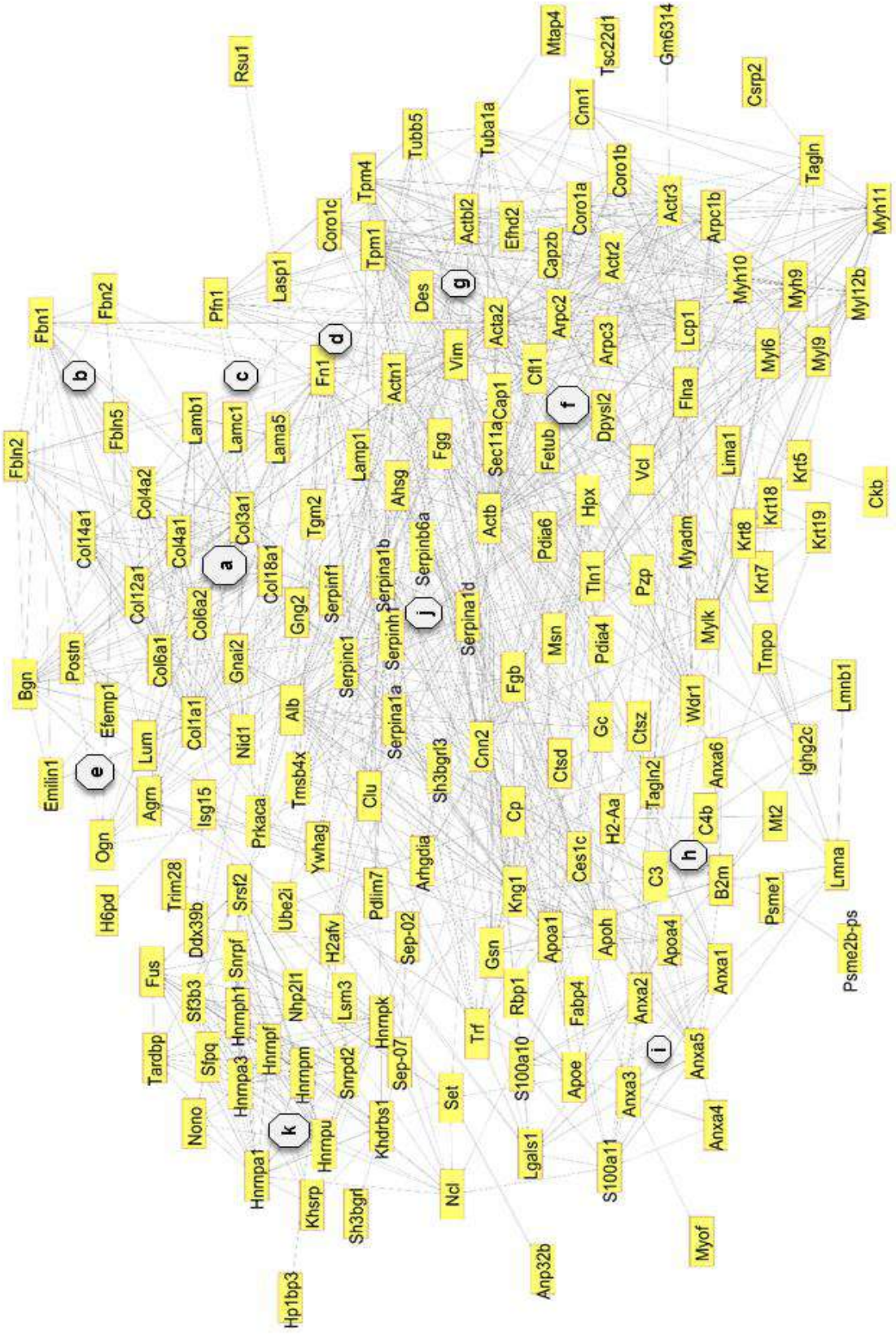

Figure 3.11: Network of protein-protein interactions of UUO-overexpressed proteins. Network of known and predicted protein-protein interactions was designed in STRING (http://string-db.org) using the list of proteins overexpressed in UUO kidney. A confidence of at least 0.4 (middle confidence in STRING) was chosen as threshold for the interactions identified. Results were exported on Cytoscape (http://www.cytoscape.org) for graphical visualisation.

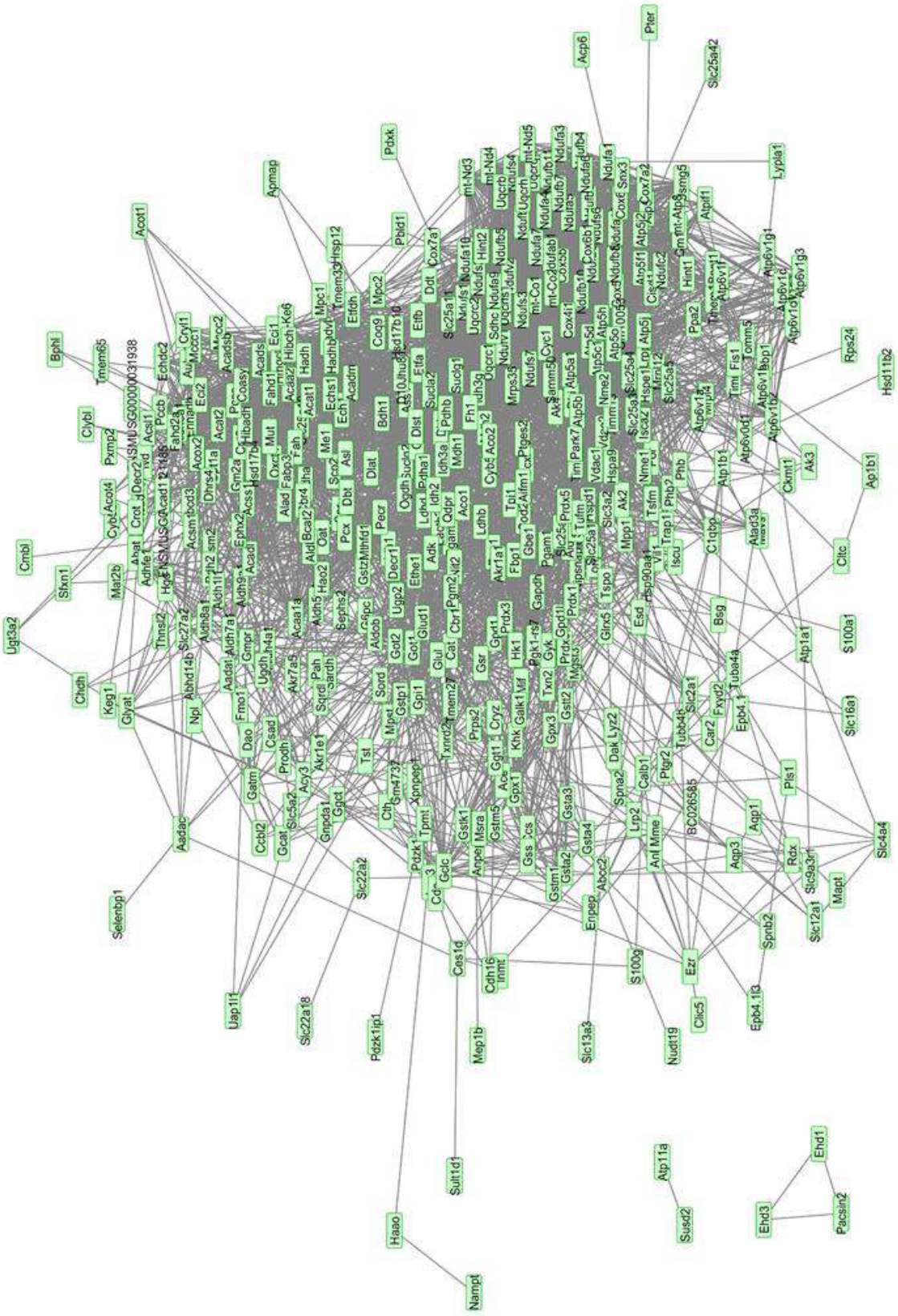

Figure 3.12: Network of protein-protein interactions of UUO-underexpressed proteins. Network of known and predicted protein-protein interactions was designed in STRING (http://string-db.org) using the list of proteins underexpressed in UUO. A confidence of at least 0.4 (middle confidence in STRING) was chosen as threshold for the interactions identified. Results were exported on Cytoscape (http://www.cytoscape.org) for graphical visualisation.

3.4.5 SWATH-MS approach allows to identify a larger amount of proteins significantly altered in UUO kidneys in comparison with previous studies

The UUO-differentially expressed proteins were compared to those obtained previously in rat in the same model of CKD (**Table 3.13**).

Table 3.13: Summary of the most recent proteomic studies performed on UUO models.

Protein list from	Treatment	Sample	Technique	Total proteins detected	UUO differentially expressed proteins	Of which Overexpressed
Yuan et al. (Sci Rep, 2015)	UUO 1 week and 3 weeks	Urine	LC-MS/MS DDA (Triple TOF 5600 mass spectrometer - SCIEX, Canada)	500 proteins	23 (7 after 1 week and 18 after 3 weeks	23
Zhao et al. (Int.J Clin Exp Path, 2015)	UUO 12, 24 and 72 hours	Tissue	2-DE + MALDI-TOF/TOF (ABI 4800 Proteomics Analyzer mass spectrometer, Applied Biosystems, USA).	~ 800 spots/ gel	39 (21 after 12 hr, 9 after 24 hr and 12 after 72 hr)	31
Current Study	UUO 3 weeks	Tissue	LC-MS/MS SWATH-DIA (Triple TOF 5600 mass spectrometer - SCIEX, Canada)	2106	653	195

Table 3.14 displays all the proteins identified as differentially expressed in UUO by Yuan and colleagues and Zhao and colleagues (Yuan, et al. 2015, Zhao, et al. 2015b) and investigates their identification in the current proteomic study.

Of the 23 proteins identified as overexpressed in UUO by Yuan et al. (Yuan, et al. 2015), 10 were also identified as overexpressed in our model, of which seven at a significant level (confidence > 80%) and three at a less significant level (50<confidence<80, displayed in **Suppl. Table 3.1**) (**Table 3.14**). Four proteins were instead found underexpressed in the current study, of which one, aminopeptidase N, at a significant level. This is understandable if we consider that aminopeptidase N is an early urine marker for this study (Yuan, et al. 2015) and can either be downregulated at later stages of the disease or be mainly identified in urine upon UUO.

At 21 days post-UUO, which is the same time-point of advanced fibrosis employed in the current study, 18 were the proteins identified by Yuan et al. (Yuan, et al. 2015) of which eight were identified by the current study, six at a significant level and two at a confidence level between 50 and 80% (**Table 3.14**). In general, the 30.4% of proteins suggested as urinary markers by Yuan et al. were significantly identified in the UUO model by SWATH-MS, number that rises to 43.5% if we consider also the less significant proteins (confidence <0.8). If we narrow the analysis to the sole proteins upregulated in urine at 21 days, 33.3% of proteins

were significantly (confidence≥0.8) identified by SWATH-MS which rises to 44.4% if we lower the confidence level to 50% (**Table 3.14**).

A different situation was found when the current study was compared to the list of proteins identified by Zhao et al. in 2015 (Zhao, et al. 2015b) (**Table 3.14**). In this latter work, in fact, despite whole kidney lysates were employed as in the current study, early time points were used (less than a week), ending up with the identification of early marker of inflammatory or ischemic reaction and not markers of an advanced fibrosis. Of the 31 proteins found overexpressed in the UUO model at either 12, 24 or 72 h by Zhao and colleagues, only 10 (32.2%) were found overexpressed in our SWATH-MS analysis at 21 days post UUO, of which 7 in a significant manner (22.6%)(**Table 3.14**). Interestingly, 19 proteins were found underexpressed in our model (61.3%), of which 15 in a significant manner (48.4%), and three at a confidence between 0.5 and 0.8 (9.7%) (**Table 3.14**). These proteins were mostly markers of the earlier time-points (12-24 h), and are likely to be proteins overexpressed as an immediate inflammatory response or antioxidant response to ischemia, then underexpressed when the fibrosis is at its late stages. Only two proteins (6.4%) were not detected at all (**Table 3.14**). Zhao and colleagues also identified nine proteins as significantly underexpressed in UUO (two at 24 hr and 7 at 72 h); of these proteins, seven (77.8%) were found significantly downregulated also by SWATH-MS, while two were found overexpressed, one significantly at a confidence higher than 0.8 and one less significantly (confidence 0.77) (**Table 3.14**).

The comparison of the current study with both papers was collected in **Suppl. Table 3.13**, that provides an alternative way to see the results, showing only the proteins detected by SWATH-MS and the corresponding expression in previous literature. **Suppl. Table 3.14** summarizes the overlap between the previous analyses and the UUO-overexpressed proteins in the current study.

In summary, of the 54 proteins found overexpressed in UUO either in urine or in tissue by the two recent papers using a less sensitive technique, 19 were detected also SWATH-MS, of which 13 in a significant manner [C(FC)≥0.8]. These proteins represent approximately the 8% of all the proteins detected by SWATH-MS. 23 of these proteins were instead found underexpressed in our model, of which 15 were significant (80% confidence).

Table 3.14: List of proteins reported as differentially expressed in the UUO model from recent literature and corresponding detection in the current study. Legend: +, red = overexpressed proteins in the study (positive fold change from the Sham operated control); -, green =underexpressed proteins in the study (negative fold change from the Sham operated control); in increasing shades of grey = absolute fold change from the sham operated control in the current study (the more intense, the more overexpressed or underexpressed depending on the direction of difference) ; bright yellow = confidence ≥ 0.8 in the current study (considered significant in the current study); pale yellow = 0.5 > confidence < 0.8 in the current study; * = A1AT1 as example value, but also other isoforms (A1AT2, A1AT4 and A1AT5) were detected as overexpressed ** = MUP2 as example value, but also MUP6 was detected as overexpressed, while MUP3 was detected as underexpressed.

Proteins Identified as differentially expressed in UUO by Yuan et al., 2015 IN URINE				**Current study**		
Name		days post UUO	Direction of difference	FC (UUO/Sham)		C(FC)
Alpha-actinin 1	ACTN1	21	+	+	4.22	0.96
Alpha-actinin 4	ACTN4	21	+	+	1.46	0.70
Aminopeptidase N	AMPN	7	+	-	3.83	0.95
Annexin A1	ANXA1	21	+	+	8.17	0.84
Cathepsin D	CATD	7	+	+	2.65	0.82
Clusterin	CLUS	21	+	+	5.35	0.81
Complement component C9	CO9	21	+			
Golgi resident protein GCP-60	GCP60	21	+			
Cluster of Histone H1-4	H14	21	+	-	1.32	0.18
Intraflagellar transport protein 172 homolog	IF172	7	+			
Ig gamma-1 chain C region	IGHG1	21	+			
Galectin 3 - binding protein	LG3BP	7	+	+	5.78	0.67
Lumican	LUM	21	+	+	6.55	0.87
Moesin	MOES	21	+	+	1.52	0.81
Periaxin	PRAX	21	+			
Glycogen phosphorylase	PYGM	7, 21	+			
Protein S100-A8	S10A8	21	+			
Protein S100-A9	S10A9	7, 21	+	+	3.03	0.54
Solute carrier family 12 member 7	S12A7	7	+			
Extracellular Superoxide dismutase	SODE	21	+	-	1.30	0.31
Serine protease Inhibitor A3N	SPA3N	21	+			
Transaldolase	TALDO	21	+	-	1.34	0.57
Cluster of Vimentin	VIME	21	+	+	8.56	0.90

Proteins Identifled as differentially expressed in UUO by Zhao et al., 2015 IN KIDNEY TISSUE				**Current study**		
Name		days post UUO	Direction of difference	Fold change UUO/Sham		Confidence
3-hydroxyantharanilate 3,4-dioxygenase	3HAO	72	+	-	15.56	0.85
Alpha-1 antiproteinase	A1AT	72	+	+	3.07 *	0.86
abhydrolase domain-containing protein 14B	ABHEB	12	+	-	5.57	0.93
Actin, aortic smooth muscle	ACTA	72	-	+	3.17	0.94
Aspartoacylase-2	ACY3	72	-	-	12.43	0.80
Alanine glyoxylate aminotransferae 2, mitochondrial	AGT2	12	+	-	9.01	0.71
4'-Trimethylaminobutyraldehyde dehydrogenase	AL9A1	24	-	-	5.76	0.94
Serum albumin	ALBU	72	+	+	2.98	0.92
Aldose reductase related protein 1	ALD1	24	+	+	3.96	0.44
Annexin A1	ANXA1	12	+	+	8.17	0.84
Annexin A2	ANXA2	12	+	+	3.76	0.90
Annexin A4	ANXA4	72	+	+	1.78	0.85
Aflatoxyn B1 aldheyde reductase member 3	ARK73	12	+			
ATP synthase subunit D, mitochondrial	ATP5H	12	+	-	7.21	0.93
ATP synthase subunit beta, mitochondrial	ATPB	12	+	-	6.55	0.94
Branched chain anìmino acid aminotransferase, mitochondrial	BCAT2	12	+	-	4.38	0.89
Macboxymethylenebutenolidase homolog	CMBL	72	-	-	5.38	0.85
Electron transfer flavoprotein subunit beta	ETFB	12	+	-	8.13	0.91
Fibronogen beta chain	FIBB	12	+	+	4.00	0.86
Glycine aminotransferase, mitochondrial	GATM	24	+	-	13.91	0.87

Guanine nucleotide binding protein G(I)/G(S)/G(T) subunit beta-2	GBB2	12	+	-	1.38	0.47
Gamma glutamyltranspeptidase	GGT1	24	+	-	13.58	0.89
Gluthatione peroxydase 1	GPX1	72	-	-	3.45	0.92
Phospholipid hydroperoxide glutathione peroxidase, mitochondrial	GPX41	12	+	-	4.18	0.52
Gluthatione S-transferase Mu 2	GSTM2	12	+	+	1.29	0.17
Gluthatione S transferase P	GSTP1	24	+	-	1.77	0.94
Gluthatione S-transferase P	GSTP1	72	-	-	1.77	0.94
Isocitrate dehydrogenase (NAD) subunit alpha, mitochondrial.	IDH3A	24	-	-	4.86	0.91
Adenylate kinase isoenxyme 4, mitochondrial	KAD4	24	+	-	19.83	0.89
Meprin A subunit alpha	MEP1A	12	+	-	7.15	0.88
Mayor urinary protein	MUP	72	-	+	2.79 **	0.77
2-oxoisovalerate dehydrogenase subunit alpha, mitochondrial	ODBA	12	+	-	10.29	0.64
Pyruvate dehydrogenaseE1 component subunit beta, mitochondrial	ODPB	72	-	-	6.05	0.96
Protein disulfide isomerase A6	PDIA6	12	+	+	1.68	0.90
Phosphatidylethanolamine binding protein 1	PEBP1	12	+	-	1.92	0.92
Peroxiredoxin	PRDX1	12	+	-	2.03	0.91
Etherogenous nuclear ribonucleoproteinsA2/B1	ROA2	24	+	+	1.27	0.38
Serine protease inhibitor A3N	SPA3N	12, 24, 72	+			
Thiosulfate sulfutransferase	THTR	12	+	-	7.75	0.89
Voltage dependent anion selective channel protein 2	VDAC2	12	+	-	2.84	0.94

3.4.6 Residual analysis of SWATH-MS protein spectral results gives a lower number of protein significantly altered from prediction.

In parallel with the fold change analysis performed by OneOmics cloud processing software (SCIEX, Canada), an analysis of residuals from the linear regression lines between WT UUO and WT Sham operated spectral data was performed, as described in 3.3.8.

First, regression lines were drawn using protein intensity values in UUO (dependent variable y) and protein intensity values in Sham operated conditions (independent variable x) foreach protein hit, for every of the 16 combinations of kidney samples as described in 3.3.8. Sixteen non-overlapping regression lines were obtained, with a slope between ~0.49 and ~0.63 (**Fig. 3.13A**). A second regression line using the mean spectral values of the four UUO WT mice and the four Sham operated WT mice was produced as well, showing a slope of 0.58 and an R^2 value of 0.43 (**Fig. 3.13B**). From these results, a low correlation (R-squared between 0.30 and 0.55) was observed between the treatments, and the relationship was biased towards higher values for the Sham operated kidneys, since the slope of the regression curves was lower than one, and always around 0.5-0.6. This reflects a generally higher expression of proteins in the healthy kidney (below y=x, red dashed line), compared to the proteins overexpressed by UUO (above y=x, red dashed line), which can be associated with an increased cell death or to a more difficult homogenization of a fibrotic tissue.

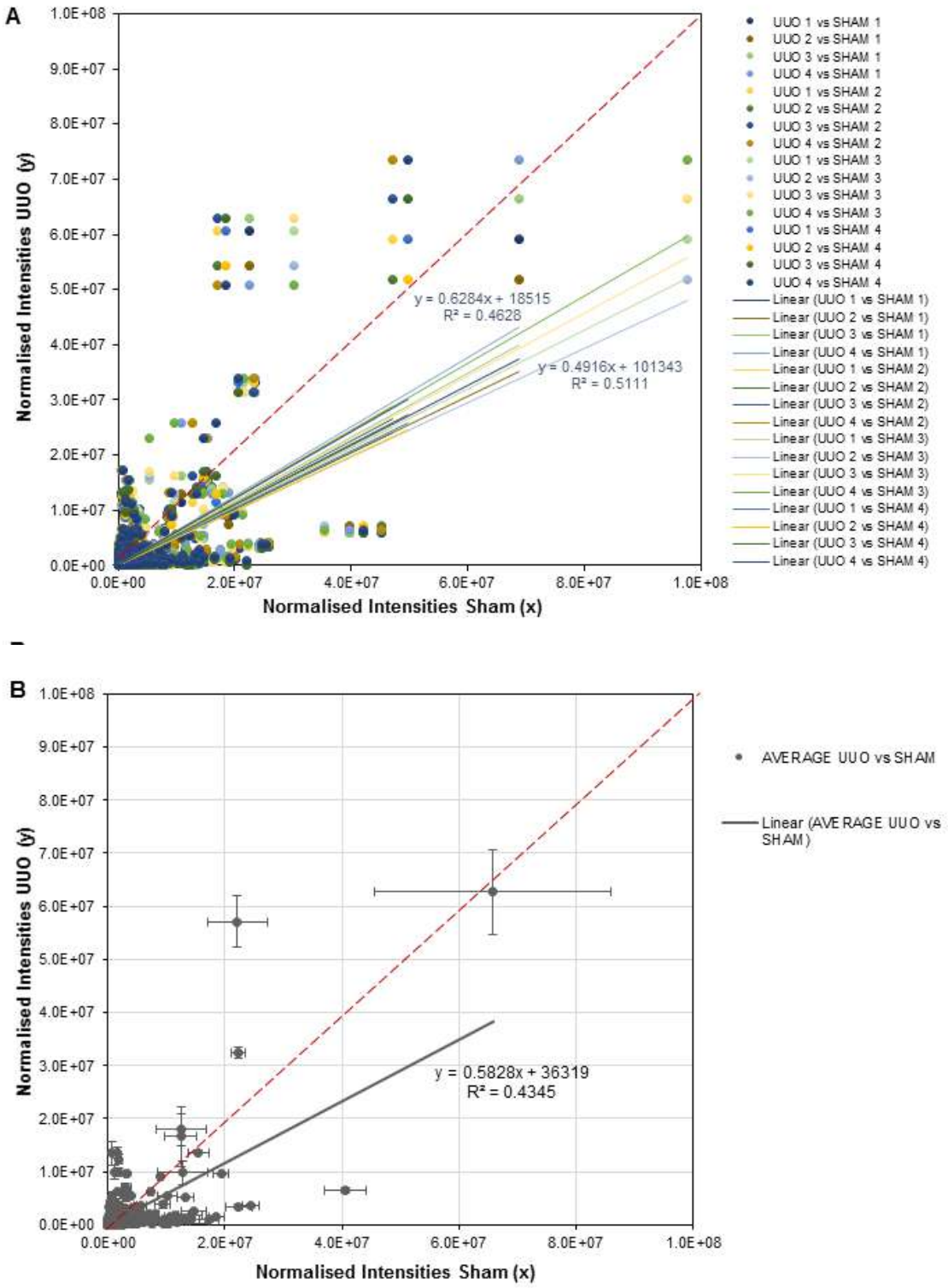

Figure 3.13: Regression lines between spectral values of UUO and Sham operated wild type mice. Regression analysis was performed on **(A)** every of the 16 combinations of UUO (dependent variable y) and Sham operated mice (independent variable x) normalized intensity values of every protein detected by SWATH-MS. Single protein points (x=intensity in Sham; y=intensity in UUO) and regression lines are shown in the graph for each combination of samples. Two representative regression line equations and R-squared values are displayed. **(B)** The same analysis was performed using the mean values of the 4 UUO and Sham operated biological replicas. Mean protein points (x= mean intensity in Sham; y=mean intensity in UUO) with relative error bars (standard deviations) are shown. The regression line is shown in black and the corresponding equation and R-squared value are displayed. In both graphs, the red dashed line is the bisector of the 1st nd 3rd quadrant, corresponding to the y=x.

Residual analysis was then performed as described in the Experimental procedure. As it can be seen in **Table 3.15**, 48 proteins were identified as significantly ($p \leq 0.05$) different from the predicted value in UUO (predicted value = y', obtained from the regression line). The exact half of these proteins (24 proteins) had positive mean of standardized residual (in increasing shades of red) and p-value lower than 0.05, and were regarded as significantly higher than the prediction. The other 24 proteins had negative mean of standardized residual (decreasing shades of green) and p-value lower than 0.05, and were considered significantly lower than the prediction.

In order to see if these variations were overlapping with the list of UUO-differentially expressed proteins reported in the previous paragraphs, the same proteins were searched in the fold change dataset obtained with OneOmics (SCIEX, Canada) (last 2 columns of **Table 3.15**). The number of proteins identified in this way by residual analysis was much smaller. No complete overlap was identified between the 2 analyses, especially for what it concerns the proteins whose residuals were significantly higher than the regression line. This is because the fold change analysis is based on the identification of proteins significantly different from an y=x assumption (bisector of the first/third quadrant, red dashed line in **Fig. 3.13**) while the residual analysis is based on the identification of proteins whose spectral value significantly different from the prediction, determined by the regression line, that, in this case, has a much lower slope (~0.5-0.6). A graphical view is presented in **Fig. 3.14** showing the regression line obtained from the mean spectral values, as well as the y=x red dashed line. In red are shown some proteins identified as significantly higher than the prediction (mean standard residual ≥ 0, $p \leq 0.05$) that were also identified as significantly overexpressed upon UUO ($FC > 1$ or $\log2(FC) > 0$, $C(FC) \geq 0.8$). These proteins are all located above both the regression line and the y=x line. In green there are some proteins identified as significantly lower than the prediction (mean standard residual ≤ 0, $p \leq 0.05$) that were also identified as significantly underexpressed upon UUO ($FC < 1$ or $\log2(FC) < 0$, $C(FC) \geq 0.8$). These proteins are all located below the regression line. Finally, in blue are shown some of proteins that, however identified as significantly higher than the prediction by residual analysis (mean standard residual ≥ 0, $p \leq 0.05$), were not significantly overexpressed during UUO. These proteins can generally be found between the regression line and the y=x line (see PPIA_MOUSE or EF1A1_MOUSE) or anyway near the bisector (such as the histone proteins H2B1P_MOUSE and H4_MOUSE) and might have a high variability in protein intensity among replicas (large error bars, as it can be seen for haemoglobin HBA_MOUSE).

Table 3.15: List of proteins identified by SWATH-MS on wild type (WT) mice having a spectral intensity significantly different from the predicted value on the regression line. Regression analysis was performed for each of the 16 possible combinations of UUO and Sham operated WT mice, and mean standard residuals were obtained for every protein identified by SWATH-MS. P-values were obtained by plotting the mean standard residuals on a normal standard distribution, and a p-value lower than 0.05 was regarded as significant. The table reports the proteins with residuals significantly positive (spectral values significantly higher than the predicted y'), in increasing shades of red, or negative (spectral values significantly lower than the predicted y'), in decreasing shades of green. Significand p-values are reported in increasing shades of blue, the more intense the more significant. The last two columns show the fold change values obtained for the given protein with the OneOmics software (SCIEX, Canada) (in increasing shades of red the positive log2 of the fold change and in decreasing shades of green negative log2 of the fold change) with the corresponding confidence highlighted in yellow if accepted as significant (higher than 0.8).

Residual analysis UUO vs SHAM				Fold Change Analysis	
Protein ID	Name	Mean Residual	P-value	Log2 (FC)	C(FC)
ALBU_MOUSE	Serum albumin	25.66	4.67E-144	1.58	0.92
HBA_MOUSE	Hemoglobin subunit alpha	14.42	2.77E-46	0.44	0.71
ACTB_MOUSE	Actin, cytoplasmic 1	11.56	4.02E-30	0.64	0.93
UROM_MOUSE	Uromodulin	7.46	3.25E-13	4.03	0.85
CO1A1_MOUSE	Collagen alpha-1(I) chain	7.19	2.38E-12	2.93	0.96
VIME_MOUSE	Vimentin	6.46	3.47E-10	3.10	0.90
H2B1P_MOUSE	Histone H2B type 1-P	6.28	1.12E-09	0.34	0.17
H4_MOUSE	Histone H4	5.50	1.07E-07	0.38	0.10
CO3A1_MOUSE	Collagen alpha-1(III) chain	5.22	4.74E-07	2.95	0.92
CO4A2_MOUSE	Collagen alpha-2(IV) chain	5.07	1.05E-06	2.17	0.80
TAGL2_MOUSE	Transgelin-2	4.50	1.60E-05	1.60	0.88
TPM4_MOUSE	Tropomyosin alpha-4 chain	2.98	4.64E-03	2.07	0.91
APOA1_MOUSE	Apolipoprotein A-I	2.97	4.87E-03	1.30	0.92
PPIA_MOUSE	Peptidyl-prolyl cis-trans isomerase A	2.89	6.21E-03	-0.23	0.32
ACTA_MOUSE	Actin, aortic smooth muscle	2.87	6.58E-03	1.67	0.94
CO1A2_MOUSE	Collagen alpha-2(I) chain	2.85	6.95E-03	3.09	0.79
MYL6_MOUSE	Myosin light polypeptide 6	2.61	1.31E-02	1.34	0.92
PROF1_MOUSE	Profilin-1	2.33	2.64E-02	1.07	0.89
EF1A1_MOUSE	Elongation factor 1-alpha 1	2.31	2.78E-02	-0.32	0.35
ABCB7_MOUSE	ATP-binding cassette sub-family B member 7, mitochondrial	2.30	2.83E-02	0.92	0.89
ECHD3_MOUSE	Enoyl-CoA hydratase domain-containing protein 3, mitochondrial	2.27	3.05E-02	-2.46	0.67
K2C8_MOUSE	Keratin, type II cytoskeletal 8	2.23	3.34E-02	2.30	0.89
LEG1_MOUSE	Galectin-1	2.22	3.41E-02	2.62	0.87
TAGL_MOUSE	Transgelin	2.06	4.78E-02	3.21	0.89
COX5B_MOUSE	Cytochrome c oxidase subunit 5B, mitochondrial	-2.08	4.58E-02	-3.04	0.91
F16P1_MOUSE	Fructose-1,6-bisphosphatase 1	-2.27	3.01E-02	-4.38	0.81
CALB1_MOUSE	Calbindin	-2.39	2.29E-02	-5.00	0.91
COX5A_MOUSE	Cytochrome c oxidase subunit 5A, mitochondrial	-2.55	1.54E-02	-3.18	0.94
COX41_MOUSE	Cytochrome c oxidase subunit 4 isoform 1, mitochondrial	-2.56	1.50E-02	-2.90	0.94
ACADM_MOUSE	Medium-chain specific acyl-CoA dehydrogenase, mitochondrial	-2.61	1.32E-02	-3.86	0.86
MMSA_MOUSE	Methylmalonate-semialdehyde dehydrogenase [acylating], mitochondrial	-2.67	1.14E-02	-3.79	0.88
MDHM_MOUSE	Malate dehydrogenase, mitochondrial	-2.71	1.03E-02	-2.73	0.96
COX2_MOUSE	Cytochrome c oxidase subunit 2	-2.76	8.87E-03	-3.00	0.87
S100G_MOUSE	Protein S100-G	-2.85	6.93E-03	-4.05	0.90
AT1B1_MOUSE	Sodium/potassium-transporting ATPase subunit beta-1	-3.03	4.00E-03	-4.29	0.87
AADAT_MOUSE	Kynurenine/alpha-aminoadipate aminotransferase, mitochondrial	-3.06	3.65E-03	-5.59	0.84
ECHP_MOUSE	Peroxisomal bifunctional enzyme	-3.06	3.64E-03	-4.32	0.84
ACSM2_MOUSE	Acyl-coenzyme A synthetase ACSM2, mitochondrial	-3.11	3.14E-03	-4.33	0.86
MDHC_MOUSE	Malate dehydrogenase, cytoplasmic	-3.13	2.97E-03	-2.30	0.95
AK1A1_MOUSE	Alcohol dehydrogenase [NADP(+)]	-3.42	1.14E-03	-3.40	0.91
ASSY_MOUSE	Argininosuccinate synthase	-3.50	8.60E-04	-4.41	0.88
ADT2_MOUSE	ADP/ATP translocase 2	-3.56	7.17E-04	-2.82	0.81
UK114_MOUSE	Ribonuclease UK114	-4.02	1.23E-04	-3.67	0.94
ALDOB_MOUSE	Fructose-bisphosphate aldolase B	-4.95	1.87E-06	-3.83	0.93
PRDX5_MOUSE	Peroxiredoxin-5, mitochondrial	-5.07	1.03E-06	-2.65	0.91
AT1A1_MOUSE	Sodium/potassium-transporting ATPase subunit alpha-1	-5.10	8.80E-07	-3.72	0.93
ATPB_MOUSE	ATP synthase subunit beta, mitochondrial	-5.65	4.59E-08	-2.71	0.94
ATPA_MOUSE	ATP synthase subunit alpha, mitochondrial	-9.15	2.72E-19	-2.69	0.96

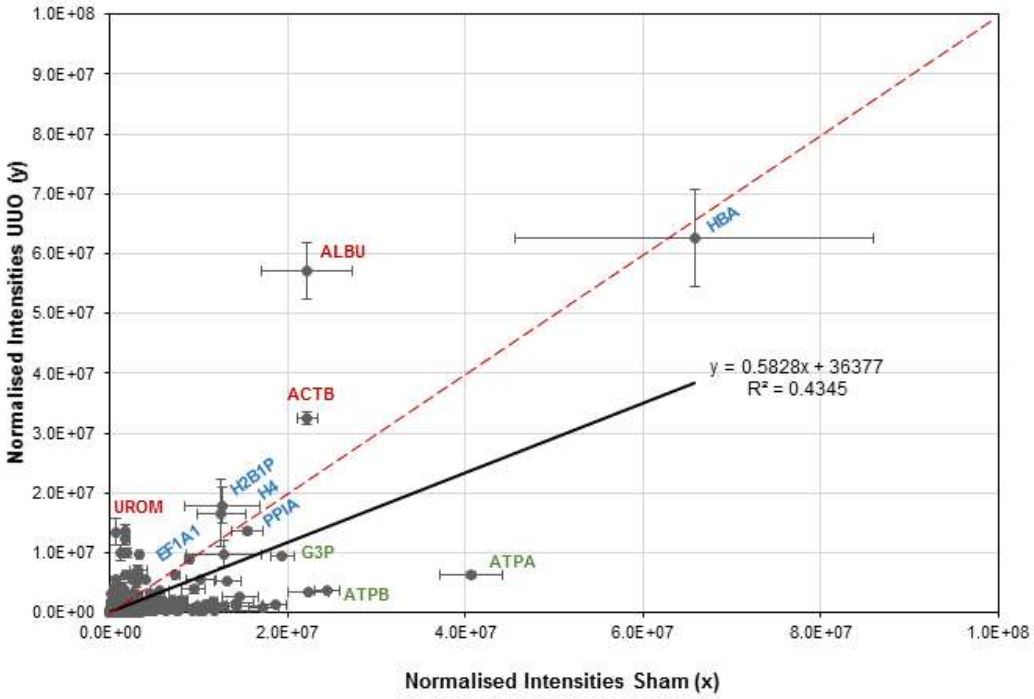

Figure 3.14: Location of specific candidates identified by residual analysis on the cartesian plane, with respect to the regression line and the y=x quadrant bisector line. Regression analysis was performed on Office Excel using the mean values of the 4 UUO and Sham operated biological replicas. Mean protein points P(x= mean intensity in Sham; y=mean intensity in UUO) with relative error bars (standard deviations) are shown. The regression line is shown in black while bisector of the quadrant, corresponding to the y=x line, is shown as a red dashed line. The name of specific proteins is shown in red (proteins with positive significant standard residuals, p≤0.05, and significantly overexpressed in UUO, confidence ≥ 0.8), blue (proteins with positive significant standard residuals, p≤0.05, but not significantly overexpressed in UUO) or green (proteins with negative significant standard residuals, p≤0.05, and significantly underexpressed in UUO, confidence ≥ 0.8).

In this chapter, residual analysis was employed as an alternative method to the fold change analysis to determine which proteins were significantly altered in the UUO comparing to the Sham operated condition. However, given the fact that the regression curves had a slope much lower than the y=x bisector curve (slope = 1), the outcome of both analyses resulted not to be comparable. The lower slope of regression curve is probably due to the fact that in the healthy (Sham) condition the proteins detected by the machine in equal amounts of total protein (from a 1 µg/µl sample concentration) were more evenly distributed in their relative intensity, while in the UUO condition the same amount of total lysate (from the same 1 µg/µl sample concentration) was represented by few highly abundant proteins, with albumin above all, and a more elevated number of less abundant proteins. Therefore, while the analysis of residuals gave us only an idea of which protein intensity in the UUO condition were significantly different from their predicted value y' obtained by the regression line, the fold change analysis performed using SCIEX OneOmics gave us a more convincing idea of which proteins were differentially expressed by UUO compared to the Sham operated condition. Production of a regression line, however, was still useful to visualize how the protein intensity were

distributed and which were the more extremely expressed protein (highly abundant or lowly abundant) such as serum albumin.

3.4.7 Analysis of the effect of TG2-KO in the UUO model of kidney fibrosis

For the aims of Chapter IV, where the interactome of TG2 in the UUO model of kidney fibrosis will be produced, use of TG2-null inbred mice next to the WT individuals was necessary. In the past, a protective role of TG2-KO in kidney fibrosis has been suggested in TG2-KO, employing different models of CKD including the UUO itself (Fisher, et al. 2009, Shweke, et al. 2008).
In this section an analysis of fibrosis development and UUO-differentially expressed proteins in TG2-KO mice subjected to UUO or Sham operation for 21 days will be provided, comparing it with the same treatments in WT mice.

3.4.7.1 Histological staining of kidney samples from UUO and Sham-operated TG2-null mice and comparison with WT

In order to qualitatively observe differences in kidney morphology in both WT and TG2-KO at 21 days post-UUO (advanced/end stage fibrosis), H&E staining was performed as described above (3.3.2) and some representative pictures are shown in **Fig. 3.15**. In Sham operated kidneys (**Fig. 3.15 a,b**) no differences in renal morphology could be observed in TG2-KO mice (**b**) in comparison with the WT conditions (**a**) (described in the 3.4.1.1 section of this chapter). In TG2-null mice (**b**), glomeruli appeared well vascularised, normally shaped and rich in mesangial cells while tubules were healthy, tightly associated and clearly bordered by epithelial cells with no differences from the Sham operated WT mice (**a**). Vascularisation appeared not dissimilar from the WT (**Fig. 3.15 a,b**).
Upon UUO (21 days), H&E highlighted a clear alteration in the organ morphology in both WT and TG2-null mice (**Fig. 3.15, c-d**). To the naked eye, no obvious difference was observed in TG2-KO mice undergoing fibrosis (**d**) comparing to the WT mice subjected to UUO (**c**) (described in 3.4.1.1). In both cases, signs of advanced-to-end stage fibrosis were highlighted, with general loss of renal structure, tubular atrophy and loss of tight tubular association, as well an advanced level of glomerulosclerosis in some glomeruli (individuated by an asterisk in **Fig. 3.15**). Eosinophilic pink staining was similar in TG2-null (**d**) and WT mice (**c**) subjected to 21 days UUO and was clearly paler than the Sham operated controls in both tubular and glomerular fractions.
These findings suggest a comparable development of fibrosis in both TG2-KO and WT mice at 21 days post-UUO, with no evident effect of TG2-KO on the level of fibrosis at 21 days post-UUO with this qualitative approach.

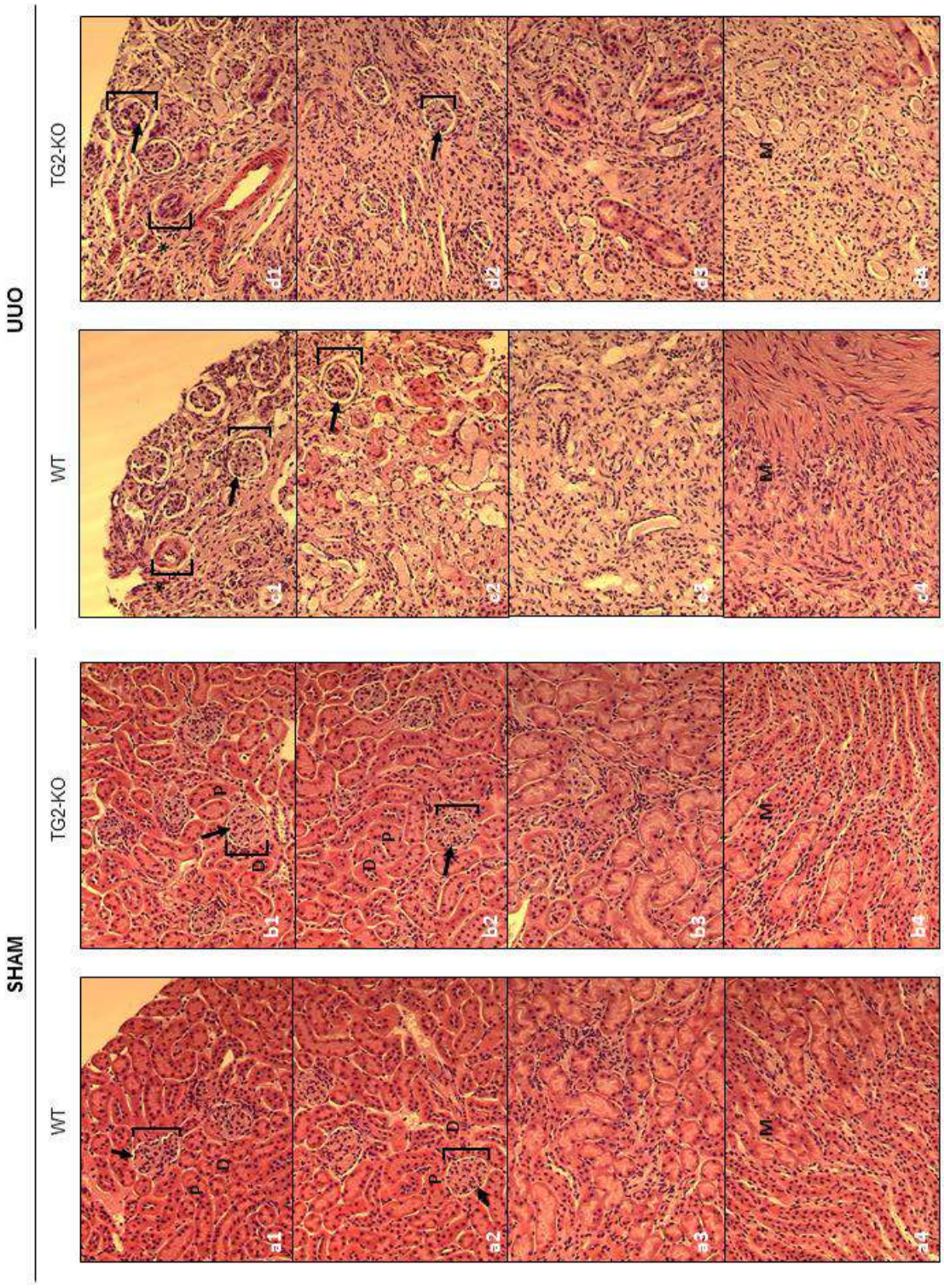

Figure 3.15: Haematoxylin and eosin (H&E) staining of kidney sections from the 21 days-UUO model in WT and TG2-KO mice. H&E staining of paraffin sections was performed at the Department of Infection, Immunity & Cardiovascular Disease of the University of Sheffield by Dr Fiona J. Wright. Pictures were taken with an Olympus BX61 fluorescent microscope with Cell^F imaging system software (Olympus, Japan). Representative images at 20X magnification are here shown. Legend: 1,2 = mostly cortical area; 3,4 = mostly medullar area; square bracket = renal corpuscule; arrow = Bowman's space; P = proximal convoluted tubule; D = distal convoluted tubule; M = medulla; * = sclerotic glomerulus.

In order to visualize fibrotic tissue accumulation in TG2-null mice subjected to UUO and compare it with the WT condition, MT staining of paraffin embedded sections was performed (**Fig. 3.16**) and the relative accumulation of fibrillary collagen was quantified as described in 3.3.2 (**Fig. 3.17**).

In Sham operated kidneys (**Fig. 3.16 a,b**), no differences in renal morphology and collagen accumulation (blue staining) was observed between TG2-null mice (**b**) and WT mice (**a**) (described in 3.4.1.2). In both cases, diffuse red staining highlighted healthy and tightly associated renal structures while minimal blue staining was limited to the interstitial space, intraglomerular space or basement membranes. No significant alteration in collagen deposition was observed between TG2-null (**b**) and WT (**a**) Sham operated mice when the blue staining corresponding to fibrillary collagen was compared to cytoplasm staining (red, **Fig. 3.17A**) (1.41±0.36, p=0.15) or nuclear staining (brown, **Fig. 3.17B**) (1.17±0.21, p=0.38).

Upon ureteral obstruction (21 days post-UUO), the level of fibrosis observed in TG2-KO mice by MT staining was similar to the one of WT mice subjected the same treatment (described in 3.4.1.2) and was comparable to and advanced/final stage of CKD (**Fig. 3.16 c,d**). Morphological alterations in fibrotic TG2-null mice (**d**) could be observed in both corpuscular and tubular portions and were comparable with what seen in WT mice subjected to UUO (**c**) (3.4.1.2 for description). In both cases, the cytosolic red staining was heavily reduced and substituted by a clear increase in fibrillary blue staining that accumulated in the areas of fibrotic tubulointerstitium and in sclerotic disrupted glomeruli. When quantification of the different staining colours was performed with Cell^F software (**Fig. 3.17**), the ratio of collagen over cytoplasm revealed a significant collagen accumulation upon UUO in both WT (10.76±3.13 fold from WT Sham, equalised to 1; p=0.002 **) and TG2-KO mice (10.08±2.70 from WT Sham, p=0.0003 ***; 7.15±2.48 fold from its own Sham operated control, P=0.0005 ***), with no significant change in collagen deposition determined by TG2-KO in UUO (p=0.99) (**Fig. 3.17A**). When, however, the accumulation of collagen was measured as ratio of collagen over the total number of cells (nuclear staining, **Fig. 3.17B**), a significant (p=0.007 **) reduction in fibrotic tissue accumulation was observed in TG2-KO mice subjected to UUO, compared to the corresponding WT mice. In TG2-KO mice, in fact, collagen accumulation was 1.64±0.30 – fold higher than the Sham operated WT (p=0.008 **) and only 1.40±0.19 higher than its own TG2-KO Sham operated control (p=0.02 *). This value was significantly (p=0.007 **) lower than the collagen accumulation in WT mice at 21 days post-UUO when it was measured with the same method (3.19±0.68, p=0.0003 ***) (**Fig. 3.17B**) and might suggest a possible protective role of TG2-KO against the progression of fibrosis, that was however difficult to observe by eye at this level of advanced disease.

In summary, by histological staining TG2-KO mice appeared to develop a level of fibrosis at 21-days post UUO that can be regarded as an advanced-to-end stage fibrosis and was similar to

WT mice subjected to the same treatment. Quantification of collagen accumulation over the total number of living cells (**Fig. 3.17B**), however, revealed a significant reduction in TG2-KO UUO mice compared to the fibrotic WT, that might suggest a protective role of TG2 abolishment in UUO. This is in line with previous findings in the same model, where however an earlier time point was employed (12 days UUO) (Shweke, et al. 2008).

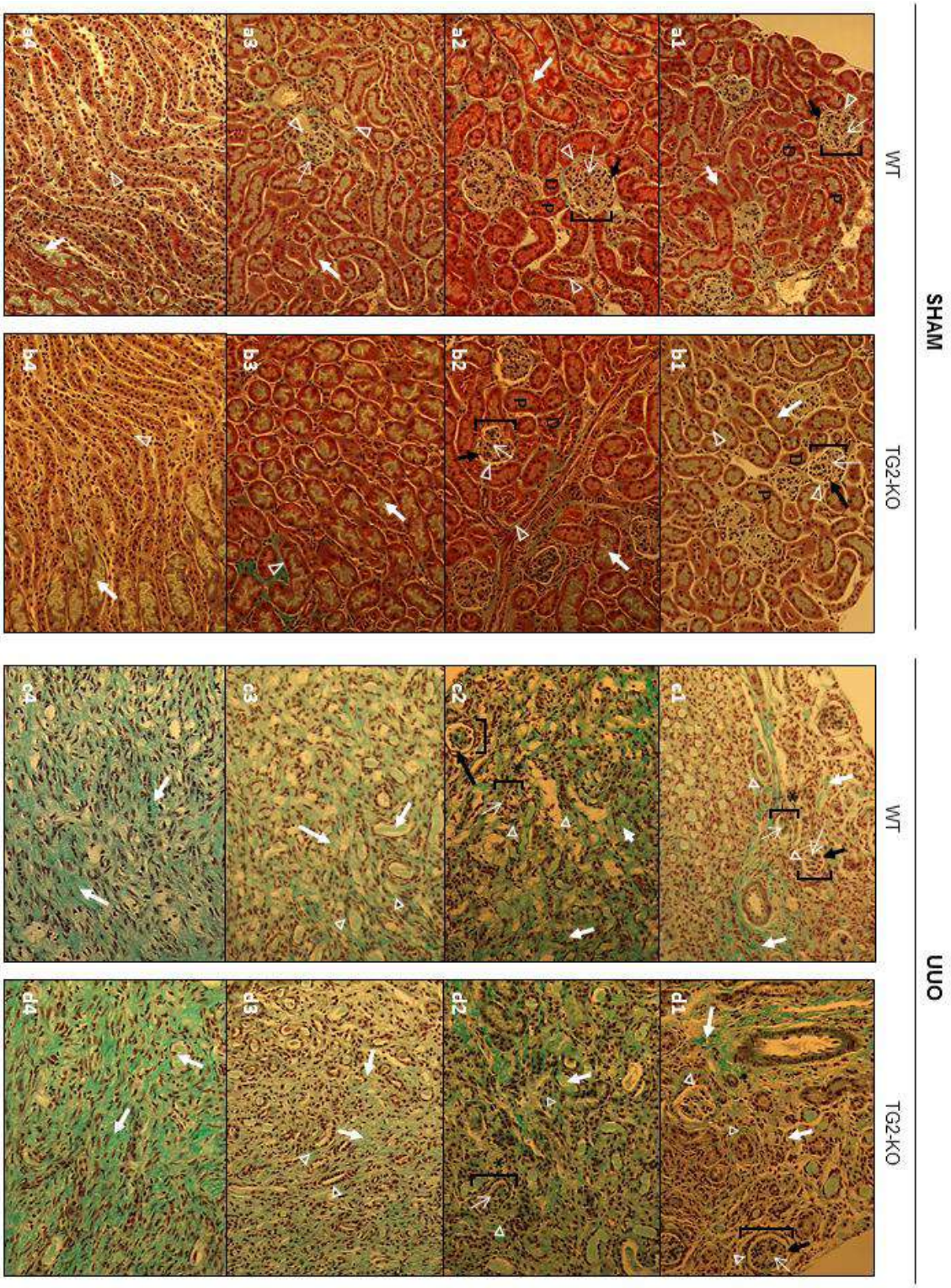

Figure 3.16: Masson's trichrome (MT) staining of kidney sections from the 21 days- UUO model in WT and TG2-KO mice. In order to visualise and quantify the development of fibrosis, MT staining of paraffin sections were performed at the Department of Infection, Immunity & Cardiovascular Disease of the University of Sheffield by Dr Fiona J. Wright. Pictures were taken with an Olympus BX61 fluorescent microscope with Cell^F imaging system software (Olympus, Japan). Representative images at 20X magnification are here shown. Legend: 1,2 = mostly cortical area; 3,4 = mostly medullar area; square bracket = renal corpuscule; arrow = Bowman's space; P = proximal convoluted tubule; D = distal convoluted tubule; * = sclerotic glomerulus; thick white arrow = interstitial space; thin white arrow = intraglomerular matrix; white triangles = basement membrane.

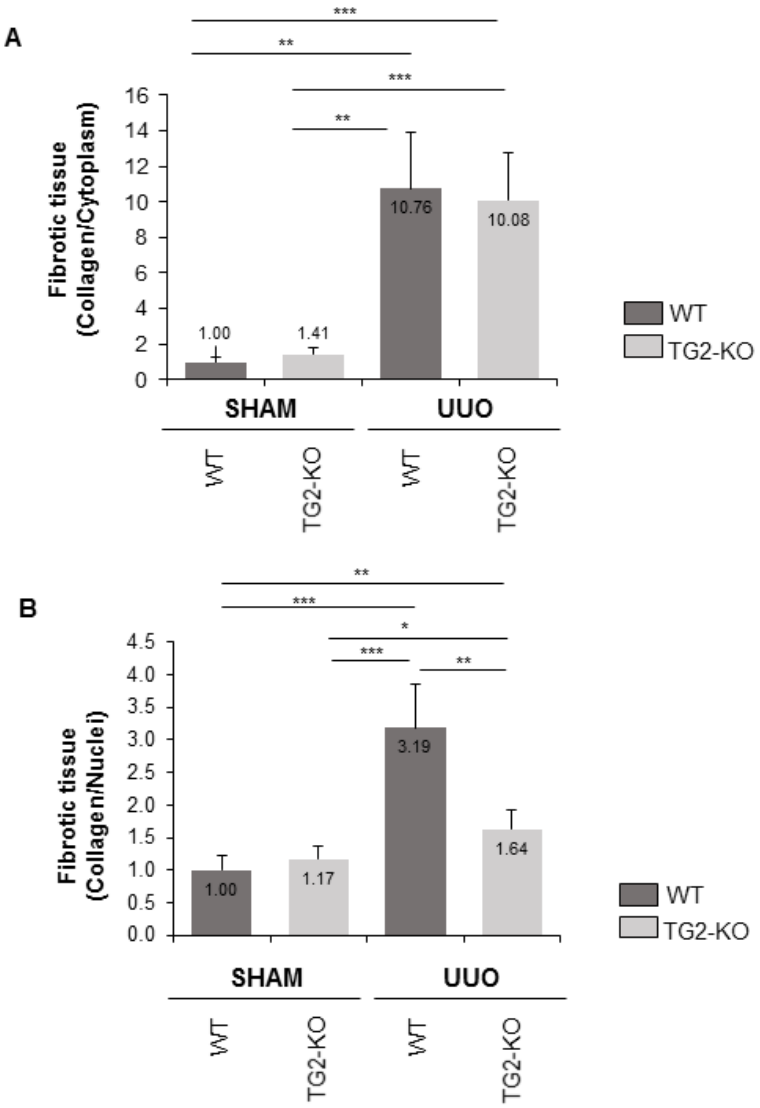

Figure 3.17: Quantification of renal fibrosis by Masson's trichrome (MT) staining. In order to quantify the level of fibrosis in WT and TG2-KO mice subjected to 21 days UUO (**Fig. 3.16**), quantification of MT-stained sections was performed with Cell^F imaging system software (Olympus, Japan). The level of fibrosis was measured as (A) ratio of phase 2 (collagen, light blue) over phase 1 (cytoplasm, pink) or as (B) ratio of phase 2 (collagen, light blue) over phase 3 (nuclei, brown). Data represent mean values expressed relative to the WT sham operated control (equalised to 1) ± SEM, n=24 different fields per treatment covering both cortical and medullar areas. Significance of the differences between treatments/phenotypes was determined by T-test: * = $p<0.05$, ** = $p<0.01$, *** = $p<0.001$, **** = $p<0.0001$.

3.4.7.2 Investigation of α-SMA expression and TGF-β1 activation in TG2-null kidneys subjected to UUO

In order to verify the knock-out of TG2 at a protein level, kidney lysates from TG2-KO mice subjected to UUO or Sham-operation (21 days) were immunoprobed for TG2 by western blotting as described in 3.3.3. Subsequently, the expression of the mesenchymal marker α-SMA was investigated in TG2-null kidneys at 21-days post-UUO by probing the same kidney lysates.

In both cases, both male (N=3) and female (N=3) randomly selected kidney samples were tested in order to examine a possible gender bias in protein expression. In all experiments, constitutively expressed cyclophilin-A (CypA) was employed as loading control.

TG2 expression was virtually absent in TG2-KO male mice subjected either to Sham operation or UUO (**Fig. 3.18A, B**), while a clear signal was observed in the WT. In females (**Fig. 3.18D, E**) TG2-immunoprobing revealed a weak signal in the TG2-null mice (**Fig. 3.18D**, asterisk), that should have a complete knock out of TG2 at a protein level (De Laurenzi and Melino 2001). This signal observed in TG2-KO females is likely to result from unspecific binding of the antibody employed to another protein, that could be also noticed in WT females, where a double band was evident (**Fig. 3.18D**, asterisk) in both UUO and Sham operated condition.

When the same samples were probed for α-SMA, the signal was absent or low in Sham operated kidneys of both TG2-null male (**Fig. 3.18A, C**) and female (**Fig. 3.18D,F**) mice; it was comparable to the one observed in WT mice subjected to the same procedure and described before in 3.4.2.2, however a small (not significant) increase in signal upon TG2-KO when band intensity was measured by densitometry.

At 21-days post-UUO, the α-SMA immunoreactive band at ~37 kDa was detected in TG2-KO mice of both genders (**Fig. 3.18A, C**, **D, F**) in line with fibrosis progression. In male mice (**Fig. 3.18A, C**) α-SMA expression in TG2-KO upon 21 days-UUO was 12.55 ± 5.93 – fold higher than the sham operated WT control (p=0.08, not significant), normalized to 1 in the graph, and 7.14 ± 4.70-fold higher than their own TG2-null control (p=0.08, not significant). The raise in α-SMA expression upon UUO was lower in mice devoid of TG2 compared to the WT ones, characterized by an average 22-fold increase in α-SMA signal, but the difference didn't appear significant by T-test (p=0.19) (**Fig. 3.18 A, C**). The noticeable drop in the fibrosis marker expression in TG2-KO mice subjected to UUO, compared to WT mice, might suggest protective role of TG2 deletion against the progression of fibrosis, in agreement with previous studies using both general TG inhibitors (Skill, et al. 2004, Johnson, et al. 2007, Huang, et al. 2009) or specific TG2-KO (Shweke, et al. 2008, Fisher, et al. 2009).

In female mice (**Fig. 3.18 D, F**)**,** again, an increase in α-SMA could be appreciated in both WT and TG2-KO individuals subjected to 21-days UUO. In TG2 null mice, the increase was 3.57 ± 1.14 – fold higher than the sham operated WT control (p=0.19, not significant), normalized to 1 in the graph, and 2.17 ± 0.79 – fold higher than its own TG2-null control (p=0.24, not significant). Again, the α-SMA expression was in average lower than the signal observed in WT mice subjected to the same procedure, but the difference wasn't regarded as significant when analyzed by T test(p=0.57). The effect was less evident in female mice than in male, and might suggest a gender bias in the rate of fibrosis development and/or in the protective effect of TG2 deletion.

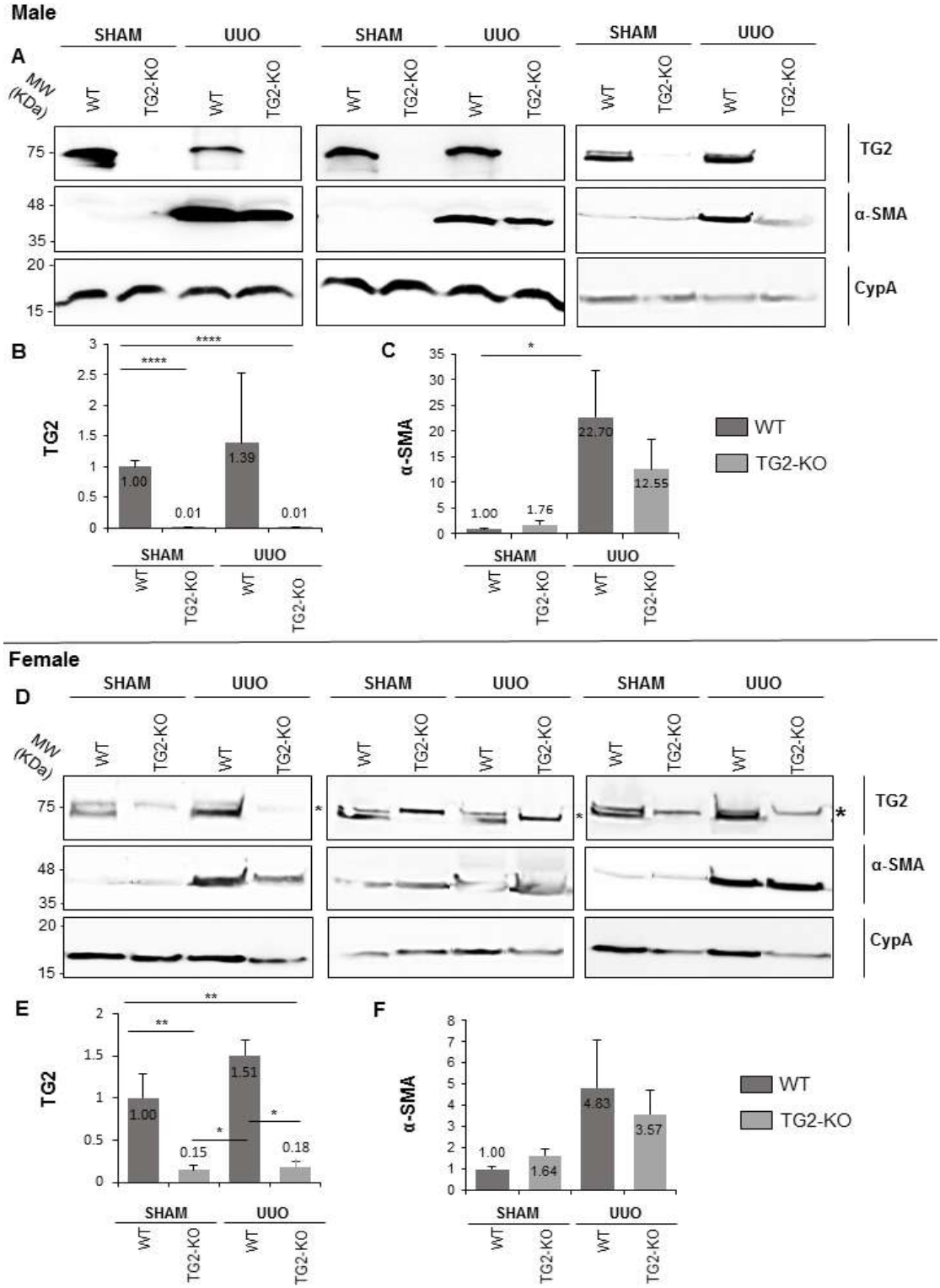

Figure 3.18: Expression of TG2 and fibrosis marker α-smooth muscle actin (α-SMA) in WT and TG2-KO kidney lysates from the UUO model at 21-days. Expression of TG2 and fibrosis marker α-SMA was detected by Western blot using the specific antibodies reported in **Table 3.2**. Experiment was performed on 3 different male kidneys (A-C) or 3 different female kidneys (D-F). Specific blots are shown on the left (A,D). Intensity of immunoreactive bands was quantified by densitometric analysis and normalised to constitutively expressed Cyclophilin A (CycA). The graphs represent mean values expressed relative to the Sham operated control (equalised to 1) ± SD, n = 3 kidney lysates per group for either male (B,C) or female (D,F) mice. Significance of the differences between treatments/phenotypes was determined by T-test: * = $p<0.05$, ** = $p<0.01$, *** = $p<0.001$, **** = $p<0.0001$.

TGF-β activation is a known marker of fibrosis progression, already shown to be increased by UUO procedure and to be significantly inhibited by TG2-KO in a model of UUO of lower severity (12 days)(Shweke, et al. 2008). In line with those findings, in this chapter, we have shown how UUO for 21 days led to a strong increase in TGF-β1 activation [3.4.3]. In order to investigate the effect of TG2-KO in our model of established UUO, a TGF-β activity bioassay was performed on TG2-null mice subjected to UUO (21 days) or Sham operation, as described in 3.3.4.

TGF-β activation was almost absent in Sham operated TG2-null kidneys (**Fig. 3.19**) and not different from the WT mice subjected to the same procedure. As described before in 3.4.3, UUO treatment for 21 days determined a strong increase of TGF-β activity in WT mice, that was almost 30-fold higher than the control ($p<0.0001$, ****). Interestingly, this activation was significantly driven back to basal levels (~1) in UUO TG2-KO mice ($p<0.0001$, ****) (**Fig. 3.19**). This confirms a crucial role for TG2 in TGF-β activation (Kojima, Nara and Rifkin 1993, Nunes, et al. 1997, Huang, et al. 2010b) while supporting the idea of a protective role of TG2-KO in this model of CKD, involving a reduced activation of the cytokine (Shweke, et al. 2008).

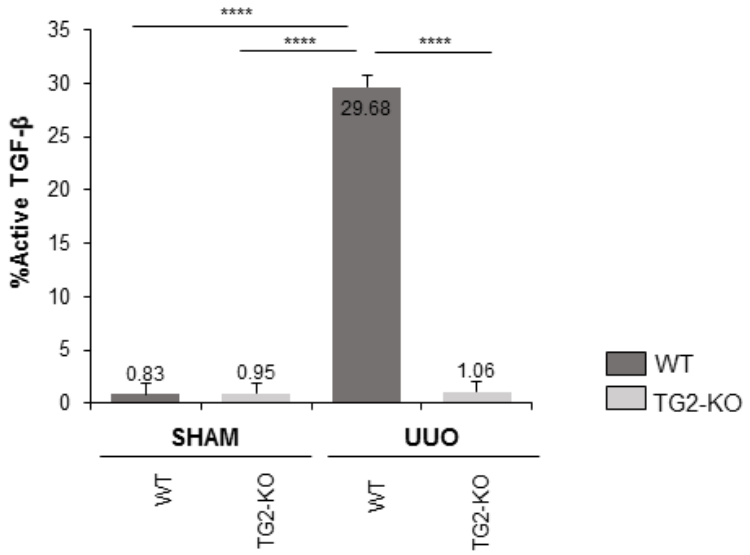

Figure 3.19: Level of active TGF-β in kidney lysates from the UUO model in WT and TG2-KO mice. In order to measure the activation of TGF-β on WT ad TG2-null mice at 21 days post-UUO, active and total TGF-β were assessed using 100 µl of 10% (w/v) kidney lysate or acid-treated lysate, both 10 times diluted, on the MLEC system. Data represent the mean % of active TGF-β ± SD, N=3. Significance of the differences between treatments/phenotypes was determined by T-test: * = $p<0.05$, ** = $p<0.01$, *** = $p<0.001$, **** = $p<0.0001$.

3.4.7.3 SWATH-MS proteomic analysis of proteins differentially expressed upon TG2-KO shows minimal alteration due to TG2 deletion.

In order to determine which were significantly altered in expression by TG2-KO in either healthy or fibrotic conditions, four randomly selected Sham operated TG2-null kidneys and four randomly selected UUO TG2-null kidneys, at 21 days post-surgery and of both genders, were analyzed by SWATH-MS as described in 3.3.6 and FC analysis was performed by OneOmics [3.3.6.2] against the spectral results of WT mice subjected to the same treatments (**Fig. 3.20**). In this way, differences between TG2-KO mice and WT mice were measured as fold change in protein expression, and, to keep consistency with the previous analysis, a confidence of fold change ≥0.8 was regarded as significant for variation. The outcome of the FC analyses between TG2-null and WT at a confidence of fold change [C(FC)] up to 0.5, can be found in the Supplementary information of this thesis (**Suppl. Table 3.2** = TG2-null and WT, Sham operated; **Suppl. Table 3.3**= TG2-null and WT, UUO).

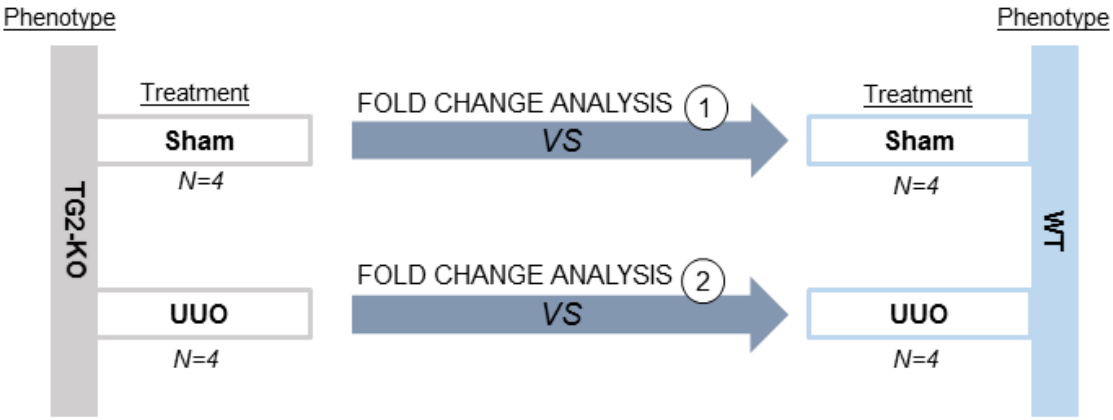

Figure 3.20: SWATH-MS Experimental setup to identify proteins significantly altered by TG2 knock-out in healthy (Sham) or fibrotic (UUO) C57BL/6J mice. (1) = Proteins significantly altered upon TG2-KO in Sham operated mice - Results in **Table 3.16A**; (2) = Proteins significantly altered upon TG2-KO in UUO mice - Results in **Table 3.16B**

Of the 2106 proteins detected by SWATH acquisition in the different samples, few were identified as differentially expressed upon TG2-KO at the chosen confidence level (C(FC)≥0.8) and are displayed in **Tables 3.16 and 3.17**.

Only 4 proteins appeared altered in TG2-null mice in Sham operated conditions, when compared to healthy WT mice (**Table 3.16**), while 31 were altered in TG2-KO mice subjected to 21 days – UUO, when compared to the WT counterpart (**Table 3.16**). In both cases, as expected, TG2 was significantly underexpressed, at a confidence higher than 80%.

In Sham operated conditions (**Table 3.16**), three proteins were overexpressed in TG2-KO animals compared to the WT: one ribosomal protein (RL24_MOUSE), one histone protein (H14_MOUSE) and another protein called calcium-binding protein 39 (CAB39_MOUSE), a

protein involved in the stimulation of the activity of serine/threonine kinases activities such as liver kinase B1 (LKB1), which has been involved in control of metabolism and proliferation in kidney cells and to be downregulated upon CKD, where its loss is associated with a pro-fibrotic phenotype of cells (Han, et al. 2016, Alexander and Walker 2011). TG2 (TGM2_MOUSE) was the only underexpressed protein, and was 9 times underexpressed comparing to WT, confirming the knock-out of the enzyme in this system (**Table 3.16**).

In order to investigate whether other proteins were differentially expressed by TG2-KO at a lower confidence of fold change, the outcome of the FC analysis between TG2-null and WT healthy mice (Sham operated) was analysed to a confidence of 0.5 (**Suppl. Table 3.2**). 50 proteins resulted increased by TG2-KO at this level of confidence, of which 26 proteins were either ribosomes or histone proteins [C(FC) generally ≥0.6]. The others were mostly associated with cell metabolism, however, few keratins resulted increased by TG2 deletions. The protein fermitin (URP2_MOUSE), involved in cell adhesion by binding integrin, was almost 6-times increased comparing to the healthy WT mice, and might reveal a compensatory effect or the KO, in response to loss of cellular adhesion. A number of proteins involved in intracellular vesicular trafficking, lysosome targeting and retromer transport were also identified.

The downregulated proteins [log2FC (TG2-KO/WT)]<0 were only 22 at this level of confidence. They included for example the exosome protein transmembrane protein 256 (TM256_MOUSE) as 1.5-fold increased compared to the WT; this might suggest a role for TG2 in the promotion of exosome trafficking.

Table 3.16: List of proteins differentially expressed (confidence ≥ 0.8) in the TG2-KO mice in Sham operated conditions, and corresponding fold change from the WT. In red the positive logarithm of FC from the WT mice (overexpression in TG2-KO comparing to WT) while in green the negative logarithm of FC (underexpression in TG2-KO comparing to WT). In shades of yellow the confidence of the change. A confidence ≥ 0.8 was regarded as significant

Proteins significantly modulated by TG2-KO in Sham operated mice (21 days)				
Protein ID	**Name**	**Log2 FC (TG2-KO Sham/ WT Sham)**	**Abs FC (TG2-KO Sham/ WT Sham)**	**C(FC)**
CAB39_MOUSE	Calcium-binding protein 39	1.88	3.69	0.81
RL24_MOUSE	60S ribosomal protein L24	0.85	1.81	0.90
H14_MOUSE	Histone H1.4	0.81	1.75	0.84
TGM2_MOUSE	Transglutaminase 2	-3.16	8.94	0.84

In UUO conditions (**Table 3.17**), the situation observed was slightly different, with a higher amount of overexpressed proteins as a consequence of TG2-KO at a confidence level of 0.8. In this case, in fact, 28 proteins were upregulated in TG2-null mice compared to the WT ones. Interestingly majority of these proteins, 19, were ribosomal, while 7 were histone proteins (**Table 3.17**). RL24_MOUSE and H14_MOUSE, that were the only ribosomal protein and the only histone protein overexpressed in TG2-null Sham operated mice (**Table 3.17**), were detected also in this list (**Table 3.17**) at C(FC)≥0.8. The remaining two proteins overexpressed in TG2-KO UUO mice compared to WT were translocator protein (TSPO_MOUSE) and mitochondrial import receptor subunit TOM5 homolog (TOM5_MOUSE), which are both mitochondrial import proteins necessary for translocation of lipids or peptides from the cytosol to the inside of the mitochondria (**Table 3.17**).

The proteins underexpressed in TG2-null mice were only two, in addition to TG2 which was more than 30-fold underexpressed: these were ATP-binding cassette sub-family B member 7 (ABCB7_MOUSE), which is mitochondrial and is involved in the export from mitochondria (the opposite direction), and fatty acid-binding protein (FABP4_MOUSE), that was already mentioned before as a protein upregulated by kidney disease (Górski, et al. 1997, Yamamoto, et al. 2007) (**Table 3.17**).

The proteins significantly altered by TG2-KO in mice subjected to UUO were analysed on STRING v10 to define possible interactions. As shown in **Fig. 3.21**, at a middle confidence level (0.4), two clear clusters of ribosomal and histone proteins were identified by STRING, while the other proteins, including TG2, were showing no interaction between themselves (not described nor predicted) or the clusters.

Table 3.17: List of proteins differentially expressed (confidence ≥ 0.8) in the TG2-KO mice at 21-UUO conditions, and corresponding fold change from the WT. In red the positive logarithm of FC from the WT mice (overexpression in TG2-KO comparing to WT) while in green the negative logarithm of FC (underexpression in TG2-KO comparing to WT). In shades of yellow the confidence of the change. A confidence ≥ 0.8 was regarded as significant

Proteins significantly modulated by TG2-KO in mice subjected to UUO (21 days)				
Protein ID	**Name**	**Log2 FC (TG2-KO UUO/ WT UUO)**	**Abs FC (TG2-KO UUO/ WT UUO)**	**Confidence**
TSPO_MOUSE	Translocator protein	1.79	3.46	1.00
H12_MOUSE	Histone H1.2	1.55	2.92	0.94
RL19_MOUSE	60S ribosomal protein L19	1.45	2.73	0.85
H10_MOUSE	Histone H1.0	1.44	2.72	0.82
H14_MOUSE	Histone H1.4	1.41	2.66	0.95
RL24_MOUSE	60S ribosomal protein L24	1.31	2.49	0.92
RL13_MOUSE	60S ribosomal protein L13	1.26	2.39	0.89
H15_MOUSE	Histone H1.5	1.24	2.35	0.88
H11_MOUSE	Histone H1.1	1.22	2.34	0.97
RL8_MOUSE	60S ribosomal protein L8	1.17	2.25	0.84
TOM5_MOUSE	Mitochondrial import receptor subunit TOM5 homolog	1.17	2.25	0.97
RL14_MOUSE	60S ribosomal protein L14	1.15	2.22	0.93
RL7A_MOUSE	60S ribosomal protein L7a	1.14	2.21	0.86
RS30_MOUSE	40S ribosomal protein S30	1.14	2.21	0.91
RS24_MOUSE	40S ribosomal protein S24	1.10	2.15	0.92
RL4_MOUSE	60S ribosomal protein L4	1.09	2.14	0.86
RL27_MOUSE	60S ribosomal protein L27	1.09	2.14	0.83
RL36_MOUSE	60S ribosomal protein L36	1.02	2.03	0.89
RL13A_MOUSE	60S ribosomal protein L13a	0.89	1.85	0.81
H4_MOUSE	Histone H4	0.89	1.85	0.82
RL17_MOUSE	60S ribosomal protein L17	0.87	1.82	0.85
RL7_MOUSE	60S ribosomal protein L7	0.85	1.80	0.91
RS18_MOUSE	40S ribosomal protein S18	0.81	1.75	0.87
RL18_MOUSE	60S ribosomal protein L18	0.79	1.73	0.87
RS29_MOUSE	40S ribosomal protein S29	0.74	1.67	0.80
RS13_MOUSE	40S ribosomal protein S13	0.68	1.60	0.86
RS25_MOUSE	40S ribosomal protein S25	0.66	1.59	0.84
H2B1P_MOUSE	Histone H2B type 1-P	0.57	1.48	0.83
ABCB7_MOUSE	ATP-binding cassette sub-family B member 7, mitochondrial	-0.39	1.31	0.88
FABP4_MOUSE	Fatty acid-binding protein, adipocyte	-1.06	2.08	0.87
TGM2_MOUSE	Transglutaminase 2	-4.97	31.44	0.85

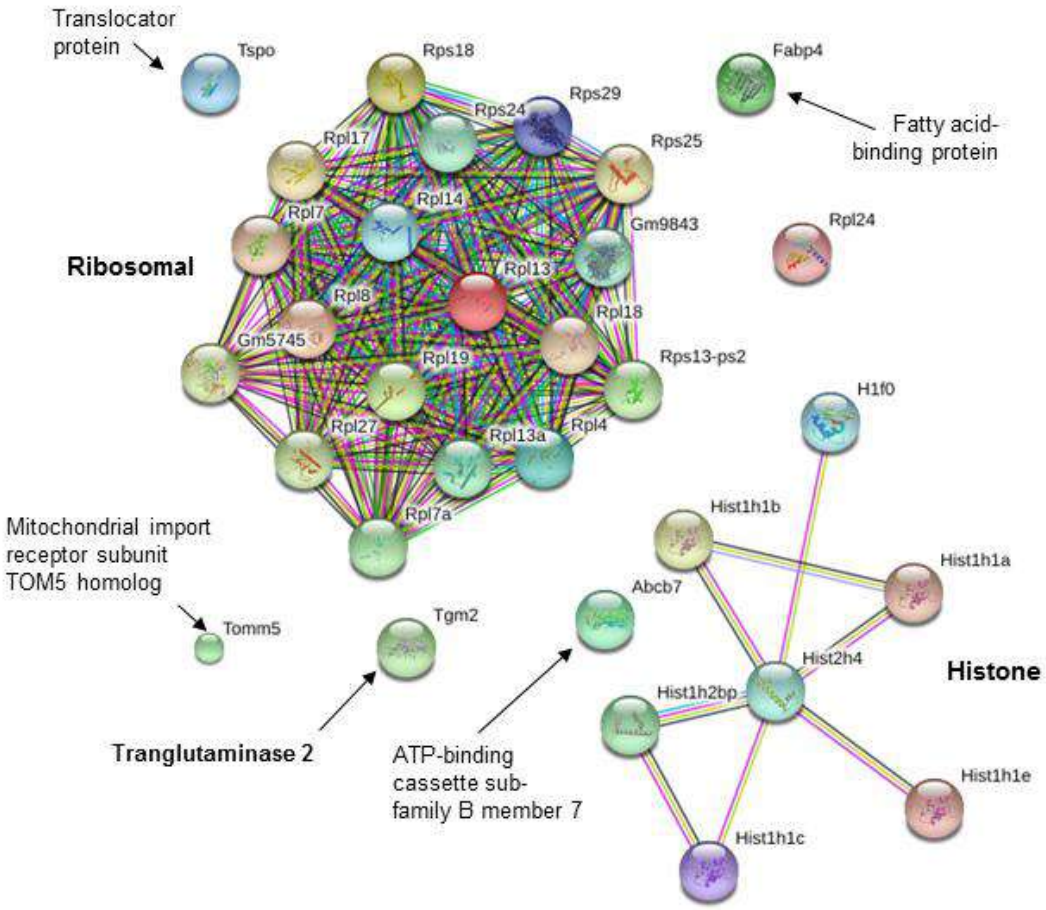

Figure 3.21: Network of protein-protein interactions of TG2-KO differentially expressed proteins in UUO mice (21 days). Network of known and predicted protein-protein interactions was designed in STRING (http://string-db.org) using the list of differentially expressed proteins of TG2-null mice subjected to UUO reported in Table 13B. A confidence of at least 0.4 (middle confidence in STRING) was chosen as threshold for the interactions identified.

When we considered a broader confidence level, higher than the 50% (displayed in **Suppl. Table 3.3**), numerous other proteins were identified as upregulated by TG2 deletion in UUO conditions. Of the 69 proteins having a positive fold change from the WT conditions at this level of confidence, 58 were either ribosomal or histone proteins, while only 11 were associated with other functions. These proteins were mostly mitochondrial and associated with cell metabolism, which might be correlated to an increased cell viability when TG2 was deleted.

At the same confidence threshold, 77 proteins appeared downregulated by TG2-KO in mice subjected to 21-days UUO. Among these proteins, only two ribosome subunits and no histone were identified. All the other proteins were associated with a plethora of intracellular and extracellular processes, and a number of them can be correlated to a bad outcome of CKD by being involved in matrix deposition, inflammation, apoptotic response, cytokine activation etc. (**Suppl. Table 3.3**), supporting the idea of a protective action of TG2 in the context of fibrosis. To cite only few examples, both collagen VI and collagen XVIII (HSPG-endostatin) were identified as downregulated by TG2-KO at a confidence higher than 60%. A number of

fibrinogen chains (FIBA_MOUSE, FIBB_MOUSE, FIBG_MOUSE) were ~2-fold downregulated at a C(FC)≥0.6, suggesting a role for TG2 on all stages of wound healing/fibrotic process (**Suppl. Table 3.3**). Thrombospondin (TSP1_MOUSE), a matrix glycoprotein known to be upregulated by TGF-β and to be significantly involved in its activation upon kidney disease (Hugo, Kang and Johnson 2002, Daniel, et al. 2004, Murphy-Ullrich, et al. 2002) was also downregulated by TG2-KO at C(FC)=0.74 (**Suppl. Table 3.3**). Cell signalling protein calmodulin (CALM_MOUSE) (C(FC)=0.76) and proteins of the 14-3-3 family [C(FC) ~0.6], known to bind phosphorylated TG2 with a possible role in cell signalling (Mishra and Murphy 2006) were also underexpressed upon KO when a lower level of significance was considered (**Suppl. Table 3.3**). Other proteins were associated with cytoskeletal remodelling and cell adhesion, and some were even involved in intracellular vesicular trafficking (**Suppl. Table 3.3**). Finally, the well-known marker of exosomal vesicles CD63 (CD63_MOUSE) was minimally downregulated by the KO [C(FC)>0.7] (**Suppl. Table 3.3**), suggesting a possible correlation between TG2 expression and exosome formation.

In summary, MS analysis of protein expression in TG2-KO mice in comparison with WT mice, in both healthy and fibrotic conditions, revealed minimal changes in protein expression at an high level of FC confidence, mostly involving an upregulation of ribosomal and histone proteins when mice were deprived of the enzyme. However, observation of expression variations at lower level of confidence highlighted a number of proteins that can be associated with a protective role for TG2 in disease, such as extracellular matrix proteins, cytoskeletal elements and signalling proteins that might control the localisation and activity of pro-fibrotic factors and cytokines. A possible involvement of TG2 in signalling and vesicular transport was also underlined by this analysis.

3.4.7.4 SWATH-MS proteomic analysis of proteins differentially expressed upon UUO in TG2-KO mice and comparison with the same analysis performed in WT mice.

Being interested in defining if the TG2-KO was determining an alteration in the list of proteins differentially expressed upon UUO, SWATH acquisition-MS was performed on 4 TG2-KO Sham operated kidneys and 4 TG2-KO UUO kidneys at 21 days post-operation, and data were acquired as described in 3.3.6. Fold change variations in proteins' expression between UUO and Sham operated TG2-null mice were calculated by OneOmics processing software, in the same way as the analysis performed in WT mice and reported in 3.4.4 (**Fig. 3.22**, **1**). The outcome of the FC analysis between UUO and Sham operated samples in TG2-null mice, at a confidence [C(FC)] higher than 0.5, can be found in the supplementary information of this thesis (**Suppl. Table 3.4**). Likewise the analysis performed in WT mice, candidates were regarded as significantly overexpressed or underexpressed upon UUO in TG2-null mice (comparing to the sham operated control in the same phenotype) at a C(FC) ≥ 0.8.

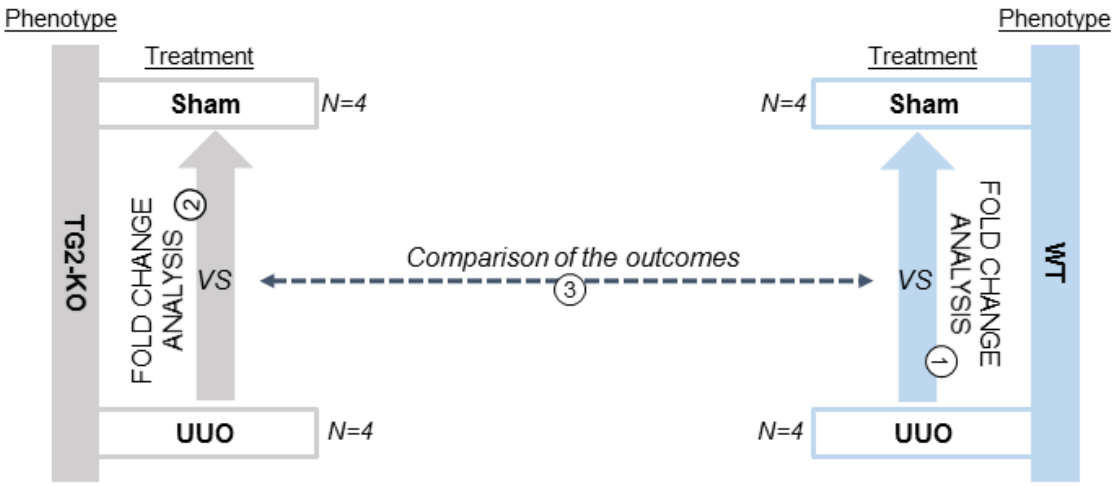

Figure 3.22: SWATH-MS experimental setup to identify proteins significantly altered by UUO in TG2-KO C57BL/6J mice. (1) = Proteins significantly altered upon UUO in WT mice – Results in 3.4.4, Lists in **Suppl. Tables 3.5 and 3.6**; **(2)** = Proteins significantly altered upon UUO in TG2-null mice – Results in **Suppl. Tables 3.15 and 16**; **(3)** = Comparison of the outcomes of the Analysis 1 and 2 - Results in **Suppl. Tables 17 and 18**.

Of the 2106 proteins detected by SWATH-MS, 668 were identified as differentially expressed in the UUO model in TG2-null mice in a significant manner (confidence ≥ 0.8), of which 186 were upregulated post UUO (**Suppl. Table 3.15**) while 482 (**Suppl. Table 3.16**) were downregulated post-UUO. These numbers were comparable, but not identical, to the number of proteins identified as significantly overexpressed (N=195, **Suppl. Table 3.5**) or underexpressed (N=458, **Suppl. Table 3.6**) in WT mice subjected to 21 days-UUO [3.3.4].

To determine if the proteins differentially expressed upon UUO in WT mice (fully analysed in 3.4.4 and listed in **Suppl. Table 3.5 and 3.6**) were similarly modulated in TG2-KO mice, and at

the same time whether new proteins were identified as significantly altered by UUO in the TG2-null phenotype, the outcomes of the 2 analyses were compared (**Fig. 3.22, 3**) and results were collected in **Suppl. Table 3.17** (UUO-Overexpressed proteins) and **Suppl. Table 3.18** (UUO-Underexpressed proteins). A summary of protein numbers and detection overlaps is reported in **Table 3.18**.

Table 3.18: Comparison of abundance (N) of UUO-differentially expressed proteins between WT and TG2-KO mice.

Phenotype:	WT		TG2-KO	
Total/Unique proteins	Total N	Unique N	Total N	Unique N
Proteins detected	2106	0	2106	0
Differentially expressed by UUO (confidence >0.8)	653	132	668	147
UUO-Overexpressed (confidence >0.8)	195	56	186	47
UUO-Underexpressed (confidence >0.8)	458	76	482	100

The main findings obtained from this comparison are reported in **Table 3.19** and **Table 3.20**. Among the 195 UUO-overexpressed proteins identified in WT mice at a confidence level of 0.8, 139 were also identified as significantly overexpressed after 21 days-UUO in TG2 null mice (labelled as COMMON in **Suppl. Table 3.17**), while 56 appeared significantly upregulated uniquely in the WT phenotype (labelled as WT ONLY in **Suppl. Table 3.17**). On the other side, 47 proteins were detected as upregulated at a confidence level higher than 0.8 only in the TG2-null mice (labelled as TG2-KO ONLY in **Suppl. Table 3.17**).

Among the UUO overexpressed proteins in both phenotypes, the more interesting finding was tapasin (TPSN_MOUSE) characterized by a substantial 36.41-fold increase in expression compared to sham operated control in WT mice at a confidence of 0.76, that can be regarded as significant, versus a more than 5-times lower fold increase upon UUO in TG2-null mice (6.71-fold from sham, confidence 0.89) (**Table 3.19**). Uromodulin (UROM_MOUSE) was more overexpressed in WT mice subjected to UUO compared to TG2-null mice (16.84 vs 9.78 – fold higher than the Sham operated control) as well as Fibrillin 1 (FBN1_MOUSE, 10.84 vs 8.05 - fold) (**Table 3.19**).

Some proteins recognised as UUO-overexpressed in WT mice were not significantly varying upon UUO in TG2-null mice, such as alpha-1-antitrypsin 1-2 (A1AT2_MOUSE), fibulin 2 (FBLN2_MOUSE) and metallothionein-2 (MT2_MOUSE). Fatty acid-binding protein (FABP4_MOUSE), even appeared downregulated (log2FC<0) by the UUO in TG2-null mice at a confidence close to 0.8 (**Table 3.19**). As a confirmation of the TG2-KO, TG2-null mice showed

no significant variation of TG2 expression upon UUO, while an overexpression was observable in WT mice (**Table 3.19, Fig 3.23**).

On the other side, collagen alpha-1(XII) chain (COCA1_MOUSE) was more overexpressed in TG2-deprived UUO mice (26.15-fold) than in WT mice (15.92 fold), and a similar difference was detected in fibrillin 2 (FBN2_MOUSE), with an overexpression upon UUO in TG2 null mice (14.52 -fold) that was almost twice the one detected in WT (7.26-fold) (**Table 3.19**).

Some proteins resulted significantly overexpressed exclusively in TG2-null mice and with a fold increase calculated from Sham higher than the WT. Examples were protein S100-A6 (S10A6_MOUSE), that was 10.94-fold overexpressed in TG2-KO UUO mice and Major urinary protein 6 (MUP6_MOUSE), 7.80-fold overexpressed (**Table 3.19**). In line with previous observation, moreover, a portion of the 47 proteins with positive fold increase significant in "TG2-KO only" at C(FC)≥0.8 were histone proteins: histone H1.5 (H15_MOUSE), histone H1.1 (H11_MOUSE), histone H2A type 1-H (H2A1H_MOUSE), histone H1.2 (H12_MOUSE), histone H2AX (H2AX_MOUSE), histone H2B type 1-P (H2B1P_MOUSE) (**Suppl. Table 3.17**), some of which already reported as significantly overexpressed upon TG2-KO in UUO mice in 3.4.7.3 section (**Table 3.17**), H12_MOUSE, H15_MOUSE, H11_MOUSE and H2B1P_MOUSE.

Table 3.19. Proteins significantly overexpressed (Confidence ≥ 0.8) in either WT or TG2-KO kidneys subjected to UUO (21 days) that show clear differences between phenotypes. In increasing shade of red the positive log2 (Log2FC) of fold change from the sham operated condition (the more intense, the more overexpressed), in decreasing shades of green the negative log2 (Log2FC) of fold change from the sham operated condition (the more intense, the more underexpressed), in increasing shades of grey the absolute fold change from the sham operated condition (ABS FC, absolute increase or decrease depending of the sign of Log2FC) while in shades of yellow the confidence of the change.

	Protein ID	Name	WT			TG2-KO		
			Log2 (FC)	Abs (FC)	C(FC)	Log2 (FC)	Abs (FC)	C(FC)
More overexpressed by UUO in WT	TPSN	Tapasin	5.19	36.41	0.76	2.75	6.71	0.89
	UROM	Uromodulin	4.03	16.34	0.85	3.29	9.78	0.88
	FBN1	Fibrillin-1	3.44	10.84	0.89	3.01	8.05	0.89
	FBLN2	Fibulin-2	3.27	9.65	0.81	2.32	4.99	0.54
	K1C19	Keratin, type I cytoskeletal 19	3.26	9.57	0.86	2.99	7.95	0.89
	C1QB	Complement C1q subcomponent subunit B	3.24	9.42	0.70	2.12	4.35	0.91
	TAGL	Transgelin	3.21	9.27	0.89	2.78	6.86	0.89
	VIME	Vimentin	3.10	8.56	0.90	2.74	6.67	0.91
	MT2	Metallothionein-2	3.02	8.11	0.84	-3.36	10.27	0.09
	A1AT2	Alpha-1-antitrypsin 1-2	2.97	7.86	0.82	1.31	2.48	0.48
	PLSL	Plastin-2	2.93	7.63	0.85	2.25	4.77	0.82
	E41L2	Band 4.1-like protein 2	2.70	6.51	0.77	1.69	3.22	0.88
	CNN2	Calponin-2	2.62	6.15	0.80	2.04	4.11	0.84
	LG3BP	Galectin-3-binding protein	2.53	5.78	0.67	1.70	3.26	0.81
	FIBA	Fibrinogen alpha chain	2.21	4.64	0.90	0.93	1.91	0.69
	CO4A2	Collagen alpha-2(IV) chain	2.17	4.50	0.80	1.45	2.73	0.79
	FIBG	Fibrinogen gamma chain	2.15	4.45	0.85	1.50	2.82	0.74
	FIBB	Fibrinogen beta chain	2.00	4.00	0.86	0.96	1.95	0.71
	K2C79	Keratin, type II cytoskeletal 79	1.61	3.05	0.91	0.65	1.57	0.56
	AGRIN	Agrin	1.11	2.16	0.92	0.73	1.66	0.67
	FABP4	Fatty acid-binding protein, adipocyte	0.86	1.82	0.85	-0.76	1.69	0.78

	TGM2	Transglutminase 2	0.78	1.71	0.90	-1.49	2.81	0.17
More overexpressed by UUO in TG2-KO	COCA1	Collagen alpha-1(XII) chain	3.99	15.92	0.82	4.71	26.15	0.83
	FBN2	Fibrillin-2	2.86	7.26	0.94	3.86	14.52	0.89
	RCN3	Reticulocalbin-3	2.73	6.65	0.74	3.22	9.30	0.84
	ELN	Elastin	1.88	3.69	0.61	2.53	5.78	0.83
	MUP6	Major urinary protein 6	1.56	2.94	0.62	2.96	7.80	0.95
	S10A6	Protein S100-A6	1.50	2.82	0.65	3.45	10.94	0.81

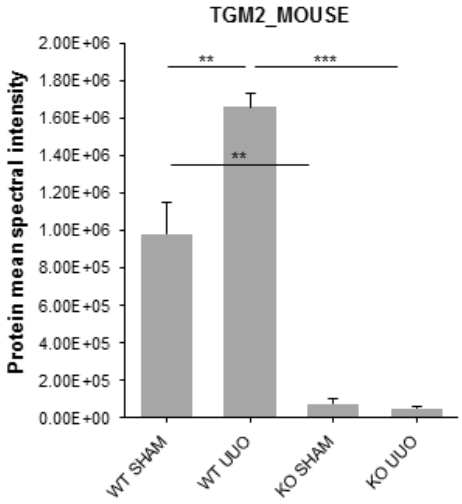

Figure 3.23: Relative quantification of TG2 expression based on normalised calculated protein spectra as detected upon UUO or Sham operation in WT or TG2-null mice by SWATH-MS data acquisition. Column show the mean normalised protein area as calculated by the software ± SD, N=4 samples per treatment. Significance of the differences between spectral means was determined by T-test: * = p<0.05, ** = p<0.01, *** = p<0.001, **** = p<0.0001.

Among the 458 UUO-underexpressed proteins identified in WT mice at a confidence level of 0.8, 382 were also identified as significantly underexpressed after 21 days-UUO in TG2 null mice at the same confidence level (labelled as COMMON in **Suppl. Table 3.18**), while 76, even if having a negative logarithm of fold change in both phenotypes, appeared significantly underexpressed uniquely in the WT phenotype (labelled as WT ONLY in **Suppl. Table 3.18**). On the other side, 100 proteins were detected as upregulated at a confidence level higher than 0.8 only in the TG2-null mice (labelled as TG2-KO ONLY in **Suppl. Table 3.18**). Few examples of proteins with different levels of underexpression between WT and TG2-KO phenotypes subjected to UUO are reported in **Table 3.20**.

The 3 most underexpressed proteins in WT mice subjected to UUO, Glucose-6-phosphatase (G6PC_MOUSE), mitochondrial Kynurenine/alpha-aminoadipate aminotransferase (AADAT_MOUSE), and Hydroxyacid oxidase (HAOX2_MOUSE), all involved in metabolic processes and energy production in the cell, were much less downregulated TG2-null individuals subjected to the same treatment. Particularly evident was the difference in the first 2 proteins, with more than 70-fold increase in WT versus less than 11 in TG2-KO (G6PC_MOUSE) and 48 -fold increase versus 11.59 (AADAT_MOUSE) (**Table 3.20**). Calbindin

(CALB1_MOUSE), an interesting protein in the context of kidney fibrosis (Steiner, et al. 1996, Armbrecht, et al. 1989, Sooy, Kohut and Christakos 2000, Hoffmann, et al. 2010), was also less downregulated in TG2-null mice. Another protein more underexpressed upon UUO in WT mice was the already mentioned mitochondrial import receptor subunit TOM5 homolog (TOM5_MOUSE)(7.94-fold increased in UUO WT mice versus 2.69 in TG2-null), already identified as significantly upregulated upon knock out of TG2 in UUO mice as reported in 3.4.7.3 section (**Table 3.17**). Some proteins, such as translocator protein (TSPO_MOUSE) and 40S ribosomal protein S24 (RS24_MOUSE) were not significantly altered by the UUO in TG2-null mice. On the other side, a number of proteins were showing a higher downregulation upon TG2-KO. The more evident examples were the bifunctional epoxide hydrolase 2 protein (HYES_MOUSE), 25.06-times underexpressed in TG2-null mice versus only 4.85-fold decrease in WT, and PDZK1-interacting protein 1, more than 90-times downregulated in the TG2-null mice subjected to UUO.

Table 3.20. Proteins significantly Underexpressed (Confidence ≥ 0.8) in either WT or TG2-KO kidneys subjected to UUO (21 days) that show clear differences between phenotypes. In increasing shade of red the positive log2 (Log2FC) of fold change from the sham operated condition (the more intense, the more overexpressed), in decreasing shades of green the negative log2 (Log2FC) of fold change from the sham operated condition (the more intense, the more underexpressed), in increasing shades of grey the absolute fold change from the sham operated condition (ABS FC, absolute increase or decrease depending of the sign of Log2FC) while in shades of yellow the confidence of the change.

	Protein ID	Name	WT			TG2-KO		
			Log2 (FC)	Abs (FC)	C(FC)	Log2 (FC)	Abs (FC)	C(FC)
More Underexpressed by UUO in WT	G6PC	Glucose-6-phosphatase	-6.17	72.24	0.86	-3.43	10.79	0.83
	AADAT	Kynurenine/alpha-aminoadipate aminotransferase, mitochondrial	-5.59	48.00	0.84	-3.54	11.59	0.80
	HAOX2	Hydroxyacid oxidase 2	-5.47	44.28	0.85	-4.18	18.08	0.88
	CALB1	Calbindin	-5.00	32.07	0.91	-4.40	21.18	0.92
	PXMP2	Peroxisomal membrane protein 2	-3.78	13.77	0.81	-2.90	7.48	0.55
	ACE	Angiotensin-converting enzyme	-3.66	12.66	0.91	-3.21	9.27	0.79
	TOM5	Mitochondrial import receptor subunit TOM5 homolog	-2.99	7.94	1.00	-1.43	2.69	0.88
	COASY	Bifunctional coenzyme A synthase	-2.97	7.83	0.85	-2.68	6.41	0.77
	TAU	Microtubule-associated protein tau	-2.96	7.76	0.83	-2.26	4.79	0.77
	PPA6	Lysophosphatidic acid phosphatase type 6	-2.95	7.74	0.85	-2.28	4.87	0.69
	MRP2	Canalicular multispecific organic anion transporter 1	-2.59	6.03	0.82	-1.17	2.25	0.24
	TSPO	Translocator protein	-1.87	3.66	0.98	0.84	1.79	0.56
	RS24	40S ribosomal protein S24	-0.99	1.99	0.88	0.81	1.75	0.37
More Underexpressed by UUO in TG2-KO	PDZ1I	PDZK1-interacting protein 1	-5.52	45.76	0.84	-6.50	90.53	0.79
	SC5A3	Sodium/myo-inositol cotransporter	-3.86	14.51	0.63	-4.79	27.69	0.86
	HYES	Bifunctional epoxide hydrolase 2	-2.28	4.85	0.81	-4.65	25.06	0.84
	CX6A1	Cytochrome c oxidase subunit 6A1, mitochondrial	-3.57	11.91	0.74	-4.43	21.54	0.80
	GATM	Glycine amidinotransferase, mitochondrial	-3.80	13.91	0.87	-4.39	20.94	0.88
	DHAK	Triokinase/FMN cyclase	-3.56	11.77	0.80	-4.16	17.82	0.79
	ACOX1	Peroxisomal acyl-coenzyme A oxidase 1	-2.33	5.01	0.78	-3.86	14.52	0.88
	BDH2	3-hydroxybutyrate dehydrogenase type 2	-3.02	8.13	0.82	-3.48	11.18	0.80
	GLNA	Glutamine synthetase	-1.97	3.91	0.83	-3.14	8.84	0.83

In conclusion, the analysis of the protein differentially expressed by UUO in TG2-null mice compared with the differentially expressed proteins in the WT phenotype highlighted few proteins whose expression might be affected by TG2 expression in UUO.

For example, despite the pattern of protein alteration at 21 days-post UUO in TG2-null mice was generally similar to the WT mice, extracellular matrix proteins such as fibrillin-1, fibulin-2, and collagen IV, and proteins involved in wound healing and fibrosis progression such as transgelin, vimentin and fibrinogen, were more strongly upregulated by UUO in WT mice compared to the mice with TG2 depletion, suggesting a protective role of the enzyme knock-out during the progression of fibrosis in mice.

3.4.8 Power calculation confirms that a sufficient number of kidneys/treatment were employed in the SWATH-MS study.

The power calculation was performed using the Dell Statistica software (Dell, Texas, USA) comparing for each detected protein the different means and standard deviation of UUO or Sham operated kidneys (T-test for dependent samples). Being unmanageable to analyse standard deviation and means of all identified proteins, nine proteins were chosen for the analysis:

1. The UUO-Overexpressed protein with lower confidence (~0.8) (FUS_MOUSE)
2. The UUO-Overexpressed protein with higher confidence (MYH9_MOUSE)
3. The UUO-Overexpressed protein with lower fold change (LAMP1_MOUSE)
4. The UUO-Overexpressed protein with higher fold change (UROM_MOUSE)
5. The UUO-Underexpressed protein with lower confidence (~0.8) (FBX50_MOUSE)
6. The UUO-Underexpressed protein with higher confidence (TOM5_MOUSE)
7. The UUO-Underexpressed protein with lower fold change (CLH1_MOUSE)
8. The UUO-Underexpressed protein with higher fold change (G6PC_MOUSE)
9. Transglutaminase 2 (TGM2_MOUSE)

In order to determine the minimum sample size N, the desired power was set to the 90% and the desired type I error rate α to 0.05. For most of the analysed proteins (**Fig. 3.24**, tables on the left and graphs in the centre), the minimum N necessary for a power higher or equal to 90% was equal or lower than 4 individuals, and most proteins were requiring a sample size of at least 3 sample, with minimal (broken line in the graph) or no change (flat line in the graph) in the power of the experiment by increasing the dimension of the group analysed. The only exception was given by clathrin (heavy chain 1, CLH1_MOUSE), which is the protein with the lowest absolute fold change among the UUO-underexpressed proteins, that gave a minimum

sample size N of 5 with power threshold set to 90%, although N=4 was still identified by a power of the experiment higher than the 80%, which is statistically acceptable (asterisk in the corresponding graph).

The trend of minimum sample size N with respect to the probability of false positive (Type I error rate α) was also analysed (**Fig. 3.24**, graphs on the right). Setting the desired power to 90%, all proteins were showing an N≤4 when α was 0.05 or lower. The only exception was again Clathrin, where the α of 0.05 was requiring a sample size of at least 5. Again, this could be lowered down by setting the power to 0.8 in the software (data not shown).

In summary, results confirmed that the experiment had a high prediction power that was always higher than 80% when using 4 samples. For this reason, a number of biological samples equal to N=4 was considered sufficient and the results of the SWATH-MS experiment statistically reliable.

FUS_MOUSE	Sample Size Calculation (Spreadsheet1) Dependent Sample t-Test H0: Mu1 = Mu2
	Value
Population Mean Mu1	377000.0000
Population Mean Mu2	868000.0000
Group 1 S.D. (Sigma1)	87200.0000
Group 2 S.D. (Sigma2)	72800.0000
Between-group Correlation	0.5442
Stand. Error of Mean Diff.	77425.8275
Standardized Effect (Es)	-6.3416
Type I Error Rate (Alpha)	0.0500
Critical Value of t	4.3027
Power Goal	0.9000
Actual Power for Required N	0.9973
Required Sample Size (N)	3.0000

MYH9_MOUSE	Sample Size Calculation (Spreadsheet1) Dependent Sample t-Test H0: Mu1 = Mu2
	Value
Population Mean Mu1	1620000.0000
Population Mean Mu2	4010000.0000
Group 1 S.D. (Sigma1)	111000.0000
Group 2 S.D. (Sigma2)	49400.0000
Between-group Correlation	0.1027
Stand. Error of Mean Diff.	116771.4932
Standardized Effect (Es)	-20.4673
Type I Error Rate (Alpha)	0.0500
Critical Value of t	12.7062
Power Goal	0.9000
Actual Power for Required N	0.9769
Required Sample Size (N)	2.0000

LAMP1_MOUSE	Sample Size Calculation (Spreadsheet1) Dependent Sample t-Test H0: Mu1 = Mu2
	Value
Population Mean Mu1	278000.0000
Population Mean Mu2	507000.0000
Group 1 S.D. (Sigma1)	23500.0000
Group 2 S.D. (Sigma2)	16600.0000
Between-group Correlation	0.4983
Stand. Error of Mean Diff.	20953.9175
Standardized Effect (Es)	-10.9287
Type I Error Rate (Alpha)	0.0500
Critical Value of t	4.3027
Power Goal	0.9000
Actual Power for Required N	1.0000
Required Sample Size (N)	3.0000

UROM_MOUSE	Sample Size Calculation (Spreadsheet1) Dependent Sample t-Test H0: Mu1 = Mu2
	Value
Population Mean Mu1	727000.0000
Population Mean Mu2	13500000.0000
Group 1 S.D. (Sigma1)	68800.0000
Group 2 S.D. (Sigma2)	2250000.0000
Between-group Correlation	0.1976
Stand. Error of Mean Diff.	2237454.0926
Standardized Effect (Es)	-5.7087
Type I Error Rate (Alpha)	0.0500
Critical Value of t	4.3027
Power Goal	0.9000
Actual Power for Required N	0.9919
Required Sample Size (N)	3.0000

FBX50_MOUSE	Sample Size Calculation (Spreadsheet1) Dependent Sample t-Test H0: Mu1 = Mu2
	Value
Population Mean Mu1	748000.0000
Population Mean Mu2	74700.0000
Group 1 S.D. (Sigma1)	124000.0000
Group 2 S.D. (Sigma2)	11800.0000
Between-group Correlation	0.1099
Stand. Error of Mean Diff.	123262.4771
Standardized Effect (Es)	5.4623
Type I Error Rate (Alpha)	0.0500
Critical Value of t	4.3027
Power Goal	0.9000
Actual Power for Required N	0.9879
Required Sample Size (N)	3.0000

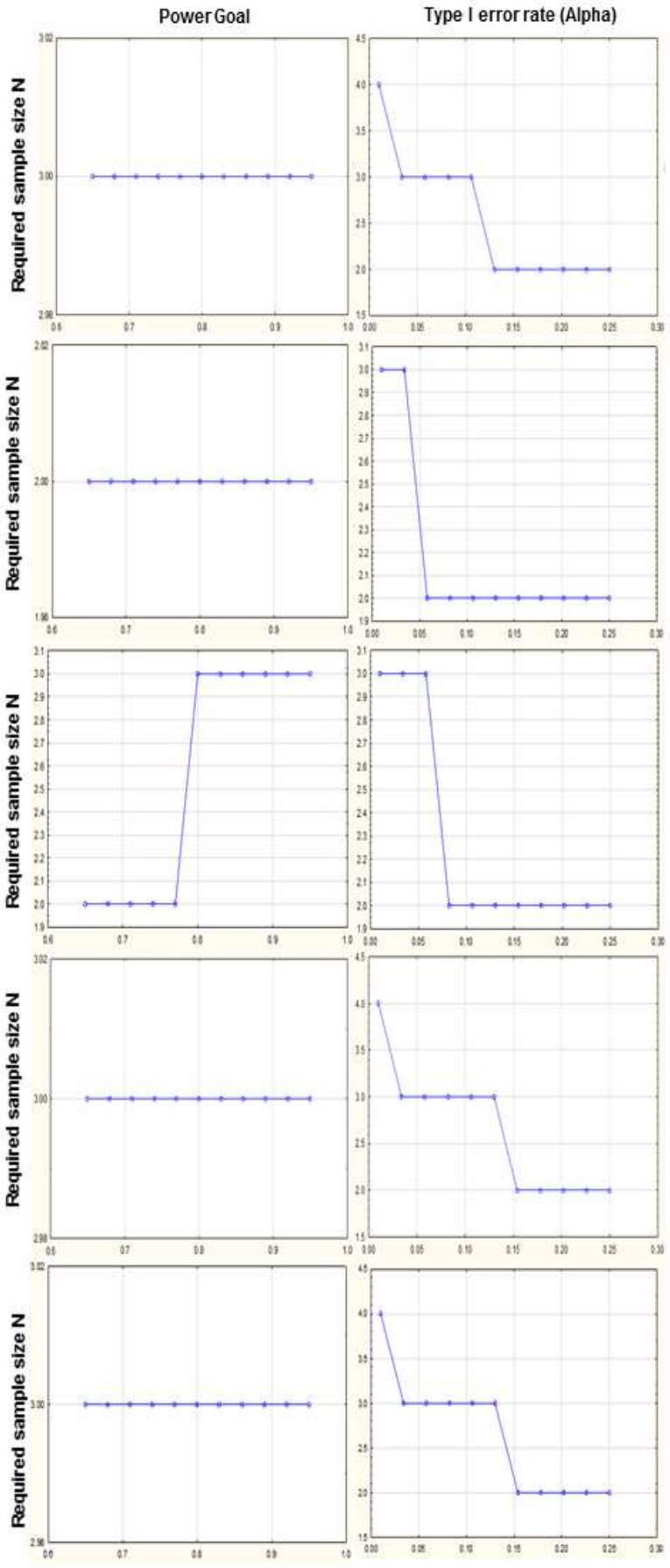

TOM5_MOUSE	Sample Size Calculation (Spreadsheet1) Dependent Sample t-Test H0: Mu1 = Mu2
	Value
Population Mean Mu1	121000.0000
Population Mean Mu2	23800.0000
Group 1 S.D. (Sigma1)	31800.0000
Group 2 S.D. (Sigma2)	16400.0000
Between-group Correlation	0.6931
Stand. Error of Mean Diff.	23607.0158
Standardized Effect (Es)	4.1174
Type I Error Rate (Alpha)	0.0500
Critical Value of t	4.3027
Power Goal	0.9000
Actual Power for Required N	0.9204
Required Sample Size (N)	3.0000

CLH1_MOUSE	Sample Size Calculation (Spreadsheet1) Dependent Sample t-Test H0: Mu1 = Mu2
	Value
Population Mean Mu1	2110000.0000
Population Mean Mu2	1260000.0000
Group 1 S.D. (Sigma1)	395000.0000
Group 2 S.D. (Sigma2)	39700.0000
Between-group Correlation	0.4929
Stand. Error of Mean Diff.	377016.5452
Standardized Effect (Es)	2.2545
Type I Error Rate (Alpha)	0.0500
Critical Value of t	2.7764
Power Goal	0.9000
Actual Power for Required N	0.9574
Required Sample Size (N)	5.0000

G6PC_MOUSE	Sample Size Calculation (Spreadsheet1) Dependent Sample t-Test H0: Mu1 = Mu2
	Value
Population Mean Mu1	636000.0000
Population Mean Mu2	21300.0000
Group 1 S.D. (Sigma1)	159000.0000
Group 2 S.D. (Sigma2)	6920.0000
Between-group Correlation	0.0327
Stand. Error of Mean Diff.	158924.0133
Standardized Effect (Es)	3.8679
Type I Error Rate (Alpha)	0.0500
Critical Value of t	3.1824
Power Goal	0.9000
Actual Power for Required N	0.9973
Required Sample Size (N)	4.0000

TGM2_MOUSE	Sample Size Calculation (Spreadsheet1) Dependent Sample t-Test H0: Mu1 = Mu2
	Value
Population Mean Mu1	981000.0000
Population Mean Mu2	1660000.0000
Group 1 S.D. (Sigma1)	145000.0000
Group 2 S.D. (Sigma2)	60900.0000
Between-group Correlation	0.5033
Stand. Error of Mean Diff.	125876.8333
Standardized Effect (Es)	-5.3942
Type I Error Rate (Alpha)	0.0500
Critical Value of t	4.3027
Power Goal	0.9000
Actual Power for Required N	0.9885
Required sample size (N)	3.0000

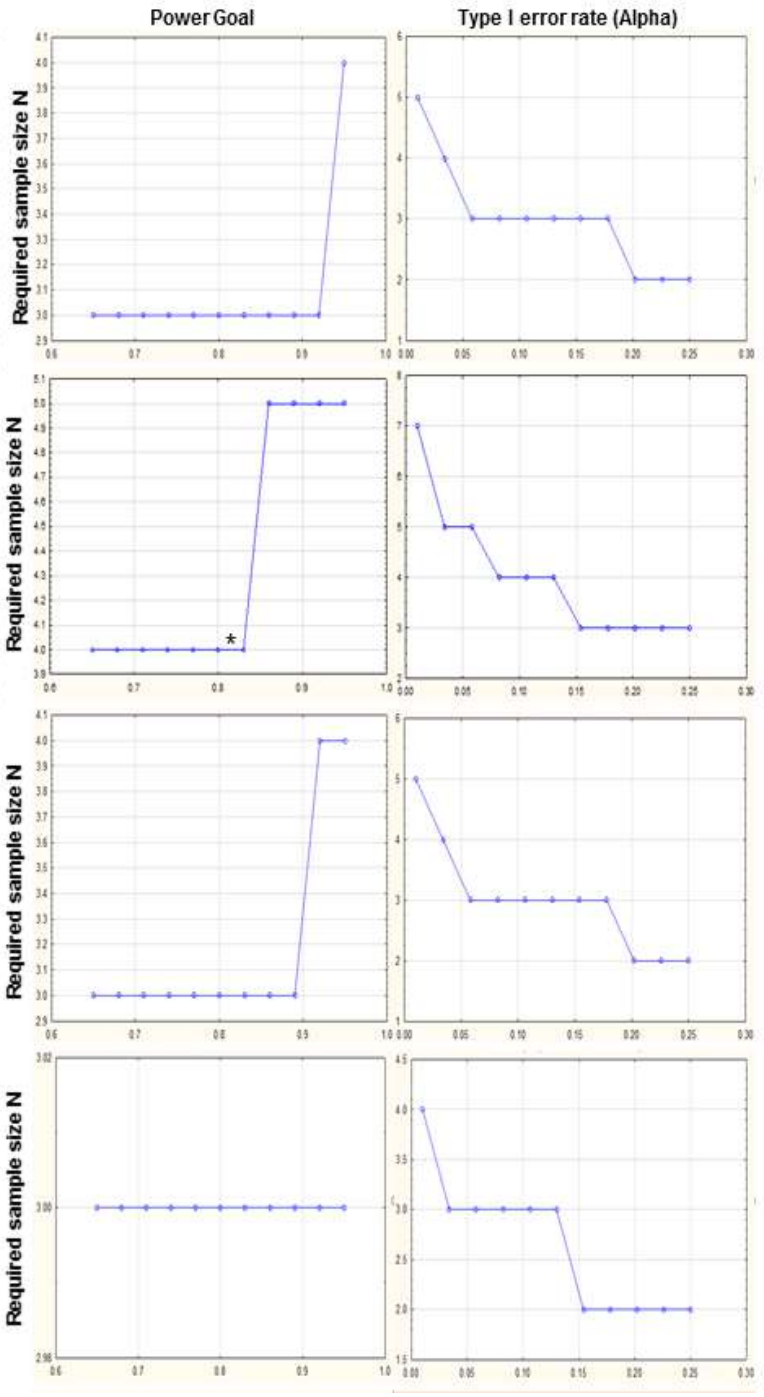

Figure 3.24: Power analysis of a representative portion of proteins identified as differentially expressed upon UUO by SWATH-MS. Power calculation was performed on Dell Statistica software (Dell, Texas, USA) comparing 2 different means (UUO or Sham) of dependent samples by T-test. Nine representative proteins were chosen for the analysis and the values obtained from four experimental replicas (mean, standard deviation, correlation) of Sham (Group 1 in the power analysis) and UUO (Group 2 in the power analysis) mice were used for the calculations. Tables on the left show the details of the calculation, with the means, standard deviation and correlation values inserted by the user and the power goal and the type I error rate fixed to 0.9 and 0.05 by the user. All the other values were calculated by the program to determine the required sample size N and its actual power. The graphs in the central column represent the required sample size (axis of ordinates) depending on the Power goal (axis of abscissae). The graphs in the right column represent the required sample size (axis of ordinates) depending on the Type I error rate (axis of abscissae).

3.5 DISCUSSION

CKD is a major healthcare problem, usually asymptomatic in the initial phases, before it progresses to a late stage of disease where it requires organ transplant. Currently classification and prognosis relies mainly on markers of renal function such as the glomerular filtration rate (eGFR) and the measure of proteinuria (specifically albuminuria). These methods, however, are have been criticized for having insufficient predictive capacity, as they are not sensitive at the early stages and highly subjected to on many factors going from age, sex and genetic background to the specific etiology of CKD and the presence of other clinical issues (Inker, et al. 2014, Levey, et al. 2009b, Levey, et al. 2009a, Rule, et al. 2004). Despite many studies have been produced in the past decades, there is still a need for the definitions of new biomarkers in CKD that could complement the current markers of renal function and even be addressed as possible clinical targets against the development of disease.

For this reason, there is a strong interest in clinical research for the identification of novel biomarker of CKD with a good correlation to fibrosis progression, early diagnostic potential and predictive capacity (Brosius and Pennathur 2013, Merchant 2015, Fassett, et al. 2011). In recent years, quantitative high resolution MS techniques have becomed a more and more suitable tool for the unbiased discovery of novel biomarkers in CKD. However, given the large spectrum of CKD causes and co-associated diseases (diabetes, hypertension, metabolic disrders, etc.) no marker has yet been confirmed as a potential clinical tool allowing early diagnostic and prediction of outcome, adding information to the current kidney function diagnostic markers (Hsu, et al. 2017).

As fibrosis is the main event associated with the progression of CKD to its late stage, novel biomarkers of CKD might be identified among the proteins associated with this pathological process, either promoters of renal scarring, such as proteins associated with inflammation, pro-fibrotic cytokines, markers of mesenchymal activation, transcription factors, etc., or products of renal scarring, such as extracellular matrix proteins and glycoproteins.

As it is well established that the progression of renal insufficiency better correlates with tubulointerstitial fibrosis than with glomerulosclerosis (Schainuck, et al. 1970), in this Chapter, we employed a well-established model of tubulointerstitial fibrosis induced by unilateral ureteric obstruction (UUO) to investigate, by a quantitative mass spectrometric approach, possible biomarkers of CKD. A blind approach should be employed in order not to miss possible markers due to the bias determined by the researcher's pre-knowledge of the pathological processes involved. A mouse model of UUO induced by 21 days surgical ligation of the left

ureter in C57BL/6J mice was used, which was compared to Sham operated mice sacrificed at the same timepoint.

Given the rapidity of this model, 21 days-UUO should be comparable to an end stage CKD, with large accumulation of fibrotic tissue and loss of parenchyma integrity (Eddy, et al. 2012, Zhao, et al. 2015a). However, the animal responses to the surgery might vary, and the progression of disease might be slower or faster.

For this reason, as a first analysis in this chapter, a validation of fibrosis development in randomly selected kidney samples was performed by both histological staining and biochemical analysis of two well-known biomarkers of the fibrotic process: α-smooth muscle actin (α-SMA) expression, as an indication of myofibroblast activation, and TGF-β activation, as a key pro-fibrotic mediator CKD. From a histological point of view, when mice were subjected to 21-days UUO, kidneys morphology and fibrotic tissue accumulation were comparable to a level of advanced kidney fibrosis. They showed a substantial loss in kidney compact structure, with parenchymal disruption, tubular atrophy, and expanded interstitial space. Sham operated mice showed healthy and functional kidneys, with no signs of structural alterations. MTstaining for fibrillar collagen deposition confirmed a significant accumulation of fibrotic tissue in kidneys from UUO-mice at this timepoint, with a collagen/cytoplasm ratio more than 10-fold higher than the sham operated mice (**Fig. 3.5 – 3.6**). The activity of the pro-fibrotic cytokine TGF-β was markedly upregulated in kidney lysates from UUO mice, while it was almost absent in Sham operated sample (less than 1% of total TGF-β, measured upon acid treatment of the lysate) (**Fig. 3.8**). These findings are in agreement with the characterization of a similar model of UUO obtained in our lab few years ago on the same mice strain, where the large accumulation of fibrillar collagen was regarded as being similar to the late stages of CKD, and a large upregulation of TGF-β activity was observed, when UUO was progressing for 21 days (Scarpellini, et al. 2014). The expression of α-SMA was also assessed in both UUO and Sham operated mice as a measure of myofibroblast proliferation, which is known to be a key feature of tubulointerstitial fibrosis and contribute to the large deposition of fibrillar matrix (Ucero, et al. 2014). As shown in **Fig. 3.7**, α-SMA was virtually absent in Sham operated mice, while clear expression was observed in kidneys upon 21-days UUO. In male mice, the upregulation of α-SMA appeared higher and more significant than in female mice subjected to the same treatment. This might be in agreement with a suggested slower rate fibrosis development in the female sex in some CKD models, as previous studies have highlighted some predisposition of male to a faster progression of non-diabetic CKD (Silbiger and Neugarten 2008, Neugarten 2002, Hu, et al. 2009, Stringer, et al. 2005); however, the analysis of more samples and different time points would be necessary to support this hypothesis.

Altogether, the analysis of the 21 days -UUO model produced for this study confirmed the development of an elevated level of CKD in the treated mice, that will be referred to as "fibrotic" mice, and the absence of any fibrotic responses in the Sham operated ones, that can be referred to as "healthy" mice.

Afterwards, the UUO proteome was identified by quantitative mass spectrometry, performed employing a high-resolution SWATH data independent acquisition (DIA) approach, followed by targeted data extraction from a spectral library produced "*a priori*". SWATH-DIA approach is a fairly recent and increasingly applied technology in MS-based proteomics. By allowing to detect all the fragment ion spectra of all the precursors in a series of sequential windows of m/z size, and to extract quantitative data by comparing them to a spectral library, this method goes beyond the discovery based shotgun proteomics or the classical targeted proteomics, as it provides a comprehensive coverage of the proteome, high reproducibility and quantitative, comparable, results (Gillet, et al. 2012, Collins, et al. 2016). Analysis of whole kidney preparations led to the identification of 2016 proteins. Analysis of the UUO and control proteome led to the identification of several proteins differentially expressed upon UUO. 195 proteins were identified as significantly upregulated upon UUO at a confidence higher than 80%, while a larger number, 458, were identified as significantly underexpressed in fibrotic kidneys at this advanced stage of disease (**Suppl. Table 3.5, 3.6**). Among these proteins, possible markers of the disease progression could be identified, as defined by a high fold increase at an elevated confidence.

Many proteins directly associated with the progression of fibrosis were identified as overexpressed in the UUO kidney (**Table 3.3**). ECM-associated proteins and structural constituents of the ECM, were strongly enriched GO terms and protein classes at 21 days post-UUO (3.4.4.4-3.4.4.5). Matrix structural proteins included an elevated number of collagens, among which collagen XII, a fibril-associated collagen, was the most upregulated at 21 days post-surgery. As expected, collagen I (more than 7-fold overexpressed) was the collagen with the highest expression, followed by collagen III and IV, all significantly upregulated by disease (**Fig. 3.9**). Other matrix proteins significantly associated with the progression of UUO in terms of upregulation were the matrix glycoproteins FN, fibrillin, fibulin and biglycan, with fibrillin 1 and biglycan being among the more strongly induced proteins post-UUO, therefore possible biomarkers of CKD, in agreement with previous findings (Schaefer, et al. 2004). Fibulin 2, a glycoprotein associated with the basement membrane and known to interact with fibrillin 1 itself (Reinhardt, et al. 1996), was almost 10-fold overexpressed in the UUO model in this study. Interestingly, all basement membrane HSPGs, known to play a role in the filtration barrier of kidney glomeruli, were also found to be induced by the UUO in the current analysis, possibly

as an effect of increased basement membrane matrix deposition, also observed in the histological specimens. However, the cell surface HSPG syndecan-4 was not induced post UUO. Annotation terms associated with the regulation of the protease activity were also significantly enriched in the list of UUO proteins. In particular, the upregulation of a number of serine protease inhibitors (serpins) was an important finding of this study and might be an interesting prognostic marker to evaluate the progression of CKD in patients. In agreement with this, the combination of the analysis of matrix proteins expression and their modification by proteases (with exposure or not of specific epitopes), has been recently suggested as possible marker of fibrosis, able to distinguish progressive from stable fibrosis (Genovese, et al. 2014)

As a possible consequence of fibroblast proliferation and myofibroblast activation, cytoskeletal-associated and cell adhesion functions were among the most significantly enriched GO terms and PANTHER protein classes. A number of mesenchymal cell markers were identified in the list of UUO overexpressed proteins, and included αSMA. The more overexpressed markers, however, were in this model vimentin and calponin 1. Transgelin, an actin-crosslinking protein expressed in proliferating cells (fibroblasts, smooth muscle), was also strongly upregulated in the disease. This might be an interesting marker of CKD, as transgelin upregulation was seen in previous studies in different models of CKD, in both glomerular and tubular fibrosis (Inomata, et al. 2011, Gerolymos, et al. 2011, Sakamaki, et al. 2011, Daniel, et al. 2012, Karagianni, et al. 2013).
Proteins involved in inflammatory response and apoptosis were also overexpressed post-UUO as well as proteins involved in transcription regulation suggesting active gene expression. The most significant pathways (KEGG and PANTHER) overrepresented in the UUO were associated with ECM-receptor interaction and integrin signaling, focal adhesion, cytoskeletal regulation by Rho GTPase and cytokine-mediated inflammatory response, in line with the notion that fibrosis is an abnormal wound healing process.

As reported before, in search of possible markers, the proteins with higher fold increase were analyzed. At a confidence level of 0.8, the protein having the highest expression was the tubulo-associated protein Uromodulin, followed by the abovementioned collagen XII and fibrillin-1. Uromodulin, however, does not appear as an interesting marker of CKD progression, as its strong upregulation in kidney lysates is more likely to be an effect of urine retention due to the ureteric obstruction process itself, being Uromodulin the more concentrated protein in urine (Bleyer, Zivna and Kmoch 2011, Devuyst 2013).
At a higher confidence level, such as 95%, only 7 proteins appeared upregulated by the UUO in this study [myosin-9, myosin regulatory light polypeptide 9, collagen alpha-1(I) chain, collagen alpha-1(XVIII) chain, alpha-actinin-1, tubulin alpha-1a chain and carboxylesterase 1C], while

38 appeared downregulated by the treatment and were in large part mitochondrial metabolic proteins.

At a confidence level higher than 70% tenascin (TENA_MOUSE), alpha-1-acid glycoprotein (A1AG1_MOUSE), neutrophil gelatinase–associated lipocalin (NGAL_MOUSE) and tapasin (TPSN_MOUSE) emerged as interesting markers of CKD progression.

Tenascin, an extracellular matrix glycoprotein for long known as a marker of mesenchymal transition in embryonic kidney (Aufderheide, Chiquet-Ehrismann and Ekblom 1987), was the most overexpressed protein of the whole proteome (79-fold overexpression post UUO at confidence of 71%). Its upregulation in CKD with different aetiologies was reported before in hypothesis-driven studies (Horstrup, et al. 2002, Masaki, et al. 1998, Truong, et al. 1994, Truong, et al. 1996) and at the time of writing this thesis Fu et al. (2016) confirmed its strong upregulation in two animal models of CKD, the UUO and the ischemia-reperfusion model, and suggested it to be crucial for the proliferation of fibroblasts. Knock down of tenascin gene is protective against fibroblast proliferation and fibrosis accumulation (Fu, et al. 2016).

Alpha-1-acid glycoprotein was as well more than 70 fold overexpressed, it is a plasma alpha globulin glycoprotein and a known acute phase protein upregulated in response to inflammation. This protein is involved in the transport of different proteins in blood, including protease inhibitors, and it has been known for a long time that the serum level of the protein is increased in patients with CKD (Docci, et al. 1985, Vasson, et al. 1991).

Notably, neutrophil gelatinase–associated lipocalin (NGAL_MOUSE) was identified as more than 9 times upregulated in UUO at 79% confidence. This is a marker of different models of kidney fibrosis also involved in cancer and cardiovascular diseases (Cernaro, et al. 2016), and the protein has been recently suggested as mediator of cell proliferation in kidney by aim of EGFR mitogenic signalling and a possible biomarker of CKD progression, with a patent filed for the study of an NGAL inhibitors (Terzi, et al. 2016).

Perhaps the most intriguing finding in this chapter was the identification of tapasin a transmembrane protein strongly induced post UUO (by 36 fold, with 76% confidence). Tapasin is mainly known to regulate ER-loading of the major histocompatibility complex I, but it is also detected on the cell surface (Teng, et al. 2002). To our knowledge, this is the first time that tapasin has emerged as a possible candidate biomarker of CKD.

The vast majority of proteins significantly underexpressed post UUO and related pathways were associated with metabolic pathways and energy production by the cells (**Suppl. Table 3.6** and **Table 3.11**). This could be a consequence of diffuse cell death by apoptosis or necrosis likely at an advanced stage of fibrosis. In agreement with this, markers of cell death such as annexins were upregulated post UUO and a generally lower protein expression was identified in UUO kidneys compared to the sham operated ones, as underlined by residual analysis (**Fig.**

3.14- 3.15). A substantial number of proteins underexpressed at 21-days UUO were having an antioxidant role (highlighted in **Table 3.4**) as dysregulation of antioxidant enzymes has been reported in diabetic and non-diabetic CKD before. Furthermore, downregulation of catalase and glutathione peroxidase activity have been correlated to the bad outcomes of different kidney diseases (Mimic-Oka, et al. 1999, Ceriello, et al. 2000, Ceballos-Picot, et al. 1996). Moreover, in models hypertensive renal disease, AngII upregulation has been suggested to induce renal oxidative stress by reducing Superoxide dismutase in the kidney (Zhao, et al. 2008).

Comparison of this study with two recent proteomic studies of the UUO using different MS acquisition approaches (Yuan, et al. 2015, Zhao, et al. 2015b) showed how the application of a SWATH-MS allows to the identification of a larger number of proteins differentially expressed upon UUO progression, as only ~8% of all the proteins detected by SWATH-MS as significantly overexpressed by UUO had been identified in the previous studies. One (Yuan, et al. 2015), was a study in late UUO (21 days), but employing urine as a sample, while the second (Zhao, et al. 2015b) was performed on whole kidney lysates as the current one, but at much earlier time point when different cellular responses take place, mainly associated with inflammation. So far, this is to our knowledge the first attempt to solve the UUO proteome at a late stage of the disease model.

An established protein implicated in CKD pathogenesis through fibrosis progression, by alteration of matrix homeostasis via protein cross-linking and recruitment of latent TGFβ, is type 2 transglutaminase (TG2). The enzyme has been object of intense research in our group at NTU and may represent a novel therapeutic target for fibrosis treatment. Our unbiased analysis of UUO proteome revealed a small but significant increase in transglutaminase-2 (TG2) post UUO (~1.71-fold increased). This is in agreement with the notion that the effect of extracellular TG2 in wound healing and fibrosis is mostly relying on an increased TG2 release from tubular epithelial cells, rather than increased expression (Scarpellini, et al. 2009, Scarpellini, et al. 2014). Although in other CKD models, including those established by us, such as the rat subtotal nephrectomy, TG2 was also found to be induced in expression (Burhan, et al. 2016), the most prominent feature related to TG2 was the increased protein crosslinking in the ECM consequent to TG2 secretion post insult (Scarpellini, et al. 2014). To establish the role played by TG2 in experimental fibrosis, UUO or a Sham operation was performed in the TG2-knockout mouse in parallel to that performed in WT mice.

The level of fibrosis developed in this phenotype upon UUO was lower when compared with the one observed in WT mice. A possible protective role of TG2-KO was suggested by biochemical analyses, with a trend in α-SMA reduction (**Fig. 3.18**) and a clear abolishment of

TGF-β activation upon UUO (**Fig. 3.19**). The inhibition of TGF-β activity in TG2-null mice subjected to UUO confirms the pivotal role for TG2 in the activation of the enzyme (Nunes, et al. 1997, Verderio, et al. 1999), which becomes especially important when the cytokine is activated in the context of fibrosis. A protective effect if TG2 KO in a CKD model was reported before and findings presented here substantially confirm and corroborate what previously reported , giving strength to the importance of TG2 in disease progression (Fisher, et al. 2009, Shweke, et al. 2008).

Analysis of the TG2-KO proteome revealed a modest alteration in protein expression between WT-proteome and TG2-null proteomes in sham operated kidneys (**Table 3.16, Suppl. Table 3.2**). No compensatory effect from other TG family members was observed in either Sham operated and UUO conditions.

There was a consistent upregulation of a number of Ribosomal subunits and histone proteins when TG2 was removed, that was particularly strong when kidneys were in fibrotic conditions. TG2 is known to be able to both crosslink and phosphorylate histone proteins (Ballestar, Boix-Chornet and Franco 2001, Kim, et al. 2002, Mishra, et al. 2006).

Among the proteins upregulated in Sham operated kidneys by TG2-KO were calcium binding protein 39 and the protein fermitin. The latter is a protein located in focal adhesion sites and involved in cell adhesion by interacting with integrins, and was strongly upregulated in TG2-null mice, hence possibly involved in a compensatory effect on cell adhesion, when TG2 is removed. Elimination of TG2 led to a the downregulation of a number of proteins otherwise overexpressed in the WT UUO kidney such as collagens VI, the HSPG collagen XVIII, a number of fibrinogen chains and thrombospondin, a protein involved in the activation of TGF-β (Hugo, Kang and Johnson 2002, Daniel, et al. 2004), as well as signalling proteins possibly associated with the enzyme activity in the cell (3.4.7.3).

One of the main finding was a clear reduction in tapasin overexpression in TG2-null mice post UUO compared to WT post UUO (**Table 3.19**) corroborating the idea of a synergy between TG2 and tapasin in CKD. This is particularly interesting in the light of independent findings by Prof. Johnson's group who recently identified tapasin as a binding partner for TG2 on the N-terminal β-sandwich domain, by employing a yeast-two-hybrid screening approach. The protein has been shown to co-localise with TG2 on the plasma membrane of renal tubular epithelial cells and knock out of the protein has been suggested to prevent TG2 export from these cells (Personal communication of Prof Timothy Johnson).

Fibrillin 1 and uromodulin, but also proteins associated with the mesenchymal phenotype such as vimentin and transgelin were less induced post UUO upon TG2 KO, proving that they potentially act in synergy with TG2 in disease progression. Fibulin 2 overexpression was significant only in WT mice, as well as the member of the serpin family α-1-antitrypsin (**Table 3.19**). Protein S100-A6, known to complex with annexin2 and be involved in plasmin

regulation and CKD (Cheng, et al. 2005), was more overexpressed in TG2-null mice upon UUO than in WT ones, where the protein resulted not significant. Similarly, mayor urinary protein 6, a small urinary globin, was also upregulated by UUO only in absence of TG2. These proteins, and other proteins differentially regulated in the TG2-null mice and reported in **Tables 3.19-3.20**, might all be associated with the protective role of TG2 in CKD, and more investigation will be needed to understand possible mechanisms involved.

In Conclusion, the establishment of UUO model of renal fibrosis and quantitative proteomics by SWATH-MS have highlighted a number of known candidate markers of fibrosis, including TG2. Knockout of TG2 in UUO has confirmed the protective role of TG2 deletion in CKD development, and quantitative proteomics has for the first time highlighted changes in UUO proteome consequent to TG2 KO in kidney. Data have revealed biomarkers of renal fibrosis which may act in synergy with TG2 in disease development.

The availability of the WT and TG2 KO proteome at a high level of resolution forms the basis of further investigations presented in the next Chapter aimed at identifying the TG2 interactome in plasma membranes isolated from UUO kidneys.

Chapter IV: The cell-matrix interactome of transglutaminase-2 in kidney fibrosis

4.1 AIMS OF THE CHAPTER

Starting from a TG2 immunoprecipitation (IP) method combined with a SWATH acquisition mass spectrometry analysis, the aim of this chapter is to define the interactome of TG2 in kidney fibrotic membranes.

It is anticipated that TG2-interacting partners will emerge that might be associated with TG2 trafficking and externalisation, leading to hypotheses on the mechanism(s) of TG2 secretion in CKD.

4.2 INTRODUCTION

4.2.1 A novel immunoprecipitation approach for the detection of TG2-associated proteins in kidney cell membranes

With the aim of analysing possible partners of TG2 secretion from kidney cells, few years ago, a preliminary MS analysis of TG2-associated proteins in kidney cell membranes was performed by our group at NTU, employing kidneys from healthy C57BL/6J mice.

The novel approach proposed by our group combined a TG2 immunoprecipitation (TG2-IP) from healthy kidneys with iTRAQ® labelling, followed by LC–MALDI-TOF/TOF analysis of the tagged samples. Importantly, it included the analysis of TG2-IPs from TG2-null mice (De Laurenzi and Melino 2001) as a background, to rule out possible false positive detections.

By comparing 5 IPs from wild type (WT) and TG2-KO mice, Dr Alessandra Scarpellini, at NTU, identified 24 proteins as significantly associated with TG2 in kidney membrane extracts (**Table 4.1**), because absent in the TG2-IP from TG2-null mice or having an intensity at least 5 fold higher in the WT than the TG2-KO (WT/TG2-KO>5), in at least 4 out of 5 IP samples. Preliminary analysis of the results was presented at the Renal Association Conference in Newcastle in 2012 by Dr Elisabetta Verderio (Elisabetta Verderio, et al. 2012), but never published. The main finding of this study was the association of TG2 with extracellular heparan sulfate proteoglycans (HSPGs) perlecan and collagen XIII (endostatin), but also the association

with the basement membrane glycoproteins nidogen-1/2 and to numerous cytoskeletal proteins (actin, myosins, plectin, vimentin, spectrins, etc.) that might be involved in the control of the enzyme's trafficking. Moreover, clathrin association was regarded as interesting at the time, being the protein involved in vesicular transport (Elisabetta Verderio, et al. 2012), and glutathione peroxidase, which is and antioxidant protein, hence possibly involved in the maintenance of the enzyme reduced-active state (Stamnaes, et al. 2010, van den Akker, et al. 2011).

This was the first attempt of identifying the TG2 interaction network in kidney samples, and set the experimental bases for the approach employed in the current study, allowing to produce results described in this chapter.

Table 4.1: TG2-associated proteins identified in healthy mice kidneys by iTRAQ® labelling and LC–MALDI-TOF/TOF.

Protein ID	Name
ACTG_MOUSE	Actin, cytoplasmic 2
ATPB_MOUSE	ATP synthase subunit beta, mitochondrial
PGBM_MOUSE	Basement membrane-specific heparan sulfate proteoglycan core protein (Perlecan)
CLH_MOUSE	Clathrin heavy chain 1
COIA1_MOUSE	Collagen alpha-1(XVIII) chain
C1QB_MOUSE	Complement C1q subcomponent subunit B
FLNB_MOUSE	Filamin-B
GPX3_MOUSE	Glutathione peroxidase 3
HSP7C_MOUSE	Heat shock cognate 71 kDa protein
ML12B_MOUSE	Myosin regulatory light chain 12B
MYH10_MOUSE	Myosin-10
MYH11_MOUSE	Myosin-11
MYH14_MOUSE	Myosin-14
MYH9_MOUSE	Myosin-9
NID1_MOUSE	Nidogen-1
NID2_MOUSE	Nidogen-2
PLEC_MOUSE	Plectin
SERPH_MOUSE	Serpin H1
AT1A1_MOUSE	Sodium/potassium-transporting ATPase subunit alpha-1
SPTA2_MOUSE	Spectrin alpha chain, brain
SPTB2_MOUSE	Spectrin beta chain, brain 1
TPM3_MOUSE	Tropomyosin alpha-3 chain
VILI_MOUSE	Villin-1
VIME_MOUSE	Vimentin

4.2.2 Preliminary work for the creation of a TG2 interactome in kidney fibrosis

This Chapter focuses on the identification of the TG2-associated proteins in the 21 days- UUO model of kidney fibrosis and their network of interactions during disease (interactome). In the preliminary work performed by our group and Prof Johnson at Nottingham Trent University and Sheffield university, a TG2 immunoprecipitation (IP) approach from UUO kidneys was combined with quantitative SWATH-Mass spectrometry (MS) (**Fig. 4.1A**).

Briefly, WT inbred mice were subjected to UUO (12 mice) or a sham operation (12 mice), and kidneys were harvested at 21-day post-surgery. To obtain a negative control for TG2-IP, TG2-null mice (TG2-KO) were also subjected to UUO (**Fig. 4.1A**). All kidneys were lysed by mechanical homogenisation in an appropriate immunoprecipitation-suitable buffer and fractionated by high speed centrifugation to separate the crude membrane extracts from the cytosolic fraction. In order to validate the appropriate fractionation of the kidney homogenates, expression of plasma membrane marker sodium potassium ATPase (Na+/K+ ATPase) in the different fractions was investigated by Western blot: as expected, an intense band at ~112kDa, corresponding to Na+/K+ ATPase, was detected in the pelleted fraction (crude membrane extract) and was completely absent in the supernatant (cytosolic extract), confirming that all the membrane fraction was collected by centrifugation, with no trace left in the cytosolic fraction (**Fig. 4.1B**).

After fractionation, extracts were combined in pairs (two extracts/sample) to increase protein amount. A total of six biological replicas per fraction were produced in this way, and TG2-associated proteins were isolated by immunoprecipitation with an anti-TG2 monoclonal antibody (IA12, University of Sheffield) crosslinked to magnetic beads. An appropriate and specific immunoprecipitation of TG2 with this antibody was confirmed by Western blot: probing of TG2 in the TG2-precipitates, in fact, confirmed the correct immunoprecipitation of TG2 in WT mice, in both cytosolic and membranous fractions while no signal, as expected, was detected in TG2-KO mice (**Fig. 1C**). Coomassie staining of the same precipitates revealed a series of proteins specifically co-precipitated in WT mice, as they were absent in the TG2-null (TG2-KO) individuals (**Fig. 4.1D**). These proteins were directly or indirectly interacting with the enzyme and, in theory, they could be detected in the subsequent mass spectrometry (MS) experiments (**Fig. 4.1A**).

The TG2-IP samples were analyzed by reverse-phase high-pressure liquid chromatography electrospray ionization tandem mass spectrometry (RP-HPLC-ESI-MS/MS) using the TripleTOF 5600+ mass spectrometer from SCIEX (Canada). The instrument is available for University staff and students at the proteomics facility lab of the John Van Geest cancer research center at Nottingham Trent University (Clifton Campus, Nottingham, UK), and mass

spectrometry runs were performed by Dr. David Boocock, assisted by Dr. Nina Schroeder, Miss Clare Coveney and Dr. Amanda Miles. In order to obtain the most quantitative and reliable results, the modern SWATH-data independent acquisition (DIA) approach (Gillet, et al. 2012) was employed for MS data acquisition (**Fig. 4.1A**). In order to ensure the most generalizable and quantitative data, five independent SWATH-MS experiment were performed, each one comparing WT and TG2-KO mice. To avoid gender bias, only male mice were employed. The different samples were subjected to cyclic data independent acquisition (DIA) using 34 Static SWATH acquisition windows of fixed dimension (m/z = 15 Da/mass) covering a mass range from 400 to 900 Da. Practically, during different cycles, an initial survey scan (TOF-MS) is performed for each window, then the following MS/MS experiments carried on the totality of the precursors detected in the window using ion collision energy, allowing to obtain the largest possible coverage of detectable proteins (Gillet, et al. 2012). After acquisition, spectral alignment and targeted data extraction was performed with an appropriate software (PeakView 2.0 SCIEX) using a reference spectral library previously generated by shotgun-MS (data dependent acquisition, DDA; FDR = 1%) on a pool of TG2-IP samples (one sample/condition) and necessary for the extrapolation of protein intensities and the production of quantitative results (**Fig. 4.1A**)[a]. The output of the analysis consisted of 3 different quantification files representing the intensity of the individual ions (the area under the intensity curve), of the different peptides (cumulative intensity of the ions) and of the proteins (cumulative intensity of the peptides).

The third file was the one used for the subsequent statistical analysis, aimed at identifying the TG2-associated proteins in UUO and Sham operated kidneys and ultimately producing the TG2 interactome in kidney fibrosis: this is the part of the analysis performed for this thesis, and the focus of this chapter.

[a] SWATH data was processed using an extraction window of 12 min and applying these parameters: 100 peptides, 5 transitions, peptide confidence of >99%, exclude shared peptides, and XIC width set at 50 ppm.

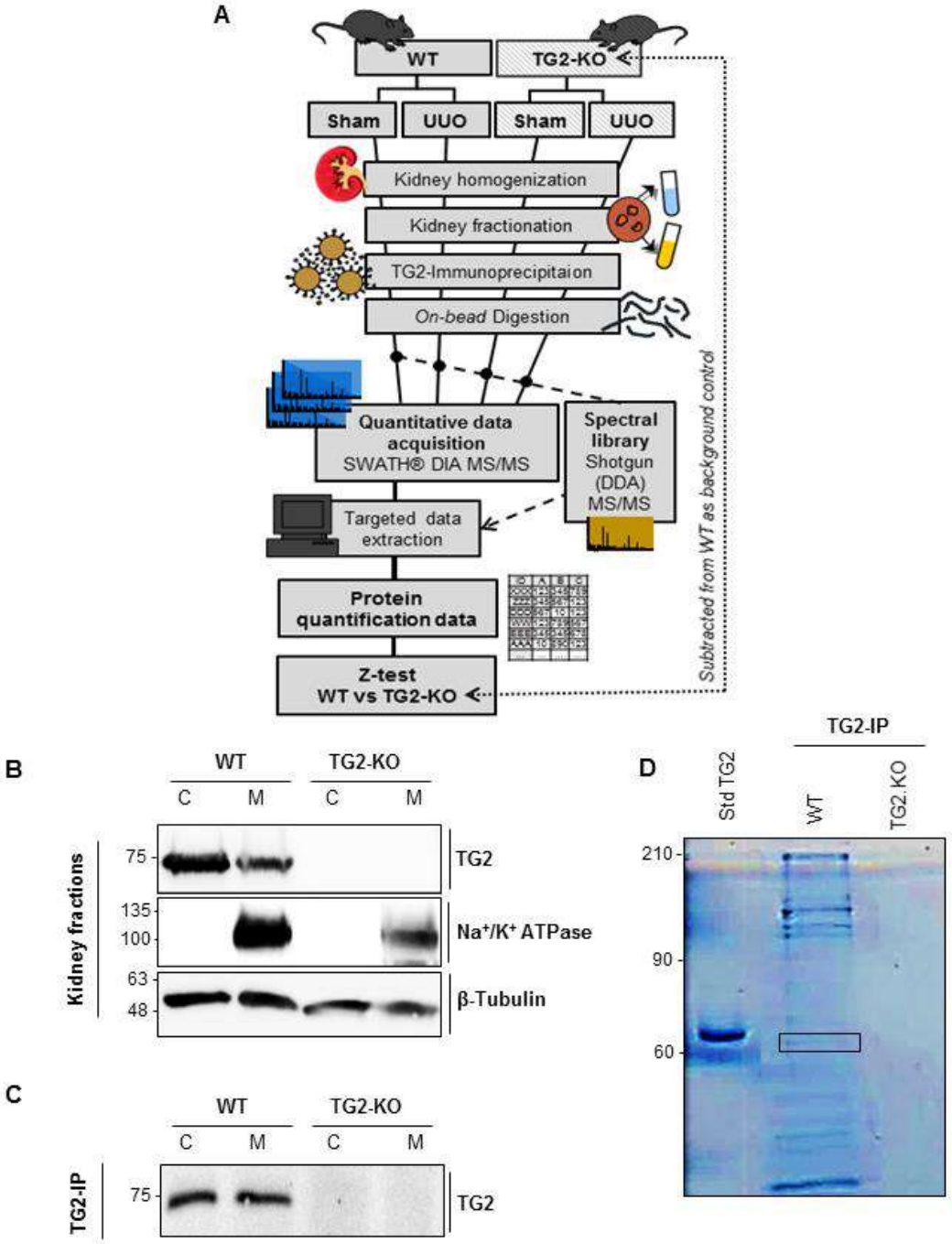

Figure 4.1: Preliminary work for the production of the TG2 interactome in kidney fibrosis. (A) Schematic outline of the experimental design for the identification of the TG2 interactome in kidney fibrosis. **(B)** 10% (w/v) kidney homogenates were prepared for both WT and TG2-KO sham operated and UUO kidneys. Kidneys were lysed in homogenization buffer (0.25 M sucrose, 10 mM Tris-HCl, 1 mM $MgCl_2$, 2 mM EDTA, pH 7.4) containing protease inhibitors (Sigma) by mechanical homogenisation (Ultra Turrax T25 homogeniser, Merck). The whole homogenate was centrifuged at 1000g for 5 min at 4°C to pellet down and remove larger particulates, then membranes (M) were separated from the cytosolic (C) fraction by centrifugation at 200,000 g at 4°C for 30 min. The pellet (crude membrane fraction, M) was re-suspended in immunoprecipitation (IP) buffer [25 mM Tris.HCl, 150 mM NaCl, 1 mM EDTA, 1% (v/v) NP40, 5% glycerol (v/v), pH 7.4] containing protease inhibitors (Sigma). Equal volumes of proteins were resolved by 12% (w/v) acrylamide SDS-PAGE under reducing condition and proteins were immunoprobed for TG2 [mouse monoclonal anti TG2 (IA12, University of Sheffield, UK)], the plasma membrane marker Na^+/K^+ ATPase [Mouse monoclonal anti-alpha 1 sodium potassium ATPase antibody [464.6] - plasma membrane marker (ab7671 Abcam)]and the loading control β-tubulin [Rabbit polyclonal anti β-tubulin (ab6046, Abcam)]. Immunoreactive bands were detected by enhanced chemiluminescence (Geneflow) after incubation with appropriate HRP-conjugated secondary

antibodies in blocking buffer. Image acquisition was performed with a LAS4000 imaging system (GE Heathcare). **(C,D)** Immunoprecipitation of TG2-associated protein (TG2-IP) was performed with an anti-TG2 monoclonal antibody (IA12) on both cytosolic (C) and membranous (M) fractions, using the Pierce™ Crosslink Magnetic IP/Co-IP Kit (Thermo Scientific) and following to the manufacturer's instructions. Proteins were eluted in 50 µl of the appropriate elution buffer provided by the kit (Thermo Scientific). (C) Equal volumes of proteins were resolved by 12% (w/v) acrylamide SDS-PAGE under reducing condition and proteins were immunoprobed for TG2. Immunoreactive bands were detected by enhanced chemiluminescence (Geneflow) after incubation with appropriate HRP-conjugated secondary antibodies in blocking buffer. Image acquisition was performed with a LAS4000 imaging system (GE Heathcare). (D) Coomassie staining of TG2-immunoprecipiates were separated by 12%(w/v) SDS-PAGE and revealed a series of specifically co-precipitated proteins in WT mice. Purified guinea pig liver TG2 was run as positive control. A black square identifies TG2.

4.2.3 Transglutaminase-2 interactions: substrates or partners?

Being a multifunctional and ubiquitous enzyme, a plethora of TG2 substrates have been identified in the literature, both in the extracellular and in the intracellular space, and including mitochondria and nucleus. Beside the notorious extracellular matrix components, substrates for TG2 crosslinking activity in the context of wound healing and scarring (fibronectin, collagen, elastin, vitronectin, etc.), also many cytoskeletal proteins have been suggested as substrates for the enzyme transamidation activity both by intramolecular and intermolecular modification (actin, tubulin, etc..). In the nucleus, histone proteins have been suggested to be crosslinked by TG2, with a role during cell death, and these are just few examples of known protein substrates.

Moreover, as described before, TG2 has also a non-enzymatic role in the cells, mainly located in the extracellular space (Kanchan, Fuxreiter and Fésüs 2015, Belkin 2011). For this reason, by immunoprecipitation, not only enzyme substrates but also a number of TG2 binding partners are likely to be detected. There is a growing interest in the non-enzymatic "binding" partners of TG2 in research, and an updated list of TG2 interacting proteins has been recently published on Cellular and Molecular Life Sciences by Khanchan and colleagues (Kanchan, Fuxreiter and Fésüs 2015). Transdab (http://genomics.dote.hu/wiki/index.php/Main_Page) is a database of known partners of the transglutaminase family and it collects both substrates and interacting partners for TG2 (Csősz, Meskó and Fésüs 2009). A list of the main TG2 partners, distinguished into substrates and binding partners, and obtained from Transdab, is provided in the Appendix (Table I), while a list of interacting partners obtained from Kanchan et al., (Kanchan, Fuxreiter and Fésüs 2015) is provided in Appendix Table II.

4.3 EXPERIMENTAL PROCEDURES

4.3.1 Z-test statistical analysis of mass spectrometric (MS) results on TG2-immunoprecipitated proteins

As mentioned in the introduction [4.2.2], five independent SWATH-MS experiments were performed, each one including an immunoprecipitation sample from each combination of mice (WT / TG2-KO), treatment (Sham / UUO) and fraction (cytosol / membrane). A graphical outline of the sample composition of each experiment is reported in **Fig.4.2A**. Starting from the five obtained datasets, in order to identify the proteins significantly associated with TG2 in both UUO and sham operated kidneys, a z-test statistical analysis (Cheadle, et al. 2003), which is conceptually similar to a t test, was performed, using the TG2-KO kidney values as background controls (**Fig. 4.2**). The TG2-KO can be considered as best possible negative control for this kind of immunoprecipitation-based studies: in fact, being lacking the protein itself, these mice will virtually not have no specifically TG2-precipitated proteins, and all the peptides identified in these samples by MS can be consider as an a-specific background not associated with TG2.

First, raw intensity values of every detected protein were normalized within the whole experiment using a Z transformation: each intensity value was transformed using the natural log transformation and then normalized by subtracting the average of the whole population (μ) and dividing for the standard deviation of the whole population (σ) as shown in equation (1) (**Fig.4.2B**). ΔZ values were then calculated by subtracting TG2-KO z-score from WT z-score for each protein in the treatment/compartment (equation 2 in **Fig.4.2B**). Finally, the Z-test (Cheadle, et al. 2003) (equation 3a in **Fig.4.2B**) was performed on the ΔZ values from the 5 experiments together in order to compare WT and TG2-KO data in the same treatment (Sham or UUO) and compartment (cytosol or membrane). In this case, being the null hypothesis H_0: $\Delta Z = 0$ (no differences in z-score between WT and KO), the test was performed by dividing the average of the ΔZ of the given protein in the experiments by the standard error of the ΔZ of the given protein in the different experiments (equation 3b in **Fig.4.2B**). The results of the z-test were plotted on a normal distribution curve to infer probability values (p-values) and identify protein whose intensity was significantly higher in WT than in the background condition [**Fig.4.2B** (4)]. The proteins whose p-value was lower than 0.05 in at least 4 out of 5 occasions (experiments)were regarded as significantly associated with TG2.

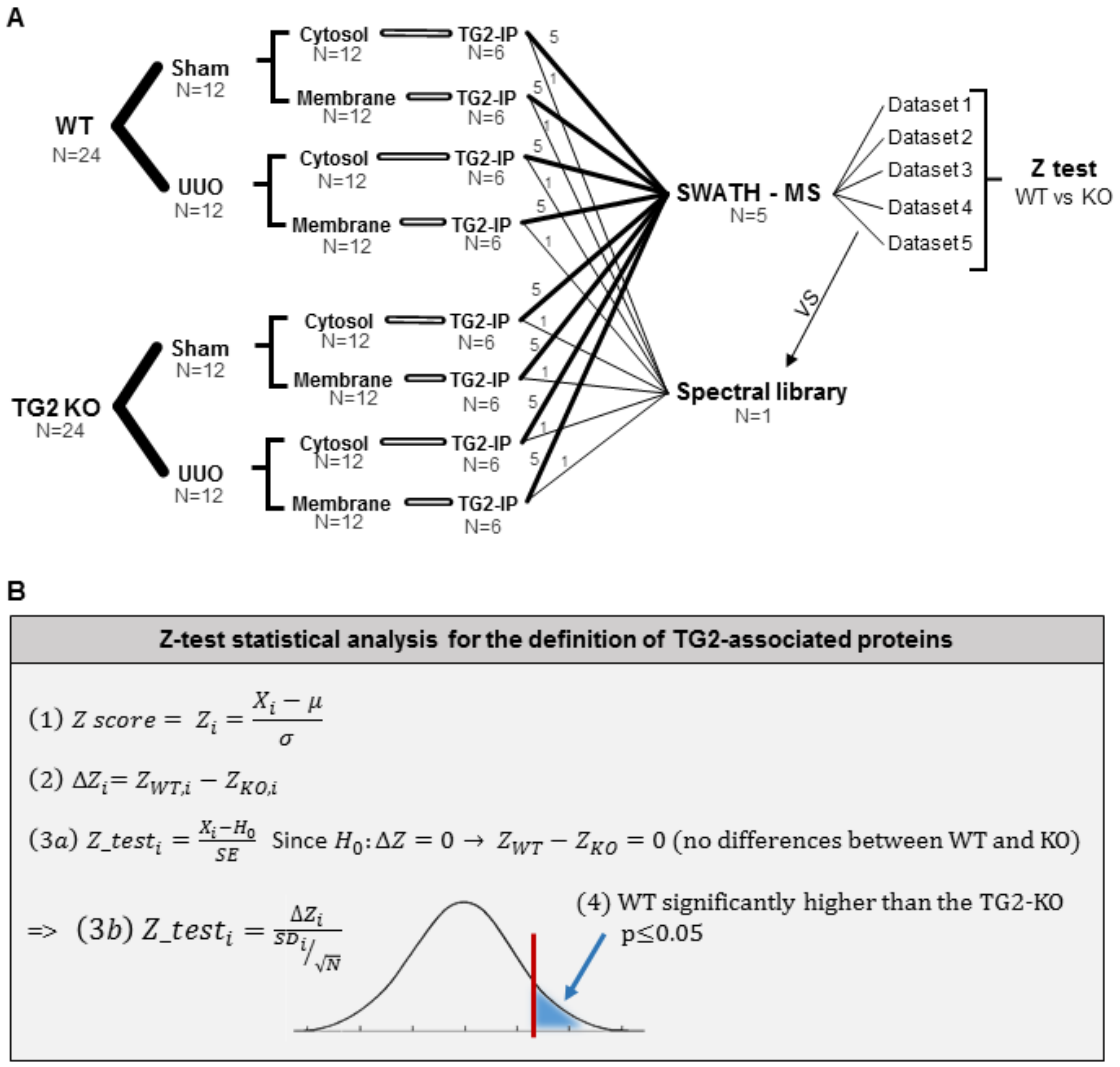

Figure 4.2: Z-test statistical analysis of SWATH-MS results on TG2-immunoprecipitated proteins. **(A)** Sample distribution in the 5 independent SWATH-MS experiments on TG2-immunoprecipitates, that were analysed by Z-test to determine TG2-associated proteins. **(B)** Z-test statistical analysis adapted from Cheadle et. al, 2003 (Cheadle, et al. 2003) for the determination of TG2 significantly associated proteins.

4.3.2 Bioinformatic analysis

4.3.2.1 Functional clustering and overrepresentation analysis

The TG2-associated proteins identified were further analysed with a series of bioinformatics approaches in order to define protein functions and determine protein-protein interactions. Initially, protein IDs where searched on UniprotKB (http://www.uniprot.org/uniprot) database to identify protein names and gather information about their functions and localisation. Based on these information, TG2-associated proteins were manually grouped into functional clusters depending on their general functions, and colour-coded to make the differences easier to observe.

Similarly to what was done for the UUO proteome and described more exhaustively in the previous chapter, functional classification and functional overrepresentation analysis were performed using both DAVID v6.7 (http://david.abcc.ncifcrf.gov) and PANTHER Database (http://www.pantherdb.org) bioinformatics resources, employing the *Mus Musculus* genome as background gene list.

Functional classification was performed using the Gene Ontology (GO) terms for "Biological Process", "Molecular Function" and "Cellular Component" in addition to PANTHER Protein Class terms and PANTHER pathways. The terms represented in the TG2-associated list in both UUO and sham operated conditions were visualized in pie charts as percentage of representation of the specific GO annotation term over the total number of class hits.

Functional overrepresentation test was performed in PANTHER using the same GO terms ("Biological Process", "Molecular Function", "Cellular Component") and PANTHER Protein class annotations. The specific description of the overrepresentation test is provided in Chapter III. A p-value lower than 0.05 was regarded as significant. To confirm the findings obtained with PANTHER, functional overrepresentation analysis was performed also by DAVID bioinformatic tool, selecting the GO terms for "Biological Process" (GOTERM_BP_FAT), "Molecular Function" (GOTERM_MF_FAT) and "Cellular Component" (GOTERM_CC_FAT). A p-value lower than 0.05 was considered significant. In order to determine which pathways were significantly overrepresented in the list of TG2-associated proteins, PANTHER Pathways overrepresentation test was carried out by PANTHER; while the same analysis using KEGG Pathway keywords was performed in DAVID.

4.3.2.2 Investigation of protein-protein interactions using STRING

The interactome of TG2 in kidney fibrosis was drawn using STRING v10.0 database (http://string-db.org). STRING allows one to identify known and predicted protein-protein interactions in the list of TG2-associated proteins. The network of interaction was obtained using a confidence level greater than 0.4 and all the unconnected proteins were removed from the final scheme. The network file was imported in Cytoscape v. 3.0.2 (http://www.cytoscape.org) to organize protein localisation and colour-code them depending on their specific functional cluster defined as above. In this way, clear clusters can be distinguished if present.

4.4 RESULTS

4.4.1 Identification of TG2 interacting proteins from SWATH acquisition mass spectrometry of TG2-precipitates

In order to identify a list of proteins that associated with TG2 in healthy and fibrotic conditions, SWATH-MS analysis was performed as described in the introduction (4.2.3). Between 800 and 1200 proteins were identified in each experiment. A total of 886 proteins were detected in at least 3 out of 5 experiments, of which 746 were detected in 4 or more experimental replicas. All the proteins identified in at least 4 out of 5 experiments and significantly more expressed (p-value lower than 0.05) than the background TG2-null control when analysed by z-test [4.3.1] were regarded as significantly associated with TG2. From this statistical analysis, 489 candidates were found significantly associated with TG2 in either UUO or sham operated conditions (243 in cytosol and 306 in crude membrane extracts, 60 in common between compartments) (**Fig. 4.3A**). Of these candidates, 243 were found significantly associated with TG2 in sham operated conditions (of which 110 in cytosol and 158 in membranes) and 316 in fibrotic conditions (UUO) (160 in cytosol and 192 in membranes). Only 70 proteins were found associated with TG2 in both conditions (35 in cytosol and 53 in membranes), suggesting that these proteins interact with the enzyme unrelatedly from the fibrosis development.

To identify the interactions involved in TG2 trafficking and extracellular activity, the proteins associated with TG2 in crude membrane extracts were analysed in detail. The TG2-associated proteins of the cytosolic fraction were collected in a separate list and are shown in **Suppl. Table 4.1** (Cytosolic fraction from UUO kidneys – 21 days) and **Suppl. Table 4.2** (Cytosolic fraction from sham operated kidneys-21 days).

Moreover, as we wanted to focus on TG2 partners at the cell-matrix interface, membrane proteins previously reported to be exclusively located in nucleus, mitochondrial or peroxisomal membranes were identified by their subcellular location as defined on UniprotKB database (Subcellular Localisation) and placed in a separate list. Nuclear proteins are displayed in **Suppl. Table 4.3**, while mitochondrial and peroxisomal are displayed in **Suppl. Table 4.4** (A=TG2 -associated proteins in UUO kidneys, B=TG2-associated proteins in sham operated kidneys). Ribosomal proteins and IgGs found in the membrane preparation were collected as well in a separate list and are reported in **Suppl. Table 4.5** (A=TG2 -associated proteins in UUO kidneys, B=TG2-associated proteins in sham operated kidneys).

Based on these criteria, 217 proteins were identified as significantly associated with TG2 ($p \leq 0.05$, $n \geq 4$) with a recorded plasma membrane or plasma membrane-associated or ECM compartmentalisation (referred to as "cell-matrix" proteins), or else a location in biological fluids (**Fig. 4.3B**). Of these proteins, 97 were found uniquely associated with TG2 in UUO

membranes, while 95 were uniquely associated with sham operated conditions. Only 25 proteins were found significantly associated with TG2 in both conditions. This little overlap suggests a marked change in TG2 interactions on kidney membranes when animals were subjected to UUO for 21 days.

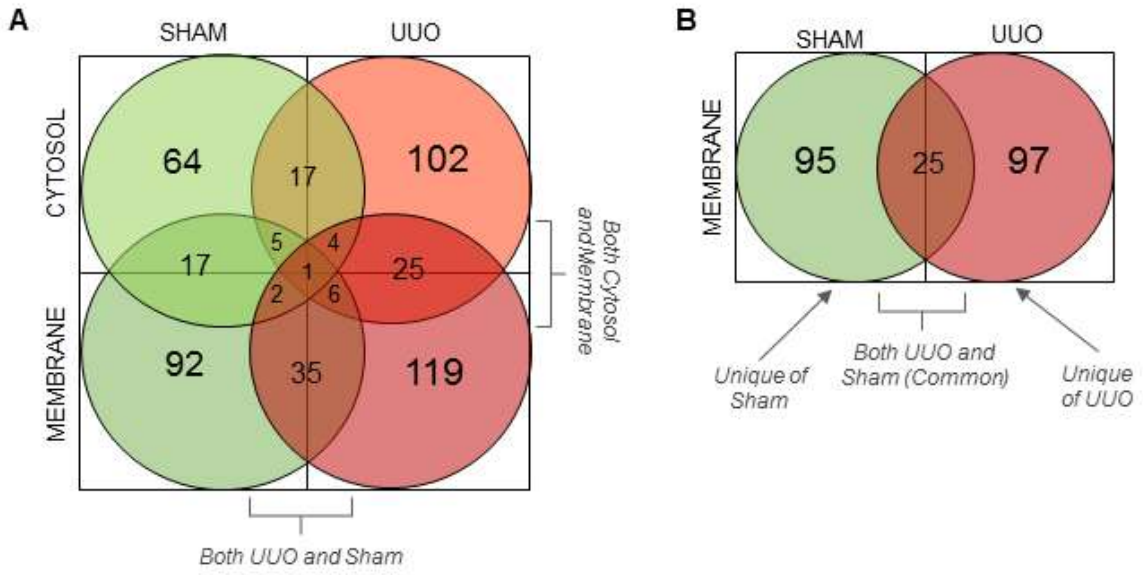

Figure 4.3: Number of TG2-associated proteins in UUO or Sham operated kidneys at 21-days post operation. (A) Number of protein identified as TG2-associated upon UUO or sham operation (21 days) by Z-test ($p \leq 0.05$ $N \geq 4$) in both cytosolic or membranous compartments. **(B)** Number of protein identified as TG2-associated in UUO or sham operated membranes (21 days) by Z analysis ($p \leq 0.05$ $N \geq 4$) after removal of specifically nuclear, mitochondrial and ribosomal proteins (reported in **Suppl. Tables 4.3-4.5**). Intersections of circles identify common proteins between the groups.

The TG2-associated candidates ($p \leq 0.05$, $n \geq 4$) in UUO and Sham operated kidney membranes (21 days) are presented in **Table 4.2** and **Table 4.3**: **Table 4.2** displays the list of 122 TG2-associated proteins in UUO (fibrotic) membranes at 21 days post-surgery, while **Table 4.2** shows the list of 120 TG2-associated proteins in sham operated, healthy, conditions at 21 days post-surgery.

Table 4.2: List of proteins significantly associated with TG2 in UUO kidney membranes (21 days). This table shows all the proteins identified as TG2-associated in UUO membranes (21 days) by z-analysis (p≤0.05 N≥4) after removal of specifically nuclear, mitochondrial and ribosomal proteins (reported in **Suppl. Tables Suppl. Tables 4.3-4.5**). In increasing shades of blue, the p-value of TG2 association obtained by z-analysis. U (red) = Uniquely expressed in UUO, C (yellow) = common between UUO and Sham.

TG2-associated proteins in UUO kidney membranes				
Sample ID	**Name**	**N**	**P value**	**Unique/ Common**
DESP_MOUSE	Desmoplakin	5	1.22E-13	U
HSP7C_MOUSE	Heat shock cognate 71 kDa protein	5	7.67E-10	U
CALM_MOUSE	Calmodulin	5	1.83E-08	C
CAZA2_MOUSE	F-actin-capping protein subunit alpha-2	5	1.97E-08	U
GPX1_MOUSE	Glutathione peroxidase 1	5	4.52E-07	U
ADH1_MOUSE	Alcohol dehydrogenase 1	5	9.40E-07	C
POSTN_MOUSE	Periostin	4	1.03E-06	U
MYO1D_MOUSE	Unconventional myosin-Id	5	3.52E-06	U
GLRX1_MOUSE	Glutaredoxin 1	4	5.61E-06	U
GLRX3_MOUSE	Glutaredoxin-3	5	1.40E-05	U
PROF1_MOUSE	Profilin-1	5	1.89E-05	U
TGM2_MOUSE	Transglutaminase 2	5	3.31E-05	C
HSPB1_MOUSE	Heat shock protein beta-1	5	3.68E-05	U
VATH_MOUSE	V-type proton ATPase subunit H	5	5.98E-05	U
ADDG_MOUSE	Gamma-adducin	5	6.66E-05	U
AT2A2_MOUSE	Sarcoplasmic/endoplasmic reticulum calcium ATPase 2	5	8.58E-05	U
SVIL_MOUSE	Supervillin	4	1.01E-04	U
COR1C_MOUSE	Coronin-1C	5	1.38E-04	U
IQGA1_MOUSE	Ras GTPase-activating-like protein IQGAP1	5	1.50E-04	C
TCPE_MOUSE	T-complex protein 1	5	3.17E-04	U
UBP5_MOUSE	Ubiquitin carboxyl-terminal hydrolase 5	5	4.59E-04	U
FLOT2_MOUSE	Flotillin-2	4	5.38E-04	U
NAMPT_MOUSE	Nicotinamide phosphoribosyltransferase	5	6.56E-04	C
PCKGC_MOUSE	Phosphoenolpyruvate carboxykinase	5	8.93E-04	C
RAB1A_MOUSE	Ras-related protein Rab-1A	5	9.16E-04	U
SDC4_MOUSE	Syndecan-4	5	9.34E-04	U
LDHA_MOUSE	L-lactate dehydrogenase A chain	4	1.04E-03	U
MYO1G_MOUSE	Unconventional myosin-Ig	5	1.21E-03	U
K1C20_MOUSE	Keratin, type I cytoskeletal 20	4	1.35E-03	U
COEA1_MOUSE	Collagen alpha-1(XIV) chain	5	1.64E-03	U
COCA1_MOUSE	Collagen alpha-1(XII) chain	4	1.68E-03	U
HIP1_MOUSE	Huntingtin-interacting protein 1	4	1.86E-03	U
LIMS1_MOUSE	LIM and senescent cell antigen-like-containing domain protein 1	5	2.47E-03	C
SAR1B_MOUSE	GTP-binding protein SAR1b	5	2.79E-03	U
SPTA1_MOUSE	Spectrin alpha chain, erythrocytic 1	5	2.92E-03	C
FLNA_MOUSE	Filamin-A	5	2.98E-03	U
ANK3_MOUSE	Ankyrin-3	5	3.03E-03	U
PSD11_MOUSE	26S proteasome non-ATPase regulatory subunit 11	5	3.09E-03	U
PGBM_MOUSE	Basement membrane-specific heparan sulfate proteoglycan core protein (Perlecan)	5	3.16E-03	U
LSP1_MOUSE	Lymphocyte-specific protein 1	5	3.53E-03	U
GELS_MOUSE	Gelsolin	5	4.61E-03	U
YKT6_MOUSE	Synaptobrevin homolog YKT6	5	4.72E-03	U
PTN6_MOUSE	Tyrosine-protein phosphatase non-receptor type 6	4	4.84E-03	C
FLNB_MOUSE	Filamin-B	5	5.03E-03	U
TLN2_MOUSE	Talin-2	5	5.28E-03	U
PGK1_MOUSE	Phosphoglycerate kinase 1	4	5.39E-03	C
PICAL_MOUSE	Phosphatidylinositol-binding clathrin assembly protein	4	5.65E-03	C
F120A_MOUSE	Constitutive coactivator of PPAR-gamma-like protein 1	5	6.27E-03	C
PRDX2_MOUSE	Peroxiredoxin-2	4	6.87E-03	C
KCC2D_MOUSE	Calcium/calmodulin-dependent protein kinase type II subunit delta	5	7.10E-03	U
RTN4_MOUSE	Reticulon-4	5	7.57E-03	U
SERA_MOUSE	D-3-phosphoglycerate dehydrogenase	5	7.78E-03	C
KC1A_MOUSE	Casein kinase I isoform alpha	5	8.06E-03	U
DCTN1_MOUSE	Dynactin subunit 1	5	8.52E-03	U
ADDA_MOUSE	Alpha-adducin	5	8.61E-03	U
PGS2_MOUSE	Decorin	5	1.09E-02	U
IF4G3_MOUSE	Eukaryotic translation initiation factor 4 gamma 3	5	1.11E-02	C
RHG18_MOUSE	Rho GTPase-activating protein 18	4	1.11E-02	U
CAPZB_MOUSE	F-actin-capping protein subunit beta	5	1.11E-02	U
MVP_MOUSE	Major vault protein	5	1.14E-02	U
TERA_MOUSE	Transitional endoplasmic reticulum ATPase	5	1.21E-02	C

ACTB_MOUSE	Actin, cytoplasmic 1	5	1.24E-02	U
PGS1_MOUSE	Biglycan	5	1.30E-02	C
K1C14_MOUSE	Keratin, type I cytoskeletal 14	5	1.33E-02	U
PLSL_MOUSE	Plastin-2	5	1.34E-02	U
AP2A2_MOUSE	AP-2 complex subunit alpha-2	5	1.52E-02	U
FINC_MOUSE	Fibronectin	5	1.57E-02	C
CLCB_MOUSE	Clathrin light chain b	5	1.65E-02	U
SNX4_MOUSE	Sorting nexin-4	5	1.67E-02	U
SPTB1_MOUSE	Spectrin beta chain, erythrocytic	5	1.73E-02	U
ZO1_MOUSE	Tight junction protein ZO-1	4	1.79E-02	U
DREB_MOUSE	Drebrin	5	1.83E-02	U
CAN1_MOUSE	Calpain1	5	1.84E-02	U
PDLI5_MOUSE	PDZ and LIM domain protein 5	5	1.85E-02	U
PUR6_MOUSE	Multifunctional protein ADE2	5	1.88E-02	U
MY18A_MOUSE	Unconventional myosin-XVIIIa	5	1.93E-02	U
CLCA_MOUSE	Clathrin light chain A	5	2.07E-02	U
IRGM1_MOUSE	Immunity-related GTPase family M protein 1	5	2.09E-02	U
NEB2_MOUSE	Neurabin-2	5	2.11E-02	U
K2C6B_MOUSE	Keratin, type II cytoskeletal 6B	5	2.14E-02	U
AP2A1_MOUSE	AP-2 complex subunit alpha-1	5	2.15E-02	U
LYPA1_MOUSE	Acyl-protein thioesterase 1	5	2.18E-02	U
PDC6I_MOUSE	Programmed cell death 6-interacting protein	5	2.38E-02	C
AP2B1_MOUSE	AP-2 complex subunit beta	5	2.43E-02	U
K1C19_MOUSE	Keratin, type I cytoskeletal 19	5	2.58E-02	U
GRP78_MOUSE	78 kDa glucose-regulated protein	5	2.59E-02	U
ARK72_MOUSE	Aflatoxin B1 aldehyde reductase member 2	5	2.61E-02	U
SNTB2_MOUSE	Beta-2-syntrophin	5	2.63E-02	U
MYO1B_MOUSE	Unconventional myosin-Ib	5	2.67E-02	U
K6PP_MOUSE	ATP-dependent 6-phosphofructokinase, platelet type	5	2.67E-02	U
C1QB_MOUSE	Complement C1q subcomponent subunit B	5	2.71E-02	U
F213A_MOUSE	Redox-regulatory protein FAM213A	5	2.79E-02	C
HS90A_MOUSE	Heat shock protein HSP 90-alpha	5	2.85E-02	U
GAK_MOUSE	Cyclin-G-associated kinase	5	2.86E-02	U
SPTN1_MOUSE	Spectrin alpha chain, non-erythrocytic 1	5	3.08E-02	C
UCK1_MOUSE	Uridine-cytidine kinase 1	5	3.12E-02	U
ECHP_MOUSE	Peroxisomal bifunctional enzyme	5	3.15E-02	C
ES8L2_MOUSE	Epidermal growth factor receptor kinase substrate 8-like protein 2	4	3.29E-02	U
MOES_MOUSE	Moesin	5	3.33E-02	U
PNCB_MOUSE	Nicotinate phosphoribosyltransferase	5	3.34E-02	U
MYH10_MOUSE	Myosin-10	5	3.59E-02	U
RBGPR_MOUSE	Rab3 GTPase-activating protein non-catalytic subunit	5	3.65E-02	U
VIME_MOUSE	Vimentin	5	3.66E-02	U
SERPH_MOUSE	Serpin H1	5	3.81E-02	U
RPN1_MOUSE	Dolichyl-diphosphooligosaccharide--protein glycosyltransferase subunit 1	4	3.89E-02	U
LAMB2_MOUSE	Laminin subunit beta-2	4	3.92E-02	C
GSTT1_MOUSE	Glutathione S-transferase theta-1	5	3.95E-02	U
TCPQ_MOUSE	T-complex protein 1	5	3.96E-02	U
TCPZ_MOUSE	T-complex protein 1	5	4.23E-02	C
IRAK4_MOUSE	Interleukin-1 receptor-associated kinase 4	5	4.24E-02	U
C1TC_MOUSE	C-1-tetrahydrofolate synthase	5	4.28E-02	U
ARC1B_MOUSE	Actin-related protein 2/3 complex subunit 1B	5	4.28E-02	U
SCFD1_MOUSE	Sec1 family domain-containing protein 1	5	4.30E-02	C
COPB2_MOUSE	Coatomer subunit beta	5	4.42E-02	U
FA49B_MOUSE	Protein FAM49B	5	4.62E-02	U
MYH14_MOUSE	Myosin-14	5	4.79E-02	U
SNX1_MOUSE	Sorting nexin-1	4	4.81E-02	U
PLST_MOUSE	Plastin-3	5	4.82E-02	U
GBP2_MOUSE	Interferon-induced guanylate-binding protein 2	5	5.00E-02	U
SYEP_MOUSE	Bifunctional glutamate/proline--tRNA ligase	5	5.17E-02	U
TCPA_MOUSE	T-complex protein 1	5	5.25E-02	U
CLIC1_MOUSE	Chloride intracellular channel protein 1	5	5.33E-02	U

Table 4.3: List of proteins significantly associated with TG2 in Sham operated kidney membranes (21 days). This table shows all the proteins identified as TG2-associated in sham operated membranes (21 days) by z-analysis ($p \leq 0.05$ $N \geq 4$) after removal of specifically nuclear, mitochondrial and ribosomal proteins (reported in **Suppl. Tables 4.3-4.5**). In increasing shades of blue, the p-value of TG2 association obtained by z-analysis. U (green) = Uniquely expressed in Sham, C (yellow) = common between UUO and Sham.

TG2-associated proteins in Sham operated kidney membranes				
Sample ID	**Name**	**N**	**p-value**	**Unique/ Common**
PRS4_MOUSE	26S protease regulatory subunit 4	5	5.22E-09	U
PSME1_MOUSE	Proteasome activator complex subunit 1	5	8.91E-07	U
NEDD4_MOUSE	E3 ubiquitin-protein ligase NEDD4	5	3.03E-05	U
K2C1B_MOUSE	Keratin, type II cytoskeletal 1b	4	8.40E-05	U
UN45A_MOUSE	Protein unc-45 homolog A	5	1.04E-04	U
TGM2_MOUSE	Transglutaminase 2	5	1.21E-04	C
PRUNE_MOUSE	Protein prune homolog	5	1.31E-04	U
NIBL1_MOUSE	Niban-like protein 1	5	1.41E-04	U
PLEC_MOUSE	Plectin	5	1.80E-04	U
IF4G3_MOUSE	Eukaryotic translation initiation factor 4 gamma 3	5	1.82E-04	C
SERA_MOUSE	D-3-phosphoglycerate dehydrogenase	5	1.85E-04	C
TERA_MOUSE	Transitional endoplasmic reticulum ATPase	5	2.49E-04	C
PH4H_MOUSE	Phenylalanine-4-hydroxylase	5	2.67E-04	U
TOM1_MOUSE	Target of Myb protein 1	4	3.37E-04	U
PTN6_MOUSE	Tyrosine-protein phosphatase non-receptor type 6	4	4.04E-04	C
ACY3_MOUSE	N-acyl-aromatic-L-amino acid amidohydrolase	4	5.54E-04	U
TCPZ_MOUSE	T-complex protein 1	5	6.52E-04	C
DEST_MOUSE	Destrin	5	8.51E-04	U
UB2D3_MOUSE	Ubiquitin-conjugating enzyme E2 D3	5	9.25E-04	U
KAD1_MOUSE	Adenylate kinase isoenzyme 1	5	9.92E-04	U
G3P_MOUSE	Glyceraldehyde-3-phosphate dehydrogenase	5	1.05E-03	U
USP9X_MOUSE	Probable ubiquitin carboxyl-terminal hydrolase FAF-X	5	1.27E-03	U
PDIA1_MOUSE	Protein disulfide-isomerase	4	1.40E-03	U
CASP3_MOUSE	Caspase-3	4	1.42E-03	U
UBP24_MOUSE	Ubiquitin carboxyl-terminal hydrolase 24	4	1.43E-03	U
MEP1A_MOUSE	Meprin A subunit alpha	5	1.68E-03	U
ARF6_MOUSE	ADP-ribosylation factor 6	5	1.88E-03	U
SPTA1_MOUSE	Spectrin alpha chain, erythrocytic 1	5	1.97E-03	C
TM55B_MOUSE	Type 1 phosphatidylinositol 4,5-bisphosphate 4-phosphatase	4	3.22E-03	U
KCRB_MOUSE	Creatine kinase B-type	5	4.11E-03	U
RHEB_MOUSE	GTP-binding protein Rheb	5	4.12E-03	U
SCFD1_MOUSE	Sec1 family domain-containing protein 1	5	4.24E-03	C
ST1A1_MOUSE	Sulfotransferase 1A1	5	4.51E-03	U
ANXA2_MOUSE	Annexin A2	5	5.38E-03	U
CALM_MOUSE	Calmodulin	5	5.39E-03	C
F120A_MOUSE	Constitutive coactivator of PPAR-gamma-like protein 1	5	5.77E-03	C
OLFM4_MOUSE	Olfactomedin-4	5	5.80E-03	U
IST1_MOUSE	IST1 homolog	5	6.01E-03	U
PRDX2_MOUSE	Peroxiredoxin-2	4	6.07E-03	C
PP1A_MOUSE	Serine/threonine-protein phosphatase PP1-alpha catalytic subunit	4	6.08E-03	U
NLTP_MOUSE	Non-specific lipid-transfer protein	5	6.29E-03	U
PPBT_MOUSE	Alkaline phosphatase, tissue-nonspecific isozyme	5	6.39E-03	U
PDC6I_MOUSE	Programmed cell death 6-interacting protein	5	6.41E-03	C
ENOA_MOUSE	Alpha-enolase	4	6.90E-03	U
FBLN1_MOUSE	Fibulin-1	5	7.33E-03	U
LIMS1_MOUSE	LIM and senescent cell antigen-like-containing domain protein 1	5	7.55E-03	C
TCPG_MOUSE	T-complex protein 1 subunit gamma	5	7.61E-03	U
GGA1_MOUSE	ADP-ribosylation factor-binding protein GGA1	5	8.30E-03	U
IRF3_MOUSE	Interferon regulatory factor 3	4	8.39E-03	U
TBB5_MOUSE	Tubulin beta-5 chain	5	8.92E-03	U
FARP1_MOUSE	FERM, RhoGEF and pleckstrin domain-containing protein 1	5	9.63E-03	U
DJB11_MOUSE	DnaJ homolog subfamily B member 11	4	1.03E-02	U
ARF5_MOUSE	ADP-ribosylation factor 5	5	1.03E-02	U
ARPC5_MOUSE	Actin-related protein 2/3 complex subunit 5	4	1.06E-02	U
ARHGC_MOUSE	Rho guanine nucleotide exchange factor 12	5	1.10E-02	U
ARL2_MOUSE	ADP-ribosylation factor-like protein 2	5	1.14E-02	U
AT1B1_MOUSE	Sodium/potassium-transporting ATPase subunit beta-1	5	1.21E-02	U
MGST3_MOUSE	Microsomal glutathione S-transferase 3	5	1.21E-02	U
NSF_MOUSE	Vesicle-fusing ATPase	5	1.28E-02	U
PGK1_MOUSE	Phosphoglycerate kinase 1	4	1.38E-02	C

ARL1_MOUSE	ADP-ribosylation factor-like protein 1	5	1.42E-02	U
AT1A1_MOUSE	Sodium/potassium-transporting ATPase subunit alpha-1	5	1.43E-02	U
CUL5_MOUSE	Cullin-5	5	1.43E-02	U
VILI_MOUSE	Villin-1	5	1.51E-02	U
S12A3_MOUSE	Solute carrier family 12 member 3	5	1.55E-02	U
KS6A3_MOUSE	Ribosomal protein S6 kinase alpha-3	5	1.58E-02	U
TBA4A_MOUSE	Tubulin alpha-4A chain	5	1.62E-02	U
VATA_MOUSE	V-type proton ATPase catalytic subunit A	5	1.70E-02	U
SYWC_MOUSE	Tryptophan--tRNA ligase	5	1.75E-02	U
CAH9_MOUSE	Carbonic anhydrase 9	4	1.76E-02	U
RAC2_MOUSE	Ras-related C3 botulinum toxin substrate 2	5	1.85E-02	U
HBA_MOUSE	Hemoglobin subunit alpha	5	1.88E-02	U
RAB10_MOUSE	Ras-related protein Rab-10	5	1.98E-02	U
PCKGC_MOUSE	Phosphoenolpyruvate carboxykinase	5	2.08E-02	C
NRK1_MOUSE	Nicotinamide riboside kinase 1	5	2.11E-02	U
VPS35_MOUSE	Vacuolar protein sorting-associated protein 35	5	2.25E-02	U
SNX3_MOUSE	Sorting nexin-3	5	2.27E-02	U
ACSA_MOUSE	Acetyl-coenzyme A synthetase	5	2.29E-02	U
DNJA2_MOUSE	DnaJ homolog subfamily A member 2	5	2.29E-02	U
ST1D1_MOUSE	Sulfotransferase 1 family member D1	5	2.40E-02	U
ANFY1_MOUSE	Rabankyrin-5	5	2.42E-02	U
GLCTK_MOUSE	Glycerate kinase	5	2.42E-02	U
ARC1A_MOUSE	Actin-related protein 2/3 complex subunit 1A	5	2.42E-02	U
PDIA6_MOUSE	Protein disulfide-isomerase A6	5	2.53E-02	U
VATB2_MOUSE	V-type proton ATPase subunit B	5	2.59E-02	U
GCYA3_MOUSE	Guanylate cyclase soluble subunit alpha-3	5	2.67E-02	U
LYPA2_MOUSE	Acyl-protein thioesterase 2	5	2.68E-02	U
RUFY3_MOUSE	Protein RUFY3	4	2.72E-02	U
PICAL_MOUSE	Phosphatidylinositol-binding clathrin assembly protein	4	2.73E-02	C
TBC9B_MOUSE	TBC1 domain family member 9B	5	2.78E-02	U
IQGA1_MOUSE	Ras GTPase-activating-like protein IQGAP1	5	2.99E-02	C
RCN1_MOUSE	Reticulocalbin-1	4	3.03E-02	U
ARP3_MOUSE	Actin-related protein 3	5	3.04E-02	U
PGS1_MOUSE	Biglycan	5	3.18E-02	C
NAMPT_MOUSE	Nicotinamide phosphoribosyltransferase	5	3.20E-02	C
ECHP_MOUSE	Peroxisomal bifunctional enzyme	5	3.21E-02	C
HS90B_MOUSE	Heat shock protein HSP 90-beta	5	3.38E-02	U
ITM2B_MOUSE	Integral membrane protein 2B	5	3.60E-02	U
MP2K2_MOUSE	Dual specificity mitogen-activated protein kinase kinase 2	5	3.62E-02	U
DHRS4_MOUSE	Dehydrogenase/reductase SDR family member 4	4	3.62E-02	U
TBA1A_MOUSE	Tubulin alpha-1A chain	5	3.66E-02	U
IF4A1_MOUSE	Eukaryotic initiation factor 4A-I	5	3.68E-02	U
OXSR1_MOUSE	Serine/threonine-protein kinase OSR1	5	3.69E-02	U
F213A_MOUSE	Redox-regulatory protein FAM213A	5	3.76E-02	C
CLIC4_MOUSE	Chloride intracellular channel protein 4	5	3.82E-02	U
VDAC1_MOUSE	Voltage-dependent anion-selective channel protein 1	5	3.87E-02	U
CAN2_MOUSE	Calpain-2 catalytic subunit	5	3.95E-02	U
NDRG3_MOUSE	Protein NDRG3	5	4.06E-02	U
CLH1_MOUSE	Clathrin heavy chain 1	5	4.11E-02	U
LAMB2_MOUSE	Laminin subunit beta-2	4	4.21E-02	C
FINC_MOUSE	Fibronectin	5	4.27E-02	C
TS101_MOUSE	Tumor susceptibility gene 101 protein	4	4.31E-02	U
DPYL3_MOUSE	Dihydropyrimidinase-related protein 3	5	4.39E-02	U
ISG15_MOUSE	Ubiquitin-like protein ISG15	5	4.53E-02	U
DRG2_MOUSE	Developmentally-regulated GTP-binding protein 2	5	4.71E-02	U
RN213_MOUSE	E3 ubiquitin-protein ligase RNF213	4	4.73E-02	U
BAX_MOUSE	Apoptosis regulator BAX	5	4.73E-02	U
ADH1_MOUSE	Alcohol dehydrogenase 1	5	4.74E-02	C
SPTN1_MOUSE	Spectrin alpha chain, non-erythrocytic 1	5	5.25E-02	C
EF1A1_MOUSE	Elongation factor 1-alpha 1	5	5.34E-02	U

Among the proteins associated with TG2 in either fibrotic or sham operated kidney membranes (**Table 4.2, 4.3**), some had been previously reported to interact with the enzyme (full list of TG2 main partners in the Appendix, **Table I**). These were either reported as known substrates of the enzyme's catalytic activity or known interacting/binding partners of TG2 non-enzymatic activity by Transdab database of TG partners (Csősz, Meskó and Fésüs 2009), and are displayed in **Table 4.4 (A,B)**.

Of the TG2 significantly associated proteins in UUO kidney membranes, as detected by TG2-IP and SWATH-MS in the current study ($p \leq 0.05$, $n \geq 4$), 39 had a reported interaction with the enzyme in literature (**Table 4.4A**), while 83 appeared as novel partners. Most of previously identified TG2-partners in UUO conditions were structural components of the ECM or adhesion proteins, with collagens (COCA1_MOUSE, COEA1_MOUSE), fibronectin (FN) (FINC_MOUSE) and the cell surface HSPGs syndecan4 (SDC4_MOUSE) among the more prominent, but many cortical cytoskeleton proteins were also identified. These included actin (ACTB_MOUSE), Filamin (FLNA_MOUSE), as substrates, and talin (TLN2_MOUSE), which is a known focal adhesion protein linking vinculin, integrin and actin cytoskeleton, as a binding partner. Ankyrin (ANK3_MOUSE) and number of spectrin chains were also identified, and are known to be substrates of TG2 crosslinking activity on the inner side of the plasma membrane, which is likely to be a result of the loss of cell integrity, and associated with a TG2-mediated cell death preventing inflammation (Orru, et al. 2003). A few chaperone proteins of the heat shock protein (HSP) family and subunits of T-complex protein 1 were also known TG2 partners identified in our study as TG2 immunoprecipitated from kidney fibrotic membranes ($p \leq 0.05$, $N=4$).

Of the TG2 significantly associated proteins in healthy (Sham operated) kidney membranes, as detected by TG2-IP and SWATH-MS in the current study ($p \leq 0.05$, $n \geq 4$), 27 had already been associated with the enzyme in literature (**Table 4.4B**), leaving out 93 possible novel partners of the enzyme. In these conditions, the only ECM protein and adhesion protein identified and already reported in literature was FN (**Table 4.4B**): no HSPG or collagen was found associated with TG2 in healthy kidney membranes, and TG2 association with FN was lower in significance compared to the UUO kidney ($p=0.043$ against $p= 0.016$). Many already reported cytoskeletal protein partners of the enzyme were identified as well in this list of candidates, of which some were Tubulins (**Table 4.4B**). Tubulins were associated with TG2 only in healthy conditions, which might be interesting, considering that TG2 has been shown to polyaminate tubulin with a role in microtubule stabilisation in brain (Song, et al. 2013). In addition, some known TG2 partners involved in cell signalling and stress response were identified as TG2-coprecipitated in the sham operated kidney membranes.

Table 4.4: TG2-immunoprecipitated candidates in UUO kidney membranes (21-days) or Sham operated membranes (p≤0.05 N≥4) with a previously reported association with TG2 (Transdab database). The two tables shows all the proteins identified as TG2-associated in UUO (A) or Sham operated (B) kidney membranes (p≤0.05 N≥4) which have already been reported as substrate or interacting partners (binding) for the enzyme, according to the Transdab database (Csősz, Meskó and Fésüs 2009). Some proteins were similar or closely related to the TG2 partners reported in the database; in this case, the name of the reported TG2-associated partner from Transdab database is provided in the legend.

A) Candidates in UUO kidney membranes with a previously reported interaction with TG2				
Sample ID	**Name**	**p-value**	**Reported interaction with TG2**	**Note**
ACTB	Actin, cytoplasmic 1	1.24E-02	Substrate	
ANK3	Ankyrin-3	3.03E-03	Substrate	
CAN1	Calpain1	1.84E-02	Substrate	
CLCA	Clathrin light chain A	2.07E-02	Substrate	(1)
CLCB	Clathrin light chain b	1.65E-02	Substrate	(1)
COCA1	Collagen alpha-1(XII) chain	1.68E-03	Substrate	
COEA1	Collagen alpha-1(XIV) chain	1.64E-03	Substrate	
FLNA	Filamin-A	2.98E-03	Substrate	
HSP7C	Heat shock cognate 71 kDa protein	7.67E-10	Substrate	
HS90A	Heat shock protein HSP 90-alpha	2.85E-02	Substrate	
HIP1	Huntingtin-interacting protein 1	1.86E-03	Substrate	(2)
MYH10	Myosin-10	3.59E-02	Substrate	
MYH14	Myosin-14	4.79E-02	Substrate	
SPTA1	Spectrin alpha chain, erythrocytic 1	2.92E-03	Substrate	
SPTN1	Spectrin alpha chain, non-erythrocytic 1	3.08E-02	Substrate	
SPTB1	Spectrin beta chain, erythrocytic	1.73E-02	Substrate	
TCPE	T-complex protein 1	3.17E-04	Substrate	
TCPQ	T-complex protein 1	3.96E-02	Substrate	
TCPZ	T-complex protein 1	4.23E-02	Substrate	
TCPA	T-complex protein 1	5.25E-02	Substrate	
MYO1B	Unconventional myosin-Ib	2.67E-02	Substrate	(3)
MYO1D	Unconventional myosin-Id	3.52E-06	Substrate	(3)
MYO1G	Unconventional myosin-Ig	1.21E-03	Substrate	(3)
MY18A	Unconventional myosin-XVIIIa	1.93E-02	Substrate	(3)
VIME	Vimentin	3.66E-02	Substrate	
FINC	Fibronectin	1.57E-02	Substrate and Binding	
GSTT1	Glutathione S-transferase theta-1	3.95E-02	Substrate and Binding	
HSPB1	Heat shock protein beta-1	3.68E-05	Substrate and Binding	
TGM2	Transglutaminase 2	3.31E-05	Substrate and Binding	
KCC2D	Calcium/calmodulin-dependent protein kinase type II subunit delta	7.10E-03	Binding	
CALM	Calmodulin	1.83E-08	Binding	
COPB2	Coatomer subunit beta	4.42E-02	Binding	
IF4G3	Eukaryotic translation initiation factor 4 gamma 3	1.11E-02	Binding	(4)
MVP	Major vault protein	1.14E-02	Binding	
MOES	Moesin	3.33E-02	Binding	(5)
PRDX2	Peroxiredoxin-2	6.87E-03	Binding	(6)
IQGA1	Ras GTPase-activating-like protein IQGAP1	1.50E-04	Binding	
SDC4	Syndecan-4	9.34E-04	Binding	
TLN2	Talin-2	5.28E-03	Binding	

B) Candidates in Sham operated kidney membranes with a previously reported interaction with TG2				
Sample ID	**Name**	**p-value**	**Reported interaction with TG2**	**note**
ANXA2	Annexin A2	5.38E-03	Substrate	(7)
CAN2	Calpain-2 catalytic subunit	3.95E-02	Substrate	
CASP3	Caspase-3	1.42E-03	Substrate	
CLH1	Clathrin heavy chain 1	4.11E-02	Substrate	
DPYL3	Dihydropyrimidinase-related protein 3	4.39E-02	Substrate	
EF1A1	Elongation factor 1-alpha 1	5.34E-02	Substrate	
IF4A1	Eukaryotic initiation factor 4A-I	3.68E-02	Substrate	(8)
G3P	Glyceraldehyde-3-phosphate dehydrogenase	1.05E-03	Substrate	
HS90B	Heat shock protein HSP 90-beta	3.38E-02	Substrate	
SPTA1	Spectrin alpha chain, erythrocytic 1	1.97E-03	Substrate	
SPTN1	Spectrin alpha chain, non-erythrocytic 1	5.25E-02	Substrate	
TCPG	T-complex protein 1	7.61E-03	Substrate	
ISG15	Ubiquitin-like protein ISG15	4.53E-02	Substrate	(9)

FINC	Fibronectin	4.27E-02	Substrate and Binding	
MGST3	Microsomal glutathione S-transferase 3	1.21E-02	Substrate and Binding	
TGM2	Transglutaminase 2	1.21E-04	Substrate and Binding	
TBB5	Tubulin beta-5 chain	8.92E-03	Substrate and Binding	
PRS4	26S protease regulatory subunit 4	5.22E-09	Binding	
BAX	Apoptosis regulator BAX	4.73E-02	Binding	
CALM	Calmodulin	5.39E-03	Binding	
IF4G3	Eukaryotic translation initiation factor 4 gamma 3	1.82E-04	Binding	(4)
PRDX2	Peroxiredoxin-2	6.07E-03	Binding	(6)
IQGA1	Ras GTPase-activating-like protein IQGAP1	2.99E-02	Binding	
RAC2	Ras-related C3 botulinum toxin substrate 2	1.85E-02	Binding	
PP1A	Serine/threonine-protein phosphatase PP1-alpha catalytic subunit	6.08E-03	Binding	
TBA1A	Tubulin alpha-1A chain	3.66E-02	Binding	
TBA4A	Tubulin alpha-4A chain	1.62E-02	Binding	

(1) Clathrin Heavy Chain, (2) Huntingtin, (3) Myosin, (4) Eukaryotic translation initiation factor 5A-1, (5) Ezrin-Radixin-Moesin binding phosphoprotein 50, (6) Peroxiredoxin-1, (7) Annexin 1, (8) Eukaryotic initiation factor 4F (eIF-4F), (9) Ubiquitin

4.4.2 Functional clusters of TG2-associated proteins in UUO and Sham operated kidney membranes

After a list of TG2-associated proteins was obtained for both fibrotic (UUO) and healthy (Sham) membranes (**Table 4.2** and **Table 4.3**), manual search of the proprieties and functions of every of them was performed, to associate each one with wide-ranging clusters depending on its role in the cell. The association of each protein with a general "functional cluster" is presented in **Suppl. Tables 4.6 – 4.8**: **Suppl. Table 4.6** displays functional clusters of the 97 proteins uniquely associated with TG2 in UUO kidney membranes, **Suppl. Table 4.7** the functional clusters of the 95 proteins uniquely associated with TG2 in sham operated kidney membranes, and **Suppl. Table 4.8** the functional clusters of the 25 proteins significantly associated withTG2 in both conditions (Common proteins). Functional clusters such as "Cytoskeletal and actin regulation", "Cell adhesion", "Vesicular Trafficking" and "Metabolism" were defined as general groups of proteins, to describe the main role/function of each TG2-associated partner in the cell.

A graphical representation of the resulting functional clustering is provided in **Figures 4.4-4.6**. In these charts the TG2-associated proteins uniquely identified in UUO kidney membranes (n=97, **Fig. 4.4**), in sham operated kidney membranes (n=95, **Fig. 4.5**), or found in both conditions (n=25, **Fig. 4.6**) were grouped depending on the functional cluster which the proteins were associated with. Each column is proportional to the significance of TG2 association as it represents the p-value in reversed logarithmic scale: the higher, the more significant the association with TG2.

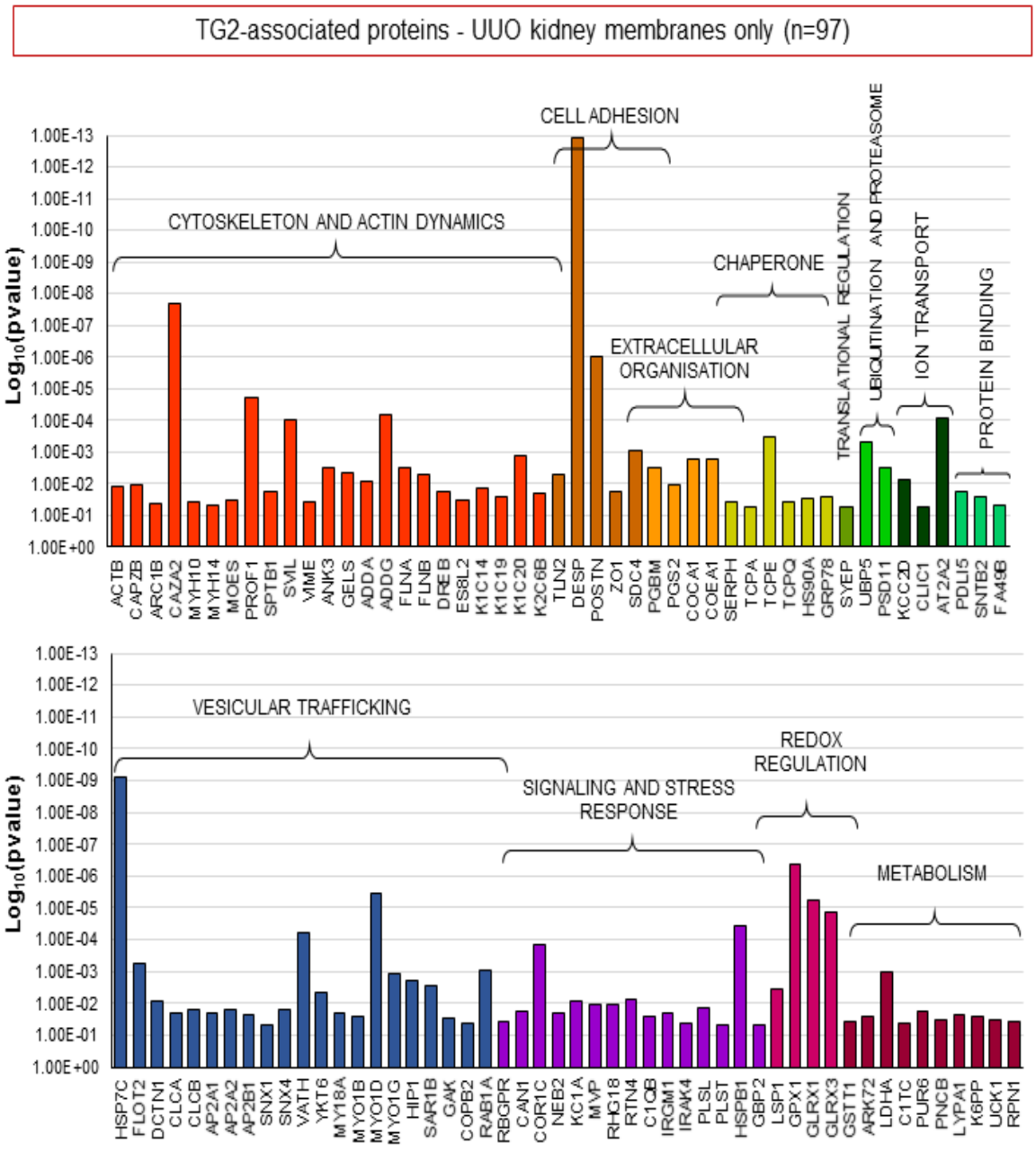

Figure 4.4: TG2-associated proteins identified uniquely in UUO kidney membranes, grouped depending on their general functions. Bars represent p-value of TG2 association (determined by z-test) of each protein identified as significantly associated with TG2 uniquely in UUO kidney membranes at 21 days post operation ($p \leq 0.05$ $N \geq 4$, marked with "U" in **Table 4.2**). Proteins were grouped and color-coded depending the general functional cluster they were associated with (**Suppl.Table 4.6**). Nuclear, mitochondrial and ribosomal proteins were removed from the list.

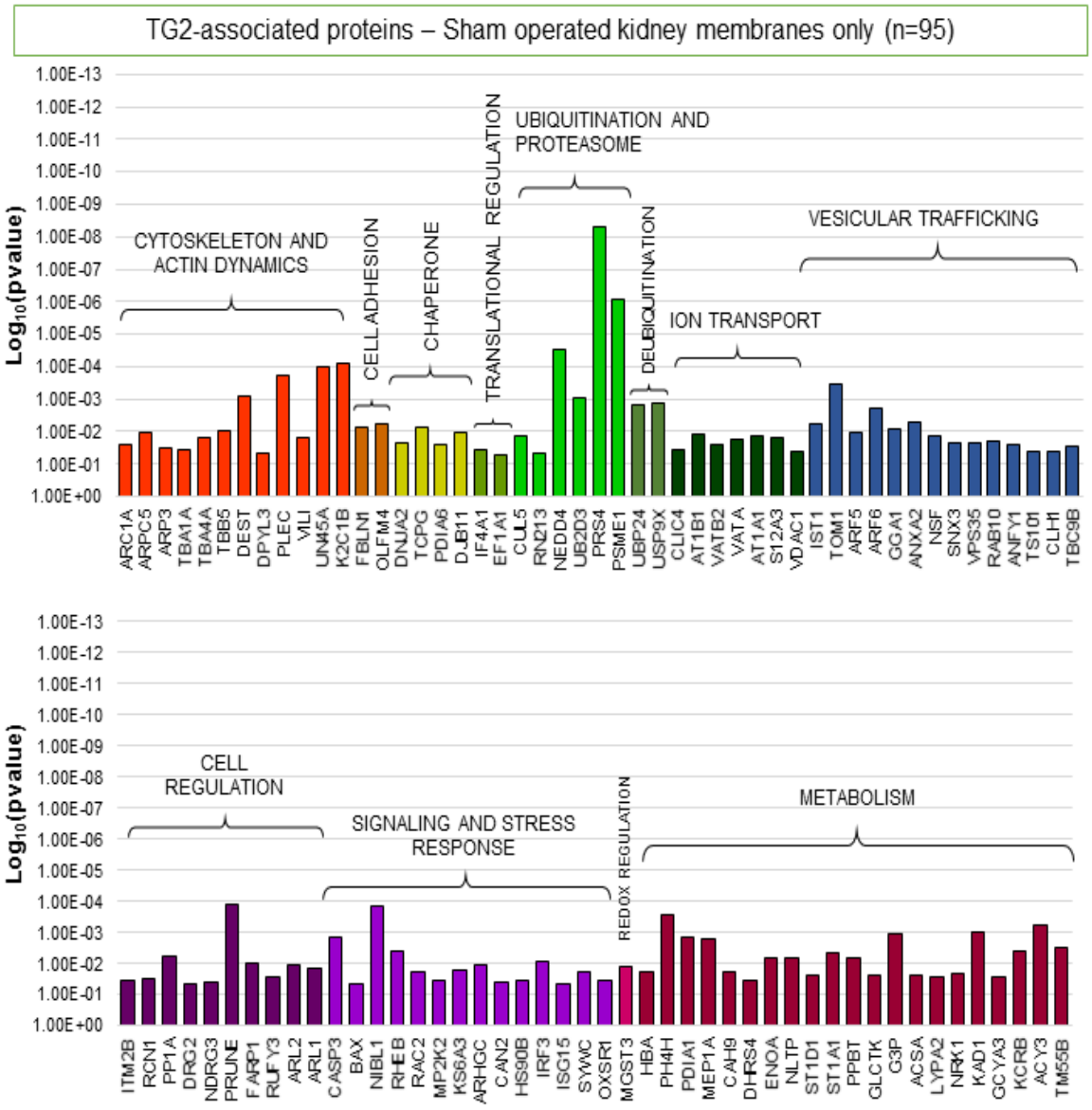

Figure 4.5: TG2-associated proteins identified uniquely in Sham operated kidney membranes, grouped depending on their general functions. Bars represent p-value of TG2 association (determined by z-test) of each protein identified as significantly associated with TG2 uniquely in sham operated kidney membranes at 21 days post operation ($p \leq 0.05$ $N \geq 4$, marked with "U" in **Table 4.3**). Proteins were grouped and color-coded depending the general functional cluster they were associated with (**Suppl.Table 4.7**). Nuclear, mitochondrial and ribosomal proteins were removed from the list.

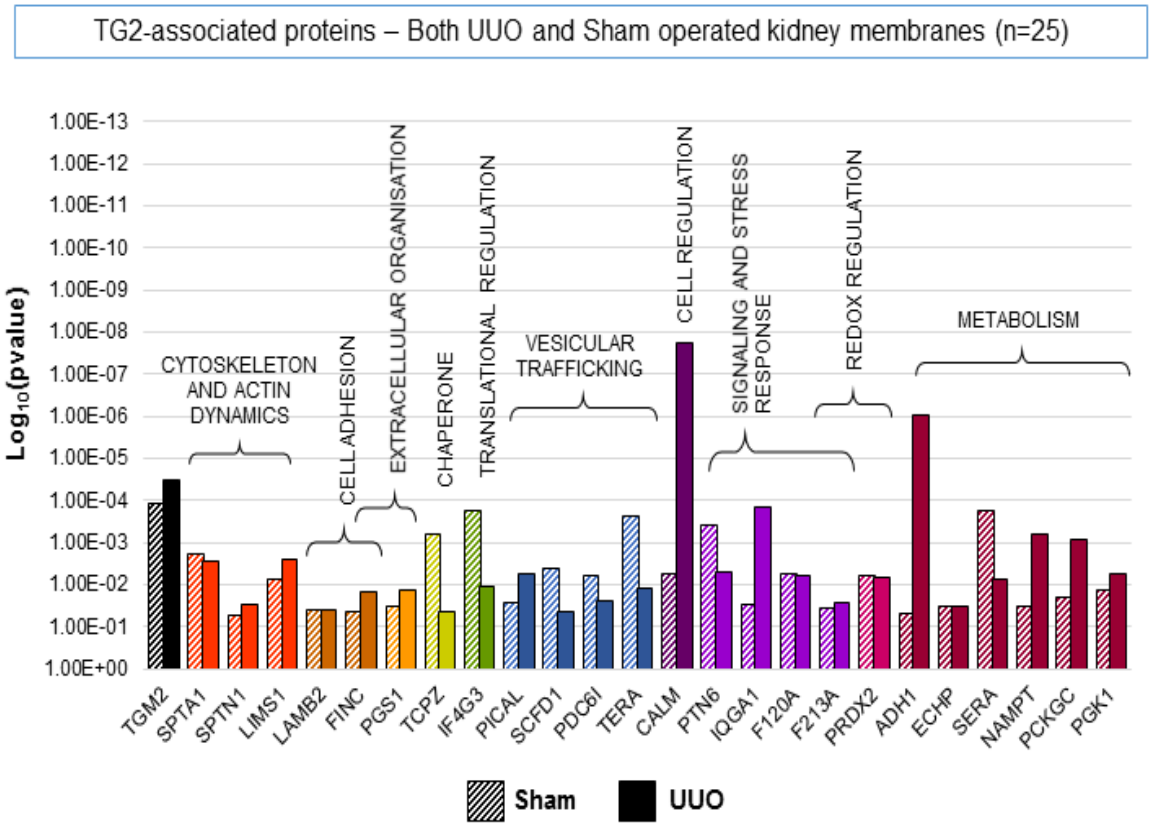

Figure 4.6: TG2-associated proteins identified in both UUO and Sham operated kidney membranes (common), grouped depending on their general functions. Bars represent p-value of TG2 association (determined by z-test) of each protein identified as significantly associated with TG2 in both UUO and sham operated kidney membranes at 21 days post operation ($p \leq 0.05$ $N \geq 4$, marked with "C" in **Tables 4.2 and 4.3**). Proteins were grouped and color-coded depending the general functional cluster they were associated with (**Suppl.Table 4.8**). Solid fill color represent the p-values for the healthy membranes, striped patterned colors represent p-values in UUO membranes. Nuclear, mitochondrial and ribosomal proteins were removed from the list.

Comparing in the same chart the TG2-associated proteins belonging to the same functional cluster, in either UUO or Sham operated kidney membranes (**Fig. 4.7**), allowed to investigate possible biases in the proteins' biological roles in association with TG2, in an established fibrotic condition comparing to a healthy state. When the numbers of TG2-associated proteins belonging to each functional cluster were presented in a pie chart as percentage of proteins in the cluster over the total number of proteins (**Fig. 4.8**), a clear difference in protein representation was evident, with different distribution of the biological functions in UUO comparing to the healthy conditions.

The first evidence was that a higher number of cytoskeletal proteins was associated with TG2 in the UUO conditions compared to the healthy status (**Fig. 4.7A, 4.8**). "Cytoskeletal and Actin dynamics" was the more represented functional cluster among the TG2-associated proteins in

fibrotic (UUO) conditions, covering the 21% of all the TG2-associated proteins in UUO kidney membranes (**Fig. 4.8A**), while in Sham operated membranes only 12% of the proteins belonged to this functional cluster (**Fig. 4.8B**). This cluster included both structural elements of the cytoskeleton and proteins involved in its remodelling, the latter important to support a series of cellular processes, going from focal adhesion and cell locomotion, endocytic and exocytic processes and intracellular movements of vesicles. In membrane extracts from kidneys subjected to 21 days-UUO (**Fig. 4.7A**), these proteins comprised actin (ACTB_MOUSE) and proteins associated with its polymerisation and remodelling proteins such as capping proteins (CAPZB_MOUSE, CAZA2_MOUSE), actin-related protein 2/3 complex (ARC1B_MOUSE), gelsolin (GELS_MOUSE), profilin (PROF1_MOUSE), etc. Other proteins, such as adducin (ADDA_MOUSE, ADDG_MOUSE), filamin (FLNA_MOUSE, FLNB_MOUSE), ankyrin (ANK3_MOUSE), moesin (MOES_MOUSE), and supervillin (SVIL_MOUSE) (**Fig. 4.7A**) are known to be present in the cortical cytoskeleton and connect it to the plasma membrane, and are frequently involved in the regulation of adhesion and plasma membrane movements. The intermediate filament protein vimentin (VIME_MOUSE), a protein specifically known as a marker of mesenchymal cells, was also associated with TG2 uniquely in UUO conditions. Myosin subtypes were also represented upon UUO, with a possible involvement in cell contraction. An increased association of TG2 with keratins (K1C14_MOUSE, K1C19_MOUSE, K1C20_MOUSE, K2C6B_MOUSE) upon kidney fibrosis is novel (**Fig. 4.7A**).

In Sham operated kidney membrane, the lower number of TG2-associated cytoskeletal proteins included mostly actin remodelling proteins such as actin-related protein 2/3 complex components (ARC1A_MOUSE, ARPC5_MOUSE, ARP3_MOUSE), destrin (DEST_MOUSE) and villin (VILI_MOUSE) (**Fig. 4.7A**), the latter mainly associated with the brush border of epithelial cells, that might be strongly lost upon induction of fibrosis. As stated before, interesting is the association of TG2 with tubulins (TBA1A_MOUSE, TBA4A_MOUSE and TBB5_MOUSE) exclusively in healthy kidney membranes (**Fig. 4.7A**). Plectin (PLEC_MOUSE), a large protein involved in the maintenance of cytoskeletal structure by connecting the different cytoskeletal filaments between them and to the plasma membrane, also lost its association with TG2 in kidney membranes when mice were subjected UUO (**Fig. 4.7A**). Spectrins appeared associated with TG2 in kidney membranes in both UUO and Sham operated conditions (**Fig. 4.7A**).

As expected, other functional clusters more represented in the group of TG2-associated candidates in the UUO conditions compared to the healthy state were “Cell adhesion” (5% against 3% in sham operated membranes) and “Extracellular Organisation” (6% against 2% in sham operated membranes) (**Fig. 4.8**), suggesting a specific upregulation of TG2 function at the cell-matrix interface upon established UUO. Matrix proteins such as FN and collagens were identified as TG2-associated in fibrotic kidney membranes, together with small matrix

proteoglycans known to be associated with CKD progression such as biglycan (PGS1_MOUSE) and decorin (PGS2_MOUSE) (Stokes, et al. 2000, Schaefer, et al. 2004) (**Fig. 4.7B**). Importantly, the cell surface HSPGs syndecan-4 (Sdc4, SDC4_MOUSE) and the basement membrane HSPG perlecan (PGBM_MOUSE), were recognised as uniquely associated with TG2 in fibrotic membranes (**Fig. 4.7B**), which is in line with previously suggested importance of HSPGs in models of kidney fibrosis, including the UUO itself (Yung, et al. 2001, Morita, et al. 1994, Fan, et al. 2003, Scarpellini, et al. 2014). Besides Sdc4, cell adhesion proteins also included talin (TLN2_MOUSE), important element of focal adhesion to the matrix, and periostin (POSTN_MOUSE), an adhesion protein known to interact with integrins (**Fig. 4.7B**). However, highly significant appeared the interaction between TG2 and desmosome protein desmoplakin (DESP_MOUSE) in UUO kidney membranes, which, together with the tight junction protein ZO1, suggests an involvement for the enzyme in the regulation of cell-cell adhesion in the context of fibrosis, that might be associated with a reepithelization process ongoing in localised sites of acute insult in the UUO kidney at this stage of disease.

Another interesting finding is the fact that redox and specifically antioxidant proteins were found associated with the enzyme mainly in UUO conditions. “Redox Regulation” proteins covered 5% of the TG2-interacting proteins in UUO membranes, against 2% in control membranes (**Fig. 4.8**). These proteins were mostly antioxidant proteins and included glutaredoxins (GLRX1_MOUSE, GLRX3_MOUSE), glutathione peroxidase (GPX1_MOUSE) and glutathione S-transferase (GSTT1_MOUSE), and peroxiredoxin (PRDX2_MOUSE) (**Fig. 4.7C**), and might be involved in the enzyme reduction and activation in the context of kidney fibrosis.

The most intriguing finding, however, was the association of TG2 with a series of proteins involved vesicular trafficking. A substantial percentage of TG2 interacting partners in UUO kidney membranes (21%) were proteins involved in different mechanisms of intracellular and extracellular vesicular trafficking, that instead represented only the 15% of the TG2-associated proteins in Sham operated conditions, suggesting that TG2 is more dynamic post UUO induction. Vesicular associated proteins included for example clathrins (CLCA_MOUSE, CLCB_MOUSE, CLH1_MOUSE) and clathin-associated proteins such as adaptor proteins (AP2A1_MOUSE, AP2A2_MOUSE, AP2B1_MOUSE), sorting nexins (SNX1_MOUSE, SNX4_MOUSE), but also known markers of extracellular vesicles such as tumour susceptibility gene 101 (TS101_MOUSE), programmed cell death 6-interacting protein/alix (PDC6I_MOUSE) and flotillin (FLOT2_MOUSE). Description of the main functions of the vesicular proteins identified as associated with TG2 is provided in a small supplement at the end of this thesis (Appendix) while a table summarizing the main proprieties is provided later in this chapter.

When the proteins less associated with TG2 in UUO kidney membranes compared to the healthy kidneys were, a general reduction in the number of metabolic proteins was observed as interacting with the enzyme (**Fig. 4.7E**). Metabolic proteins were more represented in the TG2-associated proteins in Sham operated kidney membranes (22%) compared to the fibrotic kidney membranes (12%) (**Fig. 4.8**). This might be correlated to the large underexpression of metabolic proteins at 21 days post-UUO, as described in Chapter III. "Cell regulation" proteins were associated with TG2 on kidney membranes almost uniquely in sham operated conditions (11%), while only one protein was identified as TG2-associated in UUO membranes (**Fig. 4.8**). Similarly, "Ion transport" (6% in sham against 2% in UUO membranes) and "Ubiquitination and Proteasome" (5% in sham against 2% in UUO membranes) were less associated with TG2 in UUO conditions compared to the healthy ones (**Fig. 4.8**). Functional clusters such as "Signalling and stress response" and "Translational regulation" seemed equally distributed among the TG2-associated protein in either sham and UUO fibrotic membranes, with no bias toward a specific treatment (**Fig. 4.8**).

In conclusion, while cytoskeletal components, adhesion proteins, ECM elements, antioxidants and vesicular proteins appeared more represented in the list of TG2-associated partners at 21-days post UUO, and might be involved in the enzyme's transport and pro-fibrotic activity during CKD, less metabolic proteins or proteins associated with cell functions and regulation were identified upon fibrosis when compared to the sham operated TG2 precipitates.
For the aims of this thesis, the main finding is the identification of a substantial number of vesicular proteins, that points the finger to a possible involvement of a vesicular trafficking pathway for the enzyme secretion in conditions of fibrosis.

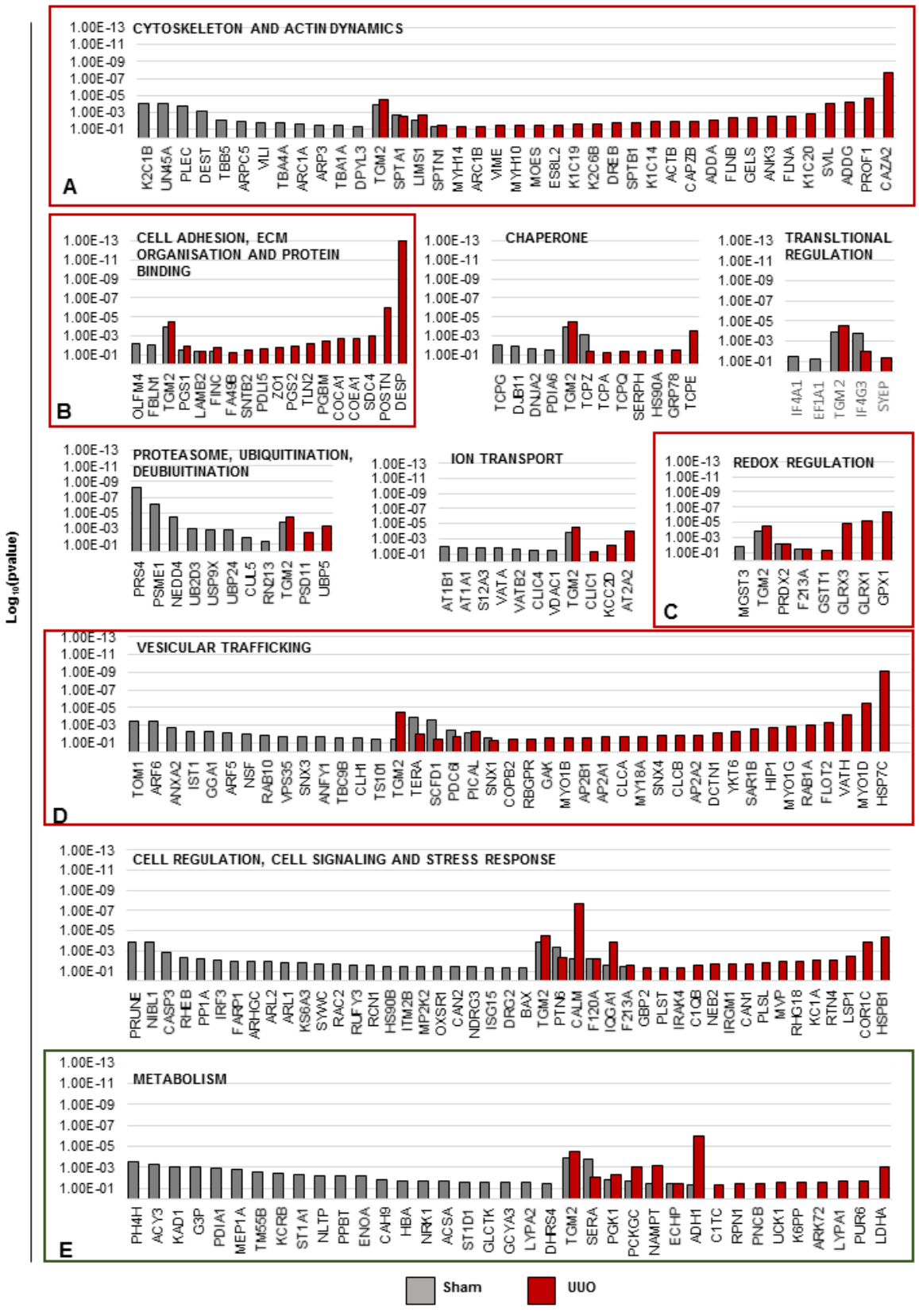

Figure 4.7: Candidate proteins significantly associated with TG2 in either Sham operated and UUO kidney membranes, grouped basing on their general functional cluster and ordered basing on their p-values. Bars represent p-value of TG2 association (determined by z-test) of each protein identified as significantly associated with TG2 in either UUO or Sham operated kidney membranes at 21 days post operation ($p \leq 0.05$ $N \geq 4$, Listed in **Table 4.2 and 4.3**). Each graph represents a specific functional cluster, as identified in **Suppl. Tables 4.6- 4.8**. TG2-associated proteins in UUO kidney membranes are in red, while TG2-associated proteins in sham operated kidney membranes are in grey.

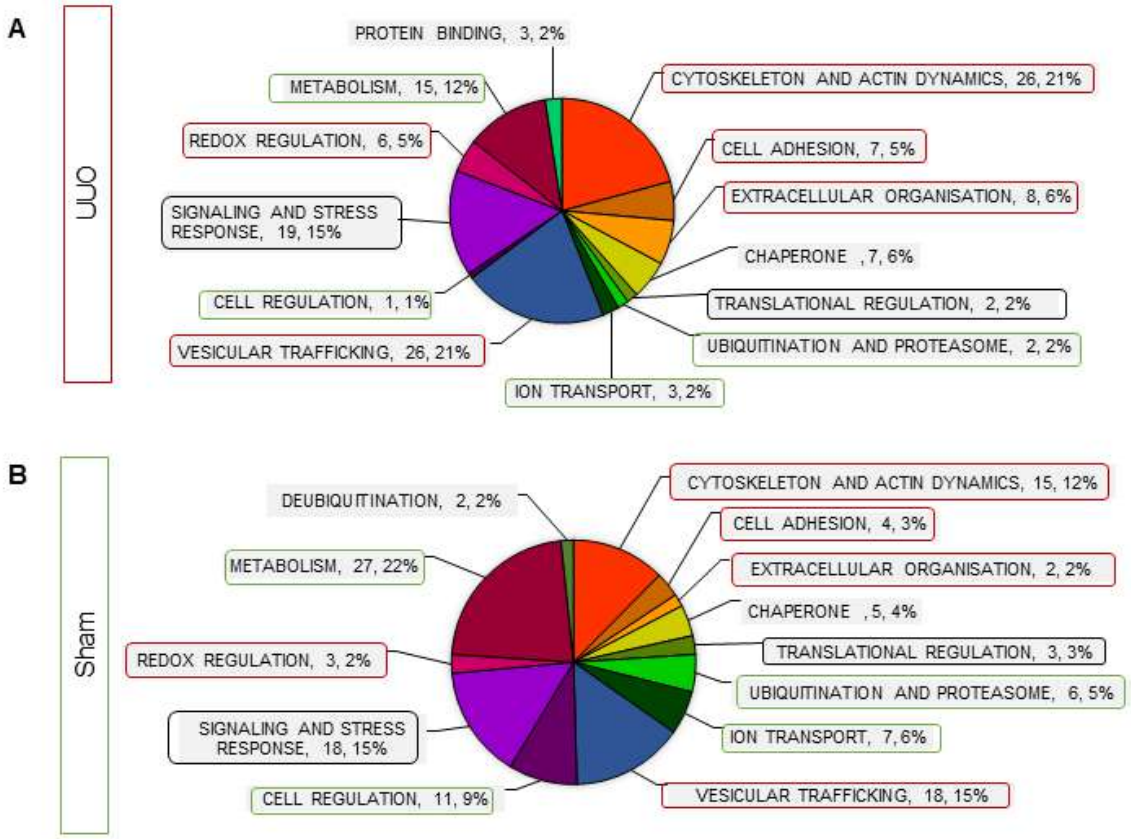

Figure 4.8: Distribution of the general functions in UUO and Sham operated kidney membranes. pie chart representing the distribution of the TG2-associated proteins in the different functional clusters (as identified in **Suppl. Tables 4-6 – 4.8**) for either UUO (A) or sham operated (B) kidney membranes at 21 days post operation ($p \leq 0.05$ $N \geq 4$). Each sector individuates the number and % of proteins in the functional cluster over the total of number of proteins). Both unique and common proteins were considered for each treatment. TG2 was excluded from the analysis. nuclear, mitochondrial and ribosomal proteins were removed from the list. Red circles indicate terms more represented as associated with TG2 in fibrotic conditions (UUO 21 days), green circles terms more represented as associated with TG2 in healthy conditions (Sham 21 days) and black circles indicate terms similarly represented in both lists.

4.4.3 Functional classification of TG2-associated proteins in UUO and Sham operated kidney membranes using Gene Ontology (GO) and PANTHER annotation terms

Functional classification of the different gene products (protein IDs) associated with TG2 was also performed in PANTHER, as described above in 4.3.2.1. GO terms for "Biological Processes", "Molecular Functions" and "Cellular Components", as well as PANTHER Protein class terms, were investigated, and results were visualized in pie charts as percentage of representation of the different annotation terms over the total class hits (**Fig. 4.9**).

For what it concerns the GO annotations terms for "Biological Processes" (**Fig. 4.9A**), the term "Cellular component organization or biogenesis" (GO:0071840) covered approximately 21% of the total class hits and 39% of the total elements of the list of TG2-associated proteins in fibrotic kidney membranes (UUO). This means that more than a third of TG2-associated proteins in UUO kidney membranes was associated with this annotation term, which is a general ancestor term that includes more specific descendant "child" terms such as "Extracellular structure organization" (GO:0043062), "Membrane and endomembrane system organization" (GO:0061024, GO:0010256), "Actin filament organization" (GO:0007015) and "Vesicle tethering" (GO:0099022). In Sham operated kidney membranes, the same term covered only 7.6% of the total number of class hits, and the 13.1% of the TG2-associated candidates (**Fig. 4.9A**). This finding is consistent with the manual clustering described before (4.4.2). On the other hand, a Biological Process GO term that was less represented among TG2-associated proteins in UUO kidney membranes, compared to the healthy ones, was "Metabolic process" (GO:0008152), in line with the functional cluster described before (4.4.2). This term covered the 22.4% of the total class hits in healthy kidney membranes, and more than a third of the total number of TG2-associated proteins in this condition (38.5%). In UUO kidney membranes, less TG2 partners were associated with this term (27.6%), that represented the 14.8% of total class hits (**Fig. 4.9A**).

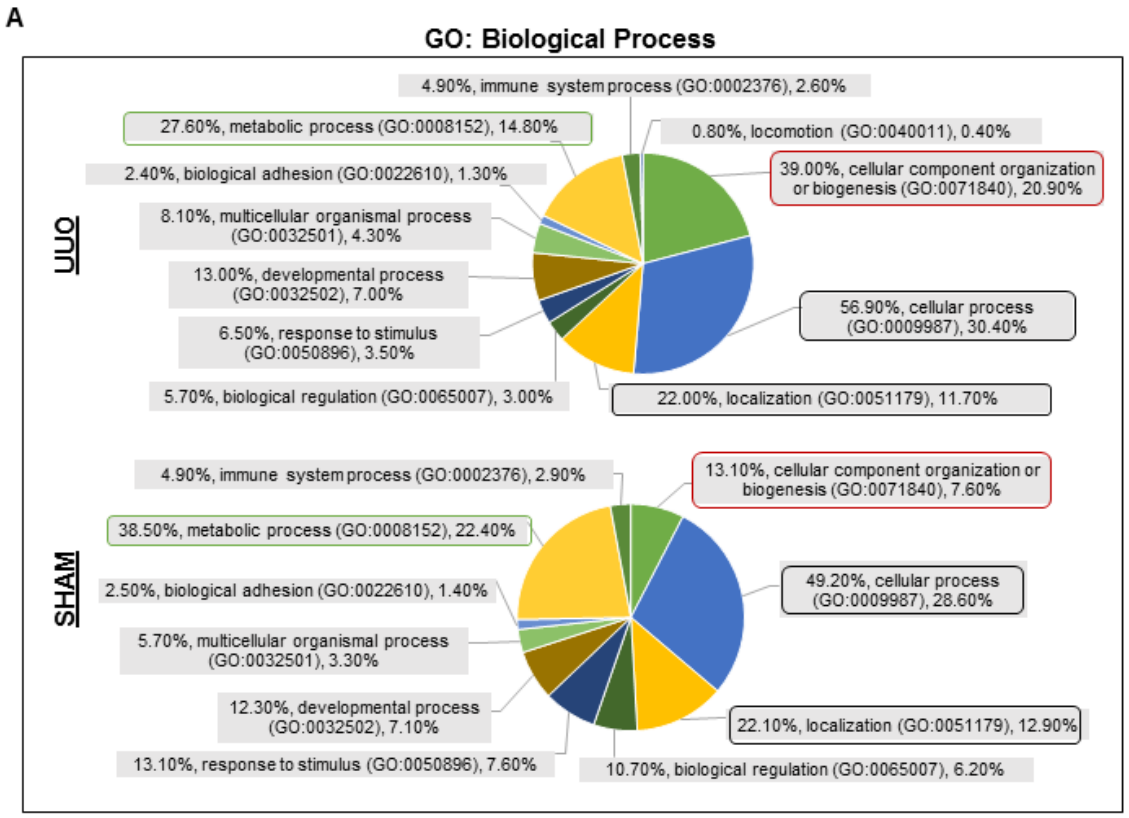

When the GO terms for "Molecular Functions" were analysed using the same approach (**Fig. 4.9B**), an elevated presence of TG2 protein partners associated with the annotation terms "Binding" (GO:0005488) and "Structural molecule activity" (GO:0005198) were identified fibrotic kidney membranes (36% and 24% of total class hits, respectively, and 39% and 26% of total number of proteins). "Binding" Molecular Function GO term is a general annotation that includes a large spectrum of more specific molecular functions such as ion binding (GO:0043167), hormone binding (GO:0042562) and extracellular matrix binding (GO:0050840), while "Structural molecule activity" term includes all the gene products implicated in the structural constitution of the cell and the extracellular space (cytoskeleton, extracellular matrix, ribosomes etc.). These functions were less represented in Sham operated kidney membranes, especially for what it concerns "Structural molecule activity" term, that was more than 2-times less represented in healthy conditions (11.5% of proteins or 11.3% of total class hits) compared to UUO (**Fig. 4.9B**). "Catalytic activity" (GO:0003824), on the other hand, was the more represented in healthy membranes, covering almost the half of the total proteins in the list (43.4%). In UUO membranes, even if still considerable, this annotation term was less represented, covering 32.3% of all the TG2-associated proteins in the list (**Fig. 4.9B**).

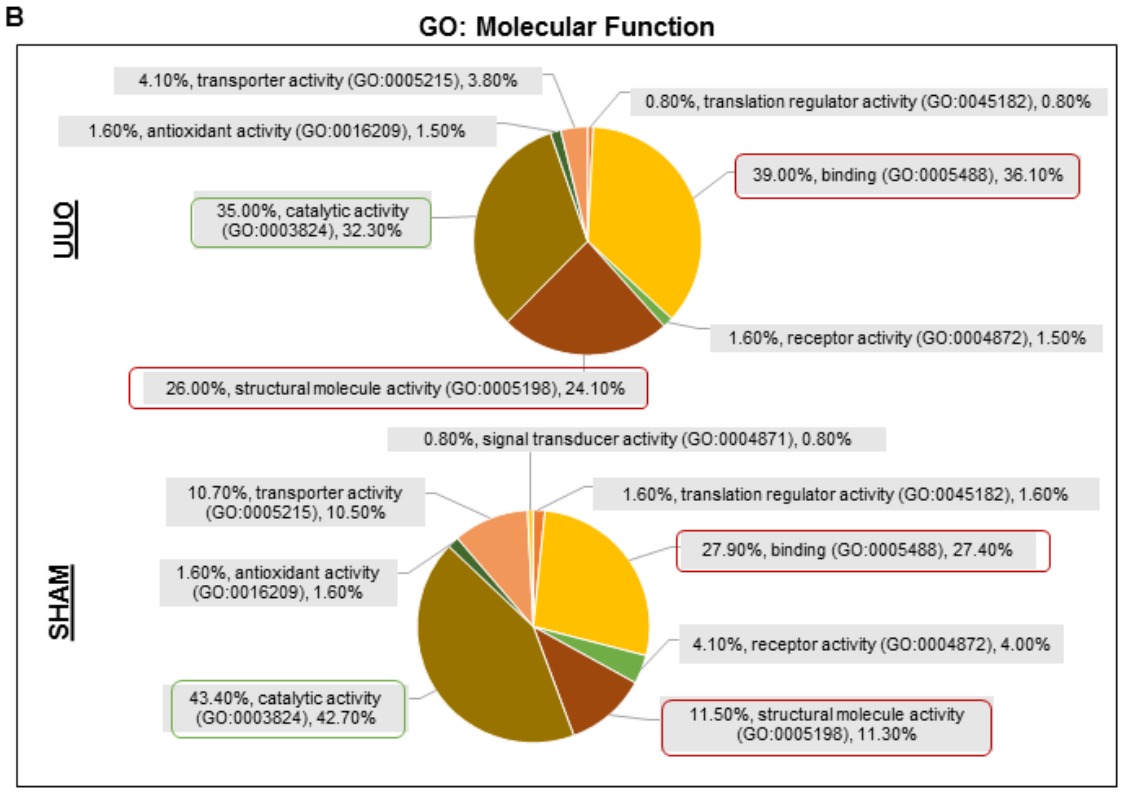

To investigate the localization of the different kidney membrane fraction TG2-associated proteins in the cells, in healthy or fibrotic conditions, GO terms for "Cellular Components" were analyzed with the same approach (**Fig. 4.9C**). Even if the distribution of the proteins in the different cellular compartments appeared similar in UUO and Sham operated conditions, some bias was noticed toward membranous and extracellular compartments for the TG2-associated proteins in UUO membranes ["Membrane" (GO:0016020) =13.0% of proteins against 4.9% in sham; "Extracellular matrix" (GO:0031012) = 2.4% against 0.8% in sham; "Extracellular region" (GO:0005576) = 4.1% against 2.5% in sham; "Cell junction" (GO:0030054) = only detected in UUO membranes, 4.9%], that were also showing an higher number of "Organelle"(GO:0043226) proteins (30.9% of proteins against 16.4% in sham) (**Fig. 4.9C**). In Sham operated kidneys, a series of proteins (at least 28%) were not associated with any annotation term for Cellular Components by the software, and the ones associated were mostly related to "Cell part" (GO:0044464) ontology, that identifies basically every intracellular component of the cell and include the plasma membrane. In healthy conditions, this term covered more than half of the total class hits, 50.6%, and the 36.1% of proteins in the list of TG2-associated proteins. In UUO kidney membranes the same term covered "only" 44.4% of total class hits, but was actually associated with more than 50% of protein candidates (**Fig. 4.9C**).

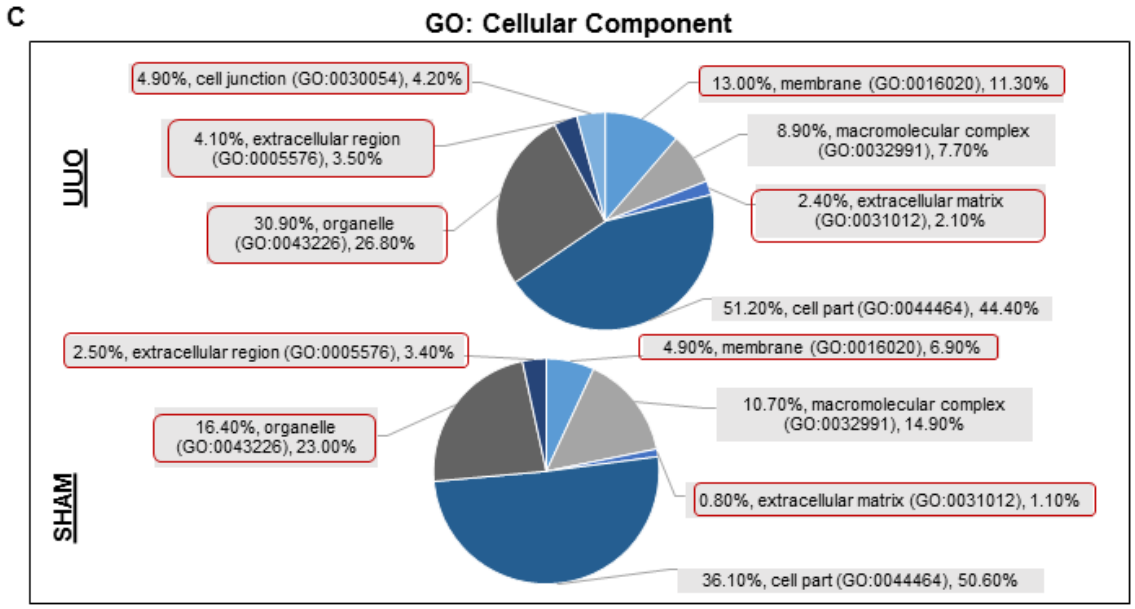

Finally, PANTHER Protein Class annotation terms analysis (Fig.4.9D) allowed us to determine more specifically to which functional group the proteins were belonging. The most represented "Protein Class" among TG2-associated proteins in UUO conditions was "Cytoskeletal protein" (PC00085), that covered almost a third of proteins (31.7%) and 25.2% of total class hits. This class was much less represented in Sham operated membranes, involving only 11.5% of proteins, or 10.5% of total class hits (**Fig. 4.9D**). TG2-associated proteins in Sham operated membranes appeared more equally distributed among the different classes. Classes involved in metabolic reactions were the more described in Sham operated conditions, and above all "Hydrolase" (PC00121) proteins represented 11.3% of the total class hits against only 3.2% in UUO. Transferases (PC00220, 8.3% vs 6.5% in UUO), transporter proteins (PC00227, 6.8% vs 3.2% in UUO) and ligases (PC00142, 4.5% vs 1.9% in UUO) were also more represented in healthy conditions (**Fig. 4.9D**). An exception was given by "Oxidoreductase" (PC00176) proteins, that were similar in both conditions, even if slightly more represented in fibrotic membranes (6.8% of total class hits in sham operated membranes and 7.1% in UUO) (**Fig. 4.9D**).

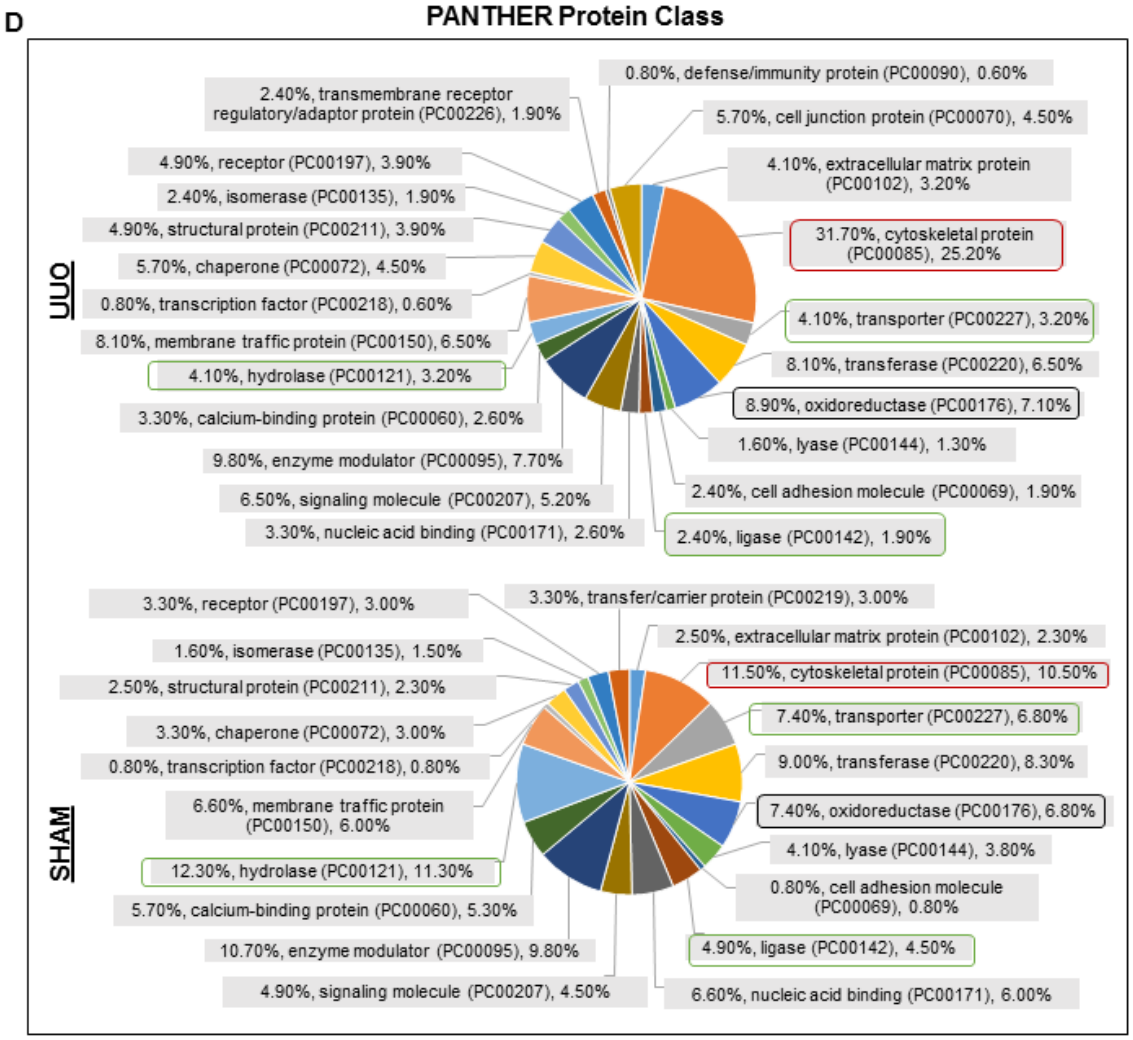

Figure 4.9: Gene Ontology (GO) annotation terms and PANTHER protein classes functional analysis of TG2-associated proteins in UUO or Sham operated kidney membranes. Functional analysis of TG2-associated candidates in UUO and Sham operated kidney membranes at 21 days post-operation was performed by PANTHER (http://www.pantherdb.org) using the annotation terms ontologies for **(A)** PANTHER GO-slim Biological Process, **(B)** PANTHER GO-slim Molecular Function, **(C)** PANTHER GO-slim Cellular Component, **(D)** PANTHER Protein Class. Labels must be read this way: % proteins belonging to the class over the number of proteins in the list; name of the annotation term; % proteins belonging to the class over the total number of class hits (for all the annotation terms individuated in the list of proteins = 100%). Red circles indicate terms more represented as associated with TG2 in fibrotic conditions (UUO 21 days), green circles terms more represented as associated with TG2 in healthy conditions (Sham 21 days), black circles indicate terms similarly represented in both lists.

The distribution of different biological pathways among TG2-associated proteins was investigated using the PANTHER Pathways annotation terms on PANTHER Database (**Table 4.5, Table 4.6**). Among the pathways identified by TG2-associated proteins in UUO membranes (**Table 4.5**), the more represented were "Integrin signaling pathway" (P00034), "Huntington disease" (P00029), "Inflammation mediated by chemokine and cytokine signalling pathway" (P00031) and "Nicotinic acetylcholine receptor signalling pathway" (P00044) (**Table 4.5,** black arrows).

Table 4.5: Pathways representation of TG2-associated proteins in UUO kidney membranes. Pathways represented among TG2-associated proteins in UUO kidneys at 21 days post-operation were analysed by PANTHER (http://www.pantherdb.org) using the annotation terms for PANTHER Pathways. The table shows the pathways represented, the number of proteins belonging to the pathway and the corresponding coverage over the total classes identified: the number of proteins belonging to the class and the percentage of representation over the total class hits are in increasing shades of red (the higher, the more intense). Black arrows identify the more represented PANTHER Pathways in the list.

PANTHER Pathways - TG2-associated proteins in UUO kidney membranes		
PANTHER Pathways	N	%
Integrin signalling pathway (P00034)	10	8.10%
Huntington disease (P00029)	9	7.30%
Inflammation mediated by chemokine and cytokine signaling pathway (P00031)	7	5.70%
Nicotinic acetylcholine receptor signaling pathway (P00044)	7	5.70%
Cytoskeletal regulation by Rho GTPase (P00016)	5	4.10%
Heterotrimeric G-protein signaling pathway-Gi alpha and Gs alpha mediated pathway (P00026)	5	4.10%
B cell activation (P00010)	4	3.30%
Parkinson disease (P00049)	3	2.40%
Heterotrimeric G-protein signaling pathway-rod outer segment phototransduction (P00028)	3	2.40%
T cell activation (P00053)	3	2.40%
Apoptosis signaling pathway (P00006)	2	1.60%
Angiogenesis (P00005)	2	1.60%
CCKR signaling map (P06959)	2	1.60%
Heterotrimeric G-protein signaling pathway-Gq alpha and Go alpha mediated pathway (P00027)	2	1.60%
Wnt signaling pathway (P00057)	2	1.60%
Ionotropic glutamate receptor pathway (P00037)	1	0.80%
p38 MAPK pathway (P05918)	1	0.80%
Interferon-gamma signaling pathway (P00035)	1	0.80%
Alzheimer disease-presenilin pathway (P00004)	1	0.80%
Dopamine receptor mediated signaling pathway (P05912)	1	0.80%
Ubiquitin proteasome pathway (P00060)	1	0.80%
Nicotine pharmacodynamics pathway (P06587)	1	0.80%
Cell cycle (P00013)	1	0.80%
Cadherin signaling pathway (P00012)	1	0.80%
Heme biosynthesis (P02746)	1	0.80%
Serine glycine biosynthesis (P02776)	1	0.80%
Salvage pyrimidine ribonucleotides (P02775)	1	0.80%
Pyruvate metabolism (P02772)	1	0.80%
VEGF signaling pathway (P00056)	1	0.80%
Hedgehog signaling pathway (P00025)	1	0.80%
Glycolysis (P00024)	1	0.80%
Toll receptor signaling pathway (P00054)	1	0.80%
FGF signaling pathway (P00021)	1	0.80%
FAS signaling pathway (P00020)	1	0.80%

In Sham operated membranes, instead, the more represented PANTHER pathways (**Table 4.6**) were, in order, "Huntington disease" (P00029), "Integrin signalling pathway" (P00034), "B cell activation" (P00010) and "CCKR signaling map" (P06959) (**Table 4.6,** black arrows).

Table 4.6: Pathways representation of TG2-associated proteins in Sham operated kidney membranes. Pathways represented among TG2-associated proteins in sham operated kidneys at 21 days post-operation were analysed by PANTHER (http://www.pantherdb.org) using the annotation terms for PANTHER Pathways. The table shows the pathways represented, the number of proteins belonging to the pathway and the corresponding coverage over the total classes identified: the number of proteins belonging to the class and the percentage of representation over the total class hits are in increasing shades of green (the higher, the more intense). Black arrows identify the more represented PANTHER Pathways in the list.

PANTHER Pathways - TG2-associated proteins in Sham operated kidney membranes		
Panther Pathways	**N**	**%**
Huntington disease (P00029)	11	9.00%
Integrin signalling pathway (P00034)	9	7.40%
B cell activation (P00010)	6	4.90%
CCKR signaling map (P06959)	6	4.90%
T cell activation (P00053)	5	4.10%
Heterotrimeric G-protein signaling pathway-Gi alpha and Gs alpha mediated pathway (P00026)	4	3.30%
Cytoskeletal regulation by Rho GTPase (P00016)	4	3.30%
Inflammation mediated by chemokine and cytokine signaling pathway (P00031)	3	2.50%
Ubiquitin proteasome pathway (P00060)	3	2.50%
Heterotrimeric G-protein signaling pathway-rod outer segment phototransduction (P00028)	3	2.50%
Glycolysis (P00024)	3	2.50%
Ras Pathway (P04393)	3	2.50%
FGF signaling pathway (P00021)	3	2.50%
Axon guidance mediated by semaphorins (P00007)	2	1.60%
Apoptosis signaling pathway (P00006)	2	1.60%
Angiogenesis (P00005)	2	1.60%
Insulin/IGF pathway-mitogen activated protein kinase kinase/MAP kinase cascade (P00032)	2	1.60%
VEGF signaling pathway (P00056)	2	1.60%
Toll receptor signaling pathway (P00054)	2	1.60%
Endothelin signaling pathway (P00019)	2	1.60%
EGF receptor signaling pathway (P00018)	2	1.60%
PDGF signaling pathway (P00047)	2	1.60%
Gonadotropin-releasing hormone receptor pathway (P06664)	2	1.60%
Axon guidance mediated by netrin (P00009)	1	0.80%
Axon guidance mediated by Slit/Robo (P00008)	1	0.80%
De novo purine biosynthesis (P02738)	1	0.80%
Ionotropic glutamate receptor pathway (P00037)	1	0.80%
Interleukin signaling pathway (P00036)	1	0.80%
Interferon-gamma signaling pathway (P00035)	1	0.80%
Nicotine pharmacodynamics pathway (P06587)	1	0.80%
Synaptic vesicle trafficking (P05734)	1	0.80%
p53 pathway (P00059)	1	0.80%
Heterotrimeric G-protein signaling pathway-Gq alpha and Go alpha mediated pathway (P00027)	1	0.80%
p53 pathway by glucose deprivation (P04397)	1	0.80%
Acetate utilization (P02722)	1	0.80%
FAS signaling pathway (P00020)	1	0.80%
p38 MAPK pathway (P05918)	1	0.80%
Serine glycine biosynthesis (P02776)	1	0.80%
Dopamine receptor mediated signaling pathway (P05912)	1	0.80%
Angiotensin II-stimulated signaling through G proteins and beta-arrestin (P05911)	1	0.80%
Pyruvate metabolism (P02772)	1	0.80%
Pyrimidine Metabolism (P02771)	1	0.80%

In order to determine which GO terms were significantly enriched among the TG2-associated candidates in either fibrotic (21 days UUO) or healthy (21 days sham) conditions, a statistical overrepresentation test was performed employing both PANTHER and DAVID bioinformatics tools, as described in the experimental procedures (4.3.2.1). For this test, both the list of TG2-associated proteins in UUO kidney membranes (n=122, **Table 4.2**) and list of TG2-associated proteins in Sham operated kidney membranes (n=120, **Table 4.3**) were analyzed, and the annotation terms' representation in the lists was compared with the terms' distribution in the whole *Mus musculus* genome to define significantly ($p \leq 0.05$) enriched classes.
Results from the test performed using PANTHER bioinformatic tool are shown in **Table 4.7**: as for the functional classification described above, the GO terms for "Biological Process", "Molecular Function" and "Cellular Component", in addition to PANTHER Protein Class terms, were analysed. A series of annotation terms were found significantly enriched (p-value lower than 0.05) and associated with TG2 in UUO conditions (in the list of UUO-overexpressed proteins). Other terms were significantly enriched among the TG2-associated proteins in sham operated kidney membranes ($p<0.05$).

Seventeen GO "Biological Process" annotation terms were identified as significantly enriched in the group of TG2-associated proteins upon UUO ($p \leq 0.05$), while only five were found significantly overexpressed in Sham operated kidneys (**Table 4.7A**). The "Biological Process" terms enriched in UUO membranes at 21-days post operation could be included into three main ancestral groups: "Cellular component organization or biogenesis" (GO:0071840) (4.93-fold enriched in UUO, $p=3.03 \cdot 10^{-19}$), "Cellular process" (GO:0009987) (1.46 fold enriched in UUO, p=0.01) and "Localization" (GO:0051179) (2.25- fold enriched in UUO, p=0.01). To this last group belong a series of sub-annotation terms (child terms) associated with intracellular transport and vesicular transport that were identified as significantly enriched among TG2-associated proteins in UUO membranes and might be involved in the enzyme movements and export (**Table 4.7A**, grey arrows). In support to this hypothesis, "Vesicle-mediated transport" (GO:0016192) was 4.54-fold enriched in UUO with a high significance of overrepresentation ($p=3.07 \cdot 10^{-7}$). The same function was significantly enriched also in sham operated kidney membranes, but with a lower fold increase and at a lower significance (3.38-fold enriched, p=0.003). Terms associated with protein transport were also enriched in Sham operated membranes, at a p-value that was similar or lower than the one of TG2-associated candidates in UUO (an asterisk identifies these terms in **Table 4.7A**).

GO "Molecular Functions" (**Table 4.7B**) significantly enriched among TG2-associated proteins in UUO kidney membranes were related to the cytoskeletal structure and actin dynamics (black arrows): "Structural constituent of cytoskeleton" (GO:0005200) was more than 10-fold

enriched at a strongly significant level ($p=7.68\cdot10^{-21}$). The term was almost 4-fold enriched also in Sham operated membranes (** in **Table 4.7B**), but at a much lower level of significance (p=0.01). Other terms significantly enriched in UUO membranes and involved in cytoskeletal dynamics (black arrows in **Table 4.7B**) were: "Actin binding" (GO:0003779) (18.34-fold enriched, $p=2.84\cdot10^{-16}$), "Cytoskeletal protein binding" (GO:0008092) (14.49-fold enriched, $p=4.30\cdot10^{-16}$), "Structural molecule activity" (GO:0005198) (6.29-fold enriched, $p=8.03\cdot10^{-15}$), in line with our previous observations on the list of proteins (4.4.2).
Two other Molecular Functions were significantly enriched in the list of TG2-associated proteins in healthy Sham operated conditions: "Catalytic activity" (GO:0003824, indicated by one circle in **Table 4.7B**) was identified as 1.89-fold overexpressed ($p=8.79\cdot10^{-5}$) while "Anion channel activity" (GO:0005253, indicated by two circles in **Table 4.7B**) was 14.35-fold enriched (p=0.03).

GO "Cellular components" overrepresented in the list of TG2-associated proteins are shown in **Table 4.7C**. In UUO kidney membranes, cytoskeletal proteins were enriched at an elevated significant level (black arrows in **Table 4.7C**). These were associated with terms such as "Actin cytoskeleton" (GO:0015629), more than 16-fold overrepresented ($p=1.43\cdot10^{-17}$), "Cytoskeleton" (GO:0005856) (7.59-fold enriched, $p=5.03\cdot10^{-14}$), "Intermediate filament cytoskeleton" (GO:0045111) (12.60-fold enriched, p=0.003). The first two terms were enriched also in Sham operated membranes, but the significance of enrichment was lower, between 0.05 and 0.01. Interestingly, "Tubulin complex" (GO:0045298) term was enriched and associated with TG2 only in sham operated kidney membranes (27.45-fold enriched, p=0.01) in line with our previous observations (4.4.1-4.4.2). Other cellular components enriched among TG2-associated proteins in UUO membranes were related to vesicular compartments (grey arrows in **Table 4.7C**). In particular, "Vesicle coat" (GO:0030120) annotation term was 17.71 fold enriched (p=0.005). In addition, it was curious to note that transmembrane proteins ("Integral to membrane", GO:0016021) were significantly underrepresented among TG2-associated proteins in both condition (white arrowhead in **Table 4.7C**).
Similar outcomes were also found by performing an overrepresentation test on the GO terms in DAVID bioinformatics resource, and results can be found in **Suppl. Table 4.9 – 4.14**.

Finally, PANTHER Protein classes significantly overrepresented were investigated in PANTHER bioinformatics resource using the same approach (**Table 4.7D**). "Protein classes" significantly overrepresented among TG2-associated proteins in kidney membranes at 21 days post-UUO were involved in both cytoskeletal dynamics (black arrows in **Table 4.7D**) and vesicular transport (gray arrows in **Table 4.7D**). The "cytoskeletal protein" (PC00085) annotation term was almost 10 times enriched in UUO membrane, with a p-value of $9.35\cdot10^{-24}$.

This annotation term resulted enriched also in healthy membranes (** in **Table 7D)**, but at a lower confidence level (p=0.015). Terms enriched uniquely in UUO membranes were proteins of the actin family (PC00041), intermediate filament proteins (PC00129) and actin binding proteins (PC00165, PC00040). The protein class of tubulins (PC00228), on the other side, was significantly enriched uniquely in sham operated kidneys (27.45-fold enriched, p=0.04), in agreement with the GO terms for "Cellular Components" described above and our previous observations (4.4.1-4.4.2). Trafficking and vesicular transport classes significantly enriched among TG2-associated proteins in kidney fibrotic membranes (gray arrows in **Table 4.7D**) were "Membrane traffic protein" (PC00150) annotation term, 5.28-fold enriched (p=0.005), and "Vesicle coat protein" (PC00235) annotation term, more than 17-times overrepresented (p=0.018). Interestingly, the protein classes identifying G-proteins (PC00020) and small GTPases (PC00208) were significantly enriched and associated with TG2 only in healthy kidney membranes at 21 days post Sham operation (3 circles in **Table 4.7D**), and might be involved in different functions of TG2 in physiological conditions.

To summarize, the annotation terms associated with both cytoskeletal organization and cell trafficking, especially vesicular, were identified as associated with TG2 in kidney fibrotic membranes and significantly enriched in this condition when compared to their expression in the whole *Mus musculus* genome. These significantly enriched proteins classes or functions might be involved in TG2 trafficking and extracellular activity during the progression of CKD. Functional classes overrepresented in Sham operated kidney were less, and mostly associated with cell regulation and metabolism.

Table 4.7: Functional Classes Overrepresentation test on TG2-associated proteins in UUO and Sham operated kidneys, performed by PANTHER. Statistical overrepresentation test was performed in PANTHER (http://www.pantherdb.org) using the annotation terms terms ontologies for **(A)** PANTHER GO-slim Biological Process, **(B)** PANTHER GO-slim Molecular Function, **(C)** PANTHER GO-slim Cellular Component, **(D)** PANTHER Protein Class. Legend: Grey arrows = Terms associated with intracellular trafficking and vesicular transport and enriched in UUO kidney membranes; * = Terms associated with intracellular trafficking and vesicular transport and enriched in Sham operated kidney membranes; Black arrows = terms associated with cytoskeletal organisation and actin binding and enriched in UUO kidney membranes; ** = terms associated with cytoskeletal organisation and actin binding and enriched in Sham operated kidney membranes; o = terms associated with catalytic activity and enriched in Sham operated kidney membranes; oo = terms associated with anion channel and enriched in Sham operated kidney membranes; ooo = terms associated with G-proteins or Small GTPases and enriched in Sham operated kidney membranes; White arrowhead = terms associated with transmembrane proteins significantly underrepresented in UUO and Sham operated kidney membranes. +, Red = overrepresented term (fold change from expected value H_0 >1); -, Green = underrepresented term (fold change from expected value H_0 <1). In increasing shades of grey = fold change from the expected value H_0 (the more intense, the higher the fold change). In increasing shades of blue = p-value (the more intense, the lower the p-value). A p-value lower than 0.05 was regarded as significant.

A

PANTHER GO-Slim Biological Process	UUO		SHAM		
	Fold change	p-value	Fold change	p-value	
cellular component organization or biogenesis (GO:0071840)	+ 4.93	3.03E-19	+ 1.66	1.00E+00	
cellular component morphogenesis (GO:0032989)	+ 9.26	3.87E-16	+ 3.11	6.28E-01	
cellular component organization (GO:0016043)	+ 4.57	1.02E-14	+ 1.57	1.00E+00	
vesicle-mediated transport (GO:0016192)	+ 4.54	3.07E-07	+ 3.38	2.82E-03	*
protein complex assembly (GO:0006461)	+ 11.07	7.79E-06	+ 5.58	5.25E-01	
protein complex biogenesis (GO:0070271)	+ 11	8.24E-06	+ 5.54	5.39E-01	
sensory perception of sound (GO:0007605)	+ 15.78	6.56E-04	- < 0.2	1.00E+00	
cytokinesis (GO:0000910)	+ 11.44	7.78E-04	+ 1.65	1.00E+00	
intracellular protein transport (GO:0006886)	+ 3.33	1.85E-03	+ 3.55	4.07E-04	*
protein transport (GO:0015031)	+ 3.27	2.43E-03	+ 3.66	1.30E-04	*
cellular component movement (GO:0006928)	+ 4.95	3.86E-03	+ 4.09	9.59E-02	
muscle contraction (GO:0006936)	+ 8.41	5.59E-03	- < 0.2	1.00E+00	
transport (GO:0006810)	+ 2.36	7.12E-03	+ 2.48	2.09E-03	*
cellular process (GO:0009987)	+ 1.46	1.04E-02	+ 1.26	1.00E+00	
localization (GO:0051179)	+ 2.25	1.14E-02	+ 2.27	9.79E-03	*
protein folding (GO:0006457)	+ 9.15	1.38E-02	+ 6.15	1.00E+00	
cellular component biogenesis (GO:0044085)	+ 4.07	2.26E-02	+ 1.86	1.00E+00	

B

PANTHER GO-Slim Molecular Function	UUO		SHAM		
	Fold change	p-value	Fold change	p-value	
structural constituent of cytoskeleton (GO:0005200)	+ 10.13	7.68E-21	+ 3.83	1.37E-02	**
actin binding (GO:0003779)	+ 18.34	2.84E-16	+ 5.84	1.10E-01	
cytoskeletal protein binding (GO:0008092)	+ 14.49	4.30E-16	+ 4.17	5.95E-01	
structural molecule activity (GO:0005198)	+ 6.29	8.03E-15	+ 2.77	9.73E-02	
protein binding (GO:0005515)	+ 2.73	5.08E-08	+ 1.66	1.00E+00	
motor activity (GO:0003774)	+ 8.85	1.21E-02	- < 0.2	1.00E+00	
catalytic activity (GO:0003824)	+ 1.52	3.21E-01	+ 1.89	8.79E-05	o
anion channel activity (GO:0005253)	+ 3.56	1.00E+00	+ 14.35	3.40E-02	oo

C

PANTHER GO-Slim Cellular Component	UUO		SHAM		
	Fold change	p-value	Fold change	p-value	
actin cytoskeleton (GO:0015629)	+ 16.29	1.43E-17	+ 5.47	1.96E-02	**
cell part (GO:0044464)	+ 2.73	3.48E-14	+ 1.92	3.09E-04	
cytoskeleton (GO:0005856)	+ 7.59	5.03E-14	+ 3.24	3.87E-02	**
intracellular (GO:0005622)	+ 2.74	6.03E-14	+ 1.92	4.58E-04	
organelle (GO:0043226)	+ 2.49	3.33E-06	+ 1.32	1.00E+00	
cell junction (GO:0030054)	+ 13.28	4.34E-04	- < 0.2	1.00E+00	
intermediate filament cytoskeleton (GO:0045111)	+ 12.6	3.30E-03	+ 2.54	1.00E+00	
vesicle coat (GO:0030120)	+ 17.71	5.21E-03	+ 8.93	1.00E+00	
cytoplasm (GO:0005737)	+ 2.21	5.42E-03	+ 2.14	1.22E-02	
integral to membrane (GO:0016021)	- < 0.2	4.27E-02	- < 0.2	4.59E-02	
tubulin complex (GO:0045298)	- < 0.2	1.00E+00	+ 27.45	1.18E-02	**

D

PANTHER Protein Class	UUO		SHAM		
	Fold change	p-value	Fold change	p-value	
cytoskeletal protein (PC00085)	+ 9.35	1.04E-24	+ 3.38	1.47E-02	**
actin family cytoskeletal protein (PC00041)	+ 13.6	4.45E-22	+ 4.26	6.00E-02	
non-motor actin binding protein (PC00165)	+ 15.99	2.13E-13	+ 4.74	8.78E-01	
actin binding motor protein (PC00040)	+ 19.1	1.84E-04	- < 0.2	1.00E+00	
chaperonin (PC00073)	+ 34.57	1.31E-03	+ 17.43	1.00E+00	
membrane traffic protein (PC00150)	+ 5.28	4.70E-03	+ 4.26	1.31E-01	
cell junction protein (PC00070)	+ 8.3	5.10E-03	- < 0.2	1.00E+00	
chaperone (PC00072)	+ 7.84	7.30E-03	+ 4.52	1.00E+00	
vesicle coat protein (PC00235)	+ 17.71	1.75E-02	+ 8.93	1.00E+00	
intermediate filament (PC00129)	+ 11.07	2.04E-02	+ 2.23	1.00E+00	
G-protein (PC00020)	+ 1.68	1.00E+00	+ 5.93	4.08E-02	ooo
small GTPase (PC00208)	+ 1.42	1.00E+00	+ 8.58	1.64E-02	ooo
tubulin (PC00228)	- < 0.2	1.00E+00	+ 27.45	3.96E-02	**

To determine which molecular pathways were significantly enriched among the TG2-associated proteins identified in this study (at a p-value lower than 0.05), statistical overrepresentation analysis was carried out using both PANTHER Pathways annotation terms on PANTHER bioinformatic tools and KEGG pathways annotation terms on DAVID database (**Table 4.8 and 4.9**).

PANTHER Pathways significantly enriched among TG2-associated proteins at 21 days post-UUO (**Table 4.8**) were, in order of significance (lower p-value): "Integrin signalling pathway" (P00034, 9.5-fold enriched, $p=2.07 \cdot 10^{-5}$), "Huntington disease" (P00029, 11.26-fold enriched, $p=2.07 \cdot 10^{-5}$), "Nicotinic acetylcholine receptor signalling pathway" (P00044, 13.37-fold enriched, $1.84E \cdot 10^{-4}$) and "Cytoskeletal regulation by Rho GTPase" (P00016, 11.49-fold enriched, p=0.01). The overrepresentation of "Nicotinic acetylcholine receptor signalling pathway" is difficult to interpret, but is known to involve myosin and actin proteins, that are well represented in the list of TG2-associated proteins. PANTHER Pathways significantly enriched among TG2-associated proteins in Sham operated conditions (**Table 4.8**) were again "Huntington disease" (P00029, 13.88-fold enriched, $p=9.94 \cdot 10^{-8}$), "Integrin signalling pathway"

(P00034, 8.62-fold enriched, p=1.99·10^{-4}), but also "B cell activation" (P00010, 15.46-fold enriched, 4.82·10^{-4}) and "T cell activation" (P00053, 9.94-fold enriched, p=0.03).

As it can be seen, integrin signalling pathway was significantly enriched in both conditions and slightly more significant in UUO kidney membranes, but curiously no integrin subunit was identified in the list. The fact that the pathway was still identified as enriched is probably due to the presence of a series of proteins interacting with integrins and identified in the lists of TG2-associated proteins such as actin-associated proteins, HSPGs, fibronectin, periostin, and TG2 itself. The presence of Huntington disease was similarly curious, but consistently identified as enriched in both conditions.

Table 4.8: PANTHER Pathway overrepresentation test on TG2-associated proteins in UUO and Sham operated kidneys. Statistical overrepresentation test was performed in PANTHER (http://www.pantherdb.org) using the annotation terms ontologies for PANTHER Pathways. Legend: +, Red = overrepresented term (fold change from expected value H_0 >1); -, Green = underrepresented term (fold change from expected value H_0 <1). In increasing shades of grey = fold change from the expected value H_0 (the more intense, the higher the fold change). In increasing shades of blue = p-value (the more intense, the lower the p-value). A p-value lower than 0.05 was regarded as significant.

PANTHER Pathways		UUO			SHAM	
		Fold change	p-value		Fold change	p-value
Integrin signalling pathway (P00034)	+	9.5	2.07E-05	+	8.62	1.99E-04
Huntington disease (P00029)	+	11.26	2.20E-05	+	13.88	9.94E-08
Nicotinic acetylcholine receptor signaling pathway (P00044)	+	13.37	1.84E-04	-	< 0.2	1.00E+00
Cytoskeletal regulation by Rho GTPase (P00016)	+	11.49	1.34E-02	+	9.26	1.56E-01
B cell activation (P00010)	+	10.22	1.09E-01	+	15.46	4.82E-04
T cell activation (P00053)	+	5.92	1.00E+00	+	9.94	2.61E-02

Overrepresented KEGG Pathways, when analyzed by DAVID (**Table 4.9**), were only partially in line with the previous analysis of PANTHER Pathways (**Table 4.8**). The most enriched pathways (lower p-value) associated with TG2 in UUO kidney membranes (**Table 4.9A**) were "Huntington's disease" (mmu05016, 4.87-fold enriched, p=3.98·10^{-4}) and "Regulation of actin cytoskeleton" (mmu04810, 4.10-fold enriched, p=0.0012), but also "Glycolysis/Gluconeogenesis" (mmu00010) KEGG pathway was identified as significantly 7-fold enriched, at a p-value equal to 0.0045. The other pathways significantly enriched, at a p-value between 0.05 and 0.01 were "Endocytosis" (mmu04144), "Adherens junction" (mmu04520) and "Focal adhesion" (mmu04510) in agreement with our previous observation of protein functions and localisation at the cortical cytoskeleton and plasma membrane, as well as with the significant presence of clathrin and clathrin-associated proteins.

In Sham operated conditions (**Table 4.9B**), the most significantly enriched pathways (lower p-value) were "Glycolysis / Gluconeogenesis" (mmu00010, 8.17-fold enriched, p=7.17·10^{-4}), in line with the previous results, followed by "Regulation of actin cytoskeleton" (mmu04810, 7.21-times overrepresented, p=0.008). The other pathways enriched in Sham operated

conditions were different from the UUO ones and were "Gap junction" (mmu04540), "Long-term potentiation" (mmu04720) and "Vascular smooth muscle contraction" (mmu04270), all overrepresented with a p-value between 0.05 and 0.01.

In summary, TG2-associated proteins in fibrotic kidney membranes were significantly (lower p-value) fitting in molecular pathways involved in both cytoskeletal organization, cell-matrix and cell-cell adhesion and vesicular trafficking. Glycolysis-Gluconeogenesis pathways, even if enriched in fibrotic conditions, was present and more overrepresented in sham operated membranes.

Table 4.9: KEGG overrepresentation test on TG2-associated proteins in UUO and Sham operated kidneys performed by DAVID. Statistical overrepresentation test was performed by DAVID (http://david.abcc.ncifcrf.gov) using the annotation terms ontologies KEGG Pathways. The number of proteins belonging to the annotation term and fold change from the expected value H_0 are in increasing shades of red for the UUO condition (the higher the more intense) (A) and of green for the Sham operated condition (the higher the more intense)(B). The p-value is shown in increasing shades of blue (the more intense, the lower the p-value). A p-value lower than 0.05 was regarded as significant.

A

KEGG Pathways-TG2-associated proteins in UUO kidney membranes				
KEGG Pathways	Count	%	PValue	Fold Enrichment
mmu05016:Huntington's disease	9	7.83	3.98E-04	4.87
mmu04810:Regulation of actin cytoskeleton	9	7.83	1.23E-03	4.10
mmu00010:Glycolysis / Gluconeogenesis	5	4.35	4.45E-03	7.27
mmu04144:Endocytosis	7	6.09	1.44E-02	3.43
mmu04520:Adherens junction	4	3.48	3.92E-02	5.21
mmu04510:Focal adhesion	6	5.22	4.57E-02	3.00

B

KEGG Pathways-TG2-associated proteins in Sham operated kidney membranes				
KEGG Pathways	Count	%	PValue	Fold Enrichment
mmu00010:Glycolysis / Gluconeogenesis	6	5.41	7.17E-04	8.17
mmu04810:Regulation of actin cytoskeleton	8	7.21	7.72E-03	3.41
mmu04540:Gap junction	5	4.50	1.28E-02	5.38
mmu04720:Long-term potentiation	4	3.60	3.78E-02	5.29
mmu04270:Vascular smooth muscle contraction	5	4.50	3.81E-02	3.86

4.4.4 The interactome of TG2 in fibrotic kidney membranes and healthy kidney membranes

The interactions existing between the TG2-coprecipitated partners in both fibrotic and healthy conditions was investigated using STRING v10.0 database tool (http://string-db.org), as described in the Experimental Procedure (4.3.2.2). The analysis was performed on the two lists of TG2-associated proteins, in UUO kidney membranes (n=122, **Table 4.2**) and Sham operated kidney membranes (n=120, **Table 4.3**), and the presence of both known and predicted protein-protein interactions was investigated at a confidence level of at least 0.4 (middle confidence), which is the default confidence level employed by STRING. STRING analysis converts the protein IDs uploaded into gene names, that are hence shown in the final interactome. The correspondence between gene names and protein IDs is shown in **Suppl. Table 4.15**.

The network of TG2 molecular interactions, or TG2-interactome, was obtained in both fibrotic (**Fig. 4.10**) and healthy kidney membranes (**Fig. 4.11**). Both networks were edited using Cytoscape, to isolate clear hubs of interacting proteins and colour code the candidates depending on their specific functions, as assigned in **Suppl. Tables 4.6-4.8** (functional clustering).

4.4.4.1 The interactome of TG2 in kidney fibrotic membranes

The interactome of TG2 in kidney fibrotic membranes is displayed in **Figure 4.10**. The picture shows an intense network of interactions between the TG2-associated proteins in fibrotic kidney membranes. The network is characterised by four main clusters of functionally-correlated proteins **(Fig 4.10A-D)** interconnected by a series of chaperone proteins (light green) or cell regulation/signalling proteins (purple/violet) that are in different ways relating to the separate clusters. Heat shock proteins (HSPs) appear to be central in the interactome, strongly associating to a series of candidates involved in different functions in the cell. The identified heat shock proteins include the chaperone proteins heat shock protein HSP 90-α (Hsp90aa1, HS90A_MOUSE) and 78 kDa glucose-regulated protein (Hspa5, GRP78_MOUSE), the stress-associated protein heat shock protein β-1 (Hspb1, HSPB1_MOUSE) and the extracellular vesicle typical protein heat shock cognate 71 kDa protein (Hspa8, HSP7C_MOUSE).

A large group of strongly interconnected cytoskeletal and actin associated proteins is present (**Fig. 4.10A**, orange). The main node is actin (Actb, ACTB_MOUSE), that is associated with many other proteins, not only cytoskeletal but also associated with cell regulation (purple), signalling and stress response (violet) such as calmodulin (Calm1, CALM_MOUSE), coronin 1C (Coro1c, COR1C_mouse), plastin 2 and 3 (Lcp1, PLSL_MOUSE; Pls3, PLST_MOUSE) and Ras GTPase-activating-like protein (Iqgap1, IQGA1_MOUSE). Actin also directly interacted with all the

abovementioned heat shock proteins. Other cytoskeletal proteins (**Fig. 4.10A**, orange) that form largely interconnecting nodes of the cluster are spectrins (Spna1, SPTA1_MOUSE; Spna2, SPTN1_MOUSE and Spnb1, SPTB1_MOUSE). These proteins directly interact with actin and other cytoskeletal proteins and might be interesting for their role at the interface with the plasma membrane, with a possible involvement in secretion (De Matteis and Morrow 2000). Important nodes are also denoted by gelsolin (Gsn, GELS_MOUSE) and vimentin (Vim, VIME_MOUSE), that provide the main connection between cytoskeletal proteins (**Fig. 4.10A**, orange) and proteins associated with cell adhesion and extracellular organisation (**Fig. 4.10B**, brown/yellow). Keratins are also present in the network of TG2-associated proteins in fibrotic membranes, of which one, keratin 14 (Krt14, K1C14_MOUSE) is directly interacting with TG2 itself.

A further protein hub identified by the interactome of TG2-associated proteins in UUO membranes is characterised by a number of cell adhesion and extracellular organisation proteins (**Fig. 4.10B**, brown/yellow), directly interacting with each other and in the same cluster with TG2 (white square). Of these proteins, fibronectin (Fn1, FINC_MOUSE) and the HSPG syndecan-4 (Sdc4, SDC4_MOUSE) are directly interacting with TG2 (**Fig. 4.10B**, brown/yellow). Another interesting HSPG specifically relating with Sdc4 in the network is the basement membrane-specific HSPG perlecan (Hspg2, PGBM_MOUSE). The HSPGs Sdc4 and perlecan are interacting with TG2 uniquely in membranes from kidneys subjected to UUO in this study, suggesting a TG2 association to these proteins upon disease. Other important proteins of the cluster are the cell adhesion protein periostin (Postn, POSTN_MOUSE), the extracellular proteoglycans biglycan and decorin (Bgn, PGS1_MOUSE; Dcn, PGS2_MOUSE), and collagens (Col12a1, COCA1_MOUSE; Col14a1, COEA1_MOUSE). The extracellular protease inhibitor serpin H1 (Serpinh1, SERPH_MOUSE) acts as a connection between this cluster and the rest of the interactome, by interacting directly with all four of the abovementioned heat shock proteins (HSPs) (**Fig. 4.10B**, brown/yellow).

A further small hub of redox related proteins is found associated with TG2 in UUO kidney membranes (**Fig. 4.10C**, pink), is linked to the network mainly by interacting with chaperone proteins (light green), including HSPs. These redox proteins are peroxiredoxin-2 (Prdx2, PRDX2_MOUSE), glutaredoxin 1 (Glrx, GLRX1_MOUSE), glutaredoxin-3 (Glrx3, GLRX3_MOUSE), glutathione peroxidase 1 (Gpx1, GPX1_MOUSE) and glutathione S-transferase theta-1 (Gstt1, GSTT1_MOUSE) (**Fig. 4.10C**, pink).

Interestingly, a main cluster identified is made of several vesicular trafficking -associated proteins (**Fig. 4.10D**, Blue). One key node of the cluster is formed by clathrin and adaptor proteins (Clta, CLCA_MOUSE; Cltb, CLCB_MOUSE; Ap2a1, AP2A1_MOUSE; Ap2a2, AP2A2_MOUSE; Ap2b1, AP2B1_MOUSE), phosphatidylinositol-binding clathrin assembly protein (Picalm, PICAL_MOUSE) and coatomer subunit beta (Copb2, COPB2_MOUSE). These

interact with the rest of the network through vesicular-associated proteins such as cyclin-G-associated kinase (Gak, GAK_MOUSE), huntingtin-interacting protein 1 (Hip1, HIP1_MOUSE) and the central heat shock cognate 71 kDa protein (Hspa8, HSP7C_MOUSE) (**Fig. 4.10D**, Blue). Elements of the retromer transport such as dynactin and sorting nexins can be observed in the same hub (Dctn1, DCTN1_MOUSE; Snx1, SNX1_MOUSE; Snx4, SNX4_MOUSE) (**Fig. 4.10D**, Blue). Unconventional myosins are known to be involved in intracellular transport and endocytic processes (Tuxworth and Titus 2000) and are part of the cluster (Myo1b, MYO1B_MOUSE; Myo1d, MYO1D_MOUSE; Myo1g; MYO1G_MOUSE; Myo18a, MY18A_MOUSE) (**Fig. 4.10D**, Blue), even if more intensely connected with the cytoskeletal proteins than with the vesicular ones. The proteins programmed cell death 6-interacting protein/alix (Pdcd6ip, PDC6I_MOUSE) and flotillin-2 (Flot2, FLOT2_MOUSE) are markers of extracellular vesicles and are both present in exosomes (See Appendix and Chapter V for more details). These proteins are both identified in the network of TG2-associated protein in fibrotic kidney membranes (**Fig. 4.10D**, Blue).

In conclusion, the network of interaction produced using STRING allowed to identify clusters of interacting proteins associated with TG2, or even directly interacting with TG2 in kidney membranes under fibrotic conditions induced by 21 days UUO. Four main groups of proteins were identified, cytoskeletal proteins, cell adhesion and extracellular organisation proteins, redox regulation proteins and vesicular proteins, and might all be involved in TG2 trafficking and pro-fibrotic activity during disease. In addition, heat shock proteins and signalling proteins involved in the regulation of cytoskeletal dynamics, such as plastin, coronin and calpain (Capn1, CAN1_MOUSE) are important elements in the network structure.

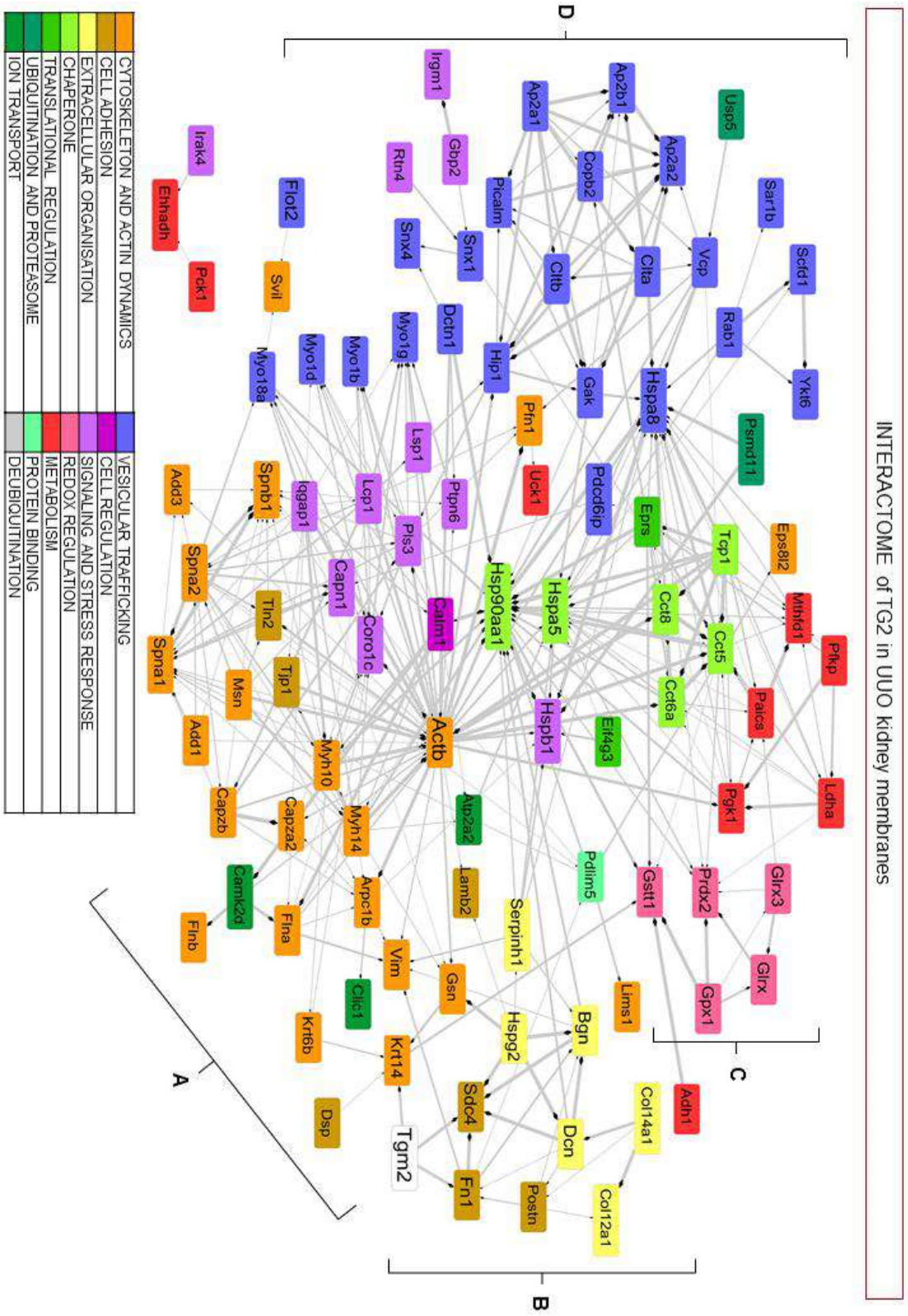

Figure 4.10: Network of protein-protein interactions of TG2-associated proteins in Fibrotic kidney membranes (UUO, 21 days). Network of known and predicted protein-protein interactions was designed in STRING (http://string-db.org) using the list of TG2-associated proteins in UUO kidney membranes. A confidence of at least 0.4 (middle confidence in STRING) was chosen as threshold for the interactions identified. Results were exported on Cytoscape (http://www.cytoscape.org) for graphical visualisation and colour coded depending on the specific functional cluster (**Suppl.Table 4.6, 4.8**). Thickness of the lines reflects the confidence of the interaction (from 0.4 to 0.99).

4.4.4.2 The interactome of TG2 in healthy kidney membranes

The interactome of TG2 in Sham operated (healthy) kidney membranes is shown in **Figure 4.11**. Similarly to what seen in the TG2-interactome in UUO conditions, a dense interrelation of proteins is observed. However, the four main clusters of functionally-correlated proteins identified in fibrotic conditions (**Fig.4.11 A-D**) are less evident in sham operated conditions, or even absent.

A series of cell regulation and cell signalling proteins are identified in the network and linking the different groups of cytoskeletal (**Fig. 4.11A**, Orange), metabolic (**Fig. 4.11C**, red) and vesicular proteins (**Fig. 4.11E**, Blue). At the centre of the network heat shock protein HSP90-β (Hsp90ab1, HS90B_MOUSE) is connected with the majority of the proteins in the network. Caspase-3 (Casp3, CASP3_MOUSE) forms another important node, connecting to cytoskeletal, metabolic and other signalling proteins, as well as directly interacting with TG2. Also Ras-related C3 botulinum toxin substrate 2 (Rac2, RAC2_MOUSE) is a cell signalling protein which represents a key node of the network, directly interacting with plasma membrane proteins and with Fibronectin. A series of chaperone proteins are also evident in the network, and in particular T-complex protein 1 subunit gamma (Cct3, TCPG_MOUSE) directly interacts with TG2.

A cluster of cytoskeletal proteins is recognized in the network (**Fig. 4.11A**, Orange). The cluster is smaller and less dense in comparison with the UUO one (**Fig. 4.11A**, Orange) and actin is not present as the central node. However, actin-associated proteins are present in the network (actin-related protein 2/3 complex subunit 1A - Arpc1a, ARC1A_MOUSE; actin-related protein 2/3 complex subunit 5 - Arpc5, ARPC5_MOUSE; actin-related protein 3 -Actr3, ARP3_MOUSE) and also two spectrin isotypes are identified and are in common with the TG2-interactome in fibrotic membranes (Spna1, SPTA1_MOUSE and Spna2, SPTN1_MOUSE). Interestingly, tubulins (tubulin alpha-1A chain - Tuba1a, TBA1A_MOUSE; tubulin alpha-4A chain - Tuba4a, TBA4A_MOUSE and tubulin beta-5 chain - Tubb5; TBB5_MOUSE) are present in the network and are uniquely associated with TG2 in Sham operated conditions.

Very few proteins involved in cell adhesion and extracellular organisation are identified in the network (**Fig. 4.11B**, Brown/yellow), of which FN (Fn1, FINC_MOUSE) was directly interacting with TG2. Unlike the network of TG2-associated proteins in fibrotic conditions, in this case no cluster of redox-associated proteins is identified, and only peroxiredoxin 2 (Prdx2, PRDX2_MOUSE) is directly connected to the main network.

Metabolic proteins are also forming a small hub of interacting candidates connected to the main network of TG2-associated proteins (**Fig. 4.11C**, Red). Among these, glyceraldehyde-3-phosphate dehydrogenase Gapdh (Gapdh, G3P_MOUSE) is central in the network and directly interacting with TG2. N-acyl-aromatic-L-amino acid amidohydrolase (aminoacylase Acy3, ACY3_MOUSE), a protein known for playing a role in kidney proximal tubules (Lindner, Täfler-

Naumann and Röhm 2008, Smith, et al. 2013, Newman, et al. 2007), is also present in the cluster and directly associates to both Gapdh and TG2 (**Fig. 4.11C**, Red).

A series of proteins associated to protein degradation by ubiquitination and proteasome (**Fig. 4.11D**, dark blue-green) are also identified in the network and form a separate hub of proteins partially interconnected with both vesicular markers and signalling proteins. E3 ubiquitin-protein ligase NEDD4 (Nedd4, NEDD4_MOUSE) and 26S proteasome regulatory subunit 4 (Psmc1, PRS4_MOUSE) are the main nodes of the cluster, followed by ubiquitin-conjugating enzyme E2 D3 (Ube2d3, UB2D3_MOUSE) and proteasome activator complex subunit 1 (Psme1, PSME1_MOUSE). Cullin 5 (Cul5, CUL5_MOUSE) is also present in the cluster. The ubiquitin-like signalling protein ubiquitin-like protein Isg15 (ISG15_MOUSE) represents the main connection between this cluster and the other members of the interactome, especially to vesicular-associated candidates **Fig. 4.11D**, dark blue-green).

Vesicular proteins (**Fig. 4.11E**, Blue) are more sparse in the network of TG2-associated proteins in healthy kidney and are forming a small protein cluster that included the vesicular trafficking regulators ADP-ribosylation factors Arf5 and Arf6 (Arf5, ARF5_MOUSE and Arf6, ARF6_MOUSE), the ADP-ribosylation factor-binding protein GGA1 (Gga1, GGA1_MOUSE), Rab10 (Rab10, RAB10_MOUSE), the vesicular protein clathrin (heavy chain Cltc, CLH1_MOUSE), phosphatidylinositol-binding clathrin assembly protein (Picalm, PICAL_MOUSE, common with UUO), and retromer-associated proteins such Vps35 and Snx3 (VPS35_MOUSE; SNX3_MOUSE) (**Fig. 4.11E**, Blue). In addition to these proteins, the programmed cell death 6-interacting protein/alix (Pdcd6ip, PDC6I_MOUSE) and the tumor susceptibility gene 101 protein (Tsg101, TS101_MOUSE), which are markers of extracellular vesicles and known to be both detectable in exosomes (See Chapter V for more details), are both present in the network of TG2-associated protein in Sham operated kidney membranes (**Fig. 4.11E**, Blue).

In conclusion, TG2-associated proteins in healthy kidney membranes form a clear network of proteins associated with different functions, and the predominance of cytoskeletal and adhesion proteins identified in fibrotic condition is reduced, as well as the presence of antioxidant proteins. Vesicular proteins are present in the network, forming a more diffuse cluster of interacting proteins. Metabolic proteins and candidates involved in proteasome degradative pathway were well represented in the network. TG2 itself is directly associated with five proteins with different roles: extracellular adhesion proteins such as FN, metabolic proteins such as Gapdh and aminoacylase Acy3, caspase 3, involved in signalling, and a T-complex chaperone protein.

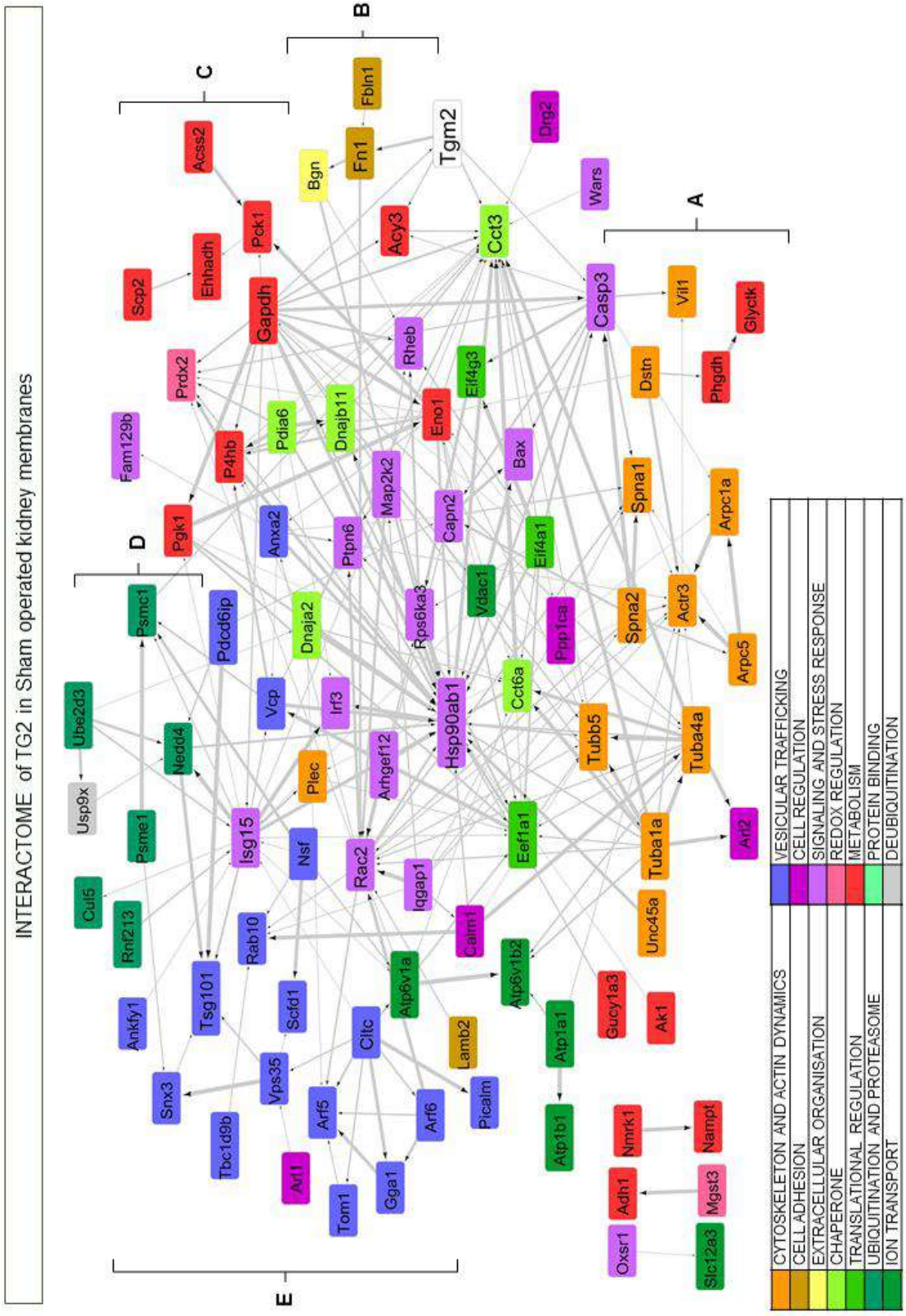

Figure 4.11: Network of protein-protein interactions of TG2-associated proteins in healthy kidney membranes (Sham operated, 21 days). Network of known and predicted protein-protein interactions was designed in STRING (http://string-db.org) using the list TG2-associated proteins in sham operated kidney membranes. A confidence of at least 0.4 (middle confidence in STRING) was chosen as threshold for the interactions identified. Results were exported on Cytoscape (http://www.cytoscape.org) for graphical visualisation and colour coded depending on the specific functional cluster (**Suppl.Table 4.6, 4.8**). Thickness of the lines reflects the confidence of the interaction (from 0.4 to 0.99).

4.4.5 TG2 association with vesicle-mediated trafficking at the cell-matrix interface

4.4.5.1 A list of TG2-associated proteins involved in vesicular trafficking

In the previous sections, it was underlined how many TG2 interacting partners were associated with vesicle-mediated trafficking in the cells. Given the interest in the possible TG2 partners in the enzyme's unconventional secretion by kidney cells during the progression of disease, the TG2-associated proteins involved in vesicle-mediated trafficking were manually investigated in literature to identify their specific function and their possible roles in secretion. The main findings of this search are reported in **Table 4.10**, displaying the main functions of each protein identified as TG2-associated in this study and having a reported involved in vesicular trafficking. A more extensive description the protein functions can be found in the Appendix. Some the proteins were recognized as mainly linked to endocytosis mechanisms, while others have been associated with exocytosis or recycling. Moreover, a number of proteins were identified as involved in the retromer trafficking from the endosome to the Golgi and/or to the plasma membrane.

Table 4.10: List of TG2-associated proteins involved in vesicular trafficking. The proteins identified as TG2-associated partners by SWATH-acquisition MS and known to play a role in intracellular and/or extracellular vesicular trafficking have been listed in this table. A more extensive description the protein functions can be found in the Appendix. For each protein, the table provides protein ID (_MOUSE), the gene name, the full protein name, and the main function associated with vesicular trafficking. Additional comments are also given for specific proteins, whose other functions might be interesting for the aims of this thesis. Finally, the conditions in which the protein has been identified as associated with TG2 in kidney membranes (Sham operated or UUO mice, or both) are provided in the last column. Abbreviations: ER=Endoplasmatic reticulum; TGN = Trans-Golgi network; PM = Plasma membrane; MVB = Multivesicular bodies.

Prot ID	Gene	Name	Main role	Other comments	SHAM/ UUO
ANFY1	*Ankfy1*	Rabankyrin-5	Endocytosis (Clathrin-mediated and Macropinocytosis)	*Also involved in retromer regulation via Rab5 - GTPase*	SHAM
ANXA2	*Anxa2*	Annexin A2	Endocytosis	*Acts by association with actin; Present in exosomes*	SHAM
AP2A1	*Ap2a1*	AP-2 complex subunit alpha-1	Endocytosis (Clathrin - mediated)	*Plasma membrane-specific adaptor*	UUO
AP2A2	*Ap2a2*	AP-2 complex subunit alpha-2			
AP2B1	*Ap2b1*	AP-2 complex subunit beta			
ARF5	*Arf5*	ADP-ribosylation factor 5	Golgi Trafficking	*Also been associated with endocytosis of α5β1 integrins*	SHAM
ARF6	*Arf6*	ADP-ribosylation factor 6	Endocytosis		SHAM
CLCA	*Clta*	Clathrin light chain A	Endocytosis (Clathrin - mediated)		UUO
CLCB	*Cltb*	Clathrin light chain b	Endocytosis (Clathrin - mediated)		UUO
CLH1	*Cltc*	Clathrin heavy chain 1	Endocytosis (Clathrin - mediated)		SHAM

COPB2	*Copb2*	Coatomer subunit beta	Trafficking through Golgi + Golgi to ER retrograde transport (COPI)		UUO
DCTN1	*Dctn1*	Dynactin subunit 1	Retromer transport	*Retrograde transport along microtubules, not only retromer*	UUO
FLOT2	*Flot2*	Flotillin-2	Endocytosis (Clathrin independent: Caveolae, Phagocytosis)	*Associated with every membrane, also present in exosomes*	UUO
GAK	*Gak*	Cyclin-G-associated kinase	Endocytosis (Clathrin - mediated)	*Clathrin uncoating, Interacts with Hsc70*	UUO
GGA1	*Gga1*	ADP-ribosylation factor-binding protein GGA1	Trafficking of Clathrin coated vesicles from TGN to endosomes/lysosomes		SHAM
HIP1	*Hip1*	Huntingtin-interacting protein 1	Endocytosis (Clathrin - mediated)		UUO
HSP7C	*Hspa8*	Heat shock cognate 71 kDa protein	Endocytosis (Clathrin - mediated) + Chaperone	*Known to be present in exosomes and enriched upon stress*	UUO
IST1	*Ist1*	IST1 homolog	Element of ESCR IIII	*Frequent in urinary exosomes*	SHAM
MY18A	*Myo18a*	Unconventional myosin-XVIIIa	Unconvetional myosins - Golgi regulation / vesicle budding	*Membrane tension/ deformation*	UUO
MYO1B	*Myo1b*	Unconventional myosin-Ib	Unconvetional myosins - intracellular vesicular movements and movements at the PM	*Golgi to PM movements, endocytosis and exocytosis; Involved in membrane tension/deformation*	UUO
MYO1D	*Myo1d*	Unconventional myosin-Id			
MYO1G	*Myo1g*	Unconventional myosin-Ig			
NSF	*Nsf*	Vesicle-fusing ATPase	Membrane fusion events - Exocytosis (SNAREs)	*Suggested to be mportant for TG2 export*	SHAM
PDC6I	*Pdcd6ip*	Programmed cell death 6-interacting protein (ALIX)	MVB biogenesis (ESCRT)- Exosome biogenesis	*Exosome marker, Associates with syndecan in exoxomes biogenesis*	COMMON
PICAL	*Picalm*	Phosphatidylinositol-binding clathrin assembly protein	Endocytosis (Clathrin - mediated)		COMMON
RAB10	*Rab10*	Ras-related protein Rab-10	Golgi to PM trafficking regulation	*Also involved in Golgi to PM transport*	SHAM
RAB1A	*Rab1A*	Ras-related protein Rab-1A	ER To Golgi trafficking regulation (COPII)		UUO
RBGPR	*Rab3gap2*	Rab3 GTPase-activating protein non-catalytic subunit	Regulated Exocytosis		UUO
SAR1B	*Sar1b*	GTP-binding protein SAR1b	ER To Golgi trafficking regulation (COPII)		UUO
SCFD1	*Scfd1*	Sec1 family domain-containing protein 1	Exocytosis (SNAREs)		COMMON
SNX1	*Snx1*	Sorting nexin-1	Retromer transport		UUO
SNX3	*Snx3*	Sorting nexin-3	Retromer transport	*Retromer transport independent from SNX-BAR*	SHAM
SNX4	*Snx4*	Sorting nexin-4	Endocytic recycling	*Interacts with Flot2 in endosomes recycling*	UUO
TBC9B	*Tbc1d9b*	TBC1 domain family member 9B	Regulation Rab GTPases (Deactivation)		SHAM
TERA	*Vcp*	Transitional endoplasmic reticulum ATPase	ER-associated Protein degradation (ERAD)		COMMON
TOM1	*Tom1*	Target of Myb protein 1	Ubiquintated protein degradation by clathrin vesicles		SHAM
TS101	*Tsg101*	Tumor susceptibility gene 101 protein	MVB biogenesis (ESCRT)- Exosome biogenesis	*Might be required for Syndecan release in exosomes*	SHAM

VATH	Atp6v1h	V-type proton ATPase subunit H	Endocytosis (Clathrin - mediated)	*Acidification of organelles and vesicular compartments*	UUO
VPS35	Vps35	Vacuolar protein sorting-associated protein 35	Retromer transport		SHAM
YKT6	Ykt6	Synaptobrevin homolog YKT6	Membrane fusion events in ER-to Golgi / Endosome to Golgi (SNAREs)	*Might be involved in exocytosis*	UUO

4.4.5.2 Search of TG2-associated candidates in the Exocarta database

As many proteins identified as TG2-associated were found to be involved in exocytosis, the top 100 exosome markers (more frequently identified in literature) per the Exocarta database (http://www.exocarta.org/) were searched among the TG2-associated partners obtained by SWATH-MS. Many top exosomal proteins were identified in the TG2 interactomes, with almost 50% (47/100) of proteins detected (**Table. 4.11**). Specifically, 28% of the proteins were identified in healthy conditions (Sham) in either cytosol or membranes, while 30% were detected in fibrotic conditions (UUO) in either cytosol or membranes. Among these proteins, the well-established exosome marker alix (PDC6I) was identified as TG2-associated in both healthy and fibrotic conditions, while heat shock proteins such as heat shock cognate 71 kD protein (HSP7C) and heat shock protein HSP90 (HS90A_MOUSE), as well as flotillin (FLOT) were detected only in fibrotic conditions (**Table. 4.11**, red circles). Tumour susceptibility gene 101 protein (TS101) was detected only in healthy membranes (**Table. 4.11**, green circles). Interestingly, none of the exosome typical tetraspanins (CD9, CD63, CD81) was detected among the TG2-associated proteins (**Table. 4.11**). In order to see if other of the proteins associated with TG2 in kidney fibrotic cell membranes had been previously reported in literature as detected in the exosomal fraction of mouse or other species (human, rat, cow) even if not belonging to the top 100 markers, all the proteins identified as TG2-associated in kidney UUO membranes by SWATH-MS were manually searched in the Exocarta database (**Suppl. Table 4.16**). Interestingly, when this analysis was performed, almost all the TG2-associated proteins in UUO kidney membranes were also reported by the Exocarta database as previously identified in the exosome compartment in literature, in at least one of the species (115/122, 94%) (**Suppl. Table 4.16**). Importantly, the proteins reported as present in exosomes by the Exocarta database included TG2 itself (**Suppl. Table 4.16**), previously identified in exosomes produced by a number of human cell lines such as hepatocellular carcinoma cells, melanoma cells, ovarian cancer cells, prostate cancer cells (He, et al. 2015, Lazar, et al. 2015, Liang, et al. 2013, Kharaziha, et al. 2015), as well as thymic tissue and urine (Gonzales, et al. 2009, Skogberg, et al. 2013), and by rat adipocytes (Lee, et al. 2015).

In conclusion, most of the proteins identified as TG2-associated in kidney fibrotic membranes had been reported to have a location in the exosomes in at least another study (**Suppl. Table 4.16**), and almost a sixth of TG2-associated proteins in either UUO or Sham operated kidney

membranes were identified as belonging to the list of top 100 exosome markers (**Table 4.11**). These results formed the hypothesis that TG2 could be secreted via exosomes by kidney cells.

Table 4.11: Top-100 exosome protein markers detection in the kidney Interactome of TG2. The top-100 proteins identified in the exosomes per the Exocarta database (http://www.exocarta.org/) were searched in the lists of TG2-associated partners obtained by SWATH-MS in both Sham operated and UUO kidneys. C= Cytosolic fraction; M= Crude membrane extract. Red circles identify examples of exosome markers that have been detected as TG2 partners in fibrotic conditions, green circles exosome markers that have been detected as TG2 partners uniquely in healthy conditions. * = The FLOT2 isoform identified in UUO crude membrane extracts.

Top 100 proteins found in exosomes (from Exocarta)			Significantly associated to TG2				
			Sham		UUO		
Gene Symbol	Protein name (_MOUSE)	Number of times identified	C	M	C	M	
CD9	CD9	98					
PDCD6IP	PDC6I	96					x
HSPA8	HSP7C	96					x
GAPDH	G3P	95					x
ACTB	ACTB	93					x
ANXA2	ANXA2	83					x
CD63	CD63	82					
SDCBP	SDCB1	78					
ENO1	ENOA	78					x
HSP90AA1	HS90A	77					x
TSG101	TS101	75					x
PKM	KPYM	72					
LDHA	LDHA	72					x
EEF1A1	EF1A1	71					x
YWHAZ	1433Z	69					x
PGK1	PGK1	69					x
EEF2	EF2	69					x
ALDOA	ALDOA	69					
HSP90AB1	HS90B	67					x
ANXA5	ANXA5	67					
FASN	FAS	66					x
YWHAE	1433E	65					x
CLTC	CLH1	64					x
CD81	CD81	64					
ALB	ALBU	63					x
VCP	TERA	62					x
TPI1	TPIS	62					x
PPIA	PPIA	62					
MSN	MOES	62					x
CFL1	COF1	62					
PRDX1	PRDX1	61					x
PFN1	PROF1	61					x
RAP1B	RAP1B	60					
ITGB1	ITB1	60					
HSPA5	GRP78	58					x
SLC3A2	4F2	57					
HIST1H4A	H4	57					x
GNB2	GBB2	57					
ATP1A1	AT1A1	57					x
YWHAQ	1433T	56					x
FLOT1	FLOT1	56				*	
FLNA	FLNA	56					x
CLIC1	CLIC1	56					x
CCT2	TCPB	56					x
CDC42	CDC42	55					x
YWHAG	1433G	54					
A2M	A2MG	54					
TUBA1B	TBA1B	53					
RAC1	RAC1	53					
LGALS3BP	LG3BP	53					
HSPA1A	HS71A	53					
GNAI2	GNAI2	53					

Top 100 proteins found in exosomes (from Exocarta)			Significantly associated to TG2				
			Sham		UUO		
Gene Symbol	Protein name (_MOUSE)	Number of times identified	C	M	C	M	
ANXA1	ANXA1	53					x
RHOA	RHOA	52					x
MFGE8	MFGM	52					
PRDX2	PRDX2	51					x
GDI2	GDIB	51					
EHD4	EHD4	51					
ACTN4	ACTN4	51					
YWHAB	1433B	50					x
RAB7A	RAB7A	50					
LDHB	LDHB	50					
GNAS	GNAS2	50					
RAB5C	RAB5C	49					
ARF1	ARF1	49					
ANXA6	ANXA6	49					
ANXA11	ANXA11	49					
ACTG1	ACTG	49					x
KPNB1	IMB1	48					x
EZR	EZRI	48					
ANXA4	ANXA4	48					
ACLY	ACLY	48					
TUBA1C	TBA1C	47					
TFRC	TFR1	47					
RAB14	RAB14	47					
HIST2H4A	H4	47					x
GNB1	GBB1	47					
THBS1	TSP1	46					
RAN	RAN	46					x
RAB5A	RAB5A	46					
PTGFRN	FPRP	46					
CCT5	TCPE	46					x
CCT3	TCPG	46					x
AHCY	SAHH	46					
UBA1	UBA1	45					
RAB5B	RAB5B	45					
RAB1A	RAB1A	45					x
LAMP2	LAMP2	45					
ITGA6	ITA6	45					
HIST1H4B	H4	45					x
BSG	BASI	45					
YWHAH	1433F	44					
TUBA1A	TBA1A	44					x
TKT	TKT	44					x
TCP1	TCPA	44					x
STOM	STOM	44					
SLC16A1	MOT1	44					
RAB8A	RAB8A	44					
MYH9	MYH9	44					
MVP	MVP	44					x
Total			28		30		47

4.4.6 Are TG2-associated proteins upon UUO significantly overexpressed by the UUO itself? A comparison between the TG2 interactome in UUO and the UUO-proteome

Once a list of TG2-associated proteins in fibrotic kidney membranes was obtained and analysed using the different bioinformatics approaches, a useful last investigation to perform was a comparison of the outcome of this TG2-immunoprecipitation study on kidney fibrotic membranes (**Table 4.2**) with the proteomic study carried out on whole kidney tissues subjected to the same treatment and shown in the previous chapter (**Suppl. Table 3.1**).

In this way, it was possible to identify which protein were at the same time upregulated in the 21 days-UUO proteome and associated with TG2 at 21-days post UUO, and which proteins were instead associated with TG2 upon UUO but not significantly altered in fibrotic conditions or even underexpressed upon UUO. The comparison of the two proteomic analyses on the UUO model is shown in **Fig 4.12** and **Table 4.12**.

From the comparison it could immediately be seen how TG2-associated proteins in UUO conditions were not necessarily significantly overexpressed in the UUO model at 21 days post UUO (**Fig. 4.12**). In fact, only 17 of the 122 TG2-associated proteins in fibrotic kidney membranes were found significantly overexpressed in the UUO proteome by SWATH-MS and fold change analysis from the Sham operated conditions [confidence of fold change C(FC)≥ 0.8]. These proteins, marked with a red arrow in **Table 4.12** and a red square in **Fig. 4.12**, were mostly associated with cytoskeletal regulation and extracellular organisation and included TG2 (TGM2_MOUSE) itself. Of these proteins, nine were cytoskeletal: profilin 1 (PROF1_MOUSE), gelsolin (GELS_MOUSE), vimentin (VIME_MOUSE), actin-related protein 2/3 (ARC1B_MOUSE), F-actin-capping protein (CAPZB_MOUSE), moesin (MOES_MOUSE), filamin-A (FLNA_MOUSE), keratin 19 (K1C19_MOUSE) and myosin 10 (MYO10_MOUSE). Other five, biglycan (PGS1_MOUSE), perlecan (PGBM_MOUSE), Fibronectin (FINC_MOUSE), Collagen (COCA1_MOUSE) and periostin (POSTN_MOUSE), were associated with either extracellular organisation or cell adhesion, and two, plastin-2 (PLSL_MOUSE) and coronin-1C (COR1C_MOUSE), were signalling proteins associated with cytoskeletal changes (**Table 4.12**, red arrows; **Fig. 4.12**, red squares).

Other 33 TG2-associated proteins in fibrotic kidney membranes were still more expressed in UUO kidney lysates compared to the sham operated conditions, but at a non-significant C(FC)(confidence lower than 0.8, marked with an asterisk in **Table 4.12**), hence were not present in the list of UUO-overexpressed proteins (**Suppl. Table 3.5**). Of these proteins, 16 had a confidence level ≥ 0.5 and are reported on the right side of the graph in **Fig. 4.12,** with no squares.

Interestingly, 12 proteins significantly associated with TG2 in kidney fibrotic membranes were identified as significantly underexpressed in whole kidney lysates under the same conditions

(green arrow in **Table 4.12,** green squares in **Fig. 4.12**). The majority of these proteins were metabolic: nicotinamide phosphoribosyltransferase (NAMPT_MOUSE), phosphoglycerate kinase 1 (PGK1_MOUSE), acyl-protein thioesterase 1 (LYPA1_MOUSE), aflatoxin B1 aldehyde reductase member 2 (ARK72_MOUSE), peroxisomal bifunctional enzyme (ECHP_MOUSE) and C-1-tetrahydrofolate synthase (C1TC_MOUSE). The redox protein glutathione peroxidase (GPX1_MOUSE) and the redox-regulatory protein FAM213A (F213A_MOUSE) were also among these proteins, together with the cytoskeletal proteins akyrin-3 (ANK3_MOUSE) and spectrin (SPTN1_MOUSE), the vesicular protein V-type proton ATPase subunit H (VATH_MOUSE) and the heat shock protein HSP 90-α (HS90A_MOUSE). Other 13 proteins resulted underexpressed at C(FC) between 0.5 and 0.8, and are reported on the left side of the graph in **Fig. 4.12,** with no squares.

In conclusion, only few of the TG2-associated proteins in fibrotic kidney membranes were found overexpressed in the UUO proteome itself when using whole kidney lysates, while a series of other proteins were found not significantly altered in the fibrotic kidney or even underexpressed. This might mean that the progression of UUO determines an increased association of the enzyme with its protein partners, and not necessarily an increase in the partners' expression. An interesting finding is that most of the vesicular partners of TG2 in UUO kidney membranes was not detected as differentially expressed in the UUO proteome, and that many antioxidant proteins were increasingly associated with the enzyme even if downregulated by the disease.

The same analysis was performed also on the list of TG2-associated proteins in healthy conditions, and results are provided in **Suppl. Table 4.17**.

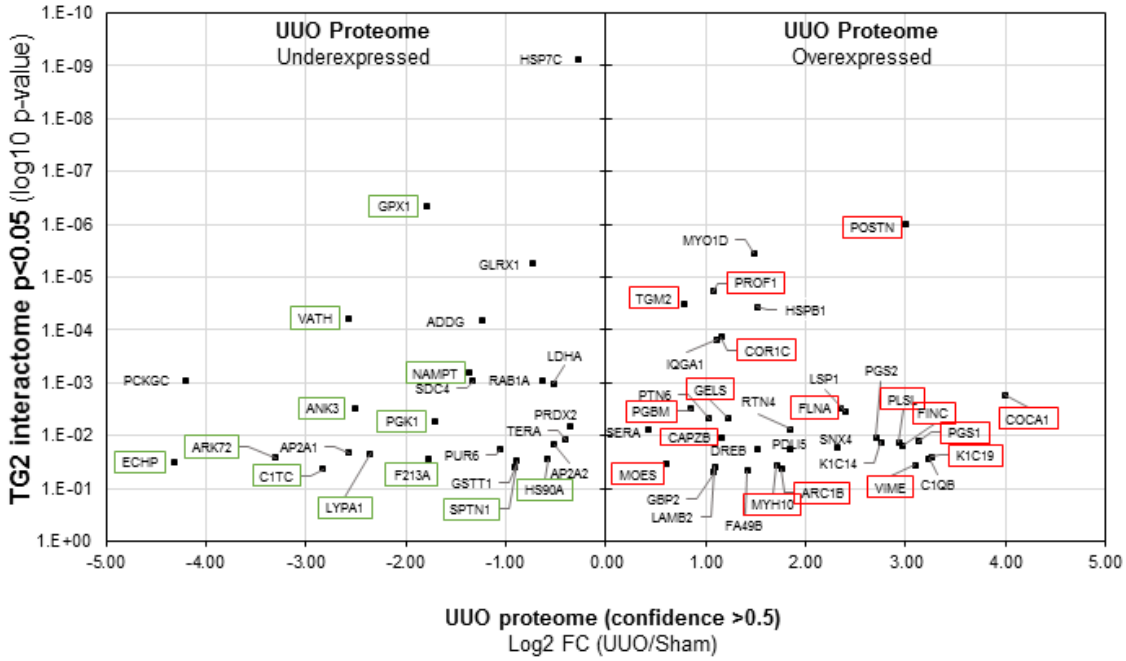

Figure 4.12: Comparison of TG2 interactome in fibrotic (UUO) kidney membranes (p≤0.05) with UUO Proteome (confidence ≥ 0.5). In order to see if the proteins significantly associated with TG2 in the UUO model were also upregulated in the whole UUO proteome, the two analyses were combined in a plot. The 122 Proteins associated with TG2 in UUO kidney membranes were plotted on the ordinate axis per the p-value of TG2-association in UUO kidney membranes (to a maximum p-value ≤ 0.05), and on the abscissa according to the log2 of the fold change (log2 FC) in the UUO proteome comparing to sham operated kidneys. A positive x value indicates overexpression upon UUO, a negative value indicates underexpression upon UUO; for this analysis, a confidence of FC ≥ 0.5 were employed, instead of the otherwise employed confidence of 0.8. Red squares identify proteins significantly overexpressed in the UUO proteome compared to the sham operated proteome at a C(FC) higher than 80%. Green squares identify proteins significantly underexpressed in the UUO proteome compared to the sham operated proteome at a C(FC) higher than 80%.

Table 4.10: Comparison of TG2 interactome in kidney fibrotic membranes (p≤0.05) with UUO Proteome. In order to see if the proteins significantly associated with TG2 in the UUO model were also overexpressed in the model itself, the two analysis in were combined in this heat-map table. On the left side, the list of TG2-associated proteins in UUO kidney membranes (21 days); in scale of blue, the p-value of TG2 association as calculated by z-test. A p-value ≤0.05 was considered as significant. On the right, the fold change from sham and confidence values for the same proteins in the UUO proteomic analysis performed on whole tissue; in red, the positive fold change (FC) in the UUO, that means overexpression, and in green the negative fold change, that means underexpression. In yellow, the level of confidence of this second analysis, bright yellow ≥ 0.8 and light yellow 0.5 ≤ C < 0.8. A confidence ≥ 0.8 was considered as significant. Legend: U=Unique; C= Common (associated with TG2 in both UUO and sham operated mice). Red arrows = proteins significantly overexpressed upon UUO; Asterisks = proteins with increase expression upon UUO but in a not significant manner (confidence < 0.8); Green arrows = proteins significantly underexpressed upon UUO.

	TG2-associated proteins in UUO membranes				Expression upon UUO in whole kidney lysates	
	Protein ID	Unique/ Common	N	p-value	Log2 FC (UUO/Sham)	Confidence
	DESP	U	5	1.22E-13		
	HSP7C	U	5	7.67E-10	-0.27	0.74
	CALM	C	5	1.83E-08	-0.51	0.41
	CAZA2	U	5	1.97E-08		
➡	GPX1	U	5	4.52E-07	-1.79	0.92
	ADH1	C	5	9.40E-07	-0.64	0.44
➡	POSTN	U	4	1.03E-06	3.01	0.80
*	MYO1D	U	5	3.52E-06	1.48	0.55
	GLRX1	U	4	5.61E-06	-0.72	0.54
	GLRX3	U	5	1.40E-05	-0.60	0.46
➡	PROF1	U	5	1.89E-05	1.07	0.89
➡	TGM2	C	5	3.31E-05	0.78	0.90
*	HSPB1	U	5	3.68E-05	1.51	0.72
➡	VATH	U	5	5.98E-05	-2.57	0.90
	ADDG	U	5	6.66E-05	-1.24	0.76
	AT2A2	U	5	8.58E-05	-0.56	0.46
	SVIL	U	4	1.01E-04		
➡	COR1C	U	5	1.38E-04	1.16	0.83
*	IQGA1	C	5	1.50E-04	1.12	0.66
	TCPE	U	5	3.17E-04	-0.54	0.31
*	UBP5	U	5	4.59E-04	1.20	0.38
*	FLOT2	U	4	5.38E-04	1.55	0.39
➡	NAMPT	C	5	6.56E-04	-1.36	0.82
	PCKGC	C	5	8.93E-04	-4.20	0.80
	RAB1A	U	5	9.16E-04	-0.64	0.71
	SDC4	U	5	9.34E-04	-1.33	0.54
	LDHA	U	4	1.04E-03	-0.52	0.72
	MYO1G	U	5	1.21E-03		
	K1C20	U	4	1.35E-03		
	COEA1	U	5	1.64E-03		
➡	COCA1	U	4	1.68E-03	3.99	0.82
	HIP1	U	4	1.86E-03		
	LIMS1	C	5	2.47E-03		
*	SAR1B	U	5	2.79E-03	0.59	0.33
	SPTA1	C	5	2.92E-03		
➡	FLNA	U	5	2.98E-03	2.34	0.93
➡	ANK3	U	5	3.03E-03	-2.51	0.85
	PSD11	U	5	3.09E-03	-0.66	0.34
➡	PGBM	U	5	3.16E-03	0.85	0.81
*	LSP1	U	5	3.53E-03	2.39	0.67
➡	GELS	U	5	4.61E-03	1.22	0.84
	YKT6	U	5	4.72E-03		
*	PTN6	C	4	4.84E-03	1.04	0.59
*	FLNB	U	5	5.03E-03	0.46	0.32
*	TLN2	U	5	5.28E-03	0.72	0.50
➡	PGK1	C	4	5.39E-03	-1.71	0.97
	PICAL	C	4	5.65E-03	-0.62	0.43
*	F120A	C	5	6.27E-03	0.59	0.33
	PRDX2	C	4	6.87E-03	-0.36	0.64
*	KCC2D	U	5	7.10E-03	1.34	0.45
*	RTN4	U	5	7.57E-03	1.85	0.72
*	SERA	C	5	7.78E-03	0.43	0.54
	KC1A	U	5	8.06E-03		
	DCTN1	U	5	8.52E-03		
	ADDA	U	5	8.61E-03	-0.67	0.47
*	PGS2	U	5	1.09E-02	2.70	0.79
	IF4G3	C	5	1.11E-02		
	RHG18	U	4	1.11E-02		
➡	CAPZB	U	5	1.11E-02	1.16	0.89
*	MVP	U	5	1.14E-02	0.48	0.33
	TERA	C	5	1.21E-02	-0.40	0.52
	ACTB	U	5	1.24E-02		
➡	PGS1	C	5	1.30E-02	3.13	0.86

	TG2-associated proteins in UUO membranes				Expression upon UUO in whole kidney lysates	
	Protein ID	Unique/ Common	N	p-value	Log2 FC (UUO/Sham)	Confidence
*	K1C14	U	5	1.33E-02	2.75	0.75
➡	PLSL	U	5	1.34E-02	2.93	0.85
	AP2A2	U	5	1.52E-02	-0.52	0.54
➡	FINC	C	5	1.57E-02	2.97	0.84
	CLCB	U	5	1.65E-02	-0.93	0.40
*	SNX4	U	5	1.67E-02	2.32	0.65
	SPTB1	U	5	1.73E-02		
*	ZO1	U	4	1.79E-02	0.78	0.40
*	DREB	U	5	1.83E-02	1.51	0.51
	CAN1	U	5	1.84E-02	-1.53	0.33
*	PDLI5	U	5	1.85E-02	1.84	0.70
	PUR6	U	5	1.88E-02	-1.06	0.79
	MY18A	U	5	1.93E-02	-3.27	0.42
	CLCA	U	5	2.07E-02	-0.64	0.34
	IRGM1	U	5	2.09E-02	-0.17	0.09
	NEB2	U	5	2.11E-02		
	K2C6B	U	5	2.14E-02		
	AP2A1	U	5	2.15E-02	-2.57	0.65
➡	LYPA1	U	5	2.18E-02	-2.36	0.90
*	PDC6I	C	5	2.38E-02	0.71	0.44
*	AP2B1	U	5	2.43E-02	0.57	0.44
➡	K1C19	U	5	2.58E-02	3.26	0.86
	GRP78	U	5	2.59E-02		
➡	ARK72	U	5	2.61E-02	-3.30	0.87
*	SNTB2	U	5	2.63E-02	1.56	0.44
	MYO1B	U	5	2.67E-02		
	K6PP	U	5	2.67E-02		
*	C1QB	U	5	2.71E-02	3.24	0.70
➡	F213A	C	5	2.79E-02	-1.77	0.89
➡	HS90A	U	5	2.85E-02	-0.58	0.81
	GAK	U	5	2.86E-02		
➡	SPTN1	C	5	3.08E-02	-0.89	0.88
	UCK1	U	5	3.12E-02		
➡	ECHP	C	5	3.15E-02	-4.32	0.84
	ES8L2	U	4	3.29E-02	-0.94	0.25
➡	MOES	U	5	3.33E-02	0.60	0.81
	PNCB	U	5	3.34E-02		
➡	MYH10	U	5	3.59E-02	1.71	0.85
	RBGPR	U	5	3.65E-02		
➡	VIME	U	5	3.66E-02	3.10	0.90
	SERPH	U	5	3.81E-02		
*	RPN1	U	4	3.89E-02	0.21	0.29
*	LAMB2	C	4	3.92E-02	1.09	0.76
	GSTT1	U	5	3.95E-02	-0.91	0.80
	TCPQ	U	5	3.96E-02		
	TCPZ	C	5	4.23E-02	-0.44	0.36
	IRAK4	U	5	4.24E-02		
➡	C1TC	U	5	4.28E-02	-2.83	0.87
➡	ARC1B	U	5	4.28E-02	1.76	0.87
*	SCFD1	C	5	4.30E-02	1.18	0.28
*	COPB2	U	5	4.42E-02	0.87	0.47
*	FA49B	U	5	4.62E-02	1.42	0.52
	MYH14	U	5	4.79E-02		
	SNX1	U	4	4.81E-02	-0.81	0.46
*	PLST	U	5	4.82E-02	0.33	0.40
*	GBP2	U	5	5.00E-02	1.08	0.56
	SYEP	U	5	5.17E-02	-0.40	0.35
*	TCPA	U	5	5.25E-02	0.56	0.31
	CLIC1	U	5	5.33E-02	-0.35	0.48

4.5 DISCUSSION

In the past few decades, several studies have highlighted the involvement of TG2 in the progression of CKD. Increased TG2 release and extracellular activity have been shown to be associated with the progression of kidney fibrosis in different models of CKD as well as in clinical biopsies. Increased extracellular TG2 expression and activity are known to contribute to kidney fibrosis by supporting matrix accumulation and resistance, TGF-β activation, and by promoting cell adhesion and contraction, acting as a structural adhesive protein.

In the previous chapter, TG2 was identified as a potential marker of fibrosis in the UUO-proteome, when compared to Sham operated conditions. The analysis of TG2-KO mice supported the idea of a protective role of TG2 inhibition against the progression of fibrosis in the UUO model, in agreement with previous studies employing both TG2-KO (Fisher, et al. 2009, Shweke, et al. 2008) or general TG inhibitors in animal models (Skill, et al. 2004, Huang, et al. 2010, Huang, et al. 2009, Johnson, et al. 2007).

TG2 has been suggested as a possible pharmacological target against the development of fibrosis, however, clinical application of a direct TG2 inhibitor is difficult, given the highly conserved catalytic core of this protein, compared to the other members of the family. One fascinating possibility would be not to aim at the inhibition of the enzymatic activity of TG2 but at the TG2 release from kidney cells into the interstitial space, where the enzyme contributes to the accumulation of fibrosis. TG2 is known to be secreted through a still not clarified unconventional secretion pathway by kidney cells (Chou, et al. 2011), which is likely to be specific for TG2 and require the interaction with certain molecular partners, with the possibility of becoming a specific target of intervention against the extracellular accumulation of the enzyme.

Given the little knowledge of TG2 export mechanism from kidney cells during CKD, we believe that the identification of the TG2 interactome on fibrotic kidney membranes is an important step to perform to accelerate the process of resolution of TG2 externalization mechanism and extracellular activity in CKD.

To achieve this purpose, in the current study, TG2-associated proteins were investigated by an original proteomic strategy that combines TG2-immunoprecipitation from whole kidney membrane preparations of WT kidneys, with negative control immunoprecipitation from TG2-null kidneys from inbred mice, in both fibrotic (21 days UUO) and Sham operated conditions, followed by a quantitative, high-throughput, MS analysis performed by SWATH-DIA. The employment of a the TG2-null background control is particularly important in the analysis and is a strength of this investigation approach, as it allows to discriminate between proteins significantly associated with the enzyme and contaminant proteins un-specifically precipitated. This, to our knowledge, represents the first unbiased (hypothesis-free) global

analysis of TG2 interacting proteins in a model of CKD. The proposed strategy could be adapted for precision targeted proteomics for the analysis of other systems.
In this Chapter, the TG2 interactome in kidney fibrotic membranes was investigated, starting from the data obtained by SWATH-MS acquisition of the TG2-IP samples. A z-test statistical analysis, conceptually similar to a T-test, was employed, to identify a list of protein significantly associated with TG2, using the TG2-null data as a background control.

Of the 746 proteins detected as TG2-immunoprecipited in at least 4 out of 5 experiments, 217 were proteins identified as significantly ($p \leq 0.05$) associated with TG2 in kidney membranes by z-test, when protein expression was compared to the TG2-null IP backgrounds. Among these proteins, 97 were identified associated with TG2 uniquely in UUO, while 95 were found exclusively in Sham operated membranes (**Fig. 4.3**). Only a small overlap (25 proteins), was found between the two conditions, suggesting a marked change of TG2 interaction on kidney membranes at this stage of UUO (**Fig. 4.3**).
When the outcome of the current SWATH-DIA analysis was compared with the TG2-associated proteins previously identified in TG2-IPs of healthy C57BL/6J mice kidney membranes by a relative quantification approach combining iTRAQ labelling and shotgun LC-MS/MS with DDA (described in 4.1.1), SWATH approach appeared as a more sensitive technology for the detection of TG2-associated proteins. Of the 24 proteins previously highlighted, 17 were also identified as significantly TG2-associated in the current study.
Among the TG2-associated proteins identified in both fibrotic or healthy conditions, only approximately ¼ had an already reported interaction with TG2 in literature, according to the Transdab database (**Table 4.4**), suggesting that the large majority of TG2-associated candidates identified with this method were novel. However, being an immunoprecipitation-based technique, some of the proteins identified as TG2-associated candidates might not be direct binding partners the enzyme, but be indirectly associated with TG2 through interaction with other TG2-binding proteins.

It was anticipated that the analysis of TG2-interacting proteins in fibrotic kidney membranes at the cell-matrix interface could lead to the discovery of candidates involved in the enzyme secretion from kidney cells and extracellular activity during the progression of fibrosis, and possibly contribute to the elucidation of the mechanism of the CKD-induced unconventional release of TG2 from kidney cells.
To examine the functional distribution of the TG2 interacting candidates in our list, as well as investigate possible pathways involved, a functional classification was performed, both manually (4.4.2) and by employment of bioinformatics supports allowing analysis of GO/PANTHER annotation terms (4.4.3-4.4.4).

Proteins involved in cytoskeletal organisation and remodelling, cell adhesion, ECM organisation and redox regulation appeared more represented among the TG2-associated proteins in fibrotic kidney membranes, compared with TG2 partners in healthy membranes (**Fig. 4.7, 4.8**), suggesting their involvement in TG2 pro-fibrotic roles during CKD.

Importantly, among the ECM organisation and adhesion proteins, the HSPGs Sdc4 and perlecan were identified in the interactome of TG2 uniquely in fibrotic conditions, in the same cluster with FN and other adhesion proteins (**Fig. 4.10**). This implies that the association of TG2 with HSPGs is induced by CKD, in line with previous findings suggesting a crucial role for HS chains in TG2 extracellular localisation and activity during the progression of fibrosis (Scarpellini, et al. 2014, Burhan, et al. 2016). The importance of Sdc4/HSPGs in CKD has been reported (Yung, et al. 2001, Morita, et al. 1994, Fan, et al. 2003) and the protective role of Sdc4-KO against the development of kidney fibrosis has been previously suggested by our group (Scarpellini, et al. 2014). Upregulation of both Sdc4 and TG2 expression during the progression of CKD has been recently shown by our group in a rat model of CKD determined by SNx, with large co-localisation of the two proteins in the interstitium of fibrotic tubules, dependent on HS chains. However, Sdc4 was not found upregulated in the UUO proteome generated in the kidney lysates (**Table 4.12**), suggesting that an increased association with TG2, more than an increased expression of the proteoglycan, is observed in UUO at this end-stage level.

A significant enrichment in TG2 association with cytoskeletal proteins was identified in UUO kidney membranes compared to the Sham operated ones. Indeed, many proteins involved in cytoskeleton remodelling were identified, that were mostly related to actin remodelling (actin related protein 2/3 complex, profilin, gelsolin, etc.) and located at the cortical cytoskeleton, at the interface with the plasma membrane (adducin, filamin, ankyrin, moesin, etc.). Vimentin was identified in the list, and already revealed in Chapter III as a largely upregulated marker of mesenchymal cells in the UUO model (**Fig. 4.6-4.7**), while α-SMA was identified as a TG2 partner in the UUO cytosol (**Suppl. Table 6.1**). Association with these proteins leads to the hypothesis of TG2 being directly involved in the large cytoskeletal reorganisation happening during the fibrotic process. Moreover, increased intracellular TG2 crosslinking activity, which is likely to target cytoskeletal proteins such as actin and vimentin (Shin, et al. 2008), has already been identified in the past as a feature of fibrosis progression in models of CKD (Johnson, et al. 1997, Johnson, et al. 2003, El Nahas, et al. 2004), contributing to the cell death (Verderio, et al. 1998) observed at the late stages. Curiously, while TG2 association with myosin was identified mainly in UUO kidney membranes, and can be explained by a larger population of cells with "smooth muscle" phenotype, tubulins were identified as associated with TG2 uniquely in healthy kidney membranes. This might be associated with a role for TG2

in the cytoskeletal stabilisation, that might be lost upon UUO; in fact, TG2 has been shown to polyaminate tubulin in neural cells, resulting in neural microtubule stabilisation and decrease in neural plasticity both *in vitro* and *in vivo* (Song, et al. 2013). Keratins were also strongly associated with TG2 in UUO fibrotic membranes, consistent with their reported upregulation in tubular cells upon CKD (Djudjaj, et al. 2016), which was confirmed in our model (Chapter III).

The identification of a number of antioxidant proteins uniquely associated with TG2 in fibrotic kidney membranes is another interesting result. Proteins with antioxidant proprieties such as glutaredoxins, glutathione peroxidase, glutathione S-transferase and peroxiredoxin, form a significant cluster in the TG2 interactome in kidney fibrotic membranes and are likely to contribute to the preservation of the enzyme reduced-active state in the interstitial space upon CKD. Interestingly, the same proteins were found as significantly downregulated in the UUO proteome at 21 days post-surgery (Chapter III and **Table 4.12**), allowing to speculate that an increase association with TG2 with these proteins is still happening even if the redox control in the organ is strongly dysregulated. This is probably a consequence of the late stages of disease, as antioxidant proteins were found upregulated in kidney lysates at the earliest stages of UUO (Zhao, et al. 2015), supporting a cooperative effect in the promotion of TG2 extracellular activity.

The most interesting finding obtained from the investigation of the TG2 interactome is the identification of a substantial number of proteins with a reported role in vesicle-mediated transport. This class of proteins was significantly enriched among the TG2 partners in both UUO and sham operated conditions (**Table 4.7**), however, protein representation was higher (21% vs 15%) (**Fig. 4.7**) and more significant in fibrotic conditions, forming a significant cluster of interacting proteins in the TG2-interactome (**Fig. 4.10**).
As a key aim of this study is the identification of potential partners of TG2 in kidney membranes that might contribute to its unconventional secretion in the interstitial space, these proteins were regarded as particularly significant, and were investigated in detail (4.4.5) (**Table 4.10**). It was highlighted that many TG2-associated proteins on kidney membranes were well-known exosome markers (**Table 4.11**). Exosomes are small extracellular vesicles (EV) (generally < 100 nm). They form at the late endosome by intraluminal vesicle budding that generate the so called multivesicular bodies (MVB), which then fuse with the plasma membrane releasing the exosomes. Among the top exosome markers obtained by the Exocarta database (Simpson, Kalra and Mathivanan 2012, Keerthikumar, et al. 2016), Alix (programmed cell death 6 – interacting protein), involved in intraluminal vesicle budding at the late exosome and responsible for exosome biogenesis through interaction with syntenin and syndecan (Hurley

and Odorizzi 2012, Colombo, et al. 2013, Ghossoub, et al. 2014, Baietti, et al. 2012), Hsp7c, a chaperone found in exosomes of most cells, and flotillin, a lipid raft associated protein, were found associated with TG2 in UUO kidney membranes, while the endosomal sorting complexes required for transport (ESCRT) machinery protein Tsg101 (Tumour susceptibility gene 101) was identified as a TG2 partner in healthy membranes. Interestingly, when a more comprehensive analysis was performed, more than 90% of the proteins identified as TG2-associated with kidney fibrotic membranes were found reported in the exosomal fraction in at least another study, and included TG2 itself (**Suppl. Table 4.16**).

Matching the TG2-associated proteins with the UUO proteome showed that the TG2 partners involved with vesicle-mediated transport and exocytosis were not increased post-UUO, suggesting a specific role in trafficking of TG2 upon disease (**Table 4.12**). On the contrary, a group of proteins involved in ECM-receptor organisation, including FN and periostin, significantly overexpressed in the UUO kidneys, were also all partners of TG2 (**Table 4.12**).

These findings suggest the existence of a pathway of TG2 secretion during fibrosis progression driven by a vesicular trafficking which is specific for TG2, and its subsequent association with an UUO-upregulated protein network responsible for ECM dynamics resulting in matrix accumulation.

We hypothesized that TG2 unconventional secretion from kidney cells to the extracellular interstitial space might be dependent on exosomes, introducing a link between TG2 and EVs in the UUO kidney. The identification of a few proteins involved in SNARE-mediated membrane fusion events, including NSF-ATPase, might support this hypothesis, as membrane fusion is required for exosome secretion. In this context, association of TG2 with several proteins mediating actin remodelling as well as signalling proteins leading to cytoskeletal reorganisation, such as plastin, coronin and calpain, which were particularly significant in kidney fibrotic membranes, might be involved in some alterations in the actin cytoskeleton suggested to favour vesicular trafficking.

In the next chapter, the hypothesis of a TG2 unconventional secretion mediated by EVs, and in particular exosomes, will be tested *in vitro* employing tubular epithelial cells (TECs). Subsequently, the involvement of HS chains / Sdc4 in the process will also be investigated on the same cells, given the specific association of this HSPG with TG2 in UUO and other models of CKD.

Chapter V: Analysis of TG2 unconventional secretion in tubular epithelial cells

5.1 AIMS OF THE CHAPTER

Work described in Chapter IV has resulted in the identification of partners of TG2 in normal and fibrotic kidney. A number of proteins involved in protein trafficking were recognised, which might play a role in the enzyme's unconventional secretion during the progression of CKD. As tubular epithelial cells (TECs) have been reported to express and release most of TG2 secreted during the progression of CKD (Johnson, et al. 1999, Johnson, et al. 2003), the aim of this chapter is to investigate the mechanism of TG2 unconventional secretion in renal TECs. To achieve this purpose, immortalised cell lines of rat TECs are utilised as a cell model of TG2 release in the present chapter. A number of unconventional secretion models are tested.

5.2 INTRODUCTION

5.2.1 Vesicular trafficking in the cell

In the eukaryotic cell, upon protein synthesis at the ribosome, proteins can be either secreted or retained into the cell. The majority of the secreted proteins are characterised by a signal peptide that determines their access into the endoplasmic reticulum (ER) for secretion (Wickner and Lodish 1985). These proteins are generally referred to as "conventionally secreted proteins". The signal peptide (leader peptide) is a short N-terminal amino acidic sequence that is added at the beginning of the protein at the moment of synthesis and directs the protein to a particular translocation channel of the ER (translocon or Sec61/TRAP/TRAM heterocomplex) (Osborne, Rapoport and van den Berg 2005, Johnson and van Waes 1999). By crossing the traslocon, proteins enter the ER and the signal peptide is then cleaved by a specific peptidase (Bussey 1988).

5.2.1.1 Intracellular trafficking

From the ER, the majority of the conventionally secreted proteins move to the cis-Golgi network, then to the trans-Golgi network (TGN) and finally to the cell surface via a well organised classical vesicular transport. Proteins are released from the ER into coat protein II (COPII)-coated vesicles (Szul and Sztul 2011). Inside the Golgi cisternae, a series of enzymes determine post translational modification of the cargo proteins that are then trafficked to the trans Golgi network (TGN) inside coat protein I (COPI)-coated vesicles, wich also mediate retrograde transport of membranes and enzymes back to the cis side of the Golgi and to ER. From the TGN, cargo proteins are released into clathrin coated vesicles.

These vesicles can be directly secreted through the plasma membrane, while others cargo-containing vesicles fuse with the late endosome (multivesicular Bodies, MVB) compartments for secretion (exosome) or degradation in the lysosome.

The endosomal compartment of the cell is a membranous compartment that sorts the different vesicles to the appropriate destination, such as lysosome (for degradation), plasma membrane (for secretion / recycling) or TGN (by retromer transport).

The endosome can be distinguished into three different compartments: the early endosome, the late endosome and the recycling endosome. Once an endocytic vesicle has formed, it generally fuses with the early endosome compartment, characterised by markers such as small GTPases Rab 4 and Rab 5 as well as early endosome antigen 1 (EEA1) and phosphatidylinositol 3-phosphate (PI3P). From the early endosome, the cargoes destined for recycling are sorted into the recycling endosome, while the remaining part of early endosome matures into the late endosome. At the late endosome, cargoes are sorted in small (< 100 nm) intraluminal vesicles (ILV) by inward budding into the lumen of the endosome, giving rise to what is called multivesicular body (MVB) or multivesicular endosome (MVE). These late endosomes / MVB either fuse with the lysosome for degradation of ILV-cargoes or with the plasma membrane for ILVs secretion as exosomes. It is believed that at last two different populations of MVBs co-exist in the same cells, which are partially dissimilar in lipid composition (Mobius, et al. 2002, Wubbolts, et al. 2003): one ”en route” for degradation and one “en route” for exosome secretion (Raposo and Stoorvogel 2013). The pathway necessary for the formation of MVBs directed to lysosome has been well described and involved the so called ESCRT (endosomal sorting complex responsible for transport) machinery. This machinery is characterised by four distinct multiprotein complexes (ESCRT-0 to ESCRT-III) and accessory proteins such as Alix and VPS4 (Wollert and Hurley 2010, Henne, Buchkovich and Emr 2011).

The retromer complex is an important component in the pathway of endosomal protein sorting (Seaman 2012). Normally, retromer complex controls the transport of proteins from the

endosomes back to the trans Golgi network, however, a role of retromer complex in protein recycling form the endosome to the plasma membrane has also being identified and might represent a different mechanism of protein secretion (Seaman 2012).

The two main elements of the retromer complex are the cargo-selective trimer (CST), constituted of three vacuolar sorting proteins (Vps35, Vps26 and Vps29), and the Snx-BAR dimer, constituted of a couple of sorting nexin proteins (Snx1 or Snx2 with Snx5 or Snx6) (van Weering, Verkade and Cullen 2010, Cullen and Korswagen 2012) and binding PI3P on the endosome suface. The CST recruitment to the endosomal membrane seems to be dependent on both the actions of the small GTPase Rab7a (Seaman, et al. 2009, Harrison, et al. 2014) and the Sorting nexin protein Snx3. Another protein that has been shown to possibly regulate the endosome to TGN trafficking mediated by the retromer is the EHD1-interacting protein rabankyrin-5, that binds CST and is likely to have a regulatory function, being a Rab5 effector (Zhang, Naslavsky and Caplan 2012, Zhang, et al. 2012). Snx5/Snx6 are able to bind dynactin (subunit 1, DCTN1) and connecting the endosomal tubule to the microtubules, thus directing the elongating endosomal tubule along them (Hong, et al. 2009, Wassmer, et al. 2009). Morover, clathrin might be associated to retromer transport, together with the molecular chaperone heat shock cognate 71 kDa protein (Hsp7c) (Popoff, et al. 2009).

Interestingly for the context of protein secretion, CST has also been reported to interact with the WASH complex through its Vps35 subuit. The WASH complex is a multimolecular complex localised on the endosomes and involved in the activation of the actin nucleation complex Arp2/3 and subsequent induction of branched actin networks formation (Puthenveedu, et al. 2010, Derivery and Gautreau 2010). WASH complex has been proposed to be central for recycling of specific proteins from the endosome to the plasma membrane through endosomal tubules elongation and budding, with crucial involvement of actin remodelling processes mediared by Arp2/3 and actin-capping proteins. Examples of proteins recycled to the plasma membrane by this WASH-dpendent mechanisma are the are the G-protein-coupled (GPCR) β2-adrenergic receptor, in a process that involves also the activity of another Snx protein, Snx27(Temkin, et al. 2011), and α5β1 integrins (Zech, et al. 2011). Also, vacuolar ATPase (VATH) recycling to the lysosome has been suggested to be mediated by WASH (Carnell, et al. 2011).

5.2.1.2 Endocytic mechanisms

Different mechanisms of endocytosis have been identified in mammalian cells, that can be generally subdivided into two categories: phagocytosis ("cell eating"/solid phase uptake) and pinocytosis ("cell drinking"/fluid phase uptake)(Conner and Schmid 2003). While phagocytosis happens only in some cells, such as leucocytes / macrophages, pinocytosis happens in all cell types and can be further subdivided into four main mechanisms (Conner and Schmid 2003): (1) clathrin mediated endocytosis (CME), (2) caveolae or lipid raft - mediated endocytosis, (3) caveolae and clathrin - independent endocytosis and (4) macropinocytosis.

CME is involved in receptor/ligand recycling, signalling and degradation by uploading into clathrin coated vesicles (CCV). The process requires adaptor proteins (AP2), associated at the membrane with phosphatidylinositol 4,5-bisphosphate [PI(4,5)P2] and dynamin (Kirchhausen, Owen and Harrison 2014). Actin dynamics also play a role in the vesicle formation (Mooren, Galletta and Cooper 2012, Grassart, et al. 2014), while auxilin and heat shock cognate 70 (HSC70) have been show to act in clathrin uncoating after budding (Kirchhausen, Owen and Harrison 2014). Lipid raft -mediated endocytosis is driven by invagination of small plasma membrane lipid microdomains regarded as caveolae or caveolin-containing lipid rafts, enriched in cholesterol and usually containing the cholesterol-binding protein caveolin (Matveev, et al. 2001, Parton and Richards 2003, Mayor, Parton and Donaldson 2014). Calveolae are particularly abundant in endothelial cells, fibroblasts and smooth muscle cells (Krajewska and Maslowska 2004). Also caveolae mediated endocytosis requires dynamin and and cortical actin dynamics contribution (Parton and Richards 2003, Mayor, Parton and Donaldson 2014). Pathways not involving clathrin nor caveolin are are involved for example in the endocytosis of (GPI)-anchored proteins and β1-integrins recycling. These pathways are usually also dynamin independent while they depend on different GTP-ases such as the plasma membrane Arf6 GTPase (Brown, et al. 2001, Sabharanjak, et al. 2002, Naslavsky, Weigert and Donaldson 2004). Finally, macropinocytosis is characterised by the formation of large cell surface ruffling/engulfment that includes large amount of liquid and solutes and result in big intracellular vacuoles named macropinosomes (Lim and Gleeson 2011, Jones 2007). Macropinosomes are generally lager and can reach up to five μm in diameter (Khalil, et al. 2006). The mechanism is similar to what happens in phagocytosis of solid particles / phagosome formation, and they are both primarily regulated by remodelling of cortical actin (Lim and Gleeson 2011, Jones 2007).

5.2.1.3 Extracellular vesicles (EV)

Cells release different kinds of vesicles in the extracellular space, generally referred to as extracellular vesicles (EVs). The two main categories of EVs released from living cells are Exosomes and Ectosomes, differing from each other on biogenesis, size and molecular markers (**Table 5.1**).

5.2.1.3.1 Exosomes

Exosomes originate in the context of the endosomal network as cargo-containing intraluminal vesicles (ILVs) of the multivesicular body (MVB) and are released by fusion of the limiting membrane of the MVB with the plasma membrane (Kowal, Tkach and Thery 2014, Cocucci and Meldolesi 2015). Exosomes size is identical to the ILVs and is generally between 30 and 100 nm of diameter, even if in some cases larger and smaller exosomes have been detected (Raposo and Stoorvogel 2013, Akers, et al. 2013). The biogenesis of the intraluminal vesicles of the MVB that is *en route* to secretion is similar to the biogenesis of intraluminal vesicles of the MVB destined to lysosome degradation. In the first case, secretory MVBs subsequently fuse with the plasma membrane to release exosomes, while the seconds, degradative MVBs, are destined to fusion with the lysosome (Raposo and Stoorvogel 2013, Cocucci and Meldolesi 2015).

An unified mechanism for secretory ILVs inward budding/exosome biogenesis has not been defined yet, as it is likely that different exosome population exist in nature and are generated through different mechanisms starting at the endosomes. Some elements of the ESCRT machinery have been shown to be also involved in the biogenesis of some exosomes (Colombo, et al. 2013): this is regarded as the ESCRT-dependent mechanism of exosomes formation. Proteins such as the ESCRTI subunit Tsg101, as well as the accessory proteins Alix and ATPase VPS4 were identified as enriched in some exosomes purifications (Thery, et al. 2001, Pisitkun, Shen and Knepper 2004, Colombo, et al. 2013) and suggested to be important for secretory ILV formation (Géminard, et al. 2004, Hurley and Odorizzi 2012, Colombo, et al. 2013). In particular, Alix has been suggested to be important for the formation of the HSPG syndecans (Sdc1-4) -baring exosomes through interaction with the Sdc - adaptor syntenin (Baietti, et al. 2012, Hurley and Odorizzi 2012) and is, togeher with Tsg101, an important marker of exosomal EVs. The recruitment of proteins into ILVs/exosomes might involve the activity of chaperone proteins such as heat shock cognate 71 kDa protein (Hsc70) (Geminard, et al. 2001, Géminard, et al. 2004), that is also regarded as a frequent marker of exosomes by the Exocarta database.

In addition to ESCRT-associated mechanisms for exosome biogenesis and relese, also ESCRT-independent mechanisms of MVE biogenesis have been suggested to exist in mammalian cells (Stuffers, et al. 2009). First of all, a lipid-mediated mechanism of exosome formation has been suggested: a lipid enrichment on the the late endosomal membrane, in fact, has been associated

with the formation of ILVs, and lipid raft domains have been suggested to be present on the endosomes in the areas of exosome formation (de Gassart, et al. 2003). The maturation of the late endosome to MVB is characterised by formation of lipid enriched domains containing cholesterol, sphingomyelin and its hydrolysis product, ceramide, that also characterize the membrane of the exosome itself (Brouwers, et al. 2013, Wubbolts, et al. 2003). The sphingolipid ceramide, in particular, has been shown to be involved in the inward budding of ILV/exosome biogenesis in a mouse oligodendroglial cell line and is considered to drive an ESCRT-independent mechanism of exosome formation (ceramide-dependent mechanism) (Trajkovic, et al. 2008, Raposo and Stoorvogel 2013). The process is controlled by neutral sphingomyelinase (N-SMase), that catalyses the formation or sphingolipid ceramide from endosomal sphingomyelin (SM). A second ESCRT-independent mechanism for exosome generation involves the formation of endosomal membrane domains enriched in particular transmembrane proteins named tetraspanins (tertraspanins enriched domains – TEMs)(Hemler 2003), of which some of the most studied in the context of exosome biogenesis are CD63, CD81, CD83 an CD4 (van Niel, et al. 2011, Perez-Hernandez, et al. 2013).
The final step of outer MVB membrane fusion with the plasma membrane has been suggested to require a SNARE membrane fusion complex and NSF-ATPase (N-ethylmaleimide-sensitive factor). Vamp7 V-SNARE and Ykt6 R-SNARE have been for example identified as important for exosomal release (Fader, et al. 2009, Gross, et al. 2012). Morover, V0 subunit of vacuolar ATPase has also been suggested to play a role in membrane fusion events leading to exosome release, possibly in association with SNAREs (Marshansky and Futai 2008).

5.2.1.3.2 Ectosomes or microvesicles (MVs)

Ectosomes, also referred to as microvesicles (MVs) or shedding vesicles, are larger vesicles originating by direct budding from the plasma membrane. They are generally bigger than the exosomes, between 100 and 2000 nm of diameter, even if smaller vesicles can bud from the plasma membrane (down to 50 nm). Given the possible overlap in sizes, the biogenesis of the vesicle and the vesicle markers are the main distinction between the two types of EVs (Akers, et al. 2013, Cocucci and Meldolesi 2015). The outward budding that determines the formation of ectosomes is regulated and happens at small plasma membrane domains with a characteristic phospholipid distribution (Akers, et al. 2013). The formation and budding of ectosomes depends on both plasma membrane phospholipids and cortical cytoskeleton. Plasma membrane asymmetry seems to play a role in membrane budding leading to microvesicle release (Hugel, et al. 2005, Akers, et al. 2013, Cocucci and Meldolesi 2015): Aminophospholipid phosphatidylserine (PS) is generally located on the inner leaflet of the plasma membrane while other lipids such as phosphatidylcholine and sphingomyelin are more represented on the outer side. PS translocation to the outer side by plasma membrane and

randomization of lipid distribution between the two layers, with subsequent loss of asymmetry, is mediated by tranlocases and scramblases, which activation is calcium dependent (increase in calcium influx triggers vesicular release). This process has been suggested to play a fundamental role in budding of ectosomal vesicles from the cell.

At the same time, vesicle shedding has been suggested to be assisted by cytoskeletal remodelling at the plasma membrane (contraction/releasing), mediated for example by myosins. Rho GTPases have been suggested to be involved in the process (de Curtis and Meldolesi 2012, Antonyak, Wilson and Cerione 2012), and in particular ADP-rybosilation factor ARF6 has been suggested to determine myosin activation through phospholipase D (PLD) that is itself involved in actomyosin contraction necessary for ectosome shedding (Muralidharan-Chari, et al. 2009, Nightingale, Cutler and Cramer 2012, Akers, et al. 2013). It has also been seen that the plasma microdomains from which ectosomes shed are, similarly to the MVB ones, enriched in cholesterol, sphingomyelin, and its product ceramide, that contribute to the process of vesicle budding itself. In glial cells, it has been seen that ectosome formation is controlled by acid sphingomyelinase (A-SMase), that catalyse the formation or sphingolipid ceramide from membrane SM (Bianco, et al. 2009, Antonucci, et al. 2012).

It is important to remember that, in general, ectosome release is quicker than exosome one, not requiring exocytosis. In most cells, the release starts in few seconds after the secretion stimulus (ATP, Calcium influx/membrane depolarisation, etc…), whereas it generally takes minutes for the exosomes to be released (Cocucci and Meldolesi 2015)

5.2.1.3.3 Destiny of EVs after release

After release, EVs can either reach another cell or dissolve in the extracellular space releasing their content (Cocucci and Meldolesi 2015). This communication and transferring of information to another cell is crucial in several processes, such as cell immune response/inflammation, nervous system/synapsis, blood coagulation and cancer (Raposo and Stoorvogel 2013). In some cases, travelling vesicles have also a role in the modulation of the extracellular matrix (ECM) itself while they move, through their transmembrane proteases that distrupt the matrix; this might allow an easier invasion by cancer cells or macrophages (Muralidharan-Chari, et al. 2010, Cocucci and Meldolesi 2015). A number of vesicles are able to travel short or long distances (navigating EVs) into biological fluid such as blood and cerebrospinal fluid, and reach target cells, where they release their content (Cocucci and Meldolesi 2015). It is believed that target cell binding is quite specific for the different secreted vesicles and might depend on adhesion proteins such as integrins and tetraspanins on their surface (Hemler 2003, Rana, et al. 2012), as well as membrane bound glycoproteins such as galectins (Klibi, et al. 2009, Barres, et al. 2010). HSPGs have also been suggested to play a role in the process (Christianson, et al. 2013).

When the EVs reach the target cell, they can fuse with the plasma membrane or be internalised by endocytosis/phagocytosis (Raposo and Stoorvogel 2013). Fusion of EVs with the plasma membrane happens through a mechanism that does not involve SNAREs (Cocucci and Meldolesi 2015) and is activated by cell surface fusogen proteins. At the moment, the retroviral proteins syncytins, that can bind receptors on the cell membrane, have been suggested as fusogen proteins for exosome fusion to the target cell (Aguilar, et al. 2013, Pérez-Vargas, et al. 2014, Vargas, et al. 2014). Currently, it is not sure that the same fusion mechanism employing syncytins is valid also for shedded ectosomes (Cocucci and Meldolesi 2015).

In other cases, an endocytic mechanism determines the internalisation of the vesicle. Endocytosis may be clathrin mediated or involve micropinocytosis and phagocytosis, and it is likely that larger vesicles employ one of the latter two mechanisms to be internalised (Feng, et al. 2010, Fitzner, et al. 2011, Tian, et al. 2014). Actin cytoskeletal proteins, phosphatilinositol-3-kinase and dynamin (Tian, et al. 2014, Barres, et al. 2010, Raposo and Stoorvogel 2013) are involved in the process of EV-endocytosis by target cells. Once endocytosed, EVs generally fuse with endosome or phagosome. From the endosome, they can release their content the cytoplasm by back fusion with the endosomal membrane or can be targeted to the lysosome to be degraded.

Some vesicles, however, dissolve in the extracellular space once secreted releasing their content. Examples are the vesicles containing IL-1β or growth factors such as FGF2 or transforming growth factor beta (TGFβ) (Cocucci and Meldolesi 2015).

5.2.1.3.4 Markers of EVs

As suggested before, exosomes and ectosomes are also characterised by different molecular markers. The databases ExoCarta (http://www.exocarta.org) (Simpson, Kalra and Mathivanan 2012, Mathivanan and Simpson 2009, Keerthikumar, et al. 2016) and Vesiclepedia (http://www.microvesicles.org) (Kalra, et al. 2012) represent collections of proteins, but also lipids and RNAs associated with exosomes and ectosomes from different species and biological tissues and are useful tools to investigate EV-markers.

Given their origin from the late endosomal compartments / MVB, typical markers of the exosomes are proteins associated with MVB biogenesis, such as ESCRT machinery components (Alix, Tsg101, etc…) (Thery, et al. 2001, Pisitkun, Shen and Knepper 2004, Colombo, et al. 2013) as well as Hsc70 (Thery, et al. 2001, Géminard, et al. 2004) and annexins (Thery, et al. 1999, Thery, et al. 2001). Proteins derived from membrane microdomains have also been found significantly enriched in the exosomes: these include both tetraspanins from TEMs (CD9, CD63, CD81, etc…) (Kleijmeer, et al. 1998, Bobrie, et al. 2011) and lipid raft markers such as flotillin and GPI-anchored proteins (Wubbolts, et al. 2003). Moving to the lipid compositions, exosomes

are also rich in cholesterol, sphingomyelin and ceramide (Wubbolts, et al. 2003, Brouwers, et al. 2013) (**Table 5.1**). Ectosome typical markers are generally less described, as they mostly vary depending on the protein and lipid composition of the plasma membrane domain they originate from. It is known, for example, that flotillin can generally be used as a marker of both ectosomes and exosomes, being associated with lipid raft domains on both endosomes and plasma membrane (**Table 5.1**). Sphingomyelin and ceramide, as well, have been described in both contexts. Some ectosomes have been suggested to be specifically enriched in membrane-associated proteins such as Integrins, Arf6 and vesicle-associated membrane protein 3 (VAMP3), or even specific matrix metalloproteases (Dolo, et al. 1998, Taraboletti, et al. 2002, Muralidharan-Chari, et al. 2009, Akers, et al. 2013). Other studies have suggested the virus-like particle TyA and complement components C1a and C1q as possible ectosomes markers (Cocucci and Meldolesi 2015, Meldolesi 2016) (**Table 5.1**).

5.2.1.3.5 Apoptotic bodies

In addition to ectosomes and exosomes, another form of extracellular vesicle can be detected. These vesicles, named apoptotic bodies or apoptosomes, are released uniquely by cells undergoing programmed cell death and apoptosis, through a mechanism of membrane blebbing (Akers, et al. 2013). These vesicles are generally larger than both ectosomes and exosomes (500-5000 nm of diameter), but in some cases, smaller apoptotic vesicles between 50 and 500 nm have been identified (Akers, et al. 2013, Simpson and Mathivanan 2012). The main marker of apoptotic bodies is Annexin V, bound to PS on the plasma membrane (Akers, et al. 2013). Moreover, thrombospondin (TSP) and Complement component C3b have been proposed as apoptotic bodies markers (Akers, et al. 2013). Generally, once released, apoptotic bodies are phagocyted by macrophages (Elmore 2007).

Table 5.1: Extracellular vesicles (EVs). Abbreviations: PM = Plasma membrane; MVB = Multivesicular bodies.

EXTRACELLULAR VESICLES			
Name	**Biogenesis**	**Diameter**	**Markers**
Exosomes	MVBs: fusion of the limiting membrane of the MVB with PM	~ 30 - 100 nm	Proteins: CD9, CD63, CD81, Alix, Tsg101, Hsp70, Flotillin etc… Lipids: Sphyngomyelin, Ceramide
Ectosomes or Microvesicles	Shedding from plasma membrane – Living cells	~ 100- 2000 nm	Proteins: Dependent on origin PM - Flotillin, Vamp3, Integrins, TyA, C1a/C1q etc.; Lipids: Phosphatidylserine (PS), Sphingomyelin, Ceramide
Apoptotic bodies	Shedding from plasma membrane – necrotic cells	~ 500-5000 nm	Annexin V, TSP, C3b

5.2.2 Mechanisms of unconventional protein secretion

5.2.2.1 Unconventionally secreted proteins

A nuber of secreted proteins have been shown to lack an N-terminal ER signal peptide and to reach the cell surface by an ER-and Golgi independent pathway (Muesch, et al. 1990). These proteins are identified as "unconventionally secreted proteins" and are a group of cell surface bound, matrix-associated or soluble proteins often involved in particular in the regulation of cell growth, differentiation and immune response (Nickel 2003, Nickel and Seedorf 2008, Nickel and Rabouille 2009, Nickel 2010). Examples of unconventionally secreted proteins are fibroblast growth factor 2 or basic fibroblast growth factor (FGF2) (Mignatti, Morimoto and Rifkin 1992), some specific interleukins (IL) (Lopez-Castejon and Brough 2011), galectins (Sato, Burdett and Hughes 1993) and the characteristic acyl-coenzyme A (CoA) - binding protein (AcbA) from yeast or *Dictyostelium discoideum* (Manjithaya, et al. 2010a). Other less studied unconventionally secreted proteins are thioredoxin (Rubartelli, et al. 1992, Nickel 2003), and peroxiredoxin 1, the export of which is regulated by cytokines such as TGF-β1 (Chang, et al. 2006). Brefeldin A (BFA), a drug that completely blocks Golgi trafficking (Orcl, et al. 1991), does not affect the export of any of these signal-peptide lacking proteins (Nickel 2003). In addition, these proteins are generally characterised by not having post-translational modifications proper of the ER/Golgi space such as N-glycosylation, even if they might have consensus sites for glycosylation (Nickel 2003).

Unconventional secretion mechanisms can be distinguished between non-vesicular and vesicular mechanisms (Rabouille, Malhotra and Nickel 2012) (**Table 5.2, Fig. 5.1**). Non-vesicular mechanisms happen by direct translocation through the plasma membrane and can involve phospholipid binding and formation of channels, as in the case of the FGF2 unconventional secretion, or protein transporters. Vesicular mechanisms involve instead different types of membranous intermediates that carry the protein cargo: this includes the formation of internal cargo-containing vesicles in the endosome (MVB) and exosome secretion, MV direct formation at the plasma membrane, and particular secretory lysosomes.

Interleukin (IL) 1β secretion is associated with the inflammasome activity and has been initially suggested to employ a vesicular pathway of unconventional secretion for its export (Andrei, et al. 1999, Andrei, et al. 2004, Qu, et al. 2007). More recently, however, a non-vesicular unconventional export has been proposed for IL-1β, involving the permeabilisation of the plasma membrane (Shirasaki, et al. 2014, Martín-Sánchez, et al. 2016).

Alternative pathways such as that involving autophagosome processes might lead to unconventional secretion (Rabouille, Malhotra and Nickel 2012), as reported for the AcbA secretion (Manjithaya and Subramani 2010, Manjithaya, et al. 2010a). Proteolytic cleavage by cysteine proteases such as caspase-1 and calpain can be involved in the unconventional

secretion of a protein, as exemplified by the inflammasome/caspase-1 dependent secretion of IL-1β and for the IL-1α secretion (Brough, et al. 2003, Brough and Rothwell 2007, Keller, et al. 2008, Groß, et al. 2012).

Another small group of unconventionally secreted proteins exists in nature (Nickel and Rabouille 2009, Nickel and Seedorf 2008, Rabouille, Malhotra and Nickel 2012) which possess the leader sequence and are driven into the ER but reach the surface either in a Golgi independent manner (Baldwin and Ostergaard 2002) or in a COPII independent manner (Fatal, et al. 2004, Karhinen, et al. 2005). Examples of Golgi-independent leader peptide-containing unconventionally secreted proteins are cystic fibrosis transmembrane conductance regulator (CFTR) (Yoo, et al. 2002, Wang, et al. 2004) and *Drosphila melanogaster* alpha-integrins (Schotman, Karhinen and Rabouille 2008).

Table 5.2: Mechanisms of unconventional protein secretion.

KNOWN UNCONVENTIONAL SECRETION MECHANISMS	
Pathway	**Main unconventionally secreted proteins**
1) NON – VESICULAR MECHANISMS OF UNCONVENTIONAL PROTEIN SECRETION (LEADERLESS PROTEINS)	
Direct translocation across the plasma membrane	Fibroblast growth factor 2 (FGF2) [Ref. in 5.2.2.2.1]; Fibroblast growth factor 1 (FGF1) [Ref. in 5.2.2.2.3]; Galectins [Ref. in 5.2.2.2.2]; Interleukin -1α (IL-1α) [Ref. in 5.2.2.2.3] Annexin A2 [Ref. in 5.2.2.2.4]; Interleukin 1β (IL-1β) [Ref. in 5.2.2.3.2]; Thioredoxin [Ref. in 5.2.2.1]
Plasma membrane transporters (ABC)	Yeast pheromone a-factor; Leishmania spp. acylated surface protein B (HASPB); Drosophila germ cell attractants [Ref. in 5.2.1.2.5] etc…
2) VESICULAR MECHANISM OF UNCONVENTIONAL PROTEIN SECRETION (LEADERLESS PROTEINS)	
Autophagosome-like structures / CUPS	Dictyostelium AcbA /Yeast Acb1 [Ref. in 5.2.2.3.1]
Secretory lysosomes / Multivesicular bodies	Interleukin 1β (IL-1β) [Ref. in 5.2.2.3.2]; Transglutaminase-2 (TG2) [Ref. in 5.3.3]?
Shedding microvesicles	Interleukin 1β (IL-1β) [Ref. in 5.2.2.3.2]; Transglutaminase-2 (TG2) [Ref. in 5.3.3]?
3) UNCONVENTIONAL SECRETION OF LEADER-CONTAINING PROTEINS	
Golgi bypass	Cystic fibrosis transmembrane conductance regulator (CFTR); CD45; yeast Ist2; Drosophila α integrin (Nickel and Rabouille, 2009; Rabouille et al., 2012)
COPII bypass	Yeast heat-shock protein 150 (Hsp150) (Nickel and Rabouille, 2009)

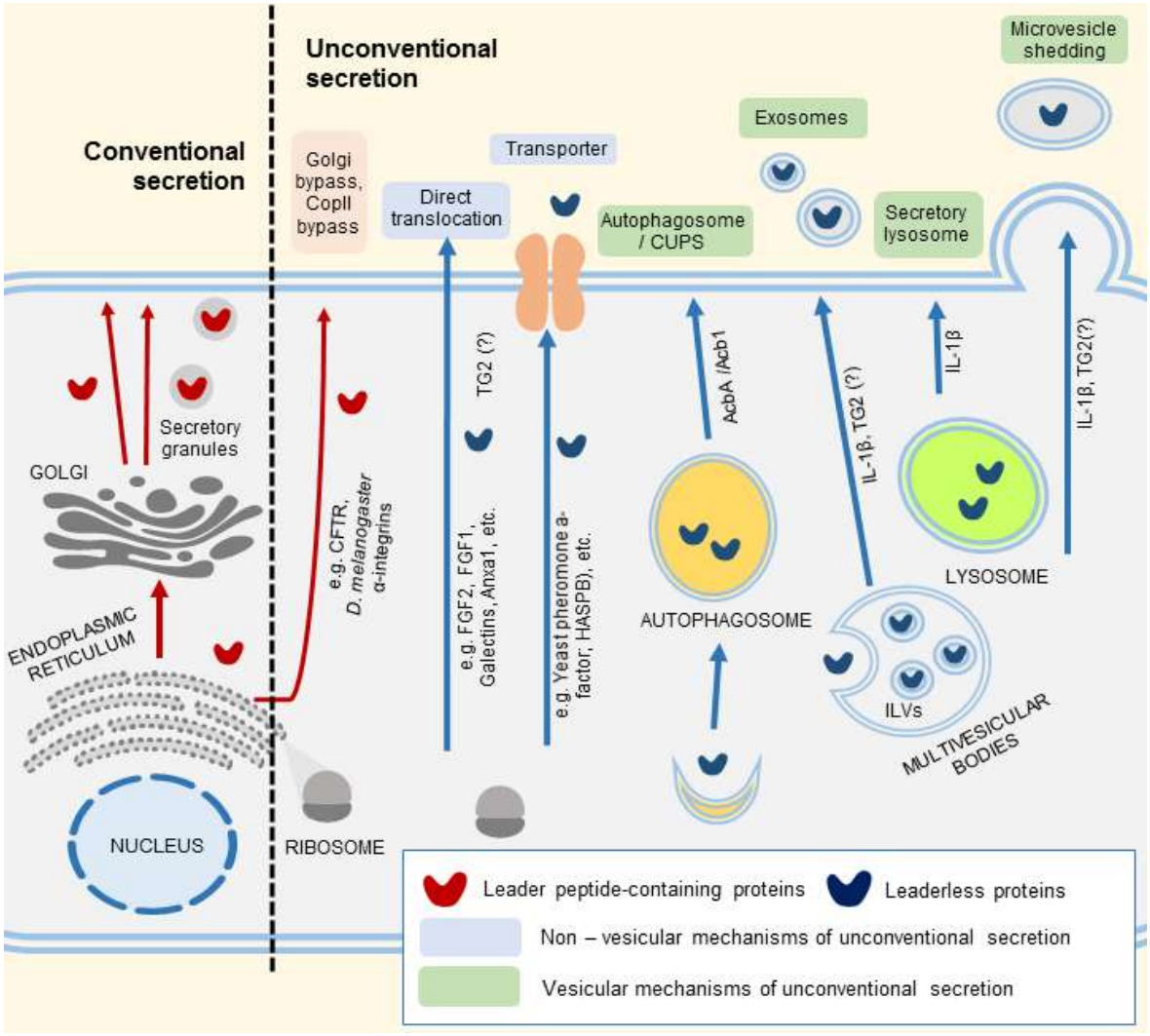

Figure 5.1: Mechanisms of unconventional protein secretion.

5.2.2.2 Non-vesicular mechanisms of unconventional protein secretion

5.2.2.2.1 Fibroblast growth factor 2 (FGF2)

The extracellular growth factor FGF2 is a protein belonging to the fibroblast growth factor family of heparin binding proteins and is involved in different functions outside the cells such as angiogenesis, wound healing, differentiation and migration (Nugent and Iozzo 2000). FGF2s lacks a signal peptide and was suggested to be secreted by an unconventional secretory pathway more than 20 years ago (Mignatti, Morimoto and Rifkin 1992). FGF2 has been reported to be secreted through a peculiar unconventional pathway that does not involve vesicular compartments (Schafer, et al. 2004, Nickel 2011, La Venuta, et al. 2015). The mechanism has been recently elucidated. FGF2 is exported by direct translocation through the plasma membrane and the process involves binding to plasma membrane phosphoinositides (PIPs) and heparan sulphate proteoglycans (HSPGs) (Temmerman, et al. 2008, Zehe, et al. 2006, Nickel 2007). According to Nickel and colleagues (Steringer, et al. 2012), FGF2 binding

to phosphatidylinositol 4,5-bisphosphate [PI(4,5)P2] on the inner side of the plasma membrane (Temmerman, et al. 2008) is the first main step: this is not only fundamental for the protein's targeting to the membrane, but also induces the oligomerisation of the protein and its inclusion in the lipidic bi-layer, with formation of an hydrophilic pore that disturbs the permeability barrier of the plasma membrane (Steringer, et al. 2012, Nickel 2011). Thereafter, HSPGs in the membrane proximity,on the extracellular surface of the plasma membrane, bind FGF2 though their long HS chains and facilitate the transport across the pore and towards the outside by means of a trapping mechanism (Zehe, et al. 2006, Nickel 2007). Curiously, FGF2 needs to be fully-folded to bind PI(4,5)P2, and through the whole process FGF2 remains in a fully-folded tertiary structure, while, normally, proteins that are transferred through conventional protein channels need be unfolded for translocation (Backhaus, et al. 2004, Torrado, et al. 2009).

FGF2 phosphorylation (Tyr83) has been suggested as a further key step to initiate the secretion of the protein. Phosphorylation is performed by a specific Tec non-receptor tyrosine kinase and might be determinant for the protein binding to phosphoinositides and translocation to the inner side of the plasma membrane (Ebert, et al. 2010, La Venuta, et al. 2016). Tec Kinase activity is itself controlled by Src- tyrosine kinases, that determine the activation of Tec and its translocation to the inner side of the plasma membrane by aims of the Tec kinase PH (plakstrin homology) domain that binds phosphoinositides (Nickel 2011). Recently, also sodium/potassium ATPase ATP1A1 has been shown to be involved in the export mechanisms by recruiting FGF2 at the inner leaflet of the plasma membrane (Zacherl, et al. 2015, La Venuta, et al. 2015).

In addition to the FGF2, other unconventionally secreted proteins have been suggested to follow a non-vesicular secretory mechanism. Among these proteins we can cite the other member of FGF family fibroblast growth factor 1 (FGF1), the plasma membrane associated proteins annexins A1 and A2 (Anxa1, Anxa2), cell surface/ECM lectins and the Leishmania hydrophilic acylated surface protein B (HASPB), that were suggested in the past to be synthesized in the cytosol and secreted by translocation across the plasma membrane that does not involve vesicular formation (Stegmayer, et al. 2005, Deora, et al. 2004, Rabouille, Malhotra and Nickel 2012, Seelenmeyer, Stegmayer and Nickel 2008). These less understood pathways are described in the next section.

5.2.2.2.2 Galectins

Lectins are a family of carbohydrate binding proteins. Among them, galectins specifically bind β-galactoside sugars and can be observed in the extracellular matrix (ECM) in association with ECM β-galactoside-containing glycoproteins or glycolipids and cell surface β-galactoside-containing counter receptors. In the extracellular space, they are involved in functions such as

receptor-mediated signalling, cell adhesion and apoptosis (Liu and Rabinovich 2005). In the past, extracellular trafficking of galectins was seen to involve blebbing of EVs from the plasma membrane (Cooper and Barondes 1990, Mehul and Hughes 1997, Hughes 1999), but more recently the formation of vesicles (either by direct blebbing or exosomes formation) was excluded at least for galectin 1 (Gal-1). Binding to cell surface β-galactoside containing glycoproteins or glycolipids (counter receptors) has been shown to be necessary for Gal-1 export across the plasma membrane with a process that might be similar to the HSPGs-FGF2 interaction. Glycoprotein/Gal-1 binding however might occur inside the cell and act in a different way in the export of the lectin (Seelenmeyer, et al. 2005). Similarly to FGF2, the export of Gal-1 happens in a fully folded state (Backhaus, et al. 2004).

5.2.2.2.3 Fibroblast growth factor 1 (FGF1)

FGF1 is a member of the fibroblast grow factor family mainly known for its role in angiogenesis and, similarly to FGF2, is characterised by an ER/Golgi-independent secretion. Differently from FGF2, that is generally secreted by the cells without the necessity of a stimulus (Florkiewicz, et al. 1995), FGF1 is secreted by the cells as a consequence of different stresses, first of all the heat shock (Jackson, et al. 1992, Jackson, et al. 1995). FGF1 was suggested to be exported by non-vesicular translocation across the plasma membrane following heat shock triggering, and to be released by the cells as a biologically inactive homodimer, formed as a result of cysteine (Cys) oxydation, which seems to be necessary for the protein secretion (Jackson, et al. 1995, Tarantini, et al. 1995). FGF1 protein is exported as part of an S100 release complex: upon stress, FGF1 is translocated in the proximity of the plasma membrane, and binding to the release complex precedes and determines the export of the protein itself (Prudovsky, et al. 2002). The complex requires S100A13, which is also an unconventionally secreted protein, structurally similar to calmodulin (Landriscina, et al. 2001). Other fundamental components are leader-less proteins 40kDa portion of synaptotagamin 1 (Syt1) (Tarantini, et al. 1998) and sphingosine kinase 1 (Soldi, et al. 2007). The stress-induced aggregation of the multiprotein complex at the inner side of the plasma membrane has been suggested to be copper(Cu^{2+}) - dependent and the components of the complex itself are all Cu^{2+}-binding proteins. Once the complex of FGF1 is formed, the translocation across the plasma membrane has been shown to happen through a complex-induced phosphatidylserine (PS) “flipping mechanism”(Kirov, et al. 2012). Similarly to FGF2, FGF1 and the components of the complex have been shown to bind acidic phospholipids such as PS and PIPs with high affinity on the inner side of the plasma membrane and induce membrane destabilisation upon binding to specific phosphatidylcholine-free membrane domains(Graziani, et al. 2006).

Interleukin -1α (IL-1α) has been reported to share most of the characteristics of FGF1 secretion, including the copper-dependent complex formation with S100A13 and phospholipid

binding- dependent translocation, however, the protein is secreted as a monomer and the secretion complex does not include Syt1. An alternative component of the complex which has been identified is calpain, another calcium binding protein that associates with annexin 2 at the plasma membrane inner side. For a reference, see (Prudovsky, et al. 2003).

5.2.2.2.4 Annexin A2

Annexin A2 (Anxa2) is a membrane binding member of the annexin family with a role in signal transduction and stress response. Anxa2 is known to bind directly PI(4,5)P2 phosphoinositides at the inner side of the plasma membrane in a calcium dependent manner (Rescher, et al. 2004) and to determine the phospholipid clustering in microdomains (Gokhale, et al. 2005, Menke, Gerke and Steinem 2005). Similarly to FGF1, Anxa2 forms an heterotetramer with the S100 protein member S100A10, which is bound to the plasma membrane through PIP2-Anxa2 binding in a Tyr phosphorylation dependent manner (Deora, et al. 2004). Also , Anxa2 is known to be able to form oligomers with FGF1-release complex, and the formation of oligomers might be involved in the process of protein translocation or FGF1 targeting to the plasma membrane (Prudovsky, et al. 2003, Prudovsky, et al. 2008, Rabouille, Malhotra and Nickel 2012).

There is no complete agreement on Anxa2 unconventional secretion, as some studies have also suggested a vesicular export through incorporation into intraluminal vesicles of MVB and subsequent release as exosomes(Valapala and Vishwanatha 2011, Deora, et al. 2004) or interaction with SNAREs (Danielsen, van Deurs and Hansen 2003).

5.2.2.2.5 Proteins employing ABC transporters for translocation

Translocation across the plasma membrane in a vesicle-independent manner is mediated by plasma membrane ATP-binding cassette (ABC) transporters. The general characteristic of proteins released through ABC transporters is to be lipidated (Rabouille, Malhotra and Nickel 2012) and the lipid chain might function for protein targeting to the inner leaflet of the plasma membrane in close proximity to the trasporter. For example, pheromone a-factor from yeast, a farnesylated protein, is externalized through the ABC transporter Ste6p (Kuchler, Sterne and Thorner 1989, Michaelis 1993). Other unconventionally secreted proteins from different eukaryotic species have been reported to be lipidated and secreted through ABC transporters, not only yeast and proteozoan parasites but also species of higher complexity such as *Drosophila spp.* (Ricardo and Lehmann 2009) suggesting ABC-transporter translocation as a common conserved mechanism of protein secretion across the plasma membrane.

5.2.2.3 Vesicular mechanisms of unconventional protein secretion

Differently from the proteins described in the previous paragraphs which follow a non-vesicular transport mechanism, a second group of leaderless proteins have been suggested to follow an unconventional secretion mechanism that involves vesicular intermediates. The two more characteristic proteins in this group are the acyl-CoA binding protein (AcbA) from Dictyostelium spp (Cabral, et al. 2010) and IL-1β.

5.2.2.3.1 Acyl-CoA binding protein (AcbA/Acb1)

AcbA is secreted by *Dictyostelium spp.* cells upon starvation, and is subsequently subjected to cleavage in the extracellular space to produce SDF-2, a smaller peptide involved in signalling and necessary for formation of spores (Richardson, Loomis and Kimmel 1994). The secretion of AcbA and its yeast homologue Acb1 has been reported to require vesicular fusion and does not involve cell surface transporters (Cabral, et al. 2010, Kinseth, et al. 2007). The secretion of AcbA/Acb1 involves a number of factors proper of autophagosome biogenesis [phosphatidylinositol (3,4,5)-trisphosphate PI(3,4,5)P3 and autophagy-related proteins (Atg) are the main examples], suggesting that the export of the AcbA/Acb1 happens through autophagosome-like vesicles (Duran, et al. 2010, Manjithaya, et al. 2010b). However, a series of elements involved in MVBs formation and endosomal fusion through SNAREs were also identified as key elements in the process (Duran, et al. 2010, Manjithaya, et al. 2010b), as well as the Golgi reassembly-stacking proteins (GRASPs, Grh1 in yeast) (Kinseth, et al. 2007, Duran, et al. 2010, Bruns, et al. 2011), primarily involved in vesicle fusion with Golgi and stacking of Golgi cisternae.

Secretion pathway starts from the formation of "cup-shaped" membranes, named CUPS (compartment for unconventional protein secretion) which form at the proximity of Sec13-containing ER exit in a starvation-dependent manner, are rich in PI(3,4,5)P3 phospholipids and contain GRASPs as well as autophagy-related proteins such as Atg9 and Atg8 (Bruns, et al. 2011, Malhotra 2013). AcbA/Acb1 are recruited in this area possibly via acylation, then the cargo containing vesicle detaches from CUPS (Malhotra 2013), reaches endosomal MVB compartment in a process that is dependent from the t-SNARE Tlg2, the Rab family GTPase Ypt6/Rab6 and ESCRT-I protein Vps24 (Duran, et al. 2010), and it is likely to be internalised as a luminal vesicle of the endosome (Malhotra 2013). While starvation dependent degradative autophagosomes end up fusing with the vacuole, these CUPS-derived secretion autophagosomes/MVBs fuse with the plasma membrane for secretion, in a process involving a specific plasma membrane tSNARE (Sso1) (Bruns, et al. 2011).

5.2.2.3.2 Interleukin 1β (IL-1β)

Interleukin 1β is another well studied unconventional secreted protein (Rubartelli, et al. 1990) and a central mediator in inflammatory response induced by inflammasome activation, also known to contribute to chronic diseases and tissue injury (Latz 2010). The main secretory stimulus is the ATP-dependent activation of purinergic receptor P2X7, a nucleotide-gated ion channel that induces inflammasome assembly and is necessary for IL-1β secretion (Ferrari, et al. 2006, Pelegrin, Barroso-Gutierrez and Surprenant 2008), supported by K^+ efflux from the channel, which is the necessary signal that triggers inflammasome assembly, and Ca^{2+} and Na^+ influx, involved in membrane depolarization and intracellular signalling. In particular, calcium influx has been proven to be necessary for microvesicle formation through depolarisation of the plasma membrane (loss of asymmetry) and dissociation of cytoskeletal actin from membrane glycoproteins (Burnier, et al. 2009). P2X7 also drives the formation of a "membrane pore", that allows the passage of larger cations through the membrane (Ferrari, et al. 2006, Browne, et al. 2013).

The inflammasome is a multi-molecular complex and its assembly determines auto-processing of pro-caspase 1 to activated caspase 1 (Kahlenberg and Dubyak 2004). The cleaveage of pro-IL-1β to active IL-1β is performed by active caspase-1 (Martinon, Burns and Tschopp 2002, Brough and Rothwell 2007, Denes, Lopez-Castejon and Brough 2012), which is itself activated by cleaveage upon iflammasome assembly (Ferrari, et al. 2006), and is thought to be important for IL-1β secretion.

In the last decades, a series of vesicular secretion pathways have been suggested for IL-1β. One involves formation of "lysosome-like" structures regarded as secretory lysosomes, lysosomes that instead of undergoing degradation are secreted at the level of the plasma membrane and contain both activated IL-1β and caspase 1 (Andrei, et al. 1999, Andrei, et al. 2004). Autophagy was also suggested to play a role in the formation of this secretory lysosomal structures (Harris, et al. 2011). In other cases, the formation of MVB and release of exosomes was suggested for IL-1β secretion (Qu, et al. 2007), while some authors where pointing at MV shedding preceded by phosphatidylserine (PS) flipping at the outer side of the membrane as a possible mechanism (MacKenzie, et al. 2001).

More recently, however, a different mechanism was suggested for IL-1β secretion, a mechanism that does not involve a vesicular compartment formation (Harris, et al. 2011), but instead happens by direct translocation through an hyperpermeabilised plasma membrane domain (Shirasaki, et al. 2014, Martín-Sánchez, et al. 2016), with phosphatidylserine (PS) flipping induced by P2X7 receptor activation, and can be due to a caspase dependent apoptotic process named pyroptosis (Martín-Sánchez, et al. 2016, Brough and Rothwell 2007), known to lead to protein leaking during inflammation (Brough and Rothwell 2007).

It is important to see that both IL-1β and the abovementioned IL-1α are synthesised by the cells as precursor proteins of the same length (31 kDa), but only IL-1β needs to be cleaved to be activated and bind the specific interleukin receptor IL-1RI, while IL-1α is active in its unprocessed form (Dinarello 1996). Calcium dependent calpain seems to be involved, instead, in IL-1α cleaveage and secretion (Groß, et al. 2012, Brough, et al. 2003). Even if not directly involved in IL-1α claveage, however, inflammasome activation and subsequent Caspase-1 activation seem to be necessary for the process of IL-1α secretion either by determining Calpain activiation (Groß, et al. 2012) or by direct cleavage of pro-IL-1α (Keller, et al. 2008). In addition to this, caspase 1 has been suggetsed to play a role in other protein secretion, such as FGF2, annexin A2, galectin 3 and peroxiredoxin 1 (Keller, et al. 2008).

5.2.3 Transglutaminase 2 is an unconventionally secreted protein

As described in Chapter I, transglutaminase-2 (TG2) is an enzyme primarily located in the cytoplasm of the cells, but it can also be localized in the plasma membrane and extracellular environment and, as a consequence, it is involved in several ECM processes. Despite being clearly released by living cells, TG2 lacks a signal peptide necessary for ER/Golgi conventional secretion (Ichinose, et al. 1990, Ikura, et al. 1988).

The TG2 unconventional secretory route has been the focus of research of different groups for many years now. Some elements have been identified in literature as important for TG2 secretion even if a complete mechanism was not elucidated.

An intact FN binding N-terminal β-sandwich domanin was suggested to be crucial for TG2 secretion (Gaudry, et al. 1999, Chou, et al. 2011). TG2 binds FN with high affinity and the binding site is located on the N-terminal side of the β-sandwich domain of TG2, independent from TG2 conformation and activity (Jeong, et al. 1995). Removal of these aminoacids was shown to prevent TG2 secretion to the cell surface of both an inducible system of Swiss 3T3 fibroblast and NRK52E renal tubular epithelial cells (Gaudry, et al. 1999, Chou, et al. 2011), however, secretion was proven not to be dependent on FN binding, as FN deletion was not affecting the export (Chou, et al. 2011). Interestingly, the motif detected (aminoacids 88-106) (Chou, et al. 2011) determines the formation of an “hairpin structure” exposed on the surface of TG2, that was suggested to be crucial for TG2 correct folding in a tertiary structure necessary for the enzyme secretion (Chou, et al. 2011). Active state conformation was found to be important for TG2 secretion in transfected 3T3 finroblasts (Balklava, et al. 2002). Moreover, TG2 binds HSPGs with high affinity, and this interaction has been proven to be central for TG2 secretion and localisation on the cell surface by our group (Scarpellini, et al. 2009, Lortat-Jacob, et al. 2012) and confirmed by others (Wang, et al. 2012).

Overall, three routes for TG2 unconventional secretion were proposed in the past few years. Belkin and colleagues showed that N-ethylmaleimide NEM, a specific inhibitor of NSF ATPase (an enzyme involved in membrane fusion), or NSF-mutant clones, led to impaired TG2 release in the ECM by NIH3T3 fibroblasts and concluded that TG2 is more likely to be secreted though an intracellular vesicular intermediate (Zemskov, et al. 2011). Indeed, it was previously shown that nitric oxide (NO) -mediated inhibition of membrane fusion, via nitrosylation of NSF-ATPase, interfered with TG2 secretion (Santhanam, Berkowitz and Belkin 2011, Jandu, et al. 2013). By immunofluorescent stainings and immunoprecipitation approaches on a model of transfected NIH3T3 fibroblasts with inducible TG2 sinthesis, it was suggested that TG2 is recruited after synthesis at the level of the Peri Nuclear Recycling Compartment (PNRC) and delivered into recycling vesicles. The small GTPase Rab11, that regulates recycling endosomes formation and delivery to the plasma membrane, was localized in the proximity of TG2 and was confirmed necessary for its secretion by siRNA tranfection, together with specific SNAREs associated with endosome-to-plasma membrane movements. The authors also suggested that phosphinositide binding [mainly PI(3)P and PI(4)P] was necessary for TG2 loading into vesicles at the level of PNRC. A phosphoinisitides binding site for TG2 was mapped in the sequence 590-KIRILGEPKQRKK-602 (Zemskov, et al. 2011), that contained the basic positively charged cluster subsequently suggested for Heparin sulphate (Lortat-Jacob, et al. 2012). By fluorescent immunostaining and immunoprecipitation, TG2 was found into the same recycling vesicles of internalized α5β1. Integrins were not necessary for TG2 loading, although the two elements were exported in complex on the cell surface (Zemskov, et al. 2011) .

J. van den Akker and co-authors from the university of Amsterdam proposed that TG2 was released from cells by microvesicle formation by smooth mucle cells, though a mechanism likely to depend on the crosslinking activity of TG2 (van den Akker, et al. 2012). TG2 crosslinking activity was suggested to be necessary for the release of these TG2-containing vesicles from the cell surface, probably involving a process of cytoskeletal remodelling necessary for the formation of the microvesicle itself (van den Akker, et al. 2012). This observation is consistent with the requirement of Ca^{2+} for TG2 secretion also reported by others (Zemskov, et al. 2011). Furthermore, a necessary stimulus for TG2 secretion in this model was TG2 redox state (Glutahione S-transferase, Thioredoxin reductase etc.) that breaks Cys-Cys disulphide bonds and allows conformational changes necessary for the Ca^{2+} dependent activation (van den Akker, et al. 2011, van den Akker, et al. 2012).

Cerione's group in the context of cancer-associated microvesicle formation (Antonyak, et al. 2011) also identified TG2 as associated with microvesicles through a MS-proteomic approach, and identified secretory microvesicles containing TG2 as independent from the conventional ER-Golgi trafficking as well as from the MVB formation. TG2 was mainly found localised on the outer side of the vesicles and FN was co-localised with TG2 on these vesicles. The authors

suggested that, despite TG2 was loaded into these vesicles, the formation of the vesicles as well as their shedding was independent from the protein itself and its catalytic activity (Antonyak, et al. 2011).

Recently, Aeschlimann's group has employed differentiated macrophages known to secrete IL-1β in a P2X7 receptor (P2X7R)/inflammasome – dependent manner, and suggested that the purinergic P2X7 receptor was necessary TG2 secretion as well (Adamczyk, et al. 2015). Using a combination of an ATP homologue for P2X7 receptor stimulation and P2X7R inhibitors, as well as transfection of P2X7R in cells naturally lacking P2X receptors, it was proposed that TG2 secretion is dependent on P2X7-receptor activation. The Ca^{2+} dependent catalytic activity of TG2 was found not to be crucial for the enzyme secretion. According to this model, although P2X7R stimulation determines an increase in extracellular vesicle secretion (shedded microvesicles/ectosomes), TG2 was secreted in soluble form and TG2 release was independent from microvesicle shedding (which is dependent on Ca^{2+} influx through P2X7R) and exosome formation. In particular, cell surface protrusions co-localised with TG2 were observed but were not detaching from the plasma membrane. Despite being attributed to P2X7R activation, TG2 release didn't involve inflammasome assemblation processes or cleaveage, neither involved the P2X7R Ca^{2+} channel function necessary for microvesicle shedding. Instead, the proposed secretion pathway involved the pore formation function of P2X7 receptor induced by ATP binding and regulated by calcium levels, and direct tranlocation of TG2 through the pore, in a catalytic activity-independent manner (Adamczyk, et al. 2015). Moreover, they suggested that Thioredoxin 1, an unconventionally secreted protein involved in redox activation of TG2 (Chapter I) was exported as well through the pore together with TG2 and might function as TG2 chaperone through secretion (Adamczyk, et al. 2015).

In conclusion, different mechanisms have been suggested for TG2 unconventional secretion in cell ines, however, no complete understanding has been obtained yet. Moreover, no investigation has been undertaken to study release *in vivo*. The association of TG2 with vesicular compartment seems to suggest a vesicular transport for TG2, however it was also shown in other systems that TG2 might not be associated directly with the vesicles.

Table 5.3: Hypotheses of TG2 unconventional secretion.

HYPOTHESES OF TG2 UNCONVENTIONAL SECRETION		
Zemskov et al., 2011; Santhanam et al, 2011	**Recycling endosome – derived secretion**	Dependent on Rab11, phosphinositide binding [PI(3)P, PI(4)P], Calcium influx, NSF-ATPase. Co-localise with integrin α5β1 in vesicles.
van den Akker et al., 2012	**Shedding microvesicles**	Release dependent on TG2 activity, dependent on reducing agent for TG2.
Antonyak et al., 2011		Independent from TG2 catalytic activity, co-localise with Fibronectin in vesicles.
Adamczyk et al., 2015	**Direct translocation through membrane pore**	Dependent on P2X7 receptor, Independent from Calcium/ TG2 activity. Co-localise with Thioredoxin 1 during export.

5.3 EXPERIMENTAL PROCEDURES

5.3.1 Experimental design

- As proteins involved in SNARE-mediated membrane fusion-exocytosis were identified in the TG2 interactome in kidney membranes, the need for membrane fusion for TG2 release is investigated in this chapter by employment of an NSF-ATPase inhibitor on TECs (**Fig. 5.2A**).
- As a number of TG2-associated proteins in kidney membranes have been found to belong to EV, mainly exosomes, this chapter also reports on the isolation of EV subpopulations and characterisation of TG2 in exosomes and ectosomes, with employment of inhibitors of EV biogenesis (**Fig. 5.2B**).
- Analysis of the known mechanisms of unconventional secretion, presented in the introduction of this chapter, has shown that many unconventionally secreted proteins are targeted to specific membranes by binding to acidic phospholipids; moreover, specific proteins' phosphorylation events were recognized to be involved in the export of some unconventionally secreted protein. For this reason, an initial analysis of both the binding capacity of TG2 to membrane phospholipids and and the degree of phosphorylation of TG2 in immunoprecipitates from TECs is provided in this chapter, as outlined in **Fig. 5.2C-D**.
- Lastly, having clathrin and CCV-associated proteins been found to be largely associated with TG2 in its interactome, the role of clathrin extracellular TG2 localisation and abundance will be examined (**Fig. 5.2E**).

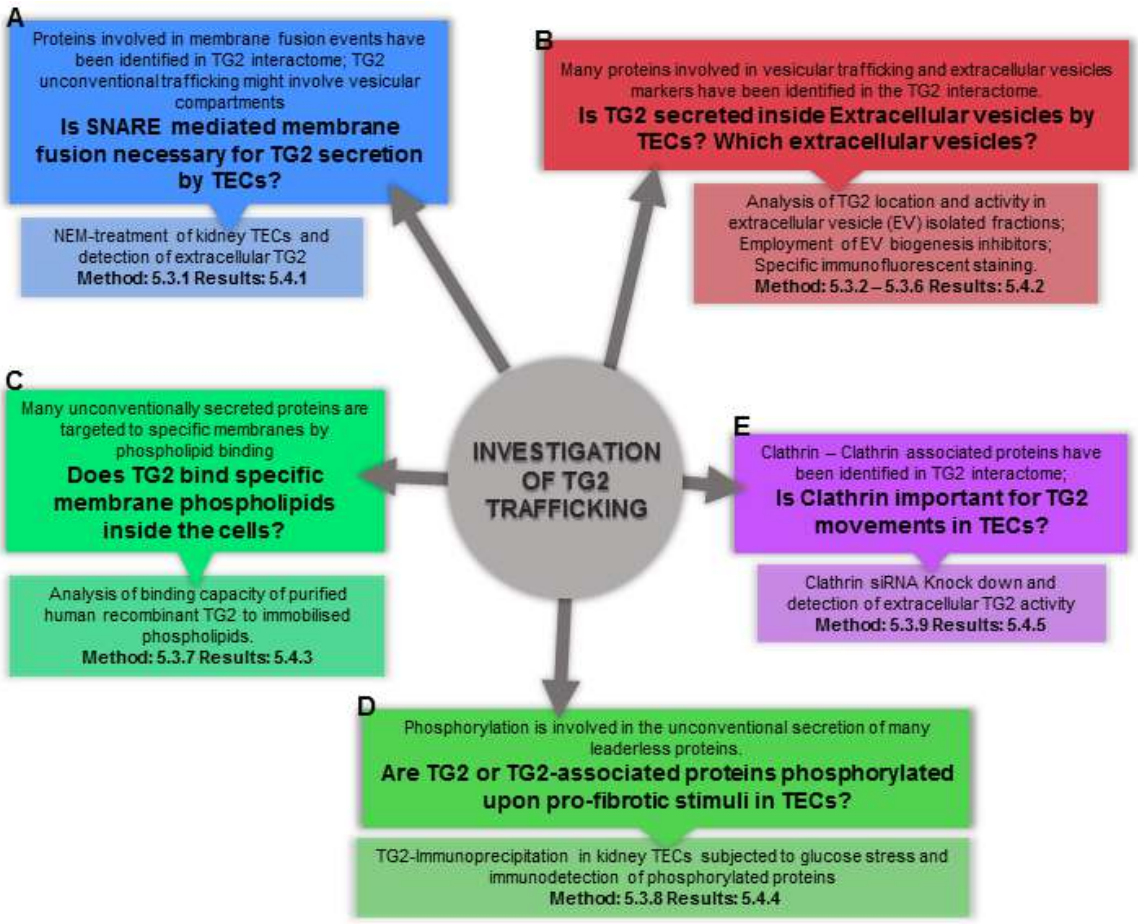

Figure 5.2: Experimental design for the investigation of TG2 unconventional secretion from TECs.

5.3.2 N-ethylmaleimide (NEM) treatment of kidney TECs

N-ethylmaleimide (NEM) is a specific inhibitor of NSF (N-ethylmaleimide-sensitive factor) ATPase, a protein necessary for the majority of intracellular vesicular trafficking and membrane fusion events. NSF-ATPase is an ATPase necessary for membrane fusion mediated by SNAREs (Zhao, Slevin and Whiteheart 2007) and is involved in both intracellular membrane fusion and secretion, including ER-Golgi derived vesicles (Block, et al. 1988, Beckers, et al. 1989), endosome membrane fusion and recycling endosomes (Rodriguez, Stirling and Woodman 1994, Mallard, et al. 2002), secretion of granules from platelets (Polgar and Reed 1999), and, importantly for the current study, exosome secretion by MVB fusion (Fader, et al. 2009). As its main function, NSF ATPase acts together with SNAPs and employs the energy of ATP hydrolysis to disassemble SNARE complexes after membrane fusion, allowing their recycling (Barnard, Morgan and Burgoyne 1997, Ryu, Jahn and Yoon 2016).

In order to test the effect of NSF ATPase inhibition on TG2 release, NRK52E WT or EGFP-TG2 overexpressing NRK52E (clone #C5) cells were cultured in normal culture conditions as described in 2.2.1, either in T-25 flasks (for biotin-cadaverine incorporation assay) or in 8-

wells chamber slides (for immunofluorescent staining), until 90% confluent. At this point, medium was supplemented with 0.6 mM NEM (E3876, Sigma) and cells were incubated for 30 min at 37°C in the presence of the inhibitor, as suggested by previous literature (Zemskov, et al. 2011). NEM stock solution was prepared in sterile water at a 100 mM concentration (12.5 mg/ml), and stored at -20°C. Aqueous solutions are reported to be instable (Sigma guidelines) hence, the solution was stored for short periods of time, and prepared fresh if older than a week.

After incubation, cell viability was measured by LDH bioassay (2.2.1.7), while the effect on extracellular TG2 was measured by either biotin-cadaverine incorporation assay performed on living cells or immunofluorescent staining of extracellular TG2, as described in the general methods (2.2.8 - 2.2.9).

5.3.3 Isolation of extracellular vesicles (EVs) from cell medium by differential centrifugation

In order to investigate the possible release of TG2 into vesicular compartments, EVs have been isolated from cell medium by differential centrifugation, by adapting the method described by Bianco and colleagues in 2009 (Bianco, et al. 2009). The different stages of the isolation are summarized in **Fig. 5.3**.

5.3.3.1 Cell culture and treatments

For EVs isolation from conditioned medium, NRK52E WT, NRK49F WT and EGFP-TG2 overexpressing NRK52E (clone #C5) cells were cultured in T-175 flasks, in the normal culture conditions described in the general methods (2.2.1.1), until 80% confluent. At this stage, cell monolayers were washed twice with PBS to remove every FBS trace, as animal serum contains vesicular components (exosomes, ectosomes and apoptotic bodies) that might interfere with the analysis (Shelke, et al. 2014, Eitan, et al. 2015). After washing, the medium was replaced with serum-free DMEM and cells were cultured for additional 36 hours.

In some cases, cells were stimulated by adding recombinant TGF-β1 (10 ng/ml) to the serum-free medium during the 36 hours of incubation, to simulate a pro-fibrotic condition *in vitro*. In other cases, glucose stress was performed by culturing the cells in a T175 culture flask in DMEM medium containing 5.5 mM D-Glucose (low glucose, physiological condition) and supplemented with 2% (v/v) heat-inactivated FBS, 2mM L-glutamine and 100 IU/mL penicillin - 100 μg/mL streptomycin until 80% confluent. The cells were then washed twice with PBS pH 7.4, the medium was replaced with serum-free medium containing either 5 mM (low) or 30

mM (high) glucose and cells were grown for a further 36 h. In specific experiments, vesicular trafficking inhibitors reported in paragraph 5.3.5 were added to the serum-free medium, and incubations were performed over appropriate times.

5.3.3.2 EVs Isolation by differential centrifugation

After incubation, conditioned medium was collected and supplemented with protease inhibitors (cOmplete™ EDTA-free protease inhibitors from Sigma). Cells monolayer was washed twice with PBS pH 7.4, scraped in PBS and the pellet collected by centrifugation at 500 g for 5 min. Pelleted cells were lysed in radiommunoprecipitation assay (RIPA) buffer [50 mM Tris-HCl pH 8, 150 mM NaCl, 1% (v/v) NP40, 0.5% (w/v) sodium deoxycholate, 0.1% (w/v) SDS] following the lysis protocol reported in 2.2.3 (**Fig.5.3**).

Conditioned medium was centrifuged 3 times at 300 g for 10 min at 4°C to remove remaining cells (P1), and supernatant (S1) was centrifuged at 1,200 g for 20 min at 4°C to remove large cell debris and apoptotic bodies (P2). Supernatant (S2) was centrifuged 10,000 g for 30 min at 4°C to collect the microvesicular/ectosomal portion (P3), and the supernatant (S3) was centrifuged at 110,000 g for 1 h at 4°C in order to collect the exosomes (P4). All pellets obtained were resuspended in equal volumes (40 µl) of RIPA buffer (**Fig.5.3**).

After the last centrifuge, the remaining EV-free medium (S4) was collected and residual proteins were precipitated using trichloroacetic acid (TCA) as it follows: 1:10 volume of TCA was added to the medium, mixed well, and the mixture was incubated for at least one hour on ice. The mixture was then divided into single conic bottom Eppendorf tubes and centrifuged for 5 min at 13,000 rpm. The supernatant was discarded and pellet was washed with cold acetone (1 ml/pellet) by centrifuging it again for 5 min at 13,000 rpm. The obtained pellet was air-dried and resuspended in 40 µl of RIPA buffer (**Fig.5.3**).

5.3.3.3 Immunoprobing of specific proteins in cell and EVs lysates

Depending on the specific experiment, equal amounts (15-25 µg) or equal volumes (40 µl) of proteins were resolved by 12% (w/v) acrylamide/bis-acrylamide SDS-PAGE under reducing condition. Immunodetection of the proteins of interest was performed by Western blot (described in Chapter II, 2.2.7) using the antibodies reported in **Table 5.4** in blocking buffer [5% (w/v) non-fat milk in TBST pH 7.4]. Flotillin-2 (Flot2) is a lipid raft protein and was employed as a marker for both ectosome and exosomes (Wubbolts, et al. 2003, Antonyak, et al. 2011). Immunoreactive bands were detected by enhanced chemiluminescence after incubation with an appropriate HRP-conjugated secondary antibody (**Table 5.4**) in blocking buffer as described in the general methods. Image acquisition was performed with a LAS4000 imaging system (GE Heathcare).

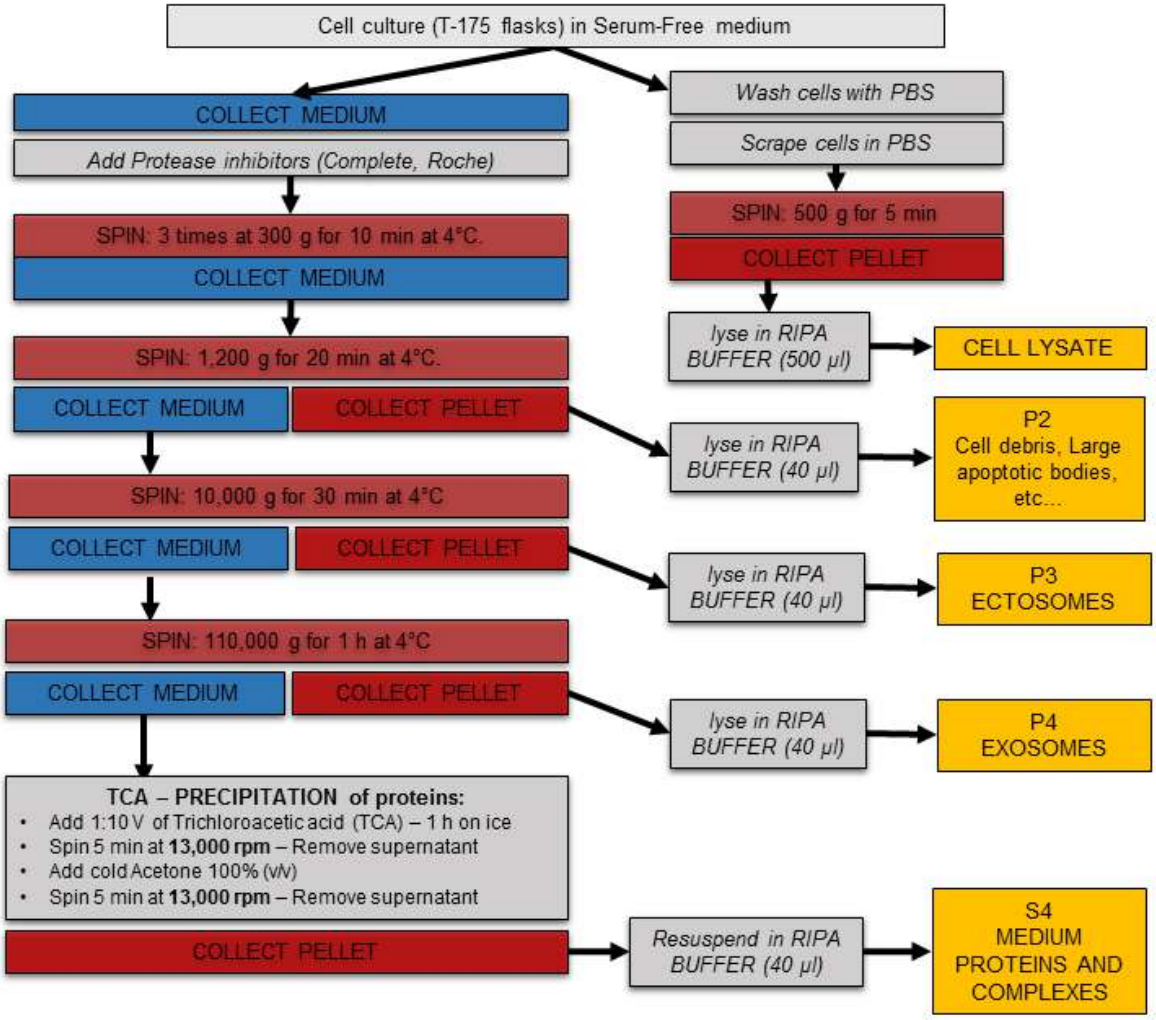

Figure 5.3: Outline of the experimental procedure for extracellular vesicles isolation by differential centrifugation. Method adapted from (Bianco, et al. 2009).

Table 5.4: Antibodies employed for extracellular vesicles (EVs) analysis. The table shows the primary and secondary antibodies employed for the immunodetection of specific proteins in cell lysates and EV fraction lysates. Antibodies' dilutions in blocking buffer [5% (w/v) non-fat milk in TBST pH 7.4] are also shown.

Primary antibodies	**Company**	**Dilution**
Rabbit polyclonal to Transglutaminase 2 (TG2) (ab421)	Abcam	1:500
Rabbit polyclonal anti-GFP (ab290)	Abcam	1:2500
Mouse Monoclonal anti-Flotillin 2 (610383)	BD Transduction Laboratories	1:5000
Secondary antibodies	**Company**	**Dilution**
Goat anti-rabbit IgG HRP conjugated	Dako	1:2000
Goat anti-mouse IgG HRP conjugated	Dako	1:1000

5.3.4 Measure of EV size by qNANO™

In order to characterize the size of the EV subpopulations obtained by differential centrifugation using the protocol described in the previous section (5.3.3.2), nanoparticle analyisis was performed by technical staff at the Institite of Neuroscience of the National Centre of Research (CNR) in Milan (Italy), using a qNANO™ (iZON, New Zeland) particle analyser (Garza-Licudine, et al. 2010). qNANO™ allows nano-scale particle analysis of biological vesicles by employing a tunable resistive pulse sensing (tRPS) method, that consents the measurement of each particle in suspension as they are passing, one at a time, though adjustable nanopores (Garza-Licudine, et al. 2010).

For the characterisation of MV size by qNANO™, EGFP-TG2 overexpressing NRK52E TECs were cultured as described in 5.3.3.1 and 36h-conditioned medium was collected and sent overnight, in ice, to the abovementioned Institite of Neuroscience. Here, EVs were isolated by differential centrifugation by technical staff, following the same method described in 5.3.3.2, and nanoparticle analysis was performed by qNANO™ on the collected EV fractions.

5.3.5 Inhibition of extracellular vesicles (EVs) release

Sphingomyelinase (SMase) is an enzyme involved in the production of ceramide by the cell, by catalysing the hydrolysis of sphingomyelin (SM) with production of phosphocholine and ceramide. Different kinds of SMases exist in nature, depending on their specific location and the pH that favours their enzymatic activity. In particular, is important to mention both neutral SMase (nSMase) and acid SMase (aSMase) in the context of lipid-induced EV formation. It has been suggested that nSMase plays a role in exosome formation (ILV budding in secretory MVBs) (Trajkovic, et al. 2008), while aSMase might be involved in MV shedding (Bianco, et al. 2009).

The following inhibitors were employed to modulate EV formation.

The inhibitor N,N′-Bis[4-(4,5-dihydro-1H-imidazol-2-yl)phenyl]-3,3′-p-phenylene-bis-acrylamide dihydrochloride, generally referred to as **GW4869** (D1692, Sigma), was employed as a cell-permeable inhibitor of nSMase (Luberto, et al. 2002) and inhibitor of exosome biogenesis (Trajkovic, et al. 2008).

Imipramine hydrochloride, or 10,11-Dihydro-N,N-dimethyl-5H-dibenz[b,f]azepine-5-propanamine hydrochloride (I0899, Sigma), a specific inhibitor of aSMase, was employed as a possible inhibitor of ectosome budding (Bianco, et al. 2009). It is also important to remember that aSMase has also been involved in endocytic pathways by micropinocytosis, and imipramine has been suggested to inhibit micropinocytosis in different cell models (Serrano, et al. 2012, Miller, et al. 2012).

Amiloride hydrochloride [N-Amidino-3,5-diamino-6-chloropyrazinecarboxamide hydrochloride hydrate] (A7410 Sigma) is an inhibitor of membrane depolarisation suggested to interfere with both EV release and macropinocytosis. This compound has been proposed to inhibit both Na^{+}/Ca^{2+} exchangers, involved in stimulated calcium influx and depolarisation, and H+/Na+ exchangers. Amiloride / N-ethyl-N-isopropyl amiloride has as mainly been involved in the inhibition of micropinocytosis, which is favoured by H+/Na+ exchange (Stelmach, Rusak and Tomasiak 2002, Koivusalo, et al. 2010). It is not yet clear wether amiloride effect on exocytosis is to associate with a lower exosome secretion by blocking channel activity (Savina, et al. 2003, Chalmin, et al. 2010, Merendino, et al. 2010), or with an inhibition of MV shedding (Stelmach, Rusak and Tomasiak 2002).

Prior to EVs extraction, treatment with the different inhibitors was performed in serum-free DMEM medium at 37°C in EGFP-TG2 overexpressing NRK52 cells (clone #C5), using the specific working concentrations and incubation times reported in **Table 5.5.** After incubation, isolation of the different vesicle subpopulations from the medium was performed following the procedure described the previous paragraph (5.3.3.2), and equal volumes (40 µl) of each fraction was analysed for TG2/EGFP-TG2 expression as described in 5.3.3.3.

Table 5.5: Inhibitors of extracellular vesicles (EVs) formation. Inhibitors used in this study to selectively interfere with EVs formation. GW4869 (N,N′-Bis[4-(4,5-dihydro-1H-imidazol-2-yl)phenyl]-3,3′-p-phenylene-bis-acrylamide dihydrochloride) was re-suspended in DMSO at stock concentration of 5 mM. Imipramine hydrochloride (10,11-Dihydro-N,N-dimethyl-5H-dibenz[b,f]azepine-5-propanamine hydochloride) and amiloride hydrochloride (N-Amidino-3,5-diamino-6-chloropyrazinecarboxamide hydrochloride hydrate) were re-suspended in water at a stock concentration of 50 and 25 mg/ml respectively (158 mM and 94 mM). All reagents were obtained from Sigma. nSMase = neutral sphingomyelinase, aSMase = acid sphingomyelinase

Inhibitor	Inhibition of	[ ]	Incubation time	Control
GW4869 (D1692 Sigma)	Selective inhibitor of nSMase	10 µM	16 h	Serum free DMEM + 0.2% (v/v) DMSO
Imipramine hydrochloride (I0899 Sigma)	Selective inhibitor of aSMase	30 µM	30 min	Serum free DMEM
Amiloride hydrochloride (A7410 Sigma)	Inhibitor of Na^{+}/H^{+} and Na^{+}/Ca^{2+} antiporter	1 mM	10 min	Serum free DMEM

5.3.6 Immunofluorescent staining of extracellular EGFP-TG2

Immunofluorescent staining of extracellular EGFP-TG2 was performed on EGFP-TG2 overexpressing NRK52E cells (Clone #C5) after treatment with specific EVs inhibitors. For these experiments, 50,000 EGFP-TG2 NRK52E cells/well were grown in an 8-well chamber slide in normal conditions for 24 h or until 80% confluent. At this stage, cells were treated as appropriate with vesicular trafficking inhibitors and/or with 10 ng/ml of recombinant TGF-β1 in complete DMEM medium, and incubated at 37°C for the times reported in **Table 5.5**.

After incubation, medium was removed carefully and cells were straight away fixed (non permeabilised) without any preliminary wash, to perturb the vesicles as little as possible. The full protocol followed for cell fixation and extracellular EGFP immunofluorescent staining (on non-permeabilised cells) is reported in the general methods (Chapter II).

5.3.7 Measurement of TG2 activity in EVs

In order to determine TG2 activity of the different extracellular vesicle subpopulations, measurement of TG2 activity was performed on both lysed and non lysed EVs of EGFP-TG2 overexpressing NRK52E TECs. EVs were isolated by differential centrifugation as described in 5.3.3, however, pellets were not lysed in RIPA buffer, but they were either lysed in a milder sucrose-based lysis buffer [0.25M sucrose, 2 mM EDTA, and 5 mM Tris-HCl, pH 7.4] (that lyses the membranous compartments but is more suitable for enzyme activity assays), or just re-suspended as whole EVs in 50 mM Tris-HCl, pH 7.4 or serum free medium. In the first case the TG2 activity detected is that of the full vesicle, while in the second case, by not lysing the EVs, the activity detected is limited to the vesicles surface.

TG2 activity was assessed using either the *in-house* total TG2 activity assay described in 2.2.9.1, or a more sensitive commercial TG2 activity "pico" assay obtained from Zedira. In both cases, assay plates were kept in gentle slow shaking during the TG2 reaction step, to make sure that all sides of the vesicles were in contact with the substrate-coated surface.

5.3.7.1 Tissue transglutaminase pico-assay

The tissue transglutaminase pico-assay kit (M003 Zedira) is a commercial kit suitable for a precise quantification of TG2 activity. The principle of the kit is very similar to the *in-house* total TG2 activity plate assay described in Chapter II: it is based on the employment of a plate coated with high molecular weight glutamine donor substrate (HA-HMS), and biotin-cadaverine as a primary amine, that is crosslinked to the substrate by catalytically active TG2 (in presence of adequate calcium and dithiothreitol – DTT). Streptavidin conjugated to horseradish peroxidase (HRP) is employed to detect biotinylated cadaverine incorporated on

the substrate and finally 3, 3', 5, 5'-tetramethylbenzidine (TMB) is used to develop the plate, through a colorimetric reaction with HRP in presence of hydrogen peroxide (H_2O_2).
50 µL of re-suspended pellet in sucrose-based lysis buffer or 50 mM Tris-HCl, pH 7.4 (both supplemented with 10 mM DTT), were tested following the manufacturer's instructions. Absorbance was read at 450 nm (TG2-activity) and 620 nm (background). TG2 activity of the given samples was measured by extrapolation from the calibration curve produced using the TG standards provided by the kit (from 0 to 10 ng/ml of TG2 or 0-500 pg/well as 50 µL are loaded per well). Calibration curve design and TG2 activity calculation for the MV extracts was performed using the statistical software GraphPad Prism 7 (http://www.graphpad.com).

5.3.8 TG2 binding to phospholipids

To analyse the ability of recombinant human TG2 to bind intracellular phospholipids, PIP Strips™ Membranes (P-23750, Molecular Probes®) were employed. PIP Strips™ are 6 cm nitrocellulose membrane containing 15 spots of different phospholipids (100 pmol each) plus a blank sample. These membranes are incubated together with the selected protein, in this case a purified TG2, and the binding to phospholipids is measured after specific washes using a dot blot – like developing approach.
First, the PIP Strips™ membrane was incubated for 1 h at room temperature using the appropriate blocking buffer (3% BSA in TBST), with gentle shaking. After blocking, the membrane was incubated overnight (15 h) at 4°C in gentle agitation with 0.5 µg/ml of commercially available recombinant human hexahistidine-tagged human TG2 produced in *E.coli* (His6-rhTG2) (T002, Zedira), in blocking buffer and in the presence of 2mM of calcium chelator EDTA, to keep TG2 in the closed conformation typical of the intracellular space (Pinkas, et al. 2007). After the incubation, the membrane was washed three times with blocking buffer (10 min wash in gentle agitation) and re-incubated as above with 0.5 µg/ml His6-rhTG2 in blocking buffer supplemented with 2mM EDTA overnight (15 h) at 4°C in gentle shaking. Washing was performed again as above and then phospholipid bound TG2 was developped by incubating the membrane with 1:1000 (v/v) dilution of mouse monoclonal anti-His6-antibody conjugated to peroxidase (Roche, Sigma) in blocking buffer at 4°C for 15 h. After incubation, the membrane was washed three times with TBST (10 min per wash in gentle agitation) and chemiluminescent spots detected by enhanced chemiluminescence (EZ-Chemiluminescence Detection Kit for HRP, Geneflow). Image acquisition was performed with a LAS4000 imaging system (GE Heathcare).

5.3.9 Detection of phosphorylation in TG2 and TG2-immunoprecipitated proteins

To determine if TG2 or TG2-associated proteins could be phosphorylated in normal conditions and upon pro-fibrotic stress, immunoprecipitation(IP) of TG2 was performed in cells subjected to glucose stress. EGFP-tagged TG2 was immunoprecipitated from the EGFP-TG2 overexpresing clones as described in 2.2.5 using a rabbit polyclonal anti-GFP antibody. An outline of the experimental procedure is reported in **Fig.5.4**.

Glucose stress to simulate a condition of diabetic nephropathy was performed in cells of NRK52 EGFP-TG2 clone #C5. Previous work from our group has proven that glucose stress determines an increase in TG2 export in this cell line, in both WT and EGFP-TG2 overexpressing NRK52E cells (Huang et al., 2016, in preparation). $2 \cdot 10^6$ cells were seeded in a T75 culture flask in complete DMEM medium but containing only 5.5 mM D-glucose (low glucose, physiological condition) and 2% (v/v) heat-inactivated FBS. After 24 h, the medium was replaced with the same medium containing either 5.5 mM (low glucose, physiological condition) or 30 mM (high glucose – "diabetic" condition) D-glucose, and grown for further 48 h. Cell lysates were produced in 500 µl of IP Lysis/Wash buffer (Thermo Scientific) as described in the general methods (2.2.5). In addition to 1% (v/v) protease inhibitors cocktail (P8340 Sigma), 1%(v/v) phosphatase inhibitors [phosphatase inhibitor cocktail 2 (P5726 Sigma) and phosphatase inhibitor cocktail 3 (P0044 Sigma)] were also added to the lysate to inhibit dephosphorylation. EGFP-immunoprecipitation was performed in equal amounts of proteins (750 µg) with 2.5 µg of rabbit polyclonal anti-GFP antibody (Ab 290, Abcam), using the Pierce™ Crosslink Magnetic IP/Co-IP Kit (Thermo Scientific), and following the protocol for IP reported in general methods (2.2.5). As a negative control, the same procedure was performed in the absence of antibody (referred to as "beads" only control). Proteins were eluted in 75 µl of acidiic elution buffer and neutralised with 7.5 µl of neutralization buffer, both from the kit.

To investigate protein phosphorylation a Western blot analysis was performed, using a range of antibodies detecting phosphotyrosine or phospho-serine/threonine at specific sites, reported in **Table 5.6.** In each blot, equal volumes of GFP-precipitates and "beads only"-precipitates were analysed for both treatments (41 µl elution product and 14 µl of 4X Laemmli buffer, deriving from 375 µg of cell lysate). As a positive control, equal amounts (37.5 µg) of total cell lysates were loaded.

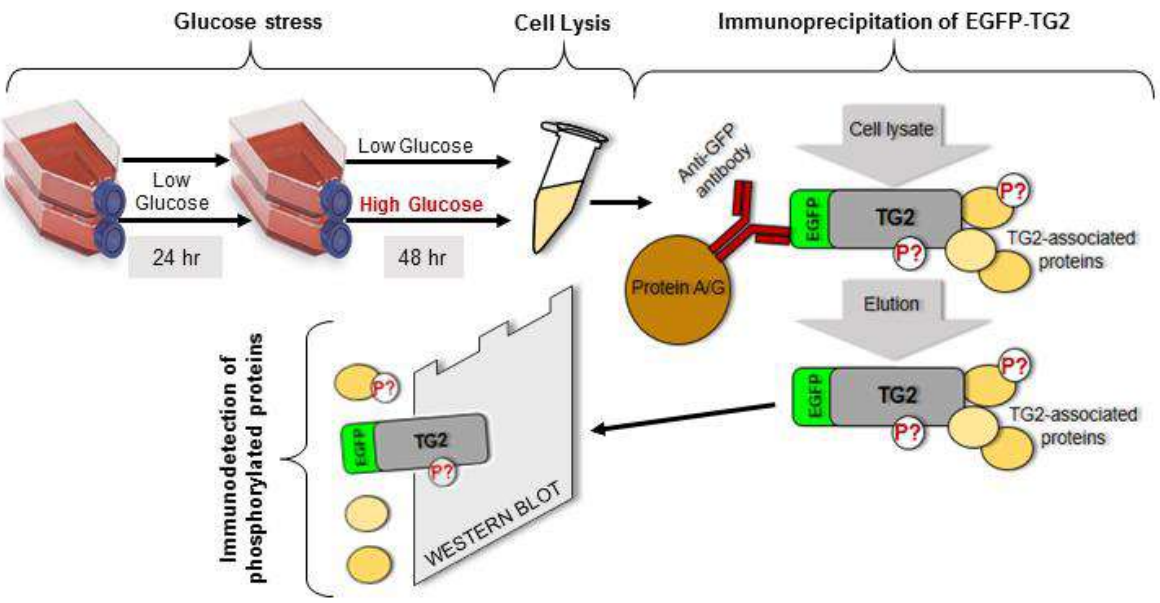

Figure 5.4: Outline of the procedure employed to investigate phosphorylation of TG2 / TG2-associated proteins, in GFP-immunoprecipitates from EGFP-TG2 overexpressing clones subjected to glucose stress.

Table 5.6: Antibodies employed to investigate phosphorylation of TG2 / TG2-associated proteins. The table shows the primary and secondary antibodies employed for Western blot immunodetection of tyrosine or serine/threonine phosphorylation, as well as the anti-GFP antibody employed to confirm the immunoprecipitation itself. Antibodies dilutions used in blocking buffer [5% (w/v) non-fat milk in TBST pH 7.4] are also shown.

	Primary antibodies	Company	Dilution
PHOSPHORYLATION	Rb polyclonal anti-phosphotyrosine	BD Transduction Laboratories	1:250
	Rb monoclonal Phospho-(Ser/Thr)AMPK Substrate (P-S/T2-102) (5759)	Cell Signaling Technology	1:1000
	Rb monoclonal Phospho-Akt Substrate (RXRXXS/T)(110B7E) (9614)	Cell Signaling Technology	1:1000
	Rb monoclonal Phospho-PKA Substrate (RRXS/T) (100G7E) (9624)	Cell Signaling Technology	1:1000
	Rb monoclonal Phospho-(Ser/Thr) ATM/ATR Substrate (S*/T*QG) (P-S/T2-100) (6966)	Cell Signaling Technology	1:1000
	Rb monoclonal Phospho-(Ser) PKC Substrate (P-S3-101) (6967)	Cell Signaling Technology	1:1000
	Rb monoclonal Phospho-(Ser) CDKs Substrate (P-S2-100) (9477)	Cell Signaling Technology	1:1000
IP Control	Rb polyclonal anti-GFP (ab290)	Abcam (UK)	1:2500
	Secondary antibodies	**Company**	**Dilution**
	Goat anti rabbit IgG HRP conjugated	Cell Signaling Technology	1:2000
	Goat anti rabbit IgG HRP conjugated	Dako	1:2000

5.3.10 SiRNA knock down of clathrin

Clathrin knock down was performed in both NRK52E WT and EGFP-TG2 overexpressing NRK52E (clone #C5) TECs, by transient transfection of rat clathrin-targeting siRNA, following the protocol for siRNA transfection reported in Chapter II (2.2.10.2).

For this specific experiment, $2 \cdot 10^5$ cells/well were cultured in a 6-well plate in antibiotic-free DMEM (Lonza, Switzerland) supplemented with 5% (v/v) heat-inactivated FBS (Gibco) and 2mM L-glutamine (Sigma) for 24 h. The day after, cells were transfected with either 100 nM rat clathrin-targeting siRNA [ON-TARGETplus Rat Cltc (54241) siRNA – SMARTpool (L-090659-02-0005) from Dharmacon, Thermo Scientific)] or non-targeting scrambled control siRNA [ON-TARGETplus Non-targeting siRNA #1 (D-001810-01-05) from Dharmacon], using DharmaFECT 1 (Dharmacon) as transfection reagent. After transfection, cells were grown for additional 24 hours.

The knock down at a protein level was measured by western blot using antibodies against clathrin [Rb monoclonal anti-clathrin heavy chain (D3C6) XP®, 4796, Cell Signalling – dilution 1:500), TG2 (Rb polyclonal anti-TG2, Ab421, Abcam – dilution 1:500) and β-tubulin (Rb Polyclonal anti-β-tubulin, Ab6046, Abcam– dilution 1:5000) as a loading control.

5.4 RESULTS

5.4.1 Membrane fusion events appear to be necessary for TG2 export from TECs

As described in Chapter IV, several proteins involved in intracellular vesicular trafficking have been found as significantly associated with TG2 in kidney membranes by SWATH™-MS in both healthy and fibrotic kidneys. Among these proteins, NSF-ATPase, that is required for intracellular SNARE-mediated membrane fusion events, including exocytosis, was itself specifically identified as TG2-associated in kidney membranes. NEM a specific inhibitor of NSF ATPase (Zhao, Slevin and Whiteheart 2007), had already been suggested to significantly interfere with TG2 secretion by Zemskov and colleagues in 2011 (Zemskov, et al. 2011). Knowing this, it was interesting to assess the effect of NSF ATPase inhibition by NEM on TG2 export by kidney TECs.

To achieve this purpose, NRK52E WT or EGFP-TG2 overexpressing NRK52E cells were employed. EGFP-TG2 overexpressing NRK52E clones had already been fully characterized in Dr Verderio laboratory (NTU) (Huang et al., 2016 manuscript in preparation), but the validation of the clones employed in this thesis, which are clone #C5, in this chapter, and both #C5 and #E6, in the next one, was repeated to confirm that the overexpression of EGF-TG2 chimera was maintained and was resulting in an higher extracellular TG2 expression compared to the wild type TECs (**Suppl. Fig. 5.1**).

NRK52E WT or EGFP-TG2 overexpressing NRK52E cells (clone #C5) were treated with 0.6 mM NEM for 30 min as described 5.3.2. Membrane integrity, measured by LDH cytotoxicity assay assay, was not significantly affected by NEM at this concentration and incubation time, in both cell lines (**Fig. 5.5A**, black arrow). Optimisation of the LDH assay for the cell lines employed was performed prior to the cytotoxicity assay as described in 2.2.1.7, and the optimal number of cells to employ was chosen depending on the results as described in **Suppl. Fig. 5.2**.

Subsequently, the effect of NEM treatment on TG2 export was assessed by biotin-cadaverine incorporation assay in FN, performed on living cells as described in 2.2.9.1 (**Fig. 5.4B**), for 2, 4 or 6 h. The optimal number of cells to employ (20,000) was chosen based on previous literature (Jones, et al. 1997) and confirmed on this line of TECs by preliminary test on a serial dilution of cells (**Suppl. Fig. 5.2**).

Results showed a progressive increase in biotinylated cadaverine incorporation (product of extracellular TG activity) with time (**Fig. 5.5B**). At each time point, pre-incubation with NEM resulted in a significant reduction of TG2 outside the cells in NRK52E WT TECs. Similarly, also

EGFP-TG2 overexpressing clones were characterised by a reduction of TG2 export upon treatment with NEM, which was significant at 2 and 4 h culture (**Fig. 5.5B**).

To support these observation, after NEM treatment, immunofluorescent staining of extracellular TG2 or EGFP-TG2 was performed in not permeabilised cells following the protocol reported in chapter II (2.2.8). NRK52E WT cells showed a punctate pattern of extracelluar TG2 antigen (red) staining that was significantly reduced upon NEM treatment (~50% of the control, $p<0.05$, *) (**Fig. 5.5C**). Similarly, also the EGFP-TG2 overexpressing cells displayed a level of extracellular EGFP-TG2 (red), which was significantly ($p<0.05$, *) reduced after NEM treatment; however, this inhibition was not as strong as the one seen in WT cells, being extracellular TG2 expression only approximately 10% lower thenthe untreated cells (**Fig. 5.5C**).

In summary, from these experiments, TG2 release appeared to be partially dependent on NSF-ATPase function, being significantly reduced by the employment of NEM. The effect appeared to be clearer on WT cells compared with the EGFP-TG2 overexpressing clone. Results suggest that vesicle fusion events requiring NSF-ATPase are at least in part involved in TG2 unconventional export from TECs, in agreement with previous findings on other cell models (Zemskov, et al. 2011).

This finding, together with the identification of several exosomal markers within the list of TG2-associated proteins in kidney membranes (shown in Chapter IV), raised the hypothesis of TG2 being secreted by the cells as an exosome cargo, by fusion of MVB outer membrane to the plasma membrane. To test this hypothesis, in the next section, TG2 presence in EV fractions was investigated.

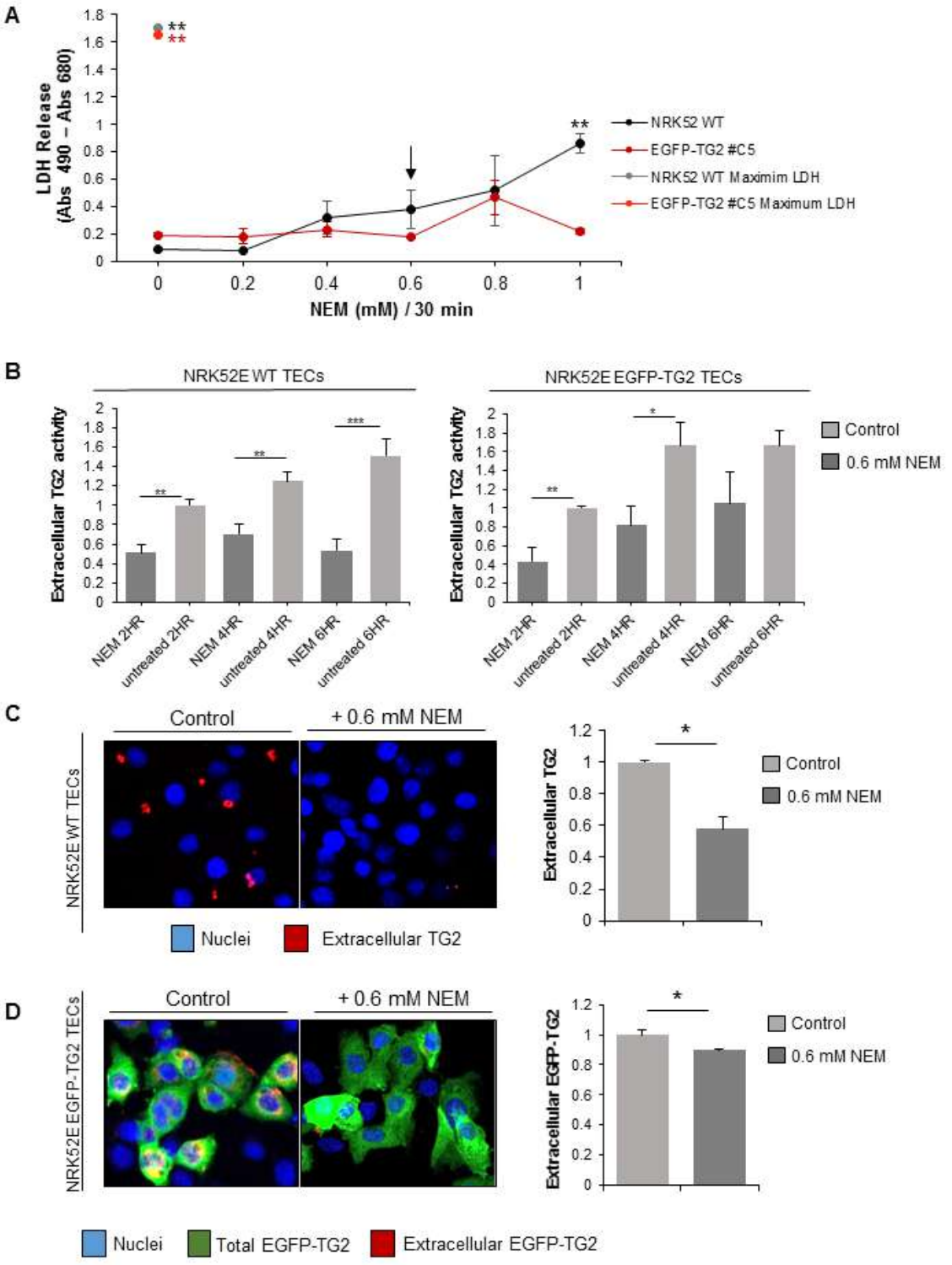

Figure 5.5: N-ethylmaleimide (NEM) treatment leads to a reduction in extracellular TG2 in kidney TECs. (A) WT or EGFP-TG2 overexpressing NRK52E TECs were incubated with different concentrations (0 to 1 μM) of N-ethylmaleimide (NEM) for 30 min. After incubation, cell viability was measured by LDH assay as described in 2.2.1.7. Data are presented as spontaneous LDH Release (Abs 490 nm – Abs 680nm) at each concentration for each cell line ± SD. Total LDH release of untreated cells (Abs 490 nm – Abs 680 nm, after cell lysis) ± SD, is also shown in the picture. **(B)** WT or EGFP-TG2 overexpressing NRK52E TECs were pre-treated with 0.6 mM NEM for 30 min. 20,000 cells/well were seeded in a 96-well plate in quadruplicates and extracellular TG2 was detected as described in 2.2.9.2, for 2, 4 and 6 h. Non-treated cells were used as a control. The values are the average Abs (450 nm) of three independent experiments, each undertaken in quadruplicates, normalised for the relative control (equalised to 1) ±

SD, N=3. **(C, D)** NRK52E WT TECs (C) and EGFP-TG2 overexpressing NRK52E TECs (D) were incubated with 0.6 μM (NEM) for 30 min. Immunofluorescent staining of estracellular TG2 or EGFP-TG2 was performed as described in 2.2.8: extracellular TG2 (C) was detected on fixed (3%PFA) but not permeabilised NRK52E WT cells using a by mouse monoclonal anti-TG2 antibody (IA12) followed by a secondary goat anti-mouse antibody Alexa Fluor® 598, with red emission. Extracellular EGFP-TG2 chimera (D) was detected on fixed (3%PFA) but not permeabilised cells using a Rb polyclonal anti-GFP antibody (Abcam) followed by a donkey anti-rabbit Alexa Fluor® 568 antibody, with red fluorescence (D). Nuclei were stained with DAPI. Representative pictures at 200X magnification are here shown. Extracellular TG2 (C) was quantified by ImageJ intensity analysis on at least 8 non-overlapping fields per treatment and presented as mean relative intensity of red over blue (nuclei), expressed relative to the control cells without NEM (equalised to 1) ± SEM. Extracellular EGFP-TG2 (D) was quantified by ImageJ intensity analysis on at least 8 non-overlapping fields per treatment and presented as mean relative intensity of red over green (total EGFP-TG2), expressed relative to the control cells without NEM (equalised to 1) ± SEM. Significance of the differences between treatments was determined by T-test: * = $p<0.05$, ** = $p<0.01$, *** = $p<0.001$, **** = $p<0.0001$.

5.4.2 The hypothesis of a TG2 vesicular export from TECs

5.4.2.1 Extracellular vesicles isolation from TECs

To investigate the possibility of TG2 being exported from kidney cells through EVs release, exosomes and ectosomes were isolated from TECs allowed to grow in serum-free medium for 36 h, following the protocol described in 5.3.3. qNANO™ analysis of particle sizes was performed on the different fractions as described in 5.3.4 and confirmed both the presence of EV subpopulation in the conditioned medium of this line of TECs and a correct separation of vesicles subpopulations with this method of isolation (**Fig. 5.6A**). Ectosomes were recovered in the P3 fraction with a mean size of 205±99.3 nm at a concentation of 2.97 x 10^7 prt/ml medium) and exosomes from the P4 fraction with a mean size of 129±50.8 nm at a concentration of 5.89 x 10^7 prt/ml medium) (**Fig. 5.6A**).

To confirm the expression of the lipid rafts marker flotillin-2 in all EV fractions produced by this cell line, the isolated pellets were lysed as described in 5.3.3 and equal amounts of proteins were subjected to Western blot analysis using a monoclonal antibody against Flot2 as reported in 5.3.3.3 (**Fig. 5.6B**). The expected molecular weight for Flot2 is was ~42 kDa. Flot2 expression was detectable in all isolated fractions, including a high expression in the cell lysate and a little expression in P2 fraction. A higher expression of Flot2 was detected in the exosomal fraction (P4) compared to the ectosomal (P3) one (**Fig. 5.6B**). As expected, no signal was detected in the vesicle-deproved medium after TCA-precipitation of proteins (S4) (**Fig 5.6B**).

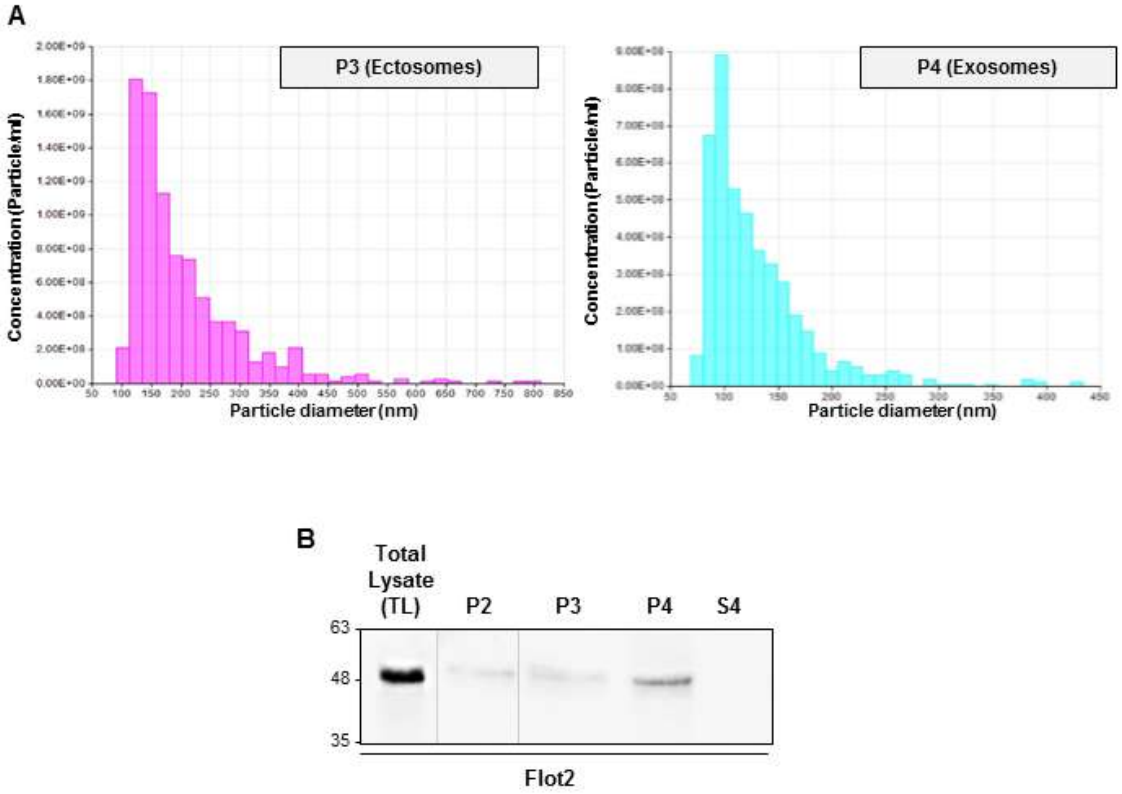

Figure 5.6: A differential centrifugation approach for the isolation of extracellular vesicles subpopulations. (A) Analysis of microparticle size distribution in fraction P3 and P4 was performed by nanoparticle tracking analysis with qNano™ (Izon) of the differential centrifugation products obtained from the conditioned medium of EGFP-TG2 overexpressing NRK52E cells, as described in 5.3.3. Ectosomes were recovered in the P3 and exosomes from the P4 fraction. **(B)** Expression of flotillin-2 (Flot2) was measured by Western blotting on equal amounts of the differential centrifugation products obtained from the conditioned medium of NRK52E cells , cultured for 36 h in serum–free conditions as described in 5.3.3.

5.4.2.2 Detection of TG2 in extracellular vesicle (EVs) fractions in TECs subjected to pro-fibrotic stimuli

To test the presence of TG2 in EVs isolated from TECs, equal amounts of proteins from the ectosome (P3) and exosome fractions (P4) of EGFP-TG2 overexpressing NRK52E cells, as well as from the vesicles-deprived medium (S4), were investigated by Western blot, following the protocol reported in 5.3.3.

The results revealed the presence of TG2 in the exosomes and ectosome fractions, as both EGFP-TG2 chimera at ~100 kDa (**Fig. 5.7A**, black arrow) and endogenous TG2 at ~80 kDa (**Fig. 5.7A**, grey arrow) were detected. Flot2 was probed as well as a lipid raft marker detectable in both exosomal and endosomal fraction, but not in soluble extracellular form.

Densitometric analysis of TG2, relative to Flot2, revealed a trend of enrichment of TG2 in the exosome fraction (P4) in the 36 h - conditioned medium compared to the ectosome (P3) (**Fig 5.7A**), suggesting a location of the enzyme predominantly in these vesicles.

Both TG2 and exogenous EGFP-TG2 were also detectable in the P2 fraction in this cell line, together with Flot2 (data not shown); this might either signify that the enzyme is present in apoptotic bodies shedding from cells undergoing programmed death or in debris of these cells present in the medium.

The same cells were also stimulated by recombinant TGF-β1 (10ng/ml) to simulate conditions of fibrogenesis *in vitro*, as described in 5.3.3.1 (**Fig 5.7B**). Incubation with recombinant TGF-β1 did not change the level of TG2 in the total cell lysate (TL), but determined an increase in the exosome-associated TG2, that was expecially evident for the endogenous enzyme (**Fig. 5.6B**). The cytokine did increase the expression of Flot2 in the TL but it did not alter Flot2 expression in the EV subpopulations, suggesting that it did not increase the exosome production in our conditions (**Fig 5.7B**). The vesicle-deprived medium was also collected and proteins recovered by TCA precipitation. The results show that a small amount of TG2 (mainly endogenous) is also present free in the culture medium but was not increased by TGFβ1 (**Fig.5.7B**).

The same experiment was performed also on WT NRK52E cells rather than in the clonal cell line to rule out artefacts determined by the exogenous protein chimera (**Fig. 5.7C**). Equal amounts of each extracted fraction as well as the vesicles-free medium proteins, was immunoprobed using antibodies against TG2 and Flot2 (**Fig. 5.7C**). Similarly to what observed in the EGFP-TG2 clone, TG2 was detectable in both exosomes (P4) and ectosomes (P3), with a prevalence in the exosomes (P4) (**Fig.5.7C**, grey arrow). Again, treatment with TGF-β1 clearly increased TG2 relative to Flot2 expression in the exosomal fraction and reduced TG2 in the cell lysate, without altering the level of Flot2 (**Fig. 5.7C**). A little amount of protein was also detected in the vesicle deprived medium (S4). Interestingly, a second band at higher molecular weight (~180 kDa) was also identified in the vesicle-deprived medium in this condition (**Fig. 5.7C**, asterisk), suggesting that free TG2 is unstable and either self-polymerises or becomes incorporated in circulating proteins. Alternatively, it might also be a product of TG2 complexing with some high molecular weight proteins in the matrix, such as perlecan or FN. TG2 expression in the medium was extremely variable (**Fig. 5.7A-C**) and we attribute this inconsistency to the experimental variability or to occasional cell leakage. This fraction was not increased by TGF-β1 (**Fig. 5.7A-C**).

Subsequently, to determine whether the location of TG2 was specific for the TEC cell lines, exosomes and ectosomes were also isolated from an established cell line of renal fibroblasts (NRK49F). Equal amounts of cells and EV fractions were probed for TG2, and also in this specific cell line TG2 was enriched in both endosomal (P3) and exosomal (P4) subpopulations, with a prevalence in the exosomal one (**Fig.5.7D**, grey arrow). TGF-β1 lowered TG2 in the total cell lysate and increased it in the exosomal and ectosomal fraction. Interestingly, Flot2 appeared to be highly expressed in the ectosomal (P3) fraction in this cell line (**Fig.5.7D**).

Finally, to check the effect of a different pro-fibrotic stress on TG2 location in the EV subpopulations, EGFP-TG2 overexpressing NRK52E cells were subjected to a glycaemic stress (30 mM glucose/36 h) to simulate conditions of diabetic nephropathy *in vitro* (**Fig.5.7E**). Equal amounts of proteins from the cellular, the ectosomal (P3) and the exosomal fractions (P4), as well as from the vesicles-free medium after TCA protein precipitation (S4), were probed for the EGFP-tag of EGFP-TG2, TG2 and Flot2, as described above. EGFP-TG2 chimera (**Fig. 5.7E**, black arrow) and endogenous TG2 (**Fig. 5.7E,** gray arrow) were identified in the ectosome (P3) and ectosome (P4) fractions, with a prevalence in the exosomal one in the 36 h - conditioned medium. In this case, however, the glucose stress didn't lead to an increase in the exosome-associated TG2 (**Fig.5.7E**). On the other side, an increase in soluble EGFP-TG2 was noticed in the vesicle-deprived medium (S4) as well as a small rise in the amount of endogenous TG2 (**Fig.5.7E**), suggesting an alternative release of the protein.

In conclusion, TG2 was suggested to be present in extracellular vesicles and to be mainly located in exosomal vesicles (P4) comparing to the shedded microvesicles in both TECs and kidney fibroblasts from rat. TGF-β1 treatment lowered TG2 in the total cell lysate and increased it in the exosomal fraction in all cell lines analysed. However, when a glucose stress was employed instead of TGF-β1, a similar effect could not be observed, suggesting that glucose is not a stimulus for TG2 loading in the vesicles.

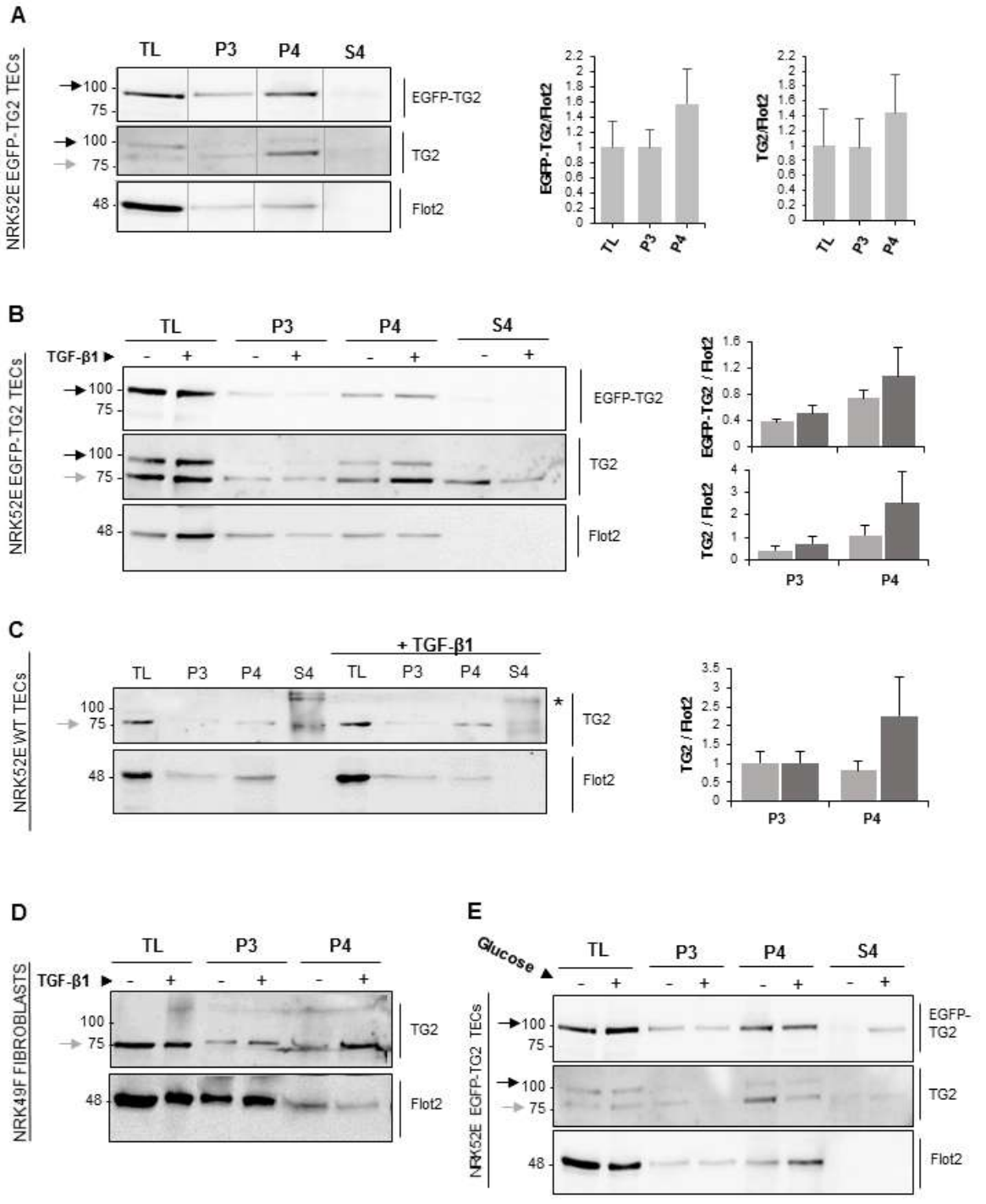

Figure 5.7: TG2 in extracellular vesicles (EV) fractions. Cells of NRK52E EGFP-TG2 stable clone #C5 (A, B), NRK52E cells (C) and NRK49F cells were grown in serum-free medium for 36 h without (A) and with supplementation of 10 ng/ml TGF-β1 (B-D). Alternatively, to simulate a glycaemic stress on the cells, NRK52E EGFP-TG2 overexpressing cells were also cultured in DMEM containing 5 mM glucose (Low glucose) for 48 h, then medium was replaced with serum-free medium containing either 5 mM (-) or 30 mM (+) glucose and grown for additional 36 h (D). After incubation, culture medium was collected and vesicular fraction separated by serial centrifugation as described in 5.3.3. Proteins from vesicles-deprived medium were concentrated by TCA precipitation (S4). Equal amounts of cell lysate (total lysate, TL), EV fraction lysates and vesicle-deprived medium (15 to 25 µg depending on the experiment) were separated by 12%SDS PAGE and immunoprobed for TG2 and flotillin-2 (Flot2) using the specific antibodies reported in **Table 5.4**. NRK52E EGFP-TG2 cells fractions (A,B,D) were also probed for the EGFP tag of EGFP-TG2 exogenous chimera using a Rb anti-GFP antibody (Abcam). All fractions were immunoprobed for TG2 and Flot2. NRK52E EGFP-TG2 cells fractions (A,B,D) were also probed for the

EGFP tag of TG2. (**A-C**) Intensity of immunoreactive bands was quantified by densitometric analysis and normalised to Flot2 expression. Densitometric data represent mean values of 3 (A) or 2 (B, C) independent experiments expressed relative to the untreated cells (equalised to 1) ± SD. Significance of the differences between treatments/fractions was determined by T-test: * = $p<0.05$, ** = $p<0.01$, *** = $p<0.001$, **** = $p<0.0001$.

To gain insights on the location of TG2 within EV, we devised an experiment aimed at measuring the catalytic activity of TG2 of whole EV and lysed EV.

To determine TG2 activity in EV-subpopulations isolated by differential centrifugation, an *in-house* TG activity assay was performed on equal volumes of the different fractions (20 μl) obtained from EGFP-TG2 overexpressing NRK52E cells, as described in 5.3.7. In this case, the fractions obtained where either lysed in a mild sucrose-based lysis buffer or kept intact by re-suspending them in fresh sterile serum-free medium. From the assay, it was evident that, even if the higher amount of TG activity was localised in the cells or on the cell surface (**Fig.5.8A**, cells), a small level of transamidating activity was also measurable in the conditioned medium EV subpopulations in both lysed (**Fig.5.8A**, inset) and intact conditions (**Fig.5.8B**, inset). In both cases, in the conditioned medium obtained (P3+P4+S4), most of the TG2 activity was localised in the exosomal fraction (P4), while less could be observed in the ectosomes (P3) and very little activity was detectable free in the medium (**Fig. 5.8A,B**). Interestingly, in the case of intact vesicles, the exosomal fraction was the only one that was showing a level of activity higher than the background activity of clean non-conditioned serum free medium in which the vesicles were re-suspended for the analysis (5.3% of the cell activity, 0.053, red dashed line in the inset of **Fig.5.8B**), while in the ectosomal fraction (P3) and the vesicle deprived condition medium (S4) where showing a TG2 activity lower than the threshold (**Fig. 5.8B**, inset).

Treatment TGF-β1 didn't affect the total TG2 activity in lysed cells, and even a small, non-significant decrease was observed in the total TG2 activity of treated EV fractions when these were lysed (**Fig. 5.8A**). On the contrary, when the transamidating activity of intact fractions was analysed, TGF-β1 appeared to significantly enhance ($p\approx0.05$) the activity of TG2 on the cell surface of the intact cells (**Fig. 5.8B**). The activity of TG2 was not significantly altered in intact ectosomes (P3) and vesicle-free medium (S4), while an increase in the enzyme activity, even if not statistically significant, could be measured in the exosomal fraction (**Fig. 5.8B**).

In order to better understand whether TG2 was more likely to be located inside or outside the extracellular vesicles of TECs, a more sensitive commercially available TG activity assay (tissue transglutaminase pico-assay kit from Zedira) was performed analysing simultaneously the activity of TG2 from lysed (in sucrose based lysis buffer) and intact (re-suspended in 50 mM Tris-HCl pH 7.4) EV-fractions, obtained from the same flask of 36 h - cultured EGFP-TG2 overexpressing TECs (**Fig. 5.8C**) as reported in 5.3.7.1. The experiment showed how the activity of TG2 is likely to be located mostly on the surface of these vesicles, rather than in their

inside, as the activity of intact vesicles (P3, P4) was not significantly different, and even a bit higher, than the lysed ones (**Fig. 5.8C**). Again, the activity was higher in the exosome compartment, followed by the ectosome, while no activity was detected in the medium by this assay (lower than the background) (**Fig. 5.8C**). Interestingly, when the cells were observed, most of the activity was again likely to locate on the cell surface of the cells, since the activity of lysed cells was only the 3% higher than the intact ones (**Fig. 5.8C**). This is in line with previous observations that TG2 is mostly in its closed catalytically inactive conformation in the intracellular environment in physiological conditions and it is typically activated after release (Pinkas, et al. 2007).

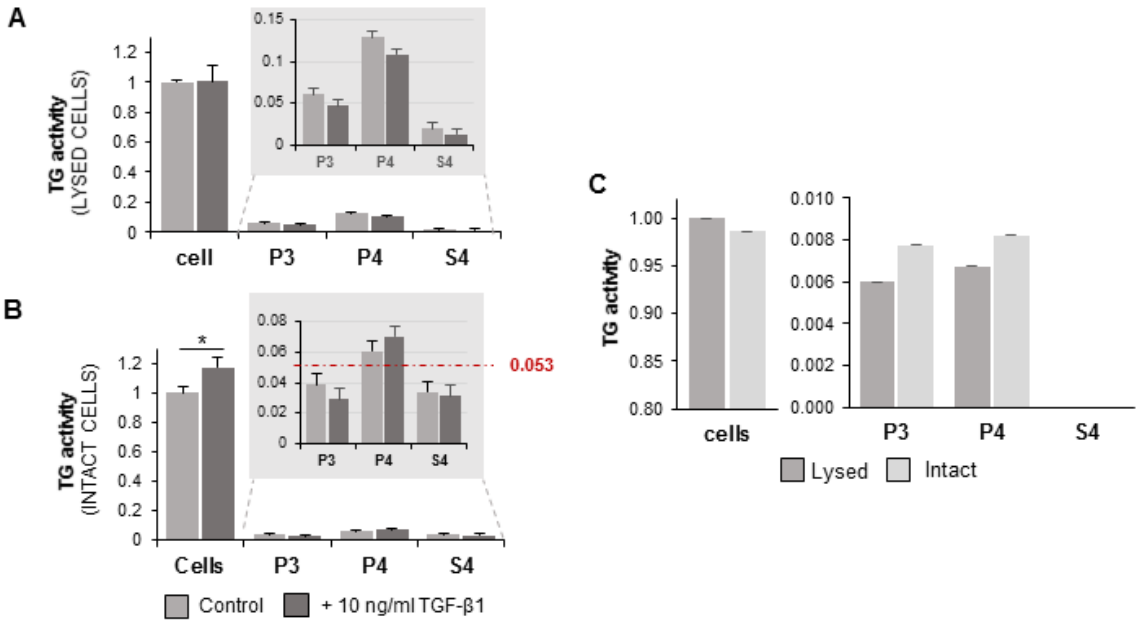

Figure 5.8: TG2 activity on intact or lysed extracellular vesicles subpopulations. (A) EGFP-TG2 overexpressing NRK52E cells (clone #C5) were grown in serum-free medium ± 10 ng/ml TGF-β1 for 36 h. Vesicular fractions were separated by serial centrifugation from culture medium and the different fractions were either lysed in a mild lysis buffer (Lysed, A) or re-suspended in serum-free sterile DMEM medium (Intact, B) depending on the expriment. Transamidating activity was measured on these extracts by *In-house* TG2 activity assay as described in 2.2.9.1. Data represent mean absorbance values (Abs 450 nm) expressed relative to the untreated cells (equalised to 1) ± SD. **(G)** NRK52E EGFP-TG2 clone #C5 cells were grown in serum-free medium for 36 h. Conditioned medium was collected and dived into two identical replicas of the same volume, one necessary to produce lysed EV fractions and one necessary for intact fractions. Vesicular fractions were separated by serial centrifugation as decribed in 5.3.2.2 and cells and EVs were either lysed in a mild lysis buffer (Lysed) or re-suspended in 50 mM Tris-HCl pH 7.4 (Intact, F). The transamidating activity was measured by Tissue Transglutaminase Pico-Assay (Zedira) as described in 5.3.7.1. Data represent mean TG2 activity values in μU/well expressed relative to the activity of lysed cells (equalised to 1). Significance of the differences between treatments and fractions was determined by T-test: * = p<0.05, ** = p<0.01, *** = p<0.001, **** = p<0.0001.

5.4.2.3 Effect of specific nSMase inhibitor GW4869

In several mammalian cell types, the biogenesis of exosomes depends on neutral sphingomyelinase activity for the production of ceramide of which exosomes are rich (Trajkovic, et al. 2008). We therefore investigated whether GW4869, which blocks neutral SMase (nSMase), affected exosome release of TG2.

EGFP-TG2 overexpressing NRK52E cells were incubated with 10μM GW4869 in serum free medium for 16 h as reported in 5.3.5. After incubation, extracellular vesicles were isolated by differential centrifugation and equal volumes (40 μl) of lysates were analysed for TG2/EGFP-TG2 expression and Flot2 expression by Western blot as described in 5.3.3.3. As a control, total cell lysed (50 μg) form treated and untreated cells were also analysed (**Fig. 5.9A-B**).

Upon 16 h treatment with 10μM GW4869 the expression of flotillin-2 was decreased in the exosomal fraction (P4), consistent with a reduction of total exosome release, and this was accompanied by a marked reduction of TG2 in the same fraction (**Fig 5.9A**). GW4869 produced no change in ectosome production (P3) and no difference in the ectosome release of TG2 was observed, which remained lower than the exosomal one (**Fig 5.9A**). A small reduction upon treatment was observed in the cell lysate (TL). When the total amount of proteins was quantified by BCA assay, the treatment with 10μM GW4869 didn't significantly change protein concentration in the cell lysate, while, in the ectosomes, the total amount of proteins appeared even increased. The exosomal proteins were just minimally reduced in this conditions, suggesting that not all the exosome production is based on the ceramide -dependent pathway.

In order to visually observe the location of extracellular EGFP-TG2, immunofluorescence staining of EGFP was performed on non-permeabilised cells as described in 5.3.6, on cells treated with 10 ng/ml of recombinant TGF-β1 and/or 10μM GW4869 (**Fig. 5.9C**). Total EGFP-TG2 (intracellular + extracellular) has spontaneous green fluorescence and is shown in green in the pictures, while extracellular EGFP, detected by immunoprobing using a red fluorocrome -conjugated secondary antibody, is show in red in the pictures.

Minimum washing of the monolayer before fixation to prevent exosome loss revealed an intense punctate pattern at the apical and basal sides of the cells (red) accompanied by bigger spots of EGFP-TG2 signal (**Fig. 5.9C**), mainly located on the apical and lateral sides of the cells. **Suppl. Fig 5.4A** shows the specific location of the signal on the cells. Specificity of the red signal for EGFP-TG2 was confirmed by providing a negative control via incubation of the non-permeabilised cell monolayer with only the secondary red fluorocrome conjugated antibody, in absence of the anti-GFP primary antibody. As expected, no red signal was observed in this condition (**Suppl. Fig 5.4B**).

Treatment of cells with TGF-β1 significantly increased the vesicular export of the EGFP-TG2 (1.56-fold higher than the untreated control, p=0.01,**), that appeared as localised in several "*puncta*" around the cells (**Fig. 5.9C**). Treatment with GW4869 markedly inhibited TG2 export

in a significant manner (65.8% of the untreated control, p=0.04, *), and clearly interfered with TGF-β1 – stimulated TG2 export, bringing exported TG2 down to the basal level (42.3% of the TGF-β1 treated control, 0.0002, ***) (**Fig. 5.9C**).

In synthesis, these data suggests that the employment of GW4869 at 10μM concentration significantly interferes with the extracellular trafficking of the EGFP-TG2 from transfected NRK52E cells and that, given the proprieties of the inhibitor itself and the characteristics of TG2 expression in EV fractions, the inhibition is likely to happen by interfering with TG2 loading on the exosome (P4) fraction during biogenesis.

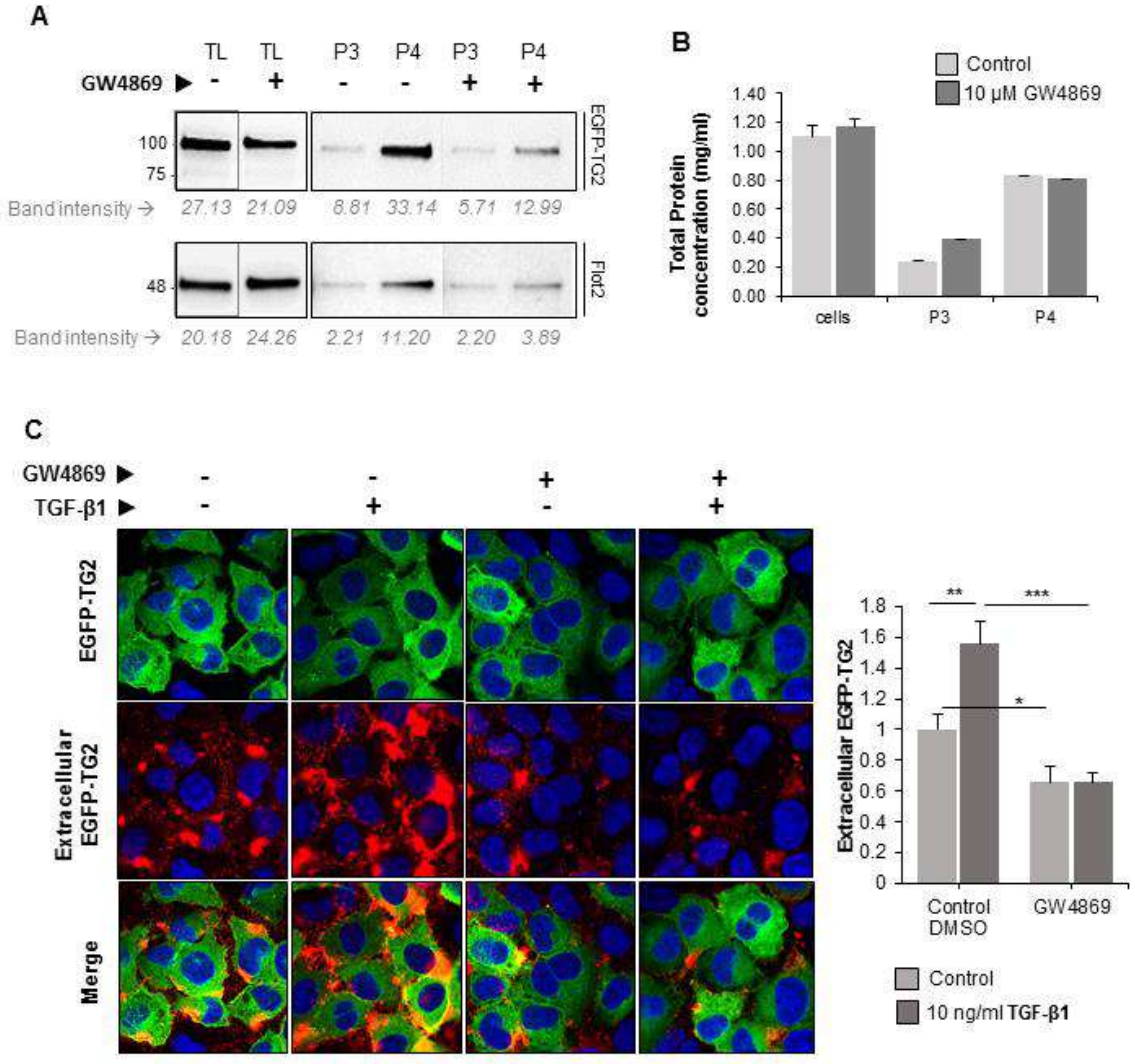

Figure 5.9. Inhibitor of exosome biogenesis GW4869 affects TG2 presence in EVs: (A,B) EGFP-TG2 overexpressing NRK52E cells (clone #C5) were grown in complete medium until 80% confluent, the cells were washed with PBS and medium replaced with serum-free medium ± 10 μM GW4869 for 16 h. After incubation, conditioned medium was collected and vesicular fraction separated by differential centrifugation as described in 5.3.3. (A) All fractions were immunoprobed for EGFP and Flot2 using the antibodies reported in Table 5.4. A representative blot is shown. Densitometric analysis of band intensity/area is shown at the bottom of the graph. (B) Total protein quantification was performed on cell lysate and vesicular fractions by BCA assay, as described in the general methods, and reported as protein concentration in mg/ml ±SD **(C)** EGFP-TG2 overexpressing NRK52E cells were grown in an 8 well chamber slide until 80% confluent, then medium was replaced with complete medium ± 10 ng/ml TGF-β1 ± 10 μM GW4869 for 16 h. Extracellular EGFP-TG2 chimera was detected on fixed (3%PFA) but not permeabilised cells as described in 2.2.8 using a rabbit polyclonal anti-GFP antibody (Abcam)

followed by a donkey anti rabbit Alexa Fluor® 568 antibody, with red fluorescence. Nuclei were stained with DAPI. Representative pictures at 200X magnification are here shown. Extracellular EGFP-TG2 was quantified by ImageJ intensity analysis on at least 8 non-overlapping fields per treatment and presented as mean relative intensity of red over green (total EGFP-TG2) ± SEM, expressed relative to the control cells without TGF-β1 (equalised to 1). Significance of the differences between treatments was determined by T-test: * = p<0.05, ** = p<0.01, *** = p<0.001, **** = p<0.0001.

5.4.2.4 Effect of two possible inhibitors of ectosome formation

As described before, acid sphingomyelinase (aSMase) has been involved in microvesicle shedding from plasma membrane(Bianco, et al. 2009), the possibility that TG2 is partly released by ceramide-mediated microvesicle shedding was investigated using the aSMase inhibitor imipramine hydrochloride. Another inhibitor employed to interfere with ectosomes secretion was the inhibitor of Na+/H+ exchanges amiloride hydrochloride. Amiloride is a known inhibitor of calcium influx dependent micropinocytosis and some types of regulated exocytosis. To investigate a possible inhibitory effect of these inhibitors on TG2 secretion by microvesicular fraction, EGFP-TG2 overexpressing cells were incubated with either 30 μM imipramine for 30 min or 1 mM amiloride for 10 min, as reported in 5.3.5.

First, extracellular TG2 activity of cells incubated with these two inhibitors was measured by biotin cadaverine incorporation assay performed on living cells, and results were compared with the extracellular TG2 activity of untreated cells (**Fig.5.10A**). Incubation with both imipramine and amiloride lead to a significant reduction of extracellular TG2 activity comparing to the control (~ 80% of the control, p = 0.0002, *** and ~86% of the control, p = 0.003 **, respectively) (**Fig. 5.10A**). Interestingly, when the effect of GW4869 on extracellular TG2 activity was tested with the same approach, no difference was observed between treatment and control (**Fig. 5.10A**). This is probably due to the short incubation time with biotinylated cadaverine after GW4869 incubation, that might not be long enough to observe the exosomes contribution to the extracellular space, as they take longer to be secreted after cells attach (Cocucci and Meldolesi 2015).

Given the ability of both imipramine and amiloride to partially reduce the level of extracellular TG2, analysis of EV fractions was performed after treatment with both inhibitors (**Fig.5.10B-C**). First, cells were treated with 30 μM imipramine for 30 min; identically to what done with GW4869 inhibitor and described in 5.4.2.3, equal volumes of treated/untreated EV fractions (40 μl) were analysed by Western blot, together with equal amounts of cell lysates as a control (20 μg) (**Fig.5.10B**). At this short time, ectosomes formed in a greater proportion than exosomes, as previously shown(Cocucci and Meldolesi 2015). Treatment with 30 μM imipramine for 30 min didn't appear to alter the level of Flot2 in any fraction (**Fig. 5.10B**). The expression of EGFP-TG2, that was particularly high in the ectosomal fraction (P3, -) of control cells after 30 min compared to the exosomal one (P4, -), was strongly reduced by treatment

with imipramine (P3, +) (**Fig.5.10B**, black arrow). This might suggest an effect of the inhibitor on the enzyme loading in MVs by regulating the formation of ceramide. Interestingly, however, employment of the inhibitor also resulted in a lower amount of EGFP-TG2 in the cell lysate (**Fig.5.10B**). No real explanation for this can be given for the moment and might reflect the effect of imipramine in the endocytosis of the protein by macropinocytosis (Serrano, et al. 2012, Miller, et al. 2012).

To test the effect of amiloride treatment on EGFP-TG2 location in the different EV fractions, EGFP-TG2 overexpressing cells were incubated with 1 mM amiloride for a short time (10 min), as suggested by previously published protocols reported in 5.3.5. After incubation, extracellular vesicles were isolated from the conditioned medium, and the expression of EGFP-TG2 and Flot2 was analysed by western blot on equal volumes of EV fractions as above (**Fig. 5.9C**). At only 10 min after medium change, ectosomes subpopulation is usually more abundant than exosomes (Cocucci and Meldolesi 2015): in agreement with this, in normal conditions, Flot2 was more expressed in the ectosomal (P3, -) fraction compared to the exosomal fraction (P4, -), where was minimal. In line with flotillin expression, also EGFP-TG2 expression was enriched in the ectosomes of untreated cells (P3, -) compared to the exosomes (P4, -) (**Fig. 5.10C**, black arrow). Amiloride incubation led to a small decrease in Flot2 in the ectosomes (P3, +) consistent with its proposed role as an inhibitor of microvesicles formation (Stelmach, Rusak and Tomasiak 2002), and a similar decrease in EGFP-TG2 in the same fraction (**Fig. 5.10C**, black arrow). No variation in both EGFP-TG2 and flotillin expression was observed under the same condition in the exosome fraction (P4, +). An increase of EGFP-TG2 was observed upon treatment in the total cell lysate, possibly underlying enzyme retention inside the cells (**Fig. 5.10C**, black arrow).

Identically to what was done with GW4869 treatment, immunofluorescent staining of extracellular EGFP-TG2 was performed on the cells after treatment with the two abovementioned inhibitors: EGFP-TG2 overexpressing TECs were treated with either with 30 μM imipramine/30 min or 1mM amiloride/10 min while a pro-fibrotic stimulus to was provided by with 10 ng/ml of recombinant TGF-β1. Immunofluorescent detection of EGFP was performed as described in the previus section. Extracellular EGFP-TG2 signal appeared as a red punctate pattern around the cells, accompanied by bigger spots of TG2 signal (**Fig. 5.10D-E**).

The first set of experiments performed after treatment with TGF-β1 and/or imipramine for 30 min (**Fig. 5.10D**) confirmed a significant effect of TGF-β1 stimulus on TG2 export in untreated cells also at this shorter incubation time, in line with what seen after 16 h treatment in **Fig. 5.9C:** treatment of cells with TGF-β1 significantly increased the vesicular export of the EGFP-

TG2 (1.47-fold higher than the untreated control, p=0.01,**), that appeared as a dense punctate pattern around the cells (**Fig. 5.10D**).

Exposure of cells to imipramine for 30 min determined only a minimal reduction of EGFP-TG2 export in control cells (less than 7% lower than the untreated control, not significant). In TGF-β1 stimulated conditions, treatment with imipramine led to a decrease extracellular TG2 export produced by TGFβ1 (~75% of the TGF-β1 stimulated untreated cells), however, this reduction was variable among the cells observed and didn't appear significant by statistical analysis (p=0.085, non significant) (**Fig. 5.10D**).

When cells were incubated with TGF-β1 and/or amiloride for only 10 min (**Fig. 5.10E**), again TGF-β1 stimulus determined a significant increase in EGFP-TG2 export even at this shorter time-point in untreated cells (1.43-fold higher than the untreated control, p=0.03, *). Amiloride incubation decreased extracellular EGFP-TG2 immunofluorescent labelling of approximately the 22% in both control and TGF-β1 stimulated cells. However, the differences in the quantification of fluorescent signal did not appear statistically significant when analysed by T-test (p=0.16 in the control cells and 0.12 in TGF-β1 stimulated cells) (**Fig. 5.10E**).

In summary, data from immunofluorescent staining of EGFP-TG2 suggest that the employment of imipramine and amiloride might partially interfer with the extracellular trafficking of the EGFP-TG2 exogenous chimera from transfected NRK52E cells. However, morphometric quantifications did not lead to statistically significant differences between untreated cells and cells treated with either imipramine or amiloride, suggesting either a low release of EGFP-TG2 in the MV/ectosomal fraction or a not complete effect of these inhibitors in the enzyme release through shedding ectosomes. Western blot analysis of ectosomal (P3) fractions after treatment with imipramine or amiloride showed a reduction in EGFP-TG2 location in this fraction compared to the untreated control. However, in the first case this was accompanied by a similar reduction of the enzyme in all fractions including the cell lysate, and was not accompanied by a similar reduction in Flot2 marker expression, while in the case of amiloride a reduction of EGFP-TG2 expression in the ectosomes was in line with the reduction of flotillin marker expression, suggesting an effective reduction in MV release mediated by the inhibitor.

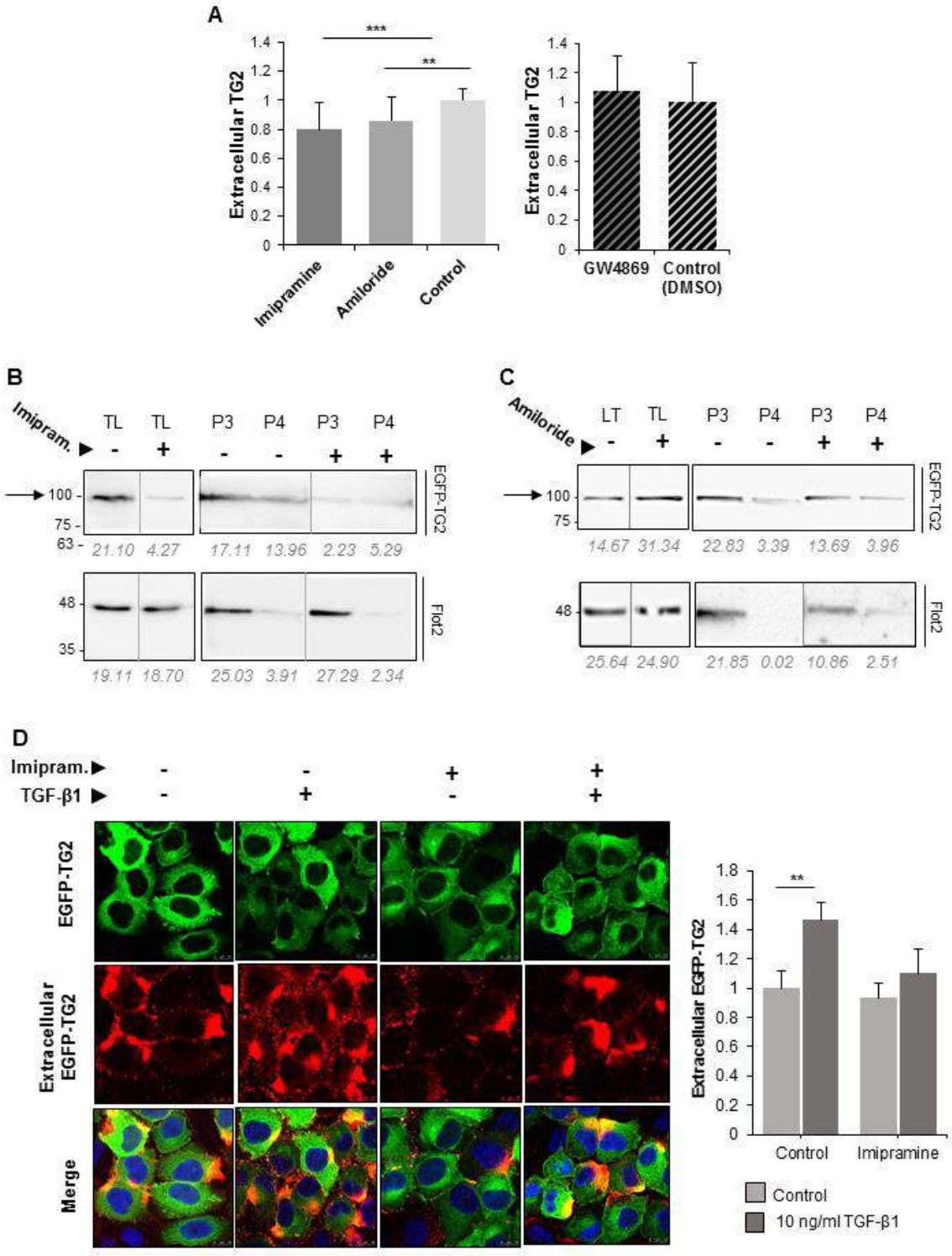
A
Extracellular TG2
***
**
Imipramine
Amiloride
Control
GW4869
Control (DMSO)
B
Imipram.
TL TL P3 P4 P3 P4
EGFP-TG2
Flot2
21.10 4.27 17.11 13.96 2.23 5.29
19.11 18.70 25.03 3.91 27.29 2.34
C
Amiloride
LT TL P3 P4 P3 P4
14.67 31.34 22.83 3.39 13.69 3.96
25.64 24.90 21.85 0.02 10.86 2.51
D
Imipram.
TGF-β1
EGFP-TG2
Extracellular EGFP-TG2
Merge
Extracellular EGFP-TG2
Control
Imipramine
Control
10 ng/ml TGF-β1

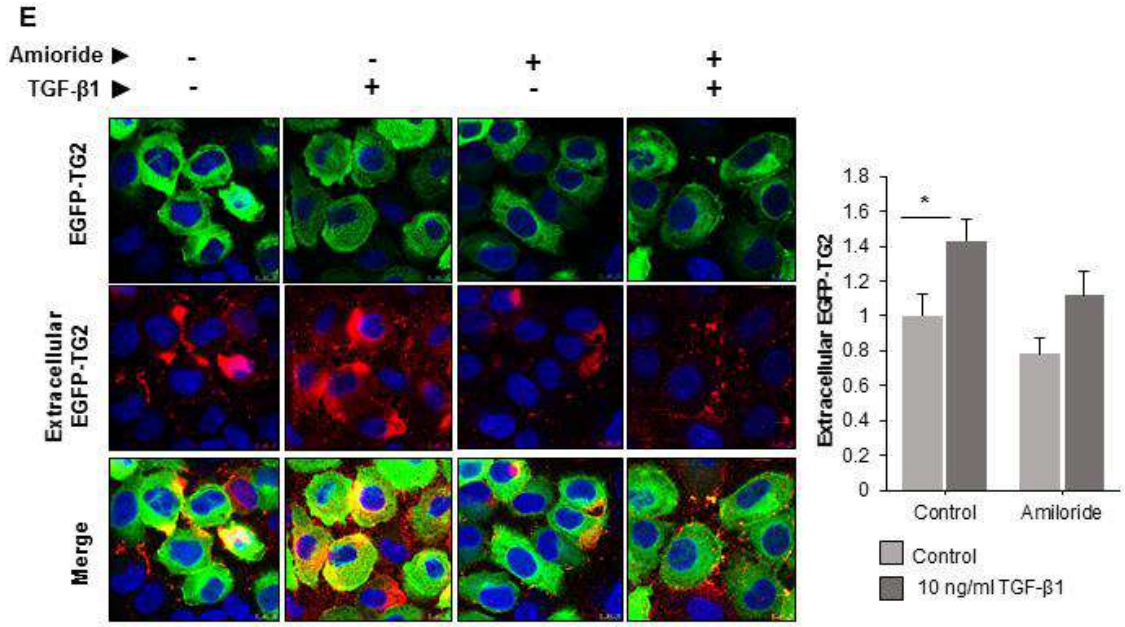

Figure 5.10: Analysis of imipramine and amiloride effects of TG2 expression in EVs. (A) EGFP-TG2 overexpressing NRK52E cells were grown in complete medium until 80% confluent, the cells were washed with PBS and medium replaced with complete medium ± specific inhibitors as described in 5.3.5. Specifically, treatments with 30 μM imipramine hydrochloride for 30 min, 1 mM amiloride hydrochloride for 10 min (complete medium as control), and 5 μM GW4869 for 16 h (0.1% DMSO in complete medium as a control) were performed. After treatment, extracellular TG2 activity was measured as described in 2.2.9.2. The values are the average Abs (450 nm) of five independent experiments, each undertaken in quadruplicates, normalised for the relative control (equalised to 1) ± SD. **(B,C)** EGFP-TG2 overexpressing NRK52E cells were grown in complete medium until 80% confluent, the cells were washed with PBS and medium replaced with serum-free medium ± 30 μM Imipramine hydrochloride for 30 min (A) or ± 1 mM amiloride hydrochloride for 10 min (B). After incubation, culture medium was collected and vesicular fraction separated by differential centrifugation as described in 5.3.3. All fractions were immunoprobed for EGFP and Flot2 as described in 5.3.3.3. Representative blots are shown. **(D,E)** EGFP-TG2 overexpressing NRK52E cells were grown in an 8 well chamber slide until 80% confluent, then medium was replaced with complete medium ± 10 ng/ml TGF-β1 ± 30 μM imipramine hydrochloride for 30 min (D) or ± 10 ng/ml TGF-β1 ± 1mM amiloride hydrochloride for 10 min (E). Extracellular EGFP-TG2 chimera was detected on fixed (3%PFA) but not permeabilised cells as described in **Fig. 5.9**. Representative pictures at 200X magnification are shown. Extracellular EGFP-TG2 was quantified by ImageJ intensity analysis on at least 8 non-overlapping fields per treatment and presented as mean relative intensity of red over green (total EGFP-TG2), expressed relative to the control cells without TGF-β1 (equalised to 1) ± SEM. Significance of the differences between treatments was determined by T-test: * = $p<0.05$, ** = $p<0.01$, *** = $p<0.001$, **** = $p<0.0001$.

5.4.3 Interaction of recombinant TG2 with immobilised phospholipids

The ability of recombinant human TG2 (rhTG2) to bind phosphoinositides (PIPs) was measured employing commercially available PIP Strips™ membranes (Molecular Probes®, Oregon, US) as described in 5.3.8. The recombinant enzyme was kept in a closed / catalytically inactive conformation by incubating it in presence of the calcium chelator EDTA (Pinkas, et al. 2007). Human TG2 bound mono-, bis- and tris- phosphorylated phosphoinositides immobilised on the membrane, with variable strength (**Fig. 5.11,** arrowheads). TG2 interacted with all three phosphoinositide monophosphate species (PI3P, PI4P and PI5P) with a preference for phosphatidylinositol 4-phosphate (PI4P), typical of the Golgi apparatus and important substrate for the stimulated formation of plasma membrane PI(4,5)P2 by phosphatidylinositol 4-phosphate 5-kinase (PIP5K) (Chong, et al. 1994, Funakoshi, Hasegawa and Kanaho 2011). The binding to PI3P, typical of early and recycling endosomes and suggested by Belkin's group as important for the enzme's unconventional secretion (Zemskov, et al. 2011), was present, but lower than the others.

TG2 did also bind all immobilised bis-phosphorylated phosphoinositides [PI(3,4)P_2, PI(3,5)P_2 and PI(4,5)P_2], with PI(3,5)P_2 and PI(4,5)P_2 , the latter typical of the plasma membrane, binding being among the highest. Interestingly, PI(3,5)P_2, having the highest binding to TG2, is known to be mainly present on the late endosomes/MVBs and lysosomes membranes and has been suggested to be upregulated in events of "lysosome exocytosis" by macrophages (Samie, et al. 2013, Li, et al. 2013).

A low but detectable binding capacity for phosphatidylinositol 3,4,5-trisphosphate [PI(3,4,5)P_2] was also noticed. No binding was detected for lysophosphatidic acid (LPA), lysophosphatidylcholine (LPC), phosphatidylinositol (PI), phosphatidylethanolamine (PE), phosphatidylcholine (PC), sphingosine-1-phosphate (S1P), phosphatidic acid (PA) and phosphatidylserine (PS) (**Fig. 5.11**).

In conclusion, TG2 showed to associate with a range of phosphoinositides typical of plasma membrane when immobilised on nitrocellulose. As TG2 was in its calcium-deprived condition it is anticipated that it can bind phosphoinositides in its closed, inactive, conformation.

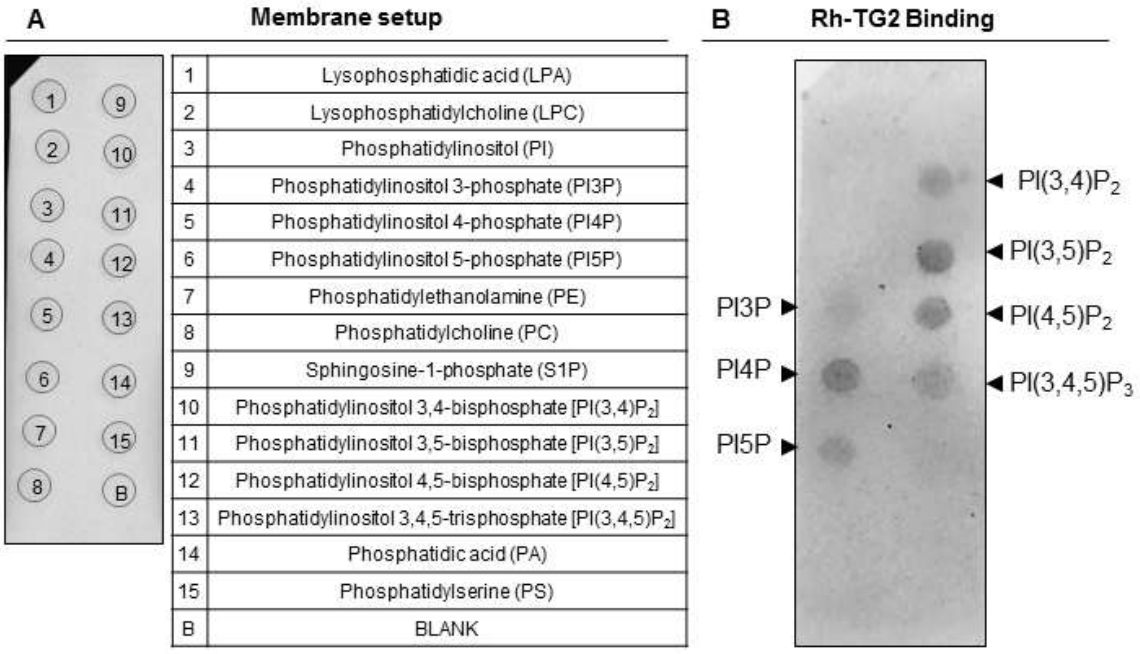

1	Lysophosphatidic acid (LPA)
2	Lysophosphatidylcholine (LPC)
3	Phosphatidylinositol (PI)
4	Phosphatidylinositol 3-phosphate (PI3P)
5	Phosphatidylinositol 4-phosphate (PI4P)
6	Phosphatidylinositol 5-phosphate (PI5P)
7	Phosphatidylethanolamine (PE)
8	Phosphatidylcholine (PC)
9	Sphingosine-1-phosphate (S1P)
10	Phosphatidylinositol 3,4-bisphosphate [PI(3,4)P_2]
11	Phosphatidylinositol 3,5-bisphosphate [PI(3,5)P_2]
12	Phosphatidylinositol 4,5-bisphosphate [PI(4,5)P_2]
13	Phosphatidylinositol 3,4,5-trisphosphate [PI(3,4,5)P_3]
14	Phosphatidic acid (PA)
15	Phosphatidylserine (PS)
B	BLANK

Figure 5.11: Phospholipid binding abilities of recombinant human TG2: The ability of recombinant His6 tagged-TG2 (T002, Zedira, Germany) to bind membrane-immobilised phospholipids was detected using commercially available PIP Strips™ membranes (Molecular Probes®, Oregon, US) following the protocol reported in 5.3.8. 2 mM EDTA was added during the reaction to keep the enzyme in the closed conformation. **(A)** Setup of the membrane: the different phospholipids immobilised on the membrane strip are reported in the table. **(B)** Phospholipid-bound recombinant TG2 was detected by incubation with anti-6His antibody conjugated to HRP (Roche, Switzerland). The immunoreactive spots were visualised by chemiluminescence after addition of ECL reagent, N=1. Arrowheads identify the phospholipid binding detected after membrane development.

5.4.4 Protein phosphorylation in TG2-immunoprecipitates from TECs subjected to glucose stress

5.4.4.1 Optimisation of IP protocol

To optimise TG2 immunoprecipitation from EGFP-TG2 transfected cells (clone #C5), cell lysates were employed to immunoprecipitate TG2 using the EGFP tag (5.3.9). A "beads-only" control was included to confirm the specificity of the binding to the antibody and washes were collected as well to assess the quality of the experiment. Immunoprobing of EGFP confirmed that EGFP-TG2 is specifically immunoprecipitated as a 100 kDa chimera by the antibody and not by the control beads (**Fig. 5.12A**). Examination of the "washes" showed an intense immunoreaction in the "beads only" control but not in the GFP-IP, confirming specificity (**Fig. 5.12A**). The heavy chain and light chain of the IgG from the antibody were also eluted with the GFP-immunoprecipitation and appear in the blot as two bands, one around 50kDa (IgG heavy chain) and one around 25 kDa (IgG light chain) (**Fig. 5.12A**, asterisk)

5.4.4.2 Analysis of protein phosphorylation in EGFP-TG2 precipitates from cells subjected to glucose stress

Putative phosphorylation sites of *Homo sapiens* TG2 protein sequence (EC:2.3.2.13) were analysed using NetPhos online tool (http://www.cbs.dtu.dk/services/NetPhos) (**Fig. 5.12B**). A series of possible serine, threonine and tyrosine phosphorylation sites were identified, at variable levels of phosphorylation potential. Among the residues at higher phosphorylation potential, several serine (S) were identified (68, 216, 253, 430, 449, etc.) as well as few threonine (T) residues (position 73, 442 etc). Some possible tyrosine (Y) phosphorylation sites were also detected, with Y-369, Y-583 and Y-503 having a score higher than 0.8, but in general threonine and tyrosine phosphorylation sites were less in number comparing to serine (**Fig. 5.12B**). TG2 documented phosphorylation sites were also searched using Phosphosite database (http://www.phosphosite.org) (**Fig. 5.12B**). A number of reported phosphorylation sites were obtained for the human TG2 protein using this database, of which the majority have been assigned to TG2 uniquely by a discovery mass spectrometric approach but have never been confirmed biochemically using site-specific methods. The only sites reported for TG2 in literature as a consequence of site-specific types of studies are Ser212, Ser215 and Ser216, largely investigated by Mishra's group (Mishra and Murphy 2006).

To study possible phosphorylation of TG2 and TG2-associated proteins under pro-fibrotic conditions, NRK52E EGFP-TG2 overexpressing clones were cultured at high glucose concentration (30mM) to simulate a diabetic status as described in 5.3.9. Previous data by the lab group had shown how increasing the level of glucose induced an increase in cell surface TG2 antigen and activity from these clones, suggesting a stress-related externalisation of the enzyme (Huang et al. 2016, in preparation). TG2 was immunoprecipitated from these cells by using the EGFP-tag, and the obtained elution was tested for phosphorylation at different residues/domains (**Fig 5.13**) as described in 5.3.9, using the antibodies reported in **Table 5.6.** Tyrosine phosphorylation (P-Y) was investigated for the precipitated EGFP-TG2, and a compatible signal for EGFP-TG2 chimera phosphorylation was detected at 100kDa (**Fig. 5.13A**, red circle), suggesting that TG2 could be phosphorylated by tyrosine kinases both in physiological and in pathological conditions.

Serine and threonine phosphorylation (P-S; P-T) (**Fig. 5.13B-G**) was analysed using antibodies detecting specific phosphorylation on distinctive consensus sequences for a range of serine/threonine (S/T) kinases. Names and consensus sequence of each S/T-kinase are reported in **Table 5.7**.

Table 5.7: Serine-threonine kinases investigated in this study

Kinase		Main roles in the cells	Consensus sequence	Reference
5' AMP-activated protein kinase	**AMPK**	Regulation of metabolism and cellular energy production	(L/M)XRXX(S/T)XXXL	(Hill, et al. 2016)
Protein kinase B	**Akt**	Apoptosis, Cell migration/proliferation, Insulin signalling pathway, Angiogenesis	RXRXX(S/T)	(Alessi, et al. 1996)
Protein Kinase A or cAMP-dependent protein kinase	**PKA**	Metabolism, Vasodilatation, Stimulation of transmembrane transport in kidney. Associates to some hormone receptors	RRX(S/T)	(Pearson and Kemp 1991)
Ataxia-telangiectasia mutated kinase / ATM- and RAD3-related kinase	**ATM/ATR**	Regulation of cell cycle I response to DNA damage	(S/T)QG	(Kastan and Lim 2000)
Protein kinase C	**PKC**	Cell signalling: cell adhesion, cell migration, cell contraction, secretion	(R/K)(R/K)XSX(R/K)	(Nishikawa, et al. 1997, Pearson and Kemp 1991)
Cyclin-dependent kinase	**CDK**	Cell cycle regulation	(K/R)SPX(K/R)	(Holmes and Solomon 1996)

Possible S/T phosphorylation of TG2 by protein kinase A (PKA) and cyclin-dependent kinase (CDK) were identified, with CDK having a more intense signal. PKA -mediated phosphorylation was identified only upon glucose stress (**Fig. 5.13D,** red circle) while CDK-mediated phosphorylation was identified in both conditions, but increased upon glucose stress (**Fig. 5.13G**, red circle). Interestingly, cyclin-G-associated kinase was identified as significantly associated with TG2 in UUO kidney membranes in the current study, as reported in Chapter IV. 5' AMP-activated protein kinase (AMPK), protein kinase B (Akt), ataxia-telangiectasia mutated kinase / ATM- and RAD3-related kinase (ATM/ATR) and protein kinase C (PKC) did not appear to phosphorylate the enzyme as no visible band was seen at 100 kDa (black arrowhead) when EGFP-precipitates were probed for these kinase's -dependent phosphorylation.

In summary, possible phosphorylation of TG2 was detected in cells subjected to glycaemic-like stress and might be involved in the secretion of the enzyme. As phosphorylation has been implicated in the unconventional secretion of HS-modulated cytokines such as FGF2 (Steringer, et al. 2012, Nickel 2007), this finding suggests that also TG2, which is HS-modulated (Scarpellini, et al. 2009, Burhan, et al. 2016, Scarpellini, et al. 2014) might share a similar release pathway.

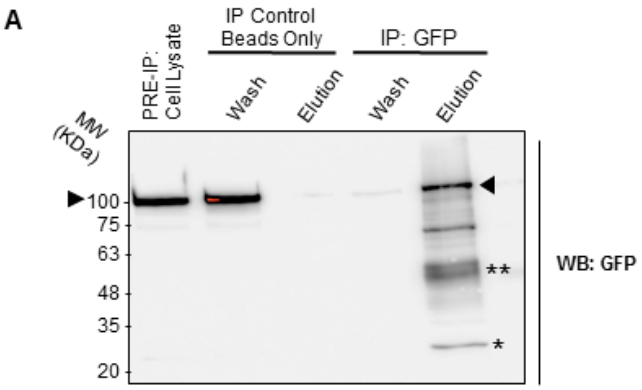

B

Potential phosphorylation sites in Human TG2 protein sequence

Position	Residue	Context	Score	Kinase	Position	Residue	Context	Score	Kinase
23	T	RDHHTADLC	0.568	CKII	295	T	LGIPTRVVT	0.517	unsp
42	T	PFWLTLHFE	0.513	PKC	299	T	TRVVTNYNS	0.622	PKG
56	S	ASVDSLTFS	0.558	unsp	303	S	TNYNSAHDQ	0.636	unsp
58	T	VDSLTFSVV	0.619	PKC	328	S	QGDKSEMIW	0.504	CKII
63	T	FSVVTGPAP	0.64	PKC	360	T	ALDPTPQEK	0.507	GSK3
68	S	GPAPSQEAG	0.99	unsp	365	S	PQEKSEGTY	0.595	unsp
73	T	QEAGTKARF	0.84	PKC	369	Y	SEGTYCCGP	0.971	unsp
91	T	DWTATVVDQ	0.67	unsp	385	S	EGDLSTKYD	0.986	unsp
101	**S**	**DCTLSLQLT**	**0.59**	**PKA**	386	T	GDLSTKYDA	0.738	PKC
106	T	LQLTTPANA	0.527	p38MAPK	411	S	QDDGSVHKS	0.73	PKC
118	S	LYRLSLEAS	0.957	unsp	415	S	SVHKSINRS	0.67	unsp
122	S	SLEASTGYQ	0.504	cdc2	419	**S**	**SINRSLIVG**	**0.614**	**PKA**
123	T	LEASTGYQG	0.516	cdc2	427	S	GLKISTKSV	0.67	PKC
129	S	YQGSSFVLG	0.607	cdc2	430	S	ISTKSVGRD	0.993	unsp
149	Y	ADAVYLDSE	0.636	unsp	442	T	DITHTYKYP	0.887	PKC
152	S	VYLDSEEER	0.813	unsp	449	S	YPEGSSEER	0.994	unsp
159	Y	ERQEYVLTQ	0.751	unsp	450	S	PEGSSEERE	0.987	unsp
162	T	EYVLTQQGF	0.531	DNAPK	496	T	FAHITNNTA	0.502	CKII
171	S	IYQGSAKFI	0.858	PKC	503	Y	TAEEYVCRL	0.877	unsp
212	S	GRDCSRRSS	0.978	unsp	515	**S**	**ARTVSYNGI**	**0.655**	**PKA**
215	S	CSRRSSPVY	0.923	unsp	528	Y	CGTKYLLNL	0.6	unsp
216	S	SRRSSPVYV	0.988	unsp	538	S	LEPFSEKSV	0.932	unsp
219	Y	SSPVYVGRV	0.695	unsp	541	**S**	**FSEKSVPLC**	**0.568**	**PKA**
225	**S**	**GRVVSGMVN**	**0.607**	**PKA**	558	S	CLTESNLIK	0.545	cdc2
245	Y	WDNNYGDGV	0.521	INSR	574	S	PVINSYLLA	0.536	cdc2
250	S	GDGVSPMSW	0.522	p38MAPK	583	Y	ERDLYLENP	0.966	unsp
253	S	VSPMSWIGS	0.992	unsp	623	T	GCTFTVEGA	0.508	CKI
286	T	AVACTVLRC	0.621	PKC	630	T	GAGLTEEQK	0.504	PKC

C

Reported phosphorylation sites in Human TG2

Residue-position	Detected by site directed assays (n° of reports)	Detected by discovery MS (n° of reports)
S56-p	0	1
S60-p	0	1
Y159-p	0	1
K202-ac	0	3
K205-ac	0	1
S212-p	1	0
S215-p	1	1
S216-p	3	5
Y219-p	0	8
Y245-p	0	1
S250-p	0	1
Y315-p	0	1
T368-p	0	8
Y369-p	0	612
S419-p	0	1
S427-p	0	1
S538-p	0	1
S541-p	0	1
Y575-p	0	1
Y583-p	0	1
S608-p	0	1
K672-ac	0	1

Figure 5.12: Optimisation of the EGFP-TG2 preciptation and identification of putative phosphorylation sites for TG2. (A) in order to optimize of EGFP-TG2 immunoprecipitation from EGFP-TG2 overexpressing clones using an anti-GFP antibody, cells were cultured in standard conditions and EGFP was immunoprecipitated from 0.75 mg of cell homogenate using 2.5 µg of rabbit polyclonal anti-GFP as described in 5.3.8. Beads only control was performed to confirm the specificity of the precipitation. Equal volumes (40 µl) of pre-elution wash (unbound proteins) and elution (IP), as well as 100 µg of total cell lysate (Pre-IP) were screened for the expression of EGFP-TG2 chimera by Western blotting with rabbit polyclonal anti-GFP antibody. Immunoreactive bands were detected by enhanced chemiluminescence (Geneflow) after incubation with appropriate HRP-conjugated secondary antibody (**Table 5.6**) in blocking buffer. Image acquisition was performed with a LAS4000 imaging system (GE Heathcare). The figure shows a representative blot. Asterisk represent co-eluted IgGs (** = Heavy Chain; *=Light Chain). **(B)** Putative phosphorylation sites of *Homo sapiens* TG2 protein sequence (EC:2.3.2.13) were analysed using NetPhos online tool (http://www.cbs.dtu.dk/services/NetPhos). Table represent all putative phosphorylation sites detected on human TG2 sequence (phosphorylation potential > threshold, set at 0.5 by default). **(C)** Documented phosphorylation sites of *Homo sapiens* TG2 protein were investigated on Phosphosite database (http://www.phosphosite.org). The table shows all the reported phosphorylation sites on TG2, and the nuber of times they have been identified by site specific analysis (second columns) or uniquely by a discovery approach-based MS (third column).

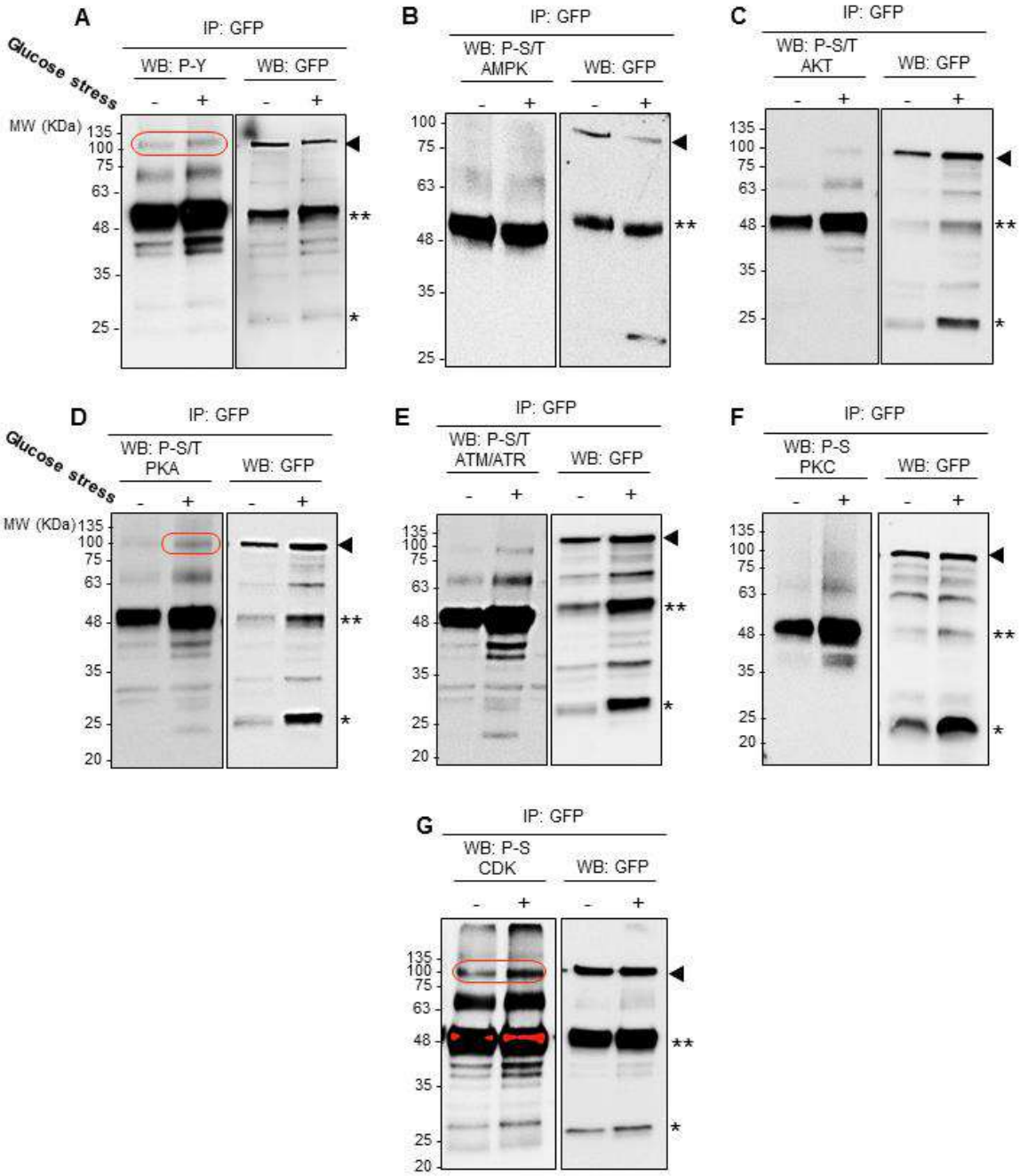

Figure 5.13: Analysis of protein phosphorylation in EGFP-TG2 precipitates from cells subjected to glucose stress. NRK52E EGFP-TG2 overexpressing clones were subjected to glucose stress to simulate a pro-fibrotic condition (5mM glucose = - / 30 mM glucose = +) and EGFP-TG2 chimera was immunoprecipitated from equal amounts of cell lysate (750 µg) with a rabbit polyclonal anti-GFP antibody (Abcam) as described in 5.3.3 Equal volumes (40 µl) of GFP-immunoprecipitated proteins (IP:GFP) were screened for the presence of phosphorylated tyrosine, serine or threonine by Western blotting using specific antibodies reported in **Table 5.6.** Immunoreactive bands were detected by enhanced chemiluminescence (Geneflow) after incubation with appropriate HRP-conjugated secondary antibody (**Table 5.6**) in blocking buffer. Image acquisition was performed with a LAS4000 imaging system. The blot was then stripped and probed with Rabbit polyclonal anti-GFP (Abcam, **Table 5.6**) followed by goat anti-rabbit IgG conjugated to HRP (Dako) to confirm the immunoprecipitation (WB: GFP). The EGFP-TG2 chimera expected MW is 100 kDa (arrowhead). Each experiment was performed in duplicates or triplicates. The figure shows representative blots for each antibody employed. Asterisk represent co-eluted IgGs (** = Heavy Chain; *=Light Chain). Red circles identify phosphorylated EGFP-TG2. A = Rabbit polyclonal anti-phosphotyrosine; B = Rabbit monoclonal Phospho-(Ser/Thr)AMPK;CF =

Rabbit monoclonal Phospho-AKT; D = Rabbit monoclonal Phospho-PKA; E = Rabbit monoclonal Phospho-(Ser/Thr) ATM/ATR; F = Rabbit monoclonal Phospho-(Ser) PKC; G = Rabbit monoclonal Phospho-(Ser) CDKs.

5.4.5 Investigation of the importance of the endocytic protein clathrin for TG2 presence on the cell surface

As reported before in chapter IV, clathrin and clathrin coated vesicles (CCV)- associated proteins were identified as TG2- partners in the enzyme's interactome by SWATH-MS in both healthy and fibrotic kidney membranes, hence might directly or indirectly interact with the enzyme itself during its trafficking. Knowing this, it was considered interesting, as an additional investigation, to study the effect of clathrin knock down on extracellular TG2.

First, to investigate the the co-precipitation of clathrin with TG2 in our cell model, NRK52E EGFP-TG2 overexpressing clones were subjected to a glucose stress (30mM) as described in the previous section (5.4.4) and immunoprecipitation of the EGFP-TG2 chimera was performed on equal amounts of cell lysates (5.3.9). Co-precipitation of clathrin was investigated on EGFP-immunoprecipitated extracts by Western blot, using a specific antibody against the heavy chain of clathrin, with predicted size of ~180 kDa. Expression of EGFP was tested as well on the same lysates, and employed as a control for protein precipitation (**Fig. 5.14A**). Immunoprobing of clathrin on EGFP-TG2 immunprecipitates revealed a faint band at high molecular weight (> 130 kDa), which is likely to be specific (**Fig. 5.14A**, arrowhead). Expression of this protein was more intense in cell stressed with high glucose, while the level of precipitated EGFP-TG2 chimera at 100 kDa remained equal in both conditions (**Fig. 5.14A**, black arrow). This suggested that clathrin is partially associated with TG2 in EGFP-TG2 overexpressing Rat TECs, and that the association with the enzyme is increased by glucose stress, probably due to an increased amount of enzyme outside the cells.

Immunofluorescent staining of both clathrin and TG2 was also performed on NRK52E WT cells following the general protocol for immunofluorescece reported in Chapter II (2.2.8). The staining revealed a partial co-localisation of TG2 (**Fig. 5.14B**, in red) with clathrin (**Fig. 5.14B**, in green) in non permeabilised cells, while it was weaker intracellularly in permeabilised cells (**Fig. 5.14B**).

Clathrin knock down was performed on both WT and EGFP-TG2 overexpressing NRK52E cells, by transient transfection of rat clathrin-targeting siRNA, as described in 5.3.10. Non-targeting scrambled siRNA was employed as a control. Transient transfection with 100 nM rat clathrin -targeting siRNA for 24 h led to a visible reduction of clathrin expression at a protein level in both WT and EGFP-TG2 overexpressing TECs, as investigated by western blot (**Fig. 5.14C,** arrowhead). Interestingly, a reduction in TG2 expression, both exogenous EGFP-tagged (100

kDa, black arrow) and endogenous (75 kDa, grey arrow), was observed in EGFP-TG2 overexpressing TECs subjected to Clathrin KO when the same lysates were probed with an anti-TG2 antibody, and might be linked to a reduced endocytosis of the enzyme itself (**Fig. 5.14 C,** red circle).

When extracellular TG2 activity was measured by biotin-cadaverine incorporation assay performed on living cells, no effect was observed on WT NRK52E cells (**Fig. 5.14D**). On the contrary, a small but significant rise (p=0.0002, ***) was detected in extracellular TG2 in EGFP-TG2 overexpressing NRK52E cells subjected to siRNA knock down of clathrin (**Fig. 5.14D**, red circle).

Results from clathrin knock down in EGFP-TG2 overexpressing TECs suggest a possible involvement of clathrin in TG2 endocytosis, with a reduced amount of TG2 inside the cells and an increased amout of extracellular/cell surface associated one upon knock out of clathrin. This is in line with previous findings of an LRP1-mediated internalisation of TG2, where the involvement of CCV was proposed (Zemskov, et al. 2007). However, it was not confirmed in WT cells in this study, suggesting that the phenomenon might happen only in conditions of TG2 overexpression, and not at a basal level of endogenous TG2.

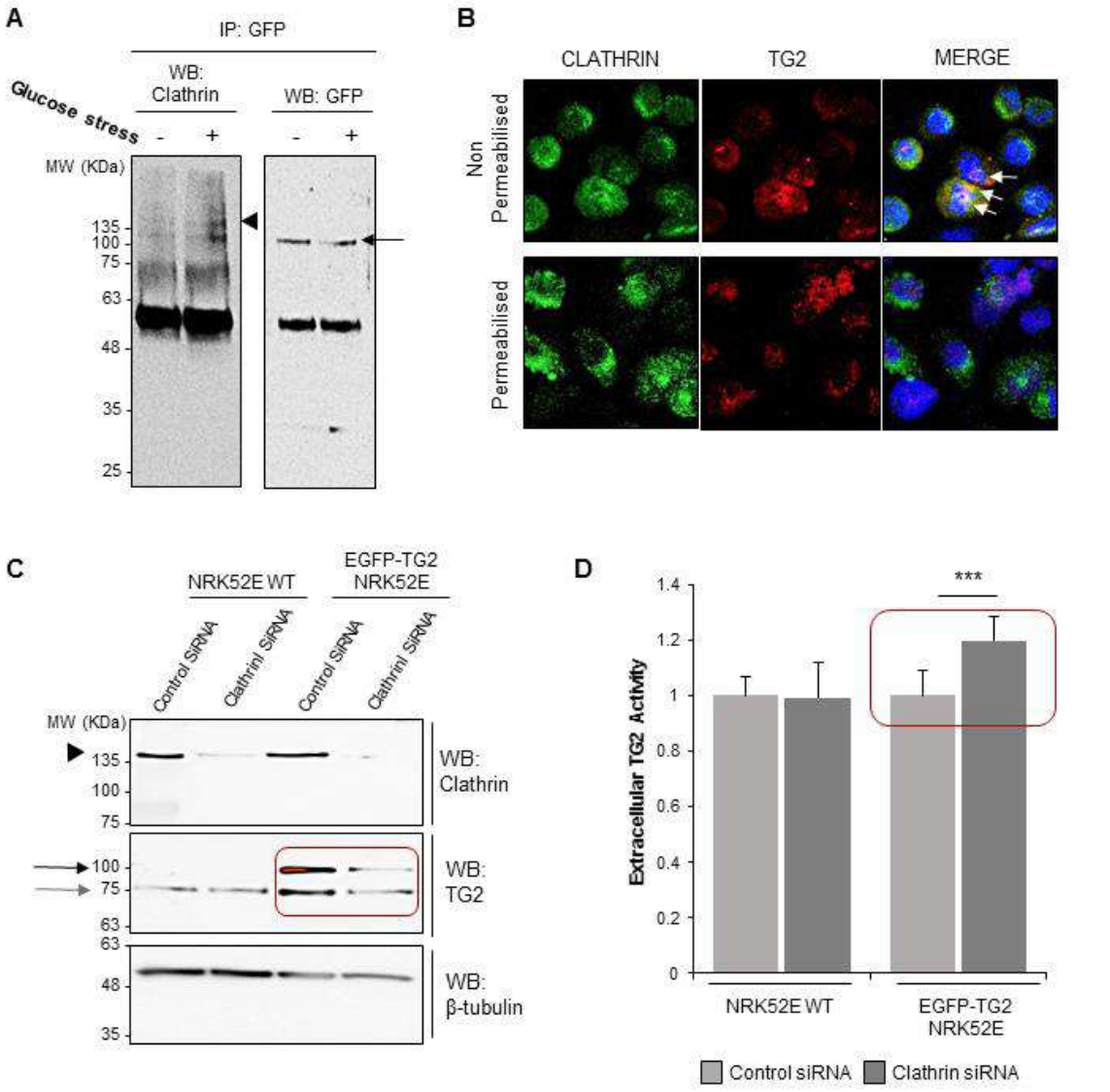

Figure 5.14: Study of interaction between Clathrin and extracellular TG2. (A) NRK52E EGFP-TG2 overexpressing clones were subjected to glucose stress and EGFP-TG2 chimera was immunoprecipitated as described in **Fig 5.13**. Equal volumes (40 µl) of GFP-immunoprecipitated proteins (IP:GFP) were screened for the presence of clathrin using a rabbit monoclonal antibody described in 5.3.10**.** GFP was also probed to confirm IP of EGFP-TG2 chimera at 100kDa (black arrow). A representative blot is here shown. Arrowhead indicates clathrin heavy chain signal > 130 kDa. **(B)** Co-Immunofluorescent staining of Clathrin and TG2 was performed on both non permeabilised and permeabilised NRK52E WT cells subjected to glucose stress (30 mM glucose), as described in 2.2.8. A rabbit monoclonal antibody against clathrin (4796, Cell Signalling,– dilution 1:400) followed by a donkey anti-rabbit Alexa Fluor® 488 antibody, with green fluorescence, and a mouse monoclonal anti-TG2 antibody (IA12, University of Sheffield - dilution 1:400) followed by a goat anti-mouse antibody Alexa Fluor® 598, with red emission were employed for the assay. White arrows indicate points of TG2 and clathrin co-localisation. **(C, D)** Clathrin knock down was performed on both NRK52E WT and EGFP-TG2 overexpressing NRK52E (clone #C5) cells, by transient transfection with rat clathrin-targeting siRNA, as described in 5.3.10. 24 h after transfection, (C) the effect of the knock down at a protein level was measured on equal amounts of proteins by immunoprobing clathrin, TG2 (Ab421, Abcam) and β-tubulin as a loading control. (D) The effect on extracellular TG2 was measured by extracellular TG2 activity assay as described in 2.2.9.2. The values are the average Abs (450 nm) of three independent experiments, each undertaken in quadruplicates, normalised for the relative scrabled siRNA control (equalised to 1) ± SD. Significance of the differences between treatments was determined by T-test: * = $p<0.05$, ** = $p<0.01$, *** = $p<0.001$, **** = $p<0.0001$.

5.5 DISCUSSION

Extracellular TG2 has been suggested to play a number of roles on the cell surface and ECM, contributing to the progression of fibrosis in the context of CKD, while its inhibition in the extracellular environment has been found to be protective against the progression of disease. Despite being primarily a cytosolic enzyme, TG2 export and extracellular activity have been shown to significantly increase during the progression of CKD in response to pro-fibrotic stimuli. The enzyme is known to be unconventionally secreted in the ECM as a leaderless protein, through a mechanism that is still not completely clarified. Here, the main objective was to understand the mechanism of TG2 unconventional secretion during fibrosis progression.
As the analysis of TG2 interactome in kidney cellular membranes highlighted a significant cluster of TG2 interacting proteins also located in extracellular vesicles, which increased in expression and complexity post UUO, it was hypothesised that TG2 could be secreted via extracellular vesicles.
As kidney tubular epithelial cells (TECs) are regarded as the main source of TG2 released in the matrix during fibrosis development (Johnson, et al. 1999, Johnson, et al. 2003) tubular epithelial cell line of NRK52E cells was selected for *in vitro* investigations of TG2 secretion. Although this established cell line expresses TG2 endogenously, rat TG2 is notoriously harder to detect by immunoassays than human TG2, especially in low protein preparations, therefore we reasoned that the EGFP reporter could facilitate the study of TG2 secretion and a clonal cell line of NRK52E cells expressing EGFP-tagged human TG2 was also employed.

The requirement of a vesicular intermediate and membrane fusion events for TG2 export was demonstrated in this cell line by the requirement of NSF-ATPase for TG2 secretion (both antigen and cell surface activity) (**Fig. 5.5**). As NSF-ATPase is necessary for a variety of membrane fusion events mediated by SNAREs (Zhao, Slevin and Whiteheart 2007) including exosome secretion by MVB fusion (Fader, et al. 2009), and was identified as associated with TG2 in kidney membranes in the previous chapter (Chapter IV), this finding suggests that vesicle fusion events mediated by SNAREs and requiring NSF-ATPase are at least in part involved in TG2 unconventional release from TECs. Although NEM has been reported to interfere with TG2 catalytic activity by promoting the formation of thiol groups (Kumazawa, et al. 1997), the fact that also the release of TG2 protein was inhibited by NEM rules out any interference with TG2 activity detection (**Fig. 5.5C**). Therefore, extracellular TG2 could be secreted through a mechanism requiring vesicle-membrane fusion, such as the recycling endosome - to - plasma membrane pathway proposed by Zemkov and colleagues (Zemskov, et al. 2011), or via MVB/exosome release.

To investigate whether TG2 was secreted via a MVB/exosome pathway, extracellular vesicles were isolated by differential centrifugation from serum-free conditioned medium, according to well established protocols which allow the separation of exosomes from vesicles shedded from plasma membrane, MV or ectosomes (Bianco, et al. 2009) (**Fig. 5.6A**). One exosomal/ectosome marker was employed in this investigation, flotillin-2 (**Fig. 5.6B**); this is a well-characterised EV protein which can be reliably detected by immunoblotting; moreover flotillin-2 emerged as a clear partner of TG2 in the UUO, indicating a co-association, either direct or indirect, with TG2 in conditions favouring the enzyme export.
TG2 presence in exosomes, as detected by Western blot on EV fractions from TECs (both WT and EGFP-TG2 overexpressing), and its further enrichment when a fibrosis-like condition was simulated in the cells by TGF-β1 addition, strongly suggest that TG2 is released via EV of intraluminal origin (exosomes) (**Fig. 5.7**). Exosomes-associated TG2 was also identified in the conditioned medium of rat renal fibroblast (NRK49F), suggesting that TG2 release into the exosomal fraction is not limited to the specific cell line. Interestingly, some TG2 was also found in larger vescicles shedded from the plasma membrane (ectosomes), although in lower amount, while the free TG2 in EV-deprived conditioned medium was generally low or absent, with some level of variability from preparation to preparation.

TG2 association with exosomes was confirmed by employing an inhibitor of ceramide synthesis by nSMase, known to interfere with exosome biogenesis (Luberto, et al. 2002, Trajkovic, et al. 2008), which significantly reduced extracellular TG2 as detected by immunofluorescence, completely abolished TGF-β1-stimulated release, and clearly lowered TG2 association with the exosomes without interfering with the microvesicle fraction (**Fig 5.9**). Employment of an inhibitor of ceramide biogenesis at the plasma membrane by aSMase, with a proposed inhibitory effect on ectosomes release (Bianco, et al. 2009), had a less singnificant consequence on TG2 relesase and a more general effect on TG2 presence in all fractions. Similarly, the employment of the inhibitor of Na+/H+ exchanges amiloride, suggested to interfer with exocytosis of micropinosomes (Falcone, et al. 2006), led to some decrease in TG2 release, but the reduction of TG2 associated with the MV fraction (P3), though observable, was not particularly strong (**Fig 5.9**). However, amiloride specificity in the inhibition of EV secretion is not yet clear as amiloride / N-ethyl-N-isopropyl amiloride (EIPA) has mainly been involved in the inhibition of micropinocytosis, which is favoured by H+/Na+ exchange (Stelmach, Rusak and Tomasiak 2002, Koivusalo, et al. 2010). In the context of EVs, only few studies have proposed an inhibitory effect of EIPA on ectosome release (Stelmach, Rusak and Tomasiak 2002) or macropinosomes release (Falcone, et al. 2006) while limited works have suggested that dimethyl amiloride inhibits calcium-regulated exosome secretion by blocking channel activity (Savina, et al. 2003, Chalmin, et al. 2010, Merendino, et al. 2010).

In summary, validation of TG2 association with exosome with inhibitor of ceramide synthesis and the finding of TG2 in EV lysate should convincingly establish that TG2 is exported via exosomes in the TEC cell line, consistent with the finding of abundant exosomal proteins in the TG2 interactome. Altogether these data suggest that, however TG2 could be identified in the ectosomal fraction, that was paticularly enriched of TG2 at the early minutes post-treatment (**Fig. 5.10**), is more likely to be release through an exosomal fraction from TECs.

In agreement with this, while this thesis was in preparation, Piacentini's group published a study on human embrionic kidney cells and mouse embryonic fibroblasts suggesting that TG2 might be secreted into exosomes and even contribute to exosome biogenesis under stress conditions, such as proteasome inhibition or the expression of mutant huntingtin (mHtt), an excessively glutaminated mutant huntingtin that is the main cause of Huntington disease (Diaz-Hidalgo, et al. 2016). They proposed that, for its secretion, TG2 was interacting with two of the main proteins involved in intraluminal vesicles biogenesis: Alix and Tsg101 (Diaz-Hidalgo, et al. 2016). In particular, they suggested that, upon stress, TG2 was able to determine the assemblage of a complex including not only the two abovementioned proteins, but also the mutant huntingtin mHtt and the co-chaperone involved in its removal from the cells, BAG3, a complex that seemed to be necessary for the selective cargo loaging mHtt/BAG3 in the exosome (Diaz-Hidalgo, et al. 2016). Previous works have identified TG2 in exosomes (Skogberg, et al. 2015, Piacentini, et al. 2014), however, the latter work and the current study form our group are the first ones trying to provide an explanation for TG2 localisation in this fraction and hypothesize a secretion pathway. Interestingly, in the current study, TG2 was identified as significantly associated with huntingtin-interacting proteins in UUO kidney membranes, and "Huntington disease" pathway was identified as significantly enriched in the list of TG2 partners cell-matrix iterface both in fibrotic and sham operated condiions. This might support the idea of an exosomal pathway for TG2 secretion that might happen under stressed conditions in different types of diseases.

There is an interest in understanding whether TG2 is present on the surface of released EVs or on their inside. This specific question is particularly relevant, considering that TG2 on the surface of vesicles can directly interact with its partners in the extracellular space such as HSPGs, FN, integrins etc., while, if the enzyme was uploaded inside the vesicle, it would require vesicle degeneration/dissolution for release in the matrix. To attempt an initial answer to his question, we developed an experimental approach aimed at measuring the catalytic activity of TG2 of whole EV and lysed EV (**Fig. 5.8**). Our preliminary results suggested that TG2 is likely to be located mostly on the surface of these vesicles, rather than in their inside, however, a better resolution approach would be necessary for the experiment to be conclusive. At the moment, we can only hypothesize that TG2 is present on the cell surface of released exosomes.

The fact that at the early times after cell medium is changed, and vesicles cleared-out by PBS wash, the exosomal fraction is minimal and substantially lower than the ectosomal, then tends to increase along the time made us speculate that many of the exosomes released might accumulate in the medium and reamain associated with the extracellular space, maybe by binding to cell surface receptors such as Sdc4 or integrins or ECM adhesion proteins such as FN. Being TG2 a known binding partner of several extracellular components, including HSPGs and FN, its presence on the exosome surface would contribute to a direct interaction of the exosomes with the matrix and their retention in the matrix. This would also explain the large retention of TG2 in the matrix as observed by immunofluorescence experiments in this Chapter.

As many pathways of unconventional protein secretion have been seen to involve protein binding to membrane phospholipid, an analysis of recombinant TG2 binding to immbilised phospholipids was performed (**Fig. 5.11**). Preliminary data obtained showed that TG2 binds with good affinity PI(4,5)P2, typical of the inner side of the plasma membrane and suggested as key element of FGF2 secretion mechanism (Steringer, et al. 2012). In the same assay, the binding to recycling endosome typical PI(3)P, suggested by Zemskov and colleagues as importat in the context of recycling endosomes-dependent TG2 trafficking, was much lower (Zemskov, et al. 2011). Interestingly, in support to our findings of TG2 association with MVB/exosomes, PI(3,5)P2 had the highest binding to TG2 and is known to be mainly present on the late endosomes/MVBs and lysosomes membranes, where is upregulated in events of "lysosome exocytosis" by macrophages (Samie, et al. 2013, Li, et al. 2013).

Phosphorylation of TG2 or TG2-associated proteins was also investigated in TECs, in conditions favouring the enzyme's export from NRK52E cells, such as a glucose stress (Huang et al., manuscript in preparation) (**Fig. 5.13**). PKA-mediated phosphorylation was identified upon stress, in line with previous studies highligting TG2 phosphorilation at Ser216 by PKA and its effect on TG2 activity and signalling (Mishra and Murphy 2006). However, highest phosphorylation was obtained by cyclin dependent kinase (CDK), a kinase primarily involved in the regulation of cell cycle. More experiments will be required to eludcidate possible consequences on TG2 export.

Finally, given the elevated numer of proteins in the TG2 interactome with a reported association with clathrin-mediated endocytosis, as an additional investigation the effect of clathrin deletion on the amount of extracellular TG2 was examined on TECs (**Fig. 5.14**). Results highlighted a possible involvement of clathrin-mediated endociytosis in the TG2 uptake from TECs, in line with previous studies of receptor-mediated TG2 internalisation (Zemskov, et al. 2007).

In conclusion, in this chapter, the hypothesis of a TG2 unconventional secretion mediated by EV was investigated, and results suggested a TG2 association with the exosomal compartment, wich is supported by the TG2 interactome analysis in kidney membranes presented in the previous chapter. The hypothesis that TG2 is secreted on the surface of exosomes, and that TG2-bearing exosomes accumulate in the extracellular matrix by binding adhesion molecules, is a fascinating hypothesis, that will be able to link a possible pathway of TG2 unconventional secretion from TECs with TG2 adhesive and pro-fibrotic role in the ECM during the process of kidney fibrosis. In support to this idea, a recent comparative analisys published on Bone has suggested that the so called "matrix vesicles", extracellular-membrane bound vesicles involved in vascular calcification, and the exosomes are homologous structures with similar markers and biogenesis (Shapiro, Landis and Risbud 2015). Moreover, exosomes have been shown to act as cell adhesion mediators in epithelial cells, fibroblasts and cancer cells, a mechanism that involved FN and in which we can hypotesize extracellular TG2 could play a role (Koumangoye, et al. 2011, Mu, Rana and Zöller 2013, Sung, et al. 2015).

If this was the case, we could postulate the existance of a population exosomes similar to matrix vesicles that are released from TECs in a profibrotic cytokine - stimulated fashion, carry TG2, and interact twith FN and HSPGs/Sdc4 in the extracellular environment, where they contribute to matrix deposition and adhesion.

As HSPGs, and in particular Sdc4, have been previously identified as important binding partners of TG2 for its secretion by mouse dermal fibroblast and *in vivo* in models of kidney fibrosis, including the UUO (Scarpellini, et al. 2009, Scarpellini, et al. 2014), and since the HSPGs Sdc4 and perlecan have been highlighted as uniquely associated with TG2 in kidney fibrotic membranes in the current study (Chapter IV), it would be interesting to investigate the involvement of cell surface HSPG Sdc4 in TG2 unconventional secretion by kidney TECs, to try to define if and at which stage the HSPGs-TG2 interaction takes place. This analysis will be the focus of the next, and last, chapter of results.

Chapter VI: The role of heparan sulfate proteoglycans (HSPGs) in TG2 secretion and extracellular retention by TECs

6.1 AIMS OF THE CHAPTER

As heparan sulfate proteoglycans (HSPGs) /syndecan 4 (Sdc4) have been suggested as potential partners of TG2 during kidney fibrosis, and since studies from my group have previously proposed a role for HSPGs, and specifically for Sdc4, in TG2 trafficking *in vivo* in kidney fibrosis models and *in vitro* in mouse dermal fibroblasts, the hypothesis of a role for HSPGs/Sdc4 in the unconventional secretion of TG2 from tubular epithelial cells (TECs) has been raised. The aim of this chapter is to investigate the role of HSPGs, and in particular Sdc4, in TG2 release and extracellular retention from kidney TECs, with a particular interest in the elucidation of the potential involvement of Sdc4 in the vesicular mechanism of TG2 unconventional secretion.

6.2 INTRODUCTION

6.2.1 Heparan sulfate proteoglycan (HSPG) biosynthesis and roles in the cells

fv6.2.1.1 Biosynthesis of HS chains in the cell

HSPGs are characterised by HS chains, particularly long GAG carbohydrates (40–300 monosaccharides, covering 20–150 nm), strongly anionic and characterised by different levels of sulfation and epimerisation (Sarrazin, Lamanna and Esko 2011). Some HSPGs are characterised by only one chain while others, such as syndecans, have up to five chains (**Fig. 6.1A**). The basic units building the HS chains are disaccharide units of β-D-Glucuronic acid (GlcA) and α-D-N-acetylglucosamine (GlcNAc), however, during biosynthesis, a series of enzymes contribute to GlcNAc N- diacylation/sulfation, O- sulfation, and epimerisation of the GlcA residues to iduronic acid (IdoA) (Sugahara and Kitagawa 2002, Whitelock and Iozzo 2005) (**Fig. 6.1B**). HS biosynthesis relies on a series of enzymatic steps happening in the Golgi apparatus and employing nucleoside-monosaccharides imported from the cytoplasm (Bishop, Schuksz and Esko 2007, Whitelock and Iozzo 2005), as schematically shown in **Fig. 6.1B**. HS biosynthesis starts at the GAG attachment sites of the core protein, which contain Serine-

Glycine sequences. The first steps of serine xylosilation and linkage region formation are in common between heparan sulfate (HS) and chondroitin sulfate (CS), while the following steps proceed differently for each type of GAG chains (Esko, Kimata and Lindahl 2009). Specific aminoacidic clusters around the attachment serine (e.g. contiguous Ser-Gly residues in the attachment sites for HS) as well as specific phosphorylation and sulfation of the linkage region are thought to be involved in the selection between the type of GAG chains assembled, being recognised by the specific enzymes involved in GAG elongation (Sugahara and Kitagawa 2002). HS elongation is shown in **Fig. 6.1B**. CS elongation is similar to HS chains, but, in this case, is formed of N-acetyl-galactose and glucuronic acid (Esko, Kimata and Lindahl 2009).

As the HS chain is growing, it simultaneously undergoes a series of modifications performed by a range of enzymes acting in the same Golgi stacks (Sugahara and Kitagawa 2002, Whitelock and Iozzo 2005) such as N- deacylation/N-sulfatation of GlcNAc to GlcNS by the enzyme GlcNAc N-deacetylase/N-sulfotransferase (Ndst), epimerisation by uronyl-C5 epimerase, which acts on the GlcA residues present in the N-sulfated domains (next to GlcNS), determining the formation of iduronic acid (IdoA) residues, and O-sulfation, which happens at different residues and is mediated by series of O-sulfotransferases (**Fig. 6.1B**). For example, 6-O sulfotransferases (Hs6st1-3), mediate the O-sulfation at C6 of N-sulfoglucosamine (GlcNS), with formation of GlcNS(6S). Rarely, also GlcNAc can be 6O-sufated. These modifications generate relatively short segments of sulfate sugars (sulfated domains) and iduronic acid alternated to variable lengths of unmodified domains. Because of these specific patterns and the strong negative charge, the HS chains can bind a great number of ligands including cytokines and growth factors, ECM structural proteins, enzymes, etc. Once HSPGs are secreted to the cell surface or ECM, they can undergo further modifications. In fact, the number of sulfated groups can be altered by plasma membrane-bound endosulfatases SULF1/2, that selectively remove sulfate groups from the HS chain, possibly as a consequence of specific signalling (Bishop, Schuksz and Esko 2007). Moreover, once exported, mammalian HS chains can be enzymatically cleaved by a specific extracellular enzyme called heparanase (endo-β-glucuronidases), that digests HS in specific sites (between GlcA-GlcNS located after IdoA-GlcNAc), determining the release of chains and associated ligands in the extracellular space (Dreyfuss, et al. 2009).

In addition to the typical HS chains, few cells can produce heparin, a highly sulfated HS chain. In heparin, more than 80% of the GlcN residues are sulfated and more than 70% GlcA is epimerized to IdoA (Esko, Kimata and Lindahl 2009). As a result, while HS chains contain only ~0.8 sulfate groups per disaccharide, heparin contains approximately 2.3 (Sarrazin, Lamanna and Esko 2011). As a proteoglycan GAG chain, heparin is produced only in the connective tissue and exclusively as a serglycin-associated chain while HS is produced virtually byall cells (Esko, Kimata and Lindahl 2009).

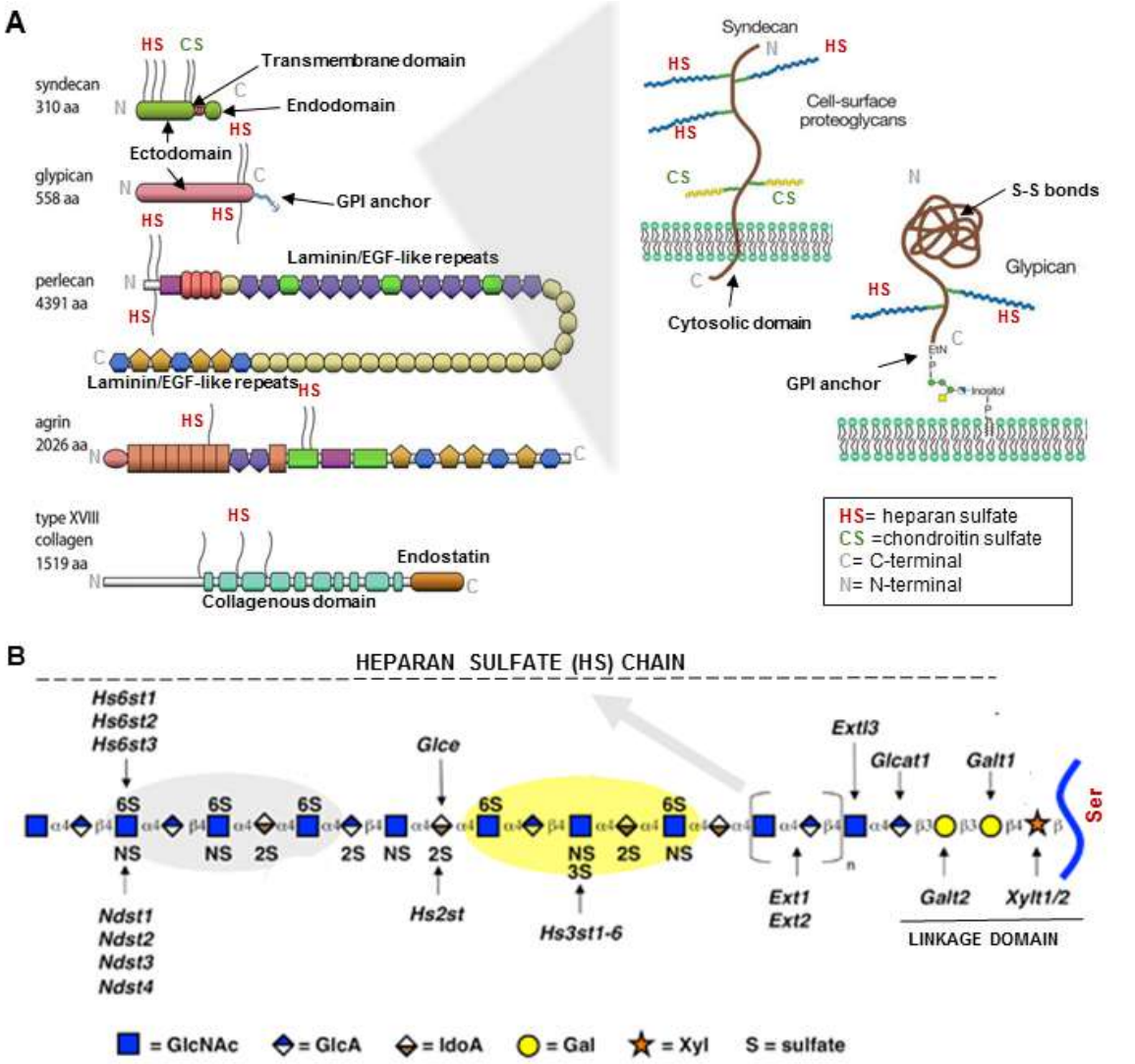

Figure 6.1: Heparan sulfate proteoglycans (HSPGs). (A) Structure of main cell surface and secreted HSPGs. Pictures adapted from (Iozzo 2001, Esko, Kimata and Lindahl 2009). Permission to reproduce these pictures has been granted by Cold Spring Harbor Laboratory Press and the American Society for Clinical Investigation. **(B)** Structure of heparan sulfate (HS) chains and enzymes involved in HS chains biogenesis and modifications. HS biosynthesis starts at the GAG attachment sites of the core protein, which contain serine-glycine sequences. The first step is the binding of a xilose to Ser residue by aim of a specific enzyme named xylosyltransferase (XylT) that employs UDP-xylose as donor. The following step is a formation of a linkage region, a tetrasaccharide sequence determined by the stepwise addition of two galactoses (Gal) and one glucuronic acid [GlcA β1-3Gal β1-3Gal β1-4Xyl β1-O-Ser] performed by specific glycosyltransferases: β1–4 galactosyltransferase, β1–3 galactosyltransferase (GalTI and GalTII) and β1–3 glucuronosyltransferase (GlcAT). HS elongation from the linkage region is initiated by the addition of a first α1–4 GlcNAc performed by an exostoses family – like (Extl) enzyme called Extl3 (GlcNAc transferase). Subsequently, an enzyme complex composed of the HS polymerases of the exostoses family (Ext), Ext1 and Ext2 (GlcA/GlcNAc Transferases), continues the HS chain elongation by alternatively adding GlcA and GlcNAc from the corresponding UDP sugars (Esko, Kimata and Lindahl 2009). N- deacylation/N-sulfatation of GlcNAc to GlcNS is perfomed by the enzyme GlcNAc ndeacetylase/nsulfotransferases (Ndst) using 3′-phosphoadenosine 5′-phosphosulfate (PAPS) as sulfate donor. Uronyl C5 epimerase acts on the GlcA residues present in the N-sulfated domains (next to GlcNS), determining the formation of iduronic acid (IdoA) residues. O-sulfotransferases mediate O-sulfation employing PAPS as sulfate donor. IdoA undergoes 2O-sulfation (sulfation at C2) performed by uronyl 2-O-sulfotransferase (Hs2st). 6-O sulfotransferases (Hs6st1-3), at the same time, mediate the O-sulfation at C6 of GlcNS or GlcNAc (rarely). 3-O-sulfotransferases (Hs3st1, 2, 3a,3b, 4, 5, 6) determine a less frequent O-sulfation at C3 of either GlcNS, GlcNS(6S)and GlcNAc with production of GlcNS(3S), GlcNS(3S+6S) and GlcNAc(3S). Adapted from (Esko, Kimata and Lindahl 2009). Permission to reproduce this picture has been granted by Cold Spring Harbor Laboratory Press.

6.2.1.2 HSPGs roles in the cells

HSPGs have been reported to bind a large number of ligands. Binding occurs mostly through their long HS chains, even if ligand associations with the core protein have also been described. For example, the core protein of syndecans is able to interact with both integrins and cytoskeletal elements [6.2.2-3], while long HSPGs such as perlecan are characterised by a series of ligand-binding independent domains (e.g. for laminin). The ability of proteins to bind HS generally depends on the presence of narrow pockets of positively charged basic amino acids (lysine, arginine and rarely histidine) on their surface in the tertiary structure (Sarrazin, Lamanna and Esko 2011, Dreyfuss, et al. 2009). For example, two consensus motifs have been proposed (XBBXBX and XBBBXXBX, where B represents a basic residue and X an hydropathic -neutral or hydrophobic- residue)(Cardin and Weintraub 1989), but they not necessarily appear on all heparin binding proteins (Dreyfuss, et al. 2009). In general, it seems that the specificity of the interactions of HS chains with particular proteins is associated with the overall organization HS chain (presence of IdoA sulfate, number of 6O sulfation, etc.) and not on a specific monosaccharide sequence (Kreuger, et al. 2006).

Ligand biding of cell surface HSPGs can induce their clustering and promote cell signalling. Given the long HS chains, that can cross the extracellular matrix, some functions of HSPGs occur both "*in cis*"(on the same cell) or "*in trans*" between neighbour cells (Bishop, Schuksz and Esko 2007). The next paragraphs will provide a general description of some of the more described roles of HSPGs in the cell (**Fig.6.2**). Specific description of syndecan functions will be provided in the next section [6.2.2-3]

HSPGs are able to bind cytokines and growth factors such as fibroblast growth factors (FGFs), transforming growth factors (TGF-β1,2), vascular endothelial growth factor (VEGF), platelet derived growth factor (PDGF), etc. (Dreyfuss, et al. 2009, Sarrazin, Lamanna and Esko 2011) through the HS chains. By binding these molecule, HSPGs play a role in controlling their activity, stability and localisation in the matrix, regulate their clustering and provide protection against proteolysis (Dreyfuss, et al. 2009, Bishop, Schuksz and Esko 2007). HSPGs can function as storage reservoirs for cytokines and growth factors in the matrix: cytokines, chemokines, growth factors etc. can be held in specific positions or stored until necessary in the matrix, from which they can be released by heparanase cleavage or core protein shedding (Dreyfuss, et al. 2009, Iozzo, Zoeller and Nyström 2009, Bishop, Schuksz and Esko 2007). Shedding of cell surface proteoglycans, specifically syndecans, by MMPs, is controlled by intracellular signalling pathways and can contribute to liberation of stored factors and chemokines.

Shedding can have a duplex role in the control of inflammation by either increasing chemokine migration in the inflammatory area or promoting chemokine release from the inflammation area (Kirkpatrick and Selleck 2007).

HS-bound chemokine gradients on endothelial cells are involved in leukocyte recruitment during inflammatory response and physiological leucocyte distribution (Wang, et al. 2005). One of the less described cell surface HSPG, betaglycan, is able to bind TGF-β through the core protein and FGF2 though the HS chains. By binding TGF-β, this proteoglycan contributes to the storage of growth factor for TGF-receptors, without directly contributing to signal transduction.

HSPGs can play a role in cellular signalling indirectly, by acting as co-receptors, or directly, by acting as receptor themselves. One of the more described HSPG ligands is FGF2, also known as basic fibroblast growth factor. Cell surface HSPGs bind FGF2 trough the HS chains, and this binding has been suggested to favour the protein's unconventional secretion (Steringer, et al. 2012, La Venuta, et al. 2015) (described in chapter V), localisation in the extracellular space, dimerization and protection from proteolytic degradation. Importantly, in this context, cell surface HSPGs have also been suggested to play a co-receptor role: it has been suggested that cell surface HSPGs can act as a co-receptor for FGF2 receptor tyrosine kinase (FGFR), favouring the formation of a ligand-receptor complex, possibly by inducing conformational changes on the bound proteins (dimerization), and, ultimately, promoting tyrosine kinase-dependent signalling (Steinfeld, Van Den Berghe and David 1996, Spivak-Kroizman, et al. 1994). The co-receptor function of HSPGs has been extended to the other members of the FGF family (Dreyfuss, et al. 2009), as well as to other growth factors such as VEGF (Ashikari-Hada, et al. 2005), PDGF (Abramsson, et al. 2007), etc. The effect of HSPGs as co-receptors can occur "*in cis*", when HSPGs and receptors are present on the same cells, or "*in trans*", when HSPGs and receptors are present on adjacent cells (Sarrazin, Lamanna and Esko 2011, Kramer and Yost 2002, Jakobsson, et al. 2006). In general, the ability of HSPGs to trans-activate adjacent cells is important to promote cellular interaction, signal transduction and cell differentiation (Sarrazin, Lamanna and Esko 2011).

Cell surface HSPGs can also act themselves as receptors, inducing a signalling cascade in a non-enzymatic, protein-kinase dependent manner. Particularly studied, in this context, are the transmembrane syndecans, characterized by specific phosphorylation sites on the cytosolic domain of the protein core and able to bind specific kinases. The best studied example is Sdc4 (Simons and Horowitz 2001), described in the next section [6.2.3].

Cell surface HSPGs, and specifically syndecans, can interact with integrins and other cell adhesion receptors, mediating cell adhesion and cell-cell interactions. One of the most common integrin binding domain present on ECM proteins is the RGD (arginine-glycine-aspartic acid) peptide sequence, that has been well described on FN. As cell surface HSPGs, and in particular syndecans, are able to bind FN on its heparin-binding domain, they can contribute to focal adhesion and stress fibres formation in collaboration with integrin or even as an

alternative cell adhesion receptor (Saoncella, et al. 1999a, Echtermeyer, et al. 1999, Alexopoulou, Multhaupt and Couchman 2007).

Another interesting function of cell surface HSPGs (both syndecans and glypicans) is the ability to act as endocytic receptors, involved in both constitutive and ligand-induced endocytosis. HSPG-mediated endocytosis appears to be both clathrin, caveolin and dynamin -independent, to be associated with lipid rafts of specific composition and to be similar to micropinocytosis (Christianson and Belting 2014). In most cases, endocytosed HSPGs are directed to the lysosome, where both HSPG and ligand is degraded. Particularly studied, in this case, is the lipoprotein degradation mediated by HS binding and endocytosis (Stanford, et al. 2010), that gives HSPGs a role in metabolic control. In the case of syndecans, internalisation can be triggered by clustering of the transmembrane and cytoplasmic domains (Fuki, et al. 1997). Cell surface syndecans have also been involved in the endocytosis of other molecules, such as FGF2 internalisation by micropinocytosis mediated by Sdc4, that involves protein-core oligomerisation (Tkachenko, et al. 2004). In some cases, internalised HSPGs can be recycled (Christianson and Belting 2014). A typical example is the Syndecan recycling together with FGF receptor (Zimmermann, et al. 2005).

Finally, extracellular matrix HSPGs such as perlecan, agrin and endostatin contribute to the definition of the basement membrane (BM) structure containing laminin, collagen and glycoproteins. The formation of a basement membrane not only contributes to the resistance of the tissue against mechanical stress, but also provide a highly charged barrier against the filtration of specific solutes (Iozzo 2005). For example, in the kidney, a thick glomerular basement membrane (GBM) rich in HS chains forms a negatively charged barrier that prevents anionic proteins from entering the ultrafiltrate. Loss of HS chains, in this context, leads to proteinuria in the urine (Raats, Van Den Born and Berden 2000).

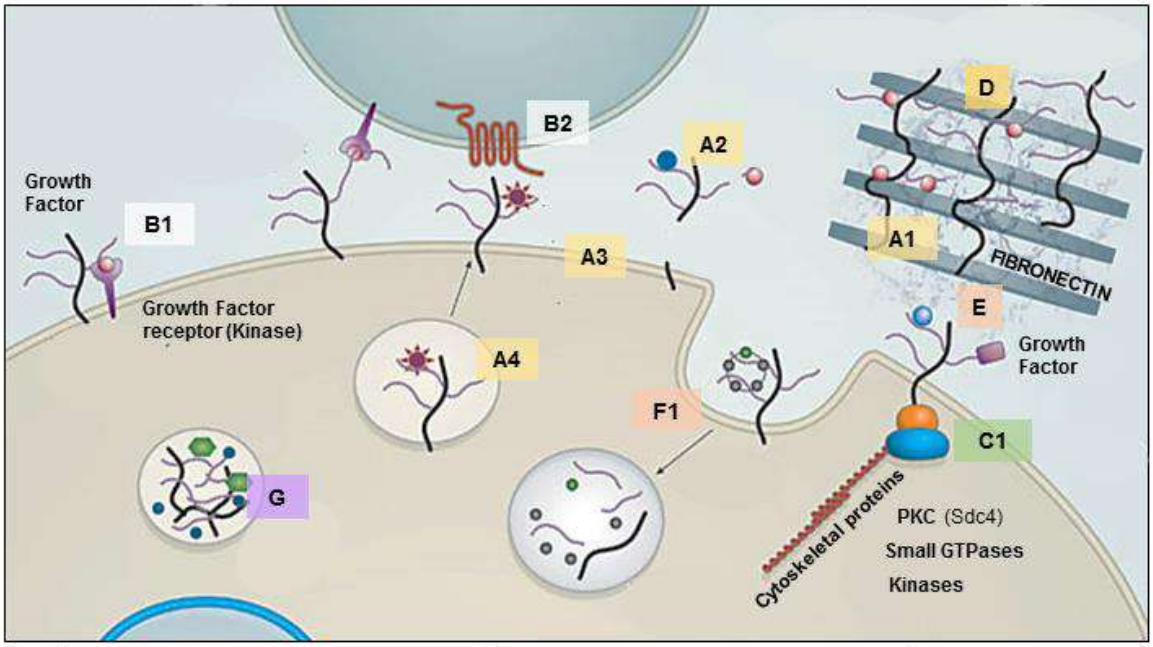

	FUNCTION	LIGANDS/PARTNERS	HSPG
A	Ligand binding and retention (Storage function)	Growth factors, Cytokines, Chemokines, Protease, protease inhibitors	Cell surface and Basement membrane
A2	Ligand regulation by Shedding/Heparanase digestion	Growth factors, Cytokines, Chemokines, Protease, protease inhibitors	Cell surface and Basement membrane
A3	Gradient formation	Chemokines and morphogens	Cell surface
A4	Transcytosis	Chemokines	Cell surface
B1	Co-receptor Function "In cis"	Growth factors, Cytokines, Chemokines, Fibronectin	Cell surface
B2	Co-receptor function "In trans"	Growth factors, Cytokines, Chemokines, Fibronectin	Cell surface
C1	Signal transduction in response to ligand (Focal adhesion and migration)	Fibronectin, Growth factors (FGF2), Cytoskeletal proteins, Kinases	Cell surface (Syndecans)
C2	Integrin regulation (cell adhesion and migration)	Integrin	Cell surface (Syndecans)
D	Barrier	/	Basement membrane
E	Mechanical tension of the matrix	ECM proteins	Cell surface and Basement membrane
F1	Endocytosis	Growth factors, Fibronectin, Cytoskeletal proteins	Cell surface (Syndecans)
F2	Recycling	Growth factors, Fibronectin, Cytoskeletal proteins	Cell surface (Syndecans)
F3	Exocytosis	Growth factors, Fibronectin, Cytoskeletal proteins	Cell surface (Syndecans)
G	Secretory granule and control of secreted proteins	Proteases, Histamine, Plasminogen activator, Tumour necrosis factor α, etc…	Serglycin

Figure 6.2: Main functions of HSPGs in cells. Figure adapted from (Bishop, Schuksz and Esko 2007). Permission to reproduce this picture has been granted by Nature Publishing Group.

6.2.2 Syndecan Family

6.2.2.1 Syndecan family and structure

The syndecan (Sdc) family is the more described family of cell surface HSPGs and is composed of 4 distinct members (Sdc1, Sdc2, Sdc3 and Sdc4) (**Fig. 6.3A**). Syndecans are type I single -pass transmembrane core proteins with covalently bound heparan sulfate (HS) chains (and chondroitin sulfate -CS- in some cases). The four members of the family have evolved from the same gene that underwent duplication followed by divergent evolution. Based on the specific origin and protein homology, two subfamilies of syndecans can be distinguished, one containing Sdc1 and Sdc3, and one characterised by Sdc2 and Sdc4 (Carey 1997). This sub-classification has also been suggested to reflect functional similarities: for example, Sdc2 and Sdc4 have been associated with cell proliferation, while Sdc1 and Sdc3 have been mainly related to its inhibition (Tkachenko, Rhodes and Simons 2005) (**Fig. 6.3A**).

The general structure of a syndecan core protein (**Fig. 6.3A**) is characterised by an N-terminal long extracellular ectodomain, with covalently bound HS or HS/CS chains, a single-pass transmembrane domain, involved in Syndecan oligomerisation, and a C-terminal short cytoplasmic domain, involved in the interaction with cytoskeleton and signal transduction.

The extracellular domain is a long region ending with its N-terminal signal peptide and is highly variable among family members (10–20% conservation)(Afratis, et al. 2016, David 1993). The ectodomain is characterised by a series of Ser-Gly attachment site for HS/CS covalent binding: both HS and CS chains can be found on Sdc1 and Sdc3, while only HS is present on Sdc2 and Sdc4. GAG chains can be located both at the distal and membrane proximal side of the ectodomain, in case of Sdc1 and Sdc3, or only in the distal part, as in Sdc2 and Sdc4 (Carey 1997, Afratis, et al. 2016). HS chains have different lengths in syndecans, going from 50 to 150 disaccharide units (Bernfield, et al. 1999).

The transmembrane domain is virtually identical among family members. Its peculiarity is to have a high affinity for self-association. The transmembrane domain contains GXXXG motifs that are fundamental for the dimerization of syndecan protein cores into homodimers (Dews and Mackenzie 2007). This oligomerisation, in particular, has been proven important for Sdc4 role in protein kinase C α (PKCα) activation.

The cytoplasmic domain is a short region (30-35 aminoacids) highly conserved among the family members. It contains binding sites for cytoskeletal proteins and phosphorylation sites for specific kinases. It is characterised by three distinct regions: two conserved regions (C1 and C2) and one variable region (V). The C1 domain binds kinases and cytoskeletal proteins such as Src non-receptor tyrosine kinase, tubulin, cortactin, and ERM family proteins (ezrin, radixin, moesin)(Afratis, et al. 2016). The C2 domains, on the other side (C-terminal), contains two

tyrosine residues and an important hydrophobic motif (C-terminal EFYA motif) that binds PDZ (PSD-95 / Discs-large / Zonula Occludens)-domain containing proteins and mediates cell adhesion and Syndecan recycling. Through this motif, Syndecans bind PDZ-containing proteins such as calcium/calmodulin dependent serine protein kinase (CASK), syntenin, synectin, synbindin, etc. (Afratis, et al. 2016). The V domain is highly heterogeneous among the four mammalian syndecans and can contain specific binding sites (Tkachenko, Rhodes and Simons 2005), for example, a specific sequence for phosphatidylinositol(4,5)bisphosphate has been observed in Sdc4 in this region.

Because of their transmembrane location and long HS chains, syndecans are able to link the intracellular space, and the actin cytoskeleton in particular, to the extracellular matrix, and have been involved in signalling transduction between ECM and intracellular space/cytoskeleton (Afratis, et al. 2016). Syndecans are involved in cell adhesion and proliferation, independently from or by interacting with integrins. They bind ECM components such as collagens (I, III, V), FN, thrombospondin etc., providing structural support for the adhesion. Moreover, they have been reported to play a role in endocytosis, recycling, exosome biosynthesis and wound repair (Tkachenko, Rhodes and Simons 2005, Afratis, et al. 2016).

Syndecans have different distribution in mammalian cells depending on the cell types and development stage (Couchman 2003, Kim, et al. 1994). Expression of the different Syndecans in cells is variably regulated by different growth factors such as TGF-β2, that upregulates Sdc4 while downregulating Sdc1 (Dobra, Nurminen and Hjerpe 2003), FGF2 (Sdc4), mechanical stress, and wound healing-associated cytokines (Sdc1 and Sdc4) (Tkachenko, Rhodes and Simons 2005). In the next paragraphs, a brief description of the four Syndecan members will be provided.

6.2.2.2 Syndecan-1 (Sdc1)

Syndecan-1 (Sdc1) is a member of syndecan family largely expressed in epithelial cells, present in plasma cells and in minor part on fibroblast/mesenchymal cells of skin, liver, lungs and kidneys. It is the main Syndecan form in keratinocytes (Kim, et al. 1994, Afratis, et al. 2016). Sdc1 is primarily involved in cell-cell adhesion and cell-matrix adhesion. Cell-cell adhesion function of Sdc1 depends on its binding *"in-trans"* to growth factors and membrane receptors on neighbouring cells, through the HS chains. In general, Sdc1 expression promotes cell adhesion and reduced migration (Altemeier, et al. 2012) while its loss promotes the cell proliferation with loss of cell-cell binding (Tkachenko, Rhodes and Simons 2005); by supporting cell-cell adhesion, Sdc1 has been suggested to be involved in the maintenance of the epithelial cells shape (Couchman, Chen and Woods 2001, Kato, et al. 1995). Sdc1 inhibition and heparanase HS digestion of Sdc1 has been shown to promote Epithelial-Mesenchymal Transition (EMT) with consequences for cell development, cancer and wound healing (Kato, et

al. 1995, Couchman, Chen and Woods 2001). This is particularly applicable to FGF2-dependent EMT induction on renal tubular epithelial cells (TECs): in renal TECs, Sdc1-HS digestion with heparanase facilitates EMT induced by FGF2, making it a possible clinical target against fibrosis (Masola, et al. 2012).

Sdc1 has been suggested to regulate the cell surface level of E-cadherin (epithelial marker), as its inhibition has been shown to correlate with the loss of E-cadherin itself. It has been suggested that the synthesis syndecan-1 and E-cadherin are themselves downregulated by the initiation of EMT, promoting loss of adhesion and conversion of the cells to a fibroblast-like shape (Sun, et al. 1998).

Similarly to Sdc4-KO [6.2.3], Sdc1-null mice are generally healthy and does not appear to have defects in development. However, defects in wound healing of the skin and cornea epithelium was observed in Sdc1-KO mice. (Stepp, et al. 2002, Pal-Ghosh, et al. 2008)

Sdc1 undergoes lipid-raft dependent endocytosis upon clustering, and the endocytosis is mediated by a specific MKKK domain on the membrane proximal C1 region. Ligand binding to Sdc1 determines MKKK-dependent phosphorylation of ERK, which itself determines the unbinding of Sdc1 and tubulin and the localisation of Sdc1 into rafts. Subsequently, MKKK mediates Src kinase phosphorylation of tyrosine residues between C1 and transmembrane region, which determines recruitment of cortactin, a mediator of actin-dependent endocytosis (Chen and Williams 2013). This process is for example involved in the removal of triglyceride-rich lipoproteins, and Sdc1 shedding impairs lipoprotein catabolism in hepatocytes (hypertriglyceridemia)(Deng, et al. 2012, Stanford, et al. 2009).

6.2.2.3 Syndecan 2 (Sdc2)

Syndecan-2 (fibroglycan, Sdc2) is well-expressed in endothelial cells, but also present in mesenchymal cells such as fibroblasts (Essner, Chen and Ekker 2006, Afratis, et al. 2016). It is strongly associated with the cytoskeleton, binding ERM-proteins on its C1 region (Granés, et al. 2003), linking the cytoskeleton to the plasma membrane.

Sdc2 has been involved in angiogenesis by modulation of VEGF signalling (Chen, Hermanson and Ekker 2004, Essner, Chen and Ekker 2006, Noguer, et al. 2009): Sdc2 shedding inhibits angiogenesis by "*in-trans*" interaction with the protein tyrosine phosphatase receptor CD148 in nearby cells, which in turn deactivates β1-containing integrins, mediating endothelial cell migration (Whiteford, et al. 2011, De Rossi, et al. 2014).

Importantly, Sdc2 has been suggested to play a role in TGF-β1 signalling: Sdc2 is in fact able to bind to both TGF-β1 and betaglycan (TGF-βRIII) though its core protein and facilitates TGF-β1-TGF-βRII binding with promotion of TGF-β1-associated Smad signalling leading to the expression of adhesion-associated proteins such as focal adhesion kinase (FAK) and integrin β1 (Chen, Klass and Woods 2004, Mytilinaiou, et al. 2013). In renal cells, Sdc2 was shown to

promote an increase in TGF-β-mediated matrix deposition; moreover, an increase in Sdc2 in renal interstitium has been associated with diabetic nephropathy (Chen, Klass and Woods 2004).

6.2.2.4 Syndecan-3 (Sdc3)

Syndecan-3 (Sdc3), also known as neural syndecan (N-syndecan) is highly expressed in neural cells and in developing musculoskeletal tissues (Afratis, et al. 2016). Its expression is highly regulated during development peaking in the first days after birth (oligodendrocyte differentiation and myelin formation) and declining in adults to basal levels (Carey, et al. 1997). Sdc3 levels in hypothalamus have been shown to regulate feeding behaviour, learning and memory, and Sdc3-KO resulted in reduced feeding response and learning/memory defects (Reizes, et al. 2001). Sdc3 knock-out has been associated with muscular dystrophy characterized by satellite cells hyperplasia and fibrosis, possibly associated with an excessive growth factor receptor activation (Cornelison, et al. 2004).

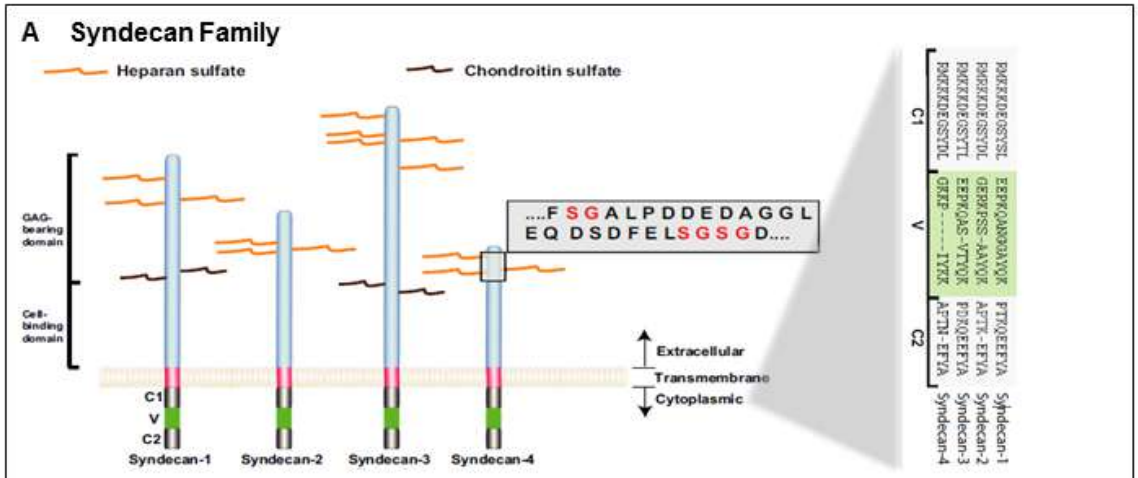

Name		Alternative name(s)	Length [aa]	MW[KDa]	Chains	Tissue specificity in mammals
Syndecan 1	Sdc1	Syndecan	310 (h) – 313 (r)	33	HS/CS	Epithelial, Plasma cells, ...
Syndecan 2	Sdc2	Fibroglycan	201 (h/r)	23	HS	Endothelial, Fibroblasts...
Syndecan 3	Sdc3	N-Syndecan	442 (h/r)	46	HS/CS	Neuronal, Musculoskeletal...
Syndecan 4	Sdc4	Ryudocan, Amphyglycan	198 (h) – 202 (r)	22	HS	Ubiquitous

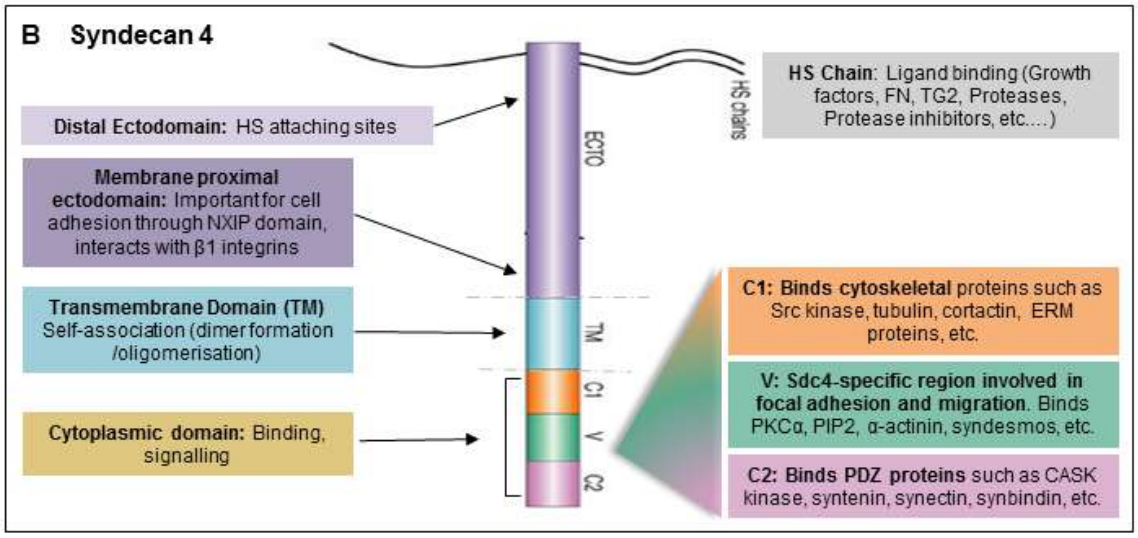

Figure 6.3: The Syndecan family of cell surface HSPGs and the specific structure of syndecan-4 (Sdc4). **(A)** The four members of the syndecan family of transmembrane HSPGs. Adapted from (Couchman, et al. 2015). Permission to reproduce this picture has been granted by John Wiley and Sons. **(B)** Specific characteristics of syndecan-4 (Sdc4) domains. Adapted from (Couchman 2003). Permission to reproduce this picture has been granted by Nature Publishing Group.

6.2.3 Syndecan-4 (Sdc4)

Syndecan-4 (Sdc4) (or ryudocan, or amphiglycan) is the most studied member of the Sdc family and is considered ubiquitously expressed in mammalian cells at all stages of development (**Fig.6.3B**). It is particularly rich in epithelial and fibroblastic cells, especially in liver and lungs, while it is lower in neuronal cells and endothelial cells. Sdc4 is considered a central mediator of cell adhesion and migration. It has a with a well-known role in wound healing and inflammatory response.

Mechanical cell stress, tissue injury and wound healing have been suggested to upregulate Sdc4 expression (Li, et al. 1997, Gallo, et al. 1997, Tkachenko, Rhodes and Simons 2005), which is also induced by growth factors such as TGF-β2 in epithelial cells (Dobra, Nurminen and Hjerpe 2003) and FGF2 (Cizmeci-Smith, et al. 1997). Expression of Sdc4 is upregulated by inflammation in cardiac cells and has a NF-κB response sequence on its promoter (Strand, et al. 2013). Expression of Sdc4 has been suggested to be important as an early inflammatory response, to accelerate the resolution of tissue inflammation limiting tissue injury and fibrosis, and for this reason it can be regarded as a possible anti-inflammatory protein (Xie, et al. 2012, Tanino, et al. 2012); however, inflammation- mediated shedding of Sdc4 ectodomain has been shown to be pro-inflammatory and to lead cell proliferation and tissue fibrosis (Strand, et al. 2013).

Similarly to Sdc1-KO mice, Sdc4-null mice are generally healthy, viable and fertile, and does not appear to have defects in development (Stepp, et al. 2002). However, defects in wound healing and impaired angiogenesis of the granulation tissue were shown in Sdc4-KO mice and were mostly associated with altered cell migration (Echtermeyer, et al. 2001).

Moreover, altered blood clothing with *thrombi* formation and excessive inflammatory response were identified. This last effect was mediated by impaired lipopolysaccharide clearance by endocytosis and excessive interleukin-1β expression from macrophages, due to impaired recruitment of transforming growth factor-β (TGF-β)(Ishiguro, Kojima and Muramatsu 2002). Sdc4-KO mice showed defects in muscular reconstruction by satellite cells, that showed altered proliferation activation and differentiation in absence of Sdc4 (Cornelison, et al. 2004). Sdc4-null mice also presented higher susceptibility to κ-carrageenan-induced nephropathy (Ishiguro, Kojima and Muramatsu 2002).

A peculiarity of Sdc4 sits in the variable cytosolic region: the cytoplasmic variable region of Sdc4 has some affinity for self-association, in addition to the transmembrane domain which is in common with the other syndecans. This leads to the formation of a “twisted clamp” structure strongly involved inSdc4 intracellular signal transduction. However, this affinity is easy to break because of C1 chains repulsion, and can be neutralised, hence stabilised, in presence of acidic phospholipids such as to phosphotidylinositol(4,5)-bisphosphate (PIP2).

In mammalian cells, Sdc4 is known to be a constitutive element of focal adhesion (FA) sites and to be largely implicated in the promotion of FA, stress fibres formation and cell spreading/migration by controlling cytosolic signalling response and actin cytoskeleton remodelling. Integrins, by themselves, are able to bind ECM adhesion molecules such as FN on their RDG binding domain ad promote cell attachment and migration, but stabilization of focal adhesion sites and formation of actin stress fibres (necessary for adhesion and migration in non -muscle cells) require the intervention of Sdc4 and its binding to the heparin binding sites of FN through the HS chains (Saoncella, et al. 1999b, Woods, et al. 2000, Mahalingam, Gallagher and Couchman 2007).

Fundamental for the mediation of FA and migration is the ability of Sdc4 to bind and activate protein kinase Cα (PKCα), a process that requires Sdc4 binding to PIP2 and oligomerisation. Briefly, upon engagement to adhesion molecules such a FN in the extracellular side, Sdc4 is able to bind PIP2 on its variable cytoplasmic region (LGKKPIYKK sequence, similar to a pleckstrin homology PH domain), which is important for the stabilisation of Sdc4 oligomers. Stable PIP2-associated oligomeric complexes of Sdc4 are able to bind the catalytic domain of PKCα on the same Sdc4 variable region, localize PKCα it in focal adhesion areas and favour its activation by auto phosphorylation (Oh, Woods and Couchman 1997, Oh, et al. 1998, Couchman, et al. 2002, Lim, et al. 2003).

PKCα activation modulates the activity of the members of the Rho family of small GTPases such as RhoA, RhoG and Rac1 (Dovas, Yoneda and Couchman 2006, Bass, et al. 2007). RhoA is mostly involved in focal adhesion and stress fibres formation and is necessary for stabilisation of focal adhesion sites required for contraction and subsequent migration, Rac1 leads the signalling cascade required for cell protrusion and migration, while RhoG is involved in a series of processes including endocytosis and cell migration and is able to determine itself the activation of Rac1 (Katoh and Negishi 2003). The control of GTPase downstream signalling depends on Sdc4 association and PKCα-dependent phosphorylation of GTPase regulation proteins such as the guanine nucleotide dissociation inhibitor RhoGDIα (that interacts with Sdc4 trough Synectin) (Brooks, Williamson and Bass 2012, Elfenbein, et al. 2009, Dovas, et al. 2010) and p190Rho–guanosine triphosphatase–activating protein (RhoGAP) (Dovas, Yoneda and Couchman 2006, Brooks, Williamson and Bass 2012, Bass, et al. 2008). By regulating Rho GTPase signalling, Sdc4 is able to transduce the extracellular signal, FN binding, to the intracellular space and regulate the signalling cascade and cytoskeletal rearrangements involved in cell adhesion and protrusion.

The Sdc4 mediated PKCα activation is also negatively controlled by the cytoplasmic domain phosphorylation at a specific serine site. In fact, PIP2 binding to Sdc4 is inhibited by phosphorylation of Serine-183 in its cytoplasmic domain, that has been suggested to be mediated by another member of PKC family, PKC-δ. When Sdc4 is Ser183 phosphorylated, it undergoes conformational changes and is unable to bind PIP2 and form PIP2-dependent oligomers. Its dephosphorylation, mediated by specific phosphatases of class II, promotes PIP2 binding to stabilise Sdc4 oligomerisation, allowing PKCα activation (Horowitz and Simons 1998, Koo, et al. 2006, Murakami, et al. 2002).

Phosphorylation-regulated binding to PIP2 is also able to control Sdc4 binding to other cytosolic proteins other than PKCα. For example, similarly to other Syndecans, Sdc4 is able to bind the PDZ domain of Syntenin on its C2 cytosolic region and the recruitment of Syntenin in proximity to the cell membrane is mediated by PIP2 binding to its PDZ domain, to which Sdc4 also binds (Zimmermann, et al. 2002) and is negatively controlled by ser-183 phosphorylation (Koo, et al. 2006).

Sdc4 has also been suggested to control cell migration and FA by regulating integrin recycling, in a process that is independent from PKCα activation, but is associated with syntenin binding and regulation of GTPse Arf6, and is controlled by Sdc4 phosphorylation by a cytosolic cSrc kinase (Morgan, et al. 2013). This suggests that Sdc4 is more likely to act as a regulator of integrins at the FA sites, rather than a co-receptor, controlling their trafficking rather than stabilisation, and to be crucial for the regulation of cell migration.
Moreover, when associated with FN, Sdc4 promotes phosphorylation of focal adhesion kinase (FAK) (Wilcox-Adelman, Denhez and Goetinck 2002) and controls cell adhesion, migration and spreading. The signal appears to be mediated by Rho GTPase but not by PKCα, and it is likely to depend on both integrin and Sdc4 cooperative signal transduction in response to FN (Bass and Humphries 2002).

Interestingly, FN-engaged Sdc4 oligomers are able to bind other cytoskeletal proteins such as α-actinin, an actin binding protein of the spectrin superfamily associated with cytoskeletal modulation by formation of actin microdomains, involved in adhesion and membrane deformation (Okina, et al. 2012, Choi, et al. 2008). Another protein that binds engaged Sdc4 intracellularly is syndesmos, that specifically binds both C1 and V domains of Sdc4 and itself interacts with paxillin, involved in FA (Denhez, et al. 2002, Baciu, et al. 2000).

To note, not only FN can induce Sdc4-mediated cell adhesion or spreading, but also other extracellular proteins, growth factors such as FGF2, and proteases. For example, Sdc4 is a cell

surface receptor for ADAM (a disintegrin and metalloprotease) -12, which promotes Sdc4 oligomerisation and activation of PKCα, that determines the accumulation of activated β1 integrins leading to β1 integrin-dependent cell spreading and stress fibres formation, with RhoA-GTPase and Rac1 GTPase as a signal mediators (Thodeti, et al. 2003). This happens also in in cell-cell adhesion of neuronal cells, where binding of Thy-1 cell surface antigen to both HS chains of Sdc4 and RGD binding sites of α5β3 integrin promotes the activation of PKC followed by cell adhesion mediated by RhoA or cell migration involving Rac1 GTPase activation/RhoA inhibition if Thy1 signal is prolonged(Avalos, et al. 2009).

Finally, Sdc4 has been suggested to be a major controller of calcium channels of the transient receptor potential canonical type (TRPC) on the cells surface. Calcium influx regulated by these channels is involved in cytoskeletal changes, by activation of proteins involved in actin modification, crosslinking, as well as of a series of calmodulin regulated enzymes. In myofibroblasts, Sdc4 controls TRPC inactivation (channel closure), which is dependent on PKC phosphorylation, and the interaction between the two proteins might involve simultaneous association with α-actinin. By blocking the channel, Sdc4 plays a key role in the formation of a myofibroblastic phenotype in these cells, characterised by α-SMA-stress fibres and focal adhesion points marked with OB-cadherin. In this context, Sdc4 deletion leads to loss of the myofibroblast mesenchymal phenotype, and to the presence of adherents junctions containing N-cadherin (Gopal, et al. 2015).

In the last few years, a number of studies have shown an involvement of syndecans, and specifically Sdc4, in protein endocytosis. In particular, Sdc4 has been shown to play a role in FGF2 internalisation by micropinocytosis, in a process that requires Sdc4 association with lipid raft domains and Sdc4-medited activation of Rac1 GTPase (Elfenbein, et al. 2012, Tkachenko, et al. 2004). FGF2 binding induces Sdc4 clustering and shifting to non – caveolar lipid rafts, leading to the uptake by micropinocytosis of both molecules.
Even if Sdc4 endocytosis has been suggested to happen synchronously with the endocytosis of caveolin-1 (“in tandem”), Sdc4 is not present in caveolar membrane lipid rafts (Tkachenko, Rhodes and Simons 2005, Tkachenko and Simons 2002). However, proximity of Sdc4 might induce caveolar endocytosis of nearby proteins upon HS-ligand binding leading to PKCα activation and activation of specific kinases (Src) or GTPases (Tkachenko, Rhodes and Simons 2005). For example, Sdc4 has been suggested to be involved in caveolin-mediated endocytosis of α5β4 integrins with a role in wound healing (Bass, et al. 2011). In this case Sdc4 supports endocytosis but is not endocytosed itself; it acts by mediating PKCα-dependent activation of RhoG upon engagement to FN (Elfenbein, et al. 2009, Bass, et al. 2011, Prieto-Sánchez, Berenjeno and Bustelo 2006).

After endocytosis, syndecans can be recycled in a process that involves alternate Syntenin – PDZ binding to the cytosolic tail and PIP2-syntenin association on the endosome. Arf6 is involved in this process by mediating PIP2 production on the endosomes trough the activation of a specific kinase (PIP5K). After being endocytosed, syndecan-binding to syntenin PDZ domains leads the HSPG to the recycling endosomal compartments, where it remains stably associated with syntenin as long as PIP2 levels are low. Subsequently, endosomal PIP2 (upregulated by Arf6 activation) binding to one or both PDZ domains determines syndecan dissociation from syntenin and drives Sdc4 recycling back to the cell surface (Zimmermann, et al. 2005). During this process, syndecans can control the recycling of HS-ligands, such as the well-described syndecan-mediated recycling of FGF2/FGF2-receptor (Zimmermann, et al. 2005) and β1 integrins, which affect cell spreading (Morgan, et al. 2013). Loss of Sdc2 binding to syntenin or syntenin inhibition lead to blockage of syndecan/syndecan cargo recycling by inhibiting its association with the recycling compartment, leads the proteins to degradation and negatively affect cell spreading. Inhibition of PIP2 binding to syntenin inhibits Syndecan recycling back to the surface and blocks it in the recycling compartment.

6.2.4 The heparin binding site of TG2

In 2012, three different research groups have attempted to describe the heparin binding site (HBS) of TG2, obtaining partially dissimilar results (Teesalu, et al. 2012b, Wang, et al. 2012, Lortat-Jacob, et al. 2012).

The first group, composed of Teesalu and colleagues (Teesalu, et al. 2012b), investigated the heparin binding sites of TG2 using synthetic peptides of 6His-tagged human recombinant TG2. They investigated five different TG2 peptides of 11-14 amino acids [P1: 202-KFLKNAGRDCSRRS-215; P2: 261-LRRWKNHGCQRVKY-274; P3: 476-RIRVGQSMNMGS-487; P4: 590-KIRILGEPKQKRKL-603; P5: 671-DKLKAVKGFRN-681] binding to immobilised heparin by surface plasmon resonance biosensor (SPR) (**Fig. 6.4A**). The two peptides that showed higher heparin affinity were P1 (202KFLKNAGRDCSRRS215) and P2 (261LRRWKNHGCQRVKY274), which also had a higher immunoreactivity for IgA anti-TG2 autoantibodies from patients with celiac disease, previously suggested to interfer with TG2-HS binding (Teesalu, et al. 2012a). P4 (590KIRILGEPKQKRKL603) showed a small affinity to heparin in SPR analysis. P2 had the higher RDG-independent effect in cell attachment assays and contains a consensus sequence proposed for heparin binding sites of different proteins (261LRRWKN266 = XBBXBX)(Cardin and Weintraub 1989). The amino acids sequences of P1 and P2 were localized in the structural model of TG2, showing that they are very close and part of the α-helical structures, on the surface of the catalytic domain; multiple alignment analysis of those sequences in different taxa and for the different human TG types revealed that they

were well conserved between taxa and but not among the other human TG (Teesalu, et al. 2012b).

A second group investigating TG2 HBS was Griffin's group (Wang, et al. 2012). Basing on the 3D arrangement of basic amino acid residues, Wang and colleagues selected two sequences, allowing simultaneous binding of FN, necessary for the adhesion function of TG2: 590-**K**I**R**ILGEP**K**Q**KRK**-602 (HS1), located at the tip of C-terminal- β barrel 2, and 202-**K**FL**K**NAG**R**DCS**RR**SSPVYVG**R**-222 plus **K**-387 (HS2), forming a shallow pocket lined with basic residues (the basic residues are in bold) (**Fig. 6.4A**). They suggested that that the HBS sequences must be in a β-sheet in order for the basic residues to face the same direction, or that the two basic residues must be at least 20 Å apart in an α-helix to permit the binding of heparin/HS. Upon structural analysis, the two clusters suggested docked well with heparin/HS when the enzyme was in a close conformation, while binding to the open conformation resulted inhibited (Wang, et al. 2012). In order to analyse the heparin binding proprieties of these suggested sequences, they produced TG2-expressing plasmids (pcDNA3.1-TG2) with mutations in the proposed HBS, substituting the basic aminoacids with alanine by site directed mutagenesis. As a result, they could compare WT TG2 (unmutated) with mutant HS1 (K600A, R601A, K602A) and mutant HS2 (K205A, R209A), that were transfected and expressed into mammalian cells, including human kidney epithelial cells. TG2 binding was measured in the transfected cell lysates applied onto heparin-sepharose column (Wang, et al. 2012). A large percentage of HS2 mutants showed no binding, suggesting that the basic residues substituted with Ala in the TG2 HS2 mutant (K205 and R209) were critic for heparin association. Moreover, they demonstrated a higher affinity of heparin-sepharose to the closed form of TG2 and the crucial role of HS2 mutant residues in this conformation (Wang, et al. 2012).

They subsequently produced a synthetic peptide P1, corresponding to the HS2 region from position 200 to position 216 of wtTG2: 200NPKFLKNAGRDCSRRSS216. The peptide represents the putative heparin binding site and was compared with a scrambled peptide P1s, used as a control. This peptide was tested in a binding-specificity assay towards Sdc4 and Sdc2. It strongly bound Sdc4, while Sdc2 binding resulted similar to the negative control without syndecans, confirming that the 200-216 TG2 region binds preferentially Sdc4. The putative HBS P1 peptide was also proven to support RDG-independent cell adhesion to syndecan in a cell attachment assay (Wang, et al. 2012). In conclusion, they suggested the region 200-NPKFLKNAGRDCSRRSS-216 as the heparin/HS binding site, with a role in cell adhesion and TG2 trafficking on the cell surface in cooperation with Sdc4 (**Table 6.2, Fig. 6.4B**). This binding site is well conserved between taxa and but not among the other human TGs (Wang, et al. 2012).

Finally, a third study was performed by our research group at NTU (Lortat-Jacob, et al. 2012) (**Table 6.1, Fig. 6.4A**). TG2 sequence was examined in search of basic residues organized into the typical consensus sequences for heparin binding (Cardin and Weintraub 1989) and two clusters were identified: RRWK (positions 262–265) and KQKRK (positions 598–602), which, even if distant on the protein sequence, are close to each other on the TG2 surface when the enzyme is its close conformation (GTP-bound). Further examination of the protein structure also revealed that three other basic residues, R19 and R28 and K634 are in close proximity to these two clusters in the close conformation of TG2 and could be involved in heparin interaction (**Table 6.1, Fig. 6.4A**). TG2 mutants targeting these domains were produced, together with other three mutants targeting K202 and K205, which form a well-exposed positively charged site on the opposite face of the protein, and R580, which is localised in GTP binding domain.

Nine different mutant human TG2 bacterial expression plasmids [pET21a(+)TG2] were produced by substitution of one or more basic residues with serine, by site-directed mutagenesis: M1a (R262S), M1b (R263S) and M1c (K265S), independently targeting 262-RRWK-265 cluster, M2 (K202S/K205S), M3 (K598S/K600S/R601S/K602S), M4 (R19S), M5 (R28S), M6 (R580S) and M7 (K634S) (Lortat-Jacob, et al. 2012) (**Table 6.1, Fig. 6.4A**). Recombinant HBM proteins were expressed and purified, and their heparin-binding ability was compared with WT TG2 (unmutated) by SPR. The requirement of each basic residue of the 262-RRWK-265 cluster for heparin binding was demonstrated, as all of the M1 mutants (a-c) had a strong decrease in affinity to heparin, compared to the WT. At the same time, also the second cluster, 598-KQKRK-602, was proven very important, as the corresponding M3 mutant was associated with an almost complete loss of heparin binding (Lortat-Jacob, et al. 2012). The mutants for the single residues Arg19 (M4) and Arg28 (M5), which were considered as putative elements of the binding site, displayed as well a reduction in the affinity, which supports their role in heparin recognition and binding. Those basic residues are very close to the two abovementioned clusters in the tri-dimensional structure. Finally, Lys634 (M7) seemed to be partially involved (slower rate of binding to heparin) in the recognition and stabilization of heparin during binding (Lortat-Jacob, et al. 2012).

From these results, it was deduced that the heparin-binding site of TG2 is probably composed of more than one element of the primary sequence, that are close to each other in the three-dimensional structure: cluster RRWK 262-265 and KQKRK 598-602 are possibly the main elements (**Table 6.1**, blue), with the participation of the basic residues Arg19, Arg28 and Lys634.

TG2 (WT or mutants) stabilisation in the open conformation determined a significant loss of heparin binding compared to the untreated enzyme. Heparin binding ability of a commercially available open-TG2, which has a stable open conformation, was tested as well and showed a

much lower affinity than WT TG2. In support to these finding, the two clusters RRWK 262-265 and KQKRK 598-602 were found spatially closed in the folded conformation, but very distant in the open "active" one. It was concluded that the binding between TG2 and heparin/HS happens when TG2 is in the closed conformation and depends on the proximity of both cluster. The research team also investigated the role of the different mutants in RGD-independent cell adhesion by plating Swiss 3T3 fibroblast on FN coated plates in presence of RGD peptide. As expected, M1c and M3 (that had no heparin affinity) failed to support RGD-independent cell adhesion, while M2 and M6 allowed some residual cell attachment.

From these results, it was concluded that the heparin binding site is made of the two clusters RRWK 262-265 and 598-KQKRK-602 (with K600 being the most important residue of the cluster). Probably the basic residues Arg19, Arg28 and Lys634 can also be involved in the binding (**Table 6.2, Fig. 6.4B**). Multiple alignment analysis of these sequences in different taxa and for the different TG types revealed that they are well conserved between taxa and typical of the TG2 (Lortat-Jacob, et al. 2012).

In summary, comparison of the three studies shows that all research groups analysed TG2 region between 200-222 as a proposed heparin binding region (Teesalu, et al. 2012b, Wang, et al. 2012, Lortat-Jacob, et al. 2012). Teesalu et al. considered 202-KFLKNAGRDCSRRS-215 (peptide P1), and Wang et al. also suggested that 202-KFLKNAGRDCSRRSSPVYVGR-222 should form a putative binding region (**Fig.6.4, Table 6.2**). In particular Wang et al. found Lys-205 and Arg-209 as critical residues for Heparin binding. Our group (Lortat-Jacob, et al. 2012) also considered two residues belonging to the region, Lys-202 and Lys-205 (mutant M2), explaining the choice with their location in the secondary structure of the protein in a well-exposed positively charged cluster on the surface of the protein and opposite to cluster 262RRWK265 (M1a-c) and 598KQKRK602 (M3) (**Table 6.1**). This residues were not found critical for heparin binding, but this could suggest that maybe the most important basic residue in that region would be Arg209, that has been substituted by mutation in mutant HS2 of Wang et al. but not our mutant M2 (Teesalu, et al. 2012b, Wang, et al. 2012, Lortat-Jacob, et al. 2012) (**Fig. 6.4, Table 6.2**).

LRRWK sequence (261-264), containing the XBBXBX consensus, was taken into consideration by Teesalu et al. (Peptide 2, 261-LRRWKNHGCQRVKY-274), who suggested it as a putative heparin binding region. Also our group (Lorat-Jacob et al.) took into consideration cluster 262RRWK265 (M1a-c) and concluded that it is likely to be a sequence involved in Heparin and HS binding of TG2. In particular, here, Arg262 was suggested to have a central position in heparin binding. The second cluster found important for heparin binding by our group is 598-KQKRK-602. This region overlaps with regions that were also studied by Teesalu et al. (peptide P4, 590KIRILGEPKQKRKL603) and Wang et al. (Mutant HS1, 590KIRILGEPKQKRK602,

mutations: K600A, R601A, K602A). In the first study, the region showed just a weak affinity to heparin while Wang et al. mutant showed no sensible differences in binding (Teesalu, et al. 2012b, Wang, et al. 2012, Lortat-Jacob, et al. 2012) (**Fig.4, Table 6.2**).

Table 6.1: Putative heparin binding sites investigated by our group (Lorat-Jacob *et al.*, 2012). The table shows the list of sites and regions investigated by the authors as possible heparin binding regions of TG2, and the mutations produced by site directed mutagenesis on full length recombinant human TG2 in order to assess the importance of the site integrity for heparin binding. Light blue indicates the TG2 heparin binding site suggested by the authors (Lortat-Jacob, et al. 2012). Tri-dimensional localisation of the putative heparin binding sites investigated by Lorat-Jacob *et al.*, 2012: tri-dimensional localisation of the sites investigated by the authors in the closed conformation of TG2. M1 and M3 sites are close to each other in this conformation, suggesting that heparin binding happens when TG2 is catalytically inactive (Lortat-Jacob, et al. 2012). Permission to reproduce this picture has been granted by the American Society for Biochemistry and Molecular Biology.

Possible heparin binding sites and regions of TG2 investigated by Dr Verderio's Group (Lortat Jacob et al., 2012).				
REGION/SITE	SEQUENCE	POSSIBLE ROLE PLAYED IN HEPARIN BINDING	MUTATION/S PERFORMED	MUTANT
262-265	RRWK	Typical consensus sequence, very close on the 3D structure of TG2 to the other cluster 598–602	R262S	M1a
262-265	RRWK		R263S	M1b
262-265	RRWK		K265S	M1c
K202; K205	K202; K205	Lys202 and Lys205 form a well exposed positively charged cluster on the opposite face of the other ones	K202S/K205S	M2
598-602	KQKRK	Typical binding consensus sequence, very close on the 3D structure of TG2 to the other cluster 262-265 and to the basic residues Arg19, Arg28 and Lys634	K598S/K600S/R601S/K602S	M3
R19	R19	Basic residue in close proximity on the 3D structure of TG2 to the 2 clusters 262-265 and 598-602.	R19S	M4
R28	R28	Basic residue in close proximity on the 3D structure of TG2 to the 2 clusters 262-265 and 598-602.	R28S	M5
R580	R580	Basic residue in the GTP binding site	R580S	M6
K634	K634	Basic residue in close proximity on the 3D structure of TG2 to the 2 clusters 262-265 and 598-602.	K634S	M7

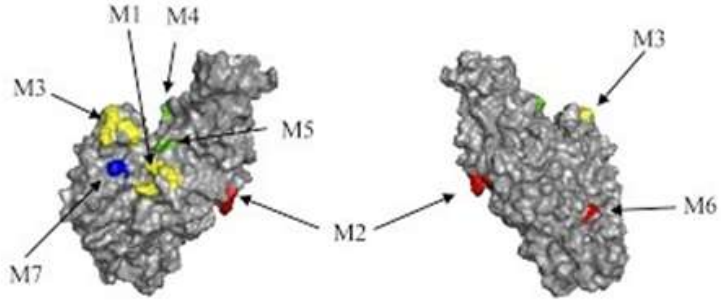

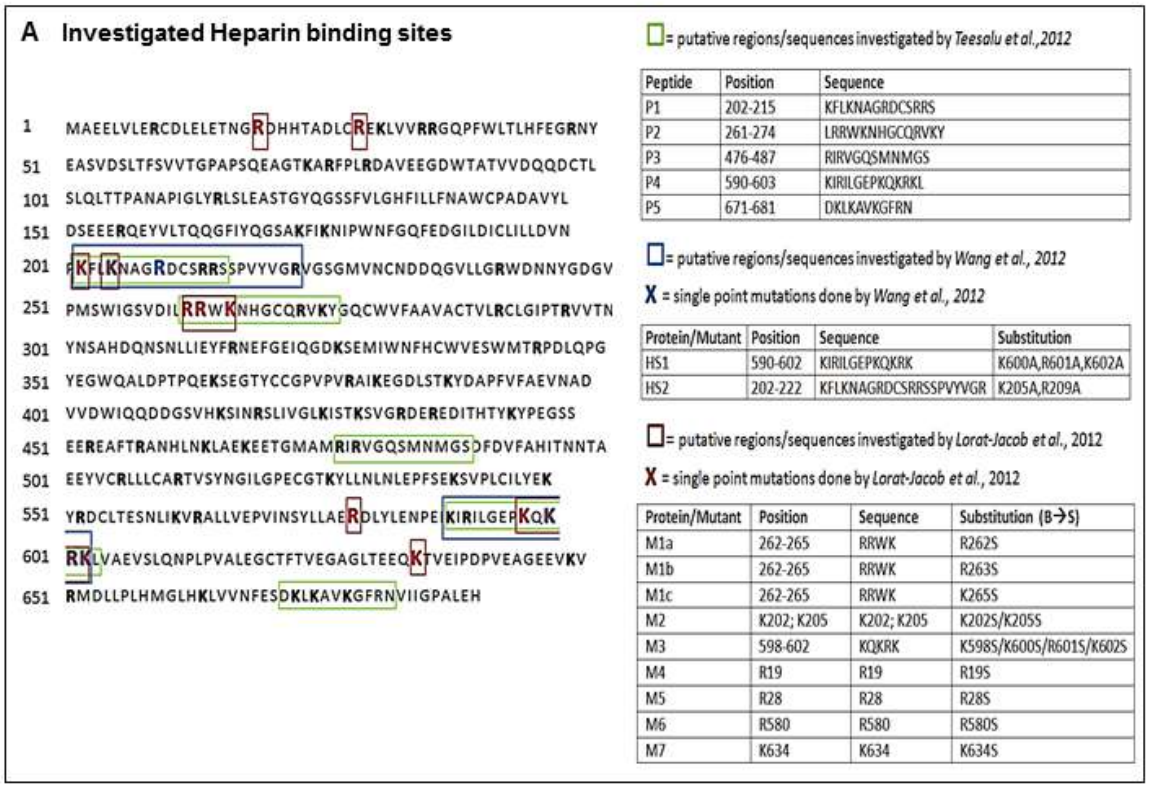

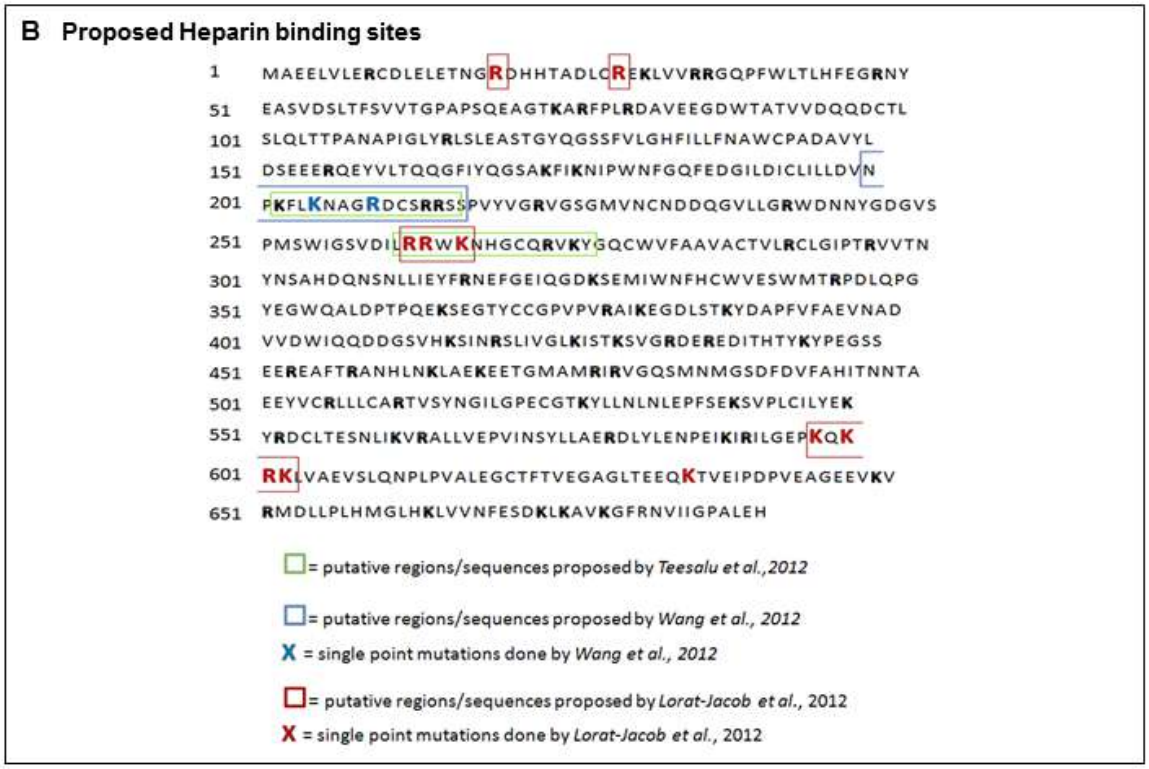

Figure 6.4: Investigation of the heparin binding site of TG2 – Comparison of investigated and proposed sites by three research groups (Teesalu, et al. 2012b, Wang, et al. 2012, Lortat-Jacob, et al. 2012). **(A)** Comparison of putative regions on amino acid sequence of TG2 (PDB code 3LY6) investigated by the three research groups **(B)** Comparison of putative amino acid sequence of TG2 (PDB code 3LY6) proposed by the three research groups. The basic residues arginine (R) and lysine (K) are in bold.

Table 6.2: Investigation of the heparin binding site of TG2 – proposed sites by three research groups (Teesalu, et al. 2012b, Wang, et al. 2012, Lortat-Jacob, et al. 2012). Proposed heparin binding sites (HBSs) of TG2 by the three research groups in 2012. The basic residues R and K are in bold. The putative important basic aminoacids investigated by mutation by Wang et al.,2012 and Lorat-Jacob et al., 2012 are underlined; the same colour (X, X, or X) indicates the same sequence or position in human TG2.

Paper	Proposed Heparin binding site(s) of TG2
Teesalu et al., J Pept Sci. 2012	L**RR**W**K**NHGCQ**R**V**K**Y 261-274 (P2) **K**FL**K**NAG**R**DCS**RR**S 202-215 (P1)
Wang et al., JBC, 2012	NP**K**FL**K**NAG**R**DCS**RR**SS 200-216 (P1)
Lortat-Jacob et al., JBC, 2012	**RR**W**K** 262-265 (M1) **K**Q**KRK** 598-602 (M3) Other important sites: Arg19 (M4), Arg28 (M5) and Lys634 (M7)

In a recent study from our group, the binding proprieties of other members of the transglutaminase family to heparin were tested by SPR (Burhan, et al. 2016). A strong binding of TG1 for heparin was detected by this assay, that was higher than TG2 affinity at the same concentration, while TG3 and FXIIIa had only a weak affinity for heparin. The TG2 Heparin binding site proposed by our group [262–RRWK-265, 598–KQKRK-602] (Lortat-Jacob, et al. 2012) has no similar sequences in TG1 and only the basic residue Arg19 was conserved and exposed on the surface of TG1 (Burhan, et al. 2016). The binding sites proposed by other groups, such as the one including the residues 202–215 (Wang, et al. 2012) are as well not conserved in TG1. These data suggest that the TG1 interaction with heparin/HS occurs through a different binding site (Burhan, et al. 2016). On the other hand, TG3 displayed two positive clusters similar to TG2 ones expose on the surface, that might act like a weak HBS [KNWK 259–262 and RVRK606–609]. FXIIIa sequence showed no similarities to TG2 HBS (Burhan, et al. 2016).

6.3 EXPERIMENTAL PROCEDURES

6.3.1 Experimental design

To investigate the role of HSPGs/Sdc4 in TG2 unconventional secretion in kidney cells (**Fig. 6.5**), an immortalized cell line of rat TECs (NRK52E), either WT or overexpressing an EGFP-tagged-TG2 protein, was employed. Sdc4 expression was modulated by transient transfection (overexpression- underexpression of Sdc4 cDNA) and inhibition of HS chains.

In specific experiments, mutations of the putative heparin binding site of TG2 was performed. An *in vitro* approach for the simulation of abundant extracellular TG2 released in the medium by neighborhood cells was also employed, and the amount of TG2 retained in ECM/cell surface before and after Sdc4 inhibition was analyzed, with particular interest to the consequences of this deposition on TGF-β activation.

Finally, the possible role of Sdc4 in the extracellular trafficking of TG2 inside vesicles has been analyzed by co-precipitation studies and transient transfections. **Fig. 6.5** outlines the different approaches employed in this results chapter.

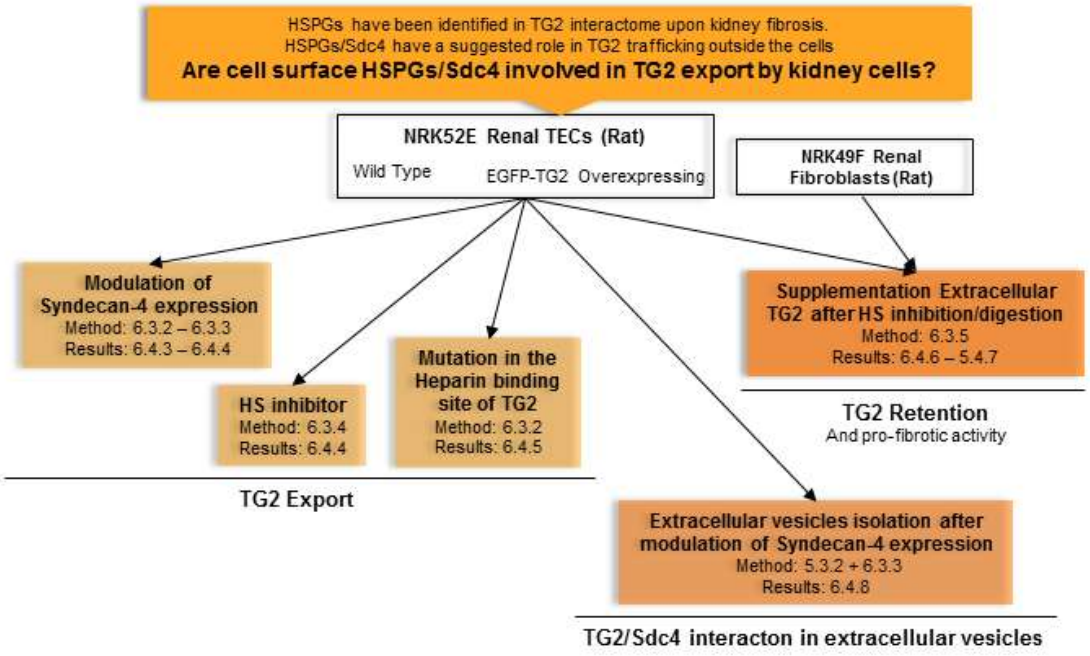

Figure 6.5: Experimental design for the investigation of HSPG/Sdc4 involvement in TG2 extracellular secretion and retention by kidney cells.

6.3.2 Immunoprecipitation of TG2 from whole kidney lysate

TG2-immunoprecipitation (TG2-IP) was performed from whole mouse (healthy female C57BL/6) and rat (male Wistar) kidney lysate (1 mg) with 2.5 μg of a mouse monoclonal anti-TG2 antibody (IA12) (University of Sheffield, UK), using the Pierce™ Crosslink Magnetic IP/Co-IP Kit (Thermo Scientific) and following the protocol for IP reported in general methods (Chapter II). Beads with no conjugated antibody were a negative control. In selected elutions, HS chains of the HSPG were digested using heparitinase I (50 mU/ml) for 2 h 37°C under constant rotation (see 6.3.5.2 for a description).

After IP, equal volumes of TG2-immunoprecipitates were separated by 12% (w/v) SDS-PAGE as described in Chapter II and immunoblotted for detection of Sdc4 using 1:500 (v/v) rabbit polyclonal anti-Sdc4 antibody (Ab24511 Abcam). Correct precipitation of TG2 was tested as well by immunoprobing with a rabbit polyclonal anti-TG2 antibody (ab80563, Abcam).

6.3.3 Transient transfection of kidney TECs

6.3.3.1 Cell transfection of syndecan-4 (Sdc4) cDNA

WT and EGFP-TG2 overexpressing NRK52E cells (clone #C5 and #E6, see Chapter II for a characterisation of these clones) were transiently transfected with human Sdc4 cDNA using two different plasmids: pcDNA3_HA-Sdc4 [expression of human Sdc4 tagged with hemagglutinin (HA) on the N-terminus] (unpublished) and pcDNA3.1(+)_Sdc4 (human Sdc4 by itself) (Scarpellini 2009). These plasmids were produced by sub-cloning in Dr Verderio laboratory at Nottingham Trent University (NTU), by, respectively, Dr Izhar Burhan and Dr Alessandra Scarpellini. Plasmid maps are reported in **Appendix** (**Fig. I**).

Plasmids were amplified by transformation of DH5α competent cells and then purified using the Midipep kit from Qiagen, as described in the general methods (Chapter II). Concentration and purity of DNA was measured by NanoDrop (Thermo scientific). In order to confirm the presence and the orientation of the insert in both plasmids, a diagnostic restriction digestion using appropriate restriction enzymes was performed.

Transient transfection with both plasmids was performed by electroporation using 5 μg of plasmid and following the general method reported in Chapter II. As a control, a mock transfection was performed. Quality of transfection was confirmed by simultaneous transient transfection of NRK52E cells with 5 μg of p-EGFP-N1 plasmid (6085-1, Clontech).

After transfection, overexpression of Sdc4 was tested at the transcript level by quantitative real time PCR (qRT-PCR, see Chapter III for the method), employing the primers and thermocycling conditions step conditions reported in **Table 6.3.** After amplification, threshold cycle (Ct) values were obtained and averaged among replica. The $2^{-\Delta\Delta Ct}$ relative quantification method

(Livak and Schmittgen 2001) was employed to calculate the level of expression of Sdc4. Efficient transfection was also assessed at a protein level by either Western blot or fluorescent immunostaining employing rabbit polyclonal anti-HA (C29F4, Cell Signalling Technology) and anti-Sdc4 (ab24511, Abcam) antibodies.

Table 6.3: Primers and thermocycling conditions for the amplification of Sdc4 cDNA by quantitative RT-PCR.

Primers				
Target Gene	**Name**	**Sequence 5'-3'**	**Tm**	**Product size**
Syndecan-4 Sdc4	Sdc4 FW	5'-GAGTCGATTCGAGAGACTGA-3'	54	366 bp
	Sdc4 RV	5'-AAAAATGTTGCTGCCCTG-3'	56	
Cyclophilin A (CycA)	Rat CycA FW	5'-AGCATACAGGTCCTGGCATC-3'	54	127 bp
	Rat CycA RV	5'-TTCACCTTCCCAAAGACCAC-3'	52	

Thermocycling conditions			
Cycles	**Step**	**T (°C)**	**Time**
1	Denaturation	95°C	10 min
40	Denaturation	95°C	30 sec
	Annealing	58 °C	20 sec
	Elongation	72 °C	20 sec
1	Melt	72 - 95°C	Hold secs on 1st step, hold 5 secs on next steps

6.3.3.2 Cell transfection with heparin binding mutant TG2 cDNA

NRK52 WT cells were transiently transfected with pEGFP-N1-TG2(M1c) and pEGFP-N1-TG2(M3) plasmids, produced in Dr Verderio's laboratory at NTU by Dr Izhar Burhan (unpublished) and expressing heparin binding site (HBS) - mutant TG2 in two different regions (Appendix, Fig II). As a TG2 control with no mutation in the heparin binding site, cells were transiently transfected with pEGFP-N1-TG2(WT) plasmid. This plasmid was produced in Dr Verderio laboratory at NTU by Dr Alessandra Scarpellini (Scarpellini 2009) (**Appendix, Fig II**). For the experimental purposes of this thesis, pEGFP-N1-TG2(WT), pEGFP-N1-TG2(M1c), pEGFP-N1- TG2(M3) plasmids, as well as pEGFP-N1 parental vector (p-EGFP-N1 plasmid, 6085-1, Clontech) were amplified and purified as described in previous section. In order to confirm the presence and the orientation of the insert in all EGFP-TG2 and mutant EGFP-TG2 plasmids, a diagnostic restriction digestion was performed.

To confirm the presence of the heparin-binding mutations, the purified pEGFP-N1-EGFP-TG2(M1c) and pEGFP-N1-EGFP-TG2(M3) plasmids were diluted in 10 mM Tris-HCl pH 8.5 at a concentration of 100 ng/µl and sequenced (Sanger sequencing) by Source Bioscience Sequencing (Nottingham, UK) using appropriate forward and reverse primers provided by the

company itself. The presence of the mutation was assessed in both plasmids by aligning the sequenced insert with WT full length TG2 cDNA on ClustalW2 web software from EMBL-EBI.
Transient transfection with all plasmids was performed by electroporation using 5 μg of plasmid and following the general method reported in 2.2.10.1. As a negative control, a mock transfection was performed. In specific experiments, pEGFP-vector alone was employed as a control. Quality of transfection was confirmed by simultaneous transient transfection of NRK52E cells with 5 μg of p-EGFP-N1 plasmid.
The expression of heparin-binding mutant and WT EGFP-TG2 chimera at ~100 kDa proteins was tested by Western blot using a rabbit polyclonal anti-GFP antibody (Ab290 Abcam).

6.3.4 SiRNA knock down of syndecan-4

Sdc4 knock down was performed on both WT and EGFP-TG2 overexpressing NRK52E (clone #C5 and #E6) cells, by transient transfection with rat Sdc4-targeting siRNA, following the protocol for siRNA transfection reported in 2.2.10.2. Briefly, $2 \cdot 10^5$ cells/well were cultured in a 6-well plate in antibiotic-free DMEM supplemented with 5% (v/v) heat-inactivated FBS and 2mM L-glutamine for 24 h. The day after, cells were transfected with either 100 nM rat Sdc4-targeting siRNA [ON-TARGETplus Rat Sdc4 (24771) siRNA from Dharmacon, Thermo Scientific] or non-targeting scrambled control siRNA [ON-TARGETplus Non-targeting siRNA #1 (D-001810-01-05) from Dharmacon, Thermo Scientific], using DharmaFECT 1 (Dharmacon, Thermo Scientific) as transfection reagent. After transfection, cells were grown for additional 24 hours. After transfection, knock-down of Sdc4 was tested at the transcript level by quantitative RT-PCR as described in 6.3.3.1 (**Table 6.3**).
When knock down of Sdc4 was followed by extracellular vesicle (EVs) isolation (as described in Chapter V), transient transfection with rat Sdc4 - targeting siRNA/ scrambled control siRNA was performed on 80% confluent EGFP-TG2 overexpressing NRK52E cells cultured in a T75 culture flask for 48 h, in 5ml antibiotic-free and serum-free medium.

6.3.5 Employment of Surfen and heparitinase to interfer with HS binding

6.3.5.1 Surfen

In order to chemically interfere with HS-binding, cells were treated with 3-12μM Surfen [bis-2-methyl-4-amino-quinolyl-6-carbamide, Sigma] (Schuksz, et al. 2008) at 37°C for 15 min or 2 h (Scarpellini 2009, Scarpellini, et al. 2009) depending on the experiment. A 30 mM stock solution of Surfen was prepared in dimethyl sulfoxide (DMSO) and stored at -20°C in the dark in glass containers, to be diluted when necessary. In specific experiments where extracellular TG2 activity was measured on living cells after treatment, Surfen was applied for 10 min on a cell suspension kept on ice, as suggested by Esko's group (Schuksz, et al. 2008). Briefly, cells were cultured in normal conditions until 80% confluent, then detached with sterile PBS containing 5mM EDTA in constant shaking at 37°C. Equal volumes of the cell suspension obtained were incubated with increasing concentration of Surfen (0, 3, 6, 9 and 12 μM) in PBS supplemented with 0.1% (w/v) BSA, for 10 minutes on ice.

6.3.5.2 Heparitinase I

Heparan sulfate chains of HSPGs were digested by incubation with 30mU/ml heparitinase I (also known as heparinase III, H8891, Sigma) at 37°C for one hour (Scarpellini 2009, Scarpellini, et al. 2009). Heparitinase I (Hep I) is was stored at -20°C as 5U/ml stock solution in an appropriate Hep I buffer [20 mM Tris-HCl, 50 mM NaCl, 4 mM $CaCl_2$, 0.01% (w/v) BSA, pH 7.5], suggested by the manufacturer. When needed, the enzyme was diluted to the working concentration (30mU/ml) in the same Hep I buffer using either water as a solvent, for experiments involving cell lysates, or complete culture DMEM medium as a solvent when the HepI treatment was performed on living cells. In this second case, generally, a 10X concentrated HepI buffer was prepared [200 mM Tris-HCl, 500 mM NaCl, 40 mM $CaCl_2$, 0.1% (w/v) BSA, pH 7.5], sterile filtered (0.2 μm filter), and diluted 1:9 with complete culture DMEM medium.

6.3.6 Employment of recombinant active TG2 to simulate high release of the enzyme in the extracellular environment

We developed an *in vitro* model simulating matrix TG2 accumulation in the extracellular milieu of rat kidney cells, where exogenous active TG2 was added to the conditioned medium of a cell monolayer (**Fig. 6.6**). Cells were cultured in 8-well chamber slides until approximately 80% confluent. At this stage, cells were washed twice with serum free medium and 250µl per well of 5 µg/ml solution of activated recombinant human TG2 was added to the cells and incubated for 1 h at 37°C.

To obtain a 5 µg/ml solution of activated TG2, 5 µg of commercially available recombinant human hexahistidine-tagged TG2 produced in *E.coli* (His6-rhTG2) (T002, Zedira) was pre-activated with 2mM DTT in a final volume of 20µl of DMEM medium supplemented with 2% (v/v) heat-inactivated FBS, 2mM L-glutamine and 100 IU/mL penicillin and 100 µg/mL streptomycin, for 15 min on ice. After incubation, 980 µl of the same supplemented medium were added in order to have 1 ml of 5 µg/ml solution of activated TG2 and dilute the DTT to a 40µM concentration, that should not interfere with cell viability.

In specific experiments, cells were pre-incubated with either 12 µM Surfen for 15 min or 30mU/ml Heparitinase I (HepI) for 1 h as described above.

6.3.6.1 Detection of TG2 and TG2 activity in situ

After incubation, cells were washed three times with sterile PBS pH 7.4 to remove all TG2 not associated with either cell surface or matrix and immunofluorescent staining of TG2 was performed on fixed (3% PFA/8 min) but not permeabilised cells following the general method for immunofluorescent staining described in Chapter II (2.2.8). Specifically, extracellular TG2 was probed with 1:150 (v/v) dilution of a mouse monoclonal anti-TG2 antibody [Cub7402] (ab2386, Abcam), followed by 1:250 (v/v) dilution of a FITC conjugated sheep anti-mouse secondary antibody. In some experiments, also extracellular collagen type I was immunostained by employing a 1:500 (v/v) dilution of rabbit polyclonal anti-collagen I antibody (Abcam) followed by a donkey anti-rabbit-Alexa Fluor® 568, with red fluorescence.

In order to detect TG2 activity *in situ*, 0.5 mM FITC - conjugated cadaverine was added to the medium during the incubation with 5 µg/ml recombinant active TG2, and cells were kept in incubation with exogenous recombinant TG2 for a longer time (6 h) to allow crosslinking activity to accumulate. After incubation, cell monolayer was washed carefully for three times with sterile PBS pH 7.4, and cells were fixed with cold methanol at -20°C for 10 min before mounting of the slide, as described in the general methods (2.2.9.3).

6.3.6.2. Immunofluorescent staining of active and total Smad3 after incubation with exogenously added TG2

Cells were grown in an 8-well chamber slide until 70% confluent and treated with 12 µM Surfen for 15 min before addition of 20 µg/ml of pre activated Rh-TG2 for 24 h. After incubation, immunofluorescent staining of total Smad3 and active Smad3 (phosphorylated) was performed on fixed (3%PFA) and permeabilised cells [0.1% (w/v) Triton X100] following the general protocol reported in 2.2.8. Cells were probed with either a 1:75 (v/v) dilution of rabbit polyclonal anti-Smad3 antibody (#9513, Cell Signalling Technology) (total Smad3) or a 1:75 (v/v) dilution of rabbit polyclonal anti-phospho(pSer$_{425}$)-Smad3 (SAB4300253, Sigma) (active Smad3), both followed by a donkey anti-rabbit Alexa Fluor® 488 secondary antibody with green fluorescence. Total and phosphorylated Smad3 were quantified by ImageJ intensity analysis and expressed relative to the number of cells (DAPI staining of nuclei), and active Smad3 was calculated as a ratio of phosho-Smad3 over Smad3 for each one of the treatments performed.

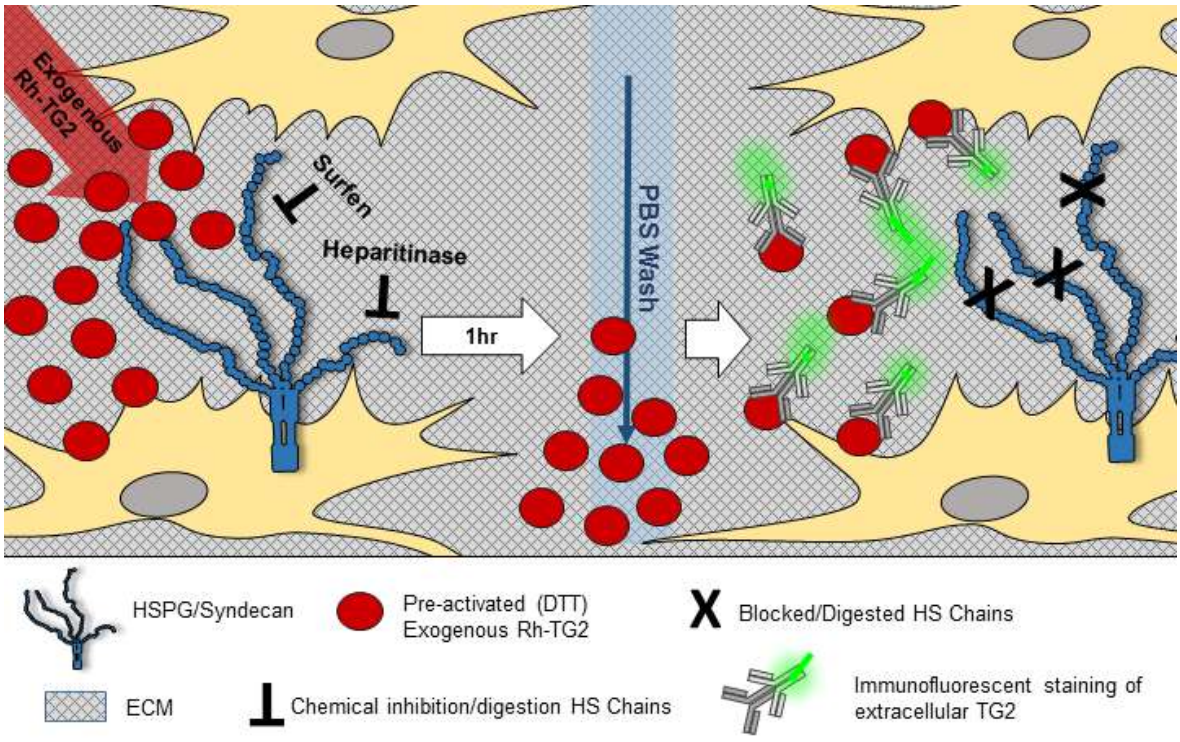

Figure 6.6: Experimental design for the simulation of abundant extracellular TG2 on a kidney cell monolayer and analysis of TG2 retention by kidney cells.

6.4 RESULTS

6.4.1 Analysis of the quality of transfection plasmids

In order to confirm the quality of transfection plasmids for transient transfection of NRK52E cells, both purity of DNA and presence/correct orientation of each plasmid employed in this chapter was analysed. Purity of plasmid DNA was measured by NanoDrop (Thermo scientific) and a clean DNA was confirmed for all plasmid preparations by a 260/280 ratio close to 2. Presence and correct orientation of the cDNA insert was confirmed in all plasmids by diagnostic restriction digestion (**Suppl. Fig. 6.1A-B**) using the appropriate restriction enzymes reported in the **Appendix (Fig. I, II)**. Correct mutations of the heparin binding site were confirmed in pEGFP-N1-EGFP-TG2(M1c) and pEGFP-N1-EGFP-TG2(M3) plasmids by Sanger sequencing and ClustalW2 sequence comparison (**Suppl. Fig. 6.1C**). Sequence alignment against the TG2(WT) plasmid sequence confirmed the presence of mutation K265S in pEGFP-N1-EGFP-TG2(M1c) and mutations K598S, K600S, R601S and K602S in pEGFP-N1-EGFP-TG2(M3), in agreement with the transfection cDNA described by Lorat-Jacob and colleagues (Lorat-Jacob et al., 2012) (**Suppl. Fig. 6.1C**).

6.4.2 TG2/Sdc4 co-precipitation in kidney lysates and co-localisation in kidney cells

In order to investigate the interaction of TG2 with Sdc4 in kidneys, TG2-immunoprecipitation (TG2-IP) was performed from whole mouse (healthy female C57BL/6) and rat (male Wistar) kidney lysate. Immunoprecipitates were probed for the presence of Sdc4 both before (-Hep) and after (+ Hep) cleavage of the HS chains by digestion with heparitinase I (HepI), as described in the experimental procedures. A double band between 25 and 35 kDa, compatible with the core protein monomer size (Echtermeyer, et al. 1999) was identified as co-precipitated with TG2, and its detection was enhanced by glycosaminoglycan (GAG) chains digestion with HepI in both mouse (**Fig. 6.7A**, grey arrowhead) and rat (**Fig. 6.7B**, grey arrowhead) kidney homogenates. In rat TG2-immunoprecipitates, a second band of ~40 kDa, compatible with Sdc4 homodimer, was also visible and its detection enhanced by treatment with HepI (**Fig. 6.7B**, grey arrow). Furthermore, HepI treatment also appeared to ease the detection of TG2 itself (**Fig. 6.7 A,B**, black arrowheads).

To visualise Sdc4, stable clones of NRK52E overexpressing EGFP-TG2 were transiently transfected with human Sdc4 cDNA tagged with hemagglutinin (HA), using pcDNA3_HA-Sdc4 as described in the experimental procedures (6.3.3.1).

The expression of the exogenous HA-Sdc4 as a chimeric protein was confirmed by Western blot of lysates of NRK52E WT cells transiently transfected with pcDNA3-HA-hSdc4 for 24, 48 and 72 h. Probing of the HA tag by Western blot confirmed expression of HA-Sdc4 starting at 24 h from transfection. Probing of the lysate with rabbit polyclonal anti-Sdc4 antibody confirmed the expression of the proteoglycan as an HA-tagged chimeric protein (**Suppl. Fig. 6.2A**). The HA tag was greatly advantageous for the detection of Sdc4, as cells transfected with a non-tagged Sdc4 cDNA (pcDNA3.1(+)_Sdc4) and immunostained with anti-Sdc4 antibody resulted into a more diffuse staining (**Suppl. Fig. 6.2B**).

As shown also in **Suppl. Fig. 6.2B**, fluorescent immunostaining of HA-Sdc4 using an anti-HA antibody revealed a predominant cell surface location of Sdc4 but also a strong peri-nuclear staining was identified in some cells (**Fig. 6.7C**). TG2 partially colocalised with Sdc4 in these compartments, as indicated by the white arrows in **Fig. 6.7C** (orange-yellow fluorescence), but it was ubiquitously expressed in the cells.

Together, these results are compatible with TG2 association with Sdc4, as the proteoglycan is precipitated with TG2 and partially co-localised with TG2 on the surface and perinucleus of NRK52 transfected cells.

In all experiments, transfection efficiency was confirmed by simultaneous transient transfection of NRK52E WT cells with 5 μg of p-EGFP-N1 plasmid, resulting in a transfection efficiency between 60 and 80%, depending on the experiment (**Suppl. Fig. 6.3**).

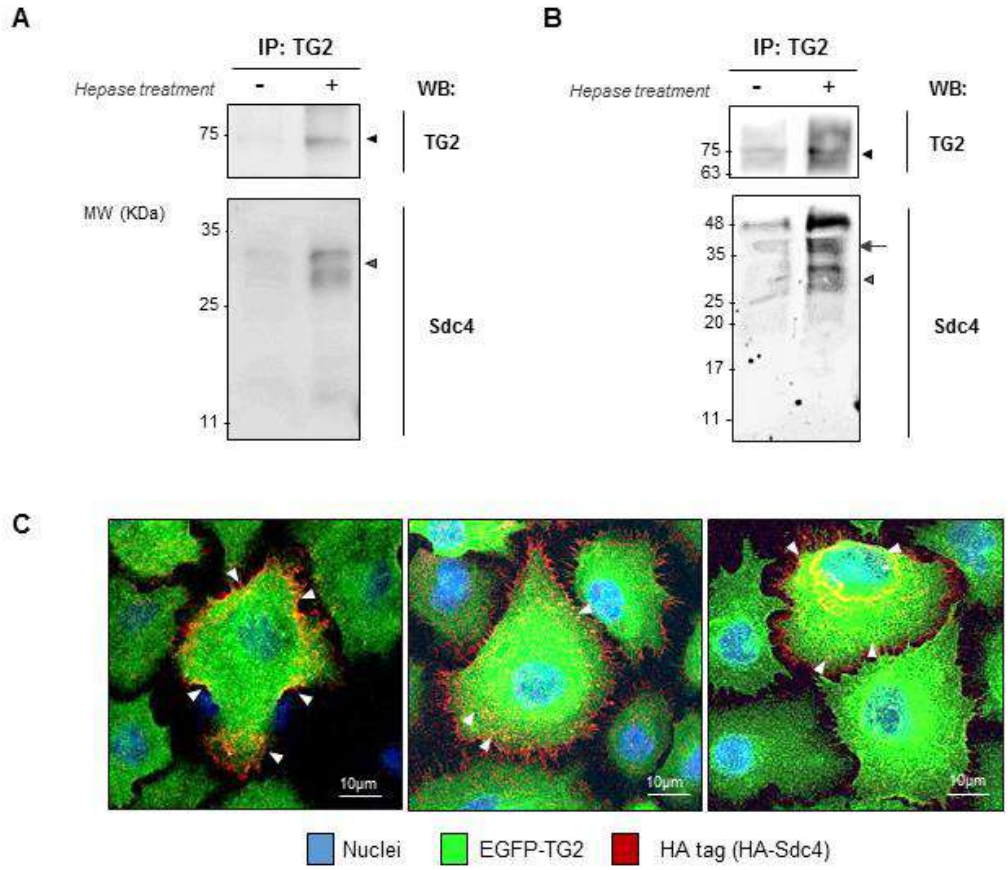

Figure 6.7: Co-precipitation of TG2 and Sdc4 from kidneys and co-localisation in kidney cells. (**A,B**) TG2-immunoprecipitation (TG2-IP) was performed on 1 mg of whole mouse (female C57BL/6) (A) and rat (male Wistar) (B) kidney homogenate with 2.5 µg of mouse monoclonal anti-TG2 antibody (IA12, University of Sheffield), using the Pierce™ Crosslink Magnetic IP/Co-IP Kit (Thermo Scientific) as described in 6.3.2. HS chains were digested using heparitinase I (Hep, 50 mU/ml). Elutions (TG2-IP) were separated by 12% (w/v) SDS-PAGE and immunoprobed with a rabbit polyclonal anti-Sdc4 antibody (ab24511, Abcam, dilution 1:500), as well as with a rabbit polyclonal anti-TG2 antibody (ab80563, Abcam, dilution 1:1000). Immunoreactive bands were detected by enhanced chemiluminescence (Geneflow) after incubation with appropriate goat anti-rabbit IgG HRP-conjugated secondary antibody (dilution 1:2000, Dako) in blocking buffer. Image acquisition was performed with a LAS4000 imaging system (GE Healthcare). Black arrowhead indicates TG2 at ~75kDa, grey arrowhead the Sdc4 bands between 25 and 35 kDa of size. **(C)** EGFP-TG2 clones were transfected by electroporation using 5 µg of pcDNA-HA-hSdc4. Fixed (3%PFA) but not permeabilized EGFP-TG2 clones were incubated with a rabbit polyclonal anti-HA antibody (C29F4, Cell Signalling Technology– dilution 1:500) followed by donkey anti-rabbit IgG H&L Alexa Fluor® 568 as secondary antibody (1:1000, red), to detect cell surface HA-Sdc4. Nuclei were stained with DAPI. Specimens (20 µm) where scanned by confocal microscopy every µm, and each picture combines all the 20 levels observed. Representative pictures of 3 fields are shown. White arrowheads indicate co'-localisation (green over red).

6.4.3 Effect of Sdc4 overexpression on TG2 extracellular deposition

In order to determine the effect of Sdc4 overexpression on TG2 export by renal TECs, cells were transiently transfected with both pcDNA3_HA-Sdc4 and pcDNA3.1(+)_Sdc4 plasmids (**Appendix, Fig.I**).

48 h transfection with both plasmids resulted into a several-fold increase in Sdc4 transcript as measured by qRT-PCR (**Fig. 6.8A**), confirming an increased expression of the protein compared to the mock transfected cells. Transfection of NRK52E WT with Sdc4 cDNA cells resulted in 8.72±2.22-fold increase of Sdc4 mRNA compared to the mock control when transfected with pcDNA3_HA-Sdc4 plasmid (p=0.03, *) and 19.93±3.41-fold increase of Sdc4 mRNA when transfected with pcDNA3.1(+)_Sdc4 (0.001,***). Similar overexpression of Sdc4 at the transcript level was confirmed upon transfection of EGFP-TG2 overexpressing clone #E6 9details of this clone in **Suppl. Fig. 5.1**) with the same plasmids: 14.32±4.11-fold increase of Sdc4 mRNA compared to the mock control upon transfection with pcDNA3_HA-Sdc4 (p=0.0006, ***) and 18.40 ± 3.87-fold increase when cells were transfected with pcDNA3.1(+)_Sdc4 (0.0001, ****). Transfection of EGFP-TG2 overexpressing clone #C5 with Sdc4 cDNA cells led to a higher increase of Sdc4 mRNA compared to the mock transfected control, with 44.63±4.45-fold rise when cells were transfected with pcDNA3_HA-Sdc4 (p=0.0001, ****) and 28.94±2.04 fold increase when pcDNA3.1(+)_Sdc4 was employed (p=0.001, ***).

In all cell lines analysed, Sdc4 overexpression was accompanied by a general increase in extracellular TG2 activity when analysed by biotin cadaverine incorporation assay on living cells, which was statistically significant expecially in the in two EGFP-TG2 overexpressing clones (**Fig 6.8B**). In NRK52E WT cells, only Sdc4 overexpression determined by pcDNA3_HA-Sdc4 led to a significant increase of extracellular TG2 activity compared to the mock transfected control (1.21 ±0.267; p=0.03, *) while no significant variation was detected when the non-tagged plasmid was employed. Similarly, also in EGFP-TG2 overexpressing clone # C5 a significant 1.68 ±0.51 -fold increase in extracellular TG2 was observed only when the HA plasmid was employed (p= 0.0007, ***) while transfection with pcDNA3.1(+)_Sdc4 plasmid led to a not significant 1.22±0.32 fold increase in TG2 export (p=0.07). The best results were obtained when Sdc4 was overexpressed in EGFP-TG2 overexpressing clone #E6: in this case, both plasmids led to a significant ~25% rise of extracellular TG2 activity (p=0.001 in the first case and p= 0.0005 in the second, ***). In all cases, a general variability in the experimental results was observed in the different experimental replica, suggesting a variable efficiency of each transfection performed and a variable cellular response to the overexpression itself (**Fig. 6.8**, bottom chart showing the single independent experimental results).

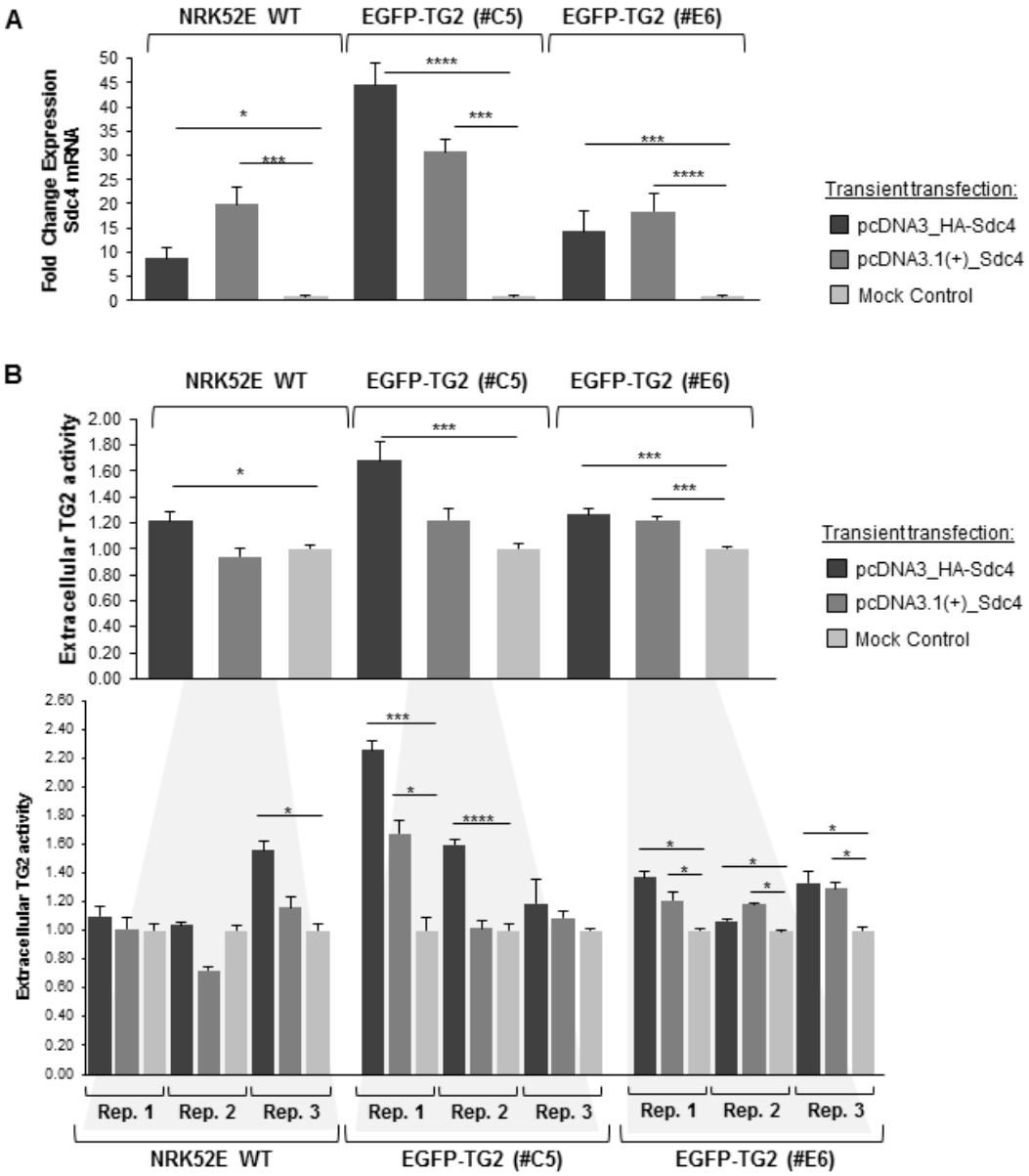

Figure 6.8: Extracellular TG2 activity in NRK52 WT cells and EGFP-TG2 clones overexpressing Sdc4. One million WT and EGFP-TG2 overexpressing (clones #C5 and E6) NRK52E cells were transfected by electroporation with human Sdc4 cDNA using 5 µg of either pcDNA3_HA-Sdc4 or pcDNA3.1(+)_Sdc4 plasmid, and seeded in a 6- well plate. Mock transfection was employed as a control. 48 h after transfection **(A)** the relative expression of Sdc4 mRNA was measured by qRT-PCR (**Table 6.3**) by $2^{-\Delta\Delta Ct}$ relative quantification method (cyclophilin-A was employed as housekeeping gene). **(B)** Extracellular TG2 activity was measured as described in 2.2.9.2. Values are the average Abs (450 nm) of three independent experiments, each undertaken in triplicates, normalised for the relative mock transfected control (equalised to 1) ± SD (top graph). Individual experimental results are shown in graph underneath. In this case, values are the average Abs (450 nm) of three replicas of each independent experiment performed, normalised for the relative mock transfected control (equalised to 1) ± SD. Significance of the differences between treatments was determined by T-test: * = $p<0.05$, ** = $p<0.01$, *** = $p<0.001$, **** = $p<0.0001$.

6.4.4 Effect of Sdc4-underexpression or chemical inhibition on TG2 extracellular deposition

In order to determine the effect of Sdc4 knock down on extracellular TG2, NRK52 cells were transiently transfected with rat Sdc4-targeting siRNA or siRNA control for 24 h, as described in the experimental procedures (6.3.4). Reduction of Sdc4 expression in rat TECs was confirmed at transcript level by qRT-PCR (**Suppl. Fig. 6.4**). There was a significant difference in residual Sdc4 transcript if cells were transfected twice with Sdc4 targeting siRNA (**Suppl. Fig. 6.4**), but since the residual expression was low in both cases (approximately 10% of the control siRNA) and the difference in residual expression small, only one siRNA transfection was applied in the subsequent experiments.

Sdc4 targeting siRNA was applied to WT NRK52 cells, resulting in 12.20 ± 0.65% of remnant Sdc4 transcript expression (p=0.005, **), and to EGFP-TG2-transfected clones #C5 and #E6 (**Suppl. Fig 5.1**), resulting into 11.85 ± 0.44% (p=0.001. ***) residual Sdc4 in clone #C5 and an almost complete Sdc4 knock down in clone #E6 (0.027 ± 0.001% of residual Sdc4 expression, p=0.005, **) (**Fig. 6.9A**).

In all cell lines analysed, Sdc4 knock down lead to a significant reduction in extracellular TG2 activity when analysed by biotin cadaverine incorporation assay in living cells (**Fig. 6.9B**). In NRK52E WT cells, TG2 extracellular activity was 45.14 ± 11.68% of that of control cells transfected with scrambled siRNA ($p = 6.66 \cdot 10^{-06}$, ****). In EGFP-TG2 overexpressing clone #C5, an approximately 20% reduction in extracellular TG2 was observed (79.99 ± 10.25% of control, p= 0.002, **), while, in the clone #E6, Sdc4 – targeting siRNA transfection led to ~40% decrease in extracellular enzyme activity (60.59 ± 12.78% of control, $p=1.17 \cdot 10^{-05}$, ****), in three independent experiments (**Fig. 6.9B**).

In order to interfere with HS-binding, cells were treated with 3-12μM Surfen, an antagonist of HS chains of HSPGs, for 10 min on ice (**Fig. 6.9C**) as previously described (Schuksz, et al. 2008). In both WT and EGFP-TG2 overexpressing NRK52 cells, HS antagonism with Surfen (6 μM) led to a significant reduction in extracellular TG2 activity. NRK52 WT cells showed a statistically significant ~27% reduction in extracellular TG2 when cells were treated with 6 μM Surfen (72.69 ±25.00 % of control cells with no Surfen, p= 0.007, **), that was further reduced if Surfen concentration was increased, as 9 or 12 μM led to, respectively, 65.26 ± 12.74% ($p=4.34 \cdot 10^{-06}$, ****) and 61.04 ±9.16% ($p=3.23 \cdot 10^{-07}$, ****) residual extracellular TG2. In the EGFP-TG2 clone #C5, treatment with 6 μM Surfen resulted in 73.62± 24.50% remnant extracellular TG2 activity compared to the untreated control (p=0.04, *) which was further decreased by a 9 μM Surfen (67.85 ± 18.24 % of control, p= 0.002, **) and a 12 μM Surfen treatment (59.15± 14.63% of control, p=0.0002, ***). Therefore, HS antagonism by Surfen led to up to a 40% reduction, approximately, in cell surface TG2 activity in NRK52E cells and EGFP-TG2 transfected clones.

LDH assay confirmed that there was no effect on cell permeability at these concentration of Surfen in both cell lines, excluding leaking of cytosolic components/loss of viability which may affect measurements of TG2 activity on the surface of cells (**Suppl. Fig. 6.5A**). Also, Surfen did not affect the total expression of TG2, at least when used at 12 μM for 2 h at 37°C (**Suppl. Fig. 6.5B**).

In summary, the two experimental approaches for HS interference described in this section propose that Sdc4 knock down and HS antagonism have a negative effect on TG2 export from TECs, suggesting the possible involvement of HSPGs/Sdc4 in the availability of TG2 at the cell surface in this cellular system.

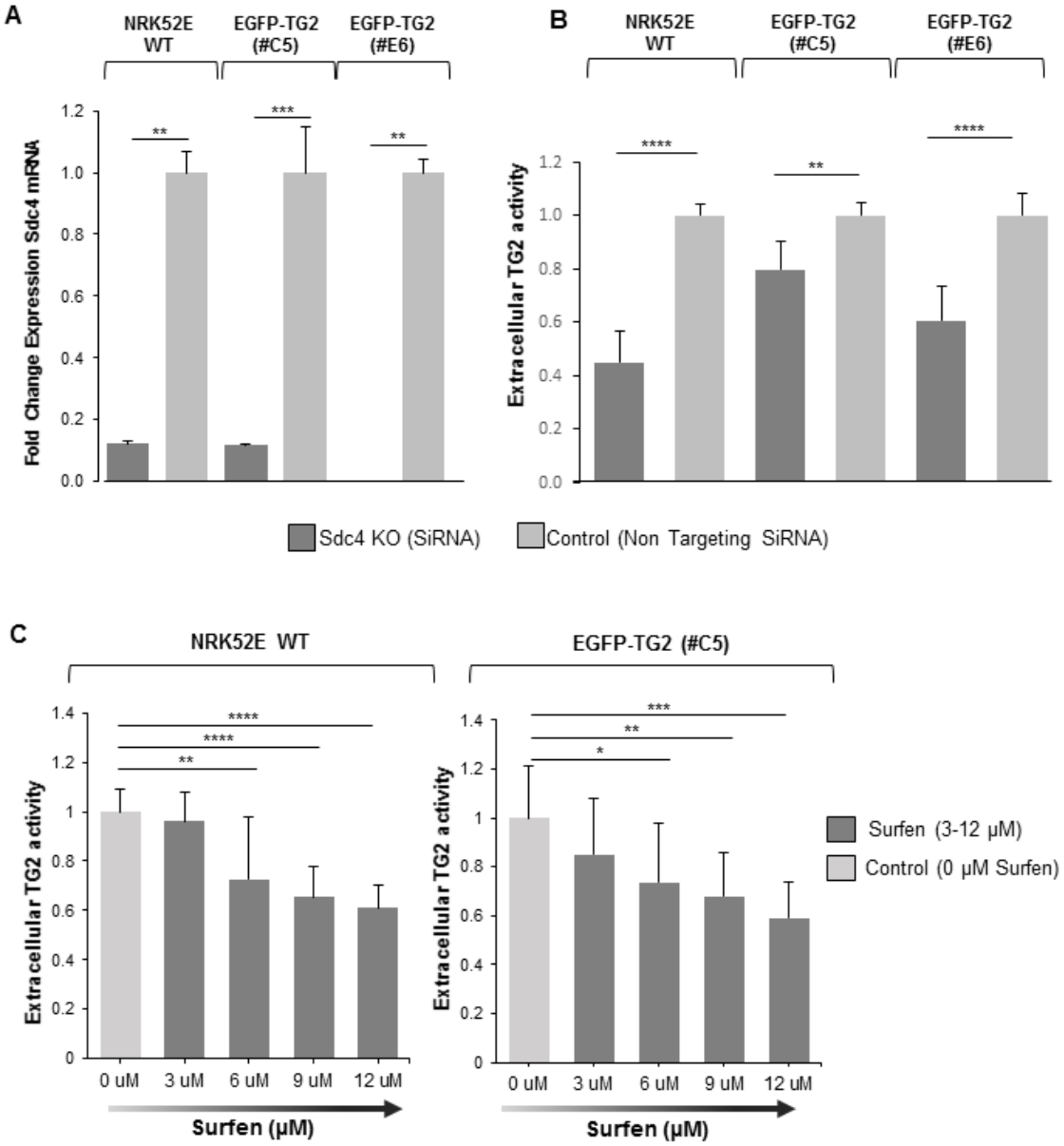

Figure 6.9: Extracellular TG2 activity in NRK52 WT cells and EGFP-TG2 clones after Sdc4 knock down. NRK52E WT and EGFP-TG2 overexpressing (clones #C5 and #E6) cells were transfected with 100 nM rat Sdc4 – targeting siRNA for 24 h as described in 6.3.4. The same cells transfected with 100 nM non-targeting scrambled SiRNA were used as control. **(A)** the relative expression of Sdc4 mRNA was measured by qRT-PCR (**Table 6.3**) by $2^{-\Delta\Delta Ct}$ relative quantification method (cyclophilin-A was employed as housekeeping gene). **(B)** Extracellular TG2 activity was measured as described in 2.2.9.2. Values are the average Abs (450 nm) of three independent experiments, each undertaken in triplicates, normalised for the relative mock transfected control (equalised to 1) ± SD. **(C)** NRK52E WT and EGFP-TG2 overexpressing (clones #C5) cells were cultured in normal conditions until 80% confluent. Cells were detached with sterile PBS containing 5mM EDTA in constant shaking at 37°C, and equal volumes of the cell suspensions obtained were incubated with increasing concentration of Surfen (0, 3, 6, 9 and 12 μM) in PBS/0.1% (w/v) BSA, for 10 min on ice. After incubation, cells were collected by centrifugation at 500 g/5 min and extracellular TG2 activity was measured as described in 2.2.9.2. Values are the average Abs (450 nm) of three independent experiments, each undertaken in triplicates, normalised for the untreated control (0 μM Surfen, equalised to 1) ± SD. Significance of the differences between treatments was determined by T-test: * = $p<0.05$, ** = $p<0.01$, *** = $p<0.001$, **** = $p<0.0001$.

6.4.5 Importance of the heparin binding site of TG2 for the enzyme's extracellular deposition

The heparin-binding site (HBS) of TG2 has been mapped to two basic clusters at position 262RRWK265 and 598KQKRK602 of TG2 by our group, forming a positively charged heparin binding pocket on the surface of the enzyme when it is in a close conformation (Lortat-Jacob, et al. 2012). The involvement of this HBS in TG2 trafficking outside the cells was investigated by transient transfection of WT NRK52E cells with EGFP-tagged heparin binding mutants of TG2 where the first (mutant M1c) and second (mutant M3) clusters were mutated by site directed mutagenesis. Cells were transfected with pEGFP-N1-TG2(M1c) and pEGFP-N1-TG2(M3) plasmids, characterised by the aforementioned point mutations in the HBS (Lortat-Jacob, et al. 2012) (**Appendix, Fig. II**). The first plasmid expresses a mutation in 262RRWK265 cluster of TG2 (M1c, mutation K265S) and the second expresses four mutations in the 598KQKRK602 of the enzyme (M3, mutations K598S, K600S, R601S and K602S) (**Suppl. Fig. 6.1C**), all mutations known to inhibit the binding of purified TG2 to heparin (Lortat-Jacob, et al. 2012). As a positive control, cells were transfected with pEGFP-N1-TG2(WT) plasmid, containing wild type human TG2 cDNA.

Transfection efficiency was assessed by fluorescent confocal microscopy by direct count of the number of green fluorescent cells (transfected) over the total (nuclei) (**Suppl. Fig. 6.6**). Transfection efficiency measured in this way was 93.42 ± 6.35% of total cells for the control pEGFP-N1-TG2(WT) plasmid, 84.63 ± 12.56% for pEGFP-N1-TG2(M1c) and 90.15 ± 15.08% for pEGFP-N1-TG2(M3). No significant difference was observed between the specific plasmids when the efficiency was measured in this way by direct count (**Suppl. Fig. 6.6**). Expression of EGFP-TG2 chimera after transfection was also assessed by western blot, and similar amount of EGFP-TG2 chimera protein was detected for both mutated and wild type TG2 (**Fig. 6.10A**).

Transfection of both Heparin binding mutant TG2 cDNA, by either pEGFP-N1-TG2(M1c) or pEGFP-N1-TG2(M3) plasmids, led to a reduction in extracellular TG2 activity compared to the control plasmid, when measured by biotinylated cadaverine incorporation assay on living cells (**Fig. 6.10B**). Transfection with both plasmids led to an approximate 40% reduction in extracellular TG2 activity, with a residual enzymatic activity of 62.15 ± 30.02 % of the control for M1c mutant and 61.11 ± 14.80% of the control for M3 mutant ($p=7.64 \cdot 10^{-07}$, ****) (**Fig. 6.10B**).

Immunofluorescent staining of extracellular EGFP-TG2 was performed on non-permeabilised cells (**Fig. 6.10C**) and reflected the observations of the above-mentioned activity assay. Transient transfection with pEGFP-N1-TG2(M1c) led to a ~35% reduction in the extracellular EGFP-TG2 (red fluorescence) compared to the TG2(WT) control (p=0.029, *), when this was measured relatively to the total transfected protein (green fluorescence) (**Fig. 6.10C**). On the

other hand, transient transfection with pEGFP-N1-TG2(M3) only led to a ~20% reduction of extracellular EGFP-TG2 compared to the TG2(WT) control (p=0.018, *) (**Fig. 6.10C**).

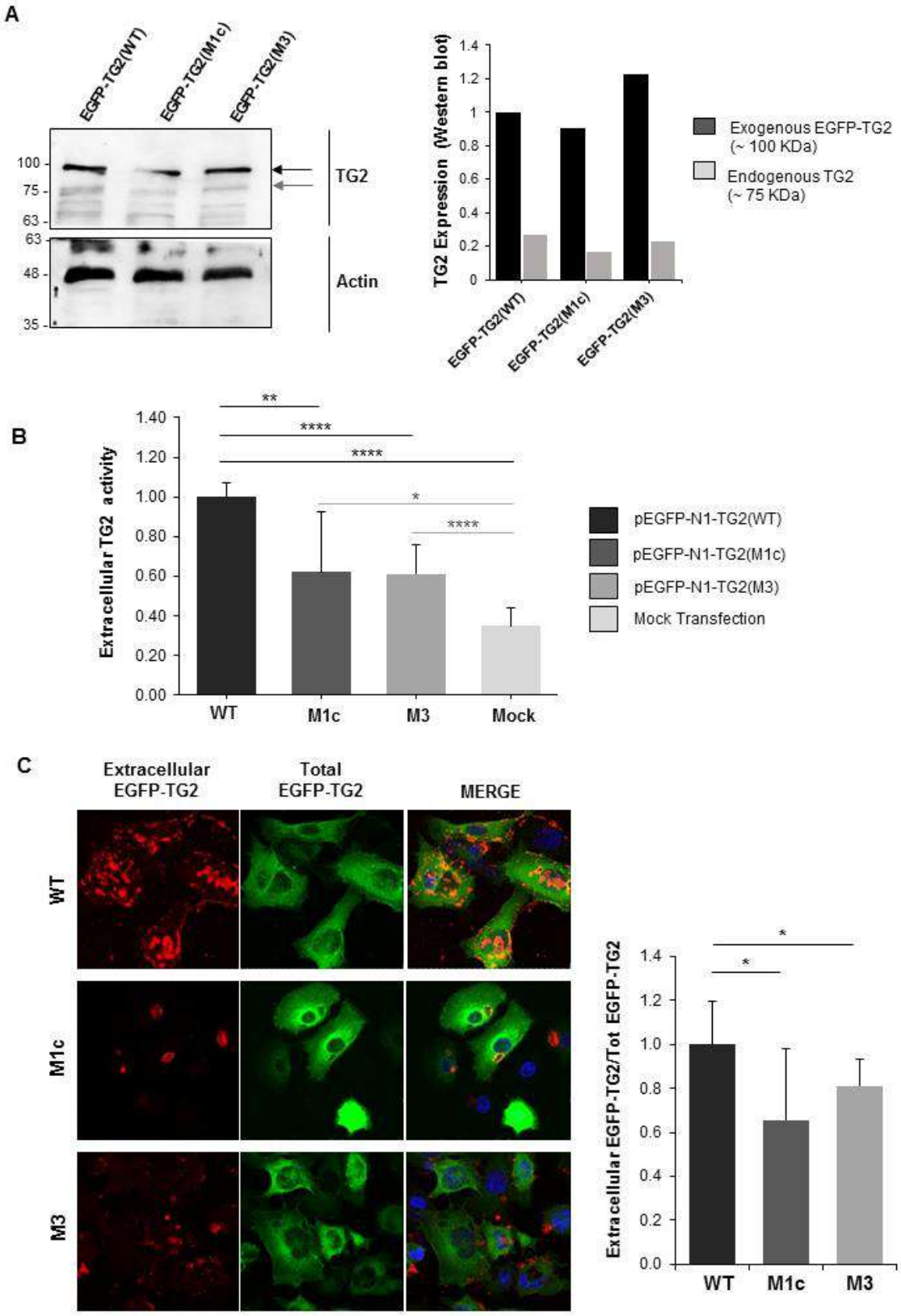

Figure 6.10: Effects of mutations in TG2 heparin binding site on extracellular TG2 localisation and activity. (A) 1 million NRK52E WT cells were transiently transfected by electroporation with 5 μg of pEGFP-N1 plasmid containing either TG2(WT), TG2(M1c) and TG2(M3) as described in 6.3.3.2 and seeded in a 6-well plate for 48 h. Equal amounts of cell lysates (30 μg) were separated by 10% SDS-PAGE and immunoprobed for TG2 using a rabbit polyclonal anti-TG2 antibody (Ab80563 Abcam, dilution 1:1000) and Actin (A5060 Sigma, dilution 1:500) as a loading control, both followed by goat anti rabbit IgG conjugated to HRP (Dako, dilution 1:2000). The immunoreactive bands were visualised by chemiluminescence after addition of ECL reagent (Biological Industries). Image acquisition was performed with a LAS4000 imaging system (GE Heathcare) and comparison of protein band intensity was obtained by Aida Image Analyzer v.4.03 (Raytest), following the manufacturer's instructions. A representative blot and relative quantification normalized for the loading control and expressed relative to the TG2(WT) transfected control (equalized to 1) are shown. Transfected EGFP-TG2 has a molecular weight of ~100 kDa, while cell endogenous TG2 appears as a lower band at ~100 kDa. **(B)** 1 million NRK52E WT cells were transiently transfected by electroporation with 5 μg of pEGFP-N1 plasmid containing either TG2(WT), TG2(M1c) and TG2(M3) as described in 6.3.3.2 and seeded in a 6-well plate for 48 h. After transfection, extracellular TG2 activity was measured as described in 2.2.9.2. Values are the average Abs (450 nm) of three independent experiments, each undertaken in quadruplicates, normalised for the control TG2(WT)-transfected cells (equalised to 1) ± SD. **(C)** 200,000 NRK52E WT cells were transiently transfected by electroporation with 5 μg of pEGFP-N1 plasmid containing either TG2(WT), TG2(M1c) and TG2(M3) as described in 6.3.3.2 and seeded in an 8-well chamber slide for 48 h. Extracellular EGFP-TG2 chimera was detected by immunofluorescent staining on fixed (3%PFA) but not permeabilised cells by a rabbit polyclonal anti-GFP antibody (ab290,Abcam,dilution 1:500) followed by a donkey anti-rabbit Alexa Fluor® 568 antibody (dilution 1:1000) secondary antibody, following the general method described in 2.2.8. Nuclei were stained with DAPI. Representative pictures at 100X magnification are here shown. Cell surface and matrix bound EGFP-TG2 was quantified by ImageJ intensity analysis (8 non-overlapping images per section) and presented as mean relative intensity of red over green (total EGFP-TG2) ± SD, expressed relative to the TG2(WT) transfected cells (equalised to 1). Significance of the differences between treatments was determined by T-test: * = $p<0.05$, ** = $p<0.01$, *** = $p<0.001$, **** = $p<0.0001$.

6.4.5.1 Investigation of the effect of altered 6-O sulfation of heparan sulfate chains on the TG2 secretion from human kidney cells

Recently, the distribution of 6-O sulfated groups in HS chains has been suggested to be important in the progression of renal fibrosis, possibly by binding specific cytokines or growth factors (Alhasan, et al. 2014). Alhasan and colleagues showed how two different enzyme families involved in 6-O sulfation of HS chains, glucosaminyl-6-O-sulfotransferases (HS6STs), which determine the formation of 6-O-sulfated glucosamine residues on HSPGs, and HS-6-O-endosulfatases (SULFs), which remove them, are able to modulate fibrotic associated cell responses *in vitro*. They also showed that the level of 6-O sulfation is upregulated in vivo in the UUO model of kidney fibrosis (Alhasan, et al. 2014).

Stable human kidney TECs overexpressing either SULF2 (HKC8 cells)(Alhasan, et al. 2014) or HS6ST (HK2 cells) (Alhasan, et al. 2014) were kindly provided by Prof Simi Ali (Newcastle University) and were employed to investigate whether the expression of these enzymes affected TG2 externalisation.

SULF2 overexpressing HKC8 clones (SULF2#S5 and SULF2 #S11)(Alhasan, et al. 2014), as well as mock transfected cells, were cultured in the appropriate selective medium until confluent and tested for both total TG2 expression/activity and extracellular TG2 activity. SULF2

overexpressing clones displayed a similar level of intracellular TG2, as determined by Western blot (**Fig.6.11A**), however the control ("mock") cells had clearly less TG2 (**Fig. 6.11A**), TG2 activity measurement on whole cell lysates (total TG2 activity), when measured by biotin cadaverine incorporation assay, confirmed a significantly lower TG2 activity in the mock transfected HKC8 clones (**Fig. 6.11B**), while the activity of the two SULF2 overexpressing clones was approximately 5-fold higher ($p<0.001$). These data suggest that increased HS-6-O-endosulfatases, predicted to raise the removal of HS-6-O sulfated groups, lead to increased expression of TG2in the cells. Alternatively, increased TG2 could be simply due to a clonal effect or a compensatory event.

When cell surface TG2 activity was measured in these cells, SULF2 overexpressing clones displayed a significantly higher level of extracellular TG2 activity compared to the mock transfected control (clone #S5 was 2.39±1.96-fold higher than the mock control, $p=0.024$, *; clone #S11 was 3.42±2.63-fold higher than the mock control, $p=0.003$, **) (**Fig.6.11C**). However, when the extracellular TG2 activity was normalised for the total TG2 activity of the cells to determine the portion of TG2 activity exported, the extracellular TG2 resulted higher in the mock transfected control HKC8 cells compared to the SULF2 overexpressing ones, suggesting that HS-6-O S groups are important for TG2 export in this cell line (**Fig. 6.11D**).

When the same analysis was performed in the HS6ST overexpressing HK2 clones (HS6ST #T5 and HS6ST #T7)(Alhasan, et al. 2014) and mock transfected HK2 cells, the SULF2 overexpressing clones displayed a ~20-25% lower TG2 compared to the stably mock transfected cells by western blot (**Fig. 6.11E**) and total TG2 activity assay (**Fig. 6.11F**). When cell surface TG2 activity was measured in these cells, HS6ST overexpressing clones were showing a significantly 20-40% lower level of extracellular TG2 activity compared to the mock transfected control (clone #T5 was 0.81 ± 0.068 of the mock control, $p =0.0002$, ***, while clone #T7 was 0.63±0.061 of the mock control, $p =2.88 \cdot 10^{-11}$, ****) (**Fig. 6.11G**). However, when the extracellular TG2 activity was normalised for the total TG2 activity of the cells to determine the portion of TG2 activity exported, the extracellular TG2 activity appeared similar between the HS6ST clone #T5 and the mock transfected cells, while the #T7 clone extracellular activity resulted still lower than the control (**Fig.6.11H**).

Overall, increased sulfation of HS-6-O by HS6ST in transfected clones was not accompanied by increased TG2 export compared to mock transfected clones (and overall led to a reduced expression of TG2) while increased de-sulfation of HS-6-O by SULF2 affected the export of TG2, although it led to its increased expression in SULF2 transfected clones.

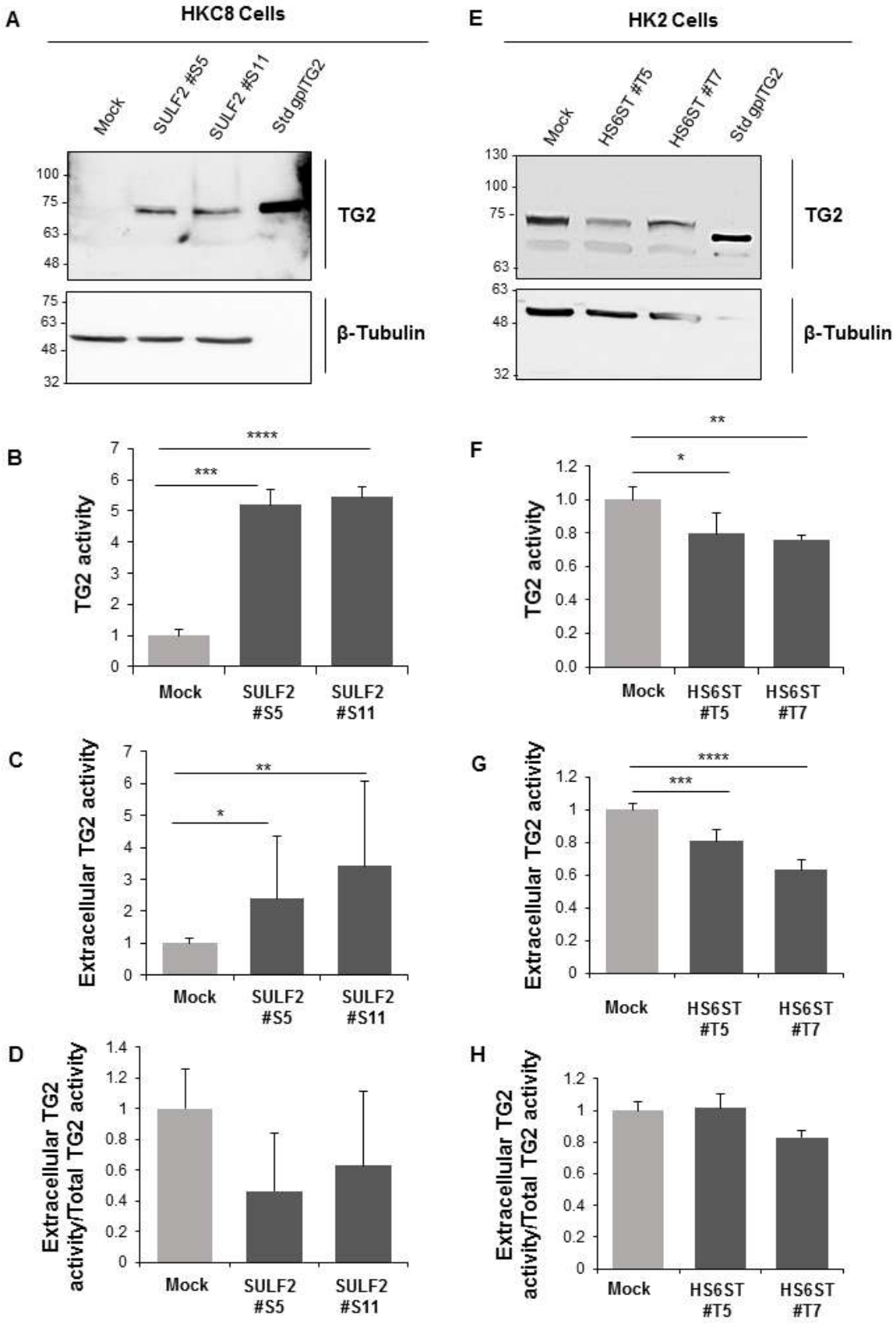

Figure 6.11: Investigation of the effect of altered 6-O sulfation of HS chains on TG2 secretion from human TECs. (A – D) HKC8 mock transfected and SULF2 overexpressing clones (#S5 and #S11) were cultured in grown in DMEM-F12 medium supplemented with 10% (v/v) heat-inactivated FBS, 2mM L-glutamine, 100 IU/mL penicillin, 100 µg/mL streptomycin and 400 µg/ml G418 (Invivogen). **(E-H)** HK2 mock transfected and HS6ST overexpressing clones (#T5 and #T7) were cultured in DMEM-F12 medium

supplemented with 10% (v/v) heat-inactivated FBS, 2mM L-glutamine, 100 IU/mL penicillin, 100 µg/mL streptomycin and 400 µg/ml Zeocin (Invivogen). **(A, B, E, F)** 90% confluent cells were lysed in a mild lysis buffer (0.25 M sucrose, 5 mM TRIS-HCl, 2 mM EDTA, pH 7.4) (**A, E**) Equal amounts of protein lysate (100 µg) were separated by 10% SDS PAGE and immunoprobed with a rabbit polyclonal anti-TG2 antibody (ab80563, Abcam, dilution 1:1000) as well as with a rabbit polyclonal anti-β-tubulin antibody (ab6046 Abcam, dilution 1:5000) as a loading control, as described in 2.2.7. 500 ng of purified guinea pig liver TG2 (gplTG2, Sigma) were also loaded as a standard positive control. Molecular weight of human TG2 immunoreactive bands is ~75kDa. **(B, F)** Total TG2 activity was measured on equal amounts of protein lysates (60 µg) as described in 2.2.9.1. Values are the average Abs (450 nm) of four replicas, expressed relative to the mock transfected control (equalised to 1) ± SD. **(C, G)** Extracellular TG2 activity was measured as described in 2.2.9.2. Values are the average Abs (450 nm) of four independent experiments, each undertaken in quadruplicates, normalised for the relative mock transfected control (equalised to 1) ± SD. Significance of the differences between treatments was determined by T-test: * = $p<0.05$, ** = $p<0.01$, *** = $p<0.001$, **** = $p<0.0001$. **(D, H)** Chart representing the extracellular TG2 activity of each clone expressed relative to the total TG2 activity of the same cells (Extracellular TG2 activity/ Total TG2 activity) and normalised for the relative mock transfected control (equalised to 1) ± SD.

6.4.6 Role of HS chains in the cell surface retention of exogenously added TG2

Having established that Sdc4 and HS can modulate the level of TG2 at the cell surface, we wanted to extend the investigation of this function in situations of abundant deposition of TG2 in the ECM, which is typically found in the context of kidney fibrosis. To do so, recombinant TG2 was added to NRK52E and NRK49F monolayers and the amount of TG2 retained in ECM/cell surface with or without HS inhibition was analyzed, with particular interest to the consequences of this deposition on TGFβ1 activation.

NRK52 cells were pre-incubated with the HS antagonist Surfen before extracellular addition of recombinant human TG2, which was pre-treated with DTT as described in 5.3.6, to allow the access to the enzyme active site (Stamnaes, et al. 2010). After washing, the level of TG2 retained to the cell surface extracellular matrix was investigated by immunofluorescence as described in 6.3.6.1 (**Fig. 6.12A**). As the monoclonal anti-TG2 antibody CUB 7402 has no reported specificity for rat TG2, no or very low background fluorescence was detected in untreated cells (**Fig. 6.12A**, - Rh-TG2). Extracellularly added recombinant TG2 was retained in the pericellular matrix of NRK52E cells (**Fig. 6.12A**, + Rh-TG2). Pre-incubation of the cell monolayer with surfen led to a significantly lower level of extracellular TG2 retention, which was 63% of the total TG2 deposited in the matrix ($p= 0.04$, *).

When TG2 activity was analysed *in situ* by FITC-cadaverine incorporation assay (Verderio, et al. 1998) (**Fig. 6.12B**), pre-incubation of the cell monolayer with Surfen reduced extracellular TG2 activity in both in cells with no additional exogenous TG2 (to 35.64±1.79%, $p=0.07$) and cells with extracellularly added enzyme (to 67.89±26.33%, $p=0.21$). Although these differences

were not statistically significant, there was a clear trend of decrease in TG2 extracellular activity upon HS antagonism by Surfen.

Treatment of the NRK52E matrix with heparitinase (HepI), which selectively cleaves HS chains at the 1-4 bounds between N-acetylglucosamine and glucuronic acid residues, led to a reduction in the exogenous TG2 deposition to approximately 66%, but this was not as significant as the reduction determined by Surfen (**Fig. 6.12C**).

As fibroblast are known to produce abundant extracellular matrix (Chapter I), NRK49F fibroblasts were also analysed using the same approach. Extracellularly added recombinant TG2 strongly accumulated in the pericellular matrix of NRK49F (**Fig. 13A**), and partially co-localized with collagen I, immunostained with an anti-collagen I polyclonal antibody followed by a secondary antibody with red fluorescence (**Fig. 6.13A**, red staining). When the NRK49 cell monolayer was pre-incubated with surfen, the amount of extracellularly retained TG2 was significantly reduced to 34% of the TG2 deposited in the matrix of untreated cells ($p=0.0008$, ***) (**Fig. 6.13A**). Pre-treatment with heparitinase (HepI) determined as well a significant reduction in TG2 deposition in the matrix, to approximately 65% of the TG2 deposited in untreated cells ($p\approx0.05$) (**Fig. 6.13B**).

In summary, HS chains are important for TG2 retention in the extracellular environment once externalised, in an autocrine or paracrine fashion, as chemical antagonism or digestion of these chains had an inhibitory effect on the enzyme deposition.

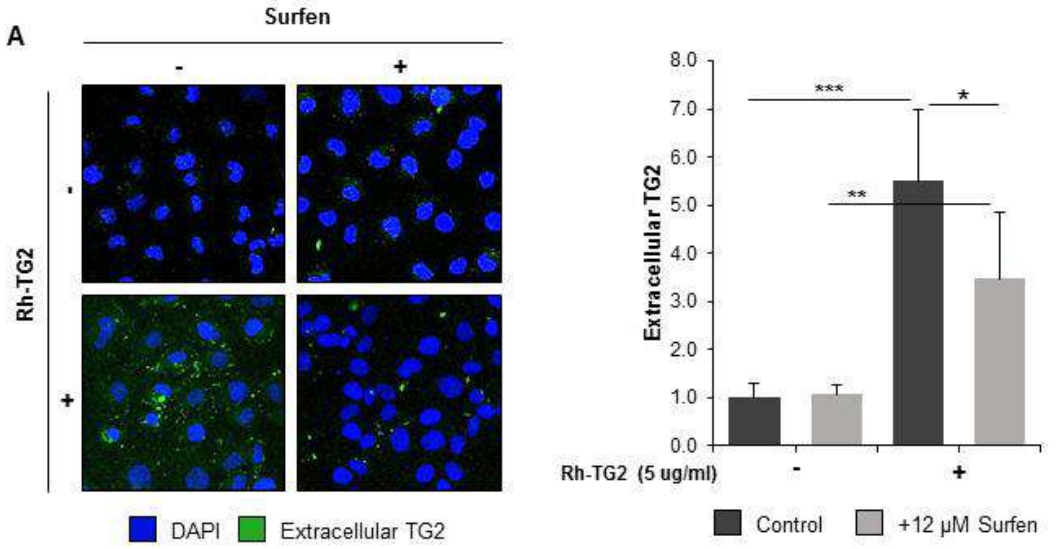
A
Surfen
-
+
Rh-TG2
DAPI
Extracellular TG2
Extracellular TG2
8.0
7.0
6.0
5.0
4.0
3.0
2.0
1.0
0.0
***
*
**
Rh-TG2 (5 ug/ml)
Control
+12 µM Surfen

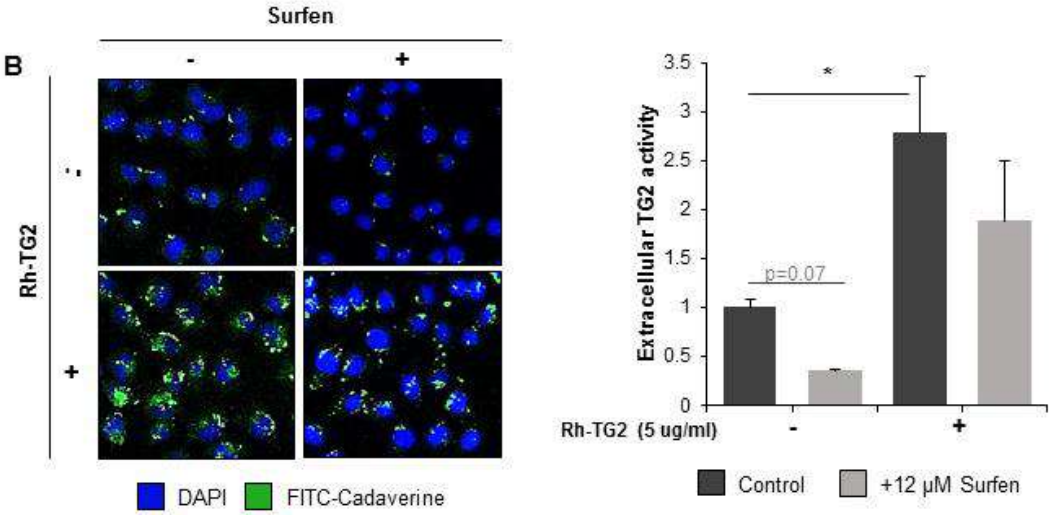
B
Surfen
Rh-TG2
DAPI
FITC-Cadaverine
Extracellular TG2 activity
3.5
3
2.5
2
1.5
1
0.5
0
*
p=0.07
Rh-TG2 (5 ug/ml)
Control
+12 µM Surfen

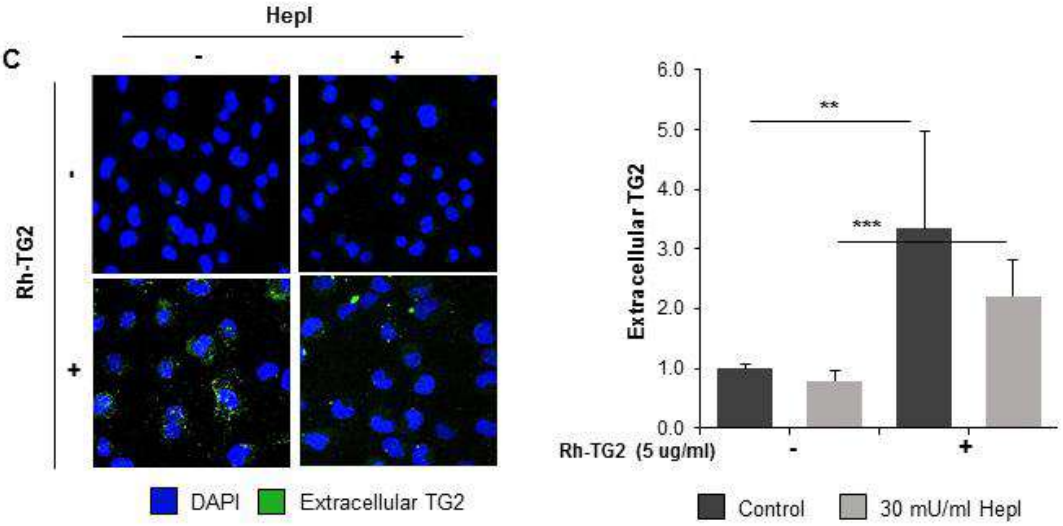
C
HepI
Rh-TG2
DAPI
Extracellular TG2
Extracellular TG2
6.0
5.0
4.0
3.0
2.0
1.0
0.0
**
***
Rh-TG2 (5 ug/ml)
Control
30 mU/ml HepI

Figure 6.12: Deposition of extracellular TG2 is reduced by employment of HS antagonist Surfen or digestion of HS chains in NRK52E TECs. (A) To assess retention of exogenous TG2 in the extracellular environment, NRK52E cells were grown in an 8-well chamber slide and treated with 12 μM Surfen for 15 min before addition of reduced human Rh-TG2 at a final concentration of 5 μg/ml for 1 h. After fixation (3%PFA), TG2 was immunostained by a mouse monoclonal anti-TG2 antibody followed by sheep anti-mouse-FITC. Nuclei were stained with DAPI. Representative figures at 100X magnification are here shown. Cell surface and matrix bound exogenous TG2 was quantified by ImageJ intensity analysis (8 non overlapping images per section) and presented as mean relative intensity of green over blue (DAPI) ± SD, expressed relative to the control without added TG2 (equalised to 1). **(B)** In order to detect TG2 extracellular activity in cells subjected to the same treatments, NRK52E cells were grown in an 8-well chamber slide and treated with 12 μM Surfen for 15 min before addition of reduced human Rh-TG2 (5 μg/ml) and FITC-conjugated cadaverine for 6 h. Cells were fixed with 90% methanol as described in 2.2.9.3 and nuclei were stained with DAPI. Representative figures at 100X magnification are here shown. Cell surface and matrix-associated TG2 activity was quantified by ImageJ intensity analysis (8 non overlapping images per section) and presented as mean relative intensity of green over blue (DAPI) ± SD, expressed relative to the control without added TG2 (equalised to 1). **(C)** In order to determine whether deposition of extracellular TG2 is reduced by digestion of HS chains in NRK52E TECs, these cells were grown in an 8-well chamber slide and treated with 30 mU/ml heparitinase I (Hep I) for 1 h before addition of 5 μg/ml reduced human Rh-TG2 for 1 h. TG2 immunostaining was performed as described above. Representative figures at 100X magnification are here shown. Cell surface and matrix bound exogenous TG2 was quantified by ImageJ intensity analysis (8 non overlapping images per section) and presented as mean relative intensity of green over blue (DAPI) ± SD, expressed relative to the control without added TG2 (equalised to 1). Significance of the differences between treatments was determined by T-test: * = $p<0.05$, ** = $p<0.01$, *** = $p<0.001$, **** = $p<0.0001$.

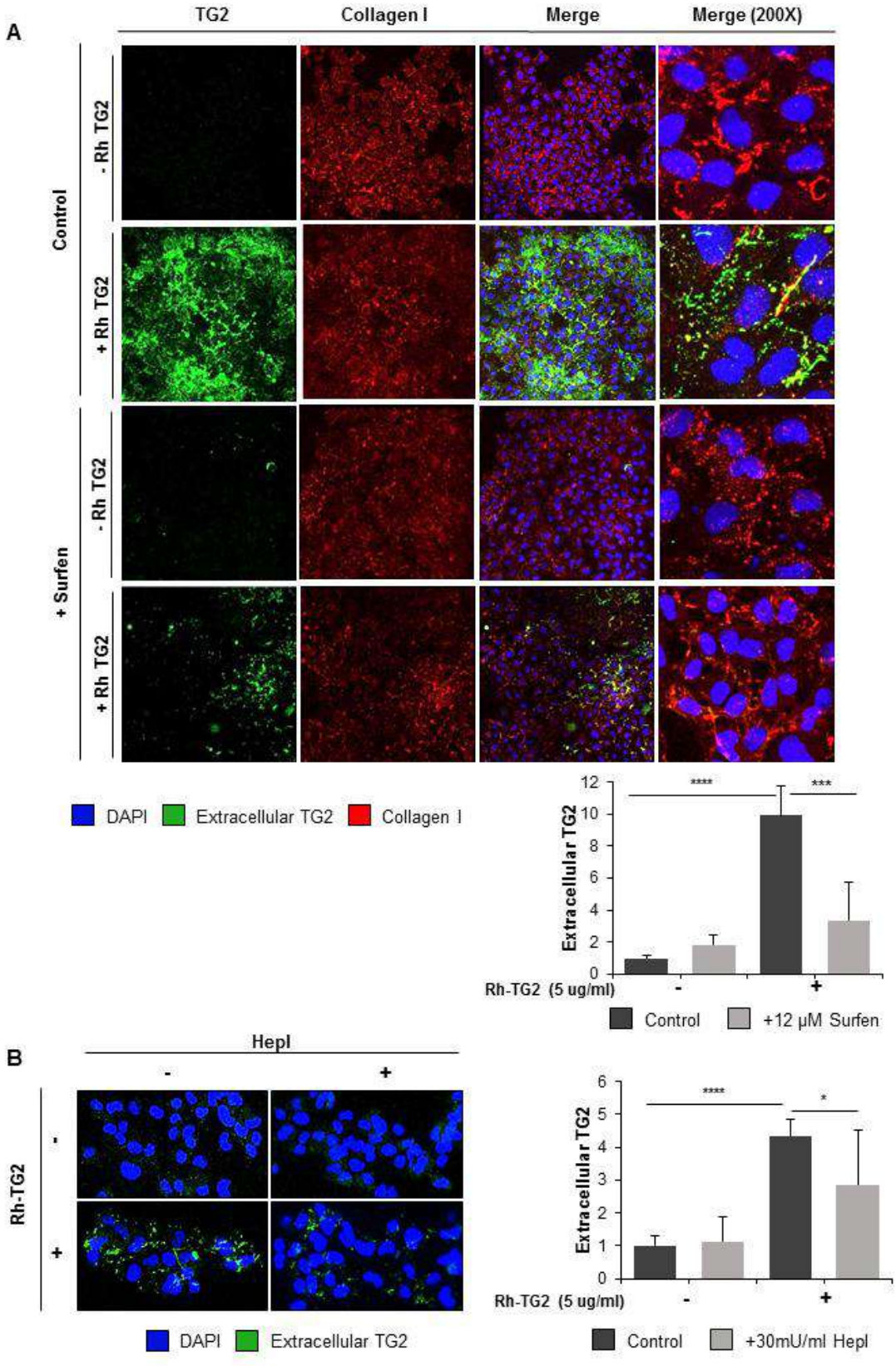
A
TG2
Collagen I
Merge
Merge (200X)
Control
+ Surfen
- Rh TG2
+ Rh TG2
- Rh TG2
+ Rh TG2
DAPI
Extracellular TG2
Collagen I
Extracellular TG2
Rh-TG2 (5 ug/ml)
Control
+12 µM Surfen
B
HepI
Rh-TG2
DAPI
Extracellular TG2
Extracellular TG2
Rh-TG2 (5 ug/ml)
Control
+30mU/ml HepI

Figure 6.13: Deposition of extracellular TG2 is inhibited by employment of HS antagonist Surfen or digestion of HS chains in NRK49F renal fibroblasts. (A) NRK49F cells were grown in an 8-well chamber slide and treated with 12 uM Surfen for 15 minutes before addition DTT-activated human Rh-TG2 at a final concentration of 5 μg/ml for 1 h. Cells were fixed with 3% PFA. Immunostaining was performed by using rabbit polyclonal anti-collagen I antibody and mouse monoclonal anti-TG2 antibody followed by donkey anti-rabbit-Alexa Fluor® 568, with red emission, and sheep anti-mouse-FITC, with green emission. Nuclei were stained with DAPI. In negative controls the primary antibodies were omitted. Representative pictures of collagen I and extracellular TG2 stainings are shown separately (40X magnification) and merged (40 and 200X magnification). Cell surface and matrix bound exogenous TG2 was quantified by ImageJ intensity analysis (8 non overlapping images per section) and presented as mean relative intensity of green over blue (DAPI) ± SD, expressed relative to the control without added TG2 (equalised to 1). **(B)** In order to determine whether deposition of extracellular TG2 is reduced by digestion of HS chains in NRK49F fibroblasts, these cells were grown in an 8-well chamber slide and treated with 30 mU/ml heparitinase I (Hep I) for 1 h before addition of 5 μg/ml reduced human Rh-TG2 for 1 h. TG2 immunostaining was performed as above. Representative figures at 100X magnification are here shown. Cell surface and matrix bound exogenous TG2 was quantified by ImageJ intensity analysis (8 non overlapping images per section) and presented as mean relative intensity of green over blue (DAPI) ± SD, expressed relative to the control without added TG2 (equalised to 1). Significance of the differences between treatments was determined by T-test: * = $p<0.05$, ** = $p<0.01$, *** = $p<0.001$, **** = $p<0.0001$.

6.4.7 Interplay between HSPG and TG2 in TGF-β activation

Having established the importance of HS chains of proteoglycans in the deposition of TG2 in the matrix, we asked the question whether extracellular TG2 leads to increased activation TGF-β signalling in TECs and the function of HS-TG2 interaction in this process. Modulation of TGF-β activity results in TGF-β receptor/ Smad3 activation, that leads to the transcriptional regulation of fibrosis-associated genes (Lan 2011, Inazaki, et al. 2004, Sato, et al. 2003).

NRK52E cells monolayer was pre-treated with Surfen before incubation with recombinant TG2, and Smad3 phosphorylation was assessed relative to total Smad3 protein by immunofluorescence using specific antibodies, as described in 6.3.6.2.

Extracellular TG2 induced Smad3 phosphorylation in the NRK52E cell monolayer (**Fig. 6.14A**), and this was greatly reduced when HS chains were blocked by Surfen (**Fig. 6.14A**). Extracellular TG2 did not change the level of total Smad3, but Surfen pre-treatment led to a decrease in total Smad3 (**Fig. 6.14B**). When the degree of Smad3 phosphorylation was expressed as a ratio between phosphorylated Smad3 and total expressed Smad3, Smad3 activation was significantly increased by extracellular exogenous TG2 (3.33±1.01 times the control without TG2, $p=3.74\cdot10^{-5}$, ****) (**Fig.6.14C**). Surfen alone did not change the level of Smad3 phosphorylation over total but had a strong inhibitory effect on Smad3 activation induced by TG2 (**Fig.6.14C**), which was only 1.50(±1.00)-fold the value of cells not supplemented with TG2 (p= 0.09) and was significantly lower than the Smad3 activation mediated by TG2 in cells without surfen (~43% of untreated cells, $p=2.77\cdot10^{-5}$,****)(**Fig. 6.14C**).

These data suggest that extracellular TG2 is sufficient to mediate TGF-β activation from TECs, when measured via Smad3 phosphorylation; moreover, they suggest that HS antagonism itself does not change the level of TGF-β activation while but TGF-β signalling is affected by interference between TG2-HS interaction in the matrix of NRK52E cells.

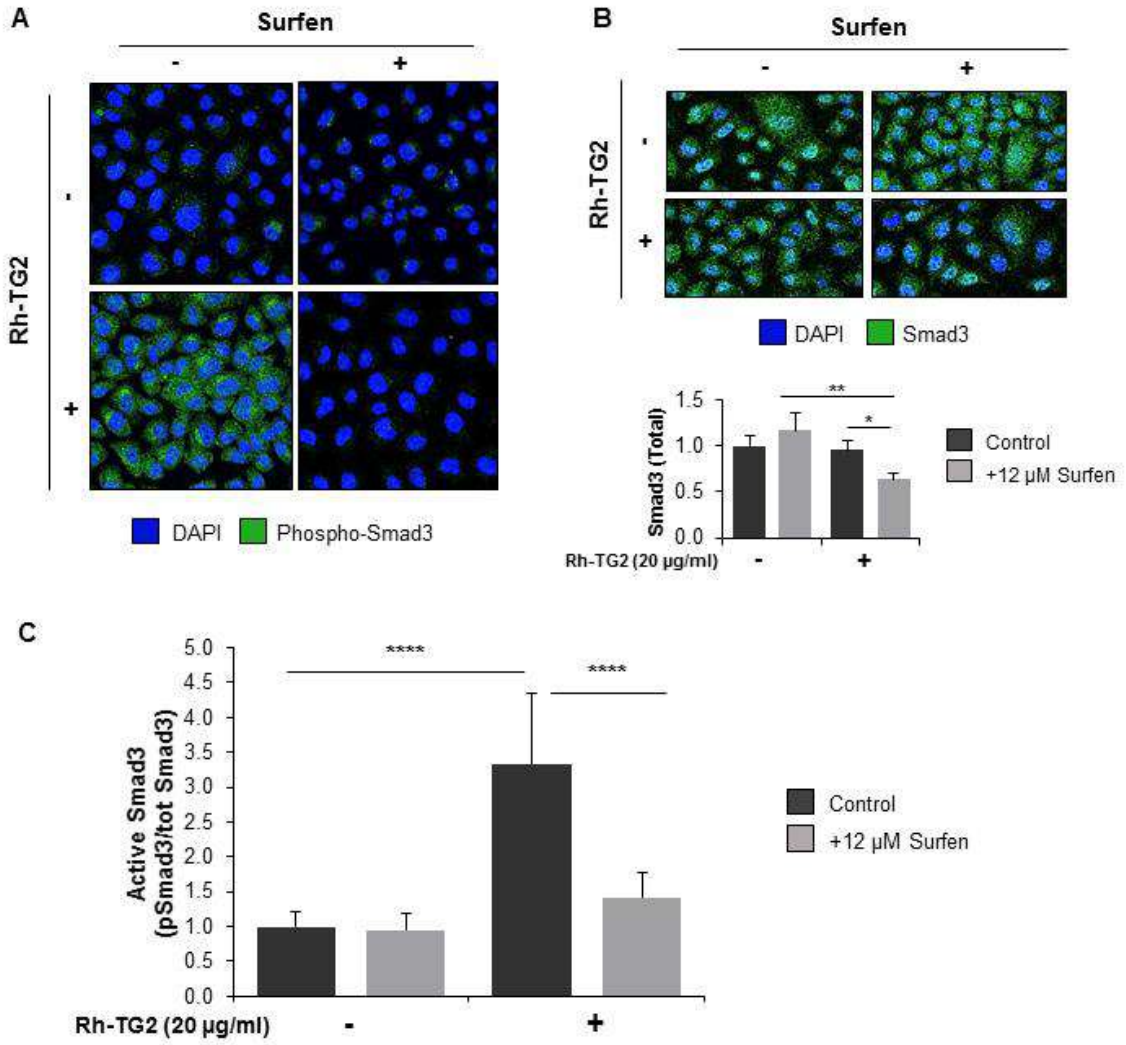

Figure 6.14: Effect of exogenously added TG2 on TGF-β-dependent Smad3 activation. (A, B) In order to assess Smad3 activation, NRK52E cells were grown in an 8-well chamber slide and treated with 12 µM Surfen for 15 minutes before addition of Rh-TG2 pre-activated with DTT, at a final concentration of 20 µg/ml for 24 hours. After fixation (3% PFA) and permeabilisation [0.1% (w/v) Triton X100], active ($pSer_{425}$) (A) and total Smad3 (B) were immunostained by rabbit polyclonal antibodies reported in 6.3.6.2, followed by donkey anti-rabbit-Alexa Fluor® 488. Nuclei were stained with DAPI. Representative figures at 100X magnification are here shown. Total Smad3 was quantified by ImageJ intensity analysis (8 non overlapping images per section) and presented as mean relative intensity of green over blue (DAPI) ± SD, expressed relative to the control without added TG2 (equalised to 1); little variation was observed in the total Smad 3 between treatments. **(C)** Active phosphorylated Smad 3 was quantified by ImageJ intensity analysis (8 non overlapping images per section) and the amount of activated Smad3 was presented as mean relative intensity of green over blue (DAPI) ± SD, normalised for the total Smad3 in the corresponding treatment and expressed relative to the control without added TG2 (equalised to 1). Significance of the differences between treatments was determined by T-test: * = $p<0.05$, ** = $p<0.01$, *** = $p<0.001$, **** = $p<0.0001$.

6.4.8 Role of Sdc4 in the proposed pathway of TG2 unconventional secretion.

In Chapter V, TG2 association with extracellular vesicles (EV) was analysed and the release of TG2 from kidney cells through a vesicular type of unconventional secretion suggested. Prior work including that reported in this chapter have shown that HS/Sdc4 are involved in TG2 export from kidney cells (Huang, et al. unpublished). As Sdc4 has been recently reported to have a role in exosome biogenesis and cargo loading by binding specific protein cargoes (Baietti, et al. 2012, Roucourt, et al. 2015, David and Zimmermann 2015), the hypothesis was formed that Sdc4 could be involved in the vesicular trafficking of TG2, with TG2 being a Sdc4-binding cargo in exosomes.

To test this hypothesis, firstly, the presence of Sdc4 in EV subpopulations obtained from rat kidney cells was investigated by Western blotting on total lysates. Sdc4 is notoriously difficult to detect by Western blotting and, being a glycoprotein, would require removal of HS chains for its correct detection (**Fig. 6.7A,B**). However my work in this chapter with cells transfected with Sdc4 cDNA constructs showed a consistent band at ~35 kDa (**Suppl. Fig. 6.2**) which intensifies after HepI treatment (**Fig. 6.7A,B**).

EGFP-TG2 overexpressing NRK52E cells were cultured in serum free medium for 36 h and the different vesicular fractions were isolated following the protocol described in the previous chapter (5.3.3) (**Fig. 6.15A**). Western blot analysis of the different fractions revealed an enrichment of Sdc4 in the exosomal fraction (P4), compared to the total cell lysate (TL), while a low almost undetectable level of Sdc4 was observed in the ectosomal portion (P3) and in the vesicle-deprived medium in the absence of Hepase treatment (**Fig. 6.15A**). Endogenous TG2 and EGFP-tagged exogenous TG2 were present in these vesicular subpopulations and more strongly associated with the exosomal portion (P4). Both Sdc4 and TG2 values were expressed as percentages of EV marker flotillin-2 (**Fig. 6.15A**).

Pro-fibrotic stimulus by recombinant TGF-β1 (10ng/ml) did not influence Sdc4 association with the exosomal fraction (**Fig. 6.15B**). This is in contrast with TG2 that appeared more strongly accumulated on the exosomal fraction upon TGF-β1 treatment (Chapter V).

When the same experiment was performed in wild type NRK52E cells, Sdc4 was also found associated with the exosomal fraction, with no or low signal in the ectosomes (P3) and in the medium (S4) under the experimental conditions employed, and Sdc4 was not affected by the treatment with recombinant TGF-β1 (**Fig. 6.15C**).

To confirm Sdc4 association in exosomes from a different renal cell type, EVs were also isolated from renal NRK49 fibroblasts. Sdc4 was also present in the exosomes subpopulation of this cell line (**Fig. 6.15D**).

Altogether, within the limits of the Sdc4 detection method, these experiments suggest that in renal cell types, Sdc4 is not only present on the surface of cells, where it serves as a receptor, but also in the exosome fraction, where TG2 can be detected too (Chapter V).

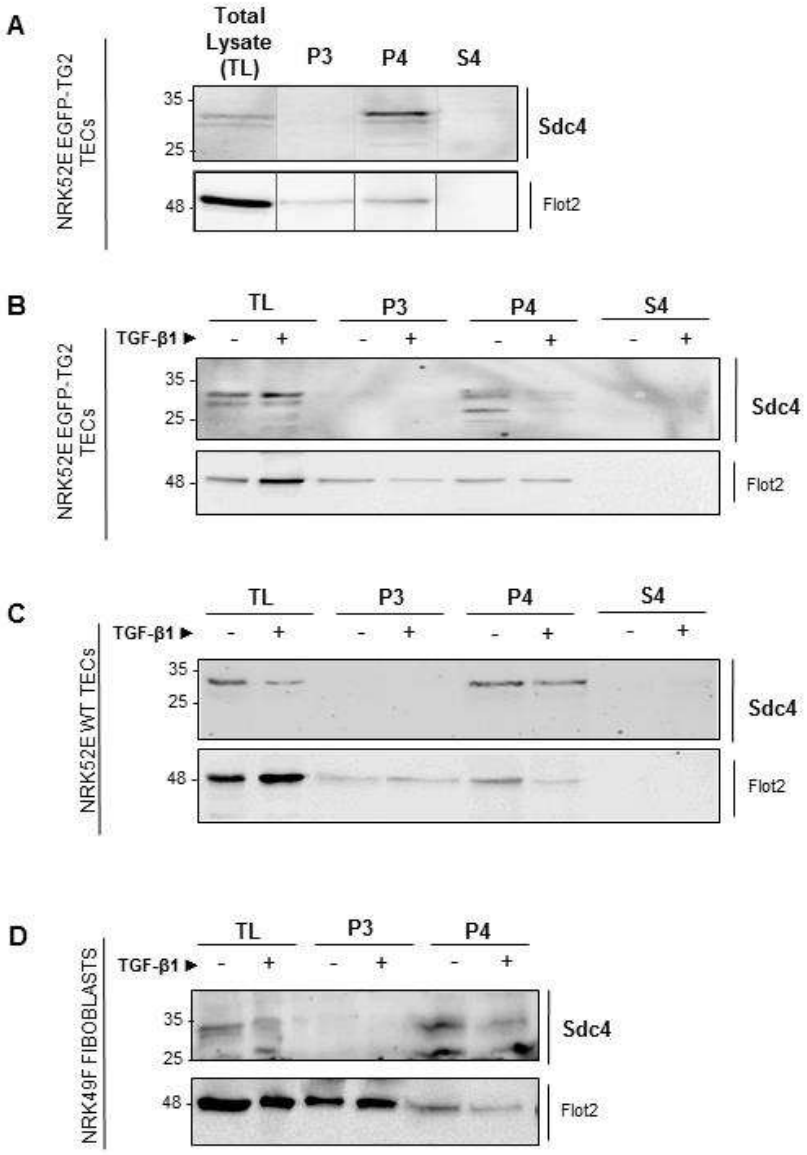

Figure 6.15: Presence of Sdc4 in extracellular vesicle (EV) fractions and cell medium. Blots from **Fig. 5.7** of Chapter V, showing EV fractions from (A) NRK52E EGFP-TG2 clone #C5 cells (B) NRK52E EGFP-TG2 clone #C5 cells ± 10 ng/ml TGF-β1, (C) NRK52E WT cells ± 10 ng/ml TGF-β1 and (D) NRK49F cells ± 10 ng/ml TGF-β1 were stripped and re-probed for Sdc4 using a rabbit polyclonal anti-Sdc4 antibody (ab24511, Abcam, dilution 1:500). Immunoreactive bands were detected by enhanced chemiluminescence (Geneflow) after incubation with appropriate HRP-conjugated secondary antibody (Goat anti-Rabbit IgG-HRP dilution 1:2000, Dako) in blocking buffer. Image acquisition was performed with a LAS4000 imaging system (GE Healthcare). For NRK52 cells, two (B,C) or three (A) independent experiments were performed. A representative blot is shown.

To investigate if TG2 and Sdc4 co-associate in these vesicles, immunoprecipitation of Sdc4 (Sdc4-IP) was performed from lysates of EV fractions, and total cell lysates as a control, obtained from EGFP-TG2 overexpressing NRK52E cells (clone #C5) using a polyclonal anti-Sdc4 antibody (**Fig. 6.16A**). In exosome lysates (P4), EGFP-tagged TG2 was shown to co-precipitate with Sdc4 (**Fig. 16A, c**), as it was seen to co-precipitate from IP of Sdc4 from total cell lysate (**Fig. 6.16A, a**). About 50% of the TG2 present in the P4 fraction associated with Sdc4, as revealed by detecting residual TG2 in the P4 "unbound" fraction (**Fig. 16A, c**). The association of TG2 with Sdc4 was proportionally lower in total cell lysate as denoted by the abundant unbound TG2 in cell lysate after Sdc4 IP (**Fig. 6.16A, a**). Sdc4 was detected via the usual 25-35 kDa double band. Immunoprecipitation of Sdc4 from the ectosomal (P3) lysate revealed that Sdc4 is indeed present in the ectosomal fraction as a 25-35 kDa double band (**Fig. 6.16A,b**), although it was not clearly visible by Western blotting of total P3 lysates as shown in **Fig. 6.15**. In contrast, only the lower Sdc4-immunoreacting band was detected in the Sdc4 immunoprecipitate from the exosomal (P4) fraction (**Fig.16A, c**). This band was intense and perhaps may result from a different degree of glycosylation of Sdc4 in exosomes (it corresponds to the size of the core protein, 20-22 kDa) (**Fig.16A, c**), although the two immunoreactive bands of Sdc4 were present in the total exosomal P4 lysate (as shown in previous **Fig 6.15**).

To assess the requirement of Sdc4 for TG2 association with the vesicles, EGFP-TG2 overexpressing NRK52E cells were transiently transfected with either rat Sdc4 targeting siRNA or scrambled control siRNA in serum-free antibiotic-free medium for 48 h, in order to knock down the expression of the proteoglycan, as described in 6.3.4. After transfection, Sdc4 reduction was confirmed by Western blotting of total cell lysate (**Fig. 6.16B**) and EV fractions isolated as above. Immunoprobing of EGFP-TG2 exogenous chimera and endogenous TG2 in these fractions showed that the knock down did not alter TG2 expression in tot cell lysate, but reduced both endogenous (TG2) and transfected (EGFP-TG2) enzyme in the exosome (P4) fractions; moreover, it lowered the level of free TG2 found in the EV-free conditioned medium (S4) (**Fig. 6.16C**). TG2 association with the ectosomes (P3) was also abolished by Sdc4 knock out (**Fig. 6.16C**).

In summary, Sdc4 was proven to associate with TG2 in extracellular vesicles, and its underexpression by siRNA knock downhad an inhibitory effect on TG2 association with the exosomal and ectosomal fraction.

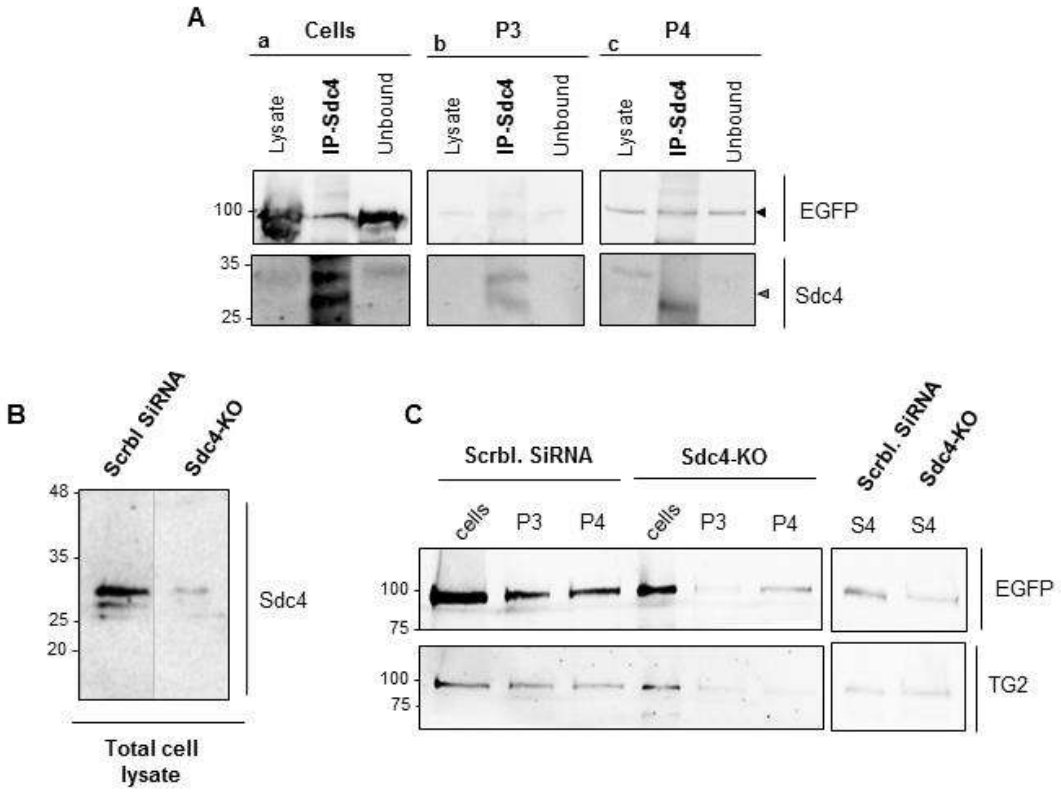

Figure 5.16: TG2 and Sdc4 interaction in extracellular vesicle (EV) fractions and cell medium. (A) NRK52E EGFP-TG2 clone #C5 cells were cultured in serum-free medium for 36 h. Culture medium was collected, the vesicular fractions were separated by differential centrifugation as described in 5.3.3 and lysed in IP Lysis/Wash Buffer (Thermo Scientific). Immunoprecipitation of Sdc4 (Sdc4-IP) was performed on these extracts and on the total cell lysate (TL) using 2.5 µg of rabbit polyclonal anti-Sdc4 antibody (ab24511, Abcam). Fraction lysates before immunoprecipitation (Lysate), Sdc4-IP and non-precipitated proteins collected as a wash-out during immunoprecipitation (Unbound) were probed for EGFP-TG2 chimera and Sdc4 by western blot using a rabbit polyclonal anti-Sdc4 antibody (ab24511, Abcam, dilution 1:500) and a rabbit polyclonal anti-GFP antibody (ab290, Abcam, dilution 1:2500) to investigate a possible co-precipitation of Sdc4 and EGFP-TG2 in vesicular extracts. Black arrowhead indicate EGFP-TG2 at ~100 kDa, grey arrowhead the Sdc4 bands between 25 and 35 kDa of size. **(B,C)** NRK52E EGFP-TG2 clone #C5 cells were transiently transfected with 100 nM rat Sdc4/targeting siRNA or scrambled control siRNA in serum-free antibiotic-free medium for 48 h as described in 6.3.4. After incubation (B) knock down of Sdc4 at a protein level was measured on equal amounts of total cell lysate by Western blot using a rabbit polyclonal antibody against Sdc4 (ab24511, Abcam, dilution 1:500) (C) culture medium was collected and vesicular fraction separated by serial centrifugation as described in 5.3.3. Proteins and complexes from vesicles-deprived medium were precipitated by TCA and collected as well. Equal volumes of all fractions were separated by 12% (w/v) SDS PAGE and immunoprobed with a rabbit polyclonal anti-TG2 antibody (ab421, Abcam) and a rabbit polyclonal anti-GFP antibody (to detect the EGFP tag of EGFP-TG2 exogenous chimera), following the general method reported in 2.2.7. A representative blot is shown for each experiment.

6.5 DISCUSSION

Heparan sulfate proteoglycans (HSPGs) have recently been involved in cell surface protein trafficking including externalisation of unconventionally secreted proteins. The HS-dependent pathway of FGF2 release from cells is one of the most understood example (Zehe, et al. 2006, Nickel 2007). TG2 has also high affinity for HS and our group was the first to report and characterise the association of TG2 with HS and then try and dissect its biological significance (Scarpellini, et al. 2009, Verderio, Scarpellini and Johnson 2009, Verderio and Scarpellini 2010). One of the main observations was that primary dermal fibroblasts KO for syndecan-4 (Sdc4) had a higher level of intracellular TG2 and a lower level of cell surface TG2 compared to wild type cells raising the hypothesis that the HS chains of Sdc4 could regulate the trafficking of TG2 (Scarpellini, et al. 2009). *In vivo*, we know that KO of Sdc4 is protective on the development of tubulointerstitial fibrosis (Scarpellini, et al. 2014), however a mechanism for this was not elucidated, as no studies have ever been performed *in vitro* employing renal cells. Work presented in this thesis has revealed that TG2 is released from cells exposed to pro-fibrogenic TGF-β1 via extracellular vesicles, predominantly exosomes. We therefore asked whether Sdc4 was involved in the release of TG2 also in TEC, and hypothesised that Sdc4 could participate in the uptake of TG2 cargo in extracellular vesicles.

Evidence for the involvement of Sdc4 in TG2 export in kidney were gained in this thesis both *in vivo* and *in vitro*. *In vivo*, it was shown that Sdc4 is part of the TG2 plasma membrane interactome specifically in the UUO kidney (Chapter IV) and that TG2 and Sdc4 co-precipitate from kidney homogenates using an anti-TG2 antibody, with increased TG2 yield upon HS cleavage (this chapter) (**Fig. 6.7**).

In this chapter, it was shown that modulation of Sdc4 expression by cell transfection of Sdc4 cDNA in NRK52E cells regulates the level of cell surface TG2 activity consequent to TG2 release (**Fig. 6.8**). This was observed both in wild type NRK52E cells and in stable cell lines of NRK52E overexpressing a EGFP-tagged TG2. Knock out of Sdc4 in the same cell lines led to a significant reduction of TG2 secretion, when assessed with the same method (**Fig. 6.9**).

Proof that TG2 association with HS was required for secretion from cells was provided by evidence of lower cells surface TG2 in NRK52E cells treated with a HS antagonist (Surfen) (**Fig. 6.9**) and by employment of NRK52E expressing TG2 mutants lacking the previously described heparin binding site of TG2 (Lortat-Jacob, et al. 2012), compared to cells expressing the wild type form of TG2 (**Fig. 6.10**).

Whether the HS-TG2 interaction occurred at the cell surface as previously suggested, as cells treated with exogenous heparitinase (which selectively cleaves HS) displayed less surface TG2 (Scarpellini, et al. 2009), or also intracellularly still remains to be elucidated. However, in the current study, Sdc4 has been detected in exosomes purified from TECs, together with TG2, and KO of Sdc4 by siRNA led to a lower level of TG2 in the exosome fraction of TECs, suggesting a direct effect of Sdc4 on TG2 secretion via exosomes (**Fig. 6.15 – 6.16**).

Sdc4 has been recently ascribed the function of contributing to exosome biogenesis. Work from Baietti et al. (2012) have proposed a role for syndecans in the biogenesis of exosomes and cargo loading into exosomes, in complex with syntenin and alix, an auxiliary component of ESCRT known to be involved in ILV formation (Baietti, et al. 2012). It was demonstrated that syndecan, syntenin and alix co-localise in a large population of exosomes (marked by CD63 as a characteristic cargo) and that ligand-mediated syndecan oligomerisation plays a central role the induction of syntenin-alix mediated intraluminal budding of these exosomes, by binding syntenin on its PDZ domain. Upon ligand binding to syndecan HS chains on the endosome, syndecan clustering has been shown to stimulate the recruitment of syntenin-alix complexes and subsequently support the budding process. Syntenin links syndecan to alix by interacting with alix through its N-terminal domain and with syndecan through its PDZ domain. Consequently, the HSPG, together with its cargoes such as FGF2 and FGFR, is found located on syntenin and alix enriched exosomes (Baietti, et al. 2012, Friand, David and Zimmermann 2015).

In the light of this, the present study cannot distinguish whether Sdc4 affects the release of TG2 by interacting with the enzyme intracellularly, because of Sdc4 implication in exosome biogenesis and cargo selection, or exclusively outside the cell, being a strong previously characterised interacting partner of the enzyme on the cell surface and extracellular space.

Whether or not TG2 interacts with Sdc4 inside the cell, it is clear that the importance of HS extends to the localisation/distribution of TG2 outside the cell, since treatment of kidney cryosections with heparitinase, which selectively cleaves HS on the surface, consistently led to loss in extracellular TG2 in the AAN and SNx model (Burhan, et al. 2016, Scarpellini, et al. 2014).

As a key feature of CKD is a large release of TG2 in the extracellular matrix, we hypothesized that extracellular HS chain largely contribute to TG2 retention and distribution in the matrix. To confirm this, we developed an *in vitro* model simulating TG2 accumulation in the extracellular milieu of renal cells, by addition of exogenous recombinant TG2 on cell monolayers (**Fig. 6.6**). This model was employed to determine the contribution of HS chains in matrix retention of the recombinant enzyme, by performing antagonism of HS chain with Surfen (Schuksz, et al. 2008) or HS digestion by heparitinase (**Fig. 6.12 – 6.13**). As secreted

TG2 is likely to be "distributed" in extracellular space from TG2-rich secreting cells (TECs) to the adjacent matrix producing cells, such as the interstitial fibroblasts, and the long HS chains are likely to contribute to the distribution of the enzyme in the matrix between adjacent cells (Verderio, Scarpellini and Johnson 2009), both TECs, known to export large TG2 during fibrosis, and renal fibroblasts (NRK49F), known to be rich in cell surface HSPGs (Clayton, et al. 2001) and produce a large amount of extracellular matrix, were analysed.
HS were confirmed to be important for the retention of extracellular TG2 in the matrix, as their removal led to la large wash out of the exogenously added enzyme, and was particularly significant on kidney fibroblasts (**Fig. 6.12 – 6.13**).

Another relevant finding in this chapter is the evidence of increased TGF-β signalling (measured by downstream Smad3 phosphorylation) induced by extracellular TG2 specifically, when added exogenously to a NRK52 monolayer, and impairment of this process by HS antagonism with Surfen (**Fig. 6.14**). TGF-β is a central mediator of kidney fibrosis and TG2 has been suggested before to promote its activation by crosslinking the latent binding protein LTBP to the matrix (Nunes, et al. 1997, Burhan, et al. 2016). In a previous chapter of this thesis, TG2 was highlighted as a central mediator of TGF-β activation in kidneys subjected to UUO, as its KO was shown to impede cytokine activation upon disease (Chapter III). A previous published work from our group has shown that also Sdc4 KO results in a strong reduction in TGF-β1 activation and inhibition of TG2 accumulation in the matrix in experimental models of CKD, with a protective role against the progression of fibrosis (Scarpellini, et al. 2014).
Here, a cooperation between HSPGs and TG2 in the activation of TGF-β from renal TECs has been highlighted. The inhibition of TGF-β activation upon HS antagonism observed in these study (**Fig.6.14**) led us to the hypothesis that HS regulates TGF-β activity by affecting the matrix deposition of TG2. Moreover, previous studies have suggested that HS chains could promote LTBP deposition in the matrix and its binding to FN (Chen, et al. 2007). Altogether, these findings led us to elucidate an interplay between TG2 and HSPGs in the activation of TGF-β, as summarized in **Fig. 6.17**. In this model, HS chains contribute to TGF-β activation recruiting both TG2 and LTBP to the ECM in association with FN. Here, TG2, which also is a binding partner for FN, promotes TGF-β activation by catalysing the incorporation of LTBP in the ECM. Moreover, TG2 promotes matrix remodelling by crosslinking FN, conferring mechanical resistance to the matrix. Large LTBP crosslinking to the matrix and matrix stiffening, on a side, and LAP binding to cell surface integrin, on the other, are thought to be sufficient to produce mechanical tension necessary for TGF-β activation. In summary, these findings suggest that controlling matrix localisation of TG2 by HS regulation has ultimately an impact not only on the extracellular TG2 enzymatic activity but also on the activation of latent TGF-β. This is particularly crucial in conditions of fibrosis, when large TG2 is secreted at the site of injury and

retained by HS chains and FN in close proximity to the secreted large latent TGFβ complex, whose secretion is also upregulated upon CKD and its localisation in the matrix also controlled by HS chains trough LTBP binding.

Lastly, access to clones of human TECs stably expressing SULF endosulfatases and HS6ST sulftransferases led us to initial data on the role of HS sulfation on TG2 availability outside the cells. It is possible that removal of 6-O-sulfated glucosamine residues leads to a lower level of TG2 release and consequent detection on the cell surface (**Fig. 6.11**). Vice versa, an increase in of 6-O-sulfation leads to a reduction in intracellular TG2 but this is not linked to a detectable incraese in TG2 on the cell surface (**Fig. 6.11**), as expected by the reasoning that 6-O-sulfation affects the degree of TG2 association with HS chains.

In conclusion, results from this Chapter suggest that HSPG Sdc4 has at least two roles in the promotion of kidney fibrosis: on a side, it contributes to TG2 export by TECs, which is likely to happen by exosome release (Chapter V), and on the other, it controls TG2 retention and deposition in the matrix in proximity to the latent TGF-β complex, contributing to the cytokine activation by TG2. Despite the importance of HS/Sdc4 for TG2 secretion by TECs has been confirmed in this study, the exact mechanism by which Sdc4 contributes to the enzyme release into exosomes has still to be elucidated, to understand whether TG2-HS binding happens inside the cell and determines TG2 loading in the exosomes during their biogenesis, or exclusively outside the cell by a so-called “trapping mechanism”. In either case, HS binding of TG2 still remains an interesting clinical target against the development of disease, as its inhibition reduces TG2 accumulation in the tubulointerstitium as well as strongly inhibiting TG2-mediated activation of the pro-fibrotic cytokine TGF-β.

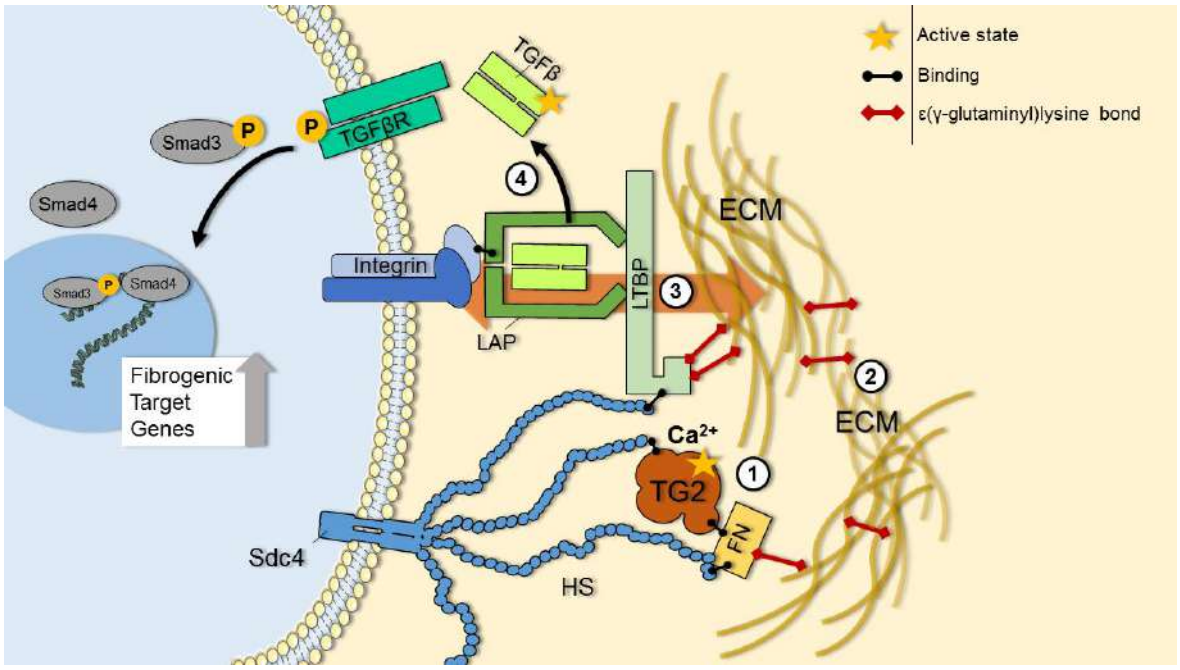

Figure 6.17: **Interplay of TG2 and HS in the mechanical activation of latent TGF-β.** TG2 is released from cells in the progression of kidney fibrosis and cell surface HS are critical for its extracellular recruitment. By calcium-dependent transamidation, extracellular TG2 increases the general degree of crosslinking of the ECM (1), produces a remodelled and stiffened matrix typical of the fibrotic condition (2) and incorporates LTBP in the ECM, storing large latent TGF-β (3). These events are a pre-requisite for the mechanical release (depicted by the background orange arrow) of soluble TGF-β dimer from large latent TGF-β complex, occurring via LAP- integrin binding on the cell side, and LTBP binding to a sufficiently remodelled ECM on the extracellular side. Under these conditions, cell contraction will result into TGF-β release, and consequently engagement with its receptor (4). HS have been reported to mediate LTBP association with the matrix. We have given new evidence that antagonism of HS lowers the recruitment and retention of TG2 to the matrix and greatly reduces activation of TGF-β by extracellular TG2.

Chapter VII: Final discussion

Transglutaminase 2 (TG2) is a multifunctional enzyme with many pathological roles in human. Its transamidating activity is strictly controlled by the low Ca^{2+}/GTP ratio inside the cell in physiological conditions; conversely, it is induced in pathological conditions when sufficient Ca^{2+} enters the cells. Therefore, as TG2 is only activated in disease, inhibition of TG2 is anticipated not to have an adverse effect in normal cells, making the enzyme an attractive target for therapy in a number of pathological conditions.

TG2 is a ubiquitous protein found in the cytosol, in mitochondria and in the nucleus, but it is also released in the extracellular environment as a leaderless unconventionally secreted protein, where the high Ca^{2+} concentration activates the protein's transamidation activity; however, TG2 has also been ascribed non-enzymatic roles in the extracellular space, binding FN, integrins and cell surface HSPGs and acting as a scaffold protein. In the extracellular environment, all these functions of TG2 concur to induce wound repair and scar formation. Examples of diseases due to TG2 malfunction are those arising from fibrosis progression and evasion of proliferation control. TG2 has been implicated in lung, liver, heart and kidney fibrosis (Verderio, et al. 2015, Small, et al. 1999, Mirza, et al. 1997, Zhao, et al. 2011, Griffin, Smith and Wynne 1979, Olsen, et al. 2011) and atherosclerosis (Williams, et al. 2010, Haroon, et al. 2001, Bakker, Pistea and VanBavel 2008).

Fibrosis can be regarded as a process of uncontrolled wound healing, determined by a chronic insult and inflammation and TG2 contributes to fibrosis in three ways: by increasing matrix deposition and stabilisation, which counteract matrix degradation, promoting the activation of TGF-β through matrix recruitment of the latent TGF-β complex, and favouring cell adhesion upon matrix degradation and tissue damage, with effects on both fibroblast proliferation and inflammatory cells recruitment.

As the carcinogenic process can be regarded as an uncontrolled wound healing process, and chronic tissue injury and inflammation are an important risk factor in the progression of malignant tumours, wound healing and malignant cancer have been suggested to have strong similarities, including matrix remodelling, cell adhesion and angiogenesis. Therefore, dissecting the pathway of TG2 export, which was the purpose of this thesis, is not only relevant to CKD but also to fibrosis at large and even cancer treatment.

Chronic kidney disease (CKD) is a pathology characterised by loss of kidney function over time, whose main feature is a progressive fibrosis of the organ, leading to kidney failure at its end stage (ESKF). The incidence of CKD is on the increase as it is linked with ageing and other conditions such as diabetes, obesity and cardiovascular diseases. Currently there is no cure for

CKD, and replacement therapy or dialysis are the only treatments currently available for ESKF patients. Moreover, risk of cardiovascular disease and death by heart failure increases with the progression of CKD, due to hypertension and arteriosclerosis as well as impaired renal filtration of uremic toxins (Herzog, et al. 2011, Sarnak, et al. 2003, Vanholder, et al. 2003, Lisowska-Myjak 2014, Moradi, Sica and Kalantar-Zadeh 2013). Beside dialysis and transplant for end stage patients, the only treatments employed at the moment are aimed to counteract CKD effects and associated syndromes, such as the control of blood pressure, anaemia and mineral bone disorder (MBD) (Yamaguchi, Tanaka and Inagi 2016, Pergola, et al. 2016, Basile, Brandenburg and Torres 2016, Carson, et al. 2009).

In this study, the fibrotic model of CKD was used as a platform to study the mechanism of TG2 externalisation to the extracellular matrix (ECM) as it precedes and determines the pro fibrogenic role of TG2. It is well established that TG2 accumulates in the tubular interstitium and glomerular matrix in several experimental models of CKD and in patients during the progression of CKD [reviewed in Chapter I and (Verderio, et al. 2015)], however, the specific mechanism of TG2 release from kidney cells is still largely unknown.
Pan inhibitors of TG convincingly reduce renal fibrosis, and in the current study (Chapter III) we have demonstrated that TG2-KO is protective in the unilateral ureteric obstruction (UUO) experimental model mimicking the late stages of CKD, with advanced tubulointerstitial fibrosis, confirming and extending the finding that TG2-KO is protective at earlier stages (Shweke, et al. 2008). Given the clear direct association of extracellular TG2 to the fibrotic process and the protective role of TG2 inhibition, TG2 can be regarded as a potential target against the progression of CKD. However, the creation of a specific TG2 inhibitor of TG2 extracellular activity is made difficult by the presence of a highly conserved catalytic core within TG family members and between TGs and a number of cysteine proteases. For example, defects in TG1 activity have been shown to determine an autosomal recessive skin disorder characterised by abnormal cornification, known as *lamellar ichthyosis* (Matsuki, et al. 1998, Huber, et al. 1995, Candi, et al. 1998), while Factor XIII-null animals have impaired coagulation and uncontrolled bleeding (Koseki-Kuno, et al. 2003).

Aware of this problem and knowing the potential uniqueness of TG2 secretion pathway, in this thesis, we suggested to interfere with the release of TG2 from kidney cells, rather than with the extracellular activity of TG2, as a way to control the pro-fibrotic role TG2 in fibrosis development. Therefore we believe that elucidation of the mechanism of TG2 unconventional secretion by tubular epithelial cells is key to control the enzyme's pathological role.
We anticipated that unbiased analysis of all TG2-interacting proteins at the cell-matrix interface in kidneys subjected to experimental CKD (the UUO model) would highlight key

partners in the enzyme's secretion. To achieve this, we proposed a novel experimental approach combining TG2 immunoprecipitation from whole kidney membrane preparations of WT kidneys with negative control immunoprecipitation from TG2-null kidneys from inbred mice (Chapter IV). TG2 associated proteins were identified with high resolution quantitative SWATH-MS acquisition. The proposed strategy could be adapted for precision targeted proteomics for the analysis of other systems.

The proteome of the UUO kidney was fully defined at the start of the project, prior to the production of the TG2 interactome. This showed upregulation of established and potentially new markers of kidney fibrosis, including a significant increase in TG2, matrix proteins and known markers of fibroblast proliferation/myofibroblast activation (Chapter III). The TG2-precipitated proteins from the UUO kidney have been identified and used to interrogate the UUO proteome.

A set of vesicular proteins potentially involved in TG2 export from kidney cells clearly emerged, and among them a striking number were exosome-associated proteins (Chapter IV). The TG2 partners involved with trafficking and exocytosis were not increased post-UUO, generating the hypothesis of their specific role in trafficking of TG2. On the contrary, a group of proteins involved in ECM-receptor organisation, a pathway that we report to be significantly overexpressed in the UUO kidneys, were also all partners of TG2. This finding is consistent with the existence of a pathway of TG2 secretion during fibrosis progression driven by vesicular trafficking specific for TG2, and its subsequent association with a protein network responsible for ECM dynamics leading to matrix accumulation.

To validate the idea of a vesicular secretion mechanism of TG2, we relied on tubular epithelial cells (TECs), known to produce and secrete the largest quota of TG2 during fibrosis (Chapter V – VI). Isolation and analysis of TG2 in extracellular vesicles revealed enrichment of TG2 mainly in vesicle of intraluminal origin (exosomes), which increases in the presence of TGF-β, therefore in situations of fibrosis (Chapter V). Evidence is presented which suggest that TG2 is located on the surface of these vesicles. Although not demonstrated in this thesis, it is possible that vesicular TG2 could contribute to the adherence of vesicles to the ECM once secreted. A portion of TG2 was also identified in larger vesicles shedded from the plasma membrane (ectosomes), which however were less enriched in TG2. Altogether, the results obtained allowed to suggest a possible secretion mechanism of TG2 from kidney cells during the progression of fibrosis, which is represented in **Figure 7.1**.

The role of EVs in kidney is only beginning to be understood (Zhang, et al. 2016). As in other systems, EVs could contribute to intercellular communication and disease spreading in physiopathological conditions and could transfer their content including TG2 to distant cells even from organ to organ.

Another main finding in this study is the specific association of TG2 with Sdc4 in the UUO kidney and not in the healthy kidney, which confirms the notion that Sdc4 cooperates with TG2 in fibrosis development (Burhan, et al. 2016, Scarpellini, et al. 2014). Here we have shown that Sdc4 is critical in TG2 extracellular trafficking by vesicles, as less TG2 is found in the EVs when Sdc4 is knocked down (Chapter VI).

It is fascinating to hypothesize an intracellular interaction between TG2 and Sdc4-HS inside the cells, that would contribute to the enzyme loading into intraluminal vesicles for secretion (**Figure 7.1**). As syndecans have been recently proposed to play a role in the exosome biogenesis and cargo loading (Roucourt, et al. 2015, Baietti, et al. 2012, Friand, David and Zimmermann 2015), it is tempting to speculate that TG2 and HS chains would interact, if present in the same vesicle.

Although we currently do not know if TG2 interacts with Sdc4/HS inside the cell, it is well established that the interaction of TG2 with HSPG/Sdc4 occurs at the cell surface/ECM, and that it is crucial for TG2 deposition *in vivo* (Burhan, et al. 2016, Scarpellini, et al. 2014) and *in vitro* (Chapter VI). Here, in TECs, requirement of TG2 interaction with HS chains for both TG2 extracellular secretion and matrix retention has been confirmed (Chapter VI), and a cooperative role for HS chains and extracellular TG2 in TGF-β activation in the ECM proposed, with some of these data recently published in Scientific Reports (Burhan, et al. 2016).

As we showed that TG2 is likely to be located on the surface of secreted exosomes, Sdc4 and other HSPGs present in the matrix (such as perlecan, another HSPG identified in the TG2 interactome post-UUO), could contribute to the retention of TG2-containing vesicles in the area via TG2-HS interaction. Therefore TG2 could promote adhesion and matrix crosslinking in this way (**Fig. 7.1**). TG2 is a known adhesive protein, but to our knowledge an adhesive role of vesicular TG2 has never been proposed. This is in line with recent thinking ascribing to EV the property of releasing ECM proteins like FN and essentially be conducive of cell adhesion and migration (Sung, et al. 2015).

In terms of "TG2 treatment" one could envisage that blocking the TG2-HS interaction by means of small inhibitors or monoclonal antibodies could lower TG2 release and accumulation in the matrix. Block of TG2 inside the cell would not lead in principle to negative effects being the enzyme mostly silent intracellularly.

TG2 is not the only matrix remodelling enzyme: lysyl oxidase proteins (LOX) and lysyl oxidase – like proteins (LOXL), which function as an extracellular amine oxidase in a copper dependent way leading to deamination of the epsilon amino group of a peptide bound lysine residue of collagen and monomers of elastin. The role of LOX in renal fibrosis is less studied (Di Donato, et al. 1997, Grau-Bove, Ruiz-Trillo and Rodriguez-Pascual 2015, Goto, et al. 2005, Yang, et al. 2010), however according to Mehal et al., LOXL2 has been suggested as a central element of

every fibrosis model, belonging to a "core pathway" of fibrosis (Mehal, Iredale and Friedman 2011). The finding that bot h LOXL2 and TG2 are overexpressed in idiopathic pulmonary fibrosis (Chien, et al. 2014, Olsen, et al. 2011) suggests that the two enzymes could co-participate to the deposition of matrix. On the other hand, it cannot be ruled out that one class of proteins could compete for the same residues.

Future work from our group will focus on the elucidation of the role of HS/Sdc4 interaction intracellularly, to understand at which stage of the TG2 secretory pathway the proteoglycan is involved. This will allow us to implement the suggested pathway of TG2 secretion and advise possible targeting strategies for the inhibition of TG2 secretion.

At the same time, a number of other proteins identified in the TG2 interactome as significantly associated to the enzyme upon disease might be investigated, with particular interest to the proteins associating to the enzyme in other compartments, such as the cytosol, the nuclear and the mitochondrial compartment, to understand their possible contribution to the large number of cellular responses happening during CKD.

The consistent identification of a TG2 association to the cytoskeletal proteins is another fascinating field of study, that might reveal additional roles for TG2 in controlling cellular responses upon disease. For example, mechanical tension produced by cytoskeletal remodelling has been shown to contribute to TGF-β activation (Giacomini, et al. 2012, Wipff and Hinz 2008, Hinz 2009, Wells and Discher 2008). If TG2 in the cortical cytoskeleton determines contraction of kidney cells, that might happen by localised calcium influx and TG2-mediated crosslinking, a dual role for the enzyme in the activation of TGF-β may be envisaged, both outside and inside the cell, where it could be transiently activated by the loss of calcium homeostasis.

Finally, having produced a the UUO proteome and highlighted a number of proteins substantially upregulated in conditions of disease, it would be useful to validate some of the novel ones as potential biomarkers of disease.

Having shown that TG2 is implicated in the development of fibrosis in the UUO model, and proposed the way TG2 might be secreted from tubular epithelial cells, which is critical to TG2-mediated matrix crosslinking leading to fibrosis, it would be of interest as a future work to confirm these findings in patients' biopsies with a view of establishing anti TG2 therapies. Work from the group of Tim Johnson (Sheffield Kidney Institute) has shown that TG2 is upregulated in patients biopsies with CKD of different aetiologies (Johnson, et al. 2003), and that increased TG2 and TG2 crosslinks can be identified in urine and may be diagnostic of fibrosis (da Silva Lodge, El Nahas and Johnson 2013, Shrestha, et al. 2014). It is anticipated that refinement of the methodology to detect TG2 and its products [current methods cannot be routinely used in clinics as not quantitative and reproducible (TS Johnson, personal

communication)] might facilitate TG2 investigation *in vivo* in clinical samples, establishing a link between the abnormal activity of TG2 and disease, thus setting the basis for TG2-targeted treatment in fibrosis.

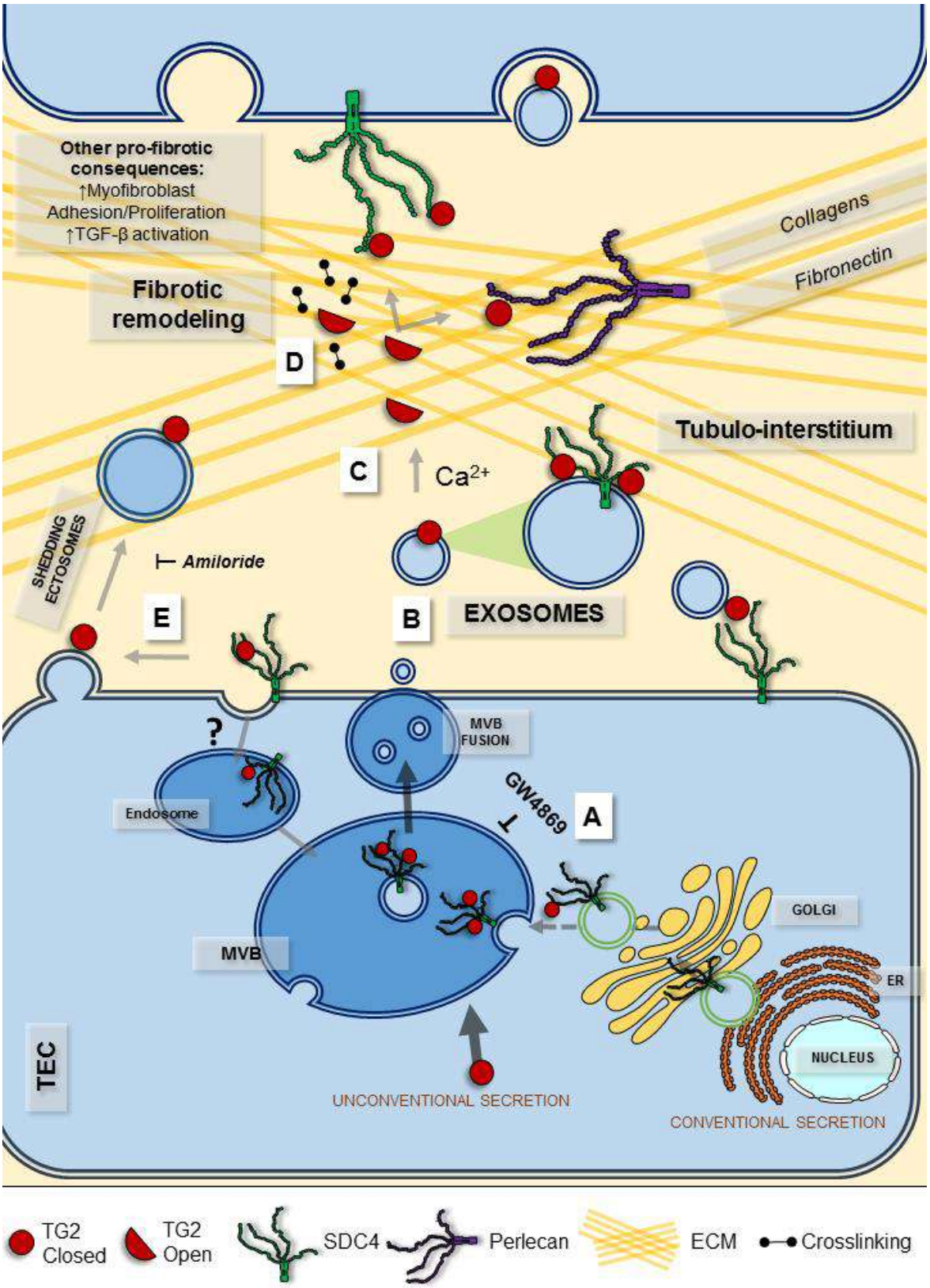

Figure 7.1: A proposed pathway for TG2 unconventional secretion and extracellular localisation by TECs. TG2 is secreted unconventionally by exosomes originating from late endosomes as multivesicular endosomes (MVB) which then fuse with the plasma membrane releasing the intraluminal vesicles (ILV) outside the cells (exosomes). **(A)** The biogenesis of TG2-bearing exosomes is mediated by ceramide, as the inhibitor of n-SMase GW4869 significantly reduces the presence of TG2 in the exosome fraction in the extracellular space (**Fig. 5.8**). TG2, which has high affinity for HS, is loaded on the surface of the ILV as a HS/SDC4 cargo, and exposed on the surface of the formed exosome. **(B)** Following fusion of the outer membrane of MVB with the plasma membrane, the TG2-bearing exosomes likely accumulate in the ECM by TG2 binding to ECM/cell surface protein partners in an "autocrine" or "paracrine" fashion. **(C)** Once released with exosomes, TG2 could also undergo a conformational change due to the high Ca^{2+}/GTP ratio of the extracellular space, with a lowering or even loss HS affinity; the free TG2 could bind the HS of other proteoglycans or other ECM partners. If this theory will be confirmed, it might explain both TG2 secretion and increased extracellular TG2 accumulation by TECs upon CKD, connecting the mechanism of export with the crucial TG2 role in matrix crosslinking as well as with its involvement in the increased cell adhesion. **(D)** In the matrix TG2 acts as an adhesive protein and matrix crosslinker promoting fibres accumulation and latent TGF-β recruitment. In the matrix, TG2 and HS/Sdc4 cooperate in the activation of TGF-β, as shown in **Fig. 6.17**. **(E)** TG2 is also present in ectosomes. It is possible that TG2 once secreted via exosomes, it is captured by the PM and retained on ectosomes shed by the PM.

THE INTERACTOME OF TRANSGLUTAMINASE 2 IN KIDNEY FIBROSIS

Uncovering a mechanism for TG2 unconventional secretion in chronic kidney disease

Giulia Furini

SUPPLEMENTARY DATA

~

APPENDIX

A thesis submitted in partial fulfilment of the
requirements of Nottingham Trent University
for the degree of Doctor of Philosophy

February 2017

Supplementary data

S.1 SUPPLEMENTARY DATA OF CHAPTER III

S.1.1 Fold Change analysis of SWATH-MS protein expression data

S.1.1.1 Fold change analysis of WT UUO vs WT Sham operated

Supplementary Table 3.1: Outcome of the fold change (FC) analysis between WT UUO mice (21 days) and WT Sham operated mice (21 days) [C(FC) ≥ 0.5].

	Protein ID	log2(FC)	Abs(FC)	C(FC)	p-value (FC)
1	sp|Q80YX1|TENA_MOUSE	6.31	79.49	0.71	4.6E-04
2	sp|P68373|TBA1C_MOUSE	6.24	75.77	0.64	2.1E-01
3	sp|Q60590|A1AG1_MOUSE	6.19	73.04	0.71	5.7E-01
4	sp|Q9R233|TPSN_MOUSE	5.19	36.41	0.76	7.4E-04
5	sp|Q07235|GDN_MOUSE	4.68	25.69	0.64	2.5E-02
6	sp|Q08619|IFI5B_MOUSE	4.25	19.08	0.60	1.7E-06
7	sp|Q9ET54|PALLD_MOUSE	4.07	16.84	0.57	8.7E-01
8	sp|Q91X17|UROM_MOUSE	4.03	16.34	0.85	3.4E-03
9	sp|Q60847|COCA1_MOUSE	3.99	15.92	0.82	9.5E-04
10	sp|Q05144|RAC2_MOUSE	3.96	15.51	0.63	7.6E-05
11	sp|Q9WVJ9|FBLN4_MOUSE	3.89	14.84	0.74	2.8E-05
12	sp|O88207|CO5A1_MOUSE	3.74	13.34	0.78	2.8E-05
13	sp|Q64449|MRC2_MOUSE	3.73	13.22	0.78	9.4E-01
14	sp|P29416|HEXA_MOUSE	3.51	11.41	0.70	1.7E-01
15	sp|Q61554|FBN1_MOUSE	3.44	10.84	0.89	4.4E-04
16	sp|Q9CZH7|MXRA7_MOUSE	3.43	10.77	0.51	1.8E-02
17	sp|P20491|FCERG_MOUSE	3.39	10.47	0.61	8.3E-01
18	sp|A6X935|ITIH4_MOUSE	3.33	10.03	0.51	2.4E-02
19	sp|P37889|FBLN2_MOUSE	3.27	9.65	0.81	3.3E-03
20	sp|P19001|K1C19_MOUSE	3.26	9.57	0.86	1.2E-03
21	sp|Q8K1B8|URP2_MOUSE	3.25	9.50	0.71	1.2E-02
22	sp|P11672|NGAL_MOUSE	3.24	9.42	0.78	2.8E-05
23	sp|P14106|C1QB_MOUSE	3.24	9.42	0.70	8.2E-07
24	sp|P37804|TAGL_MOUSE	3.21	9.27	0.89	2.7E-04
25	sp|P14483|HB2A_MOUSE	3.21	9.26	0.69	2.2E-04
26	sp|P49710|HCLS1_MOUSE	3.14	8.84	0.69	1.2E-02
27	sp|P28653|PGS1_MOUSE	3.13	8.73	0.86	1.6E-04
28	sp|Q08091|CNN1_MOUSE	3.10	8.59	0.80	6.2E-03
29	sp|P20152|VIME_MOUSE	3.10	8.56	0.90	5.4E-05
30	sp|Q01149|CO1A2_MOUSE	3.09	8.54	0.79	2.2E-03
31	sp|P02802|MT1_MOUSE	3.08	8.45	0.61	9.0E-02
32	sp|P14438|HA2U_MOUSE	3.06	8.32	0.80	1.9E-02
33	sp|P10107|ANXA1_MOUSE	3.03	8.17	0.84	2.4E-04
34	sp|Q8C4U3|SFRP1_MOUSE	3.03	8.17	0.57	1.3E-01
35	sp|P02798|MT2_MOUSE	3.02	8.11	0.84	3.9E-05
36	sp|Q62009|POSTN_MOUSE	3.01	8.04	0.80	5.9E-03
37	sp|P06800|PTPRC_MOUSE	2.99	7.95	0.78	3.3E-05
38	sp|P82198|BGH3_MOUSE	2.99	7.94	0.71	9.4E-04
39	sp|P22599|A1AT2_MOUSE	2.97	7.86	0.82	2.8E-04
40	sp|P11276|FINC_MOUSE	2.97	7.85	0.84	7.7E-03
41	sp|Q640N1|AEBP1_MOUSE	2.97	7.82	0.62	6.1E-01
42	sp|O89053|COR1A_MOUSE	2.96	7.77	0.80	1.3E-04
43	sp|P08121|CO3A1_MOUSE	2.95	7.72	0.92	1.0E-03
44	sp|Q9CYG7|TOM34_MOUSE	2.94	7.67	0.58	3.5E-04
45	sp|Q61233|PLSL_MOUSE	2.93	7.63	0.85	7.6E-05
46	sp|Q9JLI6|SCLY_MOUSE	2.93	7.61	0.53	4.1E-03
47	sp|P11087|CO1A1_MOUSE	2.93	7.61	0.96	9.4E-04
48	sp|Q04447|KCRB_MOUSE	2.92	7.56	0.83	2.7E-05
49	sp|Q71FD7|FBLI1_MOUSE	2.90	7.44	0.53	3.9E-05
50	sp|Q60710|SAMH1_MOUSE	2.89	7.41	0.74	1.3E-02
51	sp|Q9D8T7|SLIRP_MOUSE	2.89	7.39	0.56	7.6E-01

52	sp|Q61555|FBN2_MOUSE	2.86	7.26	0.94	6.9E-03
53	sp|P97290|IC1_MOUSE	2.78	6.88	0.68	1.9E-02
54	sp|Q62148|AL1A2_MOUSE	2.78	6.85	0.78	2.9E-03
55	sp|Q61781|K1C14_MOUSE	2.75	6.75	0.75	7.9E-03
56	sp|Q8VCC9|SPON1_MOUSE	2.75	6.74	0.63	6.9E-05
57	sp|Q62000|MIME_MOUSE	2.74	6.67	0.83	2.4E-03
58	sp|Q62266|SPR1A_MOUSE	2.74	6.67	0.78	8.8E-03
59	sp|Q8BH97|RCN3_MOUSE	2.73	6.65	0.74	7.1E-05
60	sp|O70456|1433S_MOUSE	2.72	6.59	0.75	4.2E-06
61	sp|Q8BMK4|CKAP4_MOUSE	2.72	6.57	0.85	4.9E-02
62	sp|P51885|LUM_MOUSE	2.71	6.55	0.87	1.8E-03
63	sp|P28654|PGS2_MOUSE	2.70	6.52	0.79	1.4E-03
64	sp|O70318|E41L2_MOUSE	2.70	6.51	0.77	4.4E-06
65	sp|Q9CX80|CYGB_MOUSE	2.67	6.36	0.67	2.2E-02
66	sp|Q8BPB5|FBLN3_MOUSE	2.66	6.33	0.80	8.3E-05
67	sp|P35441|TSP1_MOUSE	2.64	6.23	0.79	7.0E-01
68	sp|Q05186|RCN1_MOUSE	2.64	6.21	0.53	3.5E-03
69	sp|P19324|SERPH_MOUSE	2.63	6.19	0.94	1.6E-04
70	sp|Q08879|FBLN1_MOUSE	2.62	6.16	0.79	5.1E-04
71	sp|Q8VCI0|PLBL1_MOUSE	2.62	6.15	0.58	1.3E-05
72	sp|Q9Z247|FKBP9_MOUSE	2.62	6.15	0.53	5.9E-01
73	sp|Q08093|CNN2_MOUSE	2.62	6.15	0.80	6.5E-04
74	sp|P16045|LEG1_MOUSE	2.62	6.15	0.87	1.2E-04
75	sp|P21956|MFGM_MOUSE	2.61	6.12	0.54	1.2E-01
76	sp|O70400|PDLI1_MOUSE	2.61	6.10	0.76	3.6E-02
77	sp|P01631|KV2A7_MOUSE	2.60	6.05	0.71	6.6E-01
78	sp|P10923|OSTP_MOUSE	2.59	6.03	0.78	1.7E-01
79	sp|P31001|DESM_MOUSE	2.58	5.98	0.94	1.6E-03
80	sp|Q9D1H9|MFAP4_MOUSE	2.54	5.82	0.77	5.9E-04
81	sp|Q9WVH9|FBLN5_MOUSE	2.54	5.81	0.84	3.8E-04
82	sp|Q07797|LG3BP_MOUSE	2.53	5.78	0.67	6.1E-04
83	sp|Q9R111|GUAD_MOUSE	2.53	5.77	0.54	2.3E-03
84	sp|Q9CYL5|GAPR1_MOUSE	2.52	5.72	0.64	2.2E-03
85	sp|P25911|LYN_MOUSE	2.51	5.70	0.71	7.0E-01
86	sp|Q61576|FKB10_MOUSE	2.48	5.58	0.50	1.0E-02
87	sp|Q00915|RET1_MOUSE	2.48	5.56	0.83	3.6E-04
88	sp|P45377|ALD2_MOUSE	2.46	5.52	0.56	3.7E-06
89	sp|Q3TJD7|PDLI7_MOUSE	2.43	5.40	0.81	2.6E-05
90	sp|P84084|ARF5_MOUSE	2.43	5.37	0.53	9.6E-01
91	sp|Q06890|CLUS_MOUSE	2.42	5.35	0.81	2.0E-03
92	sp|P19973|LSP1_MOUSE	2.39	5.26	0.67	4.3E-04
93	sp|Q922U2|K2C5_MOUSE	2.39	5.24	0.83	2.4E-03
94	sp|O70200|AIF1_MOUSE	2.38	5.22	0.68	1.3E-03
95	sp|Q9CQW9|IFM3_MOUSE	2.37	5.17	0.57	3.0E-02
96	sp|Q03350|TSP2_MOUSE	2.37	5.16	0.53	8.6E-01
97	sp|Q9JIF0|ANM1_MOUSE	2.35	5.11	0.57	3.5E-01
98	sp|Q8BTM8|FLNA_MOUSE	2.34	5.07	0.93	1.7E-05
99	sp|Q922F4|TBB6_MOUSE	2.33	5.04	0.53	7.3E-02
100	sp|Q3U962|CO5A2_MOUSE	2.33	5.01	0.67	5.7E-03
101	sp|Q91YJ2|SNX4_MOUSE	2.32	5.01	0.65	3.5E-02
102	sp|Q69ZN7|MYOF_MOUSE	2.32	4.99	0.86	1.9E-05
103	sp|P97821|CATC_MOUSE	2.31	4.94	0.55	4.2E-03
104	sp|Q9Z0N1|IF2G_MOUSE	2.30	4.94	0.62	6.0E-01
105	sp|P11679|K2C8_MOUSE	2.30	4.93	0.89	5.5E-05
106	sp|P01901|HA1B_MOUSE	2.26	4.78	0.64	8.9E-04
107	sp|Q04857|CO6A1_MOUSE	2.26	4.78	0.88	4.7E-03
108	sp|Q02788|CO6A2_MOUSE	2.25	4.76	0.94	2.1E-03
109	sp|O35639|ANXA3_MOUSE	2.24	4.73	0.83	5.7E-05
110	sp|P11835|ITB2_MOUSE	2.22	4.67	0.54	1.0E+00
111	sp|Q8R1G6|PDLI2_MOUSE	2.22	4.67	0.55	1.1E-01
112	sp|E9PV24|FIBA_MOUSE	2.21	4.64	0.90	4.9E-02
113	sp|Q80X19|COEA1_MOUSE	2.21	4.62	0.81	3.4E-04
114	sp|Q91X72|HEMO_MOUSE	2.20	4.60	0.86	2.4E-02
115	sp|O35114|SCRB2_MOUSE	2.18	4.52	0.50	2.3E-01
116	sp|P97315|CSRP1_MOUSE	2.18	4.52	0.89	4.7E-05
117	sp|Q62188|DPYL3_MOUSE	2.18	4.52	0.67	2.5E-02
118	sp|P08122|CO4A2_MOUSE	2.17	4.50	0.80	1.3E-04
119	sp|Q8VCM7|FIBG_MOUSE	2.15	4.45	0.85	1.2E-01
120	sp|Q99K41|EMIL1_MOUSE	2.15	4.42	0.82	7.8E-05
121	sp|P68369|TBA1A_MOUSE	2.14	4.41	0.96	3.8E-04
122	sp|Q9R0P9|UCHL1_MOUSE	2.14	4.40	0.54	2.6E-02
123	sp|Q9JK53|PRELP_MOUSE	2.13	4.38	0.79	5.6E-04
124	sp|Q9WV54|ASAH1_MOUSE	2.12	4.36	0.79	5.0E-02

125	sp|P06909|CFAH_MOUSE	2.12	4.35	0.72	4.5E-02
126	sp|P20065|TYB4_MOUSE	2.12	4.35	0.88	3.5E-07
127	sp|P29788|VTNC_MOUSE	2.12	4.34	0.71	1.8E-02
128	sp|P58771|TPM1_MOUSE	2.10	4.28	0.84	4.2E-02
129	sp|Q9DCV7|K2C7_MOUSE	2.09	4.27	0.88	3.4E-05
130	sp|Q9QXS1|PLEC_MOUSE	2.09	4.25	0.73	3.6E-02
131	sp|P04441|HG2A_MOUSE	2.09	4.25	0.58	1.4E-01
132	sp|P97298|PEDF_MOUSE	2.09	4.24	0.81	1.2E-03
133	sp|Q7TPR4|ACTN1_MOUSE	2.08	4.22	0.96	8.2E-07
134	sp|Q9QZZ6|DERM_MOUSE	2.07	4.20	0.77	1.1E-03
135	sp|Q6IRU2|TPM4_MOUSE	2.07	4.19	0.91	2.2E-03
136	sp|P01837|IGKC_MOUSE	2.05	4.15	0.87	3.7E-02
137	sp|Q00898|A1AT5_MOUSE	2.04	4.10	0.65	1.2E-01
138	sp|Q8K0E8|FIBB_MOUSE	2.00	4.00	0.86	3.6E-02
139	sp|O35682|MYADM_MOUSE	2.00	4.00	0.87	3.5E-02
140	sp|Q9EP71|RAI14_MOUSE	1.98	3.95	0.70	9.9E-02
141	sp|P49300|CLC10_MOUSE	1.96	3.90	0.56	1.5E-01
142	sp|Q8C3W1|CA198_MOUSE	1.96	3.90	0.78	2.9E-05
143	sp|P01899|HA11_MOUSE	1.96	3.88	0.79	7.9E-03
144	sp|Q91VW3|SH3L3_MOUSE	1.94	3.85	0.90	3.4E-03
145	sp|O08573|LEG9_MOUSE	1.92	3.79	0.61	6.0E-04
146	sp|P70460|VASP_MOUSE	1.92	3.79	0.54	9.7E-01
147	sp|Q921I1|TRFE_MOUSE	1.92	3.78	0.91	1.4E-03
148	sp|P07356|ANXA2_MOUSE	1.91	3.76	0.90	6.9E-07
149	sp|P16110|LEG3_MOUSE	1.90	3.73	0.73	2.0E-05
150	sp|Q8CFX1|G6PE_MOUSE	1.89	3.71	0.90	3.2E-07
151	sp|P16015|CAH3_MOUSE	1.88	3.69	0.60	4.4E-01
152	sp|O35887|CALU_MOUSE	1.88	3.69	0.84	1.7E-04
153	sp|P54320|ELN_MOUSE	1.88	3.69	0.61	7.8E-04
154	sp|P42225|STAT1_MOUSE	1.88	3.68	0.54	3.2E-02
155	sp|P55002|MFAP2_MOUSE	1.87	3.65	0.58	1.0E-03
156	sp|Q61599|GDIR2_MOUSE	1.86	3.64	0.73	3.6E-03
157	sp|Q99P72|RTN4_MOUSE	1.85	3.59	0.72	5.5E-05
158	sp|P26645|MARCS_MOUSE	1.84	3.59	0.73	5.8E-02
159	sp|Q8CI51|PDLI5_MOUSE	1.84	3.58	0.70	1.7E-04
160	sp|Q9JII5|DAZP1_MOUSE	1.84	3.57	0.50	6.1E-01
161	sp|Q60854|SPB6_MOUSE	1.83	3.56	0.89	4.5E-03
162	sp|P63254|CRIP1_MOUSE	1.83	3.55	0.90	2.0E-05
163	sp|P29391|FRIL1_MOUSE	1.82	3.54	0.64	2.4E-02
164	sp|Q9D8Y0|EFHD2_MOUSE	1.82	3.52	0.87	5.7E-05
165	sp|P20918|PLMN_MOUSE	1.82	3.52	0.73	1.7E-03
166	sp|Q3U7R1|ESYT1_MOUSE	1.81	3.52	0.82	5.6E-04
167	sp|P48678|LMNA_MOUSE	1.80	3.49	0.94	1.0E-04
168	sp|P01029|CO4B_MOUSE	1.78	3.44	0.86	2.1E-03
169	sp|Q8K4G1|LTBP4_MOUSE	1.78	3.43	0.58	7.4E-05
170	sp|Q6ZWM4|LSM8_MOUSE	1.76	3.40	0.57	8.1E-01
171	sp|Q9WV32|ARC1B_MOUSE	1.76	3.38	0.87	1.2E-04
172	sp|Q62048|PEA15_MOUSE	1.74	3.34	0.63	3.6E-03
173	sp|P99024|TBB5_MOUSE	1.74	3.33	0.88	1.3E-05
174	sp|Q8CHH9|SEPT8_MOUSE	1.73	3.32	0.61	1.9E-04
175	sp|P08226|APOE_MOUSE	1.73	3.31	0.87	3.9E-04
176	sp|P84096|RHOG_MOUSE	1.72	3.29	0.77	3.4E-04
177	sp|O08638|MYH11_MOUSE	1.71	3.28	0.87	8.5E-05
178	sp|Q61879|MYH10_MOUSE	1.71	3.27	0.85	1.6E-03
179	sp|P29699|FETUA_MOUSE	1.71	3.27	0.90	1.6E-01
180	sp|Q62219|TGFI1_MOUSE	1.70	3.26	0.79	1.9E-05
181	sp|P01831|THY1_MOUSE	1.70	3.25	0.79	2.8E-05
182	sp|Q3TZZ7|ESYT2_MOUSE	1.69	3.23	0.86	6.6E-07
183	sp|Q9EPB4|ASC_MOUSE	1.68	3.21	0.76	3.8E-03
184	sp|P01864|GCAB_MOUSE	1.68	3.21	0.91	5.6E-02
185	sp|P63044|VAMP2_MOUSE	1.67	3.19	0.63	9.4E-02
186	sp|P58774|TPM2_MOUSE	1.67	3.19	0.79	1.4E-03
187	sp|P62737|ACTA_MOUSE	1.67	3.17	0.94	2.5E-06
188	sp|P23198|CBX3_MOUSE	1.66	3.16	0.78	3.3E-03
189	sp|O35206|COFA1_MOUSE	1.66	3.15	0.78	1.3E-01
190	sp|P70202|LXN_MOUSE	1.65	3.14	0.58	8.8E-04
191	sp|P21614|VTDB_MOUSE	1.65	3.13	0.93	1.1E-05
192	sp|P23953|EST1C_MOUSE	1.64	3.11	0.95	1.3E-01
193	sp|P20060|HEXB_MOUSE	1.64	3.11	0.53	1.6E-01
194	sp|O08677|KNG1_MOUSE	1.63	3.09	0.91	1.4E-04
195	sp|Q9CQ19|MYL9_MOUSE	1.62	3.08	0.98	7.9E-05
196	sp|Q61703|ITIH2_MOUSE	1.62	3.08	0.57	4.8E-01
197	sp|P50543|S10AB_MOUSE	1.62	3.08	0.88	2.7E-04

198	sp|P07758|A1AT1_MOUSE	1.62	3.07	0.86	1.7E-02
199	sp|P01867|IGG2B_MOUSE	1.62	3.07	0.81	3.2E-01
200	sp|Q9JJU8|SH3L1_MOUSE	1.61	3.06	0.86	4.1E-03
201	sp|Q8VED5|K2C79_MOUSE	1.61	3.05	0.91	8.1E-04
202	sp|Q9WVA4|TAGL2_MOUSE	1.60	3.04	0.88	3.9E-07
203	sp|Q9CPW4|ARPC5_MOUSE	1.60	3.03	0.76	3.8E-02
204	sp|P01869|IGH1M_MOUSE	1.60	3.03	0.59	9.1E-02
205	sp|P31725|S10A9_MOUSE	1.60	3.03	0.54	1.7E-01
206	sp|Q6IFZ6|K2C1B_MOUSE	1.59	3.02	0.61	4.6E-02
207	sp|P05784|K1C18_MOUSE	1.58	2.99	0.94	2.3E-03
208	sp|P07724|ALBU_MOUSE	1.58	2.98	0.92	4.1E-05
209	sp|O54724|PTRF_MOUSE	1.57	2.96	0.84	1.6E-02
210	sp|Q62465|VAT1_MOUSE	1.56	2.96	0.90	1.9E-05
211	sp|O55131|SEPT7_MOUSE	1.56	2.95	0.82	1.0E-03
212	sp|P43406|ITAV_MOUSE	1.56	2.94	0.61	2.9E-03
213	sp|P02762|MUP6_MOUSE	1.56	2.94	0.62	2.3E-01
214	sp|P28667|MRP_MOUSE	1.55	2.92	0.67	1.4E-03
215	sp|Q6P5H2|NEST_MOUSE	1.55	2.92	0.70	2.5E-04
216	sp|Q9ESB3|HRG_MOUSE	1.54	2.91	0.79	1.7E-03
217	sp|P97372|PSME2_MOUSE	1.54	2.91	0.88	1.1E-02
218	sp|P01887|B2MG_MOUSE	1.52	2.88	0.82	2.8E-04
219	sp|P07091|S10A4_MOUSE	1.52	2.87	0.64	9.6E-03
220	sp|Q61147|CERU_MOUSE	1.52	2.86	0.80	2.9E-02
221	sp|P14602|HSPB1_MOUSE	1.51	2.85	0.72	1.0E-02
222	sp|Q9QXS6|DREB_MOUSE	1.51	2.85	0.51	1.9E-02
223	sp|Q8R1F1|NIBL1_MOUSE	1.51	2.84	0.56	6.4E-01
224	sp|Q9QZ85|IIGP1_MOUSE	1.50	2.83	0.57	6.4E-02
225	sp|P42208|SEPT2_MOUSE	1.50	2.83	0.82	7.9E-05
226	sp|Q9EQH2|ERAP1_MOUSE	1.50	2.82	0.54	1.9E-02
227	sp|P47753|CAZA1_MOUSE	1.50	2.82	0.57	1.6E-03
228	sp|P14069|S10A6_MOUSE	1.50	2.82	0.65	2.4E-05
229	sp|Q9JK48|SHLB1_MOUSE	1.49	2.80	0.57	1.4E-02
230	sp|Q5SYD0|MYO1D_MOUSE	1.48	2.80	0.55	2.3E-01
231	sp|P11589|MUP2_MOUSE	1.48	2.79	0.77	7.9E-02
232	sp|P06281|RENI1_MOUSE	1.47	2.77	0.78	3.6E-01
233	sp|P30681|HMGB2_MOUSE	1.46	2.75	0.52	8.3E-02
234	sp|P18760|COF1_MOUSE	1.45	2.74	0.87	2.2E-04
235	sp|P43025|TETN_MOUSE	1.45	2.74	0.76	3.3E-02
236	sp|Q8CGP6|H2A1H_MOUSE	1.45	2.73	0.64	5.2E-03
237	sp|P46935|NEDD4_MOUSE	1.45	2.72	0.68	1.9E-01
238	sp|Q00897|A1AT4_MOUSE	1.44	2.72	0.83	3.1E-02
239	sp|P14824|ANXA6_MOUSE	1.44	2.71	0.89	3.9E-04
240	sp|Q8C1B7|SEP11_MOUSE	1.44	2.71	0.80	2.9E-06
241	sp|P54923|ADPRH_MOUSE	1.44	2.71	0.86	3.3E-04
242	sp|O08553|DPYL2_MOUSE	1.42	2.68	0.88	1.8E-04
243	sp|P02463|CO4A1_MOUSE	1.42	2.67	0.88	6.6E-03
244	sp|Q921M7|FA49B_MOUSE	1.42	2.67	0.52	1.0E-03
245	sp|P27546|MAP4_MOUSE	1.41	2.66	0.82	2.5E-05
246	sp|P18242|CATD_MOUSE	1.41	2.65	0.82	1.8E-03
247	sp|P63213|GBG2_MOUSE	1.40	2.65	0.81	2.2E-03
248	sp|A2ADY9|DDI2_MOUSE	1.40	2.64	0.58	8.5E-01
249	sp|P49312|ROA1_MOUSE	1.40	2.63	0.88	3.4E-03
250	sp|Q64339|ISG15_MOUSE	1.39	2.62	0.84	1.6E-01
251	sp|Q9QXC1|FETUB_MOUSE	1.39	2.61	0.89	4.7E-05
252	sp|Q8VDD5|MYH9_MOUSE	1.39	2.61	0.99	1.5E-06
253	sp|P01027|CO3_MOUSE	1.38	2.59	0.87	2.3E-03
254	sp|Q6PDN3|MYLK_MOUSE	1.37	2.59	0.80	1.1E-05
255	sp|P08207|S10AA_MOUSE	1.37	2.59	0.86	2.3E-03
256	sp|Q99KC8|VMA5A_MOUSE	1.37	2.58	0.86	3.2E-07
257	sp|P39061|COIA1_MOUSE	1.36	2.57	0.96	6.1E-07
258	sp|Q06138|CAB39_MOUSE	1.36	2.56	0.58	3.1E-01
259	sp|P68510|1433F_MOUSE	1.35	2.55	0.68	8.8E-01
260	sp|Q60605|MYL6_MOUSE	1.34	2.53	0.92	3.1E-04
261	sp|Q9WUU7|CATZ_MOUSE	1.34	2.53	0.86	5.5E-05
262	sp|Q9D554|SF3A3_MOUSE	1.34	2.53	0.52	4.7E-01
263	sp|Q62419|SH3G1_MOUSE	1.34	2.52	0.70	3.5E-05
264	sp|Q9ES28|ARHG7_MOUSE	1.33	2.51	0.69	3.7E-05
265	sp|Q921M3|SF3B3_MOUSE	1.33	2.51	0.83	1.9E-04
266	sp|P06728|APOA4_MOUSE	1.32	2.50	0.82	1.6E-01
267	sp|P40124|CAP1_MOUSE	1.32	2.50	0.92	7.3E-07
268	sp|Q01339|APOH_MOUSE	1.32	2.50	0.80	1.2E-03
269	sp|Q3UW53|NIBAN_MOUSE	1.31	2.48	0.55	8.4E-01
270	sp|Q00623|APOA1_MOUSE	1.30	2.46	0.92	4.2E-03

271	sp|Q9EQU5|SET_MOUSE	1.30	2.46	0.83	4.2E-02
272	sp|P63163|RSMN_MOUSE	1.29	2.45	0.60	9.3E-02
273	sp|Q8VIJ6|SFPQ_MOUSE	1.28	2.44	0.81	1.0E-06
274	sp|P02535|K1C10_MOUSE	1.27	2.41	0.58	1.0E-01
275	sp|P26350|PTMA_MOUSE	1.26	2.39	0.66	4.0E-02
276	sp|Q921E2|RAB31_MOUSE	1.26	2.39	0.57	6.5E-01
277	sp|Q8VE97|SRSF4_MOUSE	1.25	2.37	0.70	7.7E-03
278	sp|O70433|FHL2_MOUSE	1.25	2.37	0.59	9.4E-05
279	sp|P17918|PCNA_MOUSE	1.24	2.37	0.69	5.3E-02
280	sp|Q9QZR9|CO4A4_MOUSE	1.24	2.36	0.71	1.0E-02
281	sp|O89086|RBM3_MOUSE	1.24	2.36	0.84	5.1E-03
282	sp|Q06770|CBG_MOUSE	1.24	2.35	0.51	9.2E-03
283	sp|P09528|FRIH_MOUSE	1.23	2.35	0.56	4.2E-02
284	sp|P62500|T22D1_MOUSE	1.23	2.35	0.90	1.8E-04
285	sp|Q99PL5|RRBP1_MOUSE	1.23	2.35	0.55	3.7E-04
286	sp|Q62318|TIF1B_MOUSE	1.22	2.33	0.83	3.1E-04
287	sp|P13020|GELS_MOUSE	1.22	2.33	0.84	1.6E-05
288	sp|Q9CQW2|ARL8B_MOUSE	1.22	2.33	0.54	3.0E-01
289	sp|Q64727|VINC_MOUSE	1.22	2.33	0.94	2.7E-05
290	sp|Q3THE2|ML12B_MOUSE	1.22	2.33	0.83	7.8E-05
291	sp|P28665|MUG1_MOUSE	1.22	2.32	0.64	1.9E-01
292	sp|P14733|LMNB1_MOUSE	1.20	2.30	0.86	4.4E-06
293	sp|P53810|PIPNA_MOUSE	1.20	2.30	0.53	1.6E-03
294	sp|P48036|ANXA5_MOUSE	1.20	2.29	0.84	2.0E-03
295	sp|P97371|PSME1_MOUSE	1.19	2.28	0.84	9.7E-02
296	sp|P32261|ANT3_MOUSE	1.18	2.27	0.86	8.4E-02
297	sp|O88531|PPT1_MOUSE	1.18	2.26	0.70	7.5E-04
298	sp|Q61001|LAMA5_MOUSE	1.17	2.26	0.83	1.6E-01
299	sp|P21460|CYTC_MOUSE	1.16	2.23	0.69	1.1E-01
300	sp|Q9WUM4|COR1C_MOUSE	1.16	2.23	0.83	1.3E-05
301	sp|P47757|CAPZB_MOUSE	1.16	2.23	0.89	1.9E-03
302	sp|P19221|THRB_MOUSE	1.15	2.22	0.54	7.5E-02
303	sp|P56959|FUS_MOUSE	1.15	2.22	0.80	2.0E-03
304	sp|Q9QWR8|NAGAB_MOUSE	1.14	2.21	0.72	2.6E-01
305	sp|Q6P5E4|UGGG1_MOUSE	1.14	2.20	0.74	3.4E-01
306	sp|Q61166|MARE1_MOUSE	1.14	2.20	0.54	3.2E-04
307	sp|Q9JKF1|IQGA1_MOUSE	1.12	2.17	0.66	3.4E-02
308	sp|P97822|AN32E_MOUSE	1.12	2.17	0.58	9.8E-02
309	sp|A2ASQ1|AGRIN_MOUSE	1.11	2.16	0.92	3.3E-04
310	sp|Q9EST5|AN32B_MOUSE	1.11	2.15	0.81	8.9E-02
311	sp|P07759|SPA3K_MOUSE	1.11	2.15	0.79	7.6E-02
312	sp|Q9Z172|SUMO3_MOUSE	1.10	2.14	0.55	1.2E-01
313	sp|Q60749|KHDR1_MOUSE	1.10	2.14	0.84	6.7E-03
314	sp|Q61292|LAMB2_MOUSE	1.09	2.13	0.76	1.3E-03
315	sp|Q80UG5|SEPT9_MOUSE	1.09	2.13	0.52	8.3E-05
316	sp|P43276|H15_MOUSE	1.08	2.12	0.75	1.4E-01
317	sp|Q3UPH1|PRRC1_MOUSE	1.08	2.12	0.53	5.3E-01
318	sp|Q9Z0E6|GBP2_MOUSE	1.08	2.12	0.56	2.8E-02
319	sp|O88456|CPNS1_MOUSE	1.08	2.11	0.69	6.8E-03
320	sp|P62962|PROF1_MOUSE	1.07	2.10	0.89	4.1E-04
321	sp|P10493|NID1_MOUSE	1.07	2.10	0.92	1.2E-04
322	sp|O08529|CAN2_MOUSE	1.06	2.09	0.54	1.0E-03
323	sp|Q91VC3|IF4A3_MOUSE	1.05	2.07	0.50	1.4E-01
324	sp|Q3THW5|H2AV_MOUSE	1.05	2.07	0.86	1.2E-02
325	sp|Q9WUM3|COR1B_MOUSE	1.04	2.06	0.86	1.5E-03
326	sp|Q9CX86|ROA0_MOUSE	1.04	2.06	0.58	1.7E-02
327	sp|Q9CXY6|ILF2_MOUSE	1.04	2.06	0.56	8.0E-03
328	sp|P29351|PTN6_MOUSE	1.04	2.05	0.59	2.1E-01
329	sp|P04186|CFAB_MOUSE	1.03	2.05	0.55	5.8E-03
330	sp|Q61838|A2M_MOUSE	1.03	2.05	0.85	1.2E-02
331	sp|Q3UZ39|LRRF1_MOUSE	1.03	2.04	0.61	1.1E-02
332	sp|Q9JHU9|INO1_MOUSE	1.02	2.03	0.81	7.3E-04
333	sp|Q60972|RBBP4_MOUSE	1.02	2.02	0.57	1.3E-04
334	sp|Q9ERG0|LIMA1_MOUSE	1.02	2.02	0.87	6.5E-03
335	sp|P08752|GNAI2_MOUSE	1.01	2.02	0.83	3.3E-03
336	sp|Q9JM76|ARPC3_MOUSE	1.01	2.01	0.87	2.9E-07
337	sp|O88342|WDR1_MOUSE	1.01	2.01	0.83	7.0E-03
338	sp|Q925B0|PAWR_MOUSE	1.00	2.00	0.54	9.2E-03
339	sp|Q9WVB0|RBPMS_MOUSE	0.99	1.98	0.67	2.4E-02
340	sp|P48428|TBCA_MOUSE	0.99	1.98	0.76	5.7E-01
341	sp|P63280|UBC9_MOUSE	0.98	1.97	0.91	1.9E-06
342	sp|Q63844|MK03_MOUSE	0.98	1.97	0.62	2.6E-04
343	sp|P17225|PTBP1_MOUSE	0.97	1.97	0.56	3.7E-01

344	sp|Q07813|BAX_MOUSE	0.97	1.96	0.69	1.4E-01
345	sp|Q91W90|TXND5_MOUSE	0.97	1.96	0.50	3.9E-01
346	sp|P34928|APOC1_MOUSE	0.96	1.95	0.64	2.2E-01
347	sp|O88322|NID2_MOUSE	0.96	1.95	0.68	4.9E-01
348	sp|Q8BH43|WASF2_MOUSE	0.96	1.94	0.60	1.7E-02
349	sp|Q3TEA8|HP1B3_MOUSE	0.95	1.94	0.83	5.5E-04
350	sp|P47754|CAZA2_MOUSE	0.95	1.94	0.75	3.0E-02
351	sp|Q9DBG9|TX1B3_MOUSE	0.95	1.93	0.73	5.2E-04
352	sp|Q8C0E2|VP26B_MOUSE	0.95	1.93	0.67	1.1E-01
353	sp|P97447|FHL1_MOUSE	0.94	1.92	0.56	1.5E-02
354	sp|Q8BFZ3|ACTBL_MOUSE	0.93	1.91	0.84	2.4E-04
355	sp|P09813|APOA2_MOUSE	0.93	1.90	0.63	5.9E-02
356	sp|Q8BG05|ROA3_MOUSE	0.93	1.90	0.90	2.2E-03
357	sp|Q91YH5|ATLA3_MOUSE	0.92	1.90	0.67	2.4E-02
358	sp|Q8BP92|RCN2_MOUSE	0.92	1.90	0.54	6.0E-02
359	sp|Q99K48|NONO_MOUSE	0.92	1.90	0.91	6.0E-03
360	sp|Q61102|ABCB7_MOUSE	0.92	1.89	0.89	5.6E-05
361	sp|Q99JY9|ARP3_MOUSE	0.92	1.89	0.95	5.5E-05
362	sp|Q61207|SAP_MOUSE	0.91	1.88	0.75	3.3E-02
363	sp|Q60604|ADSV_MOUSE	0.91	1.88	0.78	7.7E-03
364	sp|Q9CVB6|ARPC2_MOUSE	0.91	1.87	0.83	3.7E-05
365	sp|Q9D0T1|NH2L1_MOUSE	0.90	1.86	0.81	9.1E-04
366	sp|Q8C522|ENDD1_MOUSE	0.90	1.86	0.71	4.9E-04
367	sp|P61750|ARF4_MOUSE	0.89	1.86	0.62	7.7E-01
368	sp|P02468|LAMC1_MOUSE	0.89	1.85	0.93	2.3E-04
369	sp|P02469|LAMB1_MOUSE	0.89	1.85	0.85	1.4E-02
370	sp|Q91VM5|RMXL1_MOUSE	0.89	1.85	0.65	1.1E-02
371	sp|Q9R0P5|DEST_MOUSE	0.89	1.85	0.80	2.6E-02
372	sp|Q62470|ITA3_MOUSE	0.89	1.85	0.66	7.4E-01
373	sp|Q7TSV4|PGM2_MOUSE	0.88	1.84	0.79	7.5E-05
374	sp|O35593|PSDE_MOUSE	0.87	1.83	0.56	9.9E-02
375	sp|Q9Z204|HNRPC_MOUSE	0.87	1.82	0.76	3.0E-01
376	sp|Q00612|G6PD1_MOUSE	0.87	1.82	0.74	4.9E-02
377	sp|Q9Z2X1|HNRPF_MOUSE	0.87	1.82	0.83	3.1E-02
378	sp|P04117|FABP4_MOUSE	0.86	1.82	0.85	1.4E-01
379	sp|Q6WVG3|KCD12_MOUSE	0.86	1.82	0.70	2.5E-02
380	sp|Q61792|LASP1_MOUSE	0.86	1.81	0.81	5.0E-01
381	sp|P43275|H11_MOUSE	0.86	1.81	0.68	8.3E-02
382	sp|Q80XU3|NUCKS_MOUSE	0.85	1.80	0.56	4.2E-03
383	sp|Q05793|PGBM_MOUSE	0.85	1.80	0.81	3.2E-01
384	sp|P84089|ERH_MOUSE	0.85	1.80	0.62	7.5E-02
385	sp|P70372|ELAV1_MOUSE	0.85	1.80	0.68	1.2E-01
386	sp|Q921F2|TADBP_MOUSE	0.85	1.80	0.81	1.8E-02
387	sp|O08810|U5S1_MOUSE	0.84	1.79	0.63	6.2E-01
388	sp|Q9EPC1|PARVA_MOUSE	0.84	1.79	0.73	1.9E-02
389	sp|P21619|LMNB2_MOUSE	0.84	1.79	0.53	1.6E-02
390	sp|P09405|NUCL_MOUSE	0.84	1.79	0.83	6.6E-02
391	sp|O08807|PRDX4_MOUSE	0.83	1.78	0.73	2.6E-04
392	sp|Q91V88|NPNT_MOUSE	0.83	1.78	0.57	5.8E-02
393	sp|Q8BL97|SRSF7_MOUSE	0.83	1.78	0.79	1.9E-03
394	sp|Q9Z1N5|DX39B_MOUSE	0.83	1.78	0.81	3.0E-03
395	sp|Q7TMK9|HNRPQ_MOUSE	0.83	1.78	0.65	1.3E-01
396	sp|P97429|ANXA4_MOUSE	0.83	1.78	0.85	1.3E-02
397	sp|P26039|TLN1_MOUSE	0.83	1.78	0.82	1.9E-02
398	sp|Q3U0V1|FUBP2_MOUSE	0.83	1.78	0.80	1.4E-01
399	sp|Q8C854|MYEF2_MOUSE	0.82	1.76	0.78	1.8E-05
400	sp|Q9QZS0|CO4A3_MOUSE	0.82	1.76	0.64	4.1E-02
401	sp|Q6ZWX6|IF2A_MOUSE	0.82	1.76	0.52	1.7E-01
402	sp|P61161|ARP2_MOUSE	0.81	1.76	0.88	2.3E-05
403	sp|Q62523|ZYX_MOUSE	0.81	1.75	0.53	3.6E-01
404	sp|P63158|HMGB1_MOUSE	0.81	1.75	0.68	8.4E-02
405	sp|P62307|RUXF_MOUSE	0.81	1.75	0.87	1.8E-03
406	sp|Q8R5J9|PRAF3_MOUSE	0.80	1.74	0.54	9.2E-01
407	sp|Q9D0E1|HNRPM_MOUSE	0.80	1.74	0.86	1.4E-02
408	sp|Q9QXA5|LSM4_MOUSE	0.79	1.73	0.79	8.4E-01
409	sp|P97314|CSRP2_MOUSE	0.78	1.72	0.82	3.5E-03
410	sp|Q501J6|DDX17_MOUSE	0.78	1.72	0.61	2.1E-02
411	sp|P21981|TGM2_MOUSE	0.78	1.71	0.90	6.0E-04
412	sp|Q9D1J3|SARNP_MOUSE	0.78	1.71	0.77	1.6E-01
413	sp|P62996|TRA2B_MOUSE	0.78	1.71	0.59	6.4E-01
414	sp|P59999|ARPC4_MOUSE	0.77	1.71	0.66	6.3E-03
415	sp|Q61029|LAP2B_MOUSE	0.77	1.71	0.80	1.2E-02
416	sp|Q62093|SRSF2_MOUSE	0.76	1.70	0.86	2.5E-02

417	sp|Q8C2Q3|RBM14_MOUSE	0.76	1.69	0.56	1.4E-03
418	sp|P17047|LAMP2_MOUSE	0.76	1.69	0.77	4.1E-04
419	sp|P11031|TCP4_MOUSE	0.75	1.69	0.62	5.2E-03
420	sp|Q9DAW9|CNN3_MOUSE	0.75	1.68	0.56	3.1E-01
421	sp|P24452|CAPG_MOUSE	0.75	1.68	0.77	1.9E-02
422	sp|Q922R8|PDIA6_MOUSE	0.75	1.68	0.90	1.3E-01
423	sp|Q8BQ47|CNPY4_MOUSE	0.74	1.68	0.63	8.0E-01
424	sp|Q9Z2N8|ACL6A_MOUSE	0.73	1.66	0.73	6.6E-02
425	sp|P61982|1433G_MOUSE	0.72	1.65	0.81	1.7E-01
426	sp|Q9Z130|HNRDL_MOUSE	0.72	1.65	0.66	1.1E-02
427	sp|O70133|DHX9_MOUSE	0.72	1.65	0.53	4.0E-02
428	sp|Q923D2|BLVRB_MOUSE	0.72	1.65	0.70	1.9E-03
429	sp|P62852|RS25_MOUSE	0.72	1.65	0.52	9.7E-01
430	sp|Q9R0P4|SMAP_MOUSE	0.71	1.64	0.88	9.1E-04
431	sp|P70168|IMB1_MOUSE	0.71	1.64	0.75	4.0E-01
432	sp|P40240|CD9_MOUSE	0.71	1.63	0.65	1.9E-01
433	sp|Q8CIB5|FERM2_MOUSE	0.70	1.63	0.53	2.4E-01
434	sp|Q9Z1X4|ILF3_MOUSE	0.70	1.63	0.57	1.5E-01
435	sp|Q61656|DDX5_MOUSE	0.70	1.63	0.80	1.7E-03
436	sp|O55023|IMPA1_MOUSE	0.69	1.62	0.67	1.6E-01
437	sp|P62311|LSM3_MOUSE	0.69	1.62	0.91	1.7E-04
438	sp|Q9Z2D6|MECP2_MOUSE	0.69	1.61	0.67	2.2E-03
439	sp|O08547|SC22B_MOUSE	0.68	1.61	0.74	1.0E-02
440	sp|P84104|SRSF3_MOUSE	0.68	1.60	0.64	5.0E-01
441	sp|Q62189|SNRPA_MOUSE	0.68	1.60	0.57	4.1E-03
442	sp|O08583|THOC4_MOUSE	0.67	1.60	0.57	7.6E-02
443	sp|Q01730|RSU1_MOUSE	0.67	1.59	0.84	4.8E-03
444	sp|Q99KF1|TMED9_MOUSE	0.67	1.59	0.78	1.3E-03
445	sp|Q9R0P6|SC11A_MOUSE	0.67	1.59	0.80	3.9E-01
446	sp|Q61937|NPM_MOUSE	0.67	1.59	0.57	5.4E-01
447	sp|Q8C166|CPNE1_MOUSE	0.67	1.59	0.52	4.5E-02
448	sp|Q9R1Z8|VINEX_MOUSE	0.67	1.59	0.68	8.2E-02
449	sp|P63085|MK01_MOUSE	0.66	1.58	0.73	1.2E-02
450	sp|P60843|IF4A1_MOUSE	0.66	1.58	0.66	1.8E-02
451	sp|P26883|FKB1A_MOUSE	0.66	1.58	0.64	9.1E-01
452	sp|Q02257|PLAK_MOUSE	0.64	1.56	0.62	7.0E-01
453	sp|O55222|ILK_MOUSE	0.64	1.56	0.69	9.4E-01
454	sp|Q4KML4|ABRAL_MOUSE	0.64	1.56	0.80	3.8E-03
455	sp|O09131|GSTO1_MOUSE	0.64	1.56	0.67	9.2E-02
456	sp|P60710|ACTB_MOUSE	0.64	1.56	0.93	1.0E-02
457	sp|Q8CI94|PYGB_MOUSE	0.63	1.55	0.59	2.4E-01
458	sp|Q99JI6|RAP1B_MOUSE	0.63	1.55	0.76	5.3E-03
459	sp|P49722|PSA2_MOUSE	0.63	1.55	0.57	2.2E-01
460	sp|Q9D8B3|CHM4B_MOUSE	0.62	1.54	0.51	7.2E-02
461	sp|Q9CYZ2|TPD54_MOUSE	0.62	1.54	0.50	5.9E-01
462	sp|Q9WVA3|BUB3_MOUSE	0.62	1.54	0.52	1.6E-02
463	sp|Q9CY50|SSRA_MOUSE	0.62	1.53	0.56	2.1E-02
464	sp|Q8VEK3|HNRPU_MOUSE	0.61	1.53	0.85	6.6E-03
465	sp|Q62426|CYTB_MOUSE	0.61	1.52	0.77	3.3E-01
466	sp|P26041|MOES_MOUSE	0.60	1.52	0.81	7.1E-04
467	sp|Q61990|PCBP2_MOUSE	0.60	1.52	0.68	2.1E-01
468	sp|Q60598|SRC8_MOUSE	0.60	1.51	0.56	9.3E-01
469	sp|Q99PT1|GDIR1_MOUSE	0.60	1.51	0.84	1.1E-04
470	sp|Q9CR86|CHSP1_MOUSE	0.59	1.51	0.63	1.7E-01
471	sp|Q8R081|HNRPL_MOUSE	0.59	1.50	0.60	2.4E-03
472	sp|Q3TWW8|SRSF6_MOUSE	0.58	1.50	0.54	6.2E-02
473	sp|Q61545|EWS_MOUSE	0.58	1.50	0.58	7.2E-02
474	sp|P15864|H12_MOUSE	0.58	1.49	0.53	3.1E-01
475	sp|P10605|CATB_MOUSE	0.58	1.49	0.79	1.5E-03
476	sp|Q6PDM2|SRSF1_MOUSE	0.58	1.49	0.56	6.1E-03
477	sp|P34022|RANG_MOUSE	0.57	1.49	0.53	3.4E-01
478	sp|Q8VE37|RCC1_MOUSE	0.57	1.49	0.64	1.9E-03
479	sp|Q9JHL1|NHRF2_MOUSE	0.57	1.49	0.54	6.5E-01
480	sp|Q9CQV8|1433B_MOUSE	0.57	1.49	0.75	4.6E-03
481	sp|P62320|SMD3_MOUSE	0.57	1.48	0.74	6.1E-03
482	sp|P00493|HPRT_MOUSE	0.56	1.48	0.71	5.1E-02
483	sp|P63024|VAMP3_MOUSE	0.56	1.48	0.78	6.6E-02
484	sp|O35737|HNRH1_MOUSE	0.56	1.48	0.87	1.0E-04
485	sp|Q9CQS8|SC61B_MOUSE	0.56	1.47	0.69	3.8E-02
486	sp|P62317|SMD2_MOUSE	0.56	1.47	0.81	6.5E-03
487	sp|Q7TNG5|EMAL2_MOUSE	0.55	1.47	0.51	5.6E-02
488	sp|P57780|ACTN4_MOUSE	0.55	1.46	0.70	6.7E-03
489	sp|P60867|RS20_MOUSE	0.54	1.46	0.59	2.2E-02

490	sp|P24369|PPIB_MOUSE	0.54	1.46	0.76	7.7E-03
491	sp|P68254|1433T_MOUSE	0.54	1.46	0.76	7.4E-03
492	sp|P63001|RAC1_MOUSE	0.53	1.45	0.50	9.5E-01
493	sp|P05132|KAPCA_MOUSE	0.53	1.44	0.89	6.8E-03
494	sp|Q9JHJ0|TMOD3_MOUSE	0.53	1.44	0.62	2.4E-01
495	sp|P09055|ITB1_MOUSE	0.52	1.44	0.62	6.9E-01
496	sp|Q8VBT0|TMX1_MOUSE	0.52	1.43	0.57	4.7E-02
497	sp|P62827|RAN_MOUSE	0.51	1.43	0.64	2.1E-01
498	sp|P08113|ENPL_MOUSE	0.50	1.42	0.73	4.1E-02
499	sp|P62309|RUXG_MOUSE	0.50	1.42	0.70	1.4E-01
500	sp|Q99020|ROAA_MOUSE	0.50	1.41	0.74	1.9E-02
501	sp|Q99KP6|PRP19_MOUSE	0.49	1.40	0.58	7.2E-02
502	sp|P08003|PDIA4_MOUSE	0.49	1.40	0.80	2.7E-01
503	sp|P61979|HNRPK_MOUSE	0.49	1.40	0.82	3.0E-05
504	sp|Q922Q8|LRC59_MOUSE	0.48	1.40	0.58	2.7E-04
505	sp|Q9R0Y5|KAD1_MOUSE	0.48	1.40	0.51	3.8E-01
506	sp|O89023|TPP1_MOUSE	0.48	1.39	0.69	6.1E-01
507	sp|P57776|EF1D_MOUSE	0.47	1.38	0.68	5.8E-03
508	sp|P11438|LAMP1_MOUSE	0.47	1.38	0.81	1.1E-02
509	sp|Q99M71|EPDR1_MOUSE	0.46	1.38	0.55	1.4E-02
510	sp|Q9D7X3|DUS3_MOUSE	0.46	1.38	0.57	7.1E-01
511	sp|P60766|CDC42_MOUSE	0.46	1.37	0.55	5.8E-01
512	sp|P58389|PTPA_MOUSE	0.45	1.37	0.64	6.8E-02
513	sp|Q76MZ3|2AAA_MOUSE	0.45	1.36	0.51	6.1E-01
514	sp|P21107|TPM3_MOUSE	0.44	1.36	0.67	4.0E-01
515	sp|P01942|HBA_MOUSE	0.44	1.35	0.71	9.5E-01
516	sp|P62305|RUXE_MOUSE	0.43	1.35	0.79	2.4E-01
517	sp|Q61753|SERA_MOUSE	0.43	1.35	0.54	1.7E-01
518	sp|Q9R1P4|PSA1_MOUSE	0.40	1.32	0.52	4.6E-04
519	sp|Q9D8N0|EF1G_MOUSE	0.40	1.32	0.61	1.6E-01
520	sp|P62137|PP1A_MOUSE	0.38	1.30	0.53	6.2E-02
521	sp|Q9DCD0|6PGD_MOUSE	0.37	1.29	0.65	6.1E-02
522	sp|P27773|PDIA3_MOUSE	0.35	1.28	0.56	7.6E-03
523	sp|P27661|H2AX_MOUSE	0.34	1.26	0.52	6.4E-01
524	sp|P20029|GRP78_MOUSE	0.33	1.26	0.57	3.8E-01
525	sp|P63017|HSP7C_MOUSE	-0.27	1.21	0.74	5.3E-02
526	sp|Q61171|PRDX2_MOUSE	-0.36	1.28	0.64	9.8E-02
527	sp|P40142|TKT_MOUSE	-0.40	1.32	0.51	2.4E-01
528	sp|Q01853|TERA_MOUSE	-0.40	1.32	0.52	1.1E-01
529	sp|Q9DAS9|GBG12_MOUSE	-0.40	1.32	0.51	1.7E-01
530	sp|Q93092|TALDO_MOUSE	-0.42	1.34	0.57	1.7E-02
531	sp|Q9D1G1|RAB1B_MOUSE	-0.43	1.35	0.65	5.7E-02
532	sp|Q9EQX4|AIF1L_MOUSE	-0.46	1.38	0.58	3.3E-02
533	sp|P61205|ARF3_MOUSE	-0.46	1.38	0.60	2.0E-01
534	sp|Q9QYJ0|DNJA2_MOUSE	-0.47	1.39	0.52	1.0E-01
535	sp|O54984|ASNA_MOUSE	-0.48	1.39	0.75	1.6E-03
536	sp|Q9CQ22|LTOR1_MOUSE	-0.49	1.40	0.62	2.1E-01
537	sp|P46638|RB11B_MOUSE	-0.49	1.41	0.68	3.1E-01
538	sp|Q9Z1Z0|USO1_MOUSE	-0.50	1.41	0.54	4.3E-02
539	sp|P31428|DPEP1_MOUSE	-0.51	1.43	0.76	1.1E-02
540	sp|P17427|AP2A2_MOUSE	-0.52	1.43	0.54	5.6E-03
541	sp|P06151|LDHA_MOUSE	-0.52	1.44	0.72	6.9E-02
542	sp|P26638|SYSC_MOUSE	-0.53	1.45	0.57	1.7E-01
543	sp|Q68FD5|CLH1_MOUSE	-0.56	1.47	0.88	4.2E-03
544	sp|P84091|AP2M1_MOUSE	-0.56	1.48	0.53	6.6E-01
545	sp|Q91WG5|AAKG2_MOUSE	-0.57	1.48	0.62	4.2E-01
546	sp|P10639|THIO_MOUSE	-0.57	1.49	0.75	1.6E-03
547	sp|Q8K021|SCAM1_MOUSE	-0.58	1.50	0.57	5.4E-02
548	sp|P07901|HS90A_MOUSE	-0.58	1.50	0.81	2.9E-01
549	sp|P30416|FKBP4_MOUSE	-0.61	1.53	0.68	7.1E-01
550	sp|Q8BP67|RL24_MOUSE	-0.62	1.53	0.59	6.6E-01
551	sp|Q62446|FKBP3_MOUSE	-0.62	1.53	0.67	6.1E-02
552	sp|P46412|GPX3_MOUSE	-0.63	1.54	0.83	8.4E-02
553	sp|P62821|RAB1A_MOUSE	-0.64	1.56	0.71	2.3E-02
554	sp|Q9D819|IPYR_MOUSE	-0.65	1.56	0.56	9.7E-02
555	sp|Q9CZX8|RS19_MOUSE	-0.65	1.57	0.53	9.3E-01
556	sp|P05064|ALDOA_MOUSE	-0.65	1.57	0.84	1.9E-02
557	sp|Q91V64|ISOC1_MOUSE	-0.66	1.58	0.71	9.5E-05
558	sp|P62274|RS29_MOUSE	-0.66	1.58	0.53	6.8E-01
559	sp|O09044|SNP23_MOUSE	-0.66	1.59	0.52	1.6E-01
560	sp|Q9JMH6|TRXR1_MOUSE	-0.67	1.59	0.70	2.9E-03
561	sp|Q6P8X1|SNX6_MOUSE	-0.67	1.59	0.65	2.7E-01
562	sp|Q9CPV4|GLOD4_MOUSE	-0.67	1.59	0.71	6.8E-03

563	sp|Q8K2C9|HACD3_MOUSE	-0.67	1.60	0.74	3.1E-02
564	sp|Q61249|IGBP1_MOUSE	-0.68	1.60	0.51	8.6E-01
565	sp|P08556|RASN_MOUSE	-0.68	1.61	0.70	1.6E-03
566	sp|P11881|ITPR1_MOUSE	-0.69	1.61	0.59	5.3E-04
567	sp|O55022|PGRC1_MOUSE	-0.69	1.61	0.67	3.6E-02
568	sp|Q8BFZ9|ERLN2_MOUSE	-0.69	1.62	0.66	3.4E-02
569	sp|Q68FH4|GALK2_MOUSE	-0.70	1.62	0.58	7.7E-01
570	sp|P40336|VP26A_MOUSE	-0.70	1.63	0.79	3.9E-01
571	sp|Q9R0N0|GALK1_MOUSE	-0.71	1.64	0.85	8.3E-03
572	sp|Q9QUH0|GLRX1_MOUSE	-0.72	1.65	0.54	4.0E-02
573	sp|Q9CR57|RL14_MOUSE	-0.73	1.66	0.56	3.9E-01
574	sp|Q9CQM5|TXD17_MOUSE	-0.73	1.66	0.77	7.4E-02
575	sp|Q8C7X2|EMC1_MOUSE	-0.77	1.70	0.50	2.7E-03
576	sp|Q3THS6|METK2_MOUSE	-0.77	1.70	0.69	1.1E-01
577	sp|Q6ZWV3|RL10_MOUSE	-0.77	1.71	0.64	7.4E-01
578	sp|P68372|TBB4B_MOUSE	-0.77	1.71	0.90	2.3E-04
579	sp|Q9CQ89|CUTA_MOUSE	-0.78	1.71	0.56	6.8E-02
580	sp|P63087|PP1G_MOUSE	-0.78	1.71	0.58	5.2E-02
581	sp|Q9CQB5|CISD2_MOUSE	-0.78	1.72	0.75	8.0E-02
582	sp|O70492|SNX3_MOUSE	-0.78	1.72	0.84	6.7E-02
583	sp|O88952|LIN7C_MOUSE	-0.78	1.72	0.74	2.4E-01
584	sp|Q9ES97|RTN3_MOUSE	-0.79	1.72	0.77	1.9E-03
585	sp|D3Z7P3|GLSK_MOUSE	-0.80	1.74	0.60	6.8E-03
586	sp|Q9CXA2|T3HPD_MOUSE	-0.80	1.74	0.62	3.2E-02
587	sp|P10922|H10_MOUSE	-0.80	1.74	0.52	8.4E-01
588	sp|Q91V92|ACLY_MOUSE	-0.80	1.74	0.76	3.5E-02
589	sp|P10630|IF4A2_MOUSE	-0.80	1.74	0.64	6.9E-01
590	sp|Q9EP69|SAC1_MOUSE	-0.80	1.74	0.66	5.2E-01
591	sp|Q9WTN6|S22AL_MOUSE	-0.80	1.75	0.64	2.8E-02
592	sp|Q920Q6|MSI2H_MOUSE	-0.81	1.75	0.60	5.3E-04
593	sp|Q60770|STXB3_MOUSE	-0.81	1.75	0.70	4.9E-04
594	sp|P61022|CHP1_MOUSE	-0.81	1.76	0.68	4.8E-01
595	sp|Q3TW96|UAP1L_MOUSE	-0.81	1.76	0.84	2.8E-02
596	sp|P47911|RL6_MOUSE	-0.81	1.76	0.54	8.3E-01
597	sp|P19157|GSTP1_MOUSE	-0.82	1.77	0.94	4.1E-04
598	sp|Q8K1R3|PNPT1_MOUSE	-0.83	1.77	0.59	4.3E-01
599	sp|Q9ERN0|SCAM2_MOUSE	-0.84	1.79	0.61	4.0E-01
600	sp|O70475|UGDH_MOUSE	-0.84	1.79	0.82	7.5E-03
601	sp|Q8R001|MARE2_MOUSE	-0.84	1.79	0.53	9.6E-03
602	sp|Q62261|SPTB2_MOUSE	-0.84	1.80	0.87	1.4E-02
603	sp|Q91V41|RAB14_MOUSE	-0.85	1.80	0.74	1.6E-01
604	sp|Q9WUA2|SYFB_MOUSE	-0.85	1.81	0.59	4.9E-02
605	sp|Q60676|PPP5_MOUSE	-0.86	1.82	0.53	4.7E-02
606	sp|Q8R2Y8|PTH2_MOUSE	-0.86	1.82	0.57	1.7E-02
607	sp|Q9CQ86|MIEN1_MOUSE	-0.87	1.83	0.58	2.5E-02
608	sp|Q921J2|RHEB_MOUSE	-0.87	1.83	0.56	7.4E-03
609	sp|Q9CQ80|VPS25_MOUSE	-0.88	1.84	0.55	5.3E-01
610	sp|Q99L47|F10A1_MOUSE	-0.88	1.84	0.54	2.6E-01
611	sp|P14148|RL7_MOUSE	-0.88	1.84	0.56	7.7E-01
612	sp|Q8R1V4|TMED4_MOUSE	-0.88	1.84	0.90	2.2E-03
613	sp|P35980|RL18_MOUSE	-0.88	1.85	0.66	4.5E-01
614	sp|P16546|SPTN1_MOUSE	-0.89	1.85	0.88	5.9E-05
615	sp|P12367|KAP2_MOUSE	-0.89	1.85	0.57	2.5E-01
616	sp|Q64471|GSTT1_MOUSE	-0.91	1.87	0.80	1.0E-02
617	sp|P45878|FKBP2_MOUSE	-0.91	1.88	0.74	3.8E-03
618	sp|Q99KI3|EMC3_MOUSE	-0.91	1.88	0.57	7.5E-01
619	sp|Q9R0X4|ACOT9_MOUSE	-0.91	1.88	0.71	9.5E-02
620	sp|Q8QZY2|GLCTK_MOUSE	-0.91	1.88	0.69	1.1E-02
621	sp|P54822|PUR8_MOUSE	-0.92	1.90	0.73	7.5E-03
622	sp|Q924M7|MPI_MOUSE	-0.93	1.90	0.58	6.5E-02
623	sp|Q9D1A2|CNDP2_MOUSE	-0.93	1.90	0.77	4.7E-02
624	sp|P35278|RAB5C_MOUSE	-0.93	1.91	0.74	5.4E-01
625	sp|Q9Z0P4|PALM_MOUSE	-0.93	1.91	0.73	6.1E-03
626	sp|Q9D1L0|CHCH2_MOUSE	-0.94	1.92	0.72	5.0E-02
627	sp|P70296|PEBP1_MOUSE	-0.94	1.92	0.92	2.5E-02
628	sp|Q99LB6|MAT2B_MOUSE	-0.96	1.94	0.89	2.0E-01
629	sp|Q9CY64|BIEA_MOUSE	-0.96	1.94	0.63	2.4E-01
630	sp|P28843|DPP4_MOUSE	-0.96	1.95	0.73	2.6E-02
631	sp|Q9CY27|TECR_MOUSE	-0.97	1.95	0.65	8.6E-03
632	sp|Q9WVE8|PACN2_MOUSE	-0.97	1.96	0.85	4.3E-02
633	sp|O35643|AP1B1_MOUSE	-0.97	1.97	0.82	3.5E-03
634	sp|Q8VDM4|PSMD2_MOUSE	-0.98	1.98	0.52	1.5E-01
635	sp|Q9D7S9|CHMP5_MOUSE	-0.98	1.98	0.70	3.0E-01

636	sp|P15532|NDKA_MOUSE	-0.99	1.98	0.88	2.9E-03
637	sp|P62849|RS24_MOUSE	-0.99	1.99	0.88	1.9E-01
638	sp|Q8BMA6|SRP68_MOUSE	-0.99	1.99	0.57	7.6E-01
639	sp|P12970|RL7A_MOUSE	-1.00	2.01	0.74	4.0E-01
640	sp|Q9CZW5|TOM70_MOUSE	-1.01	2.02	0.57	1.6E-02
641	sp|P06745|G6PI_MOUSE	-1.02	2.03	0.93	2.8E-04
642	sp|P35700|PRDX1_MOUSE	-1.02	2.03	0.91	9.7E-03
643	sp|P55264|ADK_MOUSE	-1.02	2.03	0.87	5.3E-04
644	sp|Q5SRX1|TM1L2_MOUSE	-1.02	2.03	0.74	9.0E-02
645	sp|Q91W52|TMM19_MOUSE	-1.03	2.04	0.71	7.2E-05
646	sp|Q9D8E6|RL4_MOUSE	-1.03	2.04	0.69	6.3E-01
647	sp|Q9CPU0|LGUL_MOUSE	-1.04	2.06	0.74	2.8E-02
648	sp|P28474|ADHX_MOUSE	-1.05	2.07	0.78	3.1E-03
649	sp|Q9DCL9|PUR6_MOUSE	-1.06	2.09	0.79	4.5E-02
650	sp|P82343|RENBP_MOUSE	-1.07	2.10	0.68	2.6E-03
651	sp|Q6ZWY3|RS27L_MOUSE	-1.07	2.10	0.77	1.9E-02
652	sp|P62855|RS26_MOUSE	-1.08	2.11	0.51	2.8E-01
653	sp|Q01768|NDKB_MOUSE	-1.08	2.11	0.95	8.8E-03
654	sp|Q3UQ44|IQGA2_MOUSE	-1.08	2.12	0.56	1.1E-02
655	sp|P55258|RAB8A_MOUSE	-1.10	2.15	0.74	2.1E-02
656	sp|O35465|FKBP8_MOUSE	-1.10	2.15	0.56	6.2E-01
657	sp|Q9DBP5|KCY_MOUSE	-1.14	2.21	0.75	1.5E-04
658	sp|Q9QYA2|TOM40_MOUSE	-1.15	2.22	0.57	2.1E-01
659	sp|O08709|PRDX6_MOUSE	-1.16	2.23	0.94	8.2E-03
660	sp|P61211|ARL1_MOUSE	-1.16	2.24	0.90	5.7E-03
661	sp|P56371|RAB4A_MOUSE	-1.17	2.25	0.80	3.7E-04
662	sp|O35857|TIM44_MOUSE	-1.17	2.25	0.83	4.3E-04
663	sp|Q9Z0M5|LICH_MOUSE	-1.18	2.27	0.58	9.0E-01
664	sp|Q9CZ42|NNRD_MOUSE	-1.18	2.27	0.78	4.1E-03
665	sp|Q9CR67|TMM33_MOUSE	-1.19	2.28	0.86	3.6E-03
666	sp|Q6GQT9|NOMO1_MOUSE	-1.19	2.28	0.53	2.4E-02
667	sp|Q6ZQI3|MLEC_MOUSE	-1.19	2.28	0.66	1.3E-02
668	sp|P16858|G3P_MOUSE	-1.19	2.29	0.92	6.5E-04
669	sp|Q91WQ3|SYYC_MOUSE	-1.20	2.30	0.57	4.1E-01
670	sp|Q8K411|PREP_MOUSE	-1.21	2.32	0.53	1.3E-01
671	sp|P47791|GSHR_MOUSE	-1.22	2.33	0.80	1.0E-01
672	sp|O55234|PSB5_MOUSE	-1.22	2.33	0.69	8.0E-03
673	sp|Q9D6U8|F162A_MOUSE	-1.23	2.35	0.51	4.4E-02
674	sp|Q9QYB5|ADDG_MOUSE	-1.24	2.36	0.76	1.5E-02
675	sp|Q9QXY6|EHD3_MOUSE	-1.24	2.37	0.86	6.4E-05
676	sp|P10649|GSTM1_MOUSE	-1.24	2.37	0.89	2.8E-04
677	sp|Q9DCZ1|GMPR1_MOUSE	-1.27	2.41	0.81	1.2E-06
678	sp|O70404|VAMP8_MOUSE	-1.27	2.41	0.77	4.8E-04
679	sp|Q9DBJ1|PGAM1_MOUSE	-1.27	2.41	0.97	2.1E-03
680	sp|Q99LX0|PARK7_MOUSE	-1.27	2.42	0.93	9.3E-03
681	sp|Q8K183|PDXK_MOUSE	-1.28	2.42	0.85	1.6E-02
682	sp|P04939|MUP3_MOUSE	-1.28	2.43	0.63	5.8E-01
683	sp|P56565|S10A1_MOUSE	-1.28	2.44	0.85	8.7E-03
684	sp|Q9R022|DJC12_MOUSE	-1.30	2.46	0.55	4.3E-02
685	sp|O70439|STX7_MOUSE	-1.32	2.49	0.76	5.3E-05
686	sp|O09117|SYPL1_MOUSE	-1.32	2.50	0.91	1.6E-03
687	sp|P17182|ENOA_MOUSE	-1.33	2.51	0.98	9.2E-04
688	sp|Q8K3A0|HSC20_MOUSE	-1.33	2.51	0.56	1.7E-01
689	sp|P15947|KLK1_MOUSE	-1.33	2.51	0.60	7.1E-01
690	sp|Q8R2K1|FUCM_MOUSE	-1.33	2.52	0.88	2.0E-02
691	sp|O35988|SDC4_MOUSE	-1.33	2.52	0.54	3.8E-05
692	sp|Q9R087|GPC6_MOUSE	-1.34	2.53	0.54	5.8E-01
693	sp|O88792|JAM1_MOUSE	-1.34	2.54	0.55	9.3E-01
694	sp|Q99KQ4|NAMPT_MOUSE	-1.36	2.57	0.82	1.5E-03
695	sp|Q9WV85|NDK3_MOUSE	-1.36	2.57	0.59	1.9E-02
696	sp|P17809|GTR1_MOUSE	-1.37	2.58	0.80	5.8E-05
697	sp|Q91XU3|PI42C_MOUSE	-1.37	2.58	0.57	4.6E-01
698	sp|Q60931|VDAC3_MOUSE	-1.37	2.59	0.74	1.4E-03
699	sp|Q9D6Y9|GLGB_MOUSE	-1.37	2.59	0.98	5.2E-05
700	sp|P56394|COX17_MOUSE	-1.37	2.59	0.69	6.4E-02
701	sp|Q9CPQ3|TOM22_MOUSE	-1.37	2.59	0.75	1.1E-03
702	sp|P47740|AL3A2_MOUSE	-1.38	2.61	0.79	5.9E-02
703	sp|Q9ESE1|LRBA_MOUSE	-1.41	2.65	0.53	3.9E-01
704	sp|Q9CQ92|FIS1_MOUSE	-1.41	2.65	0.89	3.0E-02
705	sp|P17710|HXK1_MOUSE	-1.41	2.66	0.91	3.3E-04
706	sp|Q91ZJ5|UGPA_MOUSE	-1.41	2.66	0.87	1.2E-03
707	sp|O35345|IMA7_MOUSE	-1.41	2.67	0.58	4.2E-01
708	sp|Q8VDM6|HNRL1_MOUSE	-1.42	2.67	0.58	2.7E-03

709	sp|Q8K274|KT3K_MOUSE	-1.42	2.68	0.56	4.3E-02
710	sp|Q9D5T0|ATAD1_MOUSE	-1.43	2.69	0.79	4.4E-03
711	sp|P62342|SELT_MOUSE	-1.43	2.70	0.76	1.2E-02
712	sp|Q9CYR6|AGM1_MOUSE	-1.43	2.70	0.75	1.0E-02
713	sp|P17751|TPIS_MOUSE	-1.44	2.71	0.95	1.2E-03
714	sp|Q3ULJ0|GPD1L_MOUSE	-1.44	2.72	0.87	4.2E-04
715	sp|Q9DCT1|AKCL2_MOUSE	-1.45	2.73	0.93	4.0E-05
716	sp|Q9WU84|CCS_MOUSE	-1.46	2.75	0.99	3.3E-03
717	sp|P26043|RADI_MOUSE	-1.48	2.79	0.83	3.3E-03
718	sp|P40237|CD82_MOUSE	-1.48	2.79	0.56	9.4E-01
719	sp|Q8K4Z3|NNRE_MOUSE	-1.49	2.80	0.77	3.2E-03
720	sp|P10518|HEM2_MOUSE	-1.50	2.82	0.91	2.3E-06
721	sp|Q60930|VDAC2_MOUSE	-1.50	2.84	0.94	2.9E-06
722	sp|P48193|41_MOUSE	-1.51	2.84	0.85	3.7E-04
723	sp|P27601|GNA13_MOUSE	-1.52	2.86	0.80	1.1E-02
724	sp|A3KMP2|TTC38_MOUSE	-1.52	2.87	0.87	1.2E-05
725	sp|P51906|EAA3_MOUSE	-1.52	2.88	0.50	2.2E-02
726	sp|P57016|LAD1_MOUSE	-1.53	2.89	0.66	4.4E-03
727	sp|Q3UGR5|HDHD2_MOUSE	-1.53	2.90	0.82	3.9E-01
728	sp|P59017|B2L13_MOUSE	-1.55	2.93	0.67	1.8E-01
729	sp|Q921H8|THIKA_MOUSE	-1.56	2.95	0.91	3.4E-03
730	sp|P00920|CAH2_MOUSE	-1.56	2.95	0.95	5.6E-03
731	sp|O88958|GNPI1_MOUSE	-1.56	2.96	0.89	2.9E-05
732	sp|Q60973|RBBP7_MOUSE	-1.57	2.97	0.68	4.2E-01
733	sp|Q99L04|DHRS1_MOUSE	-1.57	2.97	0.79	2.7E-02
734	sp|Q8BG51|MIRO1_MOUSE	-1.57	2.97	0.76	3.1E-04
735	sp|Q9QXW9|LAT2_MOUSE	-1.57	2.98	0.57	1.8E-04
736	sp|P50247|SAHH_MOUSE	-1.58	2.99	0.91	6.2E-04
737	sp|P28656|NP1L1_MOUSE	-1.59	3.02	0.54	8.1E-01
738	sp|P70349|HINT1_MOUSE	-1.60	3.04	0.88	4.3E-04
739	sp|Q9WVK4|EHD1_MOUSE	-1.61	3.05	0.83	1.1E-04
740	sp|Q9DD20|MET7B_MOUSE	-1.62	3.07	0.59	5.3E-03
741	sp|P97478|COQ7_MOUSE	-1.62	3.07	0.53	8.1E-02
742	sp|O35943|FRDA_MOUSE	-1.64	3.11	0.55	1.0E-02
743	sp|P56376|ACYP1_MOUSE	-1.64	3.13	0.68	2.3E-03
744	sp|P26040|EZRI_MOUSE	-1.65	3.13	0.96	5.2E-01
745	sp|P67778|PHB_MOUSE	-1.65	3.13	0.92	2.3E-03
746	sp|Q9D0F9|PGM1_MOUSE	-1.65	3.13	0.90	2.1E-04
747	sp|P46664|PURA2_MOUSE	-1.65	3.13	0.68	5.7E-01
748	sp|P03893|NU2M_MOUSE	-1.67	3.19	0.69	9.4E-03
749	sp|Q9CS42|PRPS2_MOUSE	-1.68	3.20	0.85	2.6E-04
750	sp|Q9D710|TMX2_MOUSE	-1.68	3.20	0.75	4.5E-05
751	sp|Q99J39|DCMC_MOUSE	-1.68	3.21	0.62	3.2E-03
752	sp|Q80SU7|GVIN1_MOUSE	-1.69	3.22	0.83	1.0E-01
753	sp|Q8JZQ2|AFG32_MOUSE	-1.69	3.23	0.75	6.3E-03
754	sp|P51863|VA0D1_MOUSE	-1.70	3.24	0.87	2.0E-03
755	sp|Q9D7P6|ISCU_MOUSE	-1.70	3.25	0.81	3.2E-08
756	sp|Q9QZ23|NFU1_MOUSE	-1.71	3.26	0.66	6.4E-01
757	sp|P09411|PGK1_MOUSE	-1.71	3.27	0.97	3.0E-05
758	sp|P48774|GSTM5_MOUSE	-1.71	3.27	0.87	1.3E-04
759	sp|Q9D7N9|APMAP_MOUSE	-1.71	3.28	0.84	6.0E-02
760	sp|Q9R0P3|ESTD_MOUSE	-1.72	3.28	0.86	6.8E-04
761	sp|Q64521|GPDM_MOUSE	-1.73	3.31	0.67	1.1E-01
762	sp|O09043|NAPSA_MOUSE	-1.73	3.32	0.84	3.0E-01
763	sp|P08228|SODC_MOUSE	-1.74	3.33	0.94	1.1E-02
764	sp|Q99JY0|ECHB_MOUSE	-1.75	3.37	0.87	9.0E-04
765	sp|P51660|DHB4_MOUSE	-1.76	3.39	0.95	2.5E-02
766	sp|Q9CYH2|F213A_MOUSE	-1.77	3.42	0.89	2.9E-03
767	sp|Q922B1|MACD1_MOUSE	-1.78	3.44	0.59	2.1E-01
768	sp|P11352|GPX1_MOUSE	-1.79	3.45	0.92	1.3E-02
769	sp|Q8K3J9|GPC5C_MOUSE	-1.79	3.46	0.52	1.3E-02
770	sp|Q64105|SPRE_MOUSE	-1.79	3.47	0.96	6.4E-04
771	sp|Q9JK42|PDK2_MOUSE	-1.79	3.47	0.55	4.7E-04
772	sp|Q8JZU2|TXTP_MOUSE	-1.80	3.47	0.87	3.0E-04
773	sp|P09803|CADH1_MOUSE	-1.80	3.48	0.68	6.9E-03
774	sp|Q9CZR8|EFTS_MOUSE	-1.81	3.50	0.85	3.2E-04
775	sp|P31786|ACBP_MOUSE	-1.81	3.51	0.93	8.6E-04
776	sp|Q8JZN5|ACAD9_MOUSE	-1.81	3.52	0.75	1.3E-03
777	sp|O35658|C1QBP_MOUSE	-1.82	3.52	0.83	5.7E-04
778	sp|Q9D7X8|GGCT_MOUSE	-1.83	3.55	0.99	2.0E-03
779	sp|Q3UJU9|RMD3_MOUSE	-1.83	3.55	0.75	2.2E-03
780	sp|Q9Z1G3|VATC1_MOUSE	-1.83	3.55	0.83	3.1E-07
781	sp|O70252|HMOX2_MOUSE	-1.83	3.56	0.50	4.0E-01

782	sp|Q9CPY7|AMPL_MOUSE	-1.84	3.57	0.93	2.0E-02
783	sp|Q9DCU6|RM04_MOUSE	-1.84	3.59	0.91	2.9E-06
784	sp|Q64331|MYO6_MOUSE	-1.84	3.59	0.80	2.0E-02
785	sp|P24472|GSTA4_MOUSE	-1.85	3.61	0.86	4.6E-02
786	sp|Q8CAY6|THIC_MOUSE	-1.85	3.61	0.85	2.0E-05
787	sp|Q9CQX2|CYB5B_MOUSE	-1.86	3.62	0.93	4.2E-01
788	sp|P37040|NCPR_MOUSE	-1.87	3.64	0.81	8.1E-03
789	sp|Q8K010|OPLA_MOUSE	-1.87	3.65	0.77	1.8E-04
790	sp|Q9D9V3|ECHD1_MOUSE	-1.87	3.65	0.78	7.9E-05
791	sp|P50637|TSPO_MOUSE	-1.87	3.66	0.98	1.9E-01
792	sp|P51661|DHI2_MOUSE	-1.88	3.67	0.83	2.1E-04
793	sp|P05201|AATC_MOUSE	-1.88	3.68	0.88	8.2E-04
794	sp|Q8R519|ACMSD_MOUSE	-1.88	3.69	0.69	5.3E-03
795	sp|P70245|EBP_MOUSE	-1.89	3.70	0.91	9.3E-07
796	sp|P34884|MIF_MOUSE	-1.89	3.71	0.92	1.9E-02
797	sp|Q99LP6|GRPE1_MOUSE	-1.89	3.71	0.59	5.8E-02
798	sp|O35129|PHB2_MOUSE	-1.90	3.73	0.94	1.6E-04
799	sp|P70444|BID_MOUSE	-1.90	3.74	0.74	1.0E-04
800	sp|P35802|GPM6A_MOUSE	-1.90	3.74	0.69	9.0E-05
801	sp|Q9DCJ9|NPL_MOUSE	-1.91	3.76	0.88	4.3E-03
802	sp|Q8BGC4|ZADH2_MOUSE	-1.91	3.76	0.72	2.7E-04
803	sp|P55302|AMRP_MOUSE	-1.91	3.77	0.77	3.8E-05
804	sp|O09172|GSH0_MOUSE	-1.92	3.77	0.53	4.6E-02
805	sp|Q8VDQ1|PTGR2_MOUSE	-1.92	3.79	0.89	9.8E-03
806	sp|Q8R146|APEH_MOUSE	-1.93	3.80	0.77	1.4E-03
807	sp|P70290|EM55_MOUSE	-1.93	3.82	0.91	4.5E-05
808	sp|P48962|ADT1_MOUSE	-1.93	3.82	0.83	1.0E-03
809	sp|P97449|AMPN_MOUSE	-1.94	3.83	0.95	1.8E-03
810	sp|O35969|GAMT_MOUSE	-1.94	3.83	0.64	2.0E-03
811	sp|Q9CZU6|CISY_MOUSE	-1.94	3.83	0.88	9.3E-04
812	sp|P98197|AT11A_MOUSE	-1.94	3.85	0.81	3.9E-02
813	sp|Q9Z2Z6|MCAT_MOUSE	-1.95	3.87	0.72	1.1E-01
814	sp|Q8CIM7|CP2DQ_MOUSE	-1.95	3.87	0.77	2.1E-05
815	sp|P56395|CYB5_MOUSE	-1.95	3.87	0.86	4.9E-02
816	sp|P15105|GLNA_MOUSE	-1.97	3.91	0.83	3.1E-04
817	sp|Q9D8Y1|T126A_MOUSE	-1.97	3.93	0.85	1.8E-02
818	sp|Q3TJ91|L2GL2_MOUSE	-1.98	3.94	0.71	1.0E-05
819	sp|Q9CRD0|OCAD1_MOUSE	-1.98	3.94	0.54	1.1E-02
820	sp|Q8VCF0|MAVS_MOUSE	-1.98	3.95	0.84	3.5E-04
821	sp|P58281|OPA1_MOUSE	-1.99	3.97	0.74	1.9E-02
822	sp|Q8BIJ6|SYIM_MOUSE	-1.99	3.98	0.73	4.5E-02
823	sp|P53986|MOT1_MOUSE	-1.99	3.98	0.91	6.3E-03
824	sp|O88451|RDH7_MOUSE	-1.99	3.98	0.74	2.9E-01
825	sp|P16125|LDHB_MOUSE	-2.00	3.99	0.86	1.9E-05
826	sp|Q9JHS4|CLPX_MOUSE	-2.00	3.99	0.78	2.8E-04
827	sp|Q9Z2Y8|PROSC_MOUSE	-2.00	4.01	0.90	1.8E-03
828	sp|Q791V5|MTCH2_MOUSE	-2.00	4.01	0.89	4.1E-04
829	sp|P62073|TIM10_MOUSE	-2.00	4.01	0.86	3.0E-04
830	sp|Q99L60|VATC2_MOUSE	-2.01	4.03	0.70	2.6E-04
831	sp|Q4VAE3|TMM65_MOUSE	-2.01	4.03	0.88	1.5E-02
832	sp|Q8VCA8|SCRN2_MOUSE	-2.02	4.05	0.82	5.9E-01
833	sp|P19137|LAMA1_MOUSE	-2.02	4.06	0.65	4.0E-01
834	sp|Q571I9|A16A1_MOUSE	-2.03	4.09	0.61	1.1E-03
835	sp|P18572|BASI_MOUSE	-2.03	4.09	0.87	9.2E-02
836	sp|Q9DB29|IAH1_MOUSE	-2.03	4.10	0.76	4.6E-05
837	sp|Q9DBL1|ACDSB_MOUSE	-2.04	4.10	0.93	3.9E-04
838	sp|Q8BXK9|CLIC5_MOUSE	-2.06	4.18	0.85	6.5E-03
839	sp|O70325|GPX41_MOUSE	-2.06	4.18	0.52	2.8E-04
840	sp|Q64669|NQO1_MOUSE	-2.07	4.19	0.80	2.6E-07
841	sp|Q9CR62|M2OM_MOUSE	-2.07	4.19	0.83	3.3E-03
842	sp|P06801|MAOX_MOUSE	-2.07	4.20	0.83	1.7E-02
843	sp|Q80Y14|GLRX5_MOUSE	-2.07	4.20	0.93	4.1E-04
844	sp|P16406|AMPE_MOUSE	-2.07	4.21	0.87	1.1E-02
845	sp|P30275|KCRU_MOUSE	-2.08	4.24	0.88	1.6E-04
846	sp|Q3TMH2|SCRN3_MOUSE	-2.09	4.27	0.66	4.1E-05
847	sp|P97742|CPT1A_MOUSE	-2.09	4.27	0.84	8.3E-05
848	sp|Q9D939|ST1C2_MOUSE	-2.09	4.27	0.74	4.7E-04
849	sp|P51174|ACADL_MOUSE	-2.10	4.28	0.87	1.3E-02
850	sp|Q9JLT4|TRXR2_MOUSE	-2.10	4.29	0.83	1.3E-05
851	sp|Q925I1|ATAD3_MOUSE	-2.10	4.30	0.80	2.4E-03
852	sp|Q924X2|CPT1B_MOUSE	-2.10	4.30	0.58	1.5E-03
853	sp|P10852|4F2_MOUSE	-2.12	4.34	0.91	3.5E-04
854	sp|P26443|DHE3_MOUSE	-2.13	4.37	0.92	4.0E-04

855	sp|O35855|BCAT2_MOUSE	-2.13	4.38	0.89	1.9E-05
856	sp|P57746|VATD_MOUSE	-2.14	4.40	0.89	1.5E-07
857	sp|Q6P1B1|XPP1_MOUSE	-2.14	4.40	0.87	8.8E-03
858	sp|Q3UMF0|COBL1_MOUSE	-2.14	4.40	0.54	3.0E-03
859	sp|Q99J99|THTM_MOUSE	-2.14	4.41	0.83	3.2E-04
860	sp|O35490|BHMT1_MOUSE	-2.14	4.42	0.66	1.1E-01
861	sp|Q8BJZ4|RT35_MOUSE	-2.15	4.43	0.81	3.2E-03
862	sp|Q9WVA2|TIM8A_MOUSE	-2.15	4.45	0.67	7.1E-03
863	sp|Q8BMS1|ECHA_MOUSE	-2.16	4.46	0.97	1.5E-02
864	sp|O35972|RM23_MOUSE	-2.16	4.46	0.61	9.6E-07
865	sp|P05063|ALDOC_MOUSE	-2.16	4.47	0.70	4.0E-02
866	sp|Q9CXT8|MPPB_MOUSE	-2.17	4.51	0.71	3.9E-01
867	sp|Q8BH59|CMC1_MOUSE	-2.17	4.51	0.84	7.9E-05
868	sp|Q8BFR5|EFTU_MOUSE	-2.18	4.54	0.95	1.3E-04
869	sp|Q99KB8|GLO2_MOUSE	-2.18	4.54	0.77	3.6E-03
870	sp|Q9CWS0|DDAH1_MOUSE	-2.19	4.57	0.83	8.7E-04
871	sp|P29758|OAT_MOUSE	-2.20	4.59	0.86	4.6E-02
872	sp|P08905|LYZ2_MOUSE	-2.20	4.60	0.93	1.0E-04
873	sp|O35143|ATIF1_MOUSE	-2.21	4.61	0.83	9.7E-03
874	sp|Q8CAQ8|MIC60_MOUSE	-2.22	4.65	0.92	2.4E-03
875	sp|Q8CGK3|LONM_MOUSE	-2.22	4.66	0.90	1.6E-05
876	sp|P50431|GLYC_MOUSE	-2.22	4.67	0.77	3.0E-03
877	sp|Q9WV98|TIM9_MOUSE	-2.23	4.68	0.77	1.4E-04
878	sp|Q8BGH2|SAM50_MOUSE	-2.23	4.69	0.89	5.3E-05
879	sp|Q78IK4|MIC27_MOUSE	-2.23	4.70	0.81	3.6E-06
880	sp|Q9DCB8|ISCA2_MOUSE	-2.24	4.73	0.82	1.5E-03
881	sp|O88844|IDHC_MOUSE	-2.25	4.75	0.90	2.2E-04
882	sp|O08756|HCD2_MOUSE	-2.25	4.76	0.91	8.3E-06
883	sp|P42125|ECI1_MOUSE	-2.26	4.80	0.91	4.3E-04
884	sp|P16331|PH4H_MOUSE	-2.27	4.83	0.84	3.5E-03
885	sp|Q9Z2I0|LETM1_MOUSE	-2.27	4.84	0.79	3.2E-04
886	sp|P28271|ACOC_MOUSE	-2.28	4.84	0.94	9.1E-05
887	sp|P34914|HYES_MOUSE	-2.28	4.85	0.81	1.1E-01
888	sp|Q60932|VDAC1_MOUSE	-2.28	4.85	0.96	4.0E-04
889	sp|Q9CQZ5|NDUA6_MOUSE	-2.28	4.86	0.84	4.6E-05
890	sp|Q9D6R2|IDH3A_MOUSE	-2.28	4.86	0.91	2.7E-04
891	sp|Q8VE95|CH082_MOUSE	-2.29	4.88	0.64	2.2E-02
892	sp|Q9JHW2|NIT2_MOUSE	-2.29	4.88	0.90	7.8E-04
893	sp|O88696|CLPP_MOUSE	-2.29	4.89	0.73	3.3E-06
894	sp|Q9DB15|RM12_MOUSE	-2.29	4.89	0.91	5.8E-04
895	sp|P97493|THIOM_MOUSE	-2.29	4.90	0.90	2.4E-05
896	sp|Q99J94|SO1A6_MOUSE	-2.30	4.92	0.79	8.2E-04
897	sp|P97364|SPS2_MOUSE	-2.30	4.93	0.90	1.3E-03
898	sp|P14152|MDHC_MOUSE	-2.30	4.94	0.95	6.7E-04
899	sp|P47934|CACP_MOUSE	-2.31	4.95	0.74	1.2E-03
900	sp|Q60648|SAP3_MOUSE	-2.31	4.96	0.85	1.4E-02
901	sp|Q9WV92|E41L3_MOUSE	-2.31	4.96	0.86	8.2E-04
902	sp|Q8CFA2|GCST_MOUSE	-2.32	4.98	0.69	2.7E-02
903	sp|Q60597|ODO1_MOUSE	-2.32	5.00	0.91	4.9E-07
904	sp|Q9R0H0|ACOX1_MOUSE	-2.33	5.01	0.78	1.3E-01
905	sp|Q8VDK1|NIT1_MOUSE	-2.33	5.03	0.90	2.1E-04
906	sp|P62077|TIM8B_MOUSE	-2.33	5.03	0.80	1.6E-06
907	sp|Q9QZA0|CAH5B_MOUSE	-2.33	5.03	0.56	2.3E-01
908	sp|Q8BTY1|KAT1_MOUSE	-2.34	5.05	0.69	1.3E-04
909	sp|Q8BVI4|DHPR_MOUSE	-2.34	5.07	0.88	4.0E-04
910	sp|Q60936|ADCK3_MOUSE	-2.35	5.10	0.65	1.0E-04
911	sp|Q9WTP7|KAD3_MOUSE	-2.35	5.10	0.89	2.4E-04
912	sp|P50544|ACADV_MOUSE	-2.36	5.12	0.89	4.2E-05
913	sp|P97823|LYPA1_MOUSE	-2.36	5.13	0.90	1.4E-04
914	sp|P51855|GSHB_MOUSE	-2.37	5.17	0.82	2.8E-03
915	sp|O89106|FHIT_MOUSE	-2.37	5.18	0.58	3.5E-02
916	sp|Q99M87|DNJA3_MOUSE	-2.38	5.19	0.72	5.3E-02
917	sp|Q9R112|SQRD_MOUSE	-2.38	5.20	0.92	2.4E-04
918	sp|Q3UP75|UD3A1_MOUSE	-2.38	5.20	0.72	2.3E-04
919	sp|P00158|CYB_MOUSE	-2.38	5.20	0.67	3.0E-02
920	sp|Q9WTP6|KAD2_MOUSE	-2.38	5.21	0.86	3.5E-04
921	sp|P20108|PRDX3_MOUSE	-2.39	5.23	0.90	5.7E-04
922	sp|Q8VHG0|FMO4_MOUSE	-2.39	5.24	0.52	3.6E-04
923	sp|Q8BMF4|ODP2_MOUSE	-2.39	5.25	0.98	1.4E-04
924	sp|Q6PB66|LPPRC_MOUSE	-2.40	5.26	0.88	1.0E-03
925	sp|P58137|ACOT8_MOUSE	-2.40	5.27	0.76	1.6E-03
926	sp|Q9DCQ2|ASPD_MOUSE	-2.41	5.31	0.69	4.4E-03
927	sp|P50518|VATE1_MOUSE	-2.41	5.32	0.91	1.4E-06

928	sp|Q9Z2I9|SUCB1_MOUSE	-2.42	5.33	0.97	2.2E-04
929	sp|Q07417|ACADS_MOUSE	-2.42	5.36	0.89	5.2E-03
930	sp|Q9QYR9|ACOT2_MOUSE	-2.43	5.38	0.79	1.9E-02
931	sp|Q8R1G2|CMBL_MOUSE	-2.43	5.38	0.85	2.7E-03
932	sp|Q9CQ62|DECR_MOUSE	-2.43	5.39	0.89	1.8E-03
933	sp|P47802|MTX1_MOUSE	-2.43	5.41	0.74	2.0E-01
934	sp|Q8BH86|CN159_MOUSE	-2.43	5.41	0.83	1.6E-02
935	sp|Q8BMC1|VATG3_MOUSE	-2.44	5.43	0.94	6.5E-04
936	sp|Q9D1K2|VATF_MOUSE	-2.45	5.45	0.90	7.0E-04
937	sp|O35459|ECH1_MOUSE	-2.45	5.46	0.97	5.0E-04
938	sp|Q8BLF1|NCEH1_MOUSE	-2.45	5.47	0.92	1.2E-02
939	sp|Q8R3P0|ACY2_MOUSE	-2.46	5.49	0.58	2.0E-03
940	sp|P97494|GSH1_MOUSE	-2.46	5.49	0.86	6.8E-03
941	sp|Q91WN4|KMO_MOUSE	-2.46	5.49	0.71	9.6E-04
942	sp|B2RSH2|GNAI1_MOUSE	-2.46	5.51	0.55	8.4E-03
943	sp|Q68FL4|SAHH3_MOUSE	-2.46	5.51	0.76	1.6E-01
944	sp|Q9D7J9|ECHD3_MOUSE	-2.46	5.51	0.67	5.7E-03
945	sp|P62814|VATB2_MOUSE	-2.47	5.52	0.85	1.2E-03
946	sp|Q9WV69|DEMA_MOUSE	-2.47	5.52	0.53	3.5E-03
947	sp|Q9CRB9|MIC19_MOUSE	-2.47	5.53	0.90	1.4E-02
948	sp|O09111|NDUBB_MOUSE	-2.47	5.53	0.90	1.5E-06
949	sp|Q8QZS1|HIBCH_MOUSE	-2.47	5.55	0.89	2.6E-04
950	sp|P38647|GRP75_MOUSE	-2.47	5.56	0.82	3.6E-02
951	sp|Q8VCR7|ABHEB_MOUSE	-2.48	5.57	0.93	3.6E-06
952	sp|Q8VEM8|MPCP_MOUSE	-2.48	5.57	0.90	1.9E-04
953	sp|P35486|ODPA_MOUSE	-2.48	5.58	0.92	7.5E-06
954	sp|P62075|TIM13_MOUSE	-2.48	5.58	0.96	1.3E-04
955	sp|Q9CXV1|DHSD_MOUSE	-2.49	5.60	0.60	1.4E-04
956	sp|P00375|DYR_MOUSE	-2.49	5.60	0.79	2.4E-02
957	sp|O35215|DOPD_MOUSE	-2.49	5.63	0.91	2.5E-03
958	sp|O55137|ACOT1_MOUSE	-2.49	5.63	0.85	3.5E-03
959	sp|Q922Q1|MARC2_MOUSE	-2.50	5.65	0.89	1.0E-04
960	sp|P35846|FOLR1_MOUSE	-2.50	5.66	0.64	2.7E-02
961	sp|Q8BWN8|ACOT4_MOUSE	-2.51	5.68	0.81	3.1E-02
962	sp|G5E8K5|ANK3_MOUSE	-2.51	5.70	0.85	2.5E-05
963	sp|P52825|CPT2_MOUSE	-2.51	5.70	0.88	9.9E-04
964	sp|Q921G7|ETFD_MOUSE	-2.52	5.74	0.89	1.6E-03
965	sp|Q922H2|PDK3_MOUSE	-2.52	5.75	0.66	4.3E-02
966	sp|Q9JLJ2|AL9A1_MOUSE	-2.53	5.76	0.94	5.2E-03
967	sp|Q9CQZ6|NDUB3_MOUSE	-2.53	5.76	0.76	3.9E-05
968	sp|Q9QXG4|ACSA_MOUSE	-2.53	5.76	0.65	8.7E-03
969	sp|Q9CQN1|TRAP1_MOUSE	-2.54	5.82	0.88	7.5E-04
970	sp|P47738|ALDH2_MOUSE	-2.54	5.82	0.95	1.3E-05
971	sp|Q61133|GSTT2_MOUSE	-2.55	5.84	0.87	2.8E-04
972	sp|Q9D1I5|MCEE_MOUSE	-2.55	5.85	0.76	5.6E-04
973	sp|Q8BKZ9|ODPX_MOUSE	-2.55	5.86	0.72	6.3E-04
974	sp|Q8BGD8|COA6_MOUSE	-2.55	5.87	0.67	2.2E-01
975	sp|Q91X52|DCXR_MOUSE	-2.57	5.92	0.88	7.7E-03
976	sp|Q9CQ54|NDUC2_MOUSE	-2.57	5.93	0.88	4.1E-07
977	sp|Q6DYE8|ENPP3_MOUSE	-2.57	5.94	0.71	6.1E-04
978	sp|Q8BVE3|VATH_MOUSE	-2.57	5.94	0.90	9.3E-03
979	sp|Q99JB7|AMNLS_MOUSE	-2.57	5.95	0.64	3.4E-01
980	sp|P17426|AP2A1_MOUSE	-2.57	5.95	0.65	3.2E-02
981	sp|O88441|MTX2_MOUSE	-2.58	5.96	0.79	1.8E-01
982	sp|Q9D2R6|COA3_MOUSE	-2.58	5.98	0.55	9.1E-05
983	sp|Q9DCM0|ETHE1_MOUSE	-2.58	5.99	0.92	3.6E-03
984	sp|P03888|NU1M_MOUSE	-2.58	6.00	0.74	6.4E-05
985	sp|Q8VI47|MRP2_MOUSE	-2.59	6.03	0.82	8.2E-04
986	sp|Q8K0H1|S47A1_MOUSE	-2.59	6.03	0.53	2.3E-02
987	sp|P50516|VATA_MOUSE	-2.59	6.04	0.92	1.3E-06
988	sp|Q9D051|ODPB_MOUSE	-2.60	6.05	0.96	7.1E-05
989	sp|Q8BJ64|CHDH_MOUSE	-2.60	6.06	0.88	8.9E-04
990	sp|Q9DCJ5|NDUA8_MOUSE	-2.60	6.07	0.91	3.7E-07
991	sp|P50171|DHB8_MOUSE	-2.60	6.07	0.87	5.5E-04
992	sp|P05202|AATM_MOUSE	-2.61	6.10	0.97	1.8E-04
993	sp|Q9CQJ8|NDUB9_MOUSE	-2.61	6.10	0.83	1.4E-04
994	sp|O55126|NIPS2_MOUSE	-2.62	6.13	0.66	2.1E-01
995	sp|Q9Z2H5|E41L1_MOUSE	-2.62	6.14	0.67	1.3E-01
996	sp|Q64433|CH10_MOUSE	-2.62	6.15	0.90	7.4E-04
997	sp|P03899|NU3M_MOUSE	-2.62	6.15	0.95	1.5E-03
998	sp|Q9CQQ7|AT5F1_MOUSE	-2.62	6.17	0.92	3.2E-04
999	sp|Q9D2R0|AACS_MOUSE	-2.64	6.24	0.60	1.1E-01
1000	sp|Q9QXD1|ACOX2_MOUSE	-2.64	6.24	0.84	6.1E-04

1001	sp|Q9JLF6|TGM1_MOUSE	-2.65	6.27	0.77	3.7E-03
1002	sp|Q71RI9|KAT3_MOUSE	-2.65	6.29	0.81	7.8E-03
1003	sp|P97450|ATP5J_MOUSE	-2.65	6.29	0.97	2.8E-03
1004	sp|Q8BWM0|PGES2_MOUSE	-2.65	6.29	0.89	8.1E-04
1005	sp|Q9EP89|LACTB_MOUSE	-2.65	6.30	0.72	3.8E-04
1006	sp|P99029|PRDX5_MOUSE	-2.65	6.30	0.91	5.2E-04
1007	sp|Q91YI0|ARLY_MOUSE	-2.66	6.31	0.91	3.6E-04
1008	sp|P53395|ODB2_MOUSE	-2.66	6.31	0.81	1.3E-03
1009	sp|Q9CPQ1|COX6C_MOUSE	-2.66	6.33	0.91	7.0E-04
1010	sp|Q14DH7|ACSS3_MOUSE	-2.66	6.33	0.63	1.1E-01
1011	sp|Q9DCS3|MECR_MOUSE	-2.66	6.33	0.73	6.4E-03
1012	sp|Q9D855|QCR7_MOUSE	-2.66	6.34	0.89	4.4E-03
1013	sp|Q5M8N4|D39U1_MOUSE	-2.67	6.35	0.73	1.2E-02
1014	sp|Q99JR1|SFXN1_MOUSE	-2.67	6.35	0.83	1.7E-03
1015	sp|P17665|COX7C_MOUSE	-2.67	6.35	0.80	6.1E-04
1016	sp|Q99KR7|PPIF_MOUSE	-2.67	6.36	0.57	5.2E-03
1017	sp|Q9Z1P6|NDUA7_MOUSE	-2.67	6.36	0.91	8.8E-05
1018	sp|Q9CZ13|QCR1_MOUSE	-2.67	6.37	0.94	4.0E-04
1019	sp|Q9DBX3|SUSD2_MOUSE	-2.67	6.38	0.92	8.7E-04
1020	sp|Q8R086|SUOX_MOUSE	-2.68	6.39	0.56	4.0E-02
1021	sp|Q99LB2|DHRS4_MOUSE	-2.68	6.42	0.91	1.1E-01
1022	sp|Q91WK5|GCSH_MOUSE	-2.68	6.42	0.74	1.9E-03
1023	sp|P56382|ATP5E_MOUSE	-2.68	6.42	0.61	2.4E-02
1024	sp|Q8K4F5|ABHDB_MOUSE	-2.69	6.43	0.63	3.6E-06
1025	sp|Q8VBW8|TTC36_MOUSE	-2.69	6.45	0.74	1.4E-02
1026	sp|Q03265|ATPA_MOUSE	-2.69	6.46	0.96	5.8E-04
1027	sp|Q8CC88|VWA8_MOUSE	-2.69	6.46	0.82	8.0E-04
1028	sp|Q920R6|VPP4_MOUSE	-2.69	6.46	0.78	6.0E-04
1029	sp|Q9CPP6|NDUA5_MOUSE	-2.69	6.48	0.90	3.9E-04
1030	sp|P56391|CX6B1_MOUSE	-2.70	6.48	0.92	3.2E-05
1031	sp|Q91Z53|GRHPR_MOUSE	-2.70	6.49	0.79	7.7E-03
1032	sp|Q8R2N1|AQP3_MOUSE	-2.70	6.51	0.90	2.8E-03
1033	sp|P11404|FABPH_MOUSE	-2.71	6.53	0.88	1.3E-04
1034	sp|Q99MS3|MP17L_MOUSE	-2.71	6.55	0.59	1.3E-02
1035	sp|P56480|ATPB_MOUSE	-2.71	6.55	0.94	1.5E-04
1036	sp|P97807|FUMH_MOUSE	-2.71	6.56	0.89	1.3E-07
1037	sp|P98078|DAB2_MOUSE	-2.71	6.56	0.79	1.1E-03
1038	sp|Q78IK2|USMG5_MOUSE	-2.72	6.60	0.97	1.2E-03
1039	sp|Q06185|ATP5I_MOUSE	-2.73	6.62	0.90	1.2E-03
1040	sp|P08249|MDHM_MOUSE	-2.73	6.63	0.96	6.1E-05
1041	sp|Q9DCT2|NDUS3_MOUSE	-2.73	6.64	0.96	3.1E-04
1042	sp|Q99KI0|ACON_MOUSE	-2.74	6.66	0.90	8.9E-04
1043	sp|Q8BYF6|SC5A8_MOUSE	-2.74	6.69	0.58	5.5E-03
1044	sp|Q9D172|ES1_MOUSE	-2.75	6.71	0.92	3.9E-04
1045	sp|Q91WD5|NDUS2_MOUSE	-2.75	6.72	0.91	2.9E-04
1046	sp|Q9WUR2|ECI2_MOUSE	-2.75	6.73	0.85	1.8E-03
1047	sp|A2AJL3|FGGY_MOUSE	-2.75	6.73	0.85	6.8E-04
1048	sp|Q60866|PTER_MOUSE	-2.75	6.73	0.91	2.3E-05
1049	sp|Q8VC69|S22A6_MOUSE	-2.76	6.76	0.71	3.2E-02
1050	sp|Q9Z0S1|BPNT1_MOUSE	-2.77	6.81	0.87	6.4E-05
1051	sp|Q91ZA3|PCCA_MOUSE	-2.77	6.83	0.84	5.1E-04
1052	sp|O09174|AMACR_MOUSE	-2.77	6.84	0.62	8.7E-02
1053	sp|Q9DB20|ATPO_MOUSE	-2.77	6.84	0.96	1.1E-03
1054	sp|Q9D826|SOX_MOUSE	-2.77	6.84	0.76	5.1E-02
1055	sp|Q9CQ75|NDUA2_MOUSE	-2.78	6.87	0.77	4.0E-04
1056	sp|P68368|TBA4A_MOUSE	-2.79	6.89	0.88	3.0E-05
1057	sp|Q9D2G2|ODO2_MOUSE	-2.79	6.89	0.89	6.1E-05
1058	sp|Q02013|AQP1_MOUSE	-2.79	6.91	0.80	4.8E-03
1059	sp|P55014|S12A1_MOUSE	-2.79	6.91	0.96	1.9E-04
1060	sp|Q99LC3|NDUAA_MOUSE	-2.79	6.92	0.93	1.8E-04
1061	sp|Q7TMF3|NDUAC_MOUSE	-2.79	6.93	0.76	4.4E-04
1062	sp|Q91VR2|ATPG_MOUSE	-2.80	6.96	0.90	2.5E-04
1063	sp|P03930|ATP8_MOUSE	-2.80	6.97	0.90	8.4E-04
1064	sp|Q8K3J1|NDUS8_MOUSE	-2.81	7.02	0.80	4.2E-04
1065	sp|P51881|ADT2_MOUSE	-2.82	7.06	0.81	7.5E-05
1066	sp|Q9CPX8|QCR10_MOUSE	-2.83	7.11	0.80	1.4E-02
1067	sp|Q9CPU4|MGST3_MOUSE	-2.83	7.12	0.84	2.8E-02
1068	sp|Q9CQ69|QCR8_MOUSE	-2.83	7.12	0.91	1.0E-04
1069	sp|Q922D8|C1TC_MOUSE	-2.83	7.12	0.87	4.0E-05
1070	sp|Q9DCV4|RMD1_MOUSE	-2.83	7.13	0.70	1.1E-02
1071	sp|Q9DB77|QCR2_MOUSE	-2.84	7.14	0.94	2.3E-04
1072	sp|P28825|MEP1A_MOUSE	-2.84	7.15	0.88	2.4E-03
1073	sp|Q9DBF1|AL7A1_MOUSE	-2.84	7.16	0.82	2.4E-04

1074	sp|O08749|DLDH_MOUSE	-2.84	7.18	0.94	1.2E-04
1075	sp|Q9Z2H7|GIPC2_MOUSE	-2.84	7.18	0.72	9.8E-04
1076	sp|Q91VT4|CBR4_MOUSE	-2.85	7.19	0.85	7.6E-04
1077	sp|Q9CXZ1|NDUS4_MOUSE	-2.85	7.19	0.83	2.1E-04
1078	sp|Q9QXX4|CMC2_MOUSE	-2.85	7.20	0.80	2.7E-04
1079	sp|Q9DC50|OCTC_MOUSE	-2.85	7.20	0.80	3.7E-02
1080	sp|Q9DCX2|ATP5H_MOUSE	-2.85	7.21	0.93	1.8E-03
1081	sp|Q8BH95|ECHM_MOUSE	-2.85	7.21	0.90	5.1E-05
1082	sp|Q9CQC7|NDUB4_MOUSE	-2.85	7.21	0.83	1.1E-04
1083	sp|Q99MR8|MCCA_MOUSE	-2.86	7.25	0.82	7.4E-06
1084	sp|P16332|MUTA_MOUSE	-2.86	7.27	0.81	2.3E-05
1085	sp|P56389|CDD_MOUSE	-2.86	7.28	0.81	6.7E-05
1086	sp|Q9Z0X1|AIFM1_MOUSE	-2.87	7.30	0.92	3.7E-05
1087	sp|Q62425|NDUA4_MOUSE	-2.87	7.30	0.89	5.2E-06
1088	sp|Q9CR51|VATG1_MOUSE	-2.87	7.31	0.83	5.2E-04
1089	sp|Q8C5H8|NAKD2_MOUSE	-2.87	7.33	0.95	2.5E-04
1090	sp|Q9D7B6|ACAD8_MOUSE	-2.88	7.36	0.75	1.6E-02
1091	sp|P48771|CX7A2_MOUSE	-2.88	7.37	0.92	5.2E-05
1092	sp|Q80XL6|ACD11_MOUSE	-2.89	7.41	0.80	1.3E-01
1093	sp|P19783|COX41_MOUSE	-2.90	7.46	0.94	1.4E-04
1094	sp|Q8R404|MIC13_MOUSE	-2.90	7.47	0.72	6.8E-04
1095	sp|Q9DCS2|CP013_MOUSE	-2.90	7.48	0.87	7.5E-03
1096	sp|Q9CQX8|RT36_MOUSE	-2.92	7.55	0.67	7.3E-03
1097	sp|Q91VD9|NDUS1_MOUSE	-2.92	7.55	0.94	1.1E-04
1098	sp|Q9CZB0|C560_MOUSE	-2.92	7.55	0.83	1.6E-04
1099	sp|P63038|CH60_MOUSE	-2.92	7.56	0.96	1.0E-03
1100	sp|O09173|HGD_MOUSE	-2.92	7.58	0.84	4.4E-03
1101	sp|P56392|CX7A1_MOUSE	-2.93	7.60	0.93	8.9E-05
1102	sp|A2ARV4|LRP2_MOUSE	-2.93	7.60	0.84	9.6E-04
1103	sp|Q99KP3|CRYL1_MOUSE	-2.93	7.62	0.90	3.6E-04
1104	sp|Q91WR5|AK1CL_MOUSE	-2.94	7.66	0.79	2.6E-02
1105	sp|P41216|ACSL1_MOUSE	-2.94	7.69	0.90	9.5E-03
1106	sp|P47199|QOR_MOUSE	-2.95	7.71	0.84	1.2E-04
1107	sp|P61110|ANRE_MOUSE	-2.95	7.73	0.77	1.7E-03
1108	sp|Q8BP40|PPA6_MOUSE	-2.95	7.74	0.85	3.2E-05
1109	sp|P52196|THTR_MOUSE	-2.95	7.75	0.89	4.6E-04
1110	sp|P10637|TAU_MOUSE	-2.96	7.76	0.83	2.2E-03
1111	sp|Q99LY9|NDUS5_MOUSE	-2.96	7.78	0.67	3.7E-02
1112	sp|Q9CR61|NDUB7_MOUSE	-2.96	7.79	0.84	9.2E-04
1113	sp|P61458|PHS_MOUSE	-2.96	7.81	0.80	2.5E-03
1114	sp|P32020|NLTP_MOUSE	-2.97	7.82	0.88	4.9E-02
1115	sp|Q9DBL7|COASY_MOUSE	-2.97	7.83	0.85	2.4E-03
1116	sp|Q8C165|P20D1_MOUSE	-2.97	7.83	0.53	3.9E-04
1117	sp|Q9JLZ3|AUHM_MOUSE	-2.97	7.85	0.85	1.0E-01
1118	sp|Q9CQ91|NDUA3_MOUSE	-2.98	7.86	0.89	7.5E-03
1119	sp|Q8K023|AKC1H_MOUSE	-2.98	7.87	0.56	7.5E-03
1120	sp|O08966|S22A1_MOUSE	-2.98	7.88	0.74	1.5E-01
1121	sp|Q9CR68|UCRI_MOUSE	-2.98	7.89	0.91	4.3E-04
1122	sp|Q8BWT1|THIM_MOUSE	-2.98	7.90	0.91	2.0E-03
1123	sp|P70404|IDHG1_MOUSE	-2.98	7.91	0.91	1.0E-03
1124	sp|Q8K1Z0|COQ9_MOUSE	-2.98	7.91	0.90	1.1E-04
1125	sp|B1AXP6|TOM5_MOUSE	-2.99	7.94	1.00	2.2E-03
1126	sp|Q9DCU9|HOGA1_MOUSE	-2.99	7.95	0.69	2.7E-02
1127	sp|Q9D0M3|CY1_MOUSE	-2.99	7.96	0.94	9.6E-04
1128	sp|O55060|TPMT_MOUSE	-3.00	7.98	0.93	1.3E-04
1129	sp|Q9CQA3|SDHB_MOUSE	-3.00	7.99	0.89	2.6E-04
1130	sp|P00405|COX2_MOUSE	-3.00	7.99	0.87	3.4E-03
1131	sp|Q9DBE0|CSAD_MOUSE	-3.00	8.00	0.90	6.7E-03
1132	sp|Q9ERS2|NDUAD_MOUSE	-3.00	8.00	0.89	4.1E-05
1133	sp|Q9DCZ4|MIC26_MOUSE	-3.01	8.03	0.75	4.1E-07
1134	sp|Q61391|NEP_MOUSE	-3.01	8.05	0.90	1.5E-02
1135	sp|P70441|NHRF1_MOUSE	-3.01	8.07	0.94	5.1E-03
1136	sp|P56379|68MP_MOUSE	-3.02	8.12	0.71	1.4E-03
1137	sp|Q9DCW4|ETFB_MOUSE	-3.02	8.13	0.91	4.0E-04
1138	sp|Q8JZV9|BDH2_MOUSE	-3.02	8.13	0.82	4.4E-03
1139	sp|P46656|ADX_MOUSE	-3.03	8.16	0.61	5.5E-03
1140	sp|Q9DC70|NDUS7_MOUSE	-3.03	8.16	0.94	1.4E-06
1141	sp|Q9D8I3|GLOD5_MOUSE	-3.03	8.17	0.56	2.8E-02
1142	sp|P17563|SBP1_MOUSE	-3.03	8.19	0.92	3.9E-05
1143	sp|P54071|IDHP_MOUSE	-3.04	8.21	0.93	4.2E-04
1144	sp|O35409|FOLH1_MOUSE	-3.04	8.24	0.58	2.3E-03
1145	sp|P19536|COX5B_MOUSE	-3.04	8.24	0.91	2.9E-05
1146	sp|Q8BJ03|COX15_MOUSE	-3.04	8.24	0.50	6.3E-01

1147	sp|O35683|NDUA1_MOUSE	-3.05	8.25	0.86	2.5E-03
1148	sp|P99028|QCR6_MOUSE	-3.05	8.31	0.93	1.4E-03
1149	sp|Q9D3D9|ATPD_MOUSE	-3.06	8.32	0.98	4.6E-04
1150	sp|P55096|ABCD3_MOUSE	-3.06	8.36	0.88	5.1E-03
1151	sp|Q9DC69|NDUA9_MOUSE	-3.07	8.38	0.89	6.4E-05
1152	sp|Q91YT0|NDUV1_MOUSE	-3.07	8.43	0.90	7.9E-06
1153	sp|Q91VM9|IPYR2_MOUSE	-3.09	8.50	0.83	1.4E-01
1154	sp|Q9D6J6|NDUV2_MOUSE	-3.09	8.50	0.84	1.6E-03
1155	sp|Q6P3A8|ODBB_MOUSE	-3.09	8.53	0.78	1.2E-03
1156	sp|Q9WUM5|SUCA_MOUSE	-3.10	8.55	0.94	9.3E-04
1157	sp|Q9DCS9|NDUBA_MOUSE	-3.11	8.63	0.86	3.7E-03
1158	sp|Q8K2B3|SDHA_MOUSE	-3.11	8.64	0.98	3.4E-06
1159	sp|Q99MZ7|PECR_MOUSE	-3.11	8.65	0.87	1.9E-02
1160	sp|P03921|NU5M_MOUSE	-3.12	8.67	0.88	3.1E-02
1161	sp|Q9D6J5|NDUB8_MOUSE	-3.12	8.67	0.86	3.9E-06
1162	sp|Q9DCC7|ISC2B_MOUSE	-3.12	8.68	0.71	2.6E-03
1163	sp|Q9R0M5|TPK1_MOUSE	-3.12	8.69	0.79	6.3E-03
1164	sp|Q80W22|THNS2_MOUSE	-3.12	8.70	0.83	1.2E-03
1165	sp|P52503|NDUS6_MOUSE	-3.12	8.72	0.81	2.4E-04
1166	sp|G3X9C2|FBX50_MOUSE	-3.13	8.73	0.80	5.4E-04
1167	sp|Q8R4N0|CLYBL_MOUSE	-3.13	8.75	0.80	4.1E-04
1168	sp|Q3TC72|FAHD2_MOUSE	-3.13	8.76	0.80	5.6E-04
1169	sp|P03911|NU4M_MOUSE	-3.14	8.79	0.89	1.3E-02
1170	sp|O55125|NIPS1_MOUSE	-3.14	8.81	0.91	8.3E-04
1171	sp|Q9CQR4|ACO13_MOUSE	-3.14	8.84	0.77	4.2E-04
1172	sp|P13707|GPDA_MOUSE	-3.15	8.85	0.91	8.0E-04
1173	sp|Q8CFZ5|S22AC_MOUSE	-3.15	8.90	0.78	2.7E-01
1174	sp|Q5U5V2|HYKK_MOUSE	-3.15	8.91	0.80	1.6E-02
1175	sp|Q99K67|AASS_MOUSE	-3.16	8.94	0.73	1.9E-04
1176	sp|P09242|PPBT_MOUSE	-3.17	8.99	0.74	5.9E-03
1177	sp|Q3UEG6|AGT2_MOUSE	-3.17	9.01	0.71	6.8E-05
1178	sp|Q3V0K9|PLSI_MOUSE	-3.17	9.01	0.86	1.0E-05
1179	sp|Q9CQH3|NDUB5_MOUSE	-3.17	9.01	0.85	6.9E-07
1180	sp|Q99LC5|ETFA_MOUSE	-3.18	9.07	0.93	5.5E-05
1181	sp|P12787|COX5A_MOUSE	-3.18	9.08	0.94	1.1E-03
1182	sp|P59158|S12A3_MOUSE	-3.18	9.09	0.63	8.8E-03
1183	sp|Q7TNG8|LDHD_MOUSE	-3.19	9.10	0.88	7.4E-02
1184	sp|P48758|CBR1_MOUSE	-3.19	9.11	0.92	6.1E-02
1185	sp|Q9D6Y7|MSRA_MOUSE	-3.19	9.12	0.83	1.0E-04
1186	sp|P56135|ATPK_MOUSE	-3.20	9.17	0.80	2.6E-04
1187	sp|Q9CR21|ACPM_MOUSE	-3.20	9.19	0.92	2.3E-04
1188	sp|P38060|HMGCL_MOUSE	-3.21	9.26	0.92	1.9E-03
1189	sp|Q8R1I1|QCR9_MOUSE	-3.22	9.30	0.67	3.7E-05
1190	sp|Q9D173|TOM7_MOUSE	-3.22	9.30	0.57	1.5E-02
1191	sp|Q9D0K2|SCOT1_MOUSE	-3.22	9.34	0.92	2.1E-04
1192	sp|Q8CI85|CAH12_MOUSE	-3.24	9.46	0.58	9.8E-04
1193	sp|Q9JIZ0|CMLO1_MOUSE	-3.24	9.47	0.67	2.9E-02
1194	sp|Q8BWF0|SSDH_MOUSE	-3.24	9.47	0.88	4.5E-04
1195	sp|P62897|CYC_MOUSE	-3.25	9.49	0.92	3.4E-04
1196	sp|Q91Y63|S13A3_MOUSE	-3.25	9.52	0.88	3.6E-05
1197	sp|Q62433|NDRG1_MOUSE	-3.25	9.52	0.99	8.0E-04
1198	sp|O88909|S22A8_MOUSE	-3.25	9.52	0.80	4.6E-03
1199	sp|Q99JW2|ACY1_MOUSE	-3.26	9.59	0.77	3.3E-01
1200	sp|Q9D8B4|NDUAB_MOUSE	-3.26	9.60	0.62	7.3E-03
1201	sp|Q9DBT9|M2GD_MOUSE	-3.27	9.68	0.78	1.6E-05
1202	sp|P62627|DLRB1_MOUSE	-3.28	9.69	0.63	6.0E-01
1203	sp|Q3UFF7|LYPL1_MOUSE	-3.28	9.71	0.73	1.5E-02
1204	sp|Q91WS0|CISD1_MOUSE	-3.29	9.75	0.95	5.8E-04
1205	sp|Q3UIU2|NDUB6_MOUSE	-3.29	9.77	0.81	4.6E-03
1206	sp|Q61425|HCDH_MOUSE	-3.30	9.82	0.90	3.7E-03
1207	sp|Q8BGS1|E41L5_MOUSE	-3.30	9.84	0.77	1.3E-05
1208	sp|Q78KK3|S22AI_MOUSE	-3.30	9.86	0.90	2.0E-03
1209	sp|Q8CG76|ARK72_MOUSE	-3.30	9.87	0.87	9.6E-04
1210	sp|P97328|KHK_MOUSE	-3.31	9.90	0.83	1.1E-02
1211	sp|Q5SWY8|SC5AA_MOUSE	-3.31	9.93	0.63	9.1E-03
1212	sp|Q8R0Y6|AL1L1_MOUSE	-3.31	9.95	0.91	3.9E-04
1213	sp|P40936|INMT_MOUSE	-3.33	10.03	0.83	1.5E-01
1214	sp|Q99LB7|SARDH_MOUSE	-3.33	10.05	0.85	7.1E-07
1215	sp|Q9WU79|PROD_MOUSE	-3.33	10.05	0.81	2.3E-05
1216	sp|Q8QZT1|THIL_MOUSE	-3.34	10.10	0.95	1.9E-02
1217	sp|Q9JHI5|IVD_MOUSE	-3.34	10.14	0.88	4.2E-04
1218	sp|Q91W43|GCSP_MOUSE	-3.35	10.20	0.57	2.1E-01
1219	sp|P50136|ODBA_MOUSE	-3.36	10.29	0.64	1.0E-03

1220	sp|P50285|FMO1_MOUSE	-3.37	10.33	0.82	3.8E-05
1221	sp|Q8R0F8|FAHD1_MOUSE	-3.38	10.39	0.84	6.0E-05
1222	sp|Q99KR3|LACB2_MOUSE	-3.38	10.39	0.82	1.2E-01
1223	sp|Q8JZN7|MIRO2_MOUSE	-3.38	10.40	0.55	2.2E-01
1224	sp|Q9Z2I8|SUCB2_MOUSE	-3.38	10.42	0.94	1.3E-04
1225	sp|Q6ZQM8|UD17C_MOUSE	-3.39	10.51	0.75	9.6E-03
1226	sp|Q99L13|3HIDH_MOUSE	-3.40	10.55	0.94	1.3E-08
1227	sp|Q9JII6|AK1A1_MOUSE	-3.40	10.56	0.91	4.1E-04
1228	sp|Q91V76|CK054_MOUSE	-3.41	10.61	0.82	2.8E-03
1229	sp|P30115|GSTA3_MOUSE	-3.41	10.63	0.81	1.2E-03
1230	sp|Q9JIL4|NHRF3_MOUSE	-3.42	10.71	0.86	8.2E-04
1231	sp|Q8K157|GALM_MOUSE	-3.43	10.75	0.74	2.1E-05
1232	sp|Q9WVT6|CAH14_MOUSE	-3.43	10.76	0.70	1.5E-04
1233	sp|Q8K370|ACD10_MOUSE	-3.43	10.77	0.86	1.5E-04
1234	sp|Q9QZD8|DIC_MOUSE	-3.44	10.83	0.83	8.4E-03
1235	sp|Q9DCG6|PBLD1_MOUSE	-3.45	10.91	0.87	4.3E-02
1236	sp|Q3ULD5|MCCB_MOUSE	-3.45	10.95	0.90	3.8E-04
1237	sp|Q8BGA8|ACSM5_MOUSE	-3.46	11.03	0.76	2.8E-05
1238	sp|Q5F285|TM256_MOUSE	-3.46	11.03	0.71	1.0E-02
1239	sp|Q8R164|BPHL_MOUSE	-3.47	11.09	0.87	1.2E-04
1240	sp|Q91YP0|L2HDH_MOUSE	-3.48	11.18	0.58	8.2E-05
1241	sp|Q925N2|SFXN2_MOUSE	-3.49	11.27	0.65	8.7E-02
1242	sp|Q9D0S9|HINT2_MOUSE	-3.49	11.27	0.98	2.6E-05
1243	sp|P11930|NUD19_MOUSE	-3.50	11.28	0.90	5.0E-02
1244	sp|P14246|GTR2_MOUSE	-3.50	11.30	0.72	5.0E-02
1245	sp|Q9WVD5|ORNT1_MOUSE	-3.50	11.32	0.79	1.3E-03
1246	sp|P18894|OXDA_MOUSE	-3.51	11.38	0.81	5.7E-04
1247	sp|Q9CPQ8|ATP5L_MOUSE	-3.53	11.54	0.80	6.2E-05
1248	sp|O88428|PAPS2_MOUSE	-3.53	11.56	0.77	2.2E-03
1249	sp|Q9D023|MPC2_MOUSE	-3.54	11.60	0.82	3.2E-04
1250	sp|Q8R0Y8|S2542_MOUSE	-3.54	11.63	0.86	1.4E-03
1251	sp|P09671|SODM_MOUSE	-3.54	11.66	0.93	6.7E-04
1252	sp|O88533|DDC_MOUSE	-3.55	11.69	0.74	3.6E-04
1253	sp|P00397|COX1_MOUSE	-3.55	11.70	0.90	1.1E-02
1254	sp|Q8VC30|DHAK_MOUSE	-3.56	11.77	0.80	1.6E-02
1255	sp|Q62468|VILI_MOUSE	-3.56	11.78	0.91	5.8E-09
1256	sp|Q99PG0|AAAD_MOUSE	-3.57	11.84	0.85	3.4E-03
1257	sp|Q3UNZ8|QORL2_MOUSE	-3.57	11.85	0.82	8.1E-02
1258	sp|Q64516|GLPK_MOUSE	-3.57	11.89	0.86	6.0E-05
1259	sp|P43024|CX6A1_MOUSE	-3.57	11.91	0.74	1.3E-03
1260	sp|Q8VCT4|CES1D_MOUSE	-3.58	11.96	0.83	2.3E-04
1261	sp|Q8CHT0|AL4A1_MOUSE	-3.61	12.17	0.93	9.9E-05
1262	sp|Q99MN9|PCCB_MOUSE	-3.61	12.22	0.96	1.3E-04
1263	sp|Q8CAK1|CAF17_MOUSE	-3.61	12.24	0.70	4.3E-02
1264	sp|Q9DCM2|GSTK1_MOUSE	-3.62	12.27	0.82	1.8E-04
1265	sp|O70577|S22A2_MOUSE	-3.62	12.29	0.81	2.2E-03
1266	sp|Q8BK30|NDUV3_MOUSE	-3.63	12.37	0.79	9.0E-04
1267	sp|Q91XE4|ACY3_MOUSE	-3.64	12.43	0.80	8.5E-02
1268	sp|Q9D687|S6A19_MOUSE	-3.64	12.51	0.74	1.5E-06
1269	sp|P24270|CATA_MOUSE	-3.66	12.62	0.94	1.0E-02
1270	sp|Q9WV68|DECR2_MOUSE	-3.66	12.62	0.90	6.7E-06
1271	sp|P62071|RRAS2_MOUSE	-3.66	12.64	0.58	4.3E-01
1272	sp|P09470|ACE_MOUSE	-3.66	12.66	0.91	3.4E-03
1273	sp|P52760|UK114_MOUSE	-3.67	12.69	0.94	5.5E-03
1274	sp|P63030|MPC1_MOUSE	-3.69	12.91	0.93	5.7E-04
1275	sp|Q64442|DHSO_MOUSE	-3.71	13.11	0.82	9.5E-04
1276	sp|Q8VDN2|AT1A1_MOUSE	-3.72	13.14	0.93	1.2E-04
1277	sp|P35505|FAAA_MOUSE	-3.72	13.16	0.92	5.2E-06
1278	sp|Q60759|GCDH_MOUSE	-3.72	13.17	0.77	3.4E-04
1279	sp|O88343|S4A4_MOUSE	-3.73	13.29	0.83	1.3E-04
1280	sp|Q91XE0|GLYAT_MOUSE	-3.75	13.43	0.88	1.7E-03
1281	sp|O70250|PGAM2_MOUSE	-3.75	13.44	0.88	6.6E-04
1282	sp|Q9WVL0|MAAI_MOUSE	-3.75	13.49	0.82	6.7E-07
1283	sp|Q60928|GGT1_MOUSE	-3.76	13.58	0.89	1.1E-03
1284	sp|Q3UZZ6|ST1D1_MOUSE	-3.78	13.74	0.85	5.3E-08
1285	sp|P42925|PXMP2_MOUSE	-3.78	13.77	0.81	2.8E-04
1286	sp|Q9EQ20|MMSA_MOUSE	-3.79	13.79	0.88	3.4E-04
1287	sp|O88986|KBL_MOUSE	-3.79	13.82	0.85	2.4E-05
1288	sp|P61922|GABT_MOUSE	-3.79	13.84	0.93	1.3E-03
1289	sp|Q9DCN1|NUD12_MOUSE	-3.80	13.88	0.59	1.0E-02
1290	sp|Q9D964|GATM_MOUSE	-3.80	13.91	0.87	1.7E-04
1291	sp|Q8R0N6|HOT_MOUSE	-3.82	14.07	0.84	1.0E-03
1292	sp|Q91Y97|ALDOB_MOUSE	-3.83	14.21	0.93	4.0E-05

1293	sp|Q80XN0|BDH_MOUSE	-3.83	14.24	0.89	2.7E-04
1294	sp|P85094|ISC2A_MOUSE	-3.84	14.27	0.90	3.0E-04
1295	sp|Q9Z2J0|S23A1_MOUSE	-3.84	14.29	0.78	1.5E-02
1296	sp|Q9ESG4|TMM27_MOUSE	-3.85	14.41	0.85	4.2E-05
1297	sp|P45952|ACADM_MOUSE	-3.86	14.48	0.86	1.2E-04
1298	sp|Q9JKZ2|SC5A3_MOUSE	-3.86	14.51	0.63	1.1E-02
1299	sp|Q64FW2|RETST_MOUSE	-3.88	14.71	0.76	6.6E-03
1300	sp|Q61847|MEP1B_MOUSE	-3.88	14.72	0.82	2.7E-04
1301	sp|Q9ERT9|PPR1A_MOUSE	-3.89	14.87	0.68	5.2E-04
1302	sp|O35488|S27A2_MOUSE	-3.90	14.88	0.81	1.4E-03
1303	sp|Q9QXN5|MIOX_MOUSE	-3.93	15.22	0.79	2.6E-01
1304	sp|Q78JT3|3HAO_MOUSE	-3.96	15.56	0.85	3.8E-04
1305	sp|Q60825|NPT2A_MOUSE	-3.96	15.57	0.58	1.2E-03
1306	sp|Q8BK72|RT27_MOUSE	-3.97	15.65	0.79	4.2E-01
1307	sp|Q14C51|PTCD3_MOUSE	-3.98	15.77	0.60	1.8E-01
1308	sp|Q8VCN5|CGL_MOUSE	-4.00	16.04	0.86	1.7E-03
1309	sp|Q3TLP5|ECHD2_MOUSE	-4.01	16.09	0.87	3.5E-03
1310	sp|Q923I7|SC5A2_MOUSE	-4.02	16.23	0.80	1.0E-04
1311	sp|Q9DCY0|KEG1_MOUSE	-4.03	16.36	0.88	1.7E-02
1312	sp|Q9CQN3|TOM6_MOUSE	-4.04	16.46	0.65	2.5E-02
1313	sp|Q99NB1|ACS2L_MOUSE	-4.05	16.56	0.89	1.9E-04
1314	sp|P97816|S100G_MOUSE	-4.05	16.59	0.90	3.4E-03
1315	sp|Q99N23|CAH15_MOUSE	-4.06	16.64	0.59	1.4E-03
1316	sp|Q91WG0|EST2C_MOUSE	-4.06	16.66	0.69	5.3E-02
1317	sp|Q8JZZ0|UD3A2_MOUSE	-4.06	16.72	0.83	6.6E-03
1318	sp|Q61767|3BHS4_MOUSE	-4.07	16.79	0.79	1.1E-02
1319	sp|Q04646|ATNG_MOUSE	-4.07	16.80	0.90	2.8E-04
1320	sp|Q8BH00|AL8A1_MOUSE	-4.10	17.11	0.88	3.8E-05
1321	sp|P10648|GSTA2_MOUSE	-4.10	17.14	0.85	2.0E-02
1322	sp|O54749|CP2J5_MOUSE	-4.11	17.31	0.57	6.9E-01
1323	sp|Q7TMS5|ABCG2_MOUSE	-4.12	17.42	0.79	1.8E-03
1324	sp|Q8VIM4|BSND_MOUSE	-4.14	17.65	0.77	5.0E-03
1325	sp|Q05920|PYC_MOUSE	-4.17	18.04	0.87	1.5E-03
1326	sp|Q3TNA1|XYLB_MOUSE	-4.18	18.14	0.67	3.0E-02
1327	sp|Q9WUZ9|ENTP5_MOUSE	-4.19	18.28	0.75	3.3E-04
1328	sp|Q9Z2V4|PCKGC_MOUSE	-4.20	18.41	0.80	1.4E-03
1329	sp|O88338|CAD16_MOUSE	-4.29	19.54	0.92	8.5E-04
1330	sp|P14094|AT1B1_MOUSE	-4.29	19.55	0.87	6.5E-04
1331	sp|P00416|COX3_MOUSE	-4.30	19.65	0.64	1.0E-02
1332	sp|Q9WUR9|KAD4_MOUSE	-4.31	19.83	0.89	6.5E-04
1333	sp|Q9DBM2|ECHP_MOUSE	-4.32	19.92	0.84	4.8E-03
1334	sp|Q8K0L3|ACSM2_MOUSE	-4.33	20.17	0.86	6.1E-02
1335	sp|Q91YD6|VILL_MOUSE	-4.38	20.84	0.63	7.3E-01
1336	sp|Q9QXD6|F16P1_MOUSE	-4.38	20.84	0.81	1.0E-04
1337	sp|Q91VA0|ACSM1_MOUSE	-4.38	20.87	0.83	3.8E-04
1338	sp|P16460|ASSY_MOUSE	-4.41	21.28	0.88	1.4E-03
1339	sp|Q8VEA4|MIA40_MOUSE	-4.44	21.77	0.50	9.1E-03
1340	sp|P70691|UD12_MOUSE	-4.89	29.67	0.74	6.1E-03
1341	sp|P12658|CALB1_MOUSE	-5.00	32.07	0.91	1.6E-03
1342	sp|Q8VCH0|THIKB_MOUSE	-5.10	34.19	0.75	6.8E-02
1343	sp|Q8QZW3|F151A_MOUSE	-5.39	41.95	0.79	5.6E-04
1344	sp|Q9NYQ2|HAOX2_MOUSE	-5.47	44.28	0.85	2.3E-02
1345	sp|Q9CQH0|PDZ1I_MOUSE	-5.52	45.76	0.84	5.0E-03
1346	sp|Q8C025|CHPT1_MOUSE	-5.58	47.75	0.76	5.6E-03
1347	sp|Q9WVM8|AADAT_MOUSE	-5.59	48.00	0.84	1.7E-02
1348	sp|O88576|S6A18_MOUSE	-5.82	56.31	0.63	5.7E-04
1349	sp|P35576|G6PC_MOUSE	-6.17	72.24	0.86	4.1E-03

S.1.1.2 Fold change analysis of TG2-KO Sham operated vs WT Sham operated

Supplementary Table 3.2: Outcome of the fold change (FC) analysis between TG2-KO Sham operated mice (21 days) and WT Sham operated mice (21 days) [C(FC) ≥ 0.5].

	Protein ID	log2(FC)	Abs(FC)	C(FC)	p-value (FC)
1	sp|Q9CYW4|HDHD3_MOUSE	3.44	10.87	0.52	4.27E-01
2	sp|Q99J27|ACATN_MOUSE	3.40	10.52	0.57	3.32E-01
3	sp|Q8K1B8|URP2_MOUSE	2.49	5.63	0.58	9.49E-02
4	sp|P84084|ARF5_MOUSE	2.02	4.07	0.57	2.04E-01
5	sp|Q06138|CAB39_MOUSE	1.88	3.69	0.81	2.96E-05
6	sp|Q6ZWV7|RL35_MOUSE	1.63	3.11	0.57	1.57E-01
7	sp|Q6IFZ6|K2C1B_MOUSE	1.47	2.78	0.59	1.45E-01
8	sp|Q9QZA0|CAH5B_MOUSE	1.46	2.75	0.61	2.03E-01
9	sp|P62717|RL18A_MOUSE	1.26	2.39	0.61	4.28E-01
10	sp|P47915|RL29_MOUSE	1.22	2.33	0.68	6.83E-01
11	sp|P43275|H11_MOUSE	1.05	2.07	0.58	3.34E-02
12	sp|P15864|H12_MOUSE	0.96	1.95	0.72	1.13E-02
13	sp|P10922|H10_MOUSE	0.94	1.92	0.77	3.76E-03
14	sp|Q9CPR4|RL17_MOUSE	0.90	1.87	0.76	5.00E-01
15	sp|P02535|K1C10_MOUSE	0.89	1.85	0.52	6.87E-01
16	sp|Q9D1R9|RL34_MOUSE	0.85	1.81	0.52	7.93E-01
17	sp|Q8BP67|RL24_MOUSE	0.85	1.81	0.90	1.08E-01
18	sp|Q8C0E2|VP26B_MOUSE	0.82	1.77	0.57	1.89E-01
19	sp|P43274|H14_MOUSE	0.81	1.75	0.84	3.76E-02
20	sp|P43276|H15_MOUSE	0.79	1.73	0.66	3.15E-02
21	sp|P47964|RL36_MOUSE	0.76	1.69	0.68	3.74E-02
22	sp|O09167|RL21_MOUSE	0.76	1.69	0.68	1.76E-01
23	sp|P62852|RS25_MOUSE	0.76	1.69	0.66	3.69E-01
24	sp|P84099|RL19_MOUSE	0.72	1.65	0.52	9.68E-02
25	sp|P62806|H4_MOUSE	0.72	1.64	0.74	1.73E-02
26	sp|P47963|RL13_MOUSE	0.71	1.64	0.70	4.26E-01
27	sp|P62862|RS30_MOUSE	0.70	1.62	0.69	1.79E-01
28	sp|Q8BP40|PPA6_MOUSE	0.68	1.61	0.52	3.17E-01
29	sp|Q9CRC0|VKOR1_MOUSE	0.68	1.60	0.68	1.30E-01
30	sp|Q91VW3|SH3L3_MOUSE	0.64	1.56	0.58	1.40E-01
31	sp|Q6ZWV3|RL10_MOUSE	0.64	1.55	0.56	1.03E-01
32	sp|P24668|MPRD_MOUSE	0.63	1.55	0.56	4.23E-02
33	sp|P62855|RS26_MOUSE	0.57	1.48	0.53	3.36E-01
34	sp|P84228|H32_MOUSE	0.54	1.45	0.56	1.45E-02
35	sp|P68433|H31_MOUSE	0.53	1.44	0.66	7.79E-01
36	sp|Q3THW5|H2AV_MOUSE	0.52	1.44	0.53	6.60E-02
37	sp|Q9DAS9|GBG12_MOUSE	0.52	1.43	0.75	2.60E-02
38	sp|P04117|FABP4_MOUSE	0.51	1.43	0.58	1.56E-01
39	sp|Q9QZQ8|H2AY_MOUSE	0.50	1.42	0.65	2.08E-02
40	sp|P62880|GBB2_MOUSE	0.47	1.38	0.52	4.94E-01
41	sp|P62301|RS13_MOUSE	0.43	1.35	0.50	6.23E-01
42	sp|Q14DH7|ACSS3_MOUSE	0.43	1.35	0.53	7.30E-01
43	sp|P62315|SMD1_MOUSE	0.43	1.34	0.57	4.37E-02
44	sp|P56382|ATP5E_MOUSE	0.41	1.33	0.53	1.56E-02
45	sp|P11404|FABPH_MOUSE	0.41	1.32	0.54	2.82E-01
46	sp|P63024|VAMP3_MOUSE	0.34	1.27	0.50	8.92E-01
47	sp|Q9CQ19|MYL9_MOUSE	0.32	1.24	0.63	7.37E-01
48	sp|Q99MZ7|PECR_MOUSE	0.29	1.22	0.53	9.41E-01
49	sp|P13707|GPDA_MOUSE	0.27	1.20	0.52	3.76E-01
50	sp|P63276|RS17_MOUSE	0.26	1.19	0.55	1.97E-01
51	sp|Q9DCB8|ISCA2_MOUSE	-0.31	1.24	0.54	3.15E-01
52	sp|P17563|SBP1_MOUSE	-0.31	1.24	0.57	4.44E-02
53	sp|Q9DCU6|RM04_MOUSE	-0.34	1.27	0.54	7.69E-01
54	sp|Q9DCT1|AKCL2_MOUSE	-0.35	1.28	0.55	4.39E-03
55	sp|Q61937|NPM_MOUSE	-0.41	1.33	0.62	4.20E-01
56	sp|Q9CR86|CHSP1_MOUSE	-0.51	1.42	0.54	5.96E-01
57	sp|Q9CQX2|CYB5B_MOUSE	-0.51	1.43	0.80	9.52E-02
58	sp|P51906|EAA3_MOUSE	-0.52	1.43	0.52	2.67E-02
59	sp|P05132|KAPCA_MOUSE	-0.58	1.50	0.55	9.60E-01
60	sp|Q08943|SSRP1_MOUSE	-0.63	1.55	0.56	1.33E-01
61	sp|Q5F285|TM256_MOUSE	-0.66	1.58	0.73	6.36E-02
62	sp|Q571E4|GALNS_MOUSE	-0.67	1.60	0.70	4.95E-01
63	sp|Q8BJZ4|RT35_MOUSE	-0.75	1.68	0.55	7.64E-01
64	sp|P50637|TSPO_MOUSE	-0.81	1.75	0.61	1.12E-01
65	sp|Q8CFV9|RIFK_MOUSE	-0.99	1.98	0.68	4.79E-02

66	sp|Q8K3A0|HSC20_MOUSE	-1.09	2.12	0.56	6.86E-02
67	sp|P68373|TBA1C_MOUSE	-1.12	2.17	0.67	1.47E-01
68	sp|Q9CQN3|TOM6_MOUSE	-1.24	2.37	0.62	6.39E-02
69	sp|O70252|HMOX2_MOUSE	-2.01	4.02	0.51	9.55E-01
70	sp|Q9D173|TOM7_MOUSE	-2.03	4.08	0.57	2.56E-01
71	sp|P63087|PP1G_MOUSE	-2.75	6.71	0.57	2.23E-01
72	sp|P21981|TGM2_MOUSE	-3.16	8.94	0.84	3.13E-05

S.1.1.3 Fold change analysis of TG2-KO UUO vs WT UUO

Supplementary Table 3.3: Outcome of the fold change (FC) analysis between TG2-KO UUO mice (21 days) and WT UUO mice (21 days) [C(FC) ≥ 0.5].

	Protein ID	log2(FC)	Abs(FC)	C(FC)	p-value (FC)
1	sp|Q99PG0|AAAD_MOUSE	3.08	8.48	0.51	5.25E-02
2	sp|Q8BMF3|MAON_MOUSE	2.52	5.73	0.54	6.22E-01
3	sp|Q9CXT8|MPPB_MOUSE	1.97	3.92	0.70	1.61E-01
4	sp|P50637|TSPO_MOUSE	1.79	3.46	1.00	3.76E-01
5	sp|P15864|H12_MOUSE	1.55	2.92	0.94	4.00E-02
6	sp|O35683|NDUA1_MOUSE	1.50	2.82	0.58	1.89E-01
7	sp|P84099|RL19_MOUSE	1.45	2.73	0.85	7.33E-02
8	sp|P10922|H10_MOUSE	1.44	2.72	0.82	2.40E-01
9	sp|P43274|H14_MOUSE	1.41	2.66	0.95	7.82E-02
10	sp|Q9JHU4|DYHC1_MOUSE	1.37	2.59	0.55	4.88E-01
11	sp|Q6GSS7|H2A2A_MOUSE	1.32	2.50	0.73	3.28E-02
12	sp|Q8BP67|RL24_MOUSE	1.31	2.49	0.92	2.36E-01
13	sp|P47963|RL13_MOUSE	1.26	2.39	0.89	1.24E-01
14	sp|P43276|H15_MOUSE	1.24	2.35	0.88	8.33E-02
15	sp|P43275|H11_MOUSE	1.22	2.34	0.97	2.30E-02
16	sp|P61255|RL26_MOUSE	1.19	2.28	0.58	2.32E-01
17	sp|P62918|RL8_MOUSE	1.17	2.25	0.84	8.91E-02
18	sp|B1AXP6|TOM5_MOUSE	1.17	2.25	0.97	2.81E-01
19	sp|Q9CR57|RL14_MOUSE	1.15	2.22	0.93	9.19E-02
20	sp|P12970|RL7A_MOUSE	1.14	2.21	0.86	1.97E-02
21	sp|P62862|RS30_MOUSE	1.14	2.21	0.91	7.82E-02
22	sp|Q99LX0|PARK7_MOUSE	1.13	2.19	0.51	1.58E-01
23	sp|P62849|RS24_MOUSE	1.10	2.15	0.92	1.41E-01
24	sp|Q9D8E6|RL4_MOUSE	1.09	2.14	0.86	8.61E-02
25	sp|P61358|RL27_MOUSE	1.09	2.14	0.83	2.50E-02
26	sp|P47964|RL36_MOUSE	1.02	2.03	0.89	1.25E-01
27	sp|P47911|RL6_MOUSE	1.02	2.02	0.78	1.35E-01
28	sp|P41105|RL28_MOUSE	0.98	1.97	0.80	5.36E-01
29	sp|P62843|RS15_MOUSE	0.97	1.97	0.53	1.67E-01
30	sp|P27659|RL3_MOUSE	0.97	1.96	0.55	5.04E-01
31	sp|Q6ZWV3|RL10_MOUSE	0.97	1.96	0.63	6.95E-01
32	sp|Q6ZWV7|RL35_MOUSE	0.93	1.90	0.64	4.26E-02
33	sp|P63158|HMGB1_MOUSE	0.90	1.87	0.53	7.05E-01
34	sp|P19253|RL13A_MOUSE	0.89	1.85	0.81	9.03E-01
35	sp|P62806|H4_MOUSE	0.89	1.85	0.82	2.25E-01
36	sp|Q8CGP6|H2A1H_MOUSE	0.87	1.83	0.76	2.06E-01
37	sp|Q9CPR4|RL17_MOUSE	0.87	1.82	0.85	1.71E-01
38	sp|P62855|RS26_MOUSE	0.86	1.81	0.54	3.63E-01
39	sp|P14148|RL7_MOUSE	0.85	1.80	0.91	7.32E-02
40	sp|P62270|RS18_MOUSE	0.81	1.75	0.87	1.45E-02
41	sp|Q9CZM2|RL15_MOUSE	0.81	1.75	0.61	2.10E-01
42	sp|P35980|RL18_MOUSE	0.79	1.73	0.87	9.18E-02
43	sp|Q6ZWN5|RS9_MOUSE	0.78	1.71	0.73	6.60E-02
44	sp|P62717|RL18A_MOUSE	0.77	1.70	0.68	2.68E-01
45	sp|P03987|IGHG3_MOUSE	0.76	1.69	0.66	2.92E-02
46	sp|P62281|RS11_MOUSE	0.75	1.68	0.73	3.29E-02
47	sp|P62274|RS29_MOUSE	0.74	1.67	0.80	2.19E-01
48	sp|P68433|H31_MOUSE	0.74	1.67	0.71	2.58E-01
49	sp|P62900|RL31_MOUSE	0.73	1.66	0.71	4.23E-01

50	sp|O09167|RL21_MOUSE	0.70	1.62	0.71	4.87E-01
51	sp|P62315|SMD1_MOUSE	0.68	1.61	0.79	6.96E-02
52	sp|P62301|RS13_MOUSE	0.68	1.60	0.86	3.13E-02
53	sp|P62852|RS25_MOUSE	0.66	1.59	0.84	3.02E-02
54	sp|P27661|H2AX_MOUSE	0.66	1.58	0.74	1.23E-01
55	sp|P62754|RS6_MOUSE	0.66	1.58	0.60	2.75E-01
56	sp|Q9JJI8|RL38_MOUSE	0.65	1.57	0.57	7.45E-01
57	sp|P20065|TYB4_MOUSE	0.61	1.52	0.57	8.40E-01
58	sp|Q3THW5|H2AV_MOUSE	0.60	1.52	0.62	9.36E-01
59	sp|P25444|RS2_MOUSE	0.59	1.51	0.54	7.32E-01
60	sp|Q8CGP2|H2B1P_MOUSE	0.57	1.48	0.83	1.60E-02
61	sp|P14131|RS16_MOUSE	0.54	1.46	0.54	9.45E-02
62	sp|P53026|RL10A_MOUSE	0.54	1.46	0.70	1.53E-01
63	sp|P62242|RS8_MOUSE	0.46	1.38	0.74	1.70E-01
64	sp|Q8VDM4|PSMD2_MOUSE	0.45	1.37	0.63	5.72E-01
65	sp|P62702|RS4X_MOUSE	0.45	1.37	0.59	1.59E-01
66	sp|Q9QZQ8|H2AY_MOUSE	0.44	1.35	0.78	2.92E-02
67	sp|Q6ZWY3|RS27L_MOUSE	0.42	1.34	0.62	6.84E-01
68	sp|Q9CZX8|RS19_MOUSE	0.37	1.29	0.70	3.69E-01
69	sp|P62245|RS15A_MOUSE	0.37	1.29	0.54	4.83E-02
70	sp|P17742|PPIA_MOUSE	-0.20	1.15	0.75	6.58E-02
71	sp|P57776|EF1D_MOUSE	-0.21	1.16	0.59	1.95E-01
72	sp|Q8VDW0|DX39A_MOUSE	-0.22	1.16	0.53	7.04E-01
73	sp|Q04857|CO6A1_MOUSE	-0.22	1.17	0.50	5.97E-01
74	sp|P61924|COPZ1_MOUSE	-0.22	1.17	0.51	4.60E-01
75	sp|P39061|COIA1_MOUSE	-0.23	1.17	0.60	9.51E-03
76	sp|Q99PT1|GDIR1_MOUSE	-0.23	1.17	0.60	2.72E-01
77	sp|Q61171|PRDX2_MOUSE	-0.24	1.18	0.61	3.97E-02
78	sp|P24369|PPIB_MOUSE	-0.24	1.18	0.57	4.33E-02
79	sp|Q05144|RAC2_MOUSE	-0.25	1.19	0.55	4.62E-02
80	sp|Q60972|RBBP4_MOUSE	-0.26	1.20	0.55	1.46E-02
81	sp|P68254|1433T_MOUSE	-0.26	1.20	0.60	3.58E-01
82	sp|Q02788|CO6A2_MOUSE	-0.27	1.20	0.79	5.96E-01
83	sp|P61205|ARF3_MOUSE	-0.27	1.21	0.57	1.96E-01
84	sp|O08547|SC22B_MOUSE	-0.28	1.21	0.57	5.49E-01
85	sp|Q9R0P6|SC11A_MOUSE	-0.28	1.21	0.74	7.56E-01
86	sp|P51859|HDGF_MOUSE	-0.28	1.22	0.55	5.63E-01
87	sp|P61982|1433G_MOUSE	-0.30	1.23	0.57	5.53E-01
88	sp|Q9CQR2|RS21_MOUSE	-0.31	1.24	0.67	4.01E-03
89	sp|Q922U2|K2C5_MOUSE	-0.32	1.25	0.62	9.83E-02
90	sp|Q8BGS7|CEPT1_MOUSE	-0.32	1.25	0.50	7.76E-01
91	sp|Q99KP6|PRP19_MOUSE	-0.32	1.25	0.64	2.59E-02
92	sp|P62309|RUXG_MOUSE	-0.32	1.25	0.69	5.71E-03
93	sp|P21460|CYTC_MOUSE	-0.32	1.25	0.64	1.25E-02
94	sp|P54923|ADPRH_MOUSE	-0.32	1.25	0.53	2.06E-01
95	sp|P21107|TPM3_MOUSE	-0.32	1.25	0.54	4.81E-01
96	sp|Q61233|PLSL_MOUSE	-0.33	1.25	0.64	3.05E-02
97	sp|P23953|EST1C_MOUSE	-0.34	1.26	0.76	6.95E-01
98	sp|Q9WUM3|COR1B_MOUSE	-0.34	1.27	0.53	2.20E-01
99	sp|P62259|1433E_MOUSE	-0.35	1.27	0.57	2.62E-01
100	sp|Q6IFZ6|K2C1B_MOUSE	-0.35	1.27	0.57	9.83E-02
101	sp|Q9CX80|CYGB_MOUSE	-0.36	1.29	0.60	3.32E-01
102	sp|P07759|SPA3K_MOUSE	-0.36	1.29	0.51	9.54E-01
103	sp|Q8CHH9|SEPT8_MOUSE	-0.37	1.30	0.51	6.55E-01
104	sp|Q3UBX0|TM109_MOUSE	-0.38	1.30	0.54	8.71E-03
105	sp|P01029|CO4B_MOUSE	-0.38	1.30	0.70	9.02E-02
106	sp|Q9ESB3|HRG_MOUSE	-0.38	1.31	0.52	8.85E-01
107	sp|Q61102|ABCB7_MOUSE	-0.39	1.31	0.88	2.05E-03
108	sp|P18760|COF1_MOUSE	-0.40	1.32	0.52	2.27E-01
109	sp|P41731|CD63_MOUSE	-0.40	1.32	0.74	4.88E-02
110	sp|Q91YH5|ATLA3_MOUSE	-0.40	1.32	0.53	1.40E-01
111	sp|O35887|CALU_MOUSE	-0.42	1.34	0.62	2.21E-02
112	sp|O88792|JAM1_MOUSE	-0.43	1.34	0.53	6.16E-02
113	sp|P21956|MFGM_MOUSE	-0.43	1.35	0.55	1.84E-02
114	sp|P68373|TBA1C_MOUSE	-0.44	1.35	0.57	1.25E-01
115	sp|Q9R0P4|SMAP_MOUSE	-0.44	1.36	0.57	4.38E-01
116	sp|Q99M71|EPDR1_MOUSE	-0.46	1.38	0.61	1.22E-03
117	sp|P01942|HBA_MOUSE	-0.46	1.38	0.69	1.16E-01
118	sp|Q62000|MIME_MOUSE	-0.49	1.40	0.50	6.48E-01
119	sp|Q99LB6|MAT2B_MOUSE	-0.51	1.43	0.55	3.78E-01
120	sp|Q00623|APOA1_MOUSE	-0.52	1.43	0.62	6.97E-01
121	sp|P35441|TSP1_MOUSE	-0.52	1.43	0.74	7.86E-01
122	sp|Q9D7X3|DUS3_MOUSE	-0.53	1.44	0.52	9.79E-02

123	sp|P08207|S10AA_MOUSE	-0.53	1.45	0.71	1.37E-01
124	sp|Q9R0P5|DEST_MOUSE	-0.56	1.48	0.72	7.50E-03
125	sp|Q91VW3|SH3L3_MOUSE	-0.57	1.48	0.60	1.57E-01
126	sp|Q9Z130|HNRDL_MOUSE	-0.66	1.58	0.54	1.26E-03
127	sp|Q91VM9|IPYR2_MOUSE	-0.68	1.60	0.53	9.55E-01
128	sp|P62204|CALM_MOUSE	-0.68	1.60	0.72	1.77E-01
129	sp|Q9D0M5|DYL2_MOUSE	-0.69	1.61	0.56	8.30E-01
130	sp|Q9Z2W1|STK25_MOUSE	-0.71	1.64	0.58	8.63E-01
131	sp|Q9D1L9|LTOR5_MOUSE	-0.78	1.71	0.64	2.58E-01
132	sp|P19096|FAS_MOUSE	-0.81	1.75	0.51	3.77E-01
133	sp|Q8VCM7|FIBG_MOUSE	-0.89	1.85	0.63	5.34E-01
134	sp|P01878|IGHA_MOUSE	-0.89	1.85	0.53	4.55E-01
135	sp|Q8K0E8|FIBB_MOUSE	-0.99	1.99	0.60	6.30E-01
136	sp|P14069|S10A6_MOUSE	-1.00	1.99	0.75	4.41E-03
137	sp|P04117|FABP4_MOUSE	-1.06	2.08	0.87	8.97E-02
138	sp|E9PV24|FIBA_MOUSE	-1.09	2.13	0.72	6.48E-01
139	sp|Q9QZ85|IIGP1_MOUSE	-1.35	2.54	0.65	7.15E-02
140	sp|Q9D1P4|CHRD1_MOUSE	-1.58	2.98	0.51	1.12E-03
141	sp|P02798|MT2_MOUSE	-1.78	3.45	0.69	6.42E-02
142	sp|Q9D7X8|GGCT_MOUSE	-1.89	3.71	0.53	5.37E-02
143	sp|Q9JKF7|RM39_MOUSE	-1.93	3.80	0.51	1.50E-01
144	sp|P01635|KV5A3_MOUSE	-4.19	18.29	0.71	6.78E-01
145	sp|P21981|TGM2_MOUSE	-4.97	31.44	0.85	9.81E-01
146	sp|Q6AW69|CGNL1_MOUSE	-7.21	148.27	0.50	8.44E-01

S.1.1.4 Fold change analysis of TG2-KO UUO vs TG2-KO Sham operated

Supplementary Table 3.4: Outcome of the Fold change (FC) analysis between TG2-KO UUO mice (21 days) and TG2-KO Sham operated mice (21 days) [C(FC) ≥ 0.5].

	Protein ID	log2(FC)	Abs(FC)	C(FC)	p-value (FC)
1	sp|Q60847|COCA1_MOUSE	4.71	26.15	0.83	8.11E-03
2	sp|Q61555|FBN2_MOUSE	3.86	14.52	0.89	9.96E-03
3	sp|Q80YX1|TENA_MOUSE	3.81	14.03	0.72	4.74E-03
4	sp|Q9CYG7|TOM34_MOUSE	3.55	11.73	0.70	6.13E-02
5	sp|P14069|S10A6_MOUSE	3.45	10.94	0.81	1.97E-01
6	sp|Q08091|CNN1_MOUSE	3.45	10.90	0.80	8.70E-04
7	sp|P28653|PGS1_MOUSE	3.30	9.86	0.87	1.97E-04
8	sp|Q91X17|UROM_MOUSE	3.29	9.78	0.88	1.00E-02
9	sp|Q07235|GDN_MOUSE	3.28	9.71	0.64	4.34E-01
10	sp|Q8BH97|RCN3_MOUSE	3.22	9.30	0.84	2.53E-09
11	sp|P15379|CD44_MOUSE	3.18	9.05	0.56	1.55E-04
12	sp|P82198|BGH3_MOUSE	3.18	9.04	0.75	3.72E-04
13	sp|Q08619|IFI5B_MOUSE	3.15	8.90	0.68	4.63E-04
14	sp|Q62009|POSTN_MOUSE	3.12	8.66	0.78	9.63E-03
15	sp|Q62241|RU1C_MOUSE	3.06	8.36	0.57	1.18E-02
16	sp|P10107|ANXA1_MOUSE	3.04	8.24	0.94	1.80E-05
17	sp|Q8K4G1|LTBP4_MOUSE	3.03	8.19	0.74	2.70E-06
18	sp|Q61554|FBN1_MOUSE	3.01	8.05	0.89	2.39E-04
19	sp|P19001|K1C19_MOUSE	2.99	7.95	0.89	5.00E-05
20	sp|P02762|MUP6_MOUSE	2.96	7.80	0.95	1.58E-03
21	sp|Q62148|AL1A2_MOUSE	2.96	7.79	0.77	4.24E-03
22	sp|P35441|TSP1_MOUSE	2.96	7.77	0.76	8.37E-02
23	sp|P14438|HA2U_MOUSE	2.95	7.75	0.74	8.04E-02
24	sp|O88207|CO5A1_MOUSE	2.92	7.56	0.83	1.27E-01
25	sp|Q921M7|FA49B_MOUSE	2.91	7.53	0.70	1.80E-06
26	sp|Q05144|RAC2_MOUSE	2.91	7.50	0.76	6.35E-02
27	sp|Q9CZH7|MXRA7_MOUSE	2.90	7.48	0.60	3.17E-02
28	sp|P07214|SPRC_MOUSE	2.90	7.45	0.57	7.89E-01
29	sp|Q62000|MIME_MOUSE	2.89	7.40	0.86	4.97E-02
30	sp|Q01149|CO1A2_MOUSE	2.86	7.25	0.71	1.56E-02
31	sp|P97290|IC1_MOUSE	2.86	7.24	0.78	1.33E-03
32	sp|P06800|PTPRC_MOUSE	2.84	7.17	0.78	1.52E-06
33	sp|Q8VCC9|SPON1_MOUSE	2.78	6.87	0.58	9.14E-04
34	sp|P37804|TAGL_MOUSE	2.78	6.86	0.89	6.99E-04
35	sp|O89053|COR1A_MOUSE	2.77	6.83	0.82	2.01E-04
36	sp|P51885|LUM_MOUSE	2.76	6.76	0.84	1.23E-03
37	sp|Q9R233|TPSN_MOUSE	2.75	6.71	0.89	1.14E-04
38	sp|Q8CHH9|SEPT8_MOUSE	2.74	6.69	0.58	4.77E-04
39	sp|P20152|VIME_MOUSE	2.74	6.67	0.91	4.16E-04
40	sp|P11087|CO1A1_MOUSE	2.73	6.64	0.96	1.55E-03
41	sp|Q9ET54|PALLD_MOUSE	2.69	6.47	0.52	9.94E-02
42	sp|Q9CYL5|GAPR1_MOUSE	2.69	6.44	0.86	6.35E-07
43	sp|P11276|FINC_MOUSE	2.66	6.31	0.89	8.72E-02
44	sp|P01831|THY1_MOUSE	2.66	6.30	0.72	7.83E-06
45	sp|Q08879|FBLN1_MOUSE	2.65	6.28	0.78	1.57E-04
46	sp|Q64449|MRC2_MOUSE	2.64	6.23	0.77	9.97E-04
47	sp|Q8BMK4|CKAP4_MOUSE	2.63	6.18	0.73	1.84E-04
48	sp|P06909|CFAH_MOUSE	2.63	6.17	0.81	1.83E-03
49	sp|P08121|CO3A1_MOUSE	2.59	6.02	0.95	3.74E-03
50	sp|Q04447|KCRB_MOUSE	2.58	5.98	0.86	3.51E-06
51	sp|Q61576|FKB10_MOUSE	2.57	5.94	0.52	2.39E-02
52	sp|P09528|FRIH_MOUSE	2.54	5.80	0.56	1.03E-01
53	sp|P54320|ELN_MOUSE	2.53	5.78	0.83	3.47E-04
54	sp|P11835|ITB2_MOUSE	2.50	5.65	0.57	4.24E-04
55	sp|Q91XV3|BASP1_MOUSE	2.49	5.64	0.78	3.67E-04
56	sp|Q62266|SPR1A_MOUSE	2.49	5.63	0.79	2.40E-02
57	sp|P31725|S10A9_MOUSE	2.47	5.55	0.50	1.48E-02
58	sp|Q61781|K1C14_MOUSE	2.47	5.55	0.81	1.45E-02
59	sp|Q8R0X7|SGPL1_MOUSE	2.46	5.50	0.62	3.69E-01
60	sp|P19324|SERPH_MOUSE	2.45	5.45	0.96	1.83E-03
61	sp|P16045|LEG1_MOUSE	2.44	5.44	0.93	5.59E-04
62	sp|Q9WVH9|FBLN5_MOUSE	2.43	5.38	0.87	4.64E-05
63	sp|Q71FD7|FBLI1_MOUSE	2.42	5.36	0.67	2.08E-05
64	sp|Q8BPB5|FBLN3_MOUSE	2.42	5.35	0.87	1.14E-04
65	sp|P49710|HCLS1_MOUSE	2.41	5.33	0.70	9.48E-03

66	sp|Q69ZN7|MYOF_MOUSE	2.38	5.21	0.81	9.22E-07
67	sp|P97298|PEDF_MOUSE	2.37	5.16	0.55	4.87E-02
68	sp|Q922U2|K2C5_MOUSE	2.37	5.15	0.84	8.21E-04
69	sp|Q3TJD7|PDLI7_MOUSE	2.36	5.13	0.64	2.59E-05
70	sp|P11672|NGAL_MOUSE	2.35	5.11	0.73	5.22E-04
71	sp|Q8R3Q6|CCD58_MOUSE	2.33	5.04	0.54	8.68E-01
72	sp|Q62188|DPYL3_MOUSE	2.32	4.99	0.70	9.77E-05
73	sp|P37889|FBLN2_MOUSE	2.32	4.99	0.54	1.35E-01
74	sp|Q00915|RET1_MOUSE	2.31	4.95	0.78	2.61E-04
75	sp|O70456|1433S_MOUSE	2.30	4.92	0.72	1.65E-03
76	sp|O70400|PDLI1_MOUSE	2.28	4.85	0.59	1.90E-02
77	sp|P21956|MFGM_MOUSE	2.26	4.79	0.52	5.61E-03
78	sp|Q99K41|EMIL1_MOUSE	2.25	4.77	0.89	1.95E-03
79	sp|Q61233|PLSL_MOUSE	2.25	4.77	0.82	1.00E-03
80	sp|P84096|RHOG_MOUSE	2.24	4.71	0.60	4.35E-04
81	sp|Q60710|SAMH1_MOUSE	2.23	4.70	0.84	4.60E-07
82	sp|Q9JK53|PRELP_MOUSE	2.23	4.68	0.89	8.02E-03
83	sp|P19973|LSP1_MOUSE	2.23	4.68	0.58	6.08E-05
84	sp|P20065|TYB4_MOUSE	2.22	4.65	0.90	3.17E-03
85	sp|P42703|LIFR_MOUSE	2.21	4.61	0.58	5.26E-03
86	sp|P31001|DESM_MOUSE	2.20	4.60	0.94	1.98E-03
87	sp|Q8BTM8|FLNA_MOUSE	2.19	4.56	0.95	3.61E-05
88	sp|P14483|HB2A_MOUSE	2.19	4.55	0.60	4.72E-01
89	sp|Q922F4|TBB6_MOUSE	2.18	4.53	0.57	1.78E-02
90	sp|Q9D132|UPK1A_MOUSE	2.18	4.52	0.56	2.61E-01
91	sp|Q8CGP6|H2A1H_MOUSE	2.17	4.49	0.85	5.65E-04
92	sp|Q60590|A1AG1_MOUSE	2.16	4.46	0.51	1.80E-01
93	sp|Q9CX80|CYGB_MOUSE	2.15	4.43	0.55	1.38E-02
94	sp|Q3U962|CO5A2_MOUSE	2.13	4.37	0.62	1.25E-03
95	sp|Q8K3A0|HSC20_MOUSE	2.12	4.35	0.50	9.29E-01
96	sp|P14106|C1QB_MOUSE	2.12	4.35	0.91	3.89E-03
97	sp|Q9WV54|ASAH1_MOUSE	2.11	4.32	0.87	2.96E-02
98	sp|P97821|CATC_MOUSE	2.11	4.30	0.53	6.11E-01
99	sp|Q06890|CLUS_MOUSE	2.10	4.30	0.86	3.18E-02
100	sp|P68369|TBA1A_MOUSE	2.10	4.28	0.91	2.25E-03
101	sp|P11679|K2C8_MOUSE	2.09	4.26	0.94	3.72E-05
102	sp|Q9QZZ6|DERM_MOUSE	2.08	4.23	0.71	2.01E-02
103	sp|Q61599|GDIR2_MOUSE	2.08	4.23	0.77	1.69E-03
104	sp|P07091|S10A4_MOUSE	2.07	4.21	0.67	1.18E-03
105	sp|P01864|GCAB_MOUSE	2.07	4.20	0.82	2.36E-02
106	sp|P28654|PGS2_MOUSE	2.06	4.16	0.70	3.01E-02
107	sp|Q08093|CNN2_MOUSE	2.04	4.11	0.84	3.60E-04
108	sp|Q8R1G6|PDLI2_MOUSE	2.03	4.09	0.82	3.22E-01
109	sp|P01869|IGH1M_MOUSE	2.03	4.08	0.50	1.86E-01
110	sp|Q9Z2C6|UPK1B_MOUSE	2.03	4.07	0.71	8.95E-02
111	sp|Q6IRU2|TPM4_MOUSE	2.02	4.06	0.91	7.97E-04
112	sp|Q03350|TSP2_MOUSE	2.02	4.05	0.51	2.32E-02
113	sp|P07309|TTHY_MOUSE	2.01	4.02	0.80	5.85E-04
114	sp|Q80X19|COEA1_MOUSE	1.97	3.93	0.83	1.15E-03
115	sp|Q99P72|RTN4_MOUSE	1.94	3.85	0.80	1.09E-02
116	sp|O70591|PFD2_MOUSE	1.93	3.81	0.53	4.00E-01
117	sp|Q7TPR4|ACTN1_MOUSE	1.89	3.72	0.96	3.26E-04
118	sp|P16110|LEG3_MOUSE	1.89	3.71	0.86	1.05E-04
119	sp|P28063|PSB8_MOUSE	1.87	3.66	0.54	1.61E-05
120	sp|P97315|CSRP1_MOUSE	1.87	3.65	0.92	2.85E-03
121	sp|Q61879|MYH10_MOUSE	1.86	3.63	0.84	4.47E-05
122	sp|Q62523|ZYX_MOUSE	1.86	3.63	0.72	2.22E-05
123	sp|O35682|MYADM_MOUSE	1.86	3.62	0.92	1.31E-04
124	sp|Q3U7R1|ESYT1_MOUSE	1.85	3.60	0.83	5.53E-02
125	sp|P54227|STMN1_MOUSE	1.84	3.59	0.51	1.25E-01
126	sp|Q04857|CO6A1_MOUSE	1.82	3.52	0.89	3.20E-07
127	sp|P63254|CRIP1_MOUSE	1.82	3.52	0.55	3.59E-03
128	sp|Q91X72|HEMO_MOUSE	1.81	3.50	0.82	4.92E-02
129	sp|Q8CFX1|G6PE_MOUSE	1.80	3.49	0.85	2.28E-06
130	sp|Q61581|IBP7_MOUSE	1.79	3.46	0.73	2.79E-01
131	sp|P58774|TPM2_MOUSE	1.78	3.44	0.82	4.72E-03
132	sp|P43025|TETN_MOUSE	1.78	3.43	0.79	2.49E-06
133	sp|P20491|FCERG_MOUSE	1.78	3.43	0.51	7.53E-05
134	sp|Q640N1|AEBP1_MOUSE	1.78	3.43	0.73	7.59E-02
135	sp|P11589|MUP2_MOUSE	1.78	3.43	1.00	5.29E-03
136	sp|Q8C129|LCAP_MOUSE	1.78	3.43	0.56	3.99E-01
137	sp|Q9DCV7|K2C7_MOUSE	1.78	3.43	0.88	2.46E-04
138	sp|P50543|S10AB_MOUSE	1.77	3.40	0.88	1.14E-03

139	sp|Q02788|CO6A2_MOUSE	1.77	3.40	0.92	7.91E-05
140	sp|P01837|IGKC_MOUSE	1.76	3.38	0.87	2.10E-03
141	sp|P29391|FRIL1_MOUSE	1.75	3.36	0.86	7.26E-03
142	sp|O08573|LEG9_MOUSE	1.75	3.36	0.55	4.02E-02
143	sp|Q8C3W1|CA198_MOUSE	1.73	3.32	0.77	6.05E-03
144	sp|Q9D8Y0|EFHD2_MOUSE	1.71	3.28	0.83	8.87E-06
145	sp|Q07797|LG3BP_MOUSE	1.70	3.26	0.81	4.86E-03
146	sp|O89086|RBM3_MOUSE	1.69	3.23	0.81	2.54E-02
147	sp|O70318|E41L2_MOUSE	1.69	3.22	0.88	6.30E-05
148	sp|P70460|VASP_MOUSE	1.68	3.21	0.74	1.72E-02
149	sp|Q9R0P9|UCHL1_MOUSE	1.67	3.19	0.64	3.42E-03
150	sp|P26645|MARCS_MOUSE	1.67	3.17	0.67	3.23E-01
151	sp|Q9WVA4|TAGL2_MOUSE	1.66	3.16	0.87	8.36E-04
152	sp|P20918|PLMN_MOUSE	1.64	3.13	0.72	3.82E-02
153	sp|P18242|CATD_MOUSE	1.64	3.12	0.81	7.99E-03
154	sp|P58771|TPM1_MOUSE	1.63	3.09	0.83	2.28E-03
155	sp|P42225|STAT1_MOUSE	1.63	3.09	0.60	3.37E-02
156	sp|Q9JJU8|SH3L1_MOUSE	1.63	3.09	0.89	4.69E-06
157	sp|P07356|ANXA2_MOUSE	1.61	3.06	0.90	8.75E-06
158	sp|P19221|THRB_MOUSE	1.61	3.05	0.78	1.27E-02
159	sp|O35639|ANXA3_MOUSE	1.61	3.05	0.82	4.42E-04
160	sp|Q3TZZ7|ESYT2_MOUSE	1.60	3.03	0.83	2.54E-05
161	sp|Q8BHD7|PTBP3_MOUSE	1.59	3.01	0.60	6.62E-03
162	sp|Q9R111|GUAD_MOUSE	1.58	3.00	0.52	4.18E-02
163	sp|Q9QXS6|DREB_MOUSE	1.58	2.98	0.68	4.50E-01
164	sp|Q9EPB4|ASC_MOUSE	1.57	2.97	0.73	1.35E-01
165	sp|Q61147|CERU_MOUSE	1.56	2.95	0.77	3.65E-02
166	sp|P46938|YAP1_MOUSE	1.56	2.94	0.53	4.84E-01
167	sp|P28667|MRP_MOUSE	1.56	2.94	0.64	2.52E-03
168	sp|P01867|IGG2B_MOUSE	1.56	2.94	0.77	9.32E-02
169	sp|Q00898|A1AT5_MOUSE	1.55	2.94	0.51	7.08E-02
170	sp|O35887|CALU_MOUSE	1.55	2.93	0.80	1.33E-03
171	sp|P70202|LXN_MOUSE	1.55	2.93	0.67	1.21E-02
172	sp|Q62465|VAT1_MOUSE	1.55	2.92	0.93	2.66E-04
173	sp|Q9ES28|ARHG7_MOUSE	1.54	2.92	0.55	4.49E-02
174	sp|Q9WV32|ARC1B_MOUSE	1.54	2.91	0.88	3.91E-07
175	sp|O35206|COFA1_MOUSE	1.54	2.90	0.63	7.07E-04
176	sp|O08638|MYH11_MOUSE	1.52	2.87	0.92	1.37E-04
177	sp|P01899|HA11_MOUSE	1.52	2.86	0.79	9.40E-05
178	sp|Q99M71|EPDR1_MOUSE	1.51	2.85	0.81	2.28E-05
179	sp|Q9DBR7|MYPT1_MOUSE	1.50	2.83	0.67	1.30E-03
180	sp|Q8VCM7|FIBG_MOUSE	1.50	2.82	0.74	2.80E-01
181	sp|Q01339|APOH_MOUSE	1.49	2.82	0.85	5.32E-04
182	sp|Q62048|PEA15_MOUSE	1.49	2.80	0.63	1.78E-01
183	sp|Q00897|A1AT4_MOUSE	1.48	2.79	0.81	2.18E-02
184	sp|P62737|ACTA_MOUSE	1.46	2.76	0.85	6.03E-02
185	sp|P01029|CO4B_MOUSE	1.46	2.75	0.83	1.11E-02
186	sp|O88531|PPT1_MOUSE	1.46	2.75	0.85	7.14E-04
187	sp|P07758|A1AT1_MOUSE	1.45	2.74	0.81	1.46E-02
188	sp|P08122|CO4A2_MOUSE	1.45	2.73	0.79	5.51E-05
189	sp|P99024|TBB5_MOUSE	1.45	2.72	0.90	1.30E-04
190	sp|P43275|H11_MOUSE	1.44	2.72	0.96	1.42E-03
191	sp|P03987|IGHG3_MOUSE	1.42	2.68	0.54	3.92E-01
192	sp|Q921I1|TRFE_MOUSE	1.42	2.67	0.89	5.42E-03
193	sp|P14602|HSPB1_MOUSE	1.41	2.67	0.85	3.94E-04
194	sp|P05784|K1C18_MOUSE	1.41	2.66	0.92	2.10E-04
195	sp|Q7TMB8|CYFP1_MOUSE	1.39	2.63	0.66	8.83E-04
196	sp|P42208|SEPT2_MOUSE	1.39	2.62	0.85	7.30E-06
197	sp|Q9QXC1|FETUB_MOUSE	1.38	2.60	0.86	1.14E-02
198	sp|Q64339|ISG15_MOUSE	1.37	2.59	0.89	6.35E-04
199	sp|P48678|LMNA_MOUSE	1.36	2.57	0.94	9.84E-05
200	sp|Q9CQ19|MYL9_MOUSE	1.35	2.56	0.98	1.27E-03
201	sp|P17918|PCNA_MOUSE	1.35	2.55	0.81	2.16E-01
202	sp|O08677|KNG1_MOUSE	1.35	2.54	0.92	4.70E-02
203	sp|P29699|FETUA_MOUSE	1.35	2.54	0.94	7.51E-05
204	sp|P43276|H15_MOUSE	1.34	2.54	0.91	8.85E-05
205	sp|Q5SYD0|MYO1D_MOUSE	1.34	2.54	0.65	6.79E-03
206	sp|Q60605|MYL6_MOUSE	1.34	2.53	0.94	2.47E-04
207	sp|P23953|EST1C_MOUSE	1.34	2.52	0.94	5.33E-03
208	sp|Q60854|SPB6_MOUSE	1.33	2.51	0.84	5.92E-04
209	sp|Q8CC35|SYNPO_MOUSE	1.33	2.51	0.67	2.04E-03
210	sp|Q8VDD5|MYH9_MOUSE	1.32	2.50	0.97	5.69E-04
211	sp|P08226|APOE_MOUSE	1.32	2.49	0.94	1.93E-02

212	sp|P06728|APOA4_MOUSE	1.30	2.47	0.83	1.64E-03
213	sp|Q8CCK0|H2AW_MOUSE	1.30	2.46	0.62	3.92E-02
214	sp|P07724|ALBU_MOUSE	1.30	2.46	0.91	2.09E-06
215	sp|P01027|CO3_MOUSE	1.29	2.45	0.87	1.41E-01
216	sp|P30681|HMGB2_MOUSE	1.29	2.45	0.85	2.13E-03
217	sp|Q06770|CBG_MOUSE	1.28	2.44	0.58	6.97E-02
218	sp|Q9JIF0|ANM1_MOUSE	1.28	2.44	0.72	2.71E-01
219	sp|Q9QWR8|NAGAB_MOUSE	1.28	2.43	0.82	6.47E-05
220	sp|Q61160|FADD_MOUSE	1.28	2.43	0.53	8.47E-01
221	sp|P47753|CAZA1_MOUSE	1.28	2.42	0.62	1.86E-03
222	sp|P15864|H12_MOUSE	1.28	2.42	0.93	9.43E-06
223	sp|O55131|SEPT7_MOUSE	1.27	2.41	0.80	2.32E-05
224	sp|Q8CI51|PDLI5_MOUSE	1.27	2.40	0.61	2.40E-03
225	sp|P40124|CAP1_MOUSE	1.26	2.40	0.92	3.84E-06
226	sp|O35350|CAN1_MOUSE	1.26	2.40	0.50	1.96E-01
227	sp|P63213|GBG2_MOUSE	1.25	2.39	0.78	9.71E-05
228	sp|Q62219|TGFI1_MOUSE	1.25	2.38	0.57	9.14E-01
229	sp|Q99KC8|VMA5A_MOUSE	1.24	2.36	0.86	2.46E-05
230	sp|Q9Z247|FKBP9_MOUSE	1.23	2.35	0.51	1.31E-02
231	sp|P08207|S10AA_MOUSE	1.23	2.35	0.74	1.19E-02
232	sp|P01887|B2MG_MOUSE	1.23	2.34	0.89	6.25E-01
233	sp|Q8C1B7|SEP11_MOUSE	1.22	2.33	0.83	1.09E-03
234	sp|Q3THE2|ML12B_MOUSE	1.21	2.32	0.73	2.77E-01
235	sp|P63163|RSMN_MOUSE	1.20	2.30	0.67	1.22E-04
236	sp|P13020|GELS_MOUSE	1.20	2.30	0.87	5.00E-08
237	sp|O54962|BAF_MOUSE	1.20	2.29	0.52	2.12E-01
238	sp|Q6PDN3|MYLK_MOUSE	1.19	2.28	0.89	8.25E-04
239	sp|P29351|PTN6_MOUSE	1.19	2.28	0.66	1.04E-03
240	sp|P21614|VTDB_MOUSE	1.19	2.28	0.89	1.34E-04
241	sp|Q61838|A2M_MOUSE	1.18	2.26	0.72	8.16E-02
242	sp|P62500|T22D1_MOUSE	1.17	2.24	0.84	1.89E-03
243	sp|Q9ESB3|HRG_MOUSE	1.15	2.22	0.77	1.57E-01
244	sp|P97371|PSME1_MOUSE	1.14	2.21	0.81	3.26E-04
245	sp|Q6ZWM4|LSM8_MOUSE	1.13	2.19	0.67	1.00E-01
246	sp|Q61074|PPM1G_MOUSE	1.13	2.19	0.51	3.59E-03
247	sp|P14733|LMNB1_MOUSE	1.13	2.19	0.88	6.74E-04
248	sp|P48036|ANXA5_MOUSE	1.13	2.19	0.87	2.00E-03
249	sp|P18760|COF1_MOUSE	1.13	2.18	0.83	6.23E-08
250	sp|P28352|APEX1_MOUSE	1.13	2.18	0.60	1.29E-02
251	sp|P27546|MAP4_MOUSE	1.12	2.17	0.81	1.23E-01
252	sp|Q9JK48|SHLB1_MOUSE	1.12	2.17	0.62	5.48E-01
253	sp|Q9DBG9|TX1B3_MOUSE	1.11	2.16	0.75	1.51E-04
254	sp|P62962|PROF1_MOUSE	1.11	2.16	0.88	8.92E-03
255	sp|Q9EQU5|SET_MOUSE	1.10	2.15	0.90	6.24E-04
256	sp|Q9EST5|AN32B_MOUSE	1.10	2.14	0.91	1.33E-02
257	sp|Q91XC8|DAP1_MOUSE	1.09	2.13	0.69	9.64E-02
258	sp|Q921E2|RAB31_MOUSE	1.09	2.12	0.55	8.81E-03
259	sp|P32261|ANT3_MOUSE	1.08	2.11	0.76	5.38E-01
260	sp|Q9WUU7|CATZ_MOUSE	1.07	2.09	0.85	2.19E-02
261	sp|Q9CPW4|ARPC5_MOUSE	1.06	2.09	0.90	8.18E-07
262	sp|P39061|COIA1_MOUSE	1.06	2.08	0.94	8.49E-02
263	sp|P07759|SPA3K_MOUSE	1.05	2.07	0.81	2.21E-01
264	sp|P26350|PTMA_MOUSE	1.05	2.07	0.61	1.01E-01
265	sp|P54923|ADPRH_MOUSE	1.04	2.06	0.84	1.92E-04
266	sp|Q91VW3|SH3L3_MOUSE	1.04	2.06	0.72	4.48E-03
267	sp|Q9JKF1|IQGA1_MOUSE	1.03	2.04	0.78	6.32E-03
268	sp|P10493|NID1_MOUSE	1.03	2.04	0.94	5.23E-04
269	sp|Q00623|APOA1_MOUSE	1.03	2.04	0.87	1.20E-01
270	sp|O08529|CAN2_MOUSE	1.03	2.04	0.60	3.24E-01
271	sp|P23198|CBX3_MOUSE	1.02	2.03	0.57	4.74E-02
272	sp|P97372|PSME2_MOUSE	1.02	2.03	0.81	5.24E-05
273	sp|P49312|ROA1_MOUSE	1.02	2.03	0.88	1.24E-03
274	sp|Q64727|VINC_MOUSE	1.02	2.03	0.92	9.42E-04
275	sp|Q9CX86|ROA0_MOUSE	1.01	2.01	0.69	1.65E-03
276	sp|P06281|RENI1_MOUSE	1.01	2.01	0.84	3.71E-03
277	sp|P02463|CO4A1_MOUSE	1.01	2.01	0.86	1.25E-04
278	sp|Q63961|EGLN_MOUSE	1.00	2.00	0.64	3.94E-01
279	sp|Q6WVG3|KCD12_MOUSE	1.00	2.00	0.66	9.52E-04
280	sp|Q62318|TIF1B_MOUSE	0.99	1.99	0.81	6.65E-03
281	sp|Q9DBG5|PLIN3_MOUSE	0.99	1.98	0.72	1.02E-02
282	sp|P14824|ANXA6_MOUSE	0.99	1.98	0.91	1.27E-02
283	sp|Q8VIJ6|SFPQ_MOUSE	0.98	1.97	0.81	1.13E-03
284	sp|Q9CQW2|ARL8B_MOUSE	0.98	1.97	0.58	9.96E-02

285	sp|Q61001|LAMA5_MOUSE	0.97	1.96	0.89	7.33E-03
286	sp|Q9WUM4|COR1C_MOUSE	0.97	1.95	0.82	9.46E-03
287	sp|Q9DBC7|KAP0_MOUSE	0.96	1.95	0.79	1.18E-04
288	sp|Q8K0E8|FIBB_MOUSE	0.96	1.95	0.71	2.06E-01
289	sp|P68510|1433F_MOUSE	0.95	1.94	0.67	1.32E-02
290	sp|Q9JM76|ARPC3_MOUSE	0.95	1.93	0.80	2.79E-03
291	sp|P63280|UBC9_MOUSE	0.94	1.92	0.91	1.11E-08
292	sp|Q80UG5|SEPT9_MOUSE	0.94	1.91	0.56	2.65E-03
293	sp|Q62186|SSRD_MOUSE	0.93	1.91	0.54	6.78E-02
294	sp|E9PV24|FIBA_MOUSE	0.93	1.91	0.69	2.16E-01
295	sp|Q920E5|FPPS_MOUSE	0.93	1.91	0.53	2.12E-02
296	sp|Q60749|KHDR1_MOUSE	0.93	1.90	0.52	5.83E-02
297	sp|P10923|OSTP_MOUSE	0.92	1.90	0.60	1.95E-04
298	sp|Q8BH43|WASF2_MOUSE	0.91	1.89	0.60	9.57E-04
299	sp|O08553|DPYL2_MOUSE	0.91	1.88	0.83	7.44E-03
300	sp|P56959|FUS_MOUSE	0.90	1.87	0.81	1.27E-04
301	sp|Q9CR86|CHSP1_MOUSE	0.89	1.85	0.58	1.84E-01
302	sp|Q9WVB0|RBPMS_MOUSE	0.89	1.85	0.71	1.58E-01
303	sp|P51125|ICAL_MOUSE	0.89	1.85	0.50	1.55E-01
304	sp|Q9JHU9|INO1_MOUSE	0.89	1.85	0.59	1.09E-01
305	sp|P02468|LAMC1_MOUSE	0.87	1.83	0.90	6.38E-03
306	sp|Q8C522|ENDD1_MOUSE	0.87	1.83	0.71	1.49E-04
307	sp|P43406|ITAV_MOUSE	0.87	1.82	0.54	2.39E-04
308	sp|Q3TEA8|HP1B3_MOUSE	0.86	1.82	0.89	5.42E-03
309	sp|Q6GSS7|H2A2A_MOUSE	0.86	1.81	0.56	5.21E-03
310	sp|Q9D8B3|CHM4B_MOUSE	0.85	1.81	0.59	6.21E-04
311	sp|Q61292|LAMB2_MOUSE	0.85	1.81	0.78	8.92E-03
312	sp|P08752|GNAI2_MOUSE	0.84	1.79	0.84	9.92E-03
313	sp|Q3THW5|H2AV_MOUSE	0.84	1.79	0.84	3.13E-04
314	sp|P50637|TSPO_MOUSE	0.84	1.79	0.56	6.94E-01
315	sp|Q9QZR9|CO4A4_MOUSE	0.83	1.78	0.74	1.41E-03
316	sp|O88322|NID2_MOUSE	0.83	1.77	0.87	2.47E-04
317	sp|Q3UZ39|LRRF1_MOUSE	0.83	1.77	0.70	1.13E-03
318	sp|Q07813|BAX_MOUSE	0.82	1.77	0.63	1.18E-01
319	sp|Q921M3|SF3B3_MOUSE	0.82	1.76	0.73	4.47E-02
320	sp|O70433|FHL2_MOUSE	0.82	1.76	0.71	7.81E-04
321	sp|P24452|CAPG_MOUSE	0.81	1.76	0.81	5.76E-04
322	sp|Q8BFZ3|ACTBL_MOUSE	0.81	1.75	0.91	1.48E-03
323	sp|P45377|ALD2_MOUSE	0.80	1.74	0.73	1.26E-04
324	sp|P47757|CAPZB_MOUSE	0.79	1.73	0.86	5.26E-03
325	sp|Q91YH5|ATLA3_MOUSE	0.78	1.72	0.69	1.86E-03
326	sp|Q8BH64|EHD2_MOUSE	0.78	1.72	0.57	1.56E-01
327	sp|Q9Z1Q9|SYVC_MOUSE	0.78	1.72	0.52	3.91E-02
328	sp|Q8VDW0|DX39A_MOUSE	0.78	1.71	0.57	6.26E-01
329	sp|Q8C854|MYEF2_MOUSE	0.77	1.71	0.65	4.10E-02
330	sp|Q99JY9|ARP3_MOUSE	0.77	1.71	0.93	5.66E-05
331	sp|Q9QXA5|LSM4_MOUSE	0.77	1.70	0.73	1.27E-03
332	sp|O88456|CPNS1_MOUSE	0.77	1.70	0.70	1.14E-03
333	sp|Q61207|SAP_MOUSE	0.76	1.70	0.82	9.42E-03
334	sp|Q60604|ADSV_MOUSE	0.76	1.69	0.58	9.73E-02
335	sp|Q91VM5|RMXL1_MOUSE	0.76	1.69	0.58	7.20E-01
336	sp|Q3U0V1|FUBP2_MOUSE	0.76	1.69	0.78	1.45E-03
337	sp|Q9Z1N5|DX39B_MOUSE	0.76	1.69	0.81	6.73E-03
338	sp|Q8BP92|RCN2_MOUSE	0.75	1.69	0.54	4.41E-02
339	sp|P84104|SRSF3_MOUSE	0.75	1.68	0.61	7.48E-01
340	sp|O54724|PTRF_MOUSE	0.74	1.67	0.69	1.96E-01
341	sp|P02469|LAMB1_MOUSE	0.74	1.67	0.84	2.86E-03
342	sp|P84089|ERH_MOUSE	0.73	1.66	0.71	5.27E-02
343	sp|A2ASQ1|AGRIN_MOUSE	0.73	1.66	0.67	1.97E-01
344	sp|Q3UTJ2|SRBS2_MOUSE	0.72	1.65	0.53	2.63E-02
345	sp|Q9CXY6|ILF2_MOUSE	0.72	1.65	0.84	3.67E-05
346	sp|P59999|ARPC4_MOUSE	0.72	1.65	0.85	4.33E-06
347	sp|P26039|TLN1_MOUSE	0.72	1.65	0.89	1.43E-03
348	sp|P97822|AN32E_MOUSE	0.72	1.65	0.68	3.30E-02
349	sp|Q00612|G6PD1_MOUSE	0.72	1.65	0.76	9.08E-05
350	sp|P27661|H2AX_MOUSE	0.72	1.64	0.83	3.13E-04
351	sp|Q9ERG0|LIMA1_MOUSE	0.71	1.64	0.62	5.72E-03
352	sp|Q62376|RU17_MOUSE	0.71	1.63	0.58	5.57E-03
353	sp|O54879|HMGB3_MOUSE	0.70	1.63	0.64	7.37E-04
354	sp|Q7TNC4|LC7L2_MOUSE	0.70	1.63	0.63	2.48E-03
355	sp|Q501J6|DDX17_MOUSE	0.70	1.63	0.76	8.56E-02
356	sp|Q7TMK9|HNRPQ_MOUSE	0.70	1.62	0.67	3.08E-01
357	sp|Q99K48|NONO_MOUSE	0.69	1.62	0.89	4.81E-03

358	sp|Q91W90|TXND5_MOUSE	0.68	1.60	0.75	4.41E-02
359	sp|P70168|IMB1_MOUSE	0.67	1.59	0.77	9.74E-02
360	sp|Q8CGP2|H2B1P_MOUSE	0.67	1.59	0.88	2.15E-03
361	sp|O88342|WDR1_MOUSE	0.67	1.59	0.65	5.67E-04
362	sp|Q61166|MARE1_MOUSE	0.67	1.59	0.64	3.48E-05
363	sp|Q922R8|PDIA6_MOUSE	0.67	1.59	0.88	9.34E-03
364	sp|Q61029|LAP2B_MOUSE	0.67	1.59	0.78	9.92E-03
365	sp|Q9D0T1|NH2L1_MOUSE	0.66	1.58	0.53	2.99E-02
366	sp|Q9Z204|HNRPC_MOUSE	0.66	1.58	0.51	4.21E-01
367	sp|Q9Z2N8|ACL6A_MOUSE	0.66	1.58	0.58	8.26E-04
368	sp|P61161|ARP2_MOUSE	0.66	1.58	0.81	5.83E-01
369	sp|Q9DCN2|NB5R3_MOUSE	0.66	1.58	0.58	5.37E-01
370	sp|Q61937|NPM_MOUSE	0.66	1.58	0.83	1.75E-02
371	sp|Q7TNG5|EMAL2_MOUSE	0.66	1.58	0.51	5.51E-01
372	sp|Q8BG05|ROA3_MOUSE	0.66	1.58	0.88	1.78E-04
373	sp|P62311|LSM3_MOUSE	0.65	1.57	0.91	1.64E-04
374	sp|Q8VED5|K2C79_MOUSE	0.65	1.57	0.56	1.06E-01
375	sp|P62315|SMD1_MOUSE	0.65	1.57	0.75	1.51E-03
376	sp|Q8C166|CPNE1_MOUSE	0.64	1.56	0.63	6.52E-02
377	sp|Q05793|PGBM_MOUSE	0.64	1.56	0.81	2.55E-03
378	sp|Q60668|HNRPD_MOUSE	0.63	1.55	0.56	6.20E-02
379	sp|Q4KML4|ABRAL_MOUSE	0.63	1.55	0.87	2.73E-02
380	sp|Q9Z2W0|DNPEP_MOUSE	0.62	1.54	0.59	1.85E-02
381	sp|Q8BL97|SRSF7_MOUSE	0.62	1.54	0.78	5.27E-06
382	sp|P61957|SUMO2_MOUSE	0.62	1.54	0.56	8.02E-01
383	sp|Q7TSV4|PGM2_MOUSE	0.62	1.54	0.65	3.71E-03
384	sp|Q62093|SRSF2_MOUSE	0.62	1.53	0.74	5.89E-01
385	sp|P63024|VAMP3_MOUSE	0.62	1.53	0.67	1.83E-02
386	sp|Q9D1J3|SARNP_MOUSE	0.61	1.53	0.58	1.89E-02
387	sp|O08807|PRDX4_MOUSE	0.61	1.53	0.89	1.02E-03
388	sp|Q922Q8|LRC59_MOUSE	0.60	1.51	0.64	8.19E-03
389	sp|Q9Z2D6|MECP2_MOUSE	0.60	1.51	0.73	4.42E-02
390	sp|Q9CY50|SSRA_MOUSE	0.60	1.51	0.63	3.78E-03
391	sp|Q9Z172|SUMO3_MOUSE	0.59	1.51	0.57	5.49E-01
392	sp|Q9D0E1|HNRPM_MOUSE	0.59	1.50	0.82	3.36E-01
393	sp|Q61792|LASP1_MOUSE	0.58	1.50	0.66	2.18E-01
394	sp|Q99020|ROAA_MOUSE	0.58	1.50	0.84	3.06E-03
395	sp|Q8CI94|PYGB_MOUSE	0.58	1.49	0.51	6.03E-01
396	sp|P97447|FHL1_MOUSE	0.57	1.49	0.55	2.79E-01
397	sp|P08003|PDIA4_MOUSE	0.57	1.48	0.88	1.81E-03
398	sp|Q01730|RSU1_MOUSE	0.57	1.48	0.68	2.83E-02
399	sp|P70372|ELAV1_MOUSE	0.57	1.48	0.63	1.14E-01
400	sp|P60766|CDC42_MOUSE	0.57	1.48	0.75	3.19E-02
401	sp|P30412|PPIC_MOUSE	0.56	1.48	0.69	1.83E-01
402	sp|P05132|KAPCA_MOUSE	0.56	1.47	0.78	9.34E-01
403	sp|P62806|H4_MOUSE	0.56	1.47	0.66	6.17E-01
404	sp|Q99KF1|TMED9_MOUSE	0.55	1.47	0.71	3.49E-04
405	sp|Q8BFY9|TNPO1_MOUSE	0.55	1.46	0.56	4.00E-02
406	sp|P09405|NUCL_MOUSE	0.55	1.46	0.85	7.74E-02
407	sp|P34022|RANG_MOUSE	0.55	1.46	0.51	2.87E-04
408	sp|Q9CVB6|ARPC2_MOUSE	0.55	1.46	0.79	2.09E-04
409	sp|O35737|HNRH1_MOUSE	0.55	1.46	0.71	6.93E-03
410	sp|P62305|RUXE_MOUSE	0.54	1.45	0.80	2.29E-03
411	sp|Q9Z2X1|HNRPF_MOUSE	0.54	1.45	0.74	7.75E-04
412	sp|Q61102|ABCB7_MOUSE	0.54	1.45	0.89	5.19E-04
413	sp|Q99JY3|GIMA4_MOUSE	0.53	1.45	0.54	3.91E-02
414	sp|Q60972|RBBP4_MOUSE	0.53	1.45	0.56	7.08E-03
415	sp|P47754|CAZA2_MOUSE	0.53	1.45	0.51	7.24E-01
416	sp|O55222|ILK_MOUSE	0.53	1.45	0.78	8.58E-03
417	sp|P63158|HMGB1_MOUSE	0.53	1.45	0.78	8.24E-02
418	sp|O08583|THOC4_MOUSE	0.53	1.44	0.72	3.68E-02
419	sp|Q8VEK3|HNRPU_MOUSE	0.53	1.44	0.84	8.83E-03
420	sp|P63085|MK01_MOUSE	0.53	1.44	0.62	1.81E-01
421	sp|Q9JHJ0|TMOD3_MOUSE	0.53	1.44	0.60	1.81E-03
422	sp|Q9QZS0|CO4A3_MOUSE	0.52	1.44	0.51	1.68E-01
423	sp|P60710|ACTB_MOUSE	0.52	1.43	0.90	6.17E-03
424	sp|O70251|EF1B_MOUSE	0.52	1.43	0.53	5.43E-01
425	sp|Q9R0P5|DEST_MOUSE	0.51	1.43	0.67	1.39E-02
426	sp|Q6PDM2|SRSF1_MOUSE	0.51	1.42	0.71	1.09E-01
427	sp|P26883|FKB1A_MOUSE	0.50	1.42	0.67	2.85E-02
428	sp|Q9EPC1|PARVA_MOUSE	0.50	1.41	0.66	2.37E-03
429	sp|Q99JI6|RAP1B_MOUSE	0.50	1.41	0.58	5.18E-01
430	sp|P97314|CSRP2_MOUSE	0.50	1.41	0.71	1.45E-03

431	sp|Q8BFW7|LPP_MOUSE	0.49	1.41	0.72	1.04E-03
432	sp|P62317|SMD2_MOUSE	0.48	1.40	0.82	2.16E-01
433	sp|O89023|TPP1_MOUSE	0.48	1.40	0.54	9.46E-02
434	sp|P97429|ANXA4_MOUSE	0.48	1.39	0.57	8.48E-02
435	sp|Q9R0Y5|KAD1_MOUSE	0.48	1.39	0.81	7.91E-03
436	sp|Q8VE37|RCC1_MOUSE	0.48	1.39	0.62	1.12E-03
437	sp|Q9R0P6|SC11A_MOUSE	0.47	1.39	0.78	2.47E-03
438	sp|Q62470|ITA3_MOUSE	0.47	1.39	0.52	3.05E-02
439	sp|Q921F2|TADBP_MOUSE	0.47	1.39	0.82	2.50E-04
440	sp|P17047|LAMP2_MOUSE	0.47	1.39	0.66	5.52E-03
441	sp|P00493|HPRT_MOUSE	0.47	1.38	0.74	4.19E-02
442	sp|Q80VD1|FA98B_MOUSE	0.47	1.38	0.57	2.42E-01
443	sp|Q61656|DDX5_MOUSE	0.47	1.38	0.77	1.43E-02
444	sp|P62320|SMD3_MOUSE	0.47	1.38	0.68	9.71E-03
445	sp|Q9DAW9|CNN3_MOUSE	0.46	1.38	0.57	4.48E-01
446	sp|Q8CIB5|FERM2_MOUSE	0.46	1.37	0.71	5.69E-02
447	sp|P43274|H14_MOUSE	0.46	1.37	0.64	3.22E-02
448	sp|P61750|ARF4_MOUSE	0.46	1.37	0.51	2.88E-02
449	sp|O08547|SC22B_MOUSE	0.45	1.36	0.64	6.80E-02
450	sp|P26041|MOES_MOUSE	0.44	1.36	0.57	9.75E-02
451	sp|P61982|1433G_MOUSE	0.43	1.35	0.65	9.62E-01
452	sp|P10605|CATB_MOUSE	0.43	1.35	0.85	1.33E-01
453	sp|Q8CCS6|PABP2_MOUSE	0.43	1.35	0.66	1.33E-02
454	sp|P46467|VPS4B_MOUSE	0.43	1.35	0.60	2.50E-01
455	sp|Q9WUM3|COR1B_MOUSE	0.42	1.34	0.55	1.96E-03
456	sp|Q61990|PCBP2_MOUSE	0.42	1.34	0.61	5.23E-04
457	sp|Q91VC3|IF4A3_MOUSE	0.42	1.33	0.51	3.16E-01
458	sp|P54823|DDX6_MOUSE	0.41	1.33	0.63	2.52E-03
459	sp|P61979|HNRPK_MOUSE	0.41	1.33	0.77	1.44E-03
460	sp|Q99K51|PLST_MOUSE	0.41	1.33	0.51	3.48E-01
461	sp|P62307|RUXF_MOUSE	0.41	1.33	0.67	2.98E-02
462	sp|Q99PT1|GDIR1_MOUSE	0.41	1.33	0.64	5.46E-03
463	sp|Q61545|EWS_MOUSE	0.40	1.32	0.53	5.18E-02
464	sp|Q9QZQ8|H2AY_MOUSE	0.40	1.32	0.70	2.88E-01
465	sp|P09055|ITB1_MOUSE	0.39	1.31	0.60	2.62E-02
466	sp|Q9R1Z8|VINEX_MOUSE	0.39	1.31	0.55	1.34E-01
467	sp|Q64213|SF01_MOUSE	0.38	1.31	0.51	7.69E-02
468	sp|Q8VDP6|CDIPT_MOUSE	0.38	1.30	0.67	2.30E-01
469	sp|Q60598|SRC8_MOUSE	0.38	1.30	0.50	1.01E-01
470	sp|P27773|PDIA3_MOUSE	0.37	1.29	0.65	3.09E-02
471	sp|Q8BT60|CPNE3_MOUSE	0.37	1.29	0.52	8.90E-03
472	sp|P58389|PTPA_MOUSE	0.36	1.29	0.62	2.88E-01
473	sp|Q61735|CD47_MOUSE	0.36	1.29	0.60	9.20E-01
474	sp|Q9CQU0|TXD12_MOUSE	0.35	1.28	0.56	2.21E-02
475	sp|P62309|RUXG_MOUSE	0.35	1.27	0.54	6.12E-01
476	sp|P62827|RAN_MOUSE	0.31	1.24	0.62	6.57E-01
477	sp|P60867|RS20_MOUSE	0.29	1.23	0.51	7.74E-01
478	sp|Q9D898|ARP5L_MOUSE	-0.30	1.23	0.60	1.76E-02
479	sp|P63017|HSP7C_MOUSE	-0.31	1.24	0.80	4.21E-02
480	sp|P14869|RLA0_MOUSE	-0.32	1.25	0.51	1.08E-01
481	sp|P17742|PPIA_MOUSE	-0.33	1.25	0.76	2.99E-02
482	sp|Q9CZ44|NSF1C_MOUSE	-0.33	1.26	0.58	8.80E-02
483	sp|Q01853|TERA_MOUSE	-0.35	1.27	0.60	4.73E-01
484	sp|P15626|GSTM2_MOUSE	-0.35	1.28	0.54	4.49E-01
485	sp|P84091|AP2M1_MOUSE	-0.36	1.28	0.55	4.46E-01
486	sp|P58021|TM9S2_MOUSE	-0.41	1.33	0.54	4.92E-02
487	sp|Q9Z1Q5|CLIC1_MOUSE	-0.41	1.33	0.59	5.91E-01
488	sp|Q8BGS7|CEPT1_MOUSE	-0.42	1.34	0.60	6.55E-01
489	sp|Q9Z1X4|ILF3_MOUSE	-0.43	1.35	0.56	6.94E-01
490	sp|Q61598|GDIB_MOUSE	-0.43	1.35	0.75	3.04E-02
491	sp|P23492|PNPH_MOUSE	-0.45	1.36	0.53	6.82E-01
492	sp|Q93092|TALDO_MOUSE	-0.45	1.36	0.61	3.86E-01
493	sp|Q61171|PRDX2_MOUSE	-0.45	1.37	0.88	2.27E-02
494	sp|P62259|1433E_MOUSE	-0.45	1.37	0.74	6.98E-02
495	sp|P62204|CALM_MOUSE	-0.46	1.38	0.50	1.05E-01
496	sp|P40142|TKT_MOUSE	-0.47	1.38	0.84	2.33E-02
497	sp|Q8C0C7|SYFA_MOUSE	-0.47	1.39	0.55	4.55E-03
498	sp|O70493|SNX12_MOUSE	-0.48	1.39	0.53	9.56E-01
499	sp|Q61469|LPP1_MOUSE	-0.48	1.39	0.54	2.24E-01
500	sp|Q11011|PSA_MOUSE	-0.48	1.39	0.51	7.85E-02
501	sp|P97384|ANX11_MOUSE	-0.48	1.40	0.50	4.45E-02
502	sp|P46471|PRS7_MOUSE	-0.49	1.41	0.64	2.98E-01
503	sp|P40237|CD82_MOUSE	-0.50	1.41	0.54	9.25E-01

504	sp|P46412|GPX3_MOUSE	-0.50	1.41	0.83	2.68E-03
505	sp|Q3TDQ1|STT3B_MOUSE	-0.50	1.42	0.58	3.95E-01
506	sp|Q8R1Q8|DC1L1_MOUSE	-0.51	1.42	0.58	8.84E-04
507	sp|Q9QUI0|RHOA_MOUSE	-0.51	1.42	0.70	3.31E-02
508	sp|P51150|RAB7A_MOUSE	-0.51	1.43	0.51	3.15E-01
509	sp|Q9Z1Z0|USO1_MOUSE	-0.51	1.43	0.65	1.82E-01
510	sp|Q91WG5|AAKG2_MOUSE	-0.52	1.43	0.58	2.08E-01
511	sp|Q60770|STXB3_MOUSE	-0.52	1.43	0.59	5.04E-03
512	sp|Q7M6Y3|PICAL_MOUSE	-0.52	1.44	0.52	3.14E-01
513	sp|O54990|PROM1_MOUSE	-0.53	1.44	0.56	2.87E-01
514	sp|P42932|TCPQ_MOUSE	-0.53	1.44	0.72	4.87E-01
515	sp|Q6P8X1|SNX6_MOUSE	-0.53	1.45	0.53	8.57E-02
516	sp|P26638|SYSC_MOUSE	-0.53	1.45	0.82	1.27E-03
517	sp|P46460|NSF_MOUSE	-0.54	1.45	0.52	5.97E-02
518	sp|Q99KN9|EPN4_MOUSE	-0.55	1.46	0.51	1.11E-02
519	sp|P62821|RAB1A_MOUSE	-0.55	1.46	0.64	8.96E-04
520	sp|P07901|HS90A_MOUSE	-0.55	1.46	0.82	5.95E-02
521	sp|P53994|RAB2A_MOUSE	-0.55	1.47	0.79	1.47E-02
522	sp|P70195|PSB7_MOUSE	-0.56	1.47	0.59	3.21E-02
523	sp|P63276|RS17_MOUSE	-0.57	1.48	0.58	2.85E-03
524	sp|Q68FD5|CLH1_MOUSE	-0.57	1.48	0.77	2.36E-04
525	sp|P35293|RAB18_MOUSE	-0.57	1.48	0.52	2.33E-02
526	sp|P61205|ARF3_MOUSE	-0.57	1.49	0.76	2.19E-03
527	sp|Q9JHR7|IDE_MOUSE	-0.59	1.51	0.53	2.13E-03
528	sp|P80317|TCPZ_MOUSE	-0.60	1.52	0.55	3.66E-01
529	sp|P06151|LDHA_MOUSE	-0.60	1.52	0.88	2.00E-02
530	sp|Q9EQX4|AIF1L_MOUSE	-0.60	1.52	0.57	6.06E-01
531	sp|Q9JL35|HMGN5_MOUSE	-0.61	1.52	0.57	1.29E-01
532	sp|Q9D1G1|RAB1B_MOUSE	-0.61	1.52	0.59	2.16E-01
533	sp|P31428|DPEP1_MOUSE	-0.61	1.53	0.86	2.94E-05
534	sp|Q62446|FKBP3_MOUSE	-0.63	1.55	0.81	4.23E-03
535	sp|Q61249|IGBP1_MOUSE	-0.63	1.55	0.54	1.27E-03
536	sp|Q9QUH0|GLRX1_MOUSE	-0.63	1.55	0.83	3.85E-03
537	sp|Q9DBH5|LMAN2_MOUSE	-0.64	1.55	0.59	9.89E-03
538	sp|P80315|TCPD_MOUSE	-0.64	1.56	0.51	3.43E-01
539	sp|Q9JMH6|TRXR1_MOUSE	-0.64	1.56	0.76	3.13E-03
540	sp|Q9QYB1|CLIC4_MOUSE	-0.67	1.59	0.54	2.13E-01
541	sp|Q8BMA6|SRP68_MOUSE	-0.67	1.59	0.56	1.27E-02
542	sp|Q91V92|ACLY_MOUSE	-0.67	1.60	0.85	6.47E-03
543	sp|O09044|SNP23_MOUSE	-0.68	1.60	0.52	5.57E-04
544	sp|Q9EP69|SAC1_MOUSE	-0.68	1.60	0.70	2.24E-02
545	sp|Q61035|SYHC_MOUSE	-0.68	1.61	0.53	2.73E-01
546	sp|Q99L47|F10A1_MOUSE	-0.68	1.61	0.85	6.55E-01
547	sp|Q9R0N0|GALK1_MOUSE	-0.69	1.61	0.64	1.41E-01
548	sp|P05064|ALDOA_MOUSE	-0.69	1.61	0.90	1.25E-04
549	sp|Q9CQ89|CUTA_MOUSE	-0.69	1.62	0.54	2.56E-01
550	sp|Q9CPV4|GLOD4_MOUSE	-0.70	1.62	0.87	5.87E-05
551	sp|P30416|FKBP4_MOUSE	-0.70	1.62	0.72	3.99E-04
552	sp|Q9D1L9|LTOR5_MOUSE	-0.70	1.62	0.62	3.17E-04
553	sp|Q3TW96|UAP1L_MOUSE	-0.70	1.63	0.84	1.54E-02
554	sp|Q8R2Y8|PTH2_MOUSE	-0.71	1.63	0.96	2.40E-03
555	sp|O54984|ASNA_MOUSE	-0.71	1.64	0.79	3.23E-01
556	sp|O55143|AT2A2_MOUSE	-0.72	1.64	0.75	7.17E-03
557	sp|O55022|PGRC1_MOUSE	-0.72	1.65	0.84	2.02E-02
558	sp|Q9QYC0|ADDA_MOUSE	-0.72	1.65	0.59	2.53E-02
559	sp|Q9WUA2|SYFB_MOUSE	-0.72	1.65	0.63	9.49E-02
560	sp|Q6ZWY3|RS27L_MOUSE	-0.73	1.65	0.86	2.19E-02
561	sp|Q99KI3|EMC3_MOUSE	-0.74	1.67	0.78	6.57E-01
562	sp|Q91VH2|SNX9_MOUSE	-0.74	1.67	0.75	1.30E-01
563	sp|P68373|TBA1C_MOUSE	-0.74	1.67	0.67	1.88E-01
564	sp|Q6IRU5|CLCB_MOUSE	-0.74	1.68	0.77	5.78E-05
565	sp|Q80SU7|GVIN1_MOUSE	-0.75	1.68	0.63	6.51E-02
566	sp|P46638|RB11B_MOUSE	-0.75	1.69	0.89	4.16E-04
567	sp|P04117|FABP4_MOUSE	-0.76	1.69	0.78	6.27E-02
568	sp|P47964|RL36_MOUSE	-0.76	1.69	0.66	1.81E-01
569	sp|Q9Z2W1|STK25_MOUSE	-0.77	1.70	0.58	7.55E-01
570	sp|P63037|DNJA1_MOUSE	-0.77	1.70	0.81	9.16E-03
571	sp|P11881|ITPR1_MOUSE	-0.77	1.70	0.83	2.03E-06
572	sp|P62880|GBB2_MOUSE	-0.77	1.70	0.63	7.34E-03
573	sp|P40336|VP26A_MOUSE	-0.78	1.72	0.92	1.63E-03
574	sp|Q68FH4|GALK2_MOUSE	-0.78	1.72	0.81	1.78E-01
575	sp|Q8K021|SCAM1_MOUSE	-0.78	1.72	0.66	8.54E-03
576	sp|P54822|PUR8_MOUSE	-0.79	1.73	0.69	2.87E-05

577	sp|O70492|SNX3_MOUSE	-0.79	1.73	0.85	2.38E-04
578	sp|Q9CQB5|CISD2_MOUSE	-0.79	1.73	0.60	9.61E-03
579	sp|Q8K2C9|HACD3_MOUSE	-0.79	1.73	0.88	7.03E-03
580	sp|P19157|GSTP1_MOUSE	-0.80	1.74	0.93	1.03E-03
581	sp|Q9D819|IPYR_MOUSE	-0.81	1.76	0.79	6.78E-01
582	sp|P50396|GDIA_MOUSE	-0.82	1.76	0.55	7.57E-02
583	sp|Q9CQM9|GLRX3_MOUSE	-0.82	1.77	0.67	1.19E-03
584	sp|P10639|THIO_MOUSE	-0.82	1.77	0.79	9.40E-05
585	sp|Q99LB6|MAT2B_MOUSE	-0.83	1.78	0.96	1.81E-02
586	sp|P35278|RAB5C_MOUSE	-0.83	1.78	0.65	6.88E-02
587	sp|P08556|RASN_MOUSE	-0.84	1.79	0.81	1.66E-03
588	sp|O88952|LIN7C_MOUSE	-0.84	1.79	0.57	9.57E-04
589	sp|Q9D1L0|CHCH2_MOUSE	-0.84	1.79	0.67	1.16E-03
590	sp|Q64133|AOFA_MOUSE	-0.85	1.80	0.72	1.84E-01
591	sp|Q91V64|ISOC1_MOUSE	-0.86	1.81	0.85	5.02E-05
592	sp|P27601|GNA13_MOUSE	-0.86	1.82	0.64	6.58E-03
593	sp|Q62261|SPTB2_MOUSE	-0.87	1.83	0.85	2.49E-04
594	sp|Q9CPU0|LGUL_MOUSE	-0.87	1.83	0.83	9.27E-04
595	sp|P16546|SPTN1_MOUSE	-0.88	1.84	0.98	1.93E-05
596	sp|Q64471|GSTT1_MOUSE	-0.88	1.84	0.85	2.50E-02
597	sp|D3Z7P3|GLSK_MOUSE	-0.88	1.84	0.76	7.61E-04
598	sp|Q9CS42|PRPS2_MOUSE	-0.89	1.85	0.58	9.00E-03
599	sp|P15947|KLK1_MOUSE	-0.90	1.87	0.63	1.67E-03
600	sp|Q8BFZ9|ERLN2_MOUSE	-0.90	1.87	0.80	2.20E-04
601	sp|Q99J56|DERL1_MOUSE	-0.91	1.88	0.54	1.22E-01
602	sp|Q9WV80|SNX1_MOUSE	-0.92	1.89	0.64	5.36E-01
603	sp|Q921Z5|TFIP8_MOUSE	-0.92	1.90	0.68	1.02E-02
604	sp|Q9DCL9|PUR6_MOUSE	-0.92	1.90	0.75	5.29E-01
605	sp|Q9CZW5|TOM70_MOUSE	-0.93	1.90	0.60	3.70E-03
606	sp|Q9D662|SC23B_MOUSE	-0.93	1.91	0.68	5.68E-01
607	sp|Q922B2|SYDC_MOUSE	-0.94	1.92	0.57	1.01E-01
608	sp|Q3UQ44|IQGA2_MOUSE	-0.94	1.92	0.55	1.44E-03
609	sp|B2RSH2|GNAI1_MOUSE	-0.95	1.93	0.64	9.32E-04
610	sp|O70404|VAMP8_MOUSE	-0.95	1.94	0.83	2.12E-04
611	sp|Q9ES97|RTN3_MOUSE	-0.95	1.94	0.88	1.68E-03
612	sp|Q3THS6|METK2_MOUSE	-0.96	1.94	0.78	2.75E-03
613	sp|P70296|PEBP1_MOUSE	-0.96	1.95	0.95	1.59E-06
614	sp|P68372|TBB4B_MOUSE	-0.96	1.95	1.00	1.10E-06
615	sp|Q9CQM5|TXD17_MOUSE	-0.96	1.95	0.87	1.90E-05
616	sp|O88587|COMT_MOUSE	-0.96	1.95	0.82	4.04E-02
617	sp|Q8R1V4|TMED4_MOUSE	-0.97	1.95	0.86	1.74E-01
618	sp|Q8K274|KT3K_MOUSE	-0.97	1.96	0.66	7.16E-01
619	sp|Q9D0M5|DYL2_MOUSE	-0.98	1.97	0.50	5.24E-01
620	sp|O09043|NAPSA_MOUSE	-0.98	1.98	0.67	3.91E-01
621	sp|Q9CR67|TMM33_MOUSE	-0.99	1.99	0.83	1.86E-03
622	sp|Q9D1A2|CNDP2_MOUSE	-1.00	2.00	0.85	2.17E-02
623	sp|Q9D358|PPAC_MOUSE	-1.01	2.01	0.65	6.32E-01
624	sp|P10630|IF4A2_MOUSE	-1.01	2.01	0.68	5.20E-03
625	sp|Q9Z0P4|PALM_MOUSE	-1.01	2.02	0.78	6.81E-06
626	sp|Q9ESE1|LRBA_MOUSE	-1.02	2.03	0.51	2.53E-03
627	sp|O08709|PRDX6_MOUSE	-1.02	2.03	0.96	7.15E-09
628	sp|Q9DBP5|KCY_MOUSE	-1.03	2.04	0.83	6.50E-04
629	sp|P12367|KAP2_MOUSE	-1.03	2.05	0.51	1.12E-04
630	sp|P28843|DPP4_MOUSE	-1.04	2.05	0.80	1.81E-03
631	sp|Q9R0X4|ACOT9_MOUSE	-1.04	2.05	0.58	8.99E-03
632	sp|P55258|RAB8A_MOUSE	-1.04	2.06	0.82	5.53E-04
633	sp|Q11136|PEPD_MOUSE	-1.04	2.06	0.50	7.47E-02
634	sp|Q9DCZ1|GMPR1_MOUSE	-1.05	2.06	0.92	2.40E-05
635	sp|P06745|G6PI_MOUSE	-1.05	2.07	0.96	7.31E-07
636	sp|Q9D6Z1|NOP56_MOUSE	-1.06	2.08	0.57	1.29E-03
637	sp|Q571I9|A16A1_MOUSE	-1.06	2.08	0.76	5.46E-05
638	sp|P22892|AP1G1_MOUSE	-1.06	2.08	0.59	4.57E-02
639	sp|Q9EQH3|VPS35_MOUSE	-1.06	2.09	0.81	1.45E-01
640	sp|O35345|IMA7_MOUSE	-1.07	2.10	0.61	6.36E-02
641	sp|Q9CY64|BIEA_MOUSE	-1.07	2.10	0.81	1.35E-04
642	sp|Q9CQU3|RER1_MOUSE	-1.08	2.11	0.52	4.49E-04
643	sp|O70475|UGDH_MOUSE	-1.08	2.12	0.82	1.92E-05
644	sp|Q9QXY6|EHD3_MOUSE	-1.09	2.12	0.57	3.75E-03
645	sp|O35643|AP1B1_MOUSE	-1.09	2.13	0.69	4.37E-02
646	sp|Q91V41|RAB14_MOUSE	-1.09	2.13	0.83	2.28E-02
647	sp|Q8R2K1|FUCM_MOUSE	-1.11	2.15	0.88	1.27E-04
648	sp|Q61699|HS105_MOUSE	-1.11	2.16	0.52	1.85E-02
649	sp|P09803|CADH1_MOUSE	-1.11	2.17	0.62	5.31E-06

650	sp|Q9Z0N2|IF2H_MOUSE	-1.12	2.17	0.57	4.45E-01
651	sp|Q9QZ23|NFU1_MOUSE	-1.12	2.18	0.67	1.18E-02
652	sp|Q8BJY1|PSMD5_MOUSE	-1.12	2.18	0.55	7.26E-04
653	sp|P16858|G3P_MOUSE	-1.13	2.18	0.90	2.07E-02
654	sp|Q9QYG0|NDRG2_MOUSE	-1.13	2.19	0.68	2.23E-04
655	sp|Q9CPQ3|TOM22_MOUSE	-1.13	2.19	0.56	2.09E-03
656	sp|P35700|PRDX1_MOUSE	-1.13	2.19	0.90	1.17E-03
657	sp|Q01768|NDKB_MOUSE	-1.14	2.20	0.90	3.54E-03
658	sp|Q8BMF3|MAON_MOUSE	-1.14	2.20	0.53	1.83E-01
659	sp|P15532|NDKA_MOUSE	-1.14	2.21	0.70	2.27E-03
660	sp|P10649|GSTM1_MOUSE	-1.15	2.22	0.89	5.92E-04
661	sp|Q9CXA2|T3HPD_MOUSE	-1.15	2.23	0.59	1.07E-02
662	sp|Q9QYB5|ADDG_MOUSE	-1.16	2.23	0.76	3.62E-04
663	sp|Q3ULJ0|GPD1L_MOUSE	-1.18	2.26	0.85	2.63E-04
664	sp|Q80SW1|SAHH2_MOUSE	-1.18	2.27	0.63	3.76E-06
665	sp|P45878|FKBP2_MOUSE	-1.19	2.28	0.64	8.36E-06
666	sp|O55234|PSB5_MOUSE	-1.19	2.29	0.76	1.76E-05
667	sp|Q9CQX2|CYB5B_MOUSE	-1.20	2.29	0.90	4.21E-02
668	sp|Q9QYA2|TOM40_MOUSE	-1.20	2.30	0.52	1.97E-05
669	sp|P55264|ADK_MOUSE	-1.21	2.31	0.83	2.10E-02
670	sp|Q8CFV9|RIFK_MOUSE	-1.21	2.31	0.53	8.25E-03
671	sp|Q9CZ42|NNRD_MOUSE	-1.21	2.32	0.82	3.33E-03
672	sp|P62342|SELT_MOUSE	-1.22	2.32	0.96	2.93E-04
673	sp|Q8QZY2|GLCTK_MOUSE	-1.23	2.34	0.74	3.91E-05
674	sp|O35988|SDC4_MOUSE	-1.23	2.34	0.61	1.20E-01
675	sp|Q8K411|PREP_MOUSE	-1.23	2.35	0.58	2.46E-04
676	sp|P47915|RL29_MOUSE	-1.24	2.37	0.54	4.11E-01
677	sp|Q9D6U8|F162A_MOUSE	-1.25	2.38	0.67	3.07E-02
678	sp|Q91V12|BACH_MOUSE	-1.25	2.38	0.81	7.23E-01
679	sp|Q9DBJ1|PGAM1_MOUSE	-1.26	2.39	0.95	2.08E-04
680	sp|Q9DAS9|GBG12_MOUSE	-1.26	2.39	0.94	2.16E-05
681	sp|P28474|ADHX_MOUSE	-1.26	2.40	0.84	6.84E-06
682	sp|O88851|RBBP9_MOUSE	-1.27	2.41	0.56	8.20E-03
683	sp|P47791|GSHR_MOUSE	-1.28	2.43	0.64	2.91E-03
684	sp|O70439|STX7_MOUSE	-1.30	2.46	0.76	1.00E-05
685	sp|Q9WVE8|PACN2_MOUSE	-1.30	2.46	0.88	1.83E-03
686	sp|Q9ERN0|SCAM2_MOUSE	-1.30	2.46	0.58	2.80E-01
687	sp|P17182|ENOA_MOUSE	-1.30	2.47	0.98	3.77E-04
688	sp|Q6ZQI3|MLEC_MOUSE	-1.32	2.49	0.55	3.56E-04
689	sp|Q9WV85|NDK3_MOUSE	-1.32	2.49	0.56	1.52E-01
690	sp|P17710|HXK1_MOUSE	-1.33	2.51	0.92	1.51E-03
691	sp|P56565|S10A1_MOUSE	-1.33	2.51	0.78	1.07E-01
692	sp|Q99JB2|STML2_MOUSE	-1.33	2.52	0.59	2.05E-02
693	sp|Q99L04|DHRS1_MOUSE	-1.34	2.53	0.71	4.08E-02
694	sp|P10518|HEM2_MOUSE	-1.34	2.54	0.91	5.02E-05
695	sp|O70325|GPX41_MOUSE	-1.35	2.55	0.66	6.14E-06
696	sp|Q9CR98|F136A_MOUSE	-1.35	2.56	0.58	2.60E-02
697	sp|P17751|TPIS_MOUSE	-1.36	2.56	0.83	2.72E-05
698	sp|Q99LX0|PARK7_MOUSE	-1.37	2.58	0.87	3.63E-02
699	sp|P50247|SAHH_MOUSE	-1.37	2.58	0.91	1.12E-04
700	sp|Q8K4Z3|NNRE_MOUSE	-1.38	2.60	0.76	2.55E-05
701	sp|Q08857|CD36_MOUSE	-1.38	2.60	0.67	2.17E-02
702	sp|O35857|TIM44_MOUSE	-1.38	2.61	0.83	4.82E-04
703	sp|Q924M7|MPI_MOUSE	-1.39	2.61	0.74	2.65E-04
704	sp|Q99N23|CAH15_MOUSE	-1.40	2.63	0.63	2.76E-03
705	sp|Q9DCB8|ISCA2_MOUSE	-1.40	2.64	0.71	2.34E-04
706	sp|Q3UGR5|HDHD2_MOUSE	-1.41	2.66	0.82	3.40E-01
707	sp|P56393|COX7B_MOUSE	-1.41	2.67	0.59	2.13E-03
708	sp|B1AXP6|TOM5_MOUSE	-1.43	2.69	0.88	1.10E-01
709	sp|Q99LP6|GRPE1_MOUSE	-1.43	2.69	0.78	2.89E-03
710	sp|Q3UMF0|COBL1_MOUSE	-1.43	2.70	0.50	1.77E-05
711	sp|O09117|SYPL1_MOUSE	-1.45	2.73	1.00	1.34E-04
712	sp|P47740|AL3A2_MOUSE	-1.45	2.74	0.86	3.41E-02
713	sp|Q91ZJ5|UGPA_MOUSE	-1.45	2.74	0.85	3.31E-04
714	sp|P36552|HEM6_MOUSE	-1.46	2.75	0.69	1.33E-01
715	sp|A3KMP2|TTC38_MOUSE	-1.46	2.75	0.79	1.13E-04
716	sp|Q9CYR6|AGM1_MOUSE	-1.47	2.76	0.59	1.36E-04
717	sp|Q9D6Y9|GLGB_MOUSE	-1.47	2.77	0.86	2.53E-06
718	sp|Q9D8X1|CUTC_MOUSE	-1.47	2.77	0.54	4.80E-01
719	sp|P57016|LAD1_MOUSE	-1.48	2.79	0.80	6.24E-04
720	sp|Q921H8|THIKA_MOUSE	-1.49	2.81	0.82	1.47E-02
721	sp|P98197|AT11A_MOUSE	-1.50	2.82	0.64	5.10E-02
722	sp|Q9JKW0|AR6P1_MOUSE	-1.50	2.83	0.56	1.84E-01

723	sp|Q14DH7|ACSS3_MOUSE	-1.50	2.83	0.71	1.44E-01
724	sp|Q06138|CAB39_MOUSE	-1.51	2.85	0.62	4.41E-02
725	sp|Q8BXK9|CLIC5_MOUSE	-1.51	2.86	0.81	1.87E-03
726	sp|P24472|GSTA4_MOUSE	-1.53	2.89	0.87	7.48E-02
727	sp|Q91W52|TMM19_MOUSE	-1.53	2.89	0.69	1.41E-04
728	sp|Q9CQ92|FIS1_MOUSE	-1.54	2.91	0.88	9.45E-06
729	sp|Q9D7N9|APMAP_MOUSE	-1.55	2.93	0.85	3.51E-02
730	sp|Q9Z1J3|NFS1_MOUSE	-1.57	2.97	0.64	3.50E-03
731	sp|P00920|CAH2_MOUSE	-1.58	2.99	0.96	5.29E-05
732	sp|Q8K183|PDXK_MOUSE	-1.59	3.01	0.92	3.18E-02
733	sp|Q3TMH2|SCRN3_MOUSE	-1.60	3.02	0.72	7.29E-04
734	sp|Q9CXJ4|ABCB8_MOUSE	-1.60	3.02	0.64	6.02E-02
735	sp|Q99KQ4|NAMPT_MOUSE	-1.60	3.03	0.61	5.59E-05
736	sp|Q6GQT9|NOMO1_MOUSE	-1.60	3.03	0.81	6.15E-04
737	sp|Q60973|RBBP7_MOUSE	-1.60	3.04	0.71	5.54E-01
738	sp|Q8BG51|MIRO1_MOUSE	-1.61	3.06	0.71	1.23E-05
739	sp|P70349|HINT1_MOUSE	-1.62	3.06	0.95	1.68E-05
740	sp|Q9CY27|TECR_MOUSE	-1.63	3.10	0.66	4.03E-01
741	sp|Q9QXE0|HACL1_MOUSE	-1.64	3.11	0.60	1.72E-02
742	sp|Q9WVK4|EHD1_MOUSE	-1.64	3.11	0.77	2.56E-05
743	sp|Q60930|VDAC2_MOUSE	-1.64	3.13	0.93	9.19E-06
744	sp|Q8VDQ1|PTGR2_MOUSE	-1.66	3.15	0.92	1.19E-03
745	sp|Q9D0F9|PGM1_MOUSE	-1.66	3.15	0.85	1.05E-03
746	sp|P70444|BID_MOUSE	-1.66	3.16	0.64	4.10E-06
747	sp|Q8JZQ2|AFG32_MOUSE	-1.66	3.16	0.79	2.87E-08
748	sp|Q9CYR0|SSBP_MOUSE	-1.66	3.17	0.58	1.30E-02
749	sp|P51863|VA0D1_MOUSE	-1.67	3.19	0.87	6.43E-04
750	sp|P70245|EBP_MOUSE	-1.67	3.19	0.71	1.67E-02
751	sp|Q9DCT1|AKCL2_MOUSE	-1.67	3.19	0.82	4.52E-08
752	sp|P56394|COX17_MOUSE	-1.68	3.19	0.70	1.91E-01
753	sp|Q60931|VDAC3_MOUSE	-1.68	3.20	0.75	5.57E-03
754	sp|Q9Z2Y8|PROSC_MOUSE	-1.68	3.21	0.89	6.85E-05
755	sp|P08228|SODC_MOUSE	-1.69	3.22	0.95	3.31E-05
756	sp|P51661|DHI2_MOUSE	-1.69	3.22	0.88	4.33E-04
757	sp|Q8JZU2|TXTP_MOUSE	-1.69	3.23	0.83	2.65E-06
758	sp|P56376|ACYP1_MOUSE	-1.70	3.25	0.77	1.05E-01
759	sp|Q8BIJ6|SYIM_MOUSE	-1.71	3.27	0.83	1.27E-03
760	sp|Q9D880|TIM50_MOUSE	-1.71	3.27	0.89	1.17E-03
761	sp|Q64105|SPRE_MOUSE	-1.72	3.28	0.96	4.15E-09
762	sp|Q9CYH2|F213A_MOUSE	-1.73	3.31	0.83	7.88E-05
763	sp|Q64331|MYO6_MOUSE	-1.73	3.31	0.85	3.65E-02
764	sp|O88958|GNPI1_MOUSE	-1.74	3.33	0.88	1.61E-05
765	sp|P61148|FGF1_MOUSE	-1.74	3.34	0.64	6.21E-02
766	sp|P09411|PGK1_MOUSE	-1.74	3.35	0.97	2.49E-05
767	sp|Q9D8Y1|T126A_MOUSE	-1.76	3.38	0.58	4.01E-04
768	sp|Q8BGC4|ZADH2_MOUSE	-1.76	3.38	0.64	8.79E-01
769	sp|P26043|RADI_MOUSE	-1.76	3.39	0.89	7.42E-04
770	sp|Q9DCJ9|NPL_MOUSE	-1.77	3.41	0.86	1.12E-02
771	sp|P26040|EZRI_MOUSE	-1.77	3.41	0.96	4.48E-06
772	sp|P31786|ACBP_MOUSE	-1.77	3.42	0.96	3.64E-04
773	sp|P82343|RENBP_MOUSE	-1.78	3.43	0.62	2.38E-01
774	sp|P67778|PHB_MOUSE	-1.79	3.45	0.93	1.38E-07
775	sp|Q9DCS3|MECR_MOUSE	-1.79	3.45	0.57	2.52E-06
776	sp|Q8R317|UBQL1_MOUSE	-1.80	3.48	0.53	8.01E-01
777	sp|Q91W43|GCSP_MOUSE	-1.81	3.50	0.66	3.22E-02
778	sp|P05201|AATC_MOUSE	-1.81	3.51	0.89	2.12E-04
779	sp|Q8VHF2|CDHR5_MOUSE	-1.82	3.53	0.56	6.46E-02
780	sp|O35969|GAMT_MOUSE	-1.82	3.54	0.75	3.01E-04
781	sp|P48193|41_MOUSE	-1.83	3.55	0.83	7.63E-07
782	sp|P55302|AMRP_MOUSE	-1.83	3.55	0.58	1.74E-02
783	sp|Q3UJU9|RMD3_MOUSE	-1.83	3.56	0.67	2.43E-03
784	sp|Q9D5T0|ATAD1_MOUSE	-1.83	3.57	0.85	2.36E-07
785	sp|Q8JZN5|ACAD9_MOUSE	-1.84	3.59	0.67	2.40E-02
786	sp|Q4VAE3|TMM65_MOUSE	-1.84	3.59	0.91	2.83E-03
787	sp|P56395|CYB5_MOUSE	-1.85	3.60	0.89	5.08E-02
788	sp|Q8R146|APEH_MOUSE	-1.85	3.60	0.77	2.82E-04
789	sp|Q8CAK1|CAF17_MOUSE	-1.85	3.60	0.61	5.24E-05
790	sp|P16406|AMPE_MOUSE	-1.85	3.60	0.86	1.11E-03
791	sp|P48774|GSTM5_MOUSE	-1.86	3.62	0.89	7.07E-04
792	sp|O35658|C1QBP_MOUSE	-1.86	3.63	0.92	8.43E-04
793	sp|Q9CPY7|AMPL_MOUSE	-1.86	3.63	0.93	2.92E-02
794	sp|Q8BTY1|KAT1_MOUSE	-1.86	3.63	0.82	1.97E-02
795	sp|P05063|ALDOC_MOUSE	-1.87	3.66	0.62	3.88E-04

796	sp|Q9R0Q6|ARC1A_MOUSE	-1.87	3.66	0.79	2.34E-04
797	sp|Q64669|NQO1_MOUSE	-1.88	3.67	0.52	8.49E-05
798	sp|Q9CZU6|CISY_MOUSE	-1.88	3.69	0.89	1.92E-05
799	sp|O35143|ATIF1_MOUSE	-1.89	3.71	0.83	2.41E-07
800	sp|P17809|GTR1_MOUSE	-1.91	3.75	0.72	1.80E-02
801	sp|Q922H2|PDK3_MOUSE	-1.92	3.77	0.69	1.03E-03
802	sp|Q9JM63|KCJ10_MOUSE	-1.92	3.79	0.77	5.64E-02
803	sp|P63321|RALA_MOUSE	-1.92	3.79	0.60	1.73E-03
804	sp|P34884|MIF_MOUSE	-1.92	3.79	0.89	2.62E-03
805	sp|Q9R0P3|ESTD_MOUSE	-1.92	3.80	0.88	3.21E-08
806	sp|Q99M87|DNJA3_MOUSE	-1.93	3.81	0.71	1.92E-04
807	sp|Q9CZR8|EFTS_MOUSE	-1.94	3.83	0.83	2.72E-04
808	sp|O35129|PHB2_MOUSE	-1.94	3.84	0.93	3.06E-06
809	sp|Q8CGK3|LONM_MOUSE	-1.95	3.87	0.90	6.16E-07
810	sp|P51660|DHB4_MOUSE	-1.95	3.87	0.94	3.07E-02
811	sp|Q64521|GPDM_MOUSE	-1.96	3.88	0.72	3.50E-02
812	sp|P37040|NCPR_MOUSE	-1.96	3.89	0.75	3.59E-04
813	sp|P11352|GPX1_MOUSE	-1.97	3.91	0.94	5.78E-03
814	sp|Q9DCV4|RMD1_MOUSE	-1.97	3.93	0.75	2.14E-05
815	sp|Q99KB8|GLO2_MOUSE	-1.97	3.93	0.70	1.04E-03
816	sp|Q9Z1G3|VATC1_MOUSE	-1.98	3.94	0.85	6.48E-05
817	sp|Q99J39|DCMC_MOUSE	-1.98	3.94	0.64	9.72E-01
818	sp|Q8BGA8|ACSM5_MOUSE	-2.00	4.00	0.60	2.06E-01
819	sp|P62073|TIM10_MOUSE	-2.00	4.01	0.74	1.58E-07
820	sp|Q5SW19|CLU_MOUSE	-2.01	4.02	0.57	4.45E-04
821	sp|Q9WTN6|S22AL_MOUSE	-2.01	4.03	0.63	3.16E-01
822	sp|Q6P1B1|XPP1_MOUSE	-2.02	4.05	0.85	7.74E-03
823	sp|Q8CFA2|GCST_MOUSE	-2.02	4.06	0.78	8.66E-06
824	sp|O09172|GSH0_MOUSE	-2.02	4.07	0.84	1.72E-03
825	sp|P47934|CACP_MOUSE	-2.04	4.11	0.82	4.37E-06
826	sp|P48962|ADT1_MOUSE	-2.04	4.11	0.85	1.43E-03
827	sp|O35683|NDUA1_MOUSE	-2.04	4.12	0.86	5.21E-04
828	sp|Q91VT4|CBR4_MOUSE	-2.05	4.13	0.72	1.82E-06
829	sp|Q8K0C4|CP51A_MOUSE	-2.05	4.14	0.78	4.60E-04
830	sp|Q9DC61|MPPA_MOUSE	-2.05	4.15	0.60	1.15E-03
831	sp|P30275|KCRU_MOUSE	-2.06	4.16	0.84	3.40E-05
832	sp|Q8VHG0|FMO4_MOUSE	-2.06	4.17	0.70	9.23E-01
833	sp|Q8K010|OPLA_MOUSE	-2.06	4.17	0.73	1.94E-04
834	sp|Q924X2|CPT1B_MOUSE	-2.06	4.17	0.53	1.84E-02
835	sp|Q9JK42|PDK2_MOUSE	-2.06	4.17	0.57	1.02E-04
836	sp|Q811D0|DLG1_MOUSE	-2.06	4.18	0.52	1.38E-02
837	sp|Q9D939|ST1C2_MOUSE	-2.07	4.19	0.50	3.91E-03
838	sp|Q9JHW2|NIT2_MOUSE	-2.07	4.19	0.90	2.70E-04
839	sp|P97742|CPT1A_MOUSE	-2.07	4.20	0.85	2.29E-03
840	sp|Q80Y14|GLRX5_MOUSE	-2.07	4.20	0.86	2.04E-07
841	sp|Q5F285|TM256_MOUSE	-2.07	4.21	0.58	2.86E-06
842	sp|O55137|ACOT1_MOUSE	-2.08	4.21	0.85	1.52E-04
843	sp|P61110|ANRE_MOUSE	-2.08	4.22	0.71	2.56E-02
844	sp|P16125|LDHB_MOUSE	-2.08	4.24	0.86	2.76E-04
845	sp|P29758|OAT_MOUSE	-2.09	4.26	0.86	1.70E-01
846	sp|P97449|AMPN_MOUSE	-2.09	4.26	0.94	3.67E-03
847	sp|P53986|MOT1_MOUSE	-2.10	4.28	0.80	8.36E-05
848	sp|Q9CR62|M2OM_MOUSE	-2.10	4.29	0.88	1.05E-08
849	sp|Q99K30|ES8L2_MOUSE	-2.10	4.29	0.65	4.43E-02
850	sp|Q791V5|MTCH2_MOUSE	-2.11	4.32	0.89	7.49E-06
851	sp|Q925I1|ATAD3_MOUSE	-2.11	4.33	0.87	9.83E-05
852	sp|G5E8K5|ANK3_MOUSE	-2.11	4.33	0.84	2.62E-05
853	sp|Q9DB29|IAH1_MOUSE	-2.12	4.35	0.82	3.41E-04
854	sp|Q9EP89|LACTB_MOUSE	-2.13	4.36	0.68	2.52E-04
855	sp|Q922B1|MACD1_MOUSE	-2.13	4.36	0.66	2.58E-04
856	sp|Q9JLI6|SCLY_MOUSE	-2.13	4.37	0.59	5.12E-01
857	sp|Q8C5H8|NAKD2_MOUSE	-2.13	4.39	0.65	8.94E-04
858	sp|P58137|ACOT8_MOUSE	-2.13	4.39	0.72	4.71E-03
859	sp|Q9CPX8|QCR10_MOUSE	-2.14	4.39	0.75	2.48E-03
860	sp|Q99JY0|ECHB_MOUSE	-2.15	4.43	0.89	1.86E-03
861	sp|Q9DCU6|RM04_MOUSE	-2.16	4.46	0.78	8.53E-05
862	sp|Q9Z2I0|LETM1_MOUSE	-2.16	4.47	0.86	8.05E-05
863	sp|P70290|EM55_MOUSE	-2.16	4.48	0.86	3.39E-05
864	sp|O88451|RDH7_MOUSE	-2.16	4.48	0.69	7.13E-02
865	sp|Q8K157|GALM_MOUSE	-2.16	4.48	0.78	1.51E-04
866	sp|Q78IK4|MIC27_MOUSE	-2.17	4.49	0.87	1.77E-01
867	sp|Q9DCQ2|ASPD_MOUSE	-2.17	4.50	0.67	1.05E-04
868	sp|Q9JJW0|PXMP4_MOUSE	-2.17	4.50	0.57	6.40E-03

869	sp|O88696|CLPP_MOUSE	-2.17	4.51	0.87	3.01E-04
870	sp|P00158|CYB_MOUSE	-2.18	4.53	0.65	7.51E-03
871	sp|P57746|VATD_MOUSE	-2.18	4.54	0.86	4.39E-05
872	sp|O89106|FHIT_MOUSE	-2.18	4.54	0.79	3.05E-02
873	sp|P46656|ADX_MOUSE	-2.18	4.55	0.78	7.22E-04
874	sp|P18572|BASI_MOUSE	-2.19	4.56	0.82	4.64E-04
875	sp|P51174|ACADL_MOUSE	-2.19	4.56	0.95	3.30E-03
876	sp|P97823|LYPA1_MOUSE	-2.21	4.62	0.88	4.97E-03
877	sp|P38647|GRP75_MOUSE	-2.21	4.62	0.85	4.91E-04
878	sp|Q8BGS1|E41L5_MOUSE	-2.21	4.64	0.64	1.86E-03
879	sp|P16331|PH4H_MOUSE	-2.22	4.66	0.78	2.67E-05
880	sp|Q8BMS1|ECHA_MOUSE	-2.22	4.67	0.96	2.35E-03
881	sp|Q8BFR5|EFTU_MOUSE	-2.24	4.73	0.95	1.60E-05
882	sp|Q8BMC1|VATG3_MOUSE	-2.25	4.74	0.84	4.73E-04
883	sp|Q9WTP7|KAD3_MOUSE	-2.25	4.75	0.89	5.27E-05
884	sp|P50431|GLYC_MOUSE	-2.25	4.75	0.85	2.84E-05
885	sp|P10637|TAU_MOUSE	-2.26	4.79	0.77	2.71E-04
886	sp|Q9D7P6|ISCU_MOUSE	-2.27	4.82	0.71	5.80E-05
887	sp|Q60676|PPP5_MOUSE	-2.27	4.83	0.57	1.02E-04
888	sp|Q61133|GSTT2_MOUSE	-2.27	4.83	0.82	2.05E-04
889	sp|Q9DB15|RM12_MOUSE	-2.27	4.83	0.93	2.29E-05
890	sp|P58281|OPA1_MOUSE	-2.28	4.84	0.86	1.65E-09
891	sp|Q9WV98|TIM9_MOUSE	-2.28	4.85	0.81	2.08E-05
892	sp|Q8VDK1|NIT1_MOUSE	-2.28	4.86	0.89	5.74E-04
893	sp|O88844|IDHC_MOUSE	-2.28	4.87	0.91	6.87E-04
894	sp|Q8VCR7|ABHEB_MOUSE	-2.28	4.87	0.91	4.43E-05
895	sp|Q8BP40|PPA6_MOUSE	-2.28	4.87	0.69	6.19E-06
896	sp|Q9DBL1|ACDSB_MOUSE	-2.29	4.89	0.94	4.00E-04
897	sp|Q9WV68|DECR2_MOUSE	-2.30	4.92	0.79	6.73E-03
898	sp|P62814|VATB2_MOUSE	-2.30	4.92	0.91	9.32E-04
899	sp|O55126|NIPS2_MOUSE	-2.30	4.93	0.78	2.03E-02
900	sp|P10852|4F2_MOUSE	-2.31	4.94	0.93	5.34E-05
901	sp|Q6PB66|LPPRC_MOUSE	-2.31	4.96	0.85	2.81E-04
902	sp|Q9QXG4|ACSA_MOUSE	-2.31	4.97	0.75	1.69E-03
903	sp|Q9D2R6|COA3_MOUSE	-2.32	4.99	0.63	2.04E-04
904	sp|O08756|HCD2_MOUSE	-2.32	5.00	0.94	9.49E-02
905	sp|Q8BH59|CMC1_MOUSE	-2.32	5.01	0.86	4.67E-05
906	sp|P97364|SPS2_MOUSE	-2.33	5.03	0.84	2.59E-04
907	sp|Q9R112|SQRD_MOUSE	-2.33	5.04	0.89	1.43E-06
908	sp|Q8BK72|RT27_MOUSE	-2.34	5.05	0.71	5.71E-04
909	sp|P97493|THIOM_MOUSE	-2.34	5.05	0.95	6.36E-04
910	sp|Q99J99|THTM_MOUSE	-2.34	5.06	0.82	1.17E-06
911	sp|Q8CAY6|THIC_MOUSE	-2.34	5.08	0.81	5.93E-04
912	sp|Q9DCC4|P5CR3_MOUSE	-2.35	5.08	0.84	7.88E-04
913	sp|O08691|ARGI2_MOUSE	-2.35	5.10	0.52	7.12E-01
914	sp|O35215|DOPD_MOUSE	-2.35	5.10	0.95	1.11E-07
915	sp|Q9CQZ5|NDUA6_MOUSE	-2.35	5.11	0.87	5.55E-05
916	sp|P26443|DHE3_MOUSE	-2.37	5.15	0.93	1.27E-03
917	sp|Q9DCN1|NUD12_MOUSE	-2.37	5.15	0.63	3.67E-03
918	sp|Q9D6R2|IDH3A_MOUSE	-2.38	5.19	0.93	1.55E-04
919	sp|Q9D2R0|AACS_MOUSE	-2.38	5.22	0.81	6.81E-02
920	sp|Q99LY9|NDUS5_MOUSE	-2.39	5.22	0.85	9.03E-05
921	sp|Q9WU84|CCS_MOUSE	-2.39	5.23	0.83	9.89E-05
922	sp|Q9DCS2|CP013_MOUSE	-2.39	5.23	0.83	8.75E-03
923	sp|P08905|LYZ2_MOUSE	-2.39	5.25	0.87	1.53E-06
924	sp|Q9Z2H7|GIPC2_MOUSE	-2.39	5.26	0.55	2.08E-01
925	sp|O35459|ECH1_MOUSE	-2.40	5.27	0.95	1.18E-03
926	sp|Q8K0D5|EFGM_MOUSE	-2.40	5.27	0.50	1.87E-03
927	sp|P28271|ACOC_MOUSE	-2.41	5.32	0.88	1.33E-06
928	sp|P62075|TIM13_MOUSE	-2.41	5.33	0.89	1.83E-07
929	sp|Q60648|SAP3_MOUSE	-2.42	5.34	0.85	2.71E-06
930	sp|Q8VCA8|SCRN2_MOUSE	-2.43	5.37	0.83	5.11E-01
931	sp|Q9D1K2|VATF_MOUSE	-2.43	5.40	0.88	4.58E-06
932	sp|P14152|MDHC_MOUSE	-2.44	5.41	0.94	9.41E-08
933	sp|Q8R086|SUOX_MOUSE	-2.44	5.41	0.79	5.24E-05
934	sp|Q8BVI4|DHPR_MOUSE	-2.45	5.45	0.91	1.16E-04
935	sp|Q8VEA4|MIA40_MOUSE	-2.45	5.45	0.86	8.70E-03
936	sp|Q9WVA2|TIM8A_MOUSE	-2.45	5.45	0.84	1.63E-04
937	sp|Q9D1H6|NDUF4_MOUSE	-2.45	5.45	0.71	1.25E-04
938	sp|P50518|VATE1_MOUSE	-2.45	5.47	0.92	8.02E-05
939	sp|Q9D517|PLCC_MOUSE	-2.45	5.47	0.80	2.00E-04
940	sp|Q9D1I5|MCEE_MOUSE	-2.45	5.48	0.59	4.46E-04
941	sp|P47738|ALDH2_MOUSE	-2.45	5.48	0.94	2.65E-04

942	sp|Q9JHS4|CLPX_MOUSE	-2.45	5.48	0.91	5.84E-04
943	sp|Q7TMF3|NDUAC_MOUSE	-2.46	5.49	0.70	8.33E-06
944	sp|Q921G7|ETFD_MOUSE	-2.46	5.49	0.90	3.66E-04
945	sp|Q60932|VDAC1_MOUSE	-2.46	5.49	0.96	6.12E-05
946	sp|P42125|ECI1_MOUSE	-2.46	5.51	0.90	2.47E-08
947	sp|Q68FL4|SAHH3_MOUSE	-2.47	5.54	0.83	1.46E-03
948	sp|Q9DCU9|HOGA1_MOUSE	-2.47	5.55	0.55	1.11E-01
949	sp|Q99KR7|PPIF_MOUSE	-2.47	5.55	0.77	1.04E-02
950	sp|P50171|DHB8_MOUSE	-2.47	5.55	0.81	7.84E-04
951	sp|Q8BGH2|SAM50_MOUSE	-2.49	5.60	0.90	4.03E-05
952	sp|P50136|ODBA_MOUSE	-2.49	5.61	0.75	1.02E-04
953	sp|P98078|DAB2_MOUSE	-2.49	5.62	0.80	6.54E-02
954	sp|Q8VCF0|MAVS_MOUSE	-2.49	5.62	0.75	6.43E-05
955	sp|Q9CQ62|DECR_MOUSE	-2.49	5.63	0.88	3.89E-03
956	sp|Q8VDG7|PAFA2_MOUSE	-2.49	5.64	0.55	5.67E-06
957	sp|P00375|DYR_MOUSE	-2.50	5.65	0.82	6.52E-04
958	sp|Q91X52|DCXR_MOUSE	-2.50	5.66	0.83	5.79E-04
959	sp|P06801|MAOX_MOUSE	-2.51	5.68	0.87	5.22E-02
960	sp|Q8BJ64|CHDH_MOUSE	-2.51	5.69	0.88	1.32E-03
961	sp|Q9DBX3|SUSD2_MOUSE	-2.52	5.75	0.93	5.04E-05
962	sp|Q60597|ODO1_MOUSE	-2.53	5.76	0.89	3.72E-07
963	sp|Q8C3K6|SC5A1_MOUSE	-2.53	5.77	0.57	1.68E-04
964	sp|O88441|MTX2_MOUSE	-2.53	5.78	0.74	1.15E-02
965	sp|Q8VEM8|MPCP_MOUSE	-2.53	5.78	0.94	5.33E-09
966	sp|P50544|ACADV_MOUSE	-2.53	5.79	0.85	1.62E-08
967	sp|P99029|PRDX5_MOUSE	-2.54	5.81	0.91	1.22E-04
968	sp|Q8BWM0|PGES2_MOUSE	-2.55	5.84	0.81	1.53E-07
969	sp|Q9CRB9|MIC19_MOUSE	-2.55	5.85	0.86	4.49E-03
970	sp|O35286|DHX15_MOUSE	-2.55	5.86	0.55	8.97E-01
971	sp|Q64433|CH10_MOUSE	-2.55	5.86	0.90	3.49E-04
972	sp|Q9DCJ5|NDUA8_MOUSE	-2.55	5.86	0.89	2.22E-05
973	sp|Q9JKF7|RM39_MOUSE	-2.55	5.87	0.56	2.17E-03
974	sp|Q8BJZ4|RT35_MOUSE	-2.55	5.87	0.68	9.07E-06
975	sp|Q8BVE3|VATH_MOUSE	-2.56	5.88	0.91	3.57E-07
976	sp|Q8BWN8|ACOT4_MOUSE	-2.56	5.92	0.69	1.80E-02
977	sp|P56392|CX7A1_MOUSE	-2.57	5.92	0.88	2.21E-04
978	sp|P50516|VATA_MOUSE	-2.57	5.96	0.93	1.90E-04
979	sp|P52825|CPT2_MOUSE	-2.58	5.99	0.85	1.83E-04
980	sp|Q9EPL9|ACOX3_MOUSE	-2.59	6.00	0.82	1.31E-01
981	sp|Q9CQN1|TRAP1_MOUSE	-2.59	6.02	0.89	7.18E-05
982	sp|P20108|PRDX3_MOUSE	-2.59	6.04	0.89	1.08E-04
983	sp|Q9WTP6|KAD2_MOUSE	-2.60	6.06	0.89	8.18E-05
984	sp|P99028|QCR6_MOUSE	-2.60	6.06	0.93	3.31E-05
985	sp|P51855|GSHB_MOUSE	-2.60	6.07	0.89	1.30E-04
986	sp|Q9D051|ODPB_MOUSE	-2.60	6.07	0.97	3.19E-05
987	sp|Q91WT8|RBM47_MOUSE	-2.61	6.09	0.63	3.25E-04
988	sp|Q9CPQ1|COX6C_MOUSE	-2.61	6.11	0.89	2.20E-09
989	sp|Q9CR51|VATG1_MOUSE	-2.61	6.13	0.78	1.61E-04
990	sp|Q9WUZ9|ENTP5_MOUSE	-2.62	6.15	0.80	3.48E-03
991	sp|O08966|S22A1_MOUSE	-2.62	6.17	0.79	4.04E-03
992	sp|Q9D020|5NT3A_MOUSE	-2.63	6.18	0.57	6.27E-01
993	sp|Q91WK5|GCSH_MOUSE	-2.63	6.19	0.71	5.39E-04
994	sp|Q8K3J1|NDUS8_MOUSE	-2.63	6.20	0.86	2.19E-04
995	sp|Q9CXV1|DHSD_MOUSE	-2.64	6.22	0.59	4.61E-05
996	sp|Q922Q1|MARC2_MOUSE	-2.64	6.22	0.91	2.55E-06
997	sp|Q3UP75|UD3A1_MOUSE	-2.64	6.24	0.84	4.17E-05
998	sp|Q9CQZ6|NDUB3_MOUSE	-2.64	6.24	0.77	9.57E-05
999	sp|Q8BMF4|ODP2_MOUSE	-2.65	6.28	0.94	3.65E-06
1000	sp|P03911|NU4M_MOUSE	-2.65	6.28	0.88	4.36E-06
1001	sp|Q91YI0|ARLY_MOUSE	-2.65	6.28	0.92	7.97E-07
1002	sp|Q07417|ACADS_MOUSE	-2.65	6.28	0.89	3.08E-03
1003	sp|Q8CAQ8|MIC60_MOUSE	-2.66	6.32	0.93	3.25E-08
1004	sp|P28656|NP1L1_MOUSE	-2.67	6.35	0.61	2.91E-01
1005	sp|P03921|NU5M_MOUSE	-2.67	6.35	0.86	3.70E-05
1006	sp|Q9JLF6|TGM1_MOUSE	-2.67	6.36	0.56	5.48E-04
1007	sp|P30115|GSTA3_MOUSE	-2.67	6.36	0.71	1.86E-03
1008	sp|Q9D6J5|NDUB8_MOUSE	-2.67	6.38	0.79	5.01E-04
1009	sp|Q9JLT4|TRXR2_MOUSE	-2.68	6.39	0.71	3.56E-03
1010	sp|P05202|AATM_MOUSE	-2.68	6.39	0.97	1.67E-04
1011	sp|Q9D172|ES1_MOUSE	-2.68	6.41	0.91	4.72E-05
1012	sp|Q9DBL7|COASY_MOUSE	-2.68	6.41	0.77	1.37E-02
1013	sp|Q9ERS2|NDUAD_MOUSE	-2.68	6.42	0.94	1.40E-07
1014	sp|P03930|ATP8_MOUSE	-2.68	6.43	0.81	3.91E-06

1015	sp|O55060|TPMT_MOUSE	-2.69	6.43	0.93	3.65E-04
1016	sp|Q9DCT2|NDUS3_MOUSE	-2.70	6.51	0.94	3.46E-05
1017	sp|Q9DCM0|ETHE1_MOUSE	-2.70	6.52	0.93	8.66E-04
1018	sp|P47802|MTX1_MOUSE	-2.71	6.53	0.66	7.69E-05
1019	sp|Q9DBE0|CSAD_MOUSE	-2.71	6.56	0.91	6.18E-03
1020	sp|P97494|GSH1_MOUSE	-2.72	6.57	0.85	1.31E-06
1021	sp|Q8BWF0|SSDH_MOUSE	-2.72	6.57	0.71	7.86E-02
1022	sp|P17665|COX7C_MOUSE	-2.72	6.57	0.80	2.37E-04
1023	sp|Q8R404|MIC13_MOUSE	-2.72	6.57	0.92	1.30E-04
1024	sp|Q91YP0|L2HDH_MOUSE	-2.72	6.58	0.69	5.33E-03
1025	sp|P50285|FMO1_MOUSE	-2.73	6.63	0.78	1.30E-02
1026	sp|O09111|NDUBB_MOUSE	-2.74	6.67	0.93	5.21E-07
1027	sp|Q9CZ13|QCR1_MOUSE	-2.74	6.69	0.93	2.59E-05
1028	sp|Q9CPU4|MGST3_MOUSE	-2.74	6.70	0.76	1.62E-03
1029	sp|P35486|ODPA_MOUSE	-2.74	6.70	0.93	5.32E-06
1030	sp|Q9DCX2|ATP5H_MOUSE	-2.75	6.70	0.94	2.27E-05
1031	sp|Q9CPP6|NDUA5_MOUSE	-2.75	6.71	0.89	5.20E-04
1032	sp|Q9D2G2|ODO2_MOUSE	-2.75	6.71	0.91	3.59E-05
1033	sp|Q9CXZ1|NDUS4_MOUSE	-2.75	6.72	0.85	4.45E-07
1034	sp|P32020|NLTP_MOUSE	-2.75	6.73	0.91	5.64E-02
1035	sp|P17426|AP2A1_MOUSE	-2.75	6.75	0.65	6.59E-04
1036	sp|P11404|FABPH_MOUSE	-2.76	6.78	0.84	3.46E-06
1037	sp|Q9QYR9|ACOT2_MOUSE	-2.76	6.79	0.80	1.89E-03
1038	sp|Q8VC69|S22A6_MOUSE	-2.76	6.79	0.77	6.60E-02
1039	sp|P70414|NAC1_MOUSE	-2.77	6.80	0.59	7.11E-05
1040	sp|O35409|FOLH1_MOUSE	-2.77	6.81	0.80	1.46E-02
1041	sp|P97807|FUMH_MOUSE	-2.77	6.82	0.89	7.21E-08
1042	sp|Q9DB20|ATPO_MOUSE	-2.77	6.83	0.96	3.32E-05
1043	sp|Q60866|PTER_MOUSE	-2.78	6.85	0.94	2.33E-07
1044	sp|Q9DC69|NDUA9_MOUSE	-2.78	6.86	0.91	1.06E-05
1045	sp|Q8BKZ9|ODPX_MOUSE	-2.78	6.87	0.51	6.01E-04
1046	sp|Q925N2|SFXN2_MOUSE	-2.79	6.90	0.82	7.15E-05
1047	sp|Q5M8N4|D39U1_MOUSE	-2.79	6.91	0.69	9.10E-04
1048	sp|Q78IK2|USMG5_MOUSE	-2.79	6.93	0.97	4.94E-06
1049	sp|Q9CWS0|DDAH1_MOUSE	-2.79	6.93	0.78	4.63E-07
1050	sp|Q9D6J6|NDUV2_MOUSE	-2.79	6.94	0.79	5.41E-07
1051	sp|Q922D8|C1TC_MOUSE	-2.80	6.96	0.79	1.85E-05
1052	sp|Q9Z1P6|NDUA7_MOUSE	-2.80	6.97	0.87	6.83E-08
1053	sp|Q9CYW4|HDHD3_MOUSE	-2.80	6.97	0.61	1.08E-03
1054	sp|P08249|MDHM_MOUSE	-2.80	6.97	0.94	2.18E-05
1055	sp|Q9CQJ8|NDUB9_MOUSE	-2.81	7.01	0.84	2.95E-04
1056	sp|Q03265|ATPA_MOUSE	-2.81	7.02	0.96	2.09E-05
1057	sp|Q9CQQ7|AT5F1_MOUSE	-2.81	7.03	0.92	5.57E-07
1058	sp|Q6ZQM8|UD17C_MOUSE	-2.81	7.03	0.76	7.48E-01
1059	sp|Q9R0M5|TPK1_MOUSE	-2.81	7.03	0.72	6.12E-03
1060	sp|Q8VCH0|THIKB_MOUSE	-2.82	7.04	0.63	7.68E-04
1061	sp|Q06185|ATP5I_MOUSE	-2.82	7.06	0.86	2.20E-06
1062	sp|P03899|NU3M_MOUSE	-2.82	7.06	0.95	8.49E-04
1063	sp|P63038|CH60_MOUSE	-2.82	7.07	0.96	6.86E-04
1064	sp|Q9Z2I9|SUCB1_MOUSE	-2.82	7.07	0.93	1.72E-06
1065	sp|Q99LB2|DHRS4_MOUSE	-2.82	7.08	0.95	4.94E-02
1066	sp|Q9JLJ2|AL9A1_MOUSE	-2.83	7.09	0.92	1.06E-03
1067	sp|Q3V0K9|PLSI_MOUSE	-2.83	7.09	0.79	4.17E-04
1068	sp|O08749|DLDH_MOUSE	-2.83	7.11	0.93	8.43E-07
1069	sp|Q9CQH3|NDUB5_MOUSE	-2.84	7.15	0.79	4.95E-05
1070	sp|P00405|COX2_MOUSE	-2.84	7.15	0.86	4.27E-05
1071	sp|Q9DBF1|AL7A1_MOUSE	-2.84	7.15	0.87	3.10E-08
1072	sp|Q91WD5|NDUS2_MOUSE	-2.84	7.15	0.86	1.28E-05
1073	sp|Q91Z53|GRHPR_MOUSE	-2.84	7.17	0.77	7.36E-04
1074	sp|Q9D7B6|ACAD8_MOUSE	-2.84	7.17	0.78	9.18E-04
1075	sp|P17563|SBP1_MOUSE	-2.84	7.18	0.89	1.15E-03
1076	sp|P51881|ADT2_MOUSE	-2.84	7.18	0.88	6.34E-05
1077	sp|P56480|ATPB_MOUSE	-2.85	7.19	0.96	2.89E-05
1078	sp|Q99JR1|SFXN1_MOUSE	-2.85	7.20	0.86	3.54E-04
1079	sp|Q9WV92|E41L3_MOUSE	-2.86	7.24	0.67	9.04E-02
1080	sp|Q9D855|QCR7_MOUSE	-2.86	7.28	0.88	4.79E-06
1081	sp|P68368|TBA4A_MOUSE	-2.86	7.28	0.81	1.88E-04
1082	sp|P97450|ATP5J_MOUSE	-2.87	7.30	0.93	5.85E-05
1083	sp|P48758|CBR1_MOUSE	-2.87	7.30	0.94	6.51E-02
1084	sp|Q9WV69|DEMA_MOUSE	-2.87	7.31	0.75	1.48E-06
1085	sp|Q920R6|VPP4_MOUSE	-2.87	7.31	0.76	4.93E-05
1086	sp|Q8R1G2|CMBL_MOUSE	-2.87	7.32	0.80	1.69E-03
1087	sp|P56391|CX6B1_MOUSE	-2.87	7.32	0.88	1.74E-04

1088	sp|Q99LC3|NDUAA_MOUSE	-2.87	7.33	0.90	2.03E-08
1089	sp|Q9Z0S1|BPNT1_MOUSE	-2.88	7.34	0.81	1.82E-05
1090	sp|Q8BLF1|NCEH1_MOUSE	-2.88	7.34	0.94	3.98E-03
1091	sp|P60603|ROMO1_MOUSE	-2.88	7.34	0.69	4.01E-06
1092	sp|P56135|ATPK_MOUSE	-2.88	7.34	0.83	3.96E-03
1093	sp|O35855|BCAT2_MOUSE	-2.88	7.36	0.89	1.16E-03
1094	sp|Q71RI9|KAT3_MOUSE	-2.88	7.36	0.82	1.07E-03
1095	sp|P19783|COX41_MOUSE	-2.88	7.37	0.93	1.81E-06
1096	sp|P52503|NDUS6_MOUSE	-2.89	7.39	0.82	8.62E-04
1097	sp|Q62425|NDUA4_MOUSE	-2.89	7.39	0.88	1.74E-04
1098	sp|Q91VM9|IPYR2_MOUSE	-2.90	7.47	0.90	6.01E-06
1099	sp|P42925|PXMP2_MOUSE	-2.90	7.48	0.55	4.26E-05
1100	sp|Q9DC70|NDUS7_MOUSE	-2.91	7.49	0.85	1.53E-05
1101	sp|P62897|CYC_MOUSE	-2.92	7.56	0.90	3.89E-04
1102	sp|Q61767|3BHS4_MOUSE	-2.92	7.58	0.81	1.15E-02
1103	sp|Q91X91|NADC_MOUSE	-2.92	7.59	0.65	3.17E-04
1104	sp|O55125|NIPS1_MOUSE	-2.93	7.62	0.90	2.14E-04
1105	sp|Q9CZB0|C560_MOUSE	-2.93	7.63	0.92	9.95E-05
1106	sp|P56379|68MP_MOUSE	-2.93	7.63	0.71	5.96E-05
1107	sp|Q9CQX8|RT36_MOUSE	-2.93	7.64	0.91	8.38E-06
1108	sp|Q99KP3|CRYL1_MOUSE	-2.93	7.64	0.89	4.23E-07
1109	sp|Q91VR2|ATPG_MOUSE	-2.94	7.65	0.92	5.23E-06
1110	sp|Q91Y63|S13A3_MOUSE	-2.94	7.65	0.84	7.64E-03
1111	sp|Q9QXX4|CMC2_MOUSE	-2.94	7.66	0.89	8.52E-06
1112	sp|Q9CPQ8|ATP5L_MOUSE	-2.94	7.67	0.71	1.52E-02
1113	sp|Q9D3D9|ATPD_MOUSE	-2.94	7.68	0.95	1.27E-04
1114	sp|Q9D0M3|CY1_MOUSE	-2.95	7.72	0.93	4.77E-05
1115	sp|Q9QZD8|DIC_MOUSE	-2.95	7.73	0.91	2.60E-03
1116	sp|Q91VD9|NDUS1_MOUSE	-2.95	7.74	0.90	1.02E-04
1117	sp|P55096|ABCD3_MOUSE	-2.95	7.75	0.90	2.14E-02
1118	sp|Q9CQ75|NDUA2_MOUSE	-2.96	7.78	0.83	1.80E-04
1119	sp|Q61391|NEP_MOUSE	-2.96	7.78	0.89	1.25E-02
1120	sp|O35972|RM23_MOUSE	-2.96	7.79	0.81	1.63E-04
1121	sp|Q8K2B3|SDHA_MOUSE	-2.96	7.80	0.97	9.18E-05
1122	sp|Q99MR8|MCCA_MOUSE	-2.97	7.81	0.82	1.09E-04
1123	sp|Q7TNG8|LDHD_MOUSE	-2.97	7.83	0.88	9.56E-02
1124	sp|Q9D8I3|GLOD5_MOUSE	-2.97	7.84	0.52	1.25E-02
1125	sp|Q9DC50|OCTC_MOUSE	-2.97	7.84	0.82	2.17E-01
1126	sp|O88986|KBL_MOUSE	-2.98	7.91	0.61	6.56E-02
1127	sp|Q6DYE8|ENPP3_MOUSE	-2.99	7.92	0.81	5.76E-03
1128	sp|P56389|CDD_MOUSE	-2.99	7.93	0.80	5.78E-02
1129	sp|Q8BH95|ECHM_MOUSE	-2.99	7.96	0.90	4.31E-05
1130	sp|Q9Z0X1|AIFM1_MOUSE	-2.99	7.96	0.92	5.94E-06
1131	sp|Q9WUR2|ECI2_MOUSE	-2.99	7.96	0.85	1.11E-02
1132	sp|P56382|ATP5E_MOUSE	-3.00	7.98	0.74	6.69E-04
1133	sp|Q8VDT1|SC5A9_MOUSE	-3.00	7.99	0.64	2.27E-01
1134	sp|Q9CQA3|SDHB_MOUSE	-3.00	8.00	0.83	7.55E-09
1135	sp|Q9CQC7|NDUB4_MOUSE	-3.01	8.03	0.83	2.86E-05
1136	sp|Q9DD20|MET7B_MOUSE	-3.01	8.04	0.65	6.36E-03
1137	sp|Q8QZW3|F151A_MOUSE	-3.01	8.04	0.76	1.21E-05
1138	sp|Q9CR61|NDUB7_MOUSE	-3.01	8.05	0.90	3.70E-04
1139	sp|Q8K023|AKC1H_MOUSE	-3.01	8.07	0.87	4.03E-04
1140	sp|Q8C165|P20D1_MOUSE	-3.02	8.10	0.77	1.71E-03
1141	sp|P12787|COX5A_MOUSE	-3.02	8.11	0.93	1.26E-04
1142	sp|A2ARV4|LRP2_MOUSE	-3.03	8.16	0.83	7.94E-04
1143	sp|Q9DB77|QCR2_MOUSE	-3.03	8.19	0.97	3.61E-09
1144	sp|O70250|PGAM2_MOUSE	-3.03	8.19	0.82	1.59E-03
1145	sp|P70404|IDHG1_MOUSE	-3.04	8.20	0.89	6.31E-05
1146	sp|P11862|GAS2_MOUSE	-3.04	8.24	0.60	2.51E-01
1147	sp|Q9D9V3|ECHD1_MOUSE	-3.04	8.24	0.86	6.69E-07
1148	sp|P59158|S12A3_MOUSE	-3.04	8.24	0.78	5.12E-03
1149	sp|Q61847|MEP1B_MOUSE	-3.05	8.27	0.80	8.60E-05
1150	sp|Q02013|AQP1_MOUSE	-3.05	8.29	0.88	1.47E-03
1151	sp|P61458|PHS_MOUSE	-3.05	8.31	0.82	2.08E-06
1152	sp|Q91ZA3|PCCA_MOUSE	-3.06	8.33	0.91	1.36E-04
1153	sp|A2AJL3|FGGY_MOUSE	-3.06	8.34	0.54	1.42E-04
1154	sp|Q62433|NDRG1_MOUSE	-3.06	8.36	0.98	9.87E-05
1155	sp|Q8CI85|CAH12_MOUSE	-3.07	8.37	0.62	4.99E-04
1156	sp|Q9DBK0|ACO12_MOUSE	-3.07	8.38	0.61	1.36E-01
1157	sp|P48771|CX7A2_MOUSE	-3.07	8.39	0.84	9.42E-04
1158	sp|Q9DCS9|NDUBA_MOUSE	-3.07	8.40	0.86	1.06E-04
1159	sp|P47199|QOR_MOUSE	-3.07	8.40	0.93	2.24E-04
1160	sp|Q9CR21|ACPM_MOUSE	-3.07	8.43	0.92	1.41E-04

1161	sp|P49429|HPPD_MOUSE	-3.07	8.43	0.79	3.73E-03
1162	sp|Q9JLB4|CUBN_MOUSE	-3.08	8.45	0.74	8.02E-04
1163	sp|Q9WVD5|ORNT1_MOUSE	-3.09	8.51	0.79	5.66E-06
1164	sp|Q9JMD3|PCTL_MOUSE	-3.10	8.56	0.68	5.85E-07
1165	sp|P54071|IDHP_MOUSE	-3.10	8.56	0.93	1.41E-04
1166	sp|Q8CC88|VWA8_MOUSE	-3.10	8.58	0.80	1.77E-02
1167	sp|Q8CG76|ARK72_MOUSE	-3.10	8.60	0.85	3.84E-05
1168	sp|P18894|OXDA_MOUSE	-3.11	8.60	0.78	6.29E-04
1169	sp|Q8BK30|NDUV3_MOUSE	-3.11	8.61	0.54	4.50E-05
1170	sp|O54749|CP2J5_MOUSE	-3.11	8.61	0.58	3.19E-03
1171	sp|Q8R0Y6|AL1L1_MOUSE	-3.11	8.63	0.92	6.60E-06
1172	sp|Q9CQ69|QCR8_MOUSE	-3.11	8.65	0.92	1.50E-02
1173	sp|Q9CR68|UCRI_MOUSE	-3.13	8.74	0.84	2.41E-06
1174	sp|P35802|GPM6A_MOUSE	-3.13	8.74	0.65	5.76E-05
1175	sp|Q8VIM4|BSND_MOUSE	-3.13	8.77	0.75	7.61E-02
1176	sp|Q8R1I1|QCR9_MOUSE	-3.13	8.77	0.68	8.33E-04
1177	sp|Q9DCW4|ETFB_MOUSE	-3.13	8.78	0.92	5.83E-05
1178	sp|P62077|TIM8B_MOUSE	-3.14	8.79	0.71	4.50E-05
1179	sp|Q80XL6|ACD11_MOUSE	-3.14	8.83	0.77	1.26E-02
1180	sp|Q9WVL0|MAAI_MOUSE	-3.14	8.83	0.82	1.08E-05
1181	sp|P15105|GLNA_MOUSE	-3.14	8.84	0.83	9.22E-02
1182	sp|P70441|NHRF1_MOUSE	-3.14	8.85	0.91	9.72E-05
1183	sp|Q9D0K2|SCOT1_MOUSE	-3.15	8.85	0.91	2.78E-04
1184	sp|Q9JI75|NQO2_MOUSE	-3.15	8.86	0.55	6.12E-02
1185	sp|Q64FW2|RETST_MOUSE	-3.15	8.86	0.58	9.52E-06
1186	sp|Q99KI0|ACON_MOUSE	-3.15	8.88	0.88	3.72E-06
1187	sp|Q8R519|ACMSD_MOUSE	-3.15	8.90	0.70	5.11E-04
1188	sp|P55014|S12A1_MOUSE	-3.15	8.90	0.85	2.08E-05
1189	sp|P00397|COX1_MOUSE	-3.16	8.92	0.73	9.49E-03
1190	sp|P09242|PPBT_MOUSE	-3.16	8.93	0.70	8.50E-05
1191	sp|Q8K370|ACD10_MOUSE	-3.16	8.94	0.89	2.66E-06
1192	sp|Q9D6Y7|MSRA_MOUSE	-3.16	8.95	0.89	1.56E-05
1193	sp|Q3TNA1|XYLB_MOUSE	-3.16	8.96	0.72	5.17E-02
1194	sp|O88428|PAPS2_MOUSE	-3.16	8.97	0.77	1.50E-03
1195	sp|Q91WR5|AK1CL_MOUSE	-3.16	8.97	0.84	1.45E-01
1196	sp|Q8R0N6|HOT_MOUSE	-3.17	8.97	0.83	1.64E-01
1197	sp|Q9WUM5|SUCA_MOUSE	-3.17	9.00	0.93	2.05E-04
1198	sp|Q8K1Z0|COQ9_MOUSE	-3.17	9.02	0.81	2.51E-04
1199	sp|Q61425|HCDH_MOUSE	-3.18	9.04	0.89	5.29E-04
1200	sp|P19536|COX5B_MOUSE	-3.18	9.07	0.90	2.25E-04
1201	sp|P16332|MUTA_MOUSE	-3.18	9.08	0.83	1.77E-07
1202	sp|P09671|SODM_MOUSE	-3.18	9.08	0.88	1.31E-06
1203	sp|Q8BWT1|THIM_MOUSE	-3.18	9.09	0.88	2.59E-04
1204	sp|Q91WG0|EST2C_MOUSE	-3.20	9.16	0.57	2.05E-01
1205	sp|Q59J78|MIMIT_MOUSE	-3.20	9.17	0.66	1.77E-03
1206	sp|O09174|AMACR_MOUSE	-3.20	9.21	0.65	2.15E-01
1207	sp|Q3UIU2|NDUB6_MOUSE	-3.21	9.22	0.80	3.92E-07
1208	sp|P09470|ACE_MOUSE	-3.21	9.27	0.79	3.90E-03
1209	sp|P38060|HMGCL_MOUSE	-3.22	9.29	0.89	4.90E-06
1210	sp|Q9ESG4|TMM27_MOUSE	-3.22	9.30	0.85	1.67E-04
1211	sp|Q9CQ54|NDUC2_MOUSE	-3.22	9.30	0.84	6.09E-05
1212	sp|Q8JZN7|MIRO2_MOUSE	-3.23	9.35	0.87	6.91E-02
1213	sp|P97478|COQ7_MOUSE	-3.23	9.37	0.65	9.76E-01
1214	sp|Q9JII6|AK1A1_MOUSE	-3.23	9.38	0.92	3.89E-04
1215	sp|Q8BH86|CN159_MOUSE	-3.23	9.39	0.77	2.25E-03
1216	sp|Q91VN4|MIC25_MOUSE	-3.23	9.40	0.61	1.78E-03
1217	sp|Q8QZT1|THIL_MOUSE	-3.24	9.43	0.96	2.06E-02
1218	sp|P52760|UK114_MOUSE	-3.25	9.50	0.90	1.16E-03
1219	sp|P24270|CATA_MOUSE	-3.25	9.51	0.94	3.86E-02
1220	sp|O35943|FRDA_MOUSE	-3.25	9.53	0.66	3.23E-04
1221	sp|Q99L13|3HIDH_MOUSE	-3.26	9.57	0.93	2.16E-04
1222	sp|Q7TNE1|SUCHY_MOUSE	-3.26	9.59	0.85	6.59E-03
1223	sp|P52196|THTR_MOUSE	-3.26	9.59	0.89	8.09E-05
1224	sp|Q8VC12|HUTU_MOUSE	-3.26	9.60	0.58	1.54E-01
1225	sp|Q9JLZ3|AUHM_MOUSE	-3.27	9.63	0.89	2.02E-04
1226	sp|Q9QXN5|MIOX_MOUSE	-3.27	9.64	0.76	1.91E-04
1227	sp|Q99LC5|ETFA_MOUSE	-3.27	9.66	0.92	1.62E-05
1228	sp|Q9JIL4|NHRF3_MOUSE	-3.27	9.66	0.90	7.00E-07
1229	sp|Q91YT0|NDUV1_MOUSE	-3.29	9.81	0.92	2.47E-05
1230	sp|Q80W22|THNS2_MOUSE	-3.30	9.82	0.82	8.56E-07
1231	sp|Q3UEG6|AGT2_MOUSE	-3.30	9.85	0.78	2.69E-05
1232	sp|P63030|MPC1_MOUSE	-3.31	9.89	0.80	1.45E-05
1233	sp|Q60825|NPT2A_MOUSE	-3.31	9.93	0.59	1.88E-05

1234	sp|Q8C025|CHPT1_MOUSE	-3.31	9.94	0.67	1.88E-03
1235	sp|Q9JHI5|IVD_MOUSE	-3.33	10.09	0.86	3.82E-04
1236	sp|Q99KR3|LACB2_MOUSE	-3.34	10.12	0.76	1.69E-02
1237	sp|Q9CQ91|NDUA3_MOUSE	-3.34	10.14	0.84	1.85E-05
1238	sp|P41216|ACSL1_MOUSE	-3.35	10.18	0.86	4.03E-03
1239	sp|O88909|S22A8_MOUSE	-3.35	10.19	0.80	1.36E-02
1240	sp|Q9DCC7|ISC2B_MOUSE	-3.35	10.22	0.72	5.81E-04
1241	sp|Q3ULD5|MCCB_MOUSE	-3.36	10.25	0.86	4.58E-06
1242	sp|Q8BGD8|COA6_MOUSE	-3.36	10.29	0.81	1.16E-01
1243	sp|Q8BYF6|SC5A8_MOUSE	-3.36	10.30	0.77	3.68E-03
1244	sp|Q99JW2|ACY1_MOUSE	-3.37	10.32	0.79	1.89E-03
1245	sp|Q9DBT9|M2GD_MOUSE	-3.37	10.33	0.83	5.64E-06
1246	sp|Q91WS0|CISD1_MOUSE	-3.37	10.36	0.94	5.52E-06
1247	sp|Q8R4N0|CLYBL_MOUSE	-3.38	10.40	0.83	4.10E-07
1248	sp|O70577|S22A2_MOUSE	-3.38	10.42	0.76	4.11E-03
1249	sp|Q9Z2I8|SUCB2_MOUSE	-3.39	10.47	0.92	6.43E-08
1250	sp|Q91YD6|VILL_MOUSE	-3.39	10.48	0.70	3.73E-01
1251	sp|Q9DCZ4|MIC26_MOUSE	-3.40	10.56	0.66	1.19E-03
1252	sp|P00416|COX3_MOUSE	-3.40	10.56	0.91	1.48E-02
1253	sp|Q8R0Y8|S2542_MOUSE	-3.40	10.58	0.71	1.62E-03
1254	sp|Q60936|ADCK3_MOUSE	-3.42	10.68	0.79	2.42E-04
1255	sp|Q8VBW8|TTC36_MOUSE	-3.42	10.69	0.77	6.20E-04
1256	sp|P28825|MEP1A_MOUSE	-3.43	10.75	0.89	5.03E-04
1257	sp|Q9D0S9|HINT2_MOUSE	-3.43	10.77	0.94	8.43E-03
1258	sp|P35576|G6PC_MOUSE	-3.43	10.79	0.83	6.92E-06
1259	sp|Q9ERT9|PPR1A_MOUSE	-3.44	10.83	0.88	1.95E-03
1260	sp|P11930|NUD19_MOUSE	-3.44	10.83	0.87	7.70E-02
1261	sp|Q91V76|CK054_MOUSE	-3.44	10.86	0.81	1.54E-07
1262	sp|Q9D826|SOX_MOUSE	-3.45	10.94	0.84	5.51E-02
1263	sp|Q9Z2J0|S23A1_MOUSE	-3.45	10.96	0.83	1.06E-02
1264	sp|Q9D8B4|NDUAB_MOUSE	-3.45	10.96	0.65	1.05E-01
1265	sp|Q9QXD1|ACOX2_MOUSE	-3.46	11.03	0.78	3.51E-04
1266	sp|Q91VA0|ACSM1_MOUSE	-3.47	11.05	0.89	1.31E-03
1267	sp|P40936|INMT_MOUSE	-3.47	11.06	0.85	6.12E-02
1268	sp|Q923I7|SC5A2_MOUSE	-3.47	11.10	0.81	4.52E-06
1269	sp|Q8JZZ0|UD3A2_MOUSE	-3.47	11.11	0.81	1.33E-02
1270	sp|Q8K4F5|ABHDB_MOUSE	-3.48	11.13	0.75	5.47E-03
1271	sp|Q60759|GCDH_MOUSE	-3.48	11.14	0.78	5.05E-07
1272	sp|Q9D7X8|GGCT_MOUSE	-3.48	11.16	0.79	1.11E-01
1273	sp|Q8JZV9|BDH2_MOUSE	-3.48	11.18	0.80	1.83E-04
1274	sp|Q8R3P0|ACY2_MOUSE	-3.49	11.20	0.78	3.56E-06
1275	sp|Q9DCM2|GSTK1_MOUSE	-3.49	11.23	0.85	2.47E-05
1276	sp|Q9JIZ0|CMLO1_MOUSE	-3.49	11.24	0.73	1.57E-03
1277	sp|Q9WU79|PROD_MOUSE	-3.49	11.25	0.80	2.03E-04
1278	sp|Q8VCT4|CES1D_MOUSE	-3.50	11.28	0.87	1.48E-06
1279	sp|Q6P3A8|ODBB_MOUSE	-3.50	11.28	0.81	3.58E-04
1280	sp|Q8VCN5|CGL_MOUSE	-3.50	11.29	0.83	2.45E-03
1281	sp|Q9D023|MPC2_MOUSE	-3.50	11.30	0.90	3.38E-05
1282	sp|Q99NB1|ACS2L_MOUSE	-3.50	11.31	0.83	2.51E-03
1283	sp|Q91WN4|KMO_MOUSE	-3.51	11.42	0.78	5.67E-05
1284	sp|Q91XE4|ACY3_MOUSE	-3.53	11.54	0.77	8.55E-02
1285	sp|Q9WVM8|AADAT_MOUSE	-3.54	11.59	0.80	1.14E-02
1286	sp|Q99J27|ACATN_MOUSE	-3.54	11.64	0.72	1.01E-04
1287	sp|Q99K67|AASS_MOUSE	-3.54	11.66	0.78	3.66E-04
1288	sp|Q7TMS5|ABCG2_MOUSE	-3.55	11.70	0.86	2.66E-04
1289	sp|Q8VDN2|AT1A1_MOUSE	-3.55	11.72	0.95	5.57E-04
1290	sp|Q9DCX8|IYD1_MOUSE	-3.55	11.72	0.86	5.50E-05
1291	sp|Q99MN9|PCCB_MOUSE	-3.55	11.73	0.90	1.84E-05
1292	sp|Q62468|VILI_MOUSE	-3.55	11.73	0.88	2.97E-09
1293	sp|Q8CFZ5|S22AC_MOUSE	-3.55	11.74	0.83	2.55E-04
1294	sp|P97816|S100G_MOUSE	-3.56	11.78	0.87	1.93E-03
1295	sp|Q8CHT0|AL4A1_MOUSE	-3.56	11.79	0.91	4.83E-05
1296	sp|P10648|GSTA2_MOUSE	-3.57	11.91	0.73	2.75E-02
1297	sp|Q9CQR4|ACO13_MOUSE	-3.60	12.10	0.88	5.84E-07
1298	sp|A2AKK5|ACNT1_MOUSE	-3.60	12.12	0.75	7.84E-02
1299	sp|P85094|ISC2A_MOUSE	-3.60	12.14	0.81	3.08E-03
1300	sp|Q8R0F8|FAHD1_MOUSE	-3.61	12.20	0.84	1.71E-03
1301	sp|Q8BH00|AL8A1_MOUSE	-3.61	12.21	0.89	5.29E-06
1302	sp|P53395|ODB2_MOUSE	-3.62	12.29	0.80	3.62E-07
1303	sp|P61922|GABT_MOUSE	-3.62	12.32	0.93	9.44E-04
1304	sp|Q8QZS1|HIBCH_MOUSE	-3.63	12.41	0.77	2.84E-04
1305	sp|Q99LB7|SARDH_MOUSE	-3.65	12.57	0.87	1.05E-04
1306	sp|Q3UFF7|LYPL1_MOUSE	-3.65	12.57	0.61	6.36E-02

1307	sp|Q8R2N1|AQP3_MOUSE	-3.66	12.64	0.85	8.99E-05
1308	sp|P14246|GTR2_MOUSE	-3.66	12.65	0.59	2.88E-01
1309	sp|Q3TLP5|ECHD2_MOUSE	-3.68	12.79	0.88	3.17E-03
1310	sp|O09173|HGD_MOUSE	-3.70	13.01	0.76	2.36E-07
1311	sp|Q99MZ7|PECR_MOUSE	-3.71	13.10	0.92	2.98E-02
1312	sp|Q60928|GGT1_MOUSE	-3.74	13.34	0.86	1.52E-03
1313	sp|Q9DBM2|ECHP_MOUSE	-3.74	13.34	0.88	1.50E-02
1314	sp|O35488|S27A2_MOUSE	-3.76	13.57	0.84	2.47E-03
1315	sp|P13707|GPDA_MOUSE	-3.77	13.65	0.84	6.88E-05
1316	sp|P35505|FAAA_MOUSE	-3.79	13.80	0.90	6.23E-05
1317	sp|Q64442|DHSO_MOUSE	-3.80	13.96	0.85	2.78E-05
1318	sp|Q80XN0|BDH_MOUSE	-3.82	14.12	0.92	2.19E-05
1319	sp|Q3TC72|FAHD2_MOUSE	-3.83	14.19	0.81	6.59E-03
1320	sp|Q8R164|BPHL_MOUSE	-3.83	14.21	0.85	1.68E-04
1321	sp|P97328|KHK_MOUSE	-3.85	14.41	0.84	3.50E-05
1322	sp|Q9R0H0|ACOX1_MOUSE	-3.86	14.52	0.88	1.92E-01
1323	sp|O88533|DDC_MOUSE	-3.87	14.63	0.69	1.96E-02
1324	sp|Q5SWY8|SC5AA_MOUSE	-3.88	14.72	0.79	8.84E-04
1325	sp|Q3UNZ8|QORL2_MOUSE	-3.90	14.96	0.83	4.57E-05
1326	sp|Q64516|GLPK_MOUSE	-3.91	14.98	0.85	4.19E-05
1327	sp|Q99J94|SO1A6_MOUSE	-3.91	15.03	0.65	1.92E-03
1328	sp|P62071|RRAS2_MOUSE	-3.92	15.16	0.53	3.82E-01
1329	sp|Q9DCG6|PBLD1_MOUSE	-3.95	15.43	0.81	3.67E-04
1330	sp|Q91Y97|ALDOB_MOUSE	-3.95	15.47	0.93	1.32E-05
1331	sp|Q3UZZ6|ST1D1_MOUSE	-3.96	15.51	0.84	7.67E-06
1332	sp|Q05920|PYC_MOUSE	-3.97	15.62	0.84	2.15E-03
1333	sp|Q04646|ATNG_MOUSE	-3.97	15.63	0.89	2.75E-04
1334	sp|Q9DCY0|KEG1_MOUSE	-3.97	15.67	0.88	7.32E-02
1335	sp|Q9EQ20|MMSA_MOUSE	-3.98	15.74	0.89	1.00E-04
1336	sp|O88338|CAD16_MOUSE	-4.00	15.95	0.89	2.33E-04
1337	sp|P45952|ACADM_MOUSE	-4.02	16.23	0.87	2.07E-08
1338	sp|P70691|UD12_MOUSE	-4.04	16.44	0.72	8.34E-03
1339	sp|P14094|AT1B1_MOUSE	-4.05	16.52	0.87	1.61E-03
1340	sp|Q91XE0|GLYAT_MOUSE	-4.05	16.55	0.86	8.85E-04
1341	sp|Q2TPA8|HSDL2_MOUSE	-4.09	17.04	0.61	4.47E-01
1342	sp|G3X9C2|FBX50_MOUSE	-4.09	17.04	0.84	3.61E-04
1343	sp|Q9Z2V4|PCKGC_MOUSE	-4.10	17.10	0.85	1.47E-03
1344	sp|Q78KK3|S22AI_MOUSE	-4.12	17.38	0.78	2.76E-02
1345	sp|P47955|RLA1_MOUSE	-4.12	17.40	0.52	1.60E-02
1346	sp|Q5U5V2|HYKK_MOUSE	-4.14	17.57	0.64	1.62E-02
1347	sp|Q49B93|SC5AC_MOUSE	-4.14	17.68	0.66	8.26E-01
1348	sp|Q8VC30|DHAK_MOUSE	-4.16	17.82	0.79	7.06E-03
1349	sp|Q9NYQ2|HAOX2_MOUSE	-4.18	18.08	0.88	6.44E-02
1350	sp|Q9QXD6|F16P1_MOUSE	-4.19	18.22	0.90	1.02E-04
1351	sp|O88343|S4A4_MOUSE	-4.19	18.31	0.78	9.32E-05
1352	sp|P03893|NU2M_MOUSE	-4.21	18.52	0.51	3.27E-01
1353	sp|O88576|S6A18_MOUSE	-4.21	18.57	0.63	4.04E-03
1354	sp|Q9WUR9|KAD4_MOUSE	-4.24	18.93	0.91	1.57E-05
1355	sp|Q78JT3|3HAO_MOUSE	-4.26	19.13	0.82	6.74E-04
1356	sp|Q99PG0|AAAD_MOUSE	-4.27	19.31	0.91	1.47E-07
1357	sp|Q8K0L3|ACSM2_MOUSE	-4.32	19.94	0.89	5.35E-02
1358	sp|Q9D964|GATM_MOUSE	-4.39	20.94	0.88	3.33E-03
1359	sp|P12658|CALB1_MOUSE	-4.40	21.18	0.92	3.61E-03
1360	sp|P16460|ASSY_MOUSE	-4.43	21.51	0.87	2.53E-04
1361	sp|P43024|CX6A1_MOUSE	-4.43	21.54	0.80	3.67E-04
1362	sp|Q9D687|S6A19_MOUSE	-4.48	22.26	0.61	5.64E-03
1363	sp|P34914|HYES_MOUSE	-4.65	25.06	0.84	1.81E-01
1364	sp|Q9JKZ2|SC5A3_MOUSE	-4.79	27.69	0.86	2.89E-03
1365	sp|Q9CQH0|PDZ1I_MOUSE	-6.50	90.53	0.79	6.71E-03

S.1.2 List of overexpressed proteins in WT mice subjected to UUO

Supplementary Table 3.5: List of proteins significantly overexpressed [C(FC)≥ 0.8] in WT kidneys subjected to UUO (21 days) and corresponding positive FC from Sham operated condition.

Protein ID	Name	Abs(FC) UUO/Sham	C(FC)
UROM_MOUSE	Uromodulin	16.34	0.85
COCA1_MOUSE	Collagen alpha-1(XII) chain	15.92	0.82
FBN1_MOUSE	Fibrillin-1	10.84	0.89
FBLN2_MOUSE	Fibulin-2	9.65	0.81
K1C19_MOUSE	Keratin, type I cytoskeletal 19	9.57	0.86
TAGL_MOUSE	Transgelin	9.27	0.89
PGS1_MOUSE	Biglycan	8.73	0.86
CNN1_MOUSE	Calponin-1	8.59	0.80
VIME_MOUSE	Vimentin	8.56	0.90
HA2U_MOUSE	H-2 class II histocompatibility antigen, A-U alpha chain	8.32	0.80
ANXA1_MOUSE	Annexin A1	8.17	0.84
MT2_MOUSE	Metallothionein-2	8.11	0.84
POSTN_MOUSE	Periostin	8.04	0.80
A1AT2_MOUSE	Alpha-1-antitrypsin 1-2	7.86	0.82
FINC_MOUSE	Fibronectin	7.85	0.84
COR1A_MOUSE	Coronin-1A	7.77	0.80
CO3A1_MOUSE	Collagen alpha-1(III) chain	7.72	0.92
PLSL_MOUSE	Plastin-2	7.63	0.85
CO1A1_MOUSE	Collagen alpha-1(I) chain	7.61	0.96
KCRB_MOUSE	Creatine kinase B-type	7.56	0.83
FBN2_MOUSE	Fibrillin-2	7.26	0.94
MIME_MOUSE	Mimecan	6.67	0.83
CKAP4_MOUSE	Cytoskeleton-associated protein 4	6.57	0.85
LUM_MOUSE	Lumican	6.55	0.87
FBLN3_MOUSE	EGF-containing fibulin-like extracellular matrix protein 1	6.33	0.80
SERPH_MOUSE	Serpin H1	6.19	0.94
CNN2_MOUSE	Calponin-2	6.15	0.80
LEG1_MOUSE	Galectin-1	6.15	0.87
DESM_MOUSE	Desmin	5.98	0.94
FBLN5_MOUSE	Fibulin-5	5.81	0.84
RET1_MOUSE	Retinol-binding protein 1	5.56	0.83
PDLI7_MOUSE	PDZ and LIM domain protein 7	5.40	0.81
CLUS_MOUSE	Clusterin	5.35	0.81
K2C5_MOUSE	Keratin, type II cytoskeletal 5	5.24	0.83
FLNA_MOUSE	Filamin-A	5.07	0.93
MYOF_MOUSE	Myoferlin	4.99	0.86
K2C8_MOUSE	Keratin, type II cytoskeletal 8	4.93	0.89
CO6A1_MOUSE	Collagen alpha-1(VI) chain	4.78	0.88
CO6A2_MOUSE	Collagen alpha-2(VI) chain	4.76	0.94
ANXA3_MOUSE	Annexin A3	4.73	0.83
FIBA_MOUSE	Fibrinogen alpha chain	4.64	0.90
COEA1_MOUSE	Collagen alpha-1(XIV) chain	4.62	0.81
HEMO_MOUSE	Hemopexin	4.60	0.86
CSRP1_MOUSE	Cysteine and glycine-rich protein 1	4.52	0.89
CO4A2_MOUSE	Collagen alpha-2(IV) chain	4.50	0.80
FIBG_MOUSE	Fibrinogen gamma chain	4.45	0.85
EMIL1_MOUSE	Emilin-1	4.42	0.82
TBA1A_MOUSE	Tubulin alpha-1A chain	4.41	0.96
TYB4_MOUSE	Thymosin beta-4	4.35	0.88
TPM1_MOUSE	Tropomyosin alpha-1 chain	4.28	0.84
K2C7_MOUSE	Keratin, type II cytoskeletal 7	4.27	0.88
PEDF_MOUSE	Pigment epithelium-derived factor	4.24	0.81
ACTN1_MOUSE	Alpha-actinin-1	4.22	0.96
TPM4_MOUSE	Tropomyosin alpha-4 chain	4.19	0.91
IGKC_MOUSE	Ig kappa chain C region	4.15	0.87
FIBB_MOUSE	Fibrinogen beta chain	4.00	0.86
MYADM_MOUSE	Myeloid-associated differentiation marker	4.00	0.87
SH3L3_MOUSE	SH3 domain-binding glutamic acid-rich-like protein 3	3.85	0.90
TRFE_MOUSE	Serotransferrin	3.78	0.91
ANXA2_MOUSE	Annexin A2	3.76	0.90
G6PE_MOUSE	GDH/6PGL endoplasmic bifunctional protein	3.71	0.90
CALU_MOUSE	Calumenin	3.69	0.84
SPB6_MOUSE	Serpin B6	3.56	0.89
CRIP1_MOUSE	Cysteine-rich protein 1	3.55	0.90

EFHD2_MOUSE	EF-hand domain-containing protein D2	3.52	0.87
ESYT1_MOUSE	Extended synaptotagmin-1	3.52	0.82
LMNA_MOUSE	Prelamin-A/C	3.49	0.94
CO4B_MOUSE	Complement C4-B	3.44	0.86
ARC1B_MOUSE	Actin-related protein 2/3 complex subunit 1B	3.38	0.87
TBB5_MOUSE	Tubulin beta-5 chain	3.33	0.88
APOE_MOUSE	Apolipoprotein E	3.31	0.87
MYH11_MOUSE	Myosin-11	3.28	0.87
MYH10_MOUSE	Myosin-10	3.27	0.85
FETUA_MOUSE	Alpha-2-HS-glycoprotein	3.27	0.90
ESYT2_MOUSE	Extended synaptotagmin-2	3.23	0.86
GCAB_MOUSE	Ig gamma-2A chain C region secreted form	3.21	0.91
ACTA_MOUSE	Actin, aortic smooth muscle	3.17	0.94
VTDB_MOUSE	Vitamin D-binding protein	3.13	0.93
EST1C_MOUSE	Carboxylesterase 1C	3.11	0.95
KNG1_MOUSE	Kininogen-1	3.09	0.91
MYL9_MOUSE	Myosin regulatory light polypeptide 9	3.08	0.98
S10AB_MOUSE	Protein S100-A11	3.08	0.88
A1AT1_MOUSE	Alpha-1-antitrypsin 1-1	3.07	0.86
IGG2B_MOUSE	Ig gamma-2B chain C region	3.07	0.81
SH3L1_MOUSE	SH3 domain-binding glutamic acid-rich-like protein	3.06	0.86
K2C79_MOUSE	Keratin, type II cytoskeletal 79	3.05	0.91
TAGL2_MOUSE	Transgelin-2	3.04	0.88
K1C18_MOUSE	Keratin, type I cytoskeletal 18	2.99	0.94
ALBU_MOUSE	Serum albumin	2.98	0.92
PTRF_MOUSE	Polymerase I and transcript release factor	2.96	0.84
VAT1_MOUSE	Synaptic vesicle membrane protein VAT-1 homolog	2.96	0.90
SEPT7_MOUSE	Septin-7	2.95	0.82
PSME2_MOUSE	Proteasome activator complex subunit 2	2.91	0.88
B2MG_MOUSE	Beta-2-microglobulin	2.88	0.82
CERU_MOUSE	Ceruloplasmin	2.86	0.80
SEPT2_MOUSE	Septin-2	2.83	0.82
COF1_MOUSE	Cofilin-1	2.74	0.87
A1AT4_MOUSE	Alpha-1-antitrypsin 1-4	2.72	0.83
ANXA6_MOUSE	Annexin A6	2.71	0.89
ADPRH_MOUSE	[Protein ADP-ribosylarginine] hydrolase	2.71	0.86
DPYL2_MOUSE	Dihydropyrimidinase-related protein 2	2.68	0.88
CO4A1_MOUSE	Collagen alpha-1(IV) chain	2.67	0.88
MAP4_MOUSE	Microtubule-associated protein 4	2.66	0.82
CATD_MOUSE	Cathepsin D	2.65	0.82
GBG2_MOUSE	Guanine nucleotide-binding protein G(I)/G(S)/G(O) subunit gamma-2	2.65	0.81
ROA1_MOUSE	Heterogeneous nuclear ribonucleoprotein A1	2.63	0.88
ISG15_MOUSE	Ubiquitin-like protein ISG15	2.62	0.84
FETUB_MOUSE	Fetuin-B	2.61	0.89
MYH9_MOUSE	Myosin-9	2.61	0.99
CO3_MOUSE	Complement C3	2.59	0.87
MYLK_MOUSE	Myosin light chain kinase, smooth muscle	2.59	0.80
S10AA_MOUSE	Protein S100-A10	2.59	0.86
VMA5A_MOUSE	von Willebrand factor A domain-containing protein 5A	2.58	0.86
COIA1_MOUSE	Collagen alpha-1(XVIII) chain	2.57	0.96
MYL6_MOUSE	Myosin light polypeptide 6	2.53	0.92
CATZ_MOUSE	Cathepsin Z	2.53	0.86
SF3B3_MOUSE	Splicing factor 3B subunit 3	2.51	0.83
APOA4_MOUSE	Apolipoprotein A-IV	2.50	0.82
CAP1_MOUSE	Adenylyl cyclase-associated protein 1	2.50	0.92
APOH_MOUSE	Beta-2-glycoprotein 1	2.50	0.80
APOA1_MOUSE	Apolipoprotein A-I	2.46	0.92
SET_MOUSE	Protein SET	2.46	0.83
SFPQ_MOUSE	Splicing factor, proline- and glutamine-rich	2.44	0.81
RBM3_MOUSE	RNA-binding protein 3	2.36	0.84
T22D1_MOUSE	TSC22 domain family protein 1	2.35	0.90
TIF1B_MOUSE	Transcription intermediary factor 1-beta	2.33	0.83
GELS_MOUSE	Gelsolin	2.33	0.84
VINC_MOUSE	Vinculin	2.33	0.94
ML12B_MOUSE	Myosin regulatory light chain 12B	2.33	0.83
LMNB1_MOUSE	Lamin-B1	2.30	0.86
ANXA5_MOUSE	Annexin A5	2.29	0.84
PSME1_MOUSE	Proteasome activator complex subunit 1	2.28	0.84
ANT3_MOUSE	Antithrombin-III	2.27	0.86
LAMA5_MOUSE	Laminin subunit alpha-5	2.26	0.83
COR1C_MOUSE	Coronin-1C	2.23	0.83
CAPZB_MOUSE	F-actin-capping protein subunit beta	2.23	0.89

FUS_MOUSE	RNA-binding protein FUS	2.22	0.80
AGRIN_MOUSE	Agrin	2.16	0.92
AN32B_MOUSE	Acidic leucine-rich nuclear phosphoprotein 32 family member B	2.15	0.81
KHDR1_MOUSE	KH domain-containing, RNA-binding, signal transduction-associated protein 1	2.14	0.84
PROF1_MOUSE	Profilin-1	2.10	0.89
NID1_MOUSE	Nidogen-1	2.10	0.92
H2AV_MOUSE	Histone H2A.V	2.07	0.86
COR1B_MOUSE	Coronin-1B	2.06	0.86
A2M_MOUSE	Pregnancy zone protein	2.05	0.85
INO1_MOUSE	Inositol-3-phosphate synthase 1	2.03	0.81
LIMA1_MOUSE	LIM domain and actin-binding protein 1	2.02	0.87
GNAI2_MOUSE	Guanine nucleotide-binding protein G(i) subunit alpha-2	2.02	0.83
ARPC3_MOUSE	Actin-related protein 2/3 complex subunit 3	2.01	0.87
WDR1_MOUSE	WD repeat-containing protein 1	2.01	0.83
UBC9_MOUSE	SUMO-conjugating enzyme UBC9	1.97	0.91
HP1B3_MOUSE	Heterochromatin protein 1-binding protein 3	1.94	0.83
ACTBL_MOUSE	Beta-actin-like protein 2	1.91	0.84
ROA3_MOUSE	Heterogeneous nuclear ribonucleoprotein A3	1.90	0.90
NONO_MOUSE	Non-POU domain-containing octamer-binding protein	1.90	0.91
ABCB7_MOUSE	ATP-binding cassette sub-family B member 7, mitochondrial	1.89	0.89
ARP3_MOUSE	Actin-related protein 3	1.89	0.95
ARPC2_MOUSE	Actin-related protein 2/3 complex subunit 2	1.87	0.83
NH2L1_MOUSE	NHP2-like protein 1	1.86	0.81
LAMC1_MOUSE	Laminin subunit gamma-1	1.85	0.93
LAMB1_MOUSE	Laminin subunit beta-1	1.85	0.85
HNRPF_MOUSE	Heterogeneous nuclear ribonucleoprotein F	1.82	0.83
FABP4_MOUSE	Fatty acid-binding protein, adipocyte	1.82	0.85
LASP1_MOUSE	LIM and SH3 domain protein 1	1.81	0.81
PGBM_MOUSE	Basement membrane-specific heparan sulfate proteoglycan core protein	1.80	0.81
TADBP_MOUSE	TAR DNA-binding protein 43	1.80	0.81
NUCL_MOUSE	Nucleolin	1.79	0.83
DX39B_MOUSE	Spliceosome RNA helicase Ddx39b	1.78	0.81
ANXA4_MOUSE	Annexin A4	1.78	0.85
TLN1_MOUSE	Talin-1	1.78	0.82
FUBP2_MOUSE	Far upstream element-binding protein 2	1.78	0.80
ARP2_MOUSE	Actin-related protein 2	1.76	0.88
RUXF_MOUSE	Small nuclear ribonucleoprotein F	1.75	0.87
HNRPM_MOUSE	Heterogeneous nuclear ribonucleoprotein M	1.74	0.86
CSRP2_MOUSE	Cysteine and glycine-rich protein 2	1.72	0.82
TGM2_MOUSE	Transglutminase 2	1.71	0.90
LAP2B_MOUSE	Lamina-associated polypeptide 2, isoforms beta/delta/epsilon/gamma	1.71	0.80
SRSF2_MOUSE	Serine/arginine-rich splicing factor 2	1.70	0.86
PDIA6_MOUSE	Protein disulfide-isomerase A6	1.68	0.90
1433G_MOUSE	14-3-3 protein gamma	1.65	0.81
SMAP_MOUSE	Small acidic protein	1.64	0.88
LSM3_MOUSE	U6 snRNA-associated Sm-like protein LSm3	1.62	0.91
RSU1_MOUSE	Ras suppressor protein 1	1.59	0.84
SC11A_MOUSE	Signal peptidase complex catalytic subunit SEC11A	1.59	0.80
ABRAL_MOUSE	Costars family protein ABRACL	1.56	0.80
ACTB_MOUSE	Actin, cytoplasmic 1	1.56	0.93
HNRPU_MOUSE	Heterogeneous nuclear ribonucleoprotein U	1.53	0.85
MOES_MOUSE	Moesin	1.52	0.81
GDIR1_MOUSE	Rho GDP-dissociation inhibitor 1	1.51	0.84
HNRH1_MOUSE	Heterogeneous nuclear ribonucleoprotein H	1.48	0.87
SMD2_MOUSE	Small nuclear ribonucleoprotein Sm D2	1.47	0.81
KAPCA_MOUSE	cAMP-dependent protein kinase catalytic subunit alpha	1.44	0.89
PDIA4_MOUSE	Protein disulfide-isomerase A4	1.40	0.80
HNRPK_MOUSE	Heterogeneous nuclear ribonucleoprotein K	1.40	0.82
LAMP1_MOUSE	Lysosome-associated membrane glycoprotein 1	1.38	0.81

S.1.3 List of underexpressed proteins in WT mice subjected to UUO

Supplementary Table 3.6: List of proteins significantly underexpressed [C(FC)≥ 0.8] in WT kidneys subjected to UUO (21 days) and corresponding negative FC from Sham operated condition.

Protein ID	Names	Abs(FC) Sham/UUO	C(FC)
G6PC_MOUSE	Glucose-6-phosphatase	72.24	0.86
AADAT_MOUSE	Kynurenine/alpha-aminoadipate aminotransferase, mitochondrial	48.00	0.84
PDZ1I_MOUSE	PDZK1-interacting protein 1	45.76	0.84
HAOX2_MOUSE	Hydroxyacid oxidase 2	44.28	0.85
CALB1_MOUSE	Calbindin	32.07	0.91
ASSY_MOUSE	Argininosuccinate synthase	21.28	0.88
ACSM1_MOUSE	Acyl-coenzyme A synthetase ACSM1, mitochondrial	20.87	0.83
F16P1_MOUSE	Fructose-1,6-bisphosphatase 1	20.84	0.81
ACSM2_MOUSE	Acyl-coenzyme A synthetase ACSM2, mitochondrial	20.17	0.86
ECHP_MOUSE	Peroxisomal bifunctional enzyme	19.92	0.84
KAD4_MOUSE	Adenylate kinase 4, mitochondrial	19.83	0.89
AT1B1_MOUSE	Sodium/potassium-transporting ATPase subunit beta-1	19.55	0.87
CAD16_MOUSE	Cadherin-16	19.54	0.92
PYC_MOUSE	Pyruvate carboxylase, mitochondrial	18.04	0.87
GSTA2_MOUSE	Glutathione S-transferase A2	17.14	0.85
AL8A1_MOUSE	Aldehyde dehydrogenase family 8 member A1	17.11	0.88
ATNG_MOUSE	Sodium/potassium-transporting ATPase subunit gamma	16.80	0.90
UD3A2_MOUSE	UDP-glucuronosyltransferase 3A2	16.72	0.83
S100G_MOUSE	Protein S100-G	16.59	0.90
ACS2L_MOUSE	Acetyl-coenzyme A synthetase 2-like, mitochondrial	16.56	0.89
KEG1_MOUSE	Glycine N-acyltransferase-like protein Keg1	16.36	0.88
SC5A2_MOUSE	Sodium/glucose cotransporter 2	16.23	0.80
ECHD2_MOUSE	Enoyl-CoA hydratase domain-containing protein 2, mitochondrial	16.09	0.87
CGL_MOUSE	Cystathionine gamma-lyase	16.04	0.86
3HAO_MOUSE	3-hydroxyanthranilate 3,4-dioxygenase	15.56	0.85
S27A2_MOUSE	Very long-chain acyl-CoA synthetase	14.88	0.81
MEP1B_MOUSE	Meprin A subunit beta	14.72	0.82
ACADM_MOUSE	Medium-chain specific acyl-CoA dehydrogenase, mitochondrial	14.48	0.86
TMM27_MOUSE	Collectrin	14.41	0.85
ISC2A_MOUSE	Isochorismatase domain-containing protein 2A	14.27	0.90
BDH_MOUSE	D-beta-hydroxybutyrate dehydrogenase, mitochondrial	14.24	0.89
ALDOB_MOUSE	Fructose-bisphosphate aldolase B	14.21	0.93
HOT_MOUSE	Hydroxyacid-oxoacid transhydrogenase, mitochondrial	14.07	0.84
GATM_MOUSE	Glycine amidinotransferase, mitochondrial	13.91	0.87
GABT_MOUSE	4-aminobutyrate aminotransferase, mitochondrial	13.84	0.93
KBL_MOUSE	2-amino-3-ketobutyrate coenzyme A ligase, mitochondrial	13.82	0.85
MMSA_MOUSE	Methylmalonate-semialdehyde dehydrogenase [acylating], mitochondrial	13.79	0.88
PXMP2_MOUSE	Peroxisomal membrane protein 2	13.77	0.81
ST1D1_MOUSE	Sulfotransferase 1 family member D1	13.74	0.85
GGT1_MOUSE	Gamma-glutamyltranspeptidase 1	13.58	0.89
MAAI_MOUSE	Maleylacetoacetate isomerase	13.49	0.82
PGAM2_MOUSE	Phosphoglycerate mutase 2	13.44	0.88
GLYAT_MOUSE	Glycine N-acyltransferase	13.43	0.88
S4A4_MOUSE	Electrogenic sodium bicarbonate cotransporter 1	13.29	0.83
FAAA_MOUSE	Fumarylacetoacetase	13.16	0.92
AT1A1_MOUSE	Sodium/potassium-transporting ATPase subunit alpha-1	13.14	0.93
DHSO_MOUSE	Sorbitol dehydrogenase	13.11	0.82
MPC1_MOUSE	Mitochondrial pyruvate carrier 1	12.91	0.93
UK114_MOUSE	Ribonuclease UK114	12.69	0.94
ACE_MOUSE	Angiotensin-converting enzyme	12.66	0.91
DECR2_MOUSE	Peroxisomal 2,4-dienoyl-CoA reductase	12.62	0.90
CATA_MOUSE	Catalase	12.62	0.94
ACY3_MOUSE	N-acyl-aromatic-L-amino acid amidohydrolase (carboxylate-forming)	12.43	0.80
S22A2_MOUSE	Solute carrier family 22 member 2	12.29	0.81
GSTK1_MOUSE	Glutathione S-transferase kappa 1	12.27	0.82
PCCB_MOUSE	Propionyl-CoA carboxylase beta chain, mitochondrial	12.22	0.96
AL4A1_MOUSE	Delta-1-pyrroline-5-carboxylate dehydrogenase, mitochondrial	12.17	0.93
CES1D_MOUSE	Carboxylesterase 1D	11.96	0.83
GLPK_MOUSE	Glycerol kinase	11.89	0.86
QORL2_MOUSE	Quinone oxidoreductase-like protein 2	11.85	0.82
AAAD_MOUSE	Arylacetamide deacetylase	11.84	0.85
VILI_MOUSE	Villin-1	11.78	0.91
DHAK_MOUSE	Triokinase/FMN cyclase	11.77	0.80

COX1_MOUSE	Cytochrome c oxidase subunit 1	11.70	0.90
SODM_MOUSE	Superoxide dismutase [Mn], mitochondrial	11.66	0.93
S2542_MOUSE	Mitochondrial coenzyme A transporter SLC25A42	11.63	0.86
MPC2_MOUSE	Mitochondrial pyruvate carrier 2	11.60	0.82
ATP5L_MOUSE	ATP synthase subunit g, mitochondrial	11.54	0.80
OXDA_MOUSE	D-amino-acid oxidase	11.38	0.81
NUD19_MOUSE	Nucleoside diphosphate-linked moiety X motif 19	11.28	0.90
HINT2_MOUSE	Histidine triad nucleotide-binding protein 2, mitochondrial	11.27	0.98
BPHL_MOUSE	Valacyclovir hydrolase	11.09	0.87
MCCB_MOUSE	Methylcrotonoyl-CoA carboxylase beta chain, mitochondrial	10.95	0.90
PBLD1_MOUSE	Phenazine biosynthesis-like domain-containing protein 1	10.91	0.87
DIC_MOUSE	Mitochondrial dicarboxylate carrier	10.83	0.83
ACD10_MOUSE	Acyl-CoA dehydrogenase family member 10	10.77	0.86
NHRF3_MOUSE	Na(+)/H(+) exchange regulatory cofactor NHE-RF3	10.71	0.86
GSTA3_MOUSE	Glutathione S-transferase A3	10.63	0.81
CK054_MOUSE	Ester hydrolase C11orf54 homolog	10.61	0.82
AK1A1_MOUSE	Alcohol dehydrogenase [NADP(+)]	10.56	0.91
3HIDH_MOUSE	3-hydroxyisobutyrate dehydrogenase, mitochondrial	10.55	0.94
SUCB2_MOUSE	Succinyl-CoA ligase [GDP-forming] subunit beta, mitochondrial	10.42	0.94
LACB2_MOUSE	Beta-lactamase-like protein 2	10.39	0.82
FAHD1_MOUSE	Acylpyruvase FAHD1, mitochondrial	10.39	0.84
FMO1_MOUSE	Dimethylaniline monooxygenase [N-oxide-forming] 1	10.33	0.82
IVD_MOUSE	Isovaleryl-CoA dehydrogenase, mitochondrial	10.14	0.88
THIL_MOUSE	Acetyl-CoA acetyltransferase, mitochondrial	10.10	0.95
PROD_MOUSE	Proline dehydrogenase 1, mitochondrial	10.05	0.81
SARDH_MOUSE	Sarcosine dehydrogenase, mitochondrial	10.05	0.85
INMT_MOUSE	Indolethylamine N-methyltransferase	10.03	0.83
AL1L1_MOUSE	Cytosolic 10-formyltetrahydrofolate dehydrogenase	9.95	0.91
KHK_MOUSE	Ketohexokinase	9.90	0.83
ARK72_MOUSE	Aflatoxin B1 aldehyde reductase member 2	9.87	0.87
S22AI_MOUSE	Solute carrier family 22 member 18	9.86	0.90
HCDH_MOUSE	Hydroxyacyl-coenzyme A dehydrogenase, mitochondrial	9.82	0.90
NDUB6_MOUSE	NADH dehydrogenase [ubiquinone] 1 beta subcomplex subunit 6	9.77	0.81
CISD1_MOUSE	CDGSH iron-sulfur domain-containing protein 1	9.75	0.95
NDRG1_MOUSE	Protein NDRG1	9.52	0.99
S13A3_MOUSE	Solute carrier family 13 member 3	9.52	0.88
CYC_MOUSE	Cytochrome c, somatic	9.49	0.92
SSDH_MOUSE	Succinate-semialdehyde dehydrogenase, mitochondrial	9.47	0.88
SCOT1_MOUSE	Succinyl-CoA:3-ketoacid coenzyme A transferase 1, mitochondrial	9.34	0.92
HMGCL_MOUSE	Hydroxymethylglutaryl-CoA lyase, mitochondrial	9.26	0.92
ACPM_MOUSE	Acyl carrier protein, mitochondrial	9.19	0.92
ATPK_MOUSE	ATP synthase subunit f, mitochondrial	9.17	0.80
MSRA_MOUSE	Mitochondrial peptide methionine sulfoxide reductase	9.12	0.83
CBR1_MOUSE	Carbonyl reductase [NADPH] 1	9.11	0.92
LDHD_MOUSE	Probable D-lactate dehydrogenase, mitochondrial	9.10	0.88
COX5A_MOUSE	Cytochrome c oxidase subunit 5A, mitochondrial	9.08	0.94
ETFA_MOUSE	Electron transfer flavoprotein subunit alpha, mitochondrial	9.07	0.93
NDUB5_MOUSE	NADH dehydrogenase [ubiquinone] 1 beta subcomplex subunit 5, mitochondrial	9.01	0.85
PLSI_MOUSE	Plastin-1	9.01	0.86
GPDA_MOUSE	Glycerol-3-phosphate dehydrogenase [NAD(+)], cytoplasmic	8.85	0.91
NIPS1_MOUSE	Protein NipSnap homolog 1	8.81	0.91
NU4M_MOUSE	NADH-ubiquinone oxidoreductase chain 4	8.79	0.89
FAHD2_MOUSE	umarylacetoacetate hydrolase domain-containing protein 2A	8.76	0.80
CLYBL_MOUSE	Citrate lyase subunit beta-like protein, mitochondrial	8.75	0.80
FBX50_MOUSE	F-box only protein 50	8.73	0.80
NDUS6_MOUSE	NADH dehydrogenase [ubiquinone] iron-sulfur protein 6, mitochondrial	8.72	0.81
THNS2_MOUSE	Threonine synthase-like 2	8.70	0.83
NDUB8_MOUSE	NADH dehydrogenase [ubiquinone] 1 beta subcomplex subunit 8, mitochondrial	8.67	0.86
NU5M_MOUSE	NADH-ubiquinone oxidoreductase chain 5	8.67	0.88
PECR_MOUSE	Peroxisomal trans-2-enoyl-CoA reductase	8.65	0.87
SDHA_MOUSE	Succinate dehydrogenase [ubiquinone] flavoprotein subunit, mitochondrial	8.64	0.98
NDUBA_MOUSE	NADH dehydrogenase [ubiquinone] 1 beta subcomplex subunit 10	8.63	0.86
SUCA_MOUSE	Succinyl-CoA ligase [ADP/GDP-forming] subunit alpha, mitochondrial	8.55	0.94
NDUV2_MOUSE	NADH dehydrogenase [ubiquinone] flavoprotein 2, mitochondrial	8.50	0.84
IPYR2_MOUSE	Inorganic pyrophosphatase 2, mitochondrial	8.50	0.83
NDUV1_MOUSE	NADH dehydrogenase [ubiquinone] flavoprotein 1, mitochondrial	8.43	0.90
NDUA9_MOUSE	NADH dehydrogenase [ubiquinone] 1 alpha subcomplex subunit 9, mitochondrial	8.38	0.89
ABCD3_MOUSE	ATP-binding cassette sub-family D member 3	8.36	0.88
ATPD_MOUSE	ATP synthase subunit delta, mitochondrial	8.32	0.98

QCR6_MOUSE	Cytochrome b-c1 complex subunit 6, mitochondrial	8.31	0.93
NDUA1_MOUSE	NADH dehydrogenase [ubiquinone] 1 alpha subcomplex subunit 1	8.25	0.86
COX5B_MOUSE	Cytochrome c oxidase subunit 5B, mitochondrial	8.24	0.91
IDHP_MOUSE	Isocitrate dehydrogenase [NADP], mitochondrial	8.21	0.93
SBP1_MOUSE	Selenium-binding protein 1	8.19	0.92
NDUS7_MOUSE	NADH dehydrogenase [ubiquinone] iron-sulfur protein 7, mitochondrial	8.16	0.94
BDH2_MOUSE	3-hydroxybutyrate dehydrogenase type 2	8.13	0.82
ETFB_MOUSE	Electron transfer flavoprotein subunit beta	8.13	0.91
NHRF1_MOUSE	Na(+)/H(+) exchange regulatory cofactor NHE-RF1	8.07	0.94
NEP_MOUSE	Neprilysin	8.05	0.90
NDUAD_MOUSE	NADH dehydrogenase [ubiquinone] 1 alpha subcomplex subunit 13	8.00	0.89
CSAD_MOUSE	Cysteine sulfinic acid decarboxylase	8.00	0.90
COX2_MOUSE	Cytochrome c oxidase subunit 2	7.99	0.87
SDHB_MOUSE	Succinate dehydrogenase [ubiquinone] iron-sulfur subunit, mitochondrial	7.99	0.89
TPMT_MOUSE	Thiopurine S-methyltransferase	7.98	0.93
CY1_MOUSE	Cytochrome c1, heme protein, mitochondrial	7.96	0.94
TOM5_MOUSE	Mitochondrial import receptor subunit TOM5 homolog	7.94	1.00
COQ9_MOUSE	Ubiquinone biosynthesis protein COQ9, mitochondrial	7.91	0.90
IDHG1_MOUSE	Isocitrate dehydrogenase [NAD] subunit gamma 1, mitochondrial	7.91	0.91
THIM_MOUSE	3-ketoacyl-CoA thiolase, mitochondrial	7.90	0.91
UCRI_MOUSE	Cytochrome b-c1 complex subunit Rieske, mitochondrial	7.89	0.91
NDUA3_MOUSE	NADH dehydrogenase [ubiquinone] 1 alpha subcomplex subunit 3	7.86	0.89
AUHM_MOUSE	Methylglutaconyl-CoA hydratase, mitochondrial	7.85	0.85
COASY_MOUSE	Bifunctional coenzyme A synthase	7.83	0.85
NLTP_MOUSE	Non-specific lipid-transfer protein	7.82	0.88
NDUB7_MOUSE	NADH dehydrogenase [ubiquinone] 1 beta subcomplex subunit 7	7.79	0.84
TAU_MOUSE	Microtubule-associated protein tau	7.76	0.83
THTR_MOUSE	Thiosulfate sulfurtransferase	7.75	0.89
PPA6_MOUSE	Lysophosphatidic acid phosphatase type 6	7.74	0.85
QOR_MOUSE	Quinone oxidoreductase	7.71	0.84
ACSL1_MOUSE	Long-chain-fatty-acid--CoA ligase 1	7.69	0.90
CRYL1_MOUSE	Lambda-crystallin homolog	7.62	0.90
LRP2_MOUSE	Low-density lipoprotein receptor-related protein 2	7.60	0.84
CX7A1_MOUSE	Cytochrome c oxidase subunit 7A1, mitochondrial	7.60	0.93
HGD_MOUSE	Homogentisate 1,2-dioxygenase	7.58	0.84
CH60_MOUSE	60 kDa heat shock protein, mitochondrial	7.56	0.96
C560_MOUSE	Succinate dehydrogenase cytochrome b560 subunit, mitochondrial	7.55	0.83
NDUS1_MOUSE	NADH-ubiquinone oxidoreductase 75 kDa subunit, mitochondrial	7.55	0.94
CP013_MOUSE	UPF0585 protein C16orf13 homolog	7.48	0.87
COX41_MOUSE	Cytochrome c oxidase subunit 4 isoform 1, mitochondrial	7.46	0.94
ACD11_MOUSE	Acyl-CoA dehydrogenase family member 11	7.41	0.80
CX7A2_MOUSE	Cytochrome c oxidase subunit 7A2, mitochondrial	7.37	0.92
NAKD2_MOUSE	NAD kinase 2, mitochondrial	7.33	0.95
VATG1_MOUSE	V-type proton ATPase subunit G 1	7.31	0.83
NDUA4_MOUSE	Cytochrome c oxidase subunit NDUFA4	7.30	0.89
AIFM1_MOUSE	Apoptosis-inducing factor 1, mitochondrial	7.30	0.92
CDD_MOUSE	Cytidine deaminase	7.28	0.81
MUTA_MOUSE	Methylmalonyl-CoA mutase, mitochondrial	7.27	0.81
MCCA_MOUSE	Methylcrotonoyl-CoA carboxylase subunit alpha, mitochondrial	7.25	0.82
NDUB4_MOUSE	NADH dehydrogenase [ubiquinone] 1 beta subcomplex subunit 4	7.21	0.83
ECHM_MOUSE	Enoyl-CoA hydratase, mitochondrial	7.21	0.90
ATP5H_MOUSE	ATP synthase subunit d, mitochondrial	7.21	0.93
OCTC_MOUSE	Peroxisomal carnitine O-octanoyltransferase	7.20	0.80
CMC2_MOUSE	Calcium-binding mitochondrial carrier protein Aralar2	7.20	0.80
NDUS4_MOUSE	NADH dehydrogenase [ubiquinone] iron-sulfur protein 4, mitochondrial	7.19	0.83
CBR4_MOUSE	Carbonyl reductase family member 4	7.19	0.85
DLDH_MOUSE	Dihydrolipoyl dehydrogenase, mitochondrial	7.18	0.94
AL7A1_MOUSE	Alpha-aminoadipic semialdehyde dehydrogenase	7.16	0.82
MEP1A_MOUSE	Meprin A subunit alpha	7.15	0.88
QCR2_MOUSE	Cytochrome b-c1 complex subunit 2, mitochondrial	7.14	0.94
C1TC_MOUSE	C-1-tetrahydrofolate synthase, cytoplasmic	7.12	0.87
QCR8_MOUSE	Cytochrome b-c1 complex subunit 8	7.12	0.91
MGST3_MOUSE	Microsomal glutathione S-transferase 3	7.12	0.84
ADT2_MOUSE	ADP/ATP translocase 2	7.06	0.81
ATP8_MOUSE	ATP synthase protein 8	6.97	0.90
ATPG_MOUSE	ATP synthase subunit gamma, mitochondrial	6.96	0.90
NDUAA_MOUSE	NADH dehydrogenase [ubiquinone] 1 alpha subcomplex subunit 10, mitochondrial	6.92	0.93
S12A1_MOUSE	Solute carrier family 12 member 1	6.91	0.96
AQP1_MOUSE	Aquaporin-1	6.91	0.80
ODO2_MOUSE	Dihydrolipoyllysine-residue succinyltransferase component of 2-oxoglutarate dehydrogenase complex, mitochondrial	6.89	0.89
TBA4A_MOUSE	Tubulin alpha-4A chain	6.89	0.88

ATPO_MOUSE	ATP synthase subunit O, mitochondrial	6.84	0.96
PCCA_MOUSE	Propionyl-CoA carboxylase alpha chain, mitochondrial	6.83	0.84
BPNT1_MOUSE	3'(2'),5'-bisphosphate nucleotidase 1	6.81	0.87
PTER_MOUSE	Phosphotriesterase-related protein	6.73	0.91
FGGY_MOUSE	FGGY carbohydrate kinase domain-containing protein	6.73	0.85
ECI2_MOUSE	Enoyl-CoA delta isomerase 2, mitochondrial	6.73	0.85
NDUS2_MOUSE	NADH dehydrogenase [ubiquinone] iron-sulfur protein 2, mitochondrial	6.72	0.91
ES1_MOUSE	ES1 protein homolog, mitochondrial	6.71	0.92
ACON_MOUSE	Aconitate hydratase, mitochondrial	6.66	0.90
NDUS3_MOUSE	NADH dehydrogenase [ubiquinone] iron-sulfur protein 3, mitochondrial	6.64	0.96
MDHM_MOUSE	Malate dehydrogenase, mitochondrial	6.63	0.96
ATP5I_MOUSE	ATP synthase subunit e, mitochondrial	6.62	0.90
USMG5_MOUSE	Up-regulated during skeletal muscle growth protein 5	6.60	0.97
FUMH_MOUSE	Fumarate hydratase, mitochondrial	6.56	0.89
ATPB_MOUSE	ATP synthase subunit beta, mitochondrial	6.55	0.94
FABPH_MOUSE	Fatty acid-binding protein, heart	6.53	0.88
AQP3_MOUSE	Aquaporin-3	6.51	0.90
CX6B1_MOUSE	Cytochrome c oxidase subunit 6B1	6.48	0.92
NDUA5_MOUSE	NADH dehydrogenase [ubiquinone] 1 alpha subcomplex subunit 5	6.48	0.90
VWA8_MOUSE	von Willebrand factor A domain-containing protein 8	6.46	0.82
ATPA_MOUSE	ATP synthase subunit alpha, mitochondrial	6.46	0.96
DHRS4_MOUSE	Dehydrogenase/reductase SDR family member 4	6.42	0.91
SUSD2_MOUSE	Sushi domain-containing protein 2	6.38	0.92
QCR1_MOUSE	Cytochrome b-c1 complex subunit 1, mitochondrial	6.37	0.94
NDUA7_MOUSE	NADH dehydrogenase [ubiquinone] 1 alpha subcomplex subunit 7	6.36	0.91
SFXN1_MOUSE	Sideroflexin-1	6.35	0.83
QCR7_MOUSE	Cytochrome b-c1 complex subunit 7	6.34	0.89
COX6C_MOUSE	Cytochrome c oxidase subunit 6C	6.33	0.91
ODB2_MOUSE	Lipoamide acyltransferase component of branched-chain alpha-keto acid dehydrogenase complex, mitochondrial	6.31	0.81
ARLY_MOUSE	Argininosuccinate lyase	6.31	0.91
PRDX5_MOUSE	Peroxiredoxin-5, mitochondrial	6.30	0.91
PGES2_MOUSE	Prostaglandin E synthase 2	6.29	0.89
ATP5J_MOUSE	ATP synthase-coupling factor 6, mitochondrial	6.29	0.97
KAT3_MOUSE	Kynurenine--oxoglutarate transaminase 3	6.29	0.81
ACOX2_MOUSE	Peroxisomal acyl-coenzyme A oxidase 2	6.24	0.84
AT5F1_MOUSE	ATP synthase F(0) complex subunit B1, mitochondrial	6.17	0.92
NU3M_MOUSE	NADH-ubiquinone oxidoreductase chain 3	6.15	0.95
CH10_MOUSE	10 kDa heat shock protein, mitochondrial	6.15	0.90
NDUB9_MOUSE	NADH dehydrogenase [ubiquinone] 1 beta subcomplex subunit 9	6.10	0.83
AATM_MOUSE	Aspartate aminotransferase, mitochondrial	6.10	0.97
DHB8_MOUSE	Estradiol 17-beta-dehydrogenase 8	6.07	0.87
NDUA8_MOUSE	NADH dehydrogenase [ubiquinone] 1 alpha subcomplex subunit 8	6.07	0.91
CHDH_MOUSE	Choline dehydrogenase, mitochondrial	6.06	0.88
ODPB_MOUSE	Pyruvate dehydrogenase E1 component subunit beta, mitochondrial	6.05	0.96
VATA_MOUSE	V-type proton ATPase catalytic subunit A	6.04	0.92
MRP2_MOUSE	Canalicular multispecific organic anion transporter 1	6.03	0.82
ETHE1_MOUSE	Persulfide dioxygenase ETHE1, mitochondrial	5.99	0.92
VATH_MOUSE	V-type proton ATPase subunit H	5.94	0.90
NDUC2_MOUSE	NADH dehydrogenase [ubiquinone] 1 subunit C2	5.93	0.88
DCXR_MOUSE	L-xylulose reductase	5.92	0.88
GSTT2_MOUSE	Glutathione S-transferase theta-2	5.84	0.87
ALDH2_MOUSE	Aldehyde dehydrogenase, mitochondrial	5.82	0.95
TRAP1_MOUSE	Heat shock protein 75 kDa, mitochondrial	5.82	0.88
AL9A1_MOUSE	4-trimethylaminobutyraldehyde dehydrogenase	5.76	0.94
ETFD_MOUSE	Electron transfer flavoprotein-ubiquinone oxidoreductase, mitochondrial	5.74	0.89
CPT2_MOUSE	Carnitine O-palmitoyltransferase 2, mitochondrial	5.70	0.88
ANK3_MOUSE	Ankyrin-3	5.70	0.85
ACOT4_MOUSE	Acyl-coenzyme A thioesterase 4	5.68	0.81
MARC2_MOUSE	Mitochondrial amidoxime reducing component 2	5.65	0.89
ACOT1_MOUSE	Acyl-coenzyme A thioesterase 1	5.63	0.85
DOPD_MOUSE	D-dopachrome decarboxylase	5.63	0.91
TIM13_MOUSE	Mitochondrial import inner membrane translocase subunit Tim13	5.58	0.96
ODPA_MOUSE	Pyruvate dehydrogenase E1 component subunit alpha, somatic form, mitochondrial	5.58	0.92
MPCP_MOUSE	Phosphate carrier protein, mitochondrial	5.57	0.90
ABHEB_MOUSE	Protein ABHD14B	5.57	0.93
GRP75_MOUSE	Stress-70 protein, mitochondrial	5.56	0.82
HIBCH_MOUSE	3-hydroxyisobutyryl-CoA hydrolase, mitochondrial	5.55	0.89
NDUBB_MOUSE	NADH dehydrogenase [ubiquinone] 1 beta subcomplex subunit 11, mitochondrial	5.53	0.90
MIC19_MOUSE	MICOS complex subunit Mic19	5.53	0.90
VATB2_MOUSE	V-type proton ATPase subunit B, brain isoform	5.52	0.85

GSH1_MOUSE	Glutamate--cysteine ligase catalytic subunit	5.49	0.86
NCEH1_MOUSE	Neutral cholesterol ester hydrolase 1	5.47	0.92
ECH1_MOUSE	Delta(3,5)-Delta(2,4)-dienoyl-CoA isomerase, mitochondrial	5.46	0.97
VATF_MOUSE	V-type proton ATPase subunit F	5.45	0.90
VATG3_MOUSE	V-type proton ATPase subunit G 3	5.43	0.94
CN159_MOUSE	UPF0317 protein C14orf159 homolog, mitochondrial	5.41	0.83
DECR_MOUSE	2,4-dienoyl-CoA reductase, mitochondrial	5.39	0.89
CMBL_MOUSE	Carboxymethylenebutenolidase homolog	5.38	0.85
ACADS_MOUSE	Short-chain specific acyl-CoA dehydrogenase, mitochondrial	5.36	0.89
SUCB1_MOUSE	Succinyl-CoA ligase [ADP-forming] subunit beta, mitochondrial	5.33	0.97
VATE1_MOUSE	V-type proton ATPase subunit E 1	5.32	0.91
LPPRC_MOUSE	Leucine-rich PPR motif-containing protein, mitochondrial	5.26	0.88
ODP2_MOUSE	Dihydrolipoyllysine-residue acetyltransferase component of pyruvate dehydrogenase complex, mitochondrial	5.25	0.98
PRDX3_MOUSE	Thioredoxin-dependent peroxide reductase, mitochondrial	5.23	0.90
KAD2_MOUSE	Adenylate kinase 2, mitochondrial	5.21	0.86
SQRD_MOUSE	Sulfide:quinone oxidoreductase, mitochondrial	5.20	0.92
GSHB_MOUSE	Glutathione synthetase	5.17	0.82
LYPA1_MOUSE	Acyl-protein thioesterase 1	5.13	0.90
ACADV_MOUSE	Very long-chain specific acyl-CoA dehydrogenase, mitochondrial	5.12	0.89
KAD3_MOUSE	GTP:AMP phosphotransferase AK3, mitochondrial	5.10	0.89
DHPR_MOUSE	Dihydropteridine reductase	5.07	0.88
NIT1_MOUSE	Nitrilase homolog 1	5.03	0.90
ODO1_MOUSE	2-oxoglutarate dehydrogenase, mitochondrial	5.00	0.91
E41L3_MOUSE	Band 4.1-like protein 3	4.96	0.86
SAP3_MOUSE	Ganglioside GM2 activator	4.96	0.85
MDHC_MOUSE	Malate dehydrogenase, cytoplasmic	4.94	0.95
SPS2_MOUSE	Selenide, water dikinase 2	4.93	0.90
THIOM_MOUSE	Thioredoxin, mitochondrial	4.90	0.90
RM12_MOUSE	39S ribosomal protein L12, mitochondrial	4.89	0.91
NIT2_MOUSE	Omega-amidase NIT2	4.88	0.90
IDH3A_MOUSE	Isocitrate dehydrogenase [NAD] subunit alpha, mitochondrial	4.86	0.91
NDUA6_MOUSE	NADH dehydrogenase [ubiquinone] 1 alpha subcomplex subunit 6	4.86	0.84
VDAC1_MOUSE	Voltage-dependent anion-selective channel protein 1	4.85	0.96
HYES_MOUSE	Bifunctional epoxide hydrolase 2	4.85	0.81
ACOC_MOUSE	Cytoplasmic aconitate hydratase	4.84	0.94
PH4H_MOUSE	Cytoplasmic aconitate hydratase	4.83	0.84
ECI1_MOUSE	Enoyl-CoA delta isomerase 1, mitochondrial	4.80	0.91
HCD2_MOUSE	3-hydroxyacyl-CoA dehydrogenase type-2	4.76	0.91
IDHC_MOUSE	Isocitrate dehydrogenase [NADP] cytoplasmic	4.75	0.90
ISCA2_MOUSE	Iron-sulfur cluster assembly 2 homolog, mitochondrial	4.73	0.82
MIC27_MOUSE	MICOS complex subunit Mic27	4.70	0.81
SAM50_MOUSE	Sorting and assembly machinery component 50 homolog	4.69	0.89
LONM_MOUSE	Lon protease homolog, mitochondrial	4.66	0.90
MIC60_MOUSE	MICOS complex subunit Mic60	4.65	0.92
ATIF1_MOUSE	ATPase inhibitor, mitochondrial	4.61	0.83
LYZ2_MOUSE	Lysozyme C-2	4.60	0.93
OAT_MOUSE	Ornithine aminotransferase, mitochondrial	4.59	0.86
DDAH1_MOUSE	N(G),N(G)-dimethylarginine dimethylaminohydrolase 1	4.57	0.83
EFTU_MOUSE	Elongation factor Tu, mitochondrial	4.54	0.95
CMC1_MOUSE	Calcium-binding mitochondrial carrier protein Aralar1	4.51	0.84
ECHA_MOUSE	Trifunctional enzyme subunit alpha, mitochondrial	4.46	0.97
RT35_MOUSE	28S ribosomal protein S35, mitochondrial	4.43	0.81
THTM_MOUSE	3-mercaptopyruvate sulfurtransferase	4.41	0.83
XPP1_MOUSE	Xaa-Pro aminopeptidase 1	4.40	0.87
VATD_MOUSE	V-type proton ATPase subunit D	4.40	0.89
BCAT2_MOUSE	Branched-chain-amino-acid aminotransferase, mitochondrial	4.38	0.89
DHE3_MOUSE	Glutamate dehydrogenase 1, mitochondrial	4.37	0.92
4F2_MOUSE	4F2 cell-surface antigen heavy chain	4.34	0.91
ATAD3_MOUSE	ATPase family AAA domain-containing protein 3	4.30	0.80
TRXR2_MOUSE	Thioredoxin reductase 2, mitochondrial	4.29	0.83
ACADL_MOUSE	Long-chain specific acyl-CoA dehydrogenase, mitochondrial	4.28	0.87
CPT1A_MOUSE	Carnitine O-palmitoyltransferase 1, liver isoform	4.27	0.84
KCRU_MOUSE	Creatine kinase U-type, mitochondrial	4.24	0.88
AMPE_MOUSE	Glutamyl aminopeptidase	4.21	0.87
GLRX5_MOUSE	Glutaredoxin-related protein 5, mitochondrial	4.20	0.93
MAOX_MOUSE	NADP-dependent malic enzyme	4.20	0.83
M2OM_MOUSE	Mitochondrial 2-oxoglutarate/malate carrier protein	4.19	0.83
CLIC5_MOUSE	Chloride intracellular channel protein 5	4.18	0.85
ACDSB_MOUSE	Short/branched chain specific acyl-CoA dehydrogenase, mitochondrial	4.10	0.93
BASI_MOUSE	Basigin	4.09	0.87
SCRN2_MOUSE	Secernin-2	4.05	0.82
TMM65_MOUSE	Transmembrane protein 65	4.03	0.88

TIM10_MOUSE	Mitochondrial import inner membrane translocase subunit Tim10	4.01	0.86
MTCH2_MOUSE	Mitochondrial carrier homolog 2	4.01	0.89
PROSC_MOUSE	Proline synthase co-transcribed bacterial homolog protein	4.01	0.90
LDHB_MOUSE	L-lactate dehydrogenase B chain	3.99	0.86
MOT1_MOUSE	Monocarboxylate transporter 1	3.98	0.91
MAVS_MOUSE	Mitochondrial antiviral-signaling protein	3.95	0.84
T126A_MOUSE	Transmembrane protein 126A	3.93	0.85
GLNA_MOUSE	Glutamine synthetase	3.91	0.83
CYB5_MOUSE	Cytochrome b5	3.87	0.86
AT11A_MOUSE	Probable phospholipid-transporting ATPase IH	3.85	0.81
CISY_MOUSE	Citrate synthase, mitochondrial	3.83	0.88
AMPN_MOUSE	Aminopeptidase N	3.83	0.95
ADT1_MOUSE	ADP/ATP translocase 1	3.82	0.83
EM55_MOUSE	55 kDa erythrocyte membrane protein	3.82	0.91
PTGR2_MOUSE	Prostaglandin reductase 2	3.79	0.89
NPL_MOUSE	N-acetylneuraminate lyase	3.76	0.88
PHB2_MOUSE	Prohibitin-2	3.73	0.94
MIF_MOUSE	Macrophage migration inhibitory factor	3.71	0.92
EBP_MOUSE	3-beta-hydroxysteroid-Delta(8),Delta(7)-isomerase	3.70	0.91
AATC_MOUSE	Aspartate aminotransferase, cytoplasmic	3.68	0.88
DHI2_MOUSE	Corticosteroid 11-beta-dehydrogenase isozyme 2	3.67	0.83
TSPO_MOUSE	Translocator protein	3.66	0.98
NCPR_MOUSE	NADPH--cytochrome P450 reductase	3.64	0.81
CYB5B_MOUSE	Cytochrome b5 type B	3.62	0.93
THIC_MOUSE	Acetyl-CoA acetyltransferase, cytosolic	3.61	0.85
GSTA4_MOUSE	Glutathione S-transferase A4	3.61	0.86
RM04_MOUSE	39S ribosomal protein L4, mitochondrial	3.59	0.91
AMPL_MOUSE	Cytosol aminopeptidase	3.57	0.93
VATC1_MOUSE	V-type proton ATPase subunit C 1	3.55	0.83
GGCT_MOUSE	Gamma-glutamylcyclotransferase	3.55	0.99
C1QBP_MOUSE	Complement component 1 Q subcomponent-binding protein, mitochondrial	3.52	0.83
ACBP_MOUSE	Acyl-CoA-binding protein	3.51	0.93
EFTS_MOUSE	Elongation factor Ts, mitochondrial	3.50	0.85
TXTP_MOUSE	Tricarboxylate transport protein, mitochondrial	3.47	0.87
SPRE_MOUSE	Sepiapterin reductase	3.47	0.96
GPX1_MOUSE	Glutathione peroxidase 1	3.45	0.92
F213A_MOUSE	Redox-regulatory protein FAM213A	3.42	0.89
DHB4_MOUSE	Peroxisomal multifunctional enzyme type 2	3.39	0.95
ECHB_MOUSE	Trifunctional enzyme subunit beta, mitochondrial	3.37	0.87
SODC_MOUSE	Superoxide dismutase [Cu-Zn]	3.33	0.94
NAPSA_MOUSE	Napsin-A	3.32	0.84
ESTD_MOUSE	S-formylglutathione hydrolase	3.28	0.86
APMAP_MOUSE	Adipocyte plasma membrane-associated protein	3.28	0.84
GSTM5_MOUSE	Glutathione S-transferase Mu 5	3.27	0.87
PGK1_MOUSE	Phosphoglycerate kinase 1	3.27	0.97
ISCU_MOUSE	Iron-sulfur cluster assembly enzyme ISCU, mitochondrial	3.25	0.81
VA0D1_MOUSE	V-type proton ATPase subunit d 1	3.24	0.87
GVIN1_MOUSE	Interferon-induced very large GTPase 1	3.22	0.83
PRPS2_MOUSE	Ribose-phosphate pyrophosphokinase 2	3.20	0.85
PGM1_MOUSE	Phosphoglucomutase-1	3.13	0.90
PHB_MOUSE	Prohibitin	3.13	0.92
EZRI_MOUSE	Ezrin	3.13	0.96
EHD1_MOUSE	EH domain-containing protein 1	3.05	0.83
HINT1_MOUSE	Histidine triad nucleotide-binding protein 1	3.04	0.88
SAHH_MOUSE	Adenosylhomocysteinase	2.99	0.91
GNPI1_MOUSE	Glucosamine-6-phosphate isomerase 1	2.96	0.89
CAH2_MOUSE	Carbonic anhydrase 2	2.95	0.95
THIKA_MOUSE	3-ketoacyl-CoA thiolase A, peroxisomal	2.95	0.91
HDHD2_MOUSE	Haloacid dehalogenase-like hydrolase domain-containing protein 2	2.90	0.82
TTC38_MOUSE	Tetratricopeptide repeat protein 38	2.87	0.87
41_MOUSE	Protein 4.1	2.84	0.85
VDAC2_MOUSE	Voltage-dependent anion-selective channel protein 2	2.84	0.94
HEM2_MOUSE	Delta-aminolevulinic acid dehydratase	2.82	0.91
RADI_MOUSE	Radixin	2.79	0.83
CCS_MOUSE	Copper chaperone for superoxide dismutase	2.75	0.99
AKCL2_MOUSE	1,5-anhydro-D-fructose reductase	2.73	0.93
GPD1L_MOUSE	Glycerol-3-phosphate dehydrogenase 1-like protein	2.72	0.87
TPIS_MOUSE	Triosephosphate isomerase	2.71	0.95
UGPA_MOUSE	UTP--glucose-1-phosphate uridylyltransferase	2.66	0.87
HXK1_MOUSE	Hexokinase-1	2.66	0.91
FIS1_MOUSE	Mitochondrial fission 1 protein	2.65	0.89
GLGB_MOUSE	1,4-alpha-glucan-branching enzyme	2.59	0.98

GTR1_MOUSE	Solute carrier family 2, facilitated glucose transporter member 1	2.58	0.80
NAMPT_MOUSE	Nicotinamide phosphoribosyltransferase	2.57	0.82
FUCM_MOUSE	Fucose mutarotase	2.52	0.88
ENOA_MOUSE	Alpha-enolase	2.51	0.98
SYPL1_MOUSE	Synaptophysin-like protein 1	2.50	0.91
S10A1_MOUSE	Protein S100-A1	2.44	0.85
PDXK_MOUSE	Pyridoxal kinase	2.42	0.85
PARK7_MOUSE	Protein deglycase DJ-1	2.42	0.93
PGAM1_MOUSE	Phosphoglycerate mutase 1	2.41	0.97
GMPR1_MOUSE	GMP reductase 1	2.41	0.81
GSTM1_MOUSE	Glutathione S-transferase Mu 1	2.37	0.89
EHD3_MOUSE	EH domain-containing protein 3	2.37	0.86
GSHR_MOUSE	Glutathione reductase, mitochondrial	2.33	0.80
G3P_MOUSE	Glyceraldehyde-3-phosphate dehydrogenase	2.29	0.92
TMM33_MOUSE	Transmembrane protein 33	2.28	0.86
TIM44_MOUSE	Mitochondrial import inner membrane translocase subunit TIM44	2.25	0.83
ARL1_MOUSE	ADP-ribosylation factor-like protein 1	2.24	0.90
PRDX6_MOUSE	Peroxiredoxin-6	2.23	0.94
NDKB_MOUSE	Nucleoside diphosphate kinase B	2.11	0.95
ADK_MOUSE	Adenosine kinase	2.03	0.87
PRDX1_MOUSE	Peroxiredoxin-1	2.03	0.91
G6PI_MOUSE	Glucose-6-phosphate isomerase	2.03	0.93
RS24_MOUSE	40S ribosomal protein S24	1.99	0.88
NDKA_MOUSE	Nucleoside diphosphate kinase A	1.98	0.88
AP1B1_MOUSE	AP-1 complex subunit beta-1	1.97	0.82
PACN2_MOUSE	Protein kinase C and casein kinase substrate in neurons protein 2	1.96	0.85
MAT2B_MOUSE	Methionine adenosyltransferase 2 subunit beta	1.94	0.89
PEBP1_MOUSE	Phosphatidylethanolamine-binding protein 1	1.92	0.92
SPTN1_MOUSE	Spectrin alpha chain, non-erythrocytic 1	1.85	0.88
TMED4_MOUSE	Transmembrane emp24 domain-containing protein 4	1.84	0.90
SPTB2_MOUSE	Spectrin beta chain, non-erythrocytic 1	1.80	0.87
UGDH_MOUSE	UDP-glucose 6-dehydrogenase	1.79	0.82
GSTP1_MOUSE	Glutathione S-transferase P 1	1.77	0.94
UAP1L_MOUSE	UDP-N-acetylhexosamine pyrophosphorylase-like protein 1	1.76	0.84
SNX3_MOUSE	Sorting nexin-3	1.72	0.84
TBB4B_MOUSE	Tubulin beta-4B chain	1.71	0.90
GALK1_MOUSE	Galactokinase	1.64	0.85
ALDOA_MOUSE	Fructose-bisphosphate aldolase A	1.57	0.84
GPX3_MOUSE	Glutathione peroxidase 3	1.54	0.83
HS90A_MOUSE	Heat shock protein HSP 90-alpha	1.50	0.81
CLH1_MOUSE	Clathrin heavy chain 1	1.47	0.88

S.1.4 List of GO Biological Process terms significantly enriched in UUO-overexpressed proteins

Supplementary Table 3.7: GO Biological Process overrepresentation test on UUO-overexpressed proteins, performed by DAVID. Statistical overrepresentation test was performed by DAVID (http://david.abcc.ncifcrf.gov) using the annotation term ontologies for Biological Process (GOTERM_BP_FAT). The number of proteins belonging to the annotation term and fold change from the expected value H_0 are in increasing shades of red (the higher the more intense). The p-value is shown in increasing shades of blue (the more intense, the lower the p-value). A p-value lower than 0.05 was regarded as significant.

GO Biological Process in UUO overexpressed	Count	%	p-value	Fold Enrichment
GO:0030029~actin filament-based process	21	11.1	6.51E-15	10.6
GO:0030036~actin cytoskeleton organization	20	10.6	2.54E-14	10.8
GO:0007010~cytoskeleton organization	23	12.2	1.22E-11	6.3
GO:0008064~regulation of actin polymerization or depolymerization	11	5.8	1.59E-10	19.5
GO:0030832~regulation of actin filament length	11	5.8	1.97E-10	19.2
GO:0032956~regulation of actin cytoskeleton organization	11	5.8	1.06E-09	16.3
GO:0032970~regulation of actin filament-based process	11	5.8	1.26E-09	16.0
GO:0051493~regulation of cytoskeleton organization	12	6.3	1.29E-08	10.8
GO:0030833~regulation of actin filament polymerization	9	4.8	3.09E-08	17.8
GO:0008380~RNA splicing	15	7.9	5.54E-08	6.6
GO:0030198~extracellular matrix organization	11	5.8	1.83E-07	9.7
GO:0032271~regulation of protein polymerization	9	4.8	2.12E-07	14.0
GO:0043254~regulation of protein complex assembly	9	4.8	6.00E-07	12.3
GO:0044087~regulation of cellular component biogenesis	10	5.3	6.42E-07	10.0
GO:0043062~extracellular structure organization	12	6.3	8.77E-07	7.2
GO:0033043~regulation of organelle organization	12	6.3	1.22E-06	6.9
GO:0006397~mRNA processing	15	7.9	1.41E-06	5.1
GO:0009611~response to wounding	17	9.0	1.70E-06	4.4
GO:0032535~regulation of cellular component size	12	6.3	1.89E-06	6.6
GO:0002526~acute inflammatory response	9	4.8	3.29E-06	9.9
GO:0043933~macromolecular complex subunit organization	17	9.0	3.51E-06	4.1
GO:0065003~macromolecular complex assembly	16	8.5	5.82E-06	4.2
GO:0016071~mRNA metabolic process	15	7.9	7.37E-06	4.4
GO:0006461~protein complex assembly	13	6.9	9.18E-06	5.1
GO:0070271~protein complex biogenesis	13	6.9	9.18E-06	5.1
GO:0034621~cellular macromolecular complex subunit organization	13	6.9	1.97E-05	4.7
GO:0043623~cellular protein complex assembly	9	4.8	2.79E-05	7.4
GO:0051235~maintenance of location	6	3.2	3.02E-05	16.1
GO:0034622~cellular macromolecular complex assembly	12	6.3	3.23E-05	4.9
GO:0007015~actin filament organization	7	3.7	3.63E-05	11.1
GO:0051258~protein polymerization	6	3.2	7.87E-05	13.3
GO:0006396~RNA processing	16	8.5	1.14E-04	3.3
GO:0050729~positive regulation of inflammatory response	5	2.6	1.34E-04	18.5
GO:0032101~regulation of response to external stimulus	8	4.2	1.54E-04	6.9
GO:0007517~muscle organ development	10	5.3	1.61E-04	5.0
GO:0007155~cell adhesion	18	9.5	1.79E-04	2.8
GO:0022610~biological adhesion	18	9.5	1.83E-04	2.8
GO:0051494~negative regulation of cytoskeleton organization	6	3.2	1.91E-04	11.1
GO:0048584~positive regulation of response to stimulus	10	5.3	2.43E-04	4.8
GO:0042060~wound healing	8	4.2	2.59E-04	6.3
GO:0006953~acute-phase response	5	2.6	3.29E-04	14.8
GO:0030865~cortical cytoskeleton organization	4	2.1	3.62E-04	27.3
GO:0050727~regulation of inflammatory response	6	3.2	4.30E-04	9.3
GO:0002891~positive regulation of immunoglobulin mediated immune response	4	2.1	4.56E-04	25.4
GO:0002714~positive regulation of B cell mediated immunity	4	2.1	4.56E-04	25.4
GO:0002824~positive regulation of adaptive immune response based on somatic recombination of immune receptors built from immunoglobulin superfamily domains	5	2.6	5.38E-04	13.1
GO:0002821~positive regulation of adaptive immune response	5	2.6	5.38E-04	13.1
GO:0010639~negative regulation of organelle organization	6	3.2	6.35E-04	8.6
GO:0030155~regulation of cell adhesion	7	3.7	6.43E-04	6.6
GO:0032103~positive regulation of response to external stimulus	5	2.6	9.13E-04	11.4
GO:0006954~inflammatory response	10	5.3	9.66E-04	3.9
GO:0002708~positive regulation of lymphocyte mediated immunity	5	2.6	1.01E-03	11.1
GO:0002705~positive regulation of leukocyte mediated immunity	5	2.6	1.01E-03	11.1
GO:0007596~blood coagulation	6	3.2	1.11E-03	7.6

GO:0050817~coagulation	6	3.2	1.11E-03	7.6
GO:0007599~hemostasis	6	3.2	1.18E-03	7.5
GO:0043244~regulation of protein complex disassembly	5	2.6	1.32E-03	10.3
GO:0002699~positive regulation of immune effector process	5	2.6	1.70E-03	9.7
GO:0050766~positive regulation of phagocytosis	4	2.1	2.06E-03	15.4
GO:0030834~regulation of actin filament depolymerization	4	2.1	2.34E-03	14.8
GO:0031032~actomyosin structure organization	4	2.1	2.63E-03	14.2
GO:0030837~negative regulation of actin filament polymerization	4	2.1	2.63E-03	14.2
GO:0051651~maintenance of location in cell	4	2.1	2.63E-03	14.2
GO:0050764~regulation of phagocytosis	4	2.1	2.63E-03	14.2
GO:0050878~regulation of body fluid levels	6	3.2	3.20E-03	6.0
GO:0031333~negative regulation of protein complex assembly	4	2.1	3.30E-03	13.2
GO:0000910~cytokinesis	4	2.1	3.30E-03	13.2
GO:0032272~negative regulation of protein polymerization	4	2.1	3.30E-03	13.2
GO:0002892~regulation of type II hypersensitivity	3	1.6	3.33E-03	33.3
GO:0001798~positive regulation of type IIa hypersensitivity	3	1.6	3.33E-03	33.3
GO:0002888~positive regulation of myeloid leukocyte mediated immunity	3	1.6	3.33E-03	33.3
GO:0001796~regulation of type IIa hypersensitivity	3	1.6	3.33E-03	33.3
GO:0002894~positive regulation of type II hypersensitivity	3	1.6	3.33E-03	33.3
GO:0002822~regulation of adaptive immune response based on somatic recombination of immune receptors built from immunoglobulin superfamily domains	5	2.6	3.52E-03	7.9
GO:0002819~regulation of adaptive immune response	5	2.6	3.52E-03	7.9
GO:0045185~maintenance of protein location	4	2.1	3.66E-03	12.7
GO:0019884~antigen processing and presentation of exogenous antigen	4	2.1	3.66E-03	12.7
GO:0030334~regulation of cell migration	6	3.2	3.69E-03	5.8
GO:0031349~positive regulation of defense response	5	2.6	3.75E-03	7.8
GO:0051129~negative regulation of cellular component organization	6	3.2	3.87E-03	5.7
GO:0050778~positive regulation of immune response	7	3.7	4.24E-03	4.6
GO:0010033~response to organic substance	14	7.4	4.39E-03	2.5
GO:0051604~protein maturation	6	3.2	4.43E-03	5.6
GO:0002712~regulation of B cell mediated immunity	4	2.1	4.47E-03	11.8
GO:0002889~regulation of immunoglobulin mediated immune response	4	2.1	4.47E-03	11.8
GO:0006958~complement activation, classical pathway	4	2.1	4.47E-03	11.8
GO:0006952~defense response	13	6.9	4.50E-03	2.6
GO:0002866~positive regulation of acute inflammatory response to antigenic stimulus	3	1.6	5.27E-03	26.6
GO:0002885~positive regulation of hypersensitivity	3	1.6	5.27E-03	26.6
GO:0034097~response to cytokine stimulus	4	2.1	5.37E-03	11.1
GO:0016064~immunoglobulin mediated immune response	5	2.6	5.38E-03	7.0
GO:0051605~protein maturation by peptide bond cleavage	5	2.6	6.01E-03	6.8
GO:0002706~regulation of lymphocyte mediated immunity	5	2.6	6.01E-03	6.8
GO:0019724~B cell mediated immunity	5	2.6	6.01E-03	6.8
GO:0045807~positive regulation of endocytosis	4	2.1	6.37E-03	10.4
GO:0002675~positive regulation of acute inflammatory response	3	1.6	6.40E-03	24.2
GO:0043242~negative regulation of protein complex disassembly	4	2.1	6.91E-03	10.1
GO:0002455~humoral immune response mediated by circulating immunoglobulin	4	2.1	6.91E-03	10.1
GO:0051270~regulation of cell motion	6	3.2	6.99E-03	5.0
GO:0044057~regulation of system process	8	4.2	7.45E-03	3.5
GO:0006956~complement activation	4	2.1	7.48E-03	9.9
GO:0002541~activation of plasma proteins involved in acute inflammatory response	4	2.1	7.48E-03	9.9
GO:0002703~regulation of leukocyte mediated immunity	5	2.6	7.79E-03	6.3
GO:0040012~regulation of locomotion	6	3.2	7.84E-03	4.8
GO:0002684~positive regulation of immune system process	8	4.2	8.47E-03	3.4
GO:0002864~regulation of acute inflammatory response to antigenic stimulus	3	1.6	8.94E-03	20.5
GO:0002863~positive regulation of inflammatory response to antigenic stimulus	3	1.6	8.94E-03	20.5
GO:0002883~regulation of hypersensitivity	3	1.6	8.94E-03	20.5
GO:0030030~cell projection organization	10	5.3	9.71E-03	2.8
GO:0010810~regulation of cell-substrate adhesion	4	2.1	1.00E-02	8.9
GO:0042692~muscle cell differentiation	6	3.2	1.01E-02	4.6
GO:0007044~cell-substrate junction assembly	3	1.6	1.04E-02	19.0
GO:0002449~lymphocyte mediated immunity	5	2.6	1.04E-02	5.8
GO:0032386~regulation of intracellular transport	4	2.1	1.15E-02	8.5
GO:0002886~regulation of myeloid leukocyte mediated immunity	3	1.6	1.19E-02	17.8
GO:0030048~actin filament-based movement	3	1.6	1.19E-02	17.8
GO:0051017~actin filament bundle formation	3	1.6	1.19E-02	17.8
GO:0051130~positive regulation of cellular component organization	6	3.2	1.19E-02	4.4
GO:0045785~positive regulation of cell adhesion	4	2.1	1.22E-02	8.3
GO:0014706~striated muscle tissue development	6	3.2	1.40E-02	4.2

GO:0002250~adaptive immune response	5	2.6	1.46E-02	5.3
GO:0002460~adaptive immune response based on somatic recombination of immune receptors built from immunoglobulin superfamily domains	5	2.6	1.46E-02	5.3
GO:0008360~regulation of cell shape	4	2.1	1.55E-02	7.6
GO:0051050~positive regulation of transport	6	3.2	1.63E-02	4.0
GO:0019882~antigen processing and presentation	5	2.6	1.64E-02	5.1
GO:0002861~regulation of inflammatory response to antigenic stimulus	3	1.6	1.69E-02	14.8
GO:0002673~regulation of acute inflammatory response	3	1.6	1.69E-02	14.8
GO:0002697~regulation of immune effector process	5	2.6	1.70E-02	5.0
GO:0032989~cellular component morphogenesis	10	5.3	1.72E-02	2.5
GO:0009719~response to endogenous stimulus	7	3.7	1.74E-02	3.4
GO:0002443~leukocyte mediated immunity	5	2.6	1.76E-02	5.0
GO:0016485~protein processing	5	2.6	1.83E-02	4.9
GO:0032880~regulation of protein localization	5	2.6	1.83E-02	4.9
GO:0060537~muscle tissue development	6	3.2	1.83E-02	3.9
GO:0016477~cell migration	8	4.2	1.83E-02	3.0
GO:0030100~regulation of endocytosis	4	2.1	2.03E-02	6.8
GO:0050818~regulation of coagulation	3	1.6	2.07E-02	13.3
GO:0043434~response to peptide hormone stimulus	5	2.6	2.19E-02	4.7
GO:0032796~uropod organization	2	1.1	2.22E-02	88.8
GO:0006959~humoral immune response	4	2.1	2.25E-02	6.6
GO:0034329~cell junction assembly	3	1.6	2.27E-02	12.7
GO:0030199~collagen fibril organization	3	1.6	2.27E-02	12.7
GO:0030835~negative regulation of actin filament depolymerization	3	1.6	2.27E-02	12.7
GO:0000902~cell morphogenesis	9	4.8	2.29E-02	2.6
GO:0048738~cardiac muscle tissue development	4	2.1	2.59E-02	6.2
GO:0006936~muscle contraction	4	2.1	2.95E-02	5.9
GO:0010811~positive regulation of cell-substrate adhesion	3	1.6	3.63E-02	9.9
GO:0009725~response to hormone stimulus	6	3.2	3.79E-02	3.2
GO:0019725~cellular homeostasis	9	4.8	3.90E-02	2.3
GO:0003012~muscle system process	4	2.1	3.91E-02	5.3
GO:0031667~response to nutrient levels	5	2.6	4.01E-02	3.9
GO:0048870~cell motility	8	4.2	4.05E-02	2.5
GO:0051674~localization of cell	8	4.2	4.05E-02	2.5
GO:0030031~cell projection assembly	4	2.1	4.36E-02	5.1
GO:0030300~regulation of intestinal cholesterol absorption	2	1.1	4.40E-02	44.4
GO:0033209~tumor necrosis factor-mediated signaling pathway	2	1.1	4.40E-02	44.4
GO:0033157~regulation of intracellular protein transport	3	1.6	4.41E-02	8.9
GO:0034330~cell junction organization	3	1.6	4.95E-02	8.3

S.1.5 List of GO Biological Process terms significantly enriched in UUO-underexpressed proteins

Supplementary Table 3.8: GO Biological Process overrepresentation test on UUO-underexpressed proteins, performed by DAVID. Statistical overrepresentation test was performed by DAVID (http://david.abcc.ncifcrf.gov) using the annotation term ontologies for Biological Process (GOTERM_BP_FAT). The number of proteins belonging to the annotation term and fold change from the expected value H_0 are in increasing shades of green (the higher the more intense). The p-value is shown in increasing shades of blue (the more intense, the lower the p-value). A p-value lower than 0.05 was regarded as significant.

GO Biological Process in UUO underexpressed	Count	%	p-value	Fold Enrichment
GO:0006091~generation of precursor metabolites and energy	105	24.14	1.50E-101	16.2
GO:0055114~oxidation reduction	140	32.18	2.90E-94	8.4
GO:0022900~electron transport chain	54	12.41	1.13E-55	19.4
GO:0045333~cellular respiration	33	7.59	2.49E-36	22.5
GO:0015980~energy derivation by oxidation of organic compounds	36	8.28	1.19E-31	14.8
GO:0006119~oxidative phosphorylation	29	6.67	1.44E-30	20.8
GO:0051186~cofactor metabolic process	44	10.11	3.16E-30	9.7
GO:0006732~coenzyme metabolic process	40	9.20	4.68E-30	11.2
GO:0044271~nitrogen compound biosynthetic process	49	11.26	1.87E-25	6.5
GO:0006631~fatty acid metabolic process	38	8.74	1.82E-23	8.3
GO:0006818~hydrogen transport	23	5.29	5.37E-22	17.4
GO:0009144~purine nucleoside triphosphate metabolic process	29	6.67	1.97E-21	11.0
GO:0009205~purine ribonucleoside triphosphate metabolic process	28	6.44	7.41E-21	11.1
GO:0015992~proton transport	22	5.06	9.55E-21	17.0
GO:0009199~ribonucleoside triphosphate metabolic process	28	6.44	9.85E-21	11.0
GO:0009145~purine nucleoside triphosphate biosynthetic process	27	6.21	1.54E-20	11.5
GO:0009142~nucleoside triphosphate biosynthetic process	27	6.21	2.07E-20	11.4
GO:0009141~nucleoside triphosphate metabolic process	29	6.67	2.19E-20	10.1
GO:0034220~ion transmembrane transport	20	4.60	4.89E-20	19.1
GO:0046034~ATP metabolic process	26	5.98	7.61E-20	11.6
GO:0015986~ATP synthesis coupled proton transport	19	4.37	9.03E-20	20.6
GO:0015985~energy coupled proton transport, down electrochemical gradient	19	4.37	9.03E-20	20.6
GO:0009201~ribonucleoside triphosphate biosynthetic process	26	5.98	1.84E-19	11.2
GO:0009206~purine ribonucleoside triphosphate biosynthetic process	26	5.98	1.84E-19	11.2
GO:0009259~ribonucleotide metabolic process	29	6.67	2.45E-19	9.3
GO:0022904~respiratory electron transport chain	17	3.91	3.29E-19	24.4
GO:0044275~cellular carbohydrate catabolic process	22	5.06	3.29E-19	14.7
GO:0009150~purine ribonucleotide metabolic process	28	6.44	7.67E-19	9.5
GO:0016052~carbohydrate catabolic process	24	5.52	1.37E-18	11.9
GO:0009260~ribonucleotide biosynthetic process	27	6.21	1.47E-18	9.8
GO:0006754~ATP biosynthetic process	24	5.52	1.86E-18	11.8
GO:0009152~purine ribonucleotide biosynthetic process	26	5.98	7.33E-18	9.8
GO:0009060~aerobic respiration	16	3.68	7.91E-18	23.8
GO:0016054~organic acid catabolic process	23	5.29	2.23E-17	11.4
GO:0046395~carboxylic acid catabolic process	23	5.29	2.23E-17	11.4
GO:0006163~purine nucleotide metabolic process	30	6.90	2.51E-17	7.5
GO:0009165~nucleotide biosynthetic process	31	7.13	2.95E-17	7.2
GO:0006164~purine nucleotide biosynthetic process	28	6.44	3.55E-17	8.2
GO:0046164~alcohol catabolic process	21	4.83	4.32E-17	13.0
GO:0006006~glucose metabolic process	28	6.44	6.33E-17	8.0
GO:0034654~nucleobase, nucleoside, nucleotide and nucleic acid biosynthetic process	31	7.13	6.66E-17	7.0
GO:0034404~nucleobase, nucleoside and nucleotide biosynthetic process	31	7.13	6.66E-17	7.0
GO:0019318~hexose metabolic process	30	6.90	1.16E-16	7.1
GO:0006084~acetyl-CoA metabolic process	16	3.68	1.24E-16	20.7
GO:0046365~monosaccharide catabolic process	19	4.37	3.30E-16	14.1
GO:0005996~monosaccharide metabolic process	31	7.13	5.30E-16	6.5
GO:0006099~tricarboxylic acid cycle	14	3.22	9.60E-16	24.5
GO:0046356~acetyl-CoA catabolic process	14	3.22	2.05E-15	23.5
GO:0006096~glycolysis	17	3.91	3.18E-15	15.5
GO:0006007~glucose catabolic process	18	4.14	3.35E-15	13.9
GO:0019320~hexose catabolic process	18	4.14	3.35E-15	13.9
GO:0009109~coenzyme catabolic process	14	3.22	5.07E-14	19.4
GO:0051187~cofactor catabolic process	14	3.22	2.43E-13	17.6
GO:0055085~transmembrane transport	42	9.66	9.51E-13	3.7

GO:0042773~ATP synthesis coupled electron transport	11	2.53	2.83E-12	24.6
GO:0006749~glutathione metabolic process	12	2.76	3.48E-12	20.1
GO:0006575~cellular amino acid derivative metabolic process	23	5.29	5.02E-12	6.6
GO:0006518~peptide metabolic process	13	2.99	6.76E-11	13.8
GO:0006790~sulfur metabolic process	18	4.14	1.27E-10	7.7
GO:0046394~carboxylic acid biosynthetic process	21	4.83	2.79E-10	6.0
GO:0016053~organic acid biosynthetic process	21	4.83	2.79E-10	6.0
GO:0043648~dicarboxylic acid metabolic process	10	2.30	4.22E-10	20.1
GO:0008652~cellular amino acid biosynthetic process	13	2.99	4.61E-10	11.9
GO:0009063~cellular amino acid catabolic process	14	3.22	4.73E-10	10.4
GO:0015672~monovalent inorganic cation transport	29	6.67	2.08E-09	3.8
GO:0009310~amine catabolic process	14	3.22	5.48E-09	8.7
GO:0010035~response to inorganic substance	16	3.68	7.05E-09	7.0
GO:0006800~oxygen and reactive oxygen species metabolic process	12	2.76	1.46E-08	10.3
GO:0042775~mitochondrial ATP synthesis coupled electron transport	8	1.84	1.60E-08	23.0
GO:0009309~amine biosynthetic process	14	3.22	2.41E-08	7.7
GO:0006979~response to oxidative stress	15	3.45	2.68E-08	6.9
GO:0000302~response to reactive oxygen species	10	2.30	1.66E-07	11.2
GO:0045454~cell redox homeostasis	12	2.76	3.05E-07	7.8
GO:0042743~hydrogen peroxide metabolic process	8	1.84	3.18E-07	16.1
GO:0051188~cofactor biosynthetic process	14	3.22	3.58E-07	6.2
GO:0006811~ion transport	42	9.66	4.08E-07	2.4
GO:0009064~glutamine family amino acid metabolic process	10	2.30	8.55E-07	9.3
GO:0009062~fatty acid catabolic process	8	1.84	9.44E-07	14.0
GO:0034637~cellular carbohydrate biosynthetic process	11	2.53	9.96E-07	7.9
GO:0042542~response to hydrogen peroxide	8	1.84	1.31E-06	13.4
GO:0006635~fatty acid beta-oxidation	7	1.61	1.45E-06	17.6
GO:0006090~pyruvate metabolic process	8	1.84	1.77E-06	12.9
GO:0019319~hexose biosynthetic process	8	1.84	1.77E-06	12.9
GO:0046165~alcohol biosynthetic process	9	2.07	2.71E-06	9.8
GO:0034614~cellular response to reactive oxygen species	7	1.61	3.21E-06	15.6
GO:0009108~coenzyme biosynthetic process	11	2.53	3.55E-06	6.9
GO:0006812~cation transport	32	7.36	4.74E-06	2.5
GO:0006536~glutamate metabolic process	6	1.38	6.25E-06	20.1
GO:0006094~gluconeogenesis	7	1.61	6.43E-06	14.1
GO:0006766~vitamin metabolic process	11	2.53	7.15E-06	6.4
GO:0046364~monosaccharide biosynthetic process	8	1.84	8.54E-06	10.4
GO:0034599~cellular response to oxidative stress	7	1.61	1.19E-05	12.8
GO:0019395~fatty acid oxidation	7	1.61	2.05E-05	11.7
GO:0034440~lipid oxidation	7	1.61	2.05E-05	11.7
GO:0009081~branched chain family amino acid metabolic process	6	1.38	2.23E-05	16.1
GO:0006558~L-phenylalanine metabolic process	5	1.15	2.40E-05	25.1
GO:0019400~alditol metabolic process	7	1.61	2.65E-05	11.3
GO:0016051~carbohydrate biosynthetic process	11	2.53	3.76E-05	5.3
GO:0006081~cellular aldehyde metabolic process	6	1.38	4.41E-05	14.2
GO:0044242~cellular lipid catabolic process	9	2.07	6.63E-05	6.5
GO:0006120~mitochondrial electron transport, NADH to ubiquinone	4	0.92	1.46E-04	32.2
GO:0070301~cellular response to hydrogen peroxide	5	1.15	1.57E-04	16.8
GO:0042744~hydrogen peroxide catabolic process	5	1.15	1.57E-04	16.8
GO:0006767~water-soluble vitamin metabolic process	7	1.61	1.66E-04	8.3
GO:0000096~sulfur amino acid metabolic process	6	1.38	2.12E-04	10.5
GO:0006559~L-phenylalanine catabolic process	4	0.92	2.86E-04	26.8
GO:0006733~oxidoreduction coenzyme metabolic process	7	1.61	3.14E-04	7.4
GO:0043603~cellular amide metabolic process	7	1.61	3.64E-04	7.2
GO:0009119~ribonucleoside metabolic process	7	1.61	3.64E-04	7.2
GO:0006820~anion transport	12	2.76	3.89E-04	3.7
GO:0019439~aromatic compound catabolic process	5	1.15	4.09E-04	13.4
GO:0009084~glutamine family amino acid biosynthetic process	5	1.15	4.09E-04	13.4
GO:0006796~phosphate metabolic process	39	8.97	4.33E-04	1.8
GO:0006793~phosphorus metabolic process	39	8.97	4.33E-04	1.8
GO:0009116~nucleoside metabolic process	8	1.84	4.43E-04	5.7
GO:0016310~phosphorylation	34	7.82	4.72E-04	1.9
GO:0006107~oxaloacetate metabolic process	4	0.92	4.91E-04	23.0
GO:0019362~pyridine nucleotide metabolic process	6	1.38	5.60E-04	8.6
GO:0019751~polyol metabolic process	7	1.61	6.26E-04	6.5
GO:0030258~lipid modification	7	1.61	1.01E-03	6.0
GO:0006637~acyl-CoA metabolic process	5	1.15	1.31E-03	10.1
GO:0019748~secondary metabolic process	8	1.84	1.57E-03	4.7
GO:0009072~aromatic amino acid family metabolic process	5	1.15	1.59E-03	9.6
GO:0006570~tyrosine metabolic process	4	0.92	1.59E-03	16.1
GO:0009065~glutamine family amino acid catabolic process	4	0.92	1.59E-03	16.1
GO:0006106~fumarate metabolic process	3	0.69	1.81E-03	40.2
GO:0000305~response to oxygen radical	4	0.92	2.15E-03	14.6

GO:0009074~aromatic amino acid family catabolic process	4	0.92	2.15E-03	14.6
GO:0006071~glycerol metabolic process	5	1.15	2.27E-03	8.7
GO:0046496~nicotinamide nucleotide metabolic process	5	1.15	2.67E-03	8.4
GO:0009820~alkaloid metabolic process	5	1.15	2.67E-03	8.4
GO:0006769~nicotinamide metabolic process	5	1.15	2.67E-03	8.4
GO:0044272~sulfur compound biosynthetic process	6	1.38	3.28E-03	5.9
GO:0006839~mitochondrial transport	6	1.38	3.65E-03	5.7
GO:0019725~cellular homeostasis	18	4.14	5.38E-03	2.1
GO:0009110~vitamin biosynthetic process	5	1.15	5.41E-03	6.9
GO:0006572~tyrosine catabolic process	3	0.69	5.84E-03	24.1
GO:0016042~lipid catabolic process	10	2.30	6.18E-03	3.0
GO:0042398~cellular amino acid derivative biosynthetic process	6	1.38	6.51E-03	5.0
GO:0009067~aspartate family amino acid biosynthetic process	4	0.92	6.66E-03	10.1
GO:0018130~heterocycle biosynthetic process	6	1.38	8.41E-03	4.7
GO:0006122~mitochondrial electron transport, ubiquinol to cytochrome c	3	0.69	8.61E-03	20.1
GO:0006108~malate metabolic process	3	0.69	8.61E-03	20.1
GO:0006801~superoxide metabolic process	4	0.92	1.09E-02	8.5
GO:0006534~cysteine metabolic process	3	0.69	1.19E-02	17.2
GO:0006577~betaine metabolic process	3	0.69	1.19E-02	17.2
GO:0019430~removal of superoxide radicals	3	0.69	1.19E-02	17.2
GO:0006633~fatty acid biosynthetic process	7	1.61	1.52E-02	3.5
GO:0015711~organic anion transport	5	1.15	1.54E-02	5.2
GO:0009083~branched chain family amino acid catabolic process	3	0.69	1.56E-02	15.1
GO:0046146~tetrahydrobiopterin metabolic process	3	0.69	1.56E-02	15.1
GO:0006750~glutathione biosynthetic process	3	0.69	1.56E-02	15.1
GO:0051881~regulation of mitochondrial membrane potential	3	0.69	1.56E-02	15.1
GO:0009069~serine family amino acid metabolic process	4	0.92	1.64E-02	7.3
GO:0042364~water-soluble vitamin biosynthetic process	4	0.92	1.64E-02	7.3
GO:0009066~aspartate family amino acid metabolic process	4	0.92	1.64E-02	7.3
GO:0042592~homeostatic process	24	5.52	1.93E-02	1.7
GO:0006525~arginine metabolic process	3	0.69	1.97E-02	13.4
GO:0006072~glycerol-3-phosphate metabolic process	3	0.69	1.97E-02	13.4
GO:0008015~blood circulation	8	1.84	2.05E-02	2.9
GO:0003013~circulatory system process	8	1.84	2.05E-02	2.9
GO:0046128~purine ribonucleoside metabolic process	4	0.92	2.08E-02	6.7
GO:0042278~purine nucleoside metabolic process	4	0.92	2.08E-02	6.7
GO:0008217~regulation of blood pressure	6	1.38	2.24E-02	3.7
GO:0043043~peptide biosynthetic process	3	0.69	2.42E-02	12.1
GO:0000303~response to superoxide	3	0.69	2.42E-02	12.1
GO:0007005~mitochondrion organization	7	1.61	3.35E-02	2.9
GO:0015800~acidic amino acid transport	3	0.69	3.43E-02	10.1
GO:0015813~L-glutamate transport	3	0.69	3.43E-02	10.1
GO:0046942~carboxylic acid transport	7	1.61	3.65E-02	2.8
GO:0015849~organic acid transport	7	1.61	3.81E-02	2.8
GO:0051289~protein homotetramerization	3	0.69	3.99E-02	9.3
GO:0010038~response to metal ion	5	1.15	4.21E-02	3.8
GO:0000097~sulfur amino acid biosynthetic process	3	0.69	4.58E-02	8.6
GO:0006739~NADP metabolic process	3	0.69	4.58E-02	8.6
GO:0019563~glycerol catabolic process	2	0.46	4.90E-02	40.2
GO:0019551~glutamate catabolic process to 2-oxoglutarate	2	0.46	4.90E-02	40.2
GO:0006532~aspartate biosynthetic process	2	0.46	4.90E-02	40.2
GO:0006097~glyoxylate cycle	2	0.46	4.90E-02	40.2
GO:0043490~malate-aspartate shuttle	2	0.46	4.90E-02	40.2
GO:0006551~leucine metabolic process	2	0.46	4.90E-02	40.2
GO:0046168~glycerol-3-phosphate catabolic process	2	0.46	4.90E-02	40.2
GO:0019550~glutamate catabolic process to aspartate	2	0.46	4.90E-02	40.2
GO:0019405~alditol catabolic process	2	0.46	4.90E-02	40.2
GO:0006059~hexitol metabolic process	2	0.46	4.90E-02	40.2
GO:0015810~aspartate transport	2	0.46	4.90E-02	40.2

S.1.6 List of GO Molecular Function terms significantly enriched in UUO-overexpressed proteins

Supplementary Table 3.9: GO Molecular Function overrepresentation test on UUO-overexpressed proteins, performed by DAVID. Statistical overrepresentation test was performed by DAVID (http://david.abcc.ncifcrf.gov) using the annotation term ontologies for Molecular Function (GOTERM_MF_FAT). The number of proteins belonging to the annotation term and fold change from the expected value H_0 are in increasing shades of red (the higher the more intense). The p-value is shown in increasing shades of blue (the more intense, the lower the p-value). A p-value lower than 0.05 was regarded as significant

GO Molecular Function in UUO overexpressed	Count	%	PValue	Fold Enrichment
GO:0003779~actin binding	32	16.9	1.19E-20	8.9
GO:0008092~cytoskeletal protein binding	34	18.0	6.34E-18	6.6
GO:0005198~structural molecule activity	30	15.9	2.26E-13	5.3
GO:0005201~extracellular matrix structural constituent	10	5.3	6.45E-11	26.7
GO:0004857~enzyme inhibitor activity	16	8.5	3.53E-07	5.3
GO:0004866~endopeptidase inhibitor activity	13	6.9	7.57E-07	6.5
GO:0030414~peptidase inhibitor activity	13	6.9	1.95E-06	5.9
GO:0051015~actin filament binding	8	4.2	2.22E-06	13.1
GO:0005544~calcium-dependent phospholipid binding	6	3.2	9.76E-06	20.0
GO:0005509~calcium ion binding	27	14.3	1.38E-05	2.6
GO:0048407~platelet-derived growth factor binding	4	2.1	1.49E-04	35.6
GO:0008289~lipid binding	14	7.4	3.71E-04	3.2
GO:0004867~serine-type endopeptidase inhibitor activity	8	4.2	5.71E-04	5.6
GO:0055102~lipase inhibitor activity	3	1.6	1.50E-03	48.0
GO:0004859~phospholipase inhibitor activity	3	1.6	1.50E-03	48.0
GO:0030898~actin-dependent ATPase activity	3	1.6	2.22E-03	40.0
GO:0050840~extracellular matrix binding	4	2.1	3.54E-03	12.8
GO:0003723~RNA binding	18	9.5	4.16E-03	2.1
GO:0001871~pattern binding	7	3.7	5.23E-03	4.4
GO:0030247~polysaccharide binding	7	3.7	5.23E-03	4.4
GO:0005200~structural constituent of cytoskeleton	4	2.1	5.42E-03	11.0
GO:0005539~glycosaminoglycan binding	6	3.2	1.38E-02	4.2
GO:0005516~calmodulin binding	6	3.2	1.38E-02	4.2
GO:0005543~phospholipid binding	6	3.2	1.63E-02	4.0
GO:0008201~heparin binding	5	2.6	1.97E-02	4.8
GO:0003774~motor activity	6	3.2	2.88E-02	3.5
GO:0019834~phospholipase A2 inhibitor activity	2	1.1	3.68E-02	53.4
GO:0008538~proteasome activator activity	2	1.1	4.88E-02	40.0
GO:0043531~ADP binding	2	1.1	4.88E-02	40.0
GO:0010860~proteasome regulator activity	2	1.1	4.88E-02	40.0

S.1.7 List of GO Molecular Function terms significantly enriched in UUO-underexpressed proteins

Supplementary Table 3.10: GO Molecular Function overrepresentation test on UUO-underexpressed proteins, performed by DAVID. Statistical overrepresentation test was performed by DAVID (http://david.abcc.ncifcrf.gov) using the annotation term ontologies for Molecular Function (GOTERM_MF_FAT). The number of proteins belonging to the annotation term and fold change from the expected value H_0 are in increasing shades of green (the higher the more intense). The p-value is shown in increasing shades of blue (the more intense, the lower the p-value). A p-value lower than 0.05 was regarded as significant

GO Molecular Function in UUO underexpressed	Count	%	p-value	Fold Enrichment
GO:0048037~cofactor binding	60	13.8	8.25E-41	9.4
GO:0050662~coenzyme binding	47	10.8	6.11E-34	10.4
GO:0015077~monovalent inorganic cation transmembrane transporter activity	35	8.0	1.95E-30	14.2
GO:0015078~hydrogen ion transmembrane transporter activity	34	7.8	4.50E-30	14.7
GO:0022890~inorganic cation transmembrane transporter activity	35	8.0	3.60E-24	9.7
GO:0016651~oxidoreductase activity, acting on NADH or NADPH	24	5.5	1.09E-22	16.6
GO:0016655~oxidoreductase activity, acting on NADH or NADPH, quinone or similar compound as acceptor	17	3.9	1.14E-18	22.3
GO:0050136~NADH dehydrogenase (quinone) activity	16	3.7	4.44E-18	23.6
GO:0003954~NADH dehydrogenase activity	16	3.7	4.44E-18	23.6
GO:0008137~NADH dehydrogenase (ubiquinone) activity	16	3.7	4.44E-18	23.6
GO:0009055~electron carrier activity	32	7.4	1.07E-14	5.6
GO:0051287~NAD or NADH binding	17	3.9	2.39E-14	13.7
GO:0042625~ATPase activity, coupled to transmembrane movement of ions	19	4.4	3.98E-13	9.7
GO:0046961~proton-transporting ATPase activity, rotational mechanism	11	2.5	7.54E-13	25.9
GO:0015405~P-P-bond-hydrolysis-driven transmembrane transporter activity	22	5.1	1.79E-12	7.3
GO:0015399~primary active transmembrane transporter activity	22	5.1	2.17E-12	7.2
GO:0016820~hydrolase activity, acting on acid anhydrides, catalyzing transmembrane movement of substances	21	4.8	2.32E-12	7.7
GO:0042626~ATPase activity, coupled to transmembrane movement of substances	21	4.8	2.32E-12	7.7
GO:0043492~ATPase activity, coupled to movement of substances	21	4.8	2.32E-12	7.7
GO:0050660~FAD binding	17	3.9	9.16E-11	8.5
GO:0016209~antioxidant activity	13	3.0	5.87E-10	11.5
GO:0019829~cation-transporting ATPase activity	11	2.5	6.37E-10	15.5
GO:0016620~oxidoreductase activity, acting on the aldehyde or oxo group of donors, NAD or NADP as acceptor	11	2.5	3.53E-09	13.4
GO:0003995~acyl-CoA dehydrogenase activity	9	2.1	3.95E-09	19.9
GO:0046933~hydrogen ion transporting ATP synthase activity, rotational mechanism	8	1.8	4.04E-09	25.7
GO:0015002~heme-copper terminal oxidase activity	10	2.3	5.94E-09	15.4
GO:0004129~cytochrome-c oxidase activity	10	2.3	5.94E-09	15.4
GO:0016675~oxidoreductase activity, acting on heme group of donors	10	2.3	5.94E-09	15.4
GO:0016676~oxidoreductase activity, acting on heme group of donors, oxygen as acceptor	10	2.3	5.94E-09	15.4
GO:0004364~glutathione transferase activity	10	2.3	2.11E-08	13.6
GO:0019842~vitamin binding	18	4.1	4.83E-08	5.3
GO:0051540~metal cluster binding	12	2.8	1.09E-07	8.5
GO:0051536~iron-sulfur cluster binding	12	2.8	1.09E-07	8.5
GO:0016408~C-acyltransferase activity	8	1.8	1.24E-07	17.7
GO:0000166~nucleotide binding	102	23.4	1.24E-07	1.7
GO:0016836~hydro-lyase activity	11	2.5	1.87E-07	9.3
GO:0016684~oxidoreductase activity, acting on peroxide as acceptor	9	2.1	7.08E-07	11.4
GO:0004601~peroxidase activity	9	2.1	7.08E-07	11.4
GO:0008553~hydrogen-exporting ATPase activity, phosphorylative mechanism	7	1.6	1.20E-06	17.7
GO:0042623~ATPase activity, coupled	22	5.1	1.38E-06	3.5
GO:0016769~transferase activity, transferring nitrogenous groups	9	2.1	2.17E-06	9.9
GO:0003857~3-hydroxyacyl-CoA dehydrogenase activity	5	1.1	3.05E-06	35.3
GO:0016878~acid-thiol ligase activity	7	1.6	4.61E-06	14.6
GO:0016877~ligase activity, forming carbon-sulfur bonds	8	1.8	9.56E-06	10.1
GO:0001882~nucleoside binding	73	16.8	1.39E-05	1.7
GO:0005506~iron ion binding	26	6.0	1.44E-05	2.7

GO:0016765~transferase activity, transferring alkyl or aryl (other than methyl) groups	10	2.3	1.52E-05	6.7
GO:0030554~adenyl nucleotide binding	72	16.6	1.57E-05	1.7
GO:0030170~pyridoxal phosphate binding	10	2.3	1.78E-05	6.5
GO:0070279~vitamin B6 binding	10	2.3	1.78E-05	6.5
GO:0051920~peroxiredoxin activity	5	1.1	2.04E-05	25.2
GO:0016885~ligase activity, forming carbon-carbon bonds	5	1.1	2.04E-05	25.2
GO:0001883~purine nucleoside binding	72	16.6	2.13E-05	1.6
GO:0031406~carboxylic acid binding	12	2.8	2.56E-05	5.0
GO:0015662~ATPase activity, coupled to transmembrane movement of ions, phosphorylative mechanism	10	2.3	2.80E-05	6.2
GO:0016667~oxidoreductase activity, acting on sulfur group of donors	8	1.8	3.05E-05	8.6
GO:0051539~4 iron, 4 sulfur cluster binding	7	1.6	3.26E-05	10.8
GO:0000287~magnesium ion binding	28	6.4	3.78E-05	2.4
GO:0008483~transaminase activity	7	1.6	4.24E-05	10.3
GO:0016887~ATPase activity	22	5.1	4.88E-05	2.8
GO:0016645~oxidoreductase activity, acting on the CH-NH group of donors	7	1.6	5.45E-05	9.9
GO:0016405~CoA-ligase activity	5	1.1	7.03E-05	19.6
GO:0004300~enoyl-CoA hydratase activity	4	0.9	8.73E-05	35.3
GO:0016453~C-acetyltransferase activity	4	0.9	8.73E-05	35.3
GO:0003988~acetyl-CoA C-acyltransferase activity	4	0.9	2.14E-04	28.3
GO:0017076~purine nucleotide binding	78	17.9	3.34E-04	1.5
GO:0008121~ubiquinol-cytochrome-c reductase activity	4	0.9	4.19E-04	23.6
GO:0016681~oxidoreductase activity, acting on diphenols and related substances as donors, cytochrome as acceptor	4	0.9	4.19E-04	23.6
GO:0016679~oxidoreductase activity, acting on diphenols and related substances as donors	4	0.9	4.19E-04	23.6
GO:0016860~intramolecular oxidoreductase activity	7	1.6	6.24E-04	6.5
GO:0015036~disulfide oxidoreductase activity	5	1.1	6.66E-04	11.8
GO:0033293~monocarboxylic acid binding	6	1.4	8.43E-04	7.9
GO:0016624~oxidoreductase activity, acting on the aldehyde or oxo group of donors, disulfide as acceptor	4	0.9	1.65E-03	15.7
GO:0016868~intramolecular transferase activity, phosphotransferases	4	0.9	2.31E-03	14.1
GO:0004602~glutathione peroxidase activity	4	0.9	2.31E-03	14.1
GO:0003985~acetyl-CoA C-acetyltransferase activity	3	0.7	2.34E-03	35.3
GO:0050661~NADP or NADPH binding	5	1.1	2.55E-03	8.4
GO:0015035~protein disulfide oxidoreductase activity	4	0.9	3.11E-03	12.9
GO:0019205~nucleobase, nucleoside, nucleotide kinase activity	6	1.4	3.20E-03	5.9
GO:0016866~intramolecular transferase activity	5	1.1	4.24E-03	7.4
GO:0016833~oxo-acid-lyase activity	3	0.7	4.59E-03	26.5
GO:0004774~succinate-CoA ligase activity	3	0.7	4.59E-03	26.5
GO:0016776~phosphotransferase activity, phosphate group as acceptor	5	1.1	6.55E-03	6.5
GO:0009374~biotin binding	3	0.7	7.51E-03	21.2
GO:0031405~lipoic acid binding	3	0.7	7.51E-03	21.2
GO:0016628~oxidoreductase activity, acting on the CH-CH group of donors, NAD or NADP as acceptor	4	0.9	7.88E-03	9.4
GO:0008430~selenium binding	5	1.1	1.08E-02	5.7
GO:0004448~isocitrate dehydrogenase activity	3	0.7	1.11E-02	17.7
GO:0016406~carnitine O-acyltransferase activity	3	0.7	1.11E-02	17.7
GO:0016668~oxidoreductase activity, acting on sulfur group of donors, NAD or NADP as acceptor	3	0.7	1.11E-02	17.7
GO:0051537~2 iron, 2 sulfur cluster binding	4	0.9	1.54E-02	7.4
GO:0005524~ATP binding	55	12.6	1.82E-02	1.3
GO:0004029~aldehyde dehydrogenase (NAD) activity	3	0.7	1.99E-02	13.3
GO:0016615~malate dehydrogenase activity	3	0.7	1.99E-02	13.3
GO:0004017~adenylate kinase activity	3	0.7	1.99E-02	13.3
GO:0032559~adenyl ribonucleotide binding	55	12.6	2.33E-02	1.3
GO:0030145~manganese ion binding	10	2.3	2.45E-02	2.4
GO:0016861~intramolecular oxidoreductase activity, interconverting aldoses and ketoses	3	0.7	2.51E-02	11.8
GO:0048038~quinone binding	3	0.7	2.51E-02	11.8
GO:0010181~FMN binding	3	0.7	3.69E-02	9.6
GO:0008237~metallopeptidase activity	11	2.5	3.95E-02	2.1
GO:0004177~aminopeptidase activity	4	0.9	4.34E-02	5.0
GO:0000062~acyl-CoA binding	3	0.7	4.35E-02	8.8
GO:0008238~exopeptidase activity	6	1.4	4.75E-02	3.0

S.1.8 List of GO Cellular Component terms significantly enriched in UUO-overexpressed proteins

Supplementary Table 3.11: GO Cellular Component overrepresentation test on UUO-overexpressed proteins, performed by DAVID. Statistical overrepresentation test was performed by DAVID (http://david.abcc.ncifcrf.gov) using the annotation term ontologies for Cellular Component (GOTERM_CC_FAT). The number of proteins belonging to the annotation term and fold change from the expected value H_0 are in increasing shades of red (the higher the more intense). The p-value is shown in increasing shades of blue (the more intense, the lower the p-value). A p-value lower than 0.05 was regarded as significant.

GO Cellular Compartment in UUO overexpressed	Count	%	p-value	Fold Enrichment
GO:0015629~actin cytoskeleton	28	14.8	2.30E-20	10.88
GO:0044421~extracellular region part	46	24.3	5.29E-19	4.73
GO:0031012~extracellular matrix	30	15.9	1.02E-17	7.73
GO:0005578~proteinaceous extracellular matrix	29	15.3	3.53E-17	7.78
GO:0005856~cytoskeleton	52	27.5	4.71E-17	3.69
GO:0005576~extracellular region	62	32.8	8.36E-16	2.94
GO:0044420~extracellular matrix part	17	9.0	2.21E-14	14.72
GO:0043232~intracellular non-membrane-bounded organelle	58	30.7	5.59E-11	2.41
GO:0043228~non-membrane-bounded organelle	58	30.7	5.59E-11	2.41
GO:0044430~cytoskeletal part	35	18.5	7.52E-11	3.60
GO:0005604~basement membrane	13	6.9	8.87E-11	14.18
GO:0005938~cell cortex	15	7.9	5.09E-10	9.48
GO:0042383~sarcolemma	9	4.8	1.02E-07	15.25
GO:0044448~cell cortex part	10	5.3	2.85E-07	10.91
GO:0001725~stress fiber	7	3.7	2.90E-07	24.24
GO:0032432~actin filament bundle	7	3.7	3.83E-07	23.23
GO:0042641~actomyosin	7	3.7	8.16E-07	20.65
GO:0030863~cortical cytoskeleton	8	4.2	9.09E-07	14.82
GO:0031252~cell leading edge	11	5.8	1.30E-06	7.82
GO:0005681~spliceosome	11	5.8	3.30E-06	7.07
GO:0005615~extracellular space	21	11.1	5.55E-06	3.27
GO:0042470~melanosome	9	4.8	1.05E-05	8.43
GO:0048770~pigment granule	9	4.8	1.05E-05	8.43
GO:0044449~contractile fiber part	9	4.8	1.14E-05	8.33
GO:0005605~basal lamina	5	2.6	1.53E-05	30.63
GO:0043292~contractile fiber	9	4.8	2.38E-05	7.55
GO:0005882~intermediate filament	10	5.3	5.35E-05	5.81
GO:0045111~intermediate filament cytoskeleton	10	5.3	6.33E-05	5.69
GO:0030016~myofibril	8	4.2	1.38E-04	7.00
GO:0043259~laminin-10 complex	3	1.6	4.60E-04	79.64
GO:0005925~focal adhesion	6	3.2	7.04E-04	8.38
GO:0005924~cell-substrate adherens junction	6	3.2	9.61E-04	7.83
GO:0016459~myosin complex	6	3.2	9.61E-04	7.83
GO:0030055~cell-substrate junction	6	3.2	1.37E-03	7.24
GO:0005829~cytosol	17	9.0	1.38E-03	2.47
GO:0005581~collagen	4	2.1	1.59E-03	16.77
GO:0016323~basolateral plasma membrane	8	4.2	1.93E-03	4.52
GO:0005912~adherens junction	7	3.7	2.10E-03	5.26
GO:0005885~Arp2/3 protein complex	3	1.6	2.24E-03	39.82
GO:0030018~Z disc	5	2.6	2.53E-03	8.66
GO:0043256~laminin complex	3	1.6	3.12E-03	34.13
GO:0030017~sarcomere	6	3.2	3.21E-03	5.97
GO:0031674~I band	5	2.6	4.25E-03	7.51
GO:0070161~anchoring junction	7	3.7	4.39E-03	4.53
GO:0016023~cytoplasmic membrane-bounded vesicle	13	6.9	5.69E-03	2.50
GO:0031988~membrane-bounded vesicle	13	6.9	6.36E-03	2.47
GO:0001772~immunological synapse	3	1.6	1.10E-02	18.38
GO:0031410~cytoplasmic vesicle	14	7.4	1.11E-02	2.19
GO:0005788~endoplasmic reticulum lumen	5	2.6	1.24E-02	5.53
GO:0042995~cell projection	15	7.9	1.28E-02	2.08
GO:0030529~ribonucleoprotein complex	13	6.9	1.30E-02	2.24
GO:0031982~vesicle	14	7.4	1.31E-02	2.15
GO:0034364~high-density lipoprotein particle	3	1.6	1.65E-02	14.93
GO:0001726~ruffle	4	2.1	2.07E-02	6.78
GO:0034399~nuclear periphery	4	2.1	2.31E-02	6.50
GO:0045177~apical part of cell	6	3.2	2.77E-02	3.51
GO:0030864~cortical actin cytoskeleton	3	1.6	3.03E-02	10.86

GO:0031594~neuromuscular junction	3	1.6	3.03E-02	10.86
GO:0016324~apical plasma membrane	5	2.6	3.53E-02	4.02
GO:0030485~smooth muscle contractile fiber	2	1.1	3.70E-02	53.10
GO:0008537~proteasome activator complex	2	1.1	3.70E-02	53.10
GO:0005577~fibrinogen complex	2	1.1	3.70E-02	53.10
GO:0045098~type III intermediate filament	2	1.1	3.70E-02	53.10
GO:0030027~lamellipodium	4	2.1	4.39E-02	5.06
GO:0032994~protein-lipid complex	3	1.6	4.43E-02	8.85
GO:0034358~plasma lipoprotein particle	3	1.6	4.43E-02	8.85
GO:0045095~keratin filament	4	2.1	4.57E-02	4.98
GO:0001527~microfibril	2	1.1	4.90E-02	39.82
GO:0005638~lamin filament	2	1.1	4.90E-02	39.82

S.1.9 List of GO Cellular Component terms significantly enriched in UUO-underexpressed proteins

Supplementary Table 3.12: GO Cellular Component overrepresentation test on UUO-underexpressed proteins, performed by DAVID. Statistical overrepresentation test was performed by DAVID (http://david.abcc.ncifcrf.gov) using the annotation term ontologies for Cellular Component (GOTERM_CC_FAT). The number of proteins belonging to the annotation term and fold change from the expected value H_0 are in increasing shades of green (the higher the more intense). The p-value is shown in increasing shades of blue (the more intense, the lower the p-value). A p-value lower than 0.05 was regarded as significant

GO Cellular Compartment in UUO underexpressed	Count	%	p-value	Fold Enrichment
GO:0005739~mitochondrion	269	61.8	2.12E-185	6.9
GO:0044429~mitochondrial part	160	36.8	7.94E-126	10.3
GO:0005743~mitochondrial inner membrane	112	25.7	1.66E-96	12.8
GO:0031966~mitochondrial membrane	121	27.8	2.15E-96	11.1
GO:0019866~organelle inner membrane	113	26.0	6.45E-95	12.3
GO:0005740~mitochondrial envelope	122	28.0	3.88E-94	10.6
GO:0031967~organelle envelope	123	28.3	6.23E-77	7.7
GO:0031975~envelope	123	28.3	9.96E-77	7.7
GO:0031090~organelle membrane	129	29.7	2.54E-61	5.4
GO:0070469~respiratory chain	43	9.9	5.68E-49	22.4
GO:0005759~mitochondrial matrix	56	12.9	7.35E-44	11.6
GO:0031980~mitochondrial lumen	56	12.9	7.35E-44	11.6
GO:0016469~proton-transporting two-sector ATPase complex	22	5.1	1.18E-21	17.7
GO:0033178~proton-transporting two-sector ATPase complex, catalytic domain	12	2.8	1.31E-13	23.9
GO:0042579~microbody	23	5.3	2.35E-13	7.5
GO:0005777~peroxisome	23	5.3	2.35E-13	7.5
GO:0044455~mitochondrial membrane part	17	3.9	3.17E-13	11.8
GO:0045259~proton-transporting ATP synthase complex	12	2.8	7.57E-13	21.4
GO:0005746~mitochondrial respiratory chain	8	1.8	9.49E-08	18.1
GO:0000276~mitochondrial proton-transporting ATP synthase complex, coupling factor F(o)	6	1.4	1.26E-07	33.9
GO:0031968~organelle outer membrane	15	3.4	2.20E-07	5.8
GO:0019867~outer membrane	15	3.4	3.39E-07	5.6
GO:0031974~membrane-enclosed lumen	66	15.2	3.78E-07	1.9
GO:0005753~mitochondrial proton-transporting ATP synthase complex	6	1.4	4.30E-07	29.0
GO:0033176~proton-transporting V-type ATPase complex	8	1.8	4.35E-07	15.1
GO:0005741~mitochondrial outer membrane	14	3.2	5.32E-07	5.9
GO:0045263~proton-transporting ATP synthase complex, coupling factor F(o)	7	1.6	8.99E-07	18.2
GO:0033177~proton-transporting two-sector ATPase complex, proton-transporting domain	8	1.8	2.10E-06	12.3
GO:0005829~cytosol	38	8.7	2.17E-06	2.3
GO:0005747~mitochondrial respiratory chain complex I	5	1.1	1.06E-05	28.2
GO:0045261~proton-transporting ATP synthase complex, catalytic core F(1)	5	1.1	1.06E-05	28.2
GO:0045271~respiratory chain complex I	5	1.1	1.06E-05	28.2
GO:0030964~NADH dehydrogenase complex	5	1.1	1.06E-05	28.2
GO:0043233~organelle lumen	59	13.6	2.14E-05	1.8
GO:0070013~intracellular organelle lumen	58	13.3	3.85E-05	1.7
GO:0033180~proton-transporting V-type ATPase, V1 domain	5	1.1	4.70E-05	21.2
GO:0005758~mitochondrial intermembrane space	7	1.6	2.04E-04	7.9
GO:0005625~soluble fraction	11	2.5	6.55E-04	3.8
GO:0005792~microsome	15	3.4	7.06E-04	2.9
GO:0042598~vesicular fraction	15	3.4	9.81E-04	2.8
GO:0031970~organelle envelope lumen	7	1.6	1.03E-03	5.9
GO:0045177~apical part of cell	12	2.8	2.25E-03	3.0
GO:0016324~apical plasma membrane	10	2.3	2.53E-03	3.4
GO:0017133~mitochondrial electron transfer flavoprotein complex	3	0.7	2.54E-03	33.9
GO:0045251~electron transfer flavoprotein complex	3	0.7	2.54E-03	33.9
GO:0000267~cell fraction	31	7.1	2.91E-03	1.8
GO:0005903~brush border	6	1.4	3.37E-03	5.8
GO:0042470~melanosome	9	2.1	3.49E-03	3.6
GO:0048770~pigment granule	9	2.1	3.49E-03	3.6
GO:0005902~microvillus	5	1.1	9.80E-03	5.8
GO:0016471~vacuolar proton-transporting V-type ATPase complex	3	0.7	1.64E-02	14.5
GO:0031903~microbody membrane	4	0.9	3.98E-02	5.2
GO:0005778~peroxisomal membrane	4	0.9	3.98E-02	5.2

S.1.10 List of proteins significantly overexpressed/underexpressed upon UUO in the current SWATH-MS study which have been previously identified in the dame model by MS.

Supplementary Table 3.13: Proteins detected in the current proteomic study that have been previously identified by MS in UUO models, according to recent literature (Yuan, Zhang et al. 2015, Zhao, Yang et al. 2015). Legend: +, red = overexpressed proteins in the study (positive fold change from the Sham operated control); -, green =underexpressed proteins in the study (positive fold change from the Sham operated control); bright yellow = confidence > 0.8 in the current study (considered significant in the current study); pale yellow = 0.5 > confidence < 0.8 in the current study.

Current study			Yuan et al., 2015		Zhao et al., 2015	
Protein	Log2 FC (UUO/Sham)	C(FC)	Over/Under expressed	Weeks post UUO	Over/Under expressed	Days Post cUUO
VIME_MOUSE	3.10	0.90	+	3		
ANXA1_MOUSE	3.03	0.84	+	3	+	12
A1AT2_MOUSE	2.97	0.82			+	72
LUM_MOUSE	2.71	0.87	+	3		
LG3BP_MOUSE	2.53	0.67	+	1		
CLUS_MOUSE	2.42	0.81	+	3		
ACTN1_MOUSE	2.08	0.96	+	3		
A1AT5_MOUSE	2.04	0.65			+	72
FIBB_MOUSE	2.00	0.86			+	12
ALD1_MOUSE	1.98	0.44			+	24
ANXA2_MOUSE	1.91	0.90			+	12
ACTA_MOUSE	1.67	0.94			-	72
A1AT1_MOUSE	1.62	0.86			+	72
S10A9_MOUSE	1.60	0.54	+	1		
ALBU_MOUSE	1.58	0.92			+	72
MUP6_MOUSE	1.56	0.62			-	72
MUP2_MOUSE	1.48	0.77			-	72
A1AT4_MOUSE	1.44	0.83			+	72
CATD_MOUSE	1.41	0.82	+	1		
ANXA4_MOUSE	0.83	0.85			+	72
PDIA6_MOUSE	0.75	0.90			+	12
MOES_MOUSE	0.60	0.81	+	3		
ACTN4_MOUSE	0.55	0.70	+	3		
GSTM2_MOUSE	0.37	0.17			+	12
ROA2_MOUSE	0.35	0.38			+	24
SODE_MOUSE	**-0.38**	**0.31**	+	3		
H14_MOUSE	**-0.40**	**0.18**	+	3		
TALDO_MOUSE	**-0.42**	**0.57**	+	3		
GBB2_MOUSE	**-0.47**	**0.47**			+	12
GSTP1_MOUSE	**-0.82**	**0.94**			+/-	24 (+); 72 (-)
PEBP1_MOUSE	**-0.94**	**0.92**			+	12
PRDX1_MOUSE	**-1.02**	**0.91**			+	12
MUP3_MOUSE	**-1.28**	**0.63**			-	72
VDAC2_MOUSE	**-1.50**	**0.94**			+	12
GPX1_MOUSE	**-1.79**	**0.92**			-	72
AMPN_MOUSE	**-1.94**	**0.95**	+	1		
GPX41_MOUSE	**-2.06**	**0.52**			+	12
BCAT2_MOUSE	**-2.13**	**0.89**			+	12
IDH3A_MOUSE	**-2.28**	**0.91**			-	24
CMBL_MOUSE	**-2.43**	**0.85**			-	72
ABHEB_MOUSE	**-2.48**	**0.93**			+	12
AL9A1_MOUSE	**-2.53**	**0.94**			-	24
ODPB_MOUSE	**-2.60**	**0.96**			-	72
ATPB_MOUSE	**-2.71**	**0.94**			+	12
MEP1A_MOUSE	**-2.84**	**0.88**			+	12
ATP5H_MOUSE	**-2.85**	**0.93**			+	12

THTR_MOUSE	-2.95	0.89			+	12
ETFB_MOUSE	-3.02	0.91			+	12
AGT2_MOUSE	-3.17	0.71			+	12
ODBA_MOUSE	-3.36	0.64			+	12
ACY3_MOUSE	-3.64	0.80			-	72
GGT1_MOUSE	-3.76	0.89			+	24
GATM_MOUSE	-3.80	0.87			+	24
3HAO_MOUSE	-3.96	0.85			+	72
KAD4_MOUSE	-4.31	0.89			+	24

Supplementary Table 3.14: Proteins detected as overexpressed in the current SWATHTM-MS study that have been previously found in other studies (Yuan, Zhang et al. 2015, Zhao, Yang et al. 2015).

	log2 FC	Confidence
VIME_MOUSE	3.10	0.90
ANXA1_MOUSE	3.03	0.84
A1AT2_MOUSE	2.97	0.82
LUM_MOUSE	2.71	0.87
CLUS_MOUSE	2.42	0.81
ACTN1_MOUSE	2.08	0.96
FIBB_MOUSE	2.00	0.86
ANXA2_MOUSE	1.91	0.90
A1AT1_MOUSE	1.62	0.86
ALBU_MOUSE	1.58	0.92
A1AT4_MOUSE	1.44	0.83
CATD_MOUSE	1.41	0.82
ANXA4_MOUSE	0.83	0.85
PDIA6_MOUSE	0.75	0.90
MOES_MOUSE	0.60	0.81
LG3BP_MOUSE	2.53	0.67
A1AT5_MOUSE	2.04	0.65
ALD1_MOUSE	1.98	0.44
S10A9_MOUSE	1.60	0.54
ACTN4_MOUSE	0.55	0.70
GSTM2_MOUSE	0.37	0.17
ROA2_MOUSE	0.35	0.38

Significantly detected by SWATH™-MS in the current study
n=15
15/195=7.7%

S.1.11 List of UUO-overexpressed proteins in TG2-KO mice

Supplementary Table 3.15: List of proteins significantly overexpressed (confidence ≥ 0.8) in TG2-KO kidneys subjected to UUO (21 days) and corresponding positive fold change from Sham operated condition.

Protein ID	Name	Abs(FC) UUO/Sham	C(FC)
COCA1_MOUSE	Collagen alpha-1(XII) chain	26.15	0.83
FBN2_MOUSE	Fibrillin-2	14.52	0.89
S10A6_MOUSE	Protein S100-A6	10.94	0.81
PGS1_MOUSE	Biglycan	9.86	0.87
UROM_MOUSE	Uromodulin	9.78	0.88
RCN3_MOUSE	Reticulocalbin-3	9.30	0.84
ANXA1_MOUSE	Annexin A1	8.24	0.94
FBN1_MOUSE	Fibrillin-1	8.05	0.89
K1C19_MOUSE	Keratin, type I cytoskeletal 19	7.95	0.89
MUP6_MOUSE	Major urinary protein 6	7.80	0.95
CO5A1_MOUSE	Collagen alpha-1(V) chain	7.56	0.83
MIME_MOUSE	Mimecan	7.40	0.86
TAGL_MOUSE	Transgelin	6.86	0.89
COR1A_MOUSE	Coronin-1A	6.83	0.82
LUM_MOUSE	Lumican	6.76	0.84
TPSN_MOUSE	Tapasin	6.71	0.89
VIME_MOUSE	Vimentin	6.67	0.91
CO1A1_MOUSE	Collagen alpha-1(I) chain	6.64	0.96
GAPR1_MOUSE	Golgi-associated plant pathogenesis-related protein 1	6.44	0.86
FINC_MOUSE	Fibronectin	6.31	0.89
CFAH_MOUSE	Complement factor H	6.17	0.81
CO3A1_MOUSE	Collagen alpha-1(III) chain	6.02	0.95
KCRB_MOUSE	Creatine kinase B-type	5.98	0.86
ELN_MOUSE	Elastin	5.78	0.83
K1C14_MOUSE	Keratin, type I cytoskeletal 14	5.55	0.81
SERPH_MOUSE	Serpin H1	5.45	0.96
LEG1_MOUSE	Galectin-1	5.44	0.93
FBLN5_MOUSE	Fibulin-5	5.38	0.87
FBLN3_MOUSE	EGF-containing fibulin-like extracellular matrix protein 1	5.35	0.87
MYOF_MOUSE	Myoferlin	5.21	0.81
K2C5_MOUSE	Keratin, type II cytoskeletal 5	5.15	0.84
EMIL1_MOUSE	Emilin-1	4.77	0.89
PLSL_MOUSE	Plastin-2	4.77	0.82
SAMH1_MOUSE	Deoxynucleoside triphosphate triphosphohydrolase SAMHD1	4.70	0.84
PRELP_MOUSE	Prolargin	4.68	0.89
TYB4_MOUSE	Thymosin beta-4	4.65	0.90
DESM_MOUSE	Desmin	4.60	0.94
FLNA_MOUSE	Filamin-A	4.56	0.95
H2A1H_MOUSE	Histone H2A type 1-H	4.49	0.85
C1QB_MOUSE	Complement C1q subcomponent subunit B	4.35	0.91
ASAH1_MOUSE	Acid ceramidase	4.32	0.87
CLUS_MOUSE	Clusterin	4.30	0.86
TBA1A_MOUSE	Tubulin alpha-1A chain	4.28	0.91
K2C8_MOUSE	Keratin, type II cytoskeletal 8	4.26	0.94
GCAB_MOUSE	Ig gamma-2A chain C region secreted form	4.20	0.82
CNN2_MOUSE	Calponin-2	4.11	0.84
PDLI2_MOUSE	PDZ and LIM domain protein 2	4.09	0.82
TPM4_MOUSE	Tropomyosin alpha-4 chain	4.06	0.91
COEA1_MOUSE	Collagen alpha-1(XIV) chain	3.93	0.83
ACTN1_MOUSE	Alpha-actinin-1	3.72	0.96
LEG3_MOUSE	Galectin-3	3.71	0.86
CSRP1_MOUSE	Cysteine and glycine-rich protein 1	3.65	0.92
MYH10_MOUSE	Myosin-10	3.63	0.84
MYADM_MOUSE	Myeloid-associated differentiation marker	3.62	0.92
ESYT1_MOUSE	Extended synaptotagmin-1	3.60	0.83
CO6A1_MOUSE	Collagen alpha-1(VI) chain	3.52	0.89
HEMO_MOUSE	Hemopexin	3.50	0.82
G6PE_MOUSE	GDH/6PGL endoplasmic bifunctional protein	3.49	0.85
TPM2_MOUSE	Tropomyosin beta chain	3.44	0.82
MUP2_MOUSE	Major urinary protein 2	3.43	1.00
K2C7_MOUSE	Keratin, type II cytoskeletal 7	3.43	0.88
S10AB_MOUSE	Protein S100-A11	3.40	0.88
CO6A2_MOUSE	Collagen alpha-2(VI) chain	3.40	0.92
IGKC_MOUSE	Ig kappa chain C region	3.38	0.87

FRIL1_MOUSE	Ferritin light chain 1	3.36	0.86
EFHD2_MOUSE	EF-hand domain-containing protein D2	3.28	0.83
LG3BP_MOUSE	Galectin-3-binding protein	3.26	0.81
RBM3_MOUSE	RNA-binding protein 3	3.23	0.81
E41L2_MOUSE	Band 4.1-like protein 2	3.22	0.88
TAGL2_MOUSE	Transgelin-2	3.16	0.87
CATD_MOUSE	Cathepsin D	3.12	0.81
TPM1_MOUSE	Tropomyosin alpha-1 chain	3.09	0.83
SH3L1_MOUSE	SH3 domain-binding glutamic acid-rich-like protein	3.09	0.89
ANXA2_MOUSE	Annexin A2	3.06	0.90
ANXA3_MOUSE	Annexin A3	3.05	0.82
ESYT2_MOUSE	Extended synaptotagmin-2	3.03	0.83
VAT1_MOUSE	Synaptic vesicle membrane protein VAT-1 homolog	2.92	0.93
ARC1B_MOUSE	Actin-related protein 2/3 complex subunit 1B	2.91	0.88
MYH11_MOUSE	Myosin-11	2.87	0.92
EPDR1_MOUSE	Mammalian ependymin-related protein 1	2.85	0.81
APOH_MOUSE	Beta-2-glycoprotein 1	2.82	0.85
A1AT4_MOUSE	Alpha-1-antitrypsin 1-4	2.79	0.81
ACTA_MOUSE	Actin, aortic smooth muscle	2.76	0.85
CO4B_MOUSE	Complement C4-B	2.75	0.83
PPT1_MOUSE	Palmitoyl-protein thioesterase 1	2.75	0.85
A1AT1_MOUSE	Alpha-1-antitrypsin 1-1	2.74	0.81
TBB5_MOUSE	Tubulin beta-5 chain	2.72	0.90
H11_MOUSE	Histone H1.1	2.72	0.96
TRFE_MOUSE	Serotransferrin	2.67	0.89
HSPB1_MOUSE	Heat shock protein beta-1	2.67	0.85
K1C18_MOUSE	Keratin, type I cytoskeletal 18	2.66	0.92
SEPT2_MOUSE	Septin-2	2.62	0.85
FETUB_MOUSE	Fetuin-B	2.60	0.86
ISG15_MOUSE	Ubiquitin-like protein ISG15	2.59	0.89
LMNA_MOUSE	Prelamin-A/C	2.57	0.94
MYL9_MOUSE	Myosin regulatory light polypeptide 9	2.56	0.98
PCNA_MOUSE	Proliferating cell nuclear antigen	2.55	0.81
KNG1_MOUSE	Kininogen-1	2.54	0.92
FETUA_MOUSE	Alpha-2-HS-glycoprotein	2.54	0.94
H15_MOUSE	Histone H1.5	2.54	0.91
MYL6_MOUSE	Myosin light polypeptide 6	2.53	0.94
EST1C_MOUSE	Carboxylesterase 1C	2.52	0.94
SPB6_MOUSE	Serpin B6	2.51	0.84
MYH9_MOUSE	Myosin-9	2.50	0.97
APOE_MOUSE	Apolipoprotein E	2.49	0.94
APOA4_MOUSE	Apolipoprotein A-IV	2.47	0.83
ALBU_MOUSE	Serum albumin	2.46	0.91
CO3_MOUSE	Complement C3	2.45	0.87
HMGB2_MOUSE	High mobility group protein B2	2.45	0.85
NAGAB_MOUSE	Alpha-N-acetylgalactosaminidase	2.43	0.82
H12_MOUSE	Histone H1.2	2.42	0.93
SEPT7_MOUSE	Septin-7	2.41	0.80
CAP1_MOUSE	Adenylyl cyclase-associated protein 1	2.40	0.92
VMA5A_MOUSE	von Willebrand factor A domain-containing protein 5A	2.36	0.86
B2MG_MOUSE	Beta-2-microglobulin	2.34	0.89
SEP11_MOUSE	Septin-11	2.33	0.83
GELS_MOUSE	Gelsolin	2.30	0.87
MYLK_MOUSE	Myosin light chain kinase, smooth muscle	2.28	0.89
VTDB_MOUSE	Vitamin D-binding protein	2.28	0.89
T22D1_MOUSE	TSC22 domain family protein 1	2.24	0.84
PSME1_MOUSE	Proteasome activator complex subunit 1	2.21	0.81
LMNB1_MOUSE	Lamin-B1	2.19	0.88
ANXA5_MOUSE	Annexin A5	2.19	0.87
COF1_MOUSE	Cofilin-1	2.18	0.83
MAP4_MOUSE	Microtubule-associated protein 4	2.17	0.81
PROF1_MOUSE	Profilin-1	2.16	0.88
SET_MOUSE	Protein SET	2.15	0.90
AN32B_MOUSE	Acidic leucine-rich nuclear phosphoprotein 32 family member B	2.14	0.91
CATZ_MOUSE	Cathepsin Z	2.09	0.85
ARPC5_MOUSE	Actin-related protein 2/3 complex subunit 5	2.09	0.90
COIA1_MOUSE	Collagen alpha-1(XVIII) chain	2.08	0.94
SPA3K_MOUSE	Serine protease inhibitor A3K	2.07	0.81
ADPRH_MOUSE	[Protein ADP-ribosylarginine] hydrolase	2.06	0.84
NID1_MOUSE	Nidogen-1	2.04	0.94
APOA1_MOUSE	Apolipoprotein A-I	2.04	0.87
PSME2_MOUSE	Proteasome activator complex subunit 2	2.03	0.81
ROA1_MOUSE	Heterogeneous nuclear ribonucleoprotein A1	2.03	0.88

VINC_MOUSE	Vinculin	2.03	0.92
RENI1_MOUSE	Renin-1	2.01	0.84
CO4A1_MOUSE	Collagen alpha-1(IV) chain	2.01	0.86
TIF1B_MOUSE	Transcription intermediary factor 1-beta	1.99	0.81
ANXA6_MOUSE	Annexin A6	1.98	0.91
SFPQ_MOUSE	Splicing factor, proline- and glutamine-rich	1.97	0.81
LAMA5_MOUSE	Laminin subunit alpha-5	1.96	0.89
COR1C_MOUSE	Coronin-1C	1.95	0.82
UBC9_MOUSE	SUMO-conjugating enzyme UBC9	1.92	0.91
DPYL2_MOUSE	Dihydropyrimidinase-related protein 2	1.88	0.83
FUS_MOUSE	RNA-binding protein FUS	1.87	0.81
LAMC1_MOUSE	Laminin subunit gamma-1	1.83	0.90
HP1B3_MOUSE	Heterochromatin protein 1-binding protein 3	1.82	0.89
GNAI2_MOUSE	Guanine nucleotide-binding protein G(i) subunit alpha-2	1.79	0.84
H2AV_MOUSE	Histone H2A.V	1.79	0.84
NID2_MOUSE	Nidogen-2	1.77	0.87
CAPG_MOUSE	Macrophage-capping protein	1.76	0.81
ACTBL_MOUSE	Beta-actin-like protein 2	1.75	0.91
CAPZB_MOUSE	F-actin-capping protein subunit beta	1.73	0.86
ARP3_MOUSE	Actin-related protein 3	1.71	0.93
SAP_MOUSE	Prosaposin	1.70	0.82
DX39B_MOUSE	Spliceosome RNA helicase Ddx39b	1.69	0.81
LAMB1_MOUSE	Laminin subunit beta-1	1.67	0.84
ILF2_MOUSE	Interleukin enhancer-binding factor 2	1.65	0.84
ARPC4_MOUSE	Actin-related protein 2/3 complex subunit 4	1.65	0.85
TLN1_MOUSE	Talin-1	1.65	0.89
H2AX_MOUSE	Histone H2AX	1.64	0.83
NONO_MOUSE	Non-POU domain-containing octamer-binding protein	1.62	0.89
H2B1P_MOUSE	Histone H2B type 1-P	1.59	0.88
PDIA6_MOUSE	Protein disulfide-isomerase A6	1.59	0.88
ARP2_MOUSE	Actin-related protein 2	1.58	0.81
NPM_MOUSE	Nucleophosmin	1.58	0.83
ROA3_MOUSE	Heterogeneous nuclear ribonucleoprotein A3	1.58	0.88
LSM3_MOUSE	U6 snRNA-associated Sm-like protein LSm3	1.57	0.91
PGBM_MOUSE	Basement membrane-specific heparan sulfate proteoglycan core protein	1.56	0.81
ABRAL_MOUSE	Costars family protein ABRACL	1.55	0.87
PRDX4_MOUSE	Peroxiredoxin-4	1.53	0.89
HNRPM_MOUSE	Heterogeneous nuclear ribonucleoprotein M	1.50	0.82
ROAA_MOUSE	Heterogeneous nuclear ribonucleoprotein A/B	1.50	0.84
PDIA4_MOUSE	Protein disulfide-isomerase A4	1.48	0.88
NUCL_MOUSE	Nucleolin	1.46	0.85
RUXE_MOUSE	Small nuclear ribonucleoprotein E	1.45	0.80
ABCB7_MOUSE	ATP-binding cassette sub-family B member 7, mitochondrial	1.45	0.89
HNRPU_MOUSE	Heterogeneous nuclear ribonucleoprotein U	1.44	0.84
ACTB_MOUSE	Actin, cytoplasmic 1	1.43	0.90
SMD2_MOUSE	Small nuclear ribonucleoprotein Sm D2	1.40	0.82
KAD1_MOUSE	Adenylate kinase isoenzyme 1	1.39	0.81
TADBP_MOUSE	TAR DNA-binding protein 43	1.39	0.82
CATB_MOUSE	Cathepsin B	1.35	0.85

S.1.12 List of UUO-underexpressed proteins in TG2-KO mice

Supplementary Table 3.16: List of proteins significantly underexpressed (confidence ≥ 0.8) in TG2-KO kidneys subjected to UUO (21 days) and corresponding negative fold change from Sham operated condition.

Protein ID	Name	Abs(FC) Sham/UUO	C(FC)
SC5A3_MOUSE	Sodium/myo-inositol cotransporter	27.69	0.86
HYES_MOUSE	Bifunctional epoxide hydrolase 2	25.06	0.84
CX6A1_MOUSE	Cytochrome c oxidase subunit 6A1, mitochondrial	21.54	0.80
ASSY_MOUSE	Argininosuccinate synthase	21.51	0.87
CALB1_MOUSE	Calbindin	21.18	0.92
GATM_MOUSE	Glycine amidinotransferase, mitochondrial	20.94	0.88
ACSM2_MOUSE	Acyl-coenzyme A synthetase ACSM2, mitochondrial	19.94	0.89
AAAD_MOUSE	Arylacetamide deacetylase	19.31	0.91
3HAO_MOUSE	3-hydroxyanthranilate 3,4-dioxygenase	19.13	0.82
KAD4_MOUSE	Adenylate kinase 4, mitochondrial	18.93	0.91
F16P1_MOUSE	Fructose-1,6-bisphosphatase 1	18.22	0.90
HAOX2_MOUSE	Hydroxyacid oxidase 2	18.08	0.88
PCKGC_MOUSE	Phosphoenolpyruvate carboxykinase, cytosolic [GTP]	17.10	0.85
FBX50_MOUSE	F-box only protein 50	17.04	0.84
GLYAT_MOUSE	Glycine N-acyltransferase	16.55	0.86
AT1B1_MOUSE	Sodium/potassium-transporting ATPase subunit beta-1	16.52	0.87
ACADM_MOUSE	Medium-chain specific acyl-CoA dehydrogenase, mitochondrial	16.23	0.87
CAD16_MOUSE	Cadherin-16	15.95	0.89
MMSA_MOUSE	Methylmalonate-semialdehyde dehydrogenase [acylating], mitochondrial	15.74	0.89
KEG1_MOUSE	Glycine N-acyltransferase-like protein Keg1	15.67	0.88
ATNG_MOUSE	Sodium/potassium-transporting ATPase subunit gamma	15.63	0.89
PYC_MOUSE	Pyruvate carboxylase, mitochondrial	15.62	0.84
ST1D1_MOUSE	Sulfotransferase 1 family member D1	15.51	0.84
ALDOB_MOUSE	Fructose-bisphosphate aldolase B	15.47	0.93
PBLD1_MOUSE	Phenazine biosynthesis-like domain-containing protein 1	15.43	0.81
GLPK_MOUSE	Glycerol kinase	14.98	0.85
QORL2_MOUSE	Quinone oxidoreductase-like protein 2	14.96	0.83
ACOX1_MOUSE	Peroxisomal acyl-coenzyme A oxidase 1	14.52	0.88
KHK_MOUSE	Ketohexokinase	14.41	0.84
BPHL_MOUSE	Valacyclovir hydrolase	14.21	0.85
FAHD2_MOUSE	umarylacetoacetate hydrolase domain-containing protein 2A	14.19	0.81
BDH_MOUSE	D-beta-hydroxybutyrate dehydrogenase, mitochondrial	14.12	0.92
DHSO_MOUSE	Sorbitol dehydrogenase	13.96	0.85
FAAA_MOUSE	Fumarylacetoacetase	13.80	0.90
GPDA_MOUSE	Glycerol-3-phosphate dehydrogenase [NAD(+)], cytoplasmic	13.65	0.84
S27A2_MOUSE	Very long-chain acyl-CoA synthetase	13.57	0.84
ECHP_MOUSE	Peroxisomal bifunctional enzyme	13.34	0.88
GGT1_MOUSE	Gamma-glutamyltranspeptidase 1	13.34	0.86
PECR_MOUSE	Peroxisomal trans-2-enoyl-CoA reductase	13.10	0.92
ECHD2_MOUSE	Enoyl-CoA hydratase domain-containing protein 2, mitochondrial	12.79	0.88
AQP3_MOUSE	Aquaporin-3	12.64	0.85
SARDH_MOUSE	Sarcosine dehydrogenase, mitochondrial	12.57	0.87
GABT_MOUSE	4-aminobutyrate aminotransferase, mitochondrial	12.32	0.93
ODB2_MOUSE	Lipoamide acyltransferase component of branched-chain alpha-keto acid dehydrogenase complex, mitochondrial	12.29	0.80
AL8A1_MOUSE	Aldehyde dehydrogenase family 8 member A1	12.21	0.89
FAHD1_MOUSE	Acylpyruvase FAHD1, mitochondrial	12.20	0.84
ISC2A_MOUSE	Isochorismatase domain-containing protein 2A	12.14	0.81
ACO13_MOUSE	Acyl-coenzyme A thioesterase 13	12.10	0.88
AL4A1_MOUSE	Delta-1-pyrroline-5-carboxylate dehydrogenase, mitochondrial	11.79	0.91
S100G_MOUSE	Protein S100-G	11.78	0.87
S22AC_MOUSE	Solute carrier family 22 member 12	11.74	0.83
VILI_MOUSE	Villin-1	11.73	0.88
PCCB_MOUSE	Propionyl-CoA carboxylase beta chain, mitochondrial	11.73	0.90
IYD1_MOUSE	Iodotyrosine deiodinase 1	11.72	0.86
AT1A1_MOUSE	Sodium/potassium-transporting ATPase subunit alpha-1	11.72	0.95
ABCG2_MOUSE	ATP-binding cassette sub-family G member 2	11.70	0.86
AADAT_MOUSE	Kynurenine/alpha-aminoadipate aminotransferase, mitochondrial	11.59	0.80
ACS2L_MOUSE	Acetyl-coenzyme A synthetase 2-like, mitochondrial	11.31	0.83
MPC2_MOUSE	Mitochondrial pyruvate carrier 2	11.30	0.90
CGL_MOUSE	Cystathionine gamma-lyase	11.29	0.83
ODBB_MOUSE	2-oxoisovalerate dehydrogenase subunit beta, mitochondrial	11.28	0.81
CES1D_MOUSE	Carboxylesterase 1D	11.28	0.87

GSTK1_MOUSE	Glutathione S-transferase kappa 1	11.23	0.85
UD3A2_MOUSE	UDP-glucuronosyltransferase 3A2	11.11	0.81
SC5A2_MOUSE	Sodium/glucose cotransporter 2	11.10	0.81
INMT_MOUSE	Indolethylamine N-methyltransferase	11.06	0.85
ACSM1_MOUSE	Acyl-coenzyme A synthetase ACSM1, mitochondrial	11.05	0.89
S23A1_MOUSE	Solute carrier family 23 member 1	10.96	0.83
SOX_MOUSE	Peroxisomal sarcosine oxidase	10.94	0.84
CK054_MOUSE	Ester hydrolase C11orf54 homolog	10.86	0.81
NUD19_MOUSE	Nucleoside diphosphate-linked moiety X motif 19	10.83	0.87
PPR1A_MOUSE	Protein phosphatase 1 regulatory subunit 1A	10.83	0.88
G6PC_MOUSE	Glucose-6-phosphatase	10.79	0.83
HINT2_MOUSE	Histidine triad nucleotide-binding protein 2, mitochondrial	10.77	0.94
MEP1A_MOUSE	Meprin A subunit alpha	10.75	0.89
COX3_MOUSE	Cytochrome c oxidase subunit 3	10.56	0.91
SUCB2_MOUSE	Succinyl-CoA ligase [GDP-forming] subunit beta, mitochondrial	10.47	0.92
CLYBL_MOUSE	Citrate lyase subunit beta-like protein, mitochondrial	10.40	0.83
CISD1_MOUSE	CDGSH iron-sulfur domain-containing protein 1	10.36	0.94
M2GD_MOUSE	Dimethylglycine dehydrogenase, mitochondrial	10.33	0.83
COA6_MOUSE	Cytochrome c oxidase assembly factor 6 homolog	10.29	0.81
MCCB_MOUSE	Methylcrotonoyl-CoA carboxylase beta chain, mitochondrial	10.25	0.86
S22A8_MOUSE	Solute carrier family 22 member 8	10.19	0.80
ACSL1_MOUSE	Long-chain-fatty-acid--CoA ligase 1	10.18	0.86
NDUA3_MOUSE	NADH dehydrogenase [ubiquinone] 1 alpha subcomplex subunit 3	10.14	0.84
IVD_MOUSE	Isovaleryl-CoA dehydrogenase, mitochondrial	10.09	0.86
MPC1_MOUSE	Mitochondrial pyruvate carrier 1	9.89	0.80
THNS2_MOUSE	Threonine synthase-like 2	9.82	0.82
NDUV1_MOUSE	NADH dehydrogenase [ubiquinone] flavoprotein 1, mitochondrial	9.81	0.92
NHRF3_MOUSE	Na(+)/H(+) exchange regulatory cofactor NHE-RF3	9.66	0.90
ETFA_MOUSE	Electron transfer flavoprotein subunit alpha, mitochondrial	9.66	0.92
AUHM_MOUSE	Methylglutaconyl-CoA hydratase, mitochondrial	9.63	0.89
THTR_MOUSE	Thiosulfate sulfurtransferase	9.59	0.89
SUCHY_MOUSE	Succinate--hydroxymethylglutarate CoA-transferase	9.59	0.85
3HIDH_MOUSE	3-hydroxyisobutyrate dehydrogenase, mitochondrial	9.57	0.93
CATA_MOUSE	Catalase	9.51	0.94
UK114_MOUSE	Ribonuclease UK114	9.50	0.90
THIL_MOUSE	Acetyl-CoA acetyltransferase, mitochondrial	9.43	0.96
AK1A1_MOUSE	Alcohol dehydrogenase [NADP(+)]	9.38	0.92
MIRO2_MOUSE	Mitochondrial Rho GTPase 2	9.35	0.87
NDUC2_MOUSE	NADH dehydrogenase [ubiquinone] 1 subunit C2	9.30	0.84
TMM27_MOUSE	Collectrin	9.30	0.85
HMGCL_MOUSE	Hydroxymethylglutaryl-CoA lyase, mitochondrial	9.29	0.89
THIM_MOUSE	3-ketoacyl-CoA thiolase, mitochondrial	9.09	0.88
SODM_MOUSE	Superoxide dismutase [Mn], mitochondrial	9.08	0.88
MUTA_MOUSE	Methylmalonyl-CoA mutase, mitochondrial	9.08	0.83
COX5B_MOUSE	Cytochrome c oxidase subunit 5B, mitochondrial	9.07	0.90
HCDH_MOUSE	Hydroxyacyl-coenzyme A dehydrogenase, mitochondrial	9.04	0.89
COQ9_MOUSE	Ubiquinone biosynthesis protein COQ9, mitochondrial	9.02	0.81
SUCA_MOUSE	Succinyl-CoA ligase [ADP/GDP-forming] subunit alpha, mitochondrial	9.00	0.93
HOT_MOUSE	Hydroxyacid-oxoacid transhydrogenase, mitochondrial	8.97	0.83
AK1CL_MOUSE	Aldo-keto reductase family 1 member C21	8.97	0.84
MSRA_MOUSE	Mitochondrial peptide methionine sulfoxide reductase	8.95	0.89
ACD10_MOUSE	Acyl-CoA dehydrogenase family member 10	8.94	0.89
S12A1_MOUSE	Solute carrier family 12 member 1	8.90	0.85
ACON_MOUSE	Aconitate hydratase, mitochondrial	8.88	0.88
SCOT1_MOUSE	Succinyl-CoA:3-ketoacid coenzyme A transferase 1, mitochondrial	8.85	0.91
NHRF1_MOUSE	Na(+)/H(+) exchange regulatory cofactor NHE-RF1	8.85	0.91
GLNA_MOUSE	Glutamine synthetase	8.84	0.83
MAAI_MOUSE	Maleylacetoacetate isomerase	8.83	0.82
ETFB_MOUSE	Electron transfer flavoprotein subunit beta	8.78	0.92
UCRI_MOUSE	Cytochrome b-c1 complex subunit Rieske, mitochondrial	8.74	0.84
QCR8_MOUSE	Cytochrome b-c1 complex subunit 8	8.65	0.92
AL1L1_MOUSE	Cytosolic 10-formyltetrahydrofolate dehydrogenase	8.63	0.92
ARK72_MOUSE	Aflatoxin B1 aldehyde reductase member 2	8.60	0.85
IDHP_MOUSE	Isocitrate dehydrogenase [NADP], mitochondrial	8.56	0.93
ACPM_MOUSE	Acyl carrier protein, mitochondrial	8.43	0.92
QOR_MOUSE	Quinone oxidoreductase	8.40	0.93
NDUBA_MOUSE	NADH dehydrogenase [ubiquinone] 1 beta subcomplex subunit 10	8.40	0.86
CX7A2_MOUSE	Cytochrome c oxidase subunit 7A2, mitochondrial	8.39	0.84
NDRG1_MOUSE	Protein NDRG1	8.36	0.98
PCCA_MOUSE	Propionyl-CoA carboxylase alpha chain, mitochondrial	8.33	0.91
PHS_MOUSE	Pterin-4-alpha-carbinolamine dehydratase	8.31	0.82
AQP1_MOUSE	Aquaporin-1	8.29	0.88
MEP1B_MOUSE	Meprin A subunit beta	8.27	0.80

ECHD1_MOUSE	Ethylmalonyl-CoA decarboxylase	8.24	0.86
IDHG1_MOUSE	Isocitrate dehydrogenase [NAD] subunit gamma 1, mitochondrial	8.20	0.89
PGAM2_MOUSE	Phosphoglycerate mutase 2	8.19	0.82
QCR2_MOUSE	Cytochrome b-c1 complex subunit 2, mitochondrial	8.19	0.97
LRP2_MOUSE	Low-density lipoprotein receptor-related protein 2	8.16	0.83
COX5A_MOUSE	Cytochrome c oxidase subunit 5A, mitochondrial	8.11	0.93
AKC1H_MOUSE	Aldo-keto reductase family 1 member C18	8.07	0.87
NDUB7_MOUSE	NADH dehydrogenase [ubiquinone] 1 beta subcomplex subunit 7	8.05	0.90
NDUB4_MOUSE	NADH dehydrogenase [ubiquinone] 1 beta subcomplex subunit 4	8.03	0.83
SDHB_MOUSE	Succinate dehydrogenase [ubiquinone] iron-sulfur subunit, mitochondrial	8.00	0.83
ECI2_MOUSE	Enoyl-CoA delta isomerase 2, mitochondrial	7.96	0.85
AIFM1_MOUSE	Apoptosis-inducing factor 1, mitochondrial	7.96	0.92
ECHM_MOUSE	Enoyl-CoA hydratase, mitochondrial	7.96	0.90
ENPP3_MOUSE	Ectonucleotide pyrophosphatase/phosphodiesterase family member 3	7.92	0.81
OCTC_MOUSE	Peroxisomal carnitine O-octanoyltransferase	7.84	0.82
LDHD_MOUSE	Probable D-lactate dehydrogenase, mitochondrial	7.83	0.88
MCCA_MOUSE	Methylcrotonoyl-CoA carboxylase subunit alpha, mitochondrial	7.81	0.82
SDHA_MOUSE	Succinate dehydrogenase [ubiquinone] flavoprotein subunit, mitochondrial	7.80	0.97
RM23_MOUSE	39S ribosomal protein L23, mitochondrial	7.79	0.81
NEP_MOUSE	Neprilysin	7.78	0.89
NDUA2_MOUSE	NADH dehydrogenase [ubiquinone] 1 alpha subcomplex subunit 2	7.78	0.83
ABCD3_MOUSE	ATP-binding cassette sub-family D member 3	7.75	0.90
NDUS1_MOUSE	NADH-ubiquinone oxidoreductase 75 kDa subunit, mitochondrial	7.74	0.90
DIC_MOUSE	Mitochondrial dicarboxylate carrier	7.73	0.91
CY1_MOUSE	Cytochrome c1, heme protein, mitochondrial	7.72	0.93
ATPD_MOUSE	ATP synthase subunit delta, mitochondrial	7.68	0.95
CMC2_MOUSE	Calcium-binding mitochondrial carrier protein Aralar2	7.66	0.89
S13A3_MOUSE	Solute carrier family 13 member 3	7.65	0.84
ATPG_MOUSE	ATP synthase subunit gamma, mitochondrial	7.65	0.92
CRYL1_MOUSE	Lambda-crystallin homolog	7.64	0.89
RT36_MOUSE	28S ribosomal protein S36, mitochondrial	7.64	0.91
C560_MOUSE	Succinate dehydrogenase cytochrome b560 subunit, mitochondrial	7.63	0.92
NIPS1_MOUSE	Protein NipSnap homolog 1	7.62	0.90
3BHS4_MOUSE	3 beta-hydroxysteroid dehydrogenase type 4	7.58	0.81
CYC_MOUSE	Cytochrome c, somatic	7.56	0.90
NDUS7_MOUSE	NADH dehydrogenase [ubiquinone] iron-sulfur protein 7, mitochondrial	7.49	0.85
IPYR2_MOUSE	Inorganic pyrophosphatase 2, mitochondrial	7.47	0.90
NDUA4_MOUSE	Cytochrome c oxidase subunit NDUFA4	7.39	0.88
NDUS6_MOUSE	NADH dehydrogenase [ubiquinone] iron-sulfur protein 6, mitochondrial	7.39	0.82
COX41_MOUSE	Cytochrome c oxidase subunit 4 isoform 1, mitochondrial	7.37	0.93
KAT3_MOUSE	Kynurenine--oxoglutarate transaminase 3	7.36	0.82
BCAT2_MOUSE	Branched-chain-amino-acid aminotransferase, mitochondrial	7.36	0.89
ATPK_MOUSE	ATP synthase subunit f, mitochondrial	7.34	0.83
NCEH1_MOUSE	Neutral cholesterol ester hydrolase 1	7.34	0.94
BPNT1_MOUSE	3'(2'),5'-bisphosphate nucleotidase 1	7.34	0.81
NDUAA_MOUSE	NADH dehydrogenase [ubiquinone] 1 alpha subcomplex subunit 10, mitochondrial	7.33	0.90
CX6B1_MOUSE	Cytochrome c oxidase subunit 6B1	7.32	0.88
CMBL_MOUSE	Carboxymethylenebutenolidase homolog	7.32	0.80
CBR1_MOUSE	Carbonyl reductase [NADPH] 1	7.30	0.94
ATP5J_MOUSE	ATP synthase-coupling factor 6, mitochondrial	7.30	0.93
TBA4A_MOUSE	Tubulin alpha-4A chain	7.28	0.81
QCR7_MOUSE	Cytochrome b-c1 complex subunit 7	7.28	0.88
SFXN1_MOUSE	Sideroflexin-1	7.20	0.86
ATPB_MOUSE	ATP synthase subunit beta, mitochondrial	7.19	0.96
ADT2_MOUSE	ADP/ATP translocase 2	7.18	0.88
SBP1_MOUSE	Selenium-binding protein 1	7.18	0.89
NDUS2_MOUSE	NADH dehydrogenase [ubiquinone] iron-sulfur protein 2, mitochondrial	7.15	0.86
AL7A1_MOUSE	Alpha-aminoadipic semialdehyde dehydrogenase	7.15	0.87
COX2_MOUSE	Cytochrome c oxidase subunit 2	7.15	0.86
DLDH_MOUSE	Dihydrolipoyl dehydrogenase, mitochondrial	7.11	0.93
AL9A1_MOUSE	4-trimethylaminobutyraldehyde dehydrogenase	7.09	0.92
DHRS4_MOUSE	Dehydrogenase/reductase SDR family member 4	7.08	0.95
SUCB1_MOUSE	Succinyl-CoA ligase [ADP-forming] subunit beta, mitochondrial	7.07	0.93
CH60_MOUSE	60 kDa heat shock protein, mitochondrial	7.07	0.96
NU3M_MOUSE	NADH-ubiquinone oxidoreductase chain 3	7.06	0.95
ATP5I_MOUSE	ATP synthase subunit e, mitochondrial	7.06	0.86
AT5F1_MOUSE	ATP synthase F(0) complex subunit B1, mitochondrial	7.03	0.92
ATPA_MOUSE	ATP synthase subunit alpha, mitochondrial	7.02	0.96
NDUB9_MOUSE	NADH dehydrogenase [ubiquinone] 1 beta subcomplex subunit 9	7.01	0.84
MDHM_MOUSE	Malate dehydrogenase, mitochondrial	6.97	0.94
NDUA7_MOUSE	NADH dehydrogenase [ubiquinone] 1 alpha subcomplex subunit 7	6.97	0.87

USMG5_MOUSE	Up-regulated during skeletal muscle growth protein 5	6.93	0.97
SFXN2_MOUSE	Sideroflexin-2	6.90	0.82
NDUA9_MOUSE	NADH dehydrogenase [ubiquinone] 1 alpha subcomplex subunit 9, mitochondrial	6.86	0.91
PTER_MOUSE	Phosphotriesterase-related protein	6.85	0.94
ATPO_MOUSE	ATP synthase subunit O, mitochondrial	6.83	0.96
FUMH_MOUSE	Fumarate hydratase, mitochondrial	6.82	0.89
FOLH1_MOUSE	Glutamate carboxypeptidase 2	6.81	0.80
ACOT2_MOUSE	Acyl-coenzyme A thioesterase 2, mitochondrial	6.79	0.80
FABPH_MOUSE	Fatty acid-binding protein, heart	6.78	0.84
NLTP_MOUSE	Non-specific lipid-transfer protein	6.73	0.91
NDUS4_MOUSE	NADH dehydrogenase [ubiquinone] iron-sulfur protein 4, mitochondrial	6.72	0.85
ODO2_MOUSE	Dihydrolipoyllysine-residue succinyltransferase component of 2-oxoglutarate dehydrogenase complex, mitochondrial	6.71	0.91
NDUA5_MOUSE	NADH dehydrogenase [ubiquinone] 1 alpha subcomplex subunit 5	6.71	0.89
ATP5H_MOUSE	ATP synthase subunit d, mitochondrial	6.70	0.94
ODPA_MOUSE	Pyruvate dehydrogenase E1 component subunit alpha, somatic form, mitochondrial	6.70	0.93
QCR1_MOUSE	Cytochrome b-c1 complex subunit 1, mitochondrial	6.69	0.93
NDUBB_MOUSE	NADH dehydrogenase [ubiquinone] 1 beta subcomplex subunit 11, mitochondrial	6.67	0.93
MIC13_MOUSE	MICOS complex subunit MIC13	6.57	0.92
COX7C_MOUSE	Cytochrome c oxidase subunit 7C, mitochondrial	6.57	0.80
GSH1_MOUSE	Glutamate--cysteine ligase catalytic subunit	6.57	0.85
CSAD_MOUSE	Cysteine sulfinic acid decarboxylase	6.56	0.91
ETHE1_MOUSE	Persulfide dioxygenase ETHE1, mitochondrial	6.52	0.93
NDUS3_MOUSE	NADH dehydrogenase [ubiquinone] iron-sulfur protein 3, mitochondrial	6.51	0.94
TPMT_MOUSE	Thiopurine S-methyltransferase	6.43	0.93
ATP8_MOUSE	ATP synthase protein 8	6.43	0.81
NDUAD_MOUSE	NADH dehydrogenase [ubiquinone] 1 alpha subcomplex subunit 13	6.42	0.94
ES1_MOUSE	ES1 protein homolog, mitochondrial	6.41	0.91
AATM_MOUSE	Aspartate aminotransferase, mitochondrial	6.39	0.97
NU5M_MOUSE	NADH-ubiquinone oxidoreductase chain 5	6.35	0.86
MIC60_MOUSE	MICOS complex subunit Mic60	6.32	0.93
ACADS_MOUSE	Short-chain specific acyl-CoA dehydrogenase, mitochondrial	6.28	0.89
ARLY_MOUSE	Argininosuccinate lyase	6.28	0.92
NU4M_MOUSE	NADH-ubiquinone oxidoreductase chain 4	6.28	0.88
ODP2_MOUSE	Dihydrolipoyllysine-residue acetyltransferase component of pyruvate dehydrogenase complex, mitochondrial	6.28	0.94
UD3A1_MOUSE	UDP-glucuronosyltransferase 3A1	6.24	0.84
MARC2_MOUSE	Mitochondrial amidoxime reducing component 2	6.22	0.91
NDUS8_MOUSE	NADH dehydrogenase [ubiquinone] iron-sulfur protein 8, mitochondrial	6.20	0.86
ENTP5_MOUSE	Ectonucleoside triphosphate diphosphohydrolase 5	6.15	0.80
COX6C_MOUSE	Cytochrome c oxidase subunit 6C	6.11	0.89
ODPB_MOUSE	Pyruvate dehydrogenase E1 component subunit beta, mitochondrial	6.07	0.97
GSHB_MOUSE	Glutathione synthetase	6.07	0.89
QCR6_MOUSE	Cytochrome b-c1 complex subunit 6, mitochondrial	6.06	0.93
KAD2_MOUSE	Adenylate kinase 2, mitochondrial	6.06	0.89
PRDX3_MOUSE	Thioredoxin-dependent peroxide reductase, mitochondrial	6.04	0.89
TRAP1_MOUSE	Heat shock protein 75 kDa, mitochondrial	6.02	0.89
ACOX3_MOUSE	Peroxisomal acyl-coenzyme A oxidase 3	6.00	0.82
CPT2_MOUSE	Carnitine O-palmitoyltransferase 2, mitochondrial	5.99	0.85
VATA_MOUSE	V-type proton ATPase catalytic subunit A	5.96	0.93
CX7A1_MOUSE	Cytochrome c oxidase subunit 7A1, mitochondrial	5.92	0.88
VATH_MOUSE	V-type proton ATPase subunit H	5.88	0.91
NDUA8_MOUSE	NADH dehydrogenase [ubiquinone] 1 alpha subcomplex subunit 8	5.86	0.89
CH10_MOUSE	10 kDa heat shock protein, mitochondrial	5.86	0.90
MIC19_MOUSE	MICOS complex subunit Mic19	5.85	0.86
PGES2_MOUSE	Prostaglandin E synthase 2	5.84	0.81
PRDX5_MOUSE	Peroxiredoxin-5, mitochondrial	5.81	0.91
ACADV_MOUSE	Very long-chain specific acyl-CoA dehydrogenase, mitochondrial	5.79	0.85
MPCP_MOUSE	Phosphate carrier protein, mitochondrial	5.78	0.94
ODO1_MOUSE	2-oxoglutarate dehydrogenase, mitochondrial	5.76	0.89
SUSD2_MOUSE	Sushi domain-containing protein 2	5.75	0.93
CHDH_MOUSE	Choline dehydrogenase, mitochondrial	5.69	0.88
MAOX_MOUSE	NADP-dependent malic enzyme	5.68	0.87
DCXR_MOUSE	L-xylulose reductase	5.66	0.83
DYR_MOUSE	Dihydrofolate reductase	5.65	0.82
DECR_MOUSE	2,4-dienoyl-CoA reductase, mitochondrial	5.63	0.88
DAB2_MOUSE	Disabled homolog 2	5.62	0.80
SAM50_MOUSE	Sorting and assembly machinery component 50 homolog	5.60	0.90
DHB8_MOUSE	Estradiol 17-beta-dehydrogenase 8	5.55	0.81
SAHH3_MOUSE	Putative adenosylhomocysteinase 3	5.54	0.83

ECI1_MOUSE	Enoyl-CoA delta isomerase 1, mitochondrial	5.51	0.90
VDAC1_MOUSE	Voltage-dependent anion-selective channel protein 1	5.49	0.96
ETFD_MOUSE	Electron transfer flavoprotein-ubiquinone oxidoreductase, mitochondrial	5.49	0.90
CLPX_MOUSE	ATP-dependent Clp protease ATP-binding subunit clpX-like, mitochondrial	5.48	0.91
ALDH2_MOUSE	Aldehyde dehydrogenase, mitochondrial	5.48	0.94
VATE1_MOUSE	V-type proton ATPase subunit E 1	5.47	0.92
TIM8A_MOUSE	Mitochondrial import inner membrane translocase subunit Tim8 A	5.45	0.84
MIA40_MOUSE	Mitochondrial intermembrane space import and assembly protein 40	5.45	0.86
DHPR_MOUSE	Dihydropteridine reductase	5.45	0.91
MDHC_MOUSE	Malate dehydrogenase, cytoplasmic	5.41	0.94
VATF_MOUSE	V-type proton ATPase subunit F	5.40	0.88
SCRN2_MOUSE	Secernin-2	5.37	0.83
SAP3_MOUSE	Ganglioside GM2 activator	5.34	0.85
TIM13_MOUSE	Mitochondrial import inner membrane translocase subunit Tim13	5.33	0.89
ACOC_MOUSE	Cytoplasmic aconitate hydratase	5.32	0.88
ECH1_MOUSE	Delta(3,5)-Delta(2,4)-dienoyl-CoA isomerase, mitochondrial	5.27	0.95
LYZ2_MOUSE	Lysozyme C-2	5.25	0.87
CP013_MOUSE	UPF0585 protein C16orf13 homolog	5.23	0.83
CCS_MOUSE	Copper chaperone for superoxide dismutase	5.23	0.83
NDUS5_MOUSE	NADH dehydrogenase [ubiquinone] iron-sulfur protein 5	5.22	0.85
AACS_MOUSE	Acetoacetyl-CoA synthetase	5.22	0.81
IDH3A_MOUSE	Isocitrate dehydrogenase [NAD] subunit alpha, mitochondrial	5.19	0.93
DHE3_MOUSE	Glutamate dehydrogenase 1, mitochondrial	5.15	0.93
NDUA6_MOUSE	NADH dehydrogenase [ubiquinone] 1 alpha subcomplex subunit 6	5.11	0.87
DOPD_MOUSE	D-dopachrome decarboxylase	5.10	0.95
P5CR3_MOUSE	Pyrroline-5-carboxylate reductase 3	5.08	0.84
THIC_MOUSE	Acetyl-CoA acetyltransferase, cytosolic	5.08	0.81
THTM_MOUSE	3-mercaptopyruvate sulfurtransferase	5.06	0.82
THIOM_MOUSE	Thioredoxin, mitochondrial	5.05	0.95
SQRD_MOUSE	Sulfide:quinone oxidoreductase, mitochondrial	5.04	0.89
SPS2_MOUSE	Selenide, water dikinase 2	5.03	0.84
CMC1_MOUSE	Calcium-binding mitochondrial carrier protein Aralar1	5.01	0.86
HCD2_MOUSE	3-hydroxyacyl-CoA dehydrogenase type-2	5.00	0.94
LPPRC_MOUSE	Leucine-rich PPR motif-containing protein, mitochondrial	4.96	0.85
4F2_MOUSE	4F2 cell-surface antigen heavy chain	4.94	0.93
VATB2_MOUSE	V-type proton ATPase subunit B, brain isoform	4.92	0.91
ACDSB_MOUSE	Short/branched chain specific acyl-CoA dehydrogenase, mitochondrial	4.89	0.94
ABHEB_MOUSE	Protein ABHD14B	4.87	0.91
IDHC_MOUSE	Isocitrate dehydrogenase [NADP] cytoplasmic	4.87	0.91
NIT1_MOUSE	Nitrilase homolog 1	4.86	0.89
TIM9_MOUSE	Mitochondrial import inner membrane translocase subunit Tim9	4.85	0.81
OPA1_MOUSE	Dynamin-like 120 kDa protein, mitochondrial	4.84	0.86
RM12_MOUSE	39S ribosomal protein L12, mitochondrial	4.83	0.93
GSTT2_MOUSE	Glutathione S-transferase theta-2	4.83	0.82
GLYC_MOUSE	Serine hydroxymethyltransferase, cytosolic	4.75	0.85
KAD3_MOUSE	GTP:AMP phosphotransferase AK3, mitochondrial	4.75	0.89
VATG3_MOUSE	V-type proton ATPase subunit G 3	4.74	0.84
EFTU_MOUSE	Elongation factor Tu, mitochondrial	4.73	0.95
ECHA_MOUSE	Trifunctional enzyme subunit alpha, mitochondrial	4.67	0.96
GRP75_MOUSE	Stress-70 protein, mitochondrial	4.62	0.85
LYPA1_MOUSE	Acyl-protein thioesterase 1	4.62	0.88
ACADL_MOUSE	Long-chain specific acyl-CoA dehydrogenase, mitochondrial	4.56	0.95
BASI_MOUSE	Basigin	4.56	0.82
VATD_MOUSE	V-type proton ATPase subunit D	4.54	0.86
CLPP_MOUSE	ATP-dependent Clp protease proteolytic subunit, mitochondrial	4.51	0.87
MIC27_MOUSE	MICOS complex subunit Mic27	4.49	0.87
EM55_MOUSE	55 kDa erythrocyte membrane protein	4.48	0.86
LETM1_MOUSE	LETM1 and EF-hand domain-containing protein 1, mitochondrial	4.47	0.86
ECHB_MOUSE	Trifunctional enzyme subunit beta, mitochondrial	4.43	0.89
IAH1_MOUSE	Isoamyl acetate-hydrolyzing esterase 1 homolog	4.35	0.82
ANK3_MOUSE	Ankyrin-3	4.33	0.84
ATAD3_MOUSE	ATPase family AAA domain-containing protein 3	4.33	0.87
MTCH2_MOUSE	Mitochondrial carrier homolog 2	4.32	0.89
M2OM_MOUSE	Mitochondrial 2-oxoglutarate/malate carrier protein	4.29	0.88
MOT1_MOUSE	Monocarboxylate transporter 1	4.28	0.80
AMPN_MOUSE	Aminopeptidase N	4.26	0.94
OAT_MOUSE	Ornithine aminotransferase, mitochondrial	4.26	0.86
LDHB_MOUSE	L-lactate dehydrogenase B chain	4.24	0.86
ACOT1_MOUSE	Acyl-coenzyme A thioesterase 1	4.21	0.85
GLRX5_MOUSE	Glutaredoxin-related protein 5, mitochondrial	4.20	0.86
CPT1A_MOUSE	Carnitine O-palmitoyltransferase 1, liver isoform	4.20	0.85
NIT2_MOUSE	Omega-amidase NIT2	4.19	0.90

KCRU_MOUSE	Creatine kinase U-type, mitochondrial	4.16	0.84
NDUA1_MOUSE	NADH dehydrogenase [ubiquinone] 1 alpha subcomplex subunit 1	4.12	0.86
ADT1_MOUSE	ADP/ATP translocase 1	4.11	0.85
CACP_MOUSE	Carnitine O-acetyltransferase	4.11	0.82
GSH0_MOUSE	Glutamate--cysteine ligase regulatory subunit	4.07	0.84
XPP1_MOUSE	Xaa-Pro aminopeptidase 1	4.05	0.85
VATC1_MOUSE	V-type proton ATPase subunit C 1	3.94	0.85
GPX1_MOUSE	Glutathione peroxidase 1	3.91	0.94
DHB4_MOUSE	Peroxisomal multifunctional enzyme type 2	3.87	0.94
LONM_MOUSE	Lon protease homolog, mitochondrial	3.87	0.90
PHB2_MOUSE	Prohibitin-2	3.84	0.93
EFTS_MOUSE	Elongation factor Ts, mitochondrial	3.83	0.83
ESTD_MOUSE	S-formylglutathione hydrolase	3.80	0.88
MIF_MOUSE	Macrophage migration inhibitory factor	3.79	0.89
ATIF1_MOUSE	ATPase inhibitor, mitochondrial	3.71	0.83
CISY_MOUSE	Citrate synthase, mitochondrial	3.69	0.89
KAT1_MOUSE	Kynurenine--oxoglutarate transaminase 1	3.63	0.82
AMPL_MOUSE	Cytosol aminopeptidase	3.63	0.93
C1QBP_MOUSE	Complement component 1 Q subcomponent-binding protein, mitochondrial	3.63	0.92
GSTM5_MOUSE	Glutathione S-transferase Mu 5	3.62	0.89
AMPE_MOUSE	Glutamyl aminopeptidase	3.60	0.86
CYB5_MOUSE	Cytochrome b5	3.60	0.89
TMM65_MOUSE	Transmembrane protein 65	3.59	0.91
ATAD1_MOUSE	ATPase family AAA domain-containing protein 1	3.57	0.85
41_MOUSE	Protein 4.1	3.55	0.83
AATC_MOUSE	Aspartate aminotransferase, cytoplasmic	3.51	0.89
PHB_MOUSE	Prohibitin	3.45	0.93
ACBP_MOUSE	Acyl-CoA-binding protein	3.42	0.96
EZRI_MOUSE	Ezrin	3.41	0.96
NPL_MOUSE	N-acetylneuraminate lyase	3.41	0.86
RADI_MOUSE	Radixin	3.39	0.89
PGK1_MOUSE	Phosphoglycerate kinase 1	3.35	0.97
GNPI1_MOUSE	Glucosamine-6-phosphate isomerase 1	3.33	0.88
MYO6_MOUSE	Unconventional myosin-VI	3.31	0.85
F213A_MOUSE	Redox-regulatory protein FAM213A	3.31	0.83
SPRE_MOUSE	Sepiapterin reductase	3.28	0.96
TIM50_MOUSE	Mitochondrial import inner membrane translocase subunit TIM50	3.27	0.89
SYIM_MOUSE	Isoleucine--tRNA ligase, mitochondrial	3.27	0.83
TXTP_MOUSE	Tricarboxylate transport protein, mitochondrial	3.23	0.83
DHI2_MOUSE	Corticosteroid 11-beta-dehydrogenase isozyme 2	3.22	0.88
SODC_MOUSE	Superoxide dismutase [Cu-Zn]	3.22	0.95
PROSC_MOUSE	Proline synthase co-transcribed bacterial homolog protein	3.21	0.89
AKCL2_MOUSE	1,5-anhydro-D-fructose reductase	3.19	0.82
VA0D1_MOUSE	V-type proton ATPase subunit d 1	3.19	0.87
PGM1_MOUSE	Phosphoglucomutase-1	3.15	0.85
PTGR2_MOUSE	Prostaglandin reductase 2	3.15	0.92
VDAC2_MOUSE	Voltage-dependent anion-selective channel protein 2	3.13	0.93
HINT1_MOUSE	Histidine triad nucleotide-binding protein 1	3.06	0.95
NOMO1_MOUSE	Nodal modulator 1	3.03	0.81
PDXK_MOUSE	Pyridoxal kinase	3.01	0.92
CAH2_MOUSE	Carbonic anhydrase 2	2.99	0.96
APMAP_MOUSE	Adipocyte plasma membrane-associated protein	2.93	0.85
FIS1_MOUSE	Mitochondrial fission 1 protein	2.91	0.88
GSTA4_MOUSE	Glutathione S-transferase A4	2.89	0.87
CLIC5_MOUSE	Chloride intracellular channel protein 5	2.86	0.81
THIKA_MOUSE	3-ketoacyl-CoA thiolase A, peroxisomal	2.81	0.82
LAD1_MOUSE	Ladinin-1	2.79	0.80
GLGB_MOUSE	1,4-alpha-glucan-branching enzyme	2.77	0.86
UGPA_MOUSE	UTP--glucose-1-phosphate uridylyltransferase	2.74	0.85
AL3A2_MOUSE	Fatty aldehyde dehydrogenase	2.74	0.86
SYPL1_MOUSE	Synaptophysin-like protein 1	2.73	1.00
TOM5_MOUSE	Mitochondrial import receptor subunit TOM5 homolog	2.69	0.88
HDHD2_MOUSE	Haloacid dehalogenase-like hydrolase domain-containing protein 2	2.66	0.82
TIM44_MOUSE	Mitochondrial import inner membrane translocase subunit TIM44	2.61	0.83
SAHH_MOUSE	Adenosylhomocysteinase	2.58	0.91
PARK7_MOUSE	Protein deglycase DJ-1	2.58	0.87
TPIS_MOUSE	Triosephosphate isomerase	2.56	0.83
HEM2_MOUSE	Delta-aminolevulinic acid dehydratase	2.54	0.91
HXK1_MOUSE	Hexokinase-1	2.51	0.92
ENOA_MOUSE	Alpha-enolase	2.47	0.98
PACN2_MOUSE	Protein kinase C and casein kinase substrate in neurons protein 2	2.46	0.88
ADHX_MOUSE	Alcohol dehydrogenase class-3	2.40	0.84

GBG12_MOUSE	Guanine nucleotide-binding protein G(I)/G(S)/G(O) subunit gamma-12	2.39	0.94
PGAM1_MOUSE	Phosphoglycerate mutase 1	2.39	0.95
BACH_MOUSE	Cytosolic acyl coenzyme A thioester hydrolase	2.38	0.81
SELT_MOUSE	Selenoprotein T	2.32	0.96
NNRD_MOUSE	ATP-dependent (S)-NAD(P)H-hydrate dehydratase	2.32	0.82
ADK_MOUSE	Adenosine kinase	2.31	0.83
CYB5B_MOUSE	Cytochrome b5 type B	2.29	0.90
GPD1L_MOUSE	Glycerol-3-phosphate dehydrogenase 1-like protein	2.26	0.85
GSTM1_MOUSE	Glutathione S-transferase Mu 1	2.22	0.89
NDKB_MOUSE	Nucleoside diphosphate kinase B	2.20	0.90
PRDX1_MOUSE	Peroxiredoxin-1	2.19	0.90
G3P_MOUSE	Glyceraldehyde-3-phosphate dehydrogenase	2.18	0.90
FUCM_MOUSE	Fucose mutarotase	2.15	0.88
RAB14_MOUSE	Ras-related protein Rab-14	2.13	0.83
UGDH_MOUSE	UDP-glucose 6-dehydrogenase	2.12	0.82
BIEA_MOUSE	Biliverdin reductase A	2.10	0.81
VPS35_MOUSE	Vacuolar protein sorting-associated protein 35	2.09	0.81
G6PI_MOUSE	Glucose-6-phosphate isomerase	2.07	0.96
GMPR1_MOUSE	GMP reductase 1	2.06	0.92
RAB8A_MOUSE	Ras-related protein Rab-8A	2.06	0.82
KCY_MOUSE	UMP-CMP kinase	2.04	0.83
PRDX6_MOUSE	Peroxiredoxin-6	2.03	0.96
CNDP2_MOUSE	Cytosolic non-specific dipeptidase	2.00	0.85
TMM33_MOUSE	Transmembrane protein 33	1.99	0.83
TMED4_MOUSE	Transmembrane emp24 domain-containing protein 4	1.95	0.86
COMT_MOUSE	Catechol O-methyltransferase	1.95	0.82
TXD17_MOUSE	Thioredoxin domain-containing protein 17	1.95	0.87
TBB4B_MOUSE	Tubulin beta-4B chain	1.95	1.00
PEBP1_MOUSE	Phosphatidylethanolamine-binding protein 1	1.95	0.95
RTN3_MOUSE	Reticulon-3	1.94	0.88
VAMP8_MOUSE	Vesicle-associated membrane protein 8	1.94	0.83
ERLN2_MOUSE	Erlin-2	1.87	0.80
GSTT1_MOUSE	Glutathione S-transferase theta-1	1.84	0.85
SPTN1_MOUSE	Spectrin alpha chain, non-erythrocytic 1	1.84	0.98
LGUL_MOUSE	Lactoylglutathione lyase	1.83	0.83
SPTB2_MOUSE	Spectrin beta chain, non-erythrocytic 1	1.83	0.85
ISOC1_MOUSE	Isochorismatase domain-containing protein 1	1.81	0.85
RASN_MOUSE	GTPase NRas	1.79	0.81
MAT2B_MOUSE	Methionine adenosyltransferase 2 subunit beta	1.78	0.96
GSTP1_MOUSE	Glutathione S-transferase P 1	1.74	0.93
HACD3_MOUSE	Very-long-chain (3R)-3-hydroxyacyl-CoA dehydratase 3	1.73	0.88
SNX3_MOUSE	Sorting nexin-3	1.73	0.85
GALK2_MOUSE	N-acetylgalactosamine kinase	1.72	0.81
VP26A_MOUSE	Vacuolar protein sorting-associated protein 26A	1.72	0.92
ITPR1_MOUSE	Inositol 1,4,5-trisphosphate receptor type 1	1.70	0.83
DNJA1_MOUSE	DnaJ homolog subfamily A member 1	1.70	0.81
RB11B_MOUSE	Ras-related protein Rab-11B	1.69	0.89
RS27L_MOUSE	40S ribosomal protein S27-like	1.65	0.86
PGRC1_MOUSE	Membrane-associated progesterone receptor component 1	1.65	0.84
PTH2_MOUSE	Peptidyl-tRNA hydrolase 2, mitochondrial	1.63	0.96
UAP1L_MOUSE	UDP-N-acetylhexosamine pyrophosphorylase-like protein 1	1.63	0.84
GLOD4_MOUSE	Glyoxalase domain-containing protein 4	1.62	0.87
ALDOA_MOUSE	Fructose-bisphosphate aldolase A	1.61	0.90
F10A1_MOUSE	Hsc70-interacting protein	1.61	0.85
ACLY_MOUSE	ATP-citrate synthase	1.60	0.85
GLRX1_MOUSE	Glutaredoxin-1	1.55	0.83
FKBP3_MOUSE	Peptidyl-prolyl cis-trans isomerase FKBP3	1.55	0.81
DPEP1_MOUSE	Dipeptidase 1	1.53	0.86
LDHA_MOUSE	L-lactate dehydrogenase A chain	1.52	0.88
HS90A_MOUSE	Heat shock protein HSP 90-alpha	1.46	0.82
SYSC_MOUSE	Serine--tRNA ligase, cytoplasmic	1.45	0.82
GPX3_MOUSE	Glutathione peroxidase 3	1.41	0.83
TKT_MOUSE	Transketolase	1.38	0.84
PRDX2_MOUSE	Peroxiredoxin-2	1.37	0.88

S.1.13 Comparison of UUO-differentially expressed proteins in WT and TG2-null mice

S.1.13.1 UUO-overexpressed proteins

Supplementary Table 3.17. List of proteins significantly overexpressed (confidence ≥ 0.8) in either WT or TG2-KO kidneys subjected to UUO (21 days) and corresponding fold change from Sham operated condition in both phenotypes. In increasing shade of red the positive log2 (Log2FC) of fold change from the sham operated condition (the more intense, the more overexpressed), in decreasing shades of green the negative log2 (Log2FC) of fold change from the sham operated condition (the more intense, the more underexpressed), in increasing shades of grey the absolute fold change from the sham operated condition (Abs FC, absolute increase or decrease depending on the sign of Log2FC) while in shades of yellow the confidence of the change (refer to the colour legend below). A confidence ≥ 0.8 was regarded as significant.

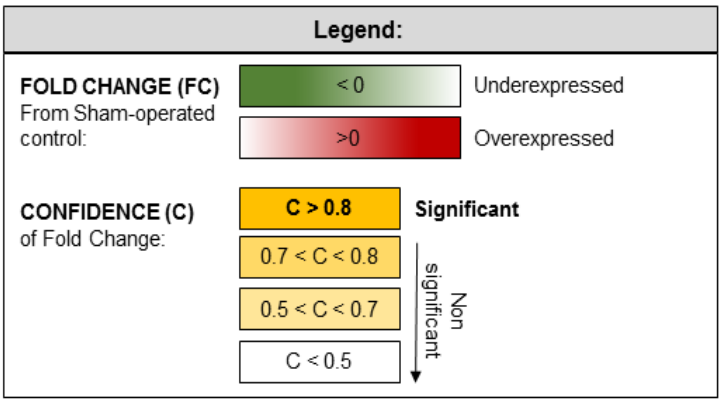

Unique/ Common	Protein ID _MOUSE	Name	WT			TG2-KO		
			Log2 (FC)	Abs (FC)	C (FC)	Log2 (FC)	Abs (FC)	C (FC)
WT ONLY	FBLN2	Fibulin-2	3.27	9.65	0.81	2.32	4.99	0.54
WT ONLY	CNN1	Calponin-1	3.10	8.59	0.80	3.45	10.90	0.80
WT ONLY	HA2U	H-2 class II histocompatibility antigen, A-U alpha chain	3.06	8.32	0.80	2.95	7.75	0.74
WT ONLY	MT2	Metallothionein-2	3.02	8.11	0.84	-3.36	10.27	0.09
WT ONLY	POSTN	Periostin	3.01	8.04	0.80	3.12	8.66	0.78
WT ONLY	A1AT2	Alpha-1-antitrypsin 1-2	2.97	7.86	0.82	1.31	2.48	0.48
WT ONLY	CKAP4	Cytoskeleton-associated protein 4	2.72	6.57	0.85	2.63	6.18	0.73
WT ONLY	RET1	Retinol-binding protein 1	2.48	5.56	0.83	2.31	4.95	0.78
WT ONLY	PDLI7	PDZ and LIM domain protein 7	2.43	5.40	0.81	2.36	5.13	0.64
WT ONLY	FIBA	Fibrinogen alpha chain	2.21	4.64	0.90	0.93	1.91	0.69
WT ONLY	CO4A2	Collagen alpha-2(IV) chain	2.17	4.50	0.80	1.45	2.73	0.79
WT ONLY	FIBG	Fibrinogen gamma chain	2.15	4.45	0.85	1.50	2.82	0.74
WT ONLY	PEDF	Pigment epithelium-derived factor	2.09	4.24	0.81	2.37	5.16	0.55
WT ONLY	FIBB	Fibrinogen beta chain	2.00	4.00	0.86	0.96	1.95	0.71
WT ONLY	SH3L3	SH3 domain-binding glutamic acid-rich-like protein 3	1.94	3.85	0.90	1.04	2.06	0.72
WT ONLY	CALU	Calumenin	1.88	3.69	0.84	1.55	2.93	0.80
WT ONLY	CRIP1	Cysteine-rich protein 1	1.83	3.55	0.90	1.82	3.52	0.55
WT ONLY	IGG2B	Ig gamma-2B chain C region	1.62	3.07	0.81	1.56	2.94	0.77
WT ONLY	K2C79	Keratin, type II cytoskeletal 79	1.61	3.05	0.91	0.65	1.57	0.56
WT ONLY	PTRF	Polymerase I and transcript release factor	1.57	2.96	0.84	0.74	1.67	0.69
WT ONLY	CERU	Ceruloplasmin	1.52	2.86	0.80	1.56	2.95	0.77
WT ONLY	GBG2	Guanine nucleotide-binding protein G(I)/G(S)/G(O) subunit gamma-2	1.40	2.65	0.81	1.25	2.39	0.78
WT ONLY	S10AA	Protein S100-A10	1.37	2.59	0.86	1.23	2.35	0.74
WT ONLY	SF3B3	Splicing factor 3B subunit 3	1.33	2.51	0.83	0.82	1.76	0.73
WT ONLY	ML12B	Myosin regulatory light chain 12B	1.22	2.33	0.83	1.21	2.32	0.73
WT ONLY	ANT3	Antithrombin-III	1.18	2.27	0.86	1.08	2.11	0.76
WT ONLY	AGRIN	Agrin	1.11	2.16	0.92	0.73	1.66	0.67
WT ONLY	KHDR1	KH domain-containing, RNA-binding, signal transduction-associated protein 1	1.10	2.14	0.84	0.93	1.90	0.52
WT ONLY	COR1B	Coronin-1B	1.04	2.06	0.86	0.42	1.34	0.55
WT ONLY	A2M	Pregnancy zone protein	1.03	2.05	0.85	1.18	2.26	0.72
WT ONLY	INO1	Inositol-3-phosphate synthase 1	1.02	2.03	0.81	0.89	1.85	0.59
WT ONLY	LIMA1	LIM domain and actin-binding protein 1	1.02	2.02	0.87	0.71	1.64	0.62
WT ONLY	ARPC3	Actin-related protein 2/3 complex subunit 3	1.01	2.01	0.87	0.95	1.93	0.80
WT ONLY	WDR1	WD repeat-containing protein 1	1.01	2.01	0.83	0.67	1.59	0.65
WT ONLY	ARPC2	Actin-related protein 2/3 complex subunit 2	0.91	1.87	0.83	0.55	1.46	0.79
WT ONLY	NH2L1	NHP2-like protein 1	0.90	1.86	0.81	0.66	1.58	0.53

WT ONLY	HNRPF	Heterogeneous nuclear ribonucleoprotein F	0.87	1.82	0.83	0.54	1.45	0.74
WT ONLY	FABP4	Fatty acid-binding protein, adipocyte	0.86	1.82	0.85	-0.76	1.69	0.78
WT ONLY	LASP1	LIM and SH3 domain protein 1	0.86	1.81	0.81	0.58	1.50	0.66
WT ONLY	ANXA4	Annexin A4	0.83	1.78	0.85	0.48	1.39	0.57
WT ONLY	FUBP2	Far upstream element-binding protein 2	0.83	1.78	0.80	0.76	1.69	0.78
WT ONLY	RUXF	Small nuclear ribonucleoprotein F	0.81	1.75	0.87	0.41	1.33	0.67
WT ONLY	CSRP2	Cysteine and glycine-rich protein 2	0.78	1.72	0.82	0.50	1.41	0.71
WT ONLY	TGM2	Transglutminase 2	0.78	1.71	0.90	-1.49	2.81	0.17
WT ONLY	LAP2B	Lamina-associated polypeptide 2, isoforms beta/delta/epsilon/gamma	0.77	1.71	0.80	0.67	1.59	0.78
WT ONLY	SRSF2	Serine/arginine-rich splicing factor 2	0.76	1.70	0.86	0.62	1.53	0.74
WT ONLY	1433G	14-3-3 protein gamma	0.72	1.65	0.81	0.43	1.35	0.65
WT ONLY	SMAP	Small acidic protein	0.71	1.64	0.88	0.36	1.28	0.24
WT ONLY	RSU1	Ras suppressor protein 1	0.67	1.59	0.84	0.57	1.48	0.68
WT ONLY	SC11A	Signal peptidase complex catalytic subunit SEC11A	0.67	1.59	0.80	0.47	1.39	0.78
WT ONLY	MOES	Moesin	0.60	1.52	0.81	0.44	1.36	0.57
WT ONLY	GDIR1	Rho GDP-dissociation inhibitor 1	0.60	1.51	0.84	0.41	1.33	0.64
WT ONLY	HNRH1	Heterogeneous nuclear ribonucleoprotein H	0.56	1.48	0.87	0.55	1.46	0.71
WT ONLY	KAPCA	cAMP-dependent protein kinase catalytic subunit alpha	0.53	1.44	0.89	0.56	1.47	0.78
WT ONLY	HNRPK	Heterogeneous nuclear ribonucleoprotein K	0.49	1.40	0.82	0.41	1.33	0.77
WT ONLY	LAMP1	Lysosome-associated membrane glycoprotein 1	0.47	1.38	0.81	0.28	1.22	0.42
COMMON	UROM	Uromodulin	4.03	16.34	0.85	3.29	9.78	0.88
COMMON	COCA1	Collagen alpha-1(XII) chain	3.99	15.92	0.82	4.71	26.15	0.83
COMMON	FBN1	Fibrillin-1	3.44	10.84	0.89	3.01	8.05	0.89
COMMON	K1C19	Keratin, type I cytoskeletal 19	3.26	9.57	0.86	2.99	7.95	0.89
COMMON	TAGL	Transgelin	3.21	9.27	0.89	2.78	6.86	0.89
COMMON	PGS1	Biglycan	3.13	8.73	0.86	3.30	9.86	0.87
COMMON	VIME	Vimentin	3.10	8.56	0.90	2.74	6.67	0.91
COMMON	ANXA1	Annexin A1	3.03	8.17	0.84	3.04	8.24	0.94
COMMON	FINC	Fibronectin	2.97	7.85	0.84	2.66	6.31	0.89
COMMON	COR1A	Coronin-1A	2.96	7.77	0.80	2.77	6.83	0.82
COMMON	CO3A1	Collagen alpha-1(III) chain	2.95	7.72	0.92	2.59	6.02	0.95
COMMON	PLSL	Plastin-2	2.93	7.63	0.85	2.25	4.77	0.82
COMMON	CO1A1	Collagen alpha-1(I) chain	2.93	7.61	0.96	2.73	6.64	0.96
COMMON	KCRB	Creatine kinase B-type	2.92	7.56	0.83	2.58	5.98	0.86
COMMON	FBN2	Fibrillin-2	2.86	7.26	0.94	3.86	14.52	0.89
COMMON	MIME	Mimecan	2.74	6.67	0.83	2.89	7.40	0.86
COMMON	LUM	Lumican	2.71	6.55	0.87	2.76	6.76	0.84
COMMON	FBLN3	EGF-containing fibulin-like extracellular matrix protein 1	2.66	6.33	0.80	2.42	5.35	0.87
COMMON	SERPH	Serpin H1	2.63	6.19	0.94	2.45	5.45	0.96
COMMON	CNN2	Calponin-2	2.62	6.15	0.80	2.04	4.11	0.84
COMMON	LEG1	Galectin-1	2.62	6.15	0.87	2.44	5.44	0.93
COMMON	DESM	Desmin	2.58	5.98	0.94	2.20	4.60	0.94
COMMON	FBLN5	Fibulin-5	2.54	5.81	0.84	2.43	5.38	0.87
COMMON	CLUS	Clusterin	2.42	5.35	0.81	2.10	4.30	0.86
COMMON	K2C5	Keratin, type II cytoskeletal 5	2.39	5.24	0.83	2.37	5.15	0.84
COMMON	FLNA	Filamin-A	2.34	5.07	0.93	2.19	4.56	0.95
COMMON	MYOF	Myoferlin	2.32	4.99	0.86	2.38	5.21	0.81
COMMON	K2C8	Keratin, type II cytoskeletal 8	2.30	4.93	0.89	2.09	4.26	0.94
COMMON	CO6A1	Collagen alpha-1(VI) chain	2.26	4.78	0.88	1.82	3.52	0.89
COMMON	CO6A2	Collagen alpha-2(VI) chain	2.25	4.76	0.94	1.77	3.40	0.92
COMMON	ANXA3	Annexin A3	2.24	4.73	0.83	1.61	3.05	0.82
COMMON	COEA1	Collagen alpha-1(XIV) chain	2.21	4.62	0.81	1.97	3.93	0.83
COMMON	HEMO	Hemopexin	2.20	4.60	0.86	1.81	3.50	0.82
COMMON	CSRP1	Cysteine and glycine-rich protein 1	2.18	4.52	0.89	1.87	3.65	0.92
COMMON	EMIL1	Emilin-1	2.15	4.42	0.82	2.25	4.77	0.89
COMMON	TBA1A	Tubulin alpha-1A chain	2.14	4.41	0.96	2.10	4.28	0.91
COMMON	TYB4	Thymosin beta-4	2.12	4.35	0.88	2.22	4.65	0.90
COMMON	TPM1	Tropomyosin alpha-1 chain	2.10	4.28	0.84	1.63	3.09	0.83
COMMON	K2C7	Keratin, type II cytoskeletal 7	2.09	4.27	0.88	1.78	3.43	0.88
COMMON	ACTN1	Alpha-actinin-1	2.08	4.22	0.96	1.89	3.72	0.96
COMMON	TPM4	Tropomyosin alpha-4 chain	2.07	4.19	0.91	2.02	4.06	0.91
COMMON	IGKC	Ig kappa chain C region	2.05	4.15	0.87	1.76	3.38	0.87
COMMON	MYADM	Myeloid-associated differentiation marker	2.00	4.00	0.87	1.86	3.62	0.92
COMMON	TRFE	Serotransferrin	1.92	3.78	0.91	1.42	2.67	0.89
COMMON	ANXA2	Annexin A2	1.91	3.76	0.90	1.61	3.06	0.90
COMMON	G6PE	GDH/6PGL endoplasmic bifunctional protein	1.89	3.71	0.90	1.80	3.49	0.85
COMMON	SPB6	Serpin B6	1.83	3.56	0.89	1.33	2.51	0.84
COMMON	EFHD2	EF-hand domain-containing protein D2	1.82	3.52	0.87	1.71	3.28	0.83
COMMON	ESYT1	Extended synaptotagmin-1	1.81	3.52	0.82	1.85	3.60	0.83
COMMON	LMNA	Prelamin-A/C	1.80	3.49	0.94	1.36	2.57	0.94
COMMON	CO4B	Complement C4-B	1.78	3.44	0.86	1.46	2.75	0.83
COMMON	ARC1B	Actin-related protein 2/3 complex subunit 1B	1.76	3.38	0.87	1.54	2.91	0.88
COMMON	TBB5	Tubulin beta-5 chain	1.74	3.33	0.88	1.45	2.72	0.90
COMMON	APOE	Apolipoprotein E	1.73	3.31	0.87	1.32	2.49	0.94
COMMON	MYH11	Myosin-11	1.71	3.28	0.87	1.52	2.87	0.92
COMMON	MYH10	Myosin-10	1.71	3.27	0.85	1.86	3.63	0.84
COMMON	FETUA	Alpha-2-HS-glycoprotein	1.71	3.27	0.90	1.35	2.54	0.94
COMMON	ESYT2	Extended synaptotagmin-2	1.69	3.23	0.86	1.60	3.03	0.83

COMMON	GCAB	Ig gamma-2A chain C region secreted form	1.68	3.21	0.91	2.07	4.20	0.82
COMMON	ACTA	Actin, aortic smooth muscle	1.67	3.17	0.94	1.46	2.76	0.85
COMMON	VTDB	Vitamin D-binding protein	1.65	3.13	0.93	1.19	2.28	0.89
COMMON	EST1C	Carboxylesterase 1C	1.64	3.11	0.95	1.34	2.52	0.94
COMMON	KNG1	Kininogen-1	1.63	3.09	0.91	1.35	2.54	0.92
COMMON	MYL9	Myosin regulatory light polypeptide 9	1.62	3.08	0.98	1.35	2.56	0.98
COMMON	S10AB	Protein S100-A11	1.62	3.08	0.88	1.77	3.40	0.88
COMMON	A1AT1	Alpha-1-antitrypsin 1-1	1.62	3.07	0.86	1.45	2.74	0.81
COMMON	SH3L1	SH3 domain-binding glutamic acid-rich-like protein	1.61	3.06	0.86	1.63	3.09	0.89
COMMON	TAGL2	Transgelin-2	1.60	3.04	0.88	1.66	3.16	0.87
COMMON	K1C18	Keratin, type I cytoskeletal 18	1.58	2.99	0.94	1.41	2.66	0.92
COMMON	ALBU	Serum albumin	1.58	2.98	0.92	1.30	2.46	0.91
COMMON	VAT1	Synaptic vesicle membrane protein VAT-1 homolog	1.56	2.96	0.90	1.55	2.92	0.93
COMMON	SEP7	Septin-7	1.56	2.95	0.82	1.27	2.41	0.80
COMMON	PSME2	Proteasome activator complex subunit 2	1.54	2.91	0.88	1.02	2.03	0.81
COMMON	B2MG	Beta-2-microglobulin	1.52	2.88	0.82	1.23	2.34	0.89
COMMON	SEP2	Septin-2	1.50	2.83	0.82	1.39	2.62	0.85
COMMON	COF1	Cofilin-1	1.45	2.74	0.87	1.13	2.18	0.83
COMMON	A1AT4	Alpha-1-antitrypsin 1-4	1.44	2.72	0.83	1.48	2.79	0.81
COMMON	ANXA6	Annexin A6	1.44	2.71	0.89	0.99	1.98	0.91
COMMON	ADPRH	[Protein ADP-ribosylarginine] hydrolase	1.44	2.71	0.86	1.04	2.06	0.84
COMMON	DPYL2	Dihydropyrimidinase-related protein 2	1.42	2.68	0.88	0.91	1.88	0.83
COMMON	CO4A1	Collagen alpha-1(IV) chain	1.42	2.67	0.88	1.01	2.01	0.86
COMMON	MAP4	Microtubule-associated protein 4	1.41	2.66	0.82	1.12	2.17	0.81
COMMON	CATD	Cathepsin D	1.41	2.65	0.82	1.64	3.12	0.81
COMMON	ROA1	Heterogeneous nuclear ribonucleoprotein A1	1.40	2.63	0.88	1.02	2.03	0.88
COMMON	ISG15	Ubiquitin-like protein ISG15	1.39	2.62	0.84	1.37	2.59	0.89
COMMON	FETUB	Fetuin-B	1.39	2.61	0.89	1.38	2.60	0.86
COMMON	MYH9	Myosin-9	1.39	2.61	0.99	1.32	2.50	0.97
COMMON	CO3	Complement C3	1.38	2.59	0.87	1.29	2.45	0.87
COMMON	MYLK	Myosin light chain kinase, smooth muscle	1.37	2.59	0.80	1.19	2.28	0.89
COMMON	VMA5A	von Willebrand factor A domain-containing protein 5A	1.37	2.58	0.86	1.24	2.36	0.86
COMMON	COIA1	Collagen alpha-1(XVIII) chain	1.36	2.57	0.96	1.06	2.08	0.94
COMMON	MYL6	Myosin light polypeptide 6	1.34	2.53	0.92	1.34	2.53	0.94
COMMON	CATZ	Cathepsin Z	1.34	2.53	0.86	1.07	2.09	0.85
COMMON	APOA4	Apolipoprotein A-IV	1.32	2.50	0.82	1.30	2.47	0.83
COMMON	CAP1	Adenylyl cyclase-associated protein 1	1.32	2.50	0.92	1.26	2.40	0.92
COMMON	APOH	Beta-2-glycoprotein 1	1.32	2.50	0.80	1.49	2.82	0.85
COMMON	APOA1	Apolipoprotein A-I	1.30	2.46	0.92	1.03	2.04	0.87
COMMON	SET	Protein SET	1.30	2.46	0.83	1.10	2.15	0.90
COMMON	SFPQ	Splicing factor, proline- and glutamine-rich	1.28	2.44	0.81	0.98	1.97	0.81
COMMON	RBM3	RNA-binding protein 3	1.24	2.36	0.84	1.69	3.23	0.81
COMMON	T22D1	TSC22 domain family protein 1	1.23	2.35	0.90	1.17	2.24	0.84
COMMON	TIF1B	Transcription intermediary factor 1-beta	1.22	2.33	0.83	0.99	1.99	0.81
COMMON	GELS	Gelsolin	1.22	2.33	0.84	1.20	2.30	0.87
COMMON	VINC	Vinculin	1.22	2.33	0.94	1.02	2.03	0.92
COMMON	LMNB1	Lamin-B1	1.20	2.30	0.86	1.13	2.19	0.88
COMMON	ANXA5	Annexin A5	1.20	2.29	0.84	1.13	2.19	0.87
COMMON	PSME1	Proteasome activator complex subunit 1	1.19	2.28	0.84	1.14	2.21	0.81
COMMON	LAMA5	Laminin subunit alpha-5	1.17	2.26	0.83	0.97	1.96	0.89
COMMON	COR1C	Coronin-1C	1.16	2.23	0.83	0.97	1.95	0.82
COMMON	CAPZB	F-actin-capping protein subunit beta	1.16	2.23	0.89	0.79	1.73	0.86
COMMON	FUS	RNA-binding protein FUS	1.15	2.22	0.80	0.90	1.87	0.81
COMMON	AN32B	Acidic leucine-rich nuclear phosphoprotein 32 family member B	1.11	2.15	0.81	1.10	2.14	0.91
COMMON	PROF1	Profilin-1	1.07	2.10	0.89	1.11	2.16	0.88
COMMON	NID1	Nidogen-1	1.07	2.10	0.92	1.03	2.04	0.94
COMMON	H2AV	Histone H2A.V	1.05	2.07	0.86	0.84	1.79	0.84
COMMON	GNAI2	Guanine nucleotide-binding protein G(i) subunit alpha-2	1.01	2.02	0.83	0.84	1.79	0.84
COMMON	UBC9	SUMO-conjugating enzyme UBC9	0.98	1.97	0.91	0.94	1.92	0.91
COMMON	HP1B3	Heterochromatin protein 1-binding protein 3	0.95	1.94	0.83	0.86	1.82	0.89
COMMON	ACTBL	Beta-actin-like protein 2	0.93	1.91	0.84	0.81	1.75	0.91
COMMON	ROA3	Heterogeneous nuclear ribonucleoprotein A3	0.93	1.90	0.90	0.66	1.58	0.88
COMMON	NONO	Non-POU domain-containing octamer-binding protein	0.92	1.90	0.91	0.69	1.62	0.89
COMMON	ABCB7	ATP-binding cassette sub-family B member 7, mitochondrial	0.92	1.89	0.89	0.54	1.45	0.89
COMMON	ARP3	Actin-related protein 3	0.92	1.89	0.95	0.77	1.71	0.93
COMMON	LAMC1	Laminin subunit gamma-1	0.89	1.85	0.93	0.87	1.83	0.90
COMMON	LAMB1	Laminin subunit beta-1	0.89	1.85	0.85	0.74	1.67	0.84
COMMON	PGBM	Basement membrane-specific heparan sulfate proteoglycan core protein	0.85	1.80	0.81	0.64	1.56	0.81
COMMON	TADBP	TAR DNA-binding protein 43	0.85	1.80	0.81	0.47	1.39	0.82
COMMON	NUCL	Nucleolin	0.84	1.79	0.83	0.55	1.46	0.85
COMMON	DX39B	Spliceosome RNA helicase Ddx39b	0.83	1.78	0.81	0.76	1.69	0.81
COMMON	TLN1	Talin-1	0.83	1.78	0.82	0.72	1.65	0.89
COMMON	ARP2	Actin-related protein 2	0.81	1.76	0.88	0.66	1.58	0.81
COMMON	HNRPM	Heterogeneous nuclear ribonucleoprotein M	0.80	1.74	0.86	0.59	1.50	0.82
COMMON	PDIA6	Protein disulfide-isomerase A6	0.75	1.68	0.90	0.67	1.59	0.88
COMMON	LSM3	U6 snRNA-associated Sm-like protein LSm3	0.69	1.62	0.91	0.65	1.57	0.91

COMMON	ABRAL	Costars family protein ABRACL	0.64	1.56	0.80	0.63	1.55	0.87
COMMON	ACTB	Actin, cytoplasmic 1	0.64	1.56	0.93	0.52	1.43	0.90
COMMON	HNRPU	Heterogeneous nuclear ribonucleoprotein U	0.61	1.53	0.85	0.53	1.44	0.84
COMMON	SMD2	Small nuclear ribonucleoprotein Sm D2	0.56	1.47	0.81	0.48	1.40	0.82
COMMON	PDIA4	Protein disulfide-isomerase A4	0.49	1.40	0.80	0.57	1.48	0.88
TG2-KO ONLY	S10A6	Protein S100-A6	1.50	2.82	0.65	3.45	10.94	0.81
TG2-KO ONLY	RCN3	Reticulocalbin-3	2.73	6.65	0.74	3.22	9.30	0.84
TG2-KO ONLY	MUP6	Major urinary protein 6	1.56	2.94	0.62	2.96	7.80	0.95
TG2-KO ONLY	CO5A1	Collagen alpha-1(V) chain	3.74	13.34	0.78	2.92	7.56	0.83
TG2-KO ONLY	TPSN	Tapasin	5.19	36.41	0.76	2.75	6.71	0.89
TG2-KO ONLY	GAPR1	Golgi-associated plant pathogenesis-related protein 1	2.52	5.72	0.64	2.69	6.44	0.86
TG2-KO ONLY	CFAH	Complement factor H	2.12	4.35	0.72	2.63	6.17	0.81
TG2-KO ONLY	ELN	Elastin	1.88	3.69	0.61	2.53	5.78	0.83
TG2-KO ONLY	K1C14	Keratin, type I cytoskeletal 14	2.75	6.75	0.75	2.47	5.55	0.81
TG2-KO ONLY	SAMH1	Deoxynucleoside triphosphate triphosphohydrolase SAMHD1	2.89	7.41	0.74	2.23	4.70	0.84
TG2-KO ONLY	PRELP	Prolargin	2.13	4.38	0.79	2.23	4.68	0.89
TG2-KO ONLY	H2A1H	Histone H2A type 1-H	1.45	2.73	0.64	2.17	4.49	0.85
TG2-KO ONLY	C1QB	Complement C1q subcomponent subunit B	3.24	9.42	0.70	2.12	4.35	0.91
TG2-KO ONLY	ASAH1	Acid ceramidase	2.12	4.36	0.79	2.11	4.32	0.87
TG2-KO ONLY	PDLI2	PDZ and LIM domain protein 2	2.22	4.67	0.55	2.03	4.09	0.82
TG2-KO ONLY	LEG3	Galectin-3	1.90	3.73	0.73	1.89	3.71	0.86
TG2-KO ONLY	TPM2	Tropomyosin beta chain	1.67	3.19	0.79	1.78	3.44	0.82
TG2-KO ONLY	MUP2	Major urinary protein 2	1.48	2.79	0.77	1.78	3.43	1.00
TG2-KO ONLY	FRIL1	Ferritin light chain 1	1.82	3.54	0.64	1.75	3.36	0.86
TG2-KO ONLY	LG3BP	Galectin-3-binding protein	2.53	5.78	0.67	1.70	3.26	0.81
TG2-KO ONLY	E41L2	Band 4.1-like protein 2	2.70	6.51	0.77	1.69	3.22	0.88
TG2-KO ONLY	EPDR1	Mammalian ependymin-related protein 1	0.46	1.38	0.55	1.51	2.85	0.81
TG2-KO ONLY	PPT1	Palmitoyl-protein thioesterase 1	1.18	2.26	0.70	1.46	2.75	0.85
TG2-KO ONLY	H11	Histone H1.1	0.86	1.81	0.68	1.44	2.72	0.96
TG2-KO ONLY	HSPB1	Heat shock protein beta-1	1.51	2.85	0.72	1.41	2.67	0.85
TG2-KO ONLY	PCNA	Proliferating cell nuclear antigen	1.24	2.37	0.69	1.35	2.55	0.81
TG2-KO ONLY	H15	Histone H1.5	1.08	2.12	0.75	1.34	2.54	0.91
TG2-KO ONLY	HMGB2	High mobility group protein B2	1.46	2.75	0.52	1.29	2.45	0.85
TG2-KO ONLY	NAGAB	Alpha-N-acetylgalactosaminidase	1.14	2.21	0.72	1.28	2.43	0.82
TG2-KO ONLY	H12	Histone H1.2	0.58	1.49	0.53	1.28	2.42	0.93
TG2-KO ONLY	SEP11	Septin-11	1.44	2.71	0.80	1.22	2.33	0.83
TG2-KO ONLY	ARPC5	Actin-related protein 2/3 complex subunit 5	1.60	3.03	0.76	1.06	2.09	0.90
TG2-KO ONLY	SPA3K	Serine protease inhibitor A3K	1.11	2.15	0.79	1.05	2.07	0.81
TG2-KO ONLY	RENI1	Renin-1	1.47	2.77	0.78	1.01	2.01	0.84
TG2-KO ONLY	NID2	Nidogen-2	0.96	1.95	0.68	0.83	1.77	0.87
TG2-KO ONLY	CAPG	Macrophage-capping protein	0.75	1.68	0.77	0.81	1.76	0.81
TG2-KO ONLY	SAP	Prosaposin	0.91	1.88	0.75	0.76	1.70	0.82
TG2-KO ONLY	ILF2	Interleukin enhancer-binding factor 2	1.04	2.06	0.56	0.72	1.65	0.84
TG2-KO ONLY	ARPC4	Actin-related protein 2/3 complex subunit 4	0.77	1.71	0.66	0.72	1.65	0.85
TG2-KO ONLY	H2AX	Histone H2AX	0.34	1.26	0.52	0.72	1.64	0.83
TG2-KO ONLY	H2B1P	Histone H2B type 1-P	0.34	1.27	0.17	0.67	1.59	0.88
TG2-KO ONLY	NPM	Nucleophosmin	0.67	1.59	0.57	0.66	1.58	0.83
TG2-KO ONLY	PRDX4	Peroxiredoxin-4	0.83	1.78	0.73	0.61	1.53	0.89
TG2-KO ONLY	ROAA	Heterogeneous nuclear ribonucleoprotein A/B	0.50	1.41	0.74	0.58	1.50	0.84
TG2-KO ONLY	RUXE	Small nuclear ribonucleoprotein E	0.43	1.35	0.79	0.54	1.45	0.80
TG2-KO ONLY	KAD1	Adenylate kinase isoenzyme 1	0.48	1.40	0.51	0.48	1.39	0.81
TG2-KO ONLY	CATB	Cathepsin B	0.58	1.49	0.79	0.43	1.35	0.85

S.1.13.2 UUO-underexpressed proteins

Supplementary Table 3.18: List of proteins significantly underexpressed (Confidence ≥ 0.8) in either WT or TG2-KO kidneys subjected to UUO (21 days) and corresponding fold change from Sham operated condition in both phenotypes. In increasing shade of red the positive log2 (Log2 FC) of fold change from the sham operated condition (the more intense, the more overexpressed), in decreasing shades of green the negative log2 (Log2 FC) of fold change from the sham operated condition (the more intense, the more underexpressed), in increasing shades of grey the absolute fold change from the sham operated condition (Abs FC, absolute increase or decrease depending of the sign of Log2 FC) while in shades of yellow the confidence of the change (refer to the colour legend below). A confidence ≥ 0.8 was regarded as significant.

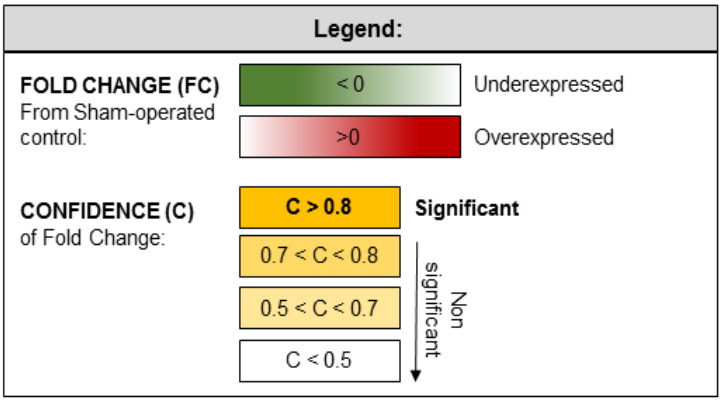

Unique/Common	Protein ID _MOUSE	Name	WT			TG2-KO		
			Log2 (FC)	Abs (FC)	C (FC)	Log2 (FC)	Abs (FC)	C (FC)
WT ONLY	PDZ1I	PDZK1-interacting protein 1	-5.52	45.76	0.84	-6.50	90.53	0.79
WT ONLY	GSTA2	Glutathione S-transferase A2	-4.10	17.14	0.85	-3.57	11.91	0.73
WT ONLY	KBL	2-amino-3-ketobutyrate coenzyme A ligase, mitochondrial	-3.79	13.82	0.85	-2.98	7.91	0.61
WT ONLY	PXMP2	Peroxisomal membrane protein 2	-3.78	13.77	0.81	-2.90	7.48	0.55
WT ONLY	S4A4	Electrogenic sodium bicarbonate cotransporter 1	-3.73	13.29	0.83	-4.19	18.31	0.78
WT ONLY	ACE	Angiotensin-converting enzyme	-3.66	12.66	0.91	-3.21	9.27	0.79
WT ONLY	DECR2	Peroxisomal 2,4-dienoyl-CoA reductase	-3.66	12.62	0.90	-2.30	4.92	0.79
WT ONLY	ACY3	N-acyl-aromatic-L-amino acid amidohydrolase (carboxylate-forming)	-3.64	12.43	0.80	-3.53	11.54	0.77
WT ONLY	S22A2	Solute carrier family 22 member 2	-3.62	12.29	0.81	-3.38	10.42	0.76
WT ONLY	DHAK	Triokinase/FMN cyclase	-3.56	11.77	0.80	-4.16	17.82	0.79
WT ONLY	COX1	Cytochrome c oxidase subunit 1	-3.55	11.70	0.90	-3.16	8.92	0.73
WT ONLY	S2542	Mitochondrial coenzyme A transporter SLC25A42	-3.54	11.63	0.86	-3.40	10.58	0.71
WT ONLY	ATP5L	ATP synthase subunit g, mitochondrial	-3.53	11.54	0.80	-2.94	7.67	0.71
WT ONLY	OXDA	D-amino-acid oxidase	-3.51	11.38	0.81	-3.11	8.60	0.78
WT ONLY	GSTA3	Glutathione S-transferase A3	-3.41	10.63	0.81	-2.67	6.36	0.71
WT ONLY	LACB2	Beta-lactamase-like protein 2	-3.38	10.39	0.82	-3.34	10.12	0.76
WT ONLY	FMO1	Dimethylaniline monooxygenase [N-oxide-forming] 1	-3.37	10.33	0.82	-2.73	6.63	0.78
WT ONLY	PROD	Proline dehydrogenase 1, mitochondrial	-3.33	10.05	0.81	-3.49	11.25	0.80
WT ONLY	S22AI	Solute carrier family 22 member 18	-3.30	9.86	0.90	-4.12	17.38	0.78
WT ONLY	NDUB6	NADH dehydrogenase [ubiquinone] 1 beta subcomplex subunit 6	-3.29	9.77	0.81	-3.21	9.22	0.80
WT ONLY	SSDH	Succinate-semialdehyde dehydrogenase, mitochondrial	-3.24	9.47	0.88	-2.72	6.57	0.71
WT ONLY	NDUB5	NADH dehydrogenase [ubiquinone] 1 beta subcomplex subunit 5, mitochondrial	-3.17	9.01	0.85	-2.84	7.15	0.79
WT ONLY	PLSI	Plastin-1	-3.17	9.01	0.86	-2.83	7.09	0.79
WT ONLY	NDUB8	NADH dehydrogenase [ubiquinone] 1 beta subcomplex subunit 8, mitochondrial	-3.12	8.67	0.86	-2.67	6.38	0.79
WT ONLY	NDUV2	NADH dehydrogenase [ubiquinone] flavoprotein 2, mitochondrial	-3.09	8.50	0.84	-2.79	6.94	0.79
WT ONLY	BDH2	3-hydroxybutyrate dehydrogenase type 2	-3.02	8.13	0.82	-3.48	11.18	0.80
WT ONLY	COASY	Bifunctional coenzyme A synthase	-2.97	7.83	0.85	-2.68	6.41	0.77
WT ONLY	TAU	Microtubule-associated protein tau	-2.96	7.76	0.83	-2.26	4.79	0.77
WT ONLY	PPA6	Lysophosphatidic acid phosphatase type 6	-2.95	7.74	0.85	-2.28	4.87	0.69
WT ONLY	HGD	Homogentisate 1,2-dioxygenase	-2.92	7.58	0.84	-3.70	13.01	0.76
WT ONLY	ACD11	Acyl-CoA dehydrogenase family member 11	-2.89	7.41	0.80	-3.14	8.83	0.77
WT ONLY	NAKD2	NAD kinase 2, mitochondrial	-2.87	7.33	0.95	-2.13	4.39	0.65
WT ONLY	VATG1	V-type proton ATPase subunit G 1	-2.87	7.31	0.83	-2.61	6.13	0.78
WT ONLY	CDD	Cytidine deaminase	-2.86	7.28	0.81	-2.99	7.93	0.80

WT ONLY	CBR4	Carbonyl reductase family member 4	-2.85	7.19	0.85	-2.05	4.13	0.72
WT ONLY	C1TC	C-1-tetrahydrofolate synthase, cytoplasmic	-2.83	7.12	0.87	-2.80	6.96	0.79
WT ONLY	MGST3	Microsomal glutathione S-transferase 3	-2.83	7.12	0.84	-2.74	6.70	0.76
WT ONLY	FGGY	FGGY carbohydrate kinase domain-containing protein	-2.75	6.73	0.85	-3.06	8.34	0.54
WT ONLY	VWA8	von Willebrand factor A domain-containing protein 8	-2.69	6.46	0.82	-3.10	8.58	0.80
WT ONLY	ACOX2	Peroxisomal acyl-coenzyme A oxidase 2	-2.64	6.24	0.84	-3.46	11.03	0.78
WT ONLY	MRP2	Canalicular multispecific organic anion transporter 1	-2.59	6.03	0.82	-1.17	2.25	0.24
WT ONLY	ACOT4	Acyl-coenzyme A thioesterase 4	-2.51	5.68	0.81	-2.56	5.92	0.69
WT ONLY	HIBCH	3-hydroxyisobutyryl-CoA hydrolase, mitochondrial	-2.47	5.55	0.89	-3.63	12.41	0.77
WT ONLY	CN159	UPF0317 protein C14orf159 homolog, mitochondrial	-2.43	5.41	0.83	-3.23	9.39	0.77
WT ONLY	E41L3	Band 4.1-like protein 3	-2.31	4.96	0.86	-2.86	7.24	0.67
WT ONLY	PH4H	Cytoplasmic aconitate hydratase	-2.27	4.83	0.84	-2.22	4.66	0.78
WT ONLY	ISCA2	Iron-sulfur cluster assembly 2 homolog, mitochondrial	-2.24	4.73	0.82	-1.40	2.64	0.71
WT ONLY	DDAH1	N(G),N(G)-dimethylarginine dimethylaminohydrolase 1	-2.19	4.57	0.83	-2.79	6.93	0.78
WT ONLY	RT35	28S ribosomal protein S35, mitochondrial	-2.15	4.43	0.81	-2.55	5.87	0.68
WT ONLY	TRXR2	Thioredoxin reductase 2, mitochondrial	-2.10	4.29	0.83	-2.68	6.39	0.71
WT ONLY	TIM10	Mitochondrial import inner membrane translocase subunit Tim10	-2.00	4.01	0.86	-2.00	4.01	0.74
WT ONLY	MAVS	Mitochondrial antiviral-signaling protein	-1.98	3.95	0.84	-2.49	5.62	0.75
WT ONLY	T126A	Transmembrane protein 126A	-1.97	3.93	0.85	-1.76	3.38	0.58
WT ONLY	AT11A	Probable phospholipid-transporting ATPase IH	-1.94	3.85	0.81	-1.50	2.82	0.64
WT ONLY	EBP	3-beta-hydroxysteroid-Delta(8),Delta(7)-isomerase	-1.89	3.70	0.91	-1.67	3.19	0.71
WT ONLY	TSPO	Translocator protein	-1.87	3.66	0.98	0.84	1.79	0.56
WT ONLY	NCPR	NADPH--cytochrome P450 reductase	-1.87	3.64	0.81	-1.96	3.89	0.75
WT ONLY	RM04	39S ribosomal protein L4, mitochondrial	-1.84	3.59	0.91	-2.16	4.46	0.78
WT ONLY	GGCT	Gamma-glutamylcyclotransferase	-1.83	3.55	0.99	-3.48	11.16	0.79
WT ONLY	NAPSA	Napsin-A	-1.73	3.32	0.84	-0.98	1.98	0.67
WT ONLY	ISCU	Iron-sulfur cluster assembly enzyme ISCU, mitochondrial	-1.70	3.25	0.81	-2.27	4.82	0.71
WT ONLY	GVIN1	Interferon-induced very large GTPase 1	-1.69	3.22	0.83	-0.75	1.68	0.63
WT ONLY	PRPS2	Ribose-phosphate pyrophosphokinase 2	-1.68	3.20	0.85	-0.89	1.85	0.58
WT ONLY	EHD1	EH domain-containing protein 1	-1.61	3.05	0.83	-1.64	3.11	0.77
WT ONLY	TTC38	Tetratricopeptide repeat protein 38	-1.52	2.87	0.87	-1.46	2.75	0.79
WT ONLY	GTR1	Solute carrier family 2, facilitated glucose transporter member 1	-1.37	2.58	0.80	-1.91	3.75	0.72
WT ONLY	NAMPT	Nicotinamide phosphoribosyltransferase	-1.36	2.57	0.82	-1.60	3.03	0.61
WT ONLY	S10A1	Protein S100-A1	-1.28	2.44	0.85	-1.33	2.51	0.78
WT ONLY	EHD3	EH domain-containing protein 3	-1.24	2.37	0.86	-1.09	2.12	0.57
WT ONLY	GSHR	Glutathione reductase, mitochondrial	-1.22	2.33	0.80	-1.28	2.43	0.64
WT ONLY	ARL1	ADP-ribosylation factor-like protein 1	-1.16	2.24	0.90	-0.27	1.20	0.38
WT ONLY	RS24	40S ribosomal protein S24	-0.99	1.99	0.88	0.81	1.75	0.37
WT ONLY	NDKA	Nucleoside diphosphate kinase A	-0.99	1.98	0.88	-1.14	2.21	0.70
WT ONLY	AP1B1	AP-1 complex subunit beta-1	-0.97	1.97	0.82	-1.09	2.13	0.69
WT ONLY	GALK1	Galactokinase	-0.71	1.64	0.85	-0.69	1.61	0.64
WT ONLY	CLH1	Clathrin heavy chain 1	-0.56	1.47	0.88	-0.57	1.48	0.77
COMMON	G6PC	Glucose-6-phosphatase	-6.17	72.24	0.86	-3.43	10.79	0.83
COMMON	AADAT	Kynurenine/alpha-aminoadipate aminotransferase, mitochondrial	-5.59	48.00	0.84	-3.54	11.59	0.80
COMMON	HAOX2	Hydroxyacid oxidase 2	-5.47	44.28	0.85	-4.18	18.08	0.88
COMMON	CALB1	Calbindin	-5.00	32.07	0.91	-4.40	21.18	0.92
COMMON	ASSY	Argininosuccinate synthase	-4.41	21.28	0.88	-4.43	21.51	0.87
COMMON	ACSM1	Acyl-coenzyme A synthetase ACSM1, mitochondrial	-4.38	20.87	0.83	-3.47	11.05	0.89
COMMON	F16P1	Fructose-1,6-bisphosphatase 1	-4.38	20.84	0.81	-4.19	18.22	0.90
COMMON	ACSM2	Acyl-coenzyme A synthetase ACSM2, mitochondrial	-4.33	20.17	0.86	-4.32	19.94	0.89
COMMON	ECHP	Peroxisomal bifunctional enzyme	-4.32	19.92	0.84	-3.74	13.34	0.88
COMMON	KAD4	Adenylate kinase 4, mitochondrial	-4.31	19.83	0.89	-4.24	18.93	0.91
COMMON	AT1B1	Sodium/potassium-transporting ATPase subunit beta-1	-4.29	19.55	0.87	-4.05	16.52	0.87
COMMON	CAD16	Cadherin-16	-4.29	19.54	0.92	-4.00	15.95	0.89
COMMON	PYC	Pyruvate carboxylase, mitochondrial	-4.17	18.04	0.87	-3.97	15.62	0.84
COMMON	AL8A1	Aldehyde dehydrogenase family 8 member A1	-4.10	17.11	0.88	-3.61	12.21	0.89
COMMON	ATNG	Sodium/potassium-transporting ATPase subunit gamma	-4.07	16.80	0.90	-3.97	15.63	0.89
COMMON	UD3A2	UDP-glucuronosyltransferase 3A2	-4.06	16.72	0.83	-3.47	11.11	0.81
COMMON	S100G	Protein S100-G	-4.05	16.59	0.90	-3.56	11.78	0.87
COMMON	ACS2L	Acetyl-coenzyme A synthetase 2-like, mitochondrial	-4.05	16.56	0.89	-3.50	11.31	0.83
COMMON	KEG1	Glycine N-acyltransferase-like protein Keg1	-4.03	16.36	0.88	-3.97	15.67	0.88
COMMON	SC5A2	Sodium/glucose cotransporter 2	-4.02	16.23	0.80	-3.47	11.10	0.81
COMMON	ECHD2	Enoyl-CoA hydratase domain-containing protein 2, mitochondrial	-4.01	16.09	0.87	-3.68	12.79	0.88
COMMON	CGL	mmthionine gamma-lyase	-4.00	16.04	0.86	-3.50	11.29	0.83

COMMON	3HAO	3-hydroxyanthranilate 3,4-dioxygenase	-3.96	15.56	0.85	-4.26	19.13	0.82
COMMON	S27A2	Very long-chain acyl-CoA synthetase	-3.90	14.88	0.81	-3.76	13.57	0.84
COMMON	MEP1B	Meprin A subunit beta	-3.88	14.72	0.82	-3.05	8.27	0.80
COMMON	ACADM	Medium-chain specific acyl-CoA dehydrogenase, mitochondrial	-3.86	14.48	0.86	-4.02	16.23	0.87
COMMON	TMM27	Collectrin	-3.85	14.41	0.85	-3.22	9.30	0.85
COMMON	ISC2A	Isochorismatase domain-containing protein 2A	-3.84	14.27	0.90	-3.60	12.14	0.81
COMMON	BDH	D-beta-hydroxybutyrate dehydrogenase, mitochondrial	-3.83	14.24	0.89	-3.82	14.12	0.92
COMMON	ALDOB	Fructose-bisphosphate aldolase B	-3.83	14.21	0.93	-3.95	15.47	0.93
COMMON	HOT	Hydroxyacid-oxoacid transhydrogenase, mitochondrial	-3.82	14.07	0.84	-3.17	8.97	0.83
COMMON	GATM	Glycine amidinotransferase, mitochondrial	-3.80	13.91	0.87	-4.39	20.94	0.88
COMMON	GABT	4-aminobutyrate aminotransferase, mitochondrial	-3.79	13.84	0.93	-3.62	12.32	0.93
COMMON	MMSA	Methylmalonate-semialdehyde dehydrogenase [acylating], mitochondrial	-3.79	13.79	0.88	-3.98	15.74	0.89
COMMON	ST1D1	Sulfotransferase 1 family member D1	-3.78	13.74	0.85	-3.96	15.51	0.84
COMMON	GGT1	Gamma-glutamyltranspeptidase 1	-3.76	13.58	0.89	-3.74	13.34	0.86
COMMON	MAAI	Maleylacetoacetate isomerase	-3.75	13.49	0.82	-3.14	8.83	0.82
COMMON	PGAM2	Phosphoglycerate mutase 2	-3.75	13.44	0.88	-3.03	8.19	0.82
COMMON	GLYAT	Glycine N-acyltransferase	-3.75	13.43	0.88	-4.05	16.55	0.86
COMMON	FAAA	Fumarylacetoacetase	-3.72	13.16	0.92	-3.79	13.80	0.90
COMMON	AT1A1	Sodium/potassium-transporting ATPase subunit alpha-1	-3.72	13.14	0.93	-3.55	11.72	0.95
COMMON	DHSO	Sorbitol dehydrogenase	-3.71	13.11	0.82	-3.80	13.96	0.85
COMMON	MPC1	Mitochondrial pyruvate carrier 1	-3.69	12.91	0.93	-3.31	9.89	0.80
COMMON	UK114	Ribonuclease UK114	-3.67	12.69	0.94	-3.25	9.50	0.90
COMMON	CATA	Catalase	-3.66	12.62	0.94	-3.25	9.51	0.94
COMMON	GSTK1	Glutathione S-transferase kappa 1	-3.62	12.27	0.82	-3.49	11.23	0.85
COMMON	PCCB	Propionyl-CoA carboxylase beta chain, mitochondrial	-3.61	12.22	0.96	-3.55	11.73	0.90
COMMON	AL4A1	Delta-1-pyrroline-5-carboxylate dehydrogenase, mitochondrial	-3.61	12.17	0.93	-3.56	11.79	0.91
COMMON	CES1D	Carboxylesterase 1D	-3.58	11.96	0.83	-3.50	11.28	0.87
COMMON	GLPK	Glycerol kinase	-3.57	11.89	0.86	-3.91	14.98	0.85
COMMON	QORL2	Quinone oxidoreductase-like protein 2	-3.57	11.85	0.82	-3.90	14.96	0.83
COMMON	AAAD	Arylacetamide deacetylase	-3.57	11.84	0.85	-4.27	19.31	0.91
COMMON	VILI	Villin-1	-3.56	11.78	0.91	-3.55	11.73	0.88
COMMON	SODM	Superoxide dismutase [Mn], mitochondrial	-3.54	11.66	0.93	-3.18	9.08	0.88
COMMON	MPC2	Mitochondrial pyruvate carrier 2	-3.54	11.60	0.82	-3.50	11.30	0.90
COMMON	NUD19	Nucleoside diphosphate-linked moiety X motif 19	-3.50	11.28	0.90	-3.44	10.83	0.87
COMMON	HINT2	Histidine triad nucleotide-binding protein 2, mitochondrial	-3.49	11.27	0.98	-3.43	10.77	0.94
COMMON	BPHL	Valacyclovir hydrolase	-3.47	11.09	0.87	-3.83	14.21	0.85
COMMON	MCCB	Methylcrotonoyl-CoA carboxylase beta chain, mitochondrial	-3.45	10.95	0.90	-3.36	10.25	0.86
COMMON	PBLD1	Phenazine biosynthesis-like domain-containing protein 1	-3.45	10.91	0.87	-3.95	15.43	0.81
COMMON	DIC	Mitochondrial dicarboxylate carrier	-3.44	10.83	0.83	-2.95	7.73	0.91
COMMON	ACD10	Acyl-CoA dehydrogenase family member 10	-3.43	10.77	0.86	-3.16	8.94	0.89
COMMON	NHRF3	Na(+)/H(+) exchange regulatory cofactor NHE-RF3	-3.42	10.71	0.86	-3.27	9.66	0.90
COMMON	CK054	Ester hydrolase C11orf54 homolog	-3.41	10.61	0.82	-3.44	10.86	0.81
COMMON	AK1A1	Alcohol dehydrogenase [NADP(+)]	-3.40	10.56	0.91	-3.23	9.38	0.92
COMMON	3HIDH	3-hydroxyisobutyrate dehydrogenase, mitochondrial	-3.40	10.55	0.94	-3.26	9.57	0.93
COMMON	SUCB2	Succinyl-CoA ligase [GDP-forming] subunit beta, mitochondrial	-3.38	10.42	0.94	-3.39	10.47	0.92
COMMON	FAHD1	Acylpyruvase FAHD1, mitochondrial	-3.38	10.39	0.84	-3.61	12.20	0.84
COMMON	IVD	Isovaleryl-CoA dehydrogenase, mitochondrial	-3.34	10.14	0.88	-3.33	10.09	0.86
COMMON	THIL	Acetyl-CoA acetyltransferase, mitochondrial	-3.34	10.10	0.95	-3.24	9.43	0.96
COMMON	SARDH	Sarcosine dehydrogenase, mitochondrial	-3.33	10.05	0.85	-3.65	12.57	0.87
COMMON	INMT	Indolethylamine N-methyltransferase	-3.33	10.03	0.83	-3.47	11.06	0.85
COMMON	AL1L1	Cytosolic 10-formyltetrahydrofolate dehydrogenase	-3.31	9.95	0.91	-3.11	8.63	0.92
COMMON	KHK	Ketohexokinase	-3.31	9.90	0.83	-3.85	14.41	0.84
COMMON	ARK72	Aflatoxin B1 aldehyde reductase member 2	-3.30	9.87	0.87	-3.10	8.60	0.85
COMMON	HCDH	Hydroxyacyl-coenzyme A dehydrogenase, mitochondrial	-3.30	9.82	0.90	-3.18	9.04	0.89
COMMON	CISD1	CDGSH iron-sulfur domain-containing protein 1	-3.29	9.75	0.95	-3.37	10.36	0.94
COMMON	NDRG1	Protein NDRG1	-3.25	9.52	0.99	-3.06	8.36	0.98
COMMON	S13A3	Solute carrier family 13 member 3	-3.25	9.52	0.88	-2.94	7.65	0.84
COMMON	CYC	Cytochrome c, somatic	-3.25	9.49	0.92	-2.92	7.56	0.90
COMMON	SCOT1	Succinyl-CoA:3-ketoacid coenzyme A transferase 1, mitochondrial	-3.22	9.34	0.92	-3.15	8.85	0.91
COMMON	HMGCL	Hydroxymethylglutaryl-CoA lyase, mitochondrial	-3.21	9.26	0.92	-3.22	9.29	0.89
COMMON	ACPM	Acyl carrier protein, mitochondrial	-3.20	9.19	0.92	-3.07	8.43	0.92
COMMON	ATPK	ATP synthase subunit f, mitochondrial	-3.20	9.17	0.80	-2.88	7.34	0.83

COMMON	MSRA	Mitochondrial peptide methionine sulfoxide reductase	-3.19	9.12	0.83	-3.16	8.95	0.89
COMMON	CBR1	Carbonyl reductase [NADPH] 1	-3.19	9.11	0.92	-2.87	7.30	0.94
COMMON	LDHD	Probable D-lactate dehydrogenase, mitochondrial	-3.19	9.10	0.88	-2.97	7.83	0.88
COMMON	COX5A	Cytochrome c oxidase subunit 5A, mitochondrial	-3.18	9.08	0.94	-3.02	8.11	0.93
COMMON	ETFA	Electron transfer flavoprotein subunit alpha, mitochondrial	-3.18	9.07	0.93	-3.27	9.66	0.92
COMMON	GPDA	Glycerol-3-phosphate dehydrogenase [NAD(+)], cytoplasmic	-3.15	8.85	0.91	-3.77	13.65	0.84
COMMON	NIPS1	Protein NipSnap homolog 1	-3.14	8.81	0.91	-2.93	7.62	0.90
COMMON	NU4M	NADH-ubiquinone oxidoreductase chain 4	-3.14	8.79	0.89	-2.65	6.28	0.88
COMMON	FAHD2	umarylacetoacetate hydrolase domain-containing protein 2A	-3.13	8.76	0.80	-3.83	14.19	0.81
COMMON	CLYBL	Citrate lyase subunit beta-like protein, mitochondrial	-3.13	8.75	0.80	-3.38	10.40	0.83
COMMON	FBX50	F-box only protein 50	-3.13	8.73	0.80	-4.09	17.04	0.84
COMMON	NDUS6	NADH dehydrogenase [ubiquinone] iron-sulfur protein 6, mitochondrial	-3.12	8.72	0.81	-2.89	7.39	0.82
COMMON	THNS2	Threonine synthase-like 2	-3.12	8.70	0.83	-3.30	9.82	0.82
COMMON	NU5M	NADH-ubiquinone oxidoreductase chain 5	-3.12	8.67	0.88	-2.67	6.35	0.86
COMMON	PECR	Peroxisomal trans-2-enoyl-CoA reductase	-3.11	8.65	0.87	-3.71	13.10	0.92
COMMON	SDHA	Succinate dehydrogenase [ubiquinone] flavoprotein subunit, mitochondrial	-3.11	8.64	0.98	-2.96	7.80	0.97
COMMON	NDUBA	NADH dehydrogenase [ubiquinone] 1 beta subcomplex subunit 10	-3.11	8.63	0.86	-3.07	8.40	0.86
COMMON	SUCA	Succinyl-CoA ligase [ADP/GDP-forming] subunit alpha, mitochondrial	-3.10	8.55	0.94	-3.17	9.00	0.93
COMMON	IPYR2	Inorganic pyrophosphatase 2, mitochondrial	-3.09	8.50	0.83	-2.90	7.47	0.90
COMMON	NDUV1	NADH dehydrogenase [ubiquinone] flavoprotein 1, mitochondrial	-3.07	8.43	0.90	-3.29	9.81	0.92
COMMON	NDUA9	NADH dehydrogenase [ubiquinone] 1 alpha subcomplex subunit 9, mitochondrial	-3.07	8.38	0.89	-2.78	6.86	0.91
COMMON	ABCD3	ATP-binding cassette sub-family D member 3	-3.06	8.36	0.88	-2.95	7.75	0.90
COMMON	ATPD	ATP synthase subunit delta, mitochondrial	-3.06	8.32	0.98	-2.94	7.68	0.95
COMMON	QCR6	Cytochrome b-c1 complex subunit 6, mitochondrial	-3.05	8.31	0.93	-2.60	6.06	0.93
COMMON	NDUA1	NADH dehydrogenase [ubiquinone] 1 alpha subcomplex subunit 1	-3.05	8.25	0.86	-2.04	4.12	0.86
COMMON	COX5B	Cytochrome c oxidase subunit 5B, mitochondrial	-3.04	8.24	0.91	-3.18	9.07	0.90
COMMON	IDHP	Isocitrate dehydrogenase [NADP], mitochondrial	-3.04	8.21	0.93	-3.10	8.56	0.93
COMMON	SBP1	Selenium-binding protein 1	-3.03	8.19	0.92	-2.84	7.18	0.89
COMMON	NDUS7	NADH dehydrogenase [ubiquinone] iron-sulfur protein 7, mitochondrial	-3.03	8.16	0.94	-2.91	7.49	0.85
COMMON	ETFB	Electron transfer flavoprotein subunit beta	-3.02	8.13	0.91	-3.13	8.78	0.92
COMMON	NHRF1	Na(+)/H(+) exchange regulatory cofactor NHE-RF1	-3.01	8.07	0.94	-3.14	8.85	0.91
COMMON	NEP	Neprilysin	-3.01	8.05	0.90	-2.96	7.78	0.89
COMMON	NDUAD	NADH dehydrogenase [ubiquinone] 1 alpha subcomplex subunit 13	-3.00	8.00	0.89	-2.68	6.42	0.94
COMMON	CSAD	Cysteine sulfinic acid decarboxylase	-3.00	8.00	0.90	-2.71	6.56	0.91
COMMON	COX2	Cytochrome c oxidase subunit 2	-3.00	7.99	0.87	-2.84	7.15	0.86
COMMON	SDHB	Succinate dehydrogenase [ubiquinone] iron-sulfur subunit, mitochondrial	-3.00	7.99	0.89	-3.00	8.00	0.83
COMMON	TPMT	Thiopurine S-methyltransferase	-3.00	7.98	0.93	-2.69	6.43	0.93
COMMON	CY1	Cytochrome c1, heme protein, mitochondrial	-2.99	7.96	0.94	-2.95	7.72	0.93
COMMON	TOM5	Mitochondrial import receptor subunit TOM5 homolog	-2.99	7.94	1.00	-1.43	2.69	0.88
COMMON	COQ9	Ubiquinone biosynthesis protein COQ9, mitochondrial	-2.98	7.91	0.90	-3.17	9.02	0.81
COMMON	IDHG1	Isocitrate dehydrogenase [NAD] subunit gamma 1, mitochondrial	-2.98	7.91	0.91	-3.04	8.20	0.89
COMMON	THIM	3-ketoacyl-CoA thiolase, mitochondrial	-2.98	7.90	0.91	-3.18	9.09	0.88
COMMON	UCRI	Cytochrome b-c1 complex subunit Rieske, mitochondrial	-2.98	7.89	0.91	-3.13	8.74	0.84
COMMON	NDUA3	NADH dehydrogenase [ubiquinone] 1 alpha subcomplex subunit 3	-2.98	7.86	0.89	-3.34	10.14	0.84
COMMON	AUHM	Methylglutaconyl-CoA hydratase, mitochondrial	-2.97	7.85	0.85	-3.27	9.63	0.89
COMMON	NLTP	Non-specific lipid-transfer protein	-2.97	7.82	0.88	-2.75	6.73	0.91
COMMON	NDUB7	NADH dehydrogenase [ubiquinone] 1 beta subcomplex subunit 7	-2.96	7.79	0.84	-3.01	8.05	0.90
COMMON	THTR	Thiosulfate sulfurtransferase	-2.95	7.75	0.89	-3.26	9.59	0.89
COMMON	QOR	Quinone oxidoreductase	-2.95	7.71	0.84	-3.07	8.40	0.93
COMMON	ACSL1	Long-chain-fatty-acid--CoA ligase 1	-2.94	7.69	0.90	-3.35	10.18	0.86
COMMON	CRYL1	Lambda-crystallin homolog	-2.93	7.62	0.90	-2.93	7.64	0.89
COMMON	LRP2	Low-density lipoprotein receptor-related protein 2	-2.93	7.60	0.84	-3.03	8.16	0.83
COMMON	CX7A1	Cytochrome c oxidase subunit 7A1, mitochondrial	-2.93	7.60	0.93	-2.57	5.92	0.88
COMMON	CH60	60 kDa heat shock protein, mitochondrial	-2.92	7.56	0.96	-2.82	7.07	0.96

COMMON	C560	Succinate dehydrogenase cytochrome b560 subunit, mitochondrial	-2.92	7.55	0.83	-2.93	7.63	0.92
COMMON	NDUS1	NADH-ubiquinone oxidoreductase 75 kDa subunit, mitochondrial	-2.92	7.55	0.94	-2.95	7.74	0.90
COMMON	CP013	UPF0585 protein C16orf13 homolog	-2.90	7.48	0.87	-2.39	5.23	0.83
COMMON	COX41	Cytochrome c oxidase subunit 4 isoform 1, mitochondrial	-2.90	7.46	0.94	-2.88	7.37	0.93
COMMON	CX7A2	Cytochrome c oxidase subunit 7A2, mitochondrial	-2.88	7.37	0.92	-3.07	8.39	0.84
COMMON	NDUA4	Cytochrome c oxidase subunit NDUFA4	-2.87	7.30	0.89	-2.89	7.39	0.88
COMMON	AIFM1	Apoptosis-inducing factor 1, mitochondrial	-2.87	7.30	0.92	-2.99	7.96	0.92
COMMON	MUTA	Methylmalonyl-CoA mutase, mitochondrial	-2.86	7.27	0.81	-3.18	9.08	0.83
COMMON	MCCA	Methylcrotonoyl-CoA carboxylase subunit alpha, mitochondrial	-2.86	7.25	0.82	-2.97	7.81	0.82
COMMON	NDUB4	NADH dehydrogenase [ubiquinone] 1 beta subcomplex subunit 4	-2.85	7.21	0.83	-3.01	8.03	0.83
COMMON	ECHM	Enoyl-CoA hydratase, mitochondrial	-2.85	7.21	0.90	-2.99	7.96	0.90
COMMON	ATP5H	ATP synthase subunit d, mitochondrial	-2.85	7.21	0.93	-2.75	6.70	0.94
COMMON	OCTC	Peroxisomal carnitine O-octanoyltransferase	-2.85	7.20	0.80	-2.97	7.84	0.82
COMMON	CMC2	Calcium-binding mitochondrial carrier protein Aralar2	-2.85	7.20	0.80	-2.94	7.66	0.89
COMMON	NDUS4	NADH dehydrogenase [ubiquinone] iron-sulfur protein 4, mitochondrial	-2.85	7.19	0.83	-2.75	6.72	0.85
COMMON	DLDH	Dihydrolipoyl dehydrogenase, mitochondrial	-2.84	7.18	0.94	-2.83	7.11	0.93
COMMON	AL7A1	Alpha-aminoadipic semialdehyde dehydrogenase	-2.84	7.16	0.82	-2.84	7.15	0.87
COMMON	MEP1A	Meprin A subunit alpha	-2.84	7.15	0.88	-3.43	10.75	0.89
COMMON	QCR2	Cytochrome b-c1 complex subunit 2, mitochondrial	-2.84	7.14	0.94	-3.03	8.19	0.97
COMMON	QCR8	Cytochrome b-c1 complex subunit 8	-2.83	7.12	0.91	-3.11	8.65	0.92
COMMON	ADT2	ADP/ATP translocase 2	-2.82	7.06	0.81	-2.84	7.18	0.88
COMMON	ATP8	ATP synthase protein 8	-2.80	6.97	0.90	-2.68	6.43	0.81
COMMON	ATPG	ATP synthase subunit gamma, mitochondrial	-2.80	6.96	0.90	-2.94	7.65	0.92
COMMON	NDUAA	NADH dehydrogenase [ubiquinone] 1 alpha subcomplex subunit 10, mitochondrial	-2.79	6.92	0.93	-2.87	7.33	0.90
COMMON	S12A1	Solute carrier family 12 member 1	-2.79	6.91	0.96	-3.15	8.90	0.85
COMMON	AQP1	Aquaporin-1	-2.79	6.91	0.80	-3.05	8.29	0.88
COMMON	ODO2	Dihydrolipoyllysine-residue succinyltransferase component of 2-oxoglutarate dehydrogenase complex, mitochondrial	-2.79	6.89	0.89	-2.75	6.71	0.91
COMMON	TBA4A	Tubulin alpha-4A chain	-2.79	6.89	0.88	-2.86	7.28	0.81
COMMON	ATPO	ATP synthase subunit O, mitochondrial	-2.77	6.84	0.96	-2.77	6.83	0.96
COMMON	PCCA	Propionyl-CoA carboxylase alpha chain, mitochondrial	-2.77	6.83	0.84	-3.06	8.33	0.91
COMMON	BPNT1	3'(2'),5'-bisphosphate nucleotidase 1	-2.77	6.81	0.87	-2.88	7.34	0.81
COMMON	PTER	Phosphotriesterase-related protein	-2.75	6.73	0.91	-2.78	6.85	0.94
COMMON	ECI2	Enoyl-CoA delta isomerase 2, mitochondrial	-2.75	6.73	0.85	-2.99	7.96	0.85
COMMON	NDUS2	NADH dehydrogenase [ubiquinone] iron-sulfur protein 2, mitochondrial	-2.75	6.72	0.91	-2.84	7.15	0.86
COMMON	ES1	ES1 protein homolog, mitochondrial	-2.75	6.71	0.92	-2.68	6.41	0.91
COMMON	ACON	Aconitate hydratase, mitochondrial	-2.74	6.66	0.90	-3.15	8.88	0.88
COMMON	NDUS3	NADH dehydrogenase [ubiquinone] iron-sulfur protein 3, mitochondrial	-2.73	6.64	0.96	-2.70	6.51	0.94
COMMON	MDHM	Malate dehydrogenase, mitochondrial	-2.73	6.63	0.96	-2.80	6.97	0.94
COMMON	ATP5I	ATP synthase subunit e, mitochondrial	-2.73	6.62	0.90	-2.82	7.06	0.86
COMMON	USMG5	Up-regulated during skeletal muscle growth protein 5	-2.72	6.60	0.97	-2.79	6.93	0.97
COMMON	FUMH	Fumarate hydratase, mitochondrial	-2.71	6.56	0.89	-2.77	6.82	0.89
COMMON	ATPB	ATP synthase subunit beta, mitochondrial	-2.71	6.55	0.94	-2.85	7.19	0.96
COMMON	FABPH	Fatty acid-binding protein, heart	-2.71	6.53	0.88	-2.76	6.78	0.84
COMMON	AQP3	Aquaporin-3	-2.70	6.51	0.90	-3.66	12.64	0.85
COMMON	CX6B1	Cytochrome c oxidase subunit 6B1	-2.70	6.48	0.92	-2.87	7.32	0.88
COMMON	NDUA5	NADH dehydrogenase [ubiquinone] 1 alpha subcomplex subunit 5	-2.69	6.48	0.90	-2.75	6.71	0.89
COMMON	ATPA	ATP synthase subunit alpha, mitochondrial	-2.69	6.46	0.96	-2.81	7.02	0.96
COMMON	DHRS4	Dehydrogenase/reductase SDR family member 4	-2.68	6.42	0.91	-2.82	7.08	0.95
COMMON	SUSD2	Sushi domain-containing protein 2	-2.67	6.38	0.92	-2.52	5.75	0.93
COMMON	QCR1	Cytochrome b-c1 complex subunit 1, mitochondrial	-2.67	6.37	0.94	-2.74	6.69	0.93
COMMON	NDUA7	NADH dehydrogenase [ubiquinone] 1 alpha subcomplex subunit 7	-2.67	6.36	0.91	-2.80	6.97	0.87
COMMON	SFXN1	Sideroflexin-1	-2.67	6.35	0.83	-2.85	7.20	0.86
COMMON	QCR7	Cytochrome b-c1 complex subunit 7	-2.66	6.34	0.89	-2.86	7.28	0.88
COMMON	COX6C	Cytochrome c oxidase subunit 6C	-2.66	6.33	0.91	-2.61	6.11	0.89
COMMON	ODB2	Lipoamide acyltransferase component of branched-chain alpha-keto acid dehydrogenase complex, mitochondrial	-2.66	6.31	0.81	-3.62	12.29	0.80
COMMON	ARLY	Argininosuccinate lyase	-2.66	6.31	0.91	-2.65	6.28	0.92
COMMON	PRDX5	Peroxiredoxin-5, mitochondrial	-2.65	6.30	0.91	-2.54	5.81	0.91
COMMON	PGES2	Prostaglandin E synthase 2	-2.65	6.29	0.89	-2.55	5.84	0.81
COMMON	ATP5J	ATP synthase-coupling factor 6, mitochondrial	-2.65	6.29	0.97	-2.87	7.30	0.93

COMMON	KAT3	Kynurenine--oxoglutarate transaminase 3	-2.65	6.29	0.81	-2.88	7.36	0.82
COMMON	AT5F1	ATP synthase F(0) complex subunit B1, mitochondrial	-2.62	6.17	0.92	-2.81	7.03	0.92
COMMON	NU3M	NADH-ubiquinone oxidoreductase chain 3	-2.62	6.15	0.95	-2.82	7.06	0.95
COMMON	CH10	10 kDa heat shock protein, mitochondrial	-2.62	6.15	0.90	-2.55	5.86	0.90
COMMON	NDUB9	NADH dehydrogenase [ubiquinone] 1 beta subcomplex subunit 9	-2.61	6.10	0.83	-2.81	7.01	0.84
COMMON	AATM	Aspartate aminotransferase, mitochondrial	-2.61	6.10	0.97	-2.68	6.39	0.97
COMMON	DHB8	Estradiol 17-beta-dehydrogenase 8	-2.60	6.07	0.87	-2.47	5.55	0.81
COMMON	NDUA8	NADH dehydrogenase [ubiquinone] 1 alpha subcomplex subunit 8	-2.60	6.07	0.91	-2.55	5.86	0.89
COMMON	CHDH	Choline dehydrogenase, mitochondrial	-2.60	6.06	0.88	-2.51	5.69	0.88
COMMON	ODPB	Pyruvate dehydrogenase E1 component subunit beta, mitochondrial	-2.60	6.05	0.96	-2.60	6.07	0.97
COMMON	VATA	V-type proton ATPase catalytic subunit A	-2.59	6.04	0.92	-2.57	5.96	0.93
COMMON	ETHE1	Persulfide dioxygenase ETHE1, mitochondrial	-2.58	5.99	0.92	-2.70	6.52	0.93
COMMON	VATH	V-type proton ATPase subunit H	-2.57	5.94	0.90	-2.56	5.88	0.91
COMMON	NDUC2	NADH dehydrogenase [ubiquinone] 1 subunit C2	-2.57	5.93	0.88	-3.22	9.30	0.84
COMMON	DCXR	L-xylulose reductase	-2.57	5.92	0.88	-2.50	5.66	0.83
COMMON	GSTT2	Glutathione S-transferase theta-2	-2.55	5.84	0.87	-2.27	4.83	0.82
COMMON	ALDH2	Aldehyde dehydrogenase, mitochondrial	-2.54	5.82	0.95	-2.45	5.48	0.94
COMMON	TRAP1	Heat shock protein 75 kDa, mitochondrial	-2.54	5.82	0.88	-2.59	6.02	0.89
COMMON	AL9A1	4-trimethylaminobutyraldehyde dehydrogenase	-2.53	5.76	0.94	-2.83	7.09	0.92
COMMON	ETFD	Electron transfer flavoprotein-ubiquinone oxidoreductase, mitochondrial	-2.52	5.74	0.89	-2.46	5.49	0.90
COMMON	CPT2	Carnitine O-palmitoyltransferase 2, mitochondrial	-2.51	5.70	0.88	-2.58	5.99	0.85
COMMON	ANK3	Ankyrin-3	-2.51	5.70	0.85	-2.11	4.33	0.84
COMMON	Mar-02	Mitochondrial amidoxime reducing component 2	-2.50	5.65	0.89	-2.64	6.22	0.91
COMMON	ACOT1	Acyl-coenzyme A thioesterase 1	-2.49	5.63	0.85	-2.08	4.21	0.85
COMMON	DOPD	D-dopachrome decarboxylase	-2.49	5.63	0.91	-2.35	5.10	0.95
COMMON	TIM13	Mitochondrial import inner membrane translocase subunit Tim13	-2.48	5.58	0.96	-2.41	5.33	0.89
COMMON	ODPA	Pyruvate dehydrogenase E1 component subunit alpha, somatic form, mitochondrial	-2.48	5.58	0.92	-2.74	6.70	0.93
COMMON	MPCP	Phosphate carrier protein, mitochondrial	-2.48	5.57	0.90	-2.53	5.78	0.94
COMMON	ABHEB	Protein ABHD14B	-2.48	5.57	0.93	-2.28	4.87	0.91
COMMON	GRP75	Stress-70 protein, mitochondrial	-2.47	5.56	0.82	-2.21	4.62	0.85
COMMON	NDUBB	NADH dehydrogenase [ubiquinone] 1 beta subcomplex subunit 11, mitochondrial	-2.47	5.53	0.90	-2.74	6.67	0.93
COMMON	MIC19	MICOS complex subunit Mic19	-2.47	5.53	0.90	-2.55	5.85	0.86
COMMON	VATB2	V-type proton ATPase subunit B, brain isoform	-2.47	5.52	0.85	-2.30	4.92	0.91
COMMON	GSH1	Glutamate--cysteine ligase catalytic subunit	-2.46	5.49	0.86	-2.72	6.57	0.85
COMMON	NCEH1	Neutral cholesterol ester hydrolase 1	-2.45	5.47	0.92	-2.88	7.34	0.94
COMMON	ECH1	Delta(3,5)-Delta(2,4)-dienoyl-CoA isomerase, mitochondrial	-2.45	5.46	0.97	-2.40	5.27	0.95
COMMON	VATF	V-type proton ATPase subunit F	-2.45	5.45	0.90	-2.43	5.40	0.88
COMMON	VATG3	V-type proton ATPase subunit G 3	-2.44	5.43	0.94	-2.25	4.74	0.84
COMMON	DECR	2,4-dienoyl-CoA reductase, mitochondrial	-2.43	5.39	0.89	-2.49	5.63	0.88
COMMON	CMBL	Carboxymethylenebutenolidase homolog	-2.43	5.38	0.85	-2.87	7.32	0.80
COMMON	ACADS	Short-chain specific acyl-CoA dehydrogenase, mitochondrial	-2.42	5.36	0.89	-2.65	6.28	0.89
COMMON	SUCB1	Succinyl-CoA ligase [ADP-forming] subunit beta, mitochondrial	-2.42	5.33	0.97	-2.82	7.07	0.93
COMMON	VATE1	V-type proton ATPase subunit E 1	-2.41	5.32	0.91	-2.45	5.47	0.92
COMMON	LPPRC	Leucine-rich PPR motif-containing protein, mitochondrial	-2.40	5.26	0.88	-2.31	4.96	0.85
COMMON	ODP2	Dihydrolipoyllysine-residue acetyltransferase component of pyruvate dehydrogenase complex, mitochondrial	-2.39	5.25	0.98	-2.65	6.28	0.94
COMMON	PRDX3	Thioredoxin-dependent peroxide reductase, mitochondrial	-2.39	5.23	0.90	-2.59	6.04	0.89
COMMON	KAD2	Adenylate kinase 2, mitochondrial	-2.38	5.21	0.86	-2.60	6.06	0.89
COMMON	SQRD	Sulfide:quinone oxidoreductase, mitochondrial	-2.38	5.20	0.92	-2.33	5.04	0.89
COMMON	GSHB	Glutathione synthetase	-2.37	5.17	0.82	-2.60	6.07	0.89
COMMON	LYPA1	Acyl-protein thioesterase 1	-2.36	5.13	0.90	-2.21	4.62	0.88
COMMON	ACADV	Very long-chain specific acyl-CoA dehydrogenase, mitochondrial	-2.36	5.12	0.89	-2.53	5.79	0.85
COMMON	KAD3	GTP:AMP phosphotransferase AK3, mitochondrial	-2.35	5.10	0.89	-2.25	4.75	0.89
COMMON	DHPR	Dihydropteridine reductase	-2.34	5.07	0.88	-2.45	5.45	0.91
COMMON	NIT1	Nitrilase homolog 1	-2.33	5.03	0.90	-2.28	4.86	0.89
COMMON	ODO1	2-oxoglutarate dehydrogenase, mitochondrial	-2.32	5.00	0.91	-2.53	5.76	0.89
COMMON	SAP3	Ganglioside GM2 activator	-2.31	4.96	0.85	-2.42	5.34	0.85
COMMON	MDHC	Malate dehydrogenase, cytoplasmic	-2.30	4.94	0.95	-2.44	5.41	0.94
COMMON	SPS2	Selenide, water dikinase 2	-2.30	4.93	0.90	-2.33	5.03	0.84
COMMON	THIOM	Thioredoxin, mitochondrial	-2.29	4.90	0.90	-2.34	5.05	0.95
COMMON	RM12	39S ribosomal protein L12, mitochondrial	-2.29	4.89	0.91	-2.27	4.83	0.93

COMMON	NIT2	Omega-amidase NIT2	-2.29	4.88	0.90	-2.07	4.19	0.90
COMMON	IDH3A	Isocitrate dehydrogenase [NAD] subunit alpha, mitochondrial	-2.28	4.86	0.91	-2.38	5.19	0.93
COMMON	NDUA6	NADH dehydrogenase [ubiquinone] 1 alpha subcomplex subunit 6	-2.28	4.86	0.84	-2.35	5.11	0.87
COMMON	VDAC1	Voltage-dependent anion-selective channel protein 1	-2.28	4.85	0.96	-2.46	5.49	0.96
COMMON	HYES	Bifunctional epoxide hydrolase 2	-2.28	4.85	0.81	-4.65	25.06	0.84
COMMON	ACOC	Cytoplasmic aconitate hydratase	-2.28	4.84	0.94	-2.41	5.32	0.88
COMMON	ECI1	Enoyl-CoA delta isomerase 1, mitochondrial	-2.26	4.80	0.91	-2.46	5.51	0.90
COMMON	HCD2	3-hydroxyacyl-CoA dehydrogenase type-2	-2.25	4.76	0.91	-2.32	5.00	0.94
COMMON	IDHC	Isocitrate dehydrogenase [NADP] cytoplasmic	-2.25	4.75	0.90	-2.28	4.87	0.91
COMMON	MIC27	MICOS complex subunit Mic27	-2.23	4.70	0.81	-2.17	4.49	0.87
COMMON	SAM50	Sorting and assembly machinery component 50 homolog	-2.23	4.69	0.89	-2.49	5.60	0.90
COMMON	LONM	Lon protease homolog, mitochondrial	-2.22	4.66	0.90	-1.95	3.87	0.90
COMMON	MIC60	MICOS complex subunit Mic60	-2.22	4.65	0.92	-2.66	6.32	0.93
COMMON	ATIF1	ATPase inhibitor, mitochondrial	-2.21	4.61	0.83	-1.89	3.71	0.83
COMMON	LYZ2	Lysozyme C-2	-2.20	4.60	0.93	-2.39	5.25	0.87
COMMON	OAT	Ornithine aminotransferase, mitochondrial	-2.20	4.59	0.86	-2.09	4.26	0.86
COMMON	EFTU	Elongation factor Tu, mitochondrial	-2.18	4.54	0.95	-2.24	4.73	0.95
COMMON	CMC1	Calcium-binding mitochondrial carrier protein Aralar1	-2.17	4.51	0.84	-2.32	5.01	0.86
COMMON	ECHA	Trifunctional enzyme subunit alpha, mitochondrial	-2.16	4.46	0.97	-2.22	4.67	0.96
COMMON	THTM	3-mercaptopyruvate sulfurtransferase	-2.14	4.41	0.83	-2.34	5.06	0.82
COMMON	XPP1	Xaa-Pro aminopeptidase 1	-2.14	4.40	0.87	-2.02	4.05	0.85
COMMON	VATD	V-type proton ATPase subunit D	-2.14	4.40	0.89	-2.18	4.54	0.86
COMMON	BCAT2	Branched-chain-amino-acid aminotransferase, mitochondrial	-2.13	4.38	0.89	-2.88	7.36	0.89
COMMON	DHE3	Glutamate dehydrogenase 1, mitochondrial	-2.13	4.37	0.92	-2.37	5.15	0.93
COMMON	4F2	4F2 cell-surface antigen heavy chain	-2.12	4.34	0.91	-2.31	4.94	0.93
COMMON	ATAD3	ATPase family AAA domain-containing protein 3	-2.10	4.30	0.80	-2.11	4.33	0.87
COMMON	ACADL	Long-chain specific acyl-CoA dehydrogenase, mitochondrial	-2.10	4.28	0.87	-2.19	4.56	0.95
COMMON	CPT1A	Carnitine O-palmitoyltransferase 1, liver isoform	-2.09	4.27	0.84	-2.07	4.20	0.85
COMMON	KCRU	Creatine kinase U-type, mitochondrial	-2.08	4.24	0.88	-2.06	4.16	0.84
COMMON	AMPE	Glutamyl aminopeptidase	-2.07	4.21	0.87	-1.85	3.60	0.86
COMMON	GLRX5	Glutaredoxin-related protein 5, mitochondrial	-2.07	4.20	0.93	-2.07	4.20	0.86
COMMON	MAOX	NADP-dependent malic enzyme	-2.07	4.20	0.83	-2.51	5.68	0.87
COMMON	M2OM	Mitochondrial 2-oxoglutarate/malate carrier protein	-2.07	4.19	0.83	-2.10	4.29	0.88
COMMON	CLIC5	Chloride intracellular channel protein 5	-2.06	4.18	0.85	-1.51	2.86	0.81
COMMON	ACDSB	Short/branched chain specific acyl-CoA dehydrogenase, mitochondrial	-2.04	4.10	0.93	-2.29	4.89	0.94
COMMON	BASI	Basigin	-2.03	4.09	0.87	-2.19	4.56	0.82
COMMON	SCRN2	Secernin-2	-2.02	4.05	0.82	-2.43	5.37	0.83
COMMON	TMM65	Transmembrane protein 65	-2.01	4.03	0.88	-1.84	3.59	0.91
COMMON	MTCH2	Mitochondrial carrier homolog 2	-2.00	4.01	0.89	-2.11	4.32	0.89
COMMON	PROSC	Proline synthase co-transcribed bacterial homolog protein	-2.00	4.01	0.90	-1.68	3.21	0.89
COMMON	LDHB	L-lactate dehydrogenase B chain	-2.00	3.99	0.86	-2.08	4.24	0.86
COMMON	MOT1	Monocarboxylate transporter 1	-1.99	3.98	0.91	-2.10	4.28	0.80
COMMON	GLNA	Glutamine synthetase	-1.97	3.91	0.83	-3.14	8.84	0.83
COMMON	CYB5	Cytochrome b5	-1.95	3.87	0.86	-1.85	3.60	0.89
COMMON	CISY	Citrate synthase, mitochondrial	-1.94	3.83	0.88	-1.88	3.69	0.89
COMMON	AMPN	Aminopeptidase N	-1.94	3.83	0.95	-2.09	4.26	0.94
COMMON	ADT1	ADP/ATP translocase 1	-1.93	3.82	0.83	-2.04	4.11	0.85
COMMON	EM55	55 kDa erythrocyte membrane protein	-1.93	3.82	0.91	-2.16	4.48	0.86
COMMON	PTGR2	Prostaglandin reductase 2	-1.92	3.79	0.89	-1.66	3.15	0.92
COMMON	NPL	N-acetylneuraminate lyase	-1.91	3.76	0.88	-1.77	3.41	0.86
COMMON	PHB2	Prohibitin-2	-1.90	3.73	0.94	-1.94	3.84	0.93
COMMON	MIF	Macrophage migration inhibitory factor	-1.89	3.71	0.92	-1.92	3.79	0.89
COMMON	AATC	Aspartate aminotransferase, cytoplasmic	-1.88	3.68	0.88	-1.81	3.51	0.89
COMMON	DHI2	Corticosteroid 11-beta-dehydrogenase isozyme 2	-1.88	3.67	0.83	-1.69	3.22	0.88
COMMON	CYB5B	Cytochrome b5 type B	-1.86	3.62	0.93	-1.20	2.29	0.90
COMMON	THIC	Acetyl-CoA acetyltransferase, cytosolic	-1.85	3.61	0.85	-2.34	5.08	0.81
COMMON	GSTA4	Glutathione S-transferase A4	-1.85	3.61	0.86	-1.53	2.89	0.87
COMMON	AMPL	Cytosol aminopeptidase	-1.84	3.57	0.93	-1.86	3.63	0.93
COMMON	VATC1	V-type proton ATPase subunit C 1	-1.83	3.55	0.83	-1.98	3.94	0.85
COMMON	C1QBP	Complement component 1 Q subcomponent-binding protein, mitochondrial	-1.82	3.52	0.83	-1.86	3.63	0.92
COMMON	ACBP	Acyl-CoA-binding protein	-1.81	3.51	0.93	-1.77	3.42	0.96
COMMON	EFTS	Elongation factor Ts, mitochondrial	-1.81	3.50	0.85	-1.94	3.83	0.83
COMMON	TXTP	Tricarboxylate transport protein, mitochondrial	-1.80	3.47	0.87	-1.69	3.23	0.83
COMMON	SPRE	Sepiapterin reductase	-1.79	3.47	0.96	-1.72	3.28	0.96
COMMON	GPX1	Glutathione peroxidase 1	-1.79	3.45	0.92	-1.97	3.91	0.94

COMMON	F213A	Redox-regulatory protein FAM213A	-1.77	3.42	0.89	-1.73	3.31	0.83
COMMON	DHB4	Peroxisomal multifunctional enzyme type 2	-1.76	3.39	0.95	-1.95	3.87	0.94
COMMON	ECHB	Trifunctional enzyme subunit beta, mitochondrial	-1.75	3.37	0.87	-2.15	4.43	0.89
COMMON	SODC	Superoxide dismutase [Cu-Zn]	-1.74	3.33	0.94	-1.69	3.22	0.95
COMMON	ESTD	S-formylglutathione hydrolase	-1.72	3.28	0.86	-1.92	3.80	0.88
COMMON	APMAP	Adipocyte plasma membrane-associated protein	-1.71	3.28	0.84	-1.55	2.93	0.85
COMMON	GSTM5	Glutathione S-transferase Mu 5	-1.71	3.27	0.87	-1.86	3.62	0.89
COMMON	PGK1	Phosphoglycerate kinase 1	-1.71	3.27	0.97	-1.74	3.35	0.97
COMMON	VA0D1	V-type proton ATPase subunit d 1	-1.70	3.24	0.87	-1.67	3.19	0.87
COMMON	PGM1	Phosphoglucomutase-1	-1.65	3.13	0.90	-1.66	3.15	0.85
COMMON	PHB	Prohibitin	-1.65	3.13	0.92	-1.79	3.45	0.93
COMMON	EZRI	Ezrin	-1.65	3.13	0.96	-1.77	3.41	0.96
COMMON	HINT1	Histidine triad nucleotide-binding protein 1	-1.60	3.04	0.88	-1.62	3.06	0.95
COMMON	SAHH	Adenosylhomocysteinase	-1.58	2.99	0.91	-1.37	2.58	0.91
COMMON	GNPI1	Glucosamine-6-phosphate isomerase 1	-1.56	2.96	0.89	-1.74	3.33	0.88
COMMON	CAH2	Carbonic anhydrase 2	-1.56	2.95	0.95	-1.58	2.99	0.96
COMMON	THIKA	3-ketoacyl-CoA thiolase A, peroxisomal	-1.56	2.95	0.91	-1.49	2.81	0.82
COMMON	HDHD2	Haloacid dehalogenase-like hydrolase domain-containing protein 2	-1.53	2.90	0.82	-1.41	2.66	0.82
COMMON	41	Protein 4.1	-1.51	2.84	0.85	-1.83	3.55	0.83
COMMON	VDAC2	Voltage-dependent anion-selective channel protein 2	-1.50	2.84	0.94	-1.64	3.13	0.93
COMMON	HEM2	Delta-aminolevulinic acid dehydratase	-1.50	2.82	0.91	-1.34	2.54	0.91
COMMON	RADI	Radixin	-1.48	2.79	0.83	-1.76	3.39	0.89
COMMON	CCS	Copper chaperone for superoxide dismutase	-1.46	2.75	0.99	-2.39	5.23	0.83
COMMON	AKCL2	1,5-anhydro-D-fructose reductase	-1.45	2.73	0.93	-1.67	3.19	0.82
COMMON	GPD1L	Glycerol-3-phosphate dehydrogenase 1-like protein	-1.44	2.72	0.87	-1.18	2.26	0.85
COMMON	TPIS	Triosephosphate isomerase	-1.44	2.71	0.95	-1.36	2.56	0.83
COMMON	UGPA	UTP--glucose-1-phosphate uridylyltransferase	-1.41	2.66	0.87	-1.45	2.74	0.85
COMMON	HXK1	Hexokinase-1	-1.41	2.66	0.91	-1.33	2.51	0.92
COMMON	FIS1	Mitochondrial fission 1 protein	-1.41	2.65	0.89	-1.54	2.91	0.88
COMMON	GLGB	1,4-alpha-glucan-branching enzyme	-1.37	2.59	0.98	-1.47	2.77	0.86
COMMON	FUCM	Fucose mutarotase	-1.33	2.52	0.88	-1.11	2.15	0.88
COMMON	ENOA	Alpha-enolase	-1.33	2.51	0.98	-1.30	2.47	0.98
COMMON	SYPL1	Synaptophysin-like protein 1	-1.32	2.50	0.91	-1.45	2.73	1.00
COMMON	PDXK	Pyridoxal kinase	-1.28	2.42	0.85	-1.59	3.01	0.92
COMMON	PARK7	Protein deglycase DJ-1	-1.27	2.42	0.93	-1.37	2.58	0.87
COMMON	PGAM1	Phosphoglycerate mutase 1	-1.27	2.41	0.97	-1.26	2.39	0.95
COMMON	GMPR1	GMP reductase 1	-1.27	2.41	0.81	-1.05	2.06	0.92
COMMON	GSTM1	Glutathione S-transferase Mu 1	-1.24	2.37	0.89	-1.15	2.22	0.89
COMMON	G3P	Glyceraldehyde-3-phosphate dehydrogenase	-1.19	2.29	0.92	-1.13	2.18	0.90
COMMON	TMM33	Transmembrane protein 33	-1.19	2.28	0.86	-0.99	1.99	0.83
COMMON	TIM44	Mitochondrial import inner membrane translocase subunit TIM44	-1.17	2.25	0.83	-1.38	2.61	0.83
COMMON	PRDX6	Peroxiredoxin-6	-1.16	2.23	0.94	-1.02	2.03	0.96
COMMON	NDKB	Nucleoside diphosphate kinase B	-1.08	2.11	0.95	-1.14	2.20	0.90
COMMON	ADK	Adenosine kinase	-1.02	2.03	0.87	-1.21	2.31	0.83
COMMON	PRDX1	Peroxiredoxin-1	-1.02	2.03	0.91	-1.13	2.19	0.90
COMMON	G6PI	Glucose-6-phosphate isomerase	-1.02	2.03	0.93	-1.05	2.07	0.96
COMMON	PACN2	Protein kinase C and casein kinase substrate in neurons protein 2	-0.97	1.96	0.85	-1.30	2.46	0.88
COMMON	MAT2B	Methionine adenosyltransferase 2 subunit beta	-0.96	1.94	0.89	-0.83	1.78	0.96
COMMON	PEBP1	Phosphatidylethanolamine-binding protein 1	-0.94	1.92	0.92	-0.96	1.95	0.95
COMMON	SPTN1	Spectrin alpha chain, non-erythrocytic 1	-0.89	1.85	0.88	-0.88	1.84	0.98
COMMON	TMED4	Transmembrane emp24 domain-containing protein 4	-0.88	1.84	0.90	-0.97	1.95	0.86
COMMON	SPTB2	Spectrin beta chain, non-erythrocytic 1	-0.84	1.80	0.87	-0.87	1.83	0.85
COMMON	UGDH	UDP-glucose 6-dehydrogenase	-0.84	1.79	0.82	-1.08	2.12	0.82
COMMON	GSTP1	Glutathione S-transferase P 1	-0.82	1.77	0.94	-0.80	1.74	0.93
COMMON	UAP1L	UDP-N-acetylhexosamine pyrophosphorylase-like protein 1	-0.81	1.76	0.84	-0.70	1.63	0.84
COMMON	SNX3	Sorting nexin-3	-0.78	1.72	0.84	-0.79	1.73	0.85
COMMON	TBB4B	Tubulin beta-4B chain	-0.77	1.71	0.90	-0.96	1.95	1.00
COMMON	ALDOA	Fructose-bisphosphate aldolase A	-0.65	1.57	0.84	-0.69	1.61	0.90
COMMON	GPX3	Glutathione peroxidase 3	-0.63	1.54	0.83	-0.50	1.41	0.83
COMMON	HS90A	Heat shock protein HSP 90-alpha	-0.58	1.50	0.81	-0.55	1.46	0.82
TG2-KO ONLY	SC5A3	Sodium/myo-inositol cotransporter	-3.86	14.51	0.63	-4.79	27.69	0.86
TG2-KO ONLY	CX6A1	Cytochrome c oxidase subunit 6A1, mitochondrial	-3.57	11.91	0.74	-4.43	21.54	0.80
TG2-KO ONLY	PCKGC	Phosphoenolpyruvate carboxykinase, cytosolic [GTP]	-4.20	18.41	0.80	-4.10	17.10	0.85
TG2-KO ONLY	ACOX1	Peroxisomal acyl-coenzyme A oxidase 1	-2.33	5.01	0.78	-3.86	14.52	0.88
TG2-KO ONLY	ACO13	Acyl-coenzyme A thioesterase 13	-3.14	8.84	0.77	-3.60	12.10	0.88
TG2-KO ONLY	S22AC	Solute carrier family 22 member 12	-3.15	8.90	0.78	-3.55	11.74	0.83
TG2-KO ONLY	IYD1	Iodotyrosine deiodinase 1	-5.13	35.04	0.44	-3.55	11.72	0.86
TG2-KO ONLY	ABCG2	ATP-binding cassette sub-family G member 2	-4.12	17.42	0.79	-3.55	11.70	0.86

TG2-KO ONLY	ODBB	2-oxoisovalerate dehydrogenase subunit beta, mitochondrial	-3.09	8.53	0.78	-3.50	11.28	0.81
TG2-KO ONLY	S23A1	Solute carrier family 23 member 1	-3.84	14.29	0.78	-3.45	10.96	0.83
TG2-KO ONLY	SOX	Peroxisomal sarcosine oxidase	-2.77	6.84	0.76	-3.45	10.94	0.84
TG2-KO ONLY	PPR1A	Protein phosphatase 1 regulatory subunit 1A	-3.89	14.87	0.68	-3.44	10.83	0.88
TG2-KO ONLY	COX3	Cytochrome c oxidase subunit 3	-4.30	19.65	0.64	-3.40	10.56	0.91
TG2-KO ONLY	M2GD	Dimethylglycine dehydrogenase, mitochondrial	-3.27	9.68	0.78	-3.37	10.33	0.83
TG2-KO ONLY	COA6	Cytochrome c oxidase assembly factor 6 homolog	-2.55	5.87	0.67	-3.36	10.29	0.81
TG2-KO ONLY	S22A8	Solute carrier family 22 member 8	-3.25	9.52	0.80	-3.35	10.19	0.80
TG2-KO ONLY	SUCHY	Succinate--hydroxymethylglutarate CoA-transferase	-3.35	10.18	0.41	-3.26	9.59	0.85
TG2-KO ONLY	MIRO2	Mitochondrial Rho GTPase 2	-3.38	10.40	0.55	-3.23	9.35	0.87
TG2-KO ONLY	AK1CL	Aldo-keto reductase family 1 member C21	-2.94	7.66	0.79	-3.16	8.97	0.84
TG2-KO ONLY	PHS	Pterin-4-alpha-carbinolamine dehydratase	-2.96	7.81	0.80	-3.05	8.31	0.82
TG2-KO ONLY	ECHD1	Ethylmalonyl-CoA decarboxylase	-1.87	3.65	0.78	-3.04	8.24	0.86
TG2-KO ONLY	AKC1H	Aldo-keto reductase family 1 member C18	-2.98	7.87	0.56	-3.01	8.07	0.87
TG2-KO ONLY	ENPP3	Ectonucleotide pyrophosphatase/phosphodiesterase family member 3	-2.57	5.94	0.71	-2.99	7.92	0.81
TG2-KO ONLY	RM23	39S ribosomal protein L23, mitochondrial	-2.16	4.46	0.61	-2.96	7.79	0.81
TG2-KO ONLY	NDUA2	NADH dehydrogenase [ubiquinone] 1 alpha subcomplex subunit 2	-2.78	6.87	0.77	-2.96	7.78	0.83
TG2-KO ONLY	RT36	28S ribosomal protein S36, mitochondrial	-2.92	7.55	0.67	-2.93	7.64	0.91
TG2-KO ONLY	3BHS4	3 beta-hydroxysteroid dehydrogenase type 4	-4.07	16.79	0.79	-2.92	7.58	0.81
TG2-KO ONLY	SFXN2	Sideroflexin-2	-3.49	11.27	0.65	-2.79	6.90	0.82
TG2-KO ONLY	FOLH1	Glutamate carboxypeptidase 2	-3.04	8.24	0.58	-2.77	6.81	0.80
TG2-KO ONLY	ACOT2	Acyl-coenzyme A thioesterase 2, mitochondrial	-2.43	5.38	0.79	-2.76	6.79	0.80
TG2-KO ONLY	MIC13	MICOS complex subunit MIC13	-2.90	7.47	0.72	-2.72	6.57	0.92
TG2-KO ONLY	COX7C	Cytochrome c oxidase subunit 7C, mitochondrial	-2.67	6.35	0.80	-2.72	6.57	0.80
TG2-KO ONLY	UD3A1	UDP-glucuronosyltransferase 3A1	-2.38	5.20	0.72	-2.64	6.24	0.84
TG2-KO ONLY	NDUS8	NADH dehydrogenase [ubiquinone] iron-sulfur protein 8, mitochondrial	-2.81	7.02	0.80	-2.63	6.20	0.86
TG2-KO ONLY	ENTP5	Ectonucleoside triphosphate diphosphohydrolase 5	-4.19	18.28	0.75	-2.62	6.15	0.80
TG2-KO ONLY	ACOX3	Peroxisomal acyl-coenzyme A oxidase 3	-3.46	11.01	0.41	-2.59	6.00	0.82
TG2-KO ONLY	DYR	Dihydrofolate reductase	-2.49	5.60	0.79	-2.50	5.65	0.82
TG2-KO ONLY	DAB2	Disabled homolog 2	-2.71	6.56	0.79	-2.49	5.62	0.80
TG2-KO ONLY	SAHH3	Putative adenosylhomocysteinase 3	-2.46	5.51	0.76	-2.47	5.54	0.83
TG2-KO ONLY	CLPX	ATP-dependent Clp protease ATP-binding subunit clpX-like, mitochondrial	-2.00	3.99	0.78	-2.45	5.48	0.91
TG2-KO ONLY	TIM8A	Mitochondrial import inner membrane translocase subunit Tim8 A	-2.15	4.45	0.67	-2.45	5.45	0.84
TG2-KO ONLY	MIA40	Mitochondrial intermembrane space import and assembly protein 40	-4.44	21.77	0.50	-2.45	5.45	0.86
TG2-KO ONLY	NDUS5	NADH dehydrogenase [ubiquinone] iron-sulfur protein 5	-2.96	7.78	0.67	-2.39	5.22	0.85
TG2-KO ONLY	AACS	Acetoacetyl-CoA synthetase	-2.64	6.24	0.60	-2.38	5.22	0.81
TG2-KO ONLY	P5CR3	Pyrroline-5-carboxylate reductase 3	-1.23	2.34	0.41	-2.35	5.08	0.84
TG2-KO ONLY	TIM9	Mitochondrial import inner membrane translocase subunit Tim9	-2.23	4.68	0.77	-2.28	4.85	0.81
TG2-KO ONLY	OPA1	Dynamin-like 120 kDa protein, mitochondrial	-1.99	3.97	0.74	-2.28	4.84	0.86
TG2-KO ONLY	GLYC	Serine hydroxymethyltransferase, cytosolic	-2.22	4.67	0.77	-2.25	4.75	0.85
TG2-KO ONLY	CLPP	ATP-dependent Clp protease proteolytic subunit, mitochondrial	-2.29	4.89	0.73	-2.17	4.51	0.87
TG2-KO ONLY	LETM1	LETM1 and EF-hand domain-containing protein 1, mitochondrial	-2.27	4.84	0.79	-2.16	4.47	0.86
TG2-KO ONLY	IAH1	Isoamyl acetate-hydrolyzing esterase 1 homolog	-2.03	4.10	0.76	-2.12	4.35	0.82
TG2-KO ONLY	CACP	Carnitine O-acetyltransferase	-2.31	4.95	0.74	-2.04	4.11	0.82
TG2-KO ONLY	GSH0	Glutamate--cysteine ligase regulatory subunit	-1.92	3.77	0.53	-2.02	4.07	0.84
TG2-KO ONLY	KAT1	Kynurenine--oxoglutarate transaminase 1	-2.34	5.05	0.69	-1.86	3.63	0.82
TG2-KO ONLY	ATAD1	ATPase family AAA domain-containing protein 1	-1.43	2.69	0.79	-1.83	3.57	0.85
TG2-KO ONLY	MYO6	Unconventional myosin-VI	-1.84	3.59	0.80	-1.73	3.31	0.85
TG2-KO ONLY	TIM50	Mitochondrial import inner membrane translocase subunit TIM50	-2.06	4.18	0.49	-1.71	3.27	0.89
TG2-KO ONLY	SYIM	Isoleucine--tRNA ligase, mitochondrial	-1.99	3.98	0.73	-1.71	3.27	0.83
TG2-KO ONLY	NOMO1	Nodal modulator 1	-1.19	2.28	0.53	-1.60	3.03	0.81
TG2-KO ONLY	LAD1	Ladinin-1	-1.53	2.89	0.66	-1.48	2.79	0.80
TG2-KO ONLY	AL3A2	Fatty aldehyde dehydrogenase	-1.38	2.61	0.79	-1.45	2.74	0.86
TG2-KO ONLY	ADHX	Alcohol dehydrogenase class-3	-1.05	2.07	0.78	-1.26	2.40	0.84
TG2-KO ONLY	GBG12	Guanine nucleotide-binding protein G(I)/G(S)/G(O) subunit gamma-12	-0.40	1.32	0.51	-1.26	2.39	0.94
TG2-KO ONLY	BACH	Cytosolic acyl coenzyme A thioester hydrolase	-1.01	2.02	0.30	-1.25	2.38	0.81
TG2-KO ONLY	SELT	Selenoprotein T	-1.43	2.70	0.76	-1.22	2.32	0.96
TG2-KO ONLY	NNRD	ATP-dependent (S)-NAD(P)H-hydrate dehydratase	-1.18	2.27	0.78	-1.21	2.32	0.82

TG2-KO ONLY	RAB14	Ras-related protein Rab-14	-0.85	1.80	0.74	-1.09	2.13	0.83
TG2-KO ONLY	BIEA	Biliverdin reductase A	-0.96	1.94	0.63	-1.07	2.10	0.81
TG2-KO ONLY	VPS35	Vacuolar protein sorting-associated protein 35	-1.06	2.09	0.50	-1.06	2.09	0.81
TG2-KO ONLY	RAB8A	Ras-related protein Rab-8A	-1.10	2.15	0.74	-1.04	2.06	0.82
TG2-KO ONLY	KCY	UMP-CMP kinase	-1.14	2.21	0.75	-1.03	2.04	0.83
TG2-KO ONLY	CNDP2	Cytosolic non-specific dipeptidase	-0.93	1.90	0.77	-1.00	2.00	0.85
TG2-KO ONLY	COMT	Catechol O-methyltransferase	-0.62	1.54	0.49	-0.96	1.95	0.82
TG2-KO ONLY	TXD17	Thioredoxin domain-containing protein 17	-0.73	1.66	0.77	-0.96	1.95	0.87
TG2-KO ONLY	RTN3	Reticulon-3	-0.79	1.72	0.77	-0.95	1.94	0.88
TG2-KO ONLY	VAMP8	Vesicle-associated membrane protein 8	-1.27	2.41	0.77	-0.95	1.94	0.83
TG2-KO ONLY	ERLN2	Erlin-2	-0.69	1.62	0.66	-0.90	1.87	0.80
TG2-KO ONLY	GSTT1	Glutathione S-transferase theta-1	-0.91	1.87	0.80	-0.88	1.84	0.85
TG2-KO ONLY	LGUL	Lactoylglutathione lyase	-1.04	2.06	0.74	-0.87	1.83	0.83
TG2-KO ONLY	ISOC1	Isochorismatase domain-containing protein 1	-0.66	1.58	0.71	-0.86	1.81	0.85
TG2-KO ONLY	RASN	GTPase NRas	-0.68	1.61	0.70	-0.84	1.79	0.81
TG2-KO ONLY	HACD3	Very-long-chain (3R)-3-hydroxyacyl-CoA dehydratase 3	-0.67	1.60	0.74	-0.79	1.73	0.88
TG2-KO ONLY	GALK2	N-acetylgalactosamine kinase	-0.70	1.62	0.58	-0.78	1.72	0.81
TG2-KO ONLY	VP26A	Vacuolar protein sorting-associated protein 26A	-0.70	1.63	0.79	-0.78	1.72	0.92
TG2-KO ONLY	ITPR1	Inositol 1,4,5-trisphosphate receptor type 1	-0.69	1.61	0.59	-0.77	1.70	0.83
TG2-KO ONLY	DNJA1	DnaJ homolog subfamily A member 1	-0.89	1.85	0.48	-0.77	1.70	0.81
TG2-KO ONLY	RB11B	Ras-related protein Rab-11B	-0.49	1.41	0.68	-0.75	1.69	0.89
TG2-KO ONLY	RS27L	40S ribosomal protein S27-like	-1.07	2.10	0.77	-0.73	1.65	0.86
TG2-KO ONLY	PGRC1	Membrane-associated progesterone receptor component 1	-0.69	1.61	0.67	-0.72	1.65	0.84
TG2-KO ONLY	PTH2	Peptidyl-tRNA hydrolase 2, mitochondrial	-0.86	1.82	0.57	-0.71	1.63	0.96
TG2-KO ONLY	GLOD4	Glyoxalase domain-containing protein 4	-0.67	1.59	0.71	-0.70	1.62	0.87
TG2-KO ONLY	F10A1	Hsc70-interacting protein	-0.88	1.84	0.54	-0.68	1.61	0.85
TG2-KO ONLY	ACLY	ATP-citrate synthase	-0.80	1.74	0.76	-0.67	1.60	0.85
TG2-KO ONLY	GLRX1	Glutaredoxin-1	-0.72	1.65	0.54	-0.63	1.55	0.83
TG2-KO ONLY	FKBP3	Peptidyl-prolyl cis-trans isomerase FKBP3	-0.62	1.53	0.67	-0.63	1.55	0.81
TG2-KO ONLY	DPEP1	Dipeptidase 1	-0.51	1.43	0.76	-0.61	1.53	0.86
TG2-KO ONLY	LDHA	L-lactate dehydrogenase A chain	-0.52	1.44	0.72	-0.60	1.52	0.88
TG2-KO ONLY	SYSC	Serine--tRNA ligase, cytoplasmic	-0.53	1.45	0.57	-0.53	1.45	0.82
TG2-KO ONLY	TKT	Transketolase	-0.40	1.32	0.51	-0.47	1.38	0.84
TG2-KO ONLY	PRDX2	Peroxiredoxin-2	-0.36	1.28	0.64	-0.45	1.37	0.88

S.2 SUPPLEMENTARY DATA FOR CHAPTER IV

S.2.1 Lists of TG2-associated proteins in the cytosolic fraction of UUO and Sham-operated kidneys at 21 days post-surgery

Supplementary Table 4.1: List of proteins significantly associated with TG2 in UUO kidneys' cytosolic fraction. This table shows all the proteins recognised as TG2-associated (z test, $p \leq 0.05$ $N \geq 4$) in the cytosolic fraction of UUO kidneys at 21 days post-operation. U = Uniquely expressed in UUO, C = common between UUO and Sham.

TG2-associated proteins in UUO kidney cytosolic faction				
Sample ID	**Name**	**N**	**p-value**	**Unique/ Common**
UBP24_MOUSE	Ubiquitin carboxyl-terminal hydrolase 24	4	0.00E+00	U
GPX41_MOUSE	Phospholipid hydroperoxide glutathione peroxidase, mitochondrial	5	0.00E+00	U
HSPB1_MOUSE	Heat shock protein beta-1	5	0.00E+00	U
CKAP4_MOUSE	Cytoskeleton-associated protein 4	4	2.88E-14	U
FBLN1_MOUSE	Fibulin-1	5	1.17E-10	U
GBP2_MOUSE	Guanylate-binding protein 1	5	1.69E-09	U
DX39B_MOUSE	Spliceosome RNA helicase Ddx39b	5	6.81E-09	C
PP6R1_MOUSE	Serine/threonine-protein phosphatase 6 regulatory subunit 1	4	8.59E-09	U
RS18_MOUSE	40S ribosomal protein S18	5	9.03E-08	U
IMB1_MOUSE	Importin subunit beta-1	5	9.38E-08	U
TES_MOUSE	Testin	4	1.42E-07	U
TCPQ_MOUSE	T-complex protein 1 subunit theta	5	1.96E-07	C
PMM2_MOUSE	Phosphomannomutase 2	5	2.92E-07	U
DCTN1_MOUSE	Dynactin subunit 1	5	2.94E-07	U
SEC13_MOUSE	Protein SEC13 homolog	5	1.10E-06	U
POSTN_MOUSE	Periostin	4	1.88E-06	U
RTN4_MOUSE	Reticulon-4	5	4.52E-06	C
PLST_MOUSE	Plastin-3	5	6.60E-06	U
DYHC1_MOUSE	Cytoplasmic dynein 1 heavy chain 1	5	8.10E-06	U
USP9X_MOUSE	Probable ubiquitin carboxyl-terminal hydrolase FAF-X	5	1.07E-05	U
ENPL_MOUSE	Endoplasmin	5	1.64E-05	U
SPTB2_MOUSE	Spectrin beta chain, non-erythrocytic 1	5	1.95E-05	U
MYO7B_MOUSE	Unconventional myosin-VIIb	5	9.33E-05	U
BAX_MOUSE	Apoptosis regulator BAX	5	1.07E-04	C
ATPA_MOUSE	ATP synthase subunit alpha, mitochondrial	5	1.10E-04	U
UB2D3_MOUSE	Ubiquitin-conjugating enzyme E2 D3	5	1.24E-04	U
RAN_MOUSE	GTP-binding nuclear protein Ran	5	1.24E-04	C
SRP68_MOUSE	Signal recognition particle subunit SRP68	5	1.67E-04	U
GRP75_MOUSE	Stress-70 protein, mitochondrial	5	1.83E-04	U
1433E_MOUSE	14-3-3 protein epsilon	5	2.07E-04	C
CB39L_MOUSE	Calcium-binding protein 39-like	5	3.18E-04	U
RL11_MOUSE	60S ribosomal protein L11	5	3.84E-04	U
HNRPM_MOUSE	Heterogeneous nuclear ribonucleoprotein M	5	4.39E-04	U
FINC_MOUSE	Fibronectin	5	4.71E-04	U
ACTA_MOUSE	Actin, aortic smooth muscle	5	5.43E-04	U
TGM2_MOUSE	Transglutaminase 2	5	5.62E-04	C
SNX12_MOUSE	Sorting nexin-12	4	5.75E-04	U
DPYL3_MOUSE	Dihydropyrimidinase-related protein 3	5	6.82E-04	U
GUAA_MOUSE	GMP synthase [glutamine-hydrolyzing]	5	6.86E-04	U
IST1_MOUSE	IST1 homolog	5	9.25E-04	U
SC31A_MOUSE	Protein transport protein Sec31A	5	1.08E-03	U
CTNB1_MOUSE	Catenin beta-1	5	1.20E-03	U
UBE2Z_MOUSE	Ubiquitin-conjugating enzyme E2 Z	5	1.21E-03	U
ANXA1_MOUSE	Annexin A1	5	1.30E-03	U
PLSL_MOUSE	Plastin-2	5	1.50E-03	U
RL15_MOUSE	60S ribosomal protein L15	5	3.27E-03	U
SYEP_MOUSE	Bifunctional glutamate/proline--tRNA ligase	5	3.63E-03	U
DNJA1_MOUSE	DnaJ homolog subfamily A member 1	5	3.98E-03	U
VPS4B_MOUSE	Vacuolar protein sorting-associated protein 4B	5	4.15E-03	U
RS9_MOUSE	40S ribosomal protein S9	4	4.27E-03	C
RS2_MOUSE	40S ribosomal protein S2	5	4.60E-03	U

1433T_MOUSE	14-3-3 protein theta	5	4.80E-03	U
CC160_MOUSE	Coiled-coil domain-containing protein 160	4	5.33E-03	U
USO1_MOUSE	General vesicular transport factor p115	5	5.63E-03	U
MP2K2_MOUSE	Dual specificity mitogen-activated protein kinase kinase 2	5	5.66E-03	C
HS90A_MOUSE	Heat shock protein HSP 90-alpha	5	5.73E-03	U
MYH10_MOUSE	Myosin-10	5	5.84E-03	U
VINC_MOUSE	Vinculin	5	6.30E-03	U
AATM_MOUSE	Aspartate aminotransferase, mitochondrial	5	6.41E-03	U
BAF_MOUSE	Barrier-to-autointegration factor	5	6.43E-03	U
K1C18_MOUSE	Keratin, type I cytoskeletal 18	5	6.51E-03	U
TPM1_MOUSE	Tropomyosin alpha-1 chain	5	7.36E-03	C
TBA1A_MOUSE	Tubulin alpha-1A chain	5	7.61E-03	U
DESM_MOUSE	Desmin	5	7.70E-03	U
AT2B2_MOUSE	Plasma membrane calcium-transporting ATPase 2	4	7.98E-03	U
VATE1_MOUSE	V-type proton ATPase subunit E 1	4	8.10E-03	C
FA49B_MOUSE	Protein FAM49B	5	8.18E-03	U
RL27A_MOUSE	60S ribosomal protein L27a	5	8.35E-03	C
VPS35_MOUSE	Vacuolar protein sorting-associated protein 35	5	8.44E-03	U
K2C8_MOUSE	Keratin, type II cytoskeletal 8	5	8.88E-03	U
BAG6_MOUSE	Large proline-rich protein BAG6	5	9.34E-03	C
ECHA_MOUSE	Trifunctional enzyme subunit alpha, mitochondrial	5	9.52E-03	U
UMPS_MOUSE	Uridine 5'-monophosphate synthase	5	9.74E-03	C
UBR4_MOUSE	E3 ubiquitin-protein ligase UBR4	5	1.01E-02	U
CTBP1_MOUSE	C-terminal-binding protein 1	5	1.06E-02	U
RL21_MOUSE	60S ribosomal protein L21	5	1.09E-02	U
EF2_MOUSE	Elongation factor 2	5	1.11E-02	C
PNCB_MOUSE	Nicotinate phosphoribosyltransferase	5	1.16E-02	U
FLNA_MOUSE	Filamin-A	5	1.20E-02	U
HSP7C_MOUSE	Heat shock cognate 71 kDa protein	5	1.22E-02	U
RL3_MOUSE	60S ribosomal protein L3	5	1.23E-02	U
MGST3_MOUSE	Microsomal glutathione S-transferase 3	5	1.25E-02	U
PSME1_MOUSE	Proteasome activator complex subunit 1	5	1.25E-02	U
TCPD_MOUSE	T-complex protein 1 subunit delta	5	1.27E-02	U
ATX10_MOUSE	Ataxin-10	5	1.31E-02	U
CTBP2_MOUSE	C-terminal-binding protein 2	5	1.33E-02	U
MEP1B_MOUSE	Meprin A subunit beta	5	1.34E-02	U
K1C14_MOUSE	Keratin, type I cytoskeletal 14	5	1.36E-02	U
KAD1_MOUSE	Adenylate kinase isoenzyme 1	5	1.37E-02	C
ROA3_MOUSE	Heterogeneous nuclear ribonucleoprotein A3	5	1.38E-02	U
PSME3_MOUSE	Proteasome activator complex subunit 3	5	1.46E-02	U
GCYB1_MOUSE	Guanylate cyclase soluble subunit beta-1	5	1.47E-02	U
ARL2_MOUSE	ADP-ribosylation factor-like protein 2	5	1.49E-02	U
UBE2N_MOUSE	Ubiquitin-conjugating enzyme E2 N	5	1.50E-02	U
MYO1E_MOUSE	Unconventional myosin-Ie	5	1.54E-02	U
PSD11_MOUSE	26S proteasome non-ATPase regulatory subunit 11	5	1.54E-02	C
SNX6_MOUSE	Sorting nexin-6	4	1.60E-02	U
DC1L2_MOUSE	Cytoplasmic dynein 1 light intermediate chain 2	5	1.60E-02	U
RS14_MOUSE	40S ribosomal protein S14	5	1.64E-02	U
PSMD5_MOUSE	26S proteasome non-ATPase regulatory subunit 5	4	1.73E-02	U
MYL6_MOUSE	Myosin light polypeptide 6	5	1.80E-02	U
VP26B_MOUSE	Vacuolar protein sorting-associated protein 26B	5	1.84E-02	U
COPA_MOUSE	Coatomer subunit alpha	5	1.95E-02	C
TLN1_MOUSE	Talin-1	5	1.96E-02	U
MBB1A_MOUSE	Myb-binding protein 1A	4	2.05E-02	U
TPC2L_MOUSE	Trafficking protein particle complex subunit 2-like protein	4	2.05E-02	U
FIBG_MOUSE	Fibrinogen gamma chain	5	2.10E-02	U
PPAC_MOUSE	Low molecular weight phosphotyrosine protein phosphatase	5	2.17E-02	U
GLSK_MOUSE	Glutaminase kidney isoform, mitochondrial	5	2.23E-02	U
DDX5_MOUSE	Probable ATP-dependent RNA helicase DDX5	5	2.29E-02	U
DLDH_MOUSE	Dihydrolipoyl dehydrogenase, mitochondrial	5	2.30E-02	U
NIBL1_MOUSE	Niban-like protein 1	5	2.37E-02	U
CH60_MOUSE	60 kDa heat shock protein, mitochondrial	5	2.43E-02	C
PRDX1_MOUSE	Peroxiredoxin-1	5	2.55E-02	U
CASP8_MOUSE	Caspase-8	5	2.57E-02	U
ACTH_MOUSE	Actin, gamma-enteric smooth muscle	5	2.59E-02	U
PLEC_MOUSE	Plectin	5	2.68E-02	U
DTX3L_MOUSE	E3 ubiquitin-protein ligase DTX3L	5	2.74E-02	U
PRS6A_MOUSE	26S protease regulatory subunit 6A	4	2.76E-02	U
ARY2_MOUSE	Arylamine N-acetyltransferase 2	5	2.78E-02	U
EFHD2_MOUSE	EF-hand domain-containing protein D2	5	2.78E-02	U
S12A3_MOUSE	Solute carrier family 12 member 3	5	2.85E-02	U
K1C19_MOUSE	Keratin, type I cytoskeletal 19	5	2.89E-02	U
IPO8_MOUSE	Importin-8	4	2.93E-02	U

IF4A2_MOUSE	Eukaryotic initiation factor 4A-II	5	3.00E-02	C
NUP98_MOUSE	Nuclear pore complex protein Nup98-Nup96	4	3.02E-02	U
RL13_MOUSE	60S ribosomal protein L13	5	3.04E-02	C
ARHG1_MOUSE	Rho guanine nucleotide exchange factor 1	5	3.18E-02	U
CYGB_MOUSE	Cytoglobin	4	3.41E-02	U
KINH_MOUSE	Kinesin-1 heavy chain	5	3.47E-02	U
PDC6I_MOUSE	Programmed cell death 6-interacting protein	5	3.51E-02	U
VIME_MOUSE	Vimentin	5	3.64E-02	U
HS90B_MOUSE	Heat shock protein HSP 90-beta	5	3.65E-02	U
DPEP1_MOUSE	Dipeptidase 1	5	3.68E-02	U
API5_MOUSE	Apoptosis inhibitor 5	5	3.79E-02	U
LSP1_MOUSE	Lymphocyte-specific protein 1	5	3.84E-02	U
TCPA_MOUSE	T-complex protein 1 subunit alpha	5	3.89E-02	U
SAE2_MOUSE	SUMO-activating enzyme subunit 2	5	3.90E-02	U
NEDD4_MOUSE	E3 ubiquitin-protein ligase NEDD4	5	3.98E-02	U
MACF1_MOUSE	Microtubule-actin cross-linking factor 1	5	4.01E-02	U
SPTA1_MOUSE	Spectrin alpha chain, erythrocytic 1	5	4.11E-02	U
DNM1L_MOUSE	Dynamin-1-like protein	5	4.11E-02	C
ACY3_MOUSE	N-acyl-aromatic-L-amino acid amidohydrolase (carboxylate-forming)	4	4.34E-02	U
DJB11_MOUSE	DnaJ homolog subfamily B member 11	4	4.35E-02	U
ML12B_MOUSE	Myosin regulatory light chain 12B	5	4.47E-02	U
RAGP1_MOUSE	Ran GTPase-activating protein 1	5	4.60E-02	U
HBA_MOUSE	Hemoglobin subunit alpha	5	4.63E-02	U
TLN2_MOUSE	Talin-2	5	4.64E-02	U
CO6A2_MOUSE	Collagen alpha-2(VI) chain	5	4.64E-02	U
TPIS_MOUSE	Triosephosphate isomerase	5	4.66E-02	C
1433B_MOUSE	14-3-3 protein beta/alpha	5	4.71E-02	U
PRS7_MOUSE	26S protease regulatory subunit 7	5	4.77E-02	U
DPM1_MOUSE	Dolichol-phosphate mannosyltransferase subunit 1	4	4.86E-02	C
EPN4_MOUSE	Clathrin interactor 1	4	5.09E-02	C
AAKG1_MOUSE	5'-AMP-activated protein kinase subunit gamma-1	5	5.13E-02	C
IPO9_MOUSE	Importin-9	5	5.17E-02	U
FLNB_MOUSE	Filamin-B	5	5.25E-02	U
CAP1_MOUSE	Adenylyl cyclase-associated protein 1	5	5.28E-02	U
DDX17_MOUSE	Probable ATP-dependent RNA helicase DDX17	5	5.28E-02	U
TRI25_MOUSE	E3 ubiquitin/ISG15 ligase TRIM25	5	5.34E-02	C

Supplementary Table 4.2: List of proteins significantly associated with TG2 in Sham operated kidneys' cytosolic fraction. This table shows all the proteins recognised as TG2-associated (z test, $p \leq 0.05$ $N \geq 4$) in the cytosolic fraction of sham operated kidneys at 21 days post-operation. U = Uniquely expressed in Sham operated conditions, C = common between UUO and Sham.

TG2-associated proteins in Sham operated kidney cytosolic faction				
Sample ID	**Name**	**N**	**P value**	**Unique/ Common**
ACAD8_MOUSE	Isobutyryl-CoA dehydrogenase, mitochondrial	4	0.00E+00	U
PLSI_MOUSE	Plastin-1	4	1.41E-07	U
TGM2_MOUSE	Transglutaminase 2	5	1.90E-07	C
ARF2_MOUSE	ADP-ribosylation factor 2	5	6.62E-07	U
GPDA_MOUSE	Glycerol-3-phosphate dehydrogenase [NAD(+)], cytoplasmic	5	8.01E-07	U
RS6_MOUSE	40S ribosomal protein S6	5	3.53E-05	U
H4_MOUSE	Histone H4	5	3.69E-05	U
CYFP2_MOUSE	Cytoplasmic FMR1-interacting protein 2	4	7.57E-05	U
NPM_MOUSE	Nucleophosmin	5	1.44E-04	U
AP2A2_MOUSE	AP-2 complex subunit alpha-2	5	1.99E-04	U
MAAI_MOUSE	Maleylacetoacetate isomerase	5	2.00E-04	U
RL13A_MOUSE	60S ribosomal protein L13a	5	2.30E-04	U
NFS1_MOUSE	Cysteine desulfurase, mitochondrial	4	2.98E-04	U
MON2_MOUSE	Protein MON2 homolog	5	3.12E-04	U
TPM3_MOUSE	Tropomyosin alpha-3 chain	5	4.38E-04	U
ISOC1_MOUSE	Isochorismatase domain-containing protein 1	5	4.38E-04	U
TRI25_MOUSE	E3 ubiquitin/ISG15 ligase TRIM25	5	4.64E-04	C
RS9_MOUSE	40S ribosomal protein S9	4	5.67E-04	C
RS30_MOUSE	40S ribosomal protein S30	5	6.12E-04	U
VATE1_MOUSE	V-type proton ATPase subunit E 1	4	6.19E-04	C
COPA_MOUSE	Coatomer subunit alpha	5	7.76E-04	C
VAT1_MOUSE	Synaptic vesicle membrane protein VAT-1 homolog	5	8.32E-04	U
RS13_MOUSE	40S ribosomal protein S13	5	9.74E-04	U
DX39B_MOUSE	Spliceosome RNA helicase Ddx39b	5	1.07E-03	C
SQRD_MOUSE	Sulfide:quinone oxidoreductase, mitochondrial	5	1.13E-03	U
AP2M1_MOUSE	AP-2 complex subunit mu	5	1.13E-03	U
IF4A1_MOUSE	Eukaryotic initiation factor 4A-I	5	1.41E-03	U
RL27A_MOUSE	60S ribosomal protein L27a	5	1.43E-03	C
PDIA6_MOUSE	Protein disulfide-isomerase A6	5	1.64E-03	U
RHG01_MOUSE	Rho GTPase-activating protein 1	5	1.73E-03	U
RCN1_MOUSE	Reticulocalbin-1	4	2.06E-03	U
RHOA_MOUSE	Transforming protein RhoA	5	2.36E-03	U
VATA_MOUSE	V-type proton ATPase catalytic subunit A	5	2.47E-03	U
IF4A2_MOUSE	Eukaryotic initiation factor 4A-II	5	2.74E-03	C
SORCN_MOUSE	Sorcin	5	3.05E-03	U
RL13_MOUSE	60S ribosomal protein L13	5	3.16E-03	C
ZADH2_MOUSE	Zinc-binding alcohol dehydrogenase domain-containing protein 2	4	3.40E-03	U
VILL_MOUSE	Villin-like protein	5	3.87E-03	U
CO3_MOUSE	Complement C3	4	4.10E-03	U
COPE_MOUSE	Coatomer subunit epsilon	5	4.20E-03	U
CPNS1_MOUSE	Calpain small subunit 1	5	5.68E-03	U
TCPQ_MOUSE	T-complex protein 1 subunit theta	5	6.01E-03	C
UCK1_MOUSE	Uridine-cytidine kinase 1	5	6.05E-03	U
GGA1_MOUSE	ADP-ribosylation factor-binding protein GGA1	5	6.25E-03	U
BAX_MOUSE	Apoptosis regulator BAX	5	7.33E-03	C
H14_MOUSE	Histone H1.4	5	7.61E-03	U
SAE1_MOUSE	SUMO-activating enzyme subunit 1	5	7.91E-03	U
TPM1_MOUSE	Tropomyosin alpha-1 chain	5	8.46E-03	C
ETHE1_MOUSE	Persulfide dioxygenase ETHE1, mitochondrial	5	8.87E-03	U
UMPS_MOUSE	Uridine 5'-monophosphate synthase	5	9.12E-03	C
RS16_MOUSE	40S ribosomal protein S16	5	1.04E-02	U
ESTD_MOUSE	S-formylglutathione hydrolase	5	1.10E-02	U
TPIS_MOUSE	Triosephosphate isomerase	5	1.13E-02	C
VMA5A_MOUSE	von Willebrand factor A domain-containing protein 5A	5	1.25E-02	U
DPM1_MOUSE	Dolichol-phosphate mannosyltransferase subunit 1	4	1.39E-02	C
SERA_MOUSE	D-3-phosphoglycerate dehydrogenase	5	1.43E-02	U
GRP78_MOUSE	78 kDa glucose-regulated protein	5	1.43E-02	U
RAN_MOUSE	GTP-binding nuclear protein Ran	5	1.57E-02	C
RTN4_MOUSE	Reticulon-4	5	1.67E-02	C
SGK2_MOUSE	Serine/threonine-protein kinase Sgk2	4	1.79E-02	U
GLRX1_MOUSE	Glutaredoxin-1	4	1.85E-02	U
PRDX3_MOUSE	Thioredoxin-dependent peroxide reductase, mitochondrial	5	1.86E-02	U
CH60_MOUSE	60 kDa heat shock protein, mitochondrial	5	1.87E-02	C

RL40_MOUSE	Ubiquitin-60S ribosomal protein L40	5	1.90E-02	U
FAS_MOUSE	Fatty acid synthase	5	1.94E-02	U
ARL8B_MOUSE	ADP-ribosylation factor-like protein 8B	5	1.97E-02	U
TKT_MOUSE	Transketolase	5	1.97E-02	U
DNM1L_MOUSE	Dynamin-1-like protein	5	2.08E-02	C
1433Z_MOUSE	14-3-3 protein zeta/delta	5	2.10E-02	U
IPO4_MOUSE	Importin-4	5	2.14E-02	U
ALBU_MOUSE	Serum albumin	5	2.19E-02	U
EPN4_MOUSE	Clathrin interactor 1	4	2.20E-02	C
EF2_MOUSE	Elongation factor 2	5	2.31E-02	C
ECHB_MOUSE	Trifunctional enzyme subunit beta, mitochondrial	5	2.52E-02	U
TOM1_MOUSE	Target of Myb protein 1	4	2.55E-02	U
PRS10_MOUSE	26S protease regulatory subunit 10B	5	2.66E-02	U
COPB2_MOUSE	Coatomer subunit beta'	5	2.93E-02	U
RL7_MOUSE	60S ribosomal protein L7	5	2.99E-02	U
DDX3Y_MOUSE	ATP-dependent RNA helicase DDX3Y	5	3.03E-02	U
ARP3_MOUSE	Actin-related protein 3	5	3.04E-02	U
ST1A1_MOUSE	Sulfotransferase 1A1	5	3.10E-02	U
ODO2_MOUSE	Dihydrolipoyllysine-residue succinyltransferase component of 2-oxoglutarate dehydrogenase complex, mitochondrial	5	3.20E-02	U
SNTB2_MOUSE	Beta-2-syntrophin	5	3.22E-02	U
MP2K2_MOUSE	Dual specificity mitogen-activated protein kinase kinase 2	5	3.22E-02	C
ASSY_MOUSE	Argininosuccinate synthase	5	3.22E-02	U
LACTB_MOUSE	Serine beta-lactamase-like protein LACTB, mitochondrial	5	3.24E-02	U
CLH1_MOUSE	Clathrin heavy chain 1	5	3.28E-02	U
KAD1_MOUSE	Adenylate kinase isoenzyme 1	5	3.33E-02	C
CALB1_MOUSE	Calbindin	5	3.38E-02	U
THIKA_MOUSE	3-ketoacyl-CoA thiolase A, peroxisomal	5	3.41E-02	U
ACADV_MOUSE	Very long-chain specific acyl-CoA dehydrogenase, mitochondrial	5	3.53E-02	U
GALK2_MOUSE	N-acetylgalactosamine kinase	5	3.60E-02	U
LYPL1_MOUSE	Lysophospholipase-like protein 1	5	3.65E-02	U
SCFD1_MOUSE	Sec1 family domain-containing protein 1	5	3.94E-02	U
ARPC4_MOUSE	Actin-related protein 2/3 complex subunit 4	5	4.06E-02	U
SYIM_MOUSE	Isoleucine--tRNA ligase, mitochondrial	4	4.23E-02	U
EHD1_MOUSE	EH domain-containing protein 1	5	4.28E-02	U
K1C20_MOUSE	Keratin, type I cytoskeletal 20	4	4.36E-02	U
1433E_MOUSE	14-3-3 protein epsilon	5	4.36E-02	C
ETFB_MOUSE	Electron transfer flavoprotein subunit beta	5	4.37E-02	U
GRAN_MOUSE	Grancalcin	5	4.58E-02	U
PSD11_MOUSE	26S proteasome non-ATPase regulatory subunit 11	5	4.60E-02	C
BAG6_MOUSE	Large proline-rich protein BAG6	5	4.63E-02	C
ANXA2_MOUSE	Annexin A2	5	4.78E-02	U
CDC42_MOUSE	Cell division control protein 42 homolog	5	4.79E-02	U
SC23B_MOUSE	Protein transport protein Sec23B	4	4.85E-02	U
ANS1A_MOUSE	Ankyrin repeat and SAM domain-containing protein 1A	4	5.20E-02	U
AAKG1_MOUSE	5'-AMP-activated protein kinase subunit gamma-1	5	5.31E-02	C
H2B1P_MOUSE	Histone H2B type 1-P	5	5.36E-02	U
DDX1_MOUSE	ATP-dependent RNA helicase DDX1	5	5.40E-02	U

S.2.2 Lists of TG2-associated proteins in the crude membrane fraction of UUO and Sham operated kidneys that have been removed from the analysis because nuclear, mitochondrial or ribosomal

Supplementary Table 4.3: List of proteins significantly associated with TG2 in UUO or Sham operated kidney membranes (21-days) and exclusively located in the nuclear cellular compartment. This table shows all the proteins recognised as TG2-associated in UUO (A) or sham operated (B) kidney membranes at 21 days (z test, p≤0.05 N≥4) and identified as uniquely associated with the nuclei. In increasing shades of blue, the p-value of TG2 association obtained by z-analysis. U = Uniquely expressed in UUO or Sham, C = common between UUO and Sham.

A

TG2-associated Nuclear proteins in UUO kidney membranes				
Sample ID	Name	N	P value	Unique/Common
ROA3_MOUSE	Heterogeneous nuclear ribonucleoprotein A3	5	7.98E-08	U
HNRPK_MOUSE	Heterogeneous nuclear ribonucleoprotein K	5	2.09E-05	U
CTBP1_MOUSE	C-terminal-binding protein 1	5	5.62E-05	C
MBB1A_MOUSE	Myb-binding protein 1A	4	2.20E-04	U
DHX9_MOUSE	ATP-dependent RNA helicase A	5	2.83E-04	C
NPM_MOUSE	Nucleophosmin	5	1.62E-03	U
HNRPU_MOUSE	Heterogeneous nuclear ribonucleoprotein U	5	1.89E-03	C
XPO2_MOUSE	Exportin-2	5	6.41E-03	U
H2AX_MOUSE	Histone H2AX	5	9.72E-03	C
DDX1_MOUSE	ATP-dependent RNA helicase DDX1	5	1.70E-02	C
RBM39_MOUSE	RNA-binding protein 39	5	1.75E-02	U
H13_MOUSE	Histone H1.3	5	1.82E-02	U
DDX46_MOUSE	Probable ATP-dependent RNA helicase DDX46	4	1.91E-02	U
DDX3Y_MOUSE	ATP-dependent RNA helicase DDX3Y	5	2.39E-02	U
SRSF2_MOUSE	Serine/arginine-rich splicing factor 2	5	2.64E-02	U
DTX3L_MOUSE	E3 ubiquitin-protein ligase DTX3L	5	2.70E-02	U
FLII_MOUSE	Protein flightless-1 homolog	5	5.28E-02	U

B

TG2-associated Nuclear proteins in Sham operated kidney membranes				
Sample ID	Name	N	p value	Unique/Common
IMB1_MOUSE	Importin subunit beta-1	5	1.43E-07	U
IPO8_MOUSE	Importin-8	4	6.06E-06	U
H2AX_MOUSE	Histone H2AX	5	2.16E-05	C
IPO9_MOUSE	Importin-9	5	6.13E-05	U
DX39B_MOUSE	Spliceosome RNA helicase Ddx39b	5	5.33E-04	U
BAF_MOUSE	Barrier-to-autointegration factor	5	2.44E-03	U
RUVB2_MOUSE	RuvB-like 2	4	3.21E-03	U
CTBP1_MOUSE	C-terminal-binding protein 1	5	1.19E-02	C
HNRPU_MOUSE	Heterogeneous nuclear ribonucleoprotein U	5	2.04E-02	C
DX39A_MOUSE	ATP-dependent RNA helicase DDX39A	5	2.12E-02	U
2AAA_MOUSE	Serine/threonine-protein phosphatase 2A 65 kDa regulatory subunit A alpha isoform	5	3.04E-02	U
U2AF2_MOUSE	Splicing factor U2AF 65 kDa subunit	5	3.37E-02	U
HP1B3_MOUSE	Heterochromatin protein 1-binding protein 3	4	3.71E-02	U
DHX9_MOUSE	ATP-dependent RNA helicase A	5	3.81E-02	C
DDX1_MOUSE	ATP-dependent RNA helicase DDX1	5	4.82E-02	C
IPO4_MOUSE	Importin-4	5	4.82E-02	U
LC7L2_MOUSE	Putative RNA-binding protein Luc7-like 2	5	5.17E-02	U

Supplementary Table 4.4: List of proteins significantly associated with TG2 in UUO or Sham operated kidney membranes (21-days) exclusively located in the mitochondrial and peroxisomal cellular compartment. This table shows all the proteins recognised as TG2-associated in UUO (A) or sham operated (B) kidney membranes at 21 days (z test, p≤0.05 N≥4) and identified as uniquely associated with mitochondria or peroxisomes. In increasing shades of blue, the p-value of TG2 association obtained by z-analysis. U = Uniquely expressed in UUO or Sham, C = common between UUO and Sham.

A

TG2-associated Mitochondrial / Peroxisomal proteins in UUO kidney membranes				
Sample ID	Name	N	P value	Unique/Common
SUCB1_MOUSE	Succinyl-CoA ligase [ADP-forming] subunit beta, mitochondrial	5	7.34E-05	U
ALDH2_MOUSE	Aldehyde dehydrogenase, mitochondrial	5	7.89E-04	U
TRAP1_MOUSE	Heat shock protein 75 kDa, mitochondrial	5	2.45E-03	U
ECI2_MOUSE	Enoyl-CoA delta isomerase 2, mitochondrial	5	2.60E-03	U
VDAC3_MOUSE	Voltage-dependent anion-selective channel protein 3	5	3.59E-03	C
ACADV_MOUSE	Very long-chain specific acyl-CoA dehydrogenase, mitochondrial	5	4.06E-03	U
ISC2A_MOUSE	Isochorismatase domain-containing protein 2A	5	4.31E-03	C
NDUA4_MOUSE	Cytochrome c oxidase subunit NDUFA4	5	6.35E-03	U
LDHD_MOUSE	Probable D-lactate dehydrogenase, mitochondrial	5	1.38E-02	U
MOSC2_MOUSE	Mitochondrial amidoxime reducing component 2	5	1.40E-02	U
ETFA_MOUSE	Electron transfer flavoprotein subunit alpha, mitochondrial	5	1.46E-02	U
COASY_MOUSE	Bifunctional coenzyme A synthase	5	1.51E-02	U
BCAT2_MOUSE	Branched-chain-amino-acid aminotransferase, mitochondrial	5	1.56E-02	U
ECHA_MOUSE	Trifunctional enzyme subunit alpha, mitochondrial	5	1.78E-02	U
THIKA_MOUSE	3-ketoacyl-CoA thiolase A, peroxisomal	5	1.83E-02	U
THIL_MOUSE	Acetyl-CoA acetyltransferase, mitochondrial	5	1.92E-02	C
M2OM_MOUSE	Mitochondrial 2-oxoglutarate/malate carrier protein	4	2.29E-02	U
SUCB2_MOUSE	Succinyl-CoA ligase [GDP-forming] subunit beta, mitochondrial	5	2.56E-02	C
DNM1L_MOUSE	Dynamin-1-like protein	5	2.69E-02	U
ES1_MOUSE	ES1 protein homolog, mitochondrial	5	3.15E-02	C
MPCP_MOUSE	Phosphate carrier protein, mitochondrial	5	3.18E-02	U
ODB2_MOUSE	Lipoamide acyltransferase component of branched-chain alpha-keto acid dehydrogenase complex, mitochondrial	5	3.88E-02	U
LACTB_MOUSE	Serine beta-lactamase-like protein LACTB, mitochondrial	5	3.89E-02	U
MMSA_MOUSE	Methylmalonate-semialdehyde dehydrogenase [acylating], mitochondrial	5	4.03E-02	C
ATPG_MOUSE	ATP synthase subunit gamma, mitochondrial	5	4.41E-02	U
KEG1_MOUSE	Glycine N-acyltransferase-like protein Keg1	4	4.67E-02	U
ACADM_MOUSE	Medium-chain specific acyl-CoA dehydrogenase, mitochondrial	5	5.48E-02	U

B

TG2-associated Mitochondrial / Peroxisomal proteins in Sham operated kidney membranes				
Sample ID	Name	N	p value	Unique/Common
VDAC3_MOUSE	Voltage-dependent anion-selective channel protein 3	5	2.08E-07	C
CH60_MOUSE	60 kDa heat shock protein, mitochondrial	5	1.80E-03	U
ISC2A_MOUSE	Isochorismatase domain-containing protein 2A	5	5.45E-03	C
MMSA_MOUSE	Methylmalonate-semialdehyde dehydrogenase [acylating], mitochondrial	5	1.08E-02	C
COX5B_MOUSE	Cytochrome c oxidase subunit 5B, mitochondrial	5	1.40E-02	U
ETHE1_MOUSE	Persulfide dioxygenase ETHE1, mitochondrial	5	1.78E-02	U
SYIM_MOUSE	Isoleucine--tRNA ligase, mitochondrial	4	2.22E-02	U
ES1_MOUSE	ES1 protein homolog, mitochondrial	5	3.92E-02	C
THIL_MOUSE	Acetyl-CoA acetyltransferase, mitochondrial	5	3.99E-02	C
SUCB2_MOUSE	Succinyl-CoA ligase [GDP-forming] subunit beta, mitochondrial	5	4.00E-02	C
DLDH_MOUSE	Dihydrolipoyl dehydrogenase, mitochondrial	5	4.02E-02	U
PRDX3_MOUSE	Thioredoxin-dependent peroxide reductase, mitochondria	5	4.28E-02	U

Supplementary Table 4.5: List of ribosomal and immunoglobulin proteins significantly associated with TG2 in UUO or Sham operated kidney membranes (21-days). (A,B) Proteins recognised as TG2-associated in UUO (A) or sham operated (B) kidney membranes at 21 days (z test, p≤0.05 N≥4) and identified as ribosomal subunits. **(C)** Proteins recognised as TG2-associated with UUO kidney membranes at 21 days (z test, p≤0.05 N≥4) and identified immunoglobulins (Ig). In increasing shades of blue, the p-value of TG2 association obtained by z-analysis. U = Uniquely expressed in UUO or Sham, C = common between UUO and Sham.

A

TG2-associated Ribosomal proteins in UUO kidney membranes				
Sample ID	Name	N	P value	Unique/Common
RL3_MOUSE	60S ribosomal protein L3	5	1.26E-09	C
RS7_MOUSE	40S ribosomal protein S7	5	5.39E-06	C
RS13_MOUSE	40S ribosomal protein S13	5	3.03E-05	C
RS3_MOUSE	40S ribosomal protein S3	5	5.17E-05	C
RL6_MOUSE	60S ribosomal protein L6	5	1.36E-04	C
RL18A_MOUSE	60S ribosomal protein L18a	5	4.63E-04	U
RS6_MOUSE	40S ribosomal protein S6	5	2.49E-03	C
RLA2_MOUSE	60S acidic ribosomal protein P2	5	2.80E-03	U
RLA0_MOUSE	60S acidic ribosomal protein P0	5	2.92E-03	C
RL35A_MOUSE	60S ribosomal protein L35a	5	3.22E-03	U
RL18A_MOUSE	60S ribosomal protein L18a	5	3.40E-03	U
RS14_MOUSE	40S ribosomal protein S14	5	6.38E-03	C
RL23_MOUSE	60S ribosomal protein L23	5	7.99E-03	U
RL11_MOUSE	60S ribosomal protein L11	5	8.87E-03	U
RL10A_MOUSE	60S ribosomal protein L10a	5	9.04E-03	U
RL9_MOUSE	60S ribosomal protein L9	5	1.04E-02	U
RL17_MOUSE	60S ribosomal protein L17	5	1.05E-02	U
RS24_MOUSE	40S ribosomal protein S24	5	1.13E-02	U
RL8_MOUSE	60S ribosomal protein L8	5	1.91E-02	U
RL4_MOUSE	60S ribosomal protein L4	5	2.54E-02	U
RL23A_MOUSE	60S ribosomal protein L23a	5	2.70E-02	U
RS15_MOUSE	40S ribosomal protein S15	5	2.71E-02	U
RL40_MOUSE	Ubiquitin-60S ribosomal protein L40	5	3.64E-02	U
RL13A_MOUSE	60S ribosomal protein L13a	5	4.35E-02	U

B

TG2-associated Ribosomal proteins in Sham operated kidney membranes				
Sample ID	Name	N	p value	Unique/Common
RS17_MOUSE	40S ribosomal protein S17	5	4.03E-03	U
RL6_MOUSE	60S ribosomal protein L6	5	6.05E-03	C
RL3_MOUSE	60S ribosomal protein L3	5	6.23E-03	C
RS3_MOUSE	40S ribosomal protein S3	5	9.02E-03	C
RS13_MOUSE	40S ribosomal protein S13	5	1.21E-02	C
RLA0_MOUSE	60S acidic ribosomal protein P0	5	1.30E-02	C
RS14_MOUSE	40S ribosomal protein S14	5	2.48E-02	C
RS6_MOUSE	40S ribosomal protein S6	5	2.73E-02	C
RS7_MOUSE	40S ribosomal protein S7	5	3.52E-02	C

C

TG2-associated Ig proteins in UUO kidney membranes				
Sample ID	Name	N	P value	Unique/Common
LAC2_MOUSE	Ig lambda-1 chain C region	5	2.66E-03	U
HVM32_MOUSE	Ig heavy chain V-III region J606	5	2.30E-02	U

S.2.3 Functional clustering of TG2-associated proteins in UUO or Sham operated kidney membranes

Supplementary Table 4.6: Functional clustering of TG2-associated proteins identified uniquely in UUO kidney membranes. Proteins identified as significantly associated with TG2 uniquely in UUO kidney membranes at 21 days post operation (p≤0.05 N≥4, marked with "U" in **Table 4.2**) were manually associated with general functional clusters depending on their main biological role in the cell, investigated by manual search of protein IDs on UniProtKB database. Nuclear, mitochondrial and ribosomal proteins were removed from the list.

TG2-associated proteins in UUO kidney membranes				
Protein ID	**Name**	**N**	**P Value**	**Functional Cluster**
DESP	Desmoplakin	5	1.22E-13	Cell Adhesion
HSP7C	Heat shock cognate 71 kDa protein	5	7.67E-10	Vesicular Trafficking
CAZA2	F-actin-capping protein subunit alpha-2	5	1.97E-08	Cytoskeleton and Actin dynamics
GPX1	Glutathione peroxidase 1	5	4.52E-07	Redox Regulation
POSTN	Periostin	4	1.03E-06	Cell Adhesion
MYO1D	Unconventional myosin-Id	5	3.52E-06	Vesicular Trafficking
GLRX1	Glutaredoxin 1	4	5.61E-06	Redox Regulation
GLRX3	Glutaredoxin-3	5	1.40E-05	Redox Regulation
PROF1	Profilin-1	5	1.89E-05	Cytoskeleton and Actin dynamics
HSPB1	Heat shock protein beta-1	5	3.68E-05	Signalling and Stress Response
VATH	V-type proton ATPase subunit H	5	5.98E-05	Vesicular Trafficking
ADDG	Gamma-adducin	5	6.66E-05	Cytoskeleton and Actin dynamics
AT2A2	Sarcoplasmic/endoplasmic reticulum calcium ATPase 2	5	8.58E-05	Ion Transport
SVIL	Supervillin	4	1.01E-04	Cytoskeleton and Actin dynamics
COR1C	Coronin-1C	5	1.38E-04	Signalling and Stress Response
TCPE	T-complex protein 1	5	3.17E-04	Chaperone
UBP5	Ubiquitin carboxyl-terminal hydrolase 5	5	4.59E-04	Ubiquitination and Proteasome
FLOT2	Flotillin-2	4	5.38E-04	Vesicular Trafficking
RAB1A	Ras-related protein Rab-1A	5	9.16E-04	Vesicular Trafficking
SDC4	Syndecan-4	5	9.34E-04	Cell Adhesion + Extracellular Organisation
LDHA	L-lactate dehydrogenase A chain	4	1.04E-03	Metabolism
MYO1G	Unconventional myosin-Ig	5	1.21E-03	Vesicular Trafficking
K1C20	Keratin, type I cytoskeletal 20	4	1.35E-03	Cytoskeleton and Actin dynamics
COEA1	Collagen alpha-1(XIV) chain	5	1.64E-03	Extracellular Organisation
COCA1	Collagen alpha-1(XII) chain	4	1.68E-03	Extracellular Organisation
HIP1	Huntingtin-interacting protein 1	4	1.86E-03	Vesicular Trafficking
SAR1B	GTP-binding protein SAR1b	5	2.79E-03	Vesicular Trafficking
FLNA	Filamin-A	5	2.98E-03	Cytoskeleton and Actin dynamics
ANK3	Ankyrin-3	5	3.03E-03	Cytoskeleton and Actin dynamics
PSD11	26S proteasome non-ATPase regulatory subunit 11	5	3.09E-03	Ubiquitination and Proteasome
PGBM	Basement membrane-specific heparan sulfate proteoglycan core protein (Perlecan)	5	3.16E-03	Extracellular Organisation
LSP1	Lymphocyte-specific protein 1	5	3.53E-03	Signalling and Stress Response
GELS	Gelsolin	5	4.61E-03	Cytoskeleton and Actin dynamics
YKT6	Synaptobrevin homolog YKT6	5	4.72E-03	Vesicular Trafficking
FLNB	Filamin-B	5	5.03E-03	Cytoskeleton and Actin dynamics
TLN2	Talin-2	5	5.28E-03	Cell Adhesion
KCC2D	Calcium/calmodulin-dependent protein kinase type II subunit delta	5	7.10E-03	Ion Transport
RTN4	Reticulon-4	5	7.57E-03	Signalling and Stress Response
KC1A	Casein kinase I isoform alpha	5	8.06E-03	Signalling and Stress Response
DCTN1	Dynactin subunit 1	5	8.52E-03	Vesicular Trafficking
ADDA	Alpha-adducin	5	8.61E-03	Cytoskeleton and Actin dynamics
PGS2	Decorin	5	1.09E-02	Extracellular Organisation
RHG18	Rho GTPase-activating protein 18	4	1.11E-02	Signalling and Stress Response
CAPZB	F-actin-capping protein subunit beta	5	1.11E-02	Cytoskeleton and Actin dynamics
MVP	Major vault protein	5	1.14E-02	Signalling and Stress Response
ACTB	Actin, cytoplasmic 1	5	1.24E-02	Cytoskeleton and Actin dynamics
K1C14	Keratin, type I cytoskeletal 14	5	1.33E-02	Cytoskeleton and Actin dynamics
PLSL	Plastin-2	5	1.34E-02	Signalling and Stress Response
AP2A2	AP-2 complex subunit alpha-2	5	1.52E-02	Vesicular Trafficking
CLCB	Clathrin light chain b	5	1.65E-02	Vesicular Trafficking
SNX4	Sorting nexin-4	5	1.67E-02	Vesicular Trafficking
SPTB1	Spectrin beta chain, erythrocytic	5	1.73E-02	Cytoskeleton and Actin dynamics

ZO1	Tight junction protein ZO-1	4	1.79E-02	Cell Adhesion	
DREB	Drebrin	5	1.83E-02	Cytoskeleton and Actin dynamics	
CAN1	Calpain1	5	1.84E-02	Signalling and Stress Response	
PDLI5	PDZ and LIM domain protein 5	5	1.85E-02	Protein Binding	
PUR6	Multifunctional protein ADE2	5	1.88E-02	Metabolism	
MY18A	Unconventional myosin-XVIIIa	5	1.93E-02	Vesicular Trafficking	
CLCA	Clathrin light chain A	5	2.07E-02	Vesicular Trafficking	
IRGM1	Immunity-related GTPase family M protein 1	5	2.09E-02	Signalling and Stress Response	
NEB2	Neurabin-2	5	2.11E-02	Signalling and Stress Response	
K2C6B	Keratin, type II cytoskeletal 6B	5	2.14E-02	Cytoskeleton and Actin dynamics	
AP2A1	AP-2 complex subunit alpha-1	5	2.15E-02	Vesicular Trafficking	
LYPA1	Acyl-protein thioesterase 1	5	2.18E-02	Metabolism	
AP2B1	AP-2 complex subunit beta	5	2.43E-02	Vesicular Trafficking	
K1C19	Keratin, type I cytoskeletal 19	5	2.58E-02	Cytoskeleton and Actin dynamics	
GRP78	78 kDa glucose-regulated protein	5	2.59E-02	Chaperone	
ARK72	Aflatoxin B1 aldehyde reductase member 2	5	2.61E-02	Metabolism	
SNTB2	Beta-2-syntrophin	5	2.63E-02	Protein Binding	
MYO1B	Unconventional myosin-Ib	5	2.67E-02	Vesicular Trafficking	
K6PP	ATP-dependent 6-phosphofructokinase, platelet type	5	2.67E-02	Metabolism	
C1QB	Complement C1q subcomponent subunit B	5	2.71E-02	Signalling and Stress Response	
HS90A	Heat shock protein HSP 90-alpha	5	2.85E-02	Chaperone	
GAK	Cyclin-G-associated kinase	5	2.86E-02	Vesicular Trafficking	
UCK1	Uridine-cytidine kinase 1	5	3.12E-02	Metabolism	
ES8L2	Epidermal growth factor receptor kinase substrate 8-like protein 2	4	3.29E-02	Cytoskeleton and Actin dynamics	
MOES	Moesin	5	3.33E-02	Cytoskeleton and Actin dynamics	
PNCB	Nicotinate phosphoribosyltransferase	5	3.34E-02	Metabolism	
MYH10	Myosin-10	5	3.59E-02	Cytoskeleton and Actin dynamics	
RBGPR	Rab3 GTPase-activating protein non-catalytic subunit	5	3.65E-02	Vesicular Trafficking	
VIME	Vimentin	5	3.66E-02	Cytoskeleton and Actin dynamics	
SERPH	Serpin H1	5	3.81E-02	Extracellular Organisation+ Chaperone	
RPN1	Dolichyl-diphosphooligosaccharide--protein glycosyltransferase subunit 1	4	3.89E-02	Metabolism	
GSTT1	Glutathione S-transferase theta-1	5	3.95E-02	Redox Regulation	
TCPQ	T-complex protein 1	5	3.96E-02	Chaperone	
IRAK4	Interleukin-1 receptor-associated kinase 4	5	4.24E-02	Signalling and Stress Response	
C1TC	C-1-tetrahydrofolate synthase	5	4.28E-02	Metabolism	
ARC1B	Actin-related protein 2/3 complex subunit 1B	5	4.28E-02	Cytoskeleton and Actin dynamics	
COPB2	Coatomer subunit beta	5	4.42E-02	Vesicular Trafficking	
FA49B	Protein FAM49B	5	4.62E-02	Protein Binding	
MYH14	Myosin-14	5	4.79E-02	Cytoskeleton and Actin dynamics	
SNX1	Sorting nexin-1	4	4.81E-02	Vesicular Trafficking	
PLST	Plastin-3	5	4.82E-02	Signalling and Stress Response	
GBP2	Interferon-induced guanylate-binding protein 2	5	5.00E-02	Signalling and Stress Response	
SYEP	Bifunctional glutamate/proline--tRNA ligase	5	5.17E-02	Translational Regulation	
TCPA	T-complex protein 1	5	5.25E-02	Chaperone	
CLIC1	Chloride intracellular channel protein 1	5	5.33E-02	Ion Transport	

Supplementary Table 4.7: Functional clustering of TG2-associated proteins identified uniquely in Sham-operated kidney membranes. Proteins identified as significantly associated with TG2 uniquely in sham operated kidney membranes at 21 days post operation (p≤0.05 N≥4, marked with "U" in **Table 4.3**) were manually associated with general functional clusters depending on their main biological role in the cell, investigated by manual search of Protein IDs on UniProtKB database. Nuclear, mitochondrial and ribosomal proteins were removed from the list.

TG2-associated proteins in Sham operated kidney membranes				
Protein ID	**Name**	**N**	**P Value**	**Functional Cluster**
PRS4	26S protease regulatory subunit 4	5	5.22E-09	Ubiquitination and Proteasome
PSME1	Proteasome activator complex subunit 1	5	8.91E-07	Ubiquitination and Proteasome
NEDD4	E3 ubiquitin-protein ligase NEDD4	5	3.03E-05	Ubiquitination and Proteasome
K2C1B	Keratin, type II cytoskeletal 1b	4	8.40E-05	Cytoskeleton and Actin dynamics
UN45A	Protein unc-45 homolog A	5	1.04E-04	Cytoskeleton and Actin dynamics
PRUNE	Protein prune homolog	5	1.31E-04	Cell Regulation
NIBL1	Niban-like protein 1	5	1.41E-04	Signalling and Stress Response
PLEC	Plectin	5	1.80E-04	Cytoskeleton and Actin dynamics
PH4H	Phenylalanine-4-hydroxylase	5	2.67E-04	Metabolism
TOM1	Target of Myb protein 1	4	3.37E-04	Vesicular Trafficking
ACY3	N-acyl-aromatic-L-amino acid amidohydrolase	4	5.54E-04	Metabolism
DEST	Destrin	5	8.51E-04	Cytoskeleton and Actin dynamics
UB2D3	Ubiquitin-conjugating enzyme E2 D3	5	9.25E-04	Ubiquitination and Proteasome
KAD1	Adenylate kinase isoenzyme 1	5	9.92E-04	Metabolism
G3P	Glyceraldehyde-3-phosphate dehydrogenase	5	1.05E-03	Metabolism
USP9X	Probable ubiquitin carboxyl-terminal hydrolase FAF-X	5	1.27E-03	Deubiquitination
PDIA1	Protein disulfide-isomerase	4	1.40E-03	Metabolism
CASP3	Caspase-3	4	1.42E-03	Signalling and Stress Response
UBP24	Ubiquitin carboxyl-terminal hydrolase 24	4	1.43E-03	Deubiquitination
MEP1A	Meprin A subunit alpha	5	1.68E-03	Metabolism
ARF6	ADP-ribosylation factor 6	5	1.88E-03	Vesicular Trafficking
TM55B	Type 1 phosphatidylinositol 4,5-bisphosphate 4-phosphatase	4	3.22E-03	Metabolism
KCRB	Creatine kinase B-type	5	4.11E-03	Metabolism
RHEB	GTP-binding protein Rheb	5	4.12E-03	Signalling and Stress Response
ST1A1	Sulfotransferase 1A1	5	4.51E-03	Metabolism
ANXA2	Annexin A2	5	5.38E-03	Vesicular Trafficking
OLFM4	Olfactomedin-4	5	5.80E-03	Cell Adhesion
IST1	IST1 homolog	5	6.01E-03	Vesicular Trafficking
PP1A	Serine/threonine-protein phosphatase PP1-alpha catalytic subunit	4	6.08E-03	Cell Regulation
NLTP	Non-specific lipid-transfer protein	5	6.29E-03	Metabolism
PPBT	Alkaline phosphatase, tissue-nonspecific isozyme	5	6.39E-03	Metabolism
ENOA	Alpha-enolase	4	6.90E-03	Metabolism
FBLN1	Fibulin-1	5	7.33E-03	Cell Adhesion
TCPG	T-complex protein 1 subunit gamma	5	7.61E-03	Chaperone
GGA1	ADP-ribosylation factor-binding protein GGA1	5	8.30E-03	Vesicular Trafficking
IRF3	Interferon regulatory factor 3	4	8.39E-03	Signalling and Stress Response
TBB5	Tubulin beta-5 chain	5	8.92E-03	Cytoskeleton and Actin dynamics
FARP1	FERM, RhoGEF and pleckstrin domain-containing protein 1	5	9.63E-03	Cell Regulation
DJB11	DnaJ homolog subfamily B member 11	4	1.03E-02	Chaperone
ARF5	ADP-ribosylation factor 5	5	1.03E-02	Vesicular Trafficking
ARPC5	Actin-related protein 2/3 complex subunit 5	4	1.06E-02	Cytoskeleton and Actin dynamics
ARHGC	Rho guanine nucleotide exchange factor 12	5	1.10E-02	Signalling and Stress Response
ARL2	ADP-ribosylation factor-like protein 2	5	1.14E-02	Cell Regulation
AT1B1	Sodium/potassium-transporting ATPase subunit beta-1	5	1.21E-02	Ion Transport
MGST3	Microsomal glutathione S-transferase 3	5	1.21E-02	Redox Regulation
NSF	Vesicle-fusing ATPase	5	1.28E-02	Vesicular Trafficking
ARL1	ADP-ribosylation factor-like protein 1	5	1.42E-02	Cell Regulation
AT1A1	Sodium/potassium-transporting ATPase subunit alpha-1	5	1.43E-02	Ion Transport
CUL5	Cullin-5	5	1.43E-02	Ubiquitination and Proteasome
VILI	Villin-1	5	1.51E-02	Cytoskeleton and Actin dynamics
S12A3	Solute carrier family 12 member 3	5	1.55E-02	Ion Transport

KS6A3	Ribosomal protein S6 kinase alpha-3	5	1.58E-02	Signalling and Stress Response	
TBA4A	Tubulin alpha-4A chain	5	1.62E-02	Cytoskeleton and Actin dynamics	
VATA	V-type proton ATPase catalytic subunit A	5	1.70E-02	Ion Transport	
SYWC	Tryptophan--tRNA ligase	5	1.75E-02	Signalling and Stress Response	
CAH9	Carbonic anhydrase 9	4	1.76E-02	Metabolism	
RAC2	Ras-related C3 botulinum toxin substrate 2	5	1.85E-02	Signalling and Stress Response	
HBA	Hemoglobin subunit alpha	5	1.88E-02	Metabolism	
RAB10	Ras-related protein Rab-10	5	1.98E-02	Vesicular Trafficking	
NRK1	Nicotinamide riboside kinase 1	5	2.11E-02	Metabolism	
VPS35	Vacuolar protein sorting-associated protein 35	5	2.25E-02	Vesicular Trafficking	
SNX3	Sorting nexin-3	5	2.27E-02	Vesicular Trafficking	
ACSA	Acetyl-coenzyme A synthetase	5	2.29E-02	Metabolism	
DNJA2	DnaJ homolog subfamily A member 2	5	2.29E-02	Chaperone	
ST1D1	Sulfotransferase 1 family member D1	5	2.40E-02	Metabolism	
ANFY1	Rabankyrin-5	5	2.42E-02	Vesicular Trafficking	
GLCTK	Glycerate kinase	5	2.42E-02	Metabolism	
ARC1A	Actin-related protein 2/3 complex subunit 1A	5	2.42E-02	Cytoskeleton and Actin dynamics	
PDIA6	Protein disulfide-isomerase A6	5	2.53E-02	Chaperone	
VATB2	V-type proton ATPase subunit B	5	2.59E-02	Ion Transport	
GCYA3	Guanylate cyclase soluble subunit alpha-3	5	2.67E-02	Metabolism	
LYPA2	Acyl-protein thioesterase 2	5	2.68E-02	Metabolism	
RUFY3	Protein RUFY3	4	2.72E-02	Cell Regulation	
TBC9B	TBC1 domain family member 9B	5	2.78E-02	Vesicular Trafficking	
RCN1	Reticulocalbin-1	4	3.03E-02	Cell Regulation	
ARP3	Actin-related protein 3	5	3.04E-02	Cytoskeleton and Actin dynamics	
HS90B	Heat shock protein HSP 90-beta	5	3.38E-02	Signalling and Stress Response	
ITM2B	Integral membrane protein 2B	5	3.60E-02	Cell Regulation	
MP2K2	Dual specificity mitogen-activated protein kinase kinase 2	5	3.62E-02	Signalling and Stress Response	
DHRS4	Dehydrogenase/reductase SDR family member 4	4	3.62E-02	Metabolism	
TBA1A	Tubulin alpha-1A chain	5	3.66E-02	Cytoskeleton and Actin dynamics	
IF4A1	Eukaryotic initiation factor 4A-I	5	3.68E-02	Traslational Regulation	
OXSR1	Serine/threonine-protein kinase OSR1	5	3.69E-02	Signalling and Stress Response	
CLIC4	Chloride intracellular channel protein 4	5	3.82E-02	Ion Transport	
VDAC1	Voltage-dependent anion-selective channel protein 1	5	3.87E-02	Ion Transport	
CAN2	Calpain-2 catalytic subunit	5	3.95E-02	Signalling and Stress Response	
NDRG3	Protein NDRG3	5	4.06E-02	Cell Regulation	
CLH1	Clathrin heavy chain 1	5	4.11E-02	Vesicular Trafficking	
TS101	Tumor susceptibility gene 101 protein	4	4.31E-02	Vesicular Trafficking	
DPYL3	Dihydropyrimidinase-related protein 3	5	4.39E-02	Cytoskeleton and Actin dynamics	
ISG15	Ubiquitin-like protein ISG15	5	4.53E-02	Signalling and Stress Response	
DRG2	Developmentally-regulated GTP-binding protein 2	5	4.71E-02	Cell Regulation	
RN213	E3 ubiquitin-protein ligase RNF213	4	4.73E-02	Ubiquitination and Proteasome	
BAX	Apoptosis regulator BAX	5	4.73E-02	Signalling and Stress Response	
EF1A1	Elongation factor 1-alpha 1	5	5.34E-02	Traslational Regulation	

Supplementary Table 4.8: Functional clustering of TG2-associated proteins identified in both UUO Sham-operated kidney membranes. Proteins identified as significantly associated with TG2 in both UUO and sham operated kidney membranes at 21 days post operation ($p \leq 0.05$ $N \geq 4$, marked with "C" in **Tables 4.2 and 4.3**) were manually associated with general functional clusters depending on their main biological role in the cell, investigated by manual search of Protein IDs on UniProtKB database. Nuclear, Mitochondrial and Ribosomal proteins were removed from the list.

TG2-associated proteins in both UUO and Sham operated kidney membranes (Common)						
Protein ID	**Name**	**N**	**Sham**	**UUO**	**Functional Cluster**	
TGM2	Transglutaminase 2	5	1.21E-04	3.31E-05	Transglutaminase	
IF4G3	Eukaryotic translation initiation factor 4 gamma 3	5	1.82E-04	1.11E-02	Traslational Regulation	
SERA	D-3-phosphoglycerate dehydrogenase	5	1.85E-04	7.78E-03	Metabolism	
TERA	Transitional endoplasmic reticulum ATPase	5	2.49E-04	1.21E-02	Vesicular Trafficking	
PTN6	Tyrosine-protein phosphatase non-receptor type 6	4	4.04E-04	4.84E-03	Signalling and Stress Response	
TCPZ	T-complex protein 1	5	6.52E-04	4.23E-02	Chaperone	
SPTA1	Spectrin alpha chain, erythrocytic 1	5	1.97E-03	2.92E-03	Cytoskeleton and Actin dynamics	
SCFD1	Sec1 family domain-containing protein 1	5	4.24E-03	4.30E-02	Vesicular Trafficking	
CALM	Calmodulin	5	5.39E-03	1.83E-08	Cell Regulation	
F120A	Constitutive coactivator of PPAR-gamma-like protein 1	5	5.77E-03	6.27E-03	Signalling and Stress Response	
PRDX2	Peroxiredoxin-2	4	6.07E-03	6.87E-03	Redox Regulation	
PDC6I	Programmed cell death 6-interacting protein	5	6.41E-03	2.38E-02	Vesicular Trafficking	
LIMS1	LIM and senescent cell antigen-like-containing domain protein 1	5	7.55E-03	2.47E-03	Cytoskeleton and Actin dynamics	
PGK1	Phosphoglycerate kinase 1	4	1.38E-02	5.39E-03	Metabolism	
PCKGC	Phosphoenolpyruvate carboxykinase	5	2.08E-02	8.93E-04	Metabolism	
PICAL	Phosphatidylinositol-binding clathrin assembly protein	4	2.73E-02	5.65E-03	Vesicular Trafficking	
IQGA1	Ras GTPase-activating-like protein IQGAP1	5	2.99E-02	1.50E-04	Signaling and Stress Response	
PGS1	Biglycan	5	3.18E-02	1.30E-02	Extracellular Organisation	
NAMPT	Nicotinamide phosphoribosyltransferase	5	3.20E-02	6.56E-04	Metabolism	
ECHP	Peroxisomal bifunctional enzyme	5	3.21E-02	3.15E-02	Metabolism	
F213A	Redox-regulatory protein FAM213A	5	3.76E-02	2.79E-02	Stress Response + Redox Regulation	
LAMB2	Laminin subunit beta-2	4	4.21E-02	3.92E-02	Cell Adhesion	
FINC	Fibronectin	5	4.27E-02	1.57E-02	Cell Adhesion + Extracellular Organisation	
ADH1	Alcohol dehydrogenase 1	5	4.74E-02	9.40E-07	Metabolism	
SPTN1	Spectrin alpha chain, non-erythrocytic 1	5	5.25E-02	3.08E-02	Cytoskeleton and Actin dynamics	

S.2.4 DAVID statistical overrepresentation test on TG2-associated proteins in fibrotic and healthy conditions

Supplementary Table 4.9: GO Biological Process overrepresentation test on TG2-associated proteins in UUO kidney membranes, performed by DAVID. Statistical overrepresentation test was performed by DAVID (http://david.abcc.ncifcrf.gov) using the annotation terms ontologies for Biological Process (GOTERM_BP_FAT). The number of proteins belonging to each annotation term and fold change from the expected value H_0 are in increasing shades of red (the higher the more intense). The p-value is shown in increasing shades of blue (the more intense, the lower the p-value). A p-value lower than 0.05 was regarded as significant. Grey arrows = Terms associated with intracellular trafficking and vesicular transport and enriched in UUO kidney membranes; Black arrows = terms associated with cytoskeletal organisation and actin binding and enriched in UUO kidney membranes.

GO Biological Process - TG2-associated proteins in UUO kidney membranes				
GO Biological Process	Count	%	PValue	Fold Enrichment
GO:0007010~cytoskeleton organization	17	14.78	1.14E-09	7.23
GO:0030029~actin filament-based process	12	10.43	4.77E-08	9.45
GO:0030036~actin cytoskeleton organization	11	9.57	2.69E-07	9.24
GO:0030833~regulation of actin filament polymerization	7	6.09	7.36E-07	21.57
GO:0030837~negative regulation of actin filament polymerization	6	5.22	7.93E-07	33.28
GO:0032272~negative regulation of protein polymerization	6	5.22	1.19E-06	30.81
GO:0031333~negative regulation of protein complex assembly	6	5.22	1.19E-06	30.81
GO:0008064~regulation of actin polymerization or depolymerization	7	6.09	1.40E-06	19.41
GO:0030832~regulation of actin filament length	7	6.09	1.57E-06	19.03
GO:0032271~regulation of protein polymerization	7	6.09	3.06E-06	17.03
GO:0032956~regulation of actin cytoskeleton organization	7	6.09	4.15E-06	16.18
GO:0032970~regulation of actin filament-based process	7	6.09	4.58E-06	15.91
GO:0016192~vesicle-mediated transport	15	13.04	5.29E-06	4.46
GO:0043254~regulation of protein complex assembly	7	6.09	6.66E-06	14.93
GO:0051693~actin filament capping	5	4.35	8.71E-06	36.49
GO:0046907~intracellular transport	14	12.17	1.13E-05	4.50
GO:0030835~negative regulation of actin filament depolymerization	5	4.35	1.33E-05	33.01
GO:0032535~regulation of cellular component size	9	7.83	1.93E-05	7.75
GO:0008104~protein localization	18	15.65	2.12E-05	3.31
GO:0051494~negative regulation of cytoskeleton organization	6	5.22	2.24E-05	17.33
GO:0030834~regulation of actin filament depolymerization	5	4.35	2.32E-05	28.89
GO:0044087~regulation of cellular component biogenesis	7	6.09	4.08E-05	10.91
GO:0007015~actin filament organization	6	5.22	4.79E-05	14.86
GO:0051129~negative regulation of cellular component organization	7	6.09	5.23E-05	10.44
GO:0034613~cellular protein localization	11	9.57	5.31E-05	5.10
GO:0070727~cellular macromolecule localization	11	9.57	5.62E-05	5.07
GO:0051493~regulation of cytoskeleton organization	7	6.09	7.43E-05	9.80
GO:0010639~negative regulation of organelle organization	6	5.22	7.84E-05	13.42
GO:0043242~negative regulation of protein complex disassembly	5	4.35	1.08E-04	19.81
GO:0006886~intracellular protein transport	10	8.70	1.55E-04	5.02
GO:0045184~establishment of protein localization	15	13.04	2.22E-04	3.17
GO:0043244~regulation of protein complex disassembly	5	4.35	2.43E-04	16.12
GO:0044271~nitrogen compound biosynthetic process	10	8.70	3.03E-04	4.59
GO:0015031~protein transport	14	12.17	7.09E-04	2.98
GO:0045103~intermediate filament-based process	4	3.48	7.24E-04	22.18
GO:0033043~regulation of organelle organization	7	6.09	8.13E-04	6.30
GO:0051186~cofactor metabolic process	7	6.09	1.92E-03	5.33
GO:0045109~intermediate filament organization	3	2.61	3.74E-03	32.00
GO:0051188~cofactor biosynthetic process	5	4.35	4.06E-03	7.62
GO:0008360~regulation of cell shape	4	3.48	4.56E-03	11.80
GO:0006790~sulfur metabolic process	5	4.35	4.56E-03	7.38
GO:0022604~regulation of cell morphogenesis	5	4.35	5.10E-03	7.15
GO:0018149~peptide cross-linking	3	2.61	6.40E-03	24.47
GO:0009165~nucleotide biosynthetic process	6	5.22	8.12E-03	4.78
GO:0034404~nucleobase, nucleoside and nucleotide biosynthetic process	6	5.22	9.12E-03	4.65
GO:0034654~nucleobase, nucleoside, nucleotide and nucleic acid biosynthetic process	6	5.22	9.12E-03	4.65
GO:0045104~intermediate filament cytoskeleton organization	3	2.61	1.06E-02	18.91
GO:0046164~alcohol catabolic process	4	3.48	1.12E-02	8.53
GO:0009611~response to wounding	8	6.96	1.20E-02	3.20
GO:0006457~protein folding	5	4.35	1.29E-02	5.46
GO:0045185~maintenance of protein location	3	2.61	1.69E-02	14.86
GO:0006732~coenzyme metabolic process	5	4.35	1.92E-02	4.85
GO:0051235~maintenance of location	3	2.61	2.31E-02	12.60
GO:0043009~chordate embryonic development	8	6.96	3.09E-02	2.63
GO:0009792~embryonic development ending in birth or egg hatching	8	6.96	3.23E-02	2.61
GO:0006091~generation of precursor metabolites and energy	6	5.22	3.90E-02	3.19
GO:0006096~glycolysis	3	2.61	3.93E-02	9.45
GO:0043623~cellular protein complex assembly	4	3.48	4.21E-02	5.14

Supplementary Table 4.10: GO Biological Process overrepresentation test on TG2-associated proteins in Sham operated kidney membranes, performed by DAVID. Statistical overrepresentation test was performed by DAVID (http://david.abcc.ncifcrf.gov) using the annotation terms ontologies for Biological Process (GOTERM_BP_FAT). The number of proteins belonging to the annotation term and fold change from the expected value H_0 are in increasing shades of green (the higher the more intense). The p-value is shown in increasing shades of blue (the more intense, the lower the p-value). A p-value lower than 0.05 was regarded as significant. * = Terms associated with intracellular trafficking and vesicular transport and enriched in sham operated kidney membranes; ** = terms associated with cytoskeletal organisation and actin binding and enriched in sham operated kidney membranes; o = terms associated with catalytic activity and enriched in sham operated kidney membranes; oo = terms associated with ion channel and enriched in sham operated kidney membranes; ooo = terms associated with G-proteins or Small GTPases and enriched in sham operated kidney membranes.

GO Biological Process - TG2-associated proteins in Sham operated kidney membranes					
	GO Biological Process	Count	%	PValue	Fold Enrichment
**	GO:0008064~regulation of actin polymerization or depolymerization	6	5.41	2.89E-05	16.47
**	GO:0030832~regulation of actin filament length	6	5.41	3.18E-05	16.15
**	GO:0032956~regulation of actin cytoskeleton organization	6	5.41	7.03E-05	13.73
**	GO:0032970~regulation of actin filament-based process	6	5.41	7.61E-05	13.50
**	GO:0030833~regulation of actin filament polymerization	5	4.50	3.02E-04	15.25
o	GO:0044271~nitrogen compound biosynthetic process	10	9.01	3.27E-04	4.54
**	GO:0051493~regulation of cytoskeleton organization	6	5.41	7.37E-04	8.32
	GO:0032271~regulation of protein polymerization	5	4.50	7.50E-04	12.04
	GO:0032535~regulation of cellular component size	7	6.31	1.08E-03	5.97
	GO:0043254~regulation of protein complex assembly	5	4.50	1.23E-03	10.56
o	GO:0009165~nucleotide biosynthetic process	7	6.31	1.61E-03	5.52
o	GO:0034404~nucleobase, nucleoside and nucleotide biosynthetic process	7	6.31	1.86E-03	5.37
o	GO:0034654~nucleobase, nucleoside, nucleotide and nucleic acid biosynthetic process	7	6.31	1.86E-03	5.37
	GO:0007264~small GTPase mediated signal transduction	8	7.21	2.61E-03	4.26
	GO:0044087~regulation of cellular component biogenesis	5	4.50	3.89E-03	7.71
	GO:0046034~ATP metabolic process	5	4.50	4.05E-03	7.63
	GO:0033043~regulation of organelle organization	6	5.41	5.11E-03	5.35
	GO:0007242~intracellular signaling cascade	15	13.51	5.83E-03	2.25
o	GO:0006163~purine nucleotide metabolic process	6	5.41	6.00E-03	5.15
o	GO:0009205~purine ribonucleoside triphosphate metabolic process	5	4.50	6.09E-03	6.79
o	GO:0009199~ribonucleoside triphosphate metabolic process	5	4.50	6.31E-03	6.73
*	GO:0015031~protein transport	12	10.81	7.13E-03	2.53
o	GO:0009144~purine nucleoside triphosphate metabolic process	5	4.50	7.21E-03	6.47
	GO:0045184~establishment of protein localization	12	10.81	7.53E-03	2.51
	GO:0008104~protein localization	13	11.71	7.82E-03	2.37
o	GO:0009141~nucleoside triphosphate metabolic process	5	4.50	9.56E-03	5.97
o	GO:0051186~cofactor metabolic process	6	5.41	1.02E-02	4.52
o	GO:0009150~purine ribonucleotide metabolic process	5	4.50	1.07E-02	5.77
o	GO:0006091~generation of precursor metabolites and energy	7	6.31	1.15E-02	3.68
o	GO:0046164~alcohol catabolic process	4	3.60	1.15E-02	8.45
o	GO:0009259~ribonucleotide metabolic process	5	4.50	1.27E-02	5.49
**	GO:0030834~regulation of actin filament depolymerization	3	2.70	1.28E-02	17.16
	GO:0006457~protein folding	5	4.50	1.34E-02	5.40
o	GO:0006766~vitamin metabolic process	4	3.60	1.35E-02	7.96
o	GO:0006164~purine nucleotide biosynthetic process	5	4.50	1.72E-02	5.01
o	GO:0006006~glucose metabolic process	5	4.50	1.85E-02	4.90
o	GO:0006732~coenzyme metabolic process	5	4.50	1.98E-02	4.80
o	GO:0006754~ATP biosynthetic process	4	3.60	2.14E-02	6.70
o	GO:0051188~cofactor biosynthetic process	4	3.60	2.80E-02	6.03
o	GO:0009201~ribonucleoside triphosphate biosynthetic process	4	3.60	2.96E-02	5.90
o	GO:0009206~purine ribonucleoside triphosphate biosynthetic process	4	3.60	2.96E-02	5.90
o	GO:0009145~purine nucleoside triphosphate biosynthetic process	4	3.60	3.04E-02	5.84
o	GO:0009142~nucleoside triphosphate biosynthetic process	4	3.60	3.13E-02	5.78
	GO:0007049~cell cycle	10	9.01	3.21E-02	2.25
	GO:0006917~induction of apoptosis	5	4.50	3.26E-02	4.11
	GO:0012502~induction of programmed cell death	5	4.50	3.26E-02	4.11
	GO:0051258~protein polymerization	3	2.70	3.36E-02	10.29
o	GO:0019318~hexose metabolic process	5	4.50	3.39E-02	4.06
	GO:0050868~negative regulation of T cell activation	3	2.70	3.68E-02	9.80
	GO:0043244~regulation of protein complex disassembly	3	2.70	3.84E-02	9.58
o	GO:0006096~glycolysis	3	2.70	4.00E-02	9.36
o	GO:0009152~purine ribonucleotide biosynthetic process	4	3.60	4.22E-02	5.13
o	GO:0009260~ribonucleotide biosynthetic process	4	3.60	4.62E-02	4.95
	GO:0048872~homeostasis of number of cells	4	3.60	4.82E-02	4.86
o	GO:0005996~monosaccharide metabolic process	5	4.50	4.93E-02	3.59

Supplementary Table 4.11: GO Molecular Function overrepresentation test on TG2-associated proteins in UUO kidney membranes, performed by DAVID. Statistical overrepresentation test was performed by DAVID (http://david.abcc.ncifcrf.gov) using the annotation terms ontologies for Molecular Function (GOTERM_MF_FAT). The number of proteins belonging to the annotation term and fold change from the expected value H_0 are in increasing shades of red (the higher the more intense). The p-value is shown in increasing shades of blue (the more intense, the lower the p-value). A p-value lower than 0.05 was regarded as significant. Grey arrows = Terms associated with intracellular trafficking and vesicular transport and enriched in UUO kidney membranes; Black arrows = terms associated with cytoskeletal organisation and actin binding and enriched in UUO kidney membranes.

GO Molecular Function - TG2-associated proteins in UUO operated kidney membranes				
GO Molecular Function	Count	%	PValue	Fold Enrichment
GO:0003779~actin binding	27	23.48	8.22E-21	11.86
GO:0008092~cytoskeletal protein binding	29	25.22	5.03E-19	8.86
GO:0005516~calmodulin binding	10	8.70	2.55E-07	11.10
GO:0005198~structural molecule activity	14	12.17	4.79E-05	3.94
GO:0032553~ribonucleotide binding	30	26.09	8.20E-05	2.11
GO:0032555~purine ribonucleotide binding	30	26.09	8.20E-05	2.11
GO:0017076~purine nucleotide binding	30	26.09	1.70E-04	2.03
GO:0051082~unfolded protein binding	6	5.22	2.16E-04	10.85
GO:0005524~ATP binding	25	21.74	2.57E-04	2.19
GO:0032559~adenyl ribonucleotide binding	25	21.74	3.07E-04	2.17
GO:0051015~actin filament binding	5	4.35	5.72E-04	12.91
GO:0030554~adenyl nucleotide binding	25	21.74	6.41E-04	2.06
GO:0001883~purine nucleoside binding	25	21.74	7.24E-04	2.04
GO:0003774~motor activity	7	6.09	7.42E-04	6.42
GO:0001882~nucleoside binding	25	21.74	7.93E-04	2.03
GO:0000166~nucleotide binding	31	26.96	1.03E-03	1.80
GO:0008565~protein transporter activity	4	3.48	1.49E-02	7.67
GO:0030276~clathrin binding	2	1.74	4.61E-02	42.18
GO:0030898~actin-dependent ATPase activity	2	1.74	4.61E-02	42.18

Supplementary Table 4.12: GO Molecular Function overrepresentation test on TG2-associated proteins in Sham-operated kidney membranes, performed on DAVID. Statistical overrepresentation test was performed by DAVID (http://david.abcc.ncifcrf.gov) using the annotation terms ontologies for Molecular Function (GOTERM_MF_FAT). The number of proteins belonging to the annotation term and fold change from the expected value H_0 are in increasing shades of green (the higher the more intense). The p-value is shown in increasing shades of blue (the more intense, the lower the p-value). A p-value lower than 0.05 was regarded as significant. o = terms associated with catalytic activity and enriched in sham operated kidney membranes; oo = terms associated with ion channel and enriched in sham operated kidney membranes; ooo = terms associated with G-proteins or Small GTPases and enriched in sham operated kidney membranes.

	GO Molecular Function - TG2-associated proteins in Sham operated kidney membranes				
	GO Molecular Function in Sham	Count	%	PValue	Fold Enrichment
	GO:0032553~ribonucleotide binding	37	33.33	3.05E-09	2.82
	GO:0032555~purine ribonucleotide binding	37	33.33	3.05E-09	2.82
	GO:0000166~nucleotide binding	41	36.94	3.60E-09	2.57
	GO:0017076~purine nucleotide binding	37	33.33	9.24E-09	2.71
	GO:0005525~GTP binding	15	13.51	2.33E-07	5.80
	GO:0032561~guanyl ribonucleotide binding	15	13.51	3.16E-07	5.66
	GO:0019001~guanyl nucleotide binding	15	13.51	3.16E-07	5.66
	GO:0005524~ATP binding	22	19.82	1.27E-03	2.09
	GO:0032559~adenyl ribonucleotide binding	22	19.82	1.48E-03	2.06
	GO:0051082~unfolded protein binding	5	4.50	1.63E-03	9.78
	GO:0030554~adenyl nucleotide binding	22	19.82	2.74E-03	1.96
	GO:0001883~purine nucleoside binding	22	19.82	3.04E-03	1.95
	GO:0001882~nucleoside binding	22	19.82	3.28E-03	1.93
	GO:0000287~magnesium ion binding	9	8.11	9.44E-03	3.01
oo	GO:0042625~ATPase activity, coupled to transmembrane movement of ions	4	3.60	1.36E-02	7.94
ooo	GO:0003924~GTPase activity	5	4.50	1.38E-02	5.35
	GO:0042623~ATPase activity, coupled	6	5.41	2.27E-02	3.69
	GO:0016860~intramolecular oxidoreductase activity	3	2.70	3.07E-02	10.81
oo	GO:0016820~hydrolase activity, acting on acid anhydrides, catalyzing transmembrane movement of substances	4	3.60	3.31E-02	5.65
oo	GO:0042626~ATPase activity, coupled to transmembrane movement of substances	4	3.60	3.31E-02	5.65
oo	GO:0043492~ATPase activity, coupled to movement of substances	4	3.60	3.31E-02	5.65
o	GO:0016836~hydro-lyase activity	3	2.70	3.69E-02	9.78
	GO:0015405~P-P-bond-hydrolysis-driven transmembrane transporter activity	4	3.60	4.23E-02	5.12
oo	GO:0015399~primary active transmembrane transporter activity	4	3.60	4.33E-02	5.07

Supplementary Table 4.13: GO Cellular Component overrepresentation test on TG2-associated proteins in UUO kidney membranes, performed by DAVID. Statistical overrepresentation test was performed in DAVID (http://david.abcc.ncifcrf.gov) using the annotation terms ontologies for Cellular Component (GOTERM_CC_FAT). The number of proteins belonging to the annotation term and fold change from the expected value H_0 are in increasing shades of red (the higher the more intense). The p-value is shown in increasing shades of blue (the more intense, the lower the p-value). A p-value lower than 0.05 was regarded as significant. Grey arrows = Terms associated with intracellular trafficking and vesicular transport and enriched in UUO kidney membranes; Black arrows = terms associated with cytoskeletal organisation and actin binding and enriched in UUO kidney membranes.

GO Cellular Component - TG2-associated proteins in UUO kidney membranes				
GO Cellular Component	Count	%	PValue	Fold Enrichment
GO:0015629~actin cytoskeleton	17	14.78	3.74E-12	10.58
GO:0005856~cytoskeleton	34	29.57	5.49E-12	3.87
GO:0009898~internal side of plasma membrane	18	15.65	6.16E-11	8.00
GO:0044430~cytoskeletal part	24	20.87	1.66E-08	3.96
GO:0005938~cell cortex	11	9.57	4.52E-08	11.14
GO:0005829~cytosol	18	15.65	9.41E-07	4.18
GO:0043228~non-membrane-bounded organelle	34	29.57	3.82E-06	2.26
GO:0043232~intracellular non-membrane-bounded organelle	34	29.57	3.82E-06	2.26
GO:0030863~cortical cytoskeleton	6	5.22	1.93E-05	17.80
GO:0031252~cell leading edge	8	6.96	2.53E-05	9.11
GO:0044459~plasma membrane part	29	25.22	2.95E-05	2.27
GO:0030117~membrane coat	6	5.22	8.38E-05	13.20
GO:0048475~coated membrane	6	5.22	8.38E-05	13.20
GO:0005905~coated pit	5	4.35	1.04E-04	19.94
GO:0016459~myosin complex	6	5.22	1.07E-04	12.55
GO:0030118~clathrin coat	5	4.35	1.32E-04	18.76
GO:0031410~cytoplasmic vesicle	14	12.17	1.44E-04	3.52
GO:0031982~vesicle	14	12.17	1.78E-04	3.44
GO:0044448~cell cortex part	6	5.22	2.51E-04	10.49
GO:0005886~plasma membrane	39	33.91	3.12E-04	1.71
GO:0016023~cytoplasmic membrane-bounded vesicle	12	10.43	3.53E-04	3.70
GO:0031988~membrane-bounded vesicle	12	10.43	3.99E-04	3.65
GO:0030018~Z disc	5	4.35	4.33E-04	13.87
GO:0042995~cell projection	14	12.17	4.80E-04	3.11
GO:0031674~I band	5	4.35	7.45E-04	12.04
GO:0016323~basolateral plasma membrane	7	6.09	7.87E-04	6.33
GO:0005925~focal adhesion	5	4.35	9.81E-04	11.19
GO:0005924~cell-substrate adherens junction	5	4.35	1.27E-03	10.46
GO:0005912~adherens junction	6	5.22	1.38E-03	7.22
GO:0030055~cell-substrate junction	5	4.35	1.70E-03	9.67
GO:0005578~proteinaceous extracellular matrix	9	7.83	2.14E-03	3.87
GO:0070161~anchoring junction	6	5.22	2.66E-03	6.22
GO:0031012~extracellular matrix	9	7.83	2.73E-03	3.72
GO:0030017~sarcomere	5	4.35	3.43E-03	7.97
GO:0030054~cell junction	11	9.57	3.45E-03	2.99
GO:0042470~melanosome	5	4.35	4.26E-03	7.51
GO:0048770~pigment granule	5	4.35	4.26E-03	7.51
GO:0044449~contractile fiber part	5	4.35	4.45E-03	7.42
GO:0030659~cytoplasmic vesicle membrane	5	4.35	4.63E-03	7.33
GO:0030016~myofibril	5	4.35	5.43E-03	7.01
GO:0044433~cytoplasmic vesicle part	5	4.35	6.32E-03	6.72
GO:0043292~contractile fiber	5	4.35	6.32E-03	6.72
GO:0005794~Golgi apparatus	13	11.30	6.37E-03	2.43
GO:0012506~vesicle membrane	5	4.35	6.80E-03	6.58
GO:0005625~soluble fraction	5	4.35	7.30E-03	6.44
GO:0030662~coated vesicle membrane	4	3.48	8.01E-03	9.63
GO:0012505~endomembrane system	11	9.57	8.44E-03	2.62
GO:0030660~Golgi-associated vesicle membrane	3	2.61	1.14E-02	18.23
GO:0030864~cortical actin cytoskeleton	3	2.61	1.24E-02	17.40
GO:0001725~stress fiber	3	2.61	1.36E-02	16.64
GO:0032432~actin filament bundle	3	2.61	1.47E-02	15.95
GO:0030131~clathrin adaptor complex	3	2.61	1.59E-02	15.31
GO:0030119~AP-type membrane coat adaptor complex	3	2.61	1.59E-02	15.31
GO:0042641~actomyosin	3	2.61	1.84E-02	14.18
GO:0030120~vesicle coat	3	2.61	1.97E-02	13.67
GO:0005882~intermediate filament	5	4.35	2.18E-02	4.66
GO:0045111~intermediate filament cytoskeleton	5	4.35	2.34E-02	4.56
GO:0005798~Golgi-associated vesicle	3	2.61	3.16E-02	10.63
GO:0030665~clathrin coated vesicle membrane	3	2.61	3.16E-02	10.63
GO:0008091~spectrin	2	1.74	3.82E-02	51.04
GO:0008290~F-actin capping protein complex	2	1.74	3.82E-02	51.04
GO:0030132~clathrin coat of coated pit	2	1.74	4.57E-02	42.53

Supplementary Table 4.14: GO Cellular Component overrepresentation test on TG2-associated proteins in UUO kidney membranes, performed by DAVID. Statistical overrepresentation test was performed by DAVID (http://david.abcc.ncifcrf.gov) using the annotation terms ontologies for Cellular Component (GOTERM_CC_FAT). The number of proteins belonging to the annotation term and fold change from the expected value H_0 are in increasing shades of green (the higher the more intense). The p-value is shown in increasing shades of blue (the more intense, the lower the p-value). A p-value lower than 0.05 was regarded as significant. * = Terms associated with intracellular trafficking and vesicular transport and enriched in sham operated kidney membranes; ** = terms associated with cytoskeletal organisation and actin binding and enriched in sham operated kidney membranes.

	GO Cellular Component- TG2-associated proteins in Sham operated kidney membranes				
	GO Cellular Component in Sham	Count	%	PValue	Fold Enrichment
	GO:0005829~cytosol	15	13.51	1.35E-05	4.07
	GO:0048770~pigment granule	6	5.41	2.47E-04	10.51
	GO:0042470~melanosome	6	5.41	2.47E-04	10.51
	GO:0044445~cytosolic part	5	4.50	7.98E-04	11.81
	GO:0000267~cell fraction	12	10.81	1.87E-03	3.00
*	GO:0005768~endosome	7	6.31	6.54E-03	4.13
	GO:0005624~membrane fraction	10	9.01	6.56E-03	2.92
	GO:0005626~insoluble fraction	10	9.01	8.16E-03	2.82
	GO:0005788~endoplasmic reticulum lumen	4	3.60	1.21E-02	8.27
	GO:0005604~basement membrane	4	3.60	1.26E-02	8.16
**	GO:0044430~cytoskeletal part	12	10.81	1.30E-02	2.31
	GO:0005886~plasma membrane	29	26.13	1.90E-02	1.49
	GO:0044420~extracellular matrix part	4	3.60	2.32E-02	6.47
	GO:0005739~mitochondrion	16	14.41	2.63E-02	1.80
**	GO:0005856~cytoskeleton	14	12.61	3.30E-02	1.86
	GO:0042995~cell projection	9	8.11	3.66E-02	2.33
	GO:0019898~extrinsic to membrane	8	7.21	3.70E-02	2.52
	GO:0042383~sarcolemma	3	2.70	3.88E-02	9.50
	GO:0005885~Arp2/3 protein complex	2	1.80	3.92E-02	49.62
**	GO:0005832~chaperonin-containing T-complex	2	1.80	4.56E-02	42.53
**	GO:0015629~actin cytoskeleton	5	4.50	4.74E-02	3.63
	GO:0005578~proteinaceous extracellular matrix	6	5.41	4.74E-02	3.01

S.2.5 Gene names corresponding to protein IDs of TG2-associated candidates

Supplementary Table 4.15: Gene names corresponding to Protein IDs of TG2-associated candidates in UUO and/or Sham operated kidney membranes. Mouse gene names corresponding to the proteins IDs significantly associated with TG2 in UUO kidney membranes (p≤0.05 N≥4, reported in **Table 4.2**) and/or Sham operated kidney membranes (p≤0.05 N≥4, reported in **Table 4.3**).

Gene Name	Protein ID	Name	Unique/ Common
Acss2	ACSA_MOUSE	Acetyl-coenzyme A synthetase	SHAM ONLY
Actb	ACTB_MOUSE	Actin, cytoplasmic 1	UUO ONLY
Actr3	ARP3_MOUSE	Actin-related protein 3	SHAM ONLY
Acy3	ACY3_MOUSE	N-acyl-aromatic-L-amino acid amidohydrolase	SHAM ONLY
Add1	ADDA_MOUSE	Alpha-adducin	UUO ONLY
Add3	ADDG_MOUSE	Gamma-adducin	UUO ONLY
Adh1	ADH1_MOUSE	Alcohol dehydrogenase 1	COMMON
Ak1	KAD1_MOUSE	Adenylate kinase isoenzyme 1	SHAM ONLY
Akr7a2	ARK72_MOUSE	Aflatoxin B1 aldehyde reductase member 2	UUO ONLY
Alpl	PPBT_MOUSE	Alkaline phosphatase, tissue-nonspecific isozyme	SHAM ONLY
Ank3	ANK3_MOUSE	Ankyrin-3	UUO ONLY
Ankfy1	ANFY1_MOUSE	Rabankyrin-5	SHAM ONLY
Anxa2	ANXA2_MOUSE	Annexin A2	SHAM ONLY
Ap2a1	AP2A1_MOUSE	AP-2 complex subunit alpha-1	UUO ONLY
Ap2a2	AP2A2_MOUSE	AP-2 complex subunit alpha-2	UUO ONLY
Ap2b1	AP2B1_MOUSE	AP-2 complex subunit beta	UUO ONLY
Arf5	ARF5_MOUSE	ADP-ribosylation factor 5	SHAM ONLY
Arf6	ARF6_MOUSE	ADP-ribosylation factor 6	SHAM ONLY
Arhgap18	RHG18_MOUSE	Rho GTPase-activating protein 18	UUO ONLY
Arhgef12	ARHGC_MOUSE	Rho guanine nucleotide exchange factor 12	SHAM ONLY
Arl1	ARL1_MOUSE	ADP-ribosylation factor-like protein 1	SHAM ONLY
Arl2	ARL2_MOUSE	ADP-ribosylation factor-like protein 2	SHAM ONLY
Arpc1a	ARC1A_MOUSE	Actin-related protein 2/3 complex subunit 1A	SHAM ONLY
Arpc1b	ARC1B_MOUSE	Actin-related protein 2/3 complex subunit 1B	UUO ONLY
Arpc5	ARPC5_MOUSE	Actin-related protein 2/3 complex subunit 5	SHAM ONLY
Atp1a1	AT1A1_MOUSE	Sodium/potassium-transporting ATPase subunit alpha-1	SHAM ONLY
Atp1b1	AT1B1_MOUSE	Sodium/potassium-transporting ATPase subunit beta-1	SHAM ONLY
Atp2a2	AT2A2_MOUSE	Sarcoplasmic/endoplasmic reticulum calcium ATPase 2	UUO ONLY
Atp6v1a	VATA_MOUSE	V-type proton ATPase catalytic subunit A	SHAM ONLY
Atp6v1b2	VATB2_MOUSE	V-type proton ATPase subunit B	SHAM ONLY
Atp6v1h	VATH_MOUSE	V-type proton ATPase subunit H	UUO ONLY
Bax	BAX_MOUSE	Apoptosis regulator BAX	SHAM ONLY
Bgn	PGS1_MOUSE	Biglycan	COMMON
C1qb	C1QB_MOUSE	Complement C1q subcomponent subunit B	UUO ONLY
Ca9	CAH9_MOUSE	Carbonic anhydrase 9	SHAM ONLY
Calm1	CALM_MOUSE	Calmodulin	COMMON
Camk2d	KCC2D_MOUSE	Calcium/calmodulin-dependent protein kinase type II subunit delta	UUO ONLY
Capn1	CAN1_MOUSE	Calpain1	UUO ONLY
Capn2	CAN2_MOUSE	Calpain-2 catalytic subunit	SHAM ONLY
Capza2	CAZA2_MOUSE	F-actin-capping protein subunit alpha-2	UUO ONLY
Capzb	CAPZB_MOUSE	F-actin-capping protein subunit beta	UUO ONLY
Casp3	CASP3_MOUSE	Caspase-3	SHAM ONLY
Cct3	TCPG_MOUSE	T-complex protein 1 subunit gamma	SHAM ONLY
Cct5	TCPE_MOUSE	T-complex protein 1	UUO ONLY
Cct6a	TCPZ_MOUSE	T-complex protein 1	COMMON
Cct8	TCPQ_MOUSE	T-complex protein 1	UUO ONLY
Ckb	KCRB_MOUSE	Creatine kinase B-type	SHAM ONLY
Clic1	CLIC1_MOUSE	Chloride intracellular channel protein 1	UUO ONLY
Clic4	CLIC4_MOUSE	Chloride intracellular channel protein 4	SHAM ONLY
Clta	CLCA_MOUSE	Clathrin light chain A	UUO ONLY
Cltb	CLCB_MOUSE	Clathrin light chain b	UUO ONLY
Cltc	CLH1_MOUSE	Clathrin heavy chain 1	SHAM ONLY
Col12a1	COCA1_MOUSE	Collagen alpha-1(XII) chain	UUO ONLY
Col14a1	COEA1_MOUSE	Collagen alpha-1(XIV) chain	UUO ONLY
Copb2	COPB2_MOUSE	Coatomer subunit beta	UUO ONLY
Coro1c	COR1C_MOUSE	Coronin-1C	UUO ONLY
Csnk1a1	KC1A_MOUSE	Casein kinase I isoform alpha	UUO ONLY
Cul5	CUL5_MOUSE	Cullin-5	SHAM ONLY
Dbn1	DREB_MOUSE	Drebrin	UUO ONLY
Dcn	PGS2_MOUSE	Decorin	UUO ONLY
Dctn1	DCTN1_MOUSE	Dynactin subunit 1	UUO ONLY
Dhrs4	DHRS4_MOUSE	Dehydrogenase/reductase SDR family member 4	SHAM ONLY
Dnaja2	DNJA2_MOUSE	DnaJ homolog subfamily A member 2	SHAM ONLY
Dnajb11	DJB11_MOUSE	DnaJ homolog subfamily B member 11	SHAM ONLY
Dpysl3	DPYL3_MOUSE	Dihydropyrimidinase-related protein 3	SHAM ONLY
Drg2	DRG2_MOUSE	Developmentally-regulated GTP-binding protein 2	SHAM ONLY
Dsp	DESP_MOUSE	Desmoplakin	UUO ONLY
Dstn	DEST_MOUSE	Destrin	SHAM ONLY

Eef1a1	EF1A1_MOUSE	Elongation factor 1-alpha 1	SHAM ONLY
Ehhadh	ECHP_MOUSE	Peroxisomal bifunctional enzyme	COMMON
Eif4a1	IF4A1_MOUSE	Eukaryotic initiation factor 4A-I	SHAM ONLY
Eif4g3	IF4G3_MOUSE	Eukaryotic translation initiation factor 4 gamma 3	COMMON
Eno1	ENOA_MOUSE	Alpha-enolase	SHAM ONLY
Eprs	SYEP_MOUSE	Bifunctional glutamate/proline--tRNA ligase	UUO ONLY
Eps8l2	ES8L2_MOUSE	Epidermal growth factor receptor kinase substrate 8-like protein 2	UUO ONLY
FAM120A	F120A_MOUSE	Constitutive coactivator of PPAR-gamma-like protein 1	COMMON
Fam129b	NIBL1_MOUSE	Niban-like protein 1	SHAM ONLY
Fam213a	F213A_MOUSE	Redox-regulatory protein FAM213A	COMMON
Fam49b	FA49B_MOUSE	Protein FAM49B	UUO ONLY
Farp1	FARP1_MOUSE	FERM, RhoGEF and pleckstrin domain-containing protein 1	SHAM ONLY
Fbln1	FBLN1_MOUSE	Fibulin-1	SHAM ONLY
Flna	FLNA_MOUSE	Filamin-A	UUO ONLY
Flnb	FLNB_MOUSE	Filamin-B	UUO ONLY
Flot2	FLOT2_MOUSE	Flotillin-2	UUO ONLY
Fn1	FINC_MOUSE	Fibronectin	COMMON
Gak	GAK_MOUSE	Cyclin-G-associated kinase	UUO ONLY
Gapdh	G3P_MOUSE	Glyceraldehyde-3-phosphate dehydrogenase	SHAM ONLY
Gbp2	GBP2_MOUSE	Interferon-induced guanylate-binding protein 2	UUO ONLY
Gga1	GGA1_MOUSE	ADP-ribosylation factor-binding protein GGA1	SHAM ONLY
Glrx	GLRX1_MOUSE	Glutaredoxin 1	UUO ONLY
Glrx3	GLRX3_MOUSE	Glutaredoxin-3	UUO ONLY
Glyctk	GLCTK_MOUSE	Glycerate kinase	SHAM ONLY
Gpx1	GPX1_MOUSE	Glutathione peroxidase 1	UUO ONLY
Gsn	GELS_MOUSE	Gelsolin	UUO ONLY
Gstt1	GSTT1_MOUSE	Glutathione S-transferase theta-1	UUO ONLY
Gucy1a3	GCYA3_MOUSE	Guanylate cyclase soluble subunit alpha-3	SHAM ONLY
Hba	HBA_MOUSE	Hemoglobin subunit alpha	SHAM ONLY
Hip1	HIP1_MOUSE	Huntingtin-interacting protein 1	UUO ONLY
Hsp90aa1	HS90A_MOUSE	Heat shock protein HSP 90-alpha	UUO ONLY
Hsp90ab1	HS90B_MOUSE	Heat shock protein HSP 90-beta	SHAM ONLY
Hspa5	GRP78_MOUSE	78 kDa glucose-regulated protein	UUO ONLY
Hspa8	HSP7C_MOUSE	Heat shock cognate 71 kDa protein	UUO ONLY
Hspb1	HSPB1_MOUSE	Heat shock protein beta-1	UUO ONLY
Hspg2	PGBM_MOUSE	Basement membrane-specific heparan sulfate proteoglycan core protein (Perlecan)	UUO ONLY
Iqgap1	IQGA1_MOUSE	Ras GTPase-activating-like protein IQGAP1	COMMON
Irak4	IRAK4_MOUSE	Interleukin-1 receptor-associated kinase 4	UUO ONLY
Irf3	IRF3_MOUSE	Interferon regulatory factor 3	SHAM ONLY
Irgm1	IRGM1_MOUSE	Immunity-related GTPase family M protein 1	UUO ONLY
Isg15	ISG15_MOUSE	Ubiquitin-like protein ISG15	SHAM ONLY
Ist1	IST1_MOUSE	IST1 homolog	SHAM ONLY
Itm2b	ITM2B_MOUSE	Integral membrane protein 2B	SHAM ONLY
Krt14	K1C14_MOUSE	Keratin, type I cytoskeletal 14	UUO ONLY
Krt19	K1C19_MOUSE	Keratin, type I cytoskeletal 19	UUO ONLY
Krt20	K1C20_MOUSE	Keratin, type I cytoskeletal 20	UUO ONLY
Krt6b	K2C6B_MOUSE	Keratin, type II cytoskeletal 6B	UUO ONLY
Krt77	K2C1B_MOUSE	Keratin, type II cytoskeletal 1b	SHAM ONLY
Lamb2	LAMB2_MOUSE	Laminin subunit beta-2	COMMON
Lcp1	PLSL_MOUSE	Plastin-2	UUO ONLY
Ldha	LDHA_MOUSE	L-lactate dehydrogenase A chain	UUO ONLY
Lims1	LIMS1_MOUSE	LIM and senescent cell antigen-like-containing domain protein 1	COMMON
Lsp1	LSP1_MOUSE	Lymphocyte-specific protein 1	UUO ONLY
Lypla1	LYPA1_MOUSE	Acyl-protein thioesterase 1	UUO ONLY
Lypla2	LYPA2_MOUSE	Acyl-protein thioesterase 2	SHAM ONLY
Map2k2	MP2K2_MOUSE	Dual specificity mitogen-activated protein kinase kinase 2	SHAM ONLY
Mep1a	MEP1A_MOUSE	Meprin A subunit alpha	SHAM ONLY
Mgst3	MGST3_MOUSE	Microsomal glutathione S-transferase 3	SHAM ONLY
Msn	MOES_MOUSE	Moesin	UUO ONLY
Mthfd1	C1TC_MOUSE	C-1-tetrahydrofolate synthase	UUO ONLY
Mvp	MVP_MOUSE	Major vault protein	UUO ONLY
Myh10	MYH10_MOUSE	Myosin-10	UUO ONLY
Myh14	MYH14_MOUSE	Myosin-14	UUO ONLY
Myo18a	MY18A_MOUSE	Unconventional myosin-XVIIIa	UUO ONLY
Myo1b	MYO1B_MOUSE	Unconventional myosin-Ib	UUO ONLY
Myo1d	MYO1D_MOUSE	Unconventional myosin-Id	UUO ONLY
Myo1g	MYO1G_MOUSE	Unconventional myosin-Ig	UUO ONLY
Nampt	NAMPT_MOUSE	Nicotinamide phosphoribosyltransferase	COMMON
Naprt	PNCB_MOUSE	Nicotinate phosphoribosyltransferase	UUO ONLY
Ndrg3	NDRG3_MOUSE	Protein NDRG3	SHAM ONLY
Nedd4	NEDD4_MOUSE	E3 ubiquitin-protein ligase NEDD4	SHAM ONLY
Nmrk1	NRK1_MOUSE	Nicotinamide riboside kinase 1	SHAM ONLY
Nsf	NSF_MOUSE	Vesicle-fusing ATPase	SHAM ONLY
Olfm4	OLFM4_MOUSE	Olfactomedin-4	SHAM ONLY
Oxsr1	OXSR1_MOUSE	Serine/threonine-protein kinase OSR1	SHAM ONLY
P4hb	PDIA1_MOUSE	Protein disulfide-isomerase	SHAM ONLY
Pah	PH4H_MOUSE	Phenylalanine-4-hydroxylase	SHAM ONLY
Paics	PUR6_MOUSE	Multifunctional protein ADE2	UUO ONLY
Pck1	PCKGC_MOUSE	Phosphoenolpyruvate carboxykinase	COMMON
Pdcd6ip	PDC6I_MOUSE	Programmed cell death 6-interacting protein	COMMON
Pdia6	PDIA6_MOUSE	Protein disulfide-isomerase A6	SHAM ONLY
Pdlim5	PDLI5_MOUSE	PDZ and LIM domain protein 5	UUO ONLY

Pfkp	K6PP_MOUSE	ATP-dependent 6-phosphofructokinase, platelet type	UUO ONLY
Pfn1	PROF1_MOUSE	Profilin-1	UUO ONLY
Pgk1	PGK1_MOUSE	Phosphoglycerate kinase 1	COMMON
Phgdh	SERA_MOUSE	D-3-phosphoglycerate dehydrogenase	COMMON
Picalm	PICAL_MOUSE	Phosphatidylinositol-binding clathrin assembly protein	COMMON
Plec	PLEC_MOUSE	Plectin	SHAM ONLY
Pls3	PLST_MOUSE	Plastin-3	UUO ONLY
Postn	POSTN_MOUSE	Periostin	UUO ONLY
Ppp1ca	PP1A_MOUSE	Serine/threonine-protein phosphatase PP1-alpha catalytic subunit	SHAM ONLY
Ppp1r9b	NEB2_MOUSE	Neurabin-2	UUO ONLY
Prdx2	PRDX2_MOUSE	Peroxiredoxin-2	COMMON
Prune	PRUNE_MOUSE	Protein prune homolog	SHAM ONLY
Psmc1	PRS4_MOUSE	26S protease regulatory subunit 4	SHAM ONLY
Psmd11	PSD11_MOUSE	26S proteasome non-ATPase regulatory subunit 11	UUO ONLY
Psme1	PSME1_MOUSE	Proteasome activator complex subunit 1	SHAM ONLY
Ptpn6	PTN6_MOUSE	Tyrosine-protein phosphatase non-receptor type 6	COMMON
Rab10	RAB10_MOUSE	Ras-related protein Rab-10	SHAM ONLY
Rab1A	RAB1A_MOUSE	Ras-related protein Rab-1A	UUO ONLY
Rab3gap2	RBGPR_MOUSE	Rab3 GTPase-activating protein non-catalytic subunit	UUO ONLY
Rac2	RAC2_MOUSE	Ras-related C3 botulinum toxin substrate 2	SHAM ONLY
Rcn1	RCN1_MOUSE	Reticulocalbin-1	SHAM ONLY
Rheb	RHEB_MOUSE	GTP-binding protein Rheb	SHAM ONLY
Rnf213	RN213_MOUSE	E3 ubiquitin-protein ligase RNF213	SHAM ONLY
Rpn1	RPN1_MOUSE	Dolichyl-diphosphooligosaccharide--protein glycosyltransferase subunit 1	UUO ONLY
Rps6ka3	KS6A3_MOUSE	Ribosomal protein S6 kinase alpha-3	SHAM ONLY
Rtn4	RTN4_MOUSE	Reticulon-4	UUO ONLY
Rufy3	RUFY3_MOUSE	Protein RUFY3	SHAM ONLY
Sar1b	SAR1B_MOUSE	GTP-binding protein SAR1b	UUO ONLY
Scfd1	SCFD1_MOUSE	Sec1 family domain-containing protein 1	COMMON
Scp2	NLTP_MOUSE	Non-specific lipid-transfer protein	SHAM ONLY
Sdc4	SDC4_MOUSE	Syndecan-4	UUO ONLY
Serpinh1	SERPH_MOUSE	Serpin H1	UUO ONLY
Slc12a3	S12A3_MOUSE	Solute carrier family 12 member 3	SHAM ONLY
Sntb2	SNTB2_MOUSE	Beta-2-syntrophin	UUO ONLY
Snx1	SNX1_MOUSE	Sorting nexin-1	UUO ONLY
Snx3	SNX3_MOUSE	Sorting nexin-3	SHAM ONLY
Snx4	SNX4_MOUSE	Sorting nexin-4	UUO ONLY
Spna1	SPTA1_MOUSE	Spectrin alpha chain, erythrocytic 1	COMMON
Spna2	SPTN1_MOUSE	Spectrin alpha chain, non-erythrocytic 1	COMMON
Spnb1	SPTB1_MOUSE	Spectrin beta chain, erythrocytic	UUO ONLY
Sult1a1	ST1A1_MOUSE	Sulfotransferase 1A1	SHAM ONLY
Sult1d1	ST1D1_MOUSE	Sulfotransferase 1 family member D1	SHAM ONLY
Svil	SVIL_MOUSE	Supervillin	UUO ONLY
Tbc1d9b	TBC9B_MOUSE	TBC1 domain family member 9B	SHAM ONLY
Tcp1	TCPA_MOUSE	T-complex protein 1	UUO ONLY
Tgm2	TGM2_MOUSE	Transglutaminase 2	COMMON
Tjp1	ZO1_MOUSE	Tight junction protein ZO-1	UUO ONLY
Tln2	TLN2_MOUSE	Talin-2	UUO ONLY
Tmem55b	TM55B_MOUSE	Type 1 phosphatidylinositol 4,5-bisphosphate 4-phosphatase	SHAM ONLY
Tom1	TOM1_MOUSE	Target of Myb protein 1	SHAM ONLY
Tsg101	TS101_MOUSE	Tumor susceptibility gene 101 protein	SHAM ONLY
Tuba1a	TBA1A_MOUSE	Tubulin alpha-1A chain	SHAM ONLY
Tuba4a	TBA4A_MOUSE	Tubulin alpha-4A chain	SHAM ONLY
Tubb5	TBB5_MOUSE	Tubulin beta-5 chain	SHAM ONLY
Ube2d3	UB2D3_MOUSE	Ubiquitin-conjugating enzyme E2 D3	SHAM ONLY
Uck1	UCK1_MOUSE	Uridine-cytidine kinase 1	UUO ONLY
Unc45a	UN45A_MOUSE	Protein unc-45 homolog A	SHAM ONLY
Usp24	UBP24_MOUSE	Ubiquitin carboxyl-terminal hydrolase 24	SHAM ONLY
Usp5	UBP5_MOUSE	Ubiquitin carboxyl-terminal hydrolase 5	UUO ONLY
Usp9x	USP9X_MOUSE	Probable ubiquitin carboxyl-terminal hydrolase FAF-X	SHAM ONLY
Vcp	TERA_MOUSE	Transitional endoplasmic reticulum ATPase	COMMON
Vdac1	VDAC1_MOUSE	Voltage-dependent anion-selective channel protein 1	SHAM ONLY
Vil1	VILI_MOUSE	Villin-1	SHAM ONLY
Vim	VIME_MOUSE	Vimentin	UUO ONLY
Vps35	VPS35_MOUSE	Vacuolar protein sorting-associated protein 35	SHAM ONLY
Wars	SYWC_MOUSE	Tryptophan--tRNA ligase	SHAM ONLY
Ykt6	YKT6_MOUSE	Synaptobrevin homolog YKT6	UUO ONLY

S.2.6 Search for TG2-associated partners in kidney fibrotic membranes on the Exocarta database

Supplementary Table 4.16: Analysis of presence of the TG2-associated proteins in kidney fibrotic membranes on the Exocarta database of exosomal proteins. The TG2-associated proteins identified in kidney fibrotic membranes were manually searched on the Exocarta database (http://www.exocarta.org/) of exosomal proteins in four different species: *Homo sapiens*, *Mus musculus*, *Rattus norvegicus* and *Bos taurus*. * = Identified only at mRNA level in the species.

TG2 associated candidates in UUO				Found in Exosomes			
Sample ID	**Name**	**p value**	**N**	*Homo Sapiens*	*Mus Muscus*	*Rattus Norvegicus*	*Bos Taurus*
DESP_MOUSE	Desmoplakin	1.22E-13	5	■			■
HSP7C_MOUSE	Heat shock cognate 71 kDa protein	7.67E-10	5	■	■	■	■
CALM_MOUSE	Calmodulin	1.83E-08	5	■		■	
CAZA2_MOUSE	F-actin-capping protein subunit alpha-2	1.97E-08	5	■	■	■	■
GPX1_MOUSE	Glutathione peroxidase 1	4.52E-07	5	■		■	■
ADH1_MOUSE	Alcohol dehydrogenase 1;Adh1;ortholog	9.40E-07	5	■		■	
POSTN_MOUSE	Periostin	1.03E-06	4	■	■	■	
MYO1D_MOUSE	Unconventional myosin-Id	3.52E-06	5	■			
GLRX1_MOUSE	Glutaredoxin 1	5.61E-06	4	■			■
GLRX3_MOUSE	Glutaredoxin-3	1.40E-05	5	■		■	■
PROF1_MOUSE	Profilin-1	1.89E-05	5	■	■	■	■
TGM2_MOUSE	Transglutaminase 2	3.31E-05	5	■		■	
HSPB1_MOUSE	Heat shock protein beta-1	3.68E-05	5	■		■	■
VATH_MOUSE	V-type proton ATPase subunit H	5.98E-05	5	■	■	■	■
ADDG_MOUSE	Gamma-adducin	6.66E-05	5				■
AT2A2_MOUSE	Sarcoplasmic/endoplasmic reticulum calcium ATPase 2	8.58E-05	5	■	■	■	
SVIL_MOUSE	Supervillin;Svil;ortholog	1.01E-04	4				■
COR1C_MOUSE	Coronin-1C	1.38E-04	5	■		■	■
IQGA1_MOUSE	Ras GTPase-activating-like protein IQGAP1	1.50E-04	5	■	■	■	
TCPE_MOUSE	T-complex protein 1	3.17E-04	5		■		
UBP5_MOUSE	Ubiquitin carboxyl-terminal hydrolase 5	4.59E-04	5				
FLOT2_MOUSE	Flotillin-2	5.38E-04	4	■		■	■
NAMPT_MOUSE	Nicotinamide phosphoribosyltransferase	6.56E-04	5	■		■	
PCKGC_MOUSE	Phosphoenolpyruvate carboxykinase	8.93E-04	5	■		■	
RAB1A_MOUSE	Ras-related protein Rab-1A	9.16E-04	5	■	■	■	■
SDC4_MOUSE	Syndecan 4	9.34E-04	5	■	■	■	■
LDHA_MOUSE	L-lactate dehydrogenase A	1.04E-03	4	■	■	■	
MYO1G_MOUSE	Unconventional myosin-Ig	1.21E-03	5	■	■		
K1C20_MOUSE	Keratin, type I cytoskeletal 20;Krt20;ortholog	1.35E-03	4	■			
COEA1_MOUSE	Collagen alpha-1(XIV) chain	1.64E-03	5	■			
COCA1_MOUSE	Collagen alpha-1(XII) chain	1.68E-03	4	■			
HIP1_MOUSE	Huntingtin-interacting protein	1.86E-03	4	■			
LIMS1_MOUSE	LIM and senescent cell antigen-like-containing domain protein 1	2.47E-03	5	■		■	
SAR1B_MOUSE	GTP-binding protein SAR1b	2.79E-03	5	■			
SPTA1_MOUSE	Spectrin alpha chain, erythrocytic 1	2.92E-03	5				
FLNA_MOUSE	Filamin-A	2.98E-03	5	■	■	■	
ANK3_MOUSE	Ankyrin-3	3.03E-03	5		*	■	
PSD11_MOUSE	26S proteasome non-ATPase regulatory subunit 11	3.09E-03	5	■	■		

PGBM_MOUSE	Basement membrane-specific heparan sulfate proteoglycan core protein (perlecan)	3.16E-03	5				
LSP1_MOUSE	Lymphocyte-specific protein 1	3.53E-03	5				
GELS_MOUSE	Gelsolin	4.61E-03	5				
YKT6_MOUSE	Synaptobrevin homolog YKT6;Ykt6;ortholog	4.72E-03	5				
PTN6_MOUSE	Tyrosine-protein phosphatase non-receptor type 6	4.84E-03	4				
FLNB_MOUSE	Filamin-B	5.03E-03	5				
TLN2_MOUSE	Talin-2	5.28E-03	5				
PGK1_MOUSE	Phosphoglycerate kinase 1	5.39E-03	4				
PICAL_MOUSE	Phosphatidylinositol-binding clathrin assembly protein	5.65E-03	4				
F120A_MOUSE	Constitutive coactivator of PPAR-gamma-like protein 1	6.27E-03	5				
PRDX2_MOUSE	Peroxiredoxin-2	6.87E-03	4				
KCC2D_MOUSE	Calcium/calmodulin-dependent protein kinase type II subunit delta	7.10E-03	5				
RTN4_MOUSE	Reticulon-4;Rtn4;ortholog	7.57E-03	5				
SERA_MOUSE	D-3-phosphoglycerate dehydrogenase	7.78E-03	5				
KC1A_MOUSE	Casein kinase I isoform alpha	8.06E-03	5				
DCTN1_MOUSE	Dynactin subunit 1	8.52E-03	5				
ADDA_MOUSE	Alpha-adducin	8.61E-03	5				
PGS2_MOUSE	Decorin	1.09E-02	5				
IF4G3_MOUSE	Eukaryotic translation initiation factor 4 gamma 3	1.11E-02	5				
RHG18_MOUSE	Rho GTPase-activating protein 18	1.11E-02	4				
CAPZB_MOUSE	F-actin-capping protein subunit beta	1.11E-02	5				
MVP_MOUSE	Major vault protein	1.14E-02	5				
TERA_MOUSE	Transitional endoplasmic reticulum ATPase	1.21E-02	5				
ACTB_MOUSE	Actin, cytoplasmic 1	1.24E-02	5				
PGS1_MOUSE	Biglycan	1.30E-02	5				
K1C14_MOUSE	Keratin, type I cytoskeletal 14	1.33E-02	5				
PLSL_MOUSE	Plastin-2	1.34E-02	5				
AP2A2_MOUSE	AP-2 complex subunit alpha-2	1.52E-02	5				
FINC_MOUSE	Fibronectin	1.57E-02	5				
CLCB_MOUSE	Clathrin light chain b	1.65E-02	5				
SNX4_MOUSE	Sorting nexin-4	1.67E-02	5				
SPTB1_MOUSE	Spectrin beta chain, erythrocytic	1.73E-02	5				
ZO1_MOUSE	Tight junction protein ZO-1	1.79E-02	4				
DREB_MOUSE	Drebrin	1.83E-02	5				
CAN1_MOUSE	Calpain1	1.84E-02	5				
PDLI5_MOUSE	PDZ and LIM domain protein 5	1.85E-02	5				
PUR6_MOUSE	Multifunctional protein ADE2	1.88E-02	5				
MY18A_MOUSE	Unconventional myosin-XVIIIa	1.93E-02	5				
CLCA_MOUSE	Clathrin light chain A	2.07E-02	5				
IRGM1_MOUSE	Immunity-related GTPase family M protein 1	2.09E-02	5				
NEB2_MOUSE	Neurabin-2	2.11E-02	5				
K2C6B_MOUSE	Keratin, type II cytoskeletal 6B	2.14E-02	5				
AP2A1_MOUSE	AP-2 complex subunit alpha-1	2.15E-02	5				
LYPA1_MOUSE	Acyl-protein thioesterase 1	2.18E-02	5				
PDC6I_MOUSE	Programmed cell death 6-interacting protein	2.38E-02	5				
AP2B1_MOUSE	AP-2 complex subunit beta	2.43E-02	5				
K1C19_MOUSE	Keratin, type I cytoskeletal 19	2.58E-02	5				
GRP78_MOUSE	78 kDa glucose-regulated protein	2.59E-02	5				

ARK72_MOUSE	Aflatoxin B1 aldehyde reductase member 2	2.61E-02	5				
SNTB2_MOUSE	Beta-2-syntrophin	2.63E-02	5				
MYO1B_MOUSE	Unconventional myosin-Ib	2.67E-02	5				
K6PP_MOUSE	ATP-dependent 6-phosphofructokinase, platelet type	2.67E-02	5				
C1QB_MOUSE	Complement C1q subcomponent subunit B	2.71E-02	5				
F213A_MOUSE	Redox-regulatory protein FAM213A	2.79E-02	5				
HS90A_MOUSE	Heat shock protein HSP 90-alpha	2.85E-02	5				
GAK_MOUSE	Cyclin-G-associated kinase	2.86E-02	5				
SPTN1_MOUSE	Spectrin alpha chain, non-erythrocytic 1	3.08E-02	5				
UCK1_MOUSE	Uridine-cytidine kinase 1	3.12E-02	5				
ECHP_MOUSE	Peroxisomal bifunctional enzyme	3.15E-02	5				
ES8L2_MOUSE	Epidermal growth factor receptor kinase substrate 8-like protein 2	3.29E-02	4				
MOES_MOUSE	Moesin	3.33E-02	5				
PNCB_MOUSE	Nicotinate phosphoribosyltransferase	3.34E-02	5				
MYH10_MOUSE	Myosin-10	3.59E-02	5				
RBGPR_MOUSE	Rab3 GTPase-activating protein non-catalytic subunit	3.65E-02	5				
VIME_MOUSE	Vimentin	3.66E-02	5				
SERPH_MOUSE	Serpin H1	3.81E-02	5				
RPN1_MOUSE	Dolichyl-diphosphooligosaccharide--protein glycosyltransferase subunit 1	3.89E-02	4				
LAMB2_MOUSE	Laminin subunit beta-2	3.92E-02	4				
GSTT1_MOUSE	Glutathione S-transferase theta-1	3.95E-02	5				
TCPQ_MOUSE	T-complex protein 1	3.96E-02	5				
TCPZ_MOUSE	T-complex protein 1	4.23E-02	5				
IRAK4_MOUSE	Interleukin-1 receptor-associated kinase 4	4.24E-02	5				
C1TC_MOUSE	C-1-tetrahydrofolate synthase, cytoplasmic	4.28E-02	5				
ARC1B_MOUSE	Actin-related protein 2/3 complex subunit 1B	4.28E-02	5				
SCFD1_MOUSE	Sec1 family domain-containing protein 1	4.30E-02	5				
COPB2_MOUSE	Coatomer subunit beta'	4.42E-02	5				
FA49B_MOUSE	Protein FAM49B;Fam49b;ortholog	4.62E-02	5				
MYH14_MOUSE	Myosin-14	4.79E-02	5				
SNX1_MOUSE	Sorting nexin-1	4.81E-02	4				
PLST_MOUSE	Plastin-3	4.82E-02	5				
GBP2_MOUSE	Interferon-induced guanylate-binding protein 2	5.00E-02	5			*	
SYEP_MOUSE	Bifunctional glutamate/proline--tRNA ligase	5.17E-02	5				
TCPA_MOUSE	T-complex protein 1	5.25E-02	5				
CLIC1_MOUSE	Chloride intracellular channel protein 1	5.33E-02	5				

S.2.7 Comparison between TG2-associated proteins in healthy kidney membranes and the proteomic analysis on the UUO model

Supplementary Table 4.17. Comparison of TG2 interactome in Sham operated kidney membranes with the UUO Proteome: To see if the proteins significantly associated with TG2 in sham operated conditions were significantly altered in the healthy mice, the two analysis in were combined in this heat-map table. On the left side, the list of TG2-associated proteins in Sham operated kidney membranes (21 days); in scale of blue, the p-value of TG2 association as calculated by z-test. A p-value ≤0.05 was regarded as significant. On the right, the fold change from sham and confidence values for the same proteins in the UUO proteomic analysis performed on whole tissue; in red, the positive fold change (FC) in the UUO, that means overexpression, and in green the negative fold change, that means underexpression. In yellow, the level of confidence of this second analysis, bright yellow ≥ 0.8 and light yellow 0.5 ≤ C < 0.8. A confidence ≥ 0.8 was considered as significant. Legend: U=Unique; C= Common (associated with TG2 in both UUO and Sham operated mice).

	TG2-associated proteins in Sham operated membranes			Expression upon UUO in whole kidney lysates	
Protein ID	Unique/ Common	N	p-value	Log2 FC (UUO/Sham)	Confidence
PRS4	U	5	5.22E-09	1.22	0.36
PSME1	U	5	8.91E-07	1.19	0.84
NEDD4	U	5	3.03E-05	1.45	0.68
K2C1B	U	4	8.40E-05	1.59	0.61
UN45A	U	5	1.04E-04		
TGM2	C	5	1.21E-04	0.78	0.90
PRUNE	U	5	1.31E-04		
NIBL1	U	5	1.41E-04	1.51	0.56
PLEC	U	5	1.80E-04	2.09	0.73
IF4G3	C	5	1.82E-04		
SERA	C	5	1.85E-04	0.43	0.54
TERA	C	5	2.49E-04	-0.40	0.52
PH4H	U	5	2.67E-04	-2.27	0.84
TOM1	U	4	3.37E-04		
PTN6	C	4	4.04E-04	1.04	0.59
ACY3	U	4	5.54E-04	-3.64	0.80
TCPZ	C	5	6.52E-04	-0.44	0.36
DEST	U	5	8.51E-04	0.89	0.80
UB2D3	U	5	9.25E-04		
KAD1	U	5	9.92E-04	0.48	0.51
G3P	U	5	1.05E-03	-1.19	0.92
USP9X	U	5	1.27E-03		
PDIA1	U	4	1.40E-03	-0.32	0.31
CASP3	U	4	1.42E-03		
UBP24	U	4	1.43E-03		
MEP1A	U	5	1.68E-03	-2.84	0.88
ARF6	U	5	1.88E-03	-0.66	0.50
SPTA1	C	5	1.97E-03		
TM55B	U	4	3.22E-03		
KCRB	U	5	4.11E-03	2.92	0.83
RHEB	U	5	4.12E-03	-0.87	0.56
SCFD1	C	5	4.24E-03	1.18	0.28
ST1A1	U	5	4.51E-03		
ANXA2	U	5	5.38E-03	0.66	0.66
CALM	C	5	5.39E-03	-0.51	0.41
F120A	C	5	5.77E-03	0.59	0.33
OLFM4	U	5	5.80E-03		
IST1	U	5	6.01E-03	1.31	0.39
PRDX2	C	4	6.07E-03	-0.36	0.64
PP1A	U	4	6.08E-03	0.38	0.53
NLTP	U	5	6.29E-03	-2.97	0.88
PPBT	U	5	6.39E-03	-3.17	0.74
PDC6I	C	5	6.41E-03	0.71	0.44
ENOA	U	4	6.90E-03	-1.33	0.98
FBLN1	U	5	7.33E-03	2.62	0.79
LIMS1	C	5	7.55E-03		
TCPG	U	5	7.61E-03	3.23	0.35
GGA1	U	5	8.30E-03		
IRF3	U	4	8.39E-03		
TBB5	U	5	8.92E-03	1.74	0.88
FARP1	U	5	9.63E-03		
DJB11	U	4	1.03E-02	-2.95	0.33
ARF5	U	5	1.03E-02	2.43	0.53
ARPC5	U	4	1.06E-02	1.60	0.76
ARHGC	U	5	1.10E-02		
ARL2	U	5	1.14E-02		
AT1B1	U	5	1.21E-02	-4.29	0.87
MGST3	U	5	1.21E-02	-2.83	0.84
NSF	U	5	1.28E-02	-0.48	0.33
PGK1	C	4	1.38E-02	-1.71	0.97
ARL1	U	5	1.42E-02	-1.16	0.90

	TG2-associated proteins in Sham operated membranes			Expression upon UUO in whole kidney lysates	
Protein ID	Unique/ Common	N	p-value	Log2 FC (UUO/Sham)	Confidence
AT1A1	U	5	1.43E-02	-3.72	0.93
CUL5	U	5	1.43E-02		
VILI	U	5	1.51E-02	-3.56	0.91
S12A3	U	5	1.55E-02	-3.18	0.63
KS6A3	U	5	1.58E-02	0.46	0.41
TBA4A	U	5	1.62E-02	-2.79	0.88
VATA	U	5	1.70E-02	-2.59	0.92
SYWC	U	5	1.75E-02	-0.92	0.32
CAH9	U	4	1.76E-02		
RAC2	U	5	1.85E-02	3.96	0.63
HBA	U	5	1.88E-02	0.44	0.71
RAB10	U	5	1.98E-02	2.64	0.53
PCKGC	C	5	2.08E-02	-4.20	0.80
NRK1	U	5	2.11E-02		
VPS35	U	5	2.25E-02		
SNX3	U	5	2.27E-02	-0.78	0.84
ACSA	U	5	2.29E-02	-2.53	0.65
DNJA2	U	5	2.29E-02	-0.47	0.52
ST1D1	U	5	2.40E-02	-3.78	0.85
ANFY1	U	5	2.42E-02		
GLCTK	U	5	2.42E-02	-0.91	0.69
ARC1A	U	5	2.42E-02	-1.77	0.43
PDIA6	U	5	2.53E-02	0.75	0.90
VATB2	U	5	2.59E-02	-2.47	0.85
GCYA3	U	5	2.67E-02		
LYPA2	U	5	2.68E-02	0.50	0.26
RUFY3	U	4	2.72E-02		
PICAL	C	4	2.73E-02	-0.62	0.43
TBC9B	U	5	2.78E-02		
IQGA1	C	5	2.99E-02	1.12	0.66
RCN1	U	4	3.03E-02	-0.54	0.47
ARP3	U	5	3.04E-02	0.92	0.95
PGS1	C	5	3.18E-02	3.13	0.86
NAMPT	C	5	3.20E-02	-1.36	0.82
ECHP	C	5	3.21E-02	-4.32	0.84
HS90B	U	5	3.38E-02	-1.56	0.47
ITM2B	U	5	3.60E-02		
MP2K2	U	5	3.62E-02		
DHRS4	U	4	3.62E-02	-2.68	0.91
TBA1A	U	5	3.66E-02	2.14	0.96
IF4A1	U	5	3.68E-02		
OXSR1	U	5	3.69E-02		
F213A	C	5	3.76E-02	-1.77	0.89
CLIC4	U	5	3.82E-02	-1.06	0.50
VDAC1	U	5	3.87E-02	-2.28	0.96
CAN2	U	5	3.95E-02	1.06	0.54
NDRG3	U	5	4.06E-02		
CLH1	U	5	4.11E-02	-0.56	0.88
LAMB2	C	4	4.21E-02	1.09	0.76
FINC	C	5	4.27E-02	2.97	0.84
TS101	U	4	4.31E-02		
DPYL3	U	5	4.39E-02	2.18	0.67
ISG15	U	5	4.53E-02	1.39	0.84
DRG2	U	5	4.71E-02	2.02	0.38
RN213	U	4	4.73E-02		
BAX	U	5	4.73E-02	0.97	0.69
ADH1	C	5	4.74E-02	-0.64	0.44
SPTN1	C	5	5.25E-02	-0.89	0.88
EF1A1	U	5	5.34E-02	-0.32	0.35

S.3 SUPPLEMENTARY DATA FOR CHAPTER V

S.3.1 Characterization of stable EGFP-TG2 overexpressing clones employed in this study

In some experiments, a stable cell line of NRK52E clones overexpressing EGFP-tagged TG2 was employed (referred as EGFP-TG2 overexpressing clones or EGFP-TG2 clones). These clones were produced in Dr Verderio laboratory (NTU) by former research assistant Raghavendran Ramaswamy, by stably transfecting NRK52E cells with a specific pEGFP-N1-TG2 plasmid (**Appendix, Fig. II**), expressing a human TG2 cDNA chimeric protein with a C-terminal EGFP tag of 100 kDa size, with green fluorescence.

These clones have already been fully characterized in Dr Verderio laboratory (NTU) and Prof Johnson laboratory (University of Sheffield) for a study of TG2 trafficking: they express an elevated level of exogenous EGFP-TG2 chimera antigen and transamidation activity, and they show a high TG2 export with a reaction to fibrotic stimuli that is comparable with the wild type (WT) cells (Huang et. al, unpublished). For the aims of this thesis, characterisation of TG2 expression and activity was repeated in the clones employed to confirm the preservation of their characteristics.

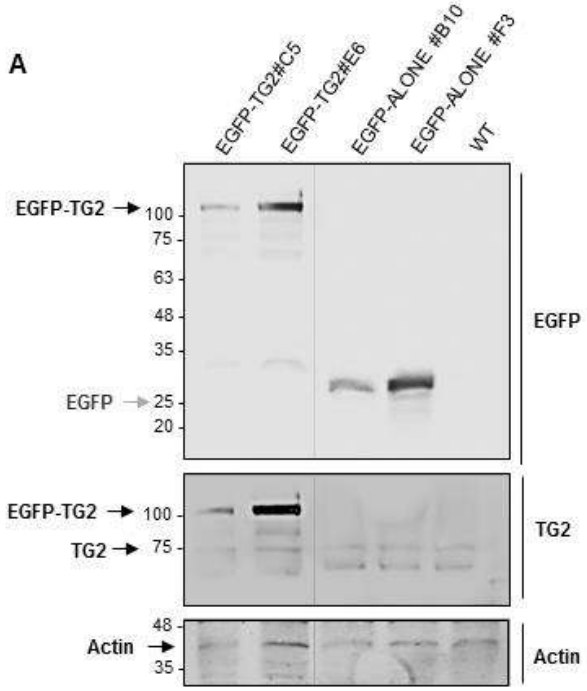

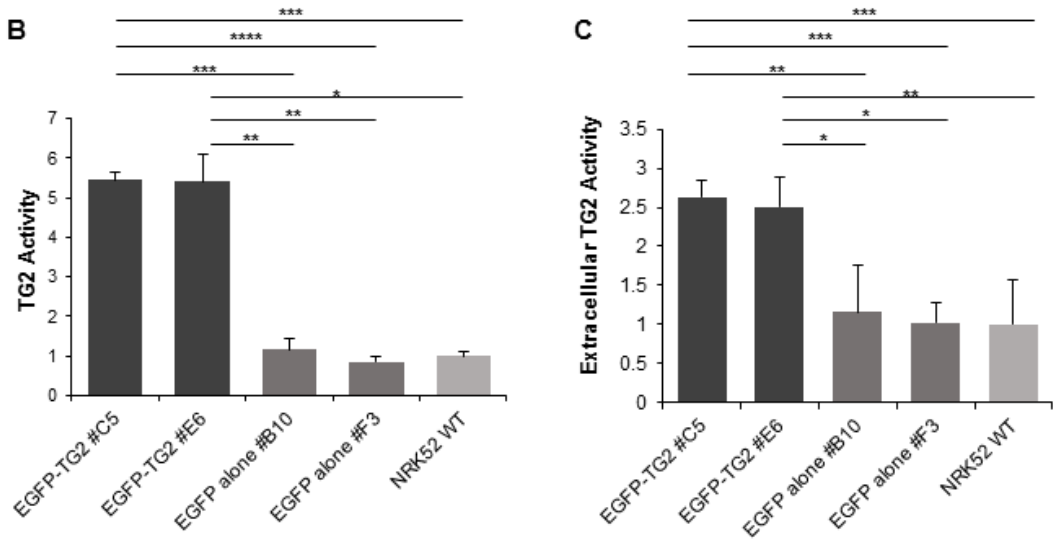

Supplementary Figure 5.1: Characterisation of EGFP-TG2 overexpressing clones employed in this thesis. Stable EGFP-TG2 overexpressing clones #C5 and #E6, together with stable clones expressing EGFP alone (#B10 and #F3) and NRK52E WT cells, were cultured as described in the general methods [2.2.1.2]. To maintain selection on stable clones, 700 µg/ml G418 (Geneticin) were added to the medium **(A)** Equal amounts of total protein lysates were separated by 12% (w/v) acrylamide/bis-acrylamide SDS PAGE and the expression of TG2 and EGFP were analysed by Western blot using a rabbit polyclonal anti-TG2 antibody (ab80563, Abcam, dilution 1:1000) or an anti-EGFP antibody (ab290, Abcam, dilution 1:2500). Actin (A2066, Sigma) was employed as a loading control. Immunoreactive bands were detected by enhanced chemiluminescence after incubation with appropriate donkey anti-rabbit IgG HRP-conjugated secondary antibody in blocking buffer. **(B)** Total TG2 was measured by biotin-cadaverine incorporation assay performed on equal amounts of total cell lysate (60 µg) in triplicates as described in 2.2.8.1, and TG2 activity was detected through the enzyme's ability of incorporating biotin-cadaverine into fibronectin for 2 h. The values are the average Abs (450 nm) of three independent experiments, each undertaken in triplicates, normalised for the WT control (equalised to 1) ± SD. **(C)** Extracellular TG2 was measured by biotin-cadaverine incorporation assay performed on 20,000 cells/well for 2 h as described in 2.2.8.2. Values are the average Abs (450 nm) of three or six independent experiments, each undertaken in triplicates, normalised for the WT control (equalised to 1) ±SD. Significance of the differences between treatments was determined by T-test: * = $p<0.05$, ** = $p<0.01$, *** = $p<0.001$, **** = $p<0.0001$.

S.3.2 Optimisation of the experimental conditions

S.3.2.1 Optimal number of cells for LDH cytotoxicity assay

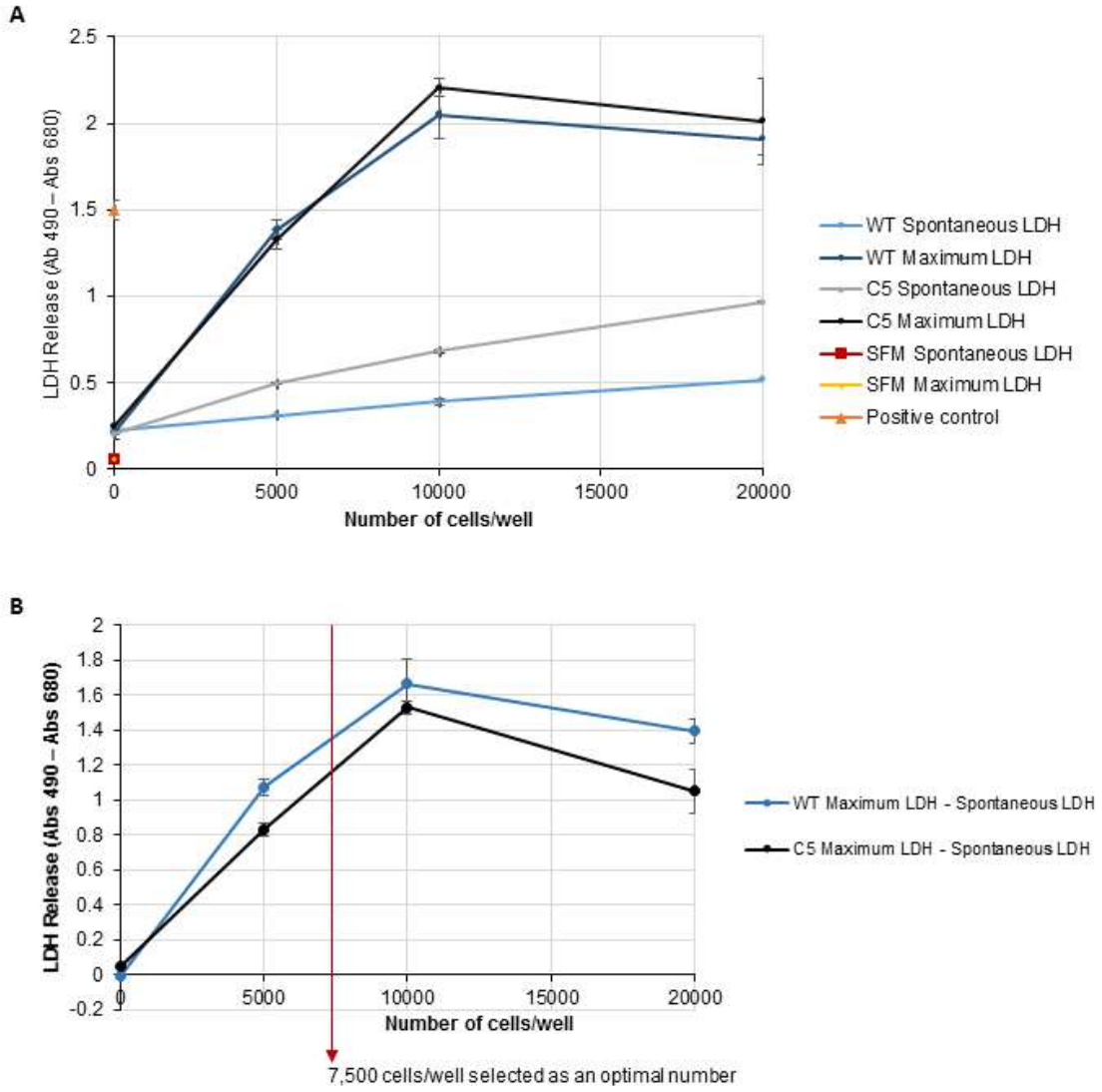

Supplementary Figure 5.2: Optimal number of cells/well for LDH cytotoxicity assay performed in a 96-well plate. In order to determine the optimal number of cells to employ using Pierce™ LDH cytotoxicity assay kit (Thermo Scientific), a serial dilution (0; 5,000; 10,000 and 20,000 cells/well) of NRK52E cells (WT) and EGFP-TG2 overexpressing clone #C5 (C5) was seeded in a 96 well plate and cultured overnight (15 h). The day after medium was collected, or cells were lysed before medium collection following the manufacturer's guidelines. Spontaneous and maximum LDH release in the medium was measured following the manufacturer's protocol as described in 2.2.1.7. **(A)** Spontaneous and maximum LDH release was measured as Abs 490 nm – Abs 680 nm in both cell lines (WT and C5) at different concentration as well as in cell free serum free medium (SFM). A positive control provided by the kit was included. Data represent mean LDH release calculated as mean Abs 490 nm- mean Abs 680 nm of three replicas, ±SD. **(B)** From the results, maximum LDH release – spontaneous LDH release ±SD was calculated for each initial cell concentration, and the optimal number of cells to employ for cytotoxicity assay was selected within the area of linear growth. 7,500 cells/well was chosen for the subsequent experiments.

S.3.2.2 Optimisation of conditions for extracellular TG2 activity assay

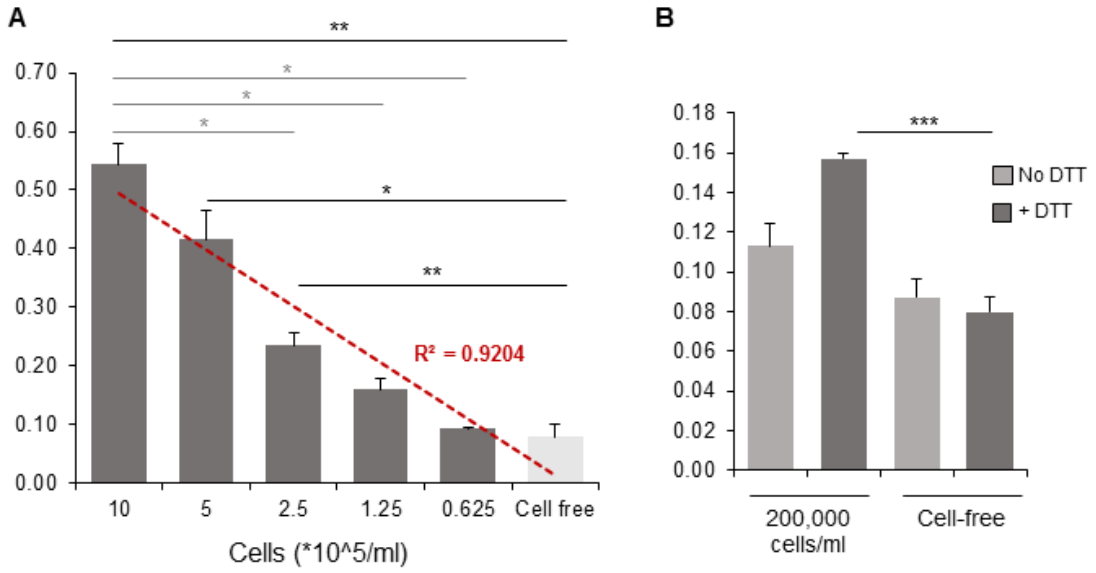

Supplementary Figure 5.3: Optimisation of extracellular TG2 activity assay in NRK52E WT cells. NRK52E WT cells were cultured in T75 flask until 80% confluent and detached with a trypsin-free buffer [5 mM EDTA in sterile PBS pH7.4] in gentle shaking at 37°C. **(A)** Extracellular TG2 activity was measured through the enzyme's ability of incorporating biotin cadaverine in fibronectin by 6,250 - 100,000 living cells/well (= 62,500 – 1 million living cells/ml) for 2 h as described in the general methods [2.2.9.2]. A number of 20,000 cells/well was chosen for the subsequent experiments **(B)** Extracellular TG2 activity was measured with the same method on 20,000 living cells/well for 2 h in presence or absence of DTT as reducing agent. Values are the average Abs (450 nm) of three replicas, normalised for the relative mock transfected control (equalised to 1) ± SD. Significance of the differences between treatments was determined by T-test: * = $p<0.05$, ** = $p<0.01$, *** = $p<0.001$, **** = $p<0.0001$.

S.3.3 Supplementary data for extracellular EGFP-TG2 immunofluorescent staining

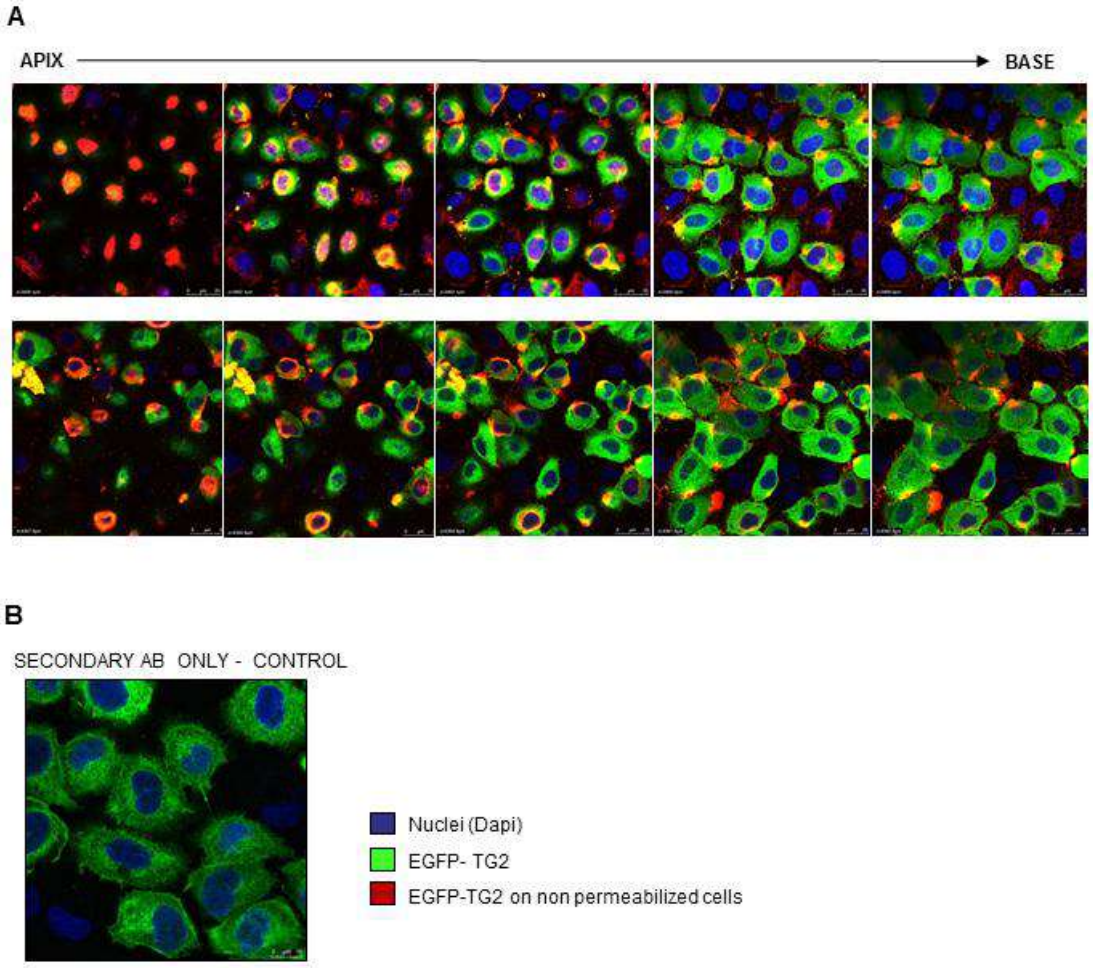

Supplementary Figure 5.4: Support data to the extracellular EGFP-TG2 immunofluorescent staining. (A) EGFP-TG2 overexpressing NRK52E cells were grown in an 8 well chamber slide until 80% confluent, then medium was replaced with complete medium ± 10 ng/ml TGF-β1 for 16 h. Extracellular EGFP-TG2 chimera was detected on fixed (3%PFA) but not permeabilised cells using a rabbit polyclonal anti-GFP antibody (Abcam) followed by a donkey anti-rabbit Alexa Fluor® 568 antibody, with red fluorescence. Nuclei were stained with DAPI. Specimens (20 µm) where scanned by confocal microscopy every µm. Pictures are showing the staining of EGFP-TG2 from the apex to the basal level. **(B)** As a control, rabbit polyclonal anti-GFP antibody (Abcam) was omitted from the experiment, and fixed (3%PFA) but not permeabilised cells were incubated with only donkey anti-rabbit Alexa Fluor® 568 antibody, with red fluorescence. Absence of the red signal after washing confirmed the specificity of the red staining observed in the experiments.

S.4 SUPPLEMENTARY DATA FOR CHAPTER VI

S.4.1 Quality of the plasmid employed

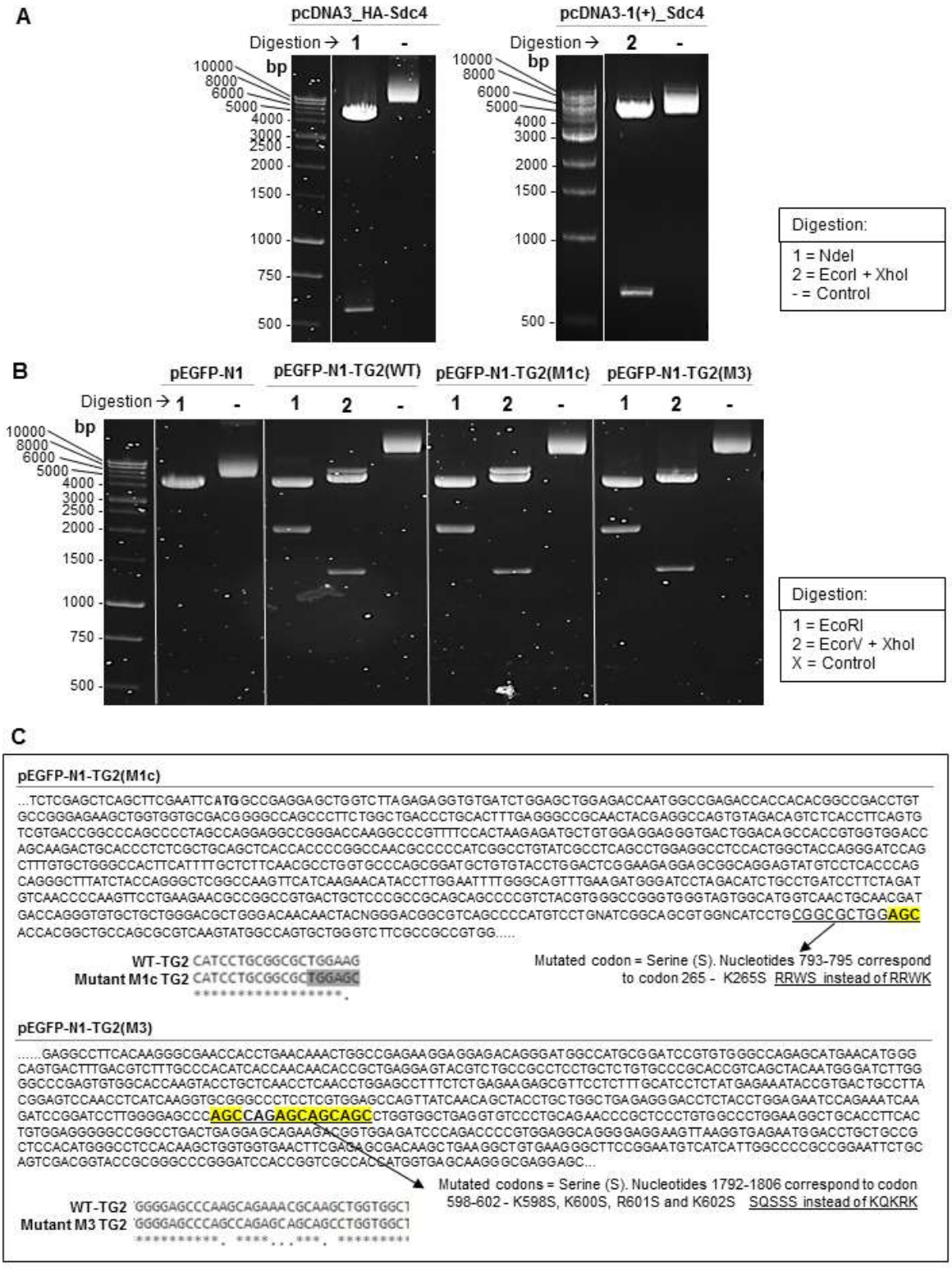

Supplementary Figure 6.1: Quality control of mammalian expression vectors employed for transient transfection of rat TECs. (A) Restriction digestion of 1 µg pcDNA3_HA-Sdc4 and pcDNA3.1(+)Sdc4 purified plasmids following the general protocol reported in chapter II. pcDNA3_HA-Sdc4 plasmid was digested using NdeI restriction enzyme (Promega) for 2 h at 37°C. pcDNA3 empty vector has only one restriction site for NdeI (cuts at 487-88); insertion of HA-Sdc4 the correct orientation introduces another NdeI restriction site, present on the N-terminal HA-tag (**Appendix Fig. I**), resulting band at 5527 bp and a lower band at 522 bp. As pcDNA3 empty vector has only one restriction site for NdeI (cuts at 487-88), insertion of HA-Sdc4 with the right orientation introduces another NdeI site, present on the HA-tag, resulting in two bands at 522 bp and 5527 bp upon digestion. pcDNA3.1(+)Sdc4 plasmid was digested using EcoRI and XhoI restriction enzymes (corresponding to cloning sites for Sdc4 cDNA, see Suppl. Figure 1B) for 2 h at 37°C. Expected bands are 5428 bp and 630 bp. In both cases, the uncut plasmid was used as a control. The picture shows the product of the restriction digestion, separated by electrophoresis on 1.5% (w/v) agarose gel. For both plasmids, band comparison with standard DNA of known size (1Kb standard ladder, Promega) confirmed the presence of the insert and its right orientation. pcDNA3_HA-Sdc4 and pcDNA3.1(+)Sdc4 plasmids were produced by Dr Izhar Burhan and Dr Alessandra Scarpellini, respectively, starting from Sdc4cDNA and HA-Sdc4 cDNA provided by Dr Mark Bass (The University of Sheffield). **(B)** Restriction digestion of pEGFP-N1 empty plasmid and pEGFP-N1-TG2 (WT or Heparin binding mutants) plasmids: 1 µg of purified plasmid was digested using restriction enzyme EcoRI or the combination of EcoRV and XhoI. EcoRI restriction site is the cloning site of the plasmid used for the introduction of the insert, digestion with this enzyme was used to confirm the presence of the insert, producing expected bands of 4733 bp (plasmid) and 2068 bp (TG2 cDNA insert)(**Appendix Fig.II**). Digestion with EcoRV and XhoI is instead used confirm the correct orientation of TG2 with EGFP. If the orientation is right the expected bands are 5456 bp and 1345 bp. In all cases, the uncut plasmid was employed as a control. The picture shows the product of the restriction digestion, separated by electrophoresis on 1.5% (w/v) agarose gel. For all plasmids, band comparison with standard DNA of known size (1Kb standard ladder, Promega) confirmed the presence of the insert and its right orientation. **(C)** Confirmation of the heparin binding site mutation in pEGFP-N1-EGFP-TG2(M1c) and pEGFP-N1-EGFP-TG2(M3) plasmids was performed by sequence alignment with wild-type full length TG2 cDNA: 100 ng/ul purified plasmids in 10 mM Tris HCl pH 8.5 were sequenced by Source Bioscience Sequencing (Nottingham UK). Sequencing results were aligned to wild type full length TG2 cDNA on ClustalW2 (EMBL-EBI) bioinformatics source.

S.4.2 Quality control and optimisation of transfections and treatments

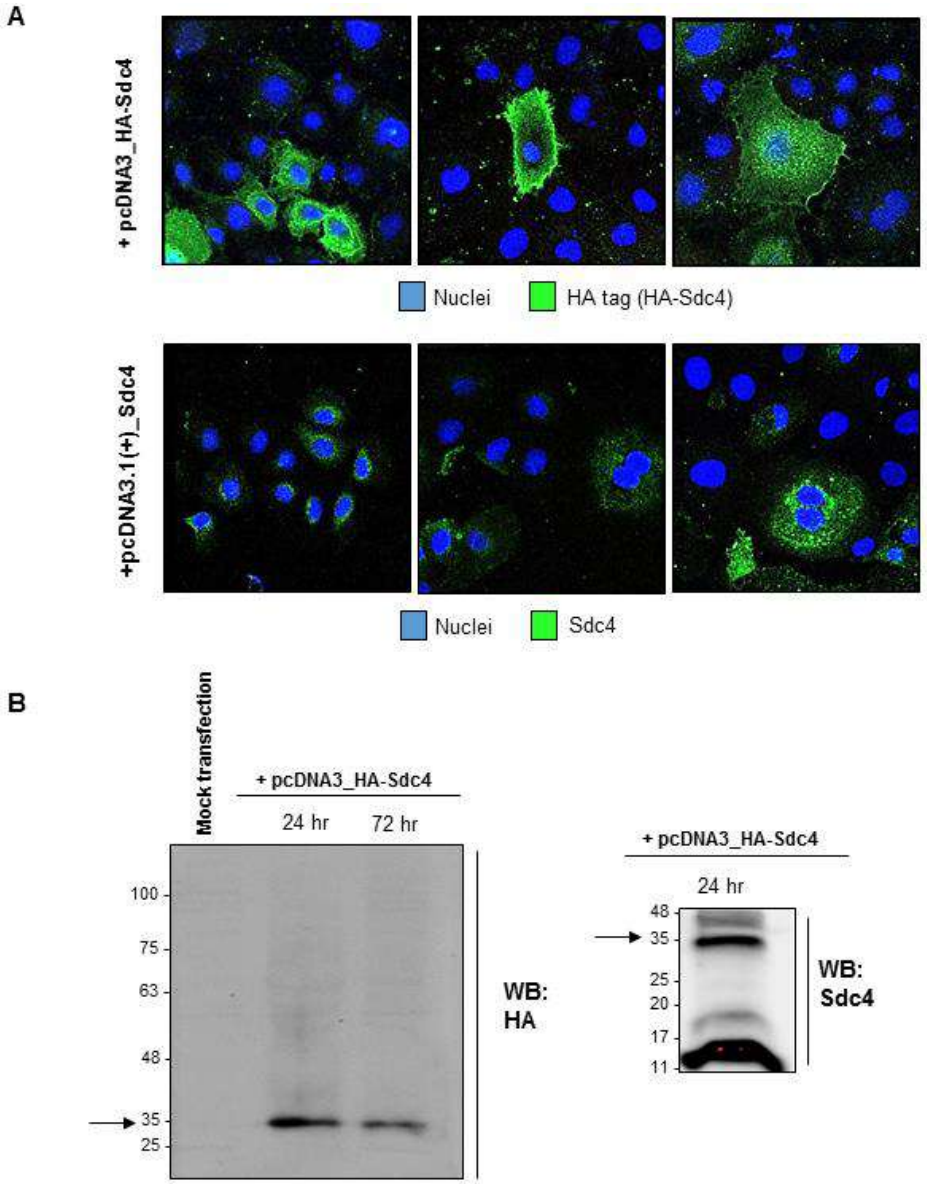

Supplementary Figure 6.2: Expression of HA-Tag and Sdc4 in NRK52E cells transfected with pcDNA3_HA-Sdc4 or pcDNA3.1(+)_Sdc4. (A) 1 million NRK52E WT cells were transfected by electroporation using 5 µg of either pcDNA3_HA-Sdc4 for 24 or 72 h. Mock transfected cells (24 h) were used as a control. Equal amounts of cell lysates (10 µg) were separated by 10% SDS-PAGE and immunoprobed with rabbit polyclonal anti-HA (Cell Technologies, dilution 1:1000) followed by Goat anti Rabbit IgG conjugated to HRP (Dako, dilution 1:2500). The immunoreactive bands were visualised by chemiluminescence after addition of ECL reagent (Biological Industries). 20 µg of proteins from the 24 h transfected lysate were also screened for the expression of Sdc4 using a rabbit polyclonal anti-Sdc4 antibody followed by goat anti-rabbit IgG conjugated to HRP. Image acquisition was performed with a LAS4000 imaging system (GE Heathcare). A representative blot is shown. **(B)** 200,000 NRK52E WT cells were transfected by electroporation with human Sdc4 cDNA using 5 µg of either pcDNA3_HA-Sdc4 or pcDNA3.1(+)_Sdc4 plasmid and seeded in an 8-well chamber slide. 48 h after transfection, cells were fixed (3%PFA/10 min) and immunostained with either a rabbit polyclonal anti-HA (C29F4, Cell Signalling Technology– dilution 1:500) in case of pcDNA3_HA-Sdc4 – transfected cells, or a rabbit polyclonal anti Sdc4 antibody (ab24511, Abcam -dilution 1:50) in case of pcDNA3.1(+)_Sdc4 – transfected cells. Both antibodies were followed by a donkey anti-rabbit IgG H&L Alexa Fluor® 488 antibody (dilution 1:1000), with green fluorescence, to detect cell surface HA-Sdc4 or cell surface Sdc4. Specimens (20 µm) where scanned by confocal microscopy every µm, and each picture combines all the 20 levels observed. Representative pictures at 100X magnification are showed.

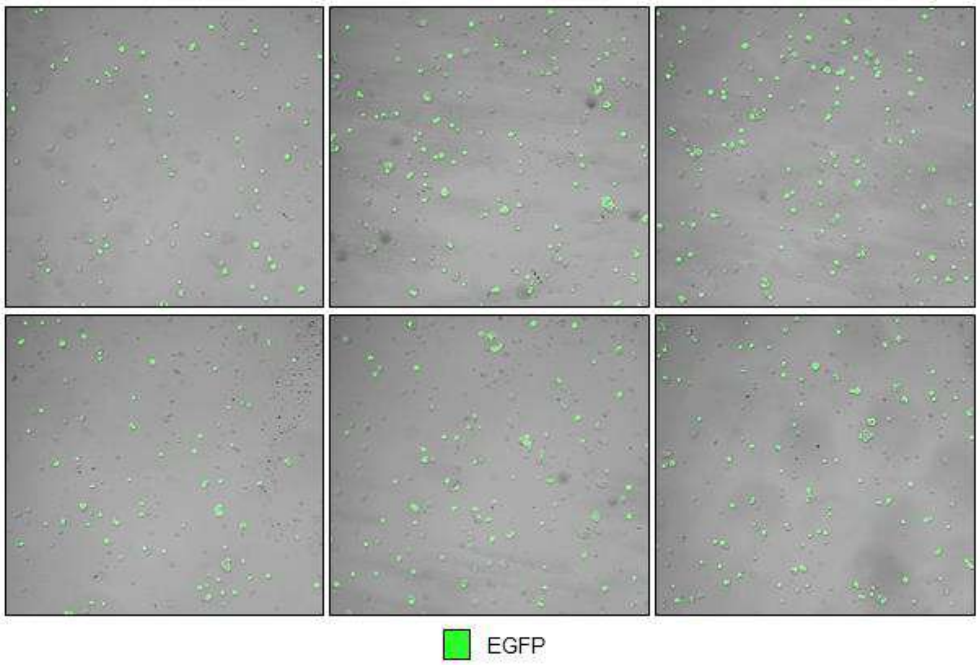

Supplementary Figure 6.3: Efficiency of NRK52E transfections. 1 million NRK52E WT cells were transfected by electroporation with 5 µg of pEGFP-N1 plasmid and seeded in a 6-well plate. 48 h after transfection, cells were detached, and ~20 µl of suspension was placed on a glass slide for direct observation by confocal microscopy. Specimens at 10X magnification were collected and transfection efficiency calculated as number of EGFP-expressing cells (green) over the total number of cells observed under bright light (bright field). Transfection efficiency was calculated as being typically between 60 and 80%

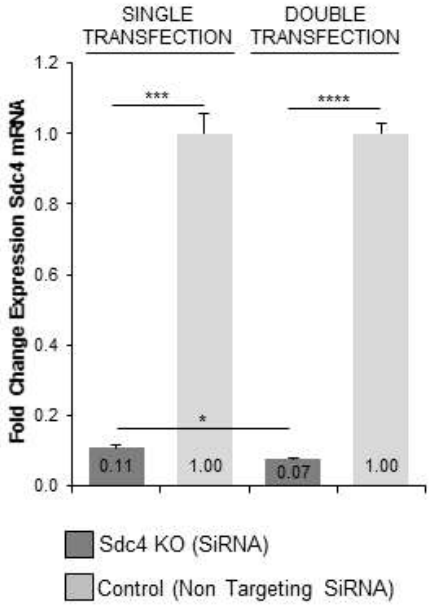

Supplementary Figure 6.4: Verification of an adequate knock down of Sdc4 from NRK52E cells by siRNA transfection. NRK52E WT cells were transfected once (single transfection for 24 h) or twice (double transfection for 24 h each) with 100 nM Rat Sdc4 – targeting siRNA as described in 6.3.4. The same cells transfected with 100 nM non-targeting scrambled siRNA were used as control. The relative expression of Sdc4 mRNA was measured by qRT-PCR (Table 4) by $2^{-\Delta\Delta Ct}$ relative quantification method (CyclophilinA was employed as housekeeping gene). The experiment was performed in triplicates. Significance of the differences between treatments was determined by T-test: * = $p<0.05$, ** = $p<0.01$, *** = $p<0.001$, **** = $p<0.0001$.

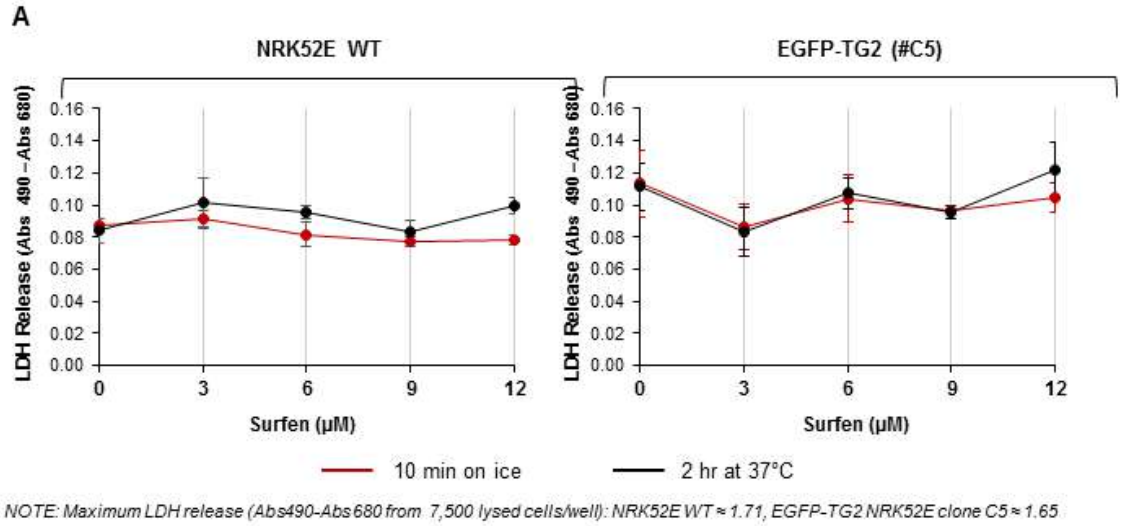

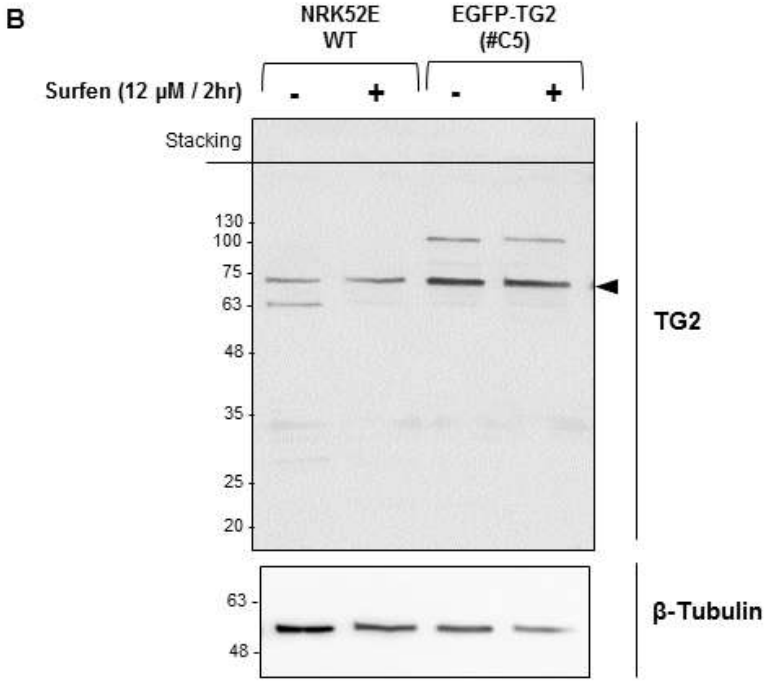

Supplementary Figure 6.5: Analysis of Surfen effect on cell permeability/leakage and TG2 expression. NRK52E WT and EGFP-TG2 overexpressing (clones #C5) cells were cultured in normal conditions until 80% confluent. At this stage, cells were incubated with 3 - 12 μM Surfen in serum free medium for 2 h at 37°C or for 10 min on ice. Incubation with serum free medium only was employed as a control. **(A)** After incubation, cell permeability was measured by LDH assay as described in the general methods (Chapter II). Data are presented as spontaneous LDH release (Abs 490 nm – Abs 680 nm) at each concentration for each cell line ± SD. Significance of the differences between treatments was determined by T-test: * = $p<0.05$, ** = $p<0.01$, *** = $p<0.001$, **** = $p<0.0001$. **(B)** After incubation with 12 μM Surfen in serum free medium for 2 h at 37°C, equal amounts of protein lysate (35 μg) were separated by 10% SDS PAGE and immunoprobed with a rabbit polyclonal anti-TG2 antibody (ab80563, Abcam, dilution 1:1000) as well as with a rabbit polyclonal anti-β-tubulin antibody (ab6046 Abcam, dilution 1:5000), as a loading control. Immunoreactive bands were detected by enhanced chemiluminescence as described in the general methods after incubation with appropriate goat anti-rabbit IgG HRP-conjugated secondary antibody (dilution 1:2000, Dako) in blocking buffer. Image acquisition was performed with a LAS4000 imaging system (GE Healthcare). Molecular weight of human TG2 immunoreactive bands is ~75kDa (arrowhead).

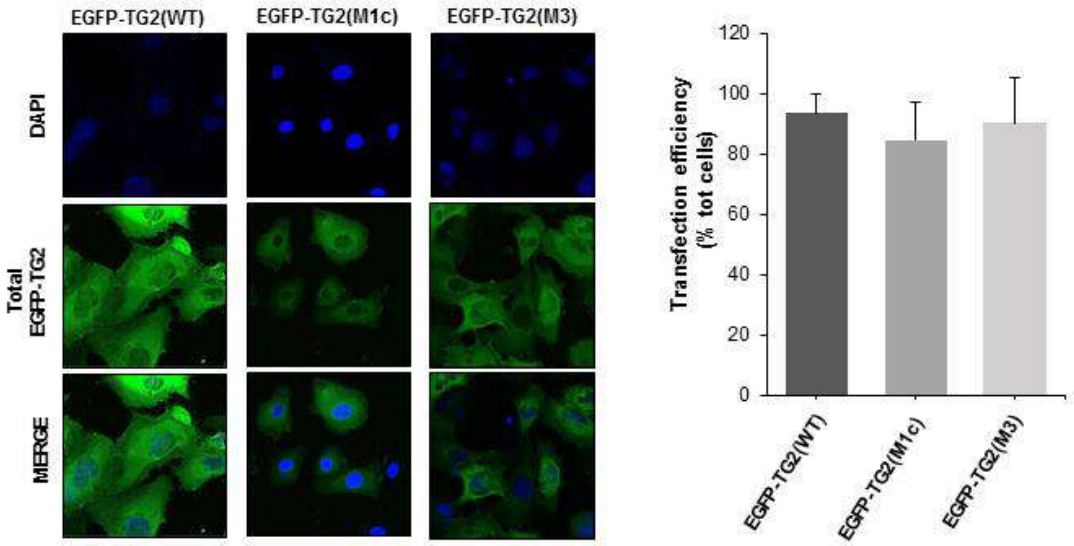

Supplementary Figure 6.6: Efficiency of NRK52E TECs transfection with heparin binding mutant TG2 cDNA by employment of pEGFP-N1 plasmids. **(A)** 200,000 NRK52E WT cells were transiently transfected by electroporation with 5 μg of pEGFP-N1 plasmid containing either TG2(WT), TG2(M1c) and TG2(M3) as described in 6.3.3.2, and seeded in an 8-well chamber slide for 48 h. Cells were fixed (3%PFA) and nuclei were stained with DAPI. Representative pictures at 100X magnification are here shown. Transfection efficiency was quantified by direct count of EGFP-expressing cells (green) over the total number of cells (blue nuclei), and presented as mean percentage of transfected cells over the total cell number (on 8 non-overlapping images per section) ± SD, expressed relative to the TG2(WT) transfected cells (equalised to 1). Significance of the differences between transfections was determined by T-test: * = $p<0.05$, ** = $p<0.01$, *** = $p<0.001$, **** = $p<0.0001$.

Appendix

A.1 THE KNOWN PARTNERS OF TRANSGLUTAMINASE 2

Table I: List known and reported partners of transglutaminase-2. According to TransDab database (Csősz, Meskó and Fésüs 2009)

TG2 partner	Type of interaction
26S proteasome non-ATPase regulatory subunit 4	BINDING
40S ribosomial protein SA	SUBSTRATE
72 kDa type IV collagenase	BINDING
Abr (Active breakpoint cluster region-related protein)	BINDING
Acidic proline rich protein	SUBSTRATE
Aconitase	SUBSTRATE
ACTH (Adrenocorticotropic hormone)	SUBSTRATE
Actin	SUBSTRATE
Adhesion G-protein coupled receptor G1	BINDING
Adipocyte plasma membrane-assoiated protein	BINDING
ADP/ATP translocase 1	SUBSTRATE
A-kinase anchor protein 13	BINDING
Aldolase A	SUBSTRATE
Alpha lactalbumin	SUBSTRATE
Alpha synuclein	SUBSTRATE
Alpha-1B adrenergic receptor	BINDING
Alpha-2 macroglobulin receptor	SUBSTRATE
Alpha-2 plasmin inhibitor	SUBSTRATE
Alpha-2-HS-glycoprotein	SUBSTRATE
Alpha-gliadin	BINDING
Alpha-ketoglutarate dehydrogenase	SUBSTRATE
Amyloid beta A4 peptide	SUBSTRATE
Androgen receptor	SUBSTRATE
Angiocidin	SUBSTRATE
Ankyrin	SUBSTRATE
Annexin I	SUBSTRATE
Antileukoproteinase	SUBSTRATE
Arginase I	SUBSTRATE
Ataxin – 1	SUBSTRATE
ATP synthase	SUBSTRATE
AT-rich interactive domain-containing protein 1A	SUBSTRATE
Band 3 anion transport protein	SUBSTRATE
Band 4.1 protein	SUBSTRATE
BAX	BINDING
Bcl-2 homologous antagonist/killer	BINDING
Bcr (Breakpoint cluster region protein)	BINDING
Bcr (Breakpoint cluster region protein)	SUBSTRATE
Beta casein	SUBSTRATE
Beta endorphin	SUBSTRATE
Beta lactoglobulin	SUBSTRATE
Beta tubulin	BINDING
Beta tubulin	SUBSTRATE
Beta-2-microglobulin	SUBSTRATE
Betaine-homocysteine S-methyltransferase	SUBSTRATE
BiP protein	SUBSTRATE
Bone sialoprotein	SUBSTRATE

C1 inhibitor	SUBSTRATE
C-1-tetrahydrofolate synthase	BINDING
Calbindin	SUBSTRATE
Calmodulin	BINDING
Calnexin	BINDING
Calpain	SUBSTRATE
Calreticulin	BINDING
Carboxypeptidase B2	SUBSTRATE
Caspase-3	SUBSTRATE
Cathepsin D	SUBSTRATE
C-CAM	SUBSTRATE
CD166 antigen/Activated leukocyte cell adhesion molecule	BINDING
CD38	SUBSTRATE
CD44 antigen	BINDING
CD98 antigen/4F2 cell-surface antigen heavy chain	BINDING
Clathrin heavy chain	SUBSTRATE
Coatomer	BINDING
Collagen	SUBSTRATE
Collagen alpha-1 (XVIII)	BINDING
Complement C3	SUBSTRATE
Crystallin	SUBSTRATE
Cyclic Thymosin beta 4	SUBSTRATE
Cytochrome C	SUBSTRATE
Deoxyribonuclease γ	SUBSTRATE
Dihydropyrimidinase-like 2 protein	SUBSTRATE
Dual leucine zipper-bearing kinase (DLK)	SUBSTRATE
E3 SUMO-protein ligase PIAS4	BINDING
EGF Receptor	SUBSTRATE
Elafin	SUBSTRATE
Elongation factor 1α	SUBSTRATE
Elongation factor 1γ	SUBSTRATE
Endostatin	BINDING
Enolase	SUBSTRATE
Envelope glycoprotein gp120	SUBSTRATE
Envelope glycoprotein gp41	SUBSTRATE
Ephrin A	SUBSTRATE
Epithelial-cadherin precursor	BINDING
Eucaryotic initiation factor 4F (eIF-4F)	SUBSTRATE
Eukaryotic translation initiation factor 5A-1	BINDING
Exendin 4	SUBSTRATE
Ezrin-Radixin-Moesin binding phosphoprotein 50	SUBSTRATE
Fatty acid synthase	SUBSTRATE
F-box only protein	SUBSTRATE
Fibrillin-1	SUBSTRATE
Fibrinogen alpha chain	SUBSTRATE
Fibrinogen gamma chain	SUBSTRATE
Fibronectin	BINDING
Fibronectin	SUBSTRATE
Filamin 1	SUBSTRATE
Fructose 1,6-bisphosphatase	SUBSTRATE
Galectin 3	SUBSTRATE
Gliadin	DEAMIDASE
Gliadin	SUBSTRATE
Gliadoralin A	SUBSTRATE
Glucagon	SUBSTRATE
Glutathione S-transferase	SUBSTRATE
Glutathione S-transferase P	BINDING
Glyceraldehyde-3-phosphate dehydrogenase	SUBSTRATE
Glycogen debranching enzyme	BINDING
Hepatitis C virus core protein	SUBSTRATE

Histamine	SUBSTRATE
Histatin	SUBSTRATE
Histone H1	KINASE
Histone H1	SUBSTRATE
Histone H2B type 1-C/E/F/G/I	BINDING
Histone H2B type 1-C/E/F/G/I	SUBSTRATE
Histone H3.1	BINDING
Histone octamer	KINASE
Histone octamer	SUBSTRATE
HIV-1 aspartyl protease	SUBSTRATE
Hsp 27	SUBSTRATE
Hsp27	BINDING
Hsp60	SUBSTRATE
Hsp70	SUBSTRATE
Hsp70/90 organizing protein	SUBSTRATE
Hsp90	SUBSTRATE
Human Clara-cell 10kDa protein	SUBSTRATE
Huntingtin	SUBSTRATE
Hyphal wall protein–1	SUBSTRATE
Hypoxia inducible factor 1	BINDING
Ig kappa chain C region	SUBSTRATE
Importin alpha3	BINDING
Importin β1 subunit	SUBSTRATE
Insulin	SUBSTRATE
Insulin-like growth factor-binding protein-1	SUBSTRATE
Insulin-like growth factor-binding protein-3	KINASE
Insulin-like growth factor-binding protein-3	SUBSTRATE
Insulin-like growth factor-binding protein-5	KINASE
Integrin beta subunit	BINDING
Integrin beta3	BINDING
Inter-alpha-inhibitor	SUBSTRATE
Intergrin alpha subunit	BINDING
Lamin A, C	SUBSTRATE
Latent transforming growth factor beta binding protein 1	SUBSTRATE
Lipoprotein A	SUBSTRATE
Long-chain-fatty-acid-CoA ligase	BINDING
Low-density lipoprotein receptor-related protein 5	BINDING
Low-density lipoprotein receptor-related protein 6	SUBSTRATE
Low-density lipoprotein receptor-related protein 6	BINDING
Major vault protein	BINDING
Melittin	SUBSTRATE
Membrane-associated progesterone receptor component 2	BINDING
Microfibril-associated glycoprotein (MAGP)	SUBSTRATE
Midkine	SUBSTRATE
Myelin basic protein	SUBSTRATE
Myoferlin	BINDING
Myosin	SUBSTRATE
NADH-cytochrome b5 reductase 3	BINDING
Neurofilament proteins	SUBSTRATE
Neuropeptide Y	SUBSTRATE
Neutral alpha-glucosidase	BINDING
NF-kappa-B inhibitor alpha	SUBSTRATE
Nidogen	SUBSTRATE
Nuclease sensitive element binding protein-1	SUBSTRATE
Nucleophosmin	SUBSTRATE
Orexin B	SUBSTRATE
Osteonectin	SUBSTRATE
Osteopontin	SUBSTRATE
Oxysterol-binding protein	BINDING
Oxytocin receptor	BINDING

Parkin	SUBSTRATE
Periphilin	SUBSTRATE
Periplakin	SUBSTRATE
Peroxiredoxin-1	BINDING
Phosphoglycerate dehydrogenase	SUBSTRATE
Phospholipase A2	SUBSTRATE
Phospholipase C delta1	BINDING
Phosphorylase kinase	SUBSTRATE
Plasminogen	SUBSTRATE
Plasminogen activator inhibitor-2	SUBSTRATE
Plasmodium falciparum liver stage antigen-1	SUBSTRATE
Platelet-derived growth factor receptor beta	BINDING
Procarboxypeptidase B/U	SUBSTRATE
Prohibitin	SUBSTRATE
Prolow-density lipoprotein receptor-related protein 1	BINDING
Protein kinase A anchoring protein 13	BINDING
Protein kinase C delta type	SUBSTRATE
Protein S100-A4	BINDING
Protein synthesis initiation factor 5A	SUBSTRATE
Proto-oncogene tyrosine-protein kinase Src	BINDING
PTEN (Phosphatase and tensin homolog)	BINDING
RAP - Alpha-2 macroglobulin related protein	SUBSTRATE
Ras GTPase-activating-like protein	BINDING
Ras-related C3 botulinum toxin substrate 1	BINDING
Retinoblastoma protein	KINASE
Retinoblastoma protein	SUBSTRATE
Retinoblastoma-associated protein	BINDING
Rho associated, coiled coil, containing protein kinase 2	SUBSTRATE
RhoA	DEAMIDASE
RhoA	SUBSTRATE
S100A10	SUBSTRATE
S100A11	SUBSTRATE
S100A7	SUBSTRATE
Seminal vesicle secretory protein IV	SUBSTRATE
Ser/Thr protein phosphatase 2A	BINDING
Serotonin	SUBSTRATE
Single-stranded DNA-bindig protein	BINDING
Small ubiquitin-related modifier 1	BINDING
SNAP-25	SUBSTRATE
SP1 transcription factor	SUBSTRATE
Spectrin	SUBSTRATE
Statherin	SUBSTRATE
Substance P	SUBSTRATE
Suprabasin	SUBSTRATE
Synapsin 1	SUBSTRATE
Synapsin I	SUBSTRATE
Syndecan-4	BINDING
Talin	BINDING
Tau protein	SUBSTRATE
T-complex protein 1ε subunit	SUBSTRATE
Thromboxane A2 receptor	BINDING
Thymosin beta 4	SUBSTRATE
Thyroglobulin	SUBSTRATE
Transcription factor AP-1	BINDING
Transcription factor p65	BINDING
Transferrin receptor	BINDING
Troponin	SUBSTRATE
Tubulin alpha	BINDING
Tubulin beta-1 chain	BINDING
Tumor protein D54	BINDING

Tumor rejection antigen-1	SUBSTRATE
Ubiquitin	SUBSTRATE
UDP-glucose:glycoprotein glucosyltransferase 1	BINDING
Uteroglobin	SUBSTRATE
UV excision repair protein RAD23 homolog B	SUBSTRATE
Valosin	SUBSTRATE
Vasoactive intestinal peptide	SUBSTRATE
VEGFR-2	SUBSTRATE
Very long-chain specific acyl-CoA dehydrogenase	BINDING
Vigilin	SUBSTRATE
Vimentin	SUBSTRATE
Vinculin	BINDING
Vitronectin	SUBSTRATE
Y-box binding protein	SUBSTRATE
Zyxin	BINDING

Table II: List of binding partners for transglutaminase-2. Adapted from (Kanchan, Fuxreiter and Fésüs 2015)

Name of the protein	Site of interaction	Proposed function
Fibronectin	ECM, plasma	Cell adhesion and migration
Integrins b1 and b3	Membrane	
Syndecan-4	Membrane, ECM	
PDGFR	Membrane	
LRP5 and LRP6	Transmembrane	Wnt/b catenin signalling pathway
LRP1	Membrane	Cell adhesion, migration, receptor mediated signalling
ACAP 13	Perinuclear, cytoplasmic areas	Involved in Rho mediated change in cell polarity, potentiates interaction between PKA and TG2
PTEN (tumor suppressor phosphatase)	Cytoplasm	Regulation of cell survival signalling
HSP 70	Membrane	Cell migration by targeting TG2 to cell surface
Endostatin	ECM	Regulation of angiogenesis and tumour growth
BCR and ABR Q12979	Cytoplasm	Cytoskeleton rearrangement through Rac activation
GPR56	ECM	Tumour progression
MMP2	ECM	Regulation of matrix composition and migration / invasion of malignant cells
Angiocidin	Cytoplasm	Regulates cell migration and adhesion by inhibiting FN incorporation to ECM
a1 adrenoceptor	Membrane	Regulates intracellular calcium signalling
PLC d1	Cytoplasm	
Oxytocin receptor	Membrane	Intracellular calcium mobilization and muscle contraction
Thromboxane receptor	Membrane	Transmembrane signalling
Calreticulin	Cytoplasm	Down-regulate both TG and GTPase activities of TG2
Importin a3	Cytoplasm, nucleus	Active transport of TG2 into the nucleus
Eukaryotic initiation factor (eIF5A)	Nucleus, cytoplasm	TGs influence the cellular localization of eIF-5A
c-Jun	Nucleus	ECM regulation and turnover
cSrc	Membrane	Cell–matrix interactions and Wnt signalling
Hypoxia-inducible factor (HIF1b)	Cytoplasm, nucleus	Protective role in the brain during its response to ischemia and stroke
Reitnoblastoma	Nucleus, cytoplasm	Transcriptional regulation
SUMO 1 (small ubiquitin-like modifier)	Nasal epithelium	Regulating oxidative stress and inflammation
PIASy (SUMO 1 ligase)	Nasal epithelium	
RAC1	Cytoplasm, membrane	Regulates allergic inflammation
Tubulin b1	Nucleus	Regulates intracellular calcium signalling
Calmodulin	Nucleus	Regulation of TG2-mediated crosslinking of huntingtin and formation of stable aggregates in Huntington's disease
Histone H3 and H2B	Nucleus	Chromatin remodelling
BAX and BAK	Cytoplasm	Stabilize efficient regulation of apoptosis
14-3-3 binding protein	Cytoplasm	Regulation of apoptosis
MFG E8	Cell surface	Phagocytosis of apoptotic cells
P62/SQSTM 1	Cytoplasm	Recognition and recruitment of ubiquitinated proteins and organelles to pre-autophagic vesicles just before its degradation by autophagolysosomes
NBR1	Cytoplasm	
HSP20	Whole cell lysate	Regulation of apoptosis by interacting with Hsp20/Hsp27 complex
Paxillin	Whole cell lysate	Regulation of cell adhesion and migration by paxillin incorporation in focal adhesion complexes

A.2 BUFFER PREPARATIONS

Table III: Buffer composition

Buffer	Composition
500 mM Tris-HCl pH 7.4 (10X Tris buffer pH 7.4)	500 mM Tris, pH 7.4 (acidified using HCl)
Blocking buffer for ELISA (3% BSA)	3% (w/v) BSA in 50mM Tris-HCl pH 7.4
Blocking buffer for Immunosfluorescence (3% BSA)	3% (w/v) BSA in PBS pH 7.4
Blocking buffer for Western blot (5% milk)	5% (w/v) non-fat milk in TBST
Diethylpyrocarbonate (DEPC)- treated water or nuclease-free water	Incubation of distilled H_2O with 0.1% (v/v) DEPC overnight (15 h), followed by autoclavation at 121 °C for 20 min
Diethylpyrocarbonate (DEPC) water	0.1% (v/v) DEPC in distilled H_2O
Fixing solution - 3%PFA	3% (w/v) PFA in PBS pH 7.4
Heparinase I Buffer	200 mM Tris-HCl, 500 mM NaCl, 40 mM $CaCl_2$, 0.1% (w/v) BSA, pH 7.5
IGEPAL- containing Lysis Buffer	20 mM Tris-HCl, 150 mM NaCl, 5 mM EDTA, 1% (v/v) IGEPAL CA-630, 0.5% (w/v) deoxycholic acid, 0.1% (w/v) SDS, pH 7.4
Laemmli buffer (4X)	250 mM Tris-HCl pH 6.8, 40% (v/v) glycerol, 8% (v/v) SDS, 20%(v/v) β-mercaptoethanol, 0.008%(w/v) bromophenol blue
Permeabilizing solution - Triton	0.1% (v/v) Triton X100 in PBS pH 7.4
Phosphate buffered saline PBS	137 mM NaCl , 2.7 mM KCl, 10 mM Na_2HPO_4, 1.8mM KH_2PO_4, pH 7.4
Ponceau Red staining	0.1% (w/v) Ponceau S, 5% (v/v) glacial acetic acid
Proteomics Lysis Buffer	9.5 M urea, 2%(w/v) DTT, 1% (w/v) N-octyl-beta-glucopyranoside (OGP)
Radioimmunoprecipitation assay buffer (RIPA buffer)	50 mM Tris-HCl, 150 mM NaCl, 1% (v/v) NP40, 0.5% sodium deoxicholate, 0.1% SDS, pH 8
Resolving Buffer (4X)	1.5 mM Tris HCl, 0.4% SDS, pH 8.8
Stacking buffer (4X)	0.5 M Tris HCl, 0.4% SDS, pH 6.8
Sucrose – based Lysis buffer	250 mM Sucrose, 2 mM EDTA, and 50 mM Tris-HCl, pH 7.4
Tank Buffer (Electrophoresis Buffer) (10X)	250mM Tris, 1.92M glycine, 1% (w/v) SDS
Transfer Buffer (Transblot Buffer) (10X)	480mM Tris, 390mM Glycine, 0.375% (w/v) SDS
Tris Buffer Saline - Tween (TBST) (10X)	10 X Tris Buffer Saline [250mM Tris-HCl, 1-5M NaCl, 20mM KCl, pH 7.4], 1%(v/v) Tween-20
Tris Buffer Saline (TBS) (10X)	250mM Tris-HCl, 1-5M NaCl, 20mM KCl, pH 7.4
Tris-Acetate-EDTA (TAE) buffer	40mM Tris, 20mM acetic acid, 1mM EDTA, pH 8.5
Tris-EDTA (TE) Buffer	10 mM Tris-HCl, 1 mM EDTA, pH 8.0
Trypsin free cell detaching buffer (For extracellular activity assay)	5 mM EDTA in sterile PBS pH 7.4

A.3 PLASMID MAPS

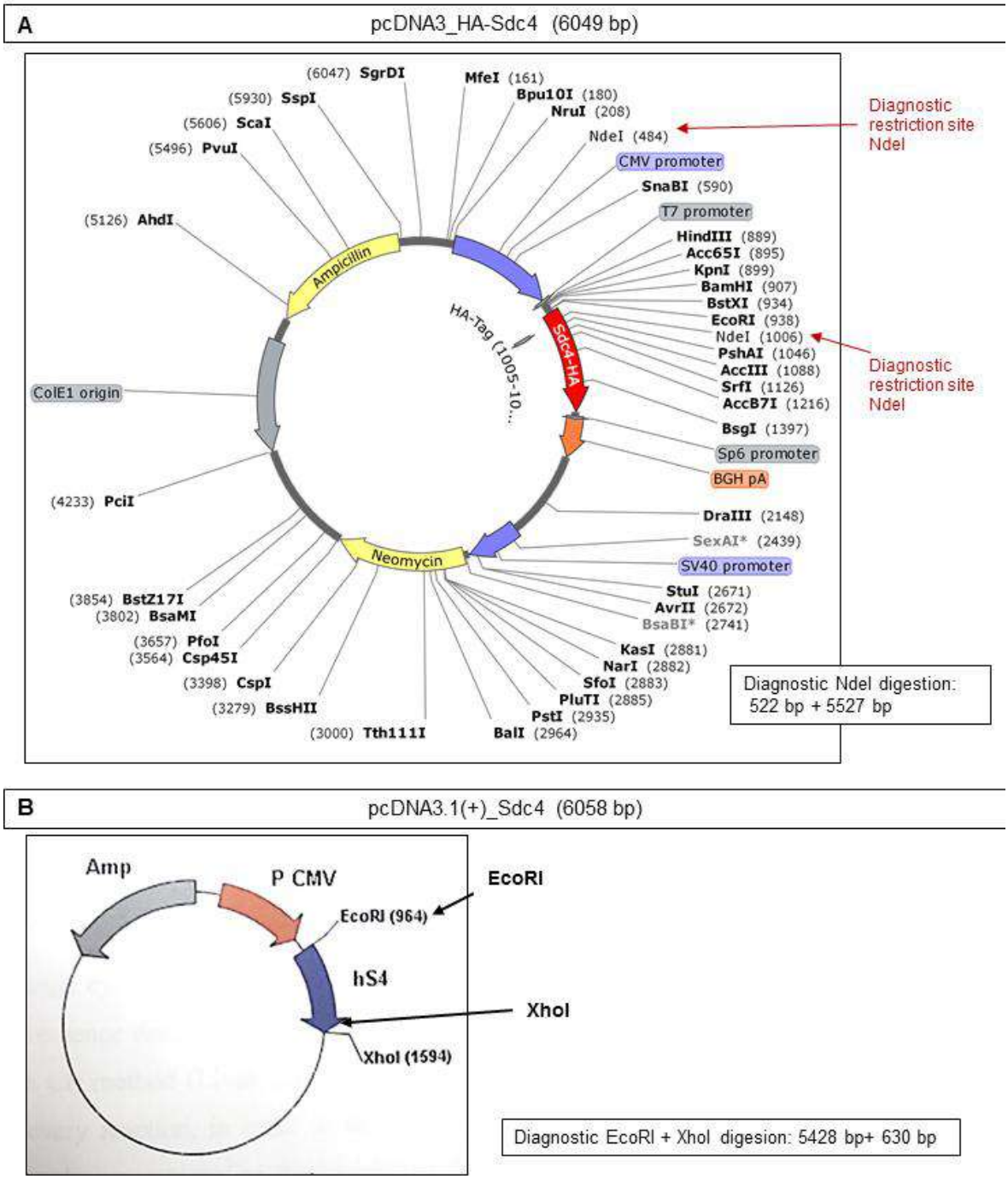

Figure I: Plasmid maps of pcDNA3_HA-Sdc4 and pcDNA3.1(+)_Sdc4. pcDNA3_HA-Sdc4 plasmid (A) was produced by Dr Izhar Burhan (unpublished) and pcDNA3.1(+)Sdc4 (B) was produced by Dr Alessandra Scarpellini (Scarpellini 2009), ~~starting~~ from Sdc4 cDNA and HA-Sdc4 cDNA provided by Dr Mark Bass (The Univesity of Sheffield). Plasmid map of pcDNA3.1(+)Sdc4 was obtained from Dr Scarpellini PhD thesis (Scarpellini 2009).

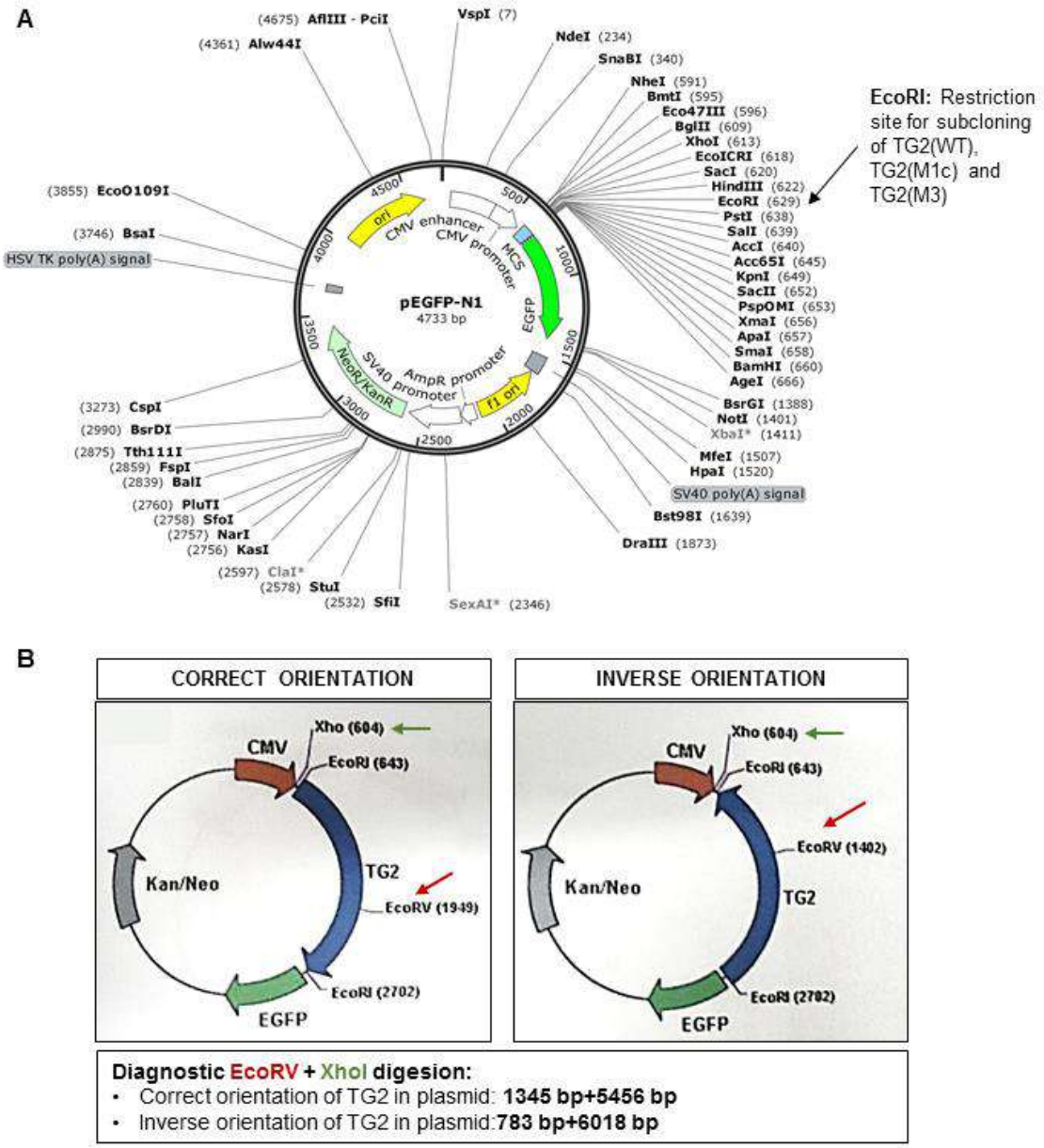

Figure II: Plasmid map of pEGFP-N1-TG2 plasmids. (A) pEGFP-N1 plasmid (ClonTech #6085-1). EcoRI restriction site was employed as cloning site for the introduction of the insert (TG2 cDNA) and the production of EGFP-TG2 chimera-expressing plasmid [pEGFP-N1-TG2(WT)] (Scarpellini 2009). Site directed mutagenesis of TG2 cDNA (Lortat-Jacob, et al. 2012) and subcloning employing the same EcoRI restriction site was performed to produce heparin binding mutant EGFP-TG2 expressing plasmid [pEGFP-N1-TG2(M1c) / pEGFP-N1-TG2(M3)]. Heparin binding mutant EGFP-TG2 expressing plasmids were produced by Dr Izhar Burhan (unpublished). **(B)** Restriction sites for diagnostic restriction digestion of pEGFP-N1-TG2 plasmids, to confirm correct orientation of TG2 with EGFP. Plasmid map of pEGFP-N1-TG2 was obtained from Dr Scarpellini PhD thesis (Scarpellini 2009).

A.4 DESCRIPTION OF THE TG2-ASSOCIATED MEMBRANE PARTNERS INVOLVED IN VESICULAR TRAFFICKING

As reported in Chapter IV, a series of proteins identified as associated ~~to~~ with TG2 in kidney membranes (either fibrotic or healthy) by SWATH™-MS analysis in the current study have been suggested to be involved in different steps of the cellular vesicular trafficking. These TG2-associated partners are putative candidates that might play a role in a possible vesicular trafficking of the enzyme. In this section, a description of the functions of all TG2-associated proteins on kidney membranes will be provided. The proteins will not all be linked to a secretory route, as some of them are mostly involved in endocytic transport.

A.4.1 Clathrin and clathrin associated proteins

Among the ~~TG2 associated~~TG2-associated proteins on kidney membranes, both Sham operated or fibrotic, a series of proteins involved in c~~C~~lathrin-~~-~~mediated endocytosis were identified.

A.4.1.1 Clathrin chains:

Clathrin chains were detected as TG2 partners in kidney membranes in both fibrotic and healthy conditions: in particular, light chains were associated with ~~to~~ TG2 upon UUO (CLCA_MOUSE, CLCB_MOUSE) while the heavy chain CLH1_MOUSE was recognised in healthy conditions. Clathrin is the key protein involved in the formation of cytoplasmic coated vesicles (clathrin-coated vesicles, CCV), ~~-~~that move in both direction, from the trans-Golgi network (TGN) to the secretory pathway, from the endosomes, and from the plasma membrane to the endosome by receptor-mediated endocytosis ~~from~~ of clathrin coated pits (CCP). Clathrin structure is called triskelion and is formed by ~~3~~ three heavy chains and ~~3~~ three light chains: the association of different triskelia to the membrane is mediated by specific adaptor proteins ~~on the membrane~~, and ~~together~~ the triskelia associate to form a lattice (skelion), that drives the membrane budding and the formation of the rounded CCV. Clathrin ~~doesn't~~ does not bind the membrane or the cargo protein directly, but needs an adaptor complex on membranous compartment the vesicle ~~will be~~is budding from. Adaptor complexes connect membrane lipids and cytosolic chains of protein cargos to clathrin during cytosolic vesicle formation. Two main type of adaptor complexes exist in nature: adaptor proteins (AP), that are associated ~~to~~ with different kind of membranes depending on the family, and the ADP-rybosilation factor (ARF)-binding protein GGA (Golgi-localised, gamma-adaptin hear containing), which is uniquely associated ~~to~~ with the TGN.

A.4.1.2 Adaptor complex-2 (AP2)

Among the TG2-associated protein in fibrotic conditions, ~~3~~ three subunits of the **a~~A~~daptor complex-2 (AP2)** were identified (AP2A1_MOUSE, AP2A2_MOUSE and AP2B1_MOUSE) while none was identified in Sham operated kidneys. Importantly, AP2 is characterised by being uniquely associated ~~to~~ with plasma membranes and to mediate in clathrin-mediated receptor-mediated endocytosis (Nakatsu and Ohno 2003). The other AP complexes present in cells, AP1, AP3 and AP4, that are instead mainly ~~associated to~~associated with the budding of vesicles from the TGN to the endosome/lysosome and from the endosome(Nakatsu and Ohno 2003), were not identified in the list of ~~TG2 associated~~TG2-associated proteins. AP2 binds cell membrane phospholipids~~,~~ ~~-~~and ~~-~~in particular ~~to~~ cell surface phosphoinositides PI(4,5)P2, targeting the adaptor to the plasma membrane (Höning, et al. 2005). Moreover AP2 might also play an additional role after endocytosis by interacting with Arf6.

A.4.1.3 ADP-rybosilation factor (ARF) binding protein GGA

The **ADP-rybosilation factor (ARF) binding protein GGA** (Golgi-localised, Gamma-adaptin hear containing) (GGA1_MOUSE) was identified as TG2 associated and is a known clathrin adaptor protein. This protein, however, is not involved in endocytosis, but is uniquely localised at the TGN, mediating the trafficking of proteins from the TGN to the endosomal/lysosomal system into ~~clathrin coated vesicles (CCV)~~ CCV. In particular, GGA adaptor proteins are involved in sorting of mannose 6-phosphate receptors/mannose-6-phospate modified proteins to the lysosome for degradation, by interaction of the receptor with the amino-terminal VHS domain of GGA (Puertollano, et al. 2003) as well as sorting of ubiquitinated proteins to the endosome/lysosome though its GAT (GGA and Tom1) domain (Shiba, et al. 2004).

A.4.1.4 Target of myb protein 1 (Tom1)

Target of myb protein 1 (Tom1)~~,~~ was ~~as well~~ detected as TG2 associated in healthy membranes (TOM1_MOUSE). This protein, similarly to GGA1, is VHS domain- and GAT domain-containing adaptor protein and is localised normally on the endosomal membrane. It has been shown to bind clathrin and probably be a mediator of ubiquitinated protein binding to clathrin vesicles (Yamakami, Yoshimori and Yokosawa 2003, Katoh, et al. 2004, Katoh, et al. 2006). It plays an important role in protein targeting for degradation (Makioka, et al. 2016).

A.4.1.5 Phosphatidylinositol clathrin assembly protein Picalm

Phosphatidylinositol clathrin assembly protein Picalm (PICAL_MOUSE) was identified as a ~~TG2-associated~~TG2-associated partner in both Sham and UUO kidney membranes. This protein interacts with both AP2 and clathrin and plays a role in the recruitment of these proteins to the plasma membrane, on the sites of formation of clathrin coated pits (Tebar, Bohlander and Sorkin 1999, Suzuki, et al. 2012).

A.4.1.6 Huntingtin interacting protein 1

Huntingtin interacting protein 1 (HIP1_MOUSE) was identified as TG2 associated in fibrotic kidney membranes. This protein is involved in the formation of CCV and receptor-mediated endocytosis, by interaction with the actin cytoskeleton (Waelter, et al. 2001, McPherson 2002). Interestingly, this protein is also involved in apoptosis by interaction with Caspase 3 (Hackam, et al. 2000, Kang, et al. 2005), a protein identified as TG2 associated in the TG2-interactome of S~~s~~ham operated kidney membranes.

A.4.1.7 Proton pump component (H subunit) of vacuolar ATPase

The **proton pump component (H subunit) of vacuolar ATPase** (VATH_MOUSE), a protein involved in endosomal compartments acidification, was a TG2-associated partner in fibrotic conditions only. VATH has been suggested to be involved in the acidification process that drives receptor-mediated endocytosis and to interact with AP2 (Forgac, et al. 1983, Mellman, Fuchs and Helenius 1986, Geyer, et al. 2002). On the other side, a role in exocytosis has also been suggested for the V0 subunit of vacuolar ATPase, which is independent from the H^+-pump activity (Marshansky and Futai 2008, Raposo and Stoorvogel 2013).

A.4.1.8 Cyclin-G associated kinase

Cyclin-G associated kinase (GAK_MOUSE), also known as **a~~A~~uxilin 2** (non-neuronal specific, ubiquitous) is another protein that interact~~s~~ed with TG2 only in fibrotic condition. Auxillin is a DnaJ homolog that has been shown to mediate CCV uncoating after endocytosis, also performed by the molecular chaperone heat shock cognate 71 KDa protein Hsc70/Hspa8 (Greener, et al. 2000, Wu 2016, Sousa and Lafer 2015), which is another TG2-associated protein in UUO kidney membranes (HSP7C_MOUSE).

A.4.2 Heat shock cognate 71 KDa protein

Heat shock cognate 71 KDa protein (HSP7C_MOUSE) was identified as a ~~TG2 associated~~TG2-associated protein in fibrotic conditions. This protein is a member of the heat shock 70 family of proteins (HSP70 family), ~~-~~and it is a constitutively expressed protein that acts as a chaperone ~~protein~~ in a GTP/GDP-dependent manner (Stricher, et al. 2013). Generally, the chaperone activity is assisted by members of the HSP40/DNAJ family of chaperones, but also other proteins, such as HSP90, can act as a co-chaperone for this protein. As a chaperone, the protein is known to be involved in several mechanisms inside the cell, including protein folding, degradation, and translocation to the nucleus, mitochondria and ER (Ngosuwan, et al. 2003, Stricher, et al. 2013). In the context of degradation, Hsp7c also plays a role in different types of autophagy (Bandyopadhyay, et al. 2008, Sahu, et al. 2011, Stricher, et al. 2013). If we focus on vesicular trafficking, Hsp7c is known to act as an ATPase in mediating the uncoating of CCVs after clathrin-dependent endocytosis. Gak and DNAJ proteins are as well involved in the process (Sousa and Lafer 2015, Greener, et al. 2000, Wu 2016, Stricher, et al. 2013). In addition, some studies have suggested a role for Hsp7c in the regulation of vesicular transport along microtubules, by acting on kinesin function(Terada, et al. 2010).

Beside the role in endocytosis and intracellular protein trafficking, the protein has also been strongly ~~associated to~~associated with the exosome compartment, being one of the most represented proteins in these extracellular vesicles, as reported on the Exocarta database ~~of reported exosomal proteins~~ (Mathivanan and Simpson 2009). Hsc70 is enriched within the exosome fraction upon cell stress/heat shock in different types of cells, and is detected in urinary exosomes after a stress such as kidney transplant (Clayton, et al. 2005, Pisitkun, et al. 2012).

A.4.3 Flotillin

Flottilin 2 (FLOT2_MOUSE), also known as r~~R~~eggie-1, was identified as well in the TG2-interactome in kidney fibrotic membranes, and is ~~an interesting~~a marker of lipid rafts. Lipid rafts are specialized lipid-rich domains on the plasma membrane, characterized by abundant cholesterol, glycosphingolipids and integral/receptor proteins (Hooper 1999, Pike 2009). In particular, flotillin proteins characterize caveolar lipid rafts, specific membrane~~-~~-invagination domains ~~associated to~~associated with caveolae-dependent, receptor-independent endocytosis and signal transduction (Hooper 1999, Pike 2009). Flotillins act as scaffolding protein in the caveolar rafts, participating, together with caveolins, in the formation of caveolar vesicles. Curiously, the protein homolog of Flot2, f~~F~~lotillin 1 or ~~/~~reggie 2, has been reported to reach the plasma membrane by unconventional Golgi-independent secretion, in a process that depends on its acylation (Morrow, et al. 2002), and Flot2 association to the lipid rafts on the plasma

membrane has been shown to be dependent on Flot2 acylation (myristoylation, palmitoylation), and homo or hetero-oligomerisation with other caveolar proteins (Neumann-Giesen, et al. 2004, Langhorst, et al. 2008).

Similarly to Hsp7c, also flotillins have been ~~associated to~~associated with the exosome fraction of the cells, with a suggested role of lipid rafts in the protein loading into/on the exosomes, and are reported in the Exocarta database as well represented proteins of the exosomes (Phuyal, et al. 2014, Frick, et al. 2007).

A.4.4 Rabankirin 5 (Rank-5)

Rabankirin 5 (Rank-5) (ANFY_MOUSE) is a PI3P-binding effector of the small GTPase Rab5 and was identified as TGg2 associated in healthy membranes. Rab GTPases are members of the Ras superfamily of G-proteins, are localised in different membranous compartments of the cell and involved in the regulation of different steps of membrane trafficking, from vesicle formation to movement and fusion, from the ER/Golgi network to the different endosomal compartments. In particular, Rab5 localises on the early endosomes and plays mostly a role in homotypic early endosomes fusion more than in heterotypic CCV-to-early endosome fusion. Both Rab5 and PI3P are known markers of early endosomes, and Rab5 plays not only a role in early endosomes lateral homotypic fusion, but also in clathrin--mediated endocytosis and liquid phase endocytosis by micropinocytosis (Bucci, et al. 1992). Together with its role in early endosome dynamics, Rank-5 has been demonstrated to play an important function as a Rab5 effector in non-clathrin mediated fluid phase endocytosis, with particular significance in polarised cells such as kidney tubular epithelial cells (Schnatwinkel, et al. 2004). Moreover, Rank-5 has been demonstrated to play a role in retromer eEndosome-to-TGN transport and regulation, again as a Rab5 effector, by interacting with Eps15 homolog domain 1 (EHD1), a protein involved in both endocytic recycling and retromer transport, and the vacuolar sorting proteins Vps26 and Vps35, belonging to the cargo selective complex (Zhang, et al. 2012).

A.4.5 ADP-ribosylation factors 5 and 6 (Arf5 and Arf6)

ADP-ribosylation factors 5 and 6 (Arf5 and Arf6) ~~were~~ are two proteins identified as significantly ~~associated to~~associated with TG2 in healthy kidney membranes (ARF5_MOUSE, ARF6_MOUSE). Arf proteins are small GTP--binding proteins (GTPases) of the Ras superfamily, a superfamily of small GTPases involved in many cell functions (Goitre, et al. 2014). Also Rab GTPases ~~proteins~~ belong to the Ras superfamily, and, together with Arf proteins regulate membrane trafficking and vesicular transport (Goitre, et al. 2014). **Arf6 GTPase** is a member of the GTP-binding protein family of ARFs, and the only component of the class III of ARF protein. The peculiarity of this protein is that is localised at the plasma membrane and is

involved in endocytic pathways (both phagocytosis and receptor-mediated endocytosis), endosomal recycling and actin remodelling, with a role in cytokinesis (cell adhesion, migration etc…) (Souza-Schorey, et al. 1995, D'Souza-Schorey and Chavrier 2006). The role in clathrin vesicles formation is carried out by interaction with PI(4,5)P2 and AP2, but the protein is also involved in other endocytic pathways such as caveolar pathways and receptor- independent endocytosis such as phagocytosis (D'Souza-Schorey and Chavrier 2006, Souza-Schorey, et al. 1995). The role in actin remodelling is itself important for localised phagocytic movements as well as for ARF6 function in cytokinesis (Balana, et al. 2005, D'Souza-Schorey and Chavrier 2006).

On the other side, **Arf5 GTPase** is a member of the class II of ARFs, together with Arf4. This class is less studied compared to the others, and has been mostly ~~associated to~~associated with Golgi trafficking and vesicles formation at the TGN (D'Souza-Schorey and Chavrier 2006). However, a work of Moravec and colleagues has suggested a role of Arf5 in clathrin-mediated endocytosis of α5β1 integrins, instead of the more likely to be involved Arf6 (Moravec, et al. 2012).

A.4.6 Annexin A2 (Anxa2)

Annexin A2 (Anxa2) (ANXA2_MOUSE) was identified as significantly ~~associated to~~associated with TG2 in healthy kidney membranes. This protein has been already mentioned in Chapter V as a well-characterised unconventionally secreted protein: is a membrane-binding protein known to interact with membrane phosphoinositides in a calcium-dependent manner (Bharadwaj, et al. 2013) and to be an important regulator of actin dynamics in the proximity of membranes (Bharadwaj, et al. 2013, Grieve, Moss and Hayes 2012). Among its many roles, Annexin A2 has been shown to be involved in clathrin mediated endocytosis by interaction with AP2, and to interact with two specific Rab5 effectors involved in endocytosis (Creutz and Snyder 2005, Urbanska, et al. 2011). At the same time, Anxa2 has also been suggested to be involved in receptor independent endocytosis by micropinocytosis, regulating the actin dynamics in the formation of the macropinosome (Hayes, et al. 2004, Grieve, Moss and Hayes 2012). In general, Anxa2 is important in a number of processes involving actin regulation in the context of membrane dynamics, with a specific importance in membrane invagination/protrusion and vesicle formation (Grieve, Moss and Hayes 2012). Some studies have also associated Anxa2 to exosomal vesicles, and its release into these vesicular compartment was suggested to be part of a pathway starting from the formation of lipid rafts rich in cholesterol (Valapala and Vishwanatha 2011, Chasserot-Golaz, et al. 2005).

A.4.7 Exocytic proteins

Moving to proteins mostly ~~associated to~~associated with exocytic pathways, two main proteins need to be mentioned, the first, programmed cell death 6 – interacting protein, better known as alix or AIP1 (PDC6I_MOUSE), was detected as TG2 associated in kidney membranes of both treatments, while the second, tumour susceptibility gene 101 protein (Tsg101) (TS101_MOUSE) was identified in Sham operated conditions only.

A.4.7.1 Alix (or Programmed cell death 6 – interacting protein or AIP1)

Alix (**or Programmed cell death 6 – interacting protein or AIP1**) (PDC6I_MOUSE) is a cytoplasmic vesicular protein sorting (Vps) protein involved in late endosomes/lysosomes regulation. The protein plays a role in the sorting of proteins into intraluminal vesicles of multivesicular bodies (MVB), generated by invagination of the limiting membrane of the late endosome, by connecting ESCRT complexes I to III and binding the atypical phospholipid lysobisphosphatidic acid (LBPA) (Matsuo, et al. 2004, Hurley and Odorizzi 2012, McCullough, Colf and Sundquist 2013). In this way, the protein regulates~~d~~ protein sorting into vesicles directed to the lysosome, but at the same time ~~they are~~it is involved in the formation of exosomes, that are intraluminal vesicles released by fusion of the limiting membrane of the multivesicular exosome with the plasma membrane (Hurley and Odorizzi 2012, McCullough, Colf and Sundquist 2013). As a matter of facts, Alix is considered one of the main exosomal markers, as mentioned on Exocarta database (Mathivanan and Simpson 2009, Keerthikumar, et al. 2016). Particularly interesting is the involvement of s~~S~~yndecan HSPGs in the exosome biogenesis ~~associated to~~in association with a~~A~~lix, and crucial in the process is the adaptor protein syntenin on the ectosome, that binds both alix and syndecan HSPGs in the formation of syntenin-containing exosomes. The process is probably dependent on the cytoplasmic domain of syndecan on the endosome, where syndecan can cluster and bind syntenin after the negatively charged extracellular domains have been cleaved (Baietti, et al. 2012, Ghossoub, et al. 2014). To confirm this, the process is favoured by the HS-~~Heparan sulphate~~ digesting enzyme heparanase (David and Zimmermann 2015, Roucourt, et al. 2015). Interestingly, one ubiquitously expressed member of the syndecan family, syndecan-~~-~~4, was identified in the list of tg2-associated proteins in kidney membranes. Moreover, the abovementioned s~~S~~mall GTPase Arf6 and its effector phospholipase D (PLD) have been suggested to be involved in the process of syntenin/alix exosome formation, possibly by the regulation of specific phosphatidic acid (PA) domains (Ghossoub, et al. 2014).

In addition to the direct functions in intraluminal vesicles / exosome formation, alix has been shown to be involved in actin dynamics on the cortical part of the cells, mediating regulation of actin polymerisation/depolymerisation and positioning of the endosome in the cell

(Cabezas, et al. 2005, Pan, et al. 2006b). Coronin, another TG2-associated protein in the kidney membrane interactome, co-localises with ~~Alix~~ alix in an actin depolymerisation process (Lin, et al. 2010).

A.4.7.2 Tumour susceptibility gene 101 protein (Tsg101)

Tumour susceptibility gene 101 protein (Tsg101) (TS101_MOUSE) is another protein involved in sorting of protein cargo into intraluminal vesicles of MVBs. It is a component of the ESCRT-I complex and recognises ubiquitinated proteins that need to be sorted into the late endosome (Babst, et al. 2000). Similarly to alix, it is likely to be required for the exosomal release of syndecan and its adaptor syntenin (Baietti, et al. 2012).

Interestingly, both Tsg101 and the abovementioned ~~Hsp7c~~ heat shock protein 70~~protein,~~ were also identified as associated with TG2 in a proteomic study of TG2-interactome, in a model of starvation mediated autophagy: the association of both proteins, together with a series of other molecular chaperones, was identified only in normal condition, and lost~~s~~ upon autophagy (Altuntas, et al. 2015). Moreover, as reported before in the context of TG2 unconventional secretion ~~hypothesis~~ (Chapter V), the enzyme was suggested to interact with Tsg101 and a~~A~~lix in the regulation of its sorting, ~~and~~ as well as other protein sorting, into secreted exosomes (Diaz-Hidalgo, et al. 2016).

A.4.7.3 Ist1 homolog

Ist1 homolog is another protein associated with the ESCRT machinery, and, similarly to Tsg101, was identified as ~~associated to~~associated with TG2 uniquely in Sham operated kidney membranes (IST_MOUSE). Ist1 has been shown to have an inhibitory effect on the ESCRT-III function (disassembly) with an important role in membrane abscission during cytokinesis (Xiao, et al. 2009, Babst, Davies and Katzmann 2011). Moreover, it has been seen to characterise a series of urinary exosome preparations (Li, et al. 2011, Raj, et al. 2012, Liu, et al. 2015).

A.4.8 Vesicle fusion associated proteins

A.4.8.1 Vesicle-fusing ATPase NSF (N-ethylmaleimide-sensitive factor)

Vesicle-fusing ATPase NSF (N-ethylmaleimide-sensitive factor) (NSF_MOUSE), well known to be involved in membrane fusion events, was identified as TG2-associated in Ssham operated kidney membranes. The protein is necessary for the process of membrane fusion and vesicle/cargo release mediated by SNAREs (vesicular and target membrane), hence is involved, in addition to its functions in intracellular fusion events, in exosome secretion by fusion of the limiting membrane (Zhao, Slevin and Whiteheart 2007, Fader, et al. 2009). As described before, TG2 secretion has been suggested to be dependent on NSF activity, as its inhibition has been shown to hamper the enzyme release (Zemskov, et al. 2011, Santhanam, Berkowitz and Belkin 2011, Jandu, et al. 2013).

A.4.8.2 Sec1 Family domain containing protein 1

A protein strictly associated with NSF and SNAREs is **Sec1 Family domain containing protein 1**, that was identified as TG2 associate in both fibrotic and healthy conditions (SCFD1_MOUSE). Sec1 is a protein specifically binding to syntaxin, a plasma membrane SNARE protein necessary, together with synaptobrevin and SNAP-25, for the formation of the SNARE complex necessary for plasma membrane fusion in constitutive and regulated exocytosis. Binding of Sec1 specifically regulates Syntaxin activity in the formation of the membrane SNARE complex (Halachmi and Lev 1996, Pevsner, et al. 1994).

A.4.8.3 Synaptobrevin homolog YKT6

Synaptobrevin homolog YKT6 was identified as TG2 associated in fibrotic conditions (YKT6_MOUSE). This protein has been shown to be involved in a vSNARE complex for membrane fusion and has mostly been associated toassociated with ER-to-Golgi transport as well as retrograde early endosome/recycling endosome to TGN transport (Zhang and Hong 2001, Xu, et al. 2002, Tai, et al. 2004). However, a study on drosophila Wnt protein has suggested its role in exosome secretion (Gross, et al. 2012).

A.4.8.4 Small GTPase Rab3 activating non catalytic protein subunit 2 (Rab3Gap2)

Small GTPase Rab3 activating non catalytic protein subunit 2 (Rab3Gap2) was identified as TG2 associated in fibrotic conditions (RBGPR_MOUSE). The protein is an activator of the Rab3 protein family, a family of small GTPases that controls the regulated, non-constitutive, exocytosis of neurotransmitters and hormones by associating to the area where Ca^{2+}-regulated membrane fusion will happenhappens (Lledo, et al. 1994, Schluter, et al. 2002, Sakane, et al. 2006). Rab3 proteins have been largely described in neural cells in the context of synaptic

secretion, but are also expressed in other cell types and in kidney cells (Liebenhoff and Rosenthal 1995, Schluter, et al. 2002). Rab3Gap complex performs the GTP-hydrolysis/inactivation of GTP-bound Rab3 and subsequent dissociation of GDP-Rab3 from the fusion area, necessary for the exocytic process to continue by membrane fusion performed by the abovementioned SNARE/Syntaxin/Synaprobrevin complex (Sakane, et al. 2006).

A.4.9 Sorting nexin 4

Sorting Nexin 4 (**Snx4**) (SNX4_MOUSE) is a member of the sorting nexin family of phosphoinositide-binding proteins, and was identified as TG2 associated in kidney fibrotic membranes. This protein binds primarily PI3P on the endosomes and is involved in the recycling of proteins such as transferrin receptor (TfnR, endocytosed by clathrin-dependent receptor-mediated endocytosis) or E-cadherin. It coordinates protein trafficking from the early endosome to the perinuclear endocytic recycling compartment by regulating minus-end directed trafficking along microtubules, in interaction with the motor protein dynein and with tubulin (Traer, et al. 2007). A more recent paper also suggested a possible interaction of Snx4 with Flot2 in the regulation of ~~recycling trafficking~~protein recycling, a process that also involves the small GTPase Rab11a (Solis, et al. 2013).

A.4.10 Unconventional myosins

In fibrotic conditions, a series of **u~~U~~nconventional myosins** (**myosin I~~i~~** class ~~- myosins~~ MYO1B_MOUSE, MYO1D_MOUSE and MYO1G_MOUSE ~~- -~~and **myosin XVIII** class - MY18A_MOUSE) were identified as ~~associated to~~associated with TG2, while no myosin was co-precipitated with the enzyme in healthy conditions. While conventional myosins (~~Class~~ class II myosins – muscle type myosins) mediate cytokinesis/cell motility in muscular and non-muscular cells and ~~obviously~~ contraction of muscular tissue, in association with actin filaments and in an ATP-dependent manner, unconventional myosins have different shapes and classes and can be ~~associated to~~associated with membrane trafficking. Myosins of class I are probably the more studied unconventional myosins and have been associated, among other functions, to the endocytic pathway. Raposo and colleagues, in 1999, have suggested that m~~M~~yosin I proteins localise in both endosome and lysosome and might mediate protein movement between the two compartments by interacting with actin and ~~joining~~linking the membranous domains to the actin cytoskeleton domains (Raposo, et al. 1999). Moreover, ~~M~~myosin I has ~~also~~ been suggested to be involved also in secretory vesicles transport from the Golgi network

(DePina and Langford 1999), in endocytosis (micropinocytosis and phagocytosis), and probably in some exocytic pathways (Mermall, Post and Mooseker 1998).

The role of mMyosin I in membrane trafficking is possibly due to its role in mediating the adhesion between membrane and cytoskeleton, that stimulates membrane tension and its subsequent deformation in the processes of endocytosis, exocytosis and vesicle budding (Nambiar, McConnell and Tyska 2009).

Myosin XVIII is another unconventional myosin possibly involved in vesicular movement. The protein, in fact, has been suggested to mediate the regulation of Golgi structures and vesicle budding from the Golgi network, by tethering the Golgi membrane to the cytoskeleton and possibly generating membrane tension and deformation (Dippold, et al. 2009, Taft, et al. 2013).

A.4.11 Retromer complex proteins

A quite substantial portion of TG2-associated proteins was recognised to be involved in the rRetromer complex mechanism (**Fig. III**).

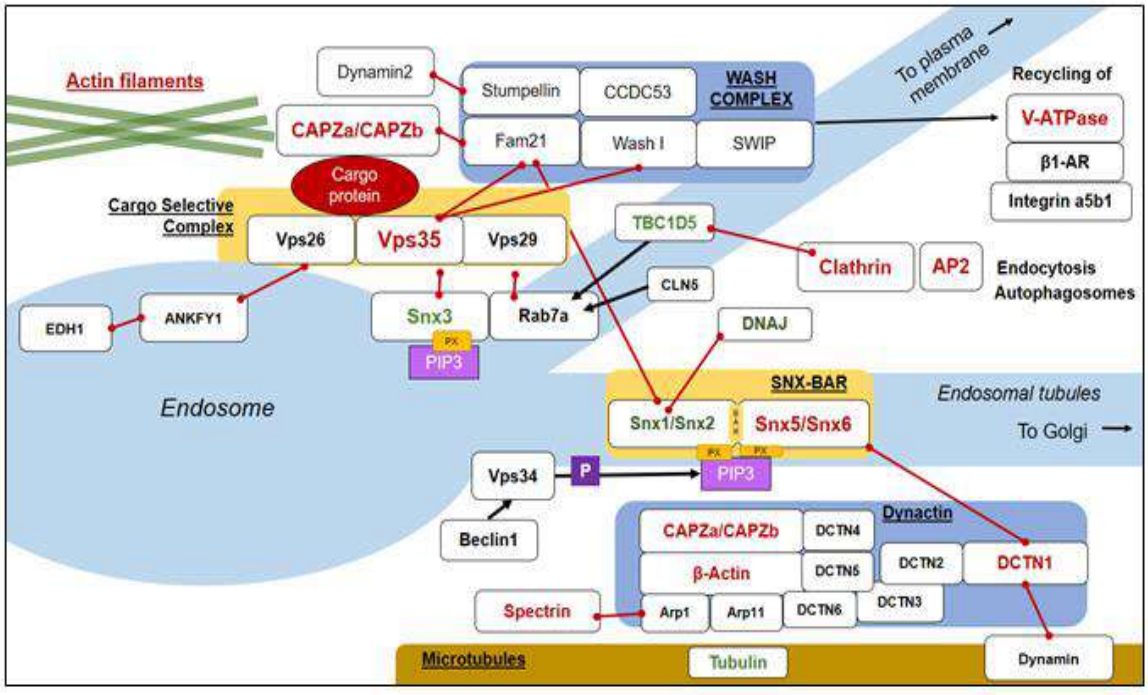

Figure III: TG2-associated partners involved in retromer complex mechanisms. The figure above summarizes the main proteins involved in retromer transport from the endosome to the Golgi and from the eEndosome to the plasma membrane. In red are highlighted the proteins identified as TG2 associated in Fibrotic fibrotic (UUO) kidney membranes by SWATH™-MS in the current study, while in green are the TG2-associated partners in healthy conditions (Chapter IV).

A.4.11.1 Sorting nexin~~s~~ 1 and sorting nexin 3

Two sorting nexin proteins, Snx1 and Snx3, were identified as ~~associated to~~associated with TG2 in kidney membranes, the first in mice subjected to UUO, and the second in Sham operated mice.

Sorting nexin 1 (Snx1) (SNX1_MOUSE) is a known member of the Snx-BAR dimer involved in tubular endosome deformation/elongation, ~~-~~necessary for the Snx-BAR retromer trafficking from the endosomal compartment to the TGN or to the plasma membrane.

Sorting nexin 3 (Snx3) (SNX3_MOUSE) is involved as well in the retromer trafficking by mediating cargo-selective trimer (CST) recruitment to the endosomal membrane together with Rab7 (Harbour, et al. 2010). It is ~~also~~ likely to act as a component of an Snx-BAR-independent/Snx3-dependent retromer complex, involved for examples in w~~W~~ingless protein trafficking to the Golgi (Harterink, et al. 2011, Zhang, et al. 2011, Cullen and Korswagen 2012).

A.4.11.2 Vacuolar sorting protein 35

Vacuolar sorting protein 35 (**Vps35**) is a key component of the ~~Cargo Selective Trimer (CST)~~CST of the retromer complex, and was identified as TG2 associated in healthy kidney membranes (VPS35_MOUSE). The protein is necessary for the selection of protein cargo to the complex; ~~,~~as part of the trimer, it plays a key role ~~acts~~ in both SNX-BAR and Snx3 retromer trafficking, ~~-~~and is also involved in binding to the WASH complex for endosome-to-~~-~~plasma membrane recycling.

A.4.11.3 Dynactin

Dynactin subunit 1, also known as p150^{Glued}~~,~~ protein, was identified as TG2 associated in ~~Fibrotic~~ fibrotic conditions (DCTN1_MOUSE). This protein is a necessary component of the dynactin complex, that mediates the binding of vesicles or organelles to the motor protein dynamin, necessary for their retrograde transport along microtubules. Dynamin-~~-~~mediated trafficking along microtubules goes from the plus-end (exposed β-tubulin subunits) of the microtubule towards the minus-end of the microtubule (exposed α-tubulin subunits), that means that the trafficking generally goes from the cell periphery towards the centrosome – microtubule organisation centre, close to the Golgi (Cooper 2000). Dynactin interacts with dynein directly through DCTN1 and mediates the connection between the organelle/vesicle to the motor protein(Vaughan and Vallee 1995). As suggested before, retromer complex associates with dynactin, and the association is needed for endosomal tubules tracking along microtubules to the minus-end where the TGN is located~~s~~ (Wassmer, et al. 2009, Hong, et al. 2009) .

A.4.12 Other vesicular-associated proteins

A.4.12.1 Small GTPase Rab1 and small GTPase Sar1b

Small GTPase Rab1 and **Small GTPase Sar1b** were both identified as TG2 associated in fibrotic kidney membranes. **Rab1** (RAB1_MOUSE) is a small GTPase of the Rab family of trafficking regulators and is involved mainly in the regulation of the vesicular trafficking from the ER to the ~~Cis~~cis-Golgi network, with a direct effect on the conventional protein secretion. The protein is involved in the budding of COPII vesicles from the ER, as well as tethering of the same vesicles at the cis-Golgi (Nuoffer, et al. 1994, Allan, Moyer and Balch 2000, Moyer, Allan and Balch 2001, Filipeanu, et al. 2004).

Sar1b (SAR1B_MOUSE), on the other side, belongs to the ARF family of small GTPases. Similarly to Rab1, the protein has been suggested to be involved in ER-to-Golgi trafficking by mediating COPII recruitment and subsequent vesicle formation. The protein is a component of the COPII coat complex, which is necessary for coat formation and cargo loading into the vesicle. The GTP-bound form of the protein (activated by Sec12 protein) binds the ER membrane and recruits a complex of COPII-coat Sec proteins (Sec23/Sec24 + Sec13/Sec31), that determine cargo protein selection to the membrane, -and membrane deformation leading to vesicle budding (Szul and Sztul 2011).

A.4.12.2 Coatomer

Coatomer subunit β protein is a TG2-associated protein identified in fibrotic kidney membrane only (COPB2_MOUSE). Coatormer proteins are members of a coatomer complex that forms COPI vesicles, mediating both anterograde trafficking trough the Golgi cisternae and retrograde Golgi-to-ER transport of proteins. The recruitment of COPI complex (coatomer proteins) to the membranes is mediated by ARF proteins of class I (Arf1, Arf2 and Arf3) and possibly class II (Arf4 and Arf5) (Szul and Sztul 2011).

A.4.12.3 Transitional endoplasmic reticulum ATPase TERA

Transitional Endoplasmic Reticulum ATPase TERA, also known as **valosin-containing protein Vcp** (TERA_MOUSE), -was identified as TG2 associated in both UUO and Sham operated kidney membranes. This protein has mainly been ~~associated to~~associated with the formation of the transitional endoplasmic reticulum (tER), the area where the newly synthesized proteins leave the ER into vesicles. It acts as a molecular chaperone and plays a role in targeting of misfolded proteins from the ER -directly to the proteasome, -for degradation by endoplasmic-reticulum-associated protein degradation (ERAD), and it generally plays a role in ubiquitin-dependent protein degradation (Dai and Li 2001, Vij 2008). Moreover, it has been shown to bind both clathrin and Hsc70 (Pleasure, Black and Keen 1993).

A.4.12.4 Small GTPase Rab10 and TBC1 domain family member 9B

Small GTPase Rab10 and TBC1-domain ~~Family~~ family member 9b were both detected as TG2 associated in Sham operated kidneys.

Small GTPase Rab10 (RAB10_MOUSE) is a known regulator of ER morphology (English and Voeltz 2013) and of conventional trafficking from TGN to the plasma membrane (Chen, et al. 2012, Wang, et al. 2010), but has also been reported to be involved in the regulation of protein recycling in polarised cells (Babbey, et al. 2006, Schuck, et al. 2007).

TBC1 domain family member 9B (TBC9B_MOUSE) is a protein characterised by the TBC-domain, a well conserved ~200 aminoacids domain typical of Rab-inactivating proteins named GAPs (GTPase-activating proteins). GAP ~~proteis~~proteins, in fact, ~~-~~promote the hydrolysis GTP to GDP, that leads to Rab inactivation (Pan, et al. 2006a, Pfeffer 2013).

References

ABDALLA, S., LOTHER, H., LANGER, A., EL FARAMAWY, Y. and QUITTERER, U., 2004. Factor XIIIA transglutaminase crosslinks AT 1 receptor dimers of monocytes at the onset of atherosclerosis. Cell, 119(3), pp. 343-354.

ABE, M., HARPEL, J., METZ, C., NUNES, I., LOSKUTOFF, D. and RIFKIN, D., 1994. An assay for transforming growth factor-β using cells transfected with a plasminogen activator inhibitor-1 promoter-luciferase construct. Analytical Biochemistry, 216(2), pp. 276-284.

ABRAMSSON, A., KURUP, S., BUSSE, M., YAMADA, S., LINDBLOM, P., SCHALLMEINER, E., STENZEL, D., SAUVAGET, D., LEDIN, J., RINGVALL, M., LANDEGREN, U., KJELLEN, L., BONDJERS, G., LI, J.P., LINDAHL, U., SPILLMANN, D., BETSHOLTZ, C. and GERHARDT, H., 2007. Defective N-sulfation of heparan sulfate proteoglycans limits PDGF-BB binding and pericyte recruitment in vascular development. Genes & development, 21(3), pp. 316-331.

ADAMCZYK, M., GRIFFITHS, R., DEWITT, S., KNAUPER, V. and AESCHLIMANN, D., 2015. P2X7 receptor activation regulates rapid unconventional export of transglutaminase-2. Journal of cell science, 128(24), pp. 4615-4628.

AESCHLIMANN, D. and PAULSSON, M., 1991. Cross-linking of laminin-nidogen complexes by tissue transglutaminase. A novel mechanism for basement membrane stabilization. The Journal of biological chemistry, 266(23), pp. 15308-15317.

AESCHLIMANN, D. and THOMAZY, V., 2000. Protein crosslinking in assembly and remodelling of extracellular matrices: the role of transglutaminases. Connective tissue research, 41(1), pp. 1-27.

AFRATIS, N.A., NIKITOVIC, D., MULTHAUPT, H.A., THEOCHARIS, A.D., COUCHMAN, J.R. and KARAMANOS, N.K., 2016. Syndecans: key regulators of cell signaling and biological functions. The FEBS Journal, .

AGUILAR, P.S., BAYLIES, M.K., FLEISSNER, A., HELMING, L., INOUE, N., PODBILEWICZ, B., WANG, H. and WONG, M., 2013. Genetic basis of cell–cell fusion mechanisms. Trends in Genetics, 29(7), pp. 427-437.

AHMAD, F., LINDH, R., TANG, Y., WESTON, M., DEGERMAN, E. and MANGANIELLO, V.C., 2007. Insulin-induced formation of macromolecular complexes involved in activation of cyclic nucleotide phosphodiesterase 3B (PDE3B) and its interaction with PKB. The Biochemical journal, 404(2), pp. 257-268.

AHN, J., KIM, M., HAHN, J., PARK, J., PARK, K., CHO, B., PARK, S. and KIM, D., 2008. Tissue transglutaminase-induced down-regulation of matrix metalloproteinase-9. Biochemical and biophysical research communications, 376(4), pp. 743-747.

AHVAZI, B., BOESHANS, K.M., IDLER, W., BAXA, U., STEINERT, P.M. and RASTINEJAD, F., 2004. Structural basis for the coordinated regulation of transglutaminase 3 by guanine nucleotides and calcium/magnesium. The Journal of biological chemistry, 279(8), pp. 7180-7192.

AKERS, J.C., GONDA, D., KIM, R., CARTER, B.S. and CHEN, C.C., 2013. Biogenesis of extracellular vesicles (EV): exosomes, microvesicles, retrovirus-like vesicles, and apoptotic bodies. Journal of neuro-oncology, 113(1), pp. 1-11.

AKIMOV, S.S. and BELKIN, A.M., 2001a. Cell surface tissue transglutaminase is involved in adhesion and migration of monocytic cells on fibronectin. Blood, 98(5), pp. 1567-1576.

AKIMOV, S.S. and BELKIN, A.M., 2001b. Cell-surface transglutaminase promotes fibronectin assembly via interaction with the gelatin-binding domain of fibronectin: a role in TGFbeta-dependent matrix deposition. Journal of cell science, 114(Pt 16), pp. 2989-3000.

AKIMOV, S.S., KRYLOV, D., FLEISCHMAN, L.F. and BELKIN, A.M., 2000. Tissue transglutaminase is an integrin-binding adhesion coreceptor for fibronectin. The Journal of cell biology, 148(4), pp. 825-838.

ALESSI, D.R., CAUDWELL, F.B., ANDJELKOVIC, M., HEMMINGS, B.A. and COHEN, P., 1996. Molecular basis for the substrate specificity of protein kinase B; comparison with MAPKAP kinase-1 and p70 S6 kinase. FEBS letters, 399(3), pp. 333-338.

ALEXANDER, A. and WALKER, C.L., 2011. The role of LKB1 and AMPK in cellular responses to stress and damage. FEBS letters, 585(7), pp. 952-957.

ALEXOPOULOU, A.N., MULTHAUPT, H.A. and COUCHMAN, J.R., 2007. Syndecans in wound healing, inflammation and vascular biology. The international journal of biochemistry & cell biology, 39(3), pp. 505-528.

ALHASAN, A.A., SPIELHOFER, J., KUSCHE-GULLBERG, M., KIRBY, J.A. and ALI, S., 2014. Role of 6-O-sulfated heparan sulfate in chronic renal fibrosis. The Journal of biological chemistry, 289(29), pp. 20295-20306.

ALLAN, B.B., MOYER, B.D. and BALCH, W.E., 2000. Rab1 recruitment of p115 into a cis-SNARE complex: programming budding COPII vesicles for fusion. Science (New York, N.Y.), 289(5478), pp. 444-448.

ALPERS, C.E. and HUDKINS, K.L., 2011. Mouse models of diabetic nephropathy. Current opinion in nephrology and hypertension, 20(3), pp. 278-284.

ALTEMEIER, W.A., SCHLESINGER, S.Y., BUELL, C.A., PARKS, W.C. and CHEN, P., 2012. Syndecan-1 controls cell migration by activating Rap1 to regulate focal adhesion disassembly. Journal of cell science, 125(Pt 21), pp. 5188-5195.

ALTUNTAS, S., ROSSIN, F., MARSELLA, C., D'ELETTO, M., DIAZ-HIDALGO, L., FARRACE, M.G., CAMPANELLA, M., ANTONIOLI, M., FIMIA, G.M. and PIACENTINI, M., 2015. The transglutaminase type 2 and pyruvate kinase isoenzyme M2 interplay in autophagy regulation. Oncotarget, 6(42), pp. 44941-44954.

ANDERSON, R.P., DEGANO, P., GODKIN, A.J., JEWELL, D.P. and HILL, A.V., 2000. In vivo antigen challenge in celiac disease identifies a single transglutaminase-modified peptide as the dominant A-gliadin T-cell epitope. Nature medicine, 6(3), pp. 337-342.

ANDERSON, S., MEYER, T.W., RENNKE, H.G. and BRENNER, B.M., 1985. Control of glomerular hypertension limits glomerular injury in rats with reduced renal mass. The Journal of clinical investigation, 76(2), pp. 612-619.

ANDREI, C., DAZZI, C., LOTTI, L., TORRISI, M.R., CHIMINI, G. and RUBARTELLI, A., 1999. The secretory route of the leaderless protein interleukin 1beta involves exocytosis of endolysosome-related vesicles. Molecular biology of the cell, 10(5), pp. 1463-1475.

REFERENCES

ANDREI, C., MARGIOCCO, P., POGGI, A., LOTTI, L.V., TORRISI, M.R. and RUBARTELLI, A., 2004. Phospholipases C and A2 control lysosome-mediated IL-1 beta secretion: Implications for inflammatory processes. Proceedings of the National Academy of Sciences of the United States of America, 101(26), pp. 9745-9750.

ANNES, J.P., MUNGER, J.S. and RIFKIN, D.B., 2003. Making sense of latent TGFbeta activation. Journal of cell science, 116(Pt 2), pp. 217-224.

ANTONUCCI, F., TUROLA, E., RIGANTI, L., CALEO, M., GABRIELLI, M., PERROTTA, C., NOVELLINO, L., CLEMENTI, E., GIUSSANI, P., VIANI, P., MATTEOLI, M. and VERDERIO, C., 2012. Microvesicles released from microglia stimulate synaptic activity via enhanced sphingolipid metabolism. The EMBO journal, 31(5), pp. 1231-1240.

ANTONYAK, M.A., JANSEN, J.M., MILLER, A.M., LY, T.K., ENDO, M. and CERIONE, R.A., 2006. Two isoforms of tissue transglutaminase mediate opposing cellular fates. Proceedings of the National Academy of Sciences of the United States of America, 103(49), pp. 18609-18614.

ANTONYAK, M.A., LI, B., BOROUGHS, L.K., JOHNSON, J.L., DRUSO, J.E., BRYANT, K.L., HOLOWKA, D.A. and CERIONE, R.A., 2011. Cancer cell-derived microvesicles induce transformation by transferring tissue transglutaminase and fibronectin to recipient cells. Proceedings of the National Academy of Sciences of the United States of America, 108(12), pp. 4852-4857.

ANTONYAK, M.A., SINGH, U.S., LEE, D.A., BOEHM, J.E., COMBS, C., ZGOLA, M.M., PAGE, R.L. and CERIONE, R.A., 2001. Effects of tissue transglutaminase on retinoic acid-induced cellular differentiation and protection against apoptosis. The Journal of biological chemistry, 276(36), pp. 33582-33587.

ANTONYAK, M.A., WILSON, K.F. and CERIONE, R.A., 2012. R (h) oads to microvesicles. Small GTPases, 3(4), pp. 219-224.

ARENTZ-HANSEN, H., KORNER, R., MOLBERG, O., QUARSTEN, H., VADER, W., KOOY, Y.M., LUNDIN, K.E., KONING, F., ROEPSTORFF, P., SOLLID, L.M. and MCADAM, S.N., 2000. The intestinal T cell response to alpha-gliadin in adult celiac disease is focused on a single deamidated glutamine targeted by tissue transglutaminase. The Journal of experimental medicine, 191(4), pp. 603-612.

ARIENS, R.A., LAI, T.S., WEISEL, J.W., GREENBERG, C.S. and GRANT, P.J., 2002. Role of factor XIII in fibrin clot formation and effects of genetic polymorphisms. Blood, 100(3), pp. 743-754.

ARMBRECHT, H., BOLTZ, M., STRONG, R., RICHARDSON, A., BRUNS, M. and CHRISTAKOS, S., 1989. Expression of Calbindin-D Decreases with Age in Intestine and Kidney*. Endocrinology, 125(6), pp. 2950-2956.

ARTHUR, W.T. and BURRIDGE, K., 2001. RhoA inactivation by p190RhoGAP regulates cell spreading and migration by promoting membrane protrusion and polarity. Molecular biology of the cell, 12(9), pp. 2711-2720.

ARUR, S., UCHE, U.E., REZAUL, K., FONG, M., SCRANTON, V., COWAN, A.E., MOHLER, W. and HAN, D.K., 2003. Annexin I is an endogenous ligand that mediates apoptotic cell engulfment. Developmental cell, 4(4), pp. 587-598.

ASHIKARI-HADA, S., HABUCHI, H., KARIYA, Y. and KIMATA, K., 2005. Heparin regulates vascular endothelial growth factor165-dependent mitogenic activity, tube formation, and its receptor phosphorylation of human endothelial cells. Comparison of the effects of heparin and modified heparins. The Journal of biological chemistry, 280(36), pp. 31508-31515.

AUFDERHEIDE, E., CHIQUET-EHRISMANN, R. and EKBLOM, P., 1987. Epithelial-mesenchymal interactions in the developing kidney lead to expression of tenascin in the mesenchyme. J Cell Biol, 105(1), pp. 599-608.

AULD, G.C., RITCHIE, H., ROBBIE, L.A. and BOOTH, N.A., 2001. Thrombin upregulates tissue transglutaminase in endothelial cells: a potential role for tissue transglutaminase in stability of atherosclerotic plaque. Arteriosclerosis, Thrombosis, and Vascular Biology, 21(10), pp. 1689-1694.

AVALOS, A.M., VALDIVIA, A.D., MUNOZ, N., HERRERA-MOLINA, R., TAPIA, J.C., LAVANDERO, S., CHIONG, M., BURRIDGE, K., SCHNEIDER, P., QUEST, A.F. and LEYTON, L., 2009. Neuronal Thy-1 induces astrocyte adhesion by engaging syndecan-4 in a cooperative interaction with alphavbeta3 integrin that activates PKCalpha and RhoA. Journal of cell science, 122(Pt 19), pp. 3462-3471.

BABBEY, C.M., AHKTAR, N., WANG, E., CHEN, C.C., GRANT, B.D. and DUNN, K.W., 2006. Rab10 regulates membrane transport through early endosomes of polarized Madin-Darby canine kidney cells. Molecular biology of the cell, 17(7), pp. 3156-3175.

BABST, M., DAVIES, B.A. and KATZMANN, D.J., 2011. Regulation of Vps4 during MVB sorting and cytokinesis. Traffic, 12(10), pp. 1298-1305.

BABST, M., ODORIZZI, G., ESTEPA, E.J. and EMR, S.D., 2000. Mammalian tumor susceptibility gene 101 (TSG101) and the yeast homologue, Vps23p, both function in late endosomal trafficking. Traffic, 1(3), pp. 248-258.

BACIU, P.C., SAONCELLA, S., LEE, S.H., DENHEZ, F., LEUTHARDT, D. and GOETINCK, P.F., 2000. Syndesmos, a protein that interacts with the cytoplasmic domain of syndecan-4, mediates cell spreading and actin cytoskeletal organization. Journal of cell science, 113 Pt 2, pp. 315-324.

BACKHAUS, R., ZEHE, C., WEGEHINGEL, S., KEHLENBACH, A., SCHWAPPACH, B. and NICKEL, W., 2004. Unconventional protein secretion: membrane translocation of FGF-2 does not require protein unfolding. Journal of cell science, 117(Pt 9), pp. 1727-1736.

BAIETTI, M.F., ZHANG, Z., MORTIER, E., MELCHIOR, A., DEGEEST, G., GEERAERTS, A., IVARSSON, Y., DEPOORTERE, F., COOMANS, C. and VERMEIREN, E., 2012. Syndecan-syntenin-ALIX regulates the biogenesis of exosomes. Nature cell biology, 14(7), pp. 677-685.

BAKKER, E.N., PISTEA, A. and VANBAVEL, E., 2008. Transglutaminases in vascular biology: relevance for vascular remodeling and atherosclerosis. Journal of vascular research, 45(4), pp. 271-278.

BALANA, M.E., NIEDERGANG, F., SUBTIL, A., ALCOVER, A., CHAVRIER, P. and DAUTRY-VARSAT, A., 2005. ARF6 GTPase controls bacterial invasion by actin remodelling. Journal of cell science, 118(Pt 10), pp. 2201-2210.

BALDWIN, T.A. and OSTERGAARD, H.L., 2002. The protein-tyrosine phosphatase CD45 reaches the cell surface via golgi-dependent and -independent pathways. The Journal of biological chemistry, 277(52), pp. 50333-50340.

BALKLAVA, Z., VERDERIO, E., COLLIGHAN, R., GROSS, S., ADAMS, J. and GRIFFIN, M., 2002. Analysis of tissue transglutaminase function in the migration of Swiss 3T3 fibroblasts: the active-state conformation of the enzyme does not affect cell motility but is important for its secretion. The Journal of biological chemistry, 277(19), pp. 16567-16575.

BALLESTAR, E., BOIX-CHORNET, M. and FRANCO, L., 2001. Conformational changes in the nucleosome followed by the selective accessibility of histone glutamines in the transglutaminase reaction: effects of ionic strength. Biochemistry, 40(7), pp. 1922-1929.

BANDYOPADHYAY, U., KAUSHIK, S., VARTICOVSKI, L. and CUERVO, A.M., 2008. The chaperone-mediated autophagy receptor organizes in dynamic protein complexes at the lysosomal membrane. Molecular and cellular biology, 28(18), pp. 5747-5763.

BARNARD, R.J., MORGAN, A. and BURGOYNE, R.D., 1997. Stimulation of NSF ATPase activity by alpha-SNAP is required for SNARE complex disassembly and exocytosis. The Journal of cell biology, 139(4), pp. 875-883.

BARRES, C., BLANC, L., BETTE-BOBILLO, P., ANDRE, S., MAMOUN, R., GABIUS, H.J. and VIDAL, M., 2010. Galectin-5 is bound onto the surface of rat reticulocyte exosomes and modulates vesicle uptake by macrophages. Blood, 115(3), pp. 696-705.

BARSIGIAN, C., STERN, A.M. and MARTINEZ, J., 1991. Tissue (type II) transglutaminase covalently incorporates itself, fibrinogen, or fibronectin into high molecular weight complexes on the extracellular surface of isolated hepatocytes. Use of 2-[(2-oxopropyl)thio] imidazolium derivatives as cellular transglutaminase inactivators. The Journal of biological chemistry, 266(33), pp. 22501-22509.

BASILE, C., BRANDENBURG, V. and TORRES, P.A.U., 2016. Natural Vitamin D in Chronic Kidney Disease. Vitamin D in Chronic Kidney Disease. Springer, pp. 465-491.

BASS, M.D. and HUMPHRIES, M.J., 2002. Cytoplasmic interactions of syndecan-4 orchestrate adhesion receptor and growth factor receptor signalling. The Biochemical journal, 368(Pt 1), pp. 1-15.

BASS, M.D., MORGAN, M.R., ROACH, K.A., SETTLEMAN, J., GORYACHEV, A.B. and HUMPHRIES, M.J., 2008. p190RhoGAP is the convergence point of adhesion signals from alpha 5 beta 1 integrin and syndecan-4. The Journal of cell biology, 181(6), pp. 1013-1026.

BASS, M.D., ROACH, K.A., MORGAN, M.R., MOSTAFAVI-POUR, Z., SCHOEN, T., MURAMATSU, T., MAYER, U., BALLESTREM, C., SPATZ, J.P. and HUMPHRIES, M.J., 2007. Syndecan-4-dependent Rac1 regulation determines directional migration in response to the extracellular matrix. The Journal of cell biology, 177(3), pp. 527-538.

BASS, M.D., WILLIAMSON, R.C., NUNAN, R.D., HUMPHRIES, J.D., BYRON, A., MORGAN, M.R., MARTIN, P. and HUMPHRIES, M.J., 2011. A syndecan-4 hair trigger initiates wound healing through caveolin-and RhoG-regulated integrin endocytosis. Developmental cell, 21(4), pp. 681-693.

BATTAGLIA, G., FARRACE, M.G., MASTROBERARDINO, P.G., VITI, I., FIMIA, G.M., VAN BEEUMEN, J., DEVREESE, B., MELINO, G., MOLINARO, G. and BUSCETI, C.L., 2007. Transglutaminase 2 ablation leads to defective function of mitochondrial respiratory complex I affecting neuronal vulnerability in experimental models of extrapyramidal disorders. Journal of neurochemistry, 100(1), pp. 36-49.

BAZZI, C., PETRINI, C., RIZZA, V., ARRIGO, G., NAPODANO, P., PAPARELLA, M. and D'AMICO, G., 2002. Urinary N-acetyl-beta-glucosaminidase excretion is a marker of tubular cell dysfunction and a predictor of outcome in primary glomerulonephritis. Nephrology, dialysis, transplantation : official publication of the European Dialysis and Transplant Association - European Renal Association, 17(11), pp. 1890-1896.

BECKERS, C.J., BLOCK, M.R., GLICK, B.S., ROTHMAN, J.E. and BALCH, W.E., 1989. Vesicular transport between the endoplasmic reticulum and the Golgi stack requires the NEM-sensitive fusion protein.

BEGG, G.E., CARRINGTON, L., STOKES, P.H., MATTHEWS, J.M., WOUTERS, M.A., HUSAIN, A., LORAND, L., IISMAA, S.E. and GRAHAM, R.M., 2006. Mechanism of allosteric regulation of transglutaminase 2 by GTP. Proceedings of the National Academy of Sciences of the United States of America, 103(52), pp. 19683-19688.

BELKIN, A.M., 2011. Extracellular TG2: emerging functions and regulation. FEBS Journal, 278(24), pp. 4704-4716.

BELKIN, A.M., AKIMOV, S.S., ZARITSKAYA, L.S., RATNIKOV, B.I., DERYUGINA, E.I. and STRONGIN, A.Y., 2001. Matrix-dependent proteolysis of surface transglutaminase by membrane-type metalloproteinase regulates cancer cell adhesion and locomotion. The Journal of biological chemistry, 276(21), pp. 18415-18422.

BELL, S.E., MAVILA, A., SALAZAR, R., BAYLESS, K.J., KANAGALA, S., MAXWELL, S.A. and DAVIS, G.E., 2001. Differential gene expression during capillary morphogenesis in 3D collagen matrices: regulated expression of genes involved in basement membrane matrix assembly, cell cycle progression, cellular differentiation and G-protein signaling. Journal of cell science, 114(Pt 15), pp. 2755-2773.

BERGIN, D.A., HURLEY, K., MCELVANEY, N.G. and REEVES, E.P., 2012. Alpha-1 antitrypsin: a potent anti-inflammatory and potential novel therapeutic agent. Archivum Immunologiae et Therapiae Experimentalis, 60(2), pp. 81-97.

BERNASSOLA, F., FEDERICI, M., CORAZZARI, M., TERRINONI, A., HRIBAL, M.L., DE LAURENZI, V., RANALLI, M., MASSA, O., SESTI, G., MCLEAN, W.H., CITRO, G., BARBETTI, F. and MELINO, G., 2002. Role of transglutaminase 2 in glucose tolerance: knockout mice studies and a putative mutation in a MODY patient. FASEB journal : official publication of the Federation of American Societies for Experimental Biology, 16(11), pp. 1371-1378.

BERNFIELD, M., GÖTTE, M., PARK, P.W., REIZES, O., FITZGERALD, M.L., LINCECUM, J. and ZAKO, M., 1999. Functions of cell surface heparan sulfate proteoglycans. Annual Review of Biochemistry, 68(1), pp. 729-777.

BERTANI, G., 1951. Studies on lysogenesis. I. The mode of phage liberation by lysogenic Escherichia coli. Journal of Bacteriology, 62(3), pp. 293-300.

BERTHELOT, L., PAPISTA, C., MACIEL, T.T., BIARNES-PELICOT, M., TISSANDIE, E., WANG, P.H., TAMOUZA, H., JAMIN, A., BEX-COUDRAT, J., GESTIN, A., BOUMEDIENE, A., ARCOS-FAJARDO, M., ENGLAND, P., PILLEBOUT, E., WALKER, F., DAUGAS, E., VRTOSVNIK, F., FLAMANT, M., BENHAMOU, M., COGNE, M., MOURA, I.C. and MONTEIRO, R.C., 2012. Transglutaminase is essential for IgA nephropathy development acting through IgA receptors. The Journal of experimental medicine, 209(4), pp. 793-806.

BHARADWAJ, A., BYDOUN, M., HOLLOWAY, R. and WAISMAN, D., 2013. Annexin A2 heterotetramer: structure and function. International journal of molecular sciences, 14(3), pp. 6259-6305.

BIANCO, F., PERROTTA, C., NOVELLINO, L., FRANCOLINI, M., RIGANTI, L., MENNA, E., SAGLIETTI, L., SCHUCHMAN, E.H., FURLAN, R., CLEMENTI, E., MATTEOLI, M. and VERDERIO, C., 2009. Acid sphingomyelinase activity triggers microparticle release from glial cells. The EMBO journal, 28(8), pp. 1043-1054.

BING, P., MAODE, L., LI, F. and SHENG, H., 2006. Expression of renal transforming growth factor-β and its receptors in a rat model of chronic cyclosporine-induced nephropathy, Transplantation proceedings 2006, Elsevier, pp. 2176-2179.

BISHOP, J.R., SCHUKSZ, M. and ESKO, J.D., 2007. Heparan sulphate proteoglycans fine-tune mammalian physiology. Nature, 446(7139), pp. 1030-1037.

REFERENCES

BLEYER, A.J., ZIVNA, M. and KMOCH, S., 2011. Uromodulin-associated kidney disease. Nephron.Clinical practice, 118(1), pp. c31-6.

BLOCK, M.R., GLICK, B.S., WILCOX, C.A., WIELAND, F.T. and ROTHMAN, J.E., 1988. Purification of an N-ethylmaleimide-sensitive protein catalyzing vesicular transport. Proceedings of the National Academy of Sciences of the United States of America, 85(21), pp. 7852-7856.

BLUMBERG, A. and BURGI, W., 1987. Behavior of beta 2-microglobulin in patients with chronic renal failure undergoing hemodialysis, hemodiafiltration and continuous ambulatory peritoneal dialysis (CAPD). Clinical nephrology, 27(5), pp. 245-249.

BOBRIE, A., COLOMBO, M., RAPOSO, G. and THÉRY, C., 2011. Exosome secretion: molecular mechanisms and roles in immune responses. Traffic, 12(12), pp. 1659-1668.

BOCHUD, M., 2015. On the rationale of population screening for chronic kidney disease: a public health perspective. Public health reviews, 36(1), pp. 1.

BOES, E., FLISER, D., RITZ, E., KONIG, P., LHOTTA, K., MANN, J.F., MULLER, G.A., NEYER, U., RIEGEL, W., RIEGLER, P. and KRONENBERG, F., 2006. Apolipoprotein A-IV predicts progression of chronic kidney disease: the mild to moderate kidney disease study. Journal of the American Society of Nephrology : JASN, 17(2), pp. 528-536.

BOTTINGER, E.P. and BITZER, M., 2002. TGF-beta signaling in renal disease. Journal of the American Society of Nephrology : JASN, 13(10), pp. 2600-2610.

BÖTTINGER, E.P., 2007. TGF-β in renal injury and disease, Seminars in nephrology 2007, Elsevier, pp. 309-320.

BROEKHUIZEN, L., LEMKES, B., MOOIJ, H.L., MEUWESE, M.C., VERBERNE, H., HOLLEMAN, F., SCHLINGEMANN, R.O., NIEUWDORP, M., STROES, E.S. and VINK, H., 2010. Effect of sulodexide on endothelial glycocalyx and vascular permeability in patients with type 2 diabetes mellitus. Diabetologia, 53(12), pp. 2646-2655.

BRONNER, F., 2001. Extracellular and intracellular regulation of calcium homeostasis. The Scientific World Journal, 1, pp. 919-925.

BROOKS, R., WILLIAMSON, R.C. and BASS, M.D., 2012. Syndecan-4 independently regulates multiple small GTPases to promote fibroblast migration during wound healing. Small GTPases, 3(2), pp. 73-79.

BROSIUS, F.C. and PENNATHUR, S., 2013. How to find a prognostic biomarker for progressive diabetic nephropathy. Kidney international, 83(6), pp. 996-998.

BROUGH, D. and ROTHWELL, N.J., 2007. Caspase-1-dependent processing of pro-interleukin-1beta is cytosolic and precedes cell death. Journal of cell science, 120(Pt 5), pp. 772-781.

BROUGH, D., LE FEUVRE, R.A., WHEELER, R.D., SOLOVYOVA, N., HILFIKER, S., ROTHWELL, N.J. and VERKHRATSKY, A., 2003. Ca2+ stores and Ca2+ entry differentially contribute to the release of IL-1 beta and IL-1 alpha from murine macrophages. Journal of immunology (Baltimore, Md.: 1950), 170(6), pp. 3029-3036.

BROUWERS, J.F., AALBERTS, M., JANSEN, J.W., VAN NIEL, G., WAUBEN, M.H., STOUT, T.A., HELMS, J.B. and STOORVOGEL, W., 2013. Distinct lipid compositions of two types of human prostasomes. Proteomics, 13(10-11), pp. 1660-1666.

BROWN, F.D., ROZELLE, A.L., YIN, H.L., BALLA, T. and DONALDSON, J.G., 2001. Phosphatidylinositol 4,5-bisphosphate and Arf6-regulated membrane traffic. The Journal of cell biology, 154(5), pp. 1007-1017.

BROWNE, L.E., COMPAN, V., BRAGG, L. and NORTH, R.A., 2013. P2X7 receptor channels allow direct permeation of nanometer-sized dyes. The Journal of neuroscience : the official journal of the Society for Neuroscience, 33(8), pp. 3557-3566.

BRUCATO, S., HARDUIN-LEPERS, A., GODARD, F., BOCQUET, J. and VILLERS, C., 2000. Expression of glypican-1, syndecan-1 and syndecan-4 mRNAs protein kinase C-regulated in rat immature Sertoli cells by semi-quantitative RT-PCR analysis. Biochimica et Biophysica Acta (BBA)-General Subjects, 1474(1), pp. 31-40.

BRUNS, C., MCCAFFERY, J.M., CURWIN, A.J., DURAN, J.M. and MALHOTRA, V., 2011. Biogenesis of a novel compartment for autophagosome-mediated unconventional protein secretion. The Journal of cell biology, 195(6), pp. 979-992.

BUCCI, C., PARTON, R.G., MATHER, I.H., STUNNENBERG, H., SIMONS, K., HOFLACK, B. and ZERIAL, M., 1992. The small GTPase rab5 functions as a regulatory factor in the early endocytic pathway. Cell, 70(5), pp. 715-728.

BUCKLEY, C.D., PILLING, D., HENRIQUEZ, N.V., PARSONAGE, G., THRELFALL, K., SCHEEL-TOELLNER, D., SIMMONS, D.L., AKBAR, A.N., LORD, J.M. and SALMON, M., 1999. RGD peptides induce apoptosis by direct caspase-3 activation. Nature, 397(6719), pp. 534-539.

BURHAN, I., FURINI, G., LORTAT-JACOB, H., ATOBATELE, A.G., SCARPELLINI, A., SCHROEDER, N., ATKINSON, J., MAAMRA, M., NUTTER, F.H., WATSON, P., VINCIGUERRA, M., JOHNSON, T.S. and VERDERIO, E.A., 2016. Interplay between transglutaminases and heparan sulphate in progressive renal scarring. Scientific reports, 6, pp. 31343.

BURNIER, L., FONTANA, P., KWAK, B.R. and ANGELILLO-SCHERRER, A., 2009. Cell-derived microparticles in haemostasis and vascular medicine. Thromb Haemost, 101(3), pp. 439-451.

BUSSEY, H., 1988. Proteases and the processing of precursors to secreted proteins in yeast. Yeast, 4(1), pp. 17-26.

CABEZAS, A., BACHE, K.G., BRECH, A. and STENMARK, H., 2005. Alix regulates cortical actin and the spatial distribution of endosomes. Journal of cell science, 118(Pt 12), pp. 2625-2635.

CABRAL, M., ANJARD, C., MALHOTRA, V., LOOMIS, W.F. and KUSPA, A., 2010. Unconventional secretion of AcbA in Dictyostelium discoideum through a vesicular intermediate. Eukaryotic cell, 9(7), pp. 1009-1017.

CAMPISI, A., CACCAMO, D., RACITI, G., CANNAVO, G., MACAIONE, V., CURRO, M., MACAIONE, S., VANELLA, A. and IENTILE, R., 2003. Glutamate-induced increases in transglutaminase activity in primary cultures of astroglial cells. Brain research, 978(1), pp. 24-30.

CANDI, E., MELINO, G., LAHM, A., CECI, R., ROSSI, A., KIM, I.G., CIANI, B. and STEINERT, P.M., 1998. Transglutaminase 1 Mutations in Lamellar Ichthyosis LOSS OF ACTIVITY DUE TO FAILURE OF ACTIVATION BY PROTEOLYTIC PROCESSING. Journal of Biological Chemistry, 273(22), pp. 13693-13702.

CANDI, E., ODDI, S., PARADISI, A., TERRINONI, A., RANALLI, M., TEOFOLI, P., CITRO, G., SCARPATO, S., PUDDU, P. and MELINO, G., 2002. Expression of transglutaminase 5 in normal and pathologic human epidermis. Journal of investigative dermatology, 119(3), pp. 670-677.

CANDI, E., ODDI, S., TERRINONI, A., PARADISI, A., RANALLI, M., FINAZZI-AGRO, A. and MELINO, G., 2001. Transglutaminase 5 cross-links loricrin, involucrin, and small proline-rich proteins in vitro. The Journal of biological chemistry, 276(37), pp. 35014-35023.

CANDI, E., PARADISI, A., TERRINONI, A., PIETRONI, V., ODDI, S., CADOT, B., JOGINI, V., MEIYAPPAN, M., CLARDY, J., FINAZZI-AGRO, A. and MELINO, G., 2004. Transglutaminase 5 is regulated by guanine-adenine nucleotides. The Biochemical journal, 381(Pt 1), pp. 313-319.

CANDI, E., SCHMIDT, R. and MELINO, G., 2005. The cornified envelope: a model of cell death in the skin. Nature reviews Molecular cell biology, 6(4), pp. 328-340.

CAO, L., PETRUSCA, D.N., SATPATHY, M., NAKSHATRI, H., PETRACHE, I. and MATEI, D., 2008. Tissue transglutaminase protects epithelial ovarian cancer cells from cisplatin-induced apoptosis by promoting cell survival signaling. Carcinogenesis, 29(10), pp. 1893-1900.

CAO, L., SHAO, M., SCHILDER, J., GUISE, T., MOHAMMAD, K. and MATEI, D., 2012. Tissue transglutaminase links TGF-β, epithelial to mesenchymal transition and a stem cell phenotype in ovarian cancer. Oncogene, 31(20), pp. 2521-2534.

CARDIN, A.D. and WEINTRAUB, H.J., 1989. Molecular modeling of protein-glycosaminoglycan interactions. Arteriosclerosis (Dallas, Tex.), 9(1), pp. 21-32.

CAREY, D.J., 1997. Syndecans: multifunctional cell-surface co-receptors. Biochemical Journal, 327(1), pp. 1-16.

CAREY, D.J., CONNER, K., ASUNDI, V.K., O'MAHONY, D.J., STAHL, R.C., SHOWALTER, L., CIZMECI-SMITH, G., HARTMAN, J. and ROTHBLUM, L.I., 1997. cDNA cloning, genomic organization, and in vivo expression of rat N-syndecan. Journal of Biological Chemistry, 272(5), pp. 2873-2879.

CARNELL, M., ZECH, T., CALAMINUS, S.D., URA, S., HAGEDORN, M., JOHNSTON, S.A., MAY, R.C., SOLDATI, T., MACHESKY, L.M. and INSALL, R.H., 2011. Actin polymerization driven by WASH causes V-ATPase retrieval and vesicle neutralization before exocytosis. The Journal of cell biology, 193(5), pp. 831-839.

CARSON, R.C., JUSZCZAK, M., DAVENPORT, A. and BURNS, A., 2009. Is maximum conservative management an equivalent treatment option to dialysis for elderly patients with significant comorbid disease? Clinical journal of the American Society of Nephrology : CJASN, 4(10), pp. 1611-1619.

CASADIO, R., POLVERINI, E., MARIANI, P., SPINOZZI, F., CARSUGHI, F., FONTANA, A., DE LAURETO, P.P., MATTEUCCI, G. and BERGAMINI, C.M., 1999. The structural basis for the regulation of tissue transglutaminase by calcium ions. European Journal of Biochemistry, 262(3), pp. 672-679.

CASSIDY, A.J., VAN STEENSEL, M.A., STEIJLEN, P.M., VAN GEEL, M., VAN DER VELDEN, J., MORLEY, S.M., TERRINONI, A., MELINO, G., CANDI, E. and MCLEAN, W.I., 2005. A homozygous missense mutation in TGM5 abolishes epidermal transglutaminase 5 activity and causes acral peeling skin syndrome. The American Journal of Human Genetics, 77(6), pp. 909-917.

CASTELHANO, A.L., DEYOUNG, L.M., KRANTZ, A., PLIURA, D.H. and VENUTI, M.C., 1990. 3, 5-substituted 4, 5-dihydroisoxazoles as transglutaminase inhibitors, .

CEBALLOS-PICOT, I., WITKO-SARSAT, V., MERAD-BOUDIA, M., NGUYEN, A.T., THÉVENIN, M., JAUDON, M.C., ZINGRAFF, J., VERGER, C., JINGERS, P. and DESCAMPS-LATSCHA, B., 1996. Glutathione antioxidant system as a marker of oxidative stress in chronic renal failure. Free Radical Biology and Medicine, 21(6), pp. 845-853.

CERIELLO, A., MOROCUTTI, A., MERCURI, F., QUAGLIARO, L., MORO, M., DAMANTE, G. and VIBERTI, G.C., 2000. Defective intracellular antioxidant enzyme production in type 1 diabetic patients with nephropathy. Diabetes, 49(12), pp. 2170-2177.

CERNARO, V., BOLIGNANO, D., BUEMI, A., LACQUANITI, A., SANTORO, D. and BUEMI, M., 2016. Overview of Neutrophil Gelatinase-Associated Lipocalin (NGAL) as a Biomarker in Nephrology. Biomarkers in Kidney Disease, , pp. 205-227.

CHALMIN, F., LADOIRE, S., MIGNOT, G., VINCENT, J., BRUCHARD, M., REMY-MARTIN, J.P., BOIREAU, W., ROULEAU, A., SIMON, B., LANNEAU, D., DE THONEL, A., MULTHOFF, G., HAMMAN, A., MARTIN, F., CHAUFFERT, B., SOLARY, E., ZITVOGEL, L., GARRIDO, C., RYFFEL, B., BORG, C., APETOH, L., REBE, C. and GHIRINGHELLI, F., 2010. Membrane-associated Hsp72 from tumor-derived exosomes mediates STAT3-dependent immunosuppressive function of mouse and human myeloid-derived suppressor cells. The Journal of clinical investigation, 120(2), pp. 457-471.

CHANG, J.W., LEE, S.H., LU, Y. and YOO, Y.J., 2006. Transforming growth factor-β1 induces the non-classical secretion of peroxiredoxin-I in A549 cells. Biochemical and biophysical research communications, 345(1), pp. 118-123.

CHASSEROT-GOLAZ, S., VITALE, N., UMBRECHT-JENCK, E., KNIGHT, D., GERKE, V. and BADER, M.F., 2005. Annexin 2 promotes the formation of lipid microdomains required for calcium-regulated exocytosis of dense-core vesicles. Molecular biology of the cell, 16(3), pp. 1108-1119.

CHAU, D.Y., COLLIGHAN, R.J., VERDERIO, E.A., ADDY, V.L. and GRIFFIN, M., 2005. The cellular response to transglutaminase-cross-linked collagen. Biomaterials, 26(33), pp. 6518-6529.

CHEADLE, C., VAWTER, M.P., FREED, W.J. and BECKER, K.G., 2003. Analysis of microarray data using Z score transformation. The Journal of molecular diagnostics, 5(2), pp. 73-81.

CHEN, D., HUANG, H.C. and YU, L., 2005. Expression and implication of tissue transglutaminase and connective tissue growth factor at fibrotic tubulointerstitium in kidneys from UUO rats. Beijing da xue xue bao.Yi xue ban = Journal of Peking University.Health sciences, 37(2), pp. 143-146.

CHEN, E., HERMANSON, S. and EKKER, S.C., 2004. Syndecan-2 is essential for angiogenic sprouting during zebrafish development. Blood, 103(5), pp. 1710-1719.

CHEN, J., MUNTNER, P., HAMM, L.L., JONES, D.W., BATUMAN, V., FONSECA, V., WHELTON, P.K. and HE, J., 2004. The metabolic syndrome and chronic kidney disease in US adults. Annals of Internal Medicine, 140(3), pp. 167-174.

CHEN, K. and WILLIAMS, K.J., 2013. Molecular mediators for raft-dependent endocytosis of syndecan-1, a highly conserved, multifunctional receptor. The Journal of biological chemistry, 288(20), pp. 13988-13999.

CHEN, L., KLASS, C. and WOODS, A., 2004. Syndecan-2 regulates transforming growth factor-beta signaling. The Journal of biological chemistry, 279(16), pp. 15715-15718.

CHEN, N.X., O'NEILL, K., CHEN, X., KIATTISUNTHORN, K., GATTONE, V.H. and MOE, S.M., 2013. Transglutaminase 2 accelerates vascular calcification in chronic kidney disease. American Journal of Nephrology, 37(3), pp. 191-198.

CHEN, P., ABACHERLI, L.E., NADLER, S.T., WANG, Y., LI, Q. and PARKS, W.C., 2009. MMP7 shedding of syndecan-1 facilitates re-epithelialization by affecting α 2 β 1 integrin activation. PloS one, 4(8), pp. e6565.

CHEN, Q., SIVAKUMAR, P., BARLEY, C., PETERS, D.M., GOMES, R.R., FARACH-CARSON, M.C. and DALLAS, S.L., 2007. Potential role for heparan sulfate proteoglycans in regulation of transforming growth factor-beta (TGF-beta) by modulating assembly of latent TGF-beta-binding protein-1. The Journal of biological chemistry, 282(36), pp. 26418-26430.

CHEN, Y., SHI-WEN, X., VAN BEEK, J., KENNEDY, L., MCLEOD, M., RENZONI, E.A., BOU-GHARIOS, G., WILCOX-ADELMAN, S., GOETINCK, P.F. and EASTWOOD, M., 2005. Matrix contraction by dermal fibroblasts requires transforming growth factor-β/activin-linked kinase 5, heparan sulfate-containing proteoglycans, and MEK/ERK: insights into pathological scarring in chronic fibrotic disease. The American journal of pathology, 167(6), pp. 1699-1711.

CHEN, Y., WANG, Y., ZHANG, J., DENG, Y., JIANG, L., SONG, E., WU, X.S., HAMMER, J.A., XU, T. and LIPPINCOTT-SCHWARTZ, J., 2012. Rab10 and myosin-Va mediate insulin-stimulated GLUT4 storage vesicle translocation in adipocytes. The Journal of cell biology, 198(4), pp. 545-560.

CHEN, Y., ZHANG, W., WANG, W., YU, X., WANG, Y., ZHANG, M. and CHEN, N., 2014. Role of moesin in renal fibrosis. PloS one, 9(11), pp. e112936.

CHENG, C., RIFAI, A., KA, S., SHUI, H., LIN, Y., LEE, W. and CHEN, A., 2005. Calcium-binding proteins annexin A2 and S100A6 are sensors of tubular injury and recovery in acute renal failure. Kidney international, 68(6), pp. 2694-2703.

CHENG, S. and LOVETT, D.H., 2003. Gelatinase A (MMP-2) is necessary and sufficient for renal tubular cell epithelial-mesenchymal transformation. The American journal of pathology, 162(6), pp. 1937-1949.

CHENG, T., HITOMI, K., VAN VLIJMEN-WILLEMS, I.M., DE JONGH, G.J., YAMAMOTO, K., NISHI, K., WATTS, C., REINHECKEL, T., SCHALKWIJK, J. and ZEEUWEN, P.L., 2006. Cystatin M/E is a high affinity inhibitor of cathepsin V and cathepsin L by a reactive site that is distinct from the legumain-binding site. A novel clue for the role of cystatin M/E in epidermal cornification. The Journal of biological chemistry, 281(23), pp. 15893-15899.

CHEVALIER, R.L., 1990. Counterbalance in functional adaptation to ureteral obstruction during development. Pediatric Nephrology, 4(4), pp. 442-444.

CHEVALIER, R.L., CHUNG, K.H., SMITH, C.D., FICENEC, M. and GOMEZ, A.R., 1996. Renal apoptosis and clusterin following ureteral obstruction: the role of maturation. The Journal of urology, 156(4), pp. 1474-1479.

CHEVALIER, R.L., FORBES, M.S. and THORNHILL, B.A., 2009. Ureteral obstruction as a model of renal interstitial fibrosis and obstructive nephropathy. Kidney international, 75(11), pp. 1145-1152.

CHIEN, J.W., RICHARDS, T.J., GIBSON, K.F., ZHANG, Y., LINDELL, K.O., SHAO, L., LYMAN, S.K., ADAMKEWICZ, J.I., SMITH, V., KAMINSKI, N. and O'RIORDAN, T., 2014. Serum lysyl oxidase-like 2 levels and idiopathic pulmonary fibrosis disease progression. The European respiratory journal, 43(5), pp. 1430-1438.

CHOI, J., NAM, S. and CHA, J., 2014. Invasion of Calponin-positive Glomerular Parietal Epithelial Cells into Glomerular Tuft Is Related to the Development of Glomerulosclerosis. Applied Microscopy, 44(4), pp. 117-122.

CHOI, Y., KIM, S., LEE, J., KO, S., LEE, W., HAN, I., WOODS, A. and OH, E., 2008. The oligomeric status of syndecan-4 regulates syndecan-4 interaction with α-actinin. European journal of cell biology, 87(10), pp. 807-815.

CHONG, L.D., TRAYNOR-KAPLAN, A., BOKOCH, G.M. and SCHWARTZ, M.A., 1994. The small GTP-binding protein Rho regulates a phosphatidylinositol 4-phosphate 5-kinase in mammalian cells. Cell, 79(3), pp. 507-513.

CHOU, C.Y., STREETS, A.J., WATSON, P.F., HUANG, L., VERDERIO, E.A. and JOHNSON, T.S., 2011. A crucial sequence for transglutaminase type 2 extracellular trafficking in renal tubular epithelial cells lies in its N-terminal beta-sandwich domain. The Journal of biological chemistry, 286(31), pp. 27825-27835.

CHRISTIANSON, H.C. and BELTING, M., 2014. Heparan sulfate proteoglycan as a cell-surface endocytosis receptor. Matrix Biology, 35, pp. 51-55.

CHRISTIANSON, H.C., SVENSSON, K.J., VAN KUPPEVELT, T.H., LI, J.P. and BELTING, M., 2013. Cancer cell exosomes depend on cell-surface heparan sulfate proteoglycans for their internalization and functional activity. Proceedings of the National Academy of Sciences of the United States of America, 110(43), pp. 17380-17385.

CITRON, B.A., SANTACRUZ, K.S., DAVIES, P.J. and FESTOFF, B.W., 2001. Intron-exon swapping of transglutaminase mRNA and neuronal Tau aggregation in Alzheimer's disease. The Journal of biological chemistry, 276(5), pp. 3295-3301.

CIZMECI-SMITH, G., LANGAN, E., YOUKEY, J., SHOWALTER, L.J. and CAREY, D.J., 1997. Syndecan-4 is a primary-response gene induced by basic fibroblast growth factor and arterial injury in vascular smooth muscle cells. Arteriosclerosis, Thrombosis, and Vascular Biology, 17(1), pp. 172-180.

CLAYTON, A., THOMAS, J., THOMAS, G.J., DAVIES, M. and STEADMAN, R., 2001. Cell surface heparan sulfate proteoglycans control the response of renal interstitial fibroblasts to fibroblast growth factor-2. Kidney international, 59(6), pp. 2084-2094.

CLAYTON, A., TURKES, A., NAVABI, H., MASON, M.D. and TABI, Z., 2005. Induction of heat shock proteins in B-cell exosomes. Journal of cell science, 118(Pt 16), pp. 3631-3638.

COCUCCI, E. and MELDOLESI, J., 2015. Ectosomes and exosomes: shedding the confusion between extracellular vesicles. Trends in cell biology, 25(6), pp. 364-372.

COLLINS, B.C., HUNTER, C.L., LIU, Y., SCHILLING, B., ROSENBERGER, G.R., BADER, S.L., CHAN, D.W., GIBSON, B.W., GINGRAS, A. and HELD, J.M., 2016. Multi-laboratory assessment of reproducibility, qualitative and quantitative performance of SWATH-mass spectrometry. bioRxiv, , pp. 074567.

COLOMBO, M., MOITA, C., VAN NIEL, G., KOWAL, J., VIGNERON, J., BENAROCH, P., MANEL, N., MOITA, L.F., THERY, C. and RAPOSO, G., 2013. Analysis of ESCRT functions in exosome biogenesis, composition and secretion highlights the heterogeneity of extracellular vesicles. Journal of cell science, 126(Pt 24), pp. 5553-5565.

CONNER, S.D. and SCHMID, S.L., 2003. Regulated portals of entry into the cell. Nature, 422(6927), pp. 37-44.

COOPER, D.N. and BARONDES, S.H., 1990. Evidence for export of a muscle lectin from cytosol to extracellular matrix and for a novel secretory mechanism. The Journal of cell biology, 110(5), pp. 1681-1691.

COOPER, G.M., 2000. Microtubule Motors and Movements.

CORDELLA-MIELE, E., MIELE, L. and MUKHERJEE, A.B., 1990. A novel transglutaminase-mediated post-translational modification of phospholipase A2 dramatically increases its catalytic activity. The Journal of biological chemistry, 265(28), pp. 17180-17188.

CORDELLA-MIELE, E., MIELE, L., BENINATI, S. and MUKHERJEE, A.B., 1993. Transglutaminase-catalyzed incorporation of polyamines into phospholipase A2. Journal of Biochemistry, 113(2), pp. 164-173.

CORESH, J., SELVIN, E., STEVENS, L.A., MANZI, J., KUSEK, J.W., EGGERS, P., VAN LENTE, F. and LEVEY, A.S., 2007. Prevalence of chronic kidney disease in the United States. Jama, 298(17), pp. 2038-2047.

CORNELISON, D.D., WILCOX-ADELMAN, S.A., GOETINCK, P.F., RAUVALA, H., RAPRAEGER, A.C. and OLWIN, B.B., 2004. Essential and separable roles for Syndecan-3 and Syndecan-4 in skeletal muscle development and regeneration. Genes & development, 18(18), pp. 2231-2236.

COUCHMAN, J.R., 2003. Syndecans: proteoglycan regulators of cell-surface microdomains? Nature Reviews Molecular Cell Biology, 4(12), pp. 926-938.

COUCHMAN, J.R., CHEN, L. and WOODS, A., 2001. Syndecans and cell adhesion. International review of cytology, 207, pp. 113-150.

COUCHMAN, J.R., GOPAL, S., LIM, H.C., NØRGAARD, S. and MULTHAUPT, H.A., 2015. Fell-Muir Lecture: Syndecans: from peripheral coreceptors to mainstream regulators of cell behaviour. International journal of experimental pathology, 96(1), pp. 1-10.

COUCHMAN, J.R., VOGT, S., LIM, S.T., LIM, Y., OH, E.S., PRESTWICH, G.D., THEIBERT, A., LEE, W. and WOODS, A., 2002. Regulation of inositol phospholipid binding and signaling through syndecan-4. The Journal of biological chemistry, 277(51), pp. 49296-49303.

CREUTZ, C.E. and SNYDER, S.L., 2005. Interactions of annexins with the mu subunits of the clathrin assembly proteins. Biochemistry, 44(42), pp. 13795-13806.

CSŐSZ, É, MESKÓ, B. and FÉSÜS, L., 2009. Transdab wiki: the interactive transglutaminase substrate database on web 2.0 surface. Amino acids, 36(4), pp. 615-617.

CULLEN, P.J. and KORSWAGEN, H.C., 2012. Sorting nexins provide diversity for retromer-dependent trafficking events. Nature cell biology, 14(1), pp. 29-37.

CUMMINS, T.D., BARATI, M.T., COVENTRY, S.C., SALYER, S.A., KLEIN, J.B. and POWELL, D.W., 2010. Quantitative mass spectrometry of diabetic kidney tubules identifies GRAP as a novel regulator of TGF-β signaling. Biochimica et Biophysica Acta (BBA)-Proteins and Proteomics, 1804(4), pp. 653-661.

DA SILVA LODGE, M., EL NAHAS, M. and JOHNSON, T., 2013. Urinary transglutaminase 2 as a potential biomarker of chronic kidney disease detection and progression. The Lancet, 381, pp. S33.

DAI, R.M. and LI, C.H., 2001. Valosin-containing protein is a multi-ubiquitin chain-targeting factor required in ubiquitin–proteasome degradation. Nature cell biology, 3(8), pp. 740-744.

DANIEL, C., LÜDKE, A., WAGNER, A., TODOROV, V.T., HOHENSTEIN, B. and HUGO, C., 2012. Transgelin is a marker of repopulating mesangial cells after injury and promotes their proliferation and migration. Laboratory investigation, 92(6), pp. 812-826.

DANIEL, C., WIEDE, J., KRUTZSCH, H.C., RIBEIRO, S.M., D ROBERTS, D., MURPHY-ULLRICH, J.E. and HUGO, C., 2004. Thrombospondin-1 is a major activator of TGF-β in fibrotic renal disease in the rat in vivo. Kidney international, 65(2), pp. 459-468.

DANIELSEN, E.M., VAN DEURS, B. and HANSEN, G.H., 2003. "Nonclassical" secretion of annexin A2 to the lumenal side of the enterocyte brush border membrane. Biochemistry, 42(49), pp. 14670-14676.

DARBY, I.A. and HEWITSON, T.D., 2007. Fibroblast differentiation in wound healing and fibrosis. International review of cytology, 257, pp. 143-179.

DARDIK, R. and INBAL, A., 2006. Complex formation between tissue transglutaminase II (tTG) and vascular endothelial growth factor receptor 2 (VEGFR-2): proposed mechanism for modulation of endothelial cell response to VEGF. Experimental cell research, 312(16), pp. 2973-2982.

DARDIK, R., LOSCALZO, J. and INBAL, A., 2006. Factor XIII (FXIII) and angiogenesis. Journal of Thrombosis and Haemostasis, 4(1), pp. 19-25.

DAVID, G. and ZIMMERMANN, P., 2015. Heparanase taylors syndecan for exosome production. Molecular & Cellular Oncology, (just-accepted), pp. 00-00.

DAVID, G., 1993. Integral membrane heparan sulfate proteoglycans. FASEB journal : official publication of the Federation of American Societies for Experimental Biology, 7(11), pp. 1023-1030.

DE CURTIS, I. and MELDOLESI, J., 2012. Cell surface dynamics - how Rho GTPases orchestrate the interplay between the plasma membrane and the cortical cytoskeleton. Journal of cell science, 125(Pt 19), pp. 4435-4444.

DE GASSART, A., GEMINARD, C., FEVRIER, B., RAPOSO, G. and VIDAL, M., 2003. Lipid raft-associated protein sorting in exosomes. Blood, 102(13), pp. 4336-4344.

DE JONG, P.E., VAN DER VELDE, M., GANSEVOORT, R.T. and ZOCCALI, C., 2008. Screening for chronic kidney disease: where does Europe go? Clinical journal of the American Society of Nephrology : CJASN, 3(2), pp. 616-623.

DE LAURENZI, V. and MELINO, G., 2001. Gene disruption of tissue transglutaminase. Molecular and cellular biology, 21(1), pp. 148-155.

DE MATTEIS, M.A. and MORROW, J.S., 2000. Spectrin tethers and mesh in the biosynthetic pathway. Journal of cell science, 113 (Pt 13)(Pt 13), pp. 2331-2343.

DE ROSSI, G., EVANS, A.R., KAY, E., WOODFIN, A., MCKAY, T.R., NOURSHARGH, S. and WHITEFORD, J.R., 2014. Shed syndecan-2 inhibits angiogenesis. Journal of cell science, 127(Pt 21), pp. 4788-4799.

DEASEY, S., SHANMUGASUNDARAM, S. and NURMINSKAYA, M., 2013. Tissue-specific responses to loss of transglutaminase 2. Amino acids, 44(1), pp. 179-187.

DEBELLE, F.D., VANHERWEGHEM, J. and NORTIER, J.L., 2008. Aristolochic acid nephropathy: a worldwide problem. Kidney international, 74(2), pp. 158-169.

DENES, A., LOPEZ-CASTEJON, G. and BROUGH, D., 2012. Caspase-1: is IL-1 just the tip of the ICEberg&quest. Cell death & disease, 3(7), pp. e338.

DENG, Y., FOLEY, E.M., GONZALES, J.C., GORDTS, P.L., LI, Y. and ESKO, J.D., 2012. Shedding of syndecan-1 from human hepatocytes alters very low density lipoprotein clearance. Hepatology, 55(1), pp. 277-286.

DENHEZ, F., WILCOX-ADELMAN, S.A., BACIU, P.C., SAONCELLA, S., LEE, S., FRENCH, B., NEVEU, W. and GOETINCK, P.F., 2002. Syndesmos, a syndecan-4 cytoplasmic domain interactor, binds to the focal adhesion adaptor proteins paxillin and Hic-5. The Journal of biological chemistry, 277(14), pp. 12270-12274.

DENNIS, G., SHERMAN, B.T., HOSACK, D.A., YANG, J., GAO, W., LANE, H.C. and LEMPICKI, R.A., 2003. DAVID: database for annotation, visualization, and integrated discovery. Genome biology, 4(9), pp. 1.

DEORA, A.B., KREITZER, G., JACOVINA, A.T. and HAJJAR, K.A., 2004. An annexin 2 phosphorylation switch mediates p11-dependent translocation of annexin 2 to the cell surface. The Journal of biological chemistry, 279(42), pp. 43411-43418.

DEPINA, A.S. and LANGFORD, G.M., 1999. Vesicle transport: the role of actin filaments and myosin motors. Microscopy research and technique, 47(2), pp. 93-106.

DERIVERY, E. and GAUTREAU, A., 2010. Evolutionary conservation of the WASH complex: An actin polymerization machine involved in endosomal fission. Communicative & integrative biology, 3(3), pp. 227-230.

DEVUYST, O., 2013. Uromodulin-associated kidney diseases, Proceedings of The Physiological Society 2013, The Physiological Society.

DEVUYST, O., ANTIGNAC, C., BINDELS, R.J., CHAUVEAU, D., EMMA, F., GANSEVOORT, R., MAXWELL, P.H., ONG, A.C., REMUZZI, G., RONCO, P. and SCHAEFER, F., 2012. The ERA-EDTA Working Group on inherited kidney disorders. Nephrology, dialysis, transplantation : official publication of the European Dialysis and Transplant Association - European Renal Association, 27(1), pp. 67-69.

DEWS, I.C. and MACKENZIE, K.R., 2007. Transmembrane domains of the syndecan family of growth factor coreceptors display a hierarchy of homotypic and heterotypic interactions. Proceedings of the National Academy of Sciences of the United States of America, 104(52), pp. 20782-20787.

DI DONATO, A., GHIGGERI, G.M., DI DUCA, M., JIVOTENKO, E., ACINNI, R., CAMPOLO, J., GINEVRI, F. and GUSMANO, R., 1997. Lysyl oxidase expression and collagen cross-linking during chronic adriamycin nephropathy. Nephron, 76(2), pp. 192-200.

DI VENERE, A., ROSSI, A., DE MATTEIS, F., ROSATO, N., AGRÒ, A.F. and MEI, G., 2000. Opposite effects of Ca2 and GTP binding on tissue transglutaminase tertiary structure. Journal of Biological Chemistry, 275(6), pp. 3915-3921.

DIAZ-HIDALGO, L., ALTUNTAS, S., ROSSIN, F., D'ELETTO, M., MARSELLA, C., FARRACE, M.G., FALASCA, L., ANTONIOLI, M., FIMIA, G.M. and PIACENTINI, M., 2016. Transglutaminase type 2-dependent selective recruitment of proteins into exosomes under stressful cellular conditions. Biochimica et Biophysica Acta (BBA)-Molecular Cell Research, 1863(8), pp. 2084-2092.

DINARELLO, C.A., 1996. Biologic basis for interleukin-1 in disease. Blood, 87(6), pp. 2095-2147.

DIPPOLD, H.C., NG, M.M., FARBER-KATZ, S.E., LEE, S., KERR, M.L., PETERMAN, M.C., SIM, R., WIHARTO, P.A., GALBRAITH, K.A. and MADHAVARAPU, S., 2009. GOLPH3 bridges phosphatidylinositol-4-phosphate and actomyosin to stretch and shape the Golgi to promote budding. Cell, 139(2), pp. 337-351.

DJUDJAJ, S., PAPASOTIRIOU, M., BÜLOW, R.D., WAGNEROVA, A., LINDENMEYER, M.T., COHEN, C.D., STRNAD, P., GOUMENOS, D.S., FLOEGE, J. and BOOR, P., 2016. Keratins are novel markers of renal epithelial cell injury. Kidney international, 89(4), pp. 792-808.

DOBRA, K., NURMINEN, M. and HJERPE, A., 2003. Growth factors regulate the expression profile of their syndecan co-receptors and the differentiation of mesothelioma cells. Anticancer Research, 23(3B), pp. 2435-2444.

DOCCI, D., BILANCIONI, R., PISTOCCHI, E., MOSCONI, G., TURCI, F., SALVI, G., BALDRATI, L. and ORSI, C., 1985. Serum alpha-1-acid glycoprotein in chronic renal failure. Nephron, 39(3), pp. 160-163.

DOLO, V., GINESTRA, A., CASSARA, D., VIOLINI, S., LUCANIA, G., TORRISI, M.R., NAGASE, H., CANEVARI, S., PAVAN, A. and VITTORELLI, M.L., 1998. Selective localization of matrix metalloproteinase 9, beta1 integrins, and human lymphocyte antigen class I molecules on membrane vesicles shed by 8701-BC breast carcinoma cells. Cancer research, 58(19), pp. 4468-4474.

DØRUM, S., QIAO, S., SOLLID, L.M. and FLECKENSTEIN, B., 2009. A quantitative analysis of transglutaminase 2-mediated deamidation of gluten peptides: implications for the T-cell response in celiac disease. Journal of proteome research, 8(4), pp. 1748-1755.

DOVAS, A., CHOI, Y., YONEDA, A., MULTHAUPT, H.A., KWON, S.H., KANG, D., OH, E.S. and COUCHMAN, J.R., 2010. Serine 34 phosphorylation of rho guanine dissociation inhibitor (RhoGDIalpha) links signaling from conventional protein kinase C to RhoGTPase in cell adhesion. The Journal of biological chemistry, 285(30), pp. 23296-23308.

DOVAS, A., YONEDA, A. and COUCHMAN, J.R., 2006. PKCbeta-dependent activation of RhoA by syndecan-4 during focal adhesion formation. Journal of cell science, 119(Pt 13), pp. 2837-2846.

DREYFUSS, J.L., REGATIERI, C.V., JARROUGE, T.R., CAVALHEIRO, R.P., SAMPAIO, L.O. and NADER, H.B., 2009. Heparan sulfate proteoglycans: structure, protein interactions and cell signaling. Anais da Academia Brasileira de Ciencias, 81(3), pp. 409-429.

D'SOUZA-SCHOREY, C. and CHAVRIER, P., 2006. ARF proteins: roles in membrane traffic and beyond. Nature reviews Molecular cell biology, 7(5), pp. 347-358.

DUBBINK, H.J., DE WAAL, L., VAN HAPEREN, R., VERKAIK, N.S., TRAPMAN, J. and ROMIJN, J.C., 1998. The human prostate-specific transglutaminase gene (TGM4): genomic organization, tissue-specific expression, and promoter characterization. Genomics, 51(3), pp. 434-444.

DUFFIELD, J.S., 2014. Cellular and molecular mechanisms in kidney fibrosis. The Journal of clinical investigation, 124(6), pp. 2299-2306.

DUNCAN, M.R., FRAZIER, K.S., ABRAMSON, S., WILLIAMS, S., KLAPPER, H., HUANG, X. and GROTENDORST, G.R., 1999. Connective tissue growth factor mediates transforming growth factor beta-induced collagen synthesis: down-regulation by cAMP. FASEB journal : official publication of the Federation of American Societies for Experimental Biology, 13(13), pp. 1774-1786.

DURAN, J.M., ANJARD, C., STEFAN, C., LOOMIS, W.F. and MALHOTRA, V., 2010. Unconventional secretion of Acb1 is mediated by autophagosomes. The Journal of cell biology, 188(4), pp. 527-536.

EBERT, A.D., LAUSSMANN, M., WEGEHINGEL, S., KADERALI, L., ERFLE, H., REICHERT, J., LECHNER, J., BEER, H., PEPPERKOK, R. and NICKEL, W., 2010. Tec-Kinase-Mediated Phosphorylation of Fibroblast Growth Factor 2 is Essential for Unconventional Secretion. Traffic, 11(6), pp. 813-826.

ECHTERMEYER, F., BACIU, P.C., SAONCELLA, S., GE, Y. and GOETINCK, P.F., 1999. Syndecan-4 core protein is sufficient for the assembly of focal adhesions and actin stress fibers. Journal of cell science, 112 (Pt 20)(Pt 20), pp. 3433-3441.

ECHTERMEYER, F., STREIT, M., WILCOX-ADELMAN, S., SAONCELLA, S., DENHEZ, F., DETMAR, M. and GOETINCK, P., 2001. Delayed wound repair and impaired angiogenesis in mice lacking syndecan-4. The Journal of clinical investigation, 107(2), pp. R9-R14.

ECKARDT, K., CORESH, J., DEVUYST, O., JOHNSON, R.J., KÖTTGEN, A., LEVEY, A.S. and LEVIN, A., 2013. Evolving importance of kidney disease: from subspecialty to global health burden. The Lancet, 382(9887), pp. 158-169.

ECKERT, R.L., FISHER, M.L., GRUN, D., ADHIKARY, G., XU, W. and KERR, C., 2015. Transglutaminase is a tumor cell and cancer stem cell survival factor. Molecular carcinogenesis, 54(10), pp. 947-958.

ECKERT, R.L., KAARTINEN, M.T., NURMINSKAYA, M., BELKIN, A.M., COLAK, G., JOHNSON, G.V. and MEHTA, K., 2014. Transglutaminase regulation of cell function. Physiological Reviews, 94(2), pp. 383-417.

ECKERT, R.L., STURNIOLO, M.T., JANS, R., KRAFT, C.A., JIANG, H. and RORKE, E.A., 2009. TIG3: a regulator of type I transglutaminase activity in epidermis. Amino acids, 36(4), pp. 739-746.

EDDY, A.A., LÓPEZ-GUISA, J.M., OKAMURA, D.M. and YAMAGUCHI, I., 2012. Investigating mechanisms of chronic kidney disease in mouse models. Pediatric nephrology, 27(8), pp. 1233-1247.

EFSTRATIADIS, G., DIVANI, M., KATSIOULIS, E. and VERGOULAS, G., 2009. Renal fibrosis. Hippokratia, 13(4), pp. 224-229.

EGBERTS, F., HEINRICH, M., JENSEN, J.M., WINOTO-MORBACH, S., PFEIFFER, S., WICKEL, M., SCHUNCK, M., STEUDE, J., SAFTIG, P., PROKSCH, E. and SCHUTZE, S., 2004. Cathepsin D is involved in the regulation of transglutaminase 1 and epidermal differentiation. Journal of cell science, 117(Pt 11), pp. 2295-2307.

EHRLICH, P., 1886. Hematoxylin sung. Z. Wiss. Micr., 3(150),.

EITAN, E., ZHANG, S., WITWER, K.W. and MATTSON, M.P., 2015. Extracellular vesicle–depleted fetal bovine and human sera have reduced capacity to support cell growth. Journal of extracellular vesicles, 4.

EKNOYAN, G., LAMEIRE, N., ECKARDT, K., KASISKE, B., WHEELER, D., LEVIN, A., STEVENS, P., BILOUS, R., LAMB, E. and CORESH, J., 2013. KDIGO 2012 clinical practice guideline for the evaluation and management of chronic kidney disease. Kidney Int, 3, pp. 5-14.

EL NAHAS, A.M., ABO-ZENAH, H., SKILL, N.J., BEX, S., WILD, G., GRIFFIN, M. and JOHNSON, T.S., 2004. Elevated epsilon-(gamma-glutamyl)lysine in human diabetic nephropathy results from increased expression and cellular release of tissue transglutaminase. Nephron.Clinical practice, 97(3), pp. c108-17.

ELFENBEIN, A., LANAHAN, A., ZHOU, T.X., YAMASAKI, A., TKACHENKO, E., MATSUDA, M. and SIMONS, M., 2012. Syndecan 4 regulates FGFR1 signaling in endothelial cells by directing macropinocytosis. Science signaling, 5(223), pp. ra36.

ELFENBEIN, A., RHODES, J.M., MELLER, J., SCHWARTZ, M.A., MATSUDA, M. and SIMONS, M., 2009. Suppression of RhoG activity is mediated by a syndecan 4-synectin-RhoGDI1 complex and is reversed by PKCalpha in a Rac1 activation pathway. The Journal of cell biology, 186(1), pp. 75-83.

ELISABETTA VERDERIO, ALESSANDRA SCARPELLINI, LINGHONG HUANG, BAHARAK VAFADAR-ISFAHANI, DAVID BOOCOCK and TIMOTHY JOHNSON, 2012. THE INTERACTOME OF TRANSGLUTAMINASE-2 (TG2) IN KIDNEY MEMBRANES P082.

ELMORE, S., 2007. Apoptosis: a review of programmed cell death. Toxicologic pathology, 35(4), pp. 495-516.

ENDO, K., TAKINO, T., MIYAMORI, H., KINSEN, H., YOSHIZAKI, T., FURUKAWA, M. and SATO, H., 2003. Cleavage of syndecan-1 by membrane type matrix metalloproteinase-1 stimulates cell migration. The Journal of biological chemistry, 278(42), pp. 40764-40770.

ENGLISH, A.R. and VOELTZ, G.K., 2013. Rab10 GTPase regulates ER dynamics and morphology. Nature cell biology, 15(2), pp. 169-178.

ESKO, J.D., KIMATA, K. and LINDAHL, U., 2009. Proteoglycans and Sulfated Glycosaminoglycans. In: A. VARKI, R.D. CUMMINGS, J.D. ESKO, H.H. FREEZE, P. STANLEY, C.R. BERTOZZI, G.W. HART and M.E. ETZLER, eds, Essentials of Glycobiology. 2nd edn. Cold Spring Harbor (NY): The Consortium of Glycobiology Editors, La Jolla, California, .

ESSNER, J.J., CHEN, E. and EKKER, S.C., 2006. Syndecan-2. The international journal of biochemistry & cell biology, 38(2), pp. 152-156.

ESTEBAN, V., LORENZO, O., RUPEREZ, M., SUZUKI, Y., MEZZANO, S., BLANCO, J., KRETZLER, M., SUGAYA, T., EGIDO, J. and RUIZ-ORTEGA, M., 2004. Angiotensin II, via AT1 and AT2 receptors and NF-kappaB pathway, regulates the inflammatory response in unilateral ureteral obstruction. Journal of the American Society of Nephrology : JASN, 15(6), pp. 1514-1529.

FADER, C.M., SÁNCHEZ, D.G., MESTRE, M.B. and COLOMBO, M.I., 2009. TI-VAMP/VAMP7 and VAMP3/cellubrevin: two v-SNARE proteins involved in specific steps of the autophagy/multivesicular body pathways. Biochimica et Biophysica Acta (BBA)-Molecular Cell Research, 1793(12), pp. 1901-1916.

FALCONE, S., COCUCCI, E., PODINI, P., KIRCHHAUSEN, T., CLEMENTI, E. and MELDOLESI, J., 2006. Macropinocytosis: regulated coordination of endocytic and exocytic membrane traffic events. Journal of cell science, 119(Pt 22), pp. 4758-4769.

FAN, J., NG, Y., HILL, P.A., NIKOLIC-PATERSON, D.J., MU, W., ATKINS, R.C. and LAN, H.Y., 1999. Transforming growth factor-&bgr; regulates tubular epithelial-myofibroblast transdifferentiation in vitro. Kidney international, 56(4), pp. 1455-1467.

FAN, Q., SHIKE, T., SHIGIHARA, T., TANIMOTO, M., GOHDA, T., MAKITA, Y., WANG, L.N., HORIKOSHI, S. and TOMINO, Y., 2003. Gene expression profile in diabetic KK/Ta mice. Kidney international, 64(6), pp. 1978-1985.

FASSETT, R.G., VENUTHURUPALLI, S.K., GOBE, G.C., COOMBES, J.S., COOPER, M.A. and HOY, W.E., 2011. Biomarkers in chronic kidney disease: a review. Kidney international, 80(8), pp. 806-821.

REFERENCES

FATAL, N., KARHINEN, L., JOKITALO, E. and MAKAROW, M., 2004. Active and specific recruitment of a soluble cargo protein for endoplasmic reticulum exit in the absence of functional COPII component Sec24p. Journal of cell science, 117(Pt 9), pp. 1665-1673.

FAVERMAN, L., MIKHAYLOVA, L., MALMQUIST, J. and NURMINSKAYA, M., 2008. Extracellular transglutaminase 2 activates β-catenin signaling in calcifying vascular smooth muscle cells. FEBS letters, 582(10), pp. 1552-1557.

FENG, D., ZHAO, W., YE, Y., BAI, X., LIU, R., CHANG, L., ZHOU, Q. and SUI, S., 2010. Cellular internalization of exosomes occurs through phagocytosis. Traffic, 11(5), pp. 675-687.

FENG, J.F., RHEE, S.G. and IM, M.J., 1996. Evidence that phospholipase delta1 is the effector in the Gh (transglutaminase II)-mediated signaling. The Journal of biological chemistry, 271(28), pp. 16451-16454.

FERRARI, D., PIZZIRANI, C., ADINOLFI, E., LEMOLI, R.M., CURTI, A., IDZKO, M., PANTHER, E. and DI VIRGILIO, F., 2006. The P2X7 receptor: a key player in IL-1 processing and release. Journal of immunology (Baltimore, Md.: 1950), 176(7), pp. 3877-3883.

FESUS, L. and PIACENTINI, M., 2002. Transglutaminase 2: an enigmatic enzyme with diverse functions. Trends in biochemical sciences, 27(10), pp. 534-539.

FÉSÜS, L. and SZONDY, Z., 2005. Transglutaminase 2 in the balance of cell death and survival. FEBS letters, 579(15), pp. 3297-3302.

FILIANO, A., TUCHOLSKI, J., DOLAN, P., COLAK, G. and JOHNSON, G., 2010. Transglutaminase 2 protects against ischemic stroke. Neurobiology of disease, 39(3), pp. 334-343.

FILIP, S., MARKOSKA, K., GLORIEUX, G., PAPADOPOULOS, T., MULLEN, W., ZOIDAKIS, J., JANKOWSKI, J., SCHANSTRA, J., VANHOLDER, R. and SPASOVSKI, G., 2015. FP308URINARY PROTEOMICS TO DECIPHER MOLECULAR PATHOPHYSIOLOGY OF CKD PROGRESSION. Nephrology Dialysis Transplantation, 30(suppl 3), pp. iii170-iii170.

FILIPEANU, C.M., ZHOU, F., CLAYCOMB, W.C. and WU, G., 2004. Regulation of the cell surface expression and function of angiotensin II type 1 receptor by Rab1-mediated endoplasmic reticulum-to-Golgi transport in cardiac myocytes. The Journal of biological chemistry, 279(39), pp. 41077-41084.

FISCHER, A.H., JACOBSON, K.A., ROSE, J. and ZELLER, R., 2008. Hematoxylin and eosin staining of tissue and cell sections. CSH protocols, 2008, pp. pdb.prot4986.

FISHER, M., JONES, R.A., HUANG, L., HAYLOR, J.L., EL NAHAS, M., GRIFFIN, M. and JOHNSON, T.S., 2009. Modulation of tissue transglutaminase in tubular epithelial cells alters extracellular matrix levels: a potential mechanism of tissue scarring. Matrix biology, 28(1), pp. 20-31.

FISHER, M.L., ADHIKARY, G., XU, W., KERR, C., KEILLOR, J.W. and ECKERT, R.L., 2015. Type II transglutaminase stimulates epidermal cancer stem cell epithelial-mesenchymal transition. Oncotarget, 6(24), pp. 20525-20539.

FITZNER, D., SCHNAARS, M., VAN ROSSUM, D., KRISHNAMOORTHY, G., DIBAJ, P., BAKHTI, M., REGEN, T., HANISCH, U.K. and SIMONS, M., 2011. Selective transfer of exosomes from oligodendrocytes to microglia by macropinocytosis. Journal of cell science, 124(Pt 3), pp. 447-458.

FITZPATRICK, S.L., KASSAM, G., CHOI, K., KANG, H., FOGG, D.K. and WAISMAN, D.M., 2000. Regulation of plasmin activity by annexin II tetramer. Biochemistry, 39(5), pp. 1021-1028.

FLORKIEWICZ, R.Z., MAJACK, R.A., BUECHLER, R.D. and FLORKIEWICZ, E., 1995. Quantitative export of FGF-2 occurs through an alternative, energy-dependent, non-ER/Golgi pathway. Journal of cellular physiology, 162(3), pp. 388-399.

FORGAC, M., CANTLEY, L., WIEDENMANN, B., ALTSTIEL, L. and BRANTON, D., 1983. Clathrin-coated vesicles contain an ATP-dependent proton pump. Proceedings of the National Academy of Sciences of the United States of America, 80(5), pp. 1300-1303.

FRAIJ, B.M. and GONZALES, R.A., 1996. A third human tissue transglutaminase homologue as a result of alternative gene transcripts. Biochimica et Biophysica Acta (BBA)-Gene Structure and Expression, 1306(1), pp. 63-74.

FRAIJ, B.M., BIRCKBICHLER, P.J., PATTERSON, M.K.,Jr, LEE, K.N. and GONZALES, R.A., 1992. A retinoic acid-inducible mRNA from human erythroleukemia cells encodes a novel tissue transglutaminase homologue. The Journal of biological chemistry, 267(31), pp. 22616-22623.

FREUND, K.F., DOSHI, K.P., GAUL, S.L., CLAREMON, D.A., REMY, D.C., BALDWIN, J.J., PITZENBERGER, S.M. and STERN, A.M., 1994. Transglutaminase inhibition by 2-[(2-oxopropyl) thio] imidazolium derivatives: mechanism of factor XIIIa inactivation. Biochemistry, 33(33), pp. 10109-10119.

FRIAND, V., DAVID, G. and ZIMMERMANN, P., 2015. Syntenin and syndecan in the biogenesis of exosomes. Biology of the Cell, 107(10), pp. 331-341.

FRICK, M., BRIGHT, N.A., RIENTO, K., BRAY, A., MERRIFIED, C. and NICHOLS, B.J., 2007. Coassembly of flotillins induces formation of membrane microdomains, membrane curvature, and vesicle budding. Current Biology, 17(13), pp. 1151-1156.

FU, H., TIAN, Y., ZHOU, L., ZHOU, D., TAN, R.J., STOLZ, D.B. and LIU, Y., 2016. Tenascin-C Is a Major Component of the Fibrogenic Niche in Kidney Fibrosis. Journal of the American Society of Nephrology, , pp. ASN. 2016020165.

FUCHS, T.C. and HEWITT, P., 2011. Biomarkers for drug-induced renal damage and nephrotoxicity—an overview for applied toxicology. The AAPS journal, 13(4), pp. 615-631.

FUKI, I.V., KUHN, K.M., LOMAZOV, I.R., ROTHMAN, V.L., TUSZYNSKI, G.P., IOZZO, R.V., SWENSON, T.L., FISHER, E.A. and WILLIAMS, K.J., 1997. The syndecan family of proteoglycans. Novel receptors mediating internalization of atherogenic lipoproteins in vitro. The Journal of clinical investigation, 100(6), pp. 1611-1622.

FUNAKOSHI, Y., HASEGAWA, H. and KANAHO, Y., 2011. Regulation of PIP5K activity by Arf6 and its physiological significance. Journal of cellular physiology, 226(4), pp. 888-895.

FURUTANI, Y., TOGUCHI, M., SHRESTHA, R. and KOJIMA, S., 2016. Phenosafranin inhibits nuclear localization of transglutaminase 2 without affecting its transamidase activity. Amino acids, , pp. 1-6.

GALLO, R., KIM, C., KOKENYESI, R., ADZICK, N.S. and BERNFIELD, M., 1997. Syndecans-1 and-4 are induced during wound repair of neonatal but not fetal skin. Journal of Investigative Dermatology, 107(5), pp. 676-683.

GANSEVOORT, R.T., CORREA-ROTTER, R., HEMMELGARN, B.R., JAFAR, T.H., HEERSPINK, H.J.L., MANN, J.F., MATSUSHITA, K. and WEN, C.P., 2013. Chronic kidney disease and cardiovascular risk: epidemiology, mechanisms, and prevention. The Lancet, 382(9889), pp. 339-352.

GARZA-LICUDINE, E., DEO, D., YU, S., UZ-ZAMAN, A. and DUNBAR, W.B., 2010. Portable nanoparticle quantization using a resizable nanopore instrument-The IZON qNano™, 2010 Annual International Conference of the IEEE Engineering in Medicine and Biology 2010, IEEE, pp. 5736-5739.

GATESMAN, A., WALKER, V.G., BAISDEN, J.M., WEED, S.A. and FLYNN, D.C., 2004. Protein kinase Calpha activates c-Src and induces podosome formation via AFAP-110. Molecular and cellular biology, 24(17), pp. 7578-7597.

GAUDRY, C.A., VERDERIO, E., AESCHLIMANN, D., COX, A., SMITH, C. and GRIFFIN, M., 1999. Cell surface localization of tissue transglutaminase is dependent on a fibronectin-binding site in its N-terminal beta-sandwich domain. The Journal of biological chemistry, 274(43), pp. 30707-30714.

GÉMINARD, C., DE GASSART, A., BLANC, L. and VIDAL, M., 2004. Degradation of AP2 during reticulocyte maturation enhances binding of hsc70 and Alix to a common site on TFR for sorting into exosomes. Traffic, 5(3), pp. 181-193.

GEMINARD, C., NAULT, F., JOHNSTONE, R.M. and VIDAL, M., 2001. Characteristics of the interaction between Hsc70 and the transferrin receptor in exosomes released during reticulocyte maturation. The Journal of biological chemistry, 276(13), pp. 9910-9916.

GENOVESE, F., MANRESA, A.A., LEEMING, D.J., KARSDAL, M.A. and BOOR, P., 2014. The extracellular matrix in the kidney: a source of novel non-invasive biomarkers of kidney fibrosis? Fibrogenesis & tissue repair, 7(1), pp. 4.

GEORGE, M.D., VOLLBERG, T.M., FLOYD, E.E., STEIN, J.P. and JETTEN, A.M., 1990. Regulation of transglutaminase type II by transforming growth factor-beta 1 in normal and transformed human epidermal keratinocytes. The Journal of biological chemistry, 265(19), pp. 11098-11104.

GEROLYMOS, M., KARAGIANNI, F., PAPASOTIRIOU, M., KALLIAKMANI, P., SOTSIOU, F., CHARONIS, A. and GOUMENOS, D.S., 2011. Expression of transgelin in human glomerulonephritis of various etiology. Nephron.Clinical practice, 119(1), pp. c74-82.

GEYER, M., YU, H., MANDIC, R., LINNEMANN, T., ZHENG, Y., FACKLER, O.T. and PETERLIN, B.M., 2002. Subunit H of the V-ATPase binds to the medium chain of adaptor protein complex 2 and connects Nef to the endocytic machinery. Journal of Biological Chemistry, 277(32), pp. 28521-28529.

GHERARDI, E., VECCHIA, L. and CALANDRA, S., 1980. Experimental nephrotic syndrome in the rat induced by puromycin aminonucleoside. Plasma and urinary lipoproteins. Experimental and molecular pathology, 32(2), pp. 128-142.

GHOSSOUB, R., LEMBO, F., RUBIO, A., GAILLARD, C.B., BOUCHET, J., VITALE, N., SLAVÍK, J., MACHALA, M. and ZIMMERMANN, P., 2014. Syntenin-ALIX exosome biogenesis and budding into multivesicular bodies are controlled by ARF6 and PLD2. Nature communications, 5.

GIACOMINI, M.M., TRAVIS, M.A., KUDO, M. and SHEPPARD, D., 2012. Epithelial cells utilize cortical actin/myosin to activate latent TGF-β through integrin α v β 6-dependent physical force. Experimental cell research, 318(6), pp. 716-722.

GILL, G.W., FROST, J.K. and MILLER, K.A., 1974. A new formula for a half-oxidized hematoxylin solution that neither overstains nor requires differentiation. Acta Cytologica, 18(4), pp. 300-311.

GILLET, L.C., NAVARRO, P., TATE, S., ROST, H., SELEVSEK, N., REITER, L., BONNER, R. and AEBERSOLD, R., 2012. Targeted data extraction of the MS/MS spectra generated by data-independent acquisition: a new concept for consistent and accurate proteome analysis. Molecular & cellular proteomics : MCP, 11(6), pp. O111.016717.

GOITRE, L., TRAPANI, E., TRABALZINI, L. and RETTA, S.F., 2014. The Ras superfamily of small GTPases: the unlocked secrets. Ras Signaling: Methods and Protocols, , pp. 1-18.

GOKHALE, N.A., ABRAHAM, A., DIGMAN, M.A., GRATTON, E. and CHO, W., 2005. Phosphoinositide specificity of and mechanism of lipid domain formation by annexin A2-p11 heterotetramer. The Journal of biological chemistry, 280(52), pp. 42831-42840.

GOKMEN, M.R. and LORD, G.M., 2012. Aristolochic acid nephropathy. BMJ (Clinical research ed.), 344, pp. e4000.

GOLDSTEIN, R.S., TARLOFF, J.B. and HOOK, J.B., 1988. Age-related nephropathy in laboratory rats. FASEB journal : official publication of the Federation of American Societies for Experimental Biology, 2(7), pp. 2241-2251.

GONG, D., CHEN, X., MIDDLEDITCH, M., HUANG, L., VAZHOOR AMARSINGH, G., REDDY, S., LU, J., ZHANG, S., RUGGIERO, K. and PHILLIPS, A.R., 2009. Quantitative proteomic profiling identifies new renal targets of copper (II)-selective chelation in the reversal of diabetic nephropathy in rats. Proteomics, 9(18), pp. 4309-4320.

GONZALES, P.A., PISITKUN, T., HOFFERT, J.D., TCHAPYJNIKOV, D., STAR, R.A., KLETA, R., WANG, N.S. and KNEPPER, M.A., 2009. Large-scale proteomics and phosphoproteomics of urinary exosomes. Journal of the American Society of Nephrology : JASN, 20(2), pp. 363-379.

GOPAL, S., SOGAARD, P., MULTHAUPT, H.A., PATAKI, C., OKINA, E., XIAN, X., PEDERSEN, M.E., STEVENS, T., GRIESBECK, O., PARK, P.W., POCOCK, R. and COUCHMAN, J.R., 2015. Transmembrane proteoglycans control stretch-activated channels to set cytosolic calcium levels. The Journal of cell biology, 210(7), pp. 1199-1211.

GÓRSKI, J., HERMENS, W.T., BORAWSKI, J., MYSLIWIEC, M. and GLATZ, J.F., 1997. Increased fatty acid-binding protein concentration in plasma of patients with chronic renal failure. Clinical chemistry, 43(1), pp. 193-195.

GOTO, Y., UCHIO-YAMADA, K., ANAN, S., YAMAMOTO, Y., OGURA, A. and MANABE, N., 2005. Transforming growth factor-β1 mediated up-regulation of lysyl oxidase in the kidneys of hereditary nephrotic mouse with chronic renal fibrosis. Virchows Archiv, 447(5), pp. 859-868.

GRANÉS, F., BERNDT, C., ROY, C., MANGEAT, P., REINA, M. and VILARÓ, S., 2003. Identification of a novel Ezrin-binding site in syndecan-2 cytoplasmic domain. FEBS letters, 547(1-3), pp. 212-216.

GRASSART, A., CHENG, A.T., HONG, S.H., ZHANG, F., ZENZER, N., FENG, Y., BRINER, D.M., DAVIS, G.D., MALKOV, D. and DRUBIN, D.G., 2014. Actin and dynamin2 dynamics and interplay during clathrin-mediated endocytosis. The Journal of cell biology, 205(5), pp. 721-735.

GRAU-BOVE, X., RUIZ-TRILLO, I. and RODRIGUEZ-PASCUAL, F., 2015. Origin and evolution of lysyl oxidases. Scientific reports, 5, pp. 10568.

GRAZIA FARRACE, M., PIREDDA, L., MATARRESE, P., CICCOSANTI, F., FALASCA, L., RODOLFO, C., GIAMMARIOLI, A.M., VERDERIO, E., GRIFFIN, M. and MALORNI, W., 2002. Transglutaminase overexpression sensitizes neuronal cell lines to apoptosis by increasing mitochondrial membrane potential and cellular oxidative stress. Journal of neurochemistry, 81(5), pp. 1061-1072.

GRAZIANI, I., BAGALÁ, C., DUARTE, M., SOLDI, R., KOLEV, V., TARANTINI, F., KUMAR, T.K.S., DOYLE, A., NEIVANDT, D. and YU, C., 2006. Release of FGF1 and p40 synaptotagmin 1 correlates with their membrane destabilizing ability. Biochemical and biophysical research communications, 349(1), pp. 192-199.

GREENE, E.L., KREN, S. and HOSTETTER, T.H., 1996. Role of aldosterone in the remnant kidney model in the rat. The Journal of clinical investigation, 98(4), pp. 1063-1068.

GREENER, T., ZHAO, X., NOJIMA, H., EISENBERG, E. and GREENE, L.E., 2000. Role of cyclin G-associated kinase in uncoating clathrin-coated vesicles from non-neuronal cells. Journal of Biological Chemistry, 275(2), pp. 1365-1370.

GRIEVE, A.G., MOSS, S.E. and HAYES, M.J., 2012. Annexin A2 at the interface of actin and membrane dynamics: a focus on its roles in endocytosis and cell polarization. International journal of cell biology, 2012.

GRIFFIN, K.A., PICKEN, M. and BIDANI, A.K., 1994. Method of renal mass reduction is a critical modulator of subsequent hypertension and glomerular injury. Journal of the American Society of Nephrology : JASN, 4(12), pp. 2023-2031.

GRIFFIN, M., CASADIO, R. and BERGAMINI, C.M., 2002. Transglutaminases: nature's biological glues. The Biochemical journal, 368(Pt 2), pp. 377-396.

GRIFFIN, M., COUTTS, I.G. and SAINT, R.E., 2004. Novel compounds and methods of using the same, .

GRIFFIN, M., JONES, R., PARRY, J. and BALKLAVA, Z., 2002. Tissue transglutaminase in tumour growth and progression: A noval strategy for tumour therapy. Minerva Biotecnologica, 14(2), pp. 213.

GRIFFIN, M., SMITH, L.L. and WYNNE, J., 1979. Changes in transglutaminase activity in an experimental model of pulmonary fibrosis induced by paraquat. British journal of experimental pathology, 60(6), pp. 653-661.

GROFFEN, A.J., RUEGG, M.A., DIJKMAN, H., VAN DE VELDEN, T.J., BUSKENS, C.A., VAN DEN BORN, J., ASSMANN, K.J., MONNENS, L.A., VEERKAMP, J.H. and VAN DEN HEUVEL, L.P., 1998. Agrin is a major heparan sulfate proteoglycan in the human glomerular basement membrane. The journal of histochemistry and cytochemistry : official journal of the Histochemistry Society, 46(1), pp. 19-27.

GRONE, H.J., WEBER, K., GRONE, E., HELMCHEN, U. and OSBORN, M., 1987. Coexpression of keratin and vimentin in damaged and regenerating tubular epithelia of the kidney. The American journal of pathology, 129(1), pp. 1-8.

GROSS, J.C., CHAUDHARY, V., BARTSCHERER, K. and BOUTROS, M., 2012. Active Wnt proteins are secreted on exosomes. Nature cell biology, 14(10), pp. 1036-1045.

GROSS, O., YAZDI, A.S., THOMAS, C.J., MASIN, M., HEINZ, L.X., GUARDA, G., QUADRONI, M., DREXLER, S.K. and TSCHOPP, J., 2012. Inflammasome activators induce interleukin-1α secretion via distinct pathways with differential requirement for the protease function of caspase-1. Immunity, 36(3), pp. 388-400.

GROSS, S.R., BALKLAVA, Z. and GRIFFIN, M., 2003. Importance of tissue transglutaminase in repair of extracellular matrices and cell death of dermal fibroblasts after exposure to a solarium ultraviolet A source. Journal of investigative dermatology, 121(2), pp. 412-423.

GROSSOWICZ, N., WAINFAN, E., BOREK, E. and WAELSCH, H., 1950. The enzymatic formation of hydroxamic acids from glutamine and asparagine. The Journal of biological chemistry, 187(1), pp. 111-125.

GUERROT, D., DUSSAULE, J., MAEL-AININ, M., XU-DUBOIS, Y., RONDEAU, E., CHATZIANTONIOU, C. and PLACIER, S., 2012. Identification of periostin as a critical marker of progression/reversal of hypertensive nephropathy. PLoS One, 7(3), pp. e31974.

GUPTA, S., CLARKSON, M.R., DUGGAN, J. and BRADY, H.R., 2000. Connective tissue growth factor: potential role in glomerulosclerosis and tubulointerstitial fibrosis. Kidney international, 58(4), pp. 1389-1399.

HACKAM, A.S., YASSA, A.S., SINGARAJA, R., METZLER, M., GUTEKUNST, C.A., GAN, L., WARBY, S., WELLINGTON, C.L., VAILLANCOURT, J., CHEN, N., GERVAIS, F.G., RAYMOND, L., NICHOLSON, D.W. and HAYDEN, M.R., 2000. Huntingtin interacting protein 1 induces apoptosis via a novel caspase-dependent death effector domain. The Journal of biological chemistry, 275(52), pp. 41299-41308.

HADDEN, H.L. and HENKE, C.A., 2000. Induction of lung fibroblast apoptosis by soluble fibronectin peptides. American journal of respiratory and critical care medicine, 162(4), pp. 1553-1560.

HALACHMI, N. and LEV, Z., 1996. The Sec1 family: a novel family of proteins involved in synaptic transmission and general secretion. Journal of neurochemistry, 66(3), pp. 889-897.

HAN, B., CHO, J., CHO, Y.D., JEONG, K., KIM, S. and LEE, B.I., 2010. Crystal structure of human transglutaminase 2 in complex with adenosine triphosphate. International journal of biological macromolecules, 47(2), pp. 190-195.

HAN, S.H., MALAGA-DIEGUEZ, L., CHINGA, F., KANG, H.M., TAO, J., REIDY, K. and SUSZTAK, K., 2016. Deletion of Lkb1 in Renal Tubular Epithelial Cells Leads to CKD by Altering Metabolism. Journal of the American Society of Nephrology : JASN, 27(2), pp. 439-453.

HANG, J., ZEMSKOV, E.A., LORAND, L. and BELKIN, A.M., 2005. Identification of a novel recognition sequence for fibronectin within the NH2-terminal beta-sandwich domain of tissue transglutaminase. The Journal of biological chemistry, 280(25), pp. 23675-23683.

HARBOUR, M.E., BREUSEGEM, S.Y., ANTROBUS, R., FREEMAN, C., REID, E. and SEAMAN, M.N., 2010. The cargo-selective retromer complex is a recruiting hub for protein complexes that regulate endosomal tubule dynamics. Journal of cell science, 123(Pt 21), pp. 3703-3717.

HAROON, Z.A., HETTASCH, J.M., LAI, T.S., DEWHIRST, M.W. and GREENBERG, C.S., 1999. Tissue transglutaminase is expressed, active, and directly involved in rat dermal wound healing and angiogenesis. FASEB journal : official publication of the Federation of American Societies for Experimental Biology, 13(13), pp. 1787-1795.

HAROON, Z.A., WANNENBURG, T., GUPTA, M., GREENBERG, C.S., WALLIN, R. and SANE, D.C., 2001. Localization of tissue transglutaminase in human carotid and coronary artery atherosclerosis: implications for plaque stability and progression. Laboratory investigation, 81(1), pp. 83-93.

HARRIS, H., 1900. On the rapid conversion of haematoxylin into haematein in staining reactions. J. Appl. Microsc., 3, pp. 777.

HARRIS, J., HARTMAN, M., ROCHE, C., ZENG, S.G., O'SHEA, A., SHARP, F.A., LAMBE, E.M., CREAGH, E.M., GOLENBOCK, D.T., TSCHOPP, J., KORNFELD, H., FITZGERALD, K.A. and LAVELLE, E.C., 2011. Autophagy controls IL-1beta secretion by targeting pro-IL-1beta for degradation. The Journal of biological chemistry, 286(11), pp. 9587-9597.

HARRISON, C., LAYTON, C., HAU, Z., BULLOCK, A., JOHNSON, T. and MACNEIL, S., 2007. Transglutaminase inhibitors induce hyperproliferation and parakeratosis in tissue-engineered skin. British Journal of Dermatology, 156(2), pp. 247-257.

HARRISON, M.S., HUNG, C.S., LIU, T.T., CHRISTIANO, R., WALTHER, T.C. and BURD, C.G., 2014. A mechanism for retromer endosomal coat complex assembly with cargo. Proceedings of the National Academy of Sciences of the United States of America, 111(1), pp. 267-272.

HARTERINK, M., PORT, F., LORENOWICZ, M.J., MCGOUGH, I.J., SILHANKOVA, M., BETIST, M.C., VAN WEERING, J.R., VAN HEESBEEN, R.G., MIDDELKOOP, T.C. and BASLER, K., 2011. A SNX3-dependent retromer pathway mediates retrograde transport of the Wnt sorting receptor Wntless and is required for Wnt secretion. Nature cell biology, 13(8), pp. 914-923.

HASEGAWA, G., SUWA, M., ICHIKAWA, Y., OHTSUKA, T., KUMAGAI, S., KIKUCHI, M., SATO, Y. and SAITO, Y., 2003. A novel function of tissue-type transglutaminase: protein disulphide isomerase. The Biochemical journal, 373(Pt 3), pp. 793-803.

HAYES, M.J., MERRIFIELD, C.J., SHAO, D., AYALA-SANMARTIN, J., SCHOREY, C.D., LEVINE, T.P., PROUST, J., CURRAN, J., BAILLY, M. and MOSS, S.E., 2004. Annexin 2 binding to phosphatidylinositol 4,5-bisphosphate on endocytic vesicles is regulated by the stress response pathway. The Journal of biological chemistry, 279(14), pp. 14157-14164.

HE, M., QIN, H., POON, T.C., SZE, S., DING, X., CO, N.N., NGAI, S., CHAN, T. and WONG, N., 2015. Hepatocellular carcinoma-derived exosomes promote motility of immortalized hepatocyte through transfer of oncogenic proteins and RNAs. Carcinogenesis, 36(9), pp. 1008-1018.

HEMLER, M.E., 2003. Tetraspanin proteins mediate cellular penetration, invasion, and fusion events and define a novel type of membrane microdomain. Annual Review of Cell and Developmental Biology, 19(1), pp. 397-422.

HENDERSON, N.C., MACKINNON, A.C., FARNWORTH, S.L., KIPARI, T., HASLETT, C., IREDALE, J.P., LIU, F., HUGHES, J. and SETHI, T., 2008. Galectin-3 expression and secretion links macrophages to the promotion of renal fibrosis. The American journal of pathology, 172(2), pp. 288-298.

HENNE, W.M., BUCHKOVICH, N.J. and EMR, S.D., 2011. The ESCRT pathway. Developmental cell, 21(1), pp. 77-91.

HERRERA, G.A., 2010. Experimental Models for Renal Diseases: Pathogenesis and Diagnosis. Karger Medical and Scientific Publishers.

HERZOG, A., KUNTZ, S., DANIEL, H. and WENZEL, U., 2004. Identification of biomarkers for the initiation of apoptosis in human preneoplastic colonocytes by proteome analysis. International journal of cancer, 109(2), pp. 220-229.

HERZOG, C.A., ASINGER, R.W., BERGER, A.K., CHARYTAN, D.M., DÍEZ, J., HART, R.G., ECKARDT, K., KASISKE, B.L., MCCULLOUGH, P.A. and PASSMAN, R.S., 2011. Cardiovascular disease in chronic kidney disease. A clinical update from Kidney Disease: Improving Global Outcomes (KDIGO). Kidney international, 80(6), pp. 572-586.

HEWITSON, T.D., 2009. Renal tubulointerstitial fibrosis: common but never simple. American journal of physiology.Renal physiology, 296(6), pp. F1239-44.

HEWITSON, T.D., 2012. Fibrosis in the kidney: is a problem shared a problem halved? Fibrogenesis & tissue repair, 5(1), pp. 1.

HIGGINS, D.F., KIMURA, K., BERNHARDT, W.M., SHRIMANKER, N., AKAI, Y., HOHENSTEIN, B., SAITO, Y., JOHNSON, R.S., KRETZLER, M., COHEN, C.D., ECKARDT, K.U., IWANO, M. and HAASE, V.H., 2007. Hypoxia promotes fibrogenesis in vivo via HIF-1 stimulation of epithelial-to-mesenchymal transition. The Journal of clinical investigation, 117(12), pp. 3810-3820.

HIGGINS, D.F., KIMURA, K., IWANO, M. and HAASE, V.H., 2008. Hypoxia-inducible factor signaling in the development of tissue fibrosis. Cell Cycle, 7(9), pp. 1128-1132.

HIIRAGI, T., SASAKI, H., NAGAFUCHI, A., SABE, H., SHEN, S.C., MATSUKI, M., YAMANISHI, K. and TSUKITA, S., 1999. Transglutaminase type 1 and its cross-linking activity are concentrated at adherens junctions in simple epithelial cells. The Journal of biological chemistry, 274(48), pp. 34148-34154.

HILL, J.L., KOBORI, N., ZHAO, J., ROZAS, N.S., HYLIN, M.J., MOORE, A.N. and DASH, P.K., 2016. Traumatic brain injury decreases AMP-activated protein kinase activity and pharmacological enhancement of its activity improves cognitive outcome. Journal of neurochemistry, 139(1), pp. 106-119.

HINZ, B., 2009. Tissue stiffness, latent TGF-β1 activation, and mechanical signal transduction: implications for the pathogenesis and treatment of fibrosis. Current rheumatology reports, 11(2), pp. 120-126.

HINZ, B., 2015. The extracellular matrix and transforming growth factor-β1: tale of a strained relationship. Matrix Biology, 47, pp. 54-65.

HINZ, B., CELETTA, G., TOMASEK, J.J., GABBIANI, G. and CHAPONNIER, C., 2001. Alpha-smooth muscle actin expression upregulates fibroblast contractile activity. Molecular biology of the cell, 12(9), pp. 2730-2741.

HINZ, B., DUGINA, V., BALLESTREM, C., WEHRLE-HALLER, B. and CHAPONNIER, C., 2003. Alpha-smooth muscle actin is crucial for focal adhesion maturation in myofibroblasts. Molecular biology of the cell, 14(6), pp. 2508-2519.

HINZ, B., MASTRANGELO, D., ISELIN, C.E., CHAPONNIER, C. and GABBIANI, G., 2001. Mechanical tension controls granulation tissue contractile activity and myofibroblast differentiation. The American journal of pathology, 159(3), pp. 1009-1020.

HITOMI, K., 2005. Transglutaminases in skin epidermis. European Journal of Dermatology, 15(5), pp. 313-319.

HITOMI, K., HORIO, Y., IKURA, K., YAMANISHI, K. and MAKI, M., 2001. Analysis of epidermal-type transglutaminase (TGase 3) expression in mouse tissues and cell lines. The international journal of biochemistry & cell biology, 33(5), pp. 491-498.

HITOMI, K., IKEDA, N. and MAKI, M., 2003. Immunological detection of proteolytically activated epidermal-type transglutaminase (TGase 3) using cleavage-site-specific antibody. Bioscience, biotechnology, and biochemistry, 67(11), pp. 2492-2494.

HOFFMANN, D., FUCHS, T.C., HENZLER, T., MATHEIS, K.A., HERGET, T., DEKANT, W., HEWITT, P. and MALLY, A., 2010. Evaluation of a urinary kidney biomarker panel in rat models of acute and subchronic nephrotoxicity. Toxicology, 277(1), pp. 49-58.

HOLINSTAT, M., KNEZEVIC, N., BROMAN, M., SAMAREL, A.M., MALIK, A.B. and MEHTA, D., 2006. Suppression of RhoA activity by focal adhesion kinase-induced activation of p190RhoGAP: role in regulation of endothelial permeability. The Journal of biological chemistry, 281(4), pp. 2296-2305.

HOLMES, J.K. and SOLOMON, M.J., 1996. A Predictive Scale for Evaluating Cyclin-dependent Kinase Substrates A COMPARISON OF p34cdc2 AND p33cdk2. Journal of Biological Chemistry, 271(41), pp. 25240-25246.

HONG, Z., YANG, Y., ZHANG, C., NIU, Y., LI, K., ZHAO, X. and LIU, J., 2009. The retromer component SNX6 interacts with dynactin p150Glued and mediates endosome-to-TGN transport. Cell research, 19(12), pp. 1334-1349.

HÖNING, S., RICOTTA, D., KRAUSS, M., SPÄTE, K., SPOLAORE, B., MOTLEY, A., ROBINSON, M., ROBINSON, C., HAUCKE, V. and OWEN, D.J., 2005. Phosphatidylinositol-(4, 5)-bisphosphate regulates sorting signal recognition by the clathrin-associated adaptor complex AP2. Molecular cell, 18(5), pp. 519-531.

HOOPER, N.M., 1999. Detergent-insoluble glycosphingolipid/cholesterol-rich membrane domains, lipid rafts and caveolae (review). Molecular membrane biology, 16(2), pp. 145-156.

HOROWITZ, A. and SIMONS, M., 1998. Phosphorylation of the cytoplasmic tail of syndecan-4 regulates activation of protein kinase Cα. Journal of Biological Chemistry, 273(40), pp. 25548-25551.

HORSTRUP, J.H., GEHRMANN, M., SCHNEIDER, B., PLOGER, A., FROESE, P., SCHIROP, T., KAMPF, D., FREI, U., NEUMANN, R. and ECKARDT, K.U., 2002. Elevation of serum and urine levels of TIMP-1 and tenascin in patients with renal disease. Nephrology, dialysis, transplantation : official publication of the European Dialysis and Transplant Association - European Renal Association, 17(6), pp. 1005-1013.

HSU, C., IRIBARREN, C., MCCULLOCH, C.E., DARBINIAN, J. and GO, A.S., 2009. Risk factors for end-stage renal disease: 25-year follow-up. Archives of Internal Medicine, 169(4), pp. 342-350.

HSU, C., XIE, D., WAIKAR, S.S., BONVENTRE, J.V., ZHANG, X., SABBISETTI, V., MIFFLIN, T.E., CORESH, J., DIAMANTIDIS, C.J. and HE, J., 2017. Urine biomarkers of tubular injury do not improve on the clinical model predicting chronic kidney disease progression. Kidney international, 91(1), pp. 196-203.

HSU, C.C., KAO, W.L., CORESH, J., PANKOW, J.S., MARSH-MANZI, J., BOERWINKLE, E. and BRAY, M.S., 2005. Apolipoprotein E and progression of chronic kidney disease. Jama, 293(23), pp. 2892-2899.

HU, H., WANG, G., BATTEUX, F. and NICCO, C., 2009. Gender differences in the susceptibility to renal ischemia-reperfusion injury in BALB/c mice. The Tohoku journal of experimental medicine, 218(4), pp. 325-329.

HUANG, L., HAYLOR, J.L., FISHER, M., HAU, Z., EL NAHAS, A.M., GRIFFIN, M. and JOHNSON, T.S., 2010. Do changes in transglutaminase activity alter latent transforming growth factor beta activation in experimental diabetic nephropathy? Nephrology, dialysis, transplantation : official publication of the European Dialysis and Transplant Association - European Renal Association, 25(12), pp. 3897-3910.

HUANG, L., HAYLOR, J.L., HAU, Z., JONES, R.A., VICKERS, M.E., WAGNER, B., GRIFFIN, M., SAINT, R.E., COUTTS, I.G. and EL NAHAS, A.M., 2009. Transglutaminase inhibition ameliorates experimental diabetic nephropathy. Kidney international, 76(4), pp. 383-394.

HUANG, L., SCARPELLINI, A., FUNCK, M., VERDERIO, E.A. and JOHNSON, T.S., 2013. Development of a chronic kidney disease model in C57BL/6 mice with relevance to human pathology. Nephron extra, 3(1), pp. 12-29.

HUANG, W., PETERS, C., ZURAKOWSKI, D., BORER, J., DIAMOND, D., BAUER, S., MCLELLAN, D. and ROSEN, S., 2006. Renal biopsy in congenital ureteropelvic junction obstruction: evidence for parenchymal maldevelopment. Kidney international, 69(1), pp. 137-143.

HUBER, M., RETTLER, I., BERNASCONI, K., FRENK, E., LAVRIJSEN, S.P., PONEC, M., BON, A., LAUTENSCHLAGER, S., SCHORDERET, D.F. and HOHL, D., 1995. Mutations of keratinocyte transglutaminase in lamellar ichthyosis. SCIENCE-NEW YORK THEN WASHINGTON-, , pp. 525-525.

HUELSZ-PRINCE, G., BELKIN, A.M., VANBAVEL, E. and BAKKER, E.N., 2013. Activation of extracellular transglutaminase 2 by mechanical force in the arterial wall. Journal of vascular research, 50(5), pp. 383-395.

HUFF, T., OTTO, A.M., MULLER, C.S., MEIER, M. and HANNAPPEL, E., 2002. Thymosin beta4 is released from human blood platelets and attached by factor XIIIa (transglutaminase) to fibrin and collagen. FASEB journal : official publication of the Federation of American Societies for Experimental Biology, 16(7), pp. 691-696.

HUGEL, B., MARTINEZ, M.C., KUNZELMANN, C. and FREYSSINET, J.M., 2005. Membrane microparticles: two sides of the coin. Physiology (Bethesda, Md.), 20, pp. 22-27.

HUGHES, R.C., 1999. Secretion of the galectin family of mammalian carbohydrate-binding proteins. Biochimica et Biophysica Acta (BBA)-General Subjects, 1473(1), pp. 172-185.

HUGO, C., KANG, D.H. and JOHNSON, R.J., 2002. Sustained expression of thrombospondin-1 is associated with the development of glomerular and tubulointerstitial fibrosis in the remnant kidney model. Nephron, 90(4), pp. 460-470.

HUMPHRIES, J.D., WANG, P., STREULI, C., GEIGER, B., HUMPHRIES, M.J. and BALLESTREM, C., 2007. Vinculin controls focal adhesion formation by direct interactions with talin and actin. The Journal of cell biology, 179(5), pp. 1043-1057.

HURLEY, J.H. and ODORIZZI, G., 2012. Get on the exosome bus with ALIX. Nature cell biology, 14(7), pp. 654-655.

HUVENEERS, S. and DANEN, E.H., 2009. Adhesion signaling - crosstalk between integrins, Src and Rho. Journal of cell science, 122(Pt 8), pp. 1059-1069.

HUVENEERS, S., TRUONG, H., FASSLER, R., SONNENBERG, A. and DANEN, E.H., 2008. Binding of soluble fibronectin to integrin alpha5 beta1 - link to focal adhesion redistribution and contractile shape. Journal of cell science, 121(Pt 15), pp. 2452-2462.

ICHINOSE, A., BOTTENUS, R., DAVIE, E., ELBRECHT, A., DIRENZO, J., SMITH, R., SHENOLIKAR, S., SATO, M., HISABORI, T. and YOSHIDA, M., 1990. Structure of transglutaminases. J Biol Chem, 265.

IENTILE, R., CACCAMO, D. and GRIFFIN, M., 2007. Tissue transglutaminase and the stress response. Amino acids, 33(2), pp. 385-394.

IENTILE, R., CACCAMO, D., MARCIANO, M.C., CURRÒ, M., MANNUCCI, C., CAMPISI, A. and CALAPAI, G., 2004. Transglutaminase activity and transglutaminase mRNA transcripts in gerbil brain ischemia. Neuroscience letters, 363(2), pp. 173-177.

IGNOTZ, R.A. and MASSAGUE, J., 1986. Transforming growth factor-beta stimulates the expression of fibronectin and collagen and their incorporation into the extracellular matrix. The Journal of biological chemistry, 261(9), pp. 4337-4345.

IHLE, B.U., BECKER, G.J., WHITWORTH, J.A., CHARLWOOD, R.A. and KINCAID-SMITH, P.S., 1989. The effect of protein restriction on the progression of renal insufficiency. New England Journal of Medicine, 321(26), pp. 1773-1777.

IISMAA, S.E., HOLMAN, S., WOUTERS, M.A., LORAND, L., GRAHAM, R.M. and HUSAIN, A., 2003. Evolutionary specialization of a tryptophan indole group for transition-state stabilization by eukaryotic transglutaminases. Proceedings of the National Academy of Sciences, 100(22), pp. 12636-12641.

IISMAA, S.E., MEARNS, B.M., LORAND, L. and GRAHAM, R.M., 2009. Transglutaminases and disease: lessons from genetically engineered mouse models and inherited disorders. Physiological Reviews, 89(3), pp. 991-1023.

IKEE, R., KOBAYASHI, S., HEMMI, N., SAIGUSA, T., NAMIKOSHI, T., YAMADA, M., IMAKIIRE, T., KIKUCHI, Y., SUZUKI, S. and MIURA, S., 2007. Involvement of transglutaminase-2 in pathological changes in renal disease. Nephron.Clinical practice, 105(3), pp. c139-46.

IKURA, K., NASU, T., YOKOTA, H., TSUCHIYA, Y., SASAKI, R. and CHIBA, H., 1988. Amino acid sequence of guinea pig liver transglutaminase from its cDNA sequence. Biochemistry, 27(8), pp. 2898-2905.

IKURA, K., SHINAGAWA, R., SUTO, N. and SASAKI, R., 1994. Increase caused by interleukin-6 in promoter activity of guinea pig liver transglutaminase gene. Bioscience, biotechnology, and biochemistry, 58(8), pp. 1540-1541.

INAZAKI, K., KANAMARU, Y., KOJIMA, Y., SUEYOSHI, N., OKUMURA, K., KANEKO, K., YAMASHIRO, Y., OGAWA, H. and NAKAO, A., 2004. Smad3 deficiency attenuates renal fibrosis, inflammation, and apoptosis after unilateral ureteral obstruction. Kidney international, 66(2), pp. 597-604.

INBAL, A. and DARDIK, R., 2006. Role of coagulation factor XIII (FXIII) in angiogenesis and tissue repair. Pathophysiology of haemostasis and thrombosis, 35(1-2), pp. 162-165.

INKER, L.A., ASTOR, B.C., FOX, C.H., ISAKOVA, T., LASH, J.P., PERALTA, C.A., TAMURA, M.K. and FELDMAN, H.I., 2014. KDOQI US commentary on the 2012 KDIGO clinical practice guideline for the evaluation and management of CKD. American Journal of Kidney Diseases, 63(5), pp. 713-735.

INOMATA, S., SAKATSUME, M., SAKAMAKI, Y., WANG, X., GOTO, S., YAMAMOTO, T., GEJYO, F. and NARITA, I., 2011. Expression of SM22alpha (transgelin) in glomerular and interstitial renal injury. Nephron.Experimental nephrology, 117(4), pp. e104-13.

IOZZO, R.V., 2001. Heparan sulfate proteoglycans: intricate molecules with intriguing functions. The Journal of clinical investigation, 108(2), pp. 165-167.

IOZZO, R.V., 2005. Basement membrane proteoglycans: from cellar to ceiling. Nature Reviews Molecular Cell Biology, 6(8), pp. 646-656.

IOZZO, R.V., ZOELLER, J.J. and NYSTRÖM, A., 2009. Basement membrane proteoglycans: modulators Par Excellence of cancer growth and angiogenesis. Molecules and cells, 27(5), pp. 503-513.

ISHIDOYA, S., MORRISSEY, J., MCCRACKEN, R., REYES, A. and KLAHR, S., 1995. Angiotensin II receptor antagonist ameliorates renal tubulointerstitial fibrosis caused by unilateral ureteral obstruction. Kidney international, 47(5), pp. 1285-1294.

ISHIGURO, K., KOJIMA, T. and MURAMATSU, T., 2002. Syndecan-4 as a molecule involved in defense mechanisms. Glycoconjugate journal, 19(4-5), pp. 315-318.

JACKSON, A., FRIEDMAN, S., ZHAN, X., ENGLEKA, K.A., FOROUGH, R. and MACIAG, T., 1992. Heat shock induces the release of fibroblast growth factor 1 from NIH 3T3 cells. Proceedings of the National Academy of Sciences of the United States of America, 89(22), pp. 10691-10695.

JACKSON, A., TARANTINI, F., GAMBLE, S., FRIEDMAN, S. and MACIAG, T., 1995. The release of fibroblast growth factor-1 from NIH 3T3 cells in response to temperature involves the function of cysteine residues. Journal of Biological Chemistry, 270(1), pp. 33-36.

JAKOBSSON, L., KREUGER, J., HOLMBORN, K., LUNDIN, L., ERIKSSON, I., KJELLÉN, L. and CLAESSON-WELSH, L., 2006. Heparan sulfate in trans potentiates VEGFR-mediated angiogenesis. Developmental cell, 10(5), pp. 625-634.

JANDU, S.K., WEBB, A.K., PAK, A., SEVINC, B., NYHAN, D., BELKIN, A.M., FLAVAHAN, N.A., BERKOWITZ, D.E. and SANTHANAM, L., 2013. Nitric oxide regulates tissue transglutaminase localization and function in the vasculature. Amino acids, 44(1), pp. 261-269.

JANG, G., JEON, J., CHO, S., SHIN, D., KIM, C., JEONG, E., BAE, H., KIM, T.W., LEE, S. and CHOI, Y., 2010. Transglutaminase 2 suppresses apoptosis by modulating caspase 3 and NF-κB activity in hypoxic tumor cells. Oncogene, 29(3), pp. 356-367.

JANG, T., LEE, D., CHOI, K., JEONG, E.M., KIM, I., KIM, Y.W., CHUN, J.N., JEON, J. and PARK, H.H., 2014. Crystal structure of transglutaminase 2 with GTP complex and amino acid sequence evidence of evolution of GTP binding site. PLoS One, 9(9), pp. e107005.

JEITNER, T.M., MUMA, N.A., BATTAILE, K.P. and COOPER, A.J., 2009. Transglutaminase activation in neurodegenerative diseases. Future neurology, 4(4), pp. 449-467.

JEONG, J., MURTHY, S.P., RADEK, J.T. and LORAND, L., 1995. The fibronectin-binding domain of transglutaminase. Journal of Biological Chemistry, 270(10), pp. 5654-5658.

JIANG, W.G. and ABLIN, R.J., 2011. Prostate transglutaminase: a unique transglutaminase and its role in prostate cancer. Biomarkers in medicine, 5(3), pp. 285-291.

JIANG, W.G., ABLIN, R., DOUGLAS-JONES, A. and MANSEL, R.E., 2003. Expression of transglutaminases in human breast cancer and their possible clinical significance. Oncology reports, 10(6), pp. 2039-2044.

JIN, X., STAMNAES, J., KLOCK, C., DIRAIMONDO, T.R., SOLLID, L.M. and KHOSLA, C., 2011. Activation of extracellular transglutaminase 2 by thioredoxin. The Journal of biological chemistry, 286(43), pp. 37866-37873.

JOHN, S., THIEBACH, L., FRIE, C., MOKKAPATI, S., BECHTEL, M., NISCHT, R., ROSSER-DAVIES, S., PAULSSON, M. and SMYTH, N., 2012. Epidermal transglutaminase (TGase 3) is required for proper hair development, but not the formation of the epidermal barrier. PLoS One, 7(4), pp. e34252.

JOHNSON, A.E. and VAN WAES, M.A., 1999. The translocon: a dynamic gateway at the ER membrane. Annual Review of Cell and Developmental Biology, 15(1), pp. 799-842.

JOHNSON, R.J., IIDA, H., ALPERS, C.E., MAJESKY, M.W., SCHWARTZ, S.M., PRITZI, P., GORDON, K. and GOWN, A.M., 1991. Expression of smooth muscle cell phenotype by rat mesangial cells in immune complex nephritis. Alpha-smooth muscle actin is a marker of mesangial cell proliferation. The Journal of clinical investigation, 87(3), pp. 847-858.

JOHNSON, T., GRIFFIN, M., THOMAS, G., YANG, B., SKILL, J., COX, A., NICHOLAS, B., KUBARA, C. and ELNAHAS, A., 1997a. Transglutaminase intracellularly crosslinks tubule cells and stabilizes the ECM in kidney fibrosis, KIDNEY INTERNATIONAL 1997a, BLACKWELL SCIENCE INC 350 MAIN ST, MALDEN, MA 02148, pp. 279-279.

JOHNSON, T.S., ABO-ZENAH, H., SKILL, J.N., BEX, S., WILD, G., BROWN, C.B., GRIFFIN, M. and EL NAHAS, A.M., 2004. Tissue transglutaminase: a mediator and predictor of chronic allograft nephropathy? Transplantation, 77(11), pp. 1667-1675.

JOHNSON, T.S., EL-KORAIE, A.F., SKILL, N.J., BADDOUR, N.M., EL NAHAS, A.M., NJLOMA, M., ADAM, A.G. and GRIFFIN, M., 2003. Tissue transglutaminase and the progression of human renal scarring. Journal of the American Society of Nephrology : JASN, 14(8), pp. 2052-2062.

JOHNSON, T.S., FISHER, M., HAYLOR, J.L., HAU, Z., SKILL, N.J., JONES, R., SAINT, R., COUTTS, I., VICKERS, M.E., EL NAHAS, A.M. and GRIFFIN, M., 2007. Transglutaminase inhibition reduces fibrosis and preserves function in experimental chronic kidney disease. Journal of the American Society of Nephrology : JASN, 18(12), pp. 3078-3088.

JOHNSON, T.S., GRIFFIN, M., THOMAS, G.L., SKILL, J., COX, A., YANG, B., NICHOLAS, B., BIRCKBICHLER, P.J., MUCHANETA-KUBARA, C. and MEGUID EL NAHAS, A., 1997b. The role of transglutaminase in the rat subtotal nephrectomy model of renal fibrosis. The Journal of clinical investigation, 99(12), pp. 2950-2960.

JOHNSON, T.S., SKILL, N.J., EL NAHAS, A.M., OLDROYD, S.D., THOMAS, G.L., DOUTHWAITE, J.A., HAYLOR, J.L. and GRIFFIN, M., 1999. Transglutaminase transcription and antigen translocation in experimental renal scarring. Journal of the American Society of Nephrology : JASN, 10(10), pp. 2146-2157.

JONES, A.T., 2007. Macropinocytosis: searching for an endocytic identity and role in the uptake of cell penetrating peptides. Journal of Cellular and Molecular Medicine, 11(4), pp. 670-684.

JONES, R., KOTSAKIS, P., JOHNSON, T., CHAU, D., ALI, S., MELINO, G. and GRIFFIN, M., 2006. Matrix changes induced by transglutaminase 2 lead to inhibition of angiogenesis and tumor growth. Cell Death & Differentiation, 13(9), pp. 1442-1453.

JONES, R.A., NICHOLAS, B., MIAN, S., DAVIES, P.J. and GRIFFIN, M., 1997. Reduced expression of tissue transglutaminase in a human endothelial cell line leads to changes in cell spreading, cell adhesion and reduced polymerisation of fibronectin. Journal of cell science, 110 (Pt 19)(Pt 19), pp. 2461-2472.

JUNN, E., RONCHETTI, R.D., QUEZADO, M.M., KIM, S.Y. and MOURADIAN, M.M., 2003. Tissue transglutaminase-induced aggregation of alpha-synuclein: Implications for Lewy body formation in Parkinson's disease and dementia with Lewy bodies. Proceedings of the National Academy of Sciences of the United States of America, 100(4), pp. 2047-2052.

KAHLENBERG, J.M. and DUBYAK, G.R., 2004. Mechanisms of caspase-1 activation by P2X7 receptor-mediated K+ release. American journal of physiology.Cell physiology, 286(5), pp. C1100-8.

KAISSLING, B., LEHIR, M. and KRIZ, W., 2013. Renal epithelial injury and fibrosis. Biochimica et Biophysica Acta (BBA)-Molecular Basis of Disease, 1832(7), pp. 931-939.

KALININ, A.E., KAJAVA, A.V. and STEINERT, P.M., 2002. Epithelial barrier function: assembly and structural features of the cornified cell envelope. Bioessays, 24(9), pp. 789-800.

KALRA, H., SIMPSON, R.J., JI, H., AIKAWA, E., ALTEVOGT, P., ASKENASE, P., BOND, V.C., BORRÀS, F.E., BREAKEFIELD, X. and BUDNIK, V., 2012. Vesiclepedia: a compendium for extracellular vesicles with continuous community annotation. PLoS Biol, 10(12), pp. e1001450.

KANCHAN, K., FUXREITER, M. and FÉSÜS, L., 2015. Physiological, pathological, and structural implications of non-enzymatic protein–protein interactions of the multifunctional human transglutaminase 2. Cellular and Molecular Life Sciences, 72(16), pp. 3009-3035.

KANETO, H., MORRISSEY, J. and KLAHR, S., 1993. Increased expression of TGF-β1 mRNA in the obstructed kidney of rats with unilateral ureteral ligation. Kidney international, 44(2), pp. 313-321.

KANG, J.E., CHOI, S., PARK, J.B. and CHUNG, K.C., 2005. Regulation of the proapoptotic activity of huntingtin interacting protein 1 by Dyrk1 and caspase-3 in hippocampal neuroprogenitor cells. Journal of neuroscience research, 81(1), pp. 62-72.

KAO, W.L., KLAG, M.J., MEONI, L.A., REICH, D., BERTHIER-SCHAAD, Y., LI, M., CORESH, J., PATTERSON, N., TANDON, A. and POWE, N.R., 2008. MYH9 is associated with nondiabetic end-stage renal disease in African Americans. Nature genetics, 40(10), pp. 1185-1192.

KARAGIANNI, F., PRAKOURA, N., KALTSA, G., POLITIS, P., ARVANITI, E., KALTEZIOTI, V., PSARRAS, S., PAGAKIS, S., KATSIMBOULAS, M. and ABED, A., 2013. Transgelin up-regulation in obstructive nephropathy. PloS one, 8(6), pp. e66887.

KARHINEN, L., BASTOS, R.N., JOKITALO, E. and MAKAROW, M., 2005. Endoplasmic reticulum exit of a secretory glycoprotein in the absence of sec24p family proteins in yeast. Traffic, 6(7), pp. 562-574.

KASTAN, M.B. and LIM, D., 2000. The many substrates and functions of ATM. Nature reviews Molecular cell biology, 1(3), pp. 179-186.

KATO, M., SAUNDERS, S., NGUYEN, H. and BERNFIELD, M., 1995. Loss of cell surface syndecan-1 causes epithelia to transform into anchorage-independent mesenchyme-like cells. Molecular biology of the cell, 6(5), pp. 559-576.

KATOH, H. and NEGISHI, M., 2003. RhoG activates Rac1 by direct interaction with the Dock180-binding protein Elmo. Nature, 424(6947), pp. 461-464.

KATOH, Y., IMAKAGURA, H., FUTATSUMORI, M. and NAKAYAMA, K., 2006. Recruitment of clathrin onto endosomes by the Tom1–Tollip complex. Biochemical and biophysical research communications, 341(1), pp. 143-149.

KATOH, Y., SHIBA, Y., MITSUHASHI, H., YANAGIDA, Y., TAKATSU, H. and NAKAYAMA, K., 2004. Tollip and Tom1 form a complex and recruit ubiquitin-conjugated proteins onto early endosomes. The Journal of biological chemistry, 279(23), pp. 24435-24443.

KAUSAR, T., SHARMA, R., HASAN, M.R., TRIPATHI, S.C., SARAYA, A., CHATTOPADHYAY, T.K., GUPTA, S.D. and RALHAN, R., 2010. Clinical significance of GPR56, transglutaminase 2, and NF-κB in esophageal squamous cell carcinoma. Cancer investigation, .

KAWAI, Y., WADA, F., SUGIMURA, Y., MAKI, M. and HITOMI, K., 2008. Transglutaminase 2 activity promotes membrane resealing after mechanical damage in the lung cancer cell line A549. Cell biology international, 32(8), pp. 928-934.

KEERTHIKUMAR, S., CHISANGA, D., ARIYARATNE, D., AL SAFFAR, H., ANAND, S., ZHAO, K., SAMUEL, M., PATHAN, M., JOIS, M. and CHILAMKURTI, N., 2016. ExoCarta: a web-based compendium of exosomal cargo. Journal of Molecular Biology, 428(4), pp. 688-692.

KELLER, M., RÜEGG, A., WERNER, S. and BEER, H., 2008. Active caspase-1 is a regulator of unconventional protein secretion. Cell, 132(5), pp. 818-831.

KENNY, H.A., KAUR, S., COUSSENS, L.M. and LENGYEL, E., 2008. The initial steps of ovarian cancer cell metastasis are mediated by MMP-2 cleavage of vitronectin and fibronectin. The Journal of clinical investigation, 118(4), pp. 1367-1379.

KHALIL, I.A., KOGURE, K., AKITA, H. and HARASHIMA, H., 2006. Uptake pathways and subsequent intracellular trafficking in nonviral gene delivery. Pharmacological reviews, 58(1), pp. 32-45.

KHARAZIHA, P., CHIOUREAS, D., RUTISHAUSER, D., BALTATZIS, G., LENNARTSSON, L., FONSECA, P., AZIMI, A., HULTENBY, K., ZUBAREV, R., ULLEN, A., YACHNIN, J., NILSSON, S. and PANARETAKIS, T., 2015. Molecular profiling of prostate cancer derived exosomes may reveal a predictive signature for response to docetaxel. Oncotarget, 6(25), pp. 21740-21754.

KIM, C.W., GOLDBERGER, O.A., GALLO, R.L. and BERNFIELD, M., 1994. Members of the syndecan family of heparan sulfate proteoglycans are expressed in distinct cell-, tissue-, and development-specific patterns. Molecular biology of the cell, 5(7), pp. 797-805.

KIM, H.C., LEWIS, M.S., GORMAN, J.J., PARK, S.C., GIRARD, J.E., FOLK, J.E. and CHUNG, S.I., 1990. Protransglutaminase E from guinea pig skin. Isolation and partial characterization. The Journal of biological chemistry, 265(35), pp. 21971-21978.

KIM, J., NAM, K.H., KWON, O., KIM, I.G., BUSTIN, M., CHOY, H.E. and PARK, S.C., 2002. Histone cross-linking by transglutaminase. Biochemical and biophysical research communications, 293(5), pp. 1453-1457.

KIM, S. and BAE, C., 1998. Calpain inhibitors reduce the cornified cell envelope formation by inhibiting proteolytic processing of transglutaminase 1. Experimental and Molecular Medicine, 30, pp. 257-262.

KIM, S.Y., CHUNG, S.I. and STEINERT, P.M., 1995. Highly active soluble processed forms of the transglutaminase 1 enzyme in epidermal keratinocytes. The Journal of biological chemistry, 270(30), pp. 18026-18035.

KIMURA, K., IWANO, M., HIGGINS, D.F., YAMAGUCHI, Y., NAKATANI, K., HARADA, K., KUBO, A., AKAI, Y., RANKIN, E.B., NEILSON, E.G., HAASE, V.H. and SAITO, Y., 2008. Stable expression of HIF-1alpha in tubular epithelial cells promotes interstitial fibrosis. American journal of physiology.Renal physiology, 295(4), pp. F1023-9.

KINSETH, M.A., ANJARD, C., FULLER, D., GUIZZUNTI, G., LOOMIS, W.F. and MALHOTRA, V., 2007. The Golgi-associated protein GRASP is required for unconventional protein secretion during development. Cell, 130(3), pp. 524-534.

KIRÁLY, R., DEMÉNY, M. and FÉSÜS, L., 2011. Protein transamidation by transglutaminase 2 in cells: a disputed Ca2 -dependent action of a multifunctional protein. FEBS Journal, 278(24), pp. 4717-4739.

KIRÁLY, R., THANGARAJU, K., NAGY, Z., COLLIGHAN, R., NEMES, Z., GRIFFIN, M. and FÉSÜS, L., 2016. Isopeptidase activity of human transglutaminase 2: disconnection from transamidation and characterization by kinetic parameters. Amino acids, 48(1), pp. 31-40.

KIRCHHAUSEN, T., OWEN, D. and HARRISON, S.C., 2014. Molecular structure, function, and dynamics of clathrin-mediated membrane traffic. Cold Spring Harbor perspectives in biology, 6(5), pp. a016725.

KIRKPATRICK, C.A. and SELLECK, S.B., 2007. Heparan sulfate proteoglycans at a glance. Journal of cell science, 120(Pt 11), pp. 1829-1832.

KIROV, A., AL-HASHIMI, H., SOLOMON, P., MAZUR, C., THORPE, P.E., SIMS, P.J., TARANTINI, F., KUMAR, T.K.S. and PRUDOVSKY, I., 2012. Phosphatidylserine externalization and membrane blebbing are involved in the nonclassical export of FGF1. Journal of cellular biochemistry, 113(3), pp. 956-966.

KLAHR, S. and MORRISSEY, J.J., 1998. The role of growth factors, cytokines, and vasoactive compounds in obstructive nephropathy. Seminars in nephrology, 18(6), pp. 622-632.

KLEIJMEER, M.J., STOORVOGEL, W., GRIFFITH, J.M., YOSHIE, O. and GEUZE, H.J., 1998. Selective enrichment of tetraspan proteins on the internal vesicles of multivesicular endosomes and on exosomes secreted by human B-lymphocytes. Journal of Biological Chemistry, 273(32), pp. 20121-20127.

KLEIN, J., KAVVADAS, P., PRAKOURA, N., KARAGIANNI, F., SCHANSTRA, J.P., BASCANDS, J. and CHARONIS, A., 2011. Renal fibrosis: insight from proteomics in animal models and human disease. Proteomics, 11(4), pp. 805-815.

KLEMAN, J., AESCHLIMANN, D., PAULSSON, M. and VAN DER REST, M., 1995. Transglutaminase-catalyzed crosslinking of fibrils of collagen V/XI in A204 rhabdomyosarcoma cells. Biochemistry, 34(42), pp. 13768-13775.

KLIBI, J., NIKI, T., RIEDEL, A., PIOCHE-DURIEU, C., SOUQUERE, S., RUBINSTEIN, E., LE MOULEC, S., GUIGAY, J., HIRASHIMA, M., GUEMIRA, F., ADHIKARY, D., MAUTNER, J. and BUSSON, P., 2009. Blood diffusion and Th1-suppressive effects of galectin-9-containing exosomes released by Epstein-Barr virus-infected nasopharyngeal carcinoma cells. Blood, 113(9), pp. 1957-1966.

KLÖCK, C., DIRAIMONDO, T.R. and KHOSLA, C., 2012. Role of transglutaminase 2 in celiac disease pathogenesis, Seminars in immunopathology 2012, Springer, pp. 513-522.

KOIVUSALO, M., WELCH, C., HAYASHI, H., SCOTT, C.C., KIM, M., ALEXANDER, T., TOURET, N., HAHN, K.M. and GRINSTEIN, S., 2010. Amiloride inhibits macropinocytosis by lowering submembranous pH and preventing Rac1 and Cdc42 signaling. The Journal of cell biology, 188(4), pp. 547-563.

KOJIMA, S., NARA, K. and RIFKIN, D.B., 1993. Requirement for transglutaminase in the activation of latent transforming growth factor-beta in bovine endothelial cells. The Journal of cell biology, 121(2), pp. 439-448.

KOLM, V., SAUER, U., OLGEMOLLER, B. and SCHLEICHER, E.D., 1996. High glucose-induced TGF-beta 1 regulates mesangial production of heparan sulfate proteoglycan. The American Journal of Physiology, 270(5 Pt 2), pp. F812-21.

KOLSET, S. and TVEIT, H., 2008. Serglycin–structure and biology. Cellular and Molecular Life Sciences, 65(7-8), pp. 1073-1085.

KOO, B., JUNG, Y.S., SHIN, J., HAN, I., MORTIER, E., ZIMMERMANN, P., WHITEFORD, J.R., COUCHMAN, J.R., OH, E. and LEE, W., 2006. Structural basis of syndecan-4 phosphorylation as a molecular switch to regulate signaling. Journal of Molecular Biology, 355(4), pp. 651-663.

KOPP, J.B., NELSON, G.W., SAMPATH, K., JOHNSON, R.C., GENOVESE, G., AN, P., FRIEDMAN, D., BRIGGS, W., DART, R., KORBET, S., MOKRZYCKI, M.H., KIMMEL, P.L., LIMOU, S., AHUJA, T.S., BERNS, J.S., FRYC, J., SIMON, E.E., SMITH, M.C., TRACHTMAN, H., MICHEL, D.M., SCHELLING, J.R., VLAHOV, D., POLLAK, M. and WINKLER, C.A., 2011. APOL1 genetic variants in focal segmental glomerulosclerosis and HIV-associated nephropathy. Journal of the American Society of Nephrology : JASN, 22(11), pp. 2129-2137.

KOSEKI-KUNO, S., YAMAKAWA, M., DICKNEITE, G. and ICHINOSE, A., 2003. Factor XIII A subunit-deficient mice developed severe uterine bleeding events and subsequent spontaneous miscarriages. Blood, 102(13), pp. 4410-4412.

KOSEKI-KUNO, S., YAMAKAWA, M., DICKNEITE, G. and ICHINOSE, A., 2003. Factor XIII A subunit-deficient mice developed severe uterine bleeding events and subsequent spontaneous miscarriages. Blood, 102(13), pp. 4410-4412.

KOTHAPALLI, D., FRAZIER, K.S., WELPLY, A., SEGARINI, P.R. and GROTENDORST, G.R., 1997. Transforming growth factor beta induces anchorage-independent growth of NRK fibroblasts via a connective tissue growth factor-dependent signaling pathway. Cell growth & differentiation : the molecular biology journal of the American Association for Cancer Research, 8(1), pp. 61-68.

KOUMANGOYE, R.B., SAKWE, A.M., GOODWIN, J.S., PATEL, T. and OCHIENG, J., 2011. Detachment of breast tumor cells induces rapid secretion of exosomes which subsequently mediate cellular adhesion and spreading. PLoS One, 6(9), pp. e24234.

KOWAL, J., TKACH, M. and THERY, C., 2014. Biogenesis and secretion of exosomes. Current opinion in cell biology, 29, pp. 116-125.

KRAJEWSKA, W.M. and MASLOWSKA, I., 2004. Caveolins: structure and function in signal transduction. CELLULAR AND MOLECULAR BIOLOGY LETTERS., 9(2), pp. 195-220.

KRAMER, K.L. and YOST, H.J., 2002. Ectodermal syndecan-2 mediates left-right axis formation in migrating mesoderm as a cell-nonautonomous Vg1 cofactor. Developmental cell, 2(1), pp. 115-124.

KREN, S. and HOSTETTER, T.H., 1999. The course of the remnant kidney model in mice. Kidney international, 56(1), pp. 333-337.

KREUGER, J., SPILLMANN, D., LI, J.P. and LINDAHL, U., 2006. Interactions between heparan sulfate and proteins: the concept of specificity. The Journal of cell biology, 174(3), pp. 323-327.

KUCHLER, K., STERNE, R.E. and THORNER, J., 1989. Saccharomyces cerevisiae STE6 gene product: a novel pathway for protein export in eukaryotic cells. The EMBO journal, 8(13), pp. 3973-3984.

KUMAR, A., XU, J., SUNG, B., KUMAR, S., YU, D., AGGARWAL, B.B. and MEHTA, K., 2012. Evidence that GTP-binding domain but not catalytic domain of transglutaminase 2 is essential for epithelial-to-mesenchymal transition in mammary epithelial cells. Breast Cancer Research, 14(1), pp. R4.

KUMAZAWA, Y., OHTSUKA, T., NINOMIYA, D. and SEGURO, K., 1997. Purification and calcium dependence of transglutaminases from sheep hair follicles. Bioscience, biotechnology, and biochemistry, 61(7), pp. 1086-1090.

KUNCIO, G., TSYGANSKAYA, M., ZHU, J., LIU, S. and ZERN, M., 1996. TNF-alpha modulates expression of the tissue transglutaminase gene in human HEPG2 cells. Hepatology 1996, WB SAUNDERS CO INDEPENDENCE SQUARE WEST CURTIS CENTER, STE 300, PHILADELPHIA, PA 19106-3399, pp. 813-813.

KUWABARA, A., SATOH, M., TOMITA, N., SASAKI, T. and KASHIHARA, N., 2010. Deterioration of glomerular endothelial surface layer induced by oxidative stress is implicated in altered permeability of macromolecules in Zucker fatty rats. Diabetologia, 53(9), pp. 2056-2065.

KVIST, A.J., JOHNSON, A.E., MORGELIN, M., GUSTAFSSON, E., BENGTSSON, E., LINDBLOM, K., ASZODI, A., FASSLER, R., SASAKI, T., TIMPL, R. and ASPBERG, A., 2006. Chondroitin sulfate perlecan enhances collagen fibril formation. Implications for perlecan chondrodysplasias. The Journal of biological chemistry, 281(44), pp. 33127-33139.

LA VENUTA, G., WEGEHINGEL, S., SEHR, P., MULLER, H.M., DIMOU, E., STERINGER, J.P., GROTWINKEL, M., HENTZE, N., MAYER, M.P., WILL, D.W., UHRIG, U., LEWIS, J.D. and NICKEL, W., 2016. Small Molecule Inhibitors Targeting Tec Kinase Block Unconventional Secretion of Fibroblast Growth Factor 2. The Journal of biological chemistry, 291(34), pp. 17787-17803.

LA VENUTA, G., ZEITLER, M., STERINGER, J.P., MULLER, H.M. and NICKEL, W., 2015. The Startling Properties of Fibroblast Growth Factor 2: How to Exit Mammalian Cells without a Signal Peptide at Hand. The Journal of biological chemistry, 290(45), pp. 27015-27020.

LAI, T., HAUSLADEN, A., SLAUGHTER, T., EU, J., STAMLER, J. and GREENBERG, C., 2001. Calcium regulates S-nitrosylation, denitrosylation, and activity of tissue transglutaminase. Biochemistry, 40(16), pp. 4904-4910.

LAI, T.S., LIU, Y., LI, W. and GREENBERG, C.S., 2007. Identification of two GTP-independent alternatively spliced forms of tissue transglutaminase in human leukocytes, vascular smooth muscle, and endothelial cells. FASEB journal : official publication of the Federation of American Societies for Experimental Biology, 21(14), pp. 4131-4143.

LAM, S., VERHAGEN, N.A., STRUTZ, F., VAN DER PIJL, JOHAN W, DAHA, M.R. and VAN KOOTEN, C., 2003. Glucose-induced fibronectin and collagen type III expression in renal fibroblasts can occur independent of TGF-&bgr; 1. Kidney international, 63(3), pp. 878-888.

LAN, H.Y., 2011. Diverse roles of TGF-beta/Smads in renal fibrosis and inflammation. Int J Biol Sci, 7(7), pp. 1056-1067.

LANDRISCINA, M., SOLDI, R., BAGALA, C., MICUCCI, I., BELLUM, S., TARANTINI, F., PRUDOVSKY, I. and MACIAG, T., 2001. S100A13 participates in the release of fibroblast growth factor 1 in response to heat shock in vitro. The Journal of biological chemistry, 276(25), pp. 22544-22552.

LANGHORST, M.F., REUTER, A., JAEGER, F.A., WIPPICH, F.M., LUXENHOFER, G., PLATTNER, H. and STUERMER, C.A., 2008. Trafficking of the microdomain scaffolding protein reggie-1/flotillin-2. European journal of cell biology, 87(4), pp. 211-226.

LATZ, E., 2010. The inflammasomes: mechanisms of activation and function. Current opinion in immunology, 22(1), pp. 28-33.

LAZAR, I., CLEMENT, E., DUCOUX-PETIT, M., DENAT, L., SOLDAN, V., DAUVILLIER, S., BALOR, S., BURLET-SCHILTZ, O., LARUE, L. and MULLER, C., 2015. Proteome characterization of melanoma exosomes reveals a specific signature for metastatic cell lines. Pigment cell & melanoma research, 28(4), pp. 464-475.

LEBEAU, C., DEBELLE, F.D., ARLT, V.M., POZDZIK, A., DE PREZ, E.G., PHILLIPS, D.H., DESCHODT-LANCKMAN, M.M., VANHERWEGHEM, J.L. and NORTIER, J.L., 2005. Early proximal tubule injury in experimental aristolochic acid nephropathy: functional and histological studies. Nephrology, dialysis, transplantation : official publication of the European Dialysis and Transplant Association - European Renal Association, 20(11), pp. 2321-2332.

LEE, J., CONDELLO, S., YAKUBOV, B., EMERSON, R., CAPERELL-GRANT, A., HITOMI, K., XIE, J. and MATEI, D., 2015. Tissue Transglutaminase Mediated Tumor-Stroma Interaction Promotes Pancreatic Cancer Progression. Clinical cancer research : an official journal of the American Association for Cancer Research, 21(19), pp. 4482-4493.

LEE, J., MOON, P., LEE, I. and BAEK, M., 2015. Proteomic analysis of extracellular vesicles released by adipocytes of Otsuka Long-Evans Tokushima Fatty (OLETF) Rats. The protein journal, 34(3), pp. 220-235.

LEE, S., CHOI, J., JIN, D., KIM, J. and CHA, J., 2010. Expression of calponin in periglomerular myofibroblasts of rat kidney with experimental chronic injuries. Anatomy & cell biology, 43(2), pp. 132-139.

LEE, S.H., LEE, J.B., BAE, M.S., BALIKOV, D.A., HWANG, A., BOIRE, T.C., KWON, I.K., SUNG, H. and YANG, J.W., 2015. Current Progress in Nanotechnology Applications for Diagnosis and Treatment of Kidney Diseases. Advanced healthcare materials, 4(13), pp. 2037-2045.

LESORT, M., ATTANAVANICH, K., ZHANG, J. and JOHNSON, G.V., 1998. Distinct nuclear localization and activity of tissue transglutaminase. Journal of Biological Chemistry, 273(20), pp. 11991-11994.

LEVEY, A.S. and CORESH, J., 2012. Chronic kidney disease. The Lancet, 379(9811), pp. 165-180.

LEVEY, A.S., BOSCH, J.P., LEWIS, J.B., GREENE, T., ROGERS, N. and ROTH, D., 1999. A more accurate method to estimate glomerular filtration rate from serum creatinine: a new prediction equation. Annals of Internal Medicine, 130(6), pp. 461-470.

LEVEY, A.S., CATTRAN, D., FRIEDMAN, A., MILLER, W.G., SEDOR, J., TUTTLE, K., KASISKE, B. and HOSTETTER, T., 2009. Proteinuria as a surrogate outcome in CKD: report of a scientific workshop sponsored by the National Kidney Foundation and the US Food and Drug Administration. American Journal of Kidney Diseases, 54(2), pp. 205-226.

LEVEY, A.S., STEVENS, L.A., SCHMID, C.H., ZHANG, Y.L., CASTRO, A.F., FELDMAN, H.I., KUSEK, J.W., EGGERS, P., VAN LENTE, F. and GREENE, T., 2009. A new equation to estimate glomerular filtration rate. Annals of Internal Medicine, 150(9), pp. 604-612.

LEWIS, E.J., HUNSICKER, L.G., CLARKE, W.R., BERL, T., POHL, M.A., LEWIS, J.B., RITZ, E., ATKINS, R.C., ROHDE, R. and RAZ, I., 2001. Renoprotective effect of the angiotensin-receptor antagonist irbesartan in patients with nephropathy due to type 2 diabetes. New England Journal of Medicine, 345(12), pp. 851-860.

LI, J. and BERTRAM, J.F., 2010. Review: Endothelial-myofibroblast transition, a new player in diabetic renal fibrosis. Nephrology, 15(5), pp. 507-512.

LI, J., BROWN, L.F., LAHAM, R.J., VOLK, R. and SIMONS, M., 1997. Macrophage-dependent regulation of syndecan gene expression. Circulation research, 81(5), pp. 785-796.

LI, J.H., HUANG, X.R., ZHU, H., JOHNSON, R. and LAN, H.Y., 2003. Role of TGF-&bgr; signaling in extracellular matrix production under high glucose conditions. Kidney international, 63(6), pp. 2010-2019.

LI, X., WANG, X., ZHANG, X., ZHAO, M., TSANG, W.L., ZHANG, Y., YAU, R.G., WEISMAN, L.S. and XU, H., 2013. Genetically encoded fluorescent probe to visualize intracellular phosphatidylinositol 3,5-bisphosphate localization and dynamics. Proceedings of the National Academy of Sciences of the United States of America, 110(52), pp. 21165-21170.

LI, Y., ZHANG, Y., QIU, F. and QIU, Z., 2011. Proteomic identification of exosomal LRG1: a potential urinary biomarker for detecting NSCLC. Electrophoresis, 32(15), pp. 1976-1983.

LIANG, B., PENG, P., CHEN, S., LI, L., ZHANG, M., CAO, D., YANG, J., LI, H., GUI, T. and LI, X., 2013. Characterization and proteomic analysis of ovarian cancer-derived exosomes. Journal of proteomics, 80, pp. 171-182.

LIEBENHOFF, U. and ROSENTHAL, W., 1995. Identification of Rab3-, Rab5a-and synaptobrevin II-like proteins in a preparation of rat kidney vesicles containing the vasopressin-regulated water channel. FEBS letters, 365(2-3), pp. 209-213.

LIM, J.P. and GLEESON, P.A., 2011. Macropinocytosis: an endocytic pathway for internalising large gulps. Immunology and cell biology, 89(8), pp. 836-843.

LIM, S.T., LONGLEY, R.L., COUCHMAN, J.R. and WOODS, A., 2003. Direct binding of syndecan-4 cytoplasmic domain to the catalytic domain of protein kinase C alpha (PKC alpha) increases focal adhesion localization of PKC alpha. The Journal of biological chemistry, 278(16), pp. 13795-13802.

LIN, M.C., GALLETTA, B.J., SEPT, D. and COOPER, J.A., 2010. Overlapping and distinct functions for cofilin, coronin and Aip1 in actin dynamics in vivo. Journal of cell science, 123(Pt 8), pp. 1329-1342.

LIN, S., KISSELEVA, T., BRENNER, D.A. and DUFFIELD, J.S., 2008. Pericytes and perivascular fibroblasts are the primary source of collagen-producing cells in obstructive fibrosis of the kidney. The American journal of pathology, 173(6), pp. 1617-1627.

LINDNER, H.A., TÄFLER-NAUMANN, M. and RÖHM, K., 2008. N-acetylamino acid utilization by kidney aminoacylase-1. Biochimie, 90(5), pp. 773-780.

LISOWSKA-MYJAK, B., 2014. Uremic toxins and their effects on multiple organ systems. Nephron.Clinical practice, 128(3-4), pp. 303-311.

LIU, F. and RABINOVICH, G.A., 2005. Galectins as modulators of tumour progression. Nature Reviews Cancer, 5(1), pp. 29-41.

LIU, S., CERIONE, R.A. and CLARDY, J., 2002. Structural basis for the guanine nucleotide-binding activity of tissue transglutaminase and its regulation of transamidation activity. Proceedings of the National Academy of Sciences of the United States of America, 99(5), pp. 2743-2747.

LIU, S., LI, Y., ZHAO, H., CHEN, D., HUANG, Q., WANG, S., ZOU, W., ZHANG, Y., LI, X. and HUANG, H., 2006. Increase in extracellular cross-linking by tissue transglutaminase and reduction in expression of MMP-9 contribute differentially to focal segmental glomerulosclerosis in rats. Molecular and cellular biochemistry, 284(1-2), pp. 9-17.

REFERENCES

LIU, X., CHINELLO, C., MUSANTE, L., CAZZANIGA, M., TATARUCH, D., CALZAFERRI, G., JAMES SMITH, A., SIO, G., MAGNI, F. and ZOU, H., 2015. Intraluminal proteome and peptidome of human urinary extracellular vesicles. PROTEOMICS-Clinical Applications, 9(5-6), pp. 568-573.

LIU, Y., 2004. Epithelial to mesenchymal transition in renal fibrogenesis: pathologic significance, molecular mechanism, and therapeutic intervention. Journal of the American Society of Nephrology : JASN, 15(1), pp. 1-12.

LIU, Y., 2006. Renal fibrosis: new insights into the pathogenesis and therapeutics. Kidney international, 69(2), pp. 213-217.

LIVAK, K.J. and SCHMITTGEN, T.D., 2001. Analysis of relative gene expression data using real-time quantitative PCR and the 2− ΔΔCT method. methods, 25(4), pp. 402-408.

LLEDO, P., JOHANNES, L., VERNIER, P., ZOREC, R., DARCHEN, F., VINCENT, J., HENRY, J. and MASON, W.T., 1994. Rab3 proteins: key players in the control of exocytosis. Trends in neurosciences, 17(10), pp. 426-432.

LOPEZ-CASTEJON, G. and BROUGH, D., 2011. Understanding the mechanism of IL-1β secretion. Cytokine & growth factor reviews, 22(4), pp. 189-195.

LOPEZ-GIACOMAN, S. and MADERO, M., 2015. Biomarkers in chronic kidney disease, from kidney function to kidney damage. World journal of nephrology, 4(1), pp. 57-73.

LORAND, L. and GRAHAM, R.M., 2003. Transglutaminases: crosslinking enzymes with pleiotropic functions. Nature reviews Molecular cell biology, 4(2), pp. 140-156.

LORTAT-JACOB, H., BURHAN, I., SCARPELLINI, A., THOMAS, A., IMBERTY, A., VIVES, R.R., JOHNSON, T., GUTIERREZ, A. and VERDERIO, E.A., 2012. Transglutaminase-2 interaction with heparin: identification of a heparin binding site that regulates cell adhesion to fibronectin-transglutaminase-2 matrix. The Journal of biological chemistry, 287(22), pp. 18005-18017.

LUBERTO, C., HASSLER, D.F., SIGNORELLI, P., OKAMOTO, Y., SAWAI, H., BOROS, E., HAZEN-MARTIN, D.J., OBEID, L.M., HANNUN, Y.A. and SMITH, G.K., 2002. Inhibition of tumor necrosis factor-induced cell death in MCF7 by a novel inhibitor of neutral sphingomyelinase. The Journal of biological chemistry, 277(43), pp. 41128-41139.

LUNDE, I.G., HERUM, K.M., CARLSON, C.C. and CHRISTENSEN, G., 2016. Syndecans in heart fibrosis. Cell and tissue research, 365(3), pp. 539-552.

MA, L.J. and FOGO, A.B., 2009. PAI-1 and kidney fibrosis. Frontiers in bioscience (Landmark edition), 14, pp. 2028-2041.

MA, L.J., NAKAMURA, S., ALDIGIER, J.C., ROSSINI, M., YANG, H., LIANG, X., NAKAMURA, I., MARCANTONI, C. and FOGO, A.B., 2005. Regression of glomerulosclerosis with high-dose angiotensin inhibition is linked to decreased plasminogen activator inhibitor-1. Journal of the American Society of Nephrology : JASN, 16(4), pp. 966-976.

MACKENZIE, A., WILSON, H.L., KISS-TOTH, E., DOWER, S.K., NORTH, R.A. and SURPRENANT, A., 2001. Rapid secretion of interleukin-1β by microvesicle shedding. Immunity, 15(5), pp. 825-835.

MAEL-AININ, M., ABED, A., CONWAY, S.J., DUSSAULE, J.C. and CHATZIANTONIOU, C., 2014. Inhibition of periostin expression protects against the development of renal inflammation and fibrosis. Journal of the American Society of Nephrology : JASN, 25(8), pp. 1724-1736.

MAEZAWA, Y., TAKEMOTO, M. and YOKOTE, K., 2015. Cell biology of diabetic nephropathy: Roles of endothelial cells, tubulointerstitial cells and podocytes. Journal of diabetes investigation, 6(1), pp. 3-15.

MAHALINGAM, Y., GALLAGHER, J.T. and COUCHMAN, J.R., 2007. Cellular adhesion responses to the heparin-binding (HepII) domain of fibronectin require heparan sulfate with specific properties. The Journal of biological chemistry, 282(5), pp. 3221-3230.

MAKIOKA, K., YAMAZAKI, T., TAKATAMA, M., IKEDA, M., MURAYAMA, S., OKAMOTO, K. and IKEDA, Y., 2016. Immunolocalization of Tom1 in relation to protein degradation systems in Alzheimer's disease. Journal of the neurological sciences, 365, pp. 101-107.

MALHOTRA, V., 2013. Unconventional protein secretion: an evolving mechanism. The EMBO journal, 32(12), pp. 1660-1664.

MALLARD, F., TANG, B.L., GALLI, T., TENZA, D., SAINT-POL, A., YUE, X., ANTONY, C., HONG, W., GOUD, B. and JOHANNES, L., 2002. Early/recycling endosomes-to-TGN transport involves two SNARE complexes and a Rab6 isoform. The Journal of cell biology, 156(4), pp. 653-664.

MANGALA, L., FOK, J., ZORRILLA-CALANCHA, I., VERMA, A. and MEHTA, K., 2007. Tissue transglutaminase expression promotes cell attachment, invasion and survival in breast cancer cells. Oncogene, 26(17), pp. 2459-2470.

MANGALA, L.S. and MEHTA, K., 2005. Tissue transglutaminase (TG2) in cancer biology. Progress in experimental tumor research, 38, pp. 125-138.

MANJITHAYA, R. and SUBRAMANI, S., 2010. Role of autophagy in unconventional protein secretion. Autophagy, 6(5), pp. 650-651.

MANJITHAYA, R., ANJARD, C., LOOMIS, W.F. and SUBRAMANI, S., 2010a. Unconventional secretion of Pichia pastoris Acb1 is dependent on GRASP protein, peroxisomal functions, and autophagosome formation. The Journal of cell biology, 188(4), pp. 537-546.

MANN, A.P., VERMA, A., SETHI, G., MANAVATHI, B., WANG, H., FOK, J.Y., KUNNUMAKKARA, A.B., KUMAR, R., AGGARWAL, B.B. and MEHTA, K., 2006. Overexpression of tissue transglutaminase leads to constitutive activation of nuclear factor-kappaB in cancer cells: delineation of a novel pathway. Cancer research, 66(17), pp. 8788-8795.

MARIC, C., 2009. Sex, diabetes and the kidney. American journal of physiology.Renal physiology, 296(4), pp. F680-8.

MARIEB, E.N. and HOEHN, K., 2007. Human anatomy & physiology. Pearson Education.

MARSHANSKY, V. and FUTAI, M., 2008. The V-type H -ATPase in vesicular trafficking: targeting, regulation and function. Current opinion in cell biology, 20(4), pp. 415-426.

MARTINON, F., BURNS, K. and TSCHOPP, J., 2002. The inflammasome: a molecular platform triggering activation of inflammatory caspases and processing of proIL-β. Molecular cell, 10(2), pp. 417-426.

MARTÍN-SÁNCHEZ, F., DIAMOND, C., ZEITLER, M., GOMEZ, A., BAROJA-MAZO, A., BAGNALL, J., SPILLER, D., WHITE, M., DANIELS, M. and MORTELLARO, A., 2016. Inflammasome-dependent IL-1β release depends upon membrane permeabilisation. Cell Death & Differentiation, .

MASAKI, T., YORIOKA, N., TANIGUCHI, Y., ODA, H. and YAMAKIDO, M., 1998. Tenascin expression may reflect the activity and chronicity of human IgA nephropathy. Clinical nephrology, 50(4), pp. 205-213.

MASOLA, V., GAMBARO, G., TIBALDI, E., BRUNATI, A.M., GASTALDELLO, A., D'ANGELO, A., ONISTO, M. and LUPO, A., 2012. Heparanase and syndecan-1 interplay orchestrates fibroblast growth factor-2-induced epithelial-mesenchymal transition in renal tubular cells. The Journal of biological chemistry, 287(2), pp. 1478-1488.

MASTROBERARDINO, P., IANNICOLA, C., NARDACCI, R., BERNASSOLA, F., DE LAURENZI, V., MELINO, G., MORENO, S., PAVONE, F., OLIVERIO, S. and FESUS, L., 2002. 'Tissue'transglutaminase ablation reduces neuronal death and prolongs survival in a mouse model of Huntington's disease. Cell Death & Differentiation, 9(9),.

MASTROBERARDINO, P.G., FARRACE, M.G., VITI, I., PAVONE, F., FIMIA, G.M., MELINO, G., RODOLFO, C. and PIACENTINI, M., 2006. "Tissue" transglutaminase contributes to the formation of disulphide bridges in proteins of mitochondrial respiratory complexes. Biochimica et Biophysica Acta (BBA)-Bioenergetics, 1757(9), pp. 1357-1365.

MATHIVANAN, S. and SIMPSON, R.J., 2009. ExoCarta: A compendium of exosomal proteins and RNA. Proteomics, 9(21), pp. 4997-5000.

MATSUI, Y., IKESUE, M., DANZAKI, K., MORIMOTO, J., SATO, M., TANAKA, S., KOJIMA, T., TSUTSUI, H. and UEDE, T., 2011. Syndecan-4 prevents cardiac rupture and dysfunction after myocardial infarction. Circulation research, 108(11), pp. 1328-1339.

MATSUKI, M., YAMASHITA, F., ISHIDA-YAMAMOTO, A., YAMADA, K., KINOSHITA, C., FUSHIKI, S., UEDA, E., MORISHIMA, Y., TABATA, K., YASUNO, H., HASHIDA, M., IIZUKA, H., IKAWA, M., OKABE, M., KONDOH, G., KINOSHITA, T., TAKEDA, J. and YAMANISHI, K., 1998. Defective stratum corneum and early neonatal death in mice lacking the gene for transglutaminase 1 (keratinocyte transglutaminase). Proceedings of the National Academy of Sciences of the United States of America, 95(3), pp. 1044-1049.

MATSUO, H., CHEVALLIER, J., MAYRAN, N., LE BLANC, I., FERGUSON, C., FAURE, J., BLANC, N.S., MATILE, S., DUBOCHET, J., SADOUL, R., PARTON, R.G., VILBOIS, F. and GRUENBERG, J., 2004. Role of LBPA and Alix in multivesicular liposome formation and endosome organization. Science (New York, N.Y.), 303(5657), pp. 531-534.

MATSUO, S., LEPEZ-GUISA, J.M., CAI, X., OKAMURA, D.M., ALPERS, C.E., BUMGARNER, R.E., PETERS, M.A., ZHANG, G. and EDDY, A.A., 2005. Multifunctionality of PAI-1 in fibrogenesis: evidence from obstructive nephropathy in PAI-1–overexpressing mice. Kidney international, 67(6), pp. 2221-2238.

MATVEEV, S., LI, X., EVERSON, W. and SMART, E.J., 2001. The role of caveolae and caveolin in vesicle-dependent and vesicle-independent trafficking. Advanced Drug Delivery Reviews, 49(3), pp. 237-250.

MAYER, P., 1891. Ueber das Forben mit haematoxylin. Mitt Zool Stat Neapel, 10, pp. 170.

MAYOR, S., PARTON, R.G. and DONALDSON, J.G., 2014. Clathrin-independent pathways of endocytosis. Cold Spring Harbor perspectives in biology, 6(6), pp. 10.1101/cshperspect.a016758.

MCCULLOUGH, J., COLF, L.A. and SUNDQUIST, W.I., 2013. Membrane fission reactions of the mammalian ESCRT pathway. Annual Review of Biochemistry, 82, pp. 663-692.

MCPHERSON, P.S., 2002. The endocytic machinery at an interface with the actin cytoskeleton: a dynamic, hip intersection. Trends in cell biology, 12(7), pp. 312-315.

MEHAL, W.Z., IREDALE, J. and FRIEDMAN, S.L., 2011. Scraping fibrosis: expressway to the core of fibrosis. Nature medicine, 17(5), pp. 552-553.

MEHUL, B. and HUGHES, R.C., 1997. Plasma membrane targetting, vesicular budding and release of galectin 3 from the cytoplasm of mammalian cells during secretion. Journal of cell science, 110 (Pt 10)(Pt 10), pp. 1169-1178.

MELDOLESI, J., 2016. Ectosomes and Exosomes-Two Extracellular Vesicles That Differ Only in Some Details. Biochemistry & Molecular Biology Journal, .

MELDRUM, K.K., METCALFE, P., LESLIE, J.A., MISSERI, R., HILE, K.L. and MELDRUM, D.R., 2006. TNF-α neutralization decreases nuclear factor-κB activation and apoptosis during renal obstruction. Journal of Surgical Research, 131(2), pp. 182-188.

MELLMAN, I., FUCHS, R. and HELENIUS, A., 1986. Acidification of the endocytic and exocytic pathways. Annual Review of Biochemistry, 55(1), pp. 663-700.

MENGEL, M., BOCK, O., PRIESS, M., HALLER, H., KREIPE, H. and GWINNER, W., 2008. Expression of pro- and antifibrotic genes in protocol biopsies from renal allografts with interstitial fibrosis and tubular atrophy. Clinical nephrology, 69(6), pp. 408-416.

MENKE, M., GERKE, V. and STEINEM, C., 2005. Phosphatidylserine membrane domain clustering induced by annexin A2/S100A10 heterotetramer. Biochemistry, 44(46), pp. 15296-15303.

MERAN, S. and STEADMAN, R., 2011. Fibroblasts and myofibroblasts in renal fibrosis. International journal of experimental pathology, 92(3), pp. 158-167.

MERCHANT, M.L., 2015. Can the Urinary Peptidome Outperform Creatinine and Albumin to Predict Renal Function Decline? Journal of the American Society of Nephrology : JASN, 26(8), pp. 1760-1761.

MERENDINO, A.M., BUCCHIERI, F., CAMPANELLA, C., MARCIANÒ, V., RIBBENE, A., DAVID, S., ZUMMO, G., BURGIO, G., CORONA, D.F. and DE MACARIO, E.C., 2010. Hsp60 is actively secreted by human tumor cells. PloS one, 5(2), pp. e9247.

MERMALL, V., POST, P.L. and MOOSEKER, M.S., 1998. Unconventional myosins in cell movement, membrane traffic, and signal transduction. Science (New York, N.Y.), 279(5350), pp. 527-533.

MI, H., MURUGANUJAN, A. and THOMAS, P.D., 2013b. PANTHER in 2013: modeling the evolution of gene function, and other gene attributes, in the context of phylogenetic trees. Nucleic acids research, 41(Database issue), pp. D377-86.

MI, H., MURUGANUJAN, A., CASAGRANDE, J.T. and THOMAS, P.D., 2013a. Large-scale gene function analysis with the PANTHER classification system. Nature protocols, 8(8), pp. 1551-1566.

MICHAELIS, S., 1993. STE6, the yeast a-factor transporter, Seminars in cell biology 1993, Elsevier, pp. 17-27.

MIGNATTI, P., MORIMOTO, T. and RIFKIN, D.B., 1992. Basic fibroblast growth factor, a protein devoid of secretory signal sequence, is released by cells via a pathway independent of the endoplasmic reticulum-Golgi complex. Journal of cellular physiology, 151(1), pp. 81-93.

MILLER, M.E., ADHIKARY, S., KOLOKOLTSOV, A.A. and DAVEY, R.A., 2012. Ebolavirus requires acid sphingomyelinase activity and plasma membrane sphingomyelin for infection. Journal of virology, 86(14), pp. 7473-7483.

MIMIC-OKA, J., SIMIC, T., DJUKANOVIC, L., RELJIC, Z. and DAVICEVIC, Z., 1999. Alteration in plasma antioxidant capacity in various degrees of chronic renal failure. Clinical nephrology, 51(4), pp. 233-241.

MIOSGE, N., SIMNIOK, T., SPRYSCH, P. and HERKEN, R., 2003. The collagen type XVIII endostatin domain is co-localized with perlecan in basement membranes in vivo. The journal of histochemistry and cytochemistry : official journal of the Histochemistry Society, 51(3), pp. 285-296.

MIRZA, A., LIU, S.L., FRIZELL, E., ZHU, J., MADDUKURI, S., MARTINEZ, J., DAVIES, P., SCHWARTING, R., NORTON, P. and ZERN, M.A., 1997. A role for tissue transglutaminase in hepatic injury and fibrogenesis, and its regulation by NF-kappaB. The American Journal of Physiology, 272(2 Pt 1), pp. G281-8.

MISHRA, S. and MURPHY, L.J., 2004. Tissue transglutaminase has intrinsic kinase activity: identification of transglutaminase 2 as an insulin-like growth factor-binding protein-3 kinase. The Journal of biological chemistry, 279(23), pp. 23863-23868.

MISHRA, S. and MURPHY, L.J., 2006. Phosphorylation of transglutaminase 2 by PKA at Ser216 creates 14-3-3 binding sites. Biochemical and biophysical research communications, 347(4), pp. 1166-1170.

MISHRA, S., MELINO, G. and MURPHY, L.J., 2007. Transglutaminase 2 kinase activity facilitates protein kinase A-induced phosphorylation of retinoblastoma protein. The Journal of biological chemistry, 282(25), pp. 18108-18115.

MISHRA, S., SALEH, A., ESPINO, P.S., DAVIE, J.R. and MURPHY, L.J., 2006. Phosphorylation of histones by tissue transglutaminase. The Journal of biological chemistry, 281(9), pp. 5532-5538.

MISSERI, R., MELDRUM, D.R., DINARELLO, C.A., DAGHER, P., HILE, K.L., RINK, R.C. and MELDRUM, K.K., 2005. TNF-alpha mediates obstruction-induced renal tubular cell apoptosis and proapoptotic signaling. American journal of physiology.Renal physiology, 288(2), pp. F406-11.

MOBIUS, W., OHNO-IWASHITA, Y., VAN DONSELAAR, E.G., OORSCHOT, V.M., SHIMADA, Y., FUJIMOTO, T., HEIJNEN, H.F., GEUZE, H.J. and SLOT, J.W., 2002. Immunoelectron microscopic localization of cholesterol using biotinylated and non-cytolytic perfringolysin O. The journal of histochemistry and cytochemistry : official journal of the Histochemistry Society, 50(1), pp. 43-55.

MOE, S.M. and CHEN, N.X., 2008. Mechanisms of vascular calcification in chronic kidney disease. Journal of the American Society of Nephrology : JASN, 19(2), pp. 213-216.

MOE, S.M., SEIFERT, M.F., CHEN, N.X., SINDERS, R.M., CHEN, X., DUAN, D., HENLEY, C., MARTIN, D. and GATTONE, V.H.,2nd, 2009. R-568 reduces ectopic calcification in a rat model of chronic kidney disease-mineral bone disorder (CKD-MBD). Nephrology, dialysis, transplantation : official publication of the European Dialysis and Transplant Association - European Renal Association, 24(8), pp. 2371-2377.

MOOREN, O.L., GALLETTA, B.J. and COOPER, J.A., 2012. Roles for actin assembly in endocytosis. Biochemistry, 81(1), pp. 661.

MORADI, H., SICA, D.A. and KALANTAR-ZADEH, K., 2013. Cardiovascular burden associated with uremic toxins in patients with chronic kidney disease. American Journal of Nephrology, 38(2), pp. 136-148.

MORAVEC, R., CONGER, K.K., D'SOUZA, R., ALLISON, A.B. and CASANOVA, J.E., 2012. BRAG2/GEP100/IQSec1 interacts with clathrin and regulates alpha5beta1 integrin endocytosis through activation of ADP ribosylation factor 5 (Arf5). The Journal of biological chemistry, 287(37), pp. 31138-31147.

MORGAN, M.R., HAMIDI, H., BASS, M.D., WARWOOD, S., BALLESTREM, C. and HUMPHRIES, M.J., 2013. Syndecan-4 phosphorylation is a control point for integrin recycling. Developmental cell, 24(5), pp. 472-485.

MORITA, H., DAVID, G., MIZUTANI, A., SHINZATO, T., HABUCHI, H., MAEDA, K. and KIMATA, K., 1994. Heparan sulfate proteoglycans in the human sclerosing and scarring kidney. Extracellular Matrix in the Kidney. Karger Publishers, pp. 174-179.

MORITA, H., YOSHIMURA, A., INUI, K., IDEURA, T., WATANABE, H., WANG, L., SOININEN, R. and TRYGGVASON, K., 2005. Heparan sulfate of perlecan is involved in glomerular filtration. Journal of the American Society of Nephrology : JASN, 16(6), pp. 1703-1710.

MORROW, I.C., REA, S., MARTIN, S., PRIOR, I.A., PROHASKA, R., HANCOCK, J.F., JAMES, D.E. and PARTON, R.G., 2002. Flotillin-1/reggie-2 traffics to surface raft domains via a novel golgi-independent pathway. Identification of a novel membrane targeting domain and a role for palmitoylation. The Journal of biological chemistry, 277(50), pp. 48834-48841.

MOYER, B.D., ALLAN, B.B. and BALCH, W.E., 2001. Rab1 Interaction with a GM130 Effector Complex Regulates COPII Vesicle cis-Golgi Tethering. Traffic, 2(4), pp. 268-276.

MU, W., RANA, S. and ZÖLLER, M., 2013. Host matrix modulation by tumor exosomes promotes motility and invasiveness. Neoplasia, 15(8), pp. 875IN1-887IN4.

MUESCH, A., HARTMANN, E., ROHDE, K., RUBARTELLI, A., SITIA, R. and RAPOPORT, T.A., 1990. A novel pathway for secretory proteins? Trends in biochemical sciences, 15(3), pp. 86-88.

MURAKAMI, M., HOROWITZ, A., TANG, S., WARE, J.A. and SIMONS, M., 2002. Protein kinase C (PKC) delta regulates PKCalpha activity in a Syndecan-4-dependent manner. The Journal of biological chemistry, 277(23), pp. 20367-20371.

MURALIDHARAN-CHARI, V., CLANCY, J., PLOU, C., ROMAO, M., CHAVRIER, P., RAPOSO, G. and D'SOUZA-SCHOREY, C., 2009. ARF6-regulated shedding of tumor cell-derived plasma membrane microvesicles. Current Biology, 19(22), pp. 1875-1885.

MURPHY-ULLRICH, J.E., RIBEIRO, S.M., HUGO, C., ROBERTS, D.D. and KRUTZSCH, H.C., 2002. Use of peptides inhibitory for thrombospondin dependent TGF-β activation in the treatment of kidney disease, .

MURTHY, S.N., IISMAA, S., BEGG, G., FREYMANN, D.M., GRAHAM, R.M. and LORAND, L., 2002. Conserved tryptophan in the core domain of transglutaminase is essential for catalytic activity. Proceedings of the National Academy of Sciences of the United States of America, 99(5), pp. 2738-2742.

MURTHY, S.N., WILSON, J., GUY, S.L. and LORAND, L., 1991. Intramolecular crosslinking of monomeric fibrinogen by tissue transglutaminase. Proceedings of the National Academy of Sciences of the United States of America, 88(23), pp. 10601-10604.

MUSZBEK, L., BERECZKY, Z., BAGOLY, Z., KOMAROMI, I. and KATONA, E., 2011. Factor XIII: a coagulation factor with multiple plasmatic and cellular functions. Physiological Reviews, 91(3), pp. 931-972.

MUSZBEK, L., YEE, V.C. and HEVESSY, Z., 1999. Blood coagulation factor XIII: structure and function. Thrombosis research, 94(5), pp. 271-305.

MYCEK, M., CLARKE, D., NEIDLE, A. and WAELSCH, H., 1959. Amine incorporation into insulin as catalyzed by transglutaminase. Archives of Biochemistry and Biophysics, 84(2), pp. 528-540.

MYTILINAIOU, M., BANO, A., NIKITOVIC, D., BERDIAKI, A., VOUDOURI, K., KALOGERAKI, A., KARAMANOS, N.K. and TZANAKAKIS, G.N., 2013. Syndecan-2 is a key regulator of transforming growth factor beta 2/smad2-mediated adhesion in fibrosarcoma cells. IUBMB life, 65(2), pp. 134-143.

NAGARAJ, N. and MANN, M., 2011. Quantitative analysis of the intra-and inter-individual variability of the normal urinary proteome. Journal of proteome research, 10(2), pp. 637-645.

NAGLE, R.B., BULGER, R., CUTLER, R., JERVIS, H. and BENDITT, E., 1973. Unilateral obstructive nephropathy in the rabbit. I. Early morphologic, physiologic, and histochemical changes. Laboratory Investigation, 28(4), pp. 456-467.

NAGY, L., SAYDAK, M., SHIPLEY, N., LU, S., BASILION, J.P., YAN, Z.H., SYKA, P., CHANDRARATNA, R.A., STEIN, J.P., HEYMAN, R.A. and DAVIES, P.J., 1996. Identification and characterization of a versatile retinoid response element (retinoic acid receptor response element-retinoid X receptor response element) in the mouse tissue transglutaminase gene promoter. The Journal of biological chemistry, 271(8), pp. 4355-4365.

NAKAGAWA, T., TANABE, K., CROKER, B.P., JOHNSON, R.J., GRANT, M.B., KOSUGI, T. and LI, Q., 2011. Endothelial dysfunction as a potential contributor in diabetic nephropathy. Nature Reviews Nephrology, 7(1), pp. 36-44.

NAKAOKA, H., PEREZ, D.M., BAEK, K.J., DAS, T., HUSAIN, A., MISONO, K., IM, M. and GRAHAM, R.M., 1994. G~ h: A GTP-Binding Protein with Transglutaminase Activity and Receptor Signaling Function. SCIENCE-NEW YORK THEN WASHINGTON-, , pp. 1593-1593.

NAKATSU, F. and OHNO, H., 2003. Adaptor protein complexes as the key regulators of protein sorting in the post-Golgi network. Cell structure and function, 28(5), pp. 419-429.

NAMBIAR, R., MCCONNELL, R.E. and TYSKA, M.J., 2009. Control of cell membrane tension by myosin-I. Proceedings of the National Academy of Sciences of the United States of America, 106(29), pp. 11972-11977.

NANDA, N., IISMAA, S.E., OWENS, W.A., HUSAIN, A., MACKAY, F. and GRAHAM, R.M., 2001. Targeted inactivation of Gh/tissue transglutaminase II. The Journal of biological chemistry, 276(23), pp. 20673-20678.

NASLAVSKY, N., WEIGERT, R. and DONALDSON, J.G., 2004. Characterization of a nonclathrin endocytic pathway: membrane cargo and lipid requirements. Molecular biology of the cell, 15(8), pp. 3542-3552.

NAVARRO-MUNOZ, M., IBERNON, M., BONET, J., PEREZ, V., PASTOR, M.C., BAYES, B., CASADO-VELA, J., NAVARRO, M., ARA, J., ESPINAL, A., FLUVIA, L., SERRA, A., LOPEZ, D. and ROMERO, R., 2012. Uromodulin and alpha(1)-antitrypsin urinary peptide analysis to differentiate glomerular kidney diseases. Kidney & blood pressure research, 35(5), pp. 314-325.

NEMES, Z., MAREKOV, L.N., FÉSÜS, L. and STEINERT, P.M., 1999. A novel function for transglutaminase 1: attachment of long-chain ω-hydroxyceramides to involucrin by ester bond formation. Proceedings of the National Academy of Sciences, 96(15), pp. 8402-8407.

NEUGARTEN, J., 2002. Gender and the progression of renal disease. Journal of the American Society of Nephrology : JASN, 13(11), pp. 2807-2809.

NEUMANN-GIESEN, C., FALKENBACH, B., BEICHT, P., CLAASEN, S., LUERS, G., STUERMER, C.A., HERZOG, V. and TIKKANEN, R., 2004. Membrane and raft association of reggie-1/flotillin-2: role of myristoylation, palmitoylation and oligomerization and induction of filopodia by overexpression. The Biochemical journal, 378(Pt 2), pp. 509-518.

NEWMAN, D., ABULADZE, N., SCHOLZ, K., DEKANT, W., TSUPRUN, V., RYAZANTSEV, S., BONDAR, G., SASSANI, P., KURTZ, I. and PUSHKIN, A., 2007. Specificity of aminoacylase III-mediated deacetylation of mercapturic acids. Drug metabolism and disposition: the biological fate of chemicals, 35(1), pp. 43-50.

NGOSUWAN, J., WANG, N.M., FUNG, K.L. and CHIRICO, W.J., 2003. Roles of cytosolic Hsp70 and Hsp40 molecular chaperones in post-translational translocation of presecretory proteins into the endoplasmic reticulum. The Journal of biological chemistry, 278(9), pp. 7034-7042.

NICHOLAS, B., SMETHURST, P., VERDERIO, E., JONES, R. and GRIFFIN, M., 2003. Cross-linking of cellular proteins by tissue transglutaminase during necrotic cell death: a mechanism for maintaining tissue integrity. The Biochemical journal, 371(Pt 2), pp. 413-422.

NICKEL, W. and RABOUILLE, C., 2009. Mechanisms of regulated unconventional protein secretion. Nature Reviews Molecular Cell Biology, 10(2), pp. 148-155.

NICKEL, W. and SEEDORF, M., 2008. Unconventional mechanisms of protein transport to the cell surface of eukaryotic cells. Annual Review of Cell and Developmental Biology, 24, pp. 287-308.

NICKEL, W., 2003. The mystery of nonclassical protein secretion. European Journal of Biochemistry, 270(10), pp. 2109-2119.

NICKEL, W., 2007. Unconventional secretion: an extracellular trap for export of fibroblast growth factor 2. Journal of cell science, 120(Pt 14), pp. 2295-2299.

NICKEL, W., 2010. Pathways of unconventional protein secretion. Current opinion in biotechnology, 21(5), pp. 621-626.

NICKEL, W., 2011. The unconventional secretory machinery of fibroblast growth factor 2. Traffic, 12(7), pp. 799-805.

NIEUWDORP, M., MOOIJ, H.L., KROON, J., ATASEVER, B., SPAAN, J.A., INCE, C., HOLLEMAN, F., DIAMANT, M., HEINE, R.J., HOEKSTRA, J.B., KASTELEIN, J.J., STROES, E.S. and VINK, H., 2006. Endothelial glycocalyx damage coincides with microalbuminuria in type 1 diabetes. Diabetes, 55(4), pp. 1127-1132.

NIGHTINGALE, T.D., CUTLER, D.F. and CRAMER, L.P., 2012. Actin coats and rings promote regulated exocytosis. Trends in cell biology, 22(6), pp. 329-337.

NISHIKAWA, K., TOKER, A., JOHANNES, F., SONGYANG, Z. and CANTLEY, L.C., 1997. Determination of the specific substrate sequence motifs of protein kinase C isozymes. Journal of Biological Chemistry, 272(2), pp. 952-960.

NOGUER, O., VILLENA, J., LORITA, J., VILARÓ, S. and REINA, M., 2009. Syndecan-2 downregulation impairs angiogenesis in human microvascular endothelial cells. Experimental cell research, 315(5), pp. 795-808.

NUGENT, M.A. and IOZZO, R.V., 2000. Fibroblast growth factor-2. The international journal of biochemistry & cell biology, 32(2), pp. 115-120.

NUNES, I., GLEIZES, P.E., METZ, C.N. and RIFKIN, D.B., 1997. Latent transforming growth factor-beta binding protein domains involved in activation and transglutaminase-dependent cross-linking of latent transforming growth factor-beta. The Journal of cell biology, 136(5), pp. 1151-1163.

NUOFFER, C., DAVIDSON, H.W., MATTESON, J., MEINKOTH, J. and BALCH, W.E., 1994. A GDP-bound of rab1 inhibits protein export from the endoplasmic reticulum and transport between Golgi compartments. The Journal of cell biology, 125(2), pp. 225-237.

OFSTAD, J. and IVERSEN, B.M., 2005. Glomerular and tubular damage in normotensive and hypertensive rats. American journal of physiology.Renal physiology, 288(4), pp. F665-72.

OH, E.S., WOODS, A. and COUCHMAN, J.R., 1997. Multimerization of the cytoplasmic domain of syndecan-4 is required for its ability to activate protein kinase C. The Journal of biological chemistry, 272(18), pp. 11805-11811.

OH, E.S., WOODS, A., LIM, S.T., THEIBERT, A.W. and COUCHMAN, J.R., 1998. Syndecan-4 proteoglycan cytoplasmic domain and phosphatidylinositol 4,5-bisphosphate coordinately regulate protein kinase C activity. The Journal of biological chemistry, 273(17), pp. 10624-10629.

OKINA, E., GROSSI, A., GOPAL, S., MULTHAUPT, H. and COUCHMAN, J.R., 2012. Alpha-actinin interactions with syndecan-4 are integral to fibroblast–matrix adhesion and regulate cytoskeletal architecture. The international journal of biochemistry & cell biology, 44(12), pp. 2161-2174.

OLIVERIO, S., AMENDOLA, A., RODOLFO, C., SPINEDI, A. and PIACENTINI, M., 1999. Inhibition of "tissue" transglutaminase increases cell survival by preventing apoptosis. The Journal of biological chemistry, 274(48), pp. 34123-34128.

OLSEN, K.C., SAPINORO, R.E., KOTTMANN, R., KULKARNI, A.A., IISMAA, S.E., JOHNSON, G.V., THATCHER, T.H., PHIPPS, R.P. and SIME, P.J., 2011. Transglutaminase 2 and its role in pulmonary fibrosis. American journal of respiratory and critical care medicine, 184(6), pp. 699-707.

ORCL, L., TAGAYA, M., AMHERDT, M., PERRELET, A., DONALDSON, J.G., LIPPINCOTT-SCHWARTZ, J., KLAUSNER, R.D. and ROTHMAN, J.E., 1991. Brefeldin A, a drug that blocks secretion, prevents the assembly of non-clathrin-coated buds on Golgi cisternae. Cell, 64(6), pp. 1183-1195.

ORRU, S., CAPUTO, I., D'AMATO, A., RUOPPOLO, M. and ESPOSITO, C., 2003. Proteomics identification of acyl-acceptor and acyl-donor substrates for transglutaminase in a human intestinal epithelial cell line. Implications for celiac disease. The Journal of biological chemistry, 278(34), pp. 31766-31773.

OSBORNE, A.R., RAPOPORT, T.A. and VAN DEN BERG, B., 2005. Protein translocation by the Sec61/SecY channel. Annu.Rev.Cell Dev.Biol., 21, pp. 529-550.

PADBERG, J., WIESINGER, A., DI MARCO, G.S., REUTER, S., GRABNER, A., KENTRUP, D., LUKASZ, A., OBERLEITHNER, H., PAVENSTÄDT, H. and BRAND, M., 2014. Damage of the endothelial glycocalyx in chronic kidney disease. Atherosclerosis, 234(2), pp. 335-343.

PAL-GHOSH, S., TADVALKAR, G., JURJUS, R.A., ZIESKE, J.D. and STEPP, M.A., 2008. BALB/c and C57BL6 mouse strains vary in their ability to heal corneal epithelial debridement wounds. Experimental eye research, 87(5), pp. 478-486.

PALLET, N., CHAUVET, S., CHASSÉ, J., VINCENT, M., AVILLACH, P., LEVI, C., MEAS-YEDID, V., OLIVO-MARIN, J., NGA-MATSOGO, D. and BEAUNE, P., 2014. Urinary retinol binding protein is a marker of the extent of interstitial kidney fibrosis. PloS one, 9(1), pp. e84708.

PAN, S., WANG, R., ZHOU, X., HE, G., KOOMEN, J., KOBAYASHI, R., SUN, L., CORVERA, J., GALLICK, G.E. and KUANG, J., 2006. Involvement of the conserved adaptor protein Alix in actin cytoskeleton assembly. The Journal of biological chemistry, 281(45), pp. 34640-34650.

PAN, X., EATHIRAJ, S., MUNSON, M. and LAMBRIGHT, D.G., 2006. TBC-domain GAPs for Rab GTPases accelerate GTP hydrolysis by a dual-finger mechanism. Nature, 442(7100), pp. 303-306.

PAPASOTIRIOU, M., KALLIAKMANI, P., HUANG, L., GEROLYMOS, M., GOUMENOS, D.S. and JOHNSON, T.S., 2012. Does treatment with corticosteroids and cyclosporine reduce transglutaminase type 2 expression in the renal tissue of patients with membranous nephropathy? Nephron.Clinical practice, 121(1-2), pp. c60-7.

PARTON, R.G. and RICHARDS, A.A., 2003. Lipid rafts and caveolae as portals for endocytosis: new insights and common mechanisms. Traffic, 4(11), pp. 724-738.

PATTON, K.T., 2015. 42. Anatomy of the urinary system. Anatomy and physiology. Elsevier Health Sciences, .

PEARSON, R.B. and KEMP, B.E., 1991. [3] Protein kinase phosphorylation site sequences and consensus specificity motifs: Tabulations. Methods in enzymology, 200, pp. 62-81.

PEJLER, G., ÅBRINK, M. and WERNERSSON, S., 2009. Serglycin proteoglycan: regulating the storage and activities of hematopoietic proteases. Biofactors, 35(1), pp. 61-68.

PELEGRIN, P., BARROSO-GUTIERREZ, C. and SURPRENANT, A., 2008. P2X7 receptor differentially couples to distinct release pathways for IL-1beta in mouse macrophage. Journal of immunology (Baltimore, Md.: 1950), 180(11), pp. 7147-7157.

PEREZ-HERNANDEZ, D., GUTIERREZ-VAZQUEZ, C., JORGE, I., LOPEZ-MARTIN, S., URSA, A., SANCHEZ-MADRID, F., VAZQUEZ, J. and YANEZ-MO, M., 2013. The intracellular interactome of tetraspanin-enriched microdomains reveals their function as sorting machineries toward exosomes. The Journal of biological chemistry, 288(17), pp. 11649-11661.

PÉREZ-VARGAS, J., KREY, T., VALANSI, C., AVINOAM, O., HAOUZ, A., JAMIN, M., RAVEH-BARAK, H., PODBILEWICZ, B. and REY, F.A., 2014. Structural basis of eukaryotic cell-cell fusion. Cell, 157(2), pp. 407-419.

PERGOLA, P.E., SPINOWITZ, B.S., HARTMAN, C.S., MARONI, B.J. and HAASE, V.H., 2016. Vadadustat, a novel oral HIF stabilizer, provides effective anemia treatment in nondialysis-dependent chronic kidney disease. Kidney international, 90(5), pp. 1115-1122.

PETERS, L.L., JINDEL, H.K., GWYNN, B., KORSGREN, C., JOHN, K.M., LUX, S.E., MOHANDAS, N., COHEN, C.M., CHO, M.R., GOLAN, D.E. and BRUGNARA, C., 1999. Mild spherocytosis and altered red cell ion transport in protein 4. 2-null mice. The Journal of clinical investigation, 103(11), pp. 1527-1537.

PETERSON, P.A., EVRIN, P.E. and BERGGARD, I., 1969. Differentiation of glomerular, tubular, and normal proteinuria: determinations of urinary excretion of beta-2-macroglobulin, albumin, and total protein. The Journal of clinical investigation, 48(7), pp. 1189-1198.

PEVSNER, J., HSU, S., BRAUN, J.E., CALAKOS, N., TING, A.E., BENNETT, M.K. and SCHELLER, R.H., 1994. Specificity and regulation of a synaptic vesicle docking complex. Neuron, 13(2), pp. 353-361.

PFEFFER, S.R., 2013. Rab GTPase regulation of membrane identity. Current opinion in cell biology, 25(4), pp. 414-419.

PHATAK, V., CROFT, S., SETTY, S.R., SCARPELLINI, A., HUGHES, D., REES, R., MCARDLE, S. and VERDERIO, E., 2013. Expression of transglutaminase-2 isoforms in normal human tissues and cancer cell lines: dysregulation of alternative splicing in cancer. Amino acids, 44(1), pp. 33-44.

PHILLIPS, M.A., QIN, Q., MEHRPOUYAN, M. and RICE, R.H., 1993. Keratinocyte transglutaminase membrane anchorage: analysis of site-directed mutants. Biochemistry, 32(41), pp. 11057-11063.

PHUYAL, S., HESSVIK, N.P., SKOTLAND, T., SANDVIG, K. and LLORENTE, A., 2014. Regulation of exosome release by glycosphingolipids and flotillins. FEBS Journal, 281(9), pp. 2214-2227.

PIACENTINI, M., AMENDOLA, A., CICCOSANTI, F., FALASCA, L., FARRACE, M.G., MASTROBERARDINO, P.G., NARDACCI, R., OLIVERIO, S., PIREDDA, L., RODOLFO, C. and AUTUORI, F., 2005. Type 2 transglutaminase and cell death. Progress in experimental tumor research, 38, pp. 58-74.

PIACENTINI, M., CERU, M., DINI, L., DI RAO, M., PIREDDA, L., THOMAZY, V., DAVIES, P. and FESUS, L., 1992. In vivo and in vitro induction of 'tissue'transglutaminase in rat hepatocytes by retinoic acid. Biochimica et Biophysica Acta (BBA)-Molecular Cell Research, 1135(2), pp. 171-179.

PIACENTINI, M., D'ELETTO, M., FARRACE, M.G., RODOLFO, C., DEL NONNO, F., IPPOLITO, G. and FALASCA, L., 2014. Characterization of distinct sub-cellular location of transglutaminase type II: changes in intracellular distribution in physiological and pathological states. Cell and tissue research, 358(3), pp. 793-805.

PIETRONI, V., DI GIORGI, S., PARADISI, A., AHVAZI, B., CANDI, E. and MELINO, G., 2008. Inactive and highly active, proteolytically processed transglutaminase-5 in epithelial cells. Journal of Investigative Dermatology, 128(12), pp. 2760-2766.

PIKE, L.J., 2009. The challenge of lipid rafts. Journal of lipid research, 50 Suppl, pp. S323-8.

PINKAS, D.M., STROP, P., BRUNGER, A.T. and KHOSLA, C., 2007. Transglutaminase 2 undergoes a large conformational change upon activation. PLoS Biol, 5(12), pp. e327.

PISITKUN, T., GANDOLFO, M.T., DAS, S., KNEPPER, M.A. and BAGNASCO, S.M., 2012. Application of systems biology principles to protein biomarker discovery: urinary exosomal proteome in renal transplantation. Proteomics-Clinical Applications, 6(5-6), pp. 268-278.

PISITKUN, T., SHEN, R.F. and KNEPPER, M.A., 2004. Identification and proteomic profiling of exosomes in human urine. Proceedings of the National Academy of Sciences of the United States of America, 101(36), pp. 13368-13373.

PLEASURE, I.T., BLACK, M.M. and KEEN, J.H., 1993. Valosin-containing protein, VCP, is a ubiquitous clathrin-binding protein. Nature, 365(6445), pp. 459-462.

POLGAR, J. and REED, G.L., 1999. A critical role for N-ethylmaleimide-sensitive fusion protein (NSF) in platelet granule secretion. Blood, 94(4), pp. 1313-1318.

PONNUSAMY, M., PANG, M., ANNAMARAJU, P.K., ZHANG, Z., GONG, R., CHIN, Y.E. and ZHUANG, S., 2009. Transglutaminase-1 protects renal epithelial cells from hydrogen peroxide-induced apoptosis through activation of STAT3 and AKT signaling pathways. American journal of physiology.Renal physiology, 297(5), pp. F1361-70.

POPOFF, V., MARDONES, G.A., BAI, S., CHAMBON, V., TENZA, D., BURGOS, P.V., SHI, A., BENAROCH, P., URBÉ, S. and LAMAZE, C., 2009. Analysis of articulation between clathrin and retromer in retrograde sorting on early endosomes. Traffic, 10(12), pp. 1868-1880.

POWELL, D.W., BERTRAM, C.C., CUMMINS, T.D., BARATI, M.T., ZHENG, S., EPSTEIN, P.N. and KLEIN, J.B., 2009. Renal tubulointerstitial fibrosis in OVE26 type 1 diabetic mice. Nephron.Experimental nephrology, 111(1), pp. e11-9.

PRIETO-SÁNCHEZ, R.M., BERENJENO, I.M. and BUSTELO, X.R., 2006. Involvement of the Rho/Rac family member RhoG in caveolar endocytosis. Oncogene, 25(21), pp. 2961-2973.

PRUDOVSKY, I., BAGALA, C., TARANTINI, F., MANDINOVA, A., SOLDI, R., BELLUM, S. and MACIAG, T., 2002. The intracellular translocation of the components of the fibroblast growth factor 1 release complex precedes their assembly prior to export. The Journal of cell biology, 158(2), pp. 201-208.

PRUDOVSKY, I., MANDINOVA, A., SOLDI, R., BAGALA, C., GRAZIANI, I., LANDRISCINA, M., TARANTINI, F., DUARTE, M., BELLUM, S., DOHERTY, H. and MACIAG, T., 2003. The non-classical export routes: FGF1 and IL-1alpha point the way. Journal of cell science, 116(Pt 24), pp. 4871-4881.

PRUDOVSKY, I., TARANTINI, F., LANDRISCINA, M., NEIVANDT, D., SOLDI, R., KIROV, A., SMALL, D., KATHIR, K.M., RAJALINGAM, D. and KUMAR, T.K.S., 2008. Secretion without Golgi. Journal of cellular biochemistry, 103(5), pp. 1327-1343.

PUERTOLLANO, R., VAN DER WEL, N.N., GREENE, L.E., EISENBERG, E., PETERS, P.J. and BONIFACINO, J.S., 2003. Morphology and dynamics of clathrin/GGA1-coated carriers budding from the trans-Golgi network. Molecular biology of the cell, 14(4), pp. 1545-1557.

PUTHENVEEDU, M.A., LAUFFER, B., TEMKIN, P., VISTEIN, R., CARLTON, P., THORN, K., TAUNTON, J., WEINER, O.D., PARTON, R.G. and VON ZASTROW, M., 2010. Sequence-dependent sorting of recycling proteins by actin-stabilized endosomal microdomains. Cell, 143(5), pp. 761-773.

QU, Y., FRANCHI, L., NUNEZ, G. and DUBYAK, G.R., 2007. Nonclassical IL-1 beta secretion stimulated by P2X7 receptors is dependent on inflammasome activation and correlated with exosome release in murine macrophages. Journal of immunology (Baltimore, Md.: 1950), 179(3), pp. 1913-1925.

QUAGGIN, S.E. and KAPUS, A., 2011. Scar wars: mapping the fate of epithelial–mesenchymal–myofibroblast transition. Kidney international, 80(1), pp. 41-50.

QUAN, G., CHOI, J., LEE, D. and LEE, S., 2005. TGF-β1 up-regulates transglutaminase two and fibronectin in dermal fibroblasts: a possible mechanism for the stabilization of tissue inflammation. Archives of Dermatological Research, 297(2), pp. 84-90.

RAATS, C.I., VAN DEN BORN, J. and BERDEN, J.H., 2000. Glomerular heparan sulfate alterations: mechanisms and relevance for proteinuria. Kidney international, 57(2), pp. 385-400.

RAATS, J. and BLOEMENDAL, H., 1992. The role of protein domains in the assembly process of intermediate filaments. Progress in nucleic acid research and molecular biology, 43, pp. 67-86.

RABOUILLE, C., MALHOTRA, V. and NICKEL, W., 2012. Diversity in unconventional protein secretion. Journal of cell science, 125(Pt 22), pp. 5251-5255.

RADEK, J.T., JEONG, J.M., MURTHY, S.N., INGHAM, K.C. and LORAND, L., 1993. Affinity of human erythrocyte transglutaminase for a 42-kDa gelatin-binding fragment of human plasma fibronectin. Proceedings of the National Academy of Sciences of the United States of America, 90(8), pp. 3152-3156.

RADISKY, D.C., LEVY, D.D., LITTLEPAGE, L.E., LIU, H., NELSON, C.M., FATA, J.E., LEAKE, D., GODDEN, E.L., ALBERTSON, D.G. and NIETO, M.A., 2005. Rac1b and reactive oxygen species mediate MMP-3-induced EMT and genomic instability. Nature, 436(7047), pp. 123-127.

RAJ, D.A.A., POCSFALVI, G., CAPASSO, G. and FIUME, I., 2012. Urinary exosomes for protein biomarker research. INTECH Open Access Publisher.

RAMPOLDI, L., CARIDI, G., SANTON, D., BOARETTO, F., BERNASCONE, I., LAMORTE, G., TARDANICO, R., DAGNINO, M., COLUSSI, G., SCOLARI, F., GHIGGERI, G.M., AMOROSO, A. and CASARI, G., 2003. Allelism of MCKD, FJHN and GCKD caused by impairment of uromodulin export dynamics. Human molecular genetics, 12(24), pp. 3369-3384.

RANA, S., YUE, S., STADEL, D. and ZÖLLER, M., 2012. Toward tailored exosomes: the exosomal tetraspanin web contributes to target cell selection. The international journal of biochemistry & cell biology, 44(9), pp. 1574-1584.

RAPOSO, G. and STOORVOGEL, W., 2013. Extracellular vesicles: exosomes, microvesicles, and friends. The Journal of cell biology, 200(4), pp. 373-383.

RAPOSO, G., CORDONNIER, M.N., TENZA, D., MENICHI, B., DURRBACH, A., LOUVARD, D. and COUDRIER, E., 1999. Association of myosin I alpha with endosomes and lysosomes in mammalian cells. Molecular biology of the cell, 10(5), pp. 1477-1494.

REINHARDT, D.P., SASAKI, T., DZAMBA, B.J., KEENE, D.R., CHU, M., GÖHRING, W., TIMPL, R. and SAKAI, L.Y., 1996. Fibrillin-1 and fibulin-2 interact and are colocalized in some tissues. Journal of Biological Chemistry, 271(32), pp. 19489-19496.

REIZES, O., LINCECUM, J., WANG, Z., GOLDBERGER, O., HUANG, L., KAKSONEN, M., AHIMA, R., HINKES, M.T., BARSH, G.S. and RAUVALA, H., 2001. Transgenic expression of syndecan-1 uncovers a physiological control of feeding behavior by syndecan-3. Cell, 106(1), pp. 105-116.

REMUZZI, G., PERICO, N., MACIA, M. and RUGGENENTI, P., 2005. The role of renin-angiotensin-aldosterone system in the progression of chronic kidney disease. Kidney international, 68, pp. S57-S65.

REN, X.D., KIOSSES, W.B., SIEG, D.J., OTEY, C.A., SCHLAEPFER, D.D. and SCHWARTZ, M.A., 2000. Focal adhesion kinase suppresses Rho activity to promote focal adhesion turnover. Journal of cell science, 113 (Pt 20)(Pt 20), pp. 3673-3678.

RENAUDINEAU, Y., DEOCHARAN, B., JOUSSE, S., RENAUDINEAU, E., PUTTERMAN, C. and YOUINOU, P., 2007. Anti-alpha-actinin antibodies: a new marker of lupus nephritis. Autoimmunity reviews, 6(7), pp. 464-468.

RESCHER, U., RUHE, D., LUDWIG, C., ZOBIACK, N. and GERKE, V., 2004. Annexin 2 is a phosphatidylinositol (4,5)-bisphosphate binding protein recruited to actin assembly sites at cellular membranes. Journal of cell science, 117(Pt 16), pp. 3473-3480.

RICARDO, S. and LEHMANN, R., 2009. An ABC transporter controls export of a Drosophila germ cell attractant. Science (New York, N.Y.), 323(5916), pp. 943-946.

RICARDO, S.D., VAN GOOR, H. and EDDY, A.A., 2008. Macrophage diversity in renal injury and repair. The Journal of clinical investigation, 118(11), pp. 3522-3530.

RICHARDSON, D.L., LOOMIS, W.F. and KIMMEL, A.R., 1994. Progression of an inductive signal activates sporulation in Dictyostelium discoideum. Development (Cambridge, England), 120(10), pp. 2891-2900.

RITCHIE, H., LAWRIE, L.C., CROMBIE, P.W., MOSESSON, M.W. and BOOTH, N.A., 2000. Cross-linking of plasminogen activator inhibitor 2 and alpha 2-antiplasmin to fibrin(ogen). The Journal of biological chemistry, 275(32), pp. 24915-24920.

ROBERTS, A., HEINE, U., FLANDERS, K. and SPORN, M., 1990. TGF-β: Major role in regulation of extracellular matrix. Ann NY Acad Sci, 580, pp. 225-232.

ROBERTS, A.B., SPORN, M.B., ASSOIAN, R.K., SMITH, J.M., ROCHE, N.S., WAKEFIELD, L.M., HEINE, U.I., LIOTTA, L.A., FALANGA, V. and KEHRL, J.H., 1986. Transforming growth factor type beta: rapid induction of fibrosis and angiogenesis in vivo and stimulation of collagen formation in vitro. Proceedings of the National Academy of Sciences of the United States of America, 83(12), pp. 4167-4171.

RODRIGUEZ, L., STIRLING, C.J. and WOODMAN, P.G., 1994. Multiple N-ethylmaleimide-sensitive components are required for endosomal vesicle fusion. Molecular biology of the cell, 5(7), pp. 773-783.

ROUCOURT, B., MEEUSSEN, S., BAO, J., ZIMMERMANN, P. and DAVID, G., 2015. Heparanase activates the syndecan-syntenin-ALIX exosome pathway. Cell research, 25(4), pp. 412-428.

RUBARTELLI, A., BAJETTO, A., ALLAVENA, G., WOLLMAN, E. and SITIA, R., 1992. Secretion of thioredoxin by normal and neoplastic cells through a leaderless secretory pathway. The Journal of biological chemistry, 267(34), pp. 24161-24164.

RUBARTELLI, A., COZZOLINO, F., TALIO, M. and SITIA, R., 1990. A novel secretory pathway for interleukin-1 beta, a protein lacking a signal sequence. The EMBO journal, 9(5), pp. 1503-1510.

RUIZ, X.D., MLAKAR, L.R., YAMAGUCHI, Y., SU, Y., LARREGINA, A.T., PILEWSKI, J.M. and FEGHALI-BOSTWICK, C.A., 2012. Syndecan-2 is a novel target of insulin-like growth factor binding protein-3 and is over-expressed in fibrosis. PloS one, 7(8), pp. e43049.

RUIZ-ORTEGA, M. and EGIDO, J., 1997. Angiotensin II modulates cell growth-related events and synthesis of matrix proteins in renal interstitial fibroblasts. Kidney international, 52(6), pp. 1497-1510.

RULE, A.D., LARSON, T.S., BERGSTRALH, E.J., SLEZAK, J.M., JACOBSEN, S.J. and COSIO, F.G., 2004. Using serum creatinine to estimate glomerular filtration rate: accuracy in good health and in chronic kidney disease. Annals of Internal Medicine, 141(12), pp. 929-937.

RUSTER, C. and WOLF, G., 2006. Renin-angiotensin-aldosterone system and progression of renal disease. Journal of the American Society of Nephrology : JASN, 17(11), pp. 2985-2991.

RÜSTER, C. and WOLF, G., 2010. Models of diabetic nephropathy. Drug discovery today: Disease models, 7(1), pp. 35-41.

RYU, J., JAHN, R. and YOON, T., 2016. Review: Progresses in understanding N-ethylmaleimide sensitive factor (NSF) mediated disassembly of SNARE complexes. Biopolymers, 105(8), pp. 518-531.

SABHARANJAK, S., SHARMA, P., PARTON, R.G. and MAYOR, S., 2002. GPI-anchored proteins are delivered to recycling endosomes via a distinct cdc42-regulated, clathrin-independent pinocytic pathway. Developmental cell, 2(4), pp. 411-423.

SAHU, R., KAUSHIK, S., CLEMENT, C.C., CANNIZZO, E.S., SCHARF, B., FOLLENZI, A., POTOLICCHIO, I., NIEVES, E., CUERVO, A.M. and SANTAMBROGIO, L., 2011. Microautophagy of cytosolic proteins by late endosomes. Developmental cell, 20(1), pp. 131-139.

SAKAMAKI, Y., SAKATSUME, M., WANG, X., INOMATA, S., YAMAMOTO, T., GEJYO, F. and NARITA, I., 2011. Injured kidney cells express SM22α (transgelin): Unique features distinct from α-smooth muscle actin (αSMA). Nephrology, 16(2), pp. 211-218.

SAKANE, A., MANABE, S., ISHIZAKI, H., TANAKA-OKAMOTO, M., KIYOKAGE, E., TOIDA, K., YOSHIDA, T., MIYOSHI, J., KAMIYA, H., TAKAI, Y. and SASAKI, T., 2006. Rab3 GTPase-activating protein regulates synaptic transmission and plasticity through the inactivation of Rab3. Proceedings of the National Academy of Sciences of the United States of America, 103(26), pp. 10029-10034.

SALICIONI, A.M., GAULTIER, A., BROWNLEE, C., CHEEZUM, M.K. and GONIAS, S.L., 2004. Low density lipoprotein receptor-related protein-1 promotes beta1 integrin maturation and transport to the cell surface. The Journal of biological chemistry, 279(11), pp. 10005-10012.

SALICIONI, A.M., MIZELLE, K.S., LOUKINOVA, E., MIKHAILENKO, I., STRICKLAND, D.K. and GONIAS, S.L., 2002. The low density lipoprotein receptor-related protein mediates fibronectin catabolism and inhibits fibronectin accumulation on cell surfaces. The Journal of biological chemistry, 277(18), pp. 16160-16166.

SAMIE, M., WANG, X., ZHANG, X., GOSCHKA, A., LI, X., CHENG, X., GREGG, E., AZAR, M., ZHUO, Y. and GARRITY, A.G., 2013. A TRP channel in the lysosome regulates large particle phagocytosis via focal exocytosis. Developmental cell, 26(5), pp. 511-524.

SANTHANAM, L., BERKOWITZ, D.E. and BELKIN, A.M., 2011. Nitric oxide regulates non-classical secretion of tissue transglutaminase. Communicative & integrative biology, 4(5), pp. 584-586.

SANTHANAM, L., TUDAY, E.C., WEBB, A.K., DOWZICKY, P., KIM, J.H., OH, Y.J., SIKKA, G., KUO, M., HALUSHKA, M.K., MACGREGOR, A.M., DUNN, J., GUTBROD, S., YIN, D., SHOUKAS, A., NYHAN, D., FLAVAHAN, N.A., BELKIN, A.M. and BERKOWITZ, D.E., 2010. Decreased S-nitrosylation of tissue transglutaminase contributes to age-related increases in vascular stiffness. Circulation research, 107(1), pp. 117-125.

SANTIAGO-RABER, M., LAPORTE, C., REININGER, L. and IZUI, S., 2004. Genetic basis of murine lupus. Autoimmunity reviews, 3(1), pp. 33-39.

SAONCELLA, S., ECHTERMEYER, F., DENHEZ, F., NOWLEN, J.K., MOSHER, D.F., ROBINSON, S.D., HYNES, R.O. and GOETINCK, P.F., 1999a. Syndecan-4 signals cooperatively with integrins in a Rho-dependent manner in the assembly of focal adhesions and actin stress fibers. Proceedings of the National Academy of Sciences of the United States of America, 96(6), pp. 2805-2810.

SARDY, M., KARPATI, S., MERKL, B., PAULSSON, M. and SMYTH, N., 2002. Epidermal transglutaminase (TGase 3) is the autoantigen of dermatitis herpetiformis. The Journal of experimental medicine, 195(6), pp. 747-757.

SARNAK, M.J., LEVEY, A.S., SCHOOLWERTH, A.C., CORESH, J., CULLETON, B., HAMM, L.L., MCCULLOUGH, P.A., KASISKE, B.L., KELEPOURIS, E., KLAG, M.J., PARFREY, P., PFEFFER, M., RAIJ, L., SPINOSA, D.J., WILSON, P.W. and AMERICAN HEART ASSOCIATION COUNCILS ON KIDNEY IN CARDIOVASCULAR DISEASE, HIGH BLOOD PRESSURE RESEARCH, CLINICAL CARDIOLOGY, AND EPIDEMIOLOGY AND PREVENTION, 2003. Kidney disease as a risk factor for development of cardiovascular disease: a statement from the American Heart Association Councils on Kidney in Cardiovascular Disease, High Blood Pressure Research, Clinical Cardiology, and Epidemiology and Prevention. Circulation, 108(17), pp. 2154-2169.

SARRAZIN, S., LAMANNA, W.C. and ESKO, J.D., 2011. Heparan sulfate proteoglycans. Cold Spring Harbor perspectives in biology, 3(7), pp. 10.1101/cshperspect.a004952.

SATCHWELL, T.J., SHOEMARK, D.K., SESSIONS, R.B. and TOYE, A.M., 2009. Protein 4.2: a complex linker. Blood Cells, Molecules, and Diseases, 42(3), pp. 201-210.

SATIRAPOJ, B., WANG, Y., CHAMBERLIN, M.P., DAI, T., LAPAGE, J., PHILLIPS, L., NAST, C.C. and ADLER, S.G., 2012. Periostin: novel tissue and urinary biomarker of progressive renal injury induces a coordinated mesenchymal phenotype in tubular cells. Nephrology, dialysis, transplantation : official publication of the European Dialysis and Transplant Association - European Renal Association, 27(7), pp. 2702-2711.

SATO, M., MURAGAKI, Y., SAIKA, S., ROBERTS, A.B. and OOSHIMA, A., 2003. Targeted disruption of TGF-beta1/Smad3 signaling protects against renal tubulointerstitial fibrosis induced by unilateral ureteral obstruction. The Journal of clinical investigation, 112(10), pp. 1486-1494.

SATO, S., BURDETT, I. and HUGHES, R.C., 1993. Secretion of the baby hamster kidney 30-kDa galactose-binding lectin from polarized and nonpolarized cells: a pathway independent of the endoplasmic reticulum-Golgi complex. Experimental cell research, 207(1), pp. 8-18.

SATPATHY, M., SHAO, M., EMERSON, R., DONNER, D.B. and MATEI, D., 2009. Tissue transglutaminase regulates matrix metalloproteinase-2 in ovarian cancer by modulating cAMP-response element-binding protein activity. The Journal of biological chemistry, 284(23), pp. 15390-15399.

SAVINA, A., FURLAN, M., VIDAL, M. and COLOMBO, M.I., 2003. Exosome release is regulated by a calcium-dependent mechanism in K562 cells. The Journal of biological chemistry, 278(22), pp. 20083-20090.

SCARPELLINI, A., 2009. Syndecan-4 regulates cell-surface trafficking and biological activity of transglutaminase-2, .

SCARPELLINI, A., GERMACK, R., LORTAT-JACOB, H., MURAMATSU, T., BILLETT, E., JOHNSON, T. and VERDERIO, E.A., 2009. Heparan sulfate proteoglycans are receptors for the cell-surface trafficking and biological activity of transglutaminase-2. The Journal of biological chemistry, 284(27), pp. 18411-18423.

SCARPELLINI, A., HUANG, L., BURHAN, I., SCHROEDER, N., FUNCK, M., JOHNSON, T.S. and VERDERIO, E.A., 2014. Syndecan-4 knockout leads to reduced extracellular transglutaminase-2 and protects against tubulointerstitial fibrosis. Journal of the American Society of Nephrology : JASN, 25(5), pp. 1013-1027.

SCHAEFER, L., MIHALIK, D., BABELOVA, A., KRZYZANKOVA, M., GRÖNE, H., IOZZO, R.V., YOUNG, M.F., SEIDLER, D.G., LIN, G. and REINHARDT, D.P., 2004. Regulation of fibrillin-1 by biglycan and decorin is important for tissue preservation in the kidney during pressure-induced injury. The American journal of pathology, 165(2), pp. 383-396.

SCHAFER, T., ZENTGRAF, H., ZEHE, C., BRUGGER, B., BERNHAGEN, J. and NICKEL, W., 2004. Unconventional secretion of fibroblast growth factor 2 is mediated by direct translocation across the plasma membrane of mammalian cells. The Journal of biological chemistry, 279(8), pp. 6244-6251.

SCHAINUCK, L.I., STRIKER, G.E., CUTLER, R.E. and BENDITT, E.P., 1970. Structural-functional correlations in renal disease: Part II: the correlations. Human pathology, 1(4), pp. 631-641.

SCHELLINGS, M.W., VANHOUTTE, D., VAN ALMEN, G.C., SWINNEN, M., LEENDERS, J.J., KUBBEN, N., VAN LEEUWEN, R.E., HOFSTRA, L., HEYMANS, S. and PINTO, Y.M., 2010. Syndecan-1 amplifies angiotensin II-induced cardiac fibrosis. Hypertension (Dallas, Tex.: 1979), 55(2), pp. 249-256.

SCHINDELIN, J., RUEDEN, C.T., HINER, M.C. and ELICEIRI, K.W., 2015. The ImageJ ecosystem: An open platform for biomedical image analysis. Molecular reproduction and development, 82(7-8), pp. 518-529.

SCHLUTER, O.M., KHVOTCHEV, M., JAHN, R. and SUDHOF, T.C., 2002. Localization versus function of Rab3 proteins. Evidence for a common regulatory role in controlling fusion. The Journal of biological chemistry, 277(43), pp. 40919-40929.

SCHMITT, R., JACOBI, C., SUSNIK, N., BROECKER, V., HALLER, H. and MELK, A., 2009. Ageing mouse kidney--not always the SAME old story. Nephrology, dialysis, transplantation : official publication of the European Dialysis and Transplant Association - European Renal Association, 24(10), pp. 3002-3005.

SCHNAPER, H.W. and KOPP, J.B., 2003. Renal fibrosis. Front Biosci, 8(1), pp. 68-86.

SCHNATWINKEL, C., CHRISTOFORIDIS, S., LINDSAY, M.R., UTTENWEILER-JOSEPH, S., WILM, M., PARTON, R.G. and ZERIAL, M., 2004. The Rab5 effector Rabankyrin-5 regulates and coordinates different endocytic mechanisms. PLoS Biol, 2(9), pp. e261.

SCHOTMAN, H., KARHINEN, L. and RABOUILLE, C., 2008. dGRASP-mediated noncanonical integrin secretion is required for Drosophila epithelial remodeling. Developmental cell, 14(2), pp. 171-182.

SCHUCK, S., GERL, M.J., ANG, A., MANNINEN, A., KELLER, P., MELLMAN, I. and SIMONS, K., 2007. Rab10 is involved in basolateral transport in polarized Madin–Darby canine kidney cells. Traffic, 8(1), pp. 47-60.

SCHUKSZ, M., FUSTER, M.M., BROWN, J.R., CRAWFORD, B.E., DITTO, D.P., LAWRENCE, R., GLASS, C.A., WANG, L., TOR, Y. and ESKO, J.D., 2008. Surfen, a small molecule antagonist of heparan sulfate. Proceedings of the National Academy of Sciences of the United States of America, 105(35), pp. 13075-13080.

SCHULTZ, G.S. and WYSOCKI, A., 2009. Interactions between extracellular matrix and growth factors in wound healing. Wound repair and regeneration, 17(2), pp. 153-162.

SCOLARI, F., CARIDI, G., RAMPOLDI, L., TARDANICO, R., IZZI, C., PIRULLI, D., AMOROSO, A., CASARI, G. and GHIGGERI, G.M., 2004. Uromodulin storage diseases: clinical aspects and mechanisms. American journal of kidney diseases, 44(6), pp. 987-999.

SEAMAN, M.N., 2012. The retromer complex - endosomal protein recycling and beyond. Journal of cell science, 125(Pt 20), pp. 4693-4702.

SEAMAN, M.N., HARBOUR, M.E., TATTERSALL, D., READ, E. and BRIGHT, N., 2009. Membrane recruitment of the cargo-selective retromer subcomplex is catalysed by the small GTPase Rab7 and inhibited by the Rab-GAP TBC1D5. Journal of cell science, 122(Pt 14), pp. 2371-2382.

SEELENMEYER, C., STEGMAYER, C. and NICKEL, W., 2008. Unconventional secretion of fibroblast growth factor 2 and galectin-1 does not require shedding of plasma membrane-derived vesicles. FEBS letters, 582(9), pp. 1362-1368.

SEIKALY, M.G., HO, P., EMMETT, L., FINE, R.N. and TEJANI, A., 2003. Chronic renal insufficiency in children: the 2001 Annual Report of the NAPRTCS. Pediatric nephrology, 18(8), pp. 796-804.

SELIGER, S.L., DAVIS, C. and STEHMAN-BREEN, C., 2001. Gender and the progression of renal disease. Current opinion in nephrology and hypertension, 10(2), pp. 219-225.

SEN, K., LINDENMEYER, M.T., GASPERT, A., EICHINGER, F., NEUSSER, M.A., KRETZLER, M., SEGERER, S. and COHEN, C.D., 2011. Periostin is induced in glomerular injury and expressed de novo in interstitial renal fibrosis. The American journal of pathology, 179(4), pp. 1756-1767.

SERRANO, D., BHOWMICK, T., CHADHA, R., GARNACHO, C. and MURO, S., 2012. Intercellular adhesion molecule 1 engagement modulates sphingomyelinase and ceramide, supporting uptake of drug carriers by the vascular endothelium. Arteriosclerosis, Thrombosis, and Vascular Biology, 32(5), pp. 1178-1185.

SHAO, M., CAO, L., SHEN, C., SATPATHY, M., CHELLADURAI, B., BIGSBY, R.M., NAKSHATRI, H. and MATEI, D., 2009. Epithelial-to-mesenchymal transition and ovarian tumor progression induced by tissue transglutaminase. Cancer research, 69(24), pp. 9192-9201.

SHAPIRO, I.M., LANDIS, W.J. and RISBUD, M.V., 2015. Matrix vesicles: Are they anchored exosomes? Bone, 79, pp. 29-36.

SHARMA, A.K., MAUER, S.M., KIM, Y. and MICHAEL, A.F., 1993. Interstitial fibrosis in obstructive nephropathy. Kidney international, 44(4), pp. 774-788.

SHARMA, K., MCCUE, P. and DUNN, S.R., 2003. Diabetic kidney disease in the db/db mouse. American journal of physiology.Renal physiology, 284(6), pp. F1138-44.

SHELKE, G.V., LÄSSER, C., GHO, Y.S. and LÖTVALL, J., 2014. Importance of exosome depletion protocols to eliminate functional and RNA-containing extracellular vesicles from fetal bovine serum. Journal of extracellular vesicles, 3.

SHIBA, Y., KATOH, Y., SHIBA, T., YOSHINO, K., TAKATSU, H., KOBAYASHI, H., SHIN, H.W., WAKATSUKI, S. and NAKAYAMA, K., 2004. GAT (GGA and Tom1) domain responsible for ubiquitin binding and ubiquitination. The Journal of biological chemistry, 279(8), pp. 7105-7111.

SHIMAMURA, T. and MORRISON, A.B., 1975. A progressive glomerulosclerosis occurring in partial five-sixths nephrectomized rats. The American journal of pathology, 79(1), pp. 95-106.

SHIN, D.M., JEON, J.H., KIM, C.W., CHO, S.Y., LEE, H.J., JANG, G.Y., JEONG, E.M., LEE, D.S., KANG, J.H., MELINO, G., PARK, S.C. and KIM, I.G., 2008. TGFbeta mediates activation of transglutaminase 2 in response to oxidative stress that leads to protein aggregation. FASEB journal : official publication of the Federation of American Societies for Experimental Biology, 22(7), pp. 2498-2507.

SHIRASAKI, Y., YAMAGISHI, M., SUZUKI, N., IZAWA, K., NAKAHARA, A., MIZUNO, J., SHOJI, S., HEIKE, T., HARADA, Y. and NISHIKOMORI, R., 2014. Real-time single-cell imaging of protein secretion. Scientific reports, 4.

SHLIPAK, M.G., MATTES, M.D. and PERALTA, C.A., 2013. Update on cystatin C: incorporation into clinical practice. American Journal of Kidney Diseases, 62(3), pp. 595-603.

SHRESTHA, B., BUTT, I., DA SILVA, M., SANCHEZ-LARA, A., WAGNER, B., RAFTERY, A., JOHNSON, T. and HAYLOR, J., 2014. Upregulation of transglutaminase and epsilon (gamma-glutamyl)-lysine in the Fisher-Lewis rat model of chronic allograft nephropathy. BioMed research international, 2014, pp. 651608.

SHRESTHA, R., TATSUKAWA, H., ISHIBASHI, N., MATSUURA, T., KAGECHIKA, H., KOSE, S., HITOMI, K., IMAMOTO, N. and KOJIMA, S., 2015. Molecular mechanism by which acyclic retinoid induces nuclear localization of transglutaminase 2 in human hepatocellular carcinoma cells. Cell death & disease, 6(12), pp. e2002.

SHWEKE, N., BOULOS, N., JOUANNEAU, C., VANDERMEERSCH, S., MELINO, G., DUSSAULE, J., CHATZIANTONIOU, C., RONCO, P. and BOFFA, J., 2008. Tissue transglutaminase contributes to interstitial renal fibrosis by favoring accumulation of fibrillar collagen through TGF-β activation and cell infiltration. The American journal of pathology, 173(3), pp. 631-642.

SIEGEL, M., STRNAD, P., WATTS, R.E., CHOI, K., JABRI, B., OMARY, M.B. and KHOSLA, C., 2008. Extracellular transglutaminase 2 is catalytically inactive, but is transiently activated upon tissue injury. PloS one, 3(3), pp. e1861.

SILBIGER, S. and NEUGARTEN, J., 2008. Gender and human chronic renal disease. Gender medicine, 5, pp. S3-S10.

SIMONS, M. and HOROWITZ, A., 2001. Syndecan-4-mediated signalling. Cellular signalling, 13(12), pp. 855-862.

SIMPSON, R.J. and MATHIVANAN, S., 2012. Extracellular microvesicles: the need for internationally recognised nomenclature and stringent purification criteria. Journal of Proteomics & Bioinformatics, 2012.

SIMPSON, R.J., KALRA, H. and MATHIVANAN, S., 2012. ExoCarta as a resource for exosomal research. Journal of extracellular vesicles, 1.

SKILL, N.J., GRIFFIN, M., EL NAHAS, A.M., SANAI, T., HAYLOR, J.L., FISHER, M., JAMIE, M.F., MOULD, N.N. and JOHNSON, T.S., 2001. Increases in Renal &egr;-(&ggr;-Glutamyl)-Lysine Crosslinks Result from Compartment-Specific Changes in Tissue Transglutaminase in Early Experimental Diabetic Nephropathy: Pathologic Implications. Laboratory investigation, 81(5), pp. 705-716.

SKILL, N.J., JOHNSON, T.S., COUTTS, I.G., SAINT, R.E., FISHER, M., HUANG, L., EL NAHAS, A.M., COLLIGHAN, R.J. and GRIFFIN, M., 2004. Inhibition of transglutaminase activity reduces extracellular matrix accumulation induced by high glucose levels in proximal tubular epithelial cells. The Journal of biological chemistry, 279(46), pp. 47754-47762.

SKOGBERG, G., GUDMUNDSDOTTIR, J., VAN DER POST, S., SANDSTRÖM, K., BRUHN, S., BENSON, M., MINCHEVA-NILSSON, L., BARANOV, V., TELEMO, E. and EKWALL, O., 2013. Characterization of human thymic exosomes. PloS one, 8(7), pp. e67554.

SKOGBERG, G., LUNDBERG, V., BERGLUND, M., GUDMUNDSDOTTIR, J., TELEMO, E., LINDGREN, S. and EKWALL, O., 2015. Human thymic epithelial primary cells produce exosomes carrying tissue-restricted antigens. Immunology and cell biology, .

SMALL, K., FENG, J.F., LORENZ, J., DONNELLY, E.T., YU, A., IM, M.J., DORN, G.W.,2nd and LIGGETT, S.B., 1999. Cardiac specific overexpression of transglutaminase II (G(h)) results in a unique hypertrophy phenotype independent of phospholipase C activation. The Journal of biological chemistry, 274(30), pp. 21291-21296.

SMETHURST, P.A. and GRIFFIN, M., 1996. Measurement of tissue transglutaminase activity in a permeabilized cell system: its regulation by Ca2+ and nucleotides. The Biochemical journal, 313 (Pt 3)(Pt 3), pp. 803-808.

SMITH, M.P.W., ZOUGMAN, A., CAIRNS, D.A., WILSON, M., WIND, T., WOOD, S.L., THOMPSON, D., MESSENGER, M.P., MOONEY, A. and SELBY, P.J., 2013. Serum aminoacylase-1 is a novel biomarker with potential prognostic utility for long-term outcome in patients with delayed graft function following renal transplantation. Kidney international, 84(6), pp. 1214-1225.

SOLDI, R., MANDINOVA, A., VENKATARAMAN, K., HLA, T., VADAS, M., PITSON, S., DUARTE, M., GRAZIANI, I., KOLEV, V. and KACER, D., 2007. Sphingosine kinase 1 is a critical component of the copper-dependent FGF1 export pathway. Experimental cell research, 313(15), pp. 3308-3318.

SOLIS, G.P., HULSBUSCH, N., RADON, Y., KATANAEV, V.L., PLATTNER, H. and STUERMER, C.A., 2013. Reggies/flotillins interact with Rab11a and SNX4 at the tubulovesicular recycling compartment and function in transferrin receptor and E-cadherin trafficking. Molecular biology of the cell, 24(17), pp. 2689-2702.

SOLLID, L.M. and JABRI, B., 2011. Celiac disease and transglutaminase 2: a model for posttranslational modification of antigens and HLA association in the pathogenesis of autoimmune disorders. Current opinion in immunology, 23(6), pp. 732-738.

SONG, Y., KIRKPATRICK, L.L., SCHILLING, A.B., HELSETH, D.L., CHABOT, N., KEILLOR, J.W., JOHNSON, G.V. and BRADY, S.T., 2013. Transglutaminase and polyamination of tubulin: posttranslational modification for stabilizing axonal microtubules. Neuron, 78(1), pp. 109-123.

SOOY, K., KOHUT, J. and CHRISTAKOS, S., 2000. The role of calbindin and 1, 25dihydroxyvitamin D3 in the kidney. Current opinion in nephrology and hypertension, 9(4), pp. 341-347.

SOUSA, R. and LAFER, E.M., 2015. The role of molecular chaperones in clathrin mediated vesicular trafficking. Frontiers in molecular biosciences, 2, pp. 26.

SOUZA-SCHOREY, C.D., LI, G., COLOMBO, M.I. and STAHL, P.D., 1995. A regulatory role for ARF6 in receptor-mediated endocytosis. Science, 267(5201), pp. 1175.

SPIVAK-KROIZMAN, T., LEMMON, M., DIKIC, I., LADBURY, J., PINCHASI, D., HUANG, J., JAYE, M., CRUMLEY, G., SCHLESSINGER, J. and LAX, I., 1994. Heparin-induced oligomerization of FGF molecules is responsible for FGF receptor dimerization, activation, and cell proliferation. Cell, 79(6), pp. 1015-1024.

STAMNAES, J., PINKAS, D.M., FLECKENSTEIN, B., KHOSLA, C. and SOLLID, L.M., 2010. Redox regulation of transglutaminase 2 activity. The Journal of biological chemistry, 285(33), pp. 25402-25409.

STANFORD, K.I., BISHOP, J.R., FOLEY, E.M., GONZALES, J.C., NIESMAN, I.R., WITZTUM, J.L. and ESKO, J.D., 2009. Syndecan-1 is the primary heparan sulfate proteoglycan mediating hepatic clearance of triglyceride-rich lipoproteins in mice. The Journal of clinical investigation, 119(11), pp. 3236-3245.

STANFORD, K.I., WANG, L., CASTAGNOLA, J., SONG, D., BISHOP, J.R., BROWN, J.R., LAWRENCE, R., BAI, X., HABUCHI, H., TANAKA, M., CARDOSO, W.V., KIMATA, K. and ESKO, J.D., 2010. Heparan sulfate 2-O-sulfotransferase is required for triglyceride-rich lipoprotein clearance. The Journal of biological chemistry, 285(1), pp. 286-294.

STEGALL, M.D., CHEDID, M.F. and CORNELL, L.D., 2012. The role of complement in antibody-mediated rejection in kidney transplantation. Nature Reviews Nephrology, 8(11), pp. 670-678.

STEGMAYER, C., KEHLENBACH, A., TOURNAVITI, S., WEGEHINGEL, S., ZEHE, C., DENNY, P., SMITH, D.F., SCHWAPPACH, B. and NICKEL, W., 2005. Direct transport across the plasma membrane of mammalian cells of Leishmania HASPB as revealed by a CHO export mutant. Journal of cell science, 118(Pt 3), pp. 517-527.

STEINER, S., AICHER, L., RAYMACKERS, J., MEHEUS, L., ESQUER-BLASCO, R., ANDERSON, N.L. and CORDIER, A., 1996. Cyclosporine A decreases the protein level of the calcium-binding protein calbindin-D 28kDa in rat kidney. Biochemical pharmacology, 51(3), pp. 253-258.

STEINERT, P.M., CHUNG, S. and KIM, S., 1996. Inactive zymogen and highly active proteolytically processed membrane-bound forms of the transglutaminase 1 enzyme in human epidermal keratinocytes. Biochemical and biophysical research communications, 221(1), pp. 101-106.

STEINFELD, R., VAN DEN BERGHE, H. and DAVID, G., 1996. Stimulation of fibroblast growth factor receptor-1 occupancy and signaling by cell surface-associated syndecans and glypican. The Journal of cell biology, 133(2), pp. 405-416.

STELMACH, H., RUSAK, T. and TOMASIAK, M., 2002. The involvement of the Na /H exchanger in the formation of microvesicles by porcine platelets. Haematologia, 32(3), pp. 239-252.

STEPHENS, P., GRENARD, P., AESCHLIMANN, P., LANGLEY, M., BLAIN, E., ERRINGTON, R., KIPLING, D., THOMAS, D. and AESCHLIMANN, D., 2004. Crosslinking and G-protein functions of transglutaminase 2 contribute differentially to fibroblast wound healing responses. Journal of cell science, 117(Pt 15), pp. 3389-3403.

STEPP, M.A., GIBSON, H.E., GALA, P.H., IGLESIA, D.D., PAJOOHESH-GANJI, A., PAL-GHOSH, S., BROWN, M., AQUINO, C., SCHWARTZ, A.M., GOLDBERGER, O., HINKES, M.T. and BERNFIELD, M., 2002. Defects in keratinocyte activation during wound healing in the syndecan-1-deficient mouse. Journal of cell science, 115(Pt 23), pp. 4517-4531.

STERINGER, J.P., BLEICKEN, S., ANDREAS, H., ZACHERL, S., LAUSSMANN, M., TEMMERMAN, K., CONTRERAS, F.X., BHARAT, T.A., LECHNER, J., MULLER, H.M., BRIGGS, J.A., GARCIA-SAEZ, A.J. and NICKEL, W., 2012. Phosphatidylinositol 4,5-bisphosphate (PI(4,5)P2)-dependent oligomerization of fibroblast growth factor 2 (FGF2) triggers the formation of a lipidic membrane pore implicated in unconventional secretion. The Journal of biological chemistry, 287(33), pp. 27659-27669.

STOKES, M.B., HOLLER, S., CUI, Y., HUDKINS, K.L., EITNER, F., FOGO, A. and ALPERS, C.E., 2000. Expression of decorin, biglycan, and collagen type I in human renal fibrosing disease. Kidney international, 57(2), pp. 487-498.

STRAND, M.E., HERUM, K.M., RANA, Z.A., SKRBIC, B., ASKEVOLD, E.T., DAHL, C.P., VISTNES, M., HASIC, A., KVALØY, H. and SJAASTAD, I., 2013. Innate immune signaling induces expression and shedding of the heparan sulfate proteoglycan syndecan-4 in cardiac fibroblasts and myocytes, affecting inflammation in the pressure-overloaded heart. FEBS Journal, 280(10), pp. 2228-2247.

STRICHER, F., MACRI, C., RUFF, M. and MULLER, S., 2013. HSPA8/HSC70 chaperone protein: structure, function, and chemical targeting. Autophagy, 9(12), pp. 1937-1954.

STRINGER, K.D., KOMERS, R., OSMAN, S.A., OYAMA, T.T., LINDSLEY, J.N. and ANDERSON, S., 2005. Gender hormones and the progression of experimental polycystic kidney disease. Kidney international, 68(4), pp. 1729-1739.

STUFFERS, S., SEM WEGNER, C., STENMARK, H. and BRECH, A., 2009. Multivesicular endosome biogenesis in the absence of ESCRTs. Traffic, 10(7), pp. 925-937.

STURNIOLO, M.T., DASHTI, S.R., DEUCHER, A., RORKE, E.A., BROOME, A.M., CHANDRARATNA, R.A., KEEPERS, T. and ECKERT, R.L., 2003. A novel tumor suppressor protein promotes keratinocyte terminal differentiation via activation of type I transglutaminase. The Journal of biological chemistry, 278(48), pp. 48066-48073.

SU, G., BLAINE, S.A., QIAO, D. and FRIEDL, A., 2008. Membrane type 1 matrix metalloproteinase-mediated stromal syndecan-1 shedding stimulates breast carcinoma cell proliferation. Cancer research, 68(22), pp. 9558-9565.

SUBRAMANIAN, S.V., FITZGERALD, M.L. and BERNFIELD, M., 1997. Regulated shedding of syndecan-1 and -4 ectodomains by thrombin and growth factor receptor activation. The Journal of biological chemistry, 272(23), pp. 14713-14720.

SUGAHARA, K. and KITAGAWA, H., 2002. Heparin and heparan sulfate biosynthesis. IUBMB life, 54(4), pp. 163-175.

SUGENOYA, Y., YOSHIMURA, A., YAMAMURA, H., INUI, K., MORITA, H., YAMABE, H., UEKI, N., IDEURA, T. and TAKAHASHI, K., 2002. Smooth-muscle calponin in mesangial cells: regulation of expression and a role in suppressing glomerulonephritis. Journal of the American Society of Nephrology : JASN, 13(2), pp. 322-331.

SUN, D., MCALMON, K.R., DAVIES, J.A., BERNFIELD, M. and HAY, E.D., 1998. Simultaneous loss of expression of syndecan-1 and E-cadherin in the embryonic palate during epithelial-mesenchymal transformation. The International journal of developmental biology, 42(5), pp. 733-736.

SUNG, B.H., KETOVA, T., HOSHINO, D., ZIJLSTRA, A. and WEAVER, A.M., 2015. Directional cell movement through tissues is controlled by exosome secretion. Nature communications, 6.

SUTO, N., IKURA, K. and SASAKI, R., 1993. Expression induced by interleukin-6 of tissue-type transglutaminase in human hepatoblastoma HepG2 cells. The Journal of biological chemistry, 268(10), pp. 7469-7473.

SUZUKI, M., TANAKA, H., TANIMURA, A., TANABE, K., OE, N., RAI, S., KON, S., FUKUMOTO, M., TAKEI, K. and ABE, T., 2012. The clathrin assembly protein PICALM is required for erythroid maturation and transferrin internalization in mice. PloS one, 7(2), pp. e31854.

SZKLARCZYK, D., FRANCESCHINI, A., WYDER, S., FORSLUND, K., HELLER, D., HUERTA-CEPAS, J., SIMONOVIC, M., ROTH, A., SANTOS, A., TSAFOU, K.P., KUHN, M., BORK, P., JENSEN, L.J. and VON MERING, C., 2015. STRING v10: protein-protein interaction networks, integrated over the tree of life. Nucleic acids research, 43(Database issue), pp. D447-52.

SZONDY, Z., SARANG, Z., MOLNAR, P., NEMETH, T., PIACENTINI, M., MASTROBERARDINO, P.G., FALASCA, L., AESCHLIMANN, D., KOVACS, J., KISS, I., SZEGEZDI, E., LAKOS, G., RAJNAVOLGYI, E., BIRCKBICHLER, P.J., MELINO, G. and FESUS, L., 2003. Transglutaminase 2-/- mice reveal a phagocytosis-associated crosstalk between macrophages and apoptotic cells. Proceedings of the National Academy of Sciences of the United States of America, 100(13), pp. 7812-7817.

SZUL, T. and SZTUL, E., 2011. COPII and COPI traffic at the ER-Golgi interface. Physiology (Bethesda, Md.), 26(5), pp. 348-364.

TAFT, M.H., BEHRMANN, E., MUNSKE-WEIDEMANN, L.C., THIEL, C., RAUNSER, S. and MANSTEIN, D.J., 2013. Functional characterization of human myosin-18A and its interaction with F-actin and GOLPH3. The Journal of biological chemistry, 288(42), pp. 30029-30041.

TAI, G., LU, L., WANG, T.L., TANG, B.L., GOUD, B., JOHANNES, L. and HONG, W., 2004. Participation of the syntaxin 5/Ykt6/GS28/GS15 SNARE complex in transport from the early/recycling endosome to the trans-Golgi network. Molecular biology of the cell, 15(9), pp. 4011-4022.

TAKAHASHI, N., TAKAHASHI, Y. and PUTNAM, F.W., 1986. Primary structure of blood coagulation factor XIIIa (fibrinoligase, transglutaminase) from human placenta. Proceedings of the National Academy of Sciences of the United States of America, 83(21), pp. 8019-8023.

TANAKA, T. and NANGAKU, M., 2010. The role of hypoxia, increased oxygen consumption, and hypoxia-inducible factor-1 alpha in progression of chronic kidney disease. Current opinion in nephrology and hypertension, 19(1), pp. 43-50.

TANINO, Y., CHANG, M.Y., WANG, X., GILL, S.E., SKERRETT, S., MCGUIRE, J.K., SATO, S., NIKAIDO, T., KOJIMA, T. and MUNAKATA, M., 2012. Syndecan-4 regulates early neutrophil migration and pulmonary inflammation in response to lipopolysaccharide. American journal of respiratory cell and molecular biology, 47(2), pp. 196-202.

TAPMEIER, T., BROWN, K., TANG, Z., SACKS, S., SHEERIN, N. and WONG, W., 2008. Reimplantation of the ureter after unilateral ureteral obstruction provides a model that allows functional evaluation. Kidney international, 73(7), pp. 885-889.

TARABOLETTI, G., D'ASCENZO, S., BORSOTTI, P., GIAVAZZI, R., PAVAN, A. and DOLO, V., 2002. Shedding of the matrix metalloproteinases MMP-2, MMP-9, and MT1-MMP as membrane vesicle-associated components by endothelial cells. The American journal of pathology, 160(2), pp. 673-680.

TARANTINI, F., GAMBLE, S., JACKSON, A. and MACIAG, T., 1995. The cysteine residue responsible for the release of fibroblast growth factor-1 residues in a domain independent of the domain for phosphatidylserine binding. The Journal of biological chemistry, 270(49), pp. 29039-29042.

TARANTINI, F., LAVALLEE, T., JACKSON, A., GAMBLE, S., CARREIRA, C.M., GARFINKEL, S., BURGESS, W.H. and MACIAG, T., 1998. The extravesicular domain of synaptotagmin-1 is released with the latent fibroblast growth factor-1 homodimer in response to heat shock. Journal of Biological Chemistry, 273(35), pp. 22209-22216.

TATSUKAWA, H., FUKAYA, Y., FRAMPTON, G., MARTINEZ–FUENTES, A., SUZUKI, K., KUO, T., NAGATSUMA, K., SHIMOKADO, K., OKUNO, M. and WU, J., 2009. Role of transglutaminase 2 in liver injury via cross-linking and silencing of transcription factor Sp1. Gastroenterology, 136(5), pp. 1783-1795. e10.

TEBAR, F., BOHLANDER, S.K. and SORKIN, A., 1999. Clathrin assembly lymphoid myeloid leukemia (CALM) protein: localization in endocytic-coated pits, interactions with clathrin, and the impact of overexpression on clathrin-mediated traffic. Molecular biology of the cell, 10(8), pp. 2687-2702.

TEESALU, K., PANARINA, M., UIBO, O., UIBO, R. and UTT, M., 2012. Autoantibodies from patients with celiac disease inhibit transglutaminase 2 binding to heparin/heparan sulfate and interfere with intestinal epithelial cell adhesion. Amino acids, 42(2-3), pp. 1055-1064.

TEESALU, K., UIBO, O., UIBO, R. and UTT, M., 2012. Kinetic and functional characterisation of the heparin-binding peptides from human transglutaminase 2. Journal of Peptide Science, 18(5), pp. 350-356.

TELCI, D. and GRIFFIN, M., 2006. Tissue transglutaminase (TG2)--a wound response enzyme. Frontiers in bioscience : a journal and virtual library, 11, pp. 867-882.

TELCI, D., COLLIGHAN, R.J., BASAGA, H. and GRIFFIN, M., 2009. Increased TG2 expression can result in induction of transforming growth factor beta1, causing increased synthesis and deposition of matrix proteins, which can be regulated by nitric oxide. The Journal of biological chemistry, 284(43), pp. 29547-29558.

TELCI, D., WANG, Z., LI, X., VERDERIO, E.A., HUMPHRIES, M.J., BACCARINI, M., BASAGA, H. and GRIFFIN, M., 2008. Fibronectin-tissue transglutaminase matrix rescues RGD-impaired cell adhesion through syndecan-4 and beta1 integrin co-signaling. The Journal of biological chemistry, 283(30), pp. 20937-20947.

TEMKIN, P., LAUFFER, B., JÄGER, S., CIMERMANCIC, P., KROGAN, N.J. and VON ZASTROW, M., 2011. SNX27 mediates retromer tubule entry and endosome-to-plasma membrane trafficking of signalling receptors. Nature cell biology, 13(6), pp. 715-721.

TEMMERMAN, K., EBERT, A.D., MÜLLER, H., SINNING, I., TEWS, I. and NICKEL, W., 2008. A direct role for phosphatidylinositol-4, 5-bisphosphate in unconventional secretion of fibroblast growth factor 2. Traffic, 9(7), pp. 1204-1217.

TENG, M.S., STEPHENS, R., PASQUIER, L.D., FREEMAN, T., LINDQUIST, J.A. and TROWSDALE, J., 2002. A human TAPBP (TAPASIN)-related gene, TAPBP-R. European journal of immunology, 32(4), pp. 1059-1068.

TERADA, S., KINJO, M., AIHARA, M., TAKEI, Y. and HIROKAWA, N., 2010. Kinesin-1/Hsc70-dependent mechanism of slow axonal transport and its relation to fast axonal transport. The EMBO journal, 29(4), pp. 843-854.

TERZI, F., VIAU, A., NGUYEN, C., BURTIN, M. and EL KAROUI, K., 2016. Methods for predicting the progression and treating a chronic kidney disease in a patient, .

TESCH, G.H. and ALLEN, T.J., 2007. Rodent models of streptozotocin-induced diabetic nephropathy (Methods in Renal Research). Nephrology, 12(3), pp. 261-266.

THERMO FISHER SCIENTIFIC, NANODROP PRODUCTS, 2008-last update, T009-TECHNICAL BULLETIN NanoDrop 1000 & 8000. Available: http://www.nanodrop.com/Library/T009-NanoDrop%201000-&-NanoDrop%208000-Nucleic-Acid-Purity-Ratios.pdf.

THERY, C., BOUSSAC, M., VERON, P., RICCIARDI-CASTAGNOLI, P., RAPOSO, G., GARIN, J. and AMIGORENA, S., 2001. Proteomic analysis of dendritic cell-derived exosomes: a secreted subcellular compartment distinct from apoptotic vesicles. Journal of immunology (Baltimore, Md.: 1950), 166(12), pp. 7309-7318.

THERY, C., REGNAULT, A., GARIN, J., WOLFERS, J., ZITVOGEL, L., RICCIARDI-CASTAGNOLI, P., RAPOSO, G. and AMIGORENA, S., 1999. Molecular characterization of dendritic cell-derived exosomes. Selective accumulation of the heat shock protein hsc73. The Journal of cell biology, 147(3), pp. 599-610.

THODETI, C.K., ALBRECHTSEN, R., GRAUSLUND, M., ASMAR, M., LARSSON, C., TAKADA, Y., MERCURIO, A.M., COUCHMAN, J.R. and WEWER, U.M., 2003. ADAM12/syndecan-4 signaling promotes beta 1 integrin-dependent cell spreading through protein kinase Calpha and RhoA. The Journal of biological chemistry, 278(11), pp. 9576-9584.

THOMAS, H., BECK, K., ADAMCZYK, M., AESCHLIMANN, P., LANGLEY, M., OITA, R.C., THIEBACH, L., HILS, M. and AESCHLIMANN, D., 2013. Transglutaminase 6: a protein associated with central nervous system development and motor function. Amino acids, 44(1), pp. 161-177.

THONGBOONKERD, V., BARATI, M.T., MCLEISH, K.R., BENARAFA, C., REMOLD-O'DONNELL, E., ZHENG, S., ROVIN, B.H., PIERCE, W.M., EPSTEIN, P.N. and KLEIN, J.B., 2004. Alterations in the renal elastin-elastase system in type 1 diabetic nephropathy identified by proteomic analysis. Journal of the American Society of Nephrology : JASN, 15(3), pp. 650-662.

TIAN, T., ZHU, Y.L., ZHOU, Y.Y., LIANG, G.F., WANG, Y.Y., HU, F.H. and XIAO, Z.D., 2014. Exosome uptake through clathrin-mediated endocytosis and macropinocytosis and mediating miR-21 delivery. The Journal of biological chemistry, 289(32), pp. 22258-22267.

TKACHENKO, E. and SIMONS, M., 2002. Clustering induces redistribution of syndecan-4 core protein into raft membrane domains. The Journal of biological chemistry, 277(22), pp. 19946-19951.

TKACHENKO, E., LUTGENS, E., STAN, R.V. and SIMONS, M., 2004. Fibroblast growth factor 2 endocytosis in endothelial cells proceed via syndecan-4-dependent activation of Rac1 and a Cdc42-dependent macropinocytic pathway. Journal of cell science, 117(Pt 15), pp. 3189-3199.

TKACHENKO, E., RHODES, J.M. and SIMONS, M., 2005. Syndecans: new kids on the signaling block. Circulation research, 96(5), pp. 488-500.

TOLENTINO, P.J., WAGHRAY, A., WANG, K.K. and HAYES, R.L., 2004. Increased expression of tissue-type transglutaminase following middle cerebral artery occlusion in rats. Journal of neurochemistry, 89(5), pp. 1301-1307.

TOMASEK, J.J., GABBIANI, G., HINZ, B., CHAPONNIER, C. and BROWN, R.A., 2002. Myofibroblasts and mechano-regulation of connective tissue remodelling. Nature reviews Molecular cell biology, 3(5), pp. 349-363.

TORRADO, L.C., TEMMERMAN, K., MULLER, H.M., MAYER, M.P., SEELENMEYER, C., BACKHAUS, R. and NICKEL, W., 2009. An intrinsic quality-control mechanism ensures unconventional secretion of fibroblast growth factor 2 in a folded conformation. Journal of cell science, 122(Pt 18), pp. 3322-3329.

TRAER, C.J., RUTHERFORD, A.C., PALMER, K.J., WASSMER, T., OAKLEY, J., ATTAR, N., CARLTON, J.G., KREMERSKOTHEN, J., STEPHENS, D.J. and CULLEN, P.J., 2007. SNX4 coordinates endosomal sorting of TfnR with dynein-mediated transport into the endocytic recycling compartment. Nature cell biology, 9(12), pp. 1370-1380.

TRAJKOVIC, K., HSU, C., CHIANTIA, S., RAJENDRAN, L., WENZEL, D., WIELAND, F., SCHWILLE, P., BRUGGER, B. and SIMONS, M., 2008. Ceramide triggers budding of exosome vesicles into multivesicular endosomes. Science (New York, N.Y.), 319(5867), pp. 1244-1247.

TROUGAKOS, I.P. and GONOS, E.S., 2006. Regulation of clusterin/apolipoprotein J, a functional homologue to the small heat shock proteins, by oxidative stress in ageing and age-related diseases. Free radical research, 40(12), pp. 1324-1334.

TRUONG, L., FOSTER, S.V., BARRIOS, R., D'AGATI, V., VERANI, R.R., GONZALEZ, J.M. and SUKI, W.N., 1996. Tenascin is an ubiquitous extracellular matrix protein of human renal interstitium in normal and pathologic conditions. Nephron, 72(4), pp. 579-586.

TRUONG, L.D., PINDUR, J., BARRIOS, R., D'AGATI, V., LECHAGO, J., SUKI, W. and MAJESKY, M., 1994. Tenascin is an important component of the glomerular extracellular matrix in normal and pathologic conditions. Kidney international, 45(1), pp. 201-210.

TUMLIN, J.A., LOHAVICHAN, V. and HENNIGAR, R., 2003. Crescentic, proliferative IgA nephropathy: clinical and histological response to methylprednisolone and intravenous cyclophosphamide. Nephrology, dialysis, transplantation : official publication of the European Dialysis and Transplant Association - European Renal Association, 18(7), pp. 1321-1329.

TUMOVA, S., WOODS, A. and COUCHMAN, J.R., 2000. Heparan sulfate proteoglycans on the cell surface: versatile coordinators of cellular functions. The international journal of biochemistry & cell biology, 32(3), pp. 269-288.

TUXWORTH, R.I. and TITUS, M.A., 2000. Unconventional myosins: anchors in the membrane traffic relay. Traffic, 1(1), pp. 11-18.

UCERO, A.C., BENITO-MARTIN, A., IZQUIERDO, M.C., SANCHEZ-NIÑO, M.D., SANZ, A.B., RAMOS, A.M., BERZAL, S., RUIZ-ORTEGA, M., EGIDO, J. and ORTIZ, A., 2014. Unilateral ureteral obstruction: beyond obstruction. International urology and nephrology, 46(4), pp. 765-776.

UPCHURCH, H.F., CONWAY, E., PATTERSON, M. and MAXWELL, M.D., 1991. Localization of cellular transglutaminase on the extracellular matrix after wounding: characteristics of the matrix bound enzyme. Journal of cellular physiology, 149(3), pp. 375-382.

URBANSKA, A., SADOWSKI, L., KALAIDZIDIS, Y. and MIACZYNSKA, M., 2011. Biochemical characterization of APPL endosomes: the role of annexin A2 in APPL membrane recruitment. Traffic, 12(9), pp. 1227-1241.

VALAPALA, M. and VISHWANATHA, J.K., 2011. Lipid raft endocytosis and exosomal transport facilitate extracellular trafficking of annexin A2. The Journal of biological chemistry, 286(35), pp. 30911-30925.

VAN DEN AKKER, J., VAN WEERT, A., AFINK, G., BAKKER, E.N., VAN DER POL, E., BÖING, A.N., NIEUWLAND, R. and VANBAVEL, E., 2012. Transglutaminase 2 is secreted from smooth muscle cells by transamidation-dependent microparticle formation. Amino acids, 42(2-3), pp. 961-973.

VAN DEN AKKER, J., VANBAVEL, E., VAN GEEL, R., MATLUNG, H.L., TUNA, B.G., JANSSEN, G.M., VAN VEELEN, P.A., BOELENS, W.C., DE MEY, J.G. and BAKKER, E.N., 2011. The redox state of transglutaminase 2 controls arterial remodeling. PLoS One, 6(8), pp. e23067.

VAN NIEL, G., CHARRIN, S., SIMOES, S., ROMAO, M., ROCHIN, L., SAFTIG, P., MARKS, M.S., RUBINSTEIN, E. and RAPOSO, G., 2011. The tetraspanin CD63 regulates ESCRT-independent and-dependent endosomal sorting during melanogenesis. Developmental cell, 21(4), pp. 708-721.

VAN WAARDE, M., VAN ASSEN, A., KAMPINGA, H., KONINGS, A. and VUJASKOVIC, Z., 1997. Quantification of Transforming Growth Factor-β in Biological Material Using Cells Transfected with a Plasminogen Activator Inhibitor-1 Promoter–Luciferase Construct. Analytical Biochemistry, 247(1), pp. 45-51.

VAN WEERING, J.R., VERKADE, P. and CULLEN, P.J., 2010. SNX–BAR proteins in phosphoinositide-mediated, tubular-based endosomal sorting, Seminars in cell & developmental biology 2010, Elsevier, pp. 371-380.

VANHERWEGHEM, J., TIELEMANS, C., ABRAMOWICZ, D., DEPIERREUX, M., VANHAELEN-FASTRE, R., VANHAELEN, M., DRATWA, M., RICHARD, C., VANDERVELDE, D. and VERBEELEN, D., 1993. Rapidly progressive interstitial renal fibrosis in young women: association with slimming regimen including Chinese herbs. The Lancet, 341(8842), pp. 387-391.

VANHOLDER, R., GLORIEUX, G., LAMEIRE, N. and EUROPEAN UREMIC TOXIN WORK GROUP, 2003. Uraemic toxins and cardiovascular disease. Nephrology, dialysis, transplantation : official publication of the European Dialysis and Transplant Association - European Renal Association, 18(3), pp. 463-466.

VARGA, J., ROSENBLOOM, J. and JIMENEZ, S.A., 1987. Transforming growth factor beta (TGF beta) causes a persistent increase in steady-state amounts of type I and type III collagen and fibronectin mRNAs in normal human dermal fibroblasts. The Biochemical journal, 247(3), pp. 597-604.

VARGAS, A., ZHOU, S., ETHIER-CHIASSON, M., FLIPO, D., LAFOND, J., GILBERT, C. and BARBEAU, B., 2014. Syncytin proteins incorporated in placenta exosomes are important for cell uptake and show variation in abundance in serum exosomes from patients with preeclampsia. FASEB journal : official publication of the Federation of American Societies for Experimental Biology, 28(8), pp. 3703-3719.

VARGHESE, S.A., POWELL, T.B., BUDISAVLJEVIC, M.N., OATES, J.C., RAYMOND, J.R., ALMEIDA, J.S. and ARTHUR, J.M., 2007. Urine biomarkers predict the cause of glomerular disease. Journal of the American Society of Nephrology : JASN, 18(3), pp. 913-922.

VASSON, M.P., PAUL, J.L., COUDERC, R., ALBUISSON, E., BARGNOUX, P.J., BAGUET, J.C. and RAICHVARG, D., 1991. Serum alpha-1 acid glycoprotein in chronic renal failure and hemodialysis. The International journal of artificial organs, 14(2), pp. 92-96.

VAUGHAN, E.D., MARION, D., POPPAS, D.P. and FELSEN, D., 2004. Pathophysiology of unilateral ureteral obstruction: studies from Charlottesville to New York. The Journal of urology, 172(6), pp. 2563-2569.

VAUGHAN, K.T. and VALLEE, R.B., 1995. Cytoplasmic dynein binds dynactin through a direct interaction between the intermediate chains and p150Glued. The Journal of cell biology, 131(6 Pt 1), pp. 1507-1516.

VERDERIO, E. and SCARPELLINI, A., 2010. Significance of the syndecan-4-transglutaminase-2 interaction. Sci World J, 10, pp. 1073-1077.

VERDERIO, E., GAUDRY, C., GROSS, S., SMITH, C., DOWNES, S. and GRIFFIN, M., 1999. Regulation of cell surface tissue transglutaminase: effects on matrix storage of latent transforming growth factor-beta binding protein-1. The journal of histochemistry and cytochemistry : official journal of the Histochemistry Society, 47(11), pp. 1417-1432.

VERDERIO, E., JOHNSON, T. and GRIFFIN, M., 2004. Tissue transglutaminase in normal and abnormal wound healing: review article. Amino acids, 26(4), pp. 387-404.

VERDERIO, E., NICHOLAS, B., GROSS, S. and GRIFFIN, M., 1998. Regulated expression of tissue transglutaminase in Swiss 3T3 fibroblasts: effects on the processing of fibronectin, cell attachment, and cell death. Experimental cell research, 239(1), pp. 119-138.

VERDERIO, E., SCARPELLINI, A. and JOHNSON, T., 2009. Novel interactions of TG2 with heparan sulfate proteoglycans: reflection on physiological implications. Amino acids, 36(4), pp. 671-677.

VERDERIO, E.A., FURINI, G., BURHAN, I.W. and JOHNSON, T.S., 2015. Transglutaminases: Expression in Kidney and Relation to Kidney Fibrosis. Transglutaminases. Springer, pp. 229-262.

VERDERIO, E.A., TELCI, D., OKOYE, A., MELINO, G. and GRIFFIN, M., 2003. A novel RGD-independent cel adhesion pathway mediated by fibronectin-bound tissue transglutaminase rescues cells from anoikis. The Journal of biological chemistry, 278(43), pp. 42604-42614.

VERMA, A. and MEHTA, K., 2007. Transglutaminase-mediated activation of nuclear transcription factor-κB in cancer cells: a new therapeutic opportunity. Current cancer drug targets, 7(6), pp. 559-565.

VIELHAUER, V., ANDERS, H.J., MACK, M., CIHAK, J., STRUTZ, F., STANGASSINGER, M., LUCKOW, B., GRONE, H.J. and SCHLONDORFF, D., 2001. Obstructive nephropathy in the mouse: progressive fibrosis correlates with tubulointerstitial chemokine expression and accumulation of CC chemokine receptor 2- and 5-positive leukocytes. Journal of the American Society of Nephrology : JASN, 12(6), pp. 1173-1187.

VIJ, N., 2008. AAA ATPase p97/VCP: cellular functions, disease and therapeutic potential. Journal of Cellular and Molecular Medicine, 12(6a), pp. 2511-2518.

WAELTER, S., SCHERZINGER, E., HASENBANK, R., NORDHOFF, E., LURZ, R., GOEHLER, H., GAUSS, C., SATHASIVAM, K., BATES, G.P., LEHRACH, H. and WANKER, E.E., 2001. The huntingtin interacting protein HIP1 is a clathrin and alpha-adaptin-binding protein involved in receptor-mediated endocytosis. Human molecular genetics, 10(17), pp. 1807-1817.

WALLACE, D.P., WHITE, C., SAVINKOVA, L., NIVENS, E., REIF, G.A., PINTO, C.S., RAMAN, A., PARNELL, S.C., CONWAY, S.J. and FIELDS, T.A., 2014. Periostin promotes renal cyst growth and interstitial fibrosis in polycystic kidney disease. Kidney international, 85(4), pp. 845-854.

WANG, D., LOU, J., OUYANG, C., CHEN, W., LIU, Y., LIU, X., CAO, X., WANG, J. and LU, L., 2010. Ras-related protein Rab10 facilitates TLR4 signaling by promoting replenishment of TLR4 onto the plasma membrane. Proceedings of the National Academy of Sciences of the United States of America, 107(31), pp. 13806-13811.

WANG, L., FUSTER, M., SRIRAMARAO, P. and ESKO, J.D., 2005. Endothelial heparan sulfate deficiency impairs L-selectin-and chemokine-mediated neutrophil trafficking during inflammatory responses. Nature immunology, 6(9), pp. 902-910.

WANG, X., MATTESON, J., AN, Y., MOYER, B., YOO, J.S., BANNYKH, S., WILSON, I.A., RIORDAN, J.R. and BALCH, W.E., 2004. COPII-dependent export of cystic fibrosis transmembrane conductance regulator from the ER uses a di-acidic exit code. The Journal of cell biology, 167(1), pp. 65-74.

WANG, Z., COLLIGHAN, R.J., GROSS, S.R., DANEN, E.H., OREND, G., TELCI, D. and GRIFFIN, M., 2010. RGD-independent cell adhesion via a tissue transglutaminase-fibronectin matrix promotes fibronectin fibril deposition and requires syndecan-4/2 alpha5beta1 integrin co-signaling. The Journal of biological chemistry, 285(51), pp. 40212-40229.

WANG, Z., COLLIGHAN, R.J., PYTEL, K., RATHBONE, D.L., LI, X. and GRIFFIN, M., 2012. Characterization of heparin-binding site of tissue transglutaminase: its importance in cell surface targeting, matrix deposition, and cell signaling. The Journal of biological chemistry, 287(16), pp. 13063-13083.

WANG, Z., TELCI, D. and GRIFFIN, M., 2011. Importance of syndecan-4 and syndecan-2 in osteoblast cell adhesion and survival mediated by a tissue transglutaminase– fibronectin complex. Experimental cell research, 317(3), pp. 367-381.

WASSMER, T., ATTAR, N., HARTERINK, M., VAN WEERING, J.R., TRAER, C.J., OAKLEY, J., GOUD, B., STEPHENS, D.J., VERKADE, P. and KORSWAGEN, H.C., 2009. The retromer coat complex coordinates endosomal sorting and dynein-mediated transport, with carrier recognition by the trans-Golgi network. Developmental cell, 17(1), pp. 110-122.

WEIGERT, K., 1904. Eine Kleine Verbesserung der haematoxylin-van Gieson-Methode. Z Wiss Mikr, 2, pp. 1-5.

WELCH, T.R., BEISCHEL, L.S. and WITTE, D.P., 1993. Differential expression of complement C3 and C4 in the human kidney. The Journal of clinical investigation, 92(3), pp. 1451-1458.

WELLS, R.G. and DISCHER, D.E., 2008. Matrix elasticity, cytoskeletal tension, and TGF-beta: the insoluble and soluble meet. Science signaling, 1(10), pp. pe13.

WHITEFORD, J.R., XIAN, X., CHAUSSADE, C., VANHAESEBROECK, B., NOURSHARGH, S. and COUCHMAN, J.R., 2011. Syndecan-2 is a novel ligand for the protein tyrosine phosphatase receptor CD148. Molecular biology of the cell, 22(19), pp. 3609-3624.

WHITELOCK, J.M. and IOZZO, R.V., 2005. Heparan sulfate: a complex polymer charged with biological activity. Chemical reviews, 105(7), pp. 2745-2764.

WICKNER, W.T. and LODISH, H.F., 1985. Multiple mechanisms of protein insertion into and across membranes. Science (New York, N.Y.), 230(4724), pp. 400-407.

WILCOX-ADELMAN, S.A., DENHEZ, F. and GOETINCK, P.F., 2002. Syndecan-4 modulates focal adhesion kinase phosphorylation. The Journal of biological chemistry, 277(36), pp. 32970-32977.

WILHELMUS, M.M., GRUNBERG, S., BOL, J.G., VAN DAM, A., HOOZEMANS, J.J., ROZEMULLER, A.J. and DRUKARCH, B., 2009. Transglutaminases and Transglutaminase-Catalyzed Cross-Links Colocalize with the Pathological Lesions in Alzheimer's Disease Brain. Brain Pathology, 19(4), pp. 612-622.

WILLIAMS, H., PEASE, R.J., NEWELL, L.M., CORDELL, P.A., GRAHAM, R.M., KEARNEY, M.T., JACKSON, C.L. and GRANT, P.J., 2010. Effect of transglutaminase 2 (TG2) deficiency on atherosclerotic plaque stability in the apolipoprotein E deficient mouse. Atherosclerosis, 210(1), pp. 94-99.

WIPFF, P. and HINZ, B., 2008. Integrins and the activation of latent transforming growth factor β1–an intimate relationship. European journal of cell biology, 87(8), pp. 601-615.

WOLLERT, T. and HURLEY, J.H., 2010. Molecular mechanism of multivesicular body biogenesis by ESCRT complexes. Nature, 464(7290), pp. 864-869.

WOODS, A., LONGLEY, R.L., TUMOVA, S. and COUCHMAN, J.R., 2000. Syndecan-4 binding to the high affinity heparin-binding domain of fibronectin drives focal adhesion formation in fibroblasts. Archives of Biochemistry and Biophysics, 374(1), pp. 66-72.

WORTHINGTON, J.J., KLEMENTOWICZ, J.E. and TRAVIS, M.A., 2011. TGFβ: a sleeping giant awoken by integrins. Trends in biochemical sciences, 36(1), pp. 47-54.

WU, L., 2016. Role of Auxilin and Heat Shock Protein 70kDa in Clathrin Uncoating. Einstein Journal of Biology and Medicine, 21(2), pp. 57-62.

WUBBOLTS, R., LECKIE, R.S., VEENHUIZEN, P.T., SCHWARZMANN, G., MOBIUS, W., HOERNSCHEMEYER, J., SLOT, J.W., GEUZE, H.J. and STOORVOGEL, W., 2003. Proteomic and biochemical analyses of human B cell-derived exosomes. Potential implications for their function and multivesicular body formation. The Journal of biological chemistry, 278(13), pp. 10963-10972.

XIAO, J., CHEN, X.W., DAVIES, B.A., SALTIEL, A.R., KATZMANN, D.J. and XU, Z., 2009. Structural basis of Ist1 function and Ist1-Did2 interaction in the multivesicular body pathway and cytokinesis. Molecular biology of the cell, 20(15), pp. 3514-3524.

XIE, J., WANG, J., LI, R., DAI, Q., YONG, Y., ZONG, B., XU, Y., LI, E., FERRO, A. and XU, B., 2012. Syndecan-4 over-expression preserves cardiac function in a rat model of myocardial infarction. Journal of Molecular and Cellular Cardiology, 53(2), pp. 250-258.

XU, B.J., SHYR, Y., LIANG, X., MA, L.J., DONNERT, E.M., ROBERTS, J.D., ZHANG, X., KON, V., BROWN, N.J., CAPRIOLI, R.M. and FOGO, A.B., 2005. Proteomic patterns and prediction of glomerulosclerosis and its mechanisms. Journal of the American Society of Nephrology : JASN, 16(10), pp. 2967-2975.

XU, L., BEGUM, S., HEARN, J.D. and HYNES, R.O., 2006. GPR56, an atypical G protein-coupled receptor, binds tissue transglutaminase, TG2, and inhibits melanoma tumor growth and metastasis. Proceedings of the National Academy of Sciences of the United States of America, 103(24), pp. 9023-9028.

XU, Y., MARTIN, S., JAMES, D.E. and HONG, W., 2002. GS15 forms a SNARE complex with syntaxin 5, GS28, and Ykt6 and is implicated in traffic in the early cisternae of the Golgi apparatus. Molecular biology of the cell, 13(10), pp. 3493-3507.

XUE, H., FAN, J., CHEN, L., SU, B., LI, Z., HU, Z., LIU, X. and XU, G., 2003. Investigation of renal fibrosis induced by unilateral ureteral obstruction. Sichuan journal of zoology/Sichuan sheng ye sheng dong wu bao hu xie hui, Sse-chuan sheng dong wu xue hui, Sichuan sheng ji sheng chong bing fang zhi yan jiu suo; Jiang Dequan zhu bian, 23(1), pp. 16-20.

YAMAGUCHI, J., TANAKA, T. and INAGI, R., 2016. Effect of AST-120 in Chronic Kidney Disease Treatment: Still a Controversy. Nephron,

YAMAKAMI, M., YOSHIMORI, T. and YOKOSAWA, H., 2003. Tom1, a VHS domain-containing protein, interacts with tollip, ubiquitin, and clathrin. The Journal of biological chemistry, 278(52), pp. 52865-52872.

YAMAMOTO, T., NOIRI, E., ONO, Y., DOI, K., NEGISHI, K., KAMIJO, A., KIMURA, K., FUJITA, T., KINUKAWA, T., TANIGUCHI, H., NAKAMURA, K., GOTO, M., SHINOZAKI, N., OHSHIMA, S. and SUGAYA, T., 2007. Renal L-type fatty acid--binding protein in acute ischemic injury. Journal of the American Society of Nephrology : JASN, 18(11), pp. 2894-2902.

YANG, H., ZUO, Y. and FOGO, A.B., 2010. Models of chronic kidney disease. Drug Discovery Today: Disease Models, 7(1), pp. 13-19.

YANG, J., SHULTZ, R.W., MARS, W.M., WEGNER, R.E., LI, Y., DAI, C., NEJAK, K. and LIU, Y., 2002. Disruption of tissue-type plasminogen activator gene in mice reduces renal interstitial fibrosis in obstructive nephropathy. The Journal of clinical investigation, 110(10), pp. 1525-1538.

YANG, J., ZHANG, X., LI, Y. and LIU, Y., 2003. Downregulation of Smad transcriptional corepressors SnoN and Ski in the fibrotic kidney: an amplification mechanism for TGF-beta1 signaling. Journal of the American Society of Nephrology : JASN, 14(12), pp. 3167-3177.

YANG, L., BESSCHETNOVA, T.Y., BROOKS, C.R., SHAH, J.V. and BONVENTRE, J.V., 2010. Epithelial cell cycle arrest in G2/M mediates kidney fibrosis after injury. Nature medicine, 16(5), pp. 535-543.

YANG, L., BESSCHETNOVA, T.Y., BROOKS, C.R., SHAH, J.V. and BONVENTRE, J.V., 2010. Epithelial cell cycle arrest in G2/M mediates kidney fibrosis after injury. Nature medicine, 16(5), pp. 535-543.

YANG, Z., XIAOHUA, W., LEI, J., RUOYUN, T., MINGXIA, X., WEICHUN, H., LI, F., PING, W. and JUNWEI, Y., 2010. Uric acid increases fibronectin synthesis through upregulation of lysyl oxidase expression in rat renal tubular epithelial cells. American journal of physiology.Renal physiology, 299(2), pp. F336-46.

YOO, J.S., MOYER, B.D., BANNYKH, S., YOO, H.M., RIORDAN, J.R. and BALCH, W.E., 2002. Non-conventional trafficking of the cystic fibrosis transmembrane conductance regulator through the early secretory pathway. The Journal of biological chemistry, 277(13), pp. 11401-11409.

YUAN, Y., ZHANG, F., WU, J., SHAO, C. and GAO, Y., 2015. Urinary candidate biomarker discovery in a rat unilateral ureteral obstruction model. Scientific reports, 5, pp. 9314.

YUASA, T., YANO, R., IZAWA, T., KUWAMURA, M. and YAMATE, J., 2014. Calponin expression in renal tubulointerstitial fibrosis induced in rats by Cisplatin. Journal of toxicologic pathology, 27(1), pp. 97-103.

YUNG, S., WOODS, A., CHAN, T.M., DAVIES, M., WILLIAMS, J.D. and COUCHMAN, J.R., 2001. Syndecan-4 up-regulation in proliferative renal disease is related to microfilament organization. FASEB journal : official publication of the Federation of American Societies for Experimental Biology, 15(9), pp. 1631-1633.

YUNG, S., WOODS, A., CHAN, T.M., DAVIES, M., WILLIAMS, J.D. and COUCHMAN, J.R., 2001. Syndecan-4 up-regulation in proliferative renal disease is related to microfilament organization. FASEB journal : official publication of the Federation of American Societies for Experimental Biology, 15(9), pp. 1631-1633.

ZACHERL, S., LA VENUTA, G., MULLER, H.M., WEGEHINGEL, S., DIMOU, E., SEHR, P., LEWIS, J.D., ERFLE, H., PEPPERKOK, R. and NICKEL, W., 2015. A direct role for ATP1A1 in unconventional secretion of fibroblast growth factor 2. The Journal of biological chemistry, 290(6), pp. 3654-3665.

ZECH, T., CALAMINUS, S.D., CASWELL, P., SPENCE, H.J., CARNELL, M., INSALL, R.H., NORMAN, J. and MACHESKY, L.M., 2011. The Arp2/3 activator WASH regulates alpha5beta1-integrin-mediated invasive migration. Journal of cell science, 124(Pt 22), pp. 3753-3759.

ZEHE, C., ENGLING, A., WEGEHINGEL, S., SCHAFER, T. and NICKEL, W., 2006. Cell-surface heparan sulfate proteoglycans are essential components of the unconventional export machinery of FGF-2. Proceedings of the National Academy of Sciences of the United States of America, 103(42), pp. 15479-15484.

ZEISBERG, E.M., POTENTA, S.E., SUGIMOTO, H., ZEISBERG, M. and KALLURI, R., 2008. Fibroblasts in kidney fibrosis emerge via endothelial-to-mesenchymal transition. Journal of the American Society of Nephrology : JASN, 19(12), pp. 2282-2287.

ZEISBERG, M. and NEILSON, E.G., 2009. Biomarkers for epithelial-mesenchymal transitions. The Journal of clinical investigation, 119(6), pp. 1429-1437.

ZEMSKOV, E.A., JANIAK, A., HANG, J., WAGHRAY, A. and BELKIN, A.M., 2006. The role of tissue transglutaminase in cell-matrix interactions. Front Biosci, 11, pp. 1057-1076.

ZEMSKOV, E.A., LOUKINOVA, E., MIKHAILENKO, I., COLEMAN, R.A., STRICKLAND, D.K. and BELKIN, A.M., 2009. Regulation of platelet-derived growth factor receptor function by integrin-associated cell surface transglutaminase. The Journal of biological chemistry, 284(24), pp. 16693-16703.

ZEMSKOV, E.A., MIKHAILENKO, I., HSIA, R., ZARITSKAYA, L. and BELKIN, A.M., 2011. Unconventional secretion of tissue transglutaminase involves phospholipid-dependent delivery into recycling endosomes. PloS one, 6(4), pp. e19414.

ZEMSKOV, E.A., MIKHAILENKO, I., STRICKLAND, D.K. and BELKIN, A.M., 2007. Cell-surface transglutaminase undergoes internalization and lysosomal degradation: an essential role for LRP1. Journal of cell science, 120(Pt 18), pp. 3188-3199.

ZENG, Y., ADAMSON, R.H., CURRY, F.R. and TARBELL, J.M., 2014. Sphingosine-1-phosphate protects endothelial glycocalyx by inhibiting syndecan-1 shedding. American journal of physiology.Heart and circulatory physiology, 306(3), pp. H363-72.

ZHANG, H., AKMAN, H.O., SMITH, E.L., ZHAO, J., MURPHY-ULLRICH, J.E. and BATUMAN, O.A., 2003. Cellular response to hypoxia involves signaling via Smad proteins. Blood, 101(6), pp. 2253-2260.

ZHANG, J., NASLAVSKY, N. and CAPLAN, S., 2012. EHDs meet the retromer: Complex regulation of retrograde transport. Cellular logistics, 2(3), pp. 161-165.

ZHANG, J., REILING, C., REINECKE, J.B., PRISLAN, I., MARKY, L.A., SORGEN, P.L., NASLAVSKY, N. and CAPLAN, S., 2012. Rabankyrin-5 Interacts with EHD1 and Vps26 to Regulate Endocytic Trafficking and Retromer Function. Traffic, 13(5), pp. 745-757.

ZHANG, P., WU, Y., BELENKAYA, T.Y. and LIN, X., 2011. SNX3 controls Wingless/Wnt secretion through regulating retromer-dependent recycling of Wntless. Cell research, 21(12), pp. 1677-1690.

ZHANG, T. and HONG, W., 2001. Ykt6 forms a SNARE complex with syntaxin 5, GS28, and Bet1 and participates in a late stage in endoplasmic reticulum-Golgi transport. The Journal of biological chemistry, 276(29), pp. 27480-27487.

ZHANG, W., ZHOU, X., ZHANG, H., YAO, Q., LIU, Y. and DONG, Z., 2016. Extracellular vesicles in diagnosis and therapy of kidney diseases. American Journal of Physiology-Renal Physiology, 311(5), pp.F844-F851.

ZHANG, Z., XING, J., MA, L., GONG, R., CHIN, Y.E. and ZHUANG, S., 2009. Transglutaminase-1 regulates renal epithelial cell proliferation through activation of Stat-3. The Journal of biological chemistry, 284(5), pp. 3345-3353.

ZHAO, C., SLEVIN, J.T. and WHITEHEART, S.W., 2007. Cellular functions of NSF: not just SNAPs and SNAREs. FEBS letters, 581(11), pp. 2140-2149.

ZHAO, G., ZHANG, Z., ZHANG, B., LUO, M., SUN, Y. and WU, Z., 2011. Down-regulation of tTG expression by RNAi inhibits HSC proliferation and attenuates liver fibrosis. Int J Clin Exp Pathol, 4(5), pp. 513-520.

ZHAO, H., DONG, Y., TIAN, X., TAN, T.K., LIU, Z., ZHAO, Y., ZHANG, Y., HARRIS, D.C. and ZHENG, G., 2013. Matrix metalloproteinases contribute to kidney fibrosis in chronic kidney diseases. World journal of nephrology, 2(3), pp. 84-89.

ZHAO, Q., YANG, Y., WANG, C.L., HOU, Y. and CHEN, H., 2015. Screening and identification of the differential proteins in kidney with complete unilateral ureteral obstruction. International journal of clinical and experimental pathology, 8(3), pp. 2615-2626.

ZHAO, W., CHEN, S.S., CHEN, Y., AHOKAS, R.A. and SUN, Y., 2008. Kidney fibrosis in hypertensive rats: role of oxidative stress. American Journal of Nephrology, 28(4), pp. 548-554.

ZHAO, X., LIU, Y., HAN, Z. and XU, Y., 2015. Effect of erythropoietin on the expression of dynamin-related protein-1 in rat renal interstitial fibrosis. Experimental and therapeutic medicine, 9(6), pp. 2065-2071.

ZHENG, G., LYONS, J.G., TAN, T.K., WANG, Y., HSU, T., MIN, D., SUCCAR, L., RANGAN, G.K., HU, M. and HENDERSON, B.R., 2009. Disruption of E-cadherin by matrix metalloproteinase directly mediates epithelial-mesenchymal transition downstream of transforming growth factor-β1 in renal tubular epithelial cells. The American journal of pathology, 175(2), pp. 580-591.

ZHONG, C., CHRZANOWSKA-WODNICKA, M., BROWN, J., SHAUB, A., BELKIN, A.M. and BURRIDGE, K., 1998. Rho-mediated contractility exposes a cryptic site in fibronectin and induces fibronectin matrix assembly. The Journal of cell biology, 141(2), pp. 539-551.

ZIMMERMANN, P., MEERSCHAERT, K., REEKMANS, G., LEENAERTS, I., SMALL, J.V., VANDEKERCKHOVE, J., DAVID, G. and GETTEMANS, J., 2002. PIP 2-PDZ domain binding controls the association of syntenin with the plasma membrane. Molecular cell, 9(6), pp. 1215-1225.

ZIMMERMANN, P., ZHANG, Z., DEGEEST, G., MORTIER, E., LEENAERTS, I., COOMANS, C., SCHULZ, J., N'KULI, F., COURTOY, P.J. and DAVID, G., 2005. Syndecan Recyling Is Controlled by Syntenin-PIP 2 Interaction and Arf6. Developmental cell, 9(3), pp. 377-388.

ZOU, J., YAOITA, E., WATANABE, Y., YOSHIDA, Y., NAMETA, M., LI, H., QU, Z. and YAMAMOTO, T., 2006. Upregulation of nestin, vimentin, and desmin in rat podocytes in response to injury. Virchows Archiv, 448(4), pp. 485-492.